AD-A166 177 UNITED STATES AIR FORCE SUMMER FACULTY RESEARCH PROGRAM 1/15
1985 TECHNICAL RE (U) UNIVERSAL ENERGY SYSTEMS INC
DAYTON OH R C DARRAH ET AL. DEC 85 AFOSR-TR-86-0140

UNCLASSIFIED F49620-85-C-0013 F/G 5/1 NL

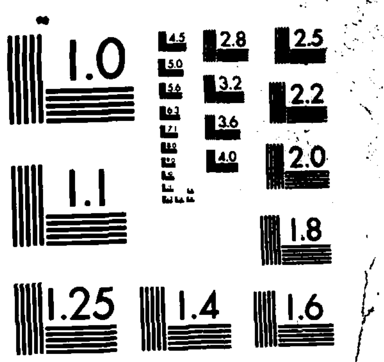

MICROCOPY RESOLUTION TEST CHART
NATIONAL BUREAU OF STANDARDS-1963-A

AD-A166 177

AIR FORCE OFFICE OF SCIENTIFIC RESEARCH

UNITED STATES AIR FORCE

SUMMER FACULTY RESEARCH PROGRAM

CONDUCTED BY
UNIVERSAL ENERGY SYSTEMS
U.E.S.

1985 TECHNICAL REPORT

VOLUME 2 OF 3

RODNEY C. DARRAH
PROGRAM DIRECTOR, UES

SUSAN K. ESPY
PROGRAM ADMINISTRATOR, UES

UNCLASSIFIED

SECURITY CLASSIFICATION OF THIS PAGE

REPORT DOCUMENTATION PAGE

1a. REPORT SECURITY CLASSIFICATION: UNCLASSIFIED

1b. RESTRICTIVE MARKINGS:

2a. SECURITY CLASSIFICATION AUTHORITY:

2b. DECLASSIFICATION/DOWNGRADING SCHEDULE:

3. DISTRIBUTION/AVAILABILITY OF REPORT: APPROVED FOR PUBLIC RELEASE; DISTRIBUTION UNLIMITED

4. PERFORMING ORGANIZATION REPORT NUMBER(S):

5. MONITORING ORGANIZATION REPORT NUMBER(S): AFOSR-TR- 86-0140

6a. NAME OF PERFORMING ORGANIZATION: Universal Energy Systems

6b. OFFICE SYMBOL (If applicable):

7a. NAME OF MONITORING ORGANIZATION: AFOSR/XOT

6c. ADDRESS (City, State and ZIP Code): 4401 Dayton-Xenia Rd. Dayton, Ohio 45432

7b. ADDRESS (City, State and ZIP Code): Building 410, Bolling AFB, DC 20332-6448

8a. NAME OF FUNDING/SPONSORING ORGANIZATION: AFOSR

8b. OFFICE SYMBOL (If applicable): XOT

9. PROCUREMENT INSTRUMENT IDENTIFICATION NUMBER: F49620-85-C-0013

8c. ADDRESS (City, State and ZIP Code): Building 410, Bolling AFB, DC 20332

10. SOURCE OF FUNDING NOS.

PROGRAM ELEMENT NO.	PROJECT NO.	TASK NO.	WORK UNIT NO.
61102F	2301	D5	

11. TITLE (Include Security Classification): United States Air Force Summer Faculty Research Program - Volume 2 - 1985

12. PERSONAL AUTHOR(S): Rodney C. Darrah, Susan K. Espy

13a. TYPE OF REPORT: Annual

13b. TIME COVERED: FROM ______ TO ______

14. DATE OF REPORT (Yr., Mo., Day): December 1985

15. PAGE COUNT:

16. SUPPLEMENTARY NOTATION:

17. COSATI CODES

FIELD	GROUP	SUB. GR.

18. SUBJECT TERMS (Continue on reverse if necessary and identify by block number):

19. ABSTRACT (Continue on reverse if necessary and identify by block number)

See Attached

20. DISTRIBUTION/AVAILABILITY OF ABSTRACT: UNCLASSIFIED/UNLIMITED ☒ SAME AS RPT. ☐ DTIC USERS ☐

21. ABSTRACT SECURITY CLASSIFICATION: UNCLASSIFIED

22a. NAME OF RESPONSIBLE INDIVIDUAL: Major Amos Otis, Program Manager

22b. TELEPHONE NUMBER (Include Area Code): (202) 767-4970

22c. OFFICE SYMBOL: XOT

DD FORM 1473, 83 APR   EDITION OF 1 JAN 73 IS OBSOLETE.

UNCLASSIFIED

SECURITY CLASSIFICATION OF THIS PAGE

TR- 86- 0190

The United States Air Force Graduate Student Summer Support Program (USAF-GSSSP) is conducted under the United States Air Force Summer Faculty Research Program. The program provides funds for selected graduate students to work at an appropriate Air Force Facility with a supervising professor who holds a concurrent Summer Faculty Research Program appointment or with a supervising Air Force Engineer. This is accomplished by the students being selected on a nationally advertised competitive basis for a ten-week assignment during the summer intersession period to perform research at Air Force laboratories/centers. Each assignment is in a subject area and at an Air Force facility mutually agreed upon by the students and the Air Force. In addition to compensation, travel and cost of living allowances are also paid. The USAF-GSSSP is sponsored by the Air Force Office of Scientific Research, Air Force Systems Command, United States Air Force, and is conducted by Universal Energy Systems, Inc.

The specific objectives of the 1985 USAF-GSSSP are:

(1) To provide a productive means for the graduate students to participate in research at the Air Force Weapons Laboratory;

(2) To stimulate continuing professional association among the Scholars and their professional peers in the Air Force;

(3) To further the research objectives of the United States Air Force;

(4) To enhance the research productivity and capabilities of the graduate students especially as these relate to Air Force technical interests.

During the summer of 1985, 92 graduate students participated. These researchers were assigned to 25 USAF laboratories/centers across the country. This two volume document is a compilation of the final reports written by the assigned students members about their summer research efforts.

AFOSR-TR- 86-0140

UNITED STATES AIR FORCE

SUMMER FACULTY RESEARCH PROGRAM

1985

PROGRAM TECHNICAL REPORT

UNIVERSAL ENERGY SYSTEMS, INC.

VOLUME II of III

Program Director, UES
Rodney C. Darrah

Program Manager, AFOSR
Major Amos L. Otis

Program Administrator, UES
Susan K. Espy

Submitted to

Air Force Office of Scientific Research

Bolling Air Force Base

Washington, DC

December 1985

86 4 1 150

PREFACE

The United States Air Force Summer Faculty Research Program (USAF-SFRP) is a program designed to introduce university, college, and technical institute faculty members to Air Force research. This is accomplished by the faculty members being selected on a nationally advertised competitive basis for a ten-week assignment during the summer intersession period to perform research at Air Force laboratories/centers. Each assignment is in a subject area and at an Air Force facility mutually agreed upon by the faculty members and the Air Force. In addition to compensation, travel and cost of living allowances are also paid. The USAF-SFRP is sponsored by the Air Force Office of Scientific Research, Air Force Systems Command, United States Air Force, and is conducted by Universal Energy Systems, Inc.

The specific objectives of the 1985 USAF-SFRP are:

(1) To provide a productive means for Scientists and Engineers holding Ph.D. degrees to participate in research at the Air Force Weapons Laboratory;

(2) To stimulate continuing professional association among the Scholars and their professional peers in the Air Force;

(3) To further the research objectives of the United States Air Force;

(4) To enhance the research productivity and capabilities of Scientists and Engineers especially as these relate to Air Force technical interests.

During the summer of 1985, 154-faculty members participated. These researchers were assigned to 25 USAF laboratories/centers across the country. This three volume document is a compilation of the final reports written by the assigned faculty members about their summer research efforts.

LIST OF PARTICIPANTS

NAME/ADDRESS	DEGREE, SPECIALTY, LABORATORY ASSIGNED
Dr. Phillip Ackerman Assistant Professor University of Minnesota Dept. of Psychology Elliott Hall 75 E. River Rd. Minneapolis, Minnesota 55455 (612) 376-3139	<u>Degree:</u> Ph.D., Philosophy in Psychology, 1984 <u>Specialty:</u> Human Abilities, Cognitive Processes, Research Methodology <u>Assigned:</u> HRL/MO
Dr. Samuel Adams Associate Professor Iowa State University Dept. of Industrial Engineering 212 Marston Hall Ames, Iowa 50011 (515) 294-5065	<u>Degree:</u> Ph.D., Industrial Engineering 1966 <u>Specialty:</u> Human Factors Engineering (Ergonomics), Biomechanics <u>Assigned:</u> AMRL
Dr. Vernon Allen Professor Tennessee Technological Univ. Dept. of Chemistry Box 5055 Cookeville, Tennessee 38505 (615) 528-3425	<u>Degree:</u> Ph.D., Polymer Science, 1960 <u>Specialty:</u> Polymer Structure - Property Relationship <u>Assigned:</u> AFWAL/ML
Dr. Jihad Alsadek Assistant Professor & Chairman Tougaloo College Department of Economics Tougaloo, Mississippi 39174 (601) 956-4941	<u>Degree:</u> Ph.D., Economics, 1983 <u>Specialty:</u> Economics <u>Assigned:</u> HRL/OT
Dr. Deborah Armstrong Assistant Professor University of Texas Division of Life Sciences San Antonio, Texas 78285 (512) 691-4458	<u>Degree:</u> Ph.D., Neuroscience, 1982 <u>Specialty:</u> Neurophysiology <u>Assigned:</u> SAM

Dr. Lucia Babcock Assistant Professor Louisiana State University Department of Chemistry Baton Rouge, Louisiana 70803 (504) 388-4694	<u>Degree:</u> <u>Specialty</u>: <u>Assigned</u>:	Ph.D., Inorganic Chemistry, 1978 Ion-Molecule Chemistry, Kinetics AFGL
Dr. Francesco Bacchialoni Associate Professor University of Lowell Dept. of Electrical Engr. 1 University Avenue Lowell, Massachusetts 01854 (617) 452-5000	<u>Degree:</u> <u>Specialty:</u> <u>Assigned:</u>	Ph.D., Engineering, 1946 Control Systems, Digital Signal Processing, Microprocessors AFGL
Dr. Mukul Banerjee Professor Meharry Medical College Physiology Department Nashville, Tennessee 37208 (615) 327-6288	<u>Degree:</u> <u>Specialty:</u> <u>Assigned:</u>	Ph.D., Animal Physiology, 1964 Respiratory Physiology, Environmental Physiology SAM
Dr. Rex Berney Associate Professor University of Dayton Physics Department 300 College Park Dayton, Ohio 45469 (513) 229-3012	<u>Degree:</u> <u>Specialty:</u> <u>Assigned:</u>	Ph.D., Solid State Physics, 1978 Digital Electronics, Photochromic Materials AFWAL/AL
Dr. Richard Bertrand Professor of Chemistry University of Colorado Department of Chemistry P. O. Box 7150 Colorado Springs, Colorado 80933-7150 (303) 593-3139	<u>Degree:</u> <u>Specialty:</u> <u>Assigned:</u>	Ph.D., Chemistry, 1969 NMR Spectroscopy, Atomic Spectroscopy FJSRL
Dr. Peter Binkert Associate Professor Oakland University Linguistics and Classics Department of Linguistics Rochester, Michigan 48063 (313) 370-2175	<u>Degree:</u> <u>Specialty:</u> <u>Assigned:</u>	Ph.D., Linguistics, 1970 Linguistic Theory, Natural Language Understanding by Computers HRL/IO

Dr. Zinny Bond
Associate Professor
Ohio University
Linguistics Department
204C Gordy Hall
Athens, Ohio 45701
(614) 594-6539

Degree: Ph.D., Linguistics, 1971
Specialty: Speech Acoustics, Speech Perception
Assigned: AMRL

Dr. Kevin Bowyer
Assistant Professor
University of South Florida
Computer Science & Engr. Dept.
Tampa, Florida 33620
(813) 974-3032

Degree: Ph.D., Computer Science, 1980
Specialty: Software Engineering, Computer Architecture, Computer Networks
Assigned: AD

Dr. Eugene Brown
Associate Professor
Virginia Polytech Institute
and State University
Blacksburg, Virginia 24060
(703) 961-7199

Degree: Ph.D., Mechanical Engineering, 1968
Specialty: Fluid Mechanics, Computational Fluid Dynamics
Assigned: WL

Dr. Linda Buehner
Assistant Professor
Wittenberg University
Education Department
P. O. Box 720
Springfield, Ohio 45501
(513) 327-6421

Degree: Ed. D., Curriculum and Instruction, 1983
Specialty: Learning and Developmental Handicaps, Reading
Assigned: HRL/LR

Dr. Connie Carrington
Assistant Professor
University of South Carolina
Mechanical Engineering Dept.
College of Engineering
Columbia, South Carolina 29208
(803) 777-7144

Degree: Ph.D., Engineering Mechanics, 1983
Specialty: Dynamics and Controls
Assigned: AFWAL/FDL

Dr. Robert Chamberlain
Assistant Professor
University of Alabama
Dept. of Aerospace Engr.
241 Hardaway Hall
University, Alabama 35486
(205) 348-7300

Degree: Ph.D., Aeronautical and Astronautical Engineering, 1984
Specialty: Computational Fluid Dynamics
Assigned: AFWAL/FDL

Dr. Jharna Chaudhuri Assistant Professor Wichita State University Mechanical Engr. Department Box 35 Wichita, Kansas 67208 (316) 689-3402	Degree: Specialty: Assigned:	Ph.D., Materials Science, 1982 Materials Science, Metallurgy, Thin Films, Electronic Materials AFWAL/AL
Dr. Lea Chen Assistant Professor The University of Iowa Dept. Mechanical Engineering 2206 EB Iowa City, Iowa 52242 (319) 353-5695	Degree: Specialty: Assigned:	Ph.D., Mechanical Engineering, 1981 Combustion AFWAL/APL
Dr. David Choate Assistant Professor Xavier University Mathematics Department New Orleans, Louisiana 70125 (504) 486-7411	Degree: Specialty: Assigned:	Ph.D., Mathematics, 1982 Algebra and Number Theory RADC
Dr. Karen Chou Assistant Professor Syracuse University Dept. of Civil Engr. Syracuse, New York 13210 (315) 423-3314	Degree: Specialty: Assigned:	Ph.D., Philosophy, Structural Engineering, 1983 Structural Engineering, Structural Reliability, Application of Probability and Statistics in Chemical Engineering ESC
Dr. Louis Chow Assistant Professor Washington State University Mechanical Engineering Dept. Pullman, Washington 99164-2920 (509) 335-1327	Degree: Specialty: Assigned:	Ph.D., Mechanical Engineering, 1978 Heat and Mass Transfer, Fluid Mechanics AFWAL/APL
Dr. Derald Chriss Instructor Southern University Department of Chemistry Baton Rouge, Louisiana 70813 (504) 771-3990	Degree: Specialty: Assigned:	M.S., Chemistry, 1981 NMR Spectroscopy, X-Ray Crystallography, Gas Chromatography, Magnetic Susceptibility Studies AFWAL/ML

Dr. David Chung Professor Howard University Department of Physics Washington, D.C. 20059 (202) 636-7903	Degree: Specialty: Assigned:	Ph.D., Solid State Physics, 1966 Fiber Optics Sensors, Ultrasound, Solid State Electronics RADC
Dr. Gale Clark Associate Professor Middle Tennessee State Univ. Chemistry Department P. O. Box 137 Murfreesboro, Tennessee 37132 (615) 898-2300	Degree: Specialty: Assigned:	Ph.D., Analytical Chemistry, 1968 HPLC using Electrochemical and Fluorescent Detection ESC
Dr. David Cochran Assistant Professor Clemson University Electrical and Computer Engineering Department Clemson, South Carolina 29631 (803) 656-3190	Degree: Specialty: Assigned:	Ph.D., Electrical Engineering, 1981 Solid State RADC
Dr. Alvin Compaan Professor Kansas State University Department of Physics Cardwell Hall Manhattan, Kansas 66506 (913) 532-6786	Degree: Specialty: Assigned:	Ph.D., Physics, 1971 Laser Interaction with Semiconductors AFWAL/AL
Dr. Thomas Connolly Professor Embry-Riddle Aeronautical University Aeronautical Science Regional Airport Daytona Beach, Florida 32014 (904) 252-5561	Degree: Specialty: Assigned:	Ed.D., Technical Education, 1979 Aviation Education, Instructional Technology HRL/OT
Dr. Hobert Corley Instructor Davis and Elkins College Computer Science Dept. Elkins, West Virginia 26241 (304) 636-1900	Degree: Specialty: Assigned:	M.S. Computer Science, 1980 Computer Science HRL/LR

Dr. Billy Covington Assistant Professor Sam Houston State University Physics Department Hunstville, Texas 77341 (409) 294-1606	<u>Degree:</u> Ph.D., Physics, 1978 <u>Specialty:</u> Solid State Physics <u>Assigned:</u> AFWAL/ML
Dr. Dennis Cravens Instructor Vernon Regional Jr. College Science and Math. Dept. 4400 College Drive Vernon, Texas 76384 (817) 552-6291	<u>Degree:</u> Ph.D., Molecular Biophysics, 1977 <u>Specialty:</u> Mathematic Models, (numerical calculations) <u>Assigned:</u> RPL
Dr. Parviz Dadras Associate Professor Wright State University Mechanics Systems Engineering Dayton, Ohio 45435 (513) 873-2944	<u>Degree:</u> Ph.D., Mechanical Engineering, 1972 <u>Specialty:</u> Mechanics, Deformation Processing, Material Properties <u>Assigned:</u> AFWAL/ML
Dr. Charles Davis Assistant Professor University of Toledo Department of Math. Toledo, Ohio 43606 (419) 537-2297	<u>Degree:</u> Ph.D. Statistics, 1976 <u>Specialty:</u> Statistics <u>Assigned:</u> AMRL
Dr. Vito DelVecchio Professor of Biology University of Scranton Scranton, Pennsylvania 18510 (717) 961-6117	<u>Degree:</u> Ph.D., Biochemical Genetics, 1967 <u>Specialty:</u> Immunochemistry and Recombinant DNA Probes <u>Assigned:</u> SAM
Dr. Hermann Donnert Professor Kansas State University Department of Nuclear Engineering Ward Hall Manhattan, Kansas 66506-7039 (913) 532-5960	<u>Degree:</u> Ph.D., Mathematics and Physics, 1951 <u>Specialty:</u> Radiation Physics, Nuclear Weapon Effects, Plasma Physics <u>Assigned:</u> FJSRL

Dr. Melvin Druelinger
Professor
University of Southern Colorado
Chemistry Department
2200 N. Bonforte Blvd.
Pueblo, Colorado 81001
(303) 549-2166

Degree: Ph.D. Chemistry, 1967
Specialty: Organic Chemistry (Mechanisms, Synthesis, Photochemistry, Energetic Materials Fluorinations)
Assigned: RPL

Dr. Charles Drummond, III
Associate Professor
The Ohio State University
Dept. of Ceramic Engineering
2041 College Road
Columbus, Ohio 43210
(614) 422-2960

Degree: Ph.D., Applied Physics, 1974
Specialty: Glass Structure and Properties and Composites
Assigned: AFWAL/ML

Dr. Leroy Eimers
Associate Professor
Cedarville College
Dept. of Science and Math.
Cedarville, Ohio 45314
(513) 766-2211

Degree: Ph.D., Theoretical Physics, 1970
Specialty: Mathematics, Physics
Assigned: AFWAL/APL

Dr. Hudson Eldridge
University of Central Arkansas
Physics Department, LSC 149
Conway, Arkansas 72032
(501) 450-3146

Degree: Ph.D., Nuclear Physics, 1967
Specialty: Experimental Nuclear Physics, Computing, Digital Electronics
Assigned: WL

Dr. Harry Emrick
Associate Professor
Colorado School of Mines
Dept. of Engineering
Golden, Colorado 80401
(303) 273-3675

Degree: Ph.D., Geodetic/Computer Science, 1973
Specialty: Positional Geodesy - Computer Applications
Assigned: FJSRL

Dr. John Erdei
Assistant Professor
University of Dayton
Dept. of Physics
300 College Park
Dayton, Ohio 45469
(513) 229-2318

Degree: Ph.D., Condensed Matter Theory, 1983
Specialty: Critical Phenomena and Field Theory
Assigned: AFWAL/APL

Dr. Dah-Nien Fan Professor Howard University Dept. of Mechanical Engr. Washington, D.C. 22059 (202) 636-6607	Degree:	Ph.D., Aerospace Engineering, 1966
	Specialty:	Fluid Mechanics, Aerodynamics, Tensor Theory, Applied Mathematics
	Assigned:	AFWAL/FDL
Dr. Mack Felton Chairman and Professor Southern University at New Orleans Biology Department 6400 Press Drive New Orleans, Louisiana 70126 (504) 282-4401	Degree:	Ph.D., Microbiology, 1973
	Specialty:	Virus Adsorption, Microbial Ecology, Physiology
	Assigned:	SAM
Dr. Edna Fiedler St. Mary's University Department Head - Psychology One Camino Santa Maria San Antonio, Texas 78284 (512) 436-3314	Degree:	Ph.D., Psychology, 1972
	Specialty:	Social and Clinical Psychology
	Assigned:	HRL/MO
Dr. John Flach Assistant Professor University of Illinois at Urbana-Champaign Aviation Research Laboratory Willard Airport Savoy, Illinois 61874 (217) 333-7749	Degree:	Ph.D., Psychology, 1984
	Specialty:	Human Performance and Engineering Psychology
	Assigned:	AMRL
Dr. John Fleming Assistant Professor Texas A&M University Dept. of Electrical Engr. College Station, Texas 77843 (409) 845-7441	Degree:	Ph.D. Electrical Engineering, 1977
	Specialty:	Systems, Control, Applied Mathematics, and Digital Signal Processing
	Assigned:	RADC
Dr. Dennis Flentge Assistant Professor Cedarville College Math and Science Dept. Cedarville, Ohio 45314 (513) 766-2211	Degree:	Ph.D., Physical Chemistry, 1974
	Specialty:	Catalysis, Infrared Spectroscopy
	Assigned:	AFWAL/APL

Dr. Bessie Foster Professor Grambling State University Department of Physics Grambling, Louisiana 71245 (318) 274-2574	<u>Degree:</u> <u>Specialty:</u> <u>Assigned:</u>	Ph.D., Science, Radiological Science, 1968 Radiological Science (Health Physics and Radiation Biology) WL
Dr. James Gallas Assistant Professor University of Texas 1604 Loop/Rt. 10 San Antonio, Texas 78250 (512) 691-5446	<u>Degree:</u> <u>Specialty:</u> <u>Assigned:</u>	Ph.D., Physics, 1981 Interaction of Light (lasers) with Biological and Polymeric Materials SAM
Dr. Chester Gardner Professor University of Illinois Electrical and Computer Engr. 1406 W. Green Urbana, Illinois 61801 (217) 333-4682	<u>Degree:</u> <u>Specialty:</u> <u>Assigned:</u>	Ph.D., Electrical Engineering, 1973 Laser Remote Sensing, Optical Communications, Fiber Optics AFGL
Dr. Doris Ginn Associate Professor Jackson State University English Department 1400 John R. Lynch Street Jackson, Mississippi 39217 (601) 968-2116	<u>Degree:</u> <u>Specialty:</u> <u>Assigned:</u>	Ph.D., Linguistics, 1979 English as a Second Language and Sociolinguistics WL
Dr. Ramana Grandhi Assistant Professor Wright State University Mechanical Systems Engineering School of Engineering Dayton, Ohio 45435 (513) 873-2079	<u>Degree:</u> <u>Specialty:</u> <u>Assigned:</u>	Ph.D., Engineering Mechanics, 1984 Structural Optimization AFWAL/FDL
Dr. Alwin Green Associate Professor State University College - Buffalo Mathematics Department 1300 Elmwood Avenue Buffalo, New York 14222 (716) 878-4420	<u>Degree:</u> <u>Specialty:</u> <u>Assigned:</u>	Ph.D., Mathematics, 1972 Graph Theory, Networks, Combinatorics, Mathematics Modeling RADC

Mr. Mahesh Greywall Professor Wichita State University Mechanical Engineering Dept. Box 35 Wichita, Kansas 67208 (316) 689-3402	Degree: Specialty: Assigned:	Ph.D., Mechanical Engineering, 1962 Fluid Mechanics AFWAL/APL
Dr. Vijay Gupta Associate Professor Central State University Chemistry Department Wilberforce, Ohio 45384 (513) 376-6423	Degree: Specialty: Assigned:	Ph.D., Chemistry, 1969 Physical Chemistry AFWAL/ML
Dr. Barry Haack Associate Professor Ball State University Dept. of Geography Muncie, Indiana 47306 (317) 285-1776	Degree: Specialty: Assigned:	Ph.D. Geography, 1977 Digital Processing of Remotely Sensed Data RADC
Dr. Je-Chin Han Associate Professor Texas A&M University Mechanical Engr. Department College Station, Texas 77843 (409) 845-3738	Degree: Specialty: Assigned:	Sc.D., Mechanical Engineering Heat Transfer, 1976 Heat Transfer AFWAL/APL
Dr. Donald Hanson Associate Professor University of Mississippi Electrical Engineering Dept. University, Mississippi 38677 (601) 232-5389	Degree: Specialty: Assigned:	Ph.D., Electromagnetics, 1976 Electromagnetic Field Theory and MOSFET VLSI Design RADC
Dr. David Hart Assistant Professor University of Florida Dept. of Mathematics 201 Walker Hall Gainesville, Florida 32611 (904) 392-6162	Degree: Specialty: Assigned:	Ph.D., Mathematics, 1980 Nonlinear Differential Equations AFWAL/FDL

Dr. Albert Heaney Professor California State University Electrical Engineering Dept. Shaw and Cedar Avenues Fresno, California 93740 (209) 294-2157	<u>Degree:</u> <u>Specialty:</u> <u>Assigned:</u>	Ph.D. Electrical Engineering, 1972 Computer Engineering RADC
Dr. Carolyn Heising Associate Professor Northeastern University Industrial Engineering Dept. 360 Huntington Ave. Boston, Massachusetts 02115 (617) 437-4948	<u>Degree:</u> <u>Specialty:</u> <u>Assigned:</u>	Ph.D., Mechanical Engineering, 1978 Reliability Analysis/Risk Assessment ESD
Dr. Troy Henson Associate Professor Louisiana Tech University Electrical Engr. Dept. Tech Station Ruston, Louisiana 71272 (318) 257-4715	<u>Degree:</u> <u>Specialty:</u> <u>Assigned:</u>	Ph.D. Electrical Engineering, 1975 Communications and Control Systems Theory, Digital Signal Processing AMRL
Dr. Astor Herrell Professor and Chairman Winston-Salem State University P. O. Box 13236 Winston-Salem, North Carolina 27110 (919) 761-2098	<u>Degree:</u> <u>Specialty:</u> <u>Assigned:</u>	Ph.D., Inorganic Chemistry, 1973 Chemistry and Physical Science AEDC
Dr. Albert Hsui Associate Professor University of Illinois Dept. of Geology 245 Nat. Hist. Bldg. 1301 W. Green Street Urbana, Illinois 61801 (217) 333-7732	<u>Degree:</u> <u>Specialty:</u> <u>Assigned:</u>	Ph.D., Geophysics and Mechanics, 1972 Geophysics, Applied Mathematics, Computer Simulation AFGL
Dr. Clifford Johnston Assistant Professor University of Florida Soil Science 2169 McCarty Hall Gainesville, Florida 32611 (904) 392-1951	<u>Degree:</u> <u>Specialty:</u> <u>Assigned:</u>	Ph.D., Soil Physical Chemistry, 1983 Vibrational Spectroscopy (laser Raman and FTIR) ESC

Dr. Betty Jones	Degree:	Ph.D., Biology, 1978
Associate Professor and Director of the Institute of Electron Microscopy	Specialty:	Medical Parasitology Tropical Medicine and Electron Microscopy
Morehouse College	Assigned:	SAM
Department of Biology		
830 Westview Drive, S.W.		
Atlanta, Georgia 30314		
(404) 681-2800		

Dr. Jeremy Jones	Degree:	M.S., Physics, 1970
Assistant Professor	Specialty:	Artificial Intelligence,
The University of West Florida		Computer Science Department
Systems Science Department	Assigned:	AFWAL/AL
Pensacola, Florida 32514-0103		
(904) 474-2551		

Dr. Patrick Jones	Degree:	Ph.D., Chemical Physics, 1980
Assistant Professor		
The Ohio State University	Specialty:	Chemical Dynamics
Chemistry Department	Assigned:	AFWAL/AL
140 W. 18th Avenue		
Columbus, Ohio 43210		
(614) 422-9489		

Dr. Walter Jones	Degree:	Ph.D., Engineering Mechanics, 1982
Assistant Professor		
University of Tennessee	Specialty:	Mechanics of Composite Materials
Dept. of Engineering Science and Mechanics	Assigned:	AFWAL/FDL
310 Perkins Hall		
Knoxville, Tennessee 37996-2030		
(615) 974-7684		

Dr. Prasad Kadaba	Degree:	Ph.D., Physics, 1950
Professor	Specialty:	Dielectric Relaxation and Magnetic Resonance: Microwave and Millimet Wave Measurements
University of Kentucky		
Electrical Engineering Dept.		
Room 453 Anderson Hall		
Lexington, Kentucky 40506	Assigned:	AFWAL/ML
(606) 257-2966		

Dr. James Kane	Degree:	Ph.D., Chemistry, 1960
Associate Professor	Specialty:	Organic, Physical Organic, Polymer Chemistry
Wright State University		
Chemistry Department	Assigned:	AFWAL/ML
Dayton, Ohio 45435		
(513) 873-2352		

Dr. Amir Karimi
Assistant Professor
University of Texas
San Antonio
Division of Engineering
San Antonio, Texas 78285
(512) 691-5514

Degree: Ph.D. Mechanical Engineering, 1982
Specialty: Thermal Sciences, Condensation, Heat Exchanger Design, Heat Transfer, Phase Change Processes, Metastable Thermodynamics
Assigned: SAM

Dr. Daisy Kimble
Instructor
Southern University
Chemistry Department
P. O. Box S.U.
Baton Rouge, Louisiana 70813
(504) 771-3990

Degree: B.S., Chemistry, 1974
Specialty: Chemistry-Analytical
Assigned: FJSRL

Dr. David Kohfeld
Professor
Southern Illinois University
at Edwardsville
Edwardsville, Illinois 62026
(618) 692-2582

Degree: Ph.D., Experimental Psychology, 1966
Specialty: Human Performance and Reaction Time, Math Models
Assigned: HRL/OT

Dr. Stephan Kolitz
Assistant Professor
University of Massachusetts
Boston
Harbor Campus
Boston, Massachusetts 02125
(617) 929-8051

Degree: Ph.D. Industrial Engineering, 1983
Specialty: Operations Research
Assigned: ESD

Dr. Lawrence Koons
Professor
Tuskegee Institute
Chemistry Department
Tuskegee Institute, Alabama 36088
(205) 727-8835

Degree: Ph.D., Physical Chemistry, 1956
Specialty: Electrochemistry
Assigned: FJSRL

Dr. Arthur Kovitz
Professor
Northwestern University
Mechanical and Nuclear Engr.
2145 Sheridan Road
Evanston, Illinois 60201
(312) 491-7066

Degree: Ph.D., Aerospace Engineering, 1957
Specialty: Fluid Mechanics, (Interfaces, Combustion, Computation)
Assigned: WL

Dr. Kurt Kraiger Assistant Professor University of Colorado at Denver Department of Psychology 1100 14th Street Denver, Colorado 80202 (303) 556-8351	Degree: Specialty: Assigned:	Ph.D., Industrial/ Organizational Psychology, 1983 I/O Psychology, Performance Appraisal, Job Attitudes, Meta-Analysis HRL/MO
Dr. Madakasira Krishna Professor South Carolina State College Mathematics and Computer Science Box 1814, State College Orangeburg, Souch Carolina 29117 (803) 536-7120	Degree: Specialty: Assigned:	Ph.D., Numerical Analysis, Fluid Mechanics Computer Science, 1974 Computational Fluid Mechanics, Numerical Analysis, Pde AD
Dr. Paul Lee Associate Professor North Carolina A&T State Univ. Dept. of Business Administration Greensboro, North Carolina 27411 (919) 379-7744	Degree: Specialty: Assigned:	Ph.D., Resource Economics, 1973 Statistics, Management Science and Computer Sciences LMDC
Dr. Benjamin Lev Professor and Chairman Temple University Department of Management School of Business Admin. Philadelphia, Pennsylvania 19122 (215) 787-8188	Degree: Specialty: Assigned:	Ph.D., Operations Research, 1970 Production Management, Mathematical Programming RADC
Dr. Edward Lewis Professor Belmont College Computer Information Systems/ Management Science 1900 Belmont Blvd. Nashville, Tennessee 37203 (615) 383-7001	Degree: Specialty: Assigned:	Ph.D., Met. Science (Operations Research and Statistics), 1978 Mathematical Modeling, Decision Support, Statistical Analysis LMC
Dr. Michael Lewis Assistant Professor Troy State University CIS Department Troy, Alabama 36082 (205) 566-3000	Degree: Specialty: Assigned:	M.S., Computer and Information Science, 1985 Advanced Microcomputer Applications LMC

Dr. Philip Lewis
Professor
Auburn University
Department of Psychology
Auburn University, Alabama 36849
(205) 826-4424

Degree: Ph.D., Clinical Psychology, 1968
Specialty: Marital Dynamics, Personality Development, Leadership
Assigned: LMDC

Dr. Irene Little-Marenin
Assistant Professor
Wellesley College
Astronomy Department
Whitin Observatory
Wellesley, Massachusetts 02181
(617) 325-0320

Degree: Ph.D., Astrophysics, 1970
Specialty: Astrophysics, Cool Stars
Assigned: AFGL

Dr. Dar-Biau Liu
Associate Professor
Old Dominion University
Dept. of Computer Sciences
Norfolk, Virginia 23508
(804) 440-3901

Degree: Ph.D., Applied Mathematics and Computer Sciences, 1972
Specialty: Computer Science
Assigned: RADC

Dr. Carl Looney
Associate Professor
University of Nevada
EE/Computer Science Dept.
Reno, Nevada 89557-0030
(702) 784-6918

Degree: Ph.D., Mathematic Analysis, 1972
Specialty: Artifical Intelligence, Tracking, Filtering
Assigned: AFWAL/AL

Dr. James Marsh
Associate Professor
University of West Florida
Department of Physics
Pensacola, Florida 32514
(904) 474-2270

Degree: Ph.D., Physics, 1966
Specialty: Optics (Physical), Electromagnetic Theory
Assigned: AD

Dr. Charles Mastin
Professor
Mississippi State University
Mathematics and Stat. Dept.
Drawer MA
Mississippi State, Mississippi 39762
(601) 325-3414

Degree: Ph.D., Mathematics, 1969
Specialty: Computational Fluid Dynamics
Assigned: AEDC

Dr. Odis McDuff
Professor
The University of Alabama
Electrical Engineering
P. O. Box 6169
University, Alabama 35486
(205) 348-6351

Degree: Ph.D., Electrical Engineering, 1966
Specialty: Lasers and Optics, Electromagnetics
Assigned: SAM

Mr. Bernard McIntyre
Associate Professor
University of Houston
Electrical Electronics Dept.
University Park
4800 Calhoun St.
Houston, Texas 77004
(713) 749-4753

Degree: Ph.D., Solid State Physics, 1970
Specialty: Space Plasma Physics
Assigned: AFGL

Dr. Leathem Mehaffey
Associate Professor
Vassar College
Biology Department
Box 410
Poughkeepsie, New York 12601
(914) 452-7000

Degree: Ph.D., Biophysics, 1971
Specialty: Neurobiology and Physiology of Vision
Assigned: SAM

Dr. Ivor Mitchell
Professor
Marketing Department
Atlanta University
223 Chestnut Street, S.W.
Atlanta, Georgia 30337
(404) 681-0251

Degree: Ph.D., Marketing and Statistics, 1977
Specialty: Marketing, Statistics
Assigned: LMDC

Dr. James Moore
Professor
University of Arkansas
Civil Engineering Dept.
Fayetteville, Arizona 72701
(501) 575-6027

Degree: Ph.D., Environmental Health Engineering, 1972
Specialty: Environmental Engineering
Assigned: ESC

Dr. Osoma Mostafa
Associate Professor
California State University
Electronics Engineering Dept.
C. S. U. C. #930
Chico, California 95929
(916) 895-5374

Degree: Ph.D., Electrical Engineering, 1975
Specialty: Systems, Automation, Artificial Intelligence
Assigned: AD

Dr. Rex Moyer Associate Professor Trinity University Biology Department 715 Stadium Drive San Antonio, Texas 78284 (512) 736-7242	<u>Degree:</u> <u>Specialty:</u> <u>Assigned</u>	Ph.D., Microbiology, 1965 Molecular Biology, Experimental Oncology SAM
Dr. James Mrotek Associate Professor Meharry Medical College Department of Physiology 1005 D. B. Todd Blvd. Nashville, Tennessee 37208 (615) 327-6979	<u>Degree:</u> <u>Specialty:</u> <u>Assigned:</u>	Ph.D., Biology, 1973 Environmental Influences on Cultured Mammalian Cells, Endocrine Cell Intracellular Exchanges SAM
Dr. Maurice Neveu Associate Professor State University College of N.Y. Chemistry Department Fredonia, New York 14063 (716) 673-3285	<u>Degree:</u> <u>Specialty:</u> <u>Assigned:</u>	Ph.D., Physical-Organic Chemistry, 1959 Physical-Organic Chemistry, Synthetic Organic Chemistry, Chemical Kinetics, Reaction Mechanisms, Explosives, Aviation Fuels AD
Dr. Robert Niebuhr Associate Professor Auburn University Dept. of Management Auburn, Alabama 36849 (205) 826-4591	<u>Degree:</u> <u>Specialty:</u> <u>Assigned:</u>	Ph.D., Management, 1977 Management Processes, Organizational Behavior LMDC
Dr. Marion Noble Professor Kansas State University Physical Education Dept. 203 Ahearn Gym Manhattan, Kansas 66506 (913) 532-6765	<u>Degree:</u> <u>Specialty:</u> <u>Assigned:</u>	Ph.D., Biomechanics, 1970 Biomechanics AMRL
Dr. Robert O'Connell Assistant Professor University of Missouri-Columbia Electrical and Engr. Dept. Columbia, Missouri 65211 (314) 882-8373	<u>Degree:</u> <u>Specialty:</u> <u>Assigned:</u>	Ph.D., Electrical Engineering, 1975 Applied Optics, Laser Effects FJSRL

Dr. Ralph Oberly Professor and Chairman Marshall University Physics Department Huntington, West Virginia 25701 (304) 696-6738	Degree: Specialty: Assigned:	Ph.D., Physics (Molecular Spectra), 1970 Molecular Spectroscopy, Optical Devices AFWAL/APL
Dr. Won Park Professor Wright State University Mathematics and Statistics Dept. Dayton, Ohio 45435 (513) 873-2837	Degree: Specialty: Assigned:	Ph.D., Mathematics, 1969 Stochastic Processes, Time Series, Reliability AFWAL/AL
Dr. Desmond Penny Assistant Professor Southern Utah State College Physical Science Department Cedar City, Utah 84720 (801) 586-7708	Degree: Specialty: Assigned:	Ph.D., Civil Engineering, 1975 Continuum Mechanics ESC
Dr. John Pierce Associate Professor University of North Alabama Department of Chemistry Florence, Alabama 35632 (205) 766-4100	Degree: Specialty: Assigned:	Ph.D., Environmental Health, 1978 Thermal Absorption of Toxicants, Analytical Methods Development OEHL
Dr. Boake Plessy Professor Dillard University Division of Natural Science 2601 Gentilly Blvd. New Orleans, Louisiana 70122 (504) 283-8822	Degree: Specialty: Assigned:	Ph.D., Physical Chemistry, 1974 Biopolymers, Proteoglycans from Corneal Tissue SAM
Dr. Arnold Polak Professor University of Cincinnati Dept. of Aerospace Engr. and Engr. Mechanics ML 70 Cincinnati, Ohio 45221 (513) 475-5133	Degree: Specialty: Assigned:	Ph.D., Aerospace Engineering, 1966 Fluid Mechanics AFWAL/APL

Dr. Justin Poland Associate Professor University of Maine Orono Mechanical Engineering Dept. 209 Boardman Hall Orono, Maine 04469 (207) 581-2123	<u>Degree:</u> <u>Specialty:</u> <u>Assigned:</u>	Ph.D., Mechanical Engineering, 1979 Thermal Sciences, Thermodynamics, Heat Transfer, Fluid Mechanics AEDC
Dr. Kuldip Rattan Associate Professor Wright State University Electrical Systems Engineering Department Fawcett Hall, Room 354 Dayton, Ohio 45435 (513) 873-2497	<u>Degree:</u> <u>Specialty:</u> <u>Assigned:</u>	Ph.D., Electrical Engineering, 1975 Digital Control Systems AFWAL/FDL
Dr. Hemen Ray Assistant Professor North Carolina A&T State Univ. Mechanical Engr. Dept. 112 Cherry Hall Greensboro, North Carolina 27411 (919) 379-7621	<u>Degree:</u> <u>Specialty:</u> <u>Assigned:</u>	Ph.D., Engineering Mechanics, 1979 Advanced Composites AFWAL/FDL
Dr. John Renie Assistant Professor University of Illinois Dept. of Mechanical and Industrial Engineering 1206 W. Green Street Urbana, Illinois 61801 (217) 333-6199	<u>Degree:</u> <u>Specialty:</u> <u>Assigned:</u>	Ph.D., Combustion/ Engineering, 1982 Combustion and Fluid Dynamics RPL
Dr. Michael Rhodes Instructor Clark College Department of Physics 240 Brawley Drive, S.W. Atlanta, Georgia 30314 (404) 681-3080	<u>Degree:</u> <u>Specialty:</u> <u>Assigned:</u>	Ph,D., Physics, 1983 Plasma Physics, Numerical Analysis AFGL
Dr. Robert Ricci Professor and Chairman Holy Cross College Chemistry Department Worcester, Massachusetts 01610 (617) 793-3380	<u>Degree:</u> <u>Specialty:</u> <u>Assigned:</u>	Ph.D., Chemistry, 1961 Physical Chemistry, Analytical Chemistry AFGL

Dr. James Riehl Associate Professor University of Missouri Department of Chemistry 8001 Natural Bridge Road St. Louis, Missouri 63121 (314) 553-5328	<u>Degree:</u> <u>Specialty:</u> <u>Assigned:</u>	PH.D., Physical Chemistry, 1975 Physical Chemistry, Theoretical Chemistry, Laser, Spectroscopy AFGL
Dr. Michael Ross Associate Professor Slippery Rock University Computer Science Department Slippery Rock, Pennsylvania 16057 (412) 794-7133	<u>Degree:</u> <u>Specialty:</u> <u>Assigned:</u>	Ph.D., Applied Mathematics, Computer Simulation, Operating Systems, Numerical Analysis AMRL
Dr. Samuel Russell Assistant Professor University of South Carolina Mechanical Engineering Dept. Columbia, South Carolina 29208 (803) 777-3241	<u>Degree:</u> <u>Specialty:</u> <u>Assigned:</u>	Ph.D., Engrineering Mechanics, 1982 Nondestructive Testing of Composite Materials AFWAL/ML
Dr. Sally Sage Assistant Professor West Georgia College Department of Math and Computer Science Carrollton, Georgia 30118 (404) 834-1380	<u>Degree:</u> <u>Specialty:</u> <u>Assigned:</u>	M.S., Computer Science, 1979 Programming Languages and Computer Simulation AD
Dr. Joseph Saliba Assistant Professor University of Dayton Civil Engr. Dept. 300 College Park Dayton, Ohio 45469 (513) 229-3847	<u>Degree:</u> <u>Specialty:</u> <u>Assigned:</u>	Ph.D., Solid Mechanics, 1983 Solid Mechanics - Structures AFWAL/FDL
Dr. Gordon Schrank Associate Professor St. Cloud State University Dept. of Biology Sciences St. Cloud, Minnesota 56301 (612) 255-2036	<u>Degree:</u> <u>Specialty:</u> <u>Assigned:</u>	Ph.D., Medical Microbiology, 1974 General Microbiology, Medical Microbiology, Electron Microscopy SAM

Dr. Ronald Sega Assistant Professor University of Colorado Department of Electrical Engr. Colorado Springs, Colorado 80933-7150 (303) 593-3510	Degree: Specialty: Assigned:	Ph.D., Electrical Engineering, 1982 Electromagnetics FJSRL
Dr. Paul Seybold Professor Wright State University Chemistry Department Dayton, Ohio 45435 (513) 873-2407	Degree: Specialty: Assigned:	Ph.D., Biophysics, 1968 Structure-Activity Relations AMRL
Dr. Shawky Shamma Professor University of West Florida Pensacola, Florida 32504 (904) 474-2281	Degree: Specialty: Assigned:	Ph.D., Applied Mathematics, Applied Mathematics AD
Dr. Ralph Sheets Professor Southwest Missouri State Univ. Department of Chemistry Springfield, Missouri 65804 (417) 836-5611	Degree: Specialty: Assigned:	Ph.D., Physical Chemistry, 1971 Chemistry (surface chemistry and catalysis environmental) OEHL
Dr. Kyle Siegrist Assistant Professor University of Alabama Mathematics Department Huntsville, Alabama 35899 (205) 895-6470	Degree: Specialty: Assigned:	Ph.D., Applied Mathematics, 1979 Probability and Stochastic Processes RADC
Dr. Ricardo Silva Professor California State University 18111 Nordhoff Street Northridge, California 91330 (818) 885-3378	Degree: Specialty: Assigned:	Ph.D., Chemistry, 1961 Organic Chemistry, Synthesis and Analysis RPL
Dr. S. Ballou Skinner Professor University of South Carolina Coastal Carolina College Physics Department P. O. Box 1954 Conway, South Carolina 29526 (803) 347-3161	Degree: Specialty: Assigned:	Ph.D., Physics, 1970 Nuclear and Radiation Physics, Gamma Ray Spectroscopy, Neutron Activation Analysis AEDC

Dr. Terrill Smith Professor Central State University Chemistry Department 100 N. University Drive Edmond, Oklahoma 73034 (405) 341-2980	Degree: Specialty: Assigned:	Ph.D., Organic Chemistry, 1959 Organic, Polymer, Fluorine, Industrial Chemistry AFWAL/ML
Dr. Siavash Sohrab Assistant Professor Northwestern University MNE Department Technical Institute Evanston, Illinois 60201 (312) 491-3572	Degree: Specialty: Assigned:	Ph.D., Engineering Physics, 1981 Combustion RPL
Dr. Richard Stebbins Assistant Professor University of Southern Maine Chemistry Department 96 Falmouth Street 360 Science Building Portland, Maine 04103 (207) 780-4232	Degree: Specialty: Assigned:	Ph.D., Physical Chemistry, 1970 Analysis of Trace Organics by ECD Gas Chromatography OEHL
Dr. Bob Stewart Assistant Professor University of Cincinnati Dept. of Mechanical Engr. M.L. #72 Cincinnati, Ohio 45221 (513) 475-4781	Degree: Specialty: Assigned:	Ph.D., Physics, 1981 General Relativity, Thermodynamics, Biomechanics WL
Dr. Lowell Stockstill Assistant Professor Wittenberg University Dept. of Business Administration P. O. Box 720 Springfield, Ohio 45501 (513) 327-7903	Degree: Specialty: Assigned:	J.D./MBA, Law, 1982 Small Business Law BRMC
Dr. William Stone Assistant Professor Meharry Medical College Dept. of Pediatrics Nashville, Tennessee 37208 (615) 327-6506	Degree: Specialty: Assigned:	Ph.D., Molecular and Cellular Biology, 1973 Lipid Biochemistry, Nutrition, Hyperbaric Medicine SAM

Dr. James Sturm Professor Lehigh University Department of Chemistry #6 Bethlehem, Pennsylvania 18015 (215) 861-3477	Degree: Specialty: Assigned:	Ph.D., Physical Chemistry, 1957 Photochemical Kinetics AFGL
Dr. Thomas Sudkamp Assistant Professor Wright State University Computer Science Department Dayton, Ohio 45435 (513) 873-2491	Degree: Specialty: Assigned:	Ph.D., Mathematics, 1978 Computer Science, Mathematics AFWAL/AL
Dr. William Sutton Assistant Professor University of Oklahoma School of Aerospace Mechanical and Nuclear Engr. Department 865 Asp Ave., Rm. 212 Norman, Oklahoma 73019 (405) 325-5011	Degree: Specialty: Assigned:	Ph.D., Mechanical Engineering, 1981 Heat Transfer, Thermal Radiation AEDC
Dr. Robert Swanson Assistant Professor Virginia Polytechnic Institute and State University Materials Engineering Dept. Blacksburg, Virginia 24061 (703) 961-5600	Degree: Specialty: Assigned:	Ph.D., Metallurgical Engineering and Materials Science, 1983 Fracture Mechanics, Environmental Cracking, Corrosion AFWAL/ML
Dr. Patrick Sweeney Professor University of Dayton Engineering Management and Systems Dept. KL 361 Dayton, Ohio 45469 (513) 229-2238	Degree: Specialty: Assigned:	Ph.D., Mechanical Engineering, 1977 Simulation, Costing, Management Systems BRMC
Dr. Charles Taylor Professor University of Florida Dept. of Engineering Science 231 Aerospace Eng. Building Gainesville, Florida 32611 (904) 392-0961	Degree: Specialty: Assigned:	Ph.D., Theory and Application Mechanics, 1953 Optical Methods of Experimental Stress Analysis AD

Dr. Joseph Tedsco Assistant Professor Auburn University Dept. of Civil Engineering 210 Ramsay Hall Auburn, Alabama 36849 (205) 826-4320	Degree: Specialty: Assigned:	Ph.D., Civil Engineering, 1982 Structural Dynamics; Concrete Structures ESC
Dr. Walter Trafton Associate Professor Gallaudet College Chemistry Department Kendall Green Washington D.C. 20002 (202) 651-5536	Degree: Specialty: Assigned:	Ph.D., Chemistry, 1973 Physical Chemistry, Kinetics and Gas Phase Reactions FJSRL
Dr. Larry Vardiman Associate Professor and Dept. Chairman Christian Heritage College Physical Sciences Dept. 2100 Greenfield Drive El Cajon, California 92021 (619) 440-3043	Degree: Specialty: Assigned:	Ph.D., Atmospheric Science, 1974 Cloud Physics and Weather Modification AFGL
Dr. Daniel Voss Assistant Professor Wright State University Dept. of Math and Stat. Dayton, Ohio 45435 (513) 873-2958	Degree: Specialty: Assigned:	Ph.D., Statistics, 1984 Experimental Design, Confounding in Factorial Exper's LC
Dr. Christian Wagner Assistant Professor Oakland University School of Engineering and Computer Science 138 Dodge Hall Rochester, Michigan 48063 (313) 370-2215	Degree: Specialty: Assigned:	Ph.D., Educational Psychology and Artificial Intelligence, 1982 Artificial Intelligence, Cognitive Psychology HRL/IO
Dr. Richard Walker Chairman Miami University Aeronautics Department 219 Culler Hall Oxford, Ohio 45056 (513) 529-5919	Degree: Specialty: Assigned:	Ph.D., Aerospace Engineering, 1970 Aircraft Design, Performance Analysis, Propulsion Aerodynamics AFWAL/FDL

Dr. Doris Walker-Dalhouse
Director of Independent/Home Study Programs
Associate Professor of Reading
Jackson State University
P. O. Box 17120
Jackson, Mississippi 39217
(601) 968-2378

Degree: Ph.D., Reading Education, 1977
Specialty: Education
Assigned: WL

Dr. Yin-min Wei
Professor
Ohio University
Computer Science Dept.
Morton Hall 573
Athens, Ohio 45701
(614) 594-6574

Degree: Ph.D., Electrical Engineering, 1966
Specialty: Signal Processing
Assigned: AMRL

Dr. Isaac Weiss
Associate Professor
Wright State University
School of Engineering
Dayton, Ohio 45435
(513) 873-3021

Degree: Ph.D., Metallurgy, 1978
Specialty: Thermomechanical Processing, Deformation Processing
Assigned: AFWAL/ML

Dr. Shih-sung Wen
Professor
Jackson State University
Psychology Department
1325 J. R. Lynch Street
Jackson, Mississippi 39217
(601) 968-2371

Degree: Ph.D., Educational Psychology, 1971
Specialty: Cognitive Psychology, Psychological Testing, Statistics
Assigned: SAM

Dr. David Wilson
Associate Professor
University of Florida
Mathematics Department
311 Walker Hall
Gainesville, Florida 32611
(904) 392-6035

Degree: Ph.D., Mathematics, Rutgers, 1969
Specialty: Geometric Topology, Grid Generation (Computer Flight Dynamics)
Assigned: AD

Dr. Jesse Williams
Associate Professor
Cheyney University
Math/CIS Department
Cheyney, Pennsylvania 19319
(215) 399-2348

Degree: M.B.A., Computer Science, 1975
Specialty: Computer Science
Assigned: LMC

Dr. Arthur Woodrum Head, Dept. of Physics Georgia Southern College Landrum Box 8031 Statesboro, Georgia 30460 (912) 681-5292	Degree: Specialty: Assigned:	Ph.D., Physics, 1968 Atmospheric Physics SAM
Dr. Billy Wooten Associate Professor Brown University Psychology Department 89 Waterman Street Providence, Rhode Island 02912 (401) 863-2330	Degree: Specialty: Assigned:	Ph.D., Experimental Psychology, 1970 Color Vision HRL/OT
Dr. Carl Wulfman Chairman University of the Pacific Department of Physics Stockton, California 95211 (209) 946-2220	Degree: Specialty: Assigned:	Ph.D., Organic Chemistry, 1957 Chemical Physics FJSRL
Dr. Hsi-Han Yeh Associate Professor University of Kentucky Dept. of E.E. Lexington, Kentucky 40506 (606) 257-4289	Degree: Specialty: Assigned:	Ph.D., Electrical Engineering, 1967 Multivariable Control AFWAL/FDL
Dr. Juin Yu Professor West Virginia Institute of Technology Mechanical Engineering Department Montgomery, West Virginia 25136 (304) 442-3248	Degree: Specialty: Assigned:	Ph.D., Mechanical Engineering Thermofluid Processes AEDC

APPENDIX II C

PARTICIPANT LABORATORY ASSIGNMENT

C. PARTICIPANT LABORATORY ASSIGNMENT (Page 1)

1985 USAF/UES SUMMER FACULTY RESEARCH PROGRAM

AERO PROPULSION LABORATORY (AFWAL/APL)
(Wright-Patterson Air Force Base)

1. Lea Der Chen
2. Louis C. Chow
3. Leroy E. Eimers
4. John E. Erdei
5. Dennis R. Flentge
6. Mahesh S. Greywall
7. Je-Chen Han
8. Ralph E. Oberly
9. Arnold Polak

AEROSPACE MEDICAL RESEARCH LABORATORY (AMRL)
(Wright-Patterson Air Force Base)

1. Samuel K. Adams
2. Zinny S. Bond
3. Charles B. Davis
4. John M. Flach
5. Troy F. Henson
6. Marion L. Noble
7. Michael D. Ross
8. Paul G. Seybold
9. Yin-min Wei

ARMAMENT LABORATORY (AD)
(Eglin Air Force Base)

1. Kevin W. Bowyer
2. Madakasira V. Krishna
3. James S. Marsh
4. Osana M. Mostafa
5. Maurice C. Neveu
6. Sally A. Sage
7. Shawky E. Shamma
8. Charles E. Taylor
9. David C. Wilson

ARNOLD ENGINEERING DEVELOPMENT CENTER (AEDC)
(Arnold Air Force Station)

1. Astor Y. Herrell
2. Charles W. Mastin
3. Justin H. Poland
4. S. Ballou Skinner
5. William H. Sutton
6. Juin S. Yu

AVIONICS LABORATORY (AFWAL/AL)
(Wright-Patterson Air Force Base)

1. Rex Barney
2. Jharna Chaudhuri
3. Alvin Compaan
4. Patrick Jones
5. Jeremy Jones
6. Carl Looney
7. Won Park
8. Thomas Sudkamp

BUSINESS RESEARCH MANAGEMENT CENTER (BRMC)
(Wright-Patterson Air Force Base)

1. Lowell E. Stockstill
2. Patrick J. Sweeney

C. PARTICIPANT LABORATORY ASSIGNMENT (Page 2)

ELECTRONICS SYSTEMS DIVISION (ESD)
(Hanscom Air Force Base)
1. Carolyn D. Heising
2. Stephan E. Kolitz

ENGINEERING AND SERVICES CENTER (ESC)
(Tyndall Air Force Base)
1. Karen Chai-Kwan Chou
2. Gale J. Clark
3. Clifford T. Johnston
4. Desmond N. Penny
5. Joseph W. Tedesco

FLIGHT DYNAMICS LABORATORY (AFWAL/FDL)
(Wright-Patterson Air Force Base)
1. Connie K. Carrington
2. Robert R. Chamberlain
3. Dah-Nien Fan
4. ramana V. Grandhi
5. David C. Hart
6. Walter F. Jones
7. Kuldip S. Rattan
8. Hemen Ray
9. Joseph E. Saliba
10. Richard C. Walker
11. Hsi-Han Yeh

FRANK J. SEILER RESEARCH LABORATORY (FJSRL)
(USAF Academy)
1. Richard D. Bertrand
2. Hermann J. Donnert
3. Harry W. Emrick
4. Daisy W. Kimble
5. Lawrence F. Koons
6. Ronald M. Sega
7. Walter E. Trafton, Jr.
8. Carl E. Wulfman

GEOPHYSICS LABORATORY (AFGL)
(Hanscom Air Force Base)
1. Lucia M. Babcock
2. Francesco L. Bacchialoni
3. Chester S. Gardner
4. Albert Tong-Kwan Hsui
5. Irene R. Little-Marenin
6. Bernard McIntyre
7. Michael B. Rhodes
8. Robert W. Ricci
9. James P. Riehl
10. James E. Strum
11. Larry Vardiman

HUMAN RESOURCES LABORATORY/LR (HRL/LR)
(Wright-Patterson Air Force Base)
1. Linda J. Buehner
2. Hobert H. Corley

HUMAN RESOURCES LABORATORY/OT (HRL/OT)
(Williams Air Force Base)
1. Thomas J. Connolly
2. David L. Kohfeld
3. Billy R. Wooten

HUMAN RESOURCES LABORATORY/MO (HRL/MO)
(Brooks Air Force Base)
1. Phillip L. Ackerman
2. Jihad A. Alsadek
3. Edna R. Fiedler
4. Kurt Kraiger

HUMAN RESOURCES LABORATORY/ID (HRL/ID)
(Lowry Air Force Base)
1. Peter J. Binkert
2. Christian C. Wagner

LEADERSHIP AND MANAGEMENT DEVELOPMENT CENTER (LMDC)
(Maxwell Air Force Base)
1. Paul S.T. Lee
2. Philip M. Lewis
3. Ivor S. Mitchell
4. Robert E. Niebuhr

LOGISTICS COMMAND (LC)
(Wright-Patterson Air Force Base)
1. Daniel T. Voss

LOGISTICS MANAGEMENT CENTER (LMC)
(Gunter Air Force Base)
1. Michael M. Lewis
2. Edward N. Lewis
3. Jesse Williams

MATERIALS LABORATORY (AFWAL/ML)
(Wright-Patterson Air Force Base)
1. Vernon R. Allen
2. Derald Chriss
3. Billy C. Covington
4. Parviz Dadras
5. Charles H. Drummond, III
6. Vijay K. Gupta
7. Prasad K. Kadaba
8. James J. Kane
9. Samuel S. Russell
10. Terrill D. Smith
11. Robert E. Swanson
12. Isaac Weiss

OCCUPATIONAL AND ENVIRONMENTAL HEALTH LABORATORY (OEHL)
(Brooks Air Force Base)
1. John T. Pierce
2. Ralph W. Sheets
3. Richard G. Stebbins

C. PARTICIPANT LABORATORY ASSIGNMENT (Page 4)

ROCKET PROPULSION LABORATORY (RPL)
(Edwards Air Force Base)

1. Dennis J. Cravens
2. Melvin L. Druelinger
3. John P. Renie
4. Ricardo A. Silva
5. Siavash H. Sohrab

ROME AIR DEVELOPMENT CENTER (RADC)
(Griffiss Air Force Base)

1. David B. Choate
2. David Y. Chung
3. David R. Cochran
4. John A. Fleming
5. Alwin C. Green
6. Barry N. Haack

7. Donald F. Hanson
5. Albert A. Heaney
6. Benjamin Lev
7. Dar-Biau Liu
8. Kyle T. Siegrist

SCHOOL OF AEROSPACE MEDICINE (SAM)
(Brooks Air Force Base)

1. Deborah L. Armstrong
2. Mukul R. Banerjee
3. Vito G. DelVecchio
4. Mack Felton
5. James M. Gallas
6. Betty R. Jones
7. Amir Karimi
8. Odis P. McDuff
9. Leathem Mehaffey
10. Rex C. Moyer
11. James J. Mrotek
12. Boake L. Plessy
13. Gordon D. Schrank
14. William L. Stone
15. Shih-sung Wen
16. Arthur Woodrum

WEAPONS LABORATORY (WL)
(Kirtland Air Force Base)

1. Eugene F. Brown
2. Hudson B. Eldridge
3. Bessie R. Foster
4. Doris O. Ginn
5. Arthur A. Kovitz
6. Robert M. O'Connell
7. Bob W. Stewart
8. Doris Walker-Dalhouse

RESEARCH REPORTS

1985 SUMMER FACULTY RESEARCH PROGRAM

76	A Study of the Electrochemical Behavior of the Bromine/Bromide Couple in Melts Composed of Aluminum Chloride and 1-Methyl-3-Ethylimidazolium Chloride	Dr. Lawrence F. Koons
77	The Thermal Layer: A Simplified Model	Dr. Arthur Kovitz
78	Analysis of Relationships Among Self, Peer, and Supervisory Ratings of Performance	Dr. Kurt Kraiger
79	Numerical Study of Detonation Near a Barrier	Dr. Madakasira V. Krishna
80	Sampling Plan for the Organizational Assessment Package Survey	Dr. Paul S. T. Lee
81	Route Planning Problem	Dr. Benjamin Lev
82	Statistical Performance Measures: Relating Air Force Mission Capability to Base Supply Measures	Dr. Edward Lewis
83	Testing the Effectiveness of some User Friendly Algorithms	Dr. Michael Lewis
84	Family Factors and the Career Intent of Air Force Enlisted Personnel	Dr. Philip M. Lewis
85	An Analysis of Low Dispersion IRAS Spectra of Carbon Stars, S Stars and M Variable Stars	Dr. Irene R. Little-Marenin
86	Preliminary Investigation on Resource Control Strategies on Distributed Computer Systems Real-Time vs. Non-Real Time	Dr. Dar-Biau Liu
87	Modelling/Analysis of Space Based Kinetic Energy Weapon Projectile Elyouts	Dr. Carl G. Looney
88	Image Formation and Processing in Superposition Eyes: Precision Location of Point Objects Using the Moire Effect	Dr. James S. Marsh
89	Control Functions in Grid Generation	Dr. C. Wayne Mastin
90	Active Mode-Locking Techniques for Ultra-Short Pulses in Nd:YAG Lasers	Dr. Odis P. McDuff

122	Indoor Radon Pollution	Dr. Ralph W. Sheets
123	Reliability of Systems with Markov Transfer of Control	Dr. Kyle Siegrist
124	The Synthesis of Reactive Intermediates	Dr. Ricardo Silva
125	Possible Targets for Testing the Neutral Particle Beam at Low Energies in the Mark I Aerospace Chamber	Dr. S. Ballou Skinner
126	Preparation of Non-Flammable Model Compounds	Dr. Terrill D. Smith
127	Studies on Combustion of Liquid Fuel Sprays in Stagnation Flows	Dr. Siavash H. Sohrab
128	Monitoring Environmental Quality by Metabolite Analysis	Dr. Richard G. Stebbins
129	Analysis of Geometric Attenuation in Ground Motion Testing	Dr. Bob W. Stewart
130	Competition Guide for Base-Level Buyers 1985	Dr. Lowell E. Stockstill
131	The Role of Antioxidants in Hyperbaric Oxygen Toxicity to the Retina	Dr. William L. Stone
132	Assessment of Maximum Entropy Method Software for Treatment of Data From the AFGL Labcede Facility	Dr. James E. Sturm
133	Inference Propagation in Emitter, System Hierarchies	Dr. Thomas A. Sudkamp
134	Particle Scattering in Plumes	Dr. William Holt Sutton
135	Thermal Stability of Aluminum-Iron-Cerium Alloys	Dr. Robert Swanson
136	The F-15 SPO Support Equipment "Tiger Team"	Dr. Patrick J. Sweeney
137	Studies in Holographic Procedures	Dr. Charles E. Taylor
138	Dynamic Stress Analysis of Layered Structures	Dr. Joseph W. Tedesco
139	An EPR Study of the Decomposition of Various Dinitrotoluenes and the Synthesis of Azo Compounds	Dr. Walter E. Trafton

1985 USAF-UES SUMMER FACULTY RESEARCH PROGRAM/

GRADUATE STUDENT SUMMER SUPPORT PROGRAM

Sponsored by the

AIR FORCE OFFICE OF SCIENTIFIC RESEARCH

Conducted by the

UNIVERSAL ENERGY SYSTEMS, INC.

FINAL REPORT

OPTIMUM DESIGN OF STRUCTURES WITH MULTIPLE CONSTRAINTS

Prepared by:	Ramana V. Grandhi
Academic Rank:	Assistant Professor
Department and University:	Mechanical Systems Engineering Wright State University
Research Location:	Flight Dynamics Laboratory Structures and Dynamics Division Analysis and Optimization Branch Design and Analysis Methods Group
USAF Research	Dr. V. B. Venkayya
Date:	September 30, 1985
Contract No:	F49620-85-C-0013

OPTIMUM DESIGN OF STRUCTURES WITH MULTIPLE CONSTRAINTS

by

Ramana V. Grandhi

Abstract

Automated design of large aerospace structures requires efficient optimization algorithms because of a large number of design variables and design constraints. Most of the difficulties associated with large structural design are solution convergence and computer resources requirements. Practical aerospace structures generally involve limitations on displacements, stresses, frequencies and flutter requirements. In this study, various mathematical programming techniques and optimality criteria methods were used for studying the relative efficiencies of these methods.

The objective of this study is to come up with a reliable and efficient optimization technique for a general complex design problem. Various optimization techniques were applied in designing several trusses and a multi-cell wing structure, and the number of structural analyses required in each technique are presented.

I Introduction

Even though thousands of papers have been published on the use of optimization algorithms to engineering design, the number of applications to practical aerospace vehicles remains very small (ref. 1). Practical aerospace structures have hundreds of design varicables and thousands of design constraints. Most of the optimization algorithms fail to converge to an optimum design when the number of design variables and design constraints is large. The behavior constraints involve stress, displacemet, frequency, aeroelastic flutter and thermal constraints. When the interdisciplinary behavior constraints are considered, optimum design is a complex task as some type of behavior constraints are inactive at one design and become active at a different design. Similarly, the active constraints become inactive as design changes. This causes oscillations of design back and forth, and never converges to an optimum.

For the last fifteen years, several techniques were developed to reduce the number of design variables using design variable linking and the number of constraints were reduced using constraint deletion (throw-away) concepts. With all these design variable linking, constraints deletetion and constraint approximation conepts, still solving a large scale design problem is a challenge to the designer. Strict application of the available mathematical programming techniques to the integrated structural synthesis problem fails to produce fully satisfactory results. Linking design variables before performing the structural design is a difficult task since there is no information on how the design variables behave during the design cycle.

II OBJECTIVES OF THE RESEARCH EFFORT

This study is undertaken with a view towards identifying the best method, improving existing methods, and developing hybrid optimization techniques. The aim of this study is to identify the strengths and weaknesses of various mathematical programming methods. Eventually, a hybrid optimization using optimality criteria and mathematical programming would be developed. The optimality criterion technqiue is very effective at the beginning of the optimization, and it becomes complex near the local optimum where the number of active constraints increases. At this point, it is more reasonable to switch to a mathematical programming method, and also design variable linking can be employed.

This work is aimed at finding an efficient and reliable mathematical programming for solving large scale problems with multiple behavior constraints. Several structures were designed to find the relative performance of various mathematical programming techniques.

III Problem Statement

The optimization task is to find a vector X of n design variables x_i, i = 1,2,...,n, which will

Minimize a multivariable function $f(X)$ subject to behavior constraints

$$g_j(X) = G_j(X) - G_{jo} \leq 0 \qquad j = 1,2,\ldots,m \qquad (1.a)$$

and side constraints

$$x_i^l \leq x_i \leq x_i^u \qquad i = 1,2,\ldots,n \qquad (1.b)$$

In structural applications, the vector X represents cross sectional areas of rods, thicknesses of plate members, etc.; the behavior constraints are limitations on displacements, stresses, frequencies and aeroelastic flutter, and $f(X)$ generally represents weight.

Two broad approaches for solving the above constrained optimization exist. The first is based on mathematical programming methods using numerical search procedures to progressively reduce weight by taking small steps toward the optimum. In the second approach, optimality criteria techniques are used, where the new designs are obtained based on conditions which are expected to exist at the optimum. The potential strength of the optimality methods is that the number of iterations needed to converge to an optimum is virtually independent of the number of design variables. The details of the mathematical programming and optimality criteria techniques considered are given in the following sections.

IV Structural Design Using Mathematical Programming Techniques

The first part of the research effort is design of large structures with multiple constraints using mathematical programming methods. Mathematical prgramming techniques which employ the general methods of linear and nonlinear programming concepts are appealing for solving the interdisciplinary design problem. These techniques employ numerical search procedures for finding the constrained minimum and have a wide selection of optimization algorithms. All algorithms are based on the iterative equation:

$$X_{k+1} = X_k + \triangle X_k \qquad k = 0, 1, 2, ... \qquad (2.a)$$

or

$$X_{k+1} = X_k + \alpha_k S_k \qquad k = 0, 1, 2, ... \qquad (2.b)$$

where $\triangle X_k$ is a change in design, k is the iteration number, α_k is a step size, S_k is a search direction, and X_o is a starting design.

In this work, four different mathematical programming techniques are used.

(a) The first one is based on methods of feasible directions. It is a direct method of constrained optimization. In this method search direction is computed such that it stays away from the constraint boundaries as much as possible. The design always stays inside the feasible domain and improves the objective function. The search direction S is computed by solving the following maximization problem.

Maximize β

such that

$$-S^T \nabla g_j + \theta_j \beta \leq 0 \qquad j \epsilon I_A$$

$$S^T \nabla f + \beta \leq 0 \qquad \theta_j \geq 0 \qquad (3)$$

$$||S|| = 1$$

where θ_j are weights, I_A is active constraint set and β is a constant. The choice of step length in eq. 2 is based on a prespecified reduction in the objective function. The method of feasible directions has been used through CONMIN (ref.2) computer program.

(b) The second mathematical programming algorithm is using a Recursive Quadratic Programming method. The algorithm is based on Pshenichny's linearization method for constrained optimization. It generates approximation to the hessian of the Lagrange function. It uses an active set strategy, so gradients of only the active constraints are calculated at each iteration. The direction of design change is obtained by solving a quadratic programming problem. This technique has been implemented using IDESIGN (refs. 3.4) computer package.

(c) The third algorithm is based on a Sequential Unconstrained Minimization Technique (SUMT). The SUMT algorithm transforms the constrained problem into a sequence of unconstrained problems using a quadratic extended interior penalty function formulation. A compound function $F(X,r)$ is introduced as:

$$F(X,r) = f(X) - r\sum_{i=1}^{m} p(g_i) \tag{4}$$

where r is the penalty parameter and the function $p(g_i)$ associated with the ith constriant is defined as:

$$p(g_i) = \frac{1}{g_i} \qquad g_i \le g_0$$

$$\frac{1}{g_0}\left[\left(\frac{g_i}{g_0}\right)^2 - 3\left(\frac{g_i}{g_0}\right) + 3\right] \qquad g_i > g_0 \tag{5}$$

$$g_0 = c\sqrt{r}$$

where g_o is the transition parameter and c is a constant.

The function $p(g_i)$ is thus defined as an interior penalty function in most of the feasible domain. It is defined as a quadratic exterior penalty function in a small part of the feasible domain ($g_i \ge g_0$) and in the infeasible domain.

The solution of the optimization problem is obtained by minimizing the function F for a decreasing sequence of r values using Newton's method with approximate second derivatives of the penalty terms.

The design vector X, that minimizes $F(X,r)$ is found using eq. 2.b iteratively. The search direction S_k is given as

$$S_k = -H_k^{-1} \nabla F_k \tag{6}$$

where H_k is the second derivatives matrix of F .

The program NEWSUMT-A (ref. 5) has been used for this technique. NEWSUMT-A iteratively modifies the design vector (Eq. 2.b) so that $f(X)$ decreases or the degree of constraint satisfaction is improved.

In this program, constraint approximations are used for improving the computational efficiency. The constraint approximations replace the basic problem statement with a sequence of relatively small, explicit problems that preserve the essential features of the original design optimization problem.

(d) Finally, a recursive quadratic programming method based on Powell's technique (ref. 6) is used. This method requires derivatives of all constraints at each iteration. It is implemented through the algorithm VMCON (refs. 6,7).

Structural analysis for stresses, displacements and frequencies is done using ANALYZE / DANALYZE (ref. 8) finite element program. Stress, displacement, and frequency constraint derivatives with respect to the decision variables are calculated using analytical expressions. Derivative calculations is done using the virtual load method.

V Structural Design Using Optimality Criteria Techniques

Optimality criteria methods for structural optimization involve: (i) the derivation of a set of necessary conditions that must be satisfied at the optimum design; and (ii) the development of an iterative redesign procedure that drives the initial trial design toward a design which satisfies the previously established set of necessary conditions.

First, the Lagrangian formulation for constrained minimization is written as

$$L(X) = f(X) + \sum_{i=1}^{m} \lambda_i g_i(X) \tag{7}$$

where $L(X)$ is the Lagrangian function and λ's are the Lagrangian multipliers.

Minimization of the Lagrangian L with respect to the design variable vector X gives the condition for the stationary value of the objective function with the constraint condition g as

$$\frac{\partial L}{\partial x_i} = \frac{\partial}{\partial x_i}\left[f(X)\right] + \sum_{j=1}^{m} \lambda_j \frac{\partial g_j}{\partial x_i} = 0 \tag{8}$$

The optimality condition can be written as

$$\sum_{j=1}^{m} e_{ij}\lambda_j = 1 \qquad\qquad i = 1, 2, ..., n \tag{9}$$

The n such equations corresponding to the n design variables can be written in the matrix form as follows:

$$[e]\lambda = \mathbf{1} \tag{10}$$

The elements of matrix $[e]$ are given by

$$e_{ij} = \frac{\partial g_j / \partial x_i}{\partial f / \partial x_i} \tag{11}$$

This equation represents the ratio of constraint to objective function gradients with respect to the design variables. These ratios can be associated with special forms of energy densities depending on the type of constraint functions.

The solution of the optimization problem involves $m + n$ unknown quantities. The additional m equations can be obtained by writing the original constraint conditions as follows:

$$\sum_{i=1}^{n} e_{ij} \rho_i x_i l_i = G_{jo} \qquad j = 1, 2, \ldots, m \tag{12}$$

Combining Eqs. 10 and 12 gives the necessary equations for determining the Lagrangian multipliers as follows

$$[H]\lambda = \mathbf{G_o} \tag{13}$$

where the matrix $[H]$ is given by

$$[H] = \mathbf{e^t}[\mathbf{A}]\mathbf{e} \tag{14}$$

$[A]$ is a diagonal matrix, and its ith diagonal element is given by

$$A_{ii} = \rho_i x_i l_i \tag{15}$$

Equations 10 and 13 are solved by iterative methods. The form of resizing algorithm is as follows:

$$X_{k+1} = X_k \Big[\sum_{j=1}^{m} c_j e_{ij}^k\Big]^{1/2} \tag{16}$$

where c_j are the weighting parameters.

For the last two decades, the optimality criteria have been applied to a wide range of design problems and have been demonstrated to be effective for large numbers of design variables (refs. 9,10). In this work, optimality criteria techniques are used for solving the structural design problems with stress and displacement constraints.

VI Numerical Results

The constraint optimization problem was solved with stress, displacement and frequency constraints. Various optimization techniquess were used to see the relative performance in solving the multiple constraint problem. A method of feasible directions method, an extended interior penalty function method, a recursive quadratic programming method based on Pshenichny's and Powell's methods were studied. The motivation of the preliminary work was to find a candidate algorithm for use in the hybrid optimization technique. The hybrid optimization technique would be based on optimality criteria and mathematical programming techniques. In all the structures, weight was considered as the objective function. A ten-bar truss, a twenty-five bar truss and a multi-cell wing structure were considered as example problems.

Ten-Bar Truss

A planar ten-bar truss shown in Fig.1 is the first example problem. The design information and the load values are given in Table 1. The structure is subjected to single load condition. The cross - sectional areas of members are the design variables. The displacement constraints are imposed at each node in x, y directions, the stress constraints are on each member and the frequency constraint is imposed on the fundamental frequency. The final designs obtained by these algorithms agree with those reported in the literature. The objective function, number of analyses are given in Table 2 for all the techniques employed.

Twenty five-Bar Truss

The second example considered is a twenty five-bar space truss shown in Fig. 2. Initial cross sectional areas, material properties, allowable stresses and load values are given in Table 3. Design variable linking is used to obtain a symmetric structure and seven design variables are used to size the 25 members of the truss. The structure is designed for two load conditions subject to tensile and compressive stresses and dispacement constraints. On nodes 1 through 6 displacement limitations are specified in x,y and z directions. The

number of analyses comparison is given in Table 4 for all the techniques.

Multi-cell Wing structure

The final example is a newly formulated multi-cell wing structure. Structural weight was minimized by taking constraints on stresses and displacements. The wing structure shown in Fig.3 has 54 elements and 54 degrees of freedom. The design information. displacement and stress limits are given in Table 5. Two load conditions were considered (Table 6). In each load condition, 54 displacement constraints and 54 stress constraints were considered. thus a total of 216 behavior constraints.

At the final design the objective function. number of constraint and gradient evaluation statistics are given in Table 7 for all the optimization technqiues employed. Dispacement constraints at the wing tip are active in z-direction in the first load condition. Most of the membrane and rod elements reached their minimum gauges.

VII RECOMMENDATIONS

The optimum design of practical structures is complicated because of convergence difficulties. The motivation for this study is to come up with a hybrid optimization method using optimality criteria and mathematical programming techniques. This work is aimed at finding an efficient and reliable mathematical programming technique among the most commonly used methods. In this report. an attempt is made to compare different optimization technqiues efficiencies in solving multiple constraint problems.

Four different mathematical programming techniques and optimality criteria methods were used with stress. displacement and frequency constraints. The number of analyses. the number of gradient calculations required for each technique are presented in Tables (2.4.7). From the results presented. optimality criteria techniques are far efficient compared to any mathematical programming method. Among the mathematical programming methods, IDESIGN peformed very well and produced the best design. VMCON performed poorly in solving complex problems. CONMIN and NEWSUMT-A are considered in between the other algorithms.

The preliminary study of the above mentioned algorithms provided information on the efficiency in solving large scale problems with multiple constraints. Further research is required in solving large scale structural problems with stress, displacement, frequency and aeroelastic flutter constraints.

ACKNOWLEDGEMENTS

This research work has been sponsored by the Air Force Systems Command, Air Force Office of Scientific Research, and the Flight Dynamics Laboratory/AFWAL. The support and assistance of all those at the Design and Analysis group, and in particular that of Dr. V. B. Venkayya and Lt. R.Canfield is gratefully acknowledged.

References

1. Ashley, H., "On Making Things the Best Aeronautical Use of Optimization," Journal of Aircraft, Vol.19, No.1, 1982, pp.5-28.

2. Vanderplaats, G.N., "CONMIN - A Fortran Program for Constrained Minimization - User's Manual," NASA TM X-62282, August 1973.

3. Arora, J.S., "Theoretical Manual for IDESIGN". Report No. ODL-85.9, College of Engineering, University of Iowa, Iowa City, 1985

4. Arora, J.S., Thanedar, P.B., and Tseng, C.H., "User's Manual for Program IDESIGN", Technical Report No. ODL 85.10, University of Iowa, Iowa City, May 1985.

5. Grandhi, R.V., Thareja, R., and Haftka, R.T., "NEWSUMT-A: A General Purpose Program for Constrained Optimization Using Constraint Approximations", ASME J. of Mechanisms, Transmissions, and Automation in Design, Vol.107, March 1985, pp. 94-99.

6. Powell, M.J.D., "A Fast Algorithm for Nonlinearly Constrained Optimization Calculations," Proceedings of the 1977 Dundee Conference on Numerical Analysis, Lecture Notes in Mathematics, Vol.630, Springer-Verlag, Berlin, 1978, pp. 144-157.

7. Crane, R.L., Hillstrom, K.E., and Minkoff, M., "Solution of the General Nonlinear Programming Problem with Subroutine VMCON", ANL-80-64.

8. Venkayya, V.B., and Tischler, V.A., "ANALYZE - Analysis of Aerospace Structures with Membrane Elements", AFFDL-TR-78-170, 1978.

9. Venkayya, V.B., Khot, N.S., and Berke, L., "Application of Optimality Criteria Approaches to Automated Design of Large Practical Structures," AGARD Second Symposium on Structural Optimization, Milan, Italy, 1973.

10. Khot, N., Berke, L., and Venkayya, V.B., "Comparison of Optimality Criteria Algorithms for Minimum Weight Design of structures," AIAA Journal, Vol.17, 1979, pp. 182-190.

Table 1

Ten-Bar Truss Design parameters	
Material:	Aluminum
Young's Modulus:	10 Mpsi
Density:	0.1 lb/in^3
Design variable lower limit:	0.1 in
Initial areas:	10.0 in
Stress limit:	25 ksi
Deflection limit:	3.0 in
Frequency limit:	22.0 Hz
Load cases:	1

Loads (lbs)		
Node #	X	Y
1	0.0	50000
2	0.0	-150000
3	0.0	50000
4	0.0	-150000

Table 2

Ten-bar Optimization Results			
# of evaluations	CONMIN	NEWSUMT-A	IDESIGN
Objective function	95	33	35
Constraints	95	33	35
Gradients	31	32	26
Optimum Weight	4755	4733	4731

Table 3

Twenty five-Bar Truss Design parameters	
Material:	Aluminum
Young's Modulus:	10 Mpsi
Density:	0.1 lb/in^3
Design variable lower limit:	0.01 in
Initial areas:	1.0 in
Stress limit:	25 ksi
Deflection limit:	0.35 in
Load cases:	2

Loads (lbs)				
Load #	Node #	X	Y	Z
1	1	1000	10000	-5000
	2	0	10000	-5000
	3	500	0	0
	6	500	0	0
2	1	0	20000	-5000
	2	0	-20000	-5000

Table 4

Twenty five-bar Truss Optimization Results				
# of evaluations	CONMIN	NEWSUMT-A	IDESIGN	VMCON
Objective function	47	30	14	39
Constraints	47	30	14	39
Gradients	14	29	11	39
Optimum Weight	545	545	545	545

Table 5

Mult-Cell Wing Box Design parameters	
Material:	Aluminum
Young's Modulus:	10 Mpsi
Density:	0.1 lb/in^3
Design variable lower limit:	0.1 in
Initial thicknesses/areas:	1.0 in
Yield Stress:	60 ksi
Shear Stress limit:	42 ksi
Deflection limit:	3.0 in
Load cases:	2

Table 6

Vertical Loads (lbs)		
Node #	Case 1	Case 2
1	1500	600
2	1500	600
3	1500	1200
4	1500	1200
5	1500	1800
6	1500	1800
7	3000	1200
8	3000	1200
9	3000	2400
10	3000	2400
11	3000	3600
12	3000	3600
13	3000	1200
14	3000	1200
15	3000	2400
16	3000	2400
17	3000	3600
18	3000	3600

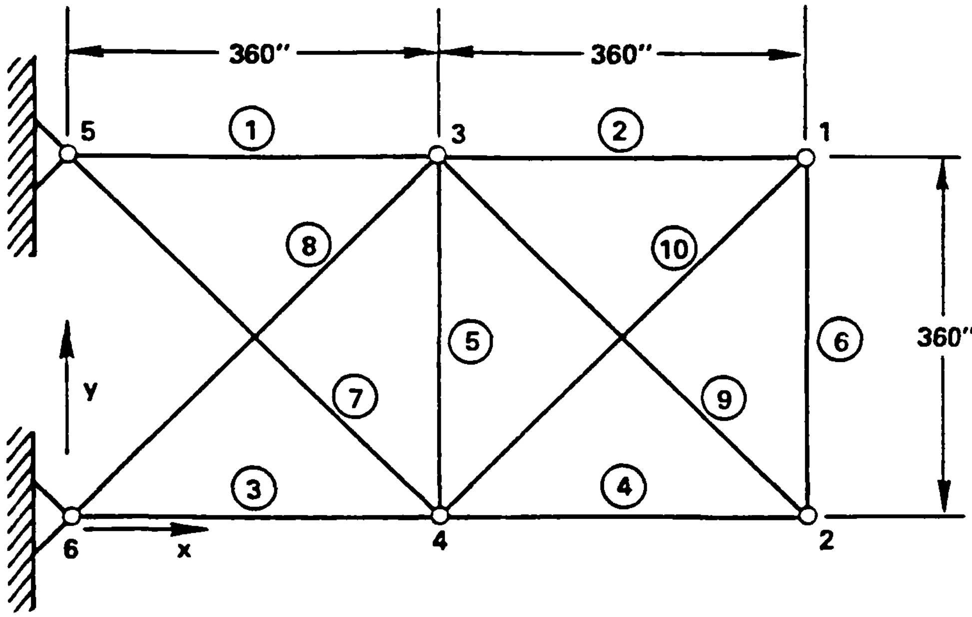

Figure 1 Planar Ten Bar Cantilever Truss.

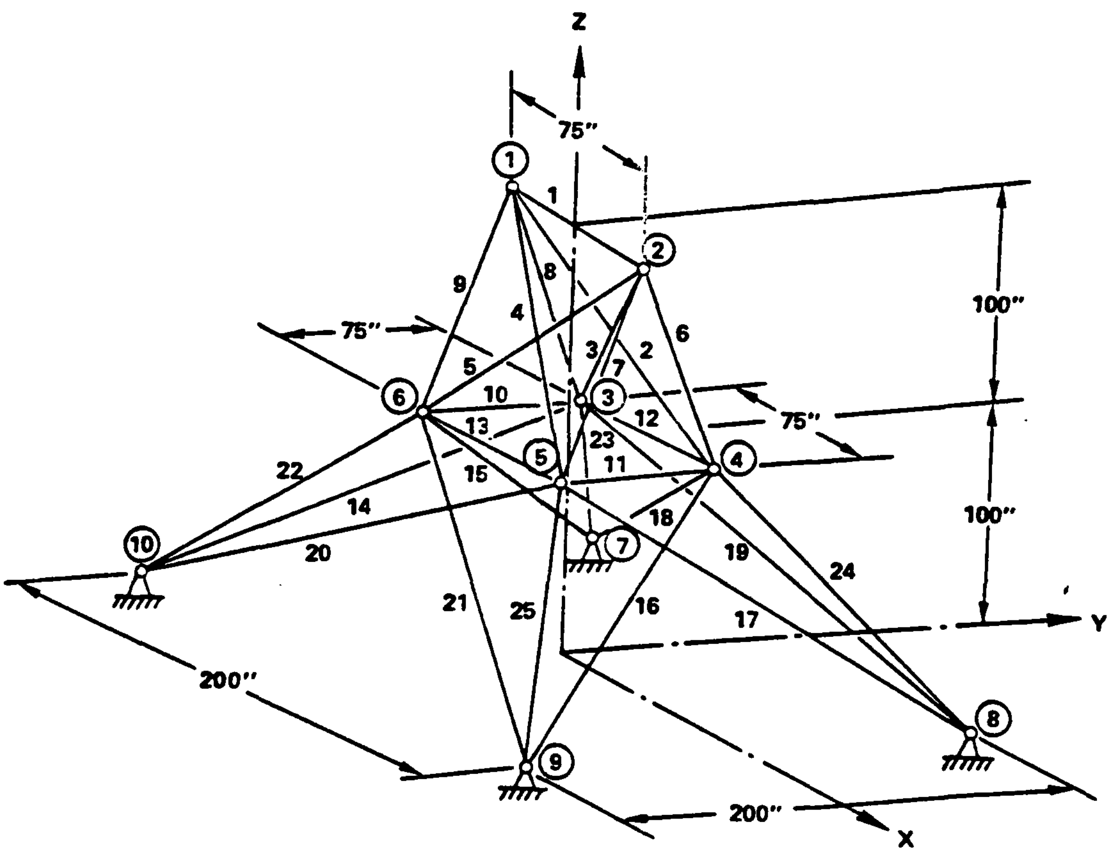

Figure 2 Twenty Five Bar Space Truss

Table 7

Optimization Results				
# of evaluations	CONMIN	NEWSUMT-A	IDESIGN	OPTSTAT
Objective function	83	32	52	15
Constraints	83	32	52	15
Gradients	22	31	46	
Optimum Weight	1858	1858	1857	1903

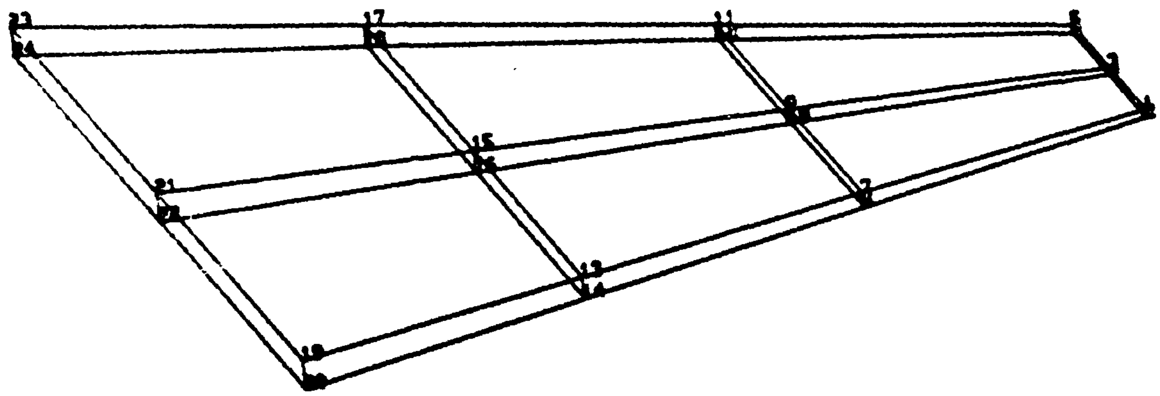

Figure 3 Multi-cell Wing Structure

1985 USAF-UES SUMMER FACULTY RESEARCH PROGRAM/

GRADUATE STUDENT SUMMER SUPPORT PROGRAM

Sponsored by the

AIR FORCE OFFICE OF SCIENTIFIC RESEARCH

Conducted by the

UNIVERSAL ENERGY SYSTEMS, INC.

FINAL REPORT

DESCRIPTIVE EXPLORATION OF PATTERNS IN OPTICAL TURBULENCE PROFILES

Prepared by:	Alwin C. Green, Ph.D.
Academic Rank:	Associate Professor
Department and	Department of Mathematics
University:	State University College at Buffalo, New York
Research Location:	Rome Air Development Center Surveillance Division (OC) Strategic Surveillance Branch (OCS) Surveillance Systems Section (OCSP) Atmospheric Optics and Remote Sensing Group
USAF Research	Norman Chonacky, Ph.D.

Date:	August 30, 1985
Contract No:	F49620-85-C-0013

ABSTRACT

A large data base of optical turbulence profiles already exists. A profile is a set of seven Cn-squared optical turbulence values which correspond to seven altitudes ranging from 2.2 km to 18.5 km. These profiles are derived from stellar scintillations due to the atmospheric optical turbulence. The profile values of any given level contain wide variations with time, and previous statistical treatments have had limited success in describing these variations. This research effort undertakes other mathematical considerations and seeks to characterize patterns of data behavior with respect to time. There is evidence of episodic behavior and several distinct modes are discussed. A primary finding is a consistent oscillation of a fundamental frequency at all altitudes with average period of about eight minutes. Another significant finding is that all altitudes may sometimes individually adopt a relatively quiescent stable mode. There are other more subtle episodic indications. The activity of individual levels of 2.2km, 7.3km, and 18.5km appear to be completely non-synchronised. However, pattern shapes of any given level is not very distinguishable from pattern shape of another level. The typical value Cn-squared turbulence decreases from the order of 10E-16 at 2.2km altitude to the order of 10E-18 at 18.5 km altitude.

ACKNOWLEDGEMENTS

I wish to thank the Air Force Systems Command(AFSC), the Air Force Office of Scientific Research(AFOSR),and the Rome Air Development Center(RADC) for their support and sponsorship of this research; for without their combined support then this project would not have been possible. I want to thank Dr. Norman Chonacky who drew me into this project and who provided to me the essential insights in the physics of optical turbulence. Also, I want to acknowledge the efforts of Donald Stebbins who provided some of the data tables and Donna Mucks who supported efforts to portray data on computer graphics. It is also important to recognize the contribution of Dr. Guy Korynen of Lawrence Livermore Laboratory who has suggested the use of Box-Jenkins type time- series analysis for these Cn-squared data profile sequences.

I. Introduction

Currently, optical instruments are being considered for many applications in the Strategic Defense Initiative effort undertaken by USAF. One significant aspect of this effort is the effect of the optical turbulance of the atmosphere on the reliability of these applications. Among others, one measure of such turbulence is the Cn-squared turbulence structure parameter. This single parameter is used as a measure by a variety of techniques and contexts. One specific instrument is the stellar scintillometer described in NOAA Technical Memorandum ERL WPL-25(1). This Star Sensor measures stellar scintillations of a single star by use of a two-dimensioned spatial frequency filter. The data is acquired as a single profile at one time which includes the Cn-squared value at seven different altitude levels ranging from 2.2km to 18.5km.

These profiles have been collected at (AOTF) RADC and (AMOS) Maui since 1979, as well as at other locations. There is an existing available data base of more than 4000 profiles. The data is known to range from 10E-19 to 10E-14 Cn-squared units. A single mission of 20 or 30 profiles may find a single level varies more than an order of magnitude during the mission. The data has been regarded in some quarters as a statistical population with some unknown distribution pattern. Efforts to analyze the distribution (2,3) have shown the entire population of logarithms of Cn-squared data is not a normal distribution; but a limited sequence of profiles may be log-normal in distribution.

The performance of the scintillometer involves the acquisition of scintillation intensity versus spatial wavelength by four passes of the spatial filter through a region near the focus of a large standard optical telescope. These four scans are composed into one averaged curve. This scintillation spectrum is then processed by computer to produce the values of the profile. The processing involves two sets of weighted response curves. One set of curves involves overlapping values and distorted peaks which are cancelled by subtraction. In some cases, an unphysical negative Cn-squared value is obtained. In this event, the entire profile is usually discarded. Also, the nature of the weighted

curves is sufficiently broad that the resolution of the system is only 5 km. Since seven assigned altitudes are distributed over only 18.5 km then the average separation between levels is less than 3 km. Therefore, any adjacent pair of levels has some resemblance because separation is less than bandpass width. In this study, only levels 1,4,7 are considered because they constitute the only subset which is reasonably independent (3).

This study is limited to the discovery of pattern and form in the numerical content of data, and discussion will not project rationales for the complex phenomena of physics which are at work.

Relevant details of my own background include bench experience of four years of electronic materiel maintenance as a U.S. Navy enlisted man with the National Security Agency; and eight years as a design engineer of arc discharge lamps with General Electric Co. I earned a Ph. D. degree in Pure Mathematics at Syracuse University, in 1972. I spent two summers with Battelle Pacific Northwest on Automata and Catastrophe Theory (1976-1977). My current interests are algorithm complexity, graph theoretic searching, pattern matching, artificial intelligence.

II. Objectives

1. To interpret the data by whatever appropriate means presented itself during a search using the methods of: graphic illustration and plotting with respect to time; catastrope theory; pattern recognition; expert systems; finite differences; and fuzzy sets.

2. To implement any feasible diagnostic technique as PASCAL software.

3. In later stages, Dr. Chonacky expressed an interest in formulating a vocabulary which describes short segments of data behavior.

III. Approach

My analysis consisted of graphic plotting. A mission is the set of profiles acquired at once and it is named by year, Julian day, and

location; e.g., 80129 MAUI or 82213 Verona. Initially, 15 of the longer missions were selected for plotting; and a total of 35 were done in all. In the beginning, each mission seemed to have unique unruly features with no common resemblance between missions. At first, all seven altitude levels were plotted and it was anticipated that some visible indication would occur that specific phenomena in one level would be passed to adjacent levels as time lapsed. There has been no evidence of this to be found.

The significant findings of this research have emerged as similarities of configuration and form without regard for quantification. There proved to be lack of consistency for a measure of amplitude which is required for application of the more elegant methods mentioned in the first objective. The positive findings pertain to various operating modes. There are suggestions that more subtle periodic episodes may be occurring over extended time intervals and effort was directed to examine longer available non-interrupted sequences of profiles. The nature of variations found in the data did not lend itself to the sophisticated techniques which were anticipated in the first objective.

IV. Significant Descriptive Discoveries

Several modes of consistent behavior have been noted. These modes belie a concept of purely random data behavior. These modes include a fundamental frequency of oscillation as well as occasional periods of stable, essentially constant values. Typical illustrations are given by plotted segments of missions in Figures 1-4 at the end of this report. Each of the plotted portions of the figure is without time interruptions between illustrated profiles. However, throughout the entire body of accumulated data, there are relatively few examples of a sequence of 30 profiles without interruptions.

A. Fast Cycle

There exists a fundamental rapid oscillation frequency throughout all levels of altitude. This frequency is not synchronised between levels, and it is consistently present for most of the time. This

frequency is super-imposed over various other longer events. A period is taken to be the interval between two relevant data peaks. The period of this fundamental frequency varies from 2-3 profiles. Sampling intervals between profiles are known to vary and this is discussed below in IV E. However, the time interval of this very evident rapid oscillation varies approximately from 5 to 15 minutes, but the average period value is the order of 6 to 8 minutes. Typical behavior of this fundamental frequency is shown in Figure 1, mission 85088 Maui. A total time interval of two hours three minutes contains the order of 15 peaks. This yields an average of about eight minutes per period. In Figure 1, level 1, there are four very rapid periods from profile 10 to profile 18. These four periods are the order of six and a half minutes each. Similar evidence is found throughout all data.

B. Longer Cycles

There is strong suggestive evidence of longer periodic episodes. When considered by the following naive method, the evidence is not scientifically conclusive, but impressive visible suggestions occur throughout the data. Let a distinguished peak be one with altitude greater than amplitude of adjacent peaks. Frequently, distinguished peaks occur in some pattern of pairing or clustering. Let such a pairing or clustering be called a distinguished event. Similar situations may occur for valleys as well as peaks.

Consider Figure 1, level 1, where there is clearly one distinguished event centered at profile 3 and another distinguished event centered at profile 33. This suggests a period of 30 profiles or about 110 minutes. Within this span, it is possible to locate somewhat less distinguished events at profiles 12, 22, and 40. This sequence of centers of 3, 12, 22, 33, 40 yield a sequence of approximate periods of length 9, 10, 11, 7 profiles. The average period is approximately nine profiles or 30 minutes.

For Figure 1, level 4, there are distinguished events centered at profiles 3, 20, and 42 and for periods of 18, 22 profiles with an average of 75 minutes. For level 4, some argument can be made that less

distinguished event centers occur at profiles 12, 33; although this particular case is tenuous. This results in centers 3, 12, 20, 33, 42 with periods 9, 8, 13, 9. The extreme negative peak at profile 30 is anomalous and may be noise external to the data. If this negative peak were discounted, then an adjustment would allow a distinguished event centered at profile 31 (or 32). This would adjust the sequence of event centers to 3,12,20,31,42 with a sequence of periods of 9,8,11,11.

For Figure 1, level 7, there are clearly distinguished valleys at profiles 6, 16, 24, 39, and 44. There is another valley at profile 32 which is distinguished in the sense that it is a strong negative peak in the center of a board positive surge. This sequence of centers 6, 16, 24, 33, 39, and 49 give a sequence of periods of 10, 8, 9, 6 and 10 profiles.

The discussion of the previous three paragraphs is admittedly only suggestive and not conclusive, but it is typical of findings for long (30 or more) consecutive sets of profiles without time interruption. There are consistently visible indications of episodic repetitions with somewhat more rapid episodes occurring at the higher levels. The exact nature of these episodes might be partially explained by effects of summing several different frequencies and by amplitude distortion of possible "aliasing" to be discussed in IV E.

C. Plateaus

There exist stable (or preferred) data plateaus over some intervals for each level. A possible exception is at level 5 (9.4 km). This is a stable mode which persists for some length of time. This is in sharp contrast to wild variations which occur part of the time. Such examples of this stable mode are clearly shown in Figure 3, level 1, where the data value is nearly constant at about 5 X 10E-16. Figure 2, level 1, shows the stable mode at about 2 X 10E-16 for profiles 1-12. Figure 1, level 1, actually has a preferred plateau at about 1.3 X 10E-16. The preferred plateau value varies from mission to mission. However, a consistent pattern develops over the entire set of missions which were examined. At level 1, the preferred plateau value falls in the range of

10E-16 to 5X10E-16 when such a plateau exists. In most cases, variations from the plateau are in the form of decreases for altitude level 1 and this is illustrated in Figures 1 and 2.

In Figure 2, level 7, there is a data plateau at about 1.8 X 10E-18 over profiles 11-23. Most data variations are increases for level 7. A majority of missions exhibit a preferred data plateau level within the range from 10E-18 to 3 X 10E-18 for altitude level 7.

Overall, the data behavior of levels 4 and 5 is very much less stable than all other levels, and this is evident in Figures 1, 2 and 4. In approximately one quarter of the missions, level 4 developed some evidence of stability at some plateau values between 10E-18 and 10E-17. Such a case is shown in Figure 3, level 4.

D. Independence

Between levels 1, 4 and 7 there is virtually no evidence that activity in any one level is dependent on another level or is directly related to activity in any other level. The fundamental frequency described in IV.A has sufficiently short periods of 2 to 3 profiles that simultaneous peaking of levels must occur among the 3 levels. However, this fundamental frequency is non-synchronous among the levels. In some missions, such as Figure 2, there is evidence of similar overall configuration of all three levels 1, 4 and 7. However, a close examination from profile to profile shows that activity varies individually among the different levels. It seems in Figure 2, that all of the levels are being concurrently influenced overall by some outside force. But the activity of any one level does not drive the activity of any other single level among levels 1, 4, 7. These results are consistent with quantitative evaluations of inter-level correlation done previously (3).

E. Aliasing

There exists an undesirable relationship between the length of the data sampling interval and the length of the period of the fundamental

frequency of the data. The actual time record on the (AMOS) Maui scintillometer indicates that sampling intervals vary from two to five minutes, with a typical value of three and a half minutes. Accurate timing on recent tests of the Verona scintillometer indicate that data acquisition (during the 4 passes by the spatial filter) always occurs during one of only four possible discrete intervals; mainly, 93 sec, 112 sec, 153 sec, or 172 sec. The data processing of the computer then fills the remainder of a data sampling interval of two and a half to four and a half minutes (with average time of about three and a half minutes). Meanwhile, from evidence such as Figure 1, the data variation period can be as short as 6 to 7 minutes. Together, these values indicate that the ratio of data sampling frequency to data fluctuation frequency can easily vary between 1:1 and 2:1. This violates the Nyquist criteria of 2:1 for minimum data sampling frequency that is sufficient to prevent data "aliasing."

Within the context of this report, data "aliasing" means that the length of the sampling interval is approximately equal to length of the period of data cycle variation. The length of the time used for actual data acquisition is a relatively short portion of the data sampling interval. Therefore, when the sampling interval is equal the data variation cycle interval, the phase difference between the two processes will play a dominating role in the determination of the actual output. If the two cycle frequencies are exactly equal then the output will be constant. If one frequency is only slightly different from the other then the output will vary at a rate equal to the difference in the two frequencies. This could lead to a very long period wave which is nearly smooth. There is substantial empirical data to indicate that the data behavior cycle varies between 5 and 15 minutes. The record also shows that the sampling interval varies commonly between 3 to 6 minutes. Hence, there is ample opportunity for coincidental matching of nearly equal periods of the two frequencies.

Possible examples of data "aliasing" can be found in Figure 1, level 1, profiles 19-24 and profiles 31-34, as well as, Figure 4 level 7, profiles 35-40. The first and third such examples are smooth concave

sections appearing abruptly between portions of the rapid fundamental frequency. The second example is three consecutive equal values between two portions of widely varying data. For the same mission 85088 (not included in Figure 1) there are actually four consecutive equal values found in profiles 69-71 level 1. Such instances of short smooth concave or flat sections data are common throughout the data. The mathematical probability of three or four consecutive equal values among random variations is negligible. When the majority of data shows vigorous variation for a major portion of the time, it stretches credibility to believe that one physical level pauses stationary for 9 to 12 minutes while data fluctuations of the adjacent levels do not pause. The more likely explanation of these brief smooth portions is data "aliasing" as both sampling frequency and data variation frequency may vary back and forth past each other.

Even with some limited measure of data "aliasing"; it is possible to detect the presence of a primary frequency. However, "aliasing" will cause amplitude distortion which may hamper technical efforts of analysis of multiple frequency components.

F. Spikes

Anomalous large spikes occur simultaneously in several levels sometimes in the data. Inspection shows that virtually all of these instances are associated with either the last profile before an interruption or the first profile after an interruption during the sequence of profiles of the mission.

G. Vocabulary

A vocabulary of behavior variations for existing data has been formally stated and transmitted to Dr. Chonacky. It is likely that this vocabulary is influenced by effects of data "aliasing." The full vocabulary is not included in this report due to limitations of brevity. Very briefly stated, the vocabulary contains: regular data fluctuations of two profiles per period; data fluctuation mixing two profiles and three profiles per period; smooth concave upward and smooth concave

downwards segments; linear segments; straight downward or straight upward linear segments; and individual spikes. Each of these primary forms may be modified with respect to amplitude or with respect to gradual sloping upward or sloping downward.

V. Obstacles to Sound Data Interpretation:

Several difficulties combine to disrupt accurate analysis of Cn-squared data.

A. It would be possible to plot existing data on whatever sampling intervals did occur and then to effect some interpolations or rounding into equal time increments for a frequency analysis. However, all Verona data has been entered onto data files of the VAX computer along with a pseudo- time base. This assigns a non-real interval of exactly two minutes to every data sampling interval. There is also no record of the actual time that the mission was undertaken, the intensity and name of the star which was used.

B. Some acquired data profiles are discarded for either of two reasons:

1. The theoretical interpolative nature of the seven altitude level response curves to the acquired raw data of the scintillometer is such that negative values of Cn-squared are calculated for some levels. It has been the practice to eliminate the entire profile from the data base in the event of at least one negative entry of the profile.

2. The entire physics of the scintillometer is not fully documented and available from the designers. The computer data processing programs of the MAUI instrument and Verona instrument appear to be distinct although the hardware is alike. In addition to Cn-squared values for each of seven altitude levels, the Verona computer program produces several other values including a value named the quality factor. If the quality factor exceeds a permissible range of 0.5 to 2.0, then the profile is discarded. The Maui computer program also records a quality factor.

C. Numerous lengthy interruptions occur during a mission due to cloud cover, electrical problems, and mechanical tracking of the focus on the star.

VI. Recommendations:

A. That a knowledgeable effort be made to apply Box-Jenkins time series analysis (4) to existing data. There exists a variety of such techniques for specific applications. At this time, it is not clear which specific techniques are applicable to data which varies in the fashion of Cn-squared data.

B. That individuals who undertake future data acquisitions be made aware of the significance and desirability of a long sequence of profiles, if possible, without avoidable interruptions.

C. That a further study of the physics of the quality factor computation be done. An effort to relate this study to environmental conditions might improve the efficiency of data gathering and reduce the number of deletions of profiles.

D. That the mechanism of triggering data acquisition in the Verona scintillometer be considered to see if the time interval between starts could become more standard and perhaps of shorter duration. This would alleviate any effect of "aliasing" and would possibly strengthen any effort to analyze future data with respect to time.

E. That a list of potentially related data be gathered and stored with Cn-squared profiles at the time the mission is completed. This data would include metrological profile such as local barometric pressure, location of surrounding high and low areas and fronts, daily navigational flight data on high altitude winds, location of jet stream, etc. This data is very difficult to collect from past archives, and storing such data concurrent with the mission would be helpful. If this sort of associated conditions were known, then it might be possible to explain such variations at the difference between Figure 1, level 1 and Figure 2, level 1.

REFERENCES

Conference and journal publications, technical memorandums:

1. Ochs, G.R., T.Wang, and F. Merrem, "Stellar Scintillometer Model II for measurement of Refractive-Turbulence Profiles," NOAA Technical Memorandum ERL WPL-25, Wave Propagation Laboratory, Boulder, Colorado, April 1977.

2. Ochs, G.R., R.S.Lawrence, and T.Wang,"Stellar Scintillation Measurement of the Vertical Profile of Refractive- Index Turbulence in the Atmosphere," Society of Photo-Optical Instrumentation Engineers Vol 75, Imaging Through Atmosphere, National Oceanic and Atmospheric Administration, Boulder, Colorado, 1976, pp 48-52.

3. Chonacky, N.J. and D.M. Stebbins, "Time-Dependent Statistics of Upper Atmospheric Optical Turbulence", SPIE Technical Symposium East '85, Arlington, Virginia, RADC, April 1985.

Textbooks:

4. Box, George and Gwilyn Jenkins,"Time Series Analysis Forecasting and Control", University of Wisconsin, Holden-Day Inc., 1976.

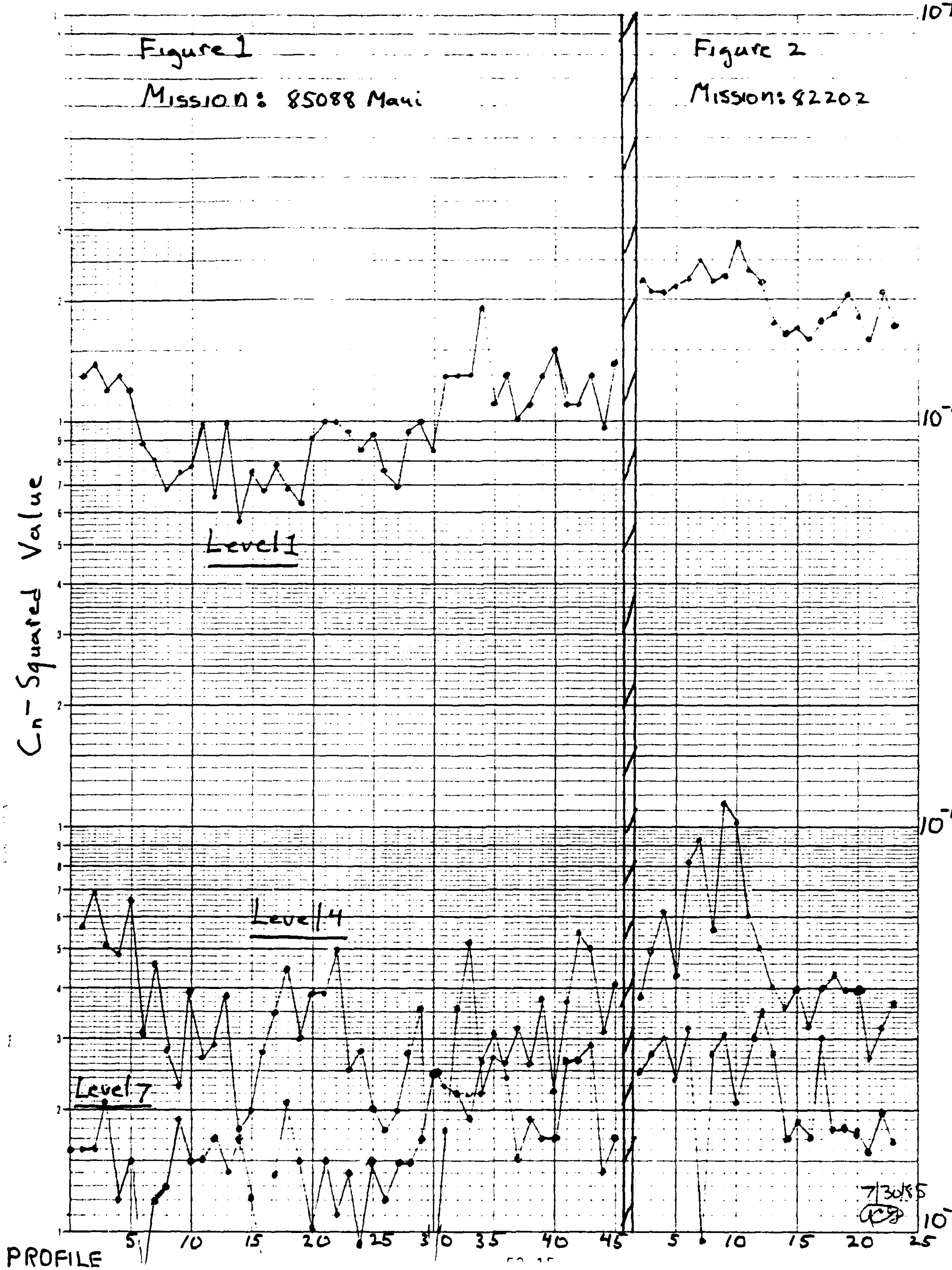
Figure 1
Mission: 85088 Maui
Figure 2
Mission: 82202
Cn - Squared Value
Level 1
Level 4
Level 7
10^{-15}
10^{-16}
10^{-17}
10^{-18}
7/30/85
5 10 15 20 25 30 35 40 45
5 10 15 20 25
PROFILE

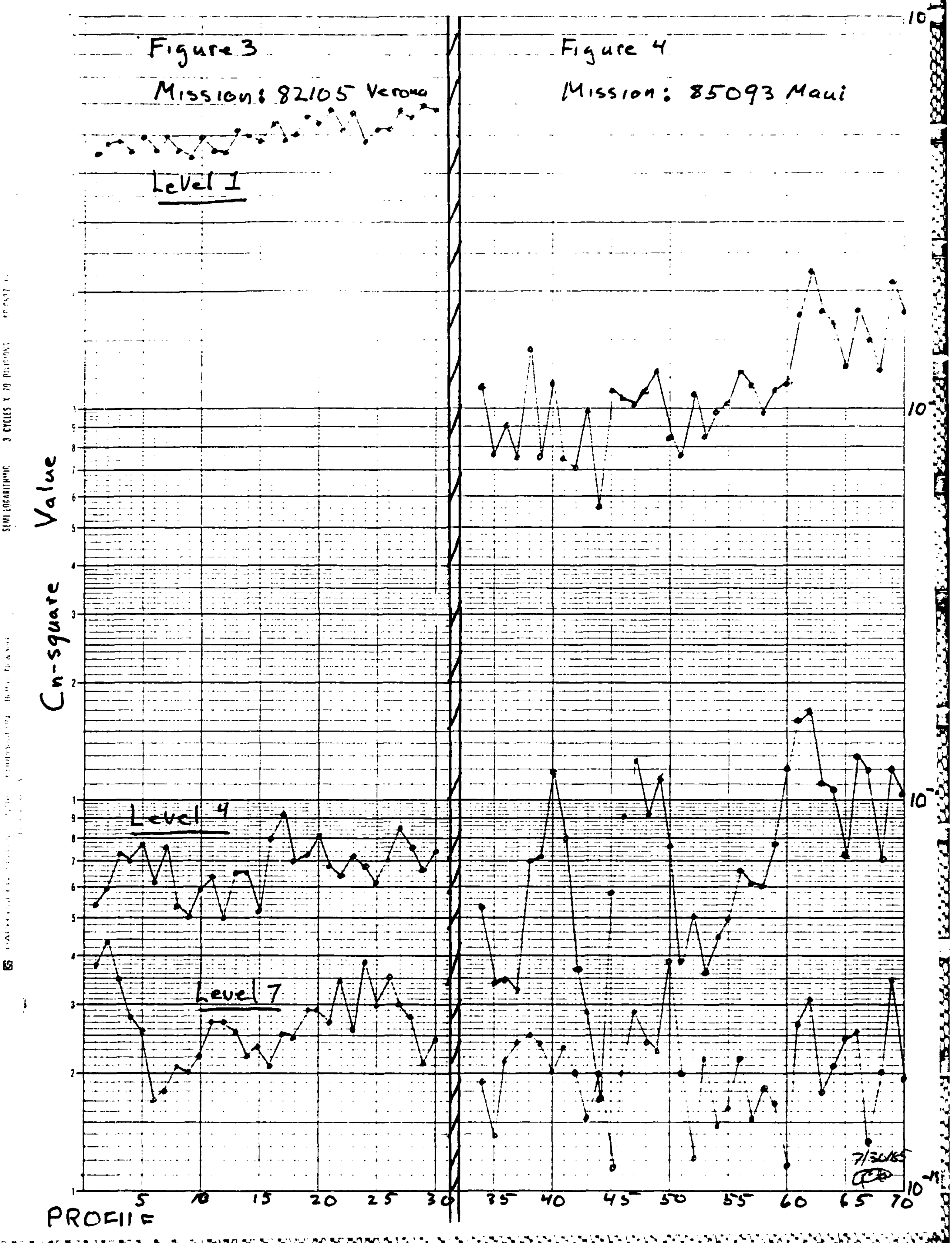

Figure 3
Mission: 82105 Verona
Level 1
Level 4
Level 7
Figure 4
Mission: 85093 Maui
Cn-square Value
PROFILE
5
10
15
20
25
30
35
40
45
50
55
60
65
70
7/30/85

1985 USAF-UES SUMMER FACULTY RESEARCH PROGRAM/

GRADUATE STUDENT SUMMER SUPPORT PROGRAM

Sponsored by the

AIR FORCE OFFICE OF SCIENTIFIC RESEARCH

Conducted by the

UNIVERSAL ENERGY SYSTEMS, INC.

FINAL REPORT

MODULAR MODELING OF SOLID-FUEL RAMJET COMBUSTOR FLOW

Prepared by:	Mahesh S. Greywall
Academic Rank:	Professor
Department and	Mechanical Engineering Department
University:	Wichita State University
Research Location:	AFWAL/PORT, Aero Propulsion Laboratory
USAF Research:	Parker L. Buckley

Date:	July 19, 1985
Contract No:	F49620-85-C-0013

MODULAR MODELING OF SOLID-FUEL RAMJET COMBUSTOR FLOW

Mahesh S. Greywall

ABSTRACT

A "modular" model for computing flow through solid-fuel dump ramjet combustors is presented. The model makes use of the modular concept, in which the combustor flow is broken down into three interacting flow components: a recirculating zone at the combustor inlet step, a recirculating zone at the aft-fuel-grain step, and a directed flow region. A code has been partially developed to compute the combustor flow along these lines, and the results of sample calculations, using the partially developed code, are presented.

ACKNOWLEDGEMENTS

I would like to thank Mr. P. L. Buckley and Dr. F. D. Stull for their help during the course of this study. I am also beholden to the rest of PORT members for lending a helping hand whenever I needed one.

The work was supported by AFOSR through the 1985 USAF-UES Summer Faculty Research Program.

I. INTRODUCTION

Solid-fuel ramjet has gained interest in the recent years as a propulsion device for specific defense applications. As the use of this device receives increasing attention, it becomes increasingly important to develop theoretical models to describe flow through the various ramjet components; in particular, the complex flow through the dump (sudden-expansion) type combustors. Theoretical studies of the combustor flow field, especially the parametric type, will lead to a better understanding of what goes on in the combustor, and thus to a better design. The insight gained by these studies will also help in planning the combustor test programs and in better understanding the test results.

Over the past several years I have been working in the area of computational fluid dynamics (see, for example, Refs. 1-3). The author has developed numerical codes for the computation of two-dimensional (Ref. 4) and three dimensional (Ref. 5) internal flows. The work was funded by NASA-Lewis.

The Ramjet Technology Branch, PORT, of AFWAL Aero Propulsion Laboratory has currently an active research and development program in the area of solid-fuel ramjet combustors. My background and interest in modeling internal flows matched the summer faculty needs of PORT.

II. OBJECTIVES OF THE RESEARCH EFFORT

Main thrust of the summer research program was to:

(1) Survey literature dealing with the modeling of solid-fuel dump ramjet combustors. Include in the survey work done on the modeling of ramjet combustors in general (i.e., not necessarily the solid-fuel type)

in so far as they may help in developing a model of the solid-fuel dump ramjet combustor.

(2) Develop a theoretical model for the solid-fuel dump ramjet combustor.

(3) Modify the code given in Ref. 4, as far as possible in the limited time available, to compute the flow through combustor-nozzle geometry according to the model developed in Step. 2.

III. LITERATURE SURVEY

Much of the analysis of SFRJ combustors in the past has dealt with correlating the fuel regression data with mass flux through the combustor. A discussion of the various correlation formulae is given in Ref. 6 (section 4.3.4). This reference also has a discussion of the more recent formulae that include, guided by one-dimensional analysis, the dependence of regression rates on the chamber pressure and the combustor inlet air temperature.

Almost all of the two-dimensional calculations of the SFRJ combustor flow, uptill now, have been carried out by Netzer, and by Netzer in cooperation with others (see, for example, Refs. 7-10). These calculations were carried out by adapting the 2-D elliptic flow codes developed by the Imperial College (11,12) to the SFRJ geometry. In Ref. 7 calculations of combustor flow were carried out using vorticity and stream function as the dependent variables. Radiation was neglected and fast chemical reaction (mixing limited combustion) was assumed. The results of calculations were in good qualitative agreement with the experimental data (also obtained by the author) for plexiglas. In Ref. 8 calculations were repeated for an all-hydrocarbon fuel. The regression rates predicted were too low and were arbitrarily increased by 30% to

obtain a more realistic value of the blowing parameter. As pointed out by the author, radiation plays a dominant role in all-hydrocarbon fuel combustors, and the neglect of radiation in his calculations was the reason for his low regression rates. Stevenson and Netzer (9) repeated the calculations of Ref. 7 using primitive variables, the results were similar to those obtained earlier with the use of vorticity-stream function variables. Metochianakis and Netzer (10) modified the earlier work (8) to include the effects of radiation. The amount of radiation striking the fuel surface depended strongly on an empirical constant ("λ") appearing in their formulation. This constant was selected to match the results of their calculations with the experimental data. Results of the calculations, carried out for plexiglas, were similar to those obtained earlier without the radiation effects. As pointed out by the authors, radiation plays an unimportant role in combustors using plexiglas fuel.

An interesting approach to the modeling of liquid-fuel dump ramjet combustors, called "modular" modeling, is presented by Edelman, et al. (13). The model makes use of the modular concept, in which the combustor flow field is broken down into various interacting components, each with its own distinct flow characteristics. This approach allows rapid calculation of the combustor flow, thus making it feasible to conduct parametric studies. Our approach to compute flow through the solid-fuel dump ramjet combustor, presented in the next section, is based on this modular concept.

IV. MODULAR MODELING OF THE SOLID-FUEL DUMP RAMJET COMBUSTOR

Flow through the solid-fuel dump ramjet combustor is considered as made up of three interacting flow regions, P, R1, and R2 (see Fig. 1a). Regions R1 and R2 represent, respectively, the recirculating zones at the combustor inlet step and the aft-fuel-grain step. Region P represents the rest of the combustor-nozzle flow. Flow through region P is a directed flow and, thus, can be computed using parabolic codes. Flow in regions R1 and R2 need to be calculated either using elliptic codes, or modeled empirically as planned in the present study.

Flow through region P is calculated using a modified version of a code developed earlier by the author (Ref. 4). The original code and the required modifications are briefly discussed next.

Original Code: The code is based on the method given in Ref. 1 for computing 2-D turbulent flows (including the energy equation) with the approximation that the flow is 'parabolic' (i.e., boundary layer type). The method uses streamline coordinates in the cross-stream plane as one of the dependent variables. Thus, it generates a body fitted coordinate system as part of its solution, this in turn makes the method attractive for computing flow through arbitrary shaped nozzles, inlets, etc. A numerical code based on this method is available in Ref. 4.

Required Modifications: Modifications to the original code required for the computation of region P flow fall into two basic classes:

Class A. The original code computes transport of a single species without any chemical reaction. The code needs to be modified to include the transport of O2, N2, Fuel, and the combustion products mass fractions. And, it needs to be modified to include chemical reaction.

Class B. The original code assumes solid boundaries, without any mass injection into the flow from the boundaries. The boundaries

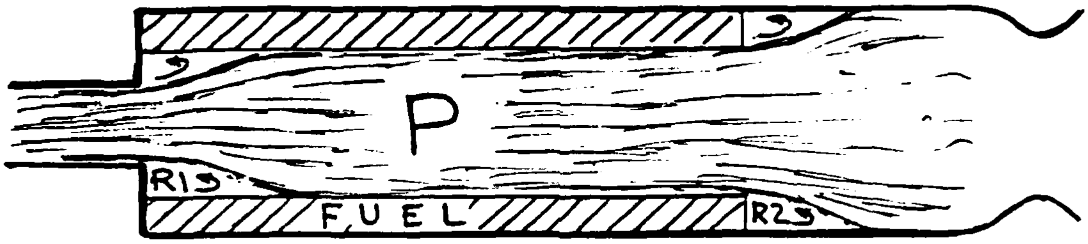

Fig. 1a. Partitioning of SFRJ combustor flow into recirculating-flow regions R_1 and R_2, and directed flow region P.

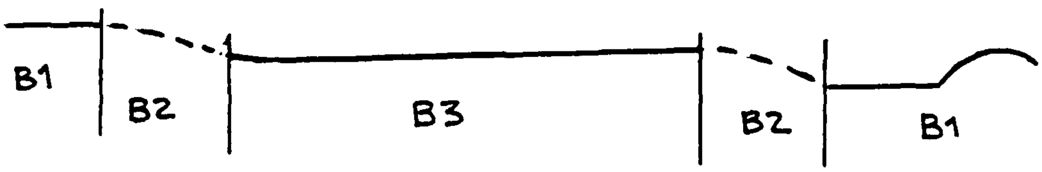

Fig. 1b. Different types of boundaries for the region P flow.

encountered in the computation of region P flow are of three different types - B1, B2, and B3 (see Fig. 1b): B1 represents the non-reacting solid boundaries. This type of boundary, as mentioned earlier, is already built into the code; B2 represents the shear layer that separates region P flow from the recirculating region flows; B3 represents the solid fuel boundary.

Code Modifications Done During the Summer:

The code was modified to include the transport of N2, O2, Fuel, and Combustion Products mass fractions. Finite difference equations for these mass fractions were derived along the lines of work given in Ref. 1 (for the sake of brevity, the gory details are omitted from this report).

Chemical reaction, such as the one used by Netzer (9), was added to the code. The combustion was considered to be mixing limited with a simple one-step chemical reaction. Thus, 1 kg of fuel and r kg of O2 (r is the stoichiometric ratio of O2 mass to fuel mass) produced (1+r) kg of combustion products, and fuel and oxygen could not co-exist. As pointed out by Muzzy and Stull (14), in solid-fuel ramjets the fuel regression rate is both kinetically and heat transfer limited. Thus, the exclusion of chemical kinetics in the present work is a serious drawback and should be remedied.

Rate of fuel evaporation from the surface, $\dot{m}_f$, was calculated from the formula,

$$\dot{m}_f \, (h_w + h_{fg}) = \dot{Q},$$

where h_w is the enthalpy of fuel grain, h_{fg} the latent heat of evaporation, and $\dot{Q}$ heat transfer to the wall. All the wall fluxes (mass, momentum, and energy) were corrected to take into account mass addition (blowing) from the wall.

At present, only the convection heat transfer is included in the code. In combustion of all-hydrocarbon fuels radiation heat transfer is very important. Thus, the code needs to be modified to include radiation heat transfer, if it is to be used for calculating all-hydrocarbon combustor flows.

V. SAMPLE CALCULATIONS

Since the code at present does not have the inlet-step recirculation zone, uses one-step chemical reaction, neglects radiation heat transfer, and uses constant specific heats, the calculations presented in this section should be looked at qualitatively. Sample calculations were carried out for flow through a 10 cm port diameter combustor and a solid fuel consisting of 75% hydroxylterminated polybutadiene and 25% cross-linked polystyrene. Fuel properties used in the computations were as follows:

Latent heat of evaporation = 2980 kJ/kg

Heat of combustion = 45,760 kJ/kg

Stoichiometric Air/Fuel ratio = 13.31

Solid phase specific heat = 1.82 kJ/kg-C

These fuel properties were supplied by PORT and are very close to those given in Ref. 6 (Table 2-11). Schadow et al. (15) have measured radial temperature distribution in the combustor for this type of fuel. In the sample calculations the combustor geometry and the starting values of the flow parameters were selected to simulate the experimental conditions of Schadow et al. (15). The flow was started with the following parameters:

Velocity = 170 M/s

Temperature = 1200 K

Pressure = 7 atm.

The fuel-wall temperature was fixed at 980 K. In calculations we used ideal gas law, fixed constant pressure specific heat equal to 1.338 kJ/kg-C (air at 2000 K), and both Prandtl and Schmidt numbers equal to one for all the species. The computations were carried out with the use of 21 streamlines (grid points normal to the flow) and an axial integration step equal to one-fifth of the combustor radius.

In Fig. 2 are shown the computed radial variations of temperature, O2, and the fuel at an axial distance of 62 cms from the start of the calculations. These distributions are what one would expect with a one-step chemical reaction model. They are in qualitative agreement with the experimental data. Figure 3 shows (solid line) the calculated axial variation of the fuel regression rate. Because the recirculation zone has been omitted in these calculations, the familiar peak at the beginning of the regression rate curve is missing. Also shown in Fig. 3 (broken line) is the radial location of the flame (defined by the position of maximum in the radial temperature distribution) along with the combustor axis.

These results, although in accord with expectations, are not in accord with reality. The predicted flame temperature of 4000 K is much too high compared to the experimental value (15) of approximately 2500 K. The predicted flame temperature is close to the local adiabatic flame temperature, The maximum predicted fuel regression rate of approximately 0.035 cm/s is lower than the value of approximately 0.05 cm/s given in Ref. 6 (Fig. 4-43) for the corresponding mass flux.

The disparity between the predicted and the experimental results is due to our assumption of fast chemical reaction (complete combustion

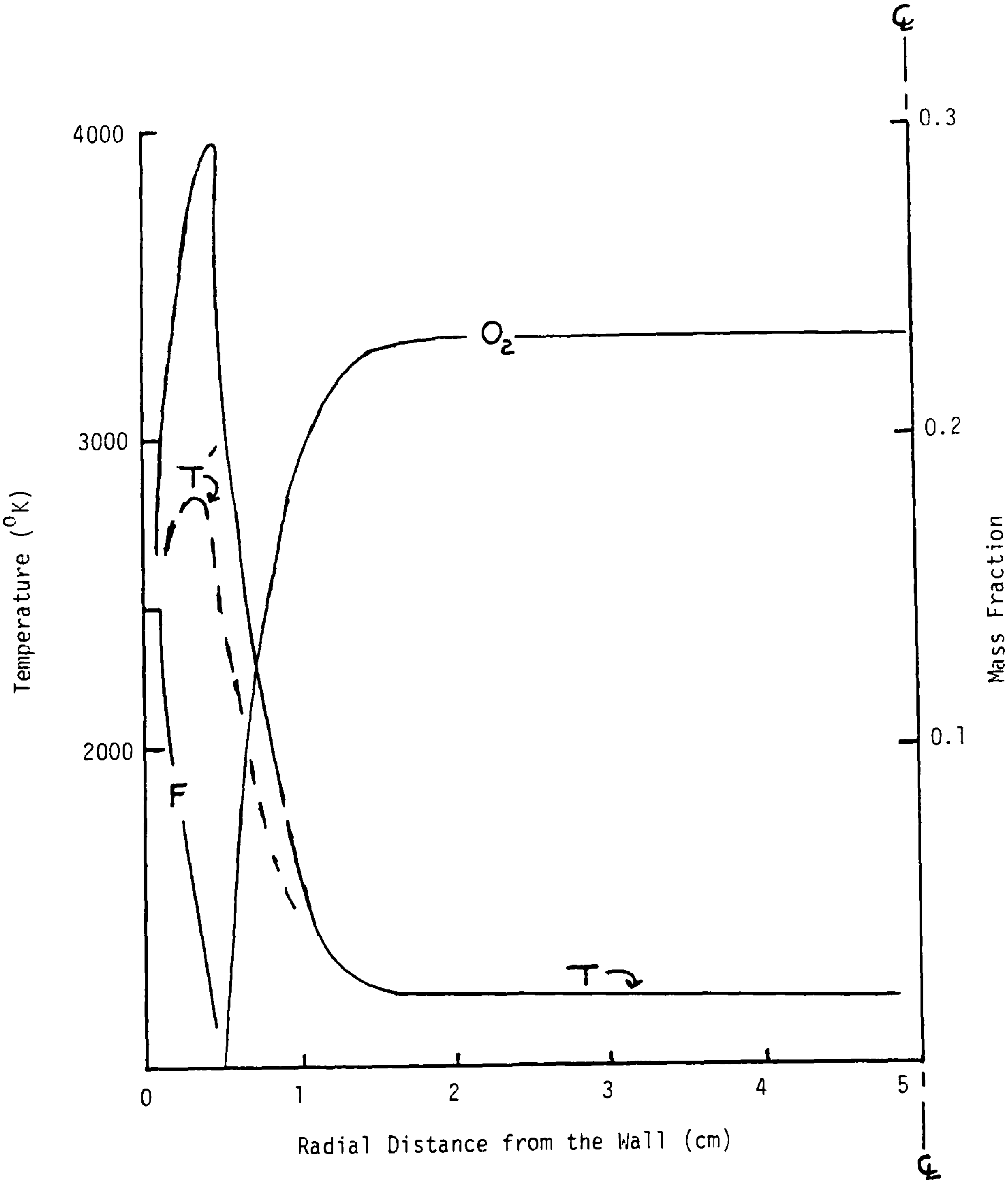

Fig. 2. Radial distributions of combustor temperature (T), and oxygen (O2) and fuel (F) mass fractions. Also shown is the radial temperature distribution (T') with the heat of combustion reduced by 25%.

AD-A166 177 UNITED STATES AIR FORCE SUMMER FACULTY RESEARCH PROGRAM 02/1
1985 TECHNICAL RE (U) UNIVERSAL ENERGY SYSTEMS INC
DAYTON OH R C DARRAH ET AL. DEC 85 AFOSR-TR-86-0140
UNCLASSIFIED F49620-85-C-0013 F/G 5/1 NL

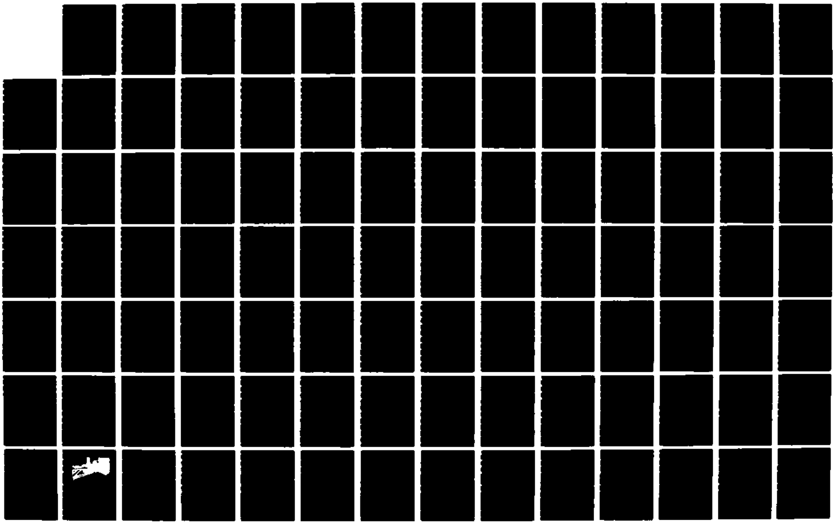

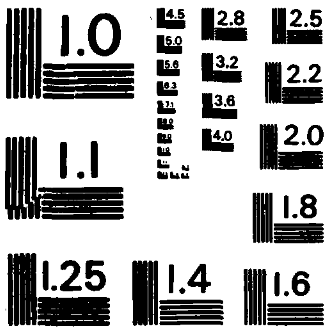

MICROCOPY RESOLUTION TEST CHART
NATIONAL BUREAU OF STANDARDS-1963-A

in a single step) and the neglect of radiation heat transfer. As the measurements of species concentration by Schadow et al. (15) show, the combustion is far from being complete. Incomplete combustion reduces the heat of reaction released locally, and thus reduces the flame temperature. Also, the high concentration of carbon particles found in such flames will lead to a substantial radiation heat transfer from the flame zone, thus further reducing the flame temperature. This radiation heat transfer will also increase the fuel regression rate by increasing the total heat transferred to the wall.

To see how incomplete combustion will effect the flame temperature calculated with the present code, the heat of combustion was artificially reduced by 25%. The resulting temperature distribution is shown in Fig. 2 with a broken line. We note that the flame temperature is reduced to 2800 K.

One thing the sample calculations show is that the use of finite reaction rates and the inclusion of radiation heat transfer are crucial in calculating flow through combustors burning all-hydrocarbon fuels. Also, since there is a large variation in the radial distribution of temperature, temperature dependence of specific heat should be included.

VI. RECOMMENDATIONS

1. Add the recirculating zone "modules" to the code to complete the modular modeling of the solid-fuel ramjet combustor.

2. Introduce finite reaction rates.

3. Add radiation heat transfer.

4. Use more accurate thermodynamic properties. At the minimum, use temperature dependent specific heat.

REFERENCES

1. Greywall, M. S., "Streamwise Computation of Duct Flows," Computer Methods in Applied Mechanics and Engineering, 21, 231, (1980).

2. Greywall, M. S., "Streamwise Computation of Three-Dimensional Parabolic Flows," Computer Methods in Applied Mechanics and Engineering, 36, 71, (1983).

3. Greywall, M. S., "Streamwise Computation of Two-Dimensional Incompressible Potential Flows," J. of Computational Physics, 59, 224, (1985).

4. Greywall, M. S., "Numerical Modeling of Two-Dimensional Confined Flows," NASA CR-162115, 1979.

5. Greywall, M. S., "Numerical Modeling of Three-Dimensional Confined Flows," NASA CR-165583; DOE/NASA/3186-2, 1981.

6. "Fundamental Combustion Technology for Ramjet Applications," CPIA 363, Vol. II, Sept. 1982.

7. Netzer, D. W., "Modeling Solid-Fuel Ramjet Combustion," Journal of Spacecraft and Rockets, Vol. 14, Dec. 1977, pp. 762-766.

8. Netzer, D. W., "Model Applications to Solid Fuel Ramjet Combustion," Journal of Spacecraft and Rockets, Vol. 15, Sep.-Oct. 1978, pp. 263-264.

9. Stevenson, C. A. and Netzer, D. W., "Primitive-Variable Model Applications to Solid-Fuel Ramjet Combustion," Journal of Spacecraft and Rockets, Vol. 18, Jan.-Feb. 1981, pp. 89-94.

10. Metochianakis, M. E., and Netzer, D. W., "Modeling Solid-Fuel Ramjet Combustion, Including Radiation to the Fuel Surface," Journal of Spacecraft and Rockets, Vol. 20, No. 4, Jul.-Aug. 1983, pp. 405-406.

11. Gosman, A. D., Pun, W. M., Runchal, A. K., Spalding, D. B., and Wolfshtein, M., "Heat and Mass Transfer in Recirculating Flows," Academic Press, New York, 1969.

12. Pun, W. M. and Spalding, D. B., "A General Computer Program for Two-Dimensional Elliptic Flows," Imperial College of Science and Technology London, Rept. HTS/76/2, Aug. 1977.

13. Edelman, R. B., Harsha, P. T., and Schmotolocha, S. N., "Modeling Techniques for the Analysis of Ramjet Combustion Processes," AIAA Journal, Vol. 19, May 1981, pp. 601-609.

14. Muzzy, R. J. and Stull, R. O., "Hybrid Combustion," Proceedings of the Tenth JANNAF Combustion Meeting, CPIA Publication No. 243, Vol. III (1973), pp. 169-179.

15. Schadow, K. C., Cordes, H. F., and Chieze, D. L., "Experimental Studies of Combustion Processes in Solid Fueled Ramjets," Proceedings of the Thirteenth JANNAF Combustion Meeting, Silver Springs, MD, Chemical Propulsion Information Agency, 1977, pp. 245-259 (CPIA Pub. 281).

1985 USAF-UES SUMMER FACULTY RESEARCH PROGRAM/

GRADUATE STUDENT SUMMER SUPPORT PROGRAM

Sponsored by the

AIR FORCE OFFICE OF SCIENTIFIC RESEARCH

Conducted by the

UNIVERSAL ENERGY SYSTEMS, INC.

FINAL REPORT

THERMAL STABILITY CHARACTERISTICS OF SOME ADVANCED SYNTHETIC BASE FLUIDS

Prepared by: Vijay K. Gupta, William Sawyer, and Lenae V. Tuggle

Academic Rank: Professor of Chemistry

Department and University: Chemistry Department, Central State University, Wilberforce, Ohio 45384

Research Location: Materials Laboratory (AFWAL/MLBT), Wright Patterson Air Force Base, Ohio

USAF Research: Mr. C.E. Snyder, Jr.

Date: September 30, 1985

Contract No: F49620-85-C-0013

THERMAL STABILTY CHARACTERISTICS OF SOME ADVANCED SYNTHE.:C BASE FLUIDS

by

Vijay K. Gupta, William Sawyer, and Lenae V. Tuggle

Abstract

Thermal stability characteristics of two Advanced Synthetic fluids MLO 82-507(silahydrocarbon and MLO 82-546 (Polyalphaolefin PAO) have been investigated. Three mixtures were prepared from two fluids with following concentrations: 25% MLO 82-507 + 75% MLO 82-546, 50% MLO 82-507 + 50% MLO 82-5 and 75% MLO 82-507 + 25% MLO 82-546. Thermal decomposition studies have been conducted as a function of time and temperature. Decomposition products were analyzed using viscosity measurements GC analysis, GC/MS analysis, and Infrared spectroscopy. It has been found that the fluid MLO 82-507 the mixture silahydrocarbon is more thermally stable than the fluid MLO 82-546. Both fluids do not show any appreciable decomposition below 357.2 C, but above this temperature rate of degradation increases significantly. The PAO MLO 82-546 decomposes almost completely in 48 hours when stressed at 371.1C, whereas the mixture silahydrocarbon takes 72 hours stress period at 371.1C for the same level of degradation. Mixing two fluids does not provide any advantage as far as the thermal stability is concerned.

Acknowledgements

The authors would like to thank the Air Force Systems Command, the Air Force Office of Scientific Research and the Universal Energy Systems Inc., for providing them with the opportunity to spend a worthwhile and interesting summer at the Materials Laboratory, Wright Patterson Air Force Base, Dayton, Ohio 45433. We would also like to thank the Nonstructural Materials Branch of the laboratory for its hospitality and excellent working conditions. The authors are thankful to Mr. Lee D. Smithson of the Analytical Services Branch, and Dr. Jeff Workamn and Dr. Chin Yu of the Technical Services Inc. for providing GC/MS analysis.

We take this opportunity to thank all the members of the Nonstructural Materials Branch and UDRI Lubricants Group for their technical assistance in conducting these studies. Finally, we would like to thank Mr. Carl E. Snyder Jr. and Ms. Lois Gschwender for suggesting this area of research and for their collaboration and helpful suggestions.

INTRODUCTION

Recent effort has led to the development of several functional fluids for use in aerospace applications such as jet engine oils, greases, .nd hydraulic fluids. Since hydraulic fluids are not expected to operate in oxidative environments, therefore thermal and hydrolytic stability are the two main areas of concern (1). In order to meet the need for a high temperature fluid, MIL-H-27601, a -40°C to 288°C hydraulic fluid was developed. A highly refined, deep-dewaxed paraffinic mineral oil was selected as the base stock for the above application, and the fluid provided satisfactory service for over ten years in the temperature range of -40°C to 288°C.

The development of the supersonic missiles, like the advanced strategic air launched missile (ASALM) has created the need for a hydraulic fluid useable over the temperature range of -54°C to 315°C. The mineral oil base stocks from which MIL-H-27601 is derived, do not have the needed viscosity temperature properties to perform satisfactorily in the temperature range of -54°C to 315°C. Synthetic hydrocarbons based on hydrogenated polyalphaolefin oligomers have also been found to be deficient both in thermal stability and viscosity temperature properties (2). However, decene oligomers have emerged as a rather unique class of synthetic hydrocarbon lubricants. These fluids are distinguished from their petroleum derived counterparts by excellent low temperature properties, improved thermal and oxidative stability, and significantly improved viscosity index. As a representative example of this type of fluid is a Gulf 4 Cst containing C_{30} oligomer. Perfluorinated fluids which have excellent thermal and oxidative stabilities, have several disadvantages such as high density, poor bulk modulus, elastomer incompatibility, and lack of suitable additives (3).

In response to the need for hydrocarbon-type fluids with improved properties, a Materials Laboratory program has led to the development of a class of compounds called silahydrocarbons. These compounds have excellent viscosity temperature properties and thermal stablity and are expected to be hydrocarbon-like in their physical and chemical properties. Therefore, silahydrocarbons are good candidates for hydraulic fluids useable over the tmeperature rnage of -54°C to 315°C. The studies on silahydrocarbon class of materials so far indicate that they are excellent candidate fluids that can be used over the temperature range of -54°C to 315°C, because fo their excellent thermal stability coupled with desired flow properties down to -54°C (4,5). However, very little effort has been focussed on the kinetics and mechanisms of the thermal degradation processes occuring in the perfluorinated fluids, synthetic hydrocarbons, and silahydrocarbons. This report describes the effort to understand the thermal stability characteristics of two synthetic base stocks of advanced hydraulic fluids. One of the fluid is a mixture silahydrocarbon labelled as MLO 82-507, and the other is a polyalphaolefin (PAO) labelled as MLO 82-546.

II. OBJECTIVES

The main objective of the summer program was to understand the thermal stability characteristics of the above fluids as a function of temperature and time in the dry environment. The other objective was to identify the thermal degradation products both in the gaseous and liquid states. One of the objectives was to determine the thermal stability characteristics of the mixtures of the synthetic polyalphaolefin fluid (PAO) with the silahydrocarbon.

III. PROPOSED EFFORT

It was proposed to study the thermal stability characteristics of the two experimental fluids which were assigned MLO numbers as indicated below:

1. MLO 82-507, a mixed silahydrocarbon consisting of the following four components: $CH_3\ Si\ (C_8H_{17})_3$, $CH_3\ Si\ (C_8H_{17})_2\ (C_{10}H_{21})_3$, $CH_3Si\ \ C_8H_{17}.(C_{10}H_{21})_3$, and $CH_3\ Si\ (C_{10}H_{21})_3$.
2. MLO 82-546, a polyalphaolefin (PAO) is a Gulf 4 Cst C_{30} oligomer containing a wide mixture of different isomers.

It was proposed to investigate the viscosity and thermal stability characteristics of the mixtures prepared from two fluids given above. Thermal studies of the above oils were proposed both as a function of temperature and time.

IV. EXPERIMENTAL

This section describes the test procedures.

Thermal Stability Test Procedure: The thermal stability tests were conducted in stainless steel bombs. The bombs were made of 9" long stainless steel tubes either 0.25' or 0.375" diameter with swagelok fittings on both ends. The bombs were cleaned with a suitable solvent such as hexane and dried in an oven at 120°C for one hour. Approximately 2.00 cc of test fluid was added to the bomb, and the lamp grade nitrogen gas was bubbled through the fluid for five minutes to remove any air and the bomb was quickly capped with the swagelok fitting. The bomb was then weighed and placed in the oven at a specific temperature (controlled within 2°C) for a specified time period. After the bomb was heated in the oven for a given length of time, the bomb was removed, allowed to cool, and was weighed again. If the pre-test and post-test

weights differed by more than 0.100 g, the test was considered to be a bad test. In normal cases the weight change was generally found to be 0.010 g to 0.020 g, but in some cases when the bomb developed leak due to some reasons, excessive weight changes were observed and those tests were repeated. The thermal degradation products from the bomb were analysed using viscosity measurements, gas chromatographic analysis for gaseous and liquid components both in the gaseous and liquid phases, and GC/MS for identification of the components. In order to analyze the gaseous components, the bomb was placed in a bath maintained at -54°C for at least 30 minutes so that the gaseous components liquify or freeze, the bomb was then taken out of the cold bath and one of the cap was replaced by a cap with a small hole containing a septum in order to facilitate the removal of sample for gas analysis by GC. The method and gas chromatographic conditions for gaseous analysis are listed in Table 1. After the gas phase sample called headspace was analysed, the bomb was opened and the liqiud sample was transferred to a glass vial for analysis of liquid components and viscosity measurements. The method and gas chromatographic conditions for the analysis of liquid phase are listed in Table 2. Both the individual fluids and the mixtures prepared from the two fluids were studied for thermal stability characteristics using the above test proceedures and the analytical methods.

V. RESULTS AND DISCUSSION

The two advanced base stock fluids MLO 82-546 and MLO 82-507 the silahydrocarbon and the mixtures 25% MLO-82-507 + 75% MLO 82-546, 50% MLO 82-507 + 50% MLO-82-546, and 75% MLO-82-507 + 25% MLO-82-546, were studied for thermal degradation characteristics. The figures 1 and 2 represent the gas chromato-

grams of MLO 82-507 and 82-546 respectively. From fig. 1, it appears that MLO 82-507 consists of four silahydrocarbon components labelled as A, B, C, and D and their concentrations are indicated accordingly. The chromatogram in fig. 2 and the GC/MS data for the MLO 82-546 indicate that there are more than 20 different isomers of the oligomer $C_{30} H_{62}$ present in this fluid.The data in table 3 gives the viscosities of the fluids MLO 82-507, MLO 82-546, and their mixtures as function of temperature. The above data when plotted on ASTM graph indicates the viscosity data to be linear except the data point at -54°C. Viscosity can be expressed as function of temperature by the equation given below:

$$\frac{1}{\phi} = \eta = A \exp \frac{E_{vis}}{RT}$$

where ϕ is the fluidity

η is the viscosity

A is the pre-exponetial factor

and E_{vis} is the activation energy for viscous flow, the energy barreir that must be overcome before the elementary flow process can occur.

The above equation in the logarithmic form can be written as

$$\log_{10} \eta = \log_{10} A + \frac{E_{vis}}{2.303 \, RT}$$

Figure 3A gives the plot of $\log_{10}\eta$ as function of 1/T. From the slopes, the activation energies have been computed and are given in table 3. Both the fluids and their mixtures have the desired viscosities in the temperature range -54 C to 98.9 C and exhibit linear relationship within the limited temperature range.

The data in table 4 and 6 and figures 4 and 6 represent the GC/MS analysis of the gaseous phase when the fluids were stressed at 700 F (371.1C). From the above data, it appears that hydrocarbons with 1-carbon atom to 10-carbon atoms are found in the degradation products of both the fluids, but in MLO 82-546, the hydrocarbons with 11-carbon atoms to 14-carbon atoms were also detected, however their amounts are very small. The data in table 5 and 7 and figures 5 and 7 represents the GC/MS analysis of the liquid phase after the two fluids were stressed at 700 F (371.1C). Various degradation products as formed under the stress conditions are listed in tables 5 and 7. As significant concentrations of small molecules are produced, the hydrocarbon chains could preferentially be breaking at the ends away from the silicon atom. The I.R. Spectra of the two fluids stressed at 700 F(371.1C) are given in figures 13 to 16. It is noted that in fig. 13 when I.R. spectra of MLO 82-507 is taken in KBr cell 0.025 mm path-length there was no band in the region 1630-1650 cm^{-1}, but when the same fluid was run in KBr cell 0.5 mm path-length, a weak band in the region 1630-1650 cm^{-1} was observed (see fig. 14). This indicates a small concentration of unsaturated hydrocarbons. In case of MLO 82-546 also I.R. spectra was taken using KBr cells with path-lengths 0.025 mm and 0.5 mm (see figures 15 and 16). The band in the region 1630-1650 cm^{-1} in case of MLO 82-546 fluid is stronger than the band in case of fluid MLO 82-507. It appears that the fluid MLO 82-546(PAO) produces more unsaturated hydrocarbons than the fluid MLO 82-507(silahydrocarbon), however the concentration of unsaturated hydrocarbons is small as indicated by GC/MS analysis.

The data in table 8 to 12 and figures 8 to 12 represents the thermal degradation data of MLO 82-507 and MLO 82-546 and their mixtures when stressed under conditions as indicated in the respective tables and figures. The

concentration values are the relative concentrations, and have been averaged when more than one data point was obtained, and the values in the parenthesis indicate standard deviation. The concentration data was fitted on a second degree polynomial, and the fitted data has been plotted in figures 8 to 12. After examining the data in table 8, it appears that the data point at 16 hours is not consistent with the rest of the data, so this point would need further experimentation. From table 8 and fig. 8, the degradation data at 700 F (371.1C) as function of time, it appears that MLO 82-507(silahydrocarbon) decomposes at a lower rate than MLO 82-546 (PAO). Similar observation is made in table 9 and fig. 9 where the two fluids were stressed at 600 F (315.6C) as function of time. It is noted that as far as degradation is concerned, viscosity is better indicator than gas chromatographic analysis, however GC analysis has its usefulness in identifying the products. Table 10 and fig. 10 represent the thermal degradation data of the two fluids stressed for 6 hours as a function of temperature, and it is observed that these fulids are quite stable in the temperature range 315.6 C to 357.2 C, but above 357.2 C the rate of decomposition increases significantly.

The degradation data of the two fluids and their mixtures stressed at 700 F(371.1C) for 6 hours, given in table 11 and fig.11, indicate a linear relationship between the extent of degradation and the mixture concentration, and MLO 82-507 (silahydrocarbon) is more thermally stable than MLO 82-546(PAO). The data in table 12 and fig. 12 indicates the degradation data of the four components of MLO 82-507 derived from the degradation data of the mixed silahydrocarbon MLO 82-507. The four components labelled as A,B,C, and D have already been identified in fig. 1. From the plots in fig. 12, it appears that there may be a slight difference in the rate of degradation of the four components, indicating the order of thermal stability as A > B > C > D. In view of

the fact that this interpretation is based on the degradation data of a mixed silahydrocarbon where one of the components, D is less than 3% and there is significant uncertainity in the experimental data, so it would be necessary to investigate the single compounds to verify this small difference in stability. A similar observation was made in a previous effort (5), when it was determined that $CH_3\ Si(C_8H_{17})_3$ decomposed about 10% whereas $CH_3\ Si\ (C_{10}H_{21})_3$ decomposed about 20% when stressed at 700 F (371.1 C) for 6 hours.

VI. CONCLUSIONS

On the basis of the results presented in the previous section, it is concluded that the silahydrocarbon candidate advanced base fluid MLO 82-507 is more thermally stable than the polyalphaolefin base fluid MLO 82-546. Both the fluids do not show any appreciable decomposition below the temperature of 357.2 C. Mixing the two fluids does not provide any advantage as far as the thermal stability is concenrned. Viscosity is a better indicator of degradation than gas chromatographic analysis. In case of silahydrocarbons, it is felt that a smaller hydrocarbon chain (alkyl group) may improve the thermal stability as compared to a longer hydrocarbon chain (alkyl group).

VII. RECOMMENDATIONS

On the basis of this effort and the results accomplished, it is felt that future effort should involve the studies of pure samples of single compounds. A large number of pure compounds should be investigated to understand the structure versus thermal stability properties. Whenever pure and single compounds are available, internal standard should be used so that quantitative data is obtained.

Table 1: Method and Gas Chromatographic Conditions for the analysis of Gases.

```
METHOD: CAR6
CHANNEL  4

1. DATA INPUT

 RUNTM    #PKS
  40.00,   100

 MV/MIN    DELAY    MIN-AR    BUNCH
   .300,    0.00,     1000,     NO

 INTEGRATOR EVENTS
      TIME    EVENT
  1    /E

 CONTROL EVENTS
      TIME    EVENT   ECM   RLY
  1    /E

2. DATA ANALYSIS

 PROC    RPRT   SUP-UNK
 ZERO,    ME,     NO

 UNITS    TITLE
 AREA %

3. USER PROGRAMS

 POST-ANAL  DIALG-PRG  PARAM-FILE
 /N

4. REPORTS

      RDVC  #RPTS
  1    T2,    1
  2    /E

DONE
```

GAS CHROMATOGRAPHIC CONDITIONS

Model: Perkin - Elmer 900
Fused Silica Capillary Column
Length: 2 5 M
Diameter: 0.22 MM
Liquid Phase: Methyl Silicone Carbowax Deactivated
Split Ratio: 100 to 1
Auxi Gas: 40 ml/min   Carrier Gas: 1 ml/min
Chart Speed: 1 cm/min
Detector: FID
Attenuation: 10 x 16
Temperatures: Injector: 220°C; Detector: 250°C
Column Temperature: -50°C to 200°C   Program Rate: 8 deg/min
Initial Hold: 0 min   Final Hold: 20 min
Sample Size: 2 ml
Sample ID: Headspace
Date: 8/24/84

Table 2: Method and Gas Chromatographic conditions for the analysis of liquids.

```
METHOD: DVK
CHANNEL  2

1. DATA INPUT

 RUNTM    #PKS
  60.00,  200

 MV/MIN   DELAY   MIN-AR   BUNCH
   .300,   0.00,      10,   NO

 INTEGRATOR EVENTS
     TIME   EVENT
  1   /E

 CONTROL EVENTS
     TIME   EVENT  ECM  RLY
  1   80.00, CY
  2   /E

2. DATA ANALYSIS

 PROC  RPRT  SUP-UNK
 ZERO,  ME,   NO

 UNITS   TITLE
 AREA %

3. USER PROGRAMS

 POST-ANAL  DIALG-PRG  PARAM-FILE
 HPGC

4. REPORTS

     RDVC #RPTS
  1   T2,    1
  2   /E
```

```
           GAS CHROMATOGRAPHIC CONDITIONS
MODEL:HP5710A
FUSED SILICA CAPILLARY COLUMN
LENGTH:12 M
DIAMETER:0.22 MM
LIQUID PHASE:METHYL SILICONE CARBOWAX DEACTIVATED
SPLIT RATIO:100 TO 1
AUX. GAS:40 ML/MIN              CARRIER GAS:1 ML/MIN
CHART SPEED:20CM/HR
DETECTOR:FID
ATTENUATION:10 X 16
TEMPERATURES:
 INJECTOR:300 DEG.C
 DETECTOR:350 DEG.C
COLUMN TEMP:70-270 DEG.C        PROGRAM RATE:8 DEG/MIN
INITIAL HOLD:2 MIN              FINAL HOLD:32 MIN
SAMPLE SIZE:STOP1
SAMPLE ID:HYDFL
DATE:8/24/84
ANALYST:DVK
```

Fig. 1: Gas Chromatogram of MLO-82-507

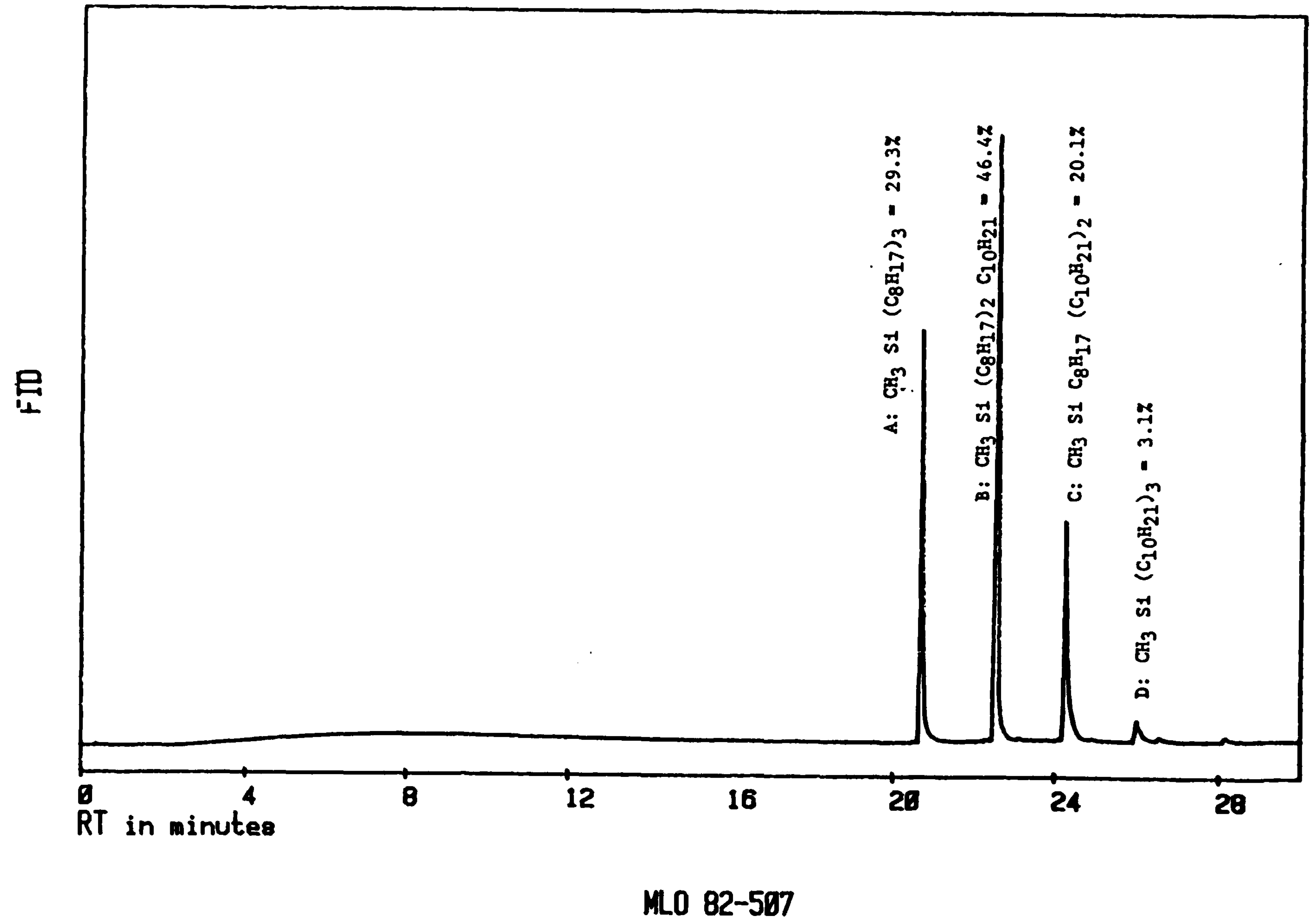

Fig. 2: Gas Chromatogram of MLO 82-546

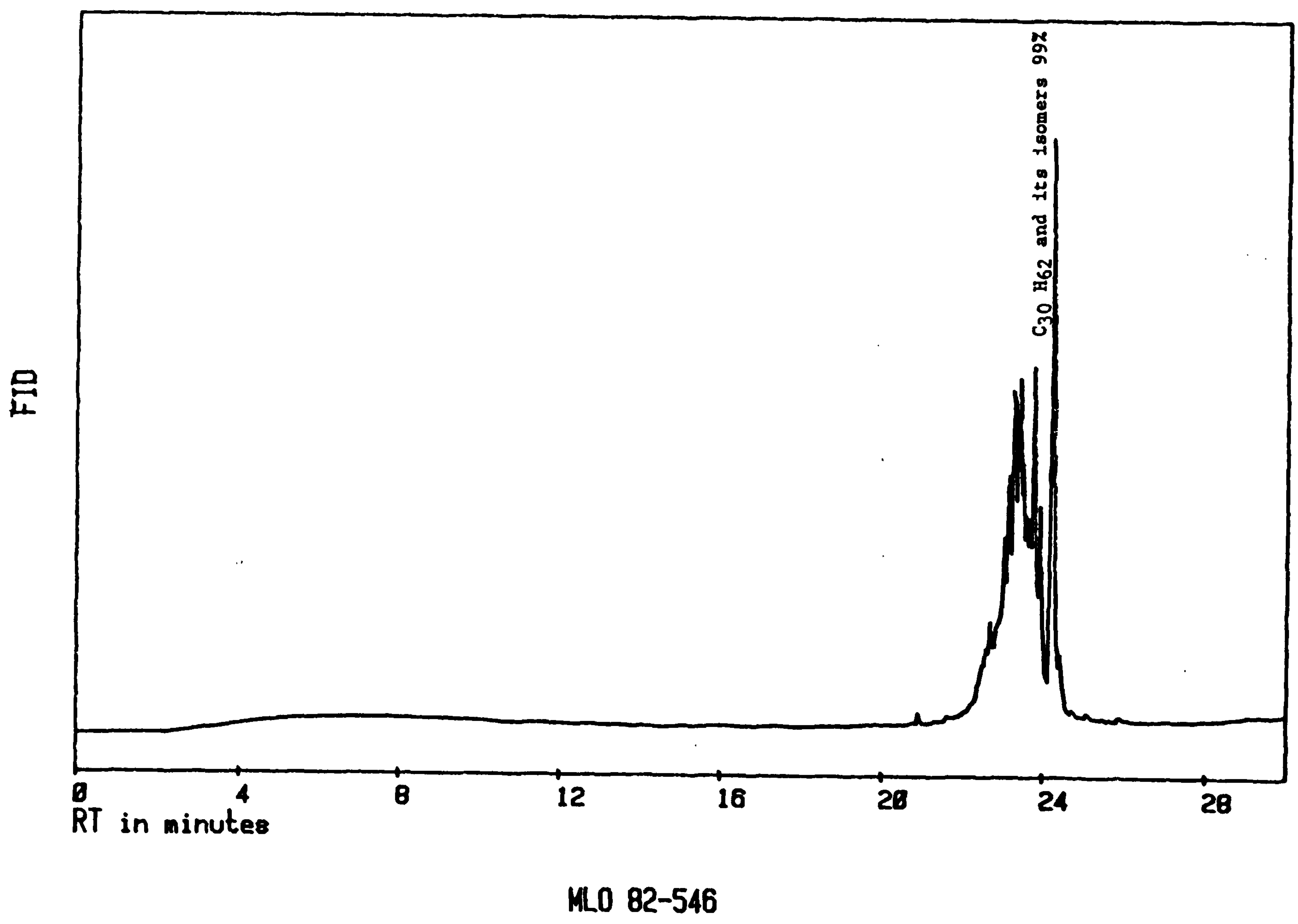

Table 3: Viscosities of the Hydraulic Fluids as a function of Temperature

Hydraulic Fluid	Viscosities (Cst) at Different Temperatures °C					
	98.9	37.8	25.0	-54	37.8*	E_{vis} (KJ/mole)
MLO 82-546	3.79	17.26	27.56	11048.45	4.3	23.79
MLO 82-507-25%+MLO82-546-75%	3.54	15.08	23.60	7349.25	5.8	22.70
MLO 82-507-50%+MLO82-546-50%	3.23	12.91	19.99	5095.71	6.3	21.74
MLO 82-507-75%+MLO82-546-25%	2.98	11.16	17.18	3130.34	6.9	20.71
MLO 82-507	2.75	9.87	14.78	2216.83	8.6	20.05

* Viscosity data after stressing the oil for 6 hours at 371.1°C.

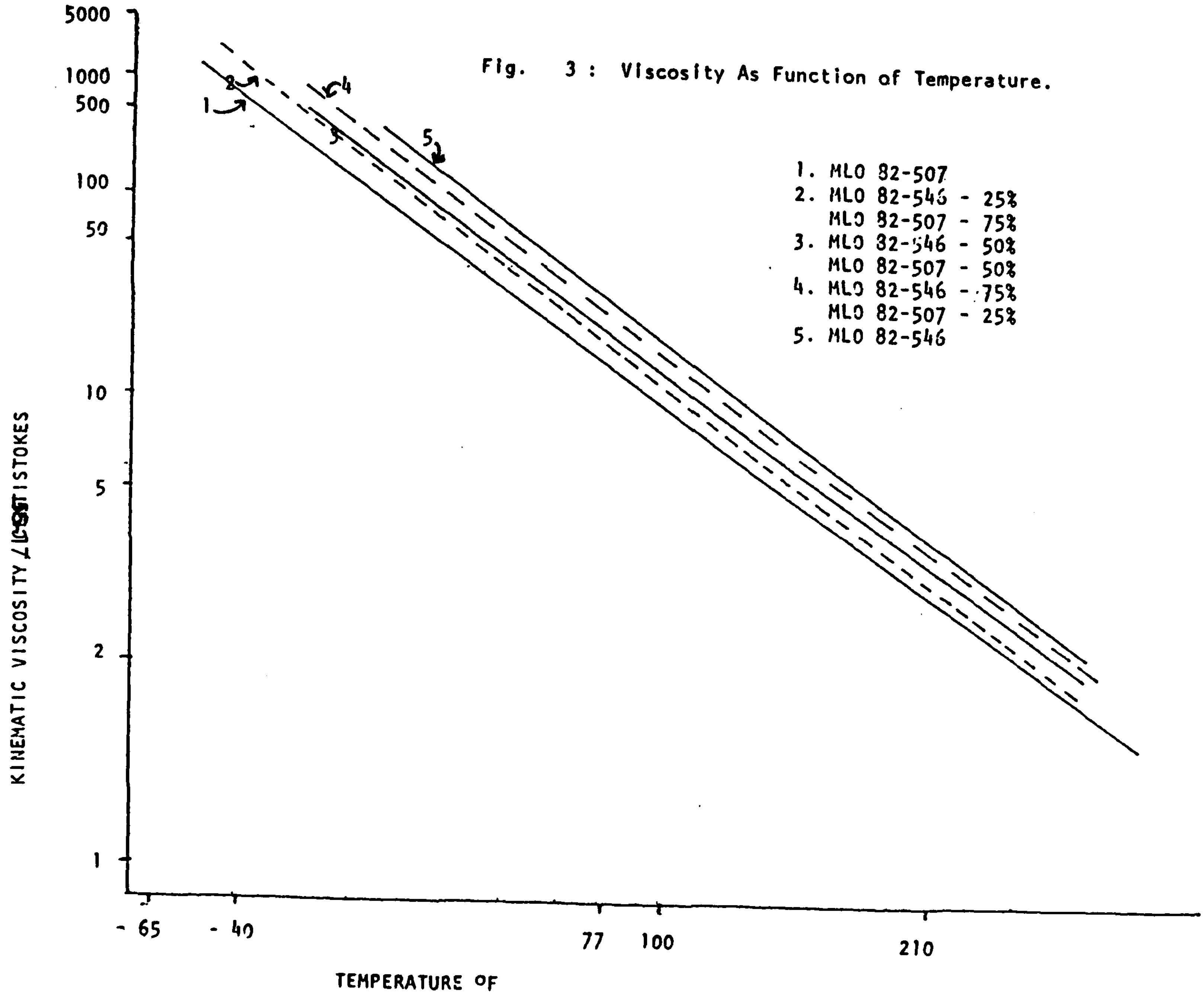

Fig. 3 : Viscosity As Function of Temperature.

Fig. 3A: VISCOSITY DATA

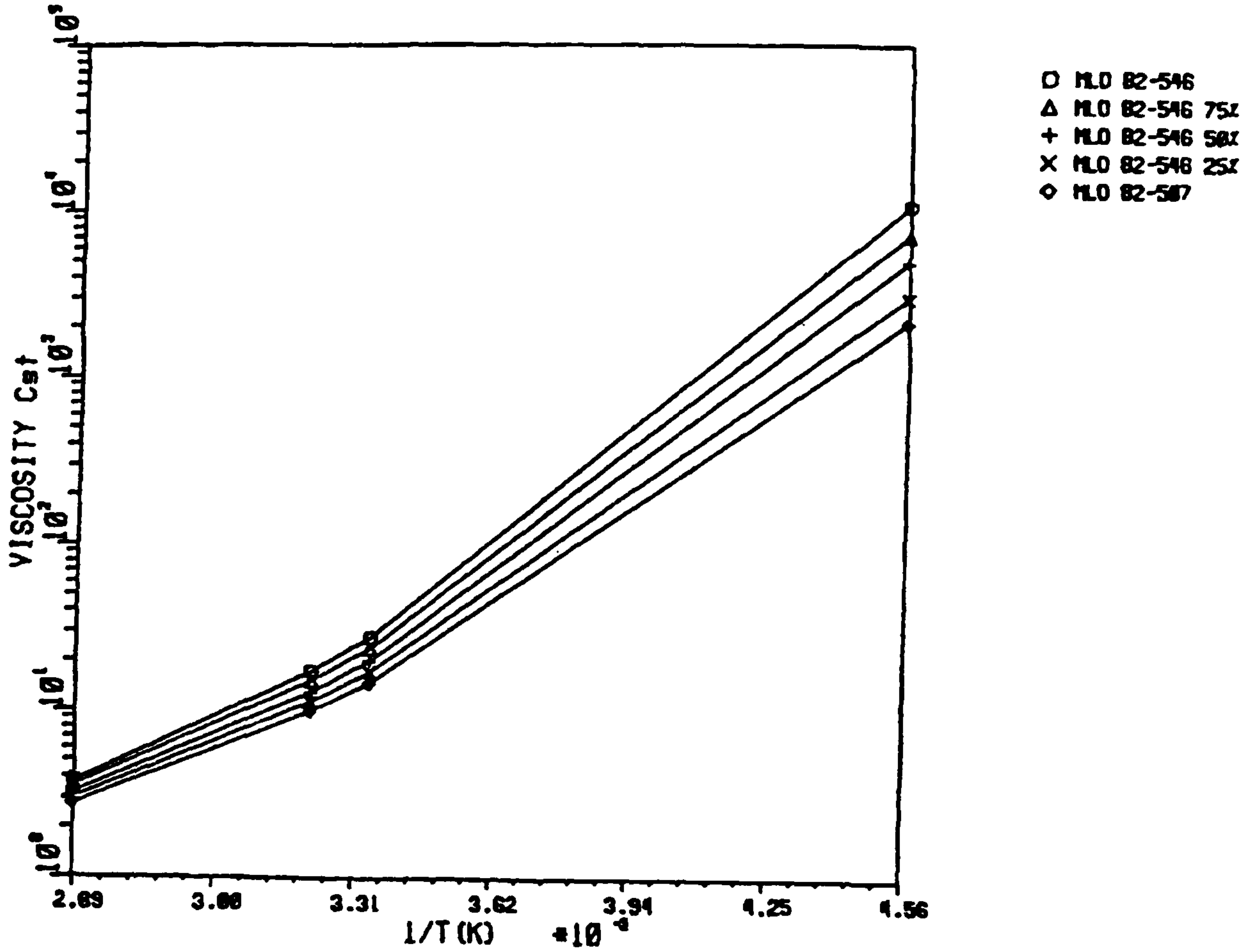

Table 4: GC/MS Analysis of the Gaseous Components of MLO 82-507 Stressed at 700 F (371.1 C) for 24 Hrs.

Scan No.	Components	% Concentration
35,36	CH_4, C_2H_4, and C_2H_6*	9;85
39	C_3H_6 and C_3H_8*	26.17
49,55	C_4H_8 and C_4H_{10}*	23.48
83	C_5H_{10}	0.90
90	C_5H_{12}	13.91
148	$(CH_3)_4$ Si**	0.48
186	C_6H_{12}	0.47
197	C_6H_{14}	12.27
300	C_7H_{16}	4.18
379	C_8H_{16} and C_8H_{18}*	2.01
450	C_9H_{18} and C_9H_{20}*	1.05
540	$C_{10}H_{20}$ and $C_{10}H_{22}$*	0.15

* These scans may be mixtures

** This has been estimated based on the past experience

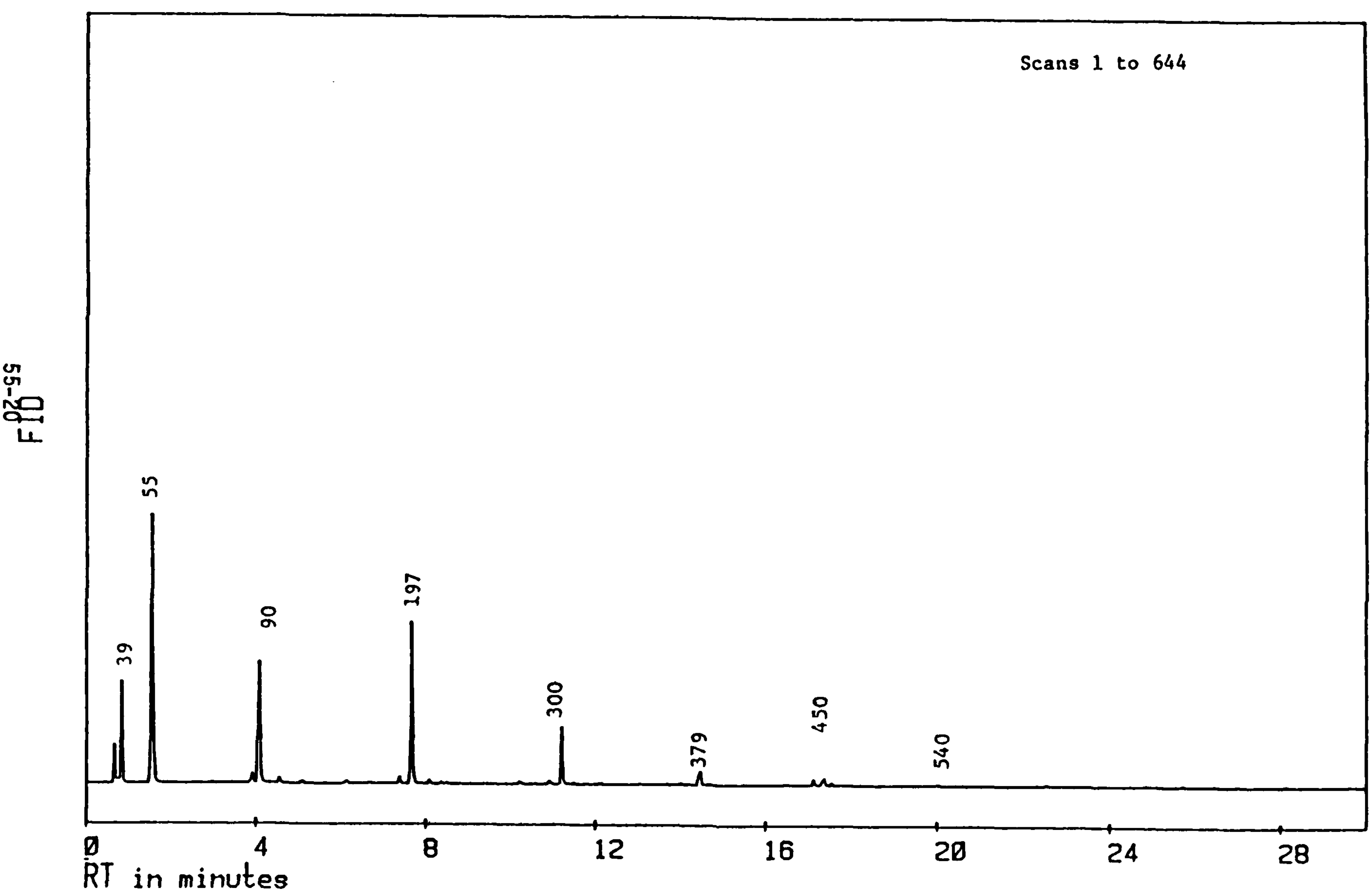

MLO 82 507 700F 24 HRS HEADSPACE

Table 5: GC/MS Analysis of the liquid components of MLO 82-507 Stressed at 700°F (371.1 C) for 24 Hrs. * Indicates may be.

Scan No.	Component	No. of C Atoms	% Concentration
49	C_5H_{10} and C_5H_{12}	5	6.60
53	C_6H_{12} and C_6H_{14}	6	5.95
55	C_7H_{14} and C_7H_{16}	7	6.95
57,59	C_8H_{16} and C_8H_{18}	8	11.65
359	$H\text{-}Si\text{-}CH_3(C_8H_{17})_2$*	17	0.26
371	$(CH_3)_2\text{-}Si\text{-}(C_8H_{17})_2$	18	4.35
404	$CH_3\text{-}Si\text{-}C_2H_5\ (C_8H_{17})_2$	19	3.31
424	$CH_3\text{-}Si\text{-}C_3H_7\ (C_8H_{17})_2$	20	2.48
433	$(CH_3)_2\text{-}Si\text{-}\ C_8H_{17}\ C_{10}H_{21}$	20	3.90
447	$CH_3\text{-}Si\text{-}(C_8H_{17})_2\ C_4H_9$	21	1.56
463	$CH_3\text{-}Si\text{-}C_2H_5\ C_8H_{17}\ C_{10}H_{21}$	21	2.74
473	$CH_3\text{-}Si\text{-}C_5H_{11}(C_8H_{17})_2$	22	1.33
481	$CH_3\text{-}Si\text{-}C_3H_7\ C_8H_{17}\ C_{10}H_{21}$	22	1.46
489	$(CH_3)_2\text{-}Si\text{-}(C_{10}H_{21})_2$	22	0.58
498	$CH_3\text{-}Si\text{-}C_6H_{13}\ (C_8H_{17})_2$*	23	1.14
502	$CH_3\text{-}Si\text{-}C_4H_9\ C_8H_{17}\ C_{10}H_{21}$	23	0.76
517	$CH_3\text{-}Si\text{-}C_2H_5(C_{10}H_{21})_2$*	23	0.25
523	$CH_3\text{-}Si\text{-}C_7H_{15}(C_8H_{17})_2$	24	1.32
525	$CH_3\text{-}Si\text{-}C_5H_{11}C_8H_{17}C_{10}H_{21}$	24	1.04
533	$CH_3\text{-}Si\text{-}C_3H_7\ (C_{10}H_{21})_2$	24	0.18
539,553	$CH_3\text{-}Si\text{-}(C_8H_{17})_3$	25	13.66
572	$CH_3\text{-}Si\text{-}C_7H_{15}C_8H_{17}C_{10}H_{21}$	26	2.03
587,602	$CH_3\text{-}Si\text{-}(C_8H_{17})_2C_{10}H_{21}$	27	17.46
618	$CH_3\text{-}Si\text{-}C_8H_{17}C_9H_{19}C_{10}H_{21}$	28	0.97
644	$CH_3\text{-}Si\text{-}C_8H_{17}(C_{10}H_{21})_2$	29	6.20
692	$CH_3\text{-}Si\text{-}(C_{10}H_{21})_3$5-21	31	1.08

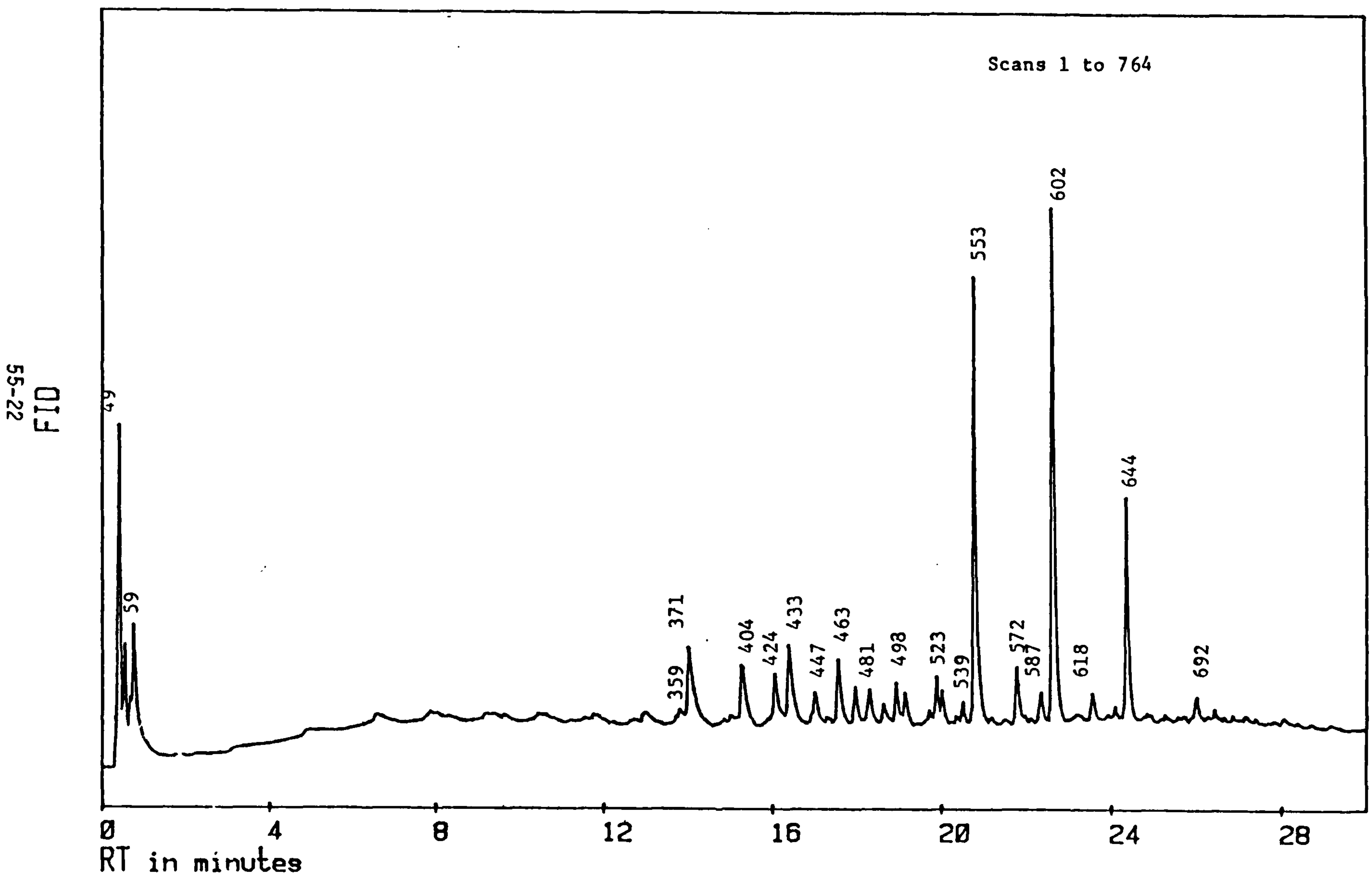

Fig. 5: MLO 82-507, 700F, 24 UPS

Table 6: GC/MS Analysis of the Gaseous Components of MLO 82-546 Stressed at 700F (371.1 C) for 6 Hrs.

Scan No.	Component	% Concentration
35	CH_4, C_2H_4, and C_2H_6*	13.06
38	C_3H_6 and C_3H_8*	31.06
47,49	C_4H_8 and C_4H_{10}*	24.94
82,89	C_5H_{10} and C_5H_{12}*	12.51
186,198	C_6H_{12} and C_6H_{14}*	6.92
301	C_7H_{16}	4.11
389	C_8H_{18}	2.46
467	C_9H_{20}	1.59
537	$C_{10}H_{22}$	0.80
601	$C_{11}H_{24}$	0.37
661	$C_{12}H_{26}$**	-
717	$C_{13}H_{28}$**	-
770	$C_{14}H_{30}$**	-
819	$C_{15}H_{32}$**	-

* These are mixtures.

** These are present only in trace amounts.

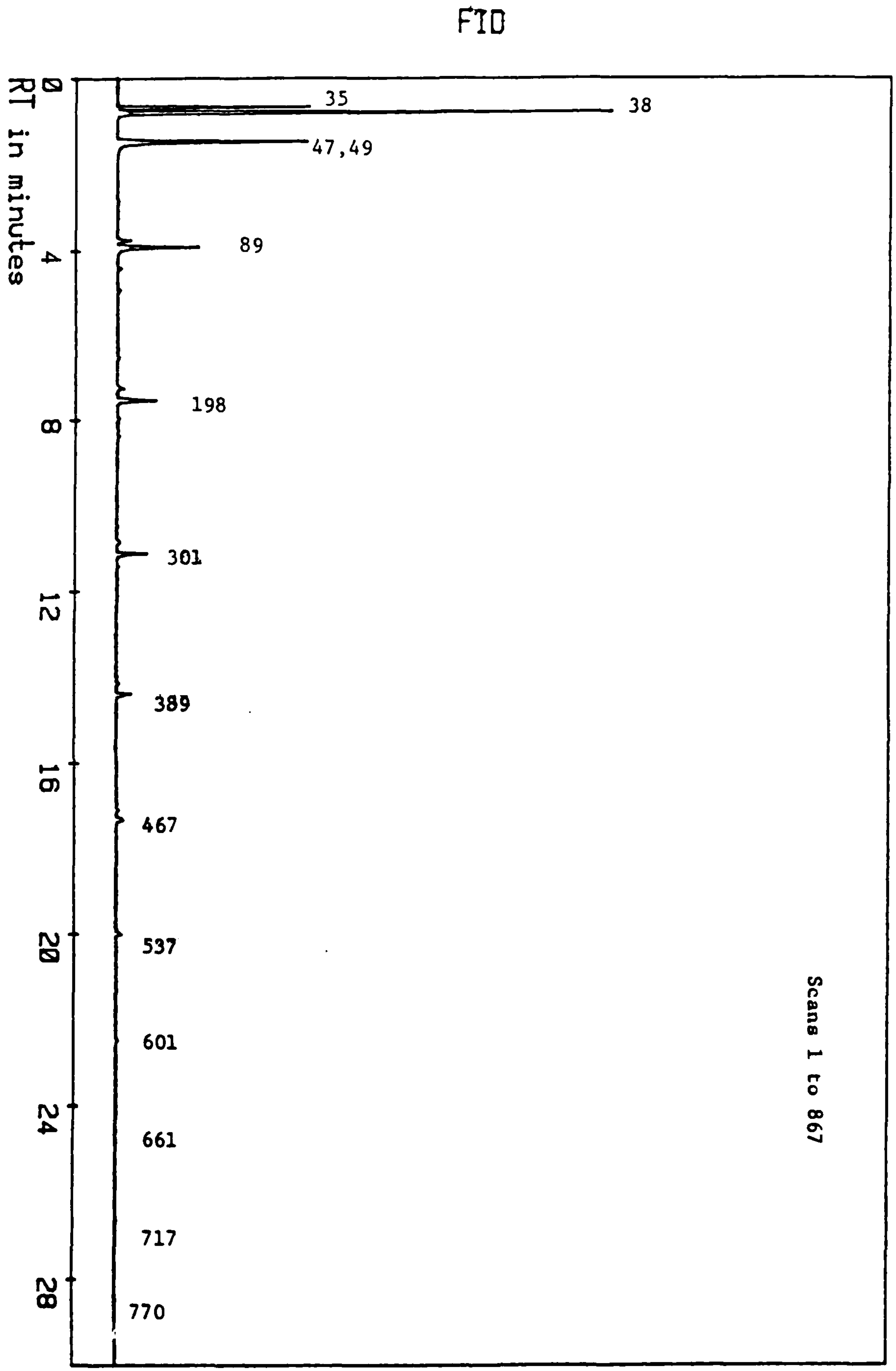

Fig. 6: MLO 82-546,700 F, 6 HRS,HEADSPACE

Table 7: GC/MS Analysis of Liquid Components of MLO 82-546 Stressed at 700F (371.1C) for 6 Hrs.

Scan No.	Component	% Concentration
49	C_5H_{12}	3.29
52	C_6H_{14}	2.97
55	C_7H_{16}	4.00
59	C_8H_{18}	5.28
71	C_9H_{20}	5.29
90	$C_{10}H_{22}$	1.08
117	$C_{11}H_{24}$*	-
150	$C_{12}H_{26}$*	-
187	$C_{13}H_{28}$*	-
225	$C_{14}H_{30}$*	-
263	$C_{15}H_{32}$*	-
300	$C_{16}H_{34}$*	-
335	$C_{17}H_{36}$	1.49
369	$C_{18}H_{38}$	1.61
402	$C_{19}H_{40}$	0.74
415	$C_{20}H_{42}$	0.37
427	$C_{21}H_{42}$	0.12
433	$C_{20}H_{42}$	0.45
445	$C_{21}H_{44}$	0.11
474	$C_{22}H_{46}$	0.16
617,627,and 640	$C_{30}H_{62}$ and its isomers	73.22

* These components are present only in trace amounts.

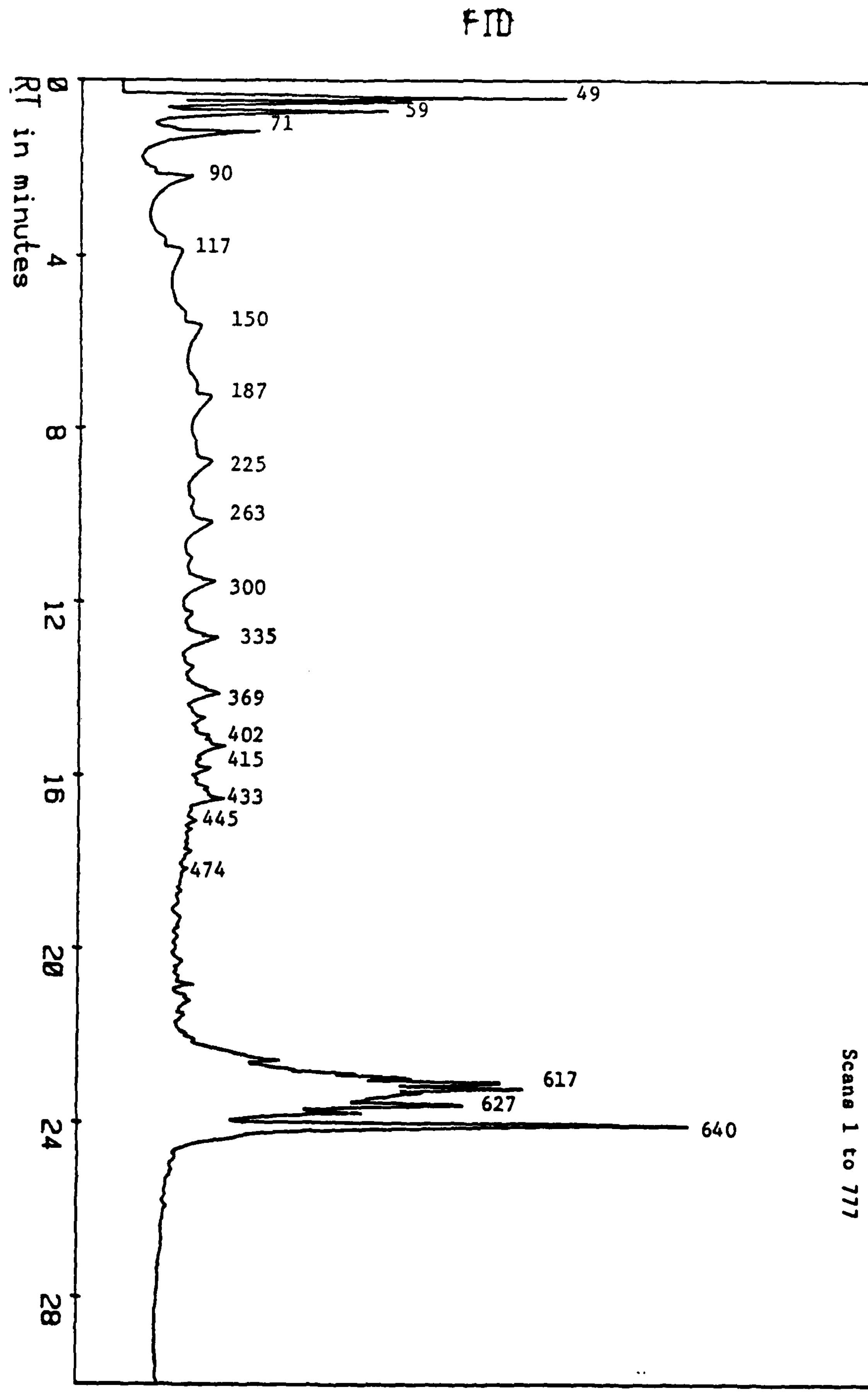

Fig. 7: MLO 82-546, 700F, 6 HRS

Table 8: Thermal Degradation Data for the Experimental Synthetic Base Stock Fluids at 700F (371.1C) as a function of time.

Time (Hrs)	MLO 82-507			MLO 82-546		
	% Conc.(*)	Visc.(cSt)(*)	% Visc**	% Conc.(*)	Visc.(cSt) (*)	% Visc.**
0(unstressed)	99.7 (0.35)	9.9 (0.00)	100.0	99.2	17.4	100.0
6	78.9 (4.27)	8.6 (0.71)	86.9	62.2(6.62)	4.4 (0.21)	25.3
16	82.6 (0.14)	9.2 (0.14)	92.9	61.3	5.9	33.9
24	37.6 (1.77)	5.8 (0.67)	58.6	53.2(7.98)	5.0 (0.49)	28.4
48	10.3 (2.68)	3.3 (0.57)	33.3	2.4(2.49)	1.7 (0.00)	9.8
72	4.4 (1.34)	2.8 (0.00)	28.2	-***	-***	

* These values indicate standard deviation.

** These values indicate % viscosity retained.

*** All of the test fluid was lost during the degradation process at 72 hours.

Fig. 8

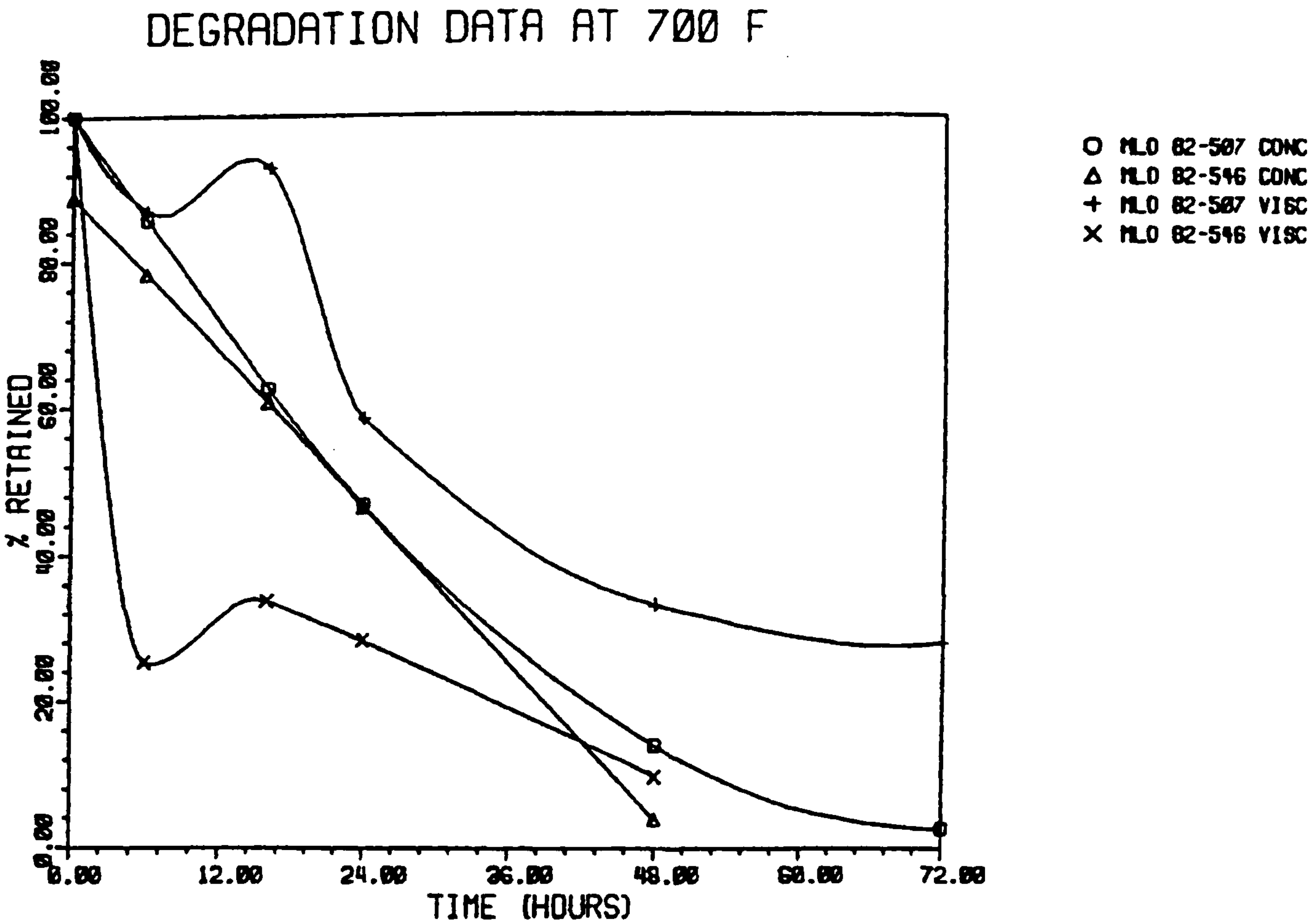
DEGRADATION DATA AT 700 F
% RETAINED
0.00
20.00
40.00
60.00
80.00
100.00
0.00
12.00
24.00
36.00
48.00
60.00
72.00
TIME (HOURS)
O MLO 82-507 CONC
Δ MLO 82-546 CONC
+ MLO 82-507 VISC
X MLO 82-546 VISC

Table 9: Thermal Degradation Data for the Experimental Synthetic Base Stock Fluids at 600F (315.6C) as a function of time.

Time (Hrs)	MLO 82-507			MLO 82-546		
	% Conc.(*)	Visc.(cSt)(*)	% Visc.**	% Conc.(*)	Visc.(cSt)(*)	% Visc.**
0(unstressed)	99.7 (0.35)	9.9 (0.00)	100.0	99.2	17.4	100.0
6	98.2	9.8	99.0	99.8	16.5	94.8
16	98.8 (0.14)	9.7 (0.00)	98.0	98.7 (0.64)	15.5 (0.71)	89.1
24	96.6 (0.07)	9.9 (0.35)	100.0	98.2 (0.07)	15.8	90.8
48	97.6	9.8	99.0	99.0	14.2 (0.71)	81.6
72	97.9	9.7 (0.21)	98.5	98.6 (0.78)	14.6 (0.21)	84.2

* These values indicate standard deviation.

** These values indicate % Viscosity retained.

Fig. 9

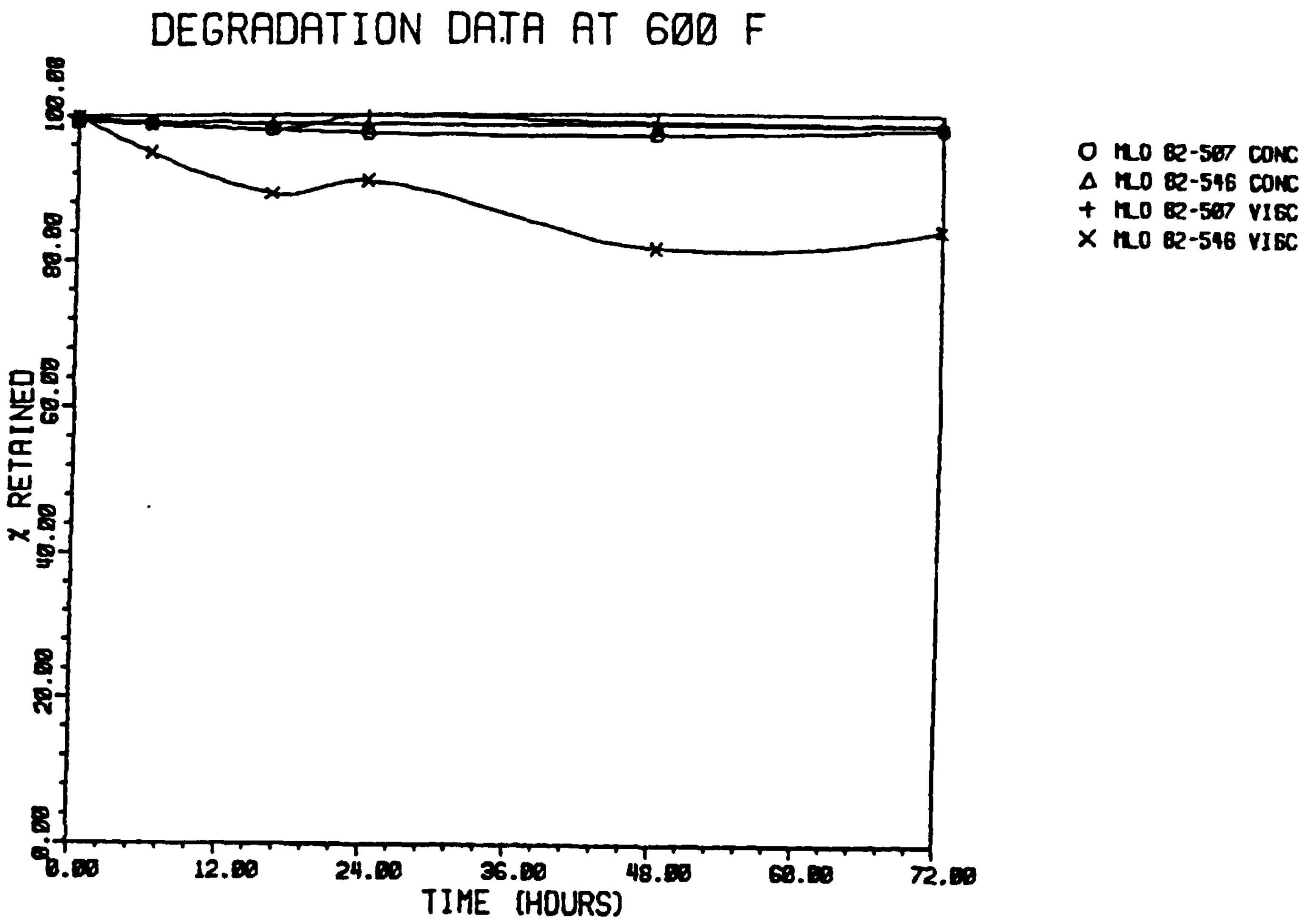
DEGRADATION DATA AT 600 F
% RETAINED
100.00
80.00
60.00
40.00
20.00
0.00
0.00
12.00
24.00
36.00
48.00
60.00
72.00
TIME (HOURS)
O MLO 82-507 CONC
Δ MLO 82-546 CONC
+ MLO 82-507 VISC
X MLO 82-546 VISC

Table 10: Thermal Degradation Data for the Experimental Synthetig Base Stock Fluids Stressed for 6 Hours as function of Temperature.

Temperature °F (°C)	MLO 82-507			MLO 82-546		
	% Conc.(*)	Visc (cSt) (*)	% Visc.**	% Conc. (*)	Visc. (cSt) (*)	% Visc.**
Unstressed	99.7 (0.35)	9.9 (0.00)	100.0	99.2	17.4	100.0
600 (315.6)	98.2	9.8	99.0	99.8	16.5	94.8
625 (329.4)	99.5 (0.14)	9.5 (0.21)	96.0	99.6 (0.21)	13.6 (0.85)	78.2
650 (343.3)	94.3 (0.00)	9.4 (0.07)	94.9	97.2 (1.98)	10.9 (0.07)	62.6
675 (357.2)	97.6 (1.98)	9.0 (0.07)	90.9	96.0 (3.18)	8.3 (0.42)	47.7
700 (371.1)	78.9 (4.27)	8.7 (0.64)	87.8	62.2 (6.62)	4.4 (0.21)	25.3

* These values indicate standard deviation.

** These values indicate % viscosity retained.

Fig. 10

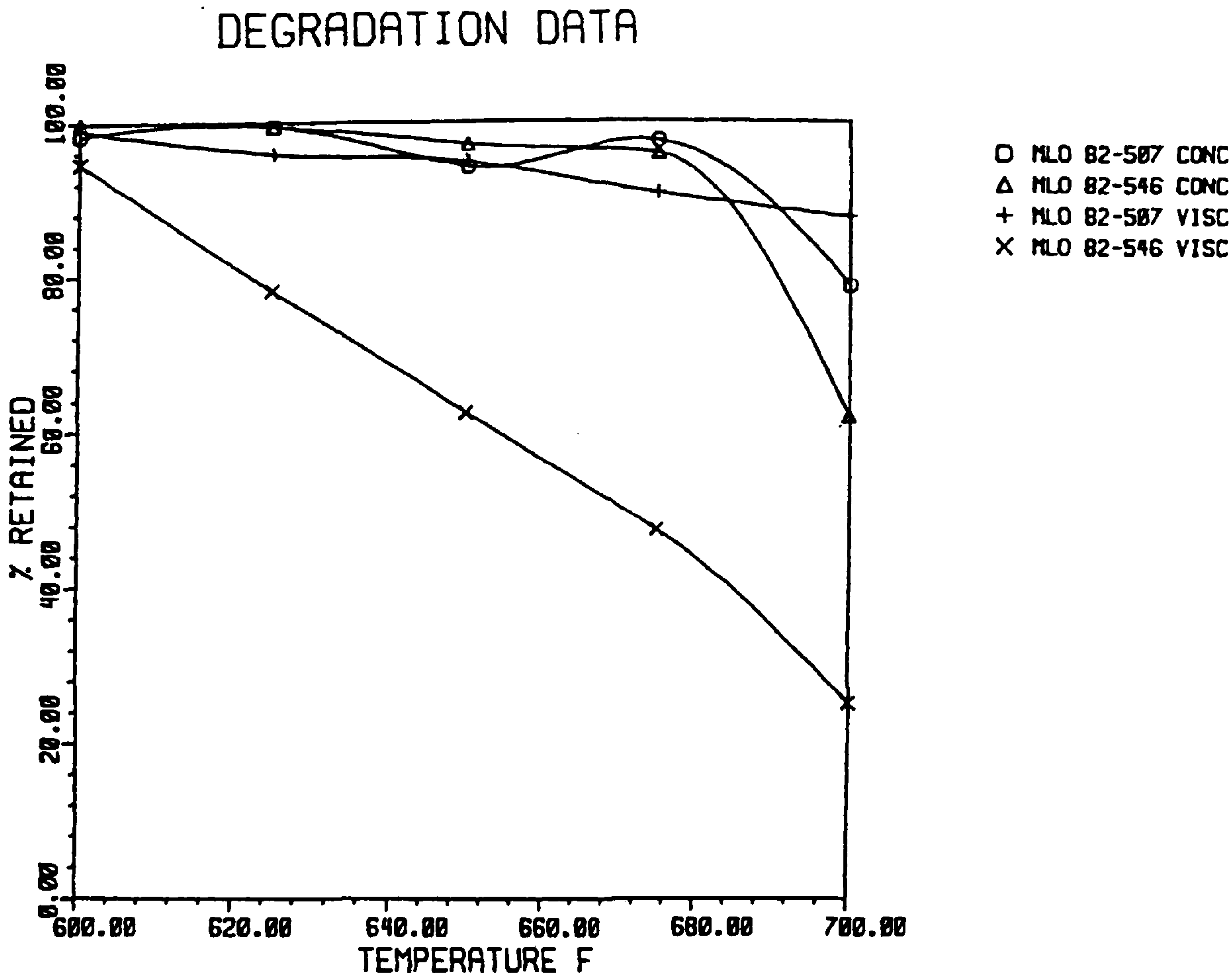
DEGRADATION DATA
100.00
80.00
60.00
40.00
20.00
0.00
% RETAINED
600.00
620.00
640.00
660.00
680.00
700.00
TEMPERATURE F
O MLO 82-507 CONC
Δ MLO 82-546 CONC
+ MLO 82-507 VISC
X MLO 82-546 VISC

Table 11: Thermal Degradation Data of MLO 82-507 and 82-546 and the Mixtures Stressed at 700 F (371.1 C) for 6 Hours.

% 82-507	% 82-546	% Conc. (*)	Visc. (cSt) (*)	Visc. (cSt)**	% Visc. Retained
0	100	62.2 (6.62)	4.4 (0.21)	17.40	25.6
25	75	64.0 (7.54)	5.8 (0.17)	15.08	38.7
50	50	75.3 (3.86)	6.2 (0.25)	12.91	48.0
75	25	84.3 (3.91)	7.2 (0.52)	11.16	64.5
100	0	78.9 (4.27)	8.7 (0.64)	9.90	87.4

* These values indicate standard deviation.

** These are the viscosities of the unstressed fluids at 100 F (37.8 C).

Fig. 11

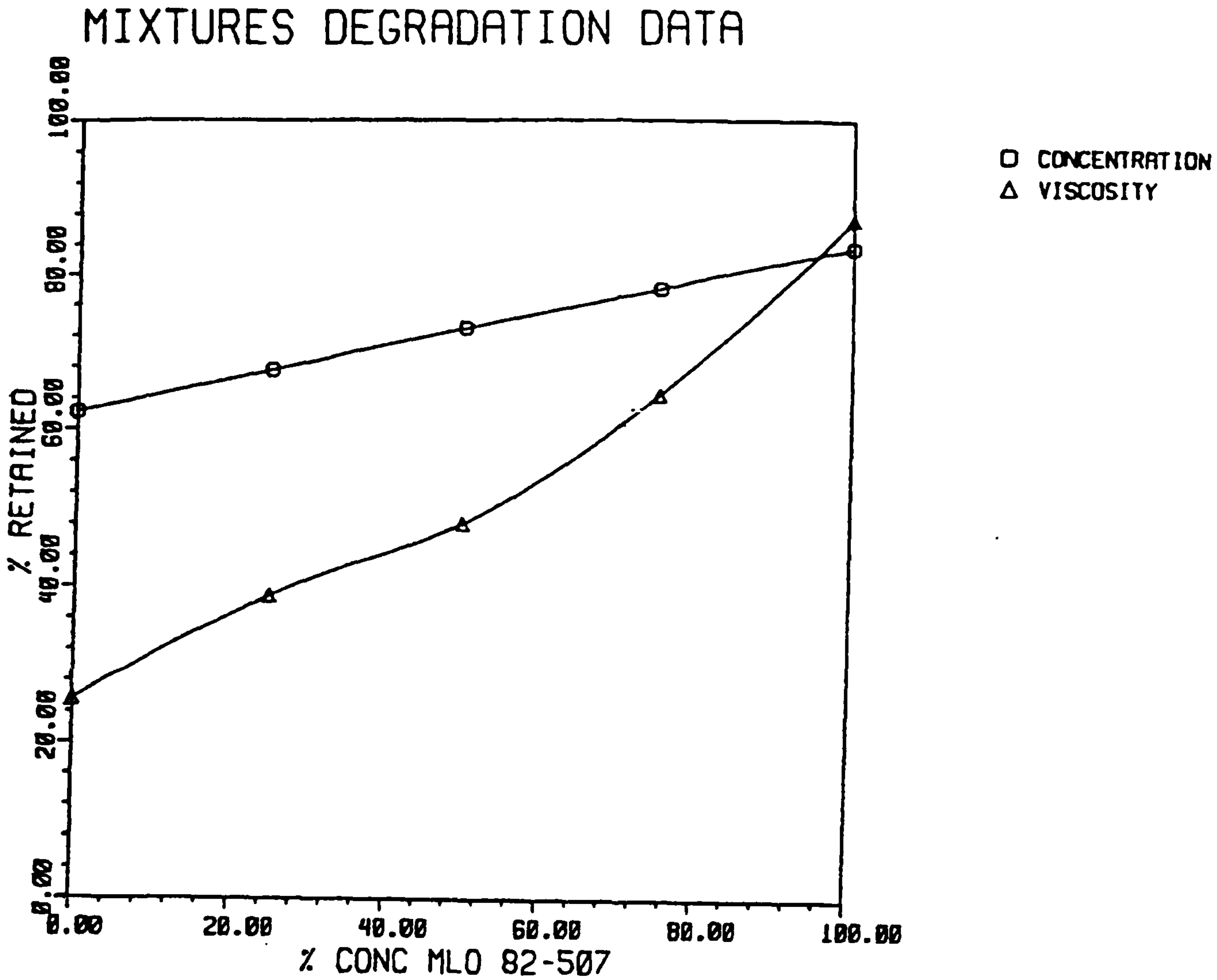

MIXTURES DEGRADATION DATA
% RETAINED
% CONC MLO 82-507
0.00
20.00
40.00
60.00
80.00
100.00
CONCENTRATION
VISCOSITY

Table 12: Thermal Degradation Data for the four components of MLO 82-507 Stressed at 700 F (371.1 C) for 6 Hours.

Time (Hrs)	Components % Conc.							
	A (*)	% A**	B (*)	% B**	C (*)	% C**	D (*)	% D**
0	28.4 (0.68)	100.0	45.6(0.70)	100.0	20.1(0.30)	100.0	2.7(0.28)	100.0
6	23.3 (1.96)	82.0	36.6(2.09)	80.2	16.6(0.35)	82.6	2.5(0.03)	92.6
16	24.1 (0.02)	84.8	38.2(0.01)	83.8	17.5(0.09)	87.0	2.7(0.02)	100.0
24	13.6 (0.66)	47.9	17.2(0.99)	37.6	6.7(0.63)	33.3	0.9(0.09)	33.3
48	3.2	11.3	3.5	7.6	1.3	6.5	0.1	3.7
72	1.7 (0.58)	6.0	2.1(0.81)	4.6	0.6(0.24)	3.0	0.0	0.0

* These values indicate standard deviation.

** These values are % concentration normalised on the scale of 0 to 100.

Fig. 12

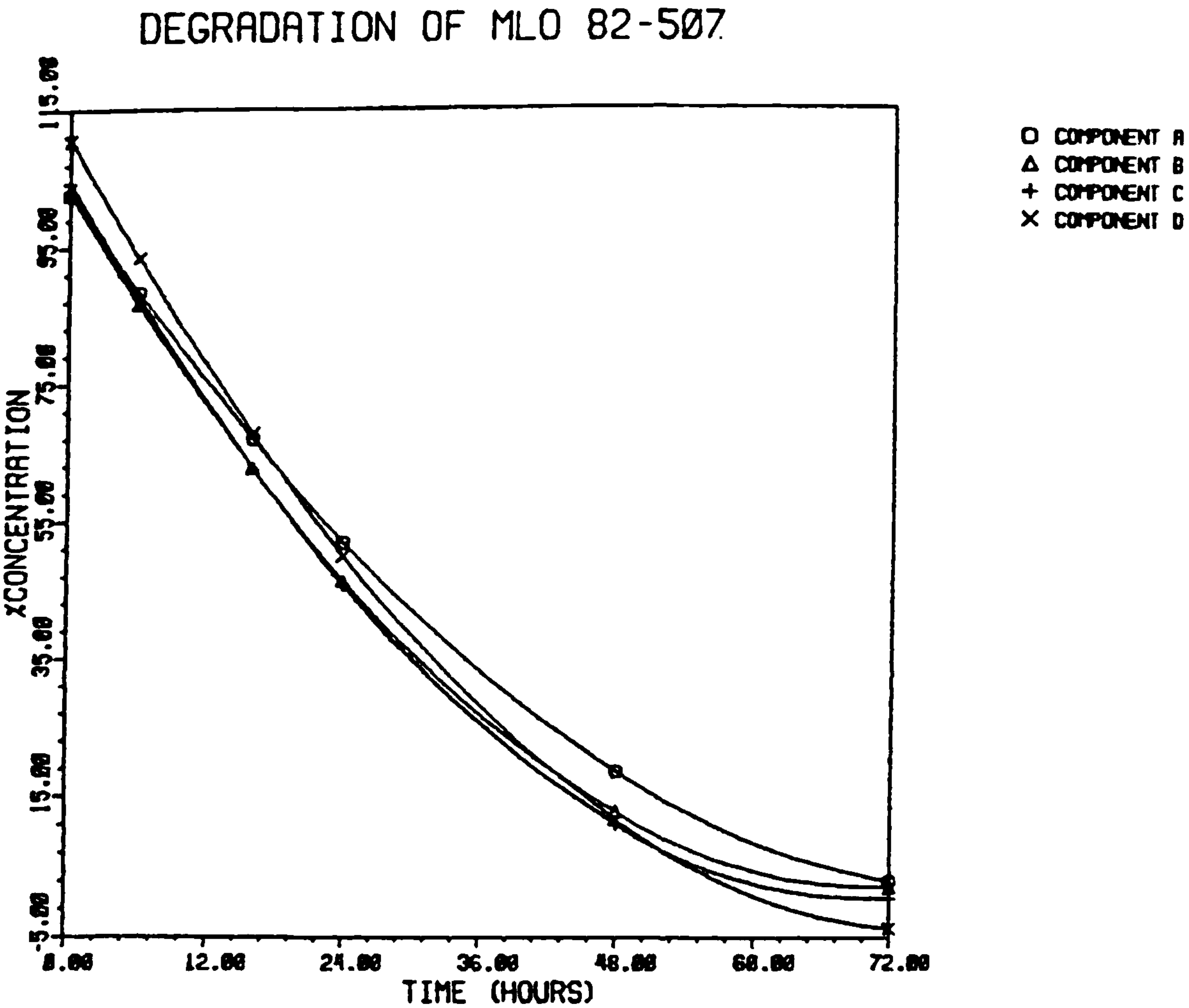

DEGRADATION OF MLO 82-507
%CONCENTRATION
TIME (HOURS)
115.00
95.00
75.00
55.00
35.00
15.00
-5.00
0.00
12.00
24.00
36.00
48.00
60.00
72.00
O COMPONENT A
Δ COMPONENT B
+ COMPONENT C
X COMPONENT D

Fig. 13: I.R. Spectra of MLO 82-507 Stressed at 700 F (371.1 C) for 24Hours using 0.025 mm. KBr cell.

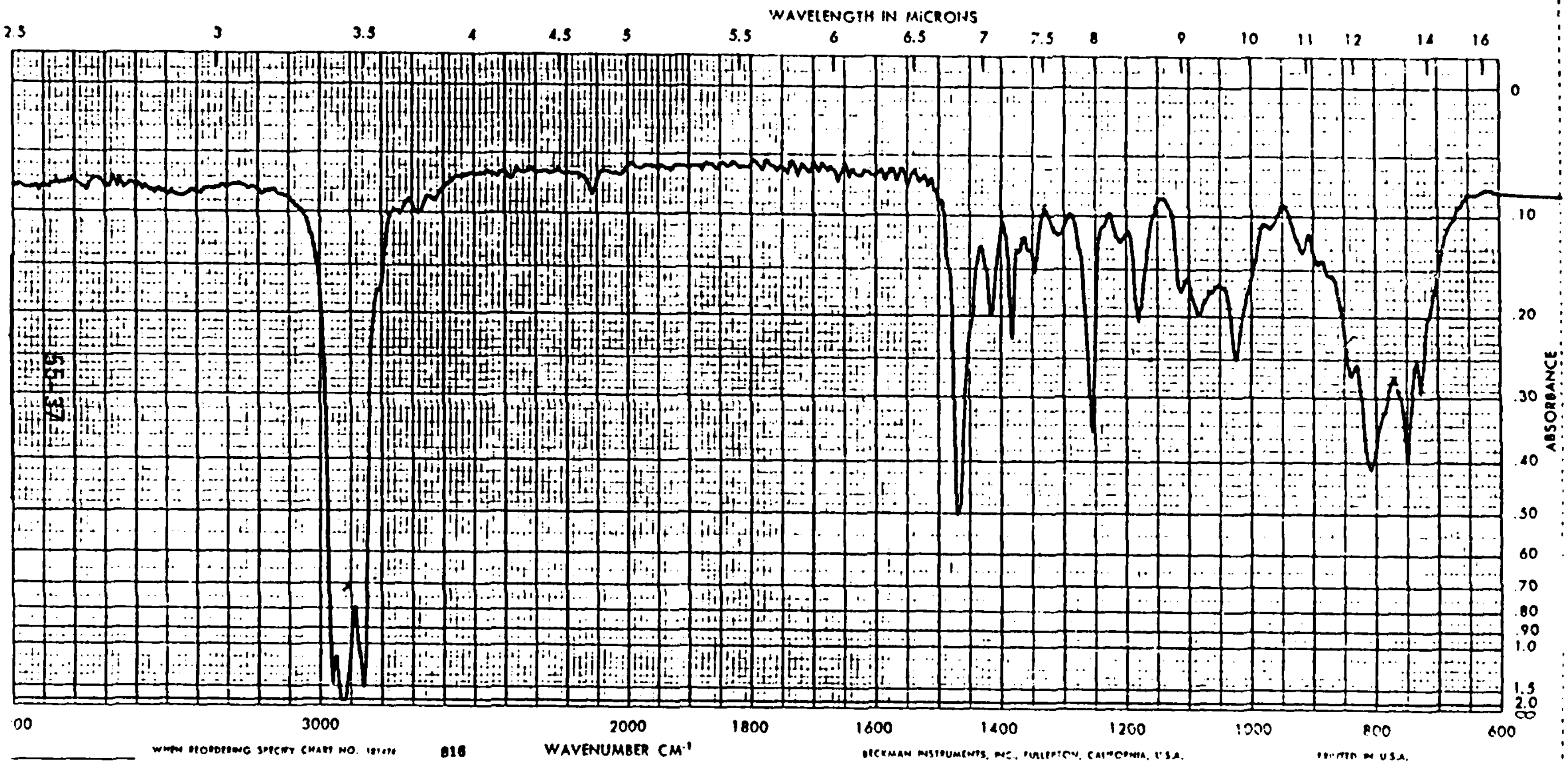

Fig. 14: I.R. Spectra of MLO 82-507 Stressed at 700 F (371.1 C) for 24Hours using 0.5 mm KBr cell.

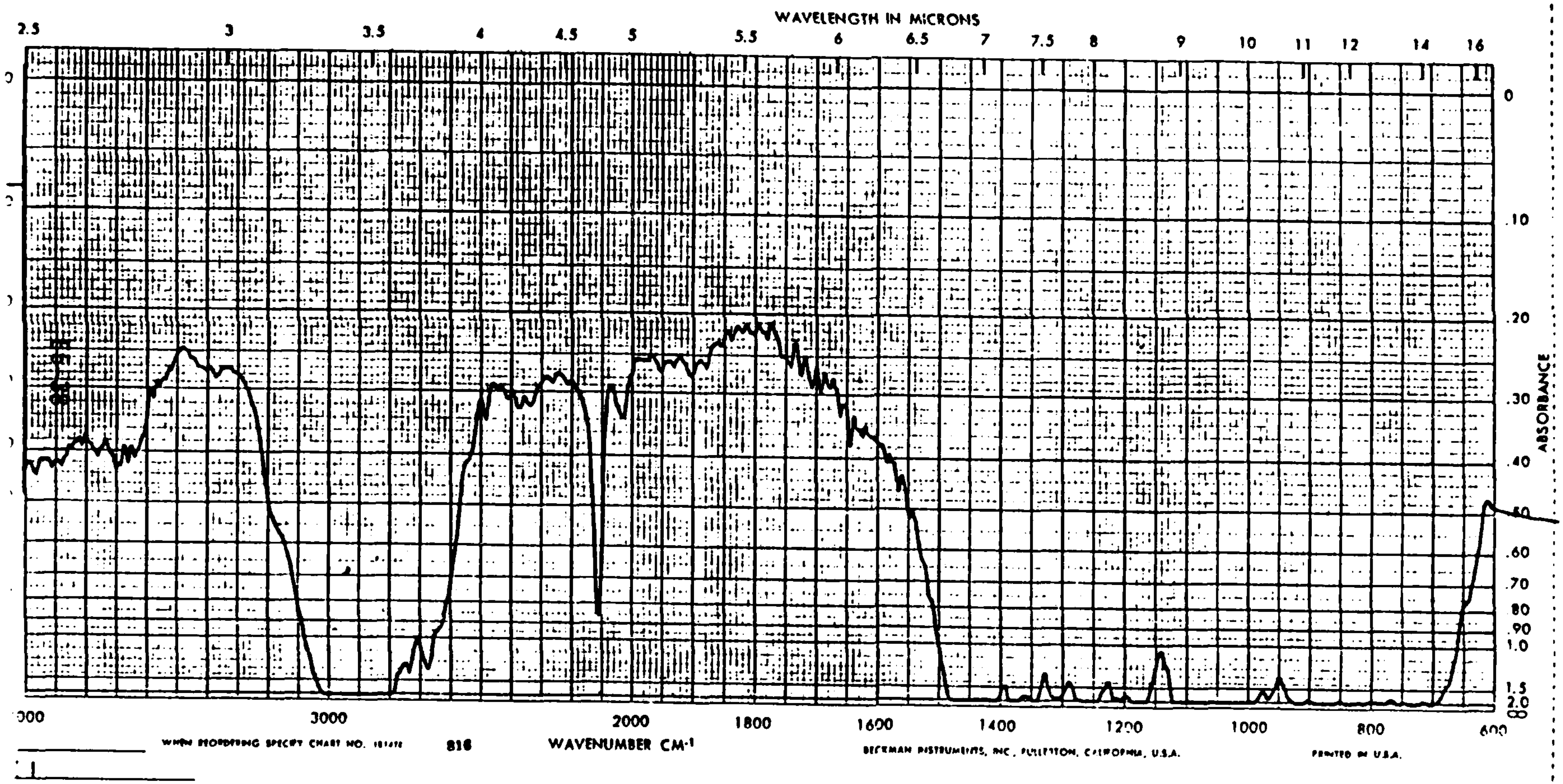

Fig. 16: I.R. Spectra of MLO 82-546 Stressed at 700 F (371.1 C) for 6 Hours using 0.5 mm KBr cell.

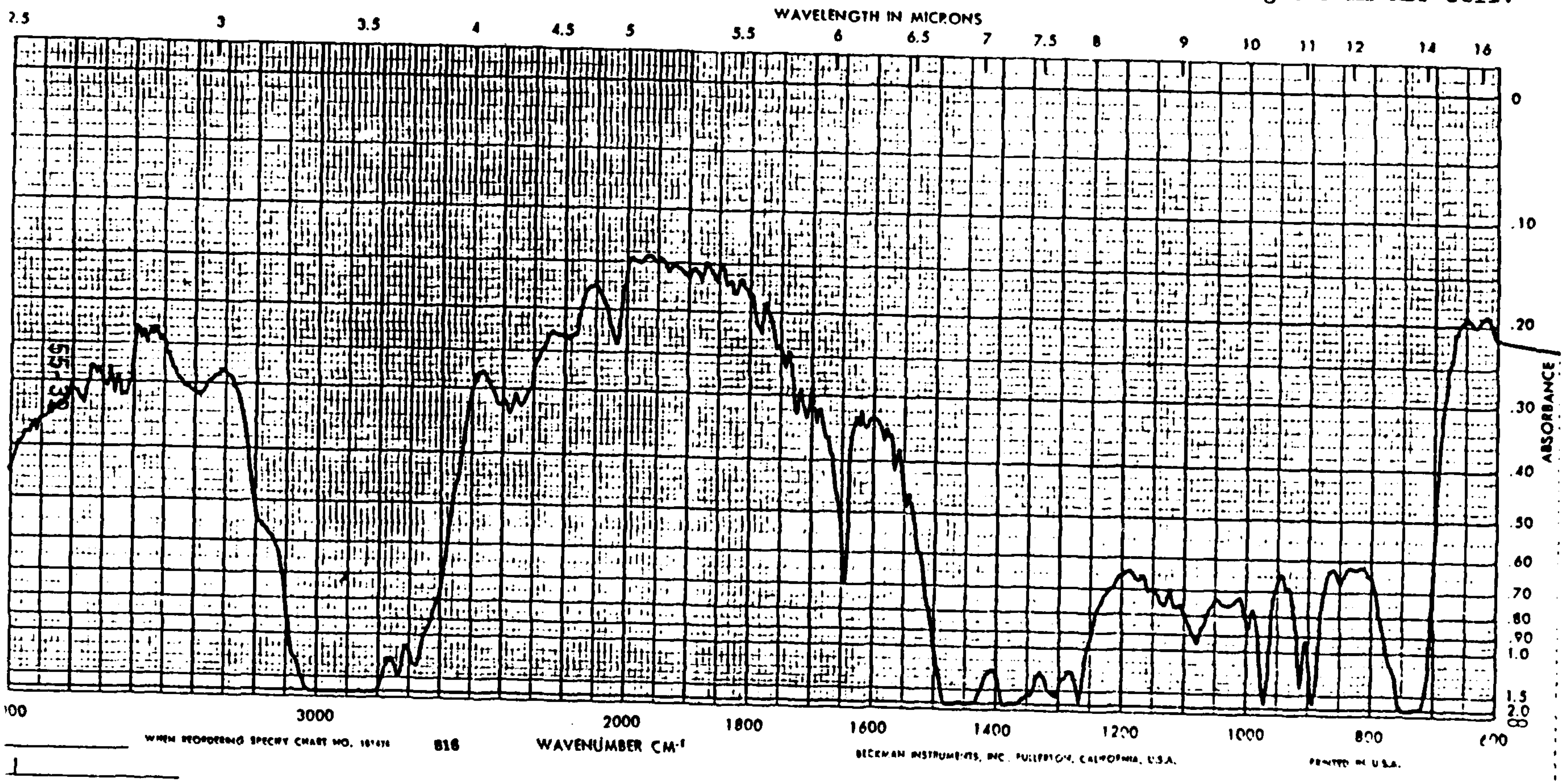

Fig. 15: I.R. Spectra of MLO 82-546 Stressed at 700 F (371.1 C) for 6 Hours using 0.025 mm KBr cell.

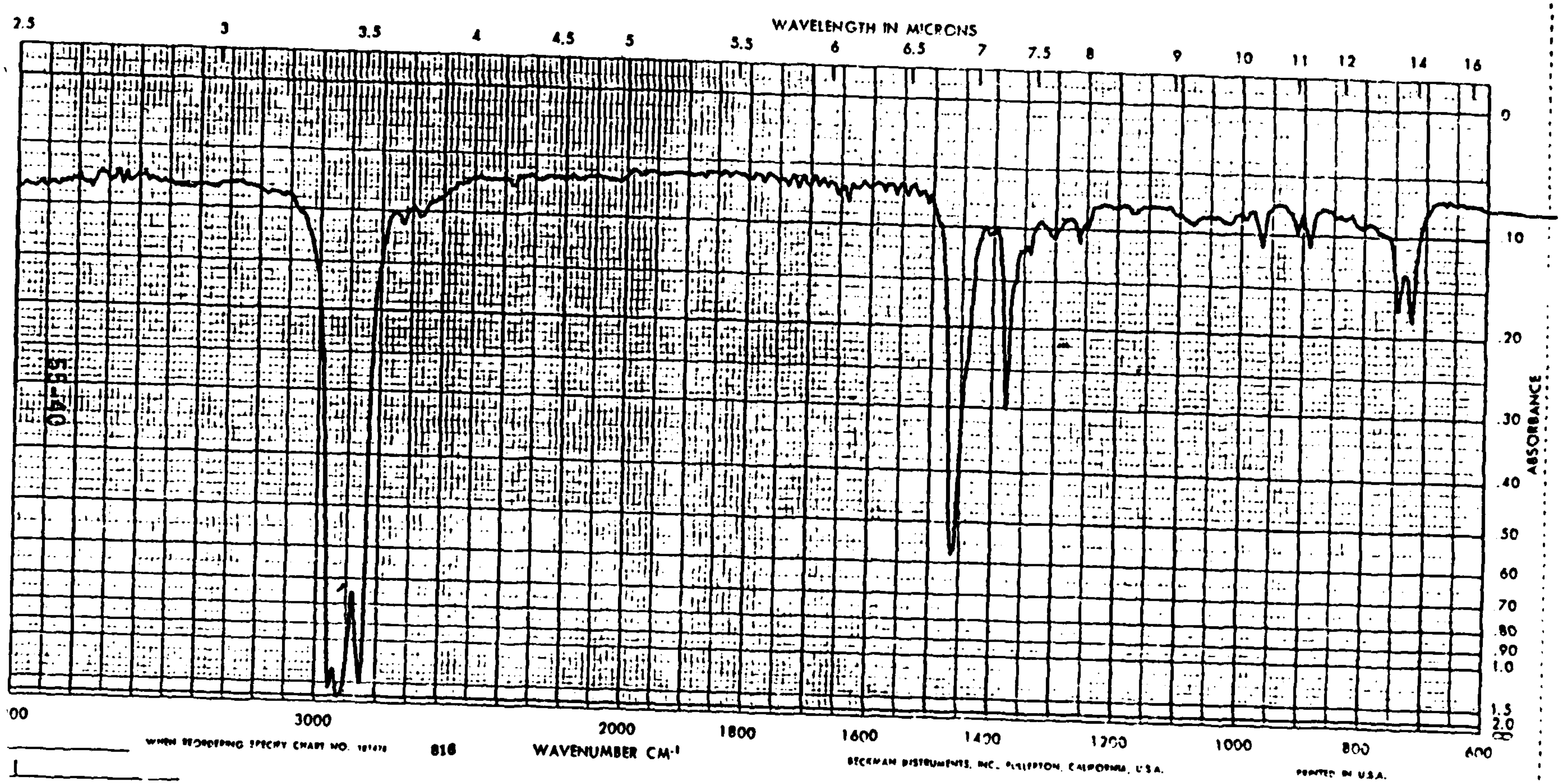

References

1. Snyder, C.E. Jr., Gschwender, L.J., and Tamborski, C., "Synthesis and Characterization of Silahydrocarbons - A Class of Thermally Stable Wide -liquid Range Functional Fluids", ASLE Trans. 25, 299-308 (1981).

2. Snyder, C.E. Jr., Tamborski, C., Gschwender, L.J., and Chen, G.J., "Development of High Temperature (-40 C to 288 C) Hydraulic Fluids for Advanced Aerospace Applications", ASLE Preprint No. 80-LC-IC-1.

3. Snyder, C.E. Jr., and Gschwender, L.J., "Development of Non-flammable Hydraulic Fluids for Aerospace Applications over a -54 C to 315 C Temperature range", Lubr. Engr. 36, 458 (1980).

4. Tamborski, C., Chen,G.J., Anderson, D.R., and Snyder, C.E. Jr., "Synthesis and Properties of Silahydrocarbons, a Class of Thermally Stable Wide-range Fluids", I & EC Product Research & Development, The American Chemical Society, 22, 172 (1983).

5. Gupta, V.K., and Weatherby, D.W., "Thermal Stability Characteristics of Silahydrocarbons", USAF-SCEEE Summer Faculty Research Program 1984, Technical Reports vol. II, # 56-1 to 56-38, (1984).

1985 USAF-UES SUMMER FACULTY RESEARCH PROGRAM

Sponsored by the

AIR FORCE OFFICE OF SCIENTIFIC RESEARCH

Conducted by the

UNIVERSAL ENERGY SYSTEMS, INC.

FINAL REPORT

USE OF TEXTURE MEASURES IN MULTISPECTRAL SCANNER DATA NUMERICAL CLASSIFICATIONS

Prepared by: Barry N. Haack

Academic Rank: Associate Professor

Department and University: Department of Public Affairs
George Mason University
Fairfax, Virginia 22030

Research Location: Rome Air Development Center
Intelligence and Reconnaissance
Image Exploitation Section
Griffiss Air Force Base
New York 13441

USAF Research Associate: Peter J. Costianes

Date: August 16, 1985

Contract No: F49620-85-C-0013

USE OF TEXTURE MEASURES IN MULTISPECTRAL SCANNER DATA NUMERICAL CLASSIFICATIONS

by

BARRY N. HAACK

ABSTRACT

Land cover information is important for many Air Force activities. One method of obtaining that information is by remote sensing, frequently using digital classification techniques. This study evaluated the use of digital texture measures with seven bands of multispectral scanner data (Thematic Mapper Simulator-TMS) for the identification of forest and nonforest land covers.

The TMS data variance by bands for representative training sites for land covers of interest were examined to select the best band for texture analysis. Variations of nine texture measures were applied to this band and the better texture measures identified. These measures were applied to the other TMS bands.

Combinations of two to seven of the best texture measures and individual spectral band data were compared for the separation of forest and nonforest areas. For combinations of three or more measurement extractors, texture was shown to be useful.

This study demonstrated the utility of texture measures in digital classification of land cover. This is particularly important because texture measures are more capable of signature extension than spectral information. Necessary continuations of this study include the examination of data for other land covers and geographic locations and the use of different spatial resolution data, such as are available from Landsat.

ACKNOWLEDGEMENTS

This work was possible under the Air Force Systems Command, Air Force Office of Scientific Research Summer Faculty Research Program. The author greatly appreciated the opportunity to participate in this excellent program. The extensive cooperation, guidance and scientific acumen of my focal point, Peter J. Costianes, of the Rome Air Development Center at Griffiss Air Force Base is gratefully acknowledged. The author also appreciated the many helpful persons at RADC and in particular the Chief of the Image Systems Branch, Vincent Nardozza, and the Chief of the Image Exploitation Section, Larry O"Dell, both of whom supported my participation in this program.

I. INTRODUCTION:

Information on conditions at the earth's surface are of interest to many individuals and organizations. Those conditions may be dynamic or static and may include such features as population density, land use or cover, topography, transportation networks or soil conditions. Many activities of the United States Air Force require current, reliable information on these and other earth surface conditions for navigation, reconnaissance and intelligence.

One tool of increasing importance in obtaining earth surface information is remote sensing. Remote sensing is frequently defined as the acquisition of information without direct contact. This tool utilizes energy within the electromagnetic spectrum. Remote sensing has recently been expanded greatly by the use of new platforms to acquire information such as earth orbiting satellites and the Shuttle Missions; the use of sensors in more portions and combinations of the electromagnetic spectrum such as active microwave, thermal infrared and multispectral scannners; and the incorporation of computers in the handling and processing of remotely sensed data.

The Rome Air Development Center of Griffiss Air Force Base in New York State has been involved in numerous remote sensing activities, particularly within the Image Systems Branch (IRR) of the Intelligence and Reconnaissance Division. To support these activities, IRR has an excellent system for numerical processing of remotely sensed data. IRR staff are actively pursuing a variety of activities to evaluate and utilize remotely sensed data for the Air Force.

The author of this report, B. N. Haack, was accepted to the 1985 USAF-UES Summer Faculty Research Program by IRR because of his interest and experience in numerical processing of remotely sensed data. Dr. Haack has previously worked with both aircraft and spacecraft obtained data from several different sensing systems. He also has experience in both visual interpretation and computer processing of this data. The ongoing projects and available resources at IRR and Dr. Haack's prior work and professional interest in remote sensing resulted in a useful and

productive summer research program.

II. OBJECTIVES OF THE RESEARCH EFFORT:

The use of multispectral scanners (MSS) on aircraft or spacecraft to measure reflected or emitted energy has been an important development in remote sensing. MSS data are frequently computer processed for image enhancement or classification of thematic features of interest using various digital pattern recognition methods. An area of considerable research interest is the examination of various methods of digital classification to improve the accuracy of theme identifications. These methods have included different data transformations; combinations of supervised, unsupervised and hybrid signature extractors; the inclusion of ancillary data in classification and different decision rules operating on either a per-pixel or a contextual basis.

Data transformations frequently include per-pixel manipulations of band reflectance or emittance values such as subtraction, addition, division or ratioing, and combinations of manipulations especially in green vegetation indices and rock type analyses. The objective of this project was to assess the usefulness of multipixel measures of texture for digital classification of MSS data.

Texture measures are important in visual analysis of remotely sensed data. Digital texture measures are the changes in digital number (DN) values from pixel to pixel within a window and are expected to be particularly useful in the identification of cover types which have a considerable variation in DN values, cover types which are difficult to classify accurately using traditional methods. The specific land covers of initial interest for this study were forest and nonforest.

II. DATA AND STUDY SITE:

The remotely sensed data utilized in this study are from a Thematic Mapper Simulator (TMS) sensor flown in an aircraft. The TMS is a seven band multispectral scanner (MSS) which includes three visible, three near to mid infrared and one thermal infrared band. The precise band widths for this sensor are contained in Table 1. The TMS is identical to the Thematic Mapper of Landsats 4 and 5, but because of the lower platform elevation, it provided data at approximately five meter spatial

resolution rather than the 30 meter resolution of the earth orbiting Landsats.

The TMS data were collected at approximately 11:00 a.m. on September 13, 1983 from a flying height of 2000 meters (6500 feet) for a rural area in central New York State near the city of Stockbridge. The study site was approximately five square kilometers; the specific study image was 512 by 418 pixels. The primary land covers in this area are forest and various active and inactive agricultural fields. Six training sites were initially selected to represent forest and nonforest covers. These sites included two for forest, a hardwood and a pine area; and four for nonforest, corn, hay, pasture and grass. They were located with the assistance of ground truth information. The means and standard deviations by bands, as well as the number of pixels in each of the training sites, are contained in Table 2.

The individual spectral bands were examined visually and statistically to determine which bands might be most useful for texture separation of forest and nonforest areas. Because of variations in tree species and the presence of shadows, the forest areas are expected to have greater texture values than the nonforest areas. Visually, several bands indicated considerable texture separability. Statistically, Band 4 appeared to have good separability because of its large range of reflected values for the entire image and because of the considerable difference in standard deviations between the forest and nonforest sites.

IV. TEXTURE MEASURES:

Texture is one of the basic elements in photo interpretation and is frequently described by terms such as smooth, rough, and coarse. Texture is a function of variations in spectral response of features adjacent to each other. Visually, texture can be used to separate field crops which have a smooth texture from inactive agriculture or pasture which have a coarse texture; or tree plantations, smooth texture, from mixed forest, coarse texture.

In digital processing, texture is the spatial distribution of pixel tones. There have been a variety of texture measures developed for digital processing. Some of the more important studies of texture, or reviews of texture measures, have been made by Hsu (1978), Weszka (1976),

Mitchell (1977) and Haralick (1973). There were nine texture measures examined in this study. Those measures and the window size for which they were initially calculated are described in Table 3.

Many of the texture measures, such as mitch, moments and mnvar, have variable input parameters to provide different results. The mitch measure is based on counts of significant local maxima or minima within a window. Significance is defined by a threshold such that local minima or maxima with amplitude greater than the threshold are retained. This thresholding is performed by a hysteresis filter which compares the current input to the current output, and leaves the output unchanged unless the deviation between input and output exceeds the threshold (Duda and Hart, 1973). The threshold value was an input variable which was altered in this study. The mitch texture measure is obtained in two stages; in the first stage the hysteresis filter is applied with a specified threshold value and in the second stage the local number of maxima or minima pixels are counted using an above or below threshold algorithm.

In the moments texture measure, the level of the moment (k) can be changed in the following formula:

(summation over x of [(x - ave)**k])/n

where: x = WIN(i,j,) = the current window intensity
ave = mean of the current window
k = k th moment
n = the number of intensities in the window.

The mnvar measure allows for various texture measures including mean, variance, statistical difference, skewness or kurtosis. The statistical difference is computed as follows. If the variance is greater than or equal to 0.1, output the pixel in the middle of the window less the mean times fifty divided by the variance and increment the result by 128, otherwise output 128 (Pratt, 1978). In this study, mnvar was utilized to determine statistical difference and skewness.

For all texture measures, the window size could be altered. The influence of window size variation on the usefulness of texture measurements is not clear. Wiersma (1976) reported some preference for

improved classification accuracy with larger window sizes while Weszka (1976) reported a decreased preference for larger windows. Larger window sizes may create difficulties near land cover boundaries when texture measures are calculated for two or more cover types within a window. Possibly some type of edge enhancement or a filter could be applied to the texture results to reduce the boundary confusions which occur with larger windows. To minimize the problem of texture measures from overlapping cover types, small window sizes were utilized in this study. The small window size is also important because one of the measures for accuracy evaluation in this study was the misclassification of the training sites themselves. A larger window size will reduce the number of sample pixels as well as their variance in a training site such that the misclassification values will be very low but not necessarily indicative of true classification accuracies for the entire study area.

V. PROCESSING METHODOLOGIES:

Processing for this study was accomplished on the Automatic Feature Extraction System (AFES) available at the Rome Air Development Center, Griffiss Air Force Base, New York. AFES has extensive software and hardware capabilities for the display and analysis of remotely sensed data.

Processing issues of concern to this study were first, which classifier to utilize; second, what evaluation techniques would indicate the relative utility of the various measurement extractors such as individual texture values and single band data for the separation of forest and nonforest areas; and third, what combinations of measurement extractors would be most useful for this separation and how would that be determined.

The classifier selected for this study was the Mahalanobian classifier which operates on a pixel by pixel basis using inverse covariance matrices obtained from training sites. This is a Baysian maximum liklihood classifier assuming gaussian statistics and equal apriori probabilities. For each image pixel, a discriminant measure from each class is calculated. The discriminant is the Mahalanobis distance minus one-half the log of the determinate of the covariance matrix. The pixel is declared to belong to the class which has the largest

discriminant value, unless it is less than the declared null class cutoff, in which case the pixel is assigned to the null class (Duda and Hart, 1973; Hsu, 1979).

Several techniques were employed for assessing the relative ability of various texture and spectral band measurement extractors for the separation of forest and nonforest land covers. These techniques included 1) a unimodal discriminant measure, 2) a probability of confusion measure, 3) misclassification of the training sites themselves and 4) classification accuracy for non-training site image areas.

The discriminant measure is useful for ranking measurement extractors when the class conditional probability distributions are approximately unimodal (Sammon, 1970). However, frequently remotely sensed data is not unimodal and therefore, the discriminant measure may not be useful with texture extractors. The probability of confusion measure is valid for any probability distribution since it essentially measures the overlap of the class conditional probabilities. It is, however, computationally much more complex than the discriminant measure. Both of these techniques operate on single measurement extractors and not combinations of extractors.

A third method for evaluating measurement extractors is to return to the training sites after extracting the necessary statistical parameters from them for the classifier, classify them and tabulate the percent of misclassification. This technique can be applied to both individual and combinations of measurement extractors.

The best technique for determining classification accuracy is to compare actual site conditions and classified results for a sample of or of the entire study site. One limitation of this approach, however, is the time and cost of such a determination when there are a large number of measurement extractors to be evaluated. A further limitation to the use of this accuracy assessment method in this study was the lack of extensive ground truth information collected near the time of data acquisition and limitations of the available classification output products. Nevertheless, this method was employed for several measurement extractor classifications.

In evaluating various measures for the separation of forest and nonforest land covers, one consideration was if the six training sites should be first grouped into classes for training and classification or if the six training sites should be treated independently until after classification and then designated as forest or nonforest. For texture measures, a grouping of sites into two classes would be appropriate because one assumes very different texture in the two classes. However, for spectral values there may be considerable difference between training site statistics within the same class of interest as indicated in Table 2. For spectral measures, it is more appropriate to maintain the individuality of each training site. At various stages in this study both grouping and nongrouping of the training sites were done prior to extractor evaluation and classification.

The research methodology for this study was to first evaluate the relative ability of the individual band spectral data to separate forest and nonforest land covers. Next, various texture measures were applied to the individual band (Band 4) which appears most useful for separating the two cover types of interest. The better texture measures as determined from the Band 4 examination were then extended to the other TMS bands. After the individual TMS band spectral data and the various texture measures had been examined independently for forest and nonforest separability, combinations of these measurement extractors were made and evaluated.

VI. RESULTS OF SINGLE EXTRACTORS:

The first aspect of this analysis was to ascertain the relative effectiveness of the available individual measurement extractors for the separation of forest and nonforest land covers. These extractors included the digital number (DN) values for each of the seven TMS bands plus the various texture measures, with internal parametric alterations, for all bands. The relative effectiveness of these measures can be ascertained by the use of the discriminate measure, probability of confusion or percent misclassification of the training sites. Furthermore, these measures and their evaluaton can be based on the six training sites independently or as grouped into two cover types.

TMS Spectral Values: The first examination was for the seven TMS spectral bands individually. The results of that examination are contained in Table 4 as band rankings for various separation evaluators. Clearly the rankings are not consistent for the different evaluations. The two class analysis groups the two forest training sites as one class and the four nonforest sites as a second class while the six class evalutation treats each site independently.

The rankings within the two class evaluation are fairly consistent. The probability of confusion is likely to be a better evaluation measure because it does not require a unimodal assumption. Certainly, when grouping various training sites as one class, one would not expect a unimodal distribution. The discriminant measure treats the data the same as the Mahalanobian classifier in assuming a gaussian distribution, which explains why it is identical to the percent misclassification at the two class level.

In the six class evaluation, the discriminant measure and probability of confusion evaluators are misleading in that they include the separation of training sites, such as corn and hay, which are subclasses of the cover types of interest, forest and nonforest. The six class percent misclassification is the best evaluator in this study because it includes only the misclassification of the training sites considered as forest or nonforest independently of the actual training sites such as hardwoods or pine. The six class percent misclassification of forest and nonforest is the evaluator applied in this study to examine measurement extractors independently or in combination.

Texture Extractors: Based on the image range of DN values and particularly the difference in standard deviations for the forest and nonforest training sites, TMS Band 4 was selected as the most likely band to provide useful texture separability of the cover types of interest. The nine texture measures in Table 3 were applied to the Band 4 data for the six training sites. Because of input parameter variations of several of the texture measures, a total of seventeen different Band 4 texture measures were obtained. A selection of these measures, including the best measures, are listed in Table 5 as evaluated by the percent forest and nonforest misclassification of the six training sites. There is not

a significant difference in the first five measures listed in Table 5, all of which use a 3 by 3 pixel window. The last two measures in this table used a 1 by 5 pixel window, which does not seem as effective.

The better texture measures, as determined by the Band 4 analysis, were applied to the other TMS bands. None of the other bands were nearly as effective as Band 4. The best of the other band texture measures was a Band 2 intensity of standard deviation misclassification of 22.8 percent.

Table 6 is a ranking of the forest and nonforest percent misclassification for the TMS spectral values and at least one texture measure for each TMS band. Several texture measures from the better bands are included in this table. This table indicates that texture measures may be more useful than a number of the TMS individual band spectral values.

VII. RESULTS OF EXTRACTOR COMBINATIONS:

The results of the single measure analysis, some of which are contained in Table 6, were utilized to develop combinations of measurement extractors for evaluation. Those combinations were composed of only DN extractors, only various texture extractors or combinations of DN and texture extractors. The combinations were evaluated by determining the percent forest or nonforest misclassification and null of the six training sites. A considerable number of different combinations of two to seven measurement extractors were examined. There were sixteen of two extractors, twenty-one of three, six of four, three of five and one for six and seven extractors. Table 7 contains the results for various combinations of two, three and four measurement extractors. The frequency of null classification is very low. Only four of the extractor combinations in Table 7 include a null percentage and the maximum amount of data not classified was 0.4 percent.

In examining Table 7, it is important to note that not all combinations of measurement extractors were made. Combinations of interest were selected using the rankings in Table 6 under the assumption that the better measures determined by individual examination would make the best combinations. Furthermore, while Table 7 contains the best several measures at each combination level, it also contains other

groupings which may not be among the better combinations but are representative of a category of combinations of interest. For example, the fourth two-measure combination is the best one DN and one texture extractor combination but there are other two DN combinations not included in this listing with lower misclassification levels.

All spectral extractors used for Table 7 are on a single pixel basis while all texture measures are for a 3 by 3 pixel window. Enlarging the window size has an impact on the classification of the training sites because there are fewer pixels sampled and because the variance of the measures are lowered. For example, the combination of Bands 2,3 and 7 DN values classified as single pixels has a percent misclassification of 0.47 but with a 3 by 3 pixel window, there is no misclassification. Retaining bands 2 and 3 at a single pixel sample and changing the band 7 measure to a 3 by 3 pixel window results in a percent misclassification of 0.32. This is very similar to combining single pixel DN and nine pixel texture extractors.

There are a number of observations which can be made from Table 7. Most importantly, there is a usefulness to combining DN and texture extractors, particularly for three or more measures. It is also evident that the combinations of extractors do not always coincide with the best single extractors as listed in Table 6. For example, the best two TMS bands are 2 and 3 but the best pair are 2 and 4. Generally, the better combinations of extractors do follow the ordering in Table 6.

Among combinations of two extractors, two DN measures are clearly better that a mix on one DN and one texture. Groupings of two texture extractors provide relatively poor results. With three extractors, there is very little accuracy variation among many different combinations. Two DN plus one texture measure provides results as good as three DN extractors. Surprisingly, in two DN and one texture groupings, the band and method for the texture measure does not seem very important. Band 4 mad-hv, band 3 rang and band 2 int-stdv texture extractors in groupings with two DN measures all provide very similar misclassification values. A combination of one DN and two texture measures provides less useful groupings than the others examined.

There are similar results with four extractors except that the three DN plus one texture combination provides better results that four DN extractors. Increasing the number of texture extractors to two or more does not provide better results.

Using different numbers of extractors in combination provides an opportunity to assess the improvement in classification as a function of the number of extractors. This assessment is documented in Table 8 for different numbers of TMS band DN values. These results are based on a misclassification of the six training sites as forest or nonforest cover types. There is considerable improvement from one to two extractors, minor improvement for two to five extractors and then a decrease in accuracy with six and seven dimensions. The six and seven grouping results both include a 0.3 null classification. The addition of more dimensions in a classification may actually produce a decrease in accuracy and certainly does not warrant the increase in processing time.

A more critical issue than the misclassification of training sites is the accuracy for data outside of the training sites. Such an accuracy can be determined on a sampled basis, either random or systematic, or for the universe of data. Two non-training site aspects of classification accuracy were examined as part of this study. The first was the relative ability of various combinations of measurement extractors to correctly identify non-training site areas of forest or nonforest and the second was the precision of boundary definition between different land covers. The ability for good boundary definition between land covers is of concern because with spatial operators such as texture, boundaries frequently become less distinct.

The accuracy of classification for non-training site areas was determined by selecting twenty-one regions of known land cover within the study site. These regions were for the six training site land covers and varied in size from 266 to 10,555 pixels. These regions included approximately 18 percent of the study area. The image was classified using three different combinations of measurement extractors. For each classified image, the error of forest and nonforest identifications for the twenty-one regions was calculated.

Based on this assessment, the best extractor combination included bands 2 and 4 DN values at a 3 by 3 pixel window and band 4 mad-hv texture measure also at a 3 by 3 window. This combination had a total misclassification of 7.93 percent. For a combination of bands 2, 3, and 4 DN values at a single pixel basis, the misclassification was 8.13 percent and for the same DN values on a 3 by 3 pixel window increased to 13.05 percent. These results again indicate the usefulness of texture extractors. The combination including the texture measure would most likely have provided better results if the DN values had been on a single pixel basis. The overall misclassification is relatively high because the intraclass reflectance variability is not accounted for with only one training site per cover type.

The boundary definition was assessed by examining the classified results for the data between cover types. This examination was for four forest and nonforest boundaries and three combinations of measurement extractors. These combinations were 1) three bands of DN values on a single pixel basis, 2) the same measures on a 3 by 3 pixel window average and 3) two bands of DN values plus a band 4 mad-hv texture measure. There were few differences between these results, however, based on the number of forest or nonforest misclassifications and null within a two pixel wide boundary, the extractor combination including the texture measure was best, the DN single pixel combination second and the DN nine pixel window third. The texture measure appears to provide a more distinct boundary than the reflectance measures. A limited examination of larger window sizes suggests a decrease in boundary definition with larger windows.

One of the expected advantages of texture measures for numerical classification is that they would have less intraclass variation than reflected or emitted DN values. The smaller intraclass variability would allow for the use of fewer same cover type training sites in classification and easier signature extension; a frequent difficulty in processing remotely sensed data.

The amount of intraclass variability was examined by obtaining the probability of confusion of seven measurement extractors independently for 1) five corn fields, 2) three hay fields and 3) five hardwood areas.

The seven extractors were band 2 DN, band 3 DN, band 4 DN, band 2 int-stdv, band 3 rang, band 4 int-stdv and band 4 mad-hv. For the five corn fields, the probability of confusion was greater for the three DN extractors than the texture extractors. The same results were obtained for the three hay fields while for the hardwood areas, two DN values had larger probability of confusion values than the four texture extractors and one, band 4, had the lowest probability of confusion. These results demonstrate the greater intraclass variability of DN reflectance values than texture values and therefore, the more likely usefulness of texture extractors in signature extension.

VIII. RECOMMENDATIONS:

This study has demonstrated that numerical measurements of texture in MSS data are useful in the digital delineation of forest and nonforest land covers. It has also been determined that there is less intraclass variability for texture extractors than with the original spectral data which indicates greater signature extension with the texture extractors. The results from this study may, however, be data specific.

One necessary continuation of this study is to assess the importance of texture with other land cover types and other remotely sensed data. The methodology developed in this analysis should be applied to other TMS data available at RADC. This data could be examined to assess signature extension for forest and nonforest separation using other study areas and assess the utility of texture for urban/nonurban separation and other land covers. Landsat TM data with 30 meter spatial resolution could also be examined with the same methodology to determine the applicability of texture measures to larger spatial resolution data. This is important because the Landsat data is essentially globally available.

Other study continuations could include the use of additional texture measures such as the spatial gray level dependency matrices (SGLDM) variations developed by Haralick (1973) and a more complete examination of the influence of window size on boundary definition and overall classification accuracy. Different methods of classification accuracy assessment should also be applied to the texture extractor results.

Various pre-classification averaging or filtering of the MSS data could be compared to post-classification smoothing as interesting extensions of this project. In addition, both the pre and post-classification processing could utilize an edge enhancement algorithm to improve boundary definitions. The AFES processing capabilities are uniquely suited to this type of analysis.

This study utilized a training site or supervised method of signature extraction. A potentially very useful and interesting approach would be to use an unsupervised or clustering approach with various texture extractors. Related to pursuing these different methods of signature extraction is the use of other decision rules or classifiers. A hierarchical classification strategy may be an extremely effective method to maximize the usefulness of texture measures.

Numerical classification of remotely sensed data is of increasing utility to many United States Air Force activities. The results of this project are very promising for improving the accuracy and usefulness of numerical classification techniques but need to be extended to other data sets for verification and modified as suggested here to more fully evaluate their importance to the Air Force.

REFERENCES

Conners, R. W. and C. A. Harlow, "A Theoretical Comparison of Texture Algorithms," IEEE Transactions on Pattern Analysis and Machine Intelligence, PAMI-2(3), 1980, pp. 204-222.

Duda, R.O. and P.E. Hart, Pattern Classification and Scene Analysis, John Wiley and Sons, New York, 1973.

Freeman, H. et. al., Pilot Digital Operations Experimentation in Feature Signature Analysis and Pattern Recognition, Rensselaer Polytechnic Institute, Troy, N.Y., 1981.

Harlow, C. A. et. al., Texture Analysis of Urban Scenes, RSIP TR 401.01, Louisiana State University.

Haralick, R. M., "A Resolution Preserving Textural Transform for Images," IEEE Proceedings of the Conference on Computer Graphics, Pattern Recognition, and Data Structure, 1975, pp. 51-61.

Haralick, R. M. et. al., "A Comparative Study of Texture Measures for Terrain Classification, " IEEE Transactions on Systems, Man and Cybernetics, SMC-3 (6), 1973, pp.610-621.

Hsu, Shin-yi, "Texture-Tone Analysis for Automated Land-Use Mapping," Photogrammetric Engineering and Remote Sensing, 44(11), 1978, pp. 1393-1404.

Hsu, Shin-yi, "The Mahalonobis Classifier with the Generalized Inverse Approach for Automated Analysis of Imagery Texture Data," Computer Graphics and Image Processing, 9, 1979, pp. 117-134.

Jensen, J. R., "Spectral and Textural Features to Classify Elusive Land Cover at the Urban Fringe," The Professional Geographer, Vol. 31 (4), 1979, pp. 400-410.

Mitchell, O. R. and S. G. Carlton, "Image Segmentation Using a Local Extrema Texture Measure," Pattern Recognition, Vol. 10, 1978, pp. 205-210.

Mitchell, O. R. et. al., "A Max-Min Measure for Image Texture Analysis," IEEE Transactions on Computers, C-26(4), 1977, pp. 408-414.

Pratt, W. K. Digital Image Processing, John Wiley and Sons, New York, 1978.

Sammon, John W. Jr., "Interactive Pattern Analysis and Classification," IEEE Transactions on Computers, C-19(7), 1970, pp. 594-616.

Weszka, J. S. et. al., "A Comparative Study of Texture Measures for Terrain Classification," IEEE Transactions on Systems, Man, and Cybernetics, SMC-6(4), 1976, pp. 269-285.

Wiersma, D. J. and D. Landgrebe, "The Use of Spatial Characteristics for the Improvement of Multispectral Classification of Remotely Sensed Data," Symposium on Machine Processing of Remotely Sensed Data, 1976, pp. 2A-18 to 2A-25.

TABLE 1

THEMATIC MAPPER SIMULATOR BANDS

Band Number	Wavelengths (microns)
1	.45 - .52
2	.52 - .60
3	.63 - .69
4	.76 - .90
5	1.55 - 1.75
6	10.40 -12.50
7	2.08 - 2.35

TABLE 2

STOCKBRIDGE TRAINING SITE STATISTICS

Training site	Number of Pixels	Band 1	2	3	4	5	6	7
Hardwood	651	39.4*	48.4	33.4	159.9	28.9	87.6	126.7
		3.4	3.4	2.4	13.7	2.2	3.7	5.0
Pine	306	36.8	41.9	30.9	98.5	23.7	80.7	118.0
		3.6	3.1	2.7	14.5	1.6	3.9	4.2
Corn	682	43.5	57.5	49.1	131.1	28.1	90.4	135.5
		3.4	1.9	1.6	3.6	1.6	3.2	2.8
Hay	638	43.5	59.3	37.5	199.3	31.9	92.0	133.3
		3.5	2.0	1.4	5.4	1.7	3.3	4.2
Grass	513	42.5	56.8	48.4	106.5	29.4	93.0	150.8
		3.2	2.8	2.5	6.5	1.4	3.4	4.3
Pasture	294	43.4	63.8	52.9	139.4	34.8	100.6	161.5
		3.7	1.8	3.2	5.5	2.2	3.8	6.5

*mean
standard deviation

TABLE 3

TEXTURE MEASURES AND WINDOW SIZES UTILIZED

System annotation	Measure	Window size (pixels)	Description
1. contr	contrast	1 x 5	sum of the difference in intensity values between each local peak or valley and the following peak or valley
2. cnt-peaks	count peaks	1 x 5	counts the number of peaks and troughs (Hsu, 1978)
3. sum-peaks	sums peaks	1 x 5	sums the heights of all peaks (Hsu, 1978)
4. mitch	Mitchell	3 x 3	counts significant local maxima or minima (Mitchell,1977)
5. rang	range	3 x 3	finds the range of intensity values
6. int-stdv	intensity of standard deviation	3 x 3	finds the standard deviation of the intensities
7. moments	moments	3 x 3	computes the k th moment
8. mad-hv	median absolute difference	3 x 3	median absolute difference between horizontal and vertical neighboring pixels
9. mnvar	mean and variance	3 x 3	computes the mean, variance, statistical difference, skewness, or kutorsis (Pratt, 1978)

TABLE 4

COMPARISON OF RANKING MEASURES FOR FOREST AND NONFOREST SEPARATION USING TMS BANDS

	Two Class *			Six Class **		
Band Number	Disc. Meas.	Prob. of Conf.	Percent Miscla.	Disc. Meas.	Prob. of Conf.	Percent Miscla.
1	5	5	5	7	7	7
2	1	1	1	4	4	1
3	2	2	2	3	3	2
4	7	4	7	1	1	4
5	6	7	6	5	5	6
6	4	6	4	6	6	5
7	3	3	3	3	2	3

*The six training site statisics are grouped into two cover types.
**Each training site is treated independently until after classification.

TABLE 5

BAND 4 TEXTURE MEASURE PERCENT MISCLASSIFICATION

Texture measure	Percent misclassification
mad-hv	8.2
rang	8.5
moments (8th)	8.8
int-stdv	9.0
mitch (thres. 12)	10.8
contr	22.8
cnt-peaks	39.0

TABLE 6

SINGLE EXTRACTION MEASURE PERCENT MISCLASSIFICATION

Measure	Percent misclassification
Band 2 DN	2.7
Band 3 DN	5.0
Band 4 mad-hv	8.2
Band 4 rang	8.5
Band 7 DN	8.7
Band 4 moments (8th)	8.8
Band 4 int-stdv	9.2
Band 4 DN	12.5
Band 6 DN	16.0
Band 5 DN	17.5
Band 1 DN	22.3
Band 2 int-stdv	22.7
Band 3 rang	28.2
Band 7 rang	32.8
Band 5 rang	34.2
Band 6 rang	39.8
Band 1 rang	48.0

TABLE 7

COMBINATIONS OF MEASUREMENT EXTRACTORS

	Two ext.	Percent misc. inc. null		Three ext.	Percent misc. inc. null		Four ext.	Percent misc. inc. null
1.	2 DN 4 DN	0.42	1.	2 DN 4 DN 4 mad-hv	0.40	1.	2 DN 3 DN 7 DN 4 mad-hv	0.25
2.	2 DN 3 DN	0.67	2.	2 DN 3 DN 4 DN	0.40	2.	2 DN 3 DN 4 DN 7 DN	0.32
3.	3 DN 4 DN	0.70	3.	2 DN 3 DN 3 rang	0.42	3.	2 DN 3 DN 4 DN 4 mad-hv	0.35
4.	2 DN 4 mad-hv	1.50	4.	2 DN 3 DN 2 int-stdv	0.43	4.	2 DN 4 DN 2 int-stdv 4 mad-hv	0.48
5.	2 DN 4 int-stdv	1.60	5.	2 DN 3 DN 4 mad-hv	0.43	5.	2 DN 3 DN 4 mad-hv 4 rang	0.50
6.	2 int-stdv 4 mad-hv	2.25	6.	2 DN 2 int-stdv 4 mad-hv	1.45	6.	2 DN 3 DN 2 int-stdv 4 mad-hv	0.53

TABLE 8

PERCENT MISCLASSIFICATION AS A FUNCTION OF THE NUMBER OF DN MEASUREMENT EXTRACTORS

Measurement	Percent misclassification including null
DN Band 2	2.73
DN Bands 2,4	0.42
DN Bands 2,3,4	0.40
DN Bands 2,3,4,7	0.32
DN Bands 2,3,4,6,7	0.28
DN Bands 2,3,4,5,6,7	0.40
DN Bands 1,2,3,4,5,6,7	0.40

1985 USAF-UES SUMMER FACULTY RESEARCH PROGRAM

Sponsored by the

AIR FORCE OFFICE OF SCIENTIFIC RESEARCH

Conducted by the

UNIVERSAL ENERGY SYSTEMS, INC.

FINAL REPORT

EFFECT OF HIGH FREE-STREAM TURBULENCE FROM A FREE JET ON FLAT PLATE TURBULENT BOUNDARY LAYER FLOW AND HEAT TRANSFER

Prepared by: Dr. Je-chin Han

Academic Rank: Associate Professor

Department and University: Department of Mechanical Engineering, Texas A&M University

Research Location: Air Force Wright Aeronautical Laboratories
Aero Propulsion Laboratory
Turbine Engine Division
Components Branch

USAF Research Contact: Dr. Richard B. Rivir

Date: 30 August 1985

Contract No.: F49620-85-C-0013

EFFECT OF HIGH FREE-STREAM TURBULENCE FROM A FREE JET ON FLAT PLATE TURBULENT BOUNDARY LAYER FLOW AND HEAT TRANSFER

by

JE-CHIN HAN

ABSTRACT

Experiments were performed to investigate the effect of high free-stream turbulence on the turbulent boundary layer flow and heat transfer. The high turbulence intensity was produced by a free jet with a diameter of 8". A electrically heated thin foil flat plate test section, with 24" wide and 120" long, was placed at the downstream of the free jet. The mean and fluctuating velocity profiles in the boundary layer were measured at three axial locations of the jet centerline, X = 1.12 D, 4.87 D, and 9.84 D, with two jet velocities, U_0 = 62 fps and 110 fps. The calculated centerline turbulence intensity at the same three locations was 5%, 12-14%, and 20%, respectively. The heat transfer coefficient distributions on the flat plate were determined. The results showed that the log-law velocity decreased with increasing turbulence intensity levels, whereas the wake flow were lower than that the flat plate results. The boundary layer transitions were affected by high turbulence; the Stanton number and the friction factor in the fully turbulent flow region increased continuously when turbulence intensity changed from 12% to 20%. The Reynolds analogy factor was much greater than unity. More measurements are required in order to conclude the combined effects of turbulence intensity, length scale, and Reynolds number on the turbulent flow heat transfer.

ACKNOWLEDGEMENTS

I wish to gratefully acknowledge the opportunity and support by the Air Force Systems Command, the Air Force Office of Scientific Research and the Universal Energy Systems, Inc.

A very special thanks is due to Dr. Richard Rivir for his suggestions, joint discussions, and technical participation during the entire course of this study. I would like to thank Mr. Tom Trame for his assistance in construction and measurements during the entire project. I wish to thank Mr. Charles MacArthur for providing valuable literature in the free jet flow.

The friendly atmosphere in the Components Branch of the Turbine Engine Division made my stay at the Aero Propulsion Laboratory very pleasant.

I. INTRODUCTION:

The effect of free-stream turbulence on turbulent boundary layer heat and momentum transfer have been recognized as one of the critical problems in turbine airfoil design. In the case of adiabatic turbulent boundary layer flow over a flat plate, many studies have consistently confirmed that increases of skin friction are caused by increased free-stream turbulence levels. However, the impacts of free-stream turbulence on the turbulent boundary layer heat transfer were contradictory as indicated by Simonich and Bradshaw [3]. Some studies [1-2], which based on low Reynolds number (Re_θ) flow experiments (transitional boundary layer flow) or used coarse boundary layer trips or unconventional free-stream turbulence generating devices (large length scale of turbulence), showed that the heat transfer rates were not affected by free-stream turbulence levels. Recently, Simonich and Bradshaw [3] and Hancock and Bradshaw [4] and Blair [5-7] indicated that the free-stream turbulence effect depends upon the free-stream turbulence intensity and length scale. Based on wind tunnel grid-generated turbulence with turbulence intensity up to 6% and length scale ratio up to 5, they found that the Stanton number increases with increasing free-stream turbulence and the increased rate of Stanton number is larger than the increased rate of skin friction which implies that the Reynolds-analogy factor ($2St/C_f$) increases. They also concluded that the Stanton number at given turbulence intensity decreases as the length scale increases, while the maximum impact of the free-stream turbulence obtained for cases where the boundary layer thickness and streamwise dissipation length scale are about the same. The skin friction and the Stanton number correlations was respectively obtained to account for the effects of turbulence intensity, length scale, and boundary layer Reynolds number (Re_θ). Blair [6] also found that the logarithmic regions of the mean velocity and temperature profiles were not affected by free-stream turbulence levels and the turbulent Prandtl number (Pr_t) increases with increasing free-stream turbulence intensity in most region of the boundary layer except that near the wall (sub-layer) region where the Pr_t decreases with increasing turbulence

intensity.

In the aforementioned studies [3-7], the effect of free-stream turbulence on turbulent heat transfer were based on the wind tunnel grid-generated turbulence with a maximum turbulence intensity of up to 6%. It is noted that the turbulence level, at the nozzle guide vane (after combustor) and the second stage stator (after rotor), can be as high as 15-20% in engine conditions. It is interesting to know whether the results obtained in [3-7] can be extended to the very high free-stream turbulence condition (15-20%). In other words, whether the Stanton number and the Reynolds-analogy factor will continued to increase with further increasing turbulence intensity or they will reach a plateau at certain high levels of intensity. More importantly, in order to improve the computational techniques (such as STAN5) in turbine heat transfer calculations, there is a need to determine the mean and fluctuating velocity and temperature profiles and the turbulent Prandtl number distributions in the boundary layer under the very high free-stream turbulence levels. However, it is very difficult, if not impossible, to obtain very high free-stream turbulence with the simulated length scale in engine conditions by using classic wind tunnel grid-generated turbulence experiments. In the present investigation, the very high free-stream turbulence was produced at the downstream of a free jet. The mean and fluctuating velocity and temperature profiles and the Stanton number were taken through a flat plate placed at the downstream of the jet. The turbulence levels could be as high as 20% at 10 jet diameters downstream from the jet.

II. OBJECTIVES OF THE RESEARCH EFFORT:

This study is aimed to investigate the effect of high free-stream turbulence from a free jet on flat plate turbulent boundary layer flow and heat transfer.

There are two types of objectives: long range and immediate. For the present investigation, the immediate objectives are restricted to the following:

1. Design and construction a free jet-flat plate test apparatus.
2. Instrumentations the test section for velocity (hot wire

anemometer) and temperature (thermocouples) measurements.

3. Calibrations and preliminary measurements for the stream flow mean and fluctuating velocity profiles across the boundary layer at several downstream locations from the jet; calculations the turbulent intensity, log-law velocity, and friction factor distributions on the corresponding measurements.

4. Wall temperature and mean temperature profile measurements; calculation the log-law temperature and heat transfer coefficients.

5. Design and construction the injection system for film cooling and heat transfer experiments.

The long range objectives are as follows:

1. Detailed measurements on mean and fluctuating velocity and temperature profiles, u, v, T, u'v', v'T', to construct log-law velocity and temperature, and turbulent Prandtl number Pr_t distributions in the boundary layer.

2. Calculate the combined effects of high turbulence intensity, length scale, and Reynolds number on the friction factor and heat transfer coefficients.

3. Do the similar measurements as items 1 and 2 with one row and two rows film cooling.

III. EXPERIMENTAL APPARATUS:

Free Jet-Flat Plate: A low speed, large scale free jet-flat plate apparatus is shown in Figure 1. The air from the 300 psi, 5 lb/sec compressor passed through a gate valve, a pressure regulator, and entered a horizontal chamber with a diameter 32" and length 60". The free jet was produced at the exit of the 8" diameter ASME nozzle which was connected to the outlet of the horizontal chamber. The contraction ratio of the nozzle was 16:1. Two pressure taps were drilled through chamber wall to measure the air pressure inside the chamber by a micromanometer. The jet velocity at the exit of the nozzle could be varied up to 200 fps. One 24 gauge iron-constantan thermocouple was place inside the chamber through chamber wall to measure the jet temperature. The jet temperature was about 80°F.

A flat plate test section placed at the downstream of the nozzle

was fabricated by a 24" width, 120" length, and 4" thickness rigid urethane foam. The side walls of the foam were enforced by a wood box, while the top surface of the foam was completely covered with a 0.050" thickness formica flat plate. Three thin stainless steel foil heaters, each had a 6" width, 100" length, and 0.002" thickness connected in series, were cemented parallelly on top of the formica plate to complete the flat plate test section. The thin foil was powered by a variac through buss bars to provide a constant surface heat flux boundary conditions during the test. The foil was instrumented by a total of 63 24-gauge iron-constantan thermocouples in the strategic locations to measure the local surface temperature distributions, as shown in Figure 2. The thermocouples were soldered underneath the thin foil through holes in the urethane foam and formica plate. An 80-channels HP3495A scanner and HP9825B calculating machine were used for thermocouples readings and data acquisition.

A travelling device, which could be moved in X-Y-Z direction, was designed to hold the hot wire probe (TSI102) for mean and fluctuating velocity and temperature profiles measurements. A 4-channels TSI IFA 100 constant temperature anemometer and 2 HP3478A precision multimeters were employed along with the HP9825B calculating machine for hot wire signal analysis and data acquisition. Figure 3 is a photo of Free Jet-Flat Plate and Travelling Device.

Injection System for Film Cooling: The injection system for film cooling experiments is shown in Figure 4. The film cooling arrangement is very similar to that in [8]. The injection system has been designed and constructed, but not yet assembled. The cold air from the 100 psi, 2½ lb/sec compressor will pass through a pressure regulator, an ASME orifice flow meter, a control valve, and enter an injection plenum. The cold air will then be injected from the injection plenum through the inclined injection tubes into the test plate. The injection plenum is oriented in the vertical direction and has a cross section of 20" by 20" and a height of 20". The injection tubes can be either one row of seven tubes or two staggered rows of thirteen tubes at an angle of 30 degrees to the direction of free jet flow. The tube has a 1" ID x 18" length,

and been connected between the top of the injection plenum and the bottom of the injection plate. The lateral distance between tubes and the axial distance between rows (in the case of two rows injection) is two and three tube diameters, respectively. The same foil-rigid urethane foam flat plate test section will be placed at the downstream of injection tubes. Three thermocouples are placed inside the injection tubes (about 6 tube diameters before entering the test section) to measure the coolant temperature (about 80°F). Both local film cooling effectiveness and heat transfer coefficient will be measured under high turbulence free jet conditions with blowing rates varied from 0.2 to 2.0 by controlling the cooling flow rate.

IV. EXPERIMENTAL RESULTS:

Mean velocity profiles and turbulence intensity distributions vs y/D along the centerline of the wall-jet are shown in Figures 5 and 6. Data for two jet velocities, U_o = 62 fps and 110 fps, at three downstream locations, X/D = 1.12, 4.87, and 9.84, are presented, where X = axial distance from the jet exit, y = vertical distance from the flat plate surface, Z = lateral distance from the centerline of the wall-jet, D = 8", jet diameter, u = local mean velocity in X-direction, u' = local fluctuating velocity in X-direction, U_m = local maximum velocity in X-direction, and U_o = jet velocity at the nozzle exit in X-direction. Three regions of wall-jet velocity profiles are indentified: Boundary layer region (close to the wall), core region (uniform velocity), and wake region (interaction with the environment). The mean velocity decreases with increasing the axial distance from the jet exit as shown in Figure 5. For two jet velocities, mean velocity profiles are very similar at the same downstream location (X/D ratio) except that the velocity gradients in the boundary layer region increase with increasing jet velocity. At the upstream location, X/D = 1.12, the velocity profiles within the core region (y/D $\le$ 0.8) are very similar to that the flow over a flat plate, i.e., the velocity profiles beyond the boundary layer region (0.1 $\le$ y/D $\le$ 0.8) are fairly uniform. At the middle downstream location, X/D = 4.87, the jet starts to lose its core region, i.e., the uniform velocity profiles only extend to y/D = 0.5 (y = 4"). At the

further downstream location, X/D = 9.84, the jet completely loses its core region, i.e., there are no uniform velocity existed.

For two jet velocities, turbulence intensity ($Tu = u'/U_m$) distributions show the similar trends at the same downstream location (X/D ratio), but the intensity slightly decreases with increasing jet velocity. The turbulence intensity increases with increasing the axial distance from the jet as shown in Figure 6. At X/D = 1.12, two maximum turbulence intensities are found, one in the boundary layer region (y/D = 0.02) and the other in the wake region (y/D = 1.0). However at X/D = 9.84, the turbulence intensity distributions over the entire region are fairly uniform. The core region turbulence intensity at X/D = 1.12, 4.87, and 9.84 is about 5%, 14%, and 20%, respectively. It is noted that the centerline turbulence intensity at X/D = 10 was about 16% in MacArthur and Schauers' wall-jet flow [12].

The log-law velocity profiles (u^+ vs y^+) are shown in Figure 7, where $u^+ = u/u^*$, u^* = friction velocity, $y^+ = y\,u^*/\nu$, ν = kinematic viscosity. The solid lines in Figure 7 represent the classic log-law velocity profiles for the case of flow over a flat plate, i.e., $u^+ = 2.44 \ln y^+ + 5.0$. The friction velocities were determined from the curve fit to the log-law profiles of the present data at the given X/D ratio. In general the logarithmic regions of the mean velocity profiles are slightly affected by high turbulence levels, and the wake region profiles are much lower than the log-law profiles. It is noted at X/D = 1.12 (Tu = 5%) the present data are pretty much followed the log-law profile and very similar to that the Blair's results [6]. However, when the turbulence intensity increases from 5% to 20% (X/D = 9.84), the logarithmic regions decreases and the data are slightly falling below the log-law profiles. This may be the nature of the wall-jet boundary layer flow.

The local wall heat transfer coefficient distributions are shown in Figures 8 and 9. The local heat transfer coefficient, h, was calculated from $h = q''/(T_w - T_o)$, where q" = uniform surface heat flux determined by the electric current and the foil resistance or by the electric current and the voltage across the foil, T_w = local wall tem-

perature, and T_o = jet temperature. The heat transfer coefficient increases with increasing jet velocity and decreases gradually with increasing the axial distance from the jet. It is seen that the heat transfer coefficients are fairly uniform in the central region of the test plate (Z = ± 2"). The present data along the centerline of the wall-jet at X/D = 1.12, 4.87, and 9.84, and U_o = 62 fps and 110 fps are summarized in Table 1, and the Stanton number (St_x) and the friction factor (C_{fx}) vs the Reynolds number (Re_x) along the centerline of the wall-jet are shown in Figure 10, where, $St_x = h/(\rho C_p U_m)$, $C_{fx} = \frac{1}{2} (u^*/U_m)^2$, $Re_x = (X U_m)/\nu$, ρ = density of jet, C_p = specific heat of jet, C_{fo}, St_o = friction factor and Stanton number, respectively, for the case of flow over a flat plate. The solid lines in Figure 10 are the classic correlations for the friction factor and the Stanton number vs Reynolds number for the laminar and turbulent flow over a flat plate. It is seen that the transitions are affected by the turbulence levels, i.e., earlier transition $Re_x \cong 2 \times 10^5$ at Tu = 5%. The friction factor and the Stanton number in the fully turbulent flow region, $Re_x > 10^6$, are higher than that the classic correlations; whereas, the C_{fx} and St_x at Tu = 20% are higher than that Tu = 12 - 14%. More data are needed in Figure 10 in order to verify the effect of high turbulence on the friction and heat transfer.

The Reynolds analogy factor ($2\ St_x/C_{fx}$), as shown in Table 1, decreases from 1.37 to 1.26 (for U_o = 62 fps) and 1.57 to 1.25 (for U_o = 110 fps), respectively, when the turbulence intensity increases from 5% to 20% (i.e., X/D = 1.12 to 9.84). The Reynolds analogy factor is greater than unity, which confirms the results of Blair's [6]. However, according to Blair [6], the $2\ St_x/C_{fx}$ should increase linearly with increasing free-stream turbulence levels. It is suspected that the length scale (λ) at the downstream from the jet may be much greater than the thickness of the boundary layer so that the effect of high turbulence intensity is reduced. Therefore in order to conclude the combined effects of Tu, λ, and Re_x on the $2\ St_x/C_{fx}$, it is necessary to measure simultaneously the length scales and velocity profiles at the same downstream location (X/D = 1.12, 4.87, and 9.84) and the same jet velocity.

V. CONCLUSIONS:

Within the past ten weeks, the wall-jet test rig was constructed and instrumented. The preliminary data were obtained and the following conclusions could be drawn.

1. The high turbulence intensity levels (5%, 14%, and 20%) were obtained at the downstream of the wall-jet, and the log-law velocity profiles were constructed at the corresponding high turbulence levels.
2. The heat transfer coefficient distributions were obtained at the downstream of the high turbulence wall-jet with two jet velocities.
3. The transitions were affected by high turbulence levels, and the Stanton number and the friction factor in the fully turbulent flow region at Tu = 20% were higher than that at Tu = 12 - 14%.
4. The Reynolds analogy factor was much greater than unity ($2\ St_x/C_{fx} = 1.25 - 1.57$).

VI. RECOMMENDATIONS:

In order to conclude the effect of high turbulence intensity, length scale, and Reynolds number on the Stanton number and the friction factor, the following investigations are recommended.

1. Improve the travelling device and extend the profiles measurements to the wall region (i.e., sublayer region, $y^+ = 10$).
2. Measure the length scales and the velocity profiles simultaneously.
3. Construct the turbulent Prandtl number (Pr_t) distributions by measuring the mean and the fluctuating quantities, u, u'v', T, v'T'.
4. Measure the film cooling effectiveness and the heat transfer coefficient with film cooling under the high turbulence conditions.

It is worthwhile to note that the present wall-jet experiment does provide high turbulence intensity, but the intensity increases, and the

velocity decreases, with increasing the axial distance from the jet. This is not exactly simulating the engine conditions in that the intensity decreases, and the velocity (except at the beginning of the pressure side of the blade) increases, with increasing the distance from the blade leading edge. Therefore additional to the present wall-jet experiment, in order to further investigate the effect of high turbulence on the turbine blade heat transfer, the following two methods which can produce high turbulence levels to simulate engine conditions are recommended.

1. In a low speed wind tunnel, the test section (flat plate, cylinder, or cascade) is placed at the downstream of the simulated wake flow which will be generated by a squirrel-cage rotation.
2. In a low speed wind tunnel, the test section (flat plate, cylinder, or cascade) is placed at the downstream of the simulated combustor flow which will be created by injection the secondary flow into the mainstream.

REFERENCES:

1. Kestin, J., "The Effect of Free-Stream Turbulence on Heat Transfer Rates," Advanced in Heat Transfer, Vol. 3, Academic Press, London, 1966.
2. Junkhan, G.H., and Serovy, G.K., "Effects of Free-Stream Turbulence and Pressure Gradient on Flat-Plate, Boundary-Layer Velocity Profiles and on Heat Transfer," ASME Journal of Heat Transfer, Vol. 89, 1967, pp. 169-176.
3. Simonich, J.C., and Bradshaw, P., "Effect of Free-Stream Turbulence on Heat Transfer Through a Turbulent Boundary Layer," ASME Journal of Heat Transfer, Vol. 100, 1978, pp. 671-677.
4. Hancock, P.E., and Bradshaw, P., "The Effect of Free-Stream Turbulence on Turbulent Boundary Layers," ASME Journal of Fluids Engineering, Vol. 105, 1983, pp. 284-289.
5. Blair, M.F., "Influence of Free-Stream Turbulence on Turbulent Boundary Layer Heat Transfer and Mean Profile Development, Part I - Experimental Data," ASME Journal of Heat Transfer, Vol. 105, 1983, pp. 33-40.
6. Blair, M.F., "Influence of Free-Stream Turbulence on Turbulent Boundary Layer Heat Transfer and Mean Profile Development, Part II - Analysis of Results," ASME Journal of Heat Transfer, Vol. 105, 1983, pp. 41-47.
7. Blair, M.F., "The Effects of Free-Stream Turbulence on the Turbulence Structure and Heat Transfer in Zero Pressure Gradient Boundary Layers," United Technologies Research Center Report: R82-915634-2, E. Hartford CT, November 1982.
8. Han, J.C., and Mehendale, A.B., "Film Cooling and Heat Transfer with Steam Injection through Inclined Circular Holes," Texas A&M University Contract Report: TEES 1600, prepared for AVCO Lycoming Division under contract N-832132-E, May, 1985.
9. MacArthur, C.D., and Schauer, J.J., "The Circular Tangential Wall Jet Flow Development and Heat Transfer," University of Dayton Contract Report, prepared for NSF under Grant CME-8012951, January, 1984.

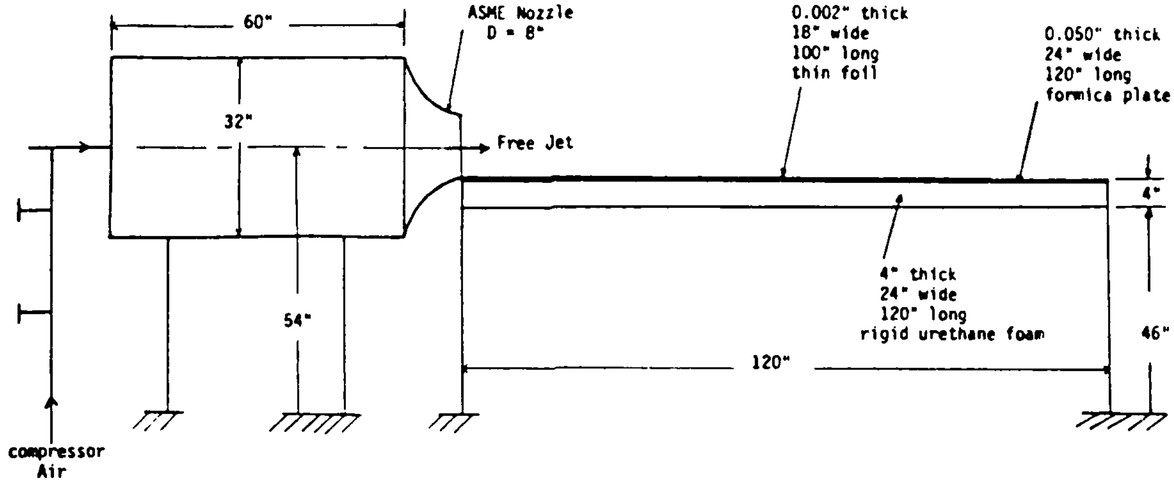

Figure 1. Schematic of the test apparatus for heat transfer

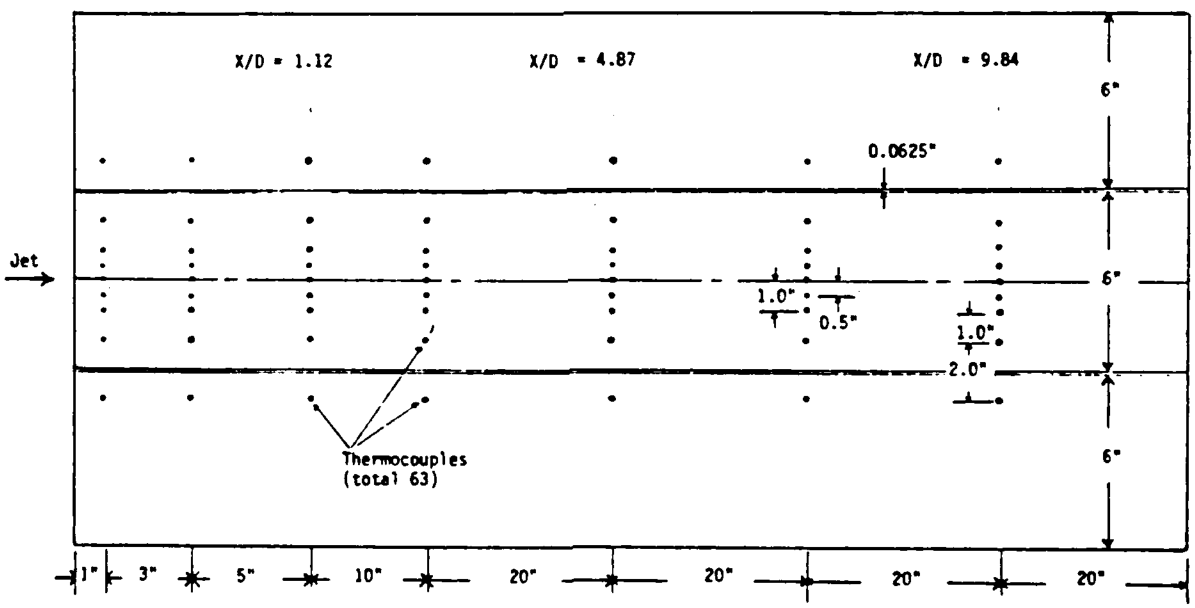

Figure 2. Detailed thermocouples locations

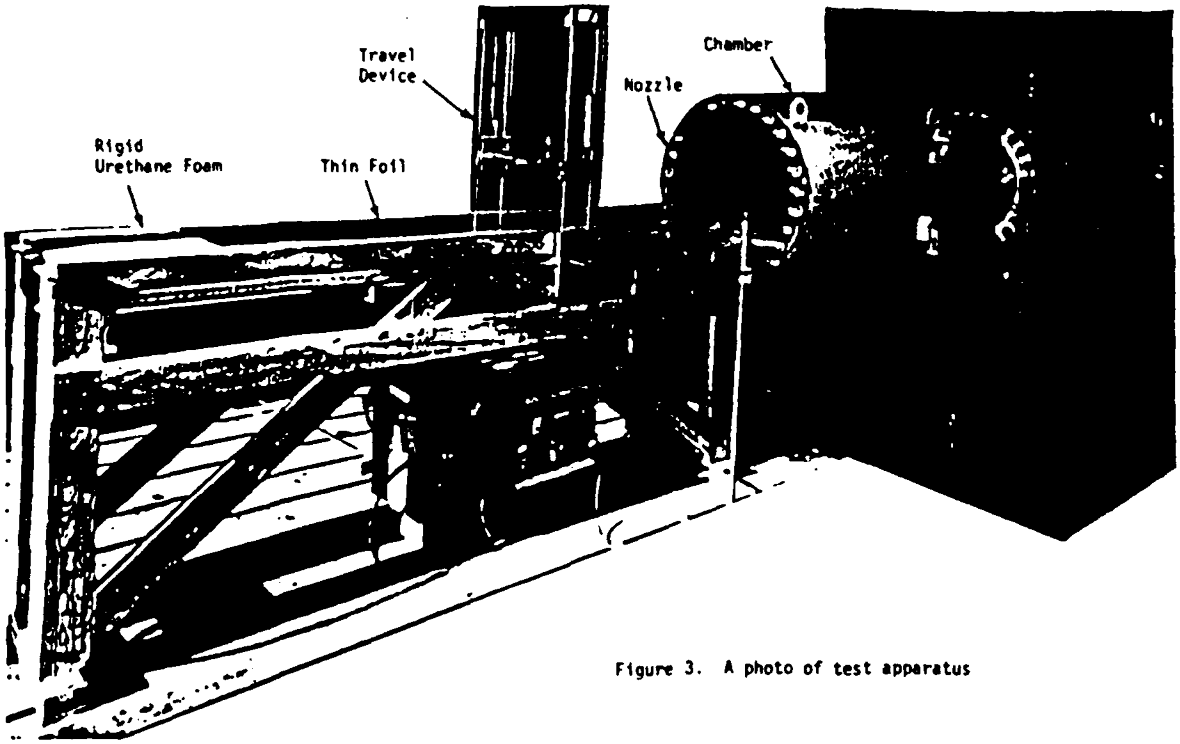

Figure 3. A photo of test apparatus

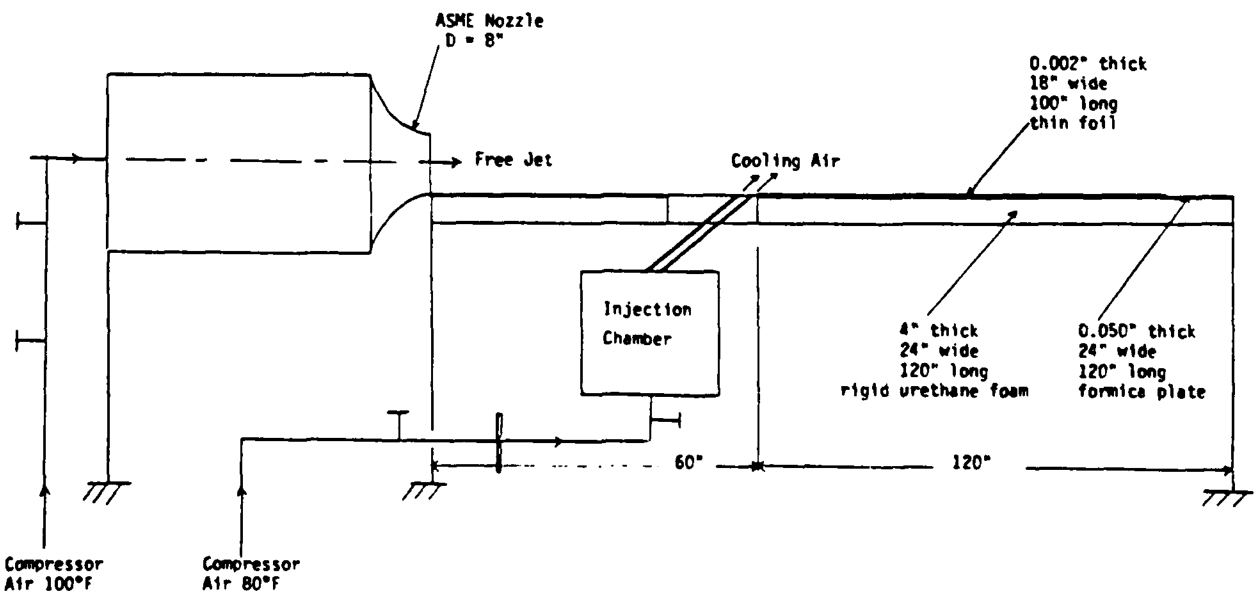

Figure 4. Schematic of the test apparatus for film cooling

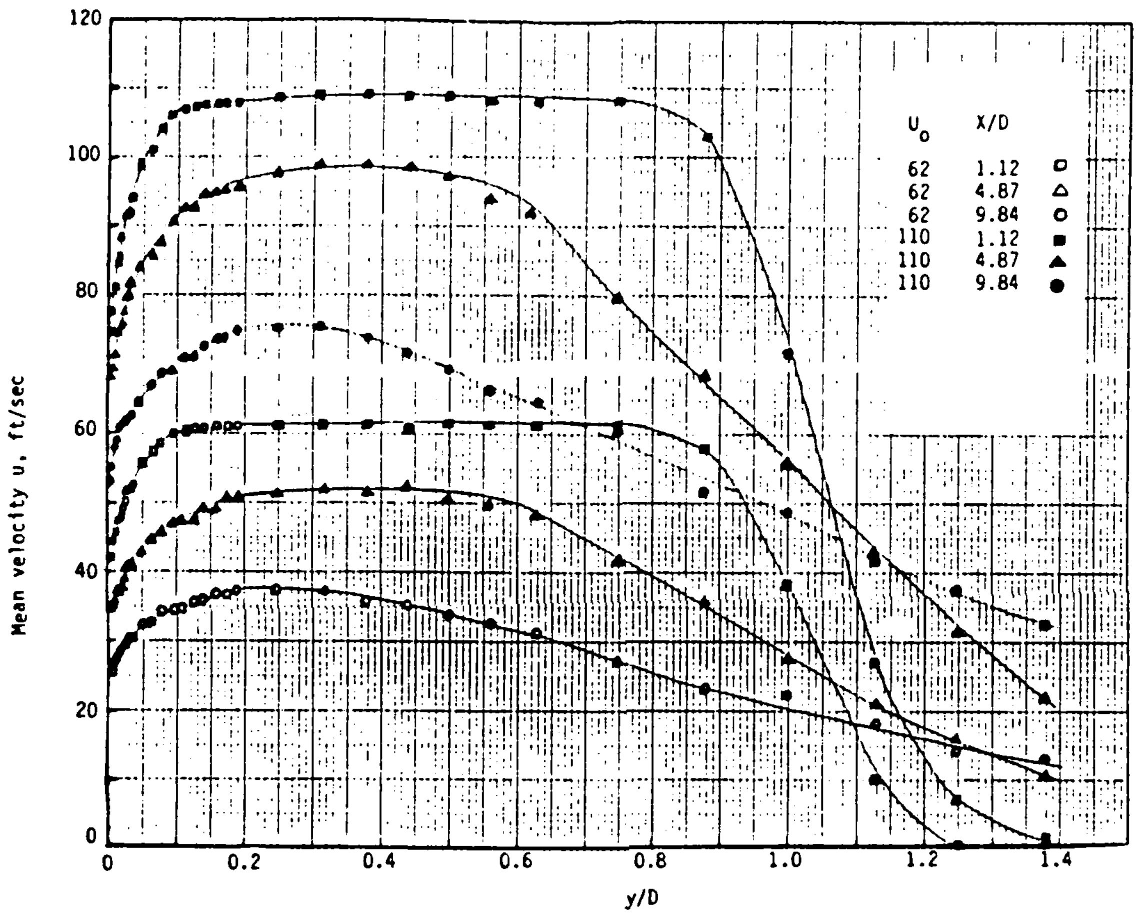

Figure 5. Mean velocity profiles along the midplane of the wall jet

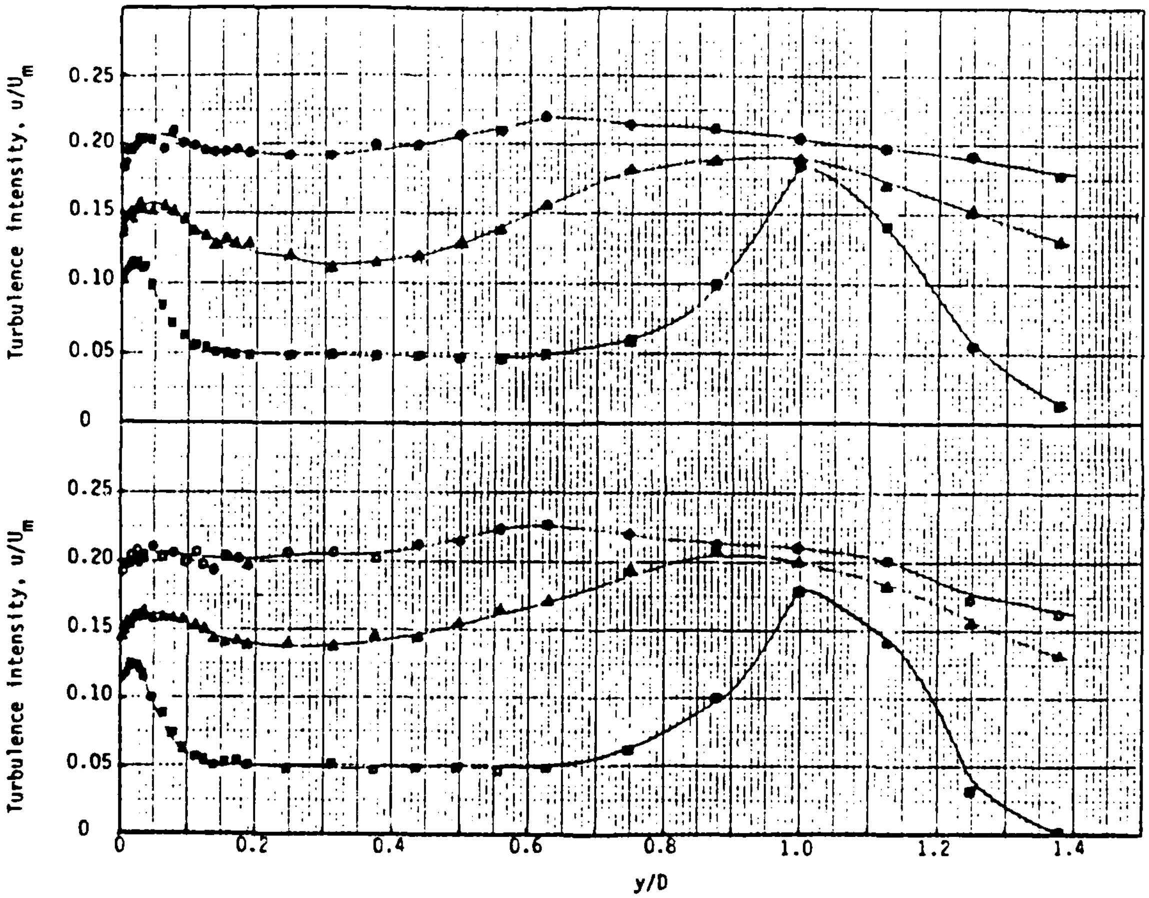

Figure 6. Turbulence intensity along the midplane of the wall jet (symbols are referred to Figure 5).

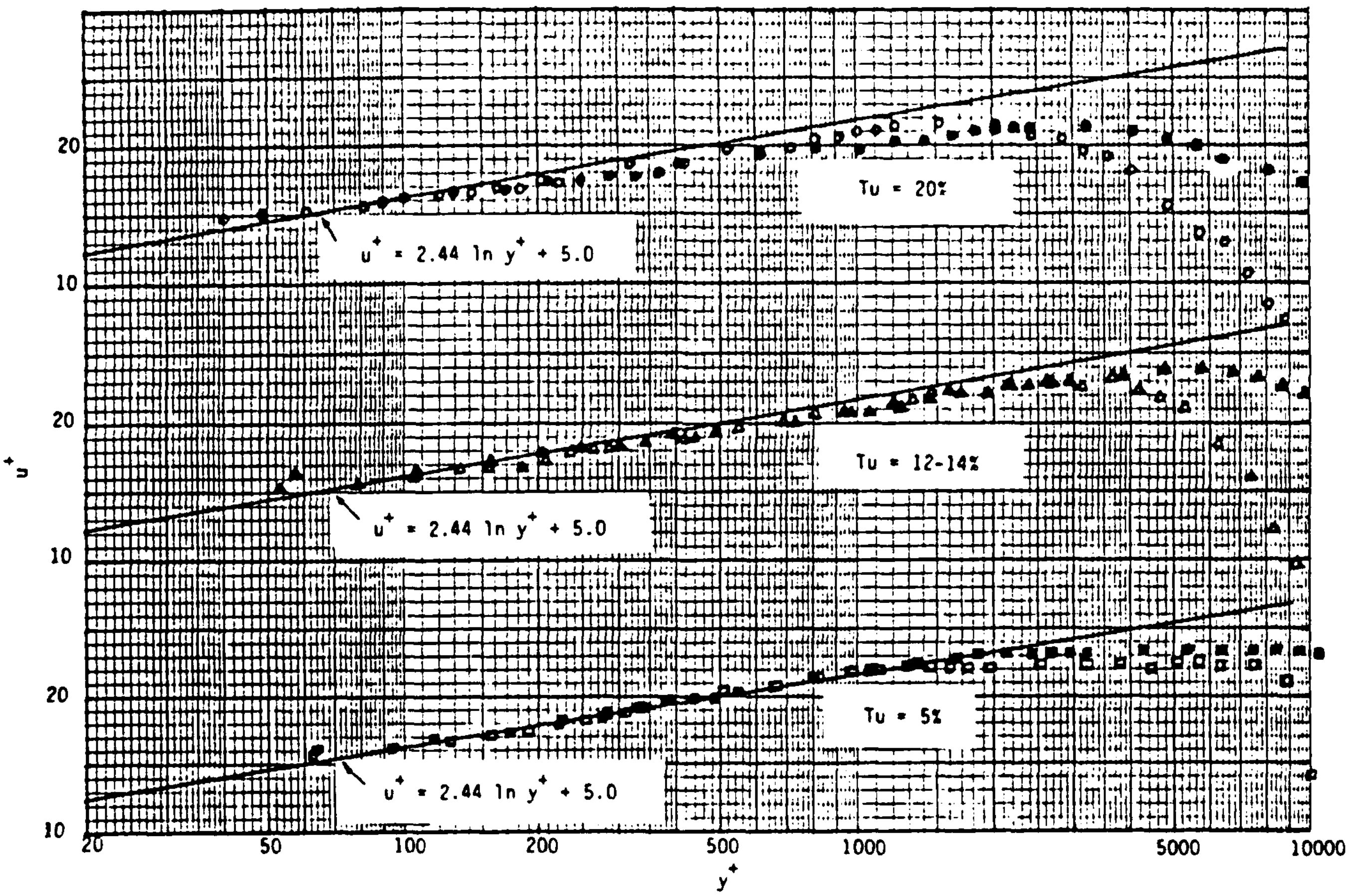

Figure 7. Log-law velocity profiles, (symbols are referred to Figure 5)

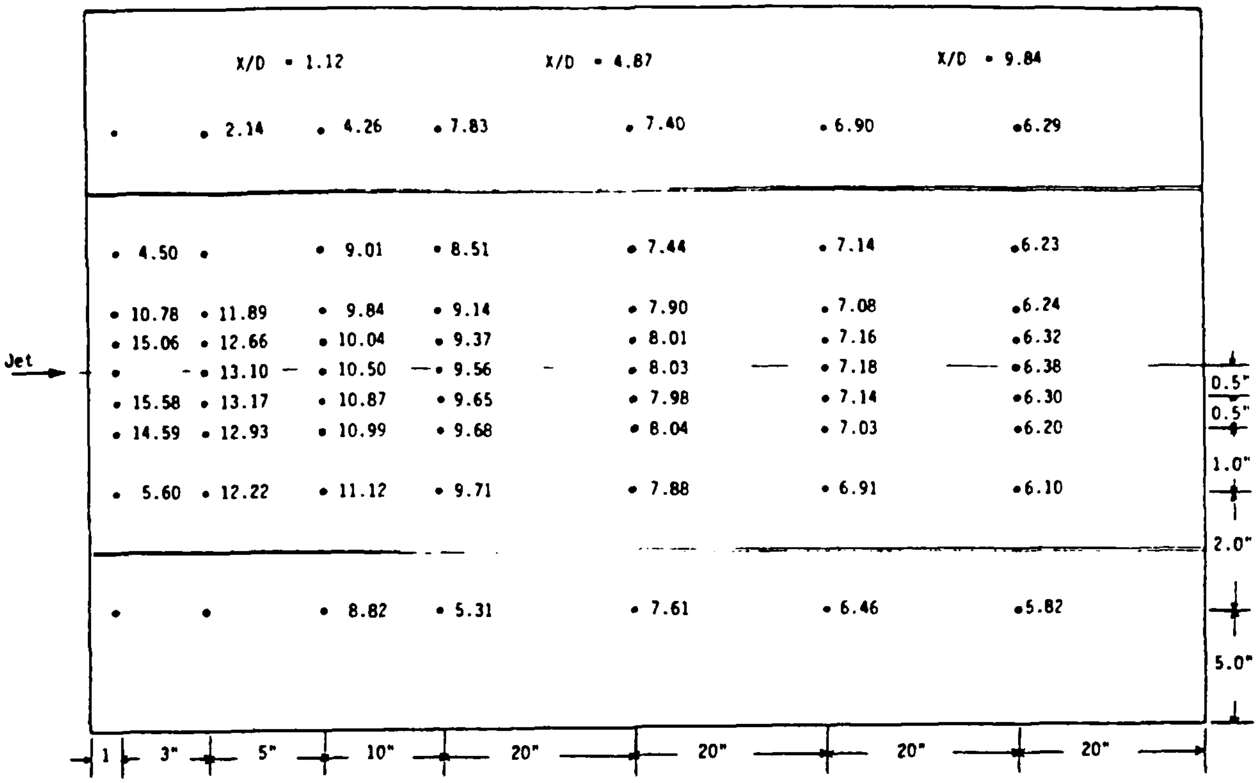

Figure 8. Local heat transfer coefficient distributions at jet velocity U_o = 62 fps, heat flux q" = 202.7 Btu/hr-ft^2-°F, jet temperature T_o = 83.2°F

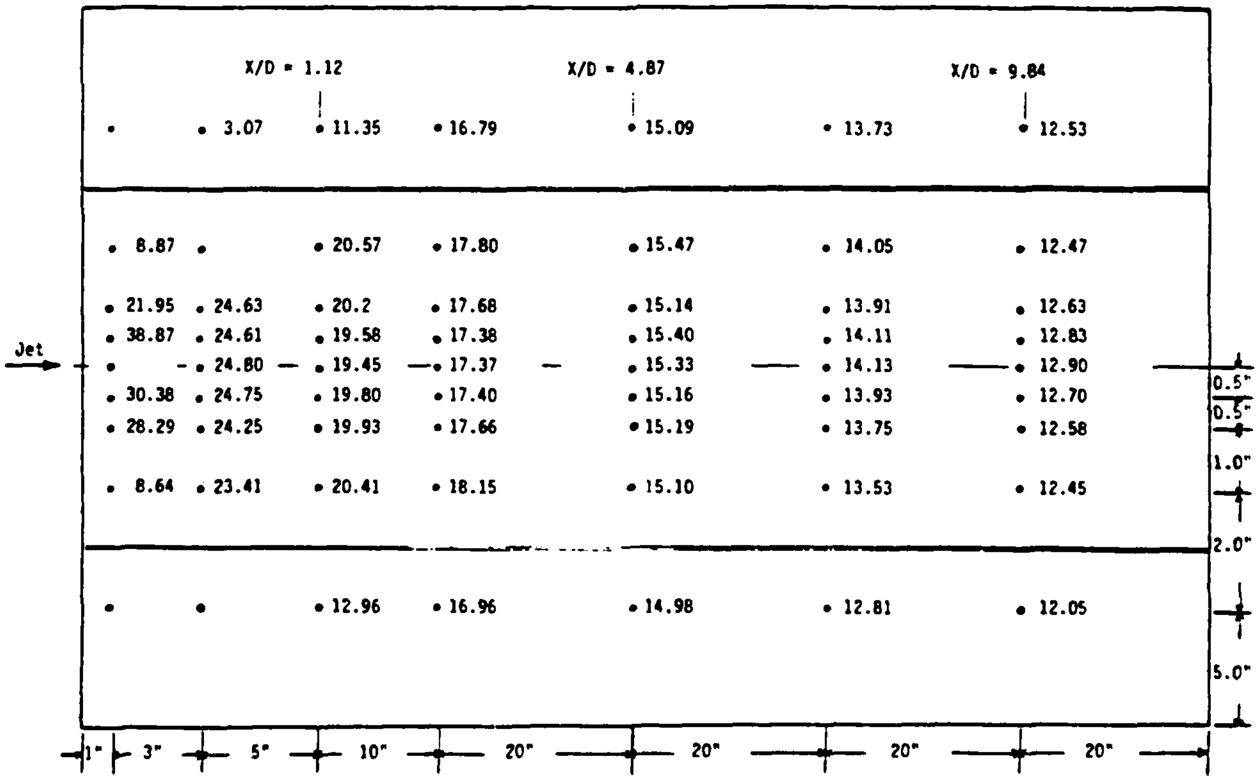

Figure 9. Local heat transfer coefficient distributions at jet velocity U_o = 110 fps, heat flux = 278.4 Btu/hr-ft^2-°F, jet temperature T_o = 80.3°F

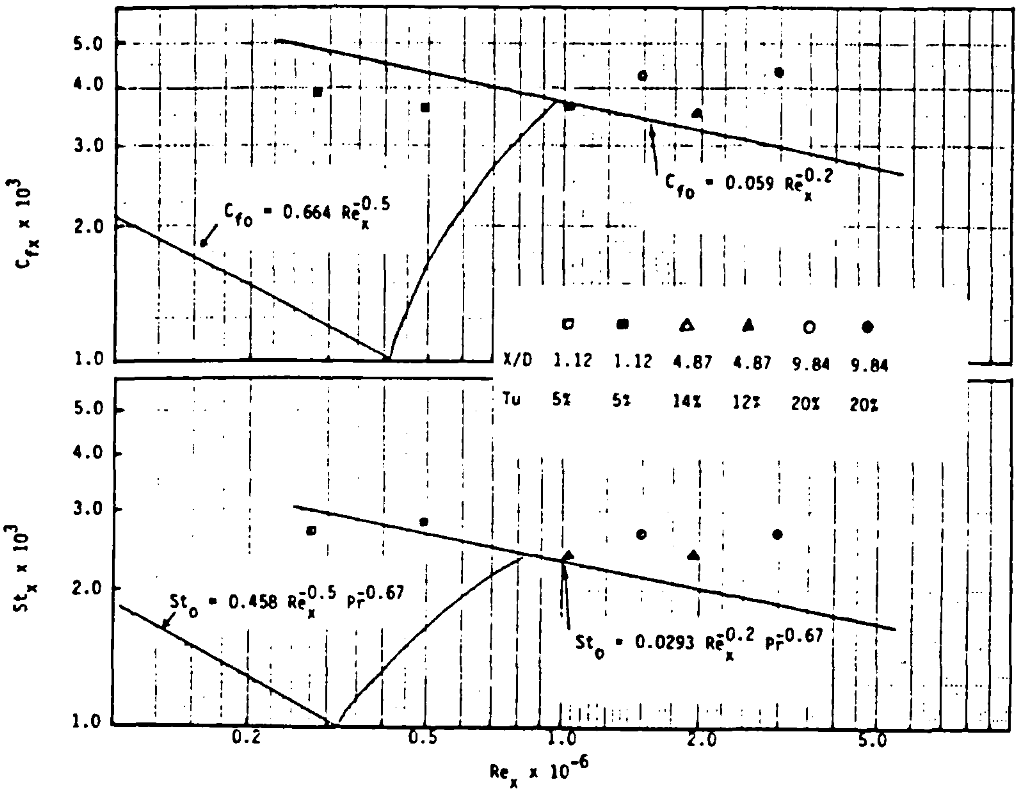

Figure 10. Friction factor and Stanton number vs Reynolds number

Table 1. Summary of test results: The first three rows data are for U_o = 62 fps, the second three rows data are for U_o = 110 fps, data in bracket are based on Laminar flow correlations

X/D	U_m fps	Tu %	Re_x $\times 10^6$	u^* fps	C_{fx} $\times 10^{-3}$	C_{fo} $\times 10^{-3}$	$(C_{fx}-C_{fo})/C_{fo}$ %	St_x $\times 10^{-3}$	St_o $\times 10^{-3}$	h_x B/HFF^2	$(St_x-St_o)/St_o$ %	$2St_x/St_o$
1.12	61.6	5	0.28	2.74	3.95	4.82 (1.26)	-18 (+213)	2.70	3.0 (0.79)	10.5 (3.06)	-10 (+242)	1.37
4.87	52.9	14	1.03	2.27	3.69	3.71	-5.4	2.41	2.31	8.03	+4.3	1.31
9.84	37.8	20	1.49	1.74	4.24	3.44	+23	2.68	2.15	6.38	+25	1.26
1.12	109	5	0.49	4.63	3.61	4.3 (0.95)	-16 (+280)	2.84	2.68 (0.6)	19.5 (4.1)	+6 (+373)	1.57
4.87	99.5	12	1.94	4.17	3.52	3.26	+8	2.44	2.03	15.3	+20	1.39
9.84	75.7	19	2.98	3.52	4.33	2.99	+45	2.70	1.87	12.9	+44	1.25

1985 USAF-UES SUMMER FACULTY RESEARCH PROGRAM

Sponsored by the

AIR FORCE OFFICE OF SCIENTIFIC RESEARCH

Conducted by the

UNIVERSAL ENERGY SYSTEMS, INC.

FINAL REPORT

A STUDY OF COPLANAR WAVEGUIDE AND ITS APPLICATION TO PHASED ARRAYS OF INTEGRATED CIRCUIT ANTENNAS

Prepared by:	Dr. Donald F. Hanson
Academic Rank:	Associate Professor
Department and University:	Department of Electrical Engineering University of Mississippi University, MS 38677
Research Location:	Rome Air Development Center EEA Hanscom AFB, MA 01731
USAF Research Contact:	Dr. Robert J. Mailloux

Date:	August 12, 1985
Contract No:	F49620-85-C-0013

A STUDY OF COPLANAR WAVEGUIDE AND ITS APPLICATION TO PHASED ARRAYS OF INTEGRATED CIRCUIT ANTENNAS

by

Donald F. Hanson

ABSTRACT

This report describes the current uses reported for coplanar waveguide (CPW). An extensive literature review on CPW is given. Particular emphasis on applications in the field of monolithic phased array antennas is made. A new quasi-TEM, quasi-static analytical solution for CPW is obtained and presented. A description of source modeling for coplanar radiating elements fed by CPW is given. Finally, techniques for modeling CPW in monolithic integrated circuit phased arrays are discussed.

ACKNOWLEDGEMENTS

The author would like to thank the personnel of RADC for providing a stimulating environment within which to work. He would like to especially thank Dr. Robert J. Mailloux for providing him with this opportunity and for suggesting this problem. He would like to acknowledge the sponsorship of the Air Force Systems Command and the Air Force Office of Scientific Research.

I. Coplanar Waveguide and Planar Structures

a) Introduction

Coplanar Waveguide uses the transmission line structure shown in Figure 1. The two outer half-planes are grounded and the signal is fed in on the center line. The thin metal structure is held in place by a dielectric half-space ($y < 0$) of dielectric constant $\epsilon_r \epsilon_0$. Its x-extent is from $0 \leq |x| < a$ and $|x| > b$. Two slots are present for $a < |x| < b$.

Coplanar waveguide (CPW) is used in many circuit applications because components can be mounted in either series or shunt. It is also especially convenient for three terminal active devices like FETs which require both shunt and series connections at the same location. The ground plane metalization then surrounds the device which makes low inductance connections to ground possible. This gives increased gain in an amplifier configuration. CPW also provides reliable microwave frequency interconnections on semiconductor surfaces for monolithic semiconductor integrated circuits. All microwave frequency interconnections can be made on a single coplanar surface. Recent work in slow-wave CPW structures has provided the ability to minimize the chip surface area required for transmission line application in exchange for increased attenuation down the line. Coplanar inductors and power FETs can be made using air bridge technology. Reliable methods for routing DC biasing lines over the CPW to the active device sites must be developed.

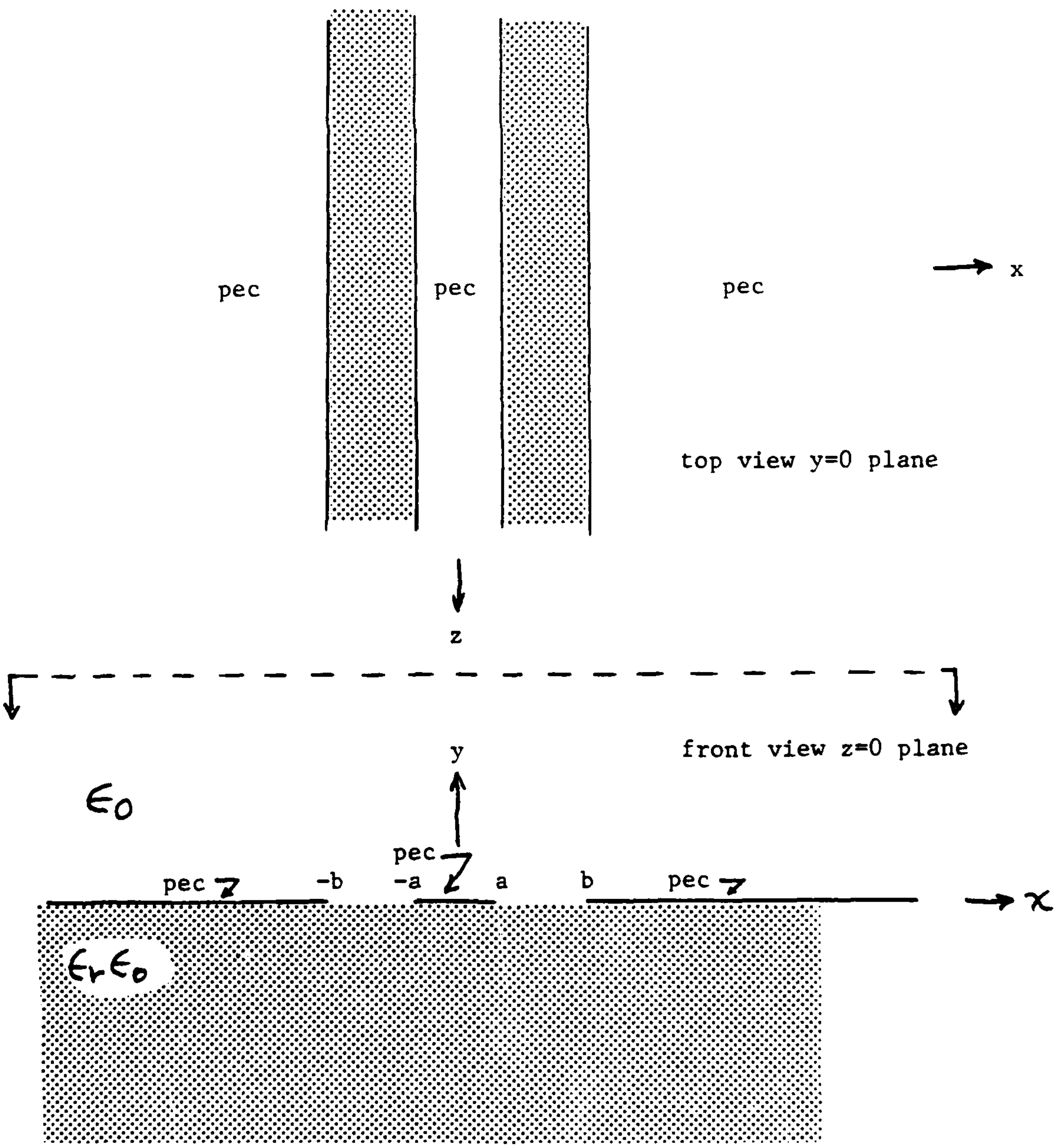

Figure 1. Coplanar Waveguide Geometry

b) Literature Review for CPW

C. P. Wen /1/ apparently first described CPW and calculated its characteristic impedance. Using conformal mapping techniques, he found it to be

$$Z_0 = \frac{\sqrt{\mu_0/\epsilon_0}}{4} \frac{1}{\sqrt{\frac{1+\epsilon_r}{2}}} \frac{K(k')}{K(k)}$$

$$k = \frac{a}{b} \qquad k' = \sqrt{1-\left(\frac{a}{b}\right)^2}$$

where K is the complete elliptical integral of the first kind. An excellent review of the pre-1979 literature on CPW is found in /2/. This list is not repeated here. The most recent literature on CPW applications, particularly relating to active devices, is described here. A recent text /3/, Applications of GaAs MESFETs, covers the use of coplanar waveguide on GaAs substrates. Pucel /4/ describes the use of CPW in monolithic microwave circuits and compares it with microstrip, coplanar strips, and slot line. He concludes that of the four, microstrip and CPW are best for GaAs monolithic circuits, but that microstrip is preferred. A recent (1983) book chapter /5/ on "Integrated Circuit Antennas" describes the use of CPW in integrated circuit antennas. They reference a large number of papers which are not repeated here.

Coplanar waveguide is an example of a planar structure to which planar theories, including duality and the Fourier Transformation, can

be applied. One recent paper /6/ looks at "Circuit Duals on Planar Transmission Media". Dual discontinuities between twin strip and CPW are illustrated. The spectral domain Green's function for planar structures has been developed /7,8/ and applied to CPW. A singular integral equation approach is used in two recent papers /9,10/ on generalized planar transmission lines.

The measurement of characteristic impedance Z_0 for CPW was done /11/ in 1971 and it closely followed the analytic result of /1/.

The properties of CPW and microstrip are compared for monolithic microwave integrated circuits (MICs) by Gopinath /12/. He concludes that the losses of the two are virtually the same. The dispersion characteristics of CPW with ferrite and dielectric media have been calculated /13,14/ using a spectral domain analysis.

Several types of CPW losses have been studied. Dielectric and conductor loss are evaluated for several CPW dimensions in /15,16/. Surface wave loss principles are described in /17/. Modifications to CPW have been proposed /18/ which reduce propagation losses.

The effect of inner conductor offset in CPW is examined by conformal mapping /19,20/ and by numerical finite differences /21/. The effect of placing a conductor backing on CPW has been examined using a full wave approach /22/ and a quasi-static numerical approach /23/. The authors of the former paper conclude that the conductor backing should be electrically connected to the top ground planes. Otherwise, propagation characteristics can be quite different than expected. In fact, two quasi-TEM modes can be supported.

The effects /24/ of finite conductor thickness have been

AD-A166 177 UNITED STATES AIR FORCE SUMMER FACULTY RESEARCH PROGRAM 03/15
1985 TECHNICAL RE.. (U) UNIVERSAL ENERGY SYSTEMS INC
DAYTON OH R C DARRAH ET AL. DEC 85 AFOSR-TR-86-0140
UNCLASSIFIED F49620-85-C-0013 F/G 5/1 NL

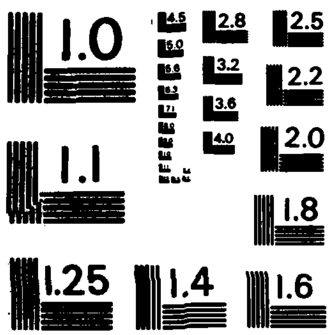

MICROCOPY RESOLUTION TEST CHART
NATIONAL BUREAU OF STANDARDS-1963-A

accounted for using a finite difference approach. A CPW with a multi-layer, anisotropic substrate has been studied /25,26/ using spectral domain techniques and the finite Fourier Transformation.

In the last three years, a new application for CPW structures has been developed by Itoh and others. This is the area of CPW on periodically doped semi-conducting substrates or on insulators above semiconductors. This provides a slow-wave structure which allows for miniaturization since lines of the same electrical length are physically shorter in the approach. A slow-wave CPW is made from a CPW underlaid with a periodically doped semiconductor substrate and Metal-Insulator-Semiconductor (MIS) or Schottky contact layers. In 1982, Bastida and others reported /27,28/ on a monolithic GaAs amplifier they fabricated which used slow-wave concepts. A photograph of their chip is shown in Figure 2. The use of CPW is evident. One CPW is seen to be crossed periodically. This slow wave structure on CPW is called Cross-Tie CPW (CTCPW).

Numerical analysis of slow-wave coplanar waveguide on periodically doped semiconductor substrates (CTCPW) has been carried out. Fukuoka and Itoh /29,30/ use Floquet's Theorem for periodic transmission lines to obtain their CTCPW solution. They have also studied Schottky periodic CTCPW /31,32/ for use as a variable slow-wave phase shifter. Jäger /33/ examines the nonlinear problem for Schottky periodic CTCPW.

CPW slow-wave devices made from Metal-Insulator-Semiconductor CPW (MISCPW) structures have been analyzed. The guide wavelength and attenuation for MISCPW have been calculated /34-38/ from .1 to 10 GHz.

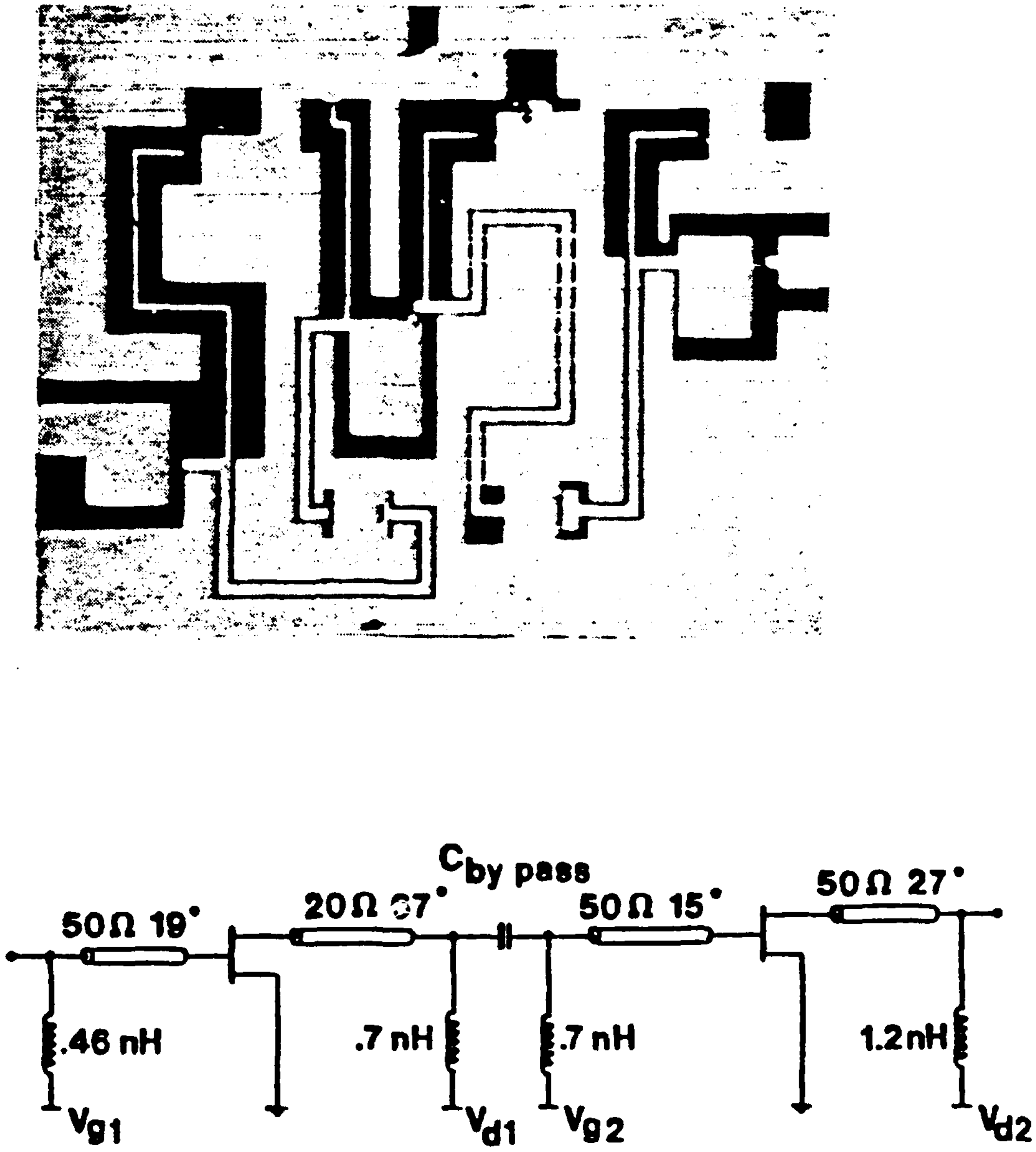

Figure 2. The Monolithic Amplifier and its Equivalent Circuit

(12th European Microwave Conference Proceedings 1982, p. 261)

for several cases. It thus appears that CPW can be used to make phase shifters and attenuators as well as to reduce size.

Conformal mapping techniques are used to analyze a CPW on GaAs with Ku-Band switchable attenuation /39/. The center conductor is forward biased to provide a large attenuation and reverse biased to provide a low attenuation. Coplanar waveguide has also been used in the design of an optically-controlled MIC phase shifter /40/, and a 22 to 24 GHz. amplifier /41/.

CPW has been used as the basis for microwave components. A computational approach for the characterization of CPW MICs has been proposed /42/ and applied to finding end inductance in CPW. The development of CPW resonators and Q-factor evaluation is given /43/ using equivalent transmission line models in the spectral domain. CPW has been used to make coplanar baluns /44,45/, coaxial test fixtures /46/, and non-reciprocal devices /47/. CPW has even been used as a microwave optical modulator /48/. Williams and Schwarz /49/ give more references for CPW components and themselves analyze CPW bandpass filters. Mixers which can easily interface with CPW are given in /50-52/ for 10 GHz and 33 GHz. W-band (75 to 110 GHz) mixers and components have been reported /53,54/ in 1985.

A final important area is CPW interfacing. Packaging using CPW input to Ultra-high speed GaAs digital integrated circuits is described /55/. Mounting external microwave components on CPW /56,57/ and matching to a coaxial input /57/ have been discussed. In one study, researchers /58/ reported interfacing microstrip to CPW. Another /59/ computes microstrip/CPW coupling characteristics. A broadband CPW-

slotline transition has been reported /60/ and experimental results presented.

II. The Quasi-Static Fields Surrounding Coplanar Waveguide

In doing the preceding literature search, it became evident that analytic expressions for the quasi-static $\vec{E}$ and $\vec{H}$ fields surrounding the conductors in CPW had apparently not been reported. Collin and Kretch /61/ recently proposed a perturbation theory for microstrip which is equally valid for CPW. This technique can be used to obtain higher order corrections to the quasi-static field expressions derived here.

The problem to be solved is shown in Figure 1. The structure is uniform in the z-direction. A free-space half-space and a dielectric half-space exist for $y > 0$ and $y < 0$, respectively. The $y=0$ plane contains a perfect electrical conducting (pec) plane for $0 < |x| < a$ and $|x| > b$. Two slots appear for $a < |x| < b$. The structure is symmetrical with respect to $x=0$.

The quasi-static electric field is present when the center conductor is held at one volt (or V volts) with respect to the ground planes which are held at zero potential. The quasi-static magnetic field is present when a total current of 1 Amp (or I Amps) is passing through the center conductor into the paper. The capacitance per unit length, C, and the inductance per unit length, L, can be determined from

the resulting electric charge and magnetic flux distributions, respectively. The characteristic impedance is then given by

$$Z_0 = \sqrt{\frac{L}{C}}$$

Wen /1/ and others use conformal mapping to avoid the computation of the field expressions themselves. Analytic field expressions in x-y space are found here.

a) Electric and Magnetic Potentials

Since a quasi-TEM wave is sought, all fields, potentials, and charge and current distributions are assumed to vary with $e^{-j\beta z}$ z-dependence and $e^{j\omega t}$ time dependence. The fields, potentials, and charge and current distributions are then

$$\vec{E}(x,y,z) = \vec{E}(x,y)\, e^{-j\beta z}$$
$$\vec{H}(x,y,z) = \vec{H}(x,y)\, e^{-j\beta z}$$
$$\phi(x,y,z) = \phi(x,y)\, e^{-j\beta z}$$
$$\vec{A}(x,y,z) = \vec{A}(x,y)\, e^{-j\beta z}$$
$$\rho(x,y,z) = \rho(x,y)\, e^{-j\beta z}$$
$$\vec{J}(x,y,z) = \vec{J}(x,y)\, e^{-j\beta z}$$

The propagation constant β is unknown and is found later.

A quasi-TEM wave is a case of TM propagation where $H_z = 0$ and where E_z is not necessarily zero. The fields can then be written in terms of transverse (t) and longitudinal (z) components as

$$\vec{H} = \vec{H}_t$$
$$\vec{E} = \vec{E}_t + \hat{z} E_z$$

For TM waves, the H field can be related to a vector potential A so that $H_z = 0$ automatically by

$$\vec{H} = \nabla \times \vec{A}$$

Maxwell's equations are

$$\nabla \times \vec{H} = j\omega\epsilon \vec{E} + \vec{J}$$
$$-\nabla \times \vec{E} = j\omega\mu \vec{H}$$

Substituting $\vec{H} = \nabla \times \vec{A}$ in the second equation, one obtains

$$\nabla \times (\vec{E} + j\omega\mu \vec{A}) = 0$$

or

$$\vec{E} = -\nabla\phi - j\omega\mu \vec{A}$$

Substituting this and $\vec{H} = \nabla \times \vec{A}$ in the first equation, one derives

$$(\nabla^2 + k^2)\vec{A}(x,y,z) = -\vec{J} + \nabla(\nabla \cdot \vec{A} + j\omega\epsilon\phi)$$

If one uses the Lorentz Gauge given by

$$\nabla \cdot \vec{A} + j\omega\epsilon\phi = 0,$$

one obtains the wave equation for $\vec{A}$ given by

$$\nabla^2 \vec{A} + k^2 \vec{A}(x,y,z) = -\vec{J}$$

Since only a z-component of current J_z exists, the vector potential $\vec{A}$ likewise has only a z-component. Therefore,

$$\vec{A}(x,y,z) = \hat{z} A_z(x,y) e^{-j\beta z}$$

The Lorentz Gauge condition can now be written as

$$-j\beta A_z(x,y) e^{-j\beta z} + j\omega\epsilon\, \phi(x,y) e^{-j\beta z} = 0$$

Therefore, the Lorentz Gauge requires that

$$A_z(x,y) = \frac{\omega\epsilon}{\beta} \phi(x,y)$$

This important condition relates the electric and magnetic potentials, ϕ and A_z, respectively. Taking the divergence of $\vec{E}$, one obtains

$$\nabla \cdot \vec{E} = \rho/\epsilon = -\nabla^2\phi - j\omega\mu\, \nabla \cdot \vec{A}$$

Applying the Lorentz condition again, the equation becomes

$$\nabla^2\phi + k^2 \phi(x,y,z) = -\rho(x,y,z)/\epsilon$$

Taking the Laplacian of $\phi(x,y,z)$, one obtains

$$\nabla^2 \phi(x,y,z) = e^{-j\beta z}(\nabla_t^2 - \beta^2)\,\phi(x,y)$$

where ∇_t^2 is the transverse Laplacian $\nabla_t^2 = \frac{\partial^2}{\partial x^2} + \frac{\partial^2}{\partial y^2}$. The wave equations for ϕ and A_z become

$$\left[\nabla_t^2 + (k^2 - \beta^2)\right]\phi(x,y) = -\rho(x,y)/\epsilon$$

$$\left[\nabla_t^2 + (k^2 - \beta^2)\right]A_z(x,y) = -J_z(x,y)$$

The current and charge densities J_z and ρ exist on the y=0 plane and are zero elsewhere. For a quasi-static approximation, we can neglect the $(k^2 - \beta^2)$ terms. More detailed analysis /61/ verifies this. Therefore, the electric and magnetic potentials satisfy Laplace's equation

$$\left.\begin{aligned} \nabla_t^2 A_z(x,y) &= 0 \\ \nabla_t^2 \phi(x,y) &= 0 \end{aligned}\right. \qquad y \neq 0$$

off of the y=0 plane subject to the boundary conditions that $\vec{E}$ tangential and $\vec{H}$ normal be zero on the metal, $\vec{E}$ and $\vec{H}$ tangential be continuous through the slots and $\vec{B}$ and $\vec{D}$ normal be continuous through the slots. The potentials also must go to zero as $\sqrt{x^2 + y^2}$ goes to infinity. The fields are found from

$$\vec{E}_t(x,y) = -\nabla_t \phi(x,y)$$

$$E_z(x,y) = \frac{1}{j\omega\epsilon}(k^2-\beta^2)A_z(x,y)$$

$$\vec{H}_t(x,y) = \nabla_t A_z(x,y) \times \hat{z}$$

$$H_z(x,y) = 0$$

provided the Lorentz Gauge condition is satisfied. Since ϵ and k are discontinuous across the y=0 plane, the second equation can be specified to the half space of applicability. The superscripts $>$ and $<$, respectively, refer to the quantities valid for $y > 0$ and $y < 0$, respectively. Therefore,

$$E_z^{>}(x,y) = \frac{1}{j\omega\epsilon^{>}}\left\{(k^{>})^2-\beta^2\right\}A_z^{>}(x,y)$$

$$E_z^{<}(x,y) = \frac{1}{j\omega\epsilon^{<}}\left\{(k^{<})^2-\beta^2\right\}A_z^{<}(x,y)$$

Similarly, the transverse fields are

$$\vec{E}_t^{\gtrless}(x,y) = -\nabla_t \phi^{\gtrless}(x,y)$$

$$\vec{H}_t^{\gtrless}(x,y) = \nabla_t A_z^{\gtrless}(x,y) \times \hat{z}$$

These expressions are valid provided the Lorentz Gauge condition

$$A_z^{\gtrless}(x,y) = \frac{\omega\epsilon^{\gtrless}}{\beta}\phi^{\gtrless}(x,y)$$

is satisfied. If $k^{<} > k^{>}$, then the propagation constant β, as yet unknown satisfies the following equation

$$k^{>} \leq \beta \leq k^{<}$$

When the dielectric half-space is replaced by free space, then $k^{>} = k^{<} = \beta$ and one has the usual TEM case where $E_z = H_z = 0$. Under this condition, the Lorentz Gauge condition is always satisfied.

b) CPW Quasi-Static Fields

The fields are found from the potentials so the potentials are solved for first. The electric potential satisfies

$$\left(\frac{\partial^2}{\partial x^2} + \frac{\partial^2}{\partial y^2}\right) \phi^{\gtrless}(x,y) = 0 \qquad y \neq 0$$

Applying the separation of variables, one has

$$\phi(x,y) = X(x)\, Y(y)$$

Substituting this in Laplace's equation, one obtains

$$\frac{1}{X} X'' + \frac{1}{Y} Y'' = 0$$

Let $Y''/Y = u^2$. Then $X''/X = -u^2$. The solutions of these equations, substituted in $\phi = XY$, gives

$$\phi(x,y) = (A_1 e^{-uy} + A_2 e^{uy})(B_1 \cos(ux) + B_2 \sin(ux))$$

No limitation has been placed on u so, in general, one can integrate

over all values

$$\phi(x,y) = \int_{u=0}^{\infty} (A_1(u)e^{-uy} + A_2(u)e^{uy})(B_1(u)\cos(ux) + B_2(u)\sin(ux))du$$

ϕ is an even function of x so $B_2(u) = 0$. To meet the requirement that ϕ goes to zero as $\sqrt{x^2 + y^2}$ goes to infinity, $A_2(u)$ is chosen to be zero for $y > 0$ and $A_1(u)$ is zero for $y < 0$. In general, then, one can express ϕ in the form

$$\phi^{>}(x,y) = \int_0^{\infty} u^{-2\alpha} A(u)\, e^{-uy} \cos ux \; du$$

$$\phi^{<}(x,y) = \int_0^{\infty} u^{-2\alpha} B(u)\, e^{uy} \cos ux \; du$$

α is a constant which one can choose at will. Similarly, the magnetic potential can be written

$$A_z^{>}(x,y) = \int_0^{\infty} u^{-2\alpha} C(u)\, e^{-uy} \cos ux \; du$$

$$A_z^{<}(x,y) = \int_0^{\infty} u^{-2\alpha} D(u)\, e^{uy} \cos ux \; du$$

The boundary conditions in the slots $a < |x| < b$ can now be written as

$$\left.\frac{\partial \phi^{>}}{\partial x}\right|_{y=0} = \left.\frac{\partial \phi^{<}}{\partial x}\right|_{y=0} \qquad \left.\frac{\partial \phi^{>}}{\partial y}\right|_{y=0} = \epsilon_r \left.\frac{\partial \phi^{<}}{\partial y}\right|_{y=0}$$

$$\left.\frac{\partial A_z^{>}}{\partial x}\right|_{y=0} = \left.\frac{\partial A_z^{<}}{\partial x}\right|_{y=0} \qquad \left.\frac{\partial A_z^{>}}{\partial y}\right|_{y=0} = \left.\frac{\partial A_z^{<}}{\partial y}\right|_{y=0}$$

Application of the first condition on each line gives

$$A(u) = B(u) \qquad \text{and} \qquad C(u) = D(u)$$

Application of the second condition on each line gives, respectively,

$$(1+\epsilon_r)\int_0^{\infty} u^{1-2\alpha} A(u) \cos ux \, du = 0 \qquad a<|x|<b$$

$$2\int_0^{\infty} u^{1-2\alpha} C(u) \cos ux \, du = 0 \qquad a<|x|<b$$

Since $\vec{E}$ tangential and $\vec{H}$ normal must be zero on the metal, one has

$$E_x = -\frac{\partial \phi}{\partial x}(x,0) = 0 \qquad \begin{array}{l} 0<|x|<a \\ b<|x| \end{array}$$

$$H_y = -\frac{\partial A_z}{\partial x}(x,0) = 0 \qquad \begin{array}{l} 0<|x|<a \\ b<|x| \end{array}$$

Therefore, the potentials on the metal must be

$$\phi(x,0) = \text{constant or zero}$$

$$A_z(x,0) = \text{constant or zero}$$

To be valid in the static case, the potentials are chosen to be zero for $|x| > b$ and $y=0$ and constant, ϕ_0 and A_0, respectively, for $0 \leq |x| < a$ and $y=0$. One then arrives at the triple integral equation for Fourier coefficient A(u)

$$\int_0^\infty u^{-2\alpha} A(u) \cos ux \, du = \phi_0 \qquad 0 \leq |x| < a$$

$$\int_0^\infty u^{1-2\alpha} A(u) \cos ux \, du = 0 \qquad a < |x| < b$$

$$\int_0^\infty u^{-2\alpha} A(u) \cos ux \, du = 0 \qquad b < |x| < \infty$$

Similarly, one obtains the triple integral equation for C(u) to be

$$\int_0^\infty u^{-2\alpha} C(u) \cos ux \, du = A_0 \qquad 0 \leq |x| < a$$

$$\int_0^\infty u^{1-2\alpha} C(u) \cos ux \, du = 0 \qquad a < |x| < b$$

$$\int_0^\infty u^{-2\alpha} C(u) \cos ux \, du = 0 \qquad b < |x| < \infty$$

Since the form of these sets of integral equations is identical, the solution for C(u) is easily obtained by substituting A_0 for ϕ_0. For $\alpha = \frac{1}{2}$, the triple integral equations become

$$\int_0^\infty u^{-1} A(u) \cos ux \, du = \phi_0 \qquad 0 \le |x| < a$$

$$\int_0^\infty A(u) \cos ux \, du = 0 \qquad a < |x| < b$$

$$\int_0^\infty u^{-1} A(u) \cos ux \, du = 0 \qquad b < |x| < \infty$$

Equations of this type have been discussed by Sneddon /62/. The third integral equation can be automatically satisfied if A(u) is chosen to be represented by the series

$$A(u) = \sum_{n=0}^{\infty} a_n J_{2n+1}(bu)$$

where the coefficients a_n are unknown and $J_{2n+1}(z)$ is the Bessel function of order 2n+1. The third equation is satisfied by virtue of the discontinuous Weber-Schafheitlin integral /63/

$$\int_0^\infty u^{-1} J_{2n+1}(bu) \cos ux \, du = \begin{cases} \frac{1}{2n+1} \cos\left\{(2n+1)\sin^{-1}\frac{x}{b}\right\} & |x| \le b \\ 0 & |x| \ge b \end{cases}$$

This can also be written in terms of Chebyshev polynomials since

$$\cos(2n+1)\sin^{-1}\frac{x}{b} = (-)^n \sqrt{1-\left(\frac{x}{b}\right)^2}\, U_{2n}(x/b)$$

where U_{2n} is the Chebyshev polynomial of the second kind. Substituting the Bessel function series in the first two equations and integrating, one obtains

$$\sum_{n=0}^{\infty} a_n \frac{1}{2n+1} \cos\left\{(2n+1)\sin^{-1}\frac{x}{b}\right\} = \phi_0 \qquad 0 \le |x| < a$$

$$\sum_{n=0}^{\infty} a_n \cos\left\{(2n+1)\sin^{-1}\frac{x}{b}\right\} = 0 \qquad a < |x| < b$$

The last equation is obtained by using the integral /63/

$$\int_0^{\infty} J_{2n+1}(bu) \cos xu \, du =$$

$$= \begin{cases} \dfrac{\cos\left\{(2n+1)\sin^{-1}\frac{x}{b}\right\}}{\sqrt{b^2-x^2}} & x < b \\ \infty \text{ or } 0 & x = b \\ \dfrac{-b^{2n+1}(-)^n}{\sqrt{x^2-b^2}\left(x+\sqrt{x^2-b^2}\right)^{2n+1}} & x > b \end{cases}$$

The triple integral equation has been converted to a dual series

equation /62/.

Before proceeding, it is easier if one makes the following substitutions

$$\frac{x}{b} = \sin\frac{\theta}{2}$$

and
$$\frac{a}{b} = \sin\frac{\phi}{2}$$

The dual series equation becomes

$$\sum_{n=0}^{\infty} a_n \frac{1}{n+\frac{1}{2}} \cos(n+\tfrac{1}{2})\theta = 2\phi_0 \qquad 0 \le \theta < \phi$$

$$\sum_{n=0}^{\infty} a_n \cos(n+\tfrac{1}{2})\theta = 0 \qquad \phi < \theta \le \pi$$

Sneddon /62, p. 165/ shows that this equation has the solution

$$a_n = \frac{2\, P_n(\cos\phi)}{K(\cos\frac{\phi}{2})}\,\phi_0$$

where $P_n(x)$ is the Legendre polynomial and $K(k)$ is the complete elliptic integral of the first kind with $k' = \cos\frac{\phi}{2} = \sqrt{1 - (\frac{a}{b})^2}$. If one makes $k = a/b$, then

$$a_n = \frac{2\, P_n(\cos\phi)}{K'(\frac{a}{b})}\,\phi_0$$

The potential then becomes

$$\phi(x,y) = \phi_0 \int_0^{\infty} u^{-1} \left\{ \sum_{n=0}^{\infty} \frac{2 P_n(\cos\phi)}{K'(\frac{a}{b})} J_{2n+1}(bu) \right\} e^{-u|y|} \cos ux \, du$$

This can be written in a number of forms. The following integral can be used /63/

$$\int_0^{\infty} u^{-1} J_{2n+1}(bu) e^{-u\alpha} du =$$

$$= \frac{1}{2n+1} \left[\frac{b}{\alpha + \sqrt{\alpha^2 + b^2}} \right]^{2n+1}$$

$$= \Gamma(2n+1) P_0^{-(2n+1)} \left[\alpha(\alpha^2+b^2)^{-\frac{1}{2}} \right]$$

The potential then becomes

$$\phi(x,y) = 2\phi_0 \frac{1}{K'(\frac{a}{b})} \sum_{n=0}^{\infty} \frac{P_n(\cos[2\sin^{-1}\frac{a}{b}])}{2n+1} \times$$

$$\times \left\{ \left(\frac{b}{y - \gamma x + \sqrt{(y-\gamma x)^2 + b^2}} \right)^{2n+1} + \left(\frac{b}{y + \gamma x + \sqrt{b^2 + (y+\gamma x)^2}} \right)^{2n+1} \right\}$$

An integral expression for $\phi(x,y)$ can be found also.

The Bessel function of order 2n+1, n=0,1, $\cdots$, can be written in integral form as

$$J_{2n+1}(x) = \frac{1}{\pi}\int_0^{\pi} \sin(x \sin\theta)\ \sin(n + \tfrac{1}{2})\theta\ d\theta$$

Substituting this in the expression for $\phi(x,y)$ given at the top of the last page results in the following expression for electric potential

$$\phi(x,y) = \frac{2\phi_0}{\pi K'(\frac{a}{b})}\int_0^{\infty} u^{-1}\int_0^{\pi} \sin(bu \sin\tfrac{\theta}{2}) \sum_{n=0}^{\infty} P_n(\cos\phi)\sin(n+\tfrac{1}{2})\theta\, d\theta \cdot e^{-u|y|}\cos ux\, du$$

An analytical expression for the series has been given by Sneddon /62, p. 59/. It is

$$\sum_{n=0}^{\infty} P_n(\cos\phi)\sin(n+\tfrac{1}{2})\theta = \frac{1}{\sqrt{2}}\frac{H(\theta-\phi)}{\sqrt{\cos\phi - \cos\theta}}$$

$$0 < \theta, \phi < \pi$$

H(x) is the Heaviside unit step and is zero for $x < 0$ and one for $x > 0$. The potential can now be written

$$\phi(x,y) = \frac{2\phi_0}{\pi K'(\frac{a}{b})}\int_0^{\infty} u^{-1}\int_0^{\pi} \frac{1}{\sqrt{2}}\frac{H(\theta-\phi)\sin(bu\sin\frac{\theta}{2})}{\sqrt{\cos\phi-\cos\theta}}\,d\theta\ e^{-u|y|}\cos ux\, du$$

The inner integral becomes

$$\frac{1}{2}\int_{\phi}^{\pi} \frac{\sin(bu \sin\frac{\theta}{2})}{\sqrt{\sin^2\frac{\theta}{2} - \sin^2\frac{\phi}{2}}}\, d\theta = \int_0^1 \frac{\sin(bu\sqrt{1-k'^2t^2})}{\sqrt{1-k'^2t^2}\,\sqrt{1-t^2}}\, dt$$

where $k' = \cos\frac{\phi}{2}$ as before. By using the complex exponential expansion for cos ux and combining this with $e^{-u|y|}$, one obtains

$$\phi(x,y) = \frac{\phi_0}{\pi K'(\frac{a}{b})}\int_0^1 \frac{1}{\sqrt{1-k'^2t^2}\,\sqrt{1-t^2}}\int_0^\infty \sin(bu\sqrt{1-k'^2t^2}) \times$$

$$\left(e^{-u(y-jx)} + e^{-u(y+jx)}\right)\frac{du}{u}\, dt$$

The infinite integral can be evaluated using the integral

$$\int_0^\infty \frac{1}{u}\sin u\alpha\, e^{-u\beta}\, du = \tan^{-1}\left(\frac{\alpha}{\beta}\right) \qquad \beta \neq 0$$

The potential integral now becomes

$$\phi(x,y) = \frac{\phi_0}{\pi K'(\frac{a}{b})}\int_0^1 \frac{\tan^{-1}\left(\frac{b\sqrt{1-k'^2t^2}}{y-jx}\right) + \tan^{-1}\left(\frac{b\sqrt{1-k'^2t^2}}{y+jx}\right)}{\sqrt{1-k'^2t^2}\,\sqrt{1-t^2}}\, dt$$

Using the standard integral /63/

$$\int_0^1 \frac{\tan^{-1}\left(\tan\lambda\sqrt{1-k^2x^2}\right)}{\sqrt{1-k^2x^2}\,\sqrt{1-x^2}}\,dx = \frac{\pi}{2}F(\lambda, k),$$

the potential becomes

$$\phi(x,y) = \frac{\varphi_0}{2K'(\frac{a}{b})}\left\{F\left(\tan^{-1}\left[\left(\frac{y}{b} - j\frac{x}{b}\right)^{-1}\right], k'\right)\right.$$

$$\left. + F\left(\tan^{-1}\left[\left(\frac{y}{b} + j\frac{x}{b}\right)^{-1}\right], k'\right)\right.$$

where

$$F(\varphi, k) = \int_0^{\varphi} \frac{d\theta}{\sqrt{1 - k^2\sin^2\theta}}$$

$$= \int_0^{\sin\varphi} \frac{ds}{\sqrt{1-k^2s^2}\,\sqrt{1-s^2}}$$

The potential can then be written as

$$\phi(x,y) = \frac{\phi_0}{2K'(\frac{a}{b})}\left\{\int_0^{b(b^2+(y-jx)^2)^{-\frac{1}{2}}} \frac{ds}{\sqrt{1-k'^2s^2}\,\sqrt{1-s^2}} + \int_0^{b(b^2+(y+jx)^2)^{-\frac{1}{2}}} \frac{ds}{\sqrt{1-k'^2s^2}\,\sqrt{1-s^2}}\right\}$$

This will apparently reduce to a single elliptic integral with real argument after using transformation formulas given by Byrd and Friedman /63a/. Another integral expression for the potential can be found

to be

$$\phi(x,y) = \frac{\phi_0}{2} - \frac{\phi_0}{K'(\frac{a}{b})}\frac{1}{\pi}\int_0^{\frac{\pi}{2}} \frac{\tan^{-1}\left(\frac{\rho^2 - b^2\Delta^2}{2b|y|\Delta}\right)}{\Delta}\, d\theta$$

where $\Delta = \sqrt{1 - k'^2 \sin^2\theta}$, $\rho^2 = x^2 + y^2$, and $k' = \cos\frac{\phi}{2}$.

An expression for $A_z(x,y)$ can be found by replacing ϕ_0 by A_0. The quasi-static fields are then found from

$$\vec{E}_t(x,y) = -\nabla_t\,\phi(x,y)$$

$$\vec{H}_t(x,y) = \nabla_t A_z(x,y) \times \hat{z}$$

The evaluation of these fields is straight-forward by differentiation.

In order to compute capacitance and inductance per unit length, the fields at y=0 need to be found. The original integrals are used to determine these fields. Using the fact that

$$\int_0^{\infty} u^{-1} \sin u\alpha \, du = \frac{\pi}{2}\,\mathrm{sgn}(\alpha),$$

one obtains

$$\int_0^{\infty} u^{-1} \sin\left(bu \sin\frac{\theta}{2}\right) \cos ux \, du = \frac{\pi}{2} H\left(b \sin\frac{\theta}{2} - x\right)$$

The integral for the potential at y=0 then becomes

$$\phi(x,0) = \frac{\phi_0}{K'(\frac{a}{b})}\frac{1}{\sqrt{2}}\int_0^{\pi} H\left(b\sin\frac{\theta}{2} - x\right)\frac{H(\theta-\phi)}{\sqrt{\cos\phi - \cos\theta}}\,d\theta$$

After changing variables three times ($\eta = \sin\frac{\theta}{2}$, $s = \sqrt{1-\eta^2}$, and $t = s/\sqrt{1-(a/b)^2}$), one obtains the result

$$\phi(x,0) = \begin{cases} \phi_0 & 0 \le |x| < a \\ \dfrac{\phi_0}{K'(\frac{a}{b})} F\left(\sin^{-1}\sqrt{\dfrac{1-(x/b)^2}{1-(a/b)^2}}, k'\right) & a < |x| < b \\ 0 & b < |x| < \infty \end{cases}$$

where F is the incomplete elliptic integral of the first kind and $k' = \sqrt{1-(a/b)^2}$. Note that this satisfies the boundary conditions on the metal. The tangential electric field in the slot can now be found.

$$E_x = -\frac{\partial\phi}{\partial x} = -\frac{\phi_0}{K'(\frac{a}{b})}\frac{\partial}{\partial x} F\left(\sin^{-1}\sqrt{\frac{1-(x/b)^2}{1-(a/b)^2}}, k'\right)$$

$$= \frac{b\,\phi_0}{k' K'(\frac{a}{b})}\frac{\operatorname{sgn}(x)}{\sqrt{(x^2-a^2)(b^2-x^2)}} \qquad a < |x| < b$$

The electric field has square root singularities at the slot edges as expected /65/. The normal magnetic field in the slot can be shown to

have the same behavior.

The y-component of electric field on the y=0 plane can be found from the $\partial\phi/\partial y$. Taking the $\partial/\partial y$ of the double integral for $\phi(x,y)$ and setting y=0, one obtains

$$\left.\frac{\partial\phi}{\partial y}\right|_{y=0} = \frac{-\operatorname{sgn}(y)\,\phi_0\,2}{\pi K'\left(\frac{a}{b}\right)} \int_0^{\pi} \frac{1}{\sqrt{2}} \int_0^{\infty} \sin\left(bu\sin\frac{\theta}{2}\right)\cos ux\,du \times \frac{H(\theta-\phi)}{\sqrt{\cos\phi-\cos\theta}}\,d\theta$$

The sgn(y) remains to differentiate between the $y=0^+$ and $y=0^-$ cases. The infinite integral can be shown to be /64/

$$\int_0^{\infty} \sin\left(bu\sin\frac{\theta}{2}\right)\cos ux\,du = \frac{-b\sin\frac{\theta}{2}}{x^2-b^2\sin^2\frac{\theta}{2}}$$

The $\partial\phi/\partial y$ then becomes

$$\left.\frac{\partial\phi}{\partial y}\right|_{y=0} = \frac{\operatorname{sgn}(y)\,\phi_0}{\pi K'\left(\frac{a}{b}\right)} \int_{\phi}^{\pi} \frac{b\sin\frac{\theta}{2}}{x^2-b^2\sin^2\frac{\theta}{2}} \frac{d\theta}{\sqrt{\sin^2\frac{\theta}{2}-\sin^2\frac{\phi}{2}}}$$

After several changes of variable, this becomes

$$\left.\frac{\partial\phi}{\partial y}\right|_{y=0} = \frac{2}{\pi}\frac{b\,\phi_0}{K'\left(\frac{a}{b}\right)}\operatorname{sgn}(y)\int_0^{\frac{\pi}{2}} \frac{d\theta}{x^2-b^2+(b^2-a^2)\sin^2\theta}$$

The value of this integral can be evaluated from integral tables. The y-component of electric field $E_y(x,0) = -\partial\phi/\partial y$ is then given by the following expression:

$$E_y(x,0) = \begin{cases} \dfrac{b\phi_0}{K'(\frac{a}{b})} \dfrac{\operatorname{sgn}(y)}{\sqrt{a^2-x^2}\sqrt{b^2-x^2}} & 0 \le |x| < a \\ 0 & a < |x| < b \\ \dfrac{-b\phi_0}{K'(\frac{a}{b})} \dfrac{\operatorname{sgn}(y)}{\sqrt{x^2-b^2}\sqrt{x^2-a^2}} & b < |x| < \infty \end{cases}$$

The x-component of magnetic field at y=0 has similar behavior as does the current density.

c) CPW Characteristic Impedance

The total charge density on the center conductor is just the charge density on the top plus that on the bottom. It becomes

$$\rho = \epsilon_0(1+\epsilon_r)\frac{b\phi_0}{K'(\frac{a}{b})}\frac{1}{\sqrt{a^2-x^2}\sqrt{b^2-x^2}}$$

The total charge on a strip of length ℓ is

$$Q = 2\int_0^{\ell}\int_0^{a}\rho\, dx\, dz = 2\epsilon_0(1+\epsilon_r)\frac{\phi_0 \ell}{K'(\frac{a}{b})}K\left(\frac{a}{b}\right)$$

The capacitance per unit length then becomes

$$C = 2\epsilon_0(1+\epsilon_r)\frac{K\left(\frac{a}{b}\right)}{K'\left(\frac{a}{b}\right)} \qquad F/m$$

The flux Ψ in a cross-section y=0, $a < |x| < b$ is

$$\Psi = \int \vec{B}\cdot\vec{ds} = \mu_0 \int \nabla\times\vec{A}\cdot\vec{ds} = \mu_0 \oint \vec{A}\cdot\vec{d\ell}$$

Since $\vec{A}$ is z-directed, one can choose a rectangular path of integration to eliminate transverse contributions to Ψ. Thus, only longitudinal contributions contribute. One has

$$\Psi = \mu_0 \ell A_z(a,0) + \mu_0 \ell A_z(b,0)$$

Upon substituting A_0 for ϕ_0 and doing the above evaluations on $A_z(x,0)$, one obtains

$$\Psi = \mu_0 \ell A_0$$

By substituting A_0 for ϕ_0 in the $\partial\phi/\partial y(x,0)$ expression, the x-component of $\vec{H}$ field is obtained from $H_x = \partial A_z(x,y)/\partial y\big|_{y=0}$. The result is

$$H_x(x,0) = \frac{-b A_0}{K'\left(\frac{a}{b}\right)}\frac{\operatorname{sgn}(y)}{\sqrt{a^2-x^2}\sqrt{b^2-x^2}}$$

$$0 \leq |x| < a$$

The surface current density then becomes

$$\vec{J}_s(x) = \hat{y} \times \left\{ \hat{x}\, H_x(x, 0^+) - \hat{x}\, H_x(x, 0^-) \right\}$$

$$= 2 \frac{b A_0}{K'\left(\frac{a}{b}\right)} \frac{1}{\sqrt{a^2 - x^2}\sqrt{b^2 - x^2}}\, \hat{z}$$

The total current i is given by

$$i = 2\int_0^a J_s(x)\, dx = 4A_0 \frac{K\left(\frac{a}{b}\right)}{K'\left(\frac{a}{b}\right)}$$

The inductance per unit length is just

$$L = \frac{\Psi}{i} = \frac{\mu_0}{4} \frac{K'\left(\frac{a}{b}\right)}{K\left(\frac{a}{b}\right)} \qquad \mathrm{H/m}$$

The characteristic impedance is now

$$Z_0 = \sqrt{\frac{L}{C}} = \frac{1}{4}\sqrt{\frac{\mu_0}{\epsilon_0}} \frac{1}{\sqrt{\frac{1+\epsilon_r}{2}}} \frac{K'\left(\frac{a}{b}\right)}{K\left(\frac{a}{b}\right)}$$

This is identical to the result Wen /1/ found by conformal mapping.

The phase velocity is

$$v = \frac{1}{\sqrt{LC}} = \frac{1}{\sqrt{\mu_0 \epsilon_0}\sqrt{\frac{1+\epsilon_r}{2}}}$$

If the propagation constant β is calculated from this, one finds

$$\beta = \omega / v = \omega \sqrt{\mu_0 \epsilon_0} \sqrt{\frac{1+\epsilon_r}{2}}$$

The relationship between ϕ_0 and A_0 can be found /61/. Since

$$\frac{\phi_0}{i} = \sqrt{\frac{L}{C}} \qquad \text{and} \qquad i = \frac{\mu_0 A_0}{L}$$

one has

$$\mu_0 A_0 = \sqrt{LC}\, \phi_0$$

or

$$\omega \mu_0 A_0 = \beta \phi_0$$

This relationship is true on the center conductor.

It is of interest to see how well the Lorentz Gauge is satisfied in this problem even though such solutions are known to be quite accurate at modeling the physical problem at low microwave frequencies. The Lorentz Gauge that must be satisfied divided by the previous equation gives

$$\frac{A_z^{\gtrless}(x,y)}{A_0} = \frac{\omega^2 \mu_0 \epsilon_0 \epsilon_r^{\gtrless}}{\omega^2 \mu_0 \epsilon_0 \sqrt{\frac{1+\epsilon_r}{2}}} \frac{\phi^{\gtrless}(x,y)}{\phi_0}$$

$$= \frac{\epsilon_r^{\gtrless}}{\sqrt{\frac{1+\epsilon_r}{2}}} \frac{\phi^{\gtrless}(x,y)}{\phi_0}$$

Since $\epsilon_r^{>} = 1$ and $\epsilon_r^{<} = \epsilon_r$, one can see that in this formulation the Lorentz Gauge is automatically satisfied in some root mean or average sense. It would be interesting to apply a perturbation theory /61/ to this problem to see if higher order corrections could be found.

III. Monolithic (Integrated Circuit) Planar Antennas for Phased Arrays on GaAs

Antennas proposed for incorporation into planar phased arrays are the microstrip dipole or patch antennas, and the slot dipole or ring antennas. Much work has been done in this area. The recent book chapter "Integrated-Circuit Antennas" /5/ covers the applicable concepts. Another book, Microstrip Antennas /66/, surveys microstrip and slot antennas and is a handy reference. A special issue of IEEE Trans. Antennas Prop. /67/ on microstrip antennas covers many aspects of the area.

The substrate that is currently most often discussed for monolithic antennas is GaAs which has a relative dielectric constant of approximately 12. This causes problems when antennas are mounted on its surface. Large amounts of power can be trapped inside the substrate instead of being radiated into space. Reciprocity is often used to calculate radiation patterns of microstrip and slot antennas.

Microstrip antennas have been modelled /68/ by coplanar cavity-backed slot antennas. This implies that a microstrip antenna should

have a coplanar cavity-backed slot equivalent. A slot-ring antenna used in a balanced mixer circuit has recently been described /69/. This is the dual of a microstrip ring resonator. A cavity-backed slot antenna has previously been studied /70/. Planar antenna principles are described in detail by Rhodes /71/.

With this introduction to some principle references in planar antenna theory, the area of active phased array modules is described. General GaAs technology references can be found in books. Two such books are Applications of GaAs MESFETs /3/ and GaAs FET Principles and Technology /72/. The former book has a brief section on the "Applications of MESFETs in Phased Array Radars". An earlier paper /73/ describes modules for active phased arrays.

The reciprocity theorem is used /74/ to determine the radiation properties of monolithic integrated circuit antennas. A recent note /75/ looks at performance bounds on monolithic phased array antennas. Another /76/ discusses considerations for millimeter wave, monolithic phased arrays.

Phased arrays can be operated in either transmit or receive mode. Power levels for receiving are generally small while those for transmitting are required to be large. Input devices are optimized for low noise while output devices are optimized for high power. Device uniformity is required for all devices in order for the array to function as expected. Matching is critical for proper operation.

IV. Applicable Source Configurations for Modeling Slot Radiators/ Receivers in Coplanar Waveguide

Several types of slot antennas fed by coplanar waveguide can be imagined. Among these are a slot-dipole antenna and a slot-ring antenna. These are sketched in Figure 3. Both types have previously been used with CPW. The interest here is in examining modeling the slots with the CPW present. This necessitates looking at the source configurations that can be used with CPW.

In modeling a slot antenna, the equivalence theorem can be used to eliminate the plane the slot is in. First, the slot is closed with metal and magnetic currents $\vec{M}_s = \vec{E} \times \hat{n}$ are added in the slot on both sides of the plane where $\vec{E}$ is the electric field in the slot. The tangential electric field in the slot is made continuous through the slot by requiring the magnetic currents to be equal, but oppositely directed on the two sides of the metal filling the slot. When one magnetic current is looking into a half-space, imaging can be used. The magnetic current doubles and, assuming the half-space is homogeneous, resides in homogeneous space. We have previously seen that the quasi-static electric field is directed across the slot in opposite directions on the plus and minus x sides. Therefore, the free-space magnetic current for CPW can be sketched as in Figure 4. The current flow is equal and opposite in the two slots--much like the situation for electric current in transmission line. The CPW is clearly a dual of the Twin Strip (or Coplanar Strip) transmission line. Since the

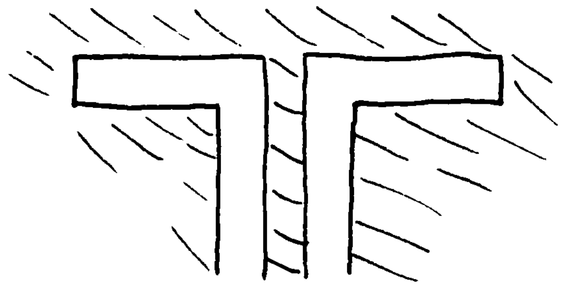

(a)

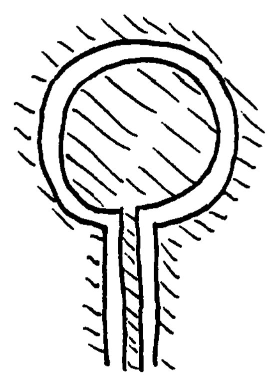

(b)

Figure 3. Slot Antennas Fed by CPW. (a) Slot-dipole Antenna

(b) Slot-ring Antenna

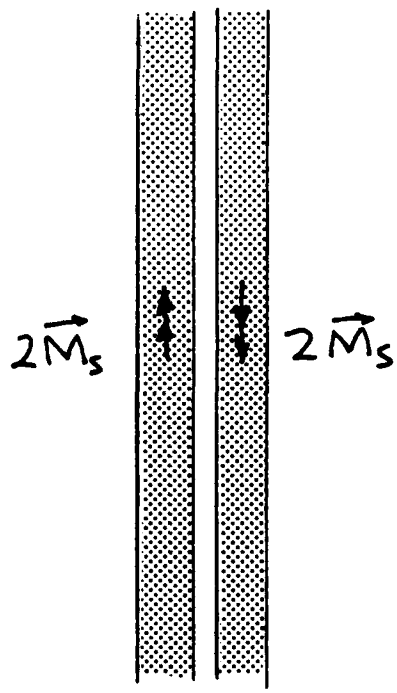

Figure 4. CPW Magnetic Currents

quasi-static electric field has an inverse square root singularity at the slot edges, the magnetic current does also. Therefore, the transverse variation of the magnetic current should be able to be built into any problem formulation.

The best source for CPW would be one which "starts" the dominant or quasi-TEM mode solved for earlier in this report. Delta function sources are more commonly used. Two types of delta function sources are available. First, current sources can be used. These are shown in Figure 5(a). For symmetry reasons, a current source $I_0/2$ is fed from each edge to the center conductor. When the magnetic current is put in place and imaged, the electric current circles the magnetic current as shown in Figure 5(b). Impedance is found by computing the voltage across the current source. Second, voltage sources can be used. Figure 6(a) shows two identical voltage sources placed to take advantage of symmetry. Figure 6(b) shows the slots shorted at the voltage source locations. This allows for current in the voltage source to be solved for. Next, Figure 6(c) shows magnetic currents looped around the slot shorts. The voltage source across the slot can be found by taking a line integral around a path which goes through the magnetic current loop and then comes back just outside of the loop. The tangential electric field on the metal is zero everywhere except on the pass just outside of the magnetic current loop and passing across the slot. From Maxwell's second equation, one obtains

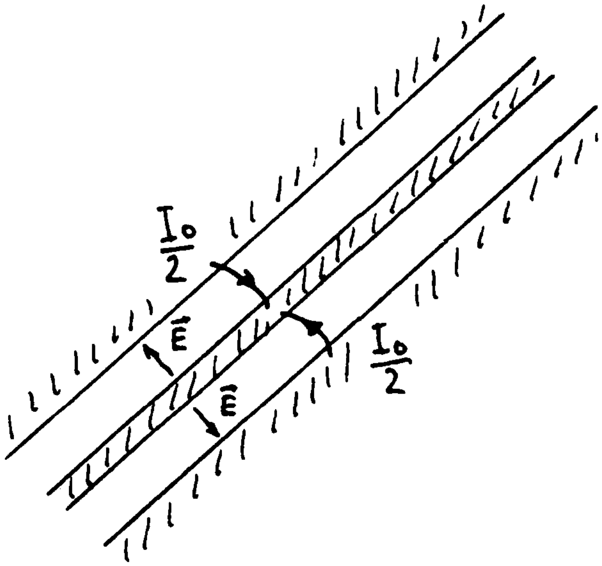

(a)

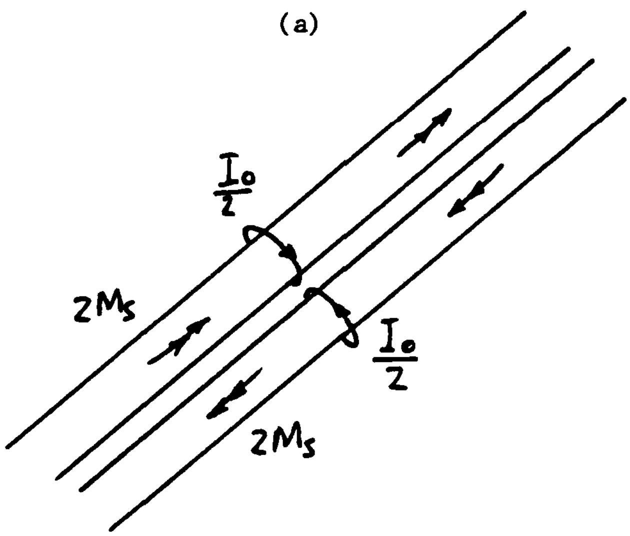

(b)

Figure 5. Current Sources for CPW (a) Electric Current Sources

(b) Modeled and Imaged Equivalent

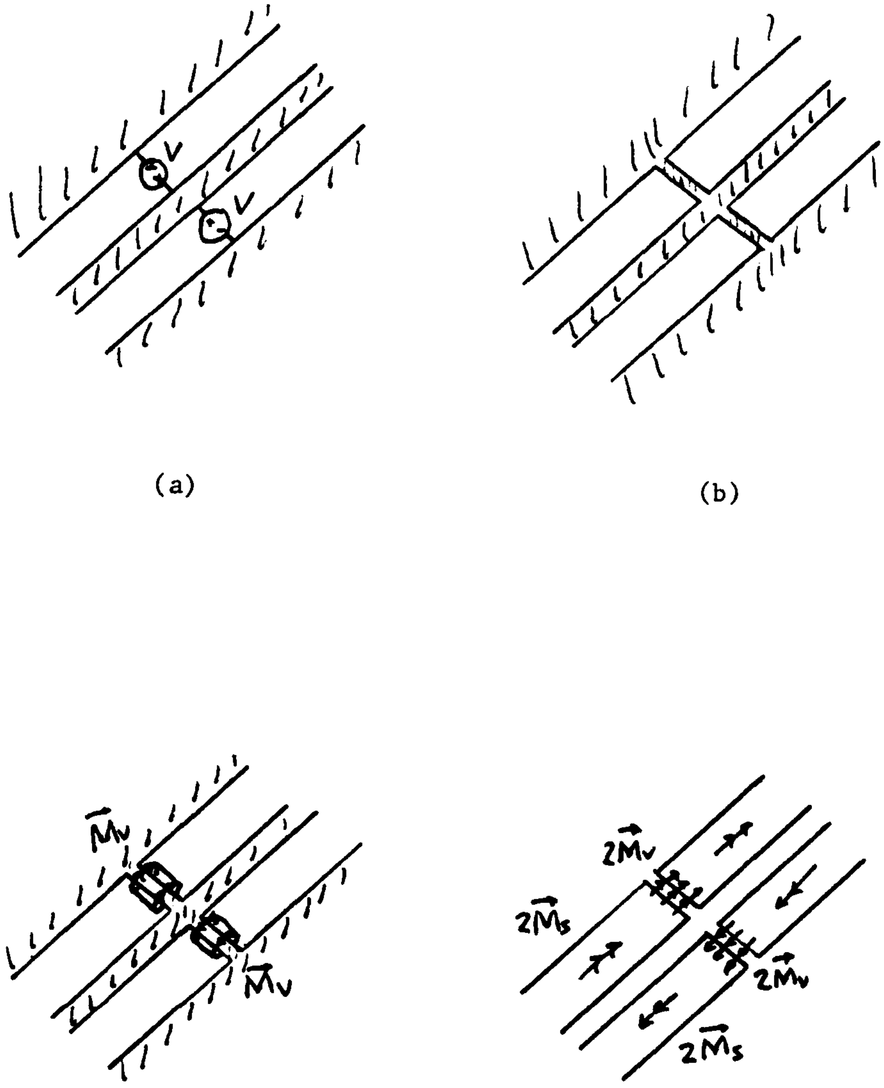

Figure 6. Voltage Sources for CPW. (a) Voltage Sources, (b) Shorted Slots, (c) Magnetic Current Voltage Sources, (d) Imaged Sources

$$V = -\oint \vec{E} \cdot \vec{d\ell} = j\omega \int \vec{B} \cdot \vec{dS} + \int \vec{M_v} \cdot \vec{dS}$$

If the path of integration is made small, the contribution from $\vec{B}$ is negligible and

$$V = M_v(b-a)$$

where b-a is the slot width. Thus, this configuration serves as a voltage source. It can also be thought of as a source of magnetic current since the magnetic current M_v doubles when imaged as shown in Figure 6(d). In general, a loop of magnetic current surrounding an electric short is equivalent to a voltage source.

A load is a resistor or other lossy device going from the center conductor to ground. Therefore, a Norton equivalent could be modeled as shown in Figure 7. This has been suggested by Harrison /76a/. In general, resistive loads would not be used because lossless matching is preferred.

A voltage source with series load can be modeled as shown in Figure 8. The same equations used before prove this. The shorted end is necessary. The magnetic current ring doubles when imaged and is just a current crossing the gap, thereby serving as a source.

Another important technique is the design of current sources from voltage sources by inserting a $\lambda/4$ section of line. This is illustrated in Figure 9. The voltage source in Figure 9(a) appears

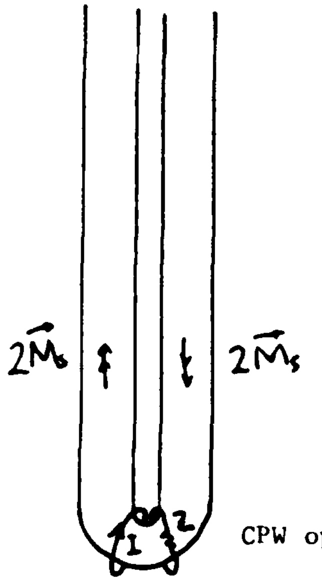

Figure 7. Norton Equivalent

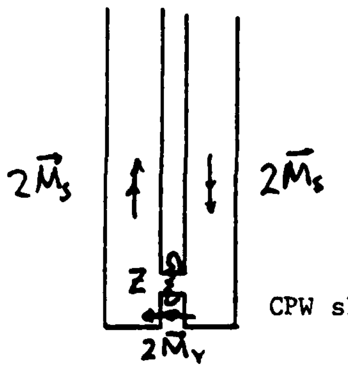

Figure 8. Thevenin Equivalent

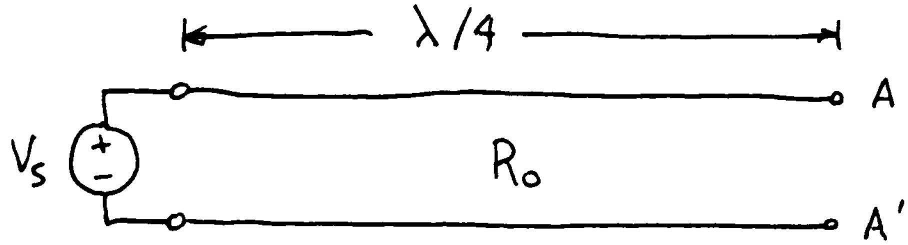

(a)

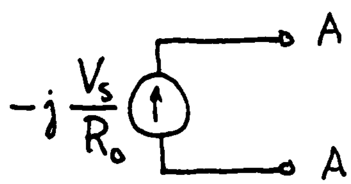

(b)

Figure 9. $\lambda/4$ Transformer. (a) Original Circuit (b) Equivalent

as a current source with respect to terminals A-A'. Hopefully, the use of such an equivalent would allow for source discontinuity problems on the transmission line to "smooth out" and give a more realistic impedance for the actual transmission line connected at A-A' to an antenna or other device.

The input impedance of an open circuited $\lambda/4$ transmission line is a short circuit. Therefore, the circuits of Figures 10(a) and 10(b) are equivalent, at least theoretically. It would be of interest to see if they are. The $\lambda/4$ open circuited line transforms into a short circuit and the current source transforms to a voltage source through the $\lambda/4$ section of line. In Figure 10(b), the magnetic current ring represents the voltage source.

Perhaps the ideal configuration for further study is given in Figure 11. King and Harrison /77/ look at slot antennas of this type.

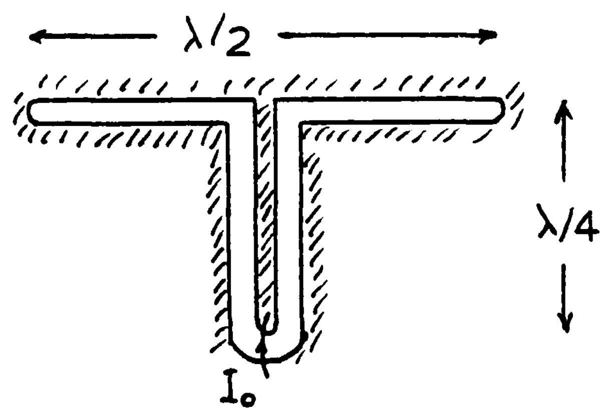

Figure 11. Another Configuration

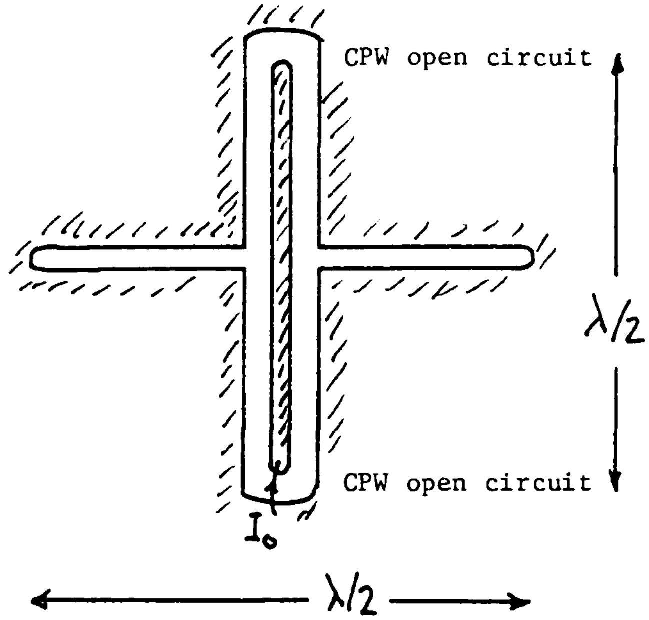

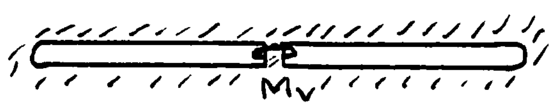

Figure 10. Using $\lambda/4$ Sections of Line. (a) Original, (b) Equivalent

V. Planar Curtain Arrays in Coplanar Waveguide

The Curtain Array /78/ is a periodic linear array of dipoles fed in series at their center by a parallel wire transmission line. A coplanar waveguide feeding a periodic array of slot-dipoles is the magnetic current dual of the coplanar strip curtain array. Figure 12 illustrates the magnetic current equivalent of a CPW Curtain Array. The slots are $\lambda/2$ apart to give broadside radiation at the center frequency. The radiation can be modeled by an appropriate valued impedance loop enclosing the imaged magnetic current in CPW as shown in Figure 13. Therefore, from a circuit point of view, a CPW Curtain Array can be considered to be a periodically loaded or lossy CPW transmission line. An infinite Curtain Array was studied to see if transmission line theory could be applied to it.

a) Finite Curtain Array Model

As stated previously, Fukuoka and Itoh /30/ use Floquet modes to analyze periodic slow-wave CPW on a periodically doped semiconductor substrate. The geometry of an infinite Curtain Array is almost the same from a computational viewpoint and should allow the same analysis technique to be applied. The Curtain Array radiates power as energy is propagated along the CPW. Attenuation also occurs for slow-wave CPW. Therefore, a brief preliminary study of an infinite Curtain Array in CPW was made using periodic transmission line techniques.

The quantity actually desired is the input impedance of the finite

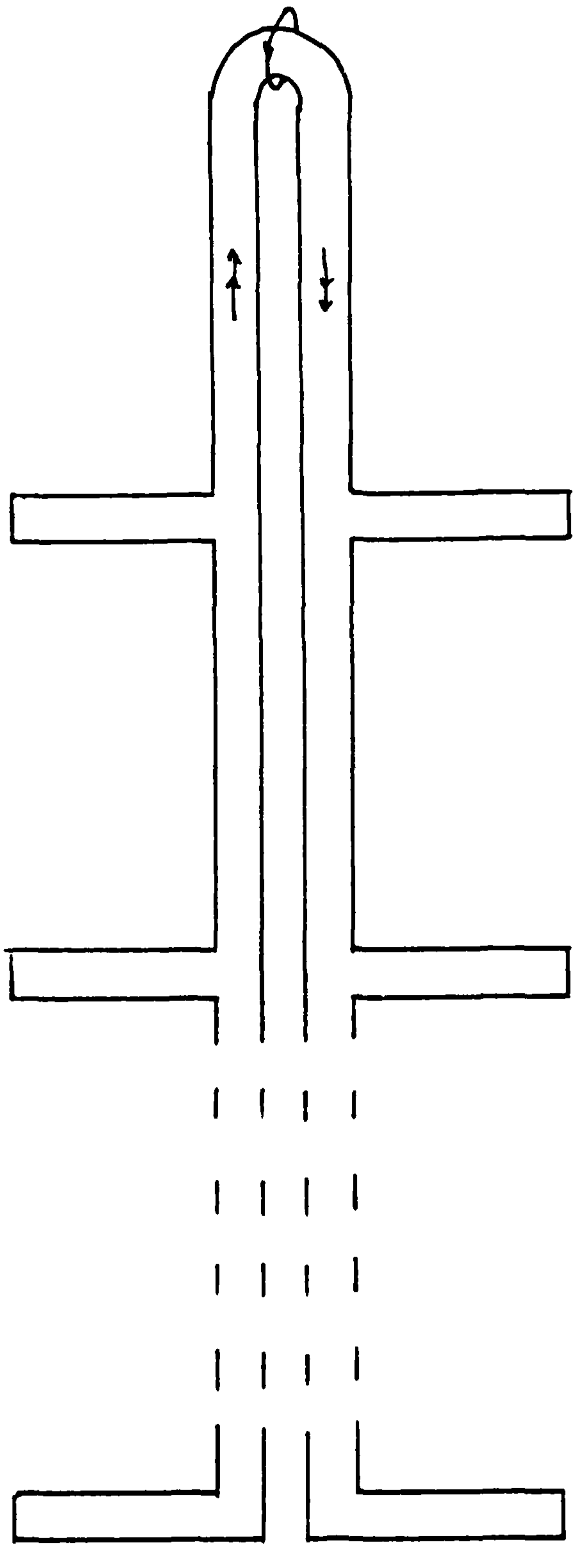

Figure 12. Magnetic Current Equivalent of CPW Curtain Array

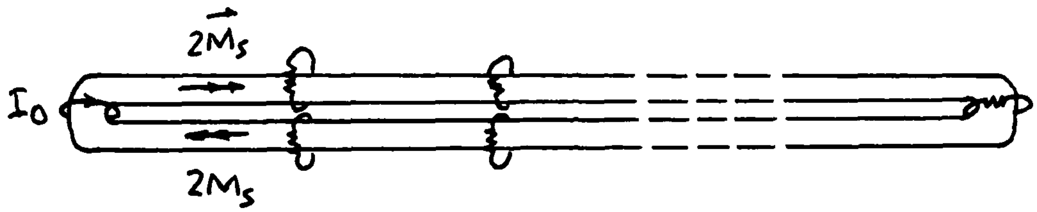

Figure 13. Loaded Magnetic Current Transmission Line Representing Curtain Array

CPW Curtain Array, such as that shown in Figure 12, versus scan (or frequency). Since radiation attenuates the available transmission line power far from the source, the infinite Curtain Array should exhibit properties similar to the finite case. Since the source is not periodic, two approaches became apparent. First, one could use reciprocity and treat this as a scattering problem. This general approach has previously been used /74/. Second, one could investigate the natural modes of the structure and do some kind of mode matching at the source. The first approach should be the easier of the two by far. This awaits further study.

Several additional references to Curtain Arrays should be given. A reference showing a coplanar array is /79/. Experimental results are given by Hudock and Mayes /80/. Two primarily experimental papers /81, 82/ have been presented by Nešić. The first examines coplanar strip Curtain Arrays and the second discusses CPW Curtain Arrays. His work /82/ appears to be the only published study of CPW Curtain Arrays.

b) Infinite Periodic Transmission Lines

The idea of modeling a Curtain Array's impedance properties by an infinite lossy transmission line was briefly examined. Although this approach totally ignores interaction or coupling between the slot-dipole antennas, a number of references were located which could be potentially useful and so they are reported here.

Collin /83,84/ has chapters on periodic lines in his textbooks. Liu, Shmoys, and Hessel /85/ model one part of a microstrip phased array with a periodic transmission line model fed periodically by a current source. Another paper /86/ investigates techniques for quasi-static solution of lines with periodic right angle protrusions such as slot-dipole antennas fed by CPW present.

Two problems were examined here. These are illustrated in Figures 14(a) and (c). Figure 14(a) shows a periodically loaded transmission line that also has periodic current sources. Since the structure is symmetrical with respect to each current source, half of the current must go in each direction as shown. Splitting each current source and placing perfect magnetic conducting walls in the center, one sees that the unit cell appears such as that shown in Figure 14(b). With the origin z=0 placed at the location of the load Y, one can write the current and voltage on each line by transmission line equations. The boundary conditions to be satisfied are

$$-I_1(-\ell) = +I_2(-\ell) = \frac{I_s}{2}$$

$$V_1(-\ell) = V_2(-\ell)$$

$$I_1(0) + I_2(0) = Y\,V_1(0) = Y\,V_2(0)$$

The final result for input impedance is

$$Z_{in} = \frac{V(-\ell)}{I_s} = \frac{R_o}{1+\frac{1}{2}YR_o}\left\{1 - j\frac{1}{2}\left(1-\frac{1}{2}YR_o\right)\cot\beta\ell\right\}$$

Several cases are of interest. For the case when $1/Y = R_0/2$, the input impedance Z_{in} is $R_0/2$. Under this condition, the input impedance is effectively invariant with line length ℓ and frequency f. The impedance for Y a short circuit is $j\frac{R_0}{2} \cot \beta\ell$. For an open circuit, it is $R_0 - j\frac{R_0}{2} \cot \beta\ell$. This yields the relationship

$$Z_{open} + Z_{short} = R_0$$

A periodic loaded transmission line ignoring coupling is illustrated in Figure 14(c). The input impedance of this structure can be found by equating the input admittance at $z=\frac{\theta}{2}$ and $z=3\frac{\theta}{2}$. After manipulation and simplification, the final result is

$$Z_{in}^2 = j R_0^2 \tan\frac{\theta}{2}\left(\frac{1 + j\frac{YR_0}{2}\tan\frac{\theta}{2}}{\frac{YR_0}{2} + j\tan\frac{\theta}{2}}\right)$$

For $\theta = \pi$, $Z_{in} \to \infty$ while for $\theta = \pi/2$, $Z_{in} = R_0\sqrt{(1+jR_0Y/2)/(1-jR_0Y/2)}$.
For $\theta = 2\pi$, $Z_{in} = 0$.

For treatment of a transmission line with coupling between elements, Floquet's Theorem is often used. This is discussed in the next section.

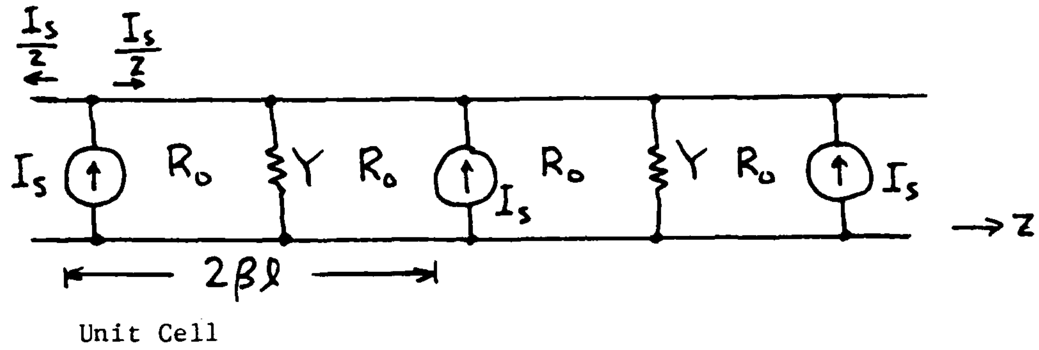

(a)

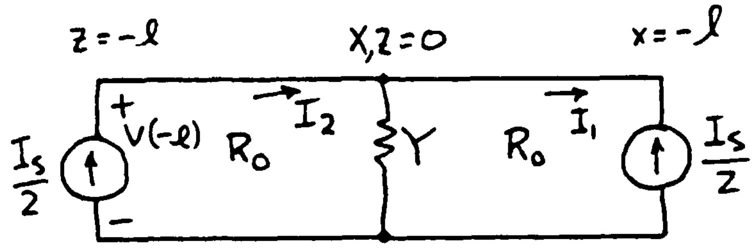

(b)

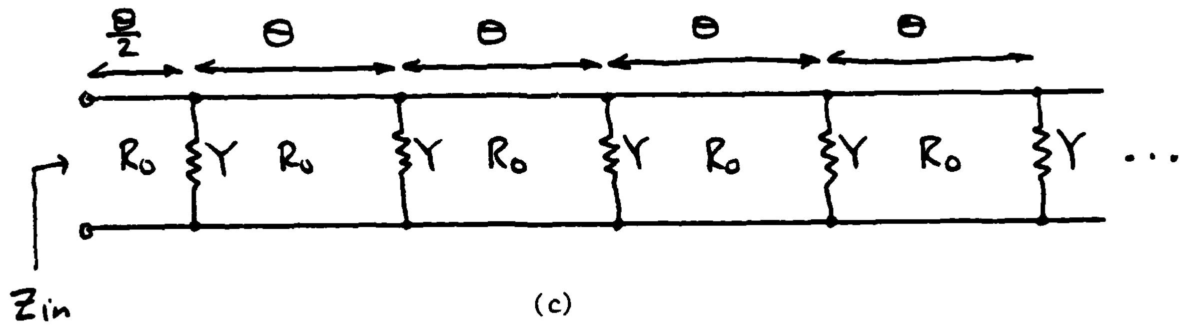

(c)

Figure 14. Transmission Line Problems. (a) Periodic Cell Approach (b) Unit Cell, (c) Periodic Load Ignoring Coupling

VI. Transmitting and Receiving Planar Phased Arrays Fed by CPW

Phased arrays are useful for providing a technical means of transmitting or receiving from a particular solid angle of space. Variable phase shifters are provided throughout the array to provide control of the scan angle. In general, the larger the array, the narrower the beam. For transmitting arrays, the more individual radiators in the array, the less power each has to handle. Individual antennas are usually spaced $\lambda/2$ apart in the grid to provide for a broadside main beam when all elements are equally fed. The basics of arrays are discussed in many textbooks. The subject of mathematical modeling of arrays of arbitrarily shaped radiators is most important for this report.

The infinite array case is most straight-forward conceptually. In this case, if one assumes that any element's currents are the same as any other element's currents except perhaps for a progressive phase shift between them and their closest neighbors, then the mathematical formulation can be limited in extent to the study of a single unit cell.

a) Floquet's Theorem

Consider the periodic array shown schematically in Figure 15. Assume the elements are slots in a ground plane and have a progressive phase shift between elements. The x-extent of a cell is D_x and the y-

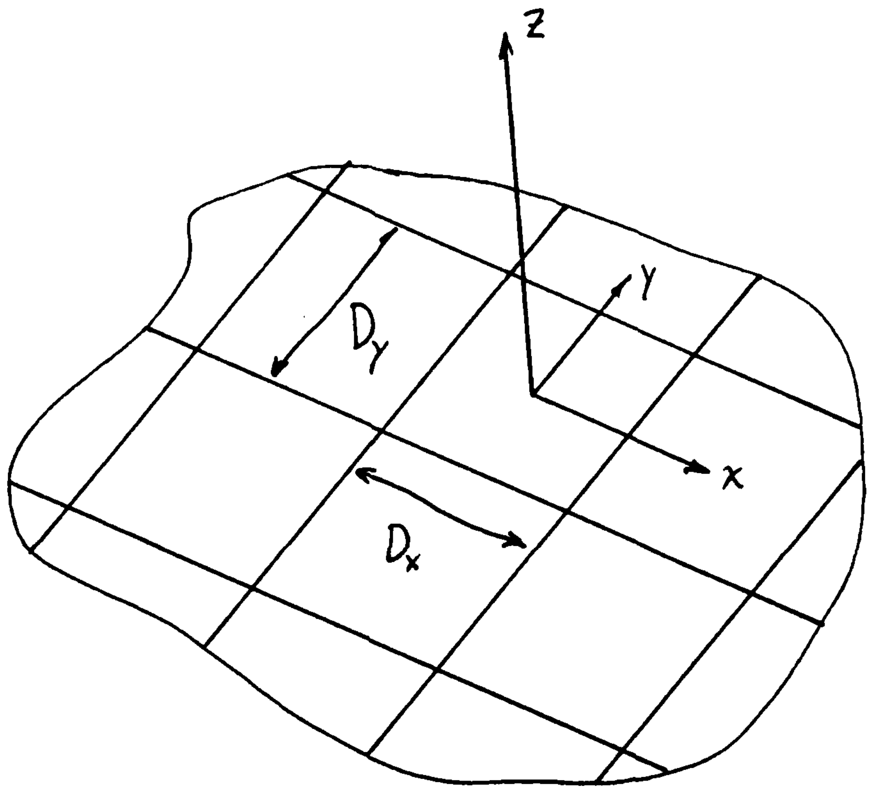

Figure 15. Phased Array

extent is D_y. The field everywhere is unique /87/ if the tangential $\vec{E}$ field is known over the planar surface z=0. By uniqueness, the $\vec{E}$ field on the plane can be replaced by a magnetic current $\vec{M}_s = \vec{E} \times \hat{z}$ on top of an unslotted plane conductor. This problem has the same solution as the original problem. This is an application of the equivalence theorem. The electric field in the slot locations is now the same as it was before and is zero elsewhere.

The magnetic current (or tangential electric field) on the z=0 surface has the following periodicity property

$$\vec{M}_s(x + mD_x, y + nD_y) =$$

$$= \vec{M}_s(x,y)\left(e^{-jk_0 u_0 D_x}\right)^m \left(e^{-jk_0 v_0 D_y}\right)^n$$

$$-\frac{D_x}{2} < x < \frac{D_x}{2}$$

$$-\frac{D_y}{2} < y < \frac{D_y}{2}$$

$$m, n \text{ integers}$$

where /88/, $u_0 = \sin\theta_0 \cos\phi_0$, $v_0 = \sin\theta_0 \sin\phi_0$. The complex exponentials account for the progressive phase shift mentioned previously and are allowed in Floquet's Theorem for solving periodic differential equations. Floquet's Theorem is formally described in several books /89-91/. Multiplying the above equation through by $\exp(jk_0u_0(x+mD_x) + jk_0v_0(y+nD_y))$, one obtains /92/

$$\vec{M}_s(x,y)\, e^{jk_0u_0x}\, e^{jk_0v_0y} =$$

$$= e^{jk_0u_0(x+mD_x)}\, e^{jk_0v_0(y+nD_y)}\, \vec{M}_s(x+mD_x,\, y+nD_y)$$

This is now written in a proper form to see the periodic nature of the function. $\vec{M}_s(x,y)$ itself is not periodic.

This periodic function is now in a form suitable for expansion in a complex exponential Fourier series.

$$\vec{M}_s(x,y)\, e^{jk_0u_0x}\, e^{jk_0v_0y} =$$

$$= \sum_{p=-\infty}^{\infty} \sum_{q=-\infty}^{\infty} \vec{A}_{pq}\, e^{-jk_0p\frac{x}{D_x}}\, e^{-jk_0q\frac{y}{D_y}}$$

The current $\vec{M}_s$ can then be written in the form

$$\vec{M}_s(x,y) = e^{-jk_0u_0x}\, e^{-jk_0v_0y} \sum_{p=-\infty}^{\infty} \sum_{q=-\infty}^{\infty} \vec{A}_{pq}\, e^{-jk_0p\frac{x}{D_x}}\, e^{-jk_0q\frac{y}{D_y}}$$

This is the form given by Floquet's Theorem /89/.

Assuming an $e^{-j\Gamma z}$ variation with z, the electric and magnetic fields due to the magnetic current can likewise be expanded in a Floquet series /91/. This can be viewed as the field in a waveguide due

to a current in the guide. The outward propagation constant is given by

$$\Gamma_{pq}^{2} = k_0^{2} - \left(k_0 u_0 + k_0 \frac{p}{D_x}\right)^{2} - \left(k_0 v_0 + k_0 \frac{q}{D_y}\right)^{2}$$

Each (p,q) represents a single Floquet mode. Green's functions for planar slots in phased arrays are given by Mailloux /88/.

b) Literature Review

Several textbooks cover topics relevant to phased arrays. Microstrip arrays are discussed by Bahl and Bhartia /66/. Finite arrays are discussed in /71/ and /91/. Periodic slow wave structures using Floquet's Theorem are covered by Bevensee /93/ and Johnson /94/.

Phased array theory and technology is covered in a review paper by Mailloux /95/. Microstrip arrays are discussed in another review paper /96/. A classic paper /97/ on phased arrays contains applicable theorems. Oliner and Knittel /98/ edited a volume of now classic papers in 1970. One of the papers from the volume is on methods of phased array analysis /99/.

The subject of infinite planar arrays has a large literature. Diamond /100/ describes a generalized approach to planar infinite arrays. Rhodes /101/ describes a fundamental principle for planar antennas. Borgiotti used modal analysis /102/. Chang /103/ studies an infinite phased dipole array. Mutual coupling in infinite arrays is examined /104/ as is the grating-lobe series for impedance variation /105/.

More recently, Pozar /106/ obtains general relations for phased arrays of printed antennas. Pozar and Schaubert /107/ study phased arrays of microstrip patches and with Kominani treat arrays on semi-infinite substrates /108/. Microstrip dipole arrays including mutual coupling have been reported /109/. Microstrip patch array response to plane waves has been studied /110/. Surface wave theory in arrays over earth have been described /111/.

REFERENCES

1. C. P. Wen, "Coplanar Waveguide: A Surface Strip Transmission Line Suitable for Nonreciprocal Gyromagnetic Device Applications", IEEE Trans. Microwave Theory Tech., Vol. MTT-17, No. 12, Dec. 1969, pp. 1087-1090.
2. K. C. Gupta, R. Garg, and I. J. Bahl, Microstrip Lines and Slotlines, Dedham, MA: Artech House, Inc., 1979.
3. R. Soares, J. Graffeuil and J. Obregon, Applications of GaAs MESFETs, Dedham, MA: Artech House, 1983.
4. R. A. Pucel, "Design Considerations for Monolithic Microwave Circuits", IEEE Trans. Microwave Theory Tech., Vol. MTT-29, June 1981, pp. 513-534.
5. K. J. Button, Infrared and Millimeter Waves, Volume 10, Millimeter Components and Techniques, Part II. New York: Academic Press, 1983. Chapter 1. "Integrated Circuit Antennas" by D. B. Rutledge, D. P. Neikirk, and D. P. Kasilingam, pp. 1-90.
6. W. J. Getsinger, "Circuit Duals on Planar Transmission Media", 1983 IEEE MTT-S International Microwave Symposium Digest, Boston, MA, pp. 154-156.
7. H. Lee and V. K. Tripathi, "New Perspectives on the Green's Function for Quasi-TEM Planar Structures", 1983 IEEE MTT-S International Microwave Symposium Digest, Boston, MA, pp. 571-573.

8. H. Lee and V. K. Tripathi, "Generalized Spectral Domain Analysis of Planar Structures Having Semi-infinite Ground Planes", 1984 IEEE MTT-S International Microwave Symposium Digest, San Francisco, CA, pp. 327-329.

9. A. S. Omar and K. Schunemann, "Space Domain Decoupling of LSE and LSM Fields in Generalized Planar Guiding Structures", 1984 IEEE MTT-S International Microwave Symposium Digest, San Francisco, CA, pp. 59-61.

10. A. S. Omar and K. Schunemann, "Formulation of the Singular Integral Equation Technique for General Planar Transmission Lines", 1985 IEEE MTT-S International Microwave Symposium Digest, St. Louis, MO, pp. 135-138.

11. H. Matino, "Characteristic Impedance Measurements of a Coplanar Waveguide", Electronics Letters, Vol. 7, No. 23, Nov. 18, 1971, pp. 678,679.

12. A. Gopinath, "A Comparison of Coplanar Waveguide and Microstrip for GaAs Monolithic Integrated Circuits", 1979 IEEE MTT-S International Microwave Symposium Digest, Orlando, FL, pp. 109-111.

13. M. Kitlinski and B. Janiczak, "Dispersion Characteristics of Single and Coupled Open Slot Lines Filled With Ferrite Medium", 12th European Microwave Conference 1982 Proceedings, Helsinki, Finland, pp. 759-764.

14. B. Janiczak, "Analysis of Multimodes Coplanar Lines for Microwave Integrated Circuits Applications", 13th European Microwave Conference 1983 Proceedings, Nurnberg, West Germany, pp. 425-430.

15. K. Koshiji, E. Shu, and S. Miki, "Dielectric and Conductor Losses in Coplanar Waveguides", Electronics and Communications in Japan, Vol. 65-B, No. 12, 1982, pp. 55-64.

16. A. M. Lerer, "Losses in the Conductors of Coplanar Waveguides", Radio Engineering and Electronic Physics (Soviet Union), Vol. 29, July 1984, pp. 69-74.

17. D. P. Kasilingam and D. B. Rutledge, "Surface-wave Losses of Coplanar Transmission Lines", 1983 IEEE MTT-S International Microwave Symposium Digest, Boston, MA, pp. 113-116.

18. D. F. Williams and S. E. Schwarz, "Reduction of Propagation Losses in Coplanar Waveguide", 1984 IEEE MTT-S International Microwave Symposium Digest, San Francisco, CA, pp. 453-454.

19. V. F. Hanna and D. Thebault, "Theoretical and Experimental Investigation of Asymmetric Coplanar Waveguides", 1984 IEEE MTT-S International Microwave Symposium Digest, San Francisco, CA, pp. 469-471.

20. V. F. Hanna and D. Thebault, "Theoretical and Experimental Investigation of Asymmetric Coplanar Waveguides", IEEE Trans. Microwave Theory Tech., Vol. MTT-32, No. 12, Dec. 1984, pp. 1649-1651.

21. K. Koshiji and E. Shu, "Effect of Inner Conductor Offset in a Coplanar Waveguide", IEEE Trans. Microwave Theory Tech., Vol. MTT-32, No. 10, Oct. 1984, pp. 1387-1390.

22. G. Leuzzi, A. Silbermann, and R. Sorrentino, "Mode Propagation in Laterally Bounded Conductor-Backed Coplanar Waveguides", 1983 IEEE MTT-S International Microwave Symposium Digest, San Francisco, CA, pp. 393-395.

23. D. A. Rowe and B. Y. Lao, "Numerical Analysis of Shielded Coplanar Waveguides", IEEE Trans. Microwave Theory Tech., Vol. MTT-31, No. 11, Nov. 1983, pp. 911-915.

24. K. Koshiji, E. Shu, and S. Miki, "An Analysis of Coplanar Waveguides with Finite Conductor Thickness--Computation and Measurement of Characteristic Impedance", Electronics and Communications in Japan, Vol. 64-B, No. 8, 1981, pp. 69-78.

25. A. Nakatani and N. G. Alexopoulos, "A Generalized Algorithm for the Modeling of the Dispersive Characteristics of Microstrip, Inverted Microstrip, Stripline, Slotline, Finline, and Coplanar Waveguide Circuits on Anisotropic Substrates", 1985 IEEE MTT-S International Microwave Symposium Digest, St. Louis, MO, pp. 457-459.

26. J. Brian Davies and D. Mirshekar-Syahkal, "Spectral Domain Solution of Arbitrary Coplanar Transmission Line with Multilayer Substrate", IEEE Trans. Microwave Theory Tech., Vol. MTT-25, No. 2, Feb. 1977, pp. 143-146.

27. E. M. Bastida, P. Bergamini, G. P. Donzelli, and N. Fanelli, "Slow-Wave and Coplanar Monolithic GaAs Circuits", 12th European Microwave Conference 1982 Proceedings, Helsinki, Finland, pp. 256-261.

28. E. M. Bastida, G. P. Donzelli, and N. Fanelli, "Slow-Wave Approach for Monolithic GaAs ICs", IEEE 1982 Microwave and Millimeter-wave Monolithic Circuits Symposium Digest, Dallas, TX, June 18, 1982, pp. 23-24.

29. Y. Fukuoka and T. Itoh, "Slow-Wave Coplanar Waveguide on Periodically Doped Semiconductor Substrate", 1983 IEEE MTT-S International Microwave Symposium Digest, Boston, MA, pp. 399-401.

30. Y. Fukuoka and T. Itoh, "Slow-Wave Coplanar Waveguide on Periodically Doped Semiconductor Substrate", IEEE Trans. Microwave Theory Techn., Vol. MTT-31, No. 12, Dec. 1983, pp. 1013-1017.

31. Y. Fukuoka and T. Itoh, "Design Consideration of Uniform and Periodic Coplanar Schottky Variable Phase Shifter", 13th European Microwave Conference 1983 Proceedings, Nurnberg, West Germany, pp. 278-282.

32. Y. Fukuoka and T. Itoh, "Coplanar Schottky Variable Phase Shifter Constructed on GaAs Substrate for Millimeter-Wave Application", Int. J. Infrared Millimeter Waves, Vol. 5, No. 6, 1984, pp. 793-801.

33. D. Jager, "Nonlinear Slow-Wave Propagation on Periodic Schottky Coplanar Lines", IEEE 1985 Microwave and Millimeter-wave Monolithic Circuits Symposium Digest, pp. 15-17.

34. P. Kennis, P. Pribetich, Ph. Gelin, M. Aubourg, J. P. Vilotte, F. Godon, and Y. Garault, "Properties of Microstrip and Coplanar Lines on Semiconductor Substrates", 12th European Microwave Conference 1982 Proceedings, Helsinki, Finland, pp. 328-333.

35. Y. C. Shih and T. Itoh, "Analysis of Printed Transmission Lines for Monolithic Integrated Circuits", 12th European Microwave Conference 1982 Proceedings, Helsinki, Finland, pp. 301-305.

36. Y. Fukuoka, Y-C. Shih, and T. Itoh, "Analysis of Slow-Wave Coplanar Waveguide for Monolithic Integrated Circuits", IEEE Trans. Microwave Theory Techn., Vol. MTT-31, No. 7, July 1983, pp. 567-573.

37. M. Aubourg, J. P. Villote, F. Godon, Y. Garault, P. Kennis, P. Pribetich, C. Seguinot, and Ph. Gelin, "Analysis of M.I.S. or Schottky Contact Coplanar Lines Using the F.E.M. and the S.D.A.", 1983 IEEE MTT-S International Microwave Symposium Digest, Boston, MA, pp. 396-398.

38. R. Sorrentino, G. Leuzzi, and A. Silbermann, "Characteristics of Metal-Insulator-Semiconductor Coplanar Waveguides for Monolithic Microwave Circuits", IEEE Trans. Microwave Theory Techn., Vol. MTT-32, No. 4, April 1984, pp. 410-416.

39. P. L. Fleming, T. Smith, H. E. Carlson, and W. A. Cox, "GaAs SAMP Device for Ku-Band Switching", 1979 IEEE MTT-S International Microwave Symposium Digest, Orlando, FL, pp. 253-255.

40. P. R. Herczfeld, A. S. Daryoush, V. M. Contarino, A. Rosen, Z. Turski, and A.P.S. Khana, "Optically Controlled Microwave Devices and Circuits", 1985 IEEE MTT-S International Microwave Symposium Digest, St. Louis, MO, pp. 211-214.

41. A. Cappello and J. Pierro, "A 22 to 24 GHz Cryogenically Cooled Low Noise FET Amplifier in Coplanar Waveguide", 1982 IEEE MTT-S International Microwave Symposium Digest, Dallas, TX, pp. 19-22.

42. R. H. Jansen and N.H.L. Koster, "A Unified CAD Basis for the Frequency Dependent Characterization of Strip, Slot, and Coplanar MIC Components", 11th European Microwave Conference 1981 Proceedings, pp. 682-687.

43. G. Ghione, C. Naldi, and R. Zich, "Q-factor Evaluation for Coplanar Resonators", Alta Frequenza, Vol. LII, N.3, May-June 1983, pp. 191-193.

44. R. G. Harrison, "A Broad-Band Frequency Divider Using Microwave Varactors", IEEE Trans. Microwave Theory Techn., Vol. MTT-25, No. 12, Dec. 1977, pp. 1055-1059.

45. J. Kohler and B. Schiek, "Broadband Microwave Frequency Doublers", The Radio and Electronic Engineer, Vol. 48, No. 1/2, Jan./Feb. 1978, pp. 29-32.

46. A Reporter, "Coaxial Test Fixture Fits Network Measurement Needs", Microwaves & RF, August 1984, p. 189.

47. Y. Naito and Y. Yamanaka, "New Nonreciprocal Devices in a Coplanar Waveguide", 1980 IEEE MTT-S International Microwave Symposium Digest, Washington, DC, pp. 235-237.

48. P. S. Cross, R. A. Baumgartner, and B. H. Kolner, "A Traveling Wave, Microwave Optical Modulator", Proc. SPIE Int. Soc. Opt. Eng., Vol. 439, Picosecond Optoelectronics, pp. 153-158.

49. D. F. Williams and S. E. Schwarz, "Design and Performance of Coplanar Waveguide Bandpass Filters", IEEE Trans. Microwave Theory Techn., Vol. MTT-31, No. 7, July 1983, pp. 558-566.

50. K. D. Stephan, N. Camilleri, and T. Itoh, "Quasi-Optical Polarization-Duplexed Balanced Mixer", 1982 IEEE MTT-S International Microwave Symposium Digest, Dallas, TX, pp. 376-378.

51. K. D. Stephan and G. Perks, "Quasi-Optical Slot Ring Mixer Noise Figure Measurements", 1985 IEEE MTT-S International Microwave Symposium Digest, St. Louis, MO, pp. 643-644.

52. J. H. Lepoff, "Mix Harmonics with Dual-Beam-Lead Diodes", Microwaves & RF, May 1984, pp. 209-212.

53. L. T. Yuan and P. G. Asher, "A W-Band Monolithic Balanced Mixer", 1985 IEEE MTT-S International Microwave Symposium Digest, St. Louis, MO, pp. 113-115.

54. L. Y. Yuan and P. G. Asher, "A W-Band Monolithic Balanced Mixer", IEEE 1985 Microwave and Millimeter-Wave Monolithic Circuits Symposium Digest, pp. 71-73.

55. T. R. Gheewala, "Packages for Ultra-High Speed GaAs ICs", 1984 IEEE Gallium Arsenide Integrated Circuit Symposium, Boston, MA, 67-70.

56. E. M. Bastida, G. P. Donzelli, G. Ghione, and C. Naldi, "A Quasi-Monolithic Approach to Microwave GaAs Integrated Circuits", 13th European Microwave Conference 1983 Proceedings, Nurnberg, West Germany, pp. 357-362.

57. P. Schmid and H. Melchior, "Coplanar Flip-chip Mounting Technique for Picosecond Devices", Rev. Sci. Instrum., Vol. 55, No. 11, Nov. 1984, pp. 1854-1858.

58. D. Mirshekar-Syahkal and J. B. Davies, "Accurate Analysis of Tapered Planar Transmission Lines for Microwave Integrated Circuits", IEEE Trans. Microwave Theory Techn., Vol. MTT-29, No. 2, Feb. 1981, pp. 123-128.

59. K. Kawamoto, K. Hirota, N. Niizaki, Y. Fujiwara, and K. Ueki, "Small Size VCO Module for 900 MHz Band Using Coupled Microstrip-Coplanar Lines", 1985 IEEE MTT-S International Microwave Symposium Digest, St. Louis, MO, pp. 689-692.

60. V. Fouad Hanna and L. Ramboz, "Broadband Planar Coplanar Waveguide-Slotline Transition", 12th European Microwave Conference 1982 Proceedings, Helsinki, Finland, pp. 628-631.

61. R. E. Collin and B. Kretch, "A Perturbation Theory for Microstrip Propagation", 1985 IEEE MTT-S International Microwave Symposium Digest, St. Louis, MO, pp. 561-562.

62. Ian N. Sneddon, Mixed Boundary Value Problems in Potential Theory, New York: John Wiley & Sons, Inc., 1966.

63. I. S. Gradshteyn and I. M. Ryzhik, Table of Integrals, Series, and Products, New York: Academic Press, 1980.

63a. P. F. Byrd and M. D. Friedman, Handbook of Elliptic Integrals for Engineers and Scientists, New York: Springer-Verlag, 1971.

64. W. Magnus, F. Oberhettinger, and R. P. Soni, Formulas and Theorems for the Special Functions of Mathematical Physics, New York: Springer-Verlag, Inc., 1966.

65. R. Mittra and S. W. Lee, Analytical Techniques in the Theory of Guided Waves, New York: The Macmillan Co., 1971.

66. I. J. Bahl and P. Bhartia, Microstrip Antennas, Dedham, MA: Artech House, 1980.

67. IEEE Trans. Antennas Prop., Vol. AP-29, No. 1, January 1981.

68. W. L. Jones and J. K. James, "Synthesis of Conformal HF and VHF Directional Arrays on Spherical Bodies Using Surface Resonator Techniques", Proc. of the IEE Second International Conference on Antennas and Propagation, Part 1: Antennas, 13-16 April 1981, University of York, Heslington, York, UK.

69. K. D. Stephan, N. Camilleri, and T. Itoh, "A Quasi-Optical Polarization-Duplexed Balanced Mixer for Millimeter-Wave Applications", IEEE Trans. Microwave Theory Techn., Vol. MTT-31, No. 2, Feb. 1983, pp. 164-170.

70. S. A. Long, "Experimental Study of the Impedance of Cavity-Backed Slot Antennas", IEEE Trans. Microwave Theory Techn., Vol. MTT-23, No. 1, Jan. 1975, pp. 1-7.

71. Donald R. Rhodes, Synthesis of Planar Antenna Sources, Oxford: Clarendon Press, 1974.

72. J. V. DiLorenzo and D. D. Khandelwal, GaAs FET Principles and Technology, Dedham, MA: Artech House, Inc., 1982.

73. J. Austin and J. R. Forrest, "Design Concepts for Active Phased-Array Modules", IEE Proc., Vol. 127, Pt. F, No. 4, Aug. 1980, pp. 290-300.

74. N. G. Alexopoulos, P. B. Kathehi, and D. B. Rutledge, "Substrate Optimization for Integrated Circuit Antennas", IEEE Trans. Microwave Theory Techn., Vol. MTT-31, No. 7, July 1983, pp. 550-557.

75. John K. Schindler, "Performance Bounds on Monolithic Phased Array Antennas", Unpublished Notes.

76. D. H. Schaubert, D. M. Pozar, K. S. Yngvesson, and R. W. Jackson, "Considerations for Millimeter Wave, Monolithic Phased Arrays", University of Massachusetts, Amherst, MA.

76a. C. W. Harrison, Jr., "Receiving Characteristics of Impedance Loaded Slot Configurations", IEEE Trans. Electromag. Compat., Vol. EMC-15, No. 3, Aug. 1973, pp. 131-136.

77. R.W.P. King and C. W. Harrison, Jr., Antennas and Waves: A Modern Approach, Cambridge, MA: The M.I.T. Press, 1969.

78. R. W. P. King, R. B. Mack, and S. S. Sandler, Arrays of Cylindrical Dipoles, London: Cambridge University Press, 1968.

79. R. W. P. King and S. S. Sandler, "Antennas with Transmission-Line Interconnections", IEEE Trans. Antennas Prop., Vol. AP-18, No. 5, Sept. 1970, pp. 616-621.

80. E. Hudock and P. E. Mayes, "Near-Field Investigation of Uniform Periodic Monopole Arrays", IEEE Trans. Antennas Prop., Vol. AP-13, No. 6, Nov. 1965, pp. 840-855.

81. A. Nesic, "A Printed Array of Symmetrical Dipoles with a Novel Feeding Configuration", Proc. of the IEE Second International Conference on Antennas and Propagation, Part I: Antennas, 13-16 April 1981, University of York, Heslington, York, UK, pp. 504-507.

82. A. Nesic, "Printed Slotted Array Excited by a Coplanar Waveguide", Proceedings of the 12th European Microwave Conference, 13-16 Sept. 1982, Helsinki, Finland, pp. 478-482.

83. R. E. Collin, Foundations for Microwave Engineering, New York: McGraw-Hill Book Company, 1966.

84. R. E. Collin, Field Theory of Guided Waves, New York: McGraw-Hill Book Company, 1960.

85. C. C. Liu, J. Shmoys, and A. Hessel, "E-Plane Performance Trade-Offs in Two-Dimensional Microstrip-Patch Element Phased Arrays", IEEE Trans. Antennas Prop., Vol. AP-30, No. 6, Nov. 1982, pp. 1201-1206.

86. A. M. Lerer, V. M. Lerer, V. D. Ryazanov, and V. A. Sledkov, "Investigation of Periodic Inhomogeneities in Strip and Microstrip Lines", Radio Engineering and Electronic Physics, (Soviet Union), V. 29, Nov. 1984, pp. 58-67.

87. R. F. Harrington, Time-Harmonic Electromagnetic Fields, New York: McGraw-Hill Book Company, 1961.

88. R. J. Mailloux, "On the Use of Metallized Cavities in Printed Slot Arrays with Dielectric Substrates", to be published.

89. F. M. Arscott, Periodic Differential Equations: An Introduction to Mathieu, Lame, and Allied Functions, New York: Macmillan, 1964.

90. W. Magnus and F. Oberhettinger, Formulas and Theorems for the Special Functions of Mathematical Physics, New York: Chelsea, 1949.

91. N. Amitay, V. Galindo, and C. P. Wu, Theory and Analysis of Phased Array Antennas, New York: Wiley-Interscience, 1972.

92. E. Argence and T. Kahan, Theory of Waveguides and Cavity Resonators, New York: Hart Publishing Co., 1968.

93. R. M. Bevensee, Electromagnetic Slow Wave Systems, New York: John Wiley & Sons, Inc., 1964.

94. C. C. Johnson, Field and Wave Electrodynamics, New York: McGraw-Hill Book Company, 1965.

95. R. J. Mailloux, "Phased Array Theory and Technology", Proc. IEEE, Vol. 70, No. 3, March 1982, pp. 246-291.

96. R. J. Mailloux, J. F. McIlvenna, and N. P. Kernweis, "Microstrip Array Technology", IEEE Trans. Antennas Prop., Vol. AP-29, No. 1, Jan. 1981, pp. 25-37.

97. D. Varon and G. I. Zysman, "Some Properties and Limitations of Electronically Steerable Phased Array Antennas", The Bell System Technical Journal, Sept. 1967, pp. 1561-1586.

98. A. A. Oliner and G. H. Knittel, Phased Array Antennas, Dedham, MA: Artech House, Inc., 1970.

99. N. Amitay, C. P. Wu, and V. Galindo, "Methods of Phased Array Analysis", Phased Array Antennas, Dedham, MA: Artech House, 1970.

100. B. L. Diamond, "A Generalized Approach to the Analysis of Infinite Planar Array Antennas", Proc. IEEE, Vol. 56, No. 11, Nov. 1968, pp. 1837-1851.

101. Donald R. Rhodes, "On a Fundamental Principle in the Theory of Planar Antennas", Proc. IEEE, Sept. 1964, pp. 1013-1021.

102. G. V. Borgiotti, "Modal Analysis of Periodic Planar Phased Arrays of Apertures", Proc. IEEE, Vol. 56, No. 11, Nov. 1968, pp. 1881-1892.

103. V. W. H. Chang, "Infinite Phased Dipole Array", Proc. IEEE, Vol. 56, No. 11, Nov. 1968, pp. 1892-1900.

104. W. Wasylkiwskyj and W. K. Kahn, "Mutual Coupling and Element Efficiency for Infinite Linear Arrays", Proc. IEEE, Vol. 56, No. 11, Nov. 1968, pp. 1901-1907.

105. H. A. Wheeler, "The Grating-Lobe Series for the Impedance Variation Antenna in a Planar Phased-Array", IEEE Trans. Antennas Prop., Vol. AP-14, No. 6, Nov. 1966, pp. 707-714.

106. D. M. Pozar, "General Relations for a Phased Array of Printed Antennas Derived from Infinite Current Sheets", IEEE Trans. Antennas Prop., Vol. AP-33, No. 5, May 1985, pp. 498-504.

107. D. M. Pozar and D. H. Schaubert, "Analysis of an Infinite Array of Rectangular Microstrip Patches with Idealized Probe Feeds", IEEE Trans. Antennas Prop., Vol. AP-32, No. 10, Oct. 1984, pp. 1101-1107.

108. M. Kominami, D. M. Pozar, and D. H. Schaubert, "Dipole and Slot Elements and Arrays on Semi-Infinite Substrates", IEEE Trans. Antennas Prop., Vol. AP-33, No. 6, June 1985, pp. 600-607.

109. R. S. Elliott and G. J. Stern, "The Design of Microstrip Dipole Arrays Including Mutual Coupling, Part I: Theory", IEEE Trans. Antennas Prop., Vol. AP-29, No. 5, Sept. 1981, pp. 757-765.

110. C-C. Liu, J. Shmoys, A. Hessel, J. D. Hanfling, and J. M. Usoff, "Plane Wave Reflection from Microstrip-Patch Arrays--Theory and Experiment", IEEE Trans. Antennas Prop., Vol. AP-33, No. 4, April 1985, pp. 426-435.

111. J. H. Richmond and R. J. Garbacz, "Surface Waves on Periodic Array of Imperfectly Conducting Verical Dipoles over the Flat Earth", IEEE Trans. Antennas Prop., Vol. AP-27, No. 6, Nov. 1979, pp. 783-789.

1985 USAF-UES SUMMER FACULTY RESEARCH PROGRAM/
GRADUATE STUDENT SUMMER SUPPORT PROGRAM

Sponsored by the

AIR FORCE OFFICE OF SCIENTIFIC RESEARCH

Conducted by the

UNIVERSAL ENERGY SYSTEMS, INC.

FINAL REPORT

THREE-DIMENSIONAL GRID GENERATION FOR HIGH-PERFORMANCE AIRCRAFT

Prepared by:	David Hart
Academic Rank:	Assistant Professor
Department and University	Department of Mathematics University of Florida
Research Location:	Wright Aeronautical Laboratory, Aerodynamics & Airframe Branch, Computational Aerodynamics Group.
USAF Research Colleague:	Joe S. Shang

Date:	26 August 1985
Contract No:	F 49620-85-C-0013

Three-Dimensional Grid Generation
For High-Performance Aircraft

by

David Hart

Abstract

A scheme is presented for constructing a computational coordinate grid about a realistic high-performance aircraft configuration. Generating schemes and geometric structure are discussed, emphasizing merger capabilities and the role of singularities.

ACKNOWLEDGEMENT

This work was prepared under the sponsorship of the Air Force Office of Scientific Research, Air Force Systems Command, and Wright Aeronautical Laboratory. The hospitality and helpful suggestions of the members of the Computational Aerodynamics Group at Wright-Patterson Air Force Base, particularly of Dr. Joseph Shang, are gratefully acknowledged.

SECTION 1
INTRODUCTION

Computational aerodynamics involves the numerical solution of differential equations on irregular domains in three-dimensional space. Exact implementation of boundary conditions requires boundary-fitting, hence curvilinear, coordinates on the flow domain. The area of mathematics whose goal is to isolate and study the properties of flows which are independent of coordinates is called the theory of dynamical systems. This field builds upon differential topology; the use of curvilinear coordinate systems is among the first lessons. Arguments are often carried out in local "coordinate patches" and the results then pieced together via change of variables transformations. The influence of computers is just beginning to be felt in these areas. "Computational geometry" and "experimental dynamics" are still in their infancy. The intellectual framework is mature, however -- it was put in place by Gauss and Riemann, over a century ago.

A goal of computational aerodynamics is to demonstrate its applicability to complicated aircraft configurations. The feasibility of this program might be established by reproducing experimental data for a well-documented example of a modern tactical fighter, the F16 "Fighting Falcon". This would build upon an earlier successful study of a lifting body aircraft, the X24C [16,19]. The geometric complexities of such an undertaking have led to the study here reported.

SECTION II

OBJECTIVES

This research studies the grid generation requirements for a particular aircraft, the F16A (see Figure 1). Particular questions concern:

1. Construction by 3D blocks vs. by stacked 2D sections;
2. The zonal structure of the aircraft surface and the surrounding space;
3. Smooth merger of coordinates constructed in separate zones.
4. Appropriate methods for constructing a grid of the type recommended.

The grid generation procedure is subject to several constraints. Foremost are the demands of the flow solver: for the X24C, the flow solution required approximately 3000 times as much CPU time as the grid generation. The grid very much affects the rate of (or lack of!) convergence of the solver, and the accuracy of the computed solution. It is desired that:

1. Few demands be made upon the flow solver - no interpolation (so no overset, refined, or adaptive grid schemes) and minimal special logic, in particular a minimum of seperate computational blocks;
2. The body must be a coordinate surface, with parallel surfaces highly clustered and complimentary lines orthogonal to the body (for modelling the turbulent boundary layer); the coordinate system should be smoothly varying (small second derivatives), nearly orthogonal everywhere, and fitted well to the shocks; and
3. Only proven technology should be used -- codes familiar to, or easily assimilated by, the personnel of the Computational Aerodynamics Group, U.S. Air Force Wright Aeronautical Laboratories.

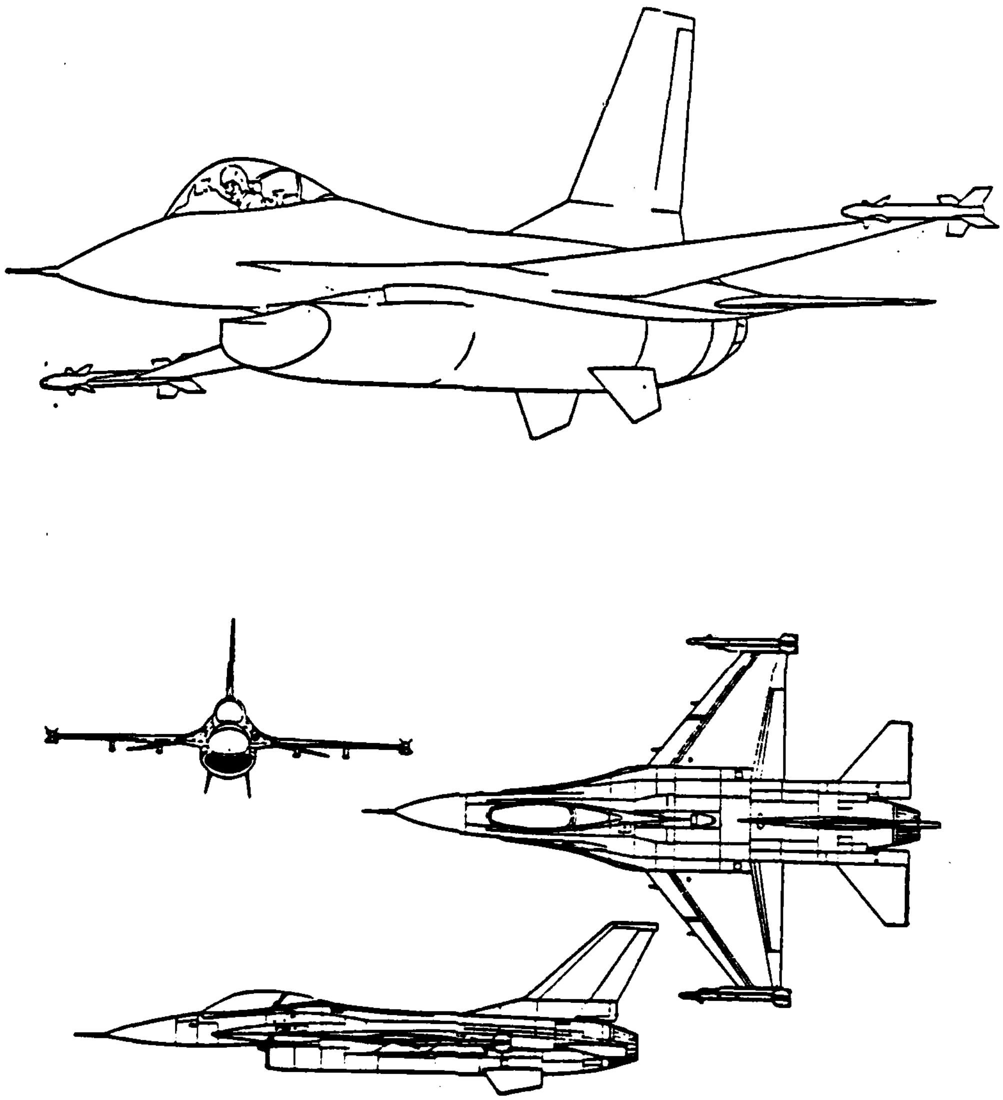

Figure 1 - F16A "Fighting Falcon"

SECTION III

GEOMETRIC CONSIDERATIONS

The gross features of nearly all aircraft include reflectional (left/right) symmetry, with natural reference axes provided by the fuselage, wings and rudder. Particular features of the F16 are the:

1. Protruding wings, strakes, stabilizers, rudder and ventral fins, which all have sharp edges; they also involve boundary slope discontinuities, as does the canopy;

2. Spike-tipped nose;

3. Separated flat-faced inlet, with a cusped diverter area above containing a corner line which merges smoothly into the fuselage;

4. Squared-off ridge along the fuselage between wing and stabilizer, with another "vanishing corner";

5. Two-part rudder, with slope discontinuity along the leading edge and bulb at the rear; and

6. Cylindrical exhaust nozzle, separated by open slits from the rudder and stabilizers.

Due to the symmetry of the aircraft and no-yaw flow regimes to be modelled, it suffices to consider one half of the total flow domain. There must be at least three computational blocks, since the sharp edges of the wings/stabilizers and ventral fins require cuts; see Shang [17], [18]. These blocks must be merged smoothly along their interfaces, for successful computation; this is a primary requirement of any generation scheme. Blocks may therefore generated from a multitude of smoothly merged subblocks, to improve generator performance and increase control. Blocks in the flow field extend/define blocks on the surface; by decomposing the surface into a number of regions, it is simpler to insure desireable properties such as appropriate clustering and streamline orientation, while avoiding undesireable properties such as winding or overlap.

SECTION IV

GENERATION SCHEMES

Minimal requirements of a coordinate transformation are homeomorphism (no overlap), with some degree of differentiability (smoothness) and conformality (angles preserved, approximately); see [11]. It should be exactly conformal and highly clustered at the boundary. The major test to be applied to competing generation schemes is the degree of control over boundary behavior, in order to handle mergers.

The use of transformations to simplify the solution of aerodynamic problems by simplifying the geometry was introduced by Joukowski [9]. He used a particular complex polynomial transformation to study flow past a specific two-dimensional configuration. The resulting coordinate system has the ultimate degree of differentiability and conformality. For more complicated configurations, analytic means are generally inadequate, and transformations must be constructed numerically. Current approaches extend Joukowski's method in two directions: transformations are constructed either "implicitly", as solutions of differential equations, just as conformal mappings satisfy the Cauchy-Riemann equations; or "algebraically", by interpolation of boundary distributions.

The leading implicit methods are based upon solving a system of elliptic PDE's. Laplace's equations allow more flexibility than the Cauchy-Riemann equations, while retaining many of their desireable traits, in particular the maximum principle quaranteeing no overlap. However, this feature may be lost in discrete approximation [15], and in any case vanishes for the Poisson equations. These are generally used, since solving them is equivalent to solving Laplace's equations and then "stretching" to provide clustering at boundaries [12]. The source terms of the Poisson equations may be used to obtain some control over clustering, boundary orthogonality and internal structure [21,22,25]. These schemes produce grids which are smooth, nearly orthogonal, and (with some care) non-overlapping. Their great disadvantage is the limited control available over boundary behavior. A variation allowing additional boundary conditions to be specified is to solve the biharmonic

equations [1]. However, no great success has been demonstrated using that approach.

Another implicit method begins by requiring orthogonality and specifying cell volume [20]. The equations which result are hyperbolic, so solvable by fast "marching" technique. They are, however, susceptible to "shocks" and overlapping, and boundary discontinuities propagate into the field. Also, there is no control whatsoever of boundary behavior in the direction of marching.

The other fast implicit method is based upon the solution of a set of parabolic equations, obtained by approximating the Poisson equations (in some not very well understood sense) [8]. This method is promising, but not very far developed. It possesses most of the advantages of the elliptic methods discussed above, and is much faster; however, it possesses most of their weaknesses as well.

Algebraic methods construct the grid by interpolation of explicit functions from the boundary of the domain into its interior. The leading scheme is called the multi-surface method [3,4,5], because a family of auxilary surfaces approximately parallel to the boundaries are introduced to control the construction. The advantages of this method are its explicit construction (cheap and easily understood) and especially the very good control of boundary behavior, achieved at the cost of increased complexity and relatively heavy demands upon the user. Moreover, internal orthogonality and even lack of overlap must be carefully monitored.

It may be possible to improve a grid, however generated. For example, "stretching functions" [24] may be used to improve clustering effects, or averaging applied to increase smoothness [16]. Two algebraic methods have been developed which may be used as generators, but are even more promising as post-processors, especially for 3D grids generated as stacked 2D sections. The "spring method" [13, 14] alters a given grid by balancing the force equations which would arise if a combination of tension and torsion springs were inserted into the physical grid, one layer at a time from the inner to the outer boundary surface. A

tridiagonal system of equations results. Both smoothness and orthogonality are improved, and by tuning the "spring constants" clustering throughout the field may be controlled. A more direct "variational method" [2, 10] sums the pointwise variation from orthogonality and uniformity (smoothness). Clustering control could presumably be easily added. The resulting function is them minimized by the conjugate direction method, with relaxation optimized by exact line searching. This is analogous to variational principles derived from integral functionals, but more direct and economical.

Finally, many variations are possible. Different methods may be used serially, as with parabolic grids as the initial iterate for an elliptic solver; this is closely related to post-processing (see section G6 of [23]). Different methods may be used jointly, as with hyperbolic generation near the body and algebraic farther out toward a shock surface [16]. The grid may be generated at several levels of refinement; patching blocks together is already a crude version of this. For elliptic methods, this can reduce the total cost by an order of magnitude, and so has been incorporated into some codes [25]. The grid may also be generated adaptively with the solution, to cluster points in high gradient regions (shocks, wakes and boundary layers) as they appear. Spectacular results have been obtained [14], showing that one may reduce the number of mesh points by half while greatly improving the accuracy of the computed solution. This variation remains extremely expensive, however.

SECTION V
RECOMMENDATIONS

The requirements of the flow solver are primary, in determining the acceptability of a grid. This leads to a demand for small second derivatives in the coordinate transformation, and an emphasis upon the singularities (those points at which derivatives vanish or become infinite). Singularities are introduced when corners or edges of the physical and computational domains are not paired. We therefore begin by discussing the corners and their treatment.

A vanishing corner, such as the F16's inlet diverter possesses, is the most difficult. If it is treated as a corner in the diverter area, the grid develops a "fake corner" singularity in sections farther toward the tail. Alternatively, if the region under the wings is fitted with cylindrical coordinates, which are carried forward and "pushed into" the diverter, additional turns (and large second derivatives) develop throughout the diverter region due to the suppressed corner and concavity. The first approach -- a fake singularity under the wings -- seems less harmful. Filling the region with a triangular block is superficially attractive; however, different (streamwise and transverse) coordinate lines would be abutted inside the diverter, requiring special logic and possibly even an additional computational block. In deference to the flow solver, such as approach must be abandoned. We recommend: that a separated subregion be gridded, "rectangular" in the diverter and "triangular" after the corner vanishes, and that this "wedge" be smoothly merged with the region under the wing, forming a noncubical computational block (see Figure 2).

A similar problem occurs where the trailing edge of the wing (and likewise the leading edge of the stabilizer) abuts the squared-off section of the fuselage: two corners merge into the smooth surface, with a cusp between them at right angles to that surface. The procedure recommended is that the grid be wrapped across (suppressing) those corners, with clustering used to reduce the size of the metrics.

Overall, we propose a grid of "H-type" as seen from the wingtip and

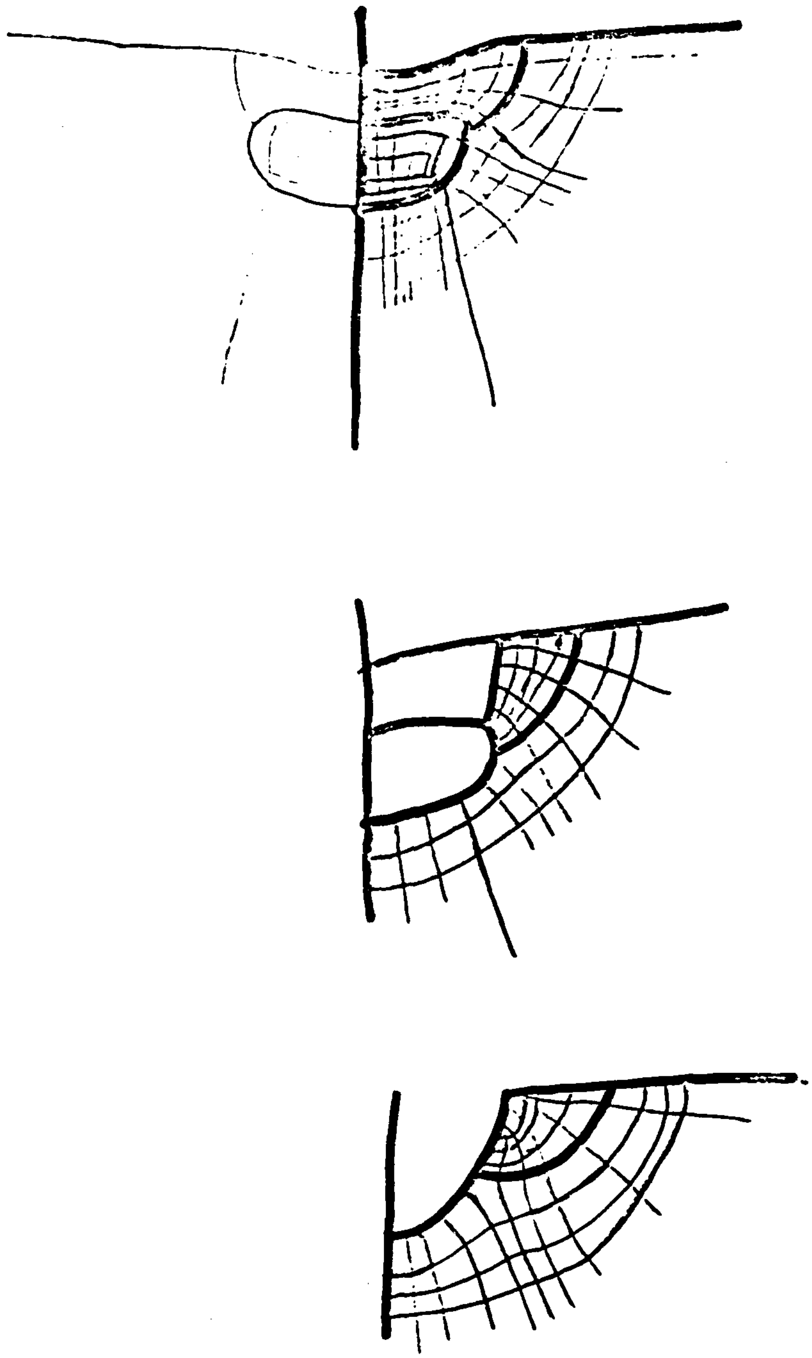

Figure 2.

of "C-type" as seen from the nose, with the curved (cylindrical) part below the wings. This seems to introduce the fewest singularities overall. Such a system clearly conforms best to the gross fuselage geometry; it also seems to cope best with some of the troublesome details. For example, the elliptical face of the inlet requires an O-type grid for proper simulation (as in [7]). To avoid a separate computational block, it must be merged and then treated by special logic (the nose may be treated similarly, see [19]). A cylindrical system is not easily blended with such a patch; however a rectangular system has even worse problems toward the tail.

Two dimensional coordinate systems are given by two families of curves; three dimensional coordinate should be thought of as given by three families of surfaces (not curves!). A major challenge is to develop a fully three-dimensional design. Visualization encounters several difficulties, for example masking (hidden lines) and the immense quantity of information involved. The classic resolution of these problems is to study a series of cross-sections. Also, three dimensional implicit generation methods are very expensive and hard to control; algebraic methods rely upon the user for control. The cross-section approach simplifies user control and remains within reach of current technology. It is greatly enhanced by the availability of three-dimensional "optimizing post-processors", which contribute to the smoothness and orthogonality of the complete three-dimensional final grid. Thus a "page construction" is recommended.

The (ξ,y,ζ)-system being proposed may be regarded as a deformation of a natural (x,y,z) Cartesian system above the wings, and of an (x,r,Θ) cylindrical system of coordinates below them. Here the x-axis is the fuselage axis, the rudder lies in the x-z plane and the wings approximate both the x-y plane ($z=0$) and the $\Theta = 0$ plane - the surfaces $y =$ constant and $r =$ constant must be merged. The wing-stabilizer cut has the equation $\zeta = 0$, and is near the plane $z = 0$. The surfaces $\xi =$ constant are deformations of the planes $x =$ constant, and are the graphs $x = x(x_o,y,z)$ where the parameter x_o indicates the surface passing through $(x,y,z) = (x_o,0,0)$.

We propose to use curved surfaces as the "pages", parametrized along the fuselage axis (x-axis), orthogonal to the body surface and bent to conform to leading/trailing edges and (as far as possible) shocks. Such surfaces are represented by an equation of the form

$$(x - x_o) + f(y) + g(z) = 0.$$

It is envisioned that the function $g(z)$ would be constructed in the $y = 0$ (symmetry) plane to be body-orthogonal and to conform to the leading edge of the rudder, by generating a grid on that surface. The grid lines ξ = const thus define g by its graph $x = x_o - g(z)$. The function $f(y)$ would be similarly constructed in $z = 0$ plane. Areas requiring particular care are the corners where the leading edges of the wings et cetera attach; surface orthogonality is inconsistant with body fitting at these points.

We have discussed the grid design from a top-down perspective; the actual construction must be from the bottom up. Thus the body surface (ξ, η) grid would be constructed before the ξ = constant pages, and the (η, ζ) grid on those pages last of all. Three blocks would be merged into the symmetry plane grid, with divisions for the leading and trailing edges of the fin, and boundary conditions from the surface grid. Seven blocks are needed for the wing plane, outside the body surface. For the surface itself, twenty blocks are proposed — more if the top and bottom of the wing (for example) are regarded as distinct generation problems. Many blocks are necessary, in order to produce a final grid satisfactory at many different boundaries. Use of many blocks also improves control, to prevent axial winding and keep the ξ = constant pages approximately orthogonal to the fuselage axis, and improves generator performance by making regions more nearly rectangular. The order in which these blocks are gridded is important, because of clustering requirements in different planes, and because the distribution generated for any block gives boundary conditions for the adjoining blocks; see Figure 3. It should be noted that blocks may lie in different coordinate surfaces; this use of three-dimensional design distinguishes this proposal from earlier full-

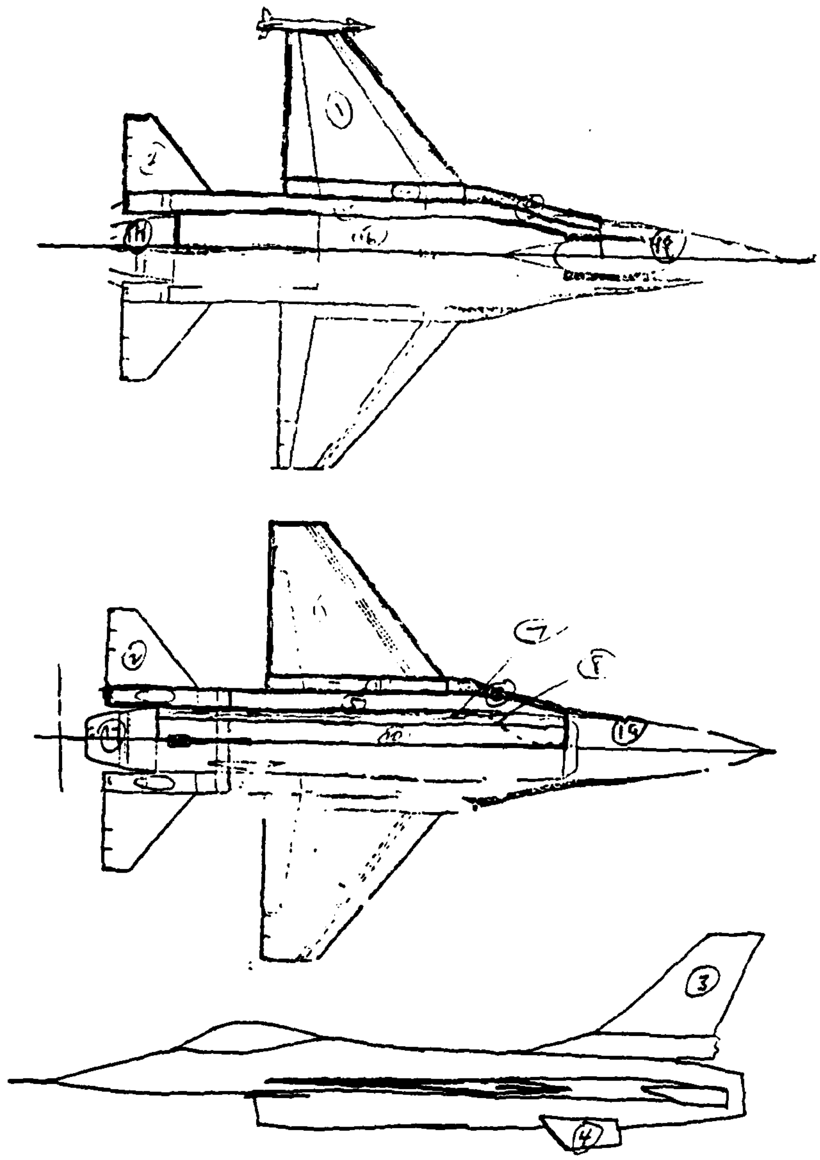

1. Wing (Top & Bottom)
2. Tail (Top & Bottom)
3. Fin
4. Stabilizer (Both Surfaces)
5. Bottom Corner Top (Diverter)
6. Bottom Corner Side
7. Bottom Corner Bottom
8. Bottom Side Fuselage
9. Bottom Mid Fuselage
10. Wing Root Bottom
11. Wing Root Top
12. Forward Wing Root Bottom
13. Forward Wing Root Top
14. Top edge fuselage
15. Top inner fuselage
16. Exhaust nozzle (top & bottom)
17. Top Nose
18. Bottom Nose
19. Side corner fuselage

Missile

1. Fore fins (4)
2. Aft fins (4)
3 Body

Figure 3.

aircraft studies [16, 27].

The grid generation algorithm recommended is Eiseman's multisurface method. It is the best method available for merging different blocks together, with smoothness through second order. Without such control, second order equations cannot be consistent, and the solution suffers. The multisurface method also seems to be the only one which can map a rectangle into a triangle reasonably well, as required by the F16 diverter's vanishing corner. A code for this method is available from NASA, but unfortunately it is only presently configured for planar problems. The extension to curved surfaces is absolutely necessary for the endeavor here contemplated; fortunately, it should not be difficult.

We also recommend the use of an algebraic post-processing scheme, Nakahashi's spring method. The page construction outlined above does not attempt to control orthogonality in the steamwise direction. It relies upon the continuity of the generation scheme to maintain smoothness. The pages would be exactly orthogonal to the body only in the symmetry and wing planes. Post-processing would alleviate all of these problems.

In summary, we recommend

1. An H-C-type grid, with a nonsquare computational block cross-section;

2. Construction using curved pages, many smoothly merged subregions, and three-dimensional post-processing; and

3. Use of an algebraic generation scheme (the multisurface method) and algebraic post-processing (the spring method).

An alternative approach may also be considered. The body grid might be constructed by parametrizing x = constant cross-sections of the fuselage (distributed "manually") according to curvature; blending with an analytically constructed grid on the wing by averaging; and constructing the fin grid analytically. The multisurface method could be used to construct the inlet diverter wedge via x = constant flat cross-sections, and then an elliptic generator used to construct and grid the curved pages. Elliptic generators for curved surfaces have been studied [6,22,26]. While the grids produced by the programs so far developed do

not handle the merger problem very well, they are not terribly bad. Derivatives (slopes and cluster rates) are approximately matched, so the grids produced might well be satisfactory, particulary after post-processing.

An immense amount of essentially mathematical work remains to be done. The entire subject of grid generation needs a serious investigation from the persepective of geometric analysis. In the control theory of elliptic generators, the most fundamental issues have not been treated. Various algorithms have been suggested for partially satisfying both Dirichlet and Neumann conditions, by constructing suitable source terms. Experience with those algorithms suggests the need for analysis: the conditions for a solution of this problem to even exist are unclear. The rate of change with respect to boundary conditions is also unstudied, and crucial to the success of the page construction approach, with its presumed practical advantages. The derivation of parabolic approximations is a related problem, and not well understood. Finally, the extension of algebraic methods to curved surfaces is pressing, would be immediately useful and very rewarding; this extension is contemplated in the very near future.

REFERENCES

[1] J.B. Bell, C.R. Shubin and A.B. Stephens, "A segmentation approach to grid generation using biharmonics," J. Comp. Ph 47, 463-472, 1982.

[2] R. Carcaillet, S.R. Kennon and G.S. Dulikravich, "Optimization of three-dimensional computational grids," AIAA paper 85-4087, 1985.

[3] P.R. Eiseman, "A multi-surface method of coordinate generation," J. Comp. Ph. 33, 118-150, 1979.

[4] P.R. Eiseman, "Coordinate generation with precise controls over mesh properties," J. Comp. Ph 47, 331-351, 1982.

[5] P.R. Eiseman, "High level continuity for coordinate generation with precise controls, "J. Comp. Ph. 47, 352-374, 1982.

[6] A. Garon and R. Camerero, "Generation of surface-fitted coordinate grids," in Advances in Grid Generation, ed. K. Ghia and U. Ghia, ASME FED-Vol. 5, 1983.

[7] J. Graham, "Subsonic boundary conditions for the XF92A configuration," to appear.

[8] J.K. Hodge, S. Leone, and R.L. McCarty, "Non-iterative parabolic grid generation for parabolized equations," AIAA paper 85-1528, 1985.

[9] N. Joukowski, "On the bound vortices," [Russian], Trans. Sect. Phys. Sci. of Soc. Nat. Sci. 13, 1906.

[10] S.R. Kennon and G.S. Dulikravich, "A posteriori optimization of computational grids," AIAA paper 85-483, 1985.

[11] C.W. Mastin, "Error induced by coordinate systems," in Numerical Grid Generation, ed. J.F. Thompson, Elsevier Science Publishing Company, New York, 1982.

[12] C.W. Mastin and J.F. Thompson, "Elliptic systems and numerical transformations," J. Math. An. Ap. 62, 52-62, 1978.

[13] K. Nakahashi and G.S. Deiwert, "A three-dimensional adoptive grid method," AIAA paper 85-486, 1985.

[14] K. Nakahashi and G.S. Peiwert, "A self-adaptive grid method with application to airfoil flow," AIAA paper 85-1525, 1985.

[15] P.J. Roache and S. Steinberg, "A new approach to grid generation using a variational formulation," AIAA paper 85-1527, 1985.

[16] S.J. Scherr and J.S. Shang, "Three-dimensional body-fitted grid system for a complete aircraft," to appear.

[17] J.S. Shang, "Numerical simulation of wing-fusalage interference," AIAA paper 81-0048, 1981.

[18] J.S. Shang, "Numerical simulation of wing-fuselage aerodynamics interaction," AIAA Jnl. 22 1345-1353, 1984.

[19] J.S. Shang and S.J. Scherr, "Navier-Stokes solution of the flow field around a complete aircraft," AIAA paper 85-1509, 1985.

[20] J.L. Steger and D.S. Chausee, "Generation of body-fitted coordinates using hyperbolic partial differential equations," SIAM J. Sci. Stat. Comput. 1, 431-437, 1980.

[21] J.L. Steger and R.L. Sorenson, "Automatic mesh-point clustering near a boundary in grid generation with elliptic partial differential equations," J. Comp. Ph. 33, 405-410, 1979.

[22] P.D. Thomas, "Construction of composite three-dimensional grids from subregion grids generated by elliptic systems," AIAA paper 81-0996, 1981.

[23] J.F. Thompson, Z.U.A. Warsi and C.W. Mastin, "Boundary-fitted coordinate systems for numerical solution of partial differential equations - a review," J. Comp. Ph. 47, 1-108, 1982.

[24] M. Vinokur, "On one-dimensional stretching functions for finite-difference calculations," J. Comp. Ph. 50, 215-234, 1983.

[25] M. Visbal and D. Knight, "Generation of orthogonal and nearly orthogonal coordinates with grid control near boundaries," AIAA Jnl. 20 305-306, 1982.

[26] A.K. Whitney and P.D. Thomas, "Construction of grids on curved surfaces described by generalized coordinates through the use of an elliptic system," in Advances in Grid Generation, ed. K. Ghia and U. Ghia, ASME FED-Vol. 5, 1983.

[27] N.J. Yu, "Grid generation and transonic flow calculations for three-dimensional configurations, AIAA paper 80-1391, 1980.

1985 USAF-UES SUMMER FACULTY RESEARCH PROGRAM/
GRADUATE STUDENT SUMMER SUPPORT PROGAM

Sponsored By The
AIR FORCE OFFICE OF SCIENTIFIC RESEARCH

Conducted By The
UNIVERSAL ENERGY SYSTEMS, INC.

FINAL REPORT

Prepared by: Albert A. Heaney

Academic Rank: Professor

Department and University: Electrical Engineering/California State University-Fresno

Research Location: RADC, Griffiss AFB, DCLW

USAF Research: James L. Davis

Date: August 8, 1985

Contract No: F49620-85-C-0013

ANALYSIS OF THE REPORT ON FILAN PERFORMANCE METRICS

by

Albert A. Heaney

ABSTRACT

RADC has been involved with the development of a local area network (LAN) suitable for DoD applications for some seven years. Such a system is designed as a means of information exchange and as a means of sharing centralized resources (e.g. memory, printers, etc.). Due to the lack of standardization in the protocol software, commercial systems are frequently not combatible with each other. This situation forces the user to choose data processing systems more for their combatability then for their capability. The DoD has addressed this problem by developing a standard interface (MIL-STD-1779) and architecture (FILAN). The Flexible Intraconnect Local Area Network (FILAN) is a high speed, baseband, polled-access local network designed for military applications. Performance evaluation of the FILAN is the basis of this report. In particular, Martin Marietta was awarded a contract by RADC to perform measurements of FILAN network capability for the purpose of ultimately characterizing total system performance. A final report has been issued on this contract by Martin Marietta and this report is an analysis of that study.

I. INTRODUCTION:

I have spent some seven years working at General Electric Ordnance Systems, Sperry Microwave Electronics and Honeywell Avionics performing research and development in the areas of computer system architectures, and fault tolerant computing. I have been continuing my research activities more recently in the area of performance monitors under contract to NASA.

The design and analysis of local area networks involves the application of computer architecture concepts. New concepts are involved in the design of a LAN system when that system does not have a centralized executive (as is the case in some classes of LAN systems). However, the Flexible Intraconnect Local Area Network (FILAN) that is being studied at RADC is centrally controlled via the Local Traffic Controller (LTC). A full evaluation of the tradeoffs made in the design of FILAN had not been made and so it was felt that my background in system architectures would be suitable to a study of this system. A final version of the design of FILAN will not be obtained until its performance capabilities are determined. My work at RADC was meant to support this effort.

II. OBJECTIVES OF THE RESEARCH EFFORT:

A problem in identifying a LAN system to satisfy a given list of user objectives exists with all such systems. The user desires to connect (n) stations to the system, he wants uninterrupted service all the time from any station, he wants no noticable delays in response, he wants access to an array of centrally located resources, he wants his system to "grow" with time, and he wants the privilege to be able to add-on any future host or resource and to be able to integrate such units without regard to the vendors that designed the units. Such capability is far from being available today. With any given system some of this capability is available up to a point. To determine the capability of FILAN (or any other LAN), two basic questions need to be asked:

1) Are there conditions that can cause the system to go unstable such that one or more stations are "locked out"?

2) What are the worse case delays tnat a station can experience and what are the conditions that produce such delays?

The goal of this study is to devise a method by which these questions can be answered in part. The study began with an analysis of the work done by Martin Marietta as described in the report entitled "FILAN PERFORMANCE METRICS." After completion of the analysis, an additional goal is to identify further work needed to be done and a realistic test bed suitable to the study.

III. FILAN PERFORMANCE METRICS: STUDY OBJECTIVES:

The primary objectives were to "characterize FILAN performance" and identify areas that might benefit from design modifications.

Observations:

The test bed appeared to be unrealistic in that it had one station that transmitted data with no receiving stations. Rather, all data were "bit-bucketed" into the destination UNIFI. No methods were provided to extrapolate the test results to realistic configurations.

Measurements delt striclty with "hardware" delays. No reference was made as to the role that software protocols play in the "delays". No reference was made to the higher layer software protocols. Test results were not correlated with physical (handshaking), link, and network protocols (the three layers involved in the measurements.)

The link layer involves the encoding of data by the DTE/PIC and the testing of incoming data by the source NAU and finally the call for retransmission of data in the event that errors are detected.

No discussion was given as to how source messages may be broken down into datagrams and how the total time to transfer these datagrams to a destination host varies with the number of active transmitting hosts (each with a differenct quantity of datagrams to be transmitted) and the number of receiving hosts. Such a discussion would involve the Network protocol layer in the NAU's and

would provide end-to-end transfer delay time measures. Note that the "Process NAU" time is left blank on Figure 4.

All contention with other application software was elliminated. No network management was used. No end-to-end user handshaking was done. The system was uni-directional, a simplex system.

No use of test results were made to identify areas that might benefit from design modifications. For example, delay times were not correlated to the clock rate of the particular CPU used in the design or any necessary processing time.

IV. INDEPENDENT VARIABLES CHOSEN FOR THIS STUDY:

Three independent variables were chosen for this study:

Block Transfer Rate - A
Block Size - B
Polling Rate - C

The Block Transfer Rate is the rate of moving a block of data across the source Standard Interface (MIL-STD-1779).

The Block Size refers to the number of 18-bit data words transferred along with a 16-word header and an 8-word trailer.

The Polling Rate refers to the number of polls per second issued to the source NAU by the LTC (see Figure 1).

A fourth parameter is formed, called the Polling coefficient, as (C/A).

Comments:

No justification for the choice of the independent variables is provided. Obvious choices for the independent variables includes the number of stations

and the load per station. In a realistic system, the Polling rate will depend on the "offered load." In order to extrapolate results to a realistic system, a relation should be formed between the Polling rate and the system "offered load." It is presumed that BLock Size and Block Transfer rate depends on message size and the "overhead" (protocols) residing within the specific DTE. A realistic range should be computed for these independent variables. For example, is it realistic to transfer a Block Size of one word (B=1) along with a 16 word header and an 8 word trailer?

V. DEPENDENT VARIABLES CHOSEN FOR THIS STUDY:

Three dependent measures are mentioned in the report:

1) Delay (A, B, C)
2) Throughput (B)
3) Utilization (B)

All three dependent measures deal only at the network level. For example "Throughput", as defined by Stallings', is the sum of successful data transfers over a network in a unit of time and is plotted as a function of "offered load". "Throughput", as defined in this study, is the maximum "rate of data being transmitted between nodes" (p. 20) with no contention.

"Delay" deals only with "handshaking" and "message" transfer rates. The word "message" also needs to be qualified; it refers to a block of data accompanied by a 16 word header and an 8 word trailer. The word "message" in a total system can refer to many blocks of data.

"Utilization" = Throughput divided by Capacity.

Comments:

As it turns out, "Delay" is the only measured dependent variable of the three. Both "Throughput" and "Utilization" are computed from the equations computed

to fit the "Delay" measures. In that there are questions concerning the validity of the "Delay" equations, the results for "Throughput" and "Utilization" are also open to question.

VI. MEASUREMENT TECHNIQUES:

a) Test Conditions:

Twenty four tests were run each with a different value of A, B, C. The values were chosen by equally spacing intermediate values between a minimum and maximum value. The spacing would then be given approximately by (MAX-MIN)/23. The MAX and MIN values were chosen as follows:

	A	B	C
	blk/sec	words/blk	polls/sec
MAX	148	500	200
MIN	1	1	2

In order to choose combinations of A, B, C that define the 24 tests, a table of random numbers was used.

Comment:

The report implied that any combination of A, B, C among the 24 values chosen for each would be realistic. However, it was observed that all 24 tests resulted in C being greater than A. As it turns out, this condition is realistic for the FILAN design. No justification was given for the range of values of each of the independent variables. In particular, it appears unrealistic to transmit one data word (B=1) along with a 16 word header and 8 word trailer.

b) Test Measurements:

For each test, 30 consecutive samples (measures) were taken from which two quantities were derived, "mean" and "peak". Assuming that all independent variables were truly held constant, any variation in a measurement must be

attributable to measurement error. The report does not mention the possibility that unknown independent variables were responsible for the variations in measurements when A, B, C were being held constant.

Comment:

Consider Test 4 of Table A.10. Note that Peak/Mean = 12.7. It follows that

MAXM is greater than 12.7 times MINM

where MAXM is the maximum measured value, and MINM is the lowest measured value. With such large variation of measured data (attributable only to measurement error), the measured data must be suspect. One then must question the exercise of performing "multiple regression analysis" on data that is itself questionable. If on the other hand the data is thought to be reliable, then all significant independent variables must be identified before an equation predicting behavior can be computed. Further, if the measured dependent variable is thought to be totally a function of the independent variable (A, B, C), then when A, B, C are held constant, each measure should produce the same constant value. What then is the significance of producing two equations, one predicting the "peak" value and one predicting the "mean" value?

c) Curve Fitting

Once all the data has been accumulated for the 24 tests, a "multiple regression analysis" is performed in order to identify that equation (a function of A, B, C) that best fits the measured data. The degree to which each of the independent variables effects the dependent variable is determined. Only when "a sufficiently large percentage of the variations are accounted for" (p. 37) by a correlation with the independent variables can an equation be generated. When such correlations cannot be found, the authors presume that the dependent variable is independent of A, B, C and therefore, is a constant.

Comment:

There appears to be no quality of fit criteria computed by the authors (e.g. standard deviation) by which they correlate a resulting equation to the measured data. A resulting equation is accepted as a "best" fit in spite of the fact that the authors recognize that in some cases the independent variables only account for a small percentage of the variance of the dependent variable. For example, the authors state that the independent variables account for only "63% of the fluctuations in source NAU word transfer time" (p. 35). They further state that "the remaining 37% of the variance is due to unaccounted-for factors (such as errors in measurement)." Obviously when the fluctuation in the dependent variable are "loosely" related to the fluctuations of the independent variables, either one of two conclusions can be drawn; (1) the dependent variable is a constant, (2) the dependent variable is a function of unaccounted for independent variables. The authors assumed the former.

Assuming the equations are a "good" fit to the measured data, and assuming they can be justified qualatatively, then the equations can be accepted as describing network behavior from a hardware point of view. If this is not the case, then further study is needed to identify all significant independent variables. Once a set of equations is obtained that provide a "good" fit to the measured data, then an understanding will be had as to where some of the low layer delays occur. This information in turn could be used to identify design modifications.

AD-A166 177 UNITED STATES AIR FORCE SUMMER FACULTY RESEARCH PROGRAM 04/15
1985 TECHNICAL RE (U) UNIVERSAL ENERGY SYSTEMS INC
DAYTON OH R C DARRAH ET AL. DEC 85 AFOSR-TR-86-0140
UNCLASSIFIED F49620-85-C-0013 F/G 5/1 NL

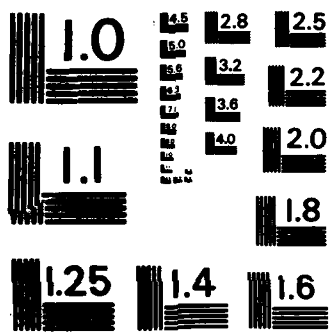

MICROCOPY RESOLUTION TEST CHART
NATIONAL BUREAU OF STANDARDS-1963-A

VII. DETAIL MEASUREMENTS:

The detail measurements can be diagramed as shown in Figure 1.

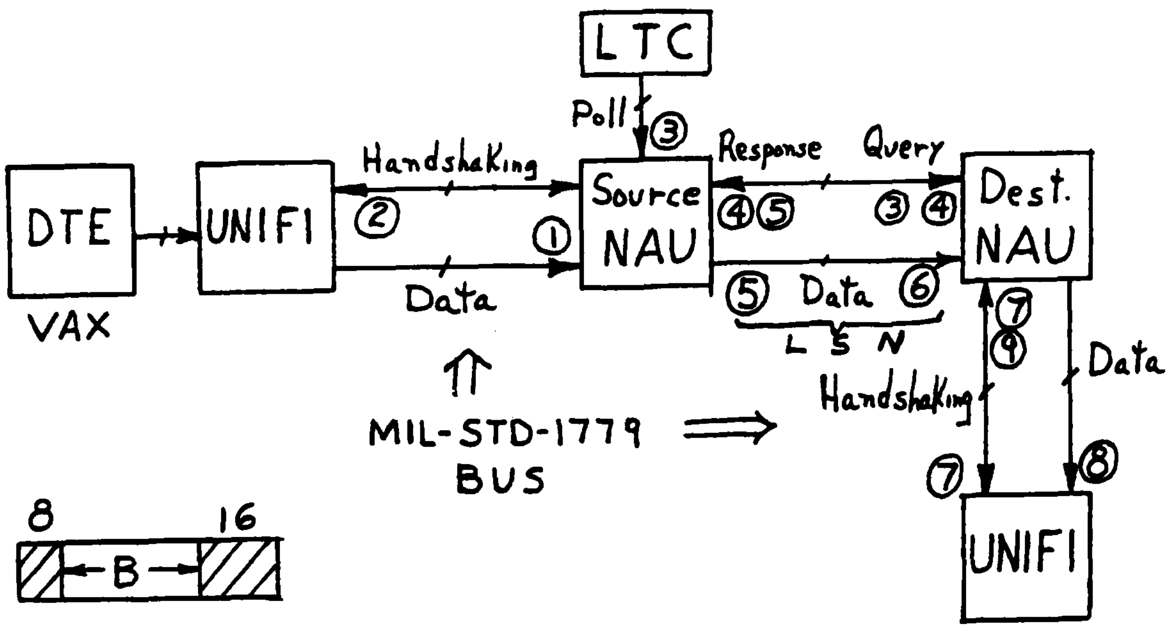

Delay Dependent Variables:

1) Source DTE Transfer Time-Time to transfer data across MIL-STD-1779.
2) Source DTE ACK/NAK Time-Time to acknowledge receipt of message by Source NAU.
3) Poll/Query Time-Poll to Source NAU to Query Dest. NAU time.
4) Query/Response Time-Query to Destination NAU response.
5) Response/Message Time-Dest. NAU response to start of Source NAU message.
6) Message Transfer Time.
7) Destination DTE Access Time-Dest. NAU ready signal to Dest. UNIFI ready signal.
8) Destination DTE Transfer Time-Message transfer time to Dest. UNIFI.
9) Destination DTE ACK/NAK Time-Time to acknowledge receipt of message by Dest. UNIFI.

FIGURE 1
TEST BED

a) Source NAU Word Transfer Time - is no doubt heavily dependent on overhead (processing) time and on system traffic. One should concentrate on the LTC and estimate the lowest polling rate as a function of "offered load."

The plot, Figure 6, does not seem to be an accurate plot of the equation.

b) Destination NAU Word Transfer Time - deals only with the time it takes to move a word through the destination NAU. Again, if total messages are broken down into datagrams and only blocks of data are being transferred at a given segment of time, the question is how long will it take to transfer a total message through the destination NAU as a function of "offered load."

One would have to question why the report shows the "peak" value of this dependent variable is a function of (A) and the "mean" value is a constant? This situation was noted throughout the report, i.e. the "peak" and "mean" values of a given dependent variable were not generally dependent on the same independent variables.

c) Source DTE Transfer Time - is defined as the time between the start of message transmission across the Standard Interface and conclusion of transmission.

Why should the "peak" value be dependent on polling rate (C)? Once transmission to the source NAU begins, does it not continue without regard to the input poll to the source NAU? Why is the "mean" value independent of Block Rate (A)? Does not the source NAU receive data at the block rate?

In spite of the fact that (B) accounts for 94% of the variance in the "mean" value, the following observation was made.

Test Number	Measured (Mean)	Equation (Mean)	Ratio
2	854	471	1.8
18	278	471	1.7

d) Source DTE ACK/NAK Time - is defined as the time between the conclusion of a message transmission and the conclusion of the acknowledgement of that message by the source NAU.

Why should that time lapse be dependent on polling rate (C) and block size (B)?

e) Destination DTE Access Time - is defined as the length of time that the destination NAU must wait after signaling that it is ready to send a message before the destination DTE (UNIFI) indicates that it is ready to receive that message.

Unless the destination DTE (UNIFI) is busy processing data, this should simply be "handshaking" time. Why was this time measured in milliseconds?

How can block rate (A) have anything to do with "handshaking" time?

The equation, again, provides a poor fit to the data as shown below:

Test Number	Measured (Peak)	Equation (Peak)	Ratio
1	5.46	1.61	3.4
6	5.7	1.51	3.8
10	4.7	1.61	2.9
13	7.15	1.54	4.6

f) Destination DTE Transfer Time - is defined as the time to transfer a message across the destination Standard Interface.

Since the equations given are a linear function of block size (B), they no doubt reflect the fact that the "word" transfer rate across the destination Standard Interface is a constant (a function of the CPU used to design the NAU). This rate would transfer 24 words (header and trailer) in a peak time of 11.8 microseconds (0.492 microseconds/word) or a mean time of 9.97 microseconds (0.415 microseconds/word). Hence the data suggests a constant word rate between destination NAU and destination UNIFI of about 0.47 microseconds/word.

VIII. END-TO-END DEPENDENT MEASURES:

It should be understood that the term "end-to-end" as used in this report refers to the time it takes the FILAN to send a word from the source DTE (VAX) to the destination DTE (UNIFI) on an otherwise unloaded system.

The end-to-end measure was broken up into two components as follows:

1) Source DTE Access Time - is defined as the time between the source DTE signaling that it is ready to send a message to the time the source NAU signals that it is ready to receive the message.

Comment:

Quite obviously if the LSN is busy, this "Time" will depend on the system "offered load." In this report the "mean" value was measured as a constant (367us). In a realistic system, this time could be much longer. Note from Table A.9 that the "mean" value varied from a low of 16 Ous to a high of 998us (a ratio of 6.2). Either there are significant measurement errors or there are other unaccounted for independent variables that are having a significant effect on this measurement.

From Table A.9, the "peak" value has the following measurements:

Test Number	Measured (Peak)	Equation (Peak)	Ratio
9	5795	1856	-3.1
10	292	2027	+6.9
14	5399	2446	-2.2
17	283	1818	+6.4

Quite obviously, the "peak" equation is a very poor fit to the data.

2) <u>End-To-End Word Transfer Time</u> - is defined as the time it takes a <u>word</u> to pass from the source to the destination Standard Interface (refer to Figure 1).

<u>Comment</u>:

In that contention for the LSN is reflected in the polling rate (C), it would be expected that this "Time" be dependent on (C). However, the report indicates that Y_{peak} is dependent only on (A).

$$Y_{peak} = 134 - A$$

Note that when (A) reaches its maximum value of 148, Y_{peak} goes negative (?). It is not clear why the "mean" value is not dependent on (A) (?). Further, it is not clear why the measured time for the various tests were so long. For example, Test #2 calls for the highest Block Rate and Polling Rate and Smallest Block Size, yet the "mean" time to move one word between the Standard Interfaces took 17 milliseconds (?).

IX. CONCLUSION:

The above analysis of the report on FILAN Performance Metrics has been a critical evaluation with the purpose of determining the completeness of the report in meeting its stated objectives. In the opinion of this analyst, the objectives were not fully addressed by the study.

The stated primary objective was to characterize "FILAN performance", but the word "performance" was never qualified and the level of performance was never defined.

The test bed used to meet the objectives was itself a compromise with no discussion as to whether the full intent of the objectives would also be compromised. In that software protocols nor systems "bottlenecks" were not dealt with or addressed, it is clear that further work is necessary in order to evaluate total system performance.

The process of collecting data should be correlated with an understanding of the internal processes of the functional units that the data passes through. The understanding of the time periods involved in processing software protocols can be used to identify all significant independent variables. When all significant independent variables are held constant (including system state), then the corresponding dependent variable should be measured at approximately a constant value. If only a subset of the independent variables are of interest, then the remaining independent variables will need to be held constant or their effects will need to be subtracted out.

Once an equation has been determined that describes the relation between the dependent and independent variables, a measure of "fitness" to the measured data should be computed. If a "good" measure of "fitness" cannot be obtained, one can conclude that there are either significant measurement errors or there are unaccounted for independent variables that are affecting the measurement. The resulting equations should be further analyzed by qualatatively justifying the need for each of the independent variables and their relative weights. In this way, the equations not only provide a quanatative measure, but also provide a basis for understanding the processes involved. With this understanding it will then be

possible to recommend design modifications which will improve system throughput. This last exercise would then correlate the results of the study (the equations) to the original objectives.

If there are limitations in the measurement methodology that prevent a qualatative understanding of the equations and their correlation to the original objectives, then this fact suggests the need to alter the test bed. On the other hand, a successful study might point to the need to extend the objectives to that of the study of a more complete system which in turn, might suggest an extended test bed.

X. ADDENDUM:

After reviewing the report entitled "FILAN PERFORMANCE METRICS" dated June 3, 1985, a second report with the same title (which will be called the FINAL REPORT) was issued dated June 20, 1985. The FINAL REPORT included a number of changes in the text, a reorganization of the sections, and the addition of subsection 3.2.2.6 and sections 4, 5, 6. The above comments are applicable to the FINAL REPORT, the following additional comments reflect an analysis of this latest report.

a) Comments On Test Bed Used:

Because of the restricted test bed used in this study, all measurements were done under controlled conditions and any conclusions drawn should keep this fact in mind. For example, "the time required to send a single message across the LSN" (p. 75, FINAL REPORT) assumes the source NAU is waiting to transfer a packet and the destination NAU is ready to receive. Hence all delays due to contention are elliminated.

There were two apparent contradictions in the FINAL REPORT relative to the test bed. The first appears on page 61 under "Interpretation" in which the authors refer to "the test receiver in the VAX" as contributing toward the measurement. On page 11 they indicated that this function of the VAX was omitted. On page 12 the authors indicate that "all non-test related applications

(of the VAX) were suspended." On the other hand, on page 72 the authors qualify the "DTE transfer" time by pointing out that the "VAX regularly gets interrupted in the middle of message transmission by VAX systems services."

b) Problems in Measuring Poll/Query Time:

The authors state "A further complication occurred whenever the polling rate exceeded the packet rate" (page 26). The authors appear to be unaware that their test conditions always produced this situation. The basic problem was that after receiving a poll, subsequent polls to the source NAU resulted in "null" responses. With many "null" responses and one "query" response to an array of polls, the equipment did not lend itself to distinquish the initial poll from subsequent polls and perform an accurate measurement. Hence in performing the poll/query time measurement, the polling system was artificially manipulated. As a result "the scope of the analysis for this measure was restricted" (page 27), Table A.5 of the first report dated (6/3/85) was omitted and replaced by "the minimum, mean, and maximum time intervals" (page 27). In addition, "the multiple regression analysis was omitted" for this measurement "and a mean poll/query time was obtained" (page 52). The authors found the "mean" value for this measurement to be 650 microseconds. This value should be contrasted to a "peak" value of 2.75 microseconds listed in the report dated (6/3/85).

c) Comments on Section 3.2.2.6:

The first sentence of this section addressses the transmit time of a message across the source MIL-STD-1779 bus. Three components are given for this measure:

1) Source DTE access time.
2) Destination DTE transfer time.
3) Source DTE ACK/NAK time.

It seems that component 2) should involve the source MIL-STD-1779 bus as do the other two components. This requires replacing $(0.47B + 9.97)$ with $(-0.0099B^2 + 13.4B + 458)$ and correcting the final equation on page 80. The

equation on page 80 was later used to generate Figure 17, hence the conclusions based on this figure are suspect.

One further comment can be made relative to component 2) above. In "bit-bucketing" data into the destination UNIFI, all "handshaking" and processing time are elliminated. Hence DTE transfer time should occur at a constant word rate. This fact is reflected in the equations shown on page 62 (0.47 microseconds/word) but was not noted under "Interpretation" (page 63).

d) Comments on Section 4.0 (CONCLUSION):

Before any conclusions can be drawn, two components are needed: an understanding of the detail operation of the system and a quanatative description of the system. In section 5.4 the authors indicate that they are not familiar with the software functions being implemented during processing intervals nor their methods of implementation. This unfamiliarity is indicated throughout the report in such statements as:

"probably an artifact of the VAX test generator" page 47
"must be due to an increase in processing time" page 58
"unaccounted for" page 66
"probably stems from the same cause" page 68

Before any measure can be qualified, and any conclusion drawn, an understanding of the processes involved is necessary. Further, it should be kept in mind that all data was measured under controlled conditions (two NAU's, undirectional data transfer, no host-to-host handshaking). In addition, as pointed out above, the "regression equations" were not rigorously developed to provide a "close fit" to the measured data nor qualified and thus any conclusions based on these equations are suspect.

In spite of the above comments, the general conclusion drawn in section 4.0 is correct, namely the LSN bus is "idle the vast majority of the time" in that transfer time is only a small fraction of processing time.

e) Comments on Section 5.0 (RECOMMENDATIONS):

The current FILAN protocol for transfer of a message across the LSN is termed "P-Q-R-M", i.e. poll-query-response-message. Section 5.0 of the REPORT proposes an alternative protocol as follows: elliminate the query, send the message immediately following a poll (assuming a message is waiting to be transmitted) and allow the destination NAU to process the header of the message and either transfer the message into its buffer space or ignore it and form an ACK/NAK response. This protocol is termed "P-M-A", i.e. poll-message-acknowledgement. If the destination NAU does not have enough space in its buffer to accept the message the condition is called "congested", otherwise it is called "uncongested". These two conditions using both protocols are diagramed in Figure 2.

As can be seen from Figure 2, the transfer interval for the two protocols is the same under the congested condition assuming under the P-M-A protocol that the destination NAU can process the header and load the message into its buffer simultaneously. For the "uncongested" condition the transfer interval for the P-Q-R-M protocol exceeds that for the P-M-A protocol by the sum of time intervals 6, 7, 8. The difference reduces to the sum of time intervals 7, 8 if the destination NAU cannot process the header and load the message into its buffer simultaneously. Further, time intervals 7, 8 are included strictly to improve data transfer reliability.

The conclusion is that the P-M-A protocol is an improvement over the P-Q-R-M protocol but not to the degree indicated in the REPORT. Further, if the destination NAU cannot process the header and load the message simultaneously, the transfer interval using the P-M-A protocol will be larger than that for the P-Q-R-M protocol under the "congested" condition and the difference reduces to that of the sum of time intervals 7, 8, under the "uncongested" condition. On the whole, however, the P-M-A protocol is preferred. It was not clear why the REPORT suggests that the processing time intervals using the P-M-A protocol would be less than using the P-Q-R-M protocol?

Figure 2

Comparing the P-Q-R-M and P-M-A Protocols

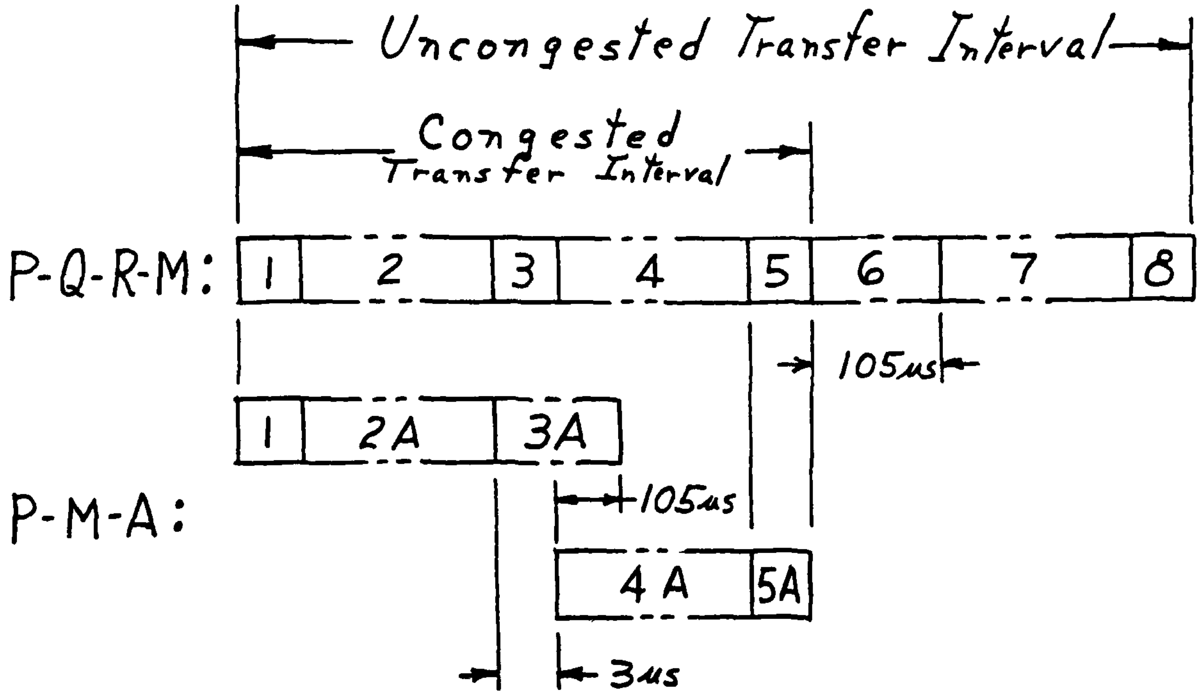

Time Interval	Description
1	LTC to Source NAU "poll" control packet transfer.
2	Source NAU process time (respond with either a "null" or a "query" packet).
3	Source to Destination NAU "query" control packet transfer.
4	Destination NAU process time (examine buffer space).
5	Destination to Source NAU "buffer full/empty" control packet transfer.
6	Source to Destination NAU message transfer (message should reside in a FIFO and be clocked out).
7	Destination NAU process time to form an "ACK" response.
8	Destination to Source NAU "ACK" control packet transfer.
2A	Source NAU process time (respond with either a "null" or a "message and header" packet).
3A	Source to Destination NAU "message and header" packet transfer.
4A	Destination NAU process time (load buffer or ignore message and prepare an "ACK/NAK" response.
5A	Destination to Source NAU "ACK/NAK" control packet transfer.

XI. RECOMMENDATIONS:

It is clear that LAN system delays are a function of network access methods, number of stations, number of protocol layers, and protocol functions needed at each node to communicate with all other nodes. It is also clear that message transmit time is a small percent of total transfer time and thus any system optimization must concentrate on protocol processing time. The FILAN system here under investigation controls access to the medium via a centrally controlled polling mechanism. Thus lower layer system delays are deterministic once an understanding of processing intervals is known, and the correlation between "offered load" and polling rate. At this point worst case delays can be computed as a function of "offered load" and the node-to-node services being offered. If the system is designed to accomodate an array of hosts such that application protocol layers are unknown as well as their language structures, then it will only be possible to study (in detail) that part of the system that connects the Standard Interfaces. This consideration reduces the number of protocol layers that may be studied in detail to four (transport, network, link, physical). The following recommendations will concentrate on the study of this aspect of the system.

It is recommended that the study of the FILAN system include both an evaluation of its design (detail analysis of each protocol service) with an "eye" to optimizing its performance (design modification) as well as its current performance limitations. The first phase should concentrate on performance limitations with design modifications using current technologies whereas the second phase should predict limitations with the current design. This approach to the evaluation of the FILAN system will then not only identify performance limitations but also will identify areas whose design modification will produce the greatest improvement in performance.

Each "service" provided by FILAN carries with it a penalty in terms of hardware, software, and system delays. It may be of interest to correlate the priority of each service with its corresponding penalty. Hence a study of FILAN might begin with identifying each "service" within each protocol and associating the services with physical devices (nodes). Each "service" is implemented within the physical devices via a processing function. We desire to optimize the processing throughput of these

functions. The following is a recommended design sequence for implementing the functions with the goal of minimizing system delays.

1) Each function should be correlated with a service within a protocol layer and ranked according to priority.

2) In implementing a particular function, identify any parallel processing that may be applicable (i.e. minimize the number of sequential operations.) For example, error detection of data blocks can be done with a dedicated unit in parallel with the data processing unit; a buffer may be loaded with data in parallel with the processing of the "header", etc.

3) Identify all functions that are candidates for a hardware implementation (e.g. encoding/decoding of data, comparators used to respond to buffer-space requests, FIFO's for loading messages, memory management units to control access to centralized resources, etc.). Use a hardware implementation wherever possible, particularly where the corresponding software implementation becomes a potential system "bottleneck."

4) When a hardware device is not available for implementing a particular function, use Table-Look-Up (firmware) rather than software processing wherever possible.

5) After completing steps 3) and 4), all remaining functions must be implemented in software. The first step in the implementation of these latter functions is to optimize a flow diagram. For example, a function should arrive at a final decision (terminal point) with as little information as possible thereby reducing to a minimum the number of processing steps.

6) Choose a CPU (microprocessor) with a "suitable" instruction set, high clock rate, large number of working registers (to minimize the number of data memory machine cycles), an instruction queue (to be able to fetch and process simultaneously), and a variety of addresing modes. Some consideration may be given to parallel processing in which several "services" are processed simultaneously.

7) After determining the "best" instruction set for the array of functions needed to be implemented, write all programs in assembler code. If very high throughput is needed, some consideration may be given to microprogramming a bit-slice microprocessor. This approach, however, is very costly in terms of the amount of hardware required and should be considered only if other methods are inadequate.

In general, an increase in processing throughput will require an increase in hardware. However, a design for maximum speed is desirable even if current requirements are surpassed in that the system will be able to "grow" to meet future demands.

It is suggested that processing time (or its range) be computed for each function implemented in either hardware, firmware, or software. Finally, tabulate all functions indicating proposed method of implementation, processing time, and the priority (need) of the function. Reviewing the protocol system, consider elliminating any redundant function. For example, should error checking be done at the network level, or be confined to the stations?

Once the above table is complete, "bottlenecks" (large system delays) can be quickly determined and correlated to hardward cost and priority. Final decisions relative to system design modification can now be made and maximim delays due to lower layer protocol processing can quickly be computed. Finally, by superimposing estimated application layer delays on the computed lower layer delays, one can compute system level delays and "size" the system in terms of maximum number of stations versus "services" provided. By comparing current design with proposed modified designs, one can not only determine performance limitations with the current design, but also project performance versus an array of design modifications.

ACKNOWLEDGMENTS

I would like to acknowledge the support of James Davis (RADC/DCLW) in obtaining pertinent reports, directing me to knowledgeable individuals, and critiquing this work. I would also like to express gratitude for the sponsorship of the Air Force Systems Command, Air Force Office of Scientific Research and the Rome Air Development Center.

REFERENCES

1. Stallings, William "Local Networks: An Introduction", Macmillan Publishing Co., 1984, page 234.

1985 USAF-UES SUMMER FACULTY RESEARCH PROGRAM/

GRADUATE STUDENT SUMMER SUPPORT PROGRAM

Sponsored by the

AIR FORCE OFFICE OF SCIENTIFIC RESEARCH

Conducted by the

UNIVERSAL ENERGY SYSTEMS, INC.

FINAL REPORT

METHODS FOR RELIABILITY WARRANTY VERIFICATION

Prepared by: Carolyn DeLane Heising - Principal Investigator

Academic Rank: Associate Professor

Department and University: Industrial Engineering Department, Northeastern University

Research Location: Electronic Systems Division (ESD)
Office of Systems Readiness Engineering
Deputy for Acquisition Logistics and Technical Operations
Hanscom AFB, MA 01731

USAF Research: Lee R. Pollock

Date: August 30, 1985

Contract No: F49620-85-C-0013

Research Assistants: Susan C. Malone, Fred C.S. Chin

METHODS FOR RELIABILITY WARRANTY VERIFICATION

by

Carolyn DeLane Heising

ABSTRACT

Methods for reliability warranty verification have been developed and applied to actual USAF systems under design and production. Two principal methods are described. The first is a procedure for predicting USAF system performance in the field (as measured by the variable Mean Time Between Failures (MTBF)), and is based on a Bayesian statistical updating approach. The second is a procedure for tracking maintenance data to verify the variable Mean Time Between Maintenance Actions (MTBMA). In addition, alternative reliability warranties are reviewed, and recommendations made as to which are preferable, particularly with respect to their ease of verification. It was found that the warranties which either guarantee the field MTBF with a verification test, or guarantee the field MTBMA are preferable to other alternatives, including the Reliability Improvement Warranty (RIW). The Bayesian procedure for updating system reliability estimates was found to be very useful in estimating USAF performance, and is recommended for implementation as a method for tracking reliability warranties in practice.

ACKNOWLEDGEMENTS

We would like to thank our Air Force research collaborator, Mr Lee Pollock, for facilitating the opportunities we have experienced this summer. We should also thank the many people who aided us during the performance of this work, either by providing information or guidance in this effort. These included Mr Steve Dizek and Dr Ruth Bordenstein of TASC, Mr Dave Goldberg of Dynamics Research, and Mr Frank Van Horn, Mr Robert Forney and Mr Ian Feltham of ESD/ALEK in the area of warranties, Lt Pete Reho, LTC Steve Sechrest, and Mr Murray Black in the area of MTBF reliability predictions, Capt Don Campbell and Col Wayne O'Hern in the area of MTBMA reliability verification, and Mr Monty Joel, Capt Don Loose, and Lt Tim Aiken in the areas of Human Factors and Human Engineering. Last, we are indebted to our sponsors, the Air Force Systems Command, Air Force Office of Scientific Research, and the Electronic Systems Division, Hanscom AFB, MA. We also thank Mr Gary Grann of ESD/XR for serving as our effort focal point, and Dr Agnes Bain of UES for providing useful information to us on the purpose and academic goals of this program.

I. Introduction

Reliability of large, technological systems is essential for maintaining a stable and growing economy, and a safe working and living environment. Over the past two decades, reliability analysis has emerged as a growing academic research area as industry and government alike strive to improve the reliability and safety of their ever more complex -- and threatening -- technological systems. The nuclear power industry has led the way in this effort, followed by the electronics and aerospace industries. More recently, the chemical and hazardous material industries have also followed suit, partially motivated by recently occuring, devastating accidents (for example, the Bhopal, India event).

One of the major areas where high reliability is required is in military defense systems, such as those being developed for use by the U.S. Air Force. Such systems are typically highly complex, and therefore expensive, and these systems must be available and ready for any possible chain of events, whether in peace or war time environments. Moreover, unreliable systems have cost the US taxpayers many millions of dollars in spare parts and maintenance actions that could have been avoided had reliability been designed into the product in the first place. Both the defense industry as producer and the military as users have cited reliability as a major priority in recent years.

The Electronic Systems Division (ESD) located at Hanscom AFB in Massachusetts serves as one of the largest procurement centers for complex systems in the USAF today. The Office of Systems Readiness Engineering at ESD has been charged with the responsibility for ensuring that contract policies will be implemented and followed that will result in highly reliable systems being procured. To this end, reliability methods for guaranteeing such performance are being developed and implemented for use. Mr Lee Pollock, Director of the Systems Readiness Engineering Division has an educational and professional background in reliability analysis, and has seen a need for improvement of reliability in these complex systems.

II. Objectives of the Research Effort

In the product assurance department of ESD at Hanscom AFB, an effort is being waged to "return to the basics" to ensure high product reliability and quality. To contribute to this effort, our research team has investigated objectives related to product assurance warranties and incentives, making recommendations for how such warranties can be written and actually implemented by ESD. We provided programmatic support to two procurement programs: the Joint Tactical Information Distribution System (JTIDS) program, and the MILSTAR EHF satellite communications system program.

Four research objectives were developed for the summer effort, the first dealing with product assurance warranties, the second with product assurance acquisition methods, the third with an assessment of the reliability of on-going ESD acquisition programs, and the fourth with human factors requirements in ESD systems acquisitions. As the summer evolved, greater emphasis was placed on the third task dealing with the programmatic support, with the results that reliability methods for warranty verification were developed, particularly a Bayesian approach for field reliability prediction. In the following report sections, these four objectives are addressed separately, with recommendations made at the report conclusion.

III. Product Assurance Warranties

A report entitled "Methods for Developing Repair Warranties" was prepared detailing work done on developing appropriate repair warranties for ESD acquisition programs (ref 1). To summarize the work done here, it is noted that the purpose of the effort was to investigate approaches for developing a generic warranty for ESD developmental systems. These included two types of warranties: (i) warranties for reliability improvement (RIW) (measuring MTBF), and (ii) field warranties for maintenance reliability (measuring MTBMA).

Professor Heising is a well-known researcher in reliability methods, and for many years taught and conducted research at MIT in the Nuclear Engineering Department where she specialized in developing procedures for analyzing the reliability of nuclear plants. Since that time, she has joined the Industrial Engineering Department at Northeastern University in Boston where she teaches undergraduate and graduate courses in reliability analysis. At Northeastern, she has been active in developing an interdisciplinary research program in reliability analysis which focuses on the analysis and comparison of risks among various technologies, including chemical and nuclear plants, dams, hazardous waste disposal and other systems. She is well-known for her work on the use of Bayesian methods to predict system performance, and has written many papers, mostly nuclear related, that deal with this subject. With her colleagues Dr Stan Kaplan of PLG and Prof George Apostolakis of UCLA, she has been influential in the recent adaptation by the nuclear industry of a Bayesian approach to nuclear power plant reliability analysis.

Recent research interests have led her to consider the reliability problems unique to military defense systems. Last year, she completed a consulting project on US air base defensability in the face of a chemical attack for Brooks AFB in Texas. There, decision analysis methods were used to develop an analytic framework useful to commanders who might one day face such a chemical attack on their air base.

Her recent interest in these areas, along with Mr Pollock's, led to the research collaboration at ESD this summer. Prof Heising has been joined in this effort by two of her students from Northeastern who recently completed course work under her direction. These were Ms Susan C. Malone, a masters degree candidate in Industrial Engineering, and Mr Fred C.S. Chin, a senior in the undergraduate Industrial Engineering Program. Both students have research interests in reliability and were gratified to find that they could apply many of the concepts taught in the classroom to the real-world systems at ESD. To them, the summer experience has been useful in this regard as well as many others.

A. The Reliability Improvement Warranty (RIW)

With regard to the RIW, the warranty is to: (a) commit the contractor to repair items furnished to the government, and (b) inherant in the repair requirement, have the incentive to improve reliability. Four objectives were outlined: (1) review past examples of reliability improvement warranties, (2) investigate the validity of the conceptual framework for reliability growth testing, (3) based upon work for the JTIDS-1 program, make policy recommendations as to which warranties are most effective, and (4) investigate possible alternatives for an effective repair warranty.

An historical review of RIWs was conducted, based upon previous work by TASC (see ref 1). It was found that most RIWs make use of an MTBF guarantee, measured in hours, for each Line Replaceable Unit (LRU) as well as the system as a whole. The guarantee is specified over a five-year period, and a reliability growth model is used to set the values which the contractor must meet.

Reliability growth testing methods were reviewed. It was found that the conceptual framework for reliability growth is theoretically sound, but it appears that many problems may arise from the actual application of these methods to a real case. Of the available methods, the Duane methodology seems most appropriate for practical application, and can provide a basis for the reliability methods to be used in determining values for MTBF versus time.

(Recommendations based on this work are found in section VII.A.1 of this report.)

B. Field Warranty (MTBMA): Reliability and Maintainability Warranty

With regard to the field warranty, it is to: (a) commit the contractor to develop equipment maintainable and more supportable in the field, and (b) provide an economic incentive to do so. Four

objectives were outlined: (1) review past examples of warranties related to maintenance actions in the field, (2) investigate possible alternatives for an effective maintenance warranty, (3) use MILSTAR programmatic support to make policy recommendations, and (4) provide an example warranty.

It was found that there have not been many MTBMA-type warranties. The MILSTAR warranty was thus used as the example warranty to be examined here. Incentives in the MILSTAR program are awarded on achieving MTBMA goals after various periods of time. Recommendations based on the MILSTAR experience are included in section VII.A.1 of this report.

IV. Product Assurance Acquisition Methods

A review was made of the ESDR 800-5 and the associated Product Assurance Handbook, the backbone of the "Back-to-Basics" emphasis. Overall, the handbook appears to provide thorough, detailed guidance to potential defense contractors. Certain good features include the specification of MTBMA requirements in addition to the standard MTBF. As discussed elsewhere in this report, MTBMA appears to be an effective and more easily verified performance measure than MTBF. Also, the Maintainability Design Criteria (see Method 10) are thorough, and this is an important reliability area often overlooked. Failures and/or errors can be inadvertently induced during maintenance, particularly if the equipment is not designed with maintainability in mind. Fortunately, in the maintainability demonstration, these induced failures are studied, in the hope of reducing their occurrence.

There are a few areas in the handbook where more emphasis may be useful, or perhaps merely a more detailed explanation would suffice. In Method 4, there appears to be a less than explicit discussion of adequate reliability predictions and verifications. In Method 5, it may be worth noting what happens once a non-standard part is approved for use; does it then become a standard part, or will it repeatedly need to go through the approval process for future use?

In Method 9, there appears to be a fair amount of subjectivity in classifying failures as relevant or non-relevant, which could lead to discrepancies between contractor and government claims. Also, in setting reliability performance specifications to be met, it may be useful to set confidence intervals rather than exact numbers. This would result in less opportunity to debate the relevancy of each failure. In addition, it should be considered a relevant failure when there is a procedural error by an operator, because there is a high probability the error will be repeated.

V. Assessment of the Reliability of On-Going ESD Acquisition Programs

This effort was split between two ESD programs; the first being the JTIDS Class 1 system and the second being the MILSTAR system. Many accomplishments were made in addressing the project research goals specific to each program, and are described separately in the following two sections. Mr Chin supported the JTIDS program, and Ms Malone the MILSTAR program.

A. The JTIDS-Class 1 System Program

Actual accomplishments performed for this program included several briefings of USAF personnel in the program offices, two memoranda by Fred Chin dealing with a Bayesian calculation of JTIDS-1 (Airborne) reliability in the field (refs 2 & 3), and a report prepared by Dr Heising documenting the Bayesian methodology used in the estimations, entitled "Bayesian Methods for Predicting USAF System Performance" (ref 4).

The focus of the support provided to the Joint Tactical Information Distribution System (JTIDS) program office was to assist in the reliability prediction of the "new" refurbished systems which have been subjected to an improved, more stringent manufacturing process.

Apparently, the manufacturer of these systems had been providing the program office with an abundance of test data from different phases of the manufacturing process as well as field data from systems already in operation. Given this information, the program office was unable to determine a method which possessed the capability of combining diverse sources of information and data together, for the purpose of conducting a reliability prediction.

After the objectives had been clearly defined, various methods for reliability analysis were researched. These included Duane Growth Curves, Weibull Analysis, Hazard Plotting and many others. As a result, a Bayesian approach was selected because of its ability to combine various sources of information together to derive a "best estimate."

Initially, with the assistance of Lt Pete Reho, a reliability engineer from the JTIDS program office, a fault tree of the system was constructed and predicted failure rates from the manufacturer's development program document dated 1978 were propagated through the tree, resulting in a mean system reliability measure of 526 hr MTBF respesenting the prior knowledge of the system. With the application of Discrete Probability Distribution (DPD) arithmetic, a distribution of the prior knowledge was determined by incorporating analyst judgement.

Next, the Binomial distribution was applied in the calculation of the likelihood function, or the updated knowledge of JTIDS. Using data from the Reliability Demonstration was believed justifiable because it was obvious that this phase of the manufacturing process closely resembled the conditions faced in the field. Calculations were performed and a likelihood distribution was drawn representing the new knowledge of the JTIDS system reliability.

Finally, via Bayes' theorem applied to discrete distributions, a posterior distribution of 'best estimate' was determined. The calculations resulted in a mean value of 182 hr MTBF - our initial prediction.

This initial analysis of the system reliability was presented to the program office under the assumption that the analysis would be refined using more relevant and recent data. Response from the program office was very positive; and enthusiasm towards the commitment to improve upon the confidence of the analysis was high (see ref 2).

Upon improving the analysis, effort was directed towards achieving results with greater confidence. First, the best data available which are the predicted failure rates from the manufacturer's development program dated 1981 (as opposed to 1978) were used in the fault tree analysis. This resulted in a new prior distribution with a mean value MTBF of 422 hrs. In addition, the intervals of MTBF were better defined to effectively illustrate the impact of the distributions on a specified MTBF interval.

Calculation of the likelihood function was performed using the Poisson distribution since it was learned that the Poisson distribution was employed to obtain conditional probabilities when the prior distribution was represented by an Inverted Gamma distribution and reliability was measured in terms of MTBF as was true in our case. Data from the Reliability Demonstration was again used in these calculations including two scenarios that were suggested by the program office (see ref 3).

B. The MILSTAR Program

Actual accomplishments performed for the MILSTAR program included a major briefing of USAF project personnel, and a report by Susan Malone dealing with a proposed method for verifying a maintenance reliability warranty (ref 5).

The objective of this method was to develop a means by which the MILSTAR program office could track Engineering Development Model (EDM) maintenance data, in order to determine system Mean Time Between Maintenance Actions (MTBMA), independently of the contractor. MTBMA is then used to calculate contractor's earned incentive, a monetary reward issued at certain milestones throughout EDM deployment, and designed to motivate the contractor to supply reliable, maintainable equipment.

Data elements such as operating hours, failure type, corrective action, and system component designators are necessary to accurately determine MTBMA, and thus any maintenance data collection system used to support MTBMA calculations must contain these elements as a minimum.

Currently, maintenance data is reported on the AFTO Form 349, and entered into the Maintenance Data Collection System (MDCS) data base. The MDCS does contain all of the necessary elements discussed above. However, this system is gradually being replaced by the Core Automated Maintenance System (CAMS), a computerized version of the MDCS. Whereas in MDCS the maintenance technicians completed printed 349 forms, in CAMS, they will enter the information directly onto a terminal at their workstation, thus the data will automatically enter the data base.

Because of the staggered implementation of CAMS, it is uncertain whether it will be fully operational at both of the MILSTAR maintenance sites at EDM deployment, thus recommendations have been made for both cases.

A thorough study was made of possible methods of MTBMA warranty tracking, in both MDCS and CAMS, and a report was prepared which summarized these methods, their advantages and disadvantages, their mode of implementation, and a timetable of what should be done when. A variety of methods were presented, some having been applied in the past, others had never before been attempted. Most were computer-based, to facilitate the collection and analysis of large quantities of data. Because of the extensive discussion accompanying the methods, they are not presented here, but the complete report is noted in ref 5.. While certain suggestions were made, all necessary facts were presented in order to allow the program office to make a final decision.

In addition to maintenance collection alternatives, a scheme was developed which would facilitate implementation of the warranty

tracking system in the program office. It is important to have the maintenance data easily accessable to the program office to enable timely analyses and MTBMA determination. In this way, the MTBMA can be calculated accurately and quickly enough to verify the contractor's claimed incentive at each milestone.

VI. Human Factors Engineering in ESD Systems Acquisitions

Human factors engineering is a technical area which seeks to make effective use of people's performance capabilities through careful design, and integration of people and their working environment. Human factors has a solid background in the military, as many military systems prompted the need for improved man-machine interfaces. However, in more recent years, it appears that, while aircraft are still well human factored, many other military systems do not have as much emphasis on human factors as necessary. The reasons for this are unclear, but it could partially be due to the diverse field of human factors getting obscured in the more well-defined complex technical areas.

During this summer effort, an attempt was made to become familiar with the role of human factors in the defense acquisition process here at ESD. The MILSTAR and PEACE SHIELD programs were looked at specifically, and also a general overview was obtained. While PEACE SHIELD appears to support a significant human factors effort, this program seems to be the exception rather than the rule. The human engineering design guidelines (eg. MIL-STD 1472C and MIL-H 46855B) are quite thorough, and if they were carefully adhered to, the systems would be well human engineered. Unfortunately, this does not appear to be the case. Whether due to a lack of understanding and/or appreciation of human factors, a scarcity of qualified human factors specialists, a need to cut corners (costwise and timewise) wherever possible, or an insufficient data base, human factors and human engineering just do not appear to receive the emphasis they deserve.

While there certainly are capable human factors specialists at ESD, there do not appear to be enough to go around for all programs, thus making enforcement of human factors standards difficult. As for cutting corners, "The investment [of time and money] in human engineering is relatively small compared to other areas, and the return on investment is relatively high" (from AFAMRL-TR-81-35 Human Engineering Procedures Guide). And it is much less costly to correct a problem in the design stage rather than during production.

Part of the problem of lack of understanding or appreciation may be that much of human engineering is seen to be abstract and theoretical. A compendium of results of practical applications may bring the area into sharper focus for those unfamiliar with it; some type of lessons learned would be valuable.

One area related to human factors and human engineering which could prove of some value to the military is Swain and Guttman's concept of Human Reliability Analysis (HRA). Rather than quantifying only equipment and parts reliability in a reliability analysis, the human operator's reliability is also considered (eg. how likely is the operator to make an error on a given task), thus resulting in more accurate reliability analyses. Swain and Guttman have focussed upon nuclear power plant applications, but there do appear to be some correlations with military systems. There is a great deal of subjectivity involved in determining these human error probabilities, but when used with caution, they could possibly provide some added insight into defense systems' reliability.

VII. Recommendations

As a consequence of the research we have performed this summer, many recommendations have resulted that may be useful to USAF personnel. Also, several ideas for follow-on research have been generated.

A. Implementation of Research Results

Recommendations for implementing our research results are now given with respect to each of the four project objectives.

A.1 Recommendations for Product Assurance Warranties

From the work performed on the reliability improvement warranty, it was recommended that thought be given toward the adoption of a warranty on total system MTBF to be based upon various possible Verification Test (VT) alternatives. The MTBF-VT warranty was recommended over the RIW because of its lesser degree of complexity and its wider applicability. Also, it is recommended that laboratory tests be scrutinized carefully for the purpose of predicting field reliability since, in worst case situations, MTBF may indeed be difficult to estimate, let alone its theoretical growth potential. It would seem a more prudent approach to have contractors guarantee an adequate field reliability, and attach to that a repair warranty if this MTBF is not met. This may be more preferable than a reliability improvement warranty. Also, this approach may prevent contractors from being rewarded for sloppy initial designs.

From the work performed on the field warranty, it is recommended that availability be the reliability measure warranted in field application, where

$$\text{Availability} = \frac{\text{MTBF}}{\text{MTBF} + \text{MTTR}} \quad \text{and MTTR} = \text{Mean Time To Repair}$$

The adoption of this approach will solve three problems:

1. If MTBF is solely warranted, there is no easy way to determine the impact on final contract costs or time-to-completion, since it is known that as MTBF improves, MTTR also grows longer, thus decreasing availability.

2. The MTTR variable is important from a human factors/ maintenance perspective, in as much as it is people who repair the systems in the field. The MTTR may actually be longer when the contractor does the repair because of longer turn-around times due to the non-proximity of the contractor to the field, so this variable should be warranted so as not to reduce system availability any further than is necessary.

3. System life-cycle costs are a direct function of availability. Thus, economic incentive for improving availability can be directly calculated.

A.2 Recommendations for Product Assurance Acquisition Methods

As a result of some of the observations noted in Section IV, certain recommendations may be worth considering for the Product Assurance Handbook.

(1) Specify how reliability predictions will be verified. This should enable the contractor to obtain a better understanding of just what is expected.

(2) Specify what becomes of a non-standard part once it is selected for use. This may have an effect on contractors' part selection approach.

(3) Be more specific on some of the relevant and non-relevant failure definitions to avoid discrepancies. Specific examples may be useful to clarify.

(4) Specify confidence intervals on reliability performance. This should eliminate the need for any subjective judgement in RVT success determination.

(5) Define operator and maintenance related failures as relevant, as their occurence during test suggests they would be even more likely to occur in the field.

If incorporated, these suggestions should result in somewhat more detailed guidelines for the contractors, leaving less room for subjectivity.

A.3 Recommendations for ESD Programs

These are given with respect to each program.

A.3.1 Recommendations for JTIDS-1

After an intensive reliability analysis of JTIDS Class 1 (Airborne), several recommendations can be presented.

(1) A simple, justifiable, and effective method for making reliability predictions must be available for engineers of the program office. The proposed Bayesian approach may be the solution to this problem. The validity of this approach has been proven in many of the technological areas, and predictions can be verified when the systems are deployed in the field and performance data is collected. Furthermore, this method may be applicable to other USAF programs.

(2) Upon data review, action must be taken to control the issue of data management since the confidence of any analysis rests on the validity and relevance of the data.

(3) It is the responsibility of the analyst to incorporate the proper data. Updating estimates is recommended to guarantee results with high confidence.

A.3.2 Recommendations for MILSTAR

The study of the MILSTAR warranty tracking system led to a variety of alternatives being presented, and some preliminary recommendations being made. Perhaps the most basic recommendation is that no additional data collection systems should be introduced. Because the necessary information is being collected now, it seems advisable to use it rather than requiring the technicians to complete additional forms. Additional forms mean more work and this may reduce the amount of time the technicians can spend on each form, possibly reducing the accuracy of the data reported.

In the MDCS, the maintenance data can be obtained either through actual retrieval, access to the Maintenance and Operational Data Access System (MODAS) a collective data base, or direct access to the individual data bases. MODAS appears to be the most efficient and least complicated method to obtain the MDCS data. CAMS has a similar collective data base which is designed for remote user access and is probably the best way to obtain that data. These collective data bases have user support and documentation, and are designed for easy access, therefore their use is recommended. Proper authorization must be obtained to access these data bases, but there is no difficulty expected in that.

Several ways exist to obtain the form 349 form narrative data elements Corrective Action and Discrepancy. These items may contain important information not easily obtained in other areas of the data base, and yet because they are in narrative form, are not coded. It may be advisable to develop codes for these data elements. Obtaining authorization to implement these codes may be difficult, but if ample time is allotted, any problems should be worked out. Other additional considerations have been outlined, along with justification for them, and can be found in detail in ref 5.

A.4 Recommendations for Human Factors in ESD Programs

There is substantial room for expansion in the area of human factors. Part of the problem is the quantity of standards which must be consulted to perform a proper human factors analysis. A "Human Factors Back-to-Basics" may be useful to develop. This could include a matrix, such that programs known to require application of certain standards may be pin-pointed, and therefore an algorithm can be designed specifying standards for certain types of programs.

Also, a human factors "lessons learned" may be useful. If part of the problem of insufficient attention to human factors is that people are unfamiliar with its significance, a lessons learned document would be valuable. Capt Don Loose of ESD/ALET is currently editing such a document; it presents situations from actual DOD programs in which human factors (either inclusion or exclusion of) appeared to have a real impact on the program's success or failure. This lessons learned is soon to be released, and is expected to have a broad distribution, thus calling the human factors issue to many people's attention.

Finally, it may be useful to explore the possibility of applying Swain and Guttman's Human Reliability Analysis method to military situations. If properly applied, it could enable more accurate reliability analyses to be performed, taking into account human reliability.

B. Suggestions for Follow-On Research

Two areas were developed as possible follow-on efforts: (i) development of a human factors simulation model of maintenance for prediction of key field reliabiliy factors, and (ii) use of a Bayesian methodology for predicting systems field reliability incorporating factory test results.

The purpose of the first effort is to develop a methodology for the prediction of key reliability factors: Mean Time To Repair (MTTR), and Mean Time Between Maintenance Actions (MTBMA). The approach to be taken would be based on a simulation model developed at the Oak Ridge National Laboratory (ORNL) in Tennessee. Other methods include the Swain-Guttmann human reliability model (THERP) and the NUS human factors model.

The purpose of the second effort is to develop a best estimate of system reliability in the field based on generic data and factory reliability tests. The approach is to develop fault trees of the system to be analyzed. Then, generic component failure rate data is propagated through the tree to calculate the "top event" failure rate distribution. The "new information" are the factory test results. The likelihood function may often take the shape of a Poisson distribution if the variable is MTBF. Once prior and likelihood distributions are known, these are discretized and combined using discrete probability distribution (DPD) arithmetic. The posterior distribution that results is then the "best estimate" of system field reliability, and includes uncertainty. This procedure allows generic data to be combined with the available experimental data. Even, and especially, when the experimental data is sparse, this procedure can result in statistically valid results.

References

1. Heising, C.D., "Methods for Developing Repair Warranties," Final Memorandum to L. Pollock and R. Forney, ESD/ALEK, Aug 22, 1985.

2. Chin, F., "A Proposed 'Bayesian' Approach for JTIDS Class 1 Reliablity Predictions," Memorandum to LTC S. Sechrest, August 9, 1985.

3. Chin, F., "A Revised Bayesian Estimate of JTIDS Class 1 Reliability Predictions," Memorandum to LTC S. Sechrest, August 30, 1985.

4. Heising, C.D., Bayesian Methods for Predicting USAF System Performance, Report, ESD/ALEK, August 1985. (for JTIDS-1 support effort)

5. Malone, S.C., "Maintenance Data Collection System for MILSTAR Warranty Tracking System," Memorandum to Capt Don Campbell, July 22, 1985.

REF. 1

22 August 1985

TO: Lee Pollock and Bob Forney

FROM: Carolyn Heising Carolyn H

Re: Methods for Developing Repair Warranties

Attached is the work I have completed on research of methods for developing repair warranties. The enclosure is similar to the draft report I left with you on July 30. This report summarizes the work done in response to the task related to the warranty work that was agreed upon in our original statement-of-research-objectives.

cc: G. Grann (MITRE)
S. Malone
F. Chin

METHODS FOR DEVELOPING REPAIR WARRANTIES

Introduction

As stated in our research objectives 1 a/b, we are to become familiar with the requirements for, purpose and wording of performance incentives and warranties, including: (1) warranties for reliability improvement (MTBF), and (2) field warranties for maintenance reliability (MTBMA). This short interim report summarizes work done to date to accomplish these objectives. This report is divided into two sections; the first deals with the reliability improvement warranty, and the second with the field warranty.

I. Reliability Improvement Warranties (MTBF)

The purpose of this effort is to investigate available approaches for developing a generic warranty for ESD developmental systems which: (a) commits the contractor to repair items furnished to the government; and (b) inherant in the repair requirement, have the incentive to improve reliability. Four objectives are outlined: (1) review past examples of reliability improvement warranties, (2) investigate the validity of the conceptual framework for reliability growth testing, (3) based upon work with the JTIDS-1 program, make policy recommendations as to which warranties are most effective, and (4) investigate possible alternatives for an effective repair warranty. Progress to date on these four objectives are reviewed here. Finally, preliminary recommendations are provided.

A. Review of Past Examples of RIWs

The TASC Corporation has been contracted by the USAF Product Performance Agreement Center (PPAC) to review various repair warranties. An historical assessment of these warranties has been conducted. We review these results here as they relate to our project this summer. Additionally, a summary of notes taken from the relevant PPAC report is included as Appendix I of this report.*

Previous use of RIWs has been on the programs listed in Table I. Characteristics of a RIW are given in Table II. Basically, the RIW is a contractual tool whose chief goal is the motivation of contractors to design into their system both enhanced reliability and/or cost support features. The contractor assumes the full responsibility for repairing or replacing the warranted items over a fixed time period. The contractor is given latitude to take whatever steps are necessary to meet specific reliability objectives. The reliability variable measured in these applications is the mean-time-between-failures (MTBF). Advantages of the RIW are reviewed in Table II, as well as disadvantages. Costs of the RIW are shown in Table III, and range between 6 to 25 percent of the total program cost.

---

* The reference is: Historical Assessment Report, TR-4632-1R, Dec 1983. Prepared by TASC for PPAC under Contract No. F33657-82-C-2207.

TABLE I

PROGRAM NAME	PPA NOMENCLATURE
1. B52 OAS Attitude Heading Reference System (AHRS)	RIW
2. C-141 AHRS	RIW with MTBF Guarantees
3. C-141 AHRS War Readiness Material Gyro	RIW
4. ALCM Inertial Navigation Element	RIW with MTBF and Availability Guarantees
5. AN/ASN-128	RIW with MTBF Guarantees
6. ARN-118 TACAN	RIW with MTBF Guarantees
7. A-10 Inertial Navigation System	RIW with MTBF Guarantees
8. B-52 OAS Controls/Displays	RIW
9. B-52 OAS Processor	RIW
10. B-52 OAS Radar, Advance Capability	RIW
11. B-52 OAS Radar Altimeter	RIW
12. Carousel IV INU	RIW with MTBF Guarantees
13. C130 Omega Navigation System	RIW with MTBF Guarantees
14. F-16 Flight Control Computer	RIW
15. F-16 Heads Up Display	RIW
16. F-16 HUD Electronics	RIW with MTBF Guarantees
17. F-16 Inertial Nav. System	RIW
18. F-16 Radar Antenna	RIW
19. F-16 Radar Computer	RIW
20. F-16 Radar Digital Signal Processor	RIW
21. F-16 Radar Low Power RF	RIW
22. F-16 Radar Transmitter	RIW
23. Standard INU	RIW with MTBF Guarantees
24. AN/ASN 92(V) CAINS	CAINS Reliability & Operational Warranty for the Navy (CROWN)

TABLE II

Objective:	Reduce failure of components during intervals between periodic overhauls.
Characteristic:	Preventive.
Applicability:	Critical, potentially high failure rate components. Fixed price type contract.
Description:	The contract contains a contractor or Air Force overhaul interval for specified components and identifies remedy required when components (on an individual or statistical basis) experience specified types of failure before the next overhaul.
Measurement:	User must maintain individual time-to-failure records for the affected component. These data will be used periodically to establish contractor conformance to requirements.
Result:	Price adjustments for failure to meet specified overhaul times; loan of spare components, accomplishment of overhaul, or repair of material; or some combination of the above.
Advantages:	Motivates contractor to provide increased equipment reliability and as a consequence minimizes disruption of operations between scheduled overhauls; Measurement parameters easily defined. Provides an additional opportunity to learn more about field performance of products. Provides an opportunity for increased profit.
Disadvantages:	Requires tracking and data collection in excess of normal requirements. Can lead to litigation particularly with regard to misuse/mistreatment of equipment. Additional contractor risks involved in sale and support of products. Must rely upon user to provide data for assessments.
General:	Used by aircraft industry for components which must be periodically overhauled/tested/inspected for soundness. Long term coverage (up to five years commencing with user's first use of the product) helps stabilize support programs for user.

FROM: The Product Performance Agreement Guide, 1980.

TABLE III

PROGRAM	TOTAL RIW COST	TOTAL PROGRAM COST	RIW COST % OF TOTAL COST	RIW COST % OF TOTAL COST PER YR	RIW COST % OF UNIT COST	RIW COST % OF UNIT COST PER YR
F-16 INS	$ 800,709	$ 5,937,780	13.5%	2.6%		
C-130 INS	654,405	2,566,272	25.0%	5.0%		
Carousel INS	4,276,589				8.0%	8.3%
ARN 118 TACAN	12,506,986	112,000,000	11.1%	3.0%	18.4%	4.9%
AN/ARN 123	197,700	2,700,000	7.3%	1.8%	10.8%	2.7%
APN-194	N/A	N/A	N/A	N/A	14.0%	7.0%
AN/APN-209	1,900,000	12,600,000	12.4%	4.6%	19.0%	6.0%
CN 494/AJB-3 Gyro	3,800,000	N/A	N/A	N/A	88.0%	18.0%
CN 494/AJB-3 Gyro (and contract)	2,500,000	N/A	N/A	N/A	58.0%	9.7%
F-111 Gyro	1,332,200	7,164,550	18.6%	3.7%	23.0%	4.6%
AHRS WRM Gyro	86,184	658,800	13.1%	2.6%		
A-24G-27 Gyro						7.3%
A-10 INU	5,641,025	33,771,844	17.0%	3.4%	26.0%	5.2%
F-14 Hydraulic Pump (ABEX)	1,600,000	6,300,000	25.4%	5.1%	25.8%	5.2%
Klystron Tube	14,784	250,000	5.9%	1.5%	6.3%	1.6%
Omega	654,360	3,766,041	17.4%	3.5%	25.5%	5.1%
F-16 Components	44M (NTE)	406,000,000	10.8%	2.7%		2-6%
Blackhawk Helicopter	6,400,000					

The TASC organization has done a comparative analysis of a situation with and without an RIW implemented. Results are shown here, and are based on a 15 year life cycle of a receiving processor.

RIW and No-RIW Costs - The RIW option yields a total cumulative discounted cost of $14,217,202. This compares with the no-RIW option whcih yields a total cumulative discounted cost of $15,565,930. Clearly, based on cost alone, the implicit choice is to apply an RIW. However, further analysis should be performed in order to validate this choice as outlined in brief below.

RIW and No RIW Cost Streams - There is no breakeven point for this example. The RIW case clearly dominates (in terms of lowest cost) from the first year. The cost streams for the two options are illustrated in Figure 1. Note that the marked increase in the RIW cost stream between years five and six is largely the result of equipping the base and depot levels with support equipment and the start of organic repair activities.

Further Analysis - Further analysis and/or program office activity should be performed at this point in the analysis. A suitable type of analysis to shed more light on the results of this example include reliability sensitivity analysis. If a decision is made to implement the RIW, analysis of the costs of two- vs three-level maintenance for the organic case after the RIW period is justified.

Most systems have experienced increased reliability and therefore lower life cycle costs. In this sense, RIWs in general have been effective. However, RIWs could have been more effective with better management and implementation procedures. As TASC notes, the ARN-118 TACAN program had a high rate of failures which was excluded from the warranty because the seals had been mistakenly broken. Also, there were excessive delays between failure notification and the issuance of Material Release Orders, as well as delays in returning failed units to the contractor for repair, which caused increased pipeline time and lower availability. Representative RIW clauses from the TASC report are provided in Appendix II here, and include:

(1) the reliability assurance warranty for the AN/ALQ-165, and

(2) the RIW for the A-10 inertial navigation unit.

Additional information on RIWs was gathered from discussions with Mr. Dave Goldberg of Dynamics Research Corporation of Wilmington, and Mr. Steve Dizek of TASC in Fairborn, Ohio. Notes from these meetings are included as Appendix III here. A review was made of the document prepared by Mr. Goldberg that outlines a possible approach to RIWs. Also, the generic RIW prepared by Mr. Dizek for PPAC was reviewed (see Appendix II).

B. Reliability Growth Testing Methods

The report entitled Reliability Growth Testing Effectiveness, RADC-TR-84-20 has been reviewed. The conceptual framework for reliability growth is theoretically sound, but it appears that many problems may arise

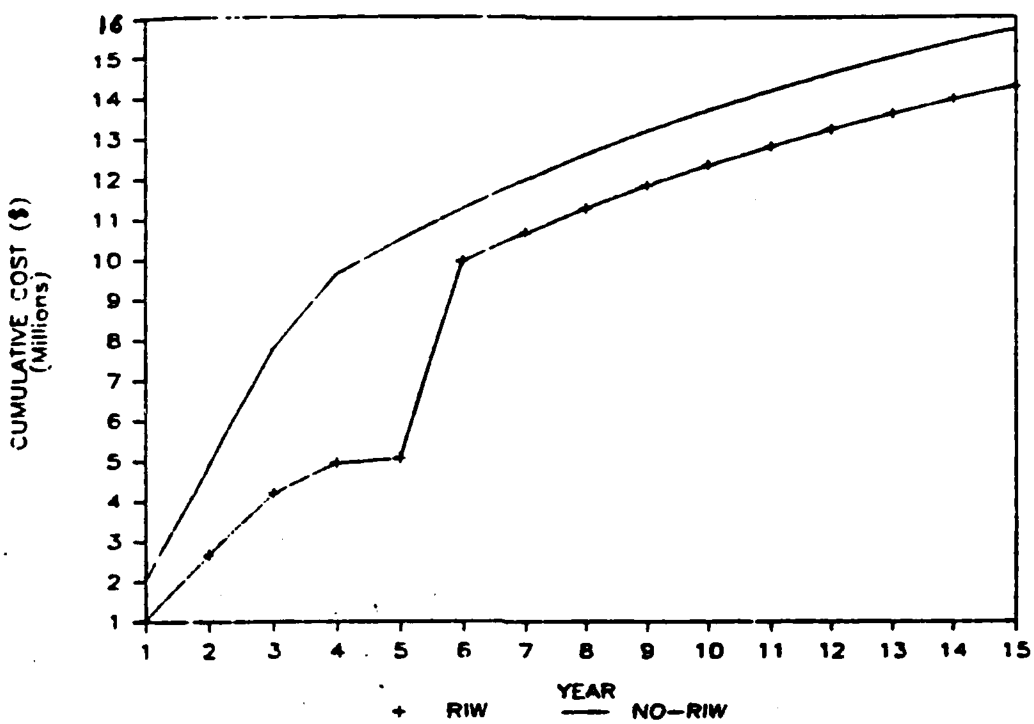

Figure 1 **Comparative Analysis (RIW vs No-RIW)**

from the actual application of these methods to the real case. First of all, it appears that there is no agreed upon format for interpreting the results of reliability tests perfomed in the laboratory, and no way of properly integrating available data sources for field reliability prediction. As a consequence of our support of the JTIDS Class 1 program, we have proposed a Bayesian approach to combining available data sources for such predictions. Apparently sequential Bayesian methods have been applied to other problem areas in the Air Force, but not to the case of field reliability estimation. (A separate memo on these methods is being prepared by myself and Fred Chin on these methods). We are proceeding to develop this approach.

Of the available reliability growth methods, the Duane methology seems most appropriate. We concur with the TASC report that such a procedure can provide a basis for the reliability methods to be used in determining values for MTBF versus time.

C. Preliminary Recommendations

We have some doubts about the ability of the project offices (SPOs) to track with confidence reliability growth per se. Our thinking is causing us to favor the MTBF-verification test warranty as somewhat more favorable than an RIW because of its lesser degree of complexity and its wider applicability. It is not always clear which systems will indeed experience reliability growth, and as Dizek points out, there have been cases where RIWs have been applied to inappropriate systems.

Also, our experience with the JTIDS system is indicating that laboratory test results must be scrutinized carefully for purpose of predicting field reliability, and in worst case situations, MTBF may indeed be difficult to estimate, let alone its theoretical growth potential. It would seem a more prudent approach to have contractors guarantee an adequate field reliability, and attach to that a repair warranty if this MTBF is not met. This may be more preferable than a reliability improvement warranty. Also, this approach may prevent contractors from being rewarded for "sloppy initial designs" (also, see preliminary recommendations, II.B below).

D. Summary: Review of RIWs

The specifications for RIWs here included MTBF versus period (see Appendix II) where incentives have been provided as a percentage of the contract cost. The data tracking system for these warranties needs to be further investigated, since the actual success of the warranty will be largely based upon how well the government can enforce the requirements. We are looking into data tracking methods for RIWs. This may be the "Achilles Heel" of RIWs.

II. FIELD WARRANTY (MTBMA): Reliability and Maintainability Warranty

The purpose of this effort is to investigate possible approaches for developing a generic warranty for ESD developmental systems which: (a) commits the contractor to develop equipment maintainable and more supportable in the field, and (b) provides an economic incentive to do so. Four objectives are outline: (1) review past examples of warranties related to maintenance actions in the field, (2) investigate possible alternatives for an

effective maintenance warranty, (3) use MILSTAR programmatic support to make policy recommendations, and (4) provide an example warranty. Progress to date on these four objectives are reviewed here. Finally, preliminary recommendations are provided.

A. Review of Past Examples of Field Warranties

An historical review of reliability and maintainability warranties was not performed by TASC for PPAC. However, TASC has written a description of a possible generic reliability and maintainability warranty (included here as Appendix IV). Moreover, MILSTAR has included an MTBMA improvement incentive in their contract (included here as Appendix V).

The MTBMA is the mean time interval between on-aircraft maintenance actions with time expressed as total operating hours. To calculate MTBMA, the following applies:

$$\text{MTBMA} = \frac{\text{total operating hours}}{\text{quantity of maintenance occurences}}$$

Incentives in the MILSTAR program are awarded based on achieving MTBMA goals afte: various periods of time. The maximum cumulative payoff of incentive fee are:

Period 1 -- 1.5 million dollars
Period 2 -- 3.5 million dollars
Period 3 -- 6.0 million dollars

B. Possible Alternatives for an Effective Maintenance Warranty/ Preliminary Recommendations

We suggest that availability be the reliability measure warranted in field applications, where

$$\text{Availability} = \frac{\text{MTBF}}{\text{MTBF} + \text{MTTR}}$$

The adoption of this approach will solve two problems:

1. If MTBF is solely warranted, there is no easy way to determine the impact on final contract costs or time-to-completion, since it is known that as MTBF improves MTTR also grows longer, thus decreasing availability.

2. The MTTR variable is important from a human factors/maintenance perspective, in as much as it is people who repair the systems in the field. The MTTR may actually be longer when the contractor does the repair, so this variable should be warranted so as not to reduce system availability any further than is necessary.

A third reason for using availability as the factor to be warranted is that system life-cycle costs are a direct function of availability. Thus, economic incentive for improving availability can be directly calculated.

General Chubb has suggested that a PPA based on maximum achievable MTBF at the state-of-the-art technology be used. This approach is a good idea if MTTR is also warrented and availability is concentrated upon. The adoption of this approach could ease the source selection procedure as well, since availability varies only between 0-1 and is almost always very close to one. Thus, a factor of 2-3 in MTBF being bid between several contractors will appear less significant when placed into an availability format. The danger of Chubb's idea is that if MTBF alone is looked at, a factor of 2-3 in MTBF will appear very important, when its actual impact on system costs may be relatively insignificant. The message is that MTTR must also be considered.

C. Data Tracking for Warranty Enforcement — Calculation of Field Reliability — Test Design

One of the major weaknesses inherent to warranties may lie with the government's capability to adequately track, and then distinguish between, defects which are attributable to the contractor (as opposed to inadvertant damage caused by the government). In fact, carefully defining which defects are the responsibility of industry is one of the major challenges of writing an effective warranty. One possible way to evaluate the appropiateness and relative effectiveness of available product performance agreements is through a preliminary evaluation of the framework available for tracking, recording, and assigning responsibilty of the defects to either the contractor or the government. These are important considerations, as indicated by their reference in the Federal Register, 9/19/83 (see notes in Appendix IV).

Sue Malone has been helping the MILSTAR SPO devise a data tracking system for maintenance actions, and her knowledge of that system is useful for evaluating the final effectiveness of the MTBMA warranty in use at MILSTAR. Similar study of RIW data tracking can give insight to its final effectiveness as a product performance measure. Experience with JTIDS indicates that problems can result when reliability data is taken without careful thought to how the data is ultimately to be used. Thus, attention must be placed on the design of the reliability assessment procedure to be utilized. Fred Chin and I have developed a procedure for JTIDS to estimate field reliability (MTBF) that makes use of the existing data collection system. This has resulted in the use of the Poisson distribution rather than the Weibull as a result of the test configuration, a comparison of the Biomial and Poisson distributions were made, slowly little actual effect on calculation results. However, the Poisson is better theoretically justified, which does not collect failure data with respect to time (i.e., failures are grouped together irrespective to their time of occurrence). However, instead of devising an approach after the data is collected, it is preferable to devise the approach first and then collect the data. Thus, test design must precede data collection, or the data may be meaningless.

APPENDIX I

<u>NOTES:</u> "Product Performance Agreement Decision Support Handbook" 2/1/85, TASC for PPAC

The Decision Support System (DSS) is a tool designed to assist the analyst by providing a framework for selecting, analyzing and structuring Product Performance Agreements (PPA).

<u>Steps:</u> (1) Data Collection
(2) Selection of Preliminary PPA
(3) Analysis of PPA Options
(3) Final Selection of PPA
(4) Structuring the PPA Contract

<u>Pg 3-9:</u> Reliability Improvement Warranty (RIW)

"The RIW is a contractual tool whose chief goal is the motivation of contractors to design into their systems both enhanced reliability and low-cost support features."

The contractor assumes <u>full</u> responsibility for repairing or replacing (as the contractor deems suitable) the warranted items over a fixed time period. The contractor is given latitude to take whatever steps are necessary to meet specific reliability, availability and/or maintainability objectives.

<u>Logistic Parameters:</u> MTBF, MTBMA, Fill Rate, Turnaround Time (TAT)

The specific parameters chosen VARY WITH EACH PROGRAM and are, <u>in fact</u>, Decision Variables to be evaluated during the Analysis of the RIW.

<u>Definition of Reliability (used by TASC for USAF) (pg 3-9):</u>

"the probability that an item will perform its stated function in a specified period of time under certain assumptions. The principal measures are MTBF, failure rates and MTBMA."

<u>Reliability Growth Estimation (pg 3-12):</u>

— need data on average operating hours, initial MTBF estimate, and Duane growth parameter.

<u>MTBF Verification Test:</u>

The MTBF-VT PPA guarantees a specified MTBF level on the warranted items in their operating environment. At the end of the warranty period, a verification test is conducted for a specified time on specified fielded units. If the MTBF is not met at the end of the verification test, the contractor must provide consignment spares to compensate the government.

A Confidence Interval Analysis is used to assess the appropriate test sample size and duration to produce a valid estimate of MTBF.

APPENDIX II

Representative RIW Clauses (MTBF Guarantees with Incentives for Growth)

1. RIW of TASC/PPAC
2. Goldberg Proposal for RIW
3. RIW for AN/ALQ-165
4. RIW for A-10 Inertial Navigation Unit

1. <u>TASC RIW</u>:

$$\text{MTBF (M)} = \frac{\text{TOH}}{\text{F}}$$

where TOH = total operating hours during a specified period;
F = total no of failures (except those exempted).

TASC recommends that the MTBF be calculated every 6 months, (so TOH = 6m x 30 days x 24hrs/day) and F be the number of relevant failures.

TOH = N x D x AOT

Where N = Average number of installed systems; D = number of days in the measurement period; and AOT = average operating time per day ($\nleq$ 24 hrs).

The MTBF guarantee is thus simply a table where the analyst/SPO office has specified a value (guaranteed value G) for each 6 month period for 60 months. Tailoring comment number 19 notes that an MTBF guarantee is used to define <u>how much</u> improvement will be required as a minimum.

The incentive is based on an operating hour adjustment, such that if the ratio of ATOH to PTOH is greater than 95% or less than 105%,

$$.95 < \frac{\text{ATOH}}{\text{PTOH}} < 1.05 \quad \text{no adjustment to contract}$$

ATOH = actual total operating hours
PTOH = projected total operating hours

If $.70 < \frac{\text{ATOH}}{\text{PTOH}} \angle .95$, adjust downward by that ratio;

If $1.05 \angle \frac{\text{ATOH}}{\text{PTOH}} \angle 1.30$, adjust upward by that ratio;

If $.70 > \frac{\text{ATOH}}{\text{PTOH}} > 1.30$, negotiate.

2. Goldberg Proposal for RIW (5/25/79)

MTBF Calculation

$$M_i = \frac{TOH_i}{F_i}$$

Where M_i = achieved MTBF of the i^{th} type unit

TOH = Total Operating Hours

= AOT x $\bar{N}$xD

Where

o AOT = Average Unit operating time per day per unit

$$= \frac{\Sigma H_i}{\Sigma T_i}$$

where

T_i = Number of days each returned unit was installed, and

H_i = Number of operating hours for each returned unit during T days

o $\bar{N}$ = average number of installed units

$$= \frac{1}{6} \sum_{j=1}^{6} \frac{N_j + N_{j-1}}{2}$$

where N_j = the number of units that are installed on the last day of each month j of the 6 month measurement period

and

N_{j-1} = the number of units installed on the last day of the previous month of the measurement period

and D = Number of days in the measurement period

The MTBF guarantee provides that the contractor specifies that the units delivered under the production contract will achieve an MTBF equal to or greater than that prescribed in the table:

MTBF Guarantee (hours)

LRU/SRU Nomenclature	LRU/SRU MTBF 1-12	13-24	25-36	37-48	49-60 MONTHS
1.					
2.					
3.					
4.					

Goldberg does not specify how these MTBF determinationa are to be made; his footnote says: "increasing MTBF guarantee hours which reflect reliability growth are encouraged; however, the offeror shall fill-in MTBF hours for each LRU/SRU for each period."

A price adjustment of the RIW is included by Goldberg such that:

$$\frac{ATOH}{PTOH} = P$$

where ATOH = actual total operating hours

PTOH = projected total operating hours

IF $P < .95$, adjust warranty price downward

IF $P > 1.05$, adjust warranty price upward

Goldberg does not indicate by how much the price would be modified. However, the government would only pay 10% of the RIW price until the MTBF could be verified.

3. RIW For AN/ALQ-165

The statement governing the warranty is a minimum Mean Flight Hour Between Removal (MFHBR) of TBD hours in an operational environment. It is specified that the CPMS shall have a minimum MFHBR of 50 hours. The warranty is in effect for 5 calender years. Verification is achieved when the device is tested on a designated tester witnessed by responsible contractor/government personnel. Any unit failing the warranty will be repaired/replaced or modified at the contractor's option and expense. The contractor makes the decision as to whether an item will be redesigned in lieu of continuing to repair or replace the same item.

The contractor is to include a list of fifteen top system warranty candidates based on the criteria of high cost and high failure:

Candidate No.	WRA	SBA	Nomenclature	Cost	MTBF(hrs)	$/.hr
01	ABC	XYX	Assy	1000	500	2.00

Additionally, the contractor shall project the total cost for each of the 15 warranty candidates over the five year life of the warranty.

4. RIW for A-10 Inertial Navigation Unit (INU)

Warranty is for a five year period. The contractor is required to correct or replace at his option at no additional cost to the government, any INU which fails during the warranty periods. A failure is defined as any warranted INU returned to the contractor because of a failure indication, a malfunction and/or a reduction in the performance of the INU below the requirements.

MTBF Guarantee

INU

Guaranteed Value	Measurement Period
N/A	Period 1: 1-6 Months
275 hours	2 7-12
325	3 13-18
365	4 19-24
400	5 25-30
428	6 31-36
453	7 37-42
477	8 43-48
497	9 49-54
525	10 55-60

Calculations of MTBF are as follows:

$$M = \frac{TOH}{F}$$

where

M = achieved MTBF of the INU

F = number of INU failures

$TOH = N \times D \times AOT$

where

N = average number of installed INUs

D = number of days in the measurement period

AOT = average operating time per day per installed INU

The government is to verify all failures using Build-in-Test.

Data Requirements

RIW data reporting and summary reports in accordance with the contract.

APPENDIX III

Discussion with Mr. Dave Goldberg (6/28/85)
Dynamics Research 685-6100; x1322

1. The Product Performance Agreement Guide (PPAG) sets the basis for warranties and guarantees. There, the advantages and disadvantages of each warranty type are discussed. The PPA center at WPAFB will implement the PPAG. Lt. Col. Tony Gunther is the contact there. TASC has a 3 year contract with the PPAC. They have provided a database for particular contracts, and track the record of failure data. The government pays for the warranty.

2. Mr. Goldberg mentioned the DD-254 syndrome. He called it an acceptance slip, and it doesn't guarantee field performance. The "COD" clause--correction of deficiencies--didn't work; it can't prove that equipment was causing failures or problems in the field.

3. Warranties and guarantees are broadly generic, and are the same things in practice. There are three main aspects: (i) what is it you want to warrant, (ii) what do you want to warrant it for or against, and (iii) how much is it worth to warrant. In answer to what do you warrant, you must warrant against critical failures, and you must perform a reliability study to do that before you can identify the key failure area.

4. A project office (SPO) may have several policy choices to choose from: (i) they may ask PPAC to write their warranty, (ii) they may write it themselves (using generic guidance from ESD or other product centers), or (iii) they may use some combination of the two approaches. (see Figure III.1).

5. RIW's-- maintenance turned over to private industry--no maintenance performed in the field--no depot. A financial incentive is provided to the contractor. How long should you specify the RIW--currently, it is 5 years. After that period, maintenance is turned back over to the USAF to perform.

Figure III.1 SPO Choice on Warranties/Guarantees

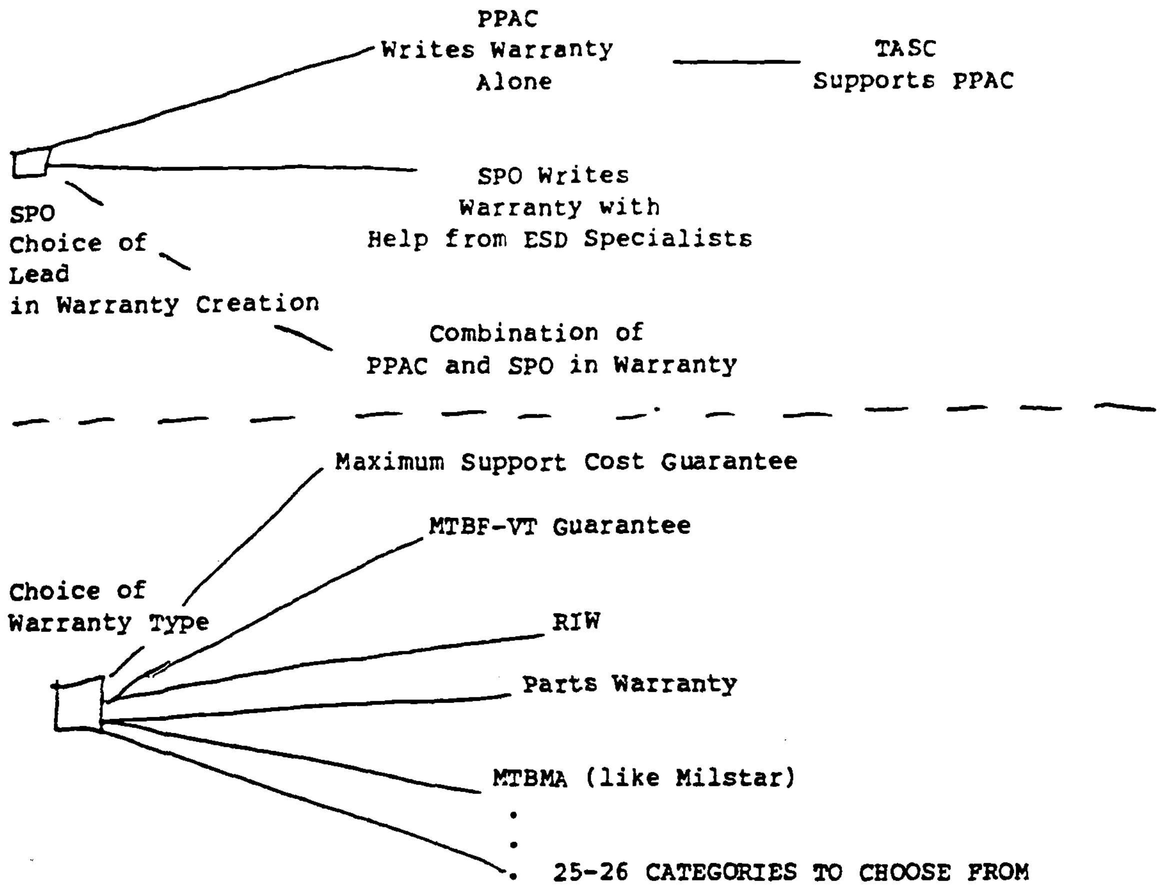

Appendix IV

Notes: Warranties --Federal Register, Vol 48, No 182, Monday, Sept 19, 1983

Definition: "Warranty" means a promise or affirmation given by a contractor to the Government regarding the nature, usefulness, or condition of the supplies or performance of services furnished under the contract.

Purposes: The principal purposes of a warranty in a contract are: (1) to delineate the rights and obligations of the contractor and the government for defective items and services, and (2) to foster quality performance.

Provisions: A warranty should provide: (1) a contractual right for the correction of defects notwithstanding any other requirement of the contract pertaining to acceptance of the supplies or services by the government, and (2) a slated period of time or use, or the occurrence of a specified event, after acceptance by the Government to assert a contractual right for correction of defects, and (3) the benefits to be derived from a warranty must be commensurate with the cost of the warranty to the government.

THE GOVERNMENT'S ABILITY TO ENFORCE THE WARRANTY IS ESSENTIAL TO THE EFFECTIVENESS OF ANY WARRANTY. There must be some assurance that an adequate administrative system for reporting defects exists or can be established.

The adequacy of a reporting system may depend upon such factors as the
(1) nature and complexity of the item
(2) location and proposed use of the item
(3) storage time for the item
(4) distance of the using activity from the source of the item,
(5) difficulty in establishing existence of defects, and
(6) difficulty in tracing responsibility for defects.

Warranties shall not be used in cost-reimbursement contracts.

WARRANTY TERMS AND CONDITIONS

To facilitate the pricing and enforcement of warranties, the contracting officer shall ensure that warranties clearly state:

(1) The exact nature of the item and its components and characteristics that the contractor warrants,
(2) Extent of the contractor's warranty including all of the contractor's obligations to the Government for breach of warranty,
(3) Specific remedies available to the government;

and

(4) Scope and duration of the warranty.

Remedies: Warranty provides as a minimum that the Government may: (a) obtain an equitable adjustment of the contract, or (b) direct the contractor to repair or replace the defective items at the contractor's expense.

Notice: The warranty shall specify a reasonable time for furnishing notice to the contractor regarding the discovery of defects.

N... ...

MEMORANDUM

TO: LTC Steve Sechrest

FROM: Fred C.S. Chin

DATE: 9 August 1985

SUBJECT: A Proposed "Bayesian" Approach for JTIDS Class 1 Reliability Predictions

Introduction

The purpose of this memorandum is to present an understandable, easy to use, and believable approach for predicting the reliability of JTIDS Class 1 (Airborne).

This method is known as the Bayesian approach using DPD arithmetic, described in reference (1), and has been applied to nuclear systems by Heising and others. It has never been used before at ESD. Bayes' theorem applied to discrete distributions can be written as:

$$P(A_i/B) = \frac{P(A_i)\ P(B/A_i)}{\sum_{i=1}^{n} P(A_i)\ P(B/A_i)}$$

where: A_i is the system reliability (either MTBF or failure rate)

- $P(A_i)$ is the initial knowledge about A_i, the prior knowledge, or simply the PRIOR
- B is the new knowledge (results of the REL DEMO)
- $P(B/A_i)$ is the probability of event B given A_i occurs, or the LIKELIHOOD function
- $P(A_i/B)$ is the best estimate of A_i given the new information B, or simply the POSTERIOR

In short, the approach being presented here is best illustrated in three parts: the Prior, the Likelihood and the Posterior.

The Prior

Before determination of the Prior distribution, a fault tree was constructed according to the system block diagram of JTIDS (fig 1). With the assistance of Lt Pete Reho, the fault tree was extended to a level for which failure data was readily available (figs 2.1 - 2.4). Data used in the fault tree analysis was extracted from the Hughes Improved Terminal (HIT) Development Program document of predicted failure rates. After propagating the failure rates through the tree, a mean value of 1.9×10^{-3} hrs was obtained. Based on this mean value, our knowledge of JTIDS Class 1 past performance, and subjective engineering judgement, a distribution was determined representing our initial knowledge (fig 3).

The Likelihood

The Likelihood function, $P(B/A_i)$, was calculated under two assumptions: (1) each hour of operation simulates a Bernoulli process (i.e. during any hour of operation, the system can exist in only one of two states: success or failure) and (2) based on the first assumption, the Binomial Distribution was assumed to be most appropriate in representing the Likelihood function (see reference (3)). This can be expressed as follows:

$$P(B/\lambda_i) = \frac{n!}{m!\,(n-m)!}\,\lambda_i^m(1-\lambda_i)^{n-m}$$

where: n is the number of hours of operation (trials)
m is the number of failures during n hours

The hours of operation, n, and the number of failures, m, were obtained from the Failure Summary Reports for HIT SS reliability demonstration process since it was acknowledged that this process most resembled the actual field operating conditions. The figures attained from the REL DEMO were 3 failures in 450 hours of operation. Using these numbers in the calculations for the Likelihood function, the distribution was thus determined (fig 4).

The Posterior

In determining the Posterior, first the product of both the Prior, $P(\lambda_i)$, and the Likelihood, $P(B/\lambda_i)$, must be found for each interval, i. Next, the Pre-Posterior, or Function Normalization Factor, $(\Sigma P(\lambda_i)\ P(B/\lambda_i))$ is calculated. After calculating the Pre-Posterior, the Posterior distribution is found by simply dividing the product of the Prior and the Likelihood by the Pre-Posterior for each interval. This resulting distribution is now our best estimate based on our prior knowledge and the results of the reliability demonstration, denoted B. Figure 5 illustrates these calculations as well as the Posterior distribution. Figure 6 compares the three resulting distributions.

Recommendations/Conclusions

Based on this preliminary analysis, a best estimate MTBF of 152 hours is expected. The intention here is to refine this estimate with more recent and relevant data. To accomplish this, the following recommendations are made:

(1) If time and funds permit, Dr Carolyn Heising and myself should visit Hughes Aircraft Company (HAC) Ground Systems Group in order to better familiarize ourselves with the Environmental Stress Screening (ESS) process and at the same time, collect more recent test data for further analysis.

(2) This method is applicable to other reliability predictions for the JTIDS program as well as all programs at ESD.

(3) It is recommended that this approach be extended and refined for field reliability prediction.

References

(1) Heising, C. D. "The Bayesian Approach Using DPD Arithmetic," Course Notes, Northeastern University, Boston, MA, 1985.

(2) Coppola, A. "Bayesian" Reliability Tests Made Practical, RADC-TC-81-106, 1981.

(3) Kececioglu, D. "Sequential Testing for the Binomial Case," Course Notes, University of Arizona, 1982.

(4) Smith, A.F.M. "Bayesian Note on Reliability Growth During a Development Testing Program," IEEE Transactions on Reliability, Vol R-26, No. 5, December 1977.

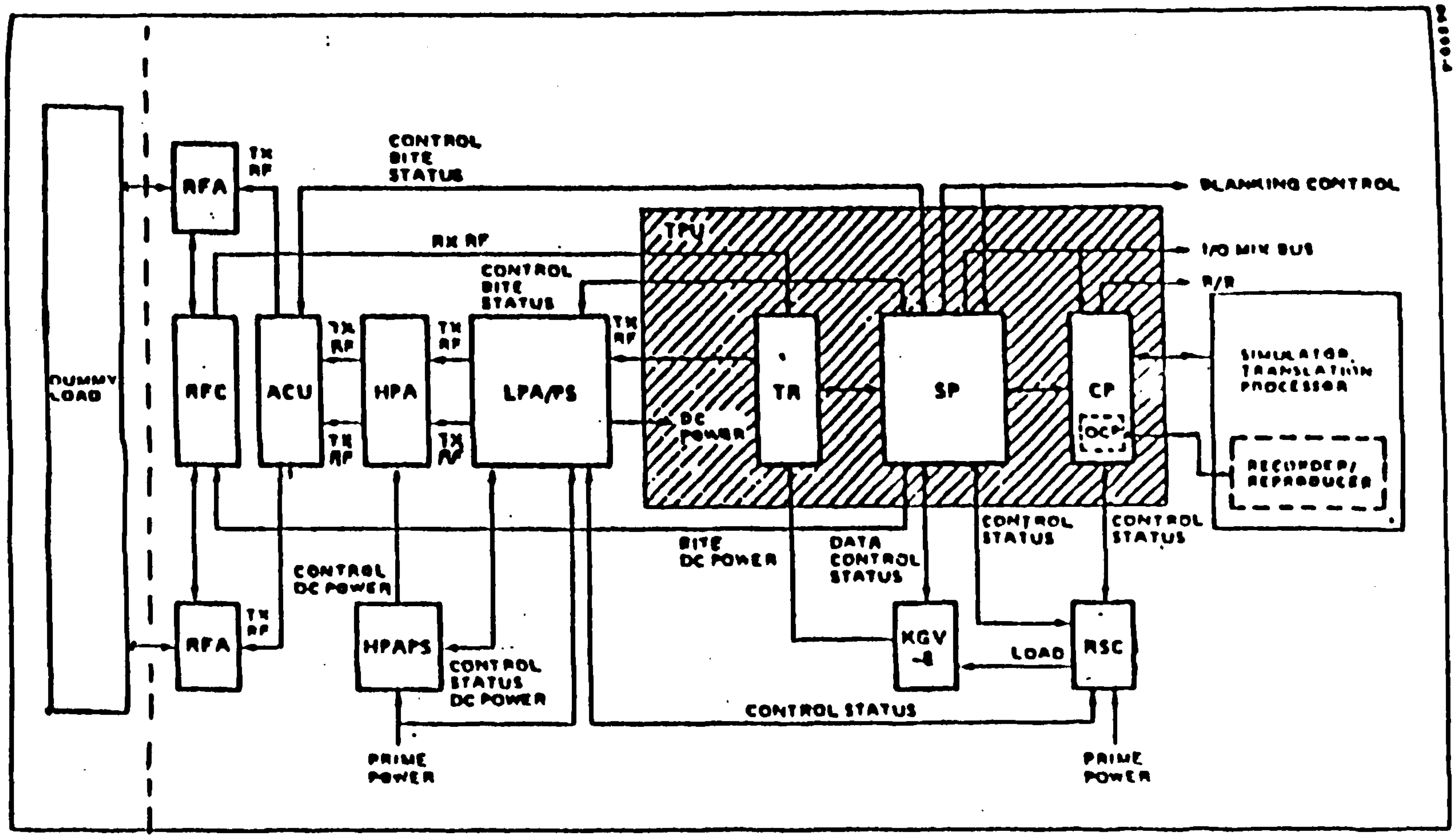

Figure 1 System Block Diagram

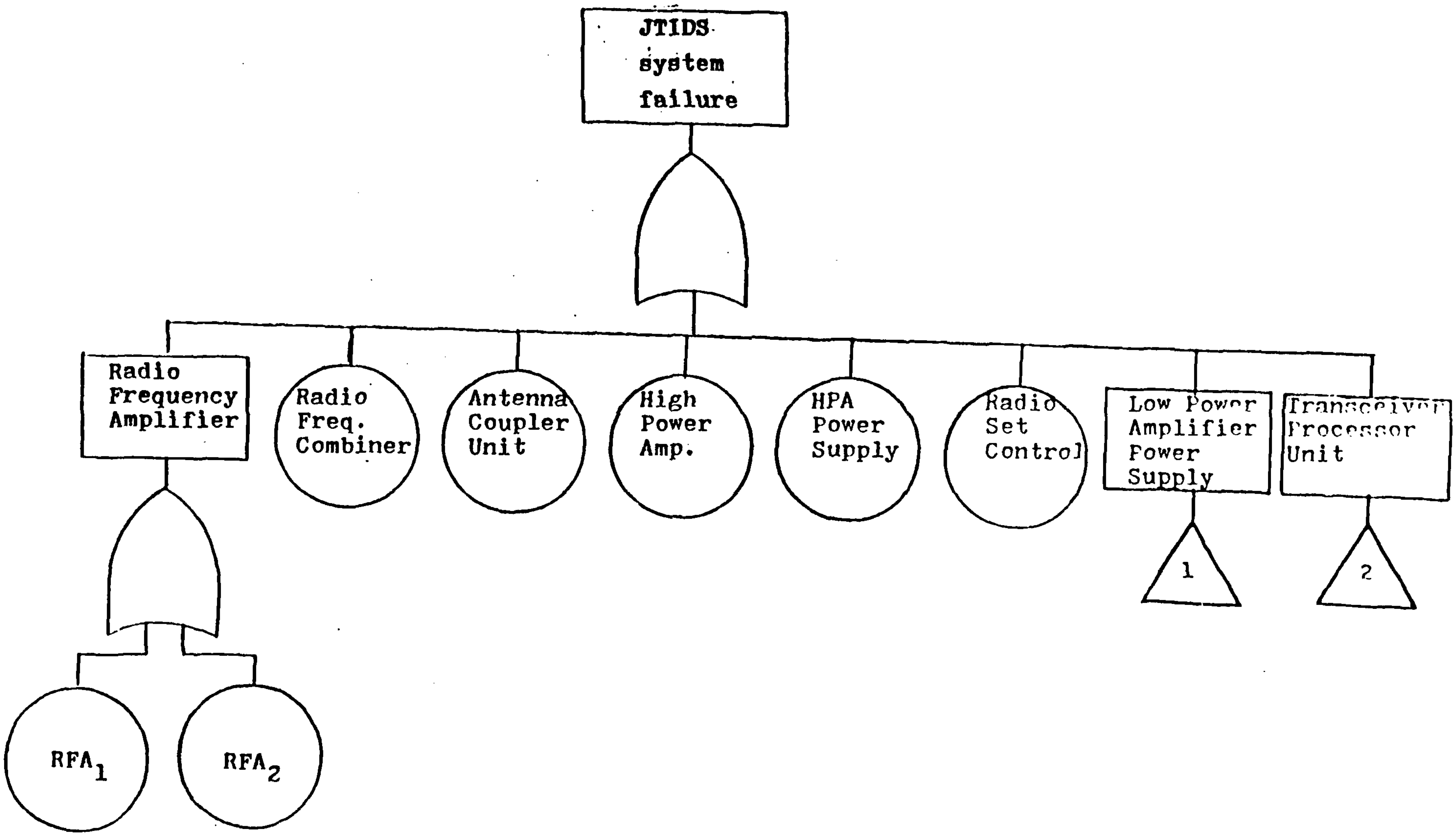
JTIDS system failure
Radio Frequency Amplifier
Radio Freq. Combiner
Antenna Coupler Unit
High Power Amp.
HPA Power Supply
Radio Set Control
Low Power Amplifier Power Supply
Transceiver Processor Unit
1
2
RFA1
RFA2

figure 2.1

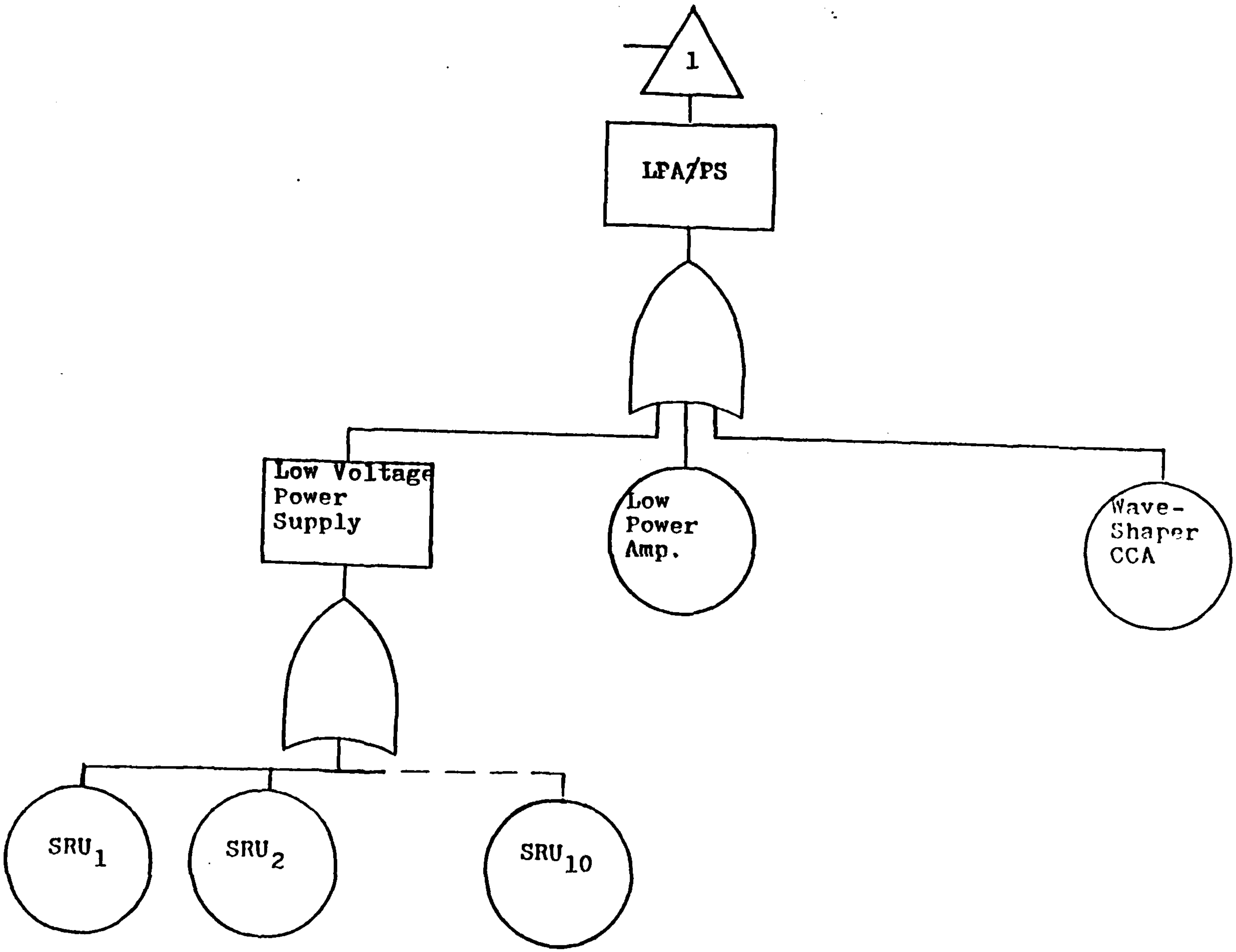
1
LFA/PS
Low Voltage Power Supply
Low Power Amp.
Wave-Shaper CCA
SRU1
SRU2
SRU10

figure 2.2

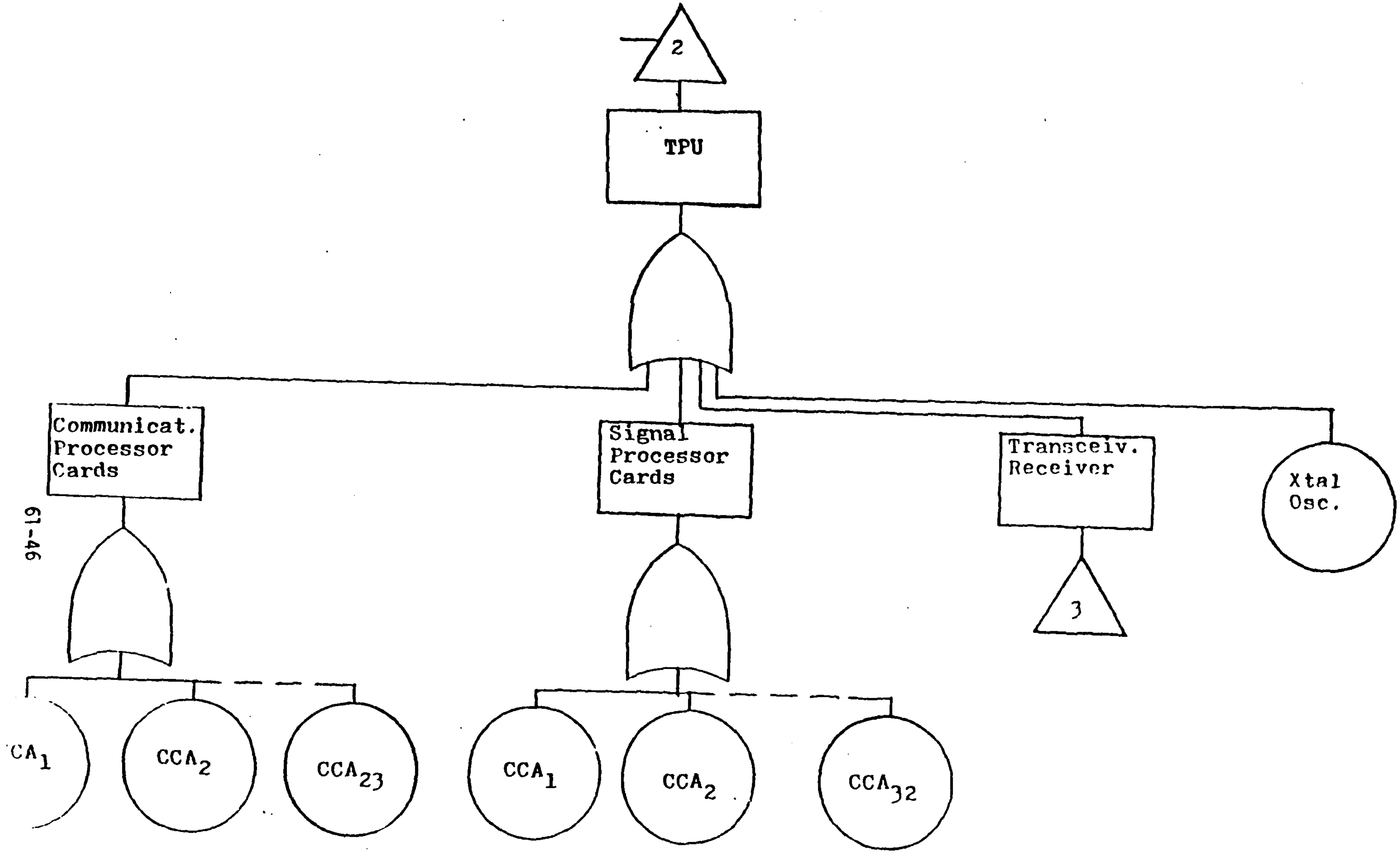
2
TPU
Communicat. Processor Cards
Signal Processor Cards
Transceiv. Receiver
Xtal Osc.
3
CA1
CCA2
CCA23
CCA1
CCA2
CCA32

figure 2.3

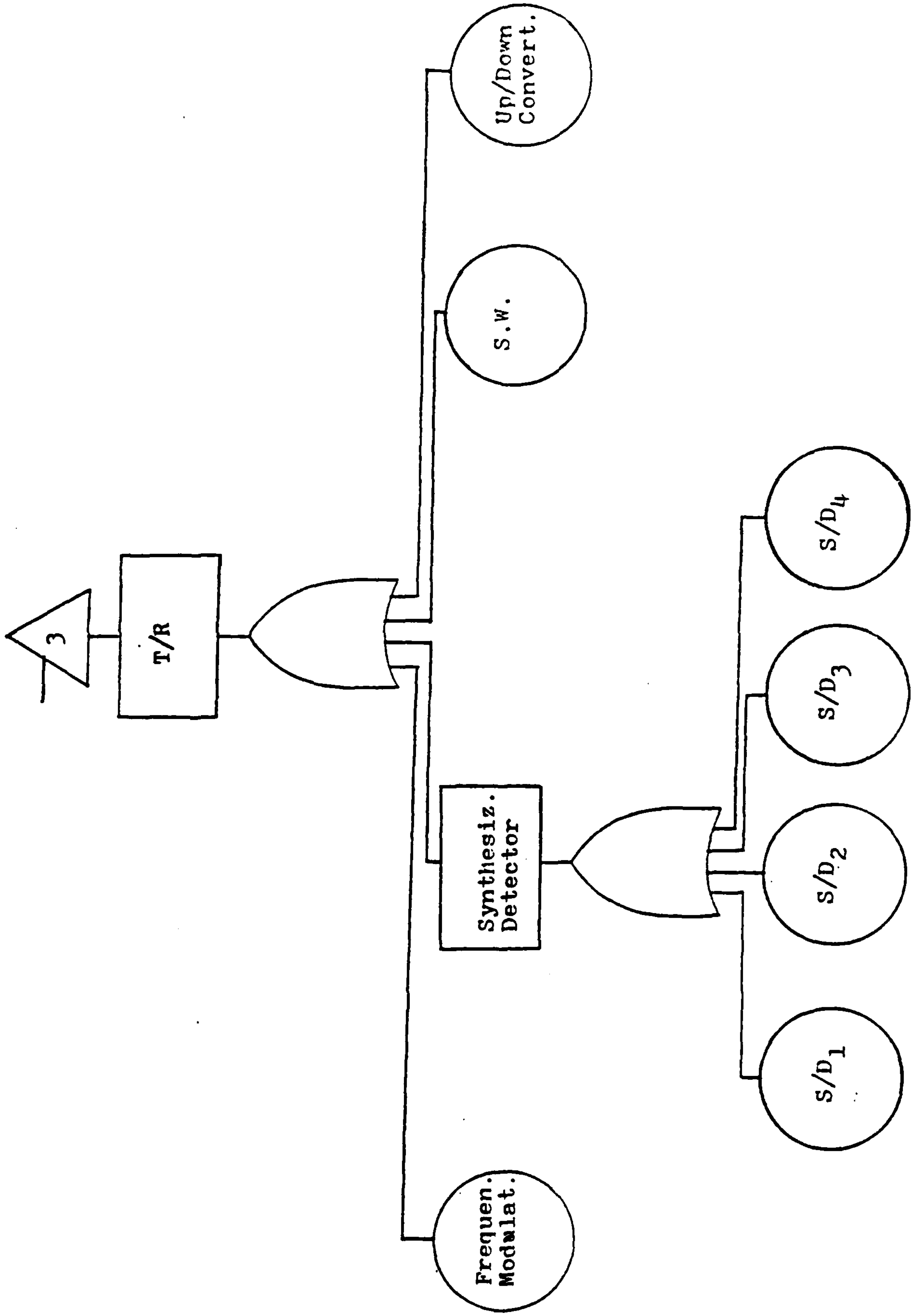
3
T/R
Up/Down
Convert.
S.W.
Synthesiz.
Detector
S/D$_4$
S/D$_3$
S/D$_2$
S/D$_1$
Frequen.
Modulat.

figure 2.4

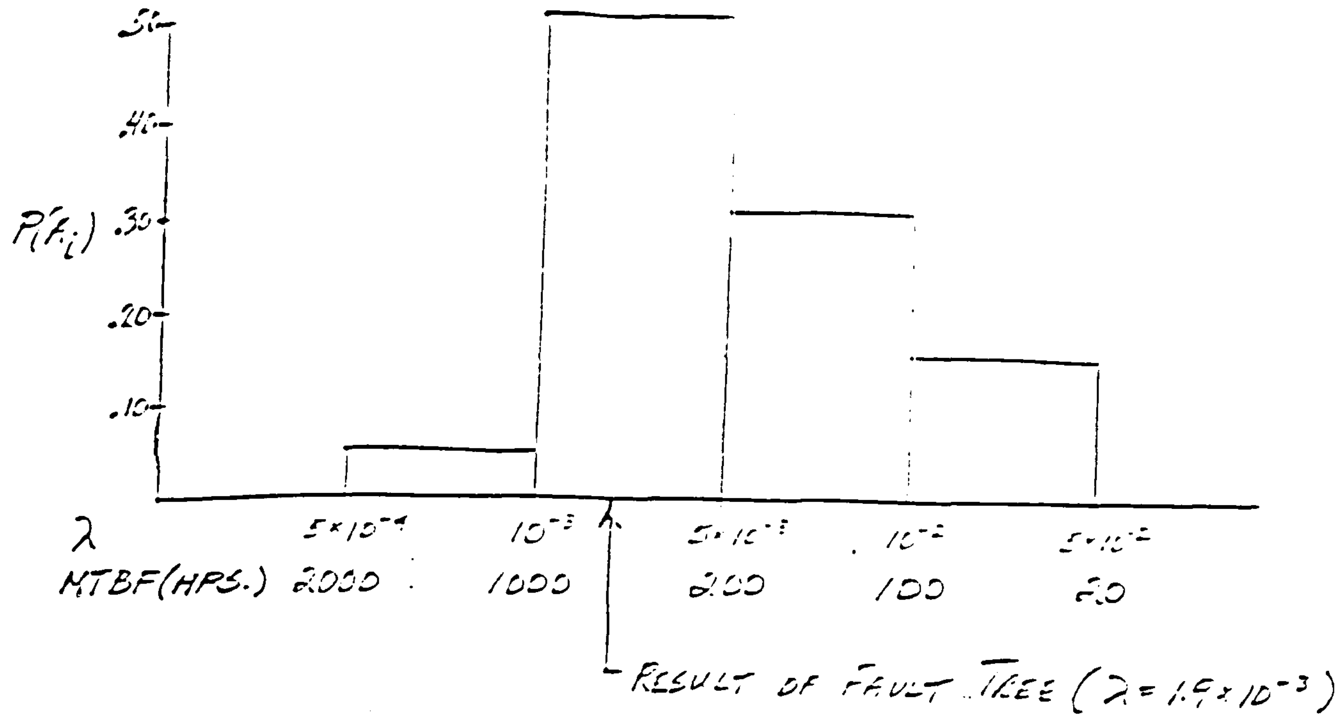

PRIOR Distribution
(Based on Fault Tree Results
and Analyst Judgement)

figure 3

NOTE: the shape of the prior resembles that of an inverted
Gamma Density Function (see reference (2))

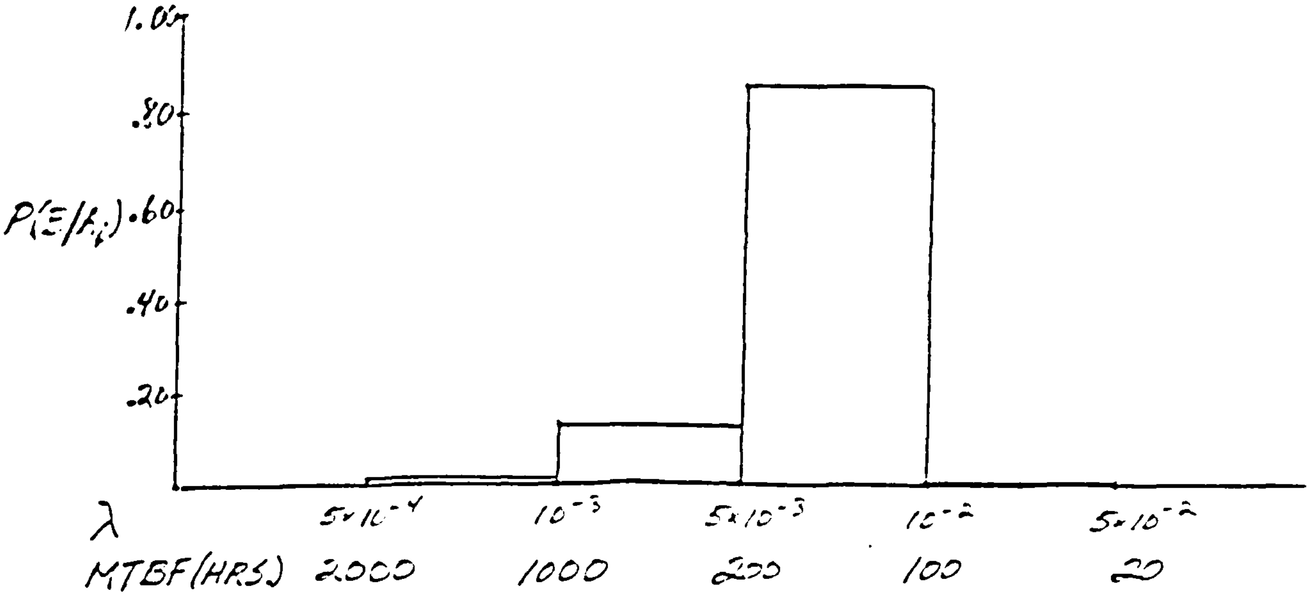

LIKELIHOOD Distribution
figure 4

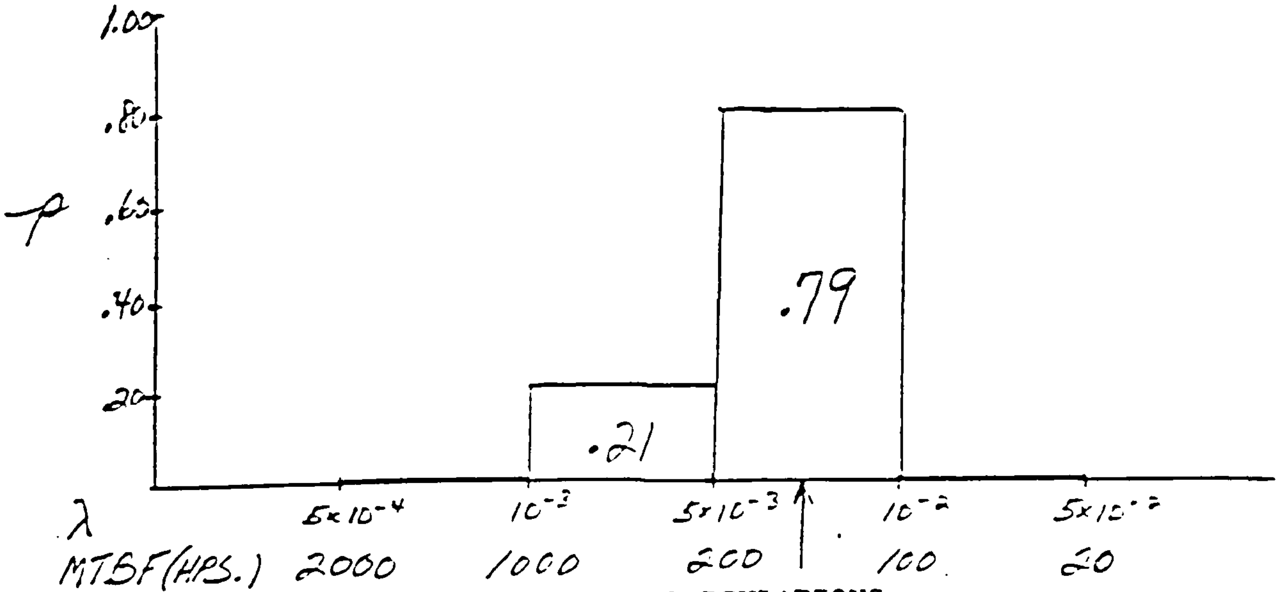

CALCULATIONS

i	1	2	3	4
A_i	7.5×10^{-4}	3×10^{-3}	7.5×10^{-3}	3×10^{-2}
$P(A_i)$	.05	.5	.30	.15
$P(B/A_i)$	4.6×10^{-3}	3.6×10^{-2}	2.2×10^{-1}	5×10^{-4}
$P(A_i)P(B/A_i)$	2.3×10^{-4}	1.8×10^{-2}	6.6×10^{-2}	7.5×10^{-5}
$\Sigma P(A_i)P(B/A_i)$	8.4×10^{-2}			
POSTERIOR	2.7×10^{-3}	2.1×10^{-1}	.79	8.9×10^{-4}

$$(2.7\times10^{-3})(7.5\times10^{-4})+(2.1\times10^{-1})(3\times10^{-3})+(.79)(7.5\times10^{-3})+(8.9\times10^{-4})(3\times1$$

$$= 6.6\times10^{-3}$$
$$= 152 \text{ HR. MTBF}$$

POSTERIOR Distribution

figure 5

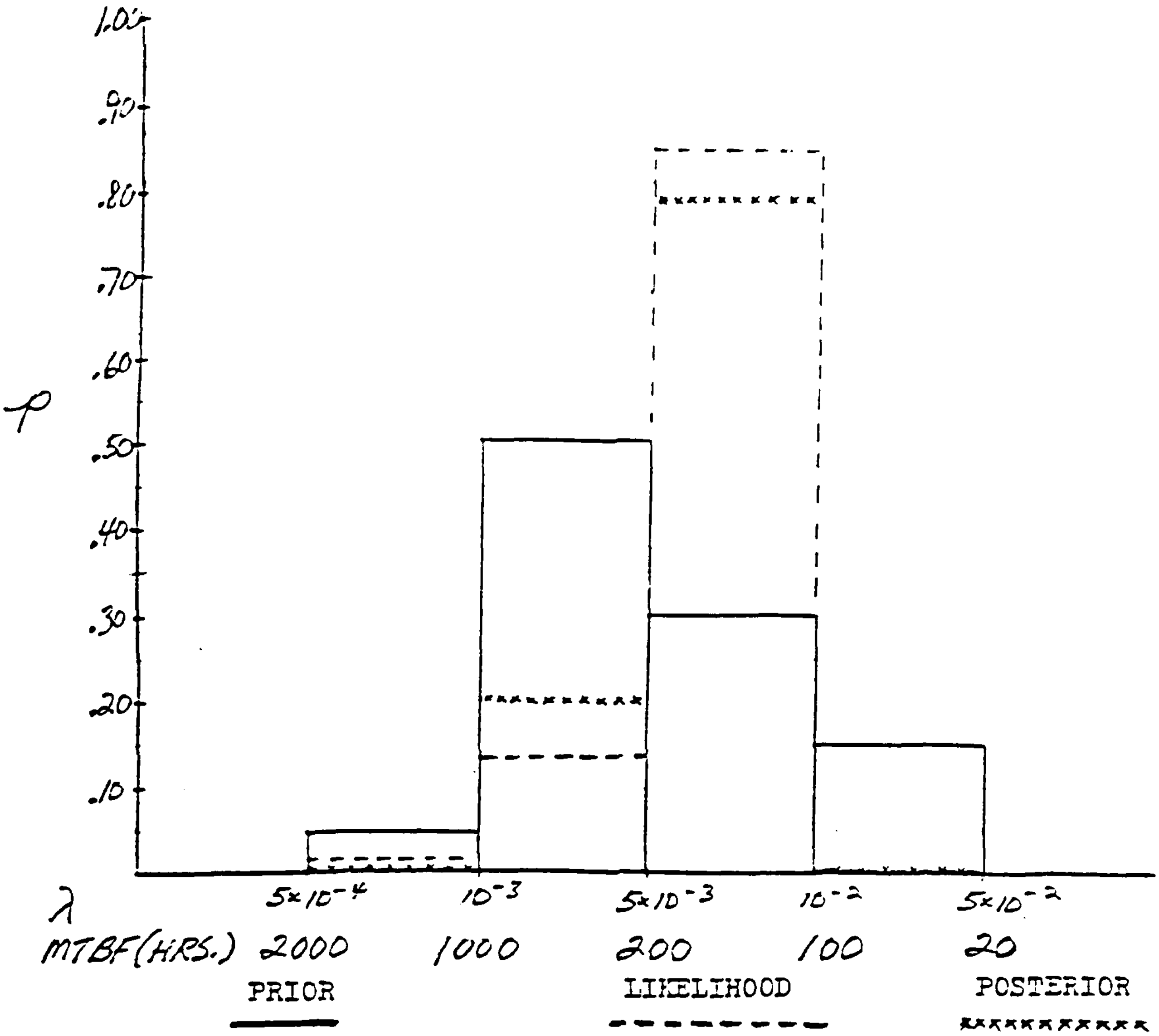
1.00
.90
.80
.70
.60
.50
.40
.30
.20
.10
P
λ
5×10⁻⁴
10⁻³
5×10⁻³
10⁻²
5×10⁻²
MTBF(HRS.)
2000
1000
200
100
20
PRIOR
LIKELIHOOD
POSTERIOR

figure 6

ATTACHMENT

DATE: 30 August 1985

RE: Corrections to memorandum addressed to LTC Sechrest dated 9 August 1985

An error in the determination of the JTIDS Class 1 system reliability was found and the appropriate corrections were made. The calculations in figure 5 of the 9 August memo should read correctly as follows:

i	1	2	3	4
A_i	7.5×10^{-4}	3×10^{-3}	7.5×10^{-3}	3×10^{-2}
$P(A_i)$	.05	.50	.30	.15
$P(B\|A_i)$	4.6×10^{-3}	1.1×10^{-1}	2.2×10^{-1}	5.0×10^{-4}
$P(A_i)P(B\|A_i)$	2.3×10^{-4}	5.3×10^{-2}	6.6×10^{-2}	7.5×10^{-5}

$\Sigma P(A_i)P(B|A_i) = .119$

POSTERIOR	1.9×10^{-3}	4.5×10^{-1}	5.5×10^{-1}	6.3×10^{-4}

$$\text{PREDICTED MTBF} = (1.9\times10^{-3})(7.5\times10^{-4}) + (4.5\times10^{-1})(3\times10^{-3}) + (5.5\times10^{-1})(7.5\times10^{-3}) + (6.3\times10^{-4})(3\times10^{-2})$$

$$= 182 \text{ HR MTBF}$$

Ref 3

MEMORANDUM

TO: LTC Steve Sechrest

FROM: Fred C.S. Chin

DATE: 30 August 1985

SUBJECT: Current "best estimate" of JTIDS Class 1 (Airborne) as of 30 August 1985

Based on the 9 August 1985 memorandum a predicted MTBF of 182 hrs was presented (see attachment). Since then refinements have been incorporated into the analysis and predictions of greater confidence were obtained. Refinements of the "upgraded" analysis are itemized as follows:

1. Data used in the fault tree analysis to obtain the distribution of prior knowledge was extracted from the Hughes Improved Terminal Development Program document# FR81-16-501 dated 24 April 1981. These more recent failure rates produced a system MTBF of 422 hrs. With this mean value and knowledge of the system's past performance, probabilities were assigned to the specified MTBF intervals to develop the distribution of prior knowledge (fig A).

2. The Poisson Distribution was assumed representative of the Likelihood function because of its appropriateness in obtaining conditional probabilities for cases of the prior distribution resembling that of an Inverted Gamma distribution (see ref.1). Furthermore, the results of calculations by applying the Poisson Distribution were compared to those of the Binomial Distribution (likelihood function for initial prediction) and no significant difference was found. However, the Binomial was not used because of its inappropriate assumption. The Likelihood function is represented as:

$$P(B/A_i) = \frac{e^{-T/\theta}\left(\frac{T}{\theta}\right)^f}{f!}$$

where,

f = # of failures

T = time (hours)

θ = MTBF

3. The intervals of MTBF were further defined to more explicitly present the uncertainty in the analysis. Also, the probabilities were reassigned to each MTBF interval in a conservative fashion and illustrating the confidence in the fault tree analysis.

4. Three scenarios were calculated to accomodate for the uncertainty in the Reliability Demonstration data: 1) 3 failures in 450 hrs 2) 1 failure in 370 hrs 3) 0 failures in 370 hrs. The resulting posterior distributions and final best estimates are shown in figures B,C and D.

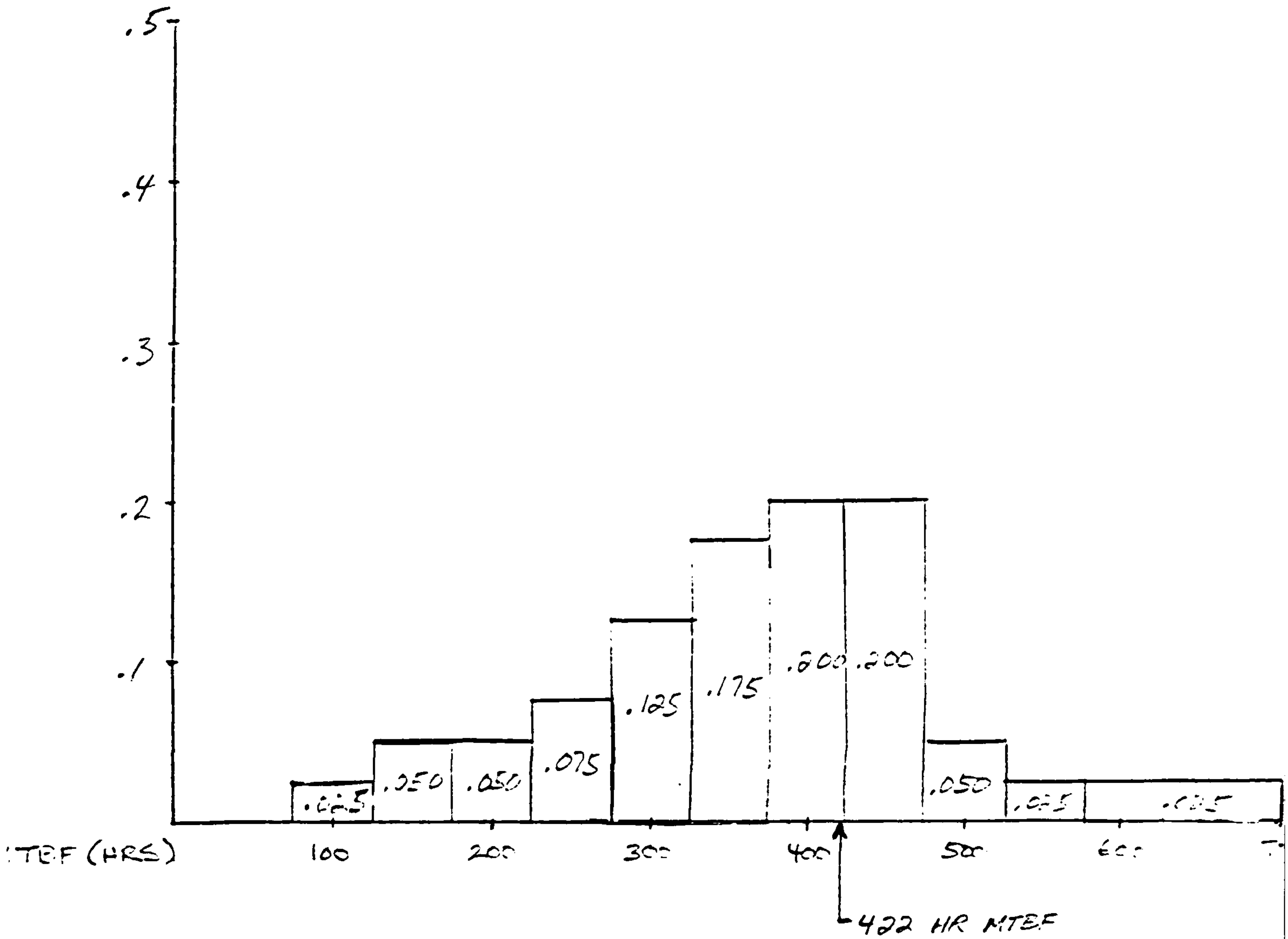

Prior Distribution

figure A

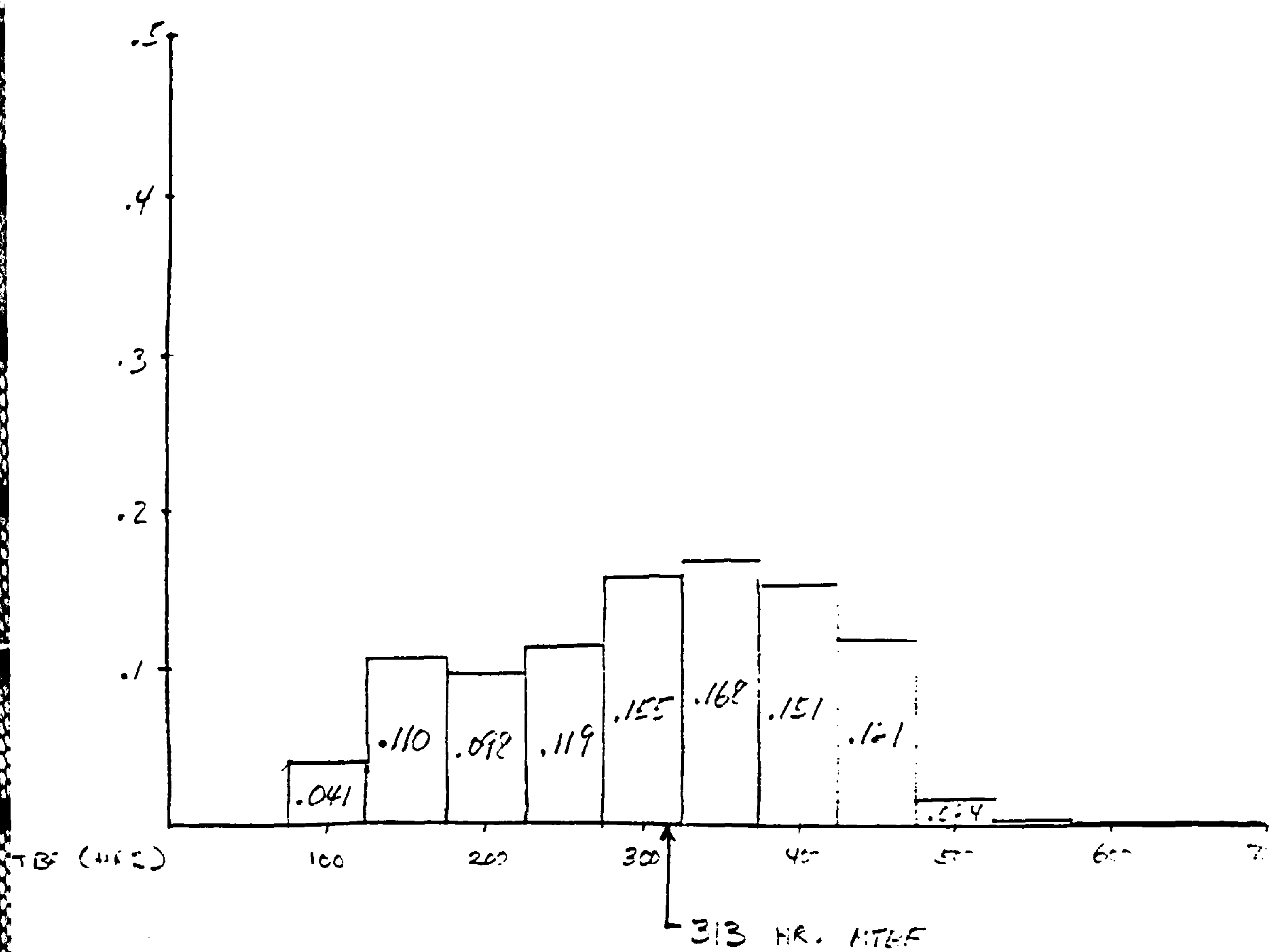

scenario 1

3 failures in 450 hours

figure B

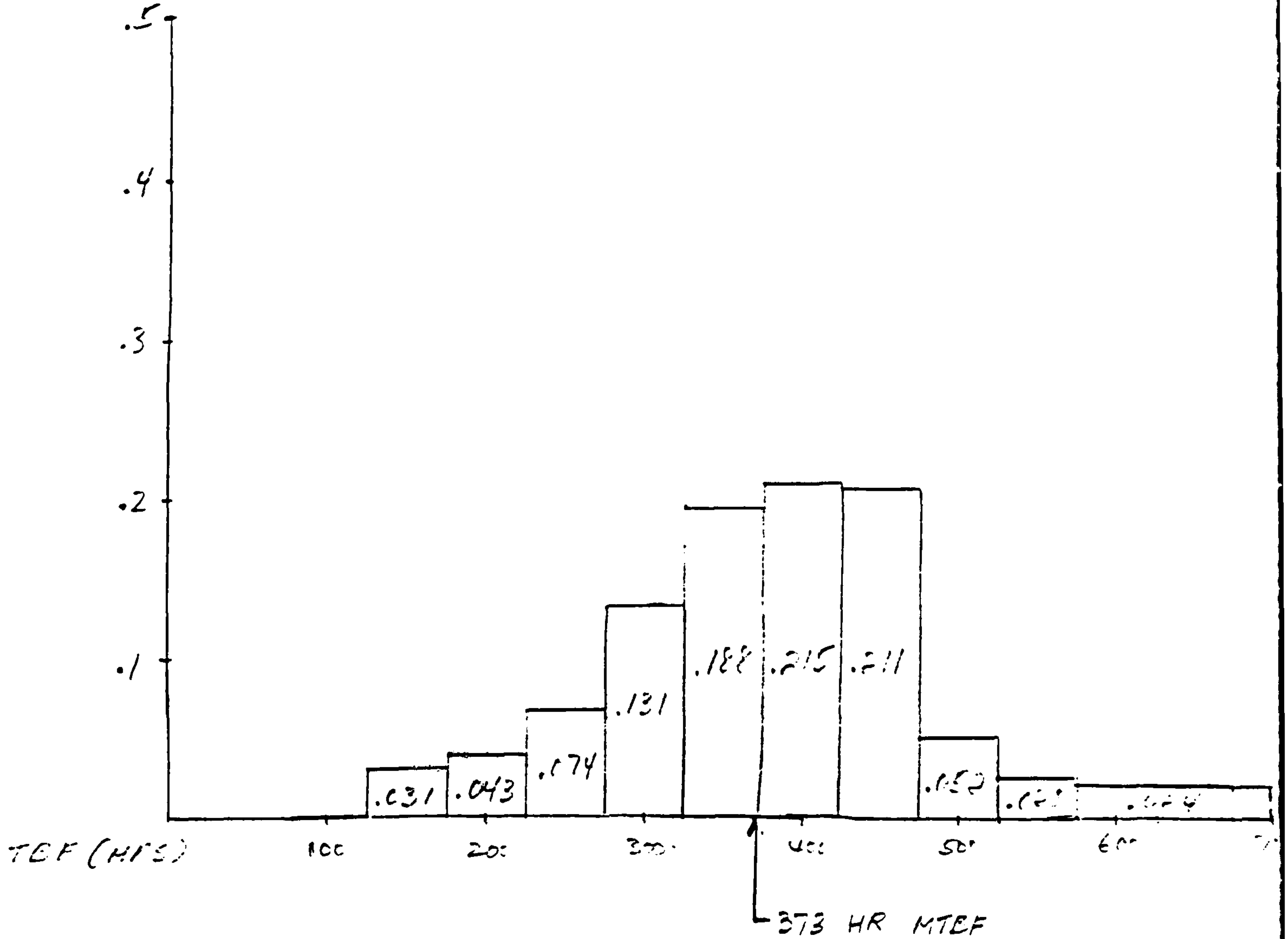

scenario 2

1 failure in 370 hours

figure C

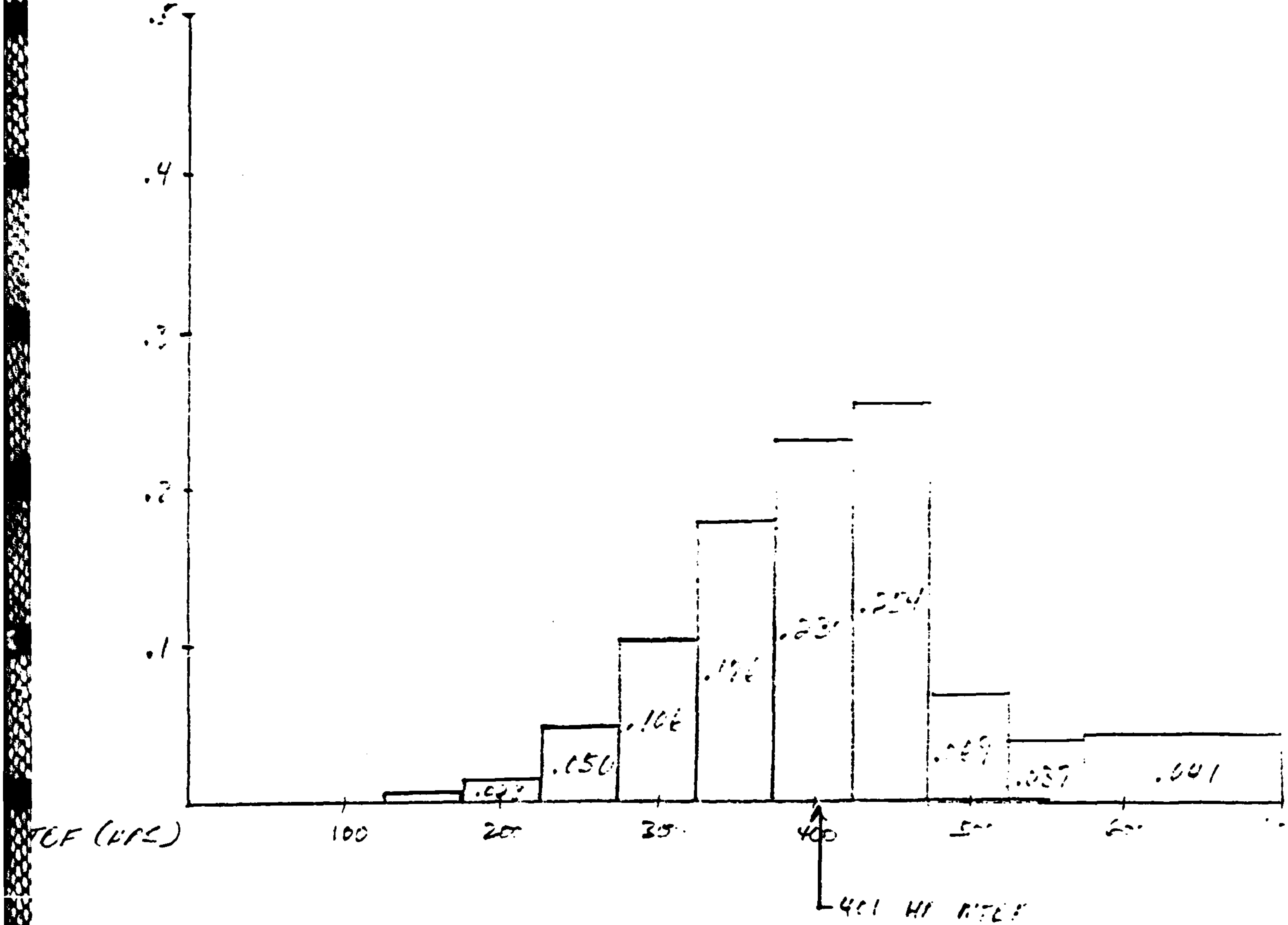

scenario 3

0 failures in 370 hours

figure D

ATTACHMENT

DATE: 30 August 1985

RE: Corrections to memorandum addressed to LTC Sechrest dated 9 August 1985

An error in the determination of the JTIDS Class 1 system reliability was found and the appropriate corrections were made. The calculations in figure 5 of the 9 August memo should read correctly as follows:

i	1	2	3	4
A_i	7.5×10^{-4}	3×10^{-3}	7.5×10^{-3}	3×10^{-2}
$P(A_i)$	.05	.50	.30	.15
$P(B\|A_i)$	4.6×10^{-3}	1.1×10^{-1}	2.2×10^{-1}	5.0×10^{-4}
$P(A_i)P(B\|A_i)$	2.3×10^{-4}	5.3×10^{-2}	6.6×10^{-2}	7.5×10^{-5}

$\Sigma P(A_i)P(B|A_i) = .119$

POSTERIOR	1.9×10^{-3}	4.5×10^{-1}	5.5×10^{-1}	6.3×10^{-4}

$$\text{PREDICTED MTBF} = (1.9\times10^{-3})(7.5\times10^{-4}) + (4.5\times10^{-1})(3\times10^{-3}) + (5.5\times10^{-1})(7.5\times10^{-3}) + (6.3\times10^{-4})(3\times10^{-2})$$

$= 182$ HR MTBF

RcF. 4

BAYESIAN METHODS FOR PREDICTING USAF SYSTEM PERFORMANCE

Dr. Carolyn D. Heising*
August 1985

Abstract

As a consequence of the programmatic support we have provided to Hanscom AFB this summer, it became apparent that the need exists to develop a practical approach to predict system field reliability. A useful Bayesian methodology has been developed in the nuclear power industry to predict system performance, and has been applied by Heising and others to several nuclear problems. This method has been applied here to estimate a well-known USAF system (JTIDS) reliability. Moreover, a body of USAF literature exists on the topic of Bayesian methodology. These methods are also reviewed here in the context of how they are related to the method we have used to estimate JTIDS reliability. It is found that a Bayesian approach can be useful for predicting USAF system performance, and can provide a practical approach to predicting system field reliability.

I. Introduction

Bayesian methods have often been used to predict system reliability. A major advantage of the Bayesian approach is the ability to combine many diverse sources of information and data together to derive a "best estimate" -- one that reflects the most current information and analyst understanding of the system. A Bayesian methodology based on the use of discrete probability distribution (DPD) arithmetic has been used here to estimate JTIDS reliability. In the following sections, Bayesian methods are further described. First, we review methodology that has been developed and applied by various USAF organizations and contractors. Second, we describe the Bayesian approach based on DPD arithmetic that we have applied here to the calculation of JTIDS reliability, and the results of that analysis. Previous work is reviewed as it relates to the JTIDS calculation methodology. Finally, conclusions and recommendations are given.

II. Review of USAF Bayesian Methods and Applications

The US Army Munitions Command suggested the use of a Bayesian approach in their proposed approach to reliability assessment (Oct, 1968, ref. 1).

The Rome Air Development Center (RADC) has investigated Bayesian methods (refs. 2-7). Also, the Analytic Sciences Corporation (TASC) has utilized such methods (ref. 8), as has TRW (refs. 9-11), Hughes (ref. 12), and others (ref. 13) in relation to USAF systems. The methods used and the applications made are reviewed here.

------

* Work performed as a USAF-UES Summer Fellow, Hanscom AFB MA, 1985. The author is an Associate Professor of Industrial Engineering at Northeastern University, Boston MA.

A. The RADC Methods

Coppola has developed a Bayesian test plan, and has shown the difference between this approach and more standard classical approaches (ref 2). In the classical case, the engineer starts by determining what values of producers and consumers risks are acceptable to him. This implies defined values for a desired MTBF and undesired MTBF (lower test bound). The engineer, by using the classical approach, completely ignores prior data which may be available on the system reliability (see Figure 1).

On the other hand, the Bayesian test procedure, outlined by Coppola, makes use of all and any previous test data available (see Figure 2). Advantages of this approach include:

(1) A favorable prior permits a shorter test with attendant savings in dollars and time (e.g., if a piece of equipment has high reliability based on commercial experience, why spend further money and time to test it -- a brief testing period is all that is required to determine whether a particular unit may be a lemon, even if the average unit is great);

(2) Each test performed can use all the previous test data as prior information; and

(3) With a Bayesian approach, continued high quality would reduce the risk of rejecting good equipment as it would successively reduce the stringency of the test.

In the method proposed by Coppola, an inverted gamma distributon is to be used as a prior (see Figure 3). (Interestingly, this distribution shape is similar to that which we have assumed for the JTIDS reliability estimation and is similar to a lognormal). The task then becomes one of fitting available data to the gamma distribution and solving for the parameters of the distribution.

Supporting this work by Coppola, several others have conducted research. Bolis, while a USAF summer faculty fellow, provided guidance for structuring Bayesian reliability test plans assuming an inverted gamma distribution of the prior and a constant failure rate of the tested equipment (ref. 3). He examined cases where these assumptions did not hold, and also presented a general estimation method called the general maximum likelihood method. This method has the advantage of being usable to update the prior when new data become available from reliability demonstration tests. Later, he extended his findings for estimating the parameters of the gamma distribution (ref. 4). He introduced a repairment assumption called instantaneous resurrection and showed that under this assumption, the number of failures of an equipment in time t is a Poisson process. This was used in the estimation of prior distribution parameters. Bolis also describes the producer's and consumer's risk as these may be formulated from a Bayesian perspective. Coppola has used these findings in his discussion of the several risk factors available as a result of a Bayesian approach to test design (ref. 2).

To summarize, the RADC methods are of a relatively theoretical and advanced mathematical detail. The application of these methods to real-world problems would need be attempted by only the most experienced analysts. However, the general conclusions reached about the benefits of a Bayesian approach are valid. The research conducted on these methods at RADC has provided a basis upon which the reliability engineer can begin to apply similar approaches, as we have done in our work reported here.

B. The Work of TASC

In the TASC work (ref. 8), a sequential Bayesian approach has been applied to an actual system of interest -- the CBU-87/B, commonly referred to as the Combined Effects Munition (CEM). A typical CEM consists of one SUV-65/B dispenser, one FZU-39/B fuze (proximity sensor), and 202 BLU-97/B Combined Effects Bomblets (CEBs). The design and construction of the bomblets is such that each one provides anti-personnel fragmentation, armor piercing and incendiary capabilities. Deployment of the weapon is shown in Figure 4.

This system was to be placed under warranty to comply with the FY84 military appropriations bill, which required that all weapon system acquisition contracts contain such product guarantees. TASC was to evaluate and then recommend a product assurance provision for the CEM system. In so doing, it was necessary to evaluate the system reliability.

TASC describes the Bayesian concept as one in which existing information about the true unit reliability is utilized to specify, before testing begins, a "prior" distribution of reliability for the age of units to be tested (see Figure 5). After additional information is gained through the testing, the prior distribution is modified with the test results to obtain a "posterior" distribution (see Figure 6). This distribution is then used to make a decision as to the ultimate reliability of the system and its acceptability. In the sequential approach used, the idea is to continue testing until a decision can be made. This is the idea behind the desiginate "sequential" in the name of the method (see Figure 7).

TASC recommended a sequential Bayesian approach be used to verify the CEM-PPA, and that such a combined approach could yield an expected benefit of at least 50 million dollars over the 5-year production period of the project. Moreover, additional benefits include:

(1) Conserving test units - not using them to verify that the reliability is in some improbable range of values;

(2) Making maximum use of knowledge gained during testing to verify with confidence if requirements are being met;

(3) Not testing any more units than necessary, by examining accept/reject criteria in a sequential manner (each time one is tested); and,

(4) Reaching a decision quickly for a population outside of specified reliability limits.

C. TRW Work

The TRW Systems Group investigated methods to combine two or more types of data (i.e.: ground and flight) (refs. 9-11). This method was used in countdown and flight reliability assessments of several Minuteman III subsystems. The need for this methodology arose as a result of the limitation in the amount of flight test data available, thus making it desirable to use data from other test sources. The use of more than one data source generates increased confidence in the reliability assessment. A "K-factor" based on the intersection or overlap of the probability density functions of the basic data and the "other" data was defined (refs. 9,10). This method was later refined to include Bayesian assumptions for binomial type data (ref. 11) so that the "K-factors" used for combining data could be based on a probability calculation. That is, instead of looking at two sets of data to see if they give the same probability of a particular reliability, it was proposed that the weighting factor be based on a comparison of the populations. It was then proposed that this factor be dependent on the probability that the true reliability of one population is greater than the other.

D. Hughes Work

A Bayesian reliability demonstration is provided in the excellent treatise by Dr. Drnas of Hughes Aircraft Co. (ref. 12). There, from a less formal point-of-view, Drnas describes Bayes Theorem in discretized form. He then performs several example calculations based on the use of this theorem, comparing the Bayesian and classical concepts. Drnas discusses the differences between Bayesian credible intervals and classical confidence intervals. Moreover, the use of the Binomial versus the Poisson distributions as likelihood functions is discussed, in addition to a review of possible prior distributions (such as the inverted gamma distribution in MTBF problems). Guidance is provided on the use of Bayesian methods for designing reliability tests. The many useful case studies provided include those that are computed with discrete probability arithmetic.

E. Others

Finally, others have investigated the use of a Bayesian approach to estimate reliability during a development test program. An example of such work is given in reference 13 by Smith, where the problem of estimating the reliability of a system which is undergoing development testing is considered from a Bayesian standpoint. Formally, M sets of binomial triads are performed under conditions which lead to an ordering, $\theta_1, \theta_2, \ldots \theta_M$, of the binomial parameters. He shows that the final underlying reliability of the system may be easily obtained as the posterior, where he has chosen to use a uniform prior for example purposes.

The U.S. Army Munitions Command proposed a Bayesian approach be used in reliability assessment (ref.1). They looked at the use of both the discrete and continuous forms of Bayes theorem. They noted that the probability theorem for combining subjective and objective information in terms of a prior probability and conditional probability density functions, respectively, yields the a posteriori density function of the parameter of concern. They suggested that Beta distributions could be used to describe component failure rates, and they derived an approach based on these distributions to combine updated flight results with laboratory component/system test results. They did not demonstrate the methods on a real-world example. However, this work is one of the earliest to recommend the use of Bayesian methodology to military reliability problems.

F. Summary of USAF Bayesian Methods and Applications

The Bayesian approaches described above have been developed and applied from differing standpoints, but all lead to one major conclusion: the Bayesian approach to system reliability predictions is more useful and practical in application than alternative approaches. Moreover, economic benefits to project management can result from the application of a Bayesian approach.

III. Bayesian Methodology Based on Discrete Probability Distribution (DPD) Arithmetic

A Bayesian methodology based on discrete probability distribution (DPD) arithmetic has been developed from work done on nuclear power plant reliability prediction (ref. 17). This methodology has been applied in several studies, including the Zion and Indian Point risk assessments (ref. 16). In Appendix A, a representative study employing these procedures is described; the ATWS study performed as part of the Oyster Creek risk assessment (ref. 19). A similar approach was taken in an analysis of core melt frequency performed by Heising and Mosleh (ref. 20). The DPD approach to Bayesian calculations is now described, and a tutorial example of how such calculations are made is provided.

A. The Bayesian Methodology Based on DPD Arithmetic (ref. 14)

It is useful for our purposes here to derive Bayes Theorem in discrete form, as we will be using it later in this form in several applications. Thus, let A and B be events. Then P(A) and P(B) are the respective probabilities of these events:

$$P(A \text{ "and" } B) = P(A \cap B) = P(A) \cdot P(B/A) \qquad (1)$$

If A and B are independent, then $P(A \cap B) = P(A) \cdot P(B)$. Thus, we can write:

$$P(A/B) = \frac{P(A \cap B)}{P(B)} = \frac{P(A) \cdot P(B/A)}{P(B)} \qquad (2)$$

Suppose we now construct a Venn diagram, and we let event A consist of four

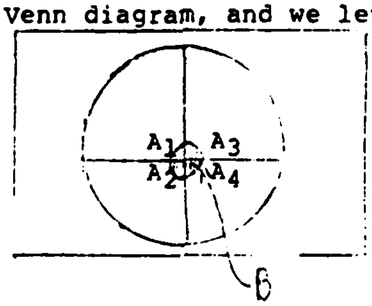

mutually exclusive events $A = A_1 \cup A_2 \cup A_3 \cup A_4$. Further, we postulate that event B may occur anywhere with respect to the four events A_i. Then we can write:

$$B = (A_1 \cap B) \cup (A_2 \cap B) \cup (A_3 \cap B) \cup (A_4 \cap B) \qquad (3)$$

We can illustrate this relation in our Venn diagram as follows so that we see that event B is made up of the union of the respective intersections with each event A_i.

We now reapply the definition in eqn. 1 above so that:

$$
\begin{aligned}
P(B) &= P(A_1)P(B/A_1) + P(A_2)P(B/A_2) \\
&\quad + P(A_3)P(B/A_3) + P(A_4)P(B/A_4) \\
&= \sum_{i=1}^{4} P(A_i)P(B/A_i)
\end{aligned} \tag{4}
$$

We can then substitute this expression into eqn. 2 as follows:

$$
P(A_i/B) = \frac{P(A_i)P(B/A_i)}{\sum_{i=1}^{4} P(A_i)P(B/A_i)} \tag{5}
$$

This is BAYES THEOREM in discretized form.

There is an important interpretation of this rule as follows:

$P(A_i)$= initial or prior information about A_i (sometimes referred to as the PRIOR),

B= new information (from experiments, tests, operating data, etc.),

$P(B/A_i)$= probability that B occurs given A assumes some particular value A_i (the LIKELIHOOD function), and

$P(A_i/B)$= updated estimate of A given new information B (the POSTERIOR)

With this interpretation of the functions related together through Bayes Theorem, we have a very powerful tool that may be applied to many important engineering reliability problems. To illustrate the approach, we look at the following illustrative example.

B. Tutorial Example--The Coin Tossing Problem Re-Visited (ref. 14)

We will now apply Bayes Theorem as we have derived it to the problem of updating your estimate on the fairness of a coin. Call the mutually exclusive events A_i the values of the frequency of observing a head, say A_1= 0.2, A_2= 0.3, A_3= 0.4, etc. Then, the probability of A_i, denoted $P(A_i)$, is just our apriori judgment about a particular coin as to the degree to which it is "fair" (where A_i= 0.5 for a "fair" coin). Suppose our apriori judgment can be encoded as shown in the histogram (Figure 8).

This histogram is based on our prior knowledge about coins, and we assume here that we have no previous experience with the particular coin we are examining. Now, we perform an experiment where we toss the coin ten times and observe seven heads. We denote this as event B, our new information about the coin. In order to determine the likelihood of observing event B (observing 7 heads out of 10 tosses), we note that coin-tossing is a Bernoulli process that can be described mathematically with the binomial distribution, where B is m heads out of n tosses:

$$P(B/A_i)=\frac{n!}{m!(n-m)!}A_i^m(1-A_i)^{n-m} \tag{6}$$

Now, we are ready to apply Bayes Theorem in eqn.5. To do so, we construct the following table where we have divided the possible frequency range for A_i into seven equally spaced intervals:

i	1	2	3	4	5	6	7
A_i	0.2	0.3	0.4	0.5	0.6	0.7	0.8
$P(A_i)$ "PRIOR"	.0025	.0025	.02	.95	.02	.0025	.0025
$P(B/A_i)$ "LIKELIHOOD"	$8x10^{-4}$	$9x10^{-3}$	.042	.117	.215	.267	.202
$P(A_i)P/B/A_i)$ "POSTERIOR"	$2x10^{-6}$	$2x10^{-5}$	$8.5x10^{-4}$	.11134	$4.3x10^{-3}$	$6.7x10^{-6}$	$5x10^{-6}$

where $P(A_i)P(B/A_i)$= .11768 and is called the pre-posterior, or simply the normalization factor.

We can illustrate the resulting histograms as shown in Figure 9. The posterior is our updated estimate about the fairness of the coin. Note that our experimental evidence has skewed the posterior distribution to the right, indicating that our coin may be biased in the direction of heads. The reader may repeat this calculation for various values of n and m, and even in a sequential fashion as further experimental evidence becomes available.

The use of the discrete form of Bayes Theorem has been extensive in nuclear power reliability studies (see refs. 15 and 16). The use of histograms instead of continuous distributions has led to a relatively new procedure for performing risk and reliability calculations based on the mathematical operations of discrete probability distribution (DPD) arithmetic (see ref. 17). This approach has many advantages, including economy-of-scale (ie: the bigger the problem, the least expensive is the DPD approach as compared to other available methods). Also, the method has the rather important advantage of being conceptually simple--large, complex and confusing continuous distributions need not be dealt with. The level of theoretical complexity is thus far reduced, leading to ease of application, particularly by project engineers who may have little or no formal statistical training.

C. Use of the Poisson Distribution for MTBF Calculations

We have illustrated the use of the binomial distribution as the likelihood function in the coin-tossing example. However, when calculations are made on system reliability problems in terms of the MTBF, the Poisson distribution is most applicable (see ref. 12). The Poisson distribution can be written as follows:

$$b(f;T,\theta)= \frac{e^{-T/\theta}\left(\frac{T}{\theta}\right)^{f}}{f!} \qquad (7)$$

where f (failures) is a random variable (=0,1,2...), T is the test time (measured in hours), and θ is the MTBF (in hours^{-1}). The use of the Poisson distribution is made in much the same way as the Binomial above, except that intervals for A_i are in MTBF units (i.e.: θ_i). This theorem is applied in the next section here.

IV. Application of the Discrete Bayesian Method to Estimate an USAF System Reliability

The following example comes from the Electronics Systems Division (ESD) at Hanscom Air Force Base near Boston, Massachusetts. The system is a communication system for USAF aircraft. The first step in the analysis was to derive a prior distribution, shown in Figure 10. This was done based upon a fault tree analysis of the system which predicted an expected value mean-time-between failures (MTBF) of 500 hours (a failure rate of $2x10^{-3}$/hr). Based upon this expected value, and the analysts judgment concerning the data used in the fault tree to derive the estimate, the prior was constructed to best reflect this "state-of-knowledge".

To calculate the likelihood function in this application, eqn. (7) was utilized where, in this case, T is the number of hours of test operation, and f is the number of failures to occur during the T hours of operation. In this application to the USAF system, failure summary reports for the reliability demonstration process were used, since this part of the overall reliability test most closely resembled actual field operating conditions. The actual figures used in the likelihood calculation were 3 failures in 450 hours of operating (see Figure 11) (Later, this data was modified to 1 failure out of 370 hours of operation since two of the three failures occurred within the last 80 hours of the reliability demonstration, leading the analyst to conclude that these 80 hours might still represent the burn-in period for the system being tested). Using the 3-out-of-450 data, a best estimate MTBF of 182 hours was calculated (see Figure 12).

V. Conclusions/Recommendations

It has been shown here that a Bayesian approach to calculating system reliability can be useful for predicting USAF system performance, particularly in the field. It is recommended that such an approach be further developed, refined, and applied to example case studies of USAF systems.

Acknowledgements

This work was performed as part of the USAF-UES Summer Fellow program. The author thanks Mr. Fred Chin, undergraduate research assistant, for performing the calculations on the JTIDS project. This work was performed at the Electronics Systems Division (ESD) at Hanscom AFB in the Product Assurance office under the direction of Mr. Lee Pollock.

References

1. A Proposec Approach to Reliability Assessment, US Army Munitions Command, App.D, October 1966.

2. Coppola, A., "Bayesian" Reliability Tests Made Practical, RADC-TR-81-106, In-House Report, July 1981.

3. Bolis, T. S., Application of Bayesian Techniques to Reliability Demonstration, Estimation, and Updating of the Prior Distribution, RADC-TR-79-121, In-House Report, April 1979.

4. Bolis, T. S., Bayesian Reliability Theory for Repairable Equipment, RADC-TR-80-30, Final Technical Report, February 1980.

5. Hughes Aircraft Company, Bayesian Reliability Demonstration: Phase-Data for the Priori Distributions, RADC-TR-69-389. (Phase II-RADC-TR-71-209; Phase III-RADC-TR-73-139).

6. Feduccia, A. J., A Bayesian/Classical Approach to Reliability Demonstration, RADC-TR-70-72.

7. Syracuse University, Design of Reliability Test Plans Based Upon Prior Distribution, RADC-TR-78-241.

8. Dizek, S. G., Fritz, A. L., and Stetzler, B. L., Product Performance Agreement Characteristics for Combined Effects Munitions, TR-4633-3-1, TASC, Reading, MA, July 1984, Section 3.3 "Sequential Bayesian Testing Approach", and Appendix B: "Sample Calculations for the Sequential Bayesian Test Concept."

9. Hottenroth, F. W., "K-Factor Generation Method," TRW, Interoffice Correspondence, March 15, 1971.

10. Hottenroth, F. W., "MK-12 Countdown and Flight Reliability Assessment Method," TRW, Interoffice Correspondence, May 10, 1971.

11. Wolf, J. E., "Proposed Weighting Factor," TRW, Interoffice Correspondence, Dec. 5, 1972.

12. Drnas, T. M., Bayesian Reliability Demonstration, Hughes Aircraft Co., Culver City, CA, 1975.

13. Smith, A. F. M., "Bayesian Note on Reliability Growth During a Development Testing Program," IEEE Trans. on Reliability, Vol R-26, No 5, December 1977.

14. Heising, C. D., "The Bayesian Approach Using DPD Arithmetic," Reliability Analysis Course Notes, Northeastern University, Boston, MA, 1985.

15. Methodology for Probabilistic Risk Assessment of Nuclear Power Plants, PLG-02209, June 1981.

16. The Zion and Indian Point Probabilistic Risk Assessments, Pickard, Lowe and Garrick, 1982.

17. Kaplan, S. "On the Method of Discrete Probability Distributions in Risk and Reliability Calculations," Risk Analysis, Vol.1, No.3, 1981, pp. 189-196.

18. Kececioglu, D., "Sequential Testing for the Binomial Case," Course Notes, University of Arizona, 1982.

19. Oyster Creek Probabilistic Safety Analysis, Main Report (Draft), August, 1979: Section 5.2.2, "Reactor Protection System," pps. 5-40--5-43; Section A.2.4.3: "A Prior Quantification," pps. A-201--A-224.

20. Heising, C. D. and Mosleh, A., "Bayesian Estimation of Core Damage Frequency Incorporating Historical Data on Precursor Events," Nuclear Safety, Vol.24, No.4, July-August 1983, pp. 485-493.

Appendix A EXAMPLE OF DPD BAYESIAN APPROACH IN APPLICATION: THE OYSTER CREEK SCRAM RELIABILITY STUDY

A more detailed analysis of the scram system (reactor protection system (RPS)) was carried out for the Oyster Creek BWR plant (ref. 17). Basically, the RPS is made up of five subsystems, shown is Figure A.1: (1) sensors, (2) logic, (3) hydraulic control units, (4) control rod devices, and (5) scram discharge volume. Each of these subsystems perform a different function in protecting the reactor from undesirable transients. The sensors first detect the undesirable circumstances (e.g., high-high reactor pressure or neutron flux) sending electrical signals to the logic circuitry, which determine whether the signals are spurious or real. At Oyster Creek, the logic used in the APRM input circuit is called a "one-out-of-two-twice" system since the signal must come from either of two sets of dual detectors twice and then be matched against the existence of a signal on the opposite channel.

In a BWR, the signals from the sensors cause the logic circuit to deenergize as each logic channel is basically a set of relays and contacts; when a detector senses a parameter out of limit, the input to the associated logic channel results in a contact being opened. The resulting open circuit leads to deenergization of a relay which in turn leads to further deenergization of other relay sets. When both logic channels are fully deenergized, the logic system causes power to all scram pilot valves to shut-off. Each of the 137 control rod drives has a hydraulic control unit (HCU) governed by the position of the scram pilot valve. The two scram pilot valves transfer to an open position and bleed the instrument air that holds two scram valves in the closed position. This exerts a change in pressure ΔP that is exerted under the control rod piston. Reactor pressure and the ΔP drive the control rods the full distance into the core.

When this happens, water is driven out of the control rod drives and is exhausted through the discharge side of the hydraulic control units. The scram discharge volume, which is the fifth sub-system, collects the water from all 137 control rod drives.

Both dependent and independent failure modes of the five sub-systems were analyzed with fault trees to arrive at histograms on the failure frequency per demand. The RPS summary fault tree for Oyster Creek is shown in Fig. A.2. Results are shown in the figure and indicate that dependent failures outweigh the independent modes of failure. The largest single contributor to the overall failure frequency is the logic sub-system followed by sensor failure, and then by the failure of 5 out of the 137 control rods to insert fully upon demand. The scram discharge volume contributes only in a minor way to the total failure frequency, but note that the dependent and independent failures are roughly equivalent. The final histograms of the failure frequency is shown in Fig A.3 and combines the histograms of the five sub-systems.

The Bayesian approach was used in the Oyster Creek study to incorporate the existing experiencial data into the calculations of scram failure per demand. Because of the uncertainty and debate surrounding the number of scram failure occurrences, and the uncertainty on the number of total tests of the scram system in the world, the Oyster Creek study points out (p. A-201):

"Subjective judgement is inevitable when dealing with uncertainty. Subjective judgement is essential. All that the Bayesian approach does is to formalize the use of judgement and make it visible and explicit so that inconsistencies will be prevented.

To use the Bayesian approach, a prior distribution must be constructed. This was done for Oyster Creek by combining the failure frequency histograms for the five sub-systems (Fig. A.3).

Next, posterior distributions were calculated from Bayes theorem (Fig. A.4) incorporating both the prior distribution derived from the systems analysis and the available experience data. The experience data consists of estimates made by EPRI and NRC on the number of scram failures r experienced out of n test trials in the world to date. The "r-out-of-n trials" is also analogous to the coin-tossing experiments discussed earlier where r= number of heads, and n= number of scrams (tests) which have occurred over the lifetime of the world's nuclear power industry. Results of the analysis for Oyster Creek are shown in Fig. A. . Note the prior distribution derived from the system fault-tree analysis and the observed data points x_i. The characteristic mean of the prior and posterior distributions are also shown.

The final result is that the best estimate of the scram failure frequency per demand is $\{WS/AT,\bar{x}\}$; i.e.; the probability distribution function of having a without scram event (WS) given an anticipated transient (demand) is conditioned on the observed data $\bar{x}$ expressed in composite form. (Note that the inferential notation allows the analyst to define the probability statement explicitly.) Numerically, the expectation of this p.d.f. is $\langle WS/AT,\bar{x}\rangle \hat{=} 5 \times 10^{-5}$/demand for Oyster Creek. However, if it is assumed that two anticipated transients are likely per reactor year, the resulting mean estimate of an ATWS event at Oyster Creek is 10^{-4} per reactor year. This value does not meet the NRC desired criterion of 10^{-6} undesirable ATWS events per reactor year. This limit can only be reached if each sub-system failure frequency is reduced to 10^{-6}. Such a risk reduction is estimated to cost several tens of millions of dollars, and is particularly expensive and costly for operating plants. Plant outage for extended retrofits such as would be required to satisfy the NRC ATWS guidelines could run into hundreds of millions of dollars because of the expense of replacement power.* Thus, a possible next step in ATWS analysis is to do a cost-benefit tradeoff between mitigation system alternatives and retrofit costs, and the expected benefits (or disbenefits) of each alternative expressed as the reduction (or increase) in public health risks. Such a study has not been done, and is certainly strongly suggested for the future.

---

* At TMI, for example, over 60% of the expense of the accident is estimated to be due to payments for replacement power.

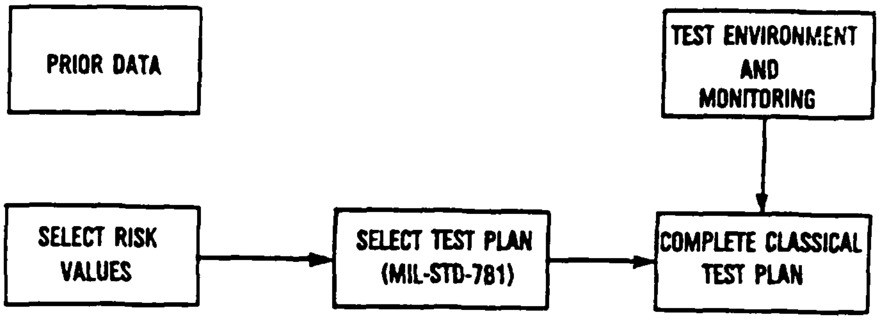

FIG. 1 DEVELOPING A CLASSICAL TEST PLAN (2)

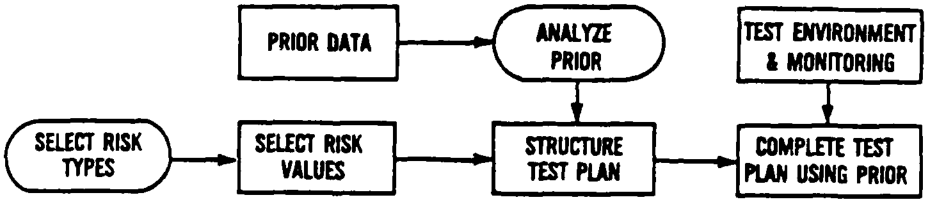

FIG. 2 DEVELOPING A BAYESIAN TEST PLAN (2)

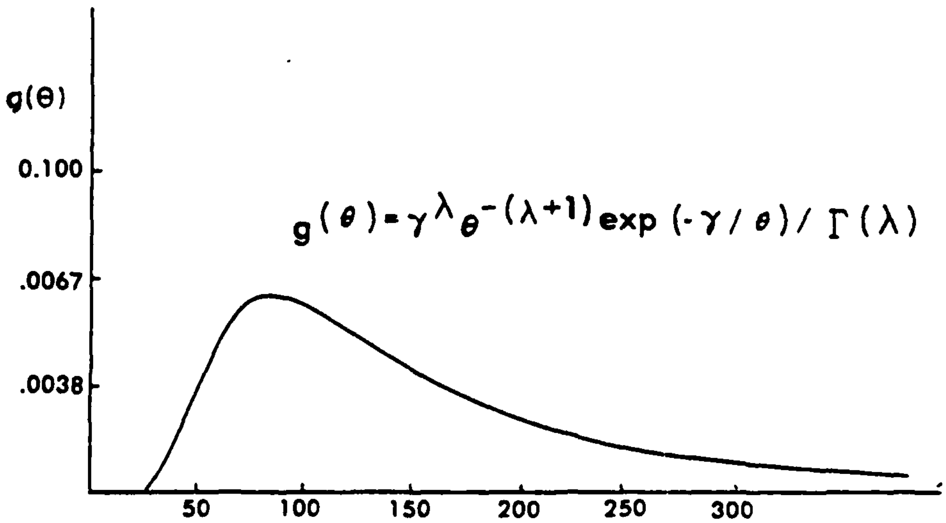

FIG. 3 INVERTED GAMMA DENSITY FUNCTION (2)
λ (SHAPE PARAMETER) = 3.5, γ (SCALE PARAMETER) = 470

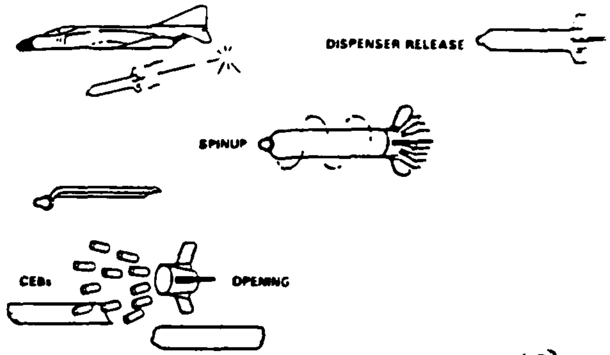

Figure 4 CBU-87/B System Bomb Deployment (8)

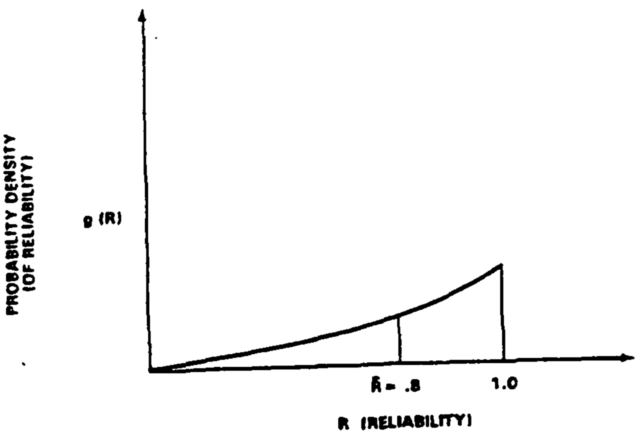

Figure 5 Example Beginning Prior Density (T=0) (8)

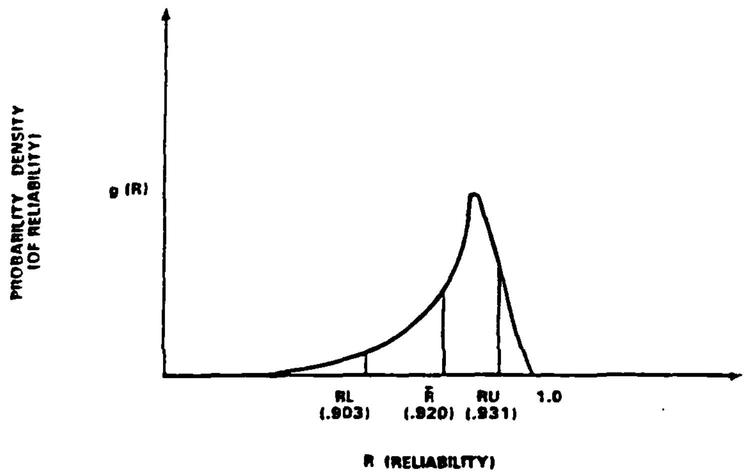

Figure 6 Example Posterior Density (T=0) (8)

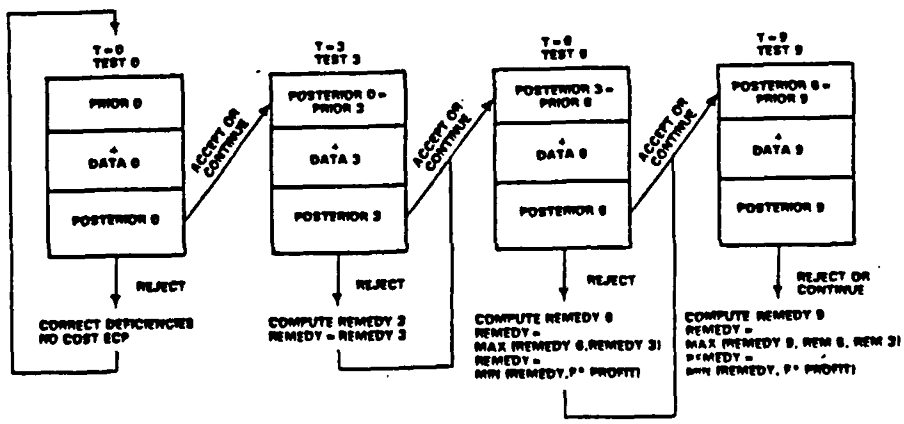

Figure 7 Sequential Bayesian Test Concept (4)

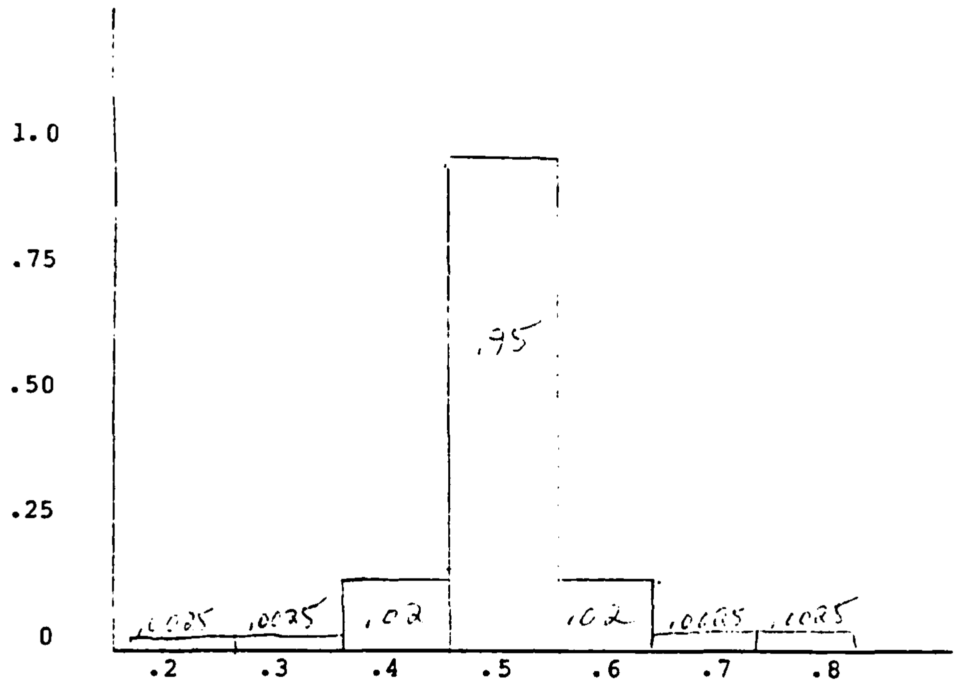

Figure 8 PRIOR DISTRIBUTION ON COIN-TOSSING EXAMPLE

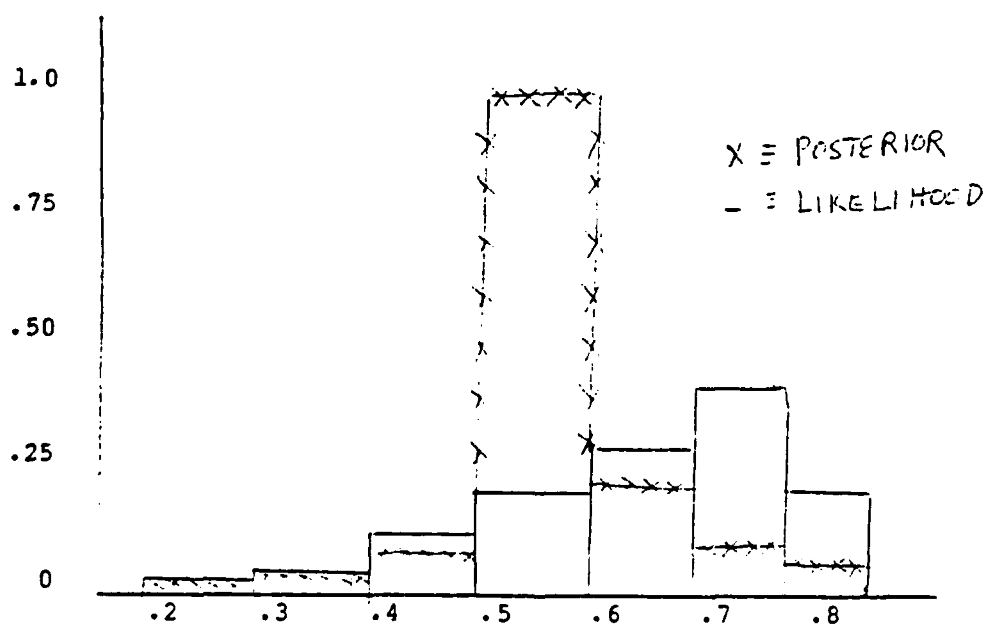

Figure 9 Comparison of Likelihood and Posterior for Coin-Tossing Example

PRIOR Distribution
(Based on Fault Tree Results
and Analyst Judgement)

figure 10

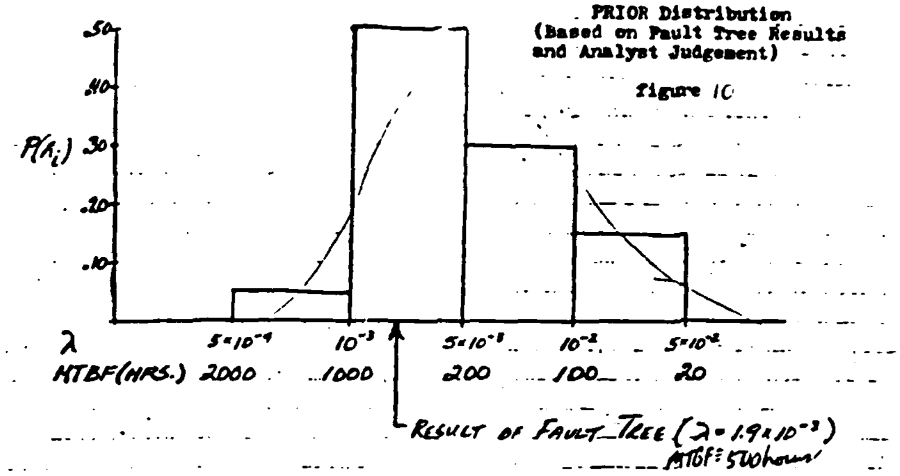

LIKELIHOOD Distribution
figure 11

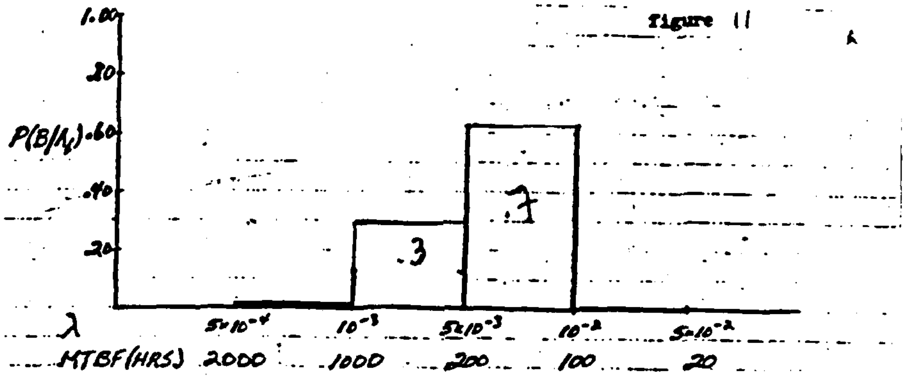

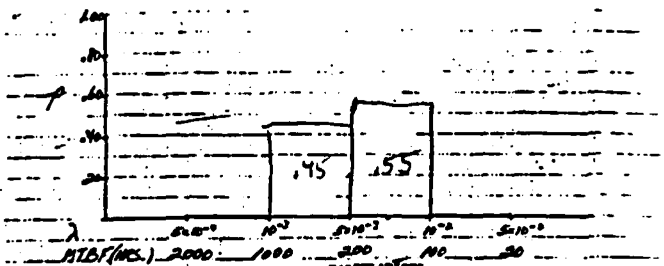

CALCULATIONS

i	1	2	3	4
λ_i	7.5×10^{-4}	3×10^{-3}	7.5×10^{-3}	3×10^{-2}
$P(\lambda_i)$	.05	.5	.30	.15
$P(B/\lambda_i)$	4.6×10^{-3}	1.1×10^{-1}	2.2×10^{-1}	5×10^{-4}
$P(\lambda_i)P(B/\lambda_i)$	2.3×10^{-4}	5.5×10^{-2}	6.6×10^{-2}	7.5×10^{-5}
$\Sigma P(\lambda_i)P(B/\lambda_i)$		1.2×10^{-1}		
POSTERIOR	2.7×10^{-3}	.45	.55	8.9×10^{-4}

$(2.7\times10^{-3})(7.5\times10^{-4}) + (2.1\times10^{-1})(3\times10^{-3}) + (.55)(2.5\times10^{-3}) + (8.9\times10^{-4})(3\times10^{-2})$

$= 6.6\times10^{-3}$

Expected Value = 183. MTBF

POSTERIOR Distribution
figure 12

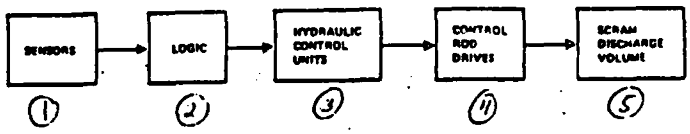

Five Subsystems of RPS
(BWR)

FIGURE A.1 REACTOR PROTECTION SYSTEM MODEL (RPS) (19)

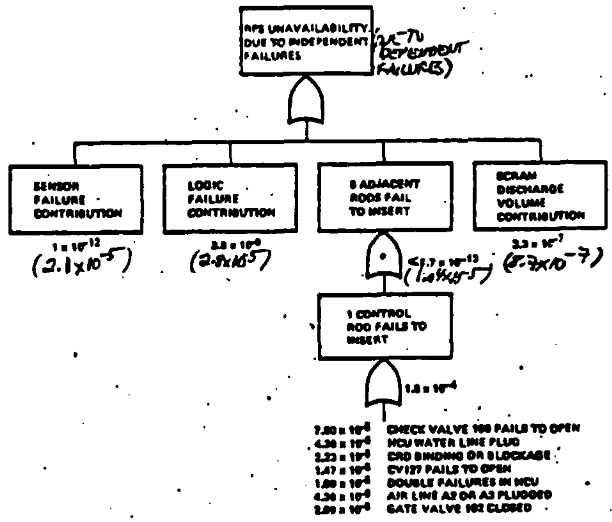

*PROBABILITY OF 8 ADJACENT ROD FAILURES CALCULATED ACCORDING TO SECTION A.2.3.5

FIGURE A.2 RPS SUMMARY FAULT TREE (19)

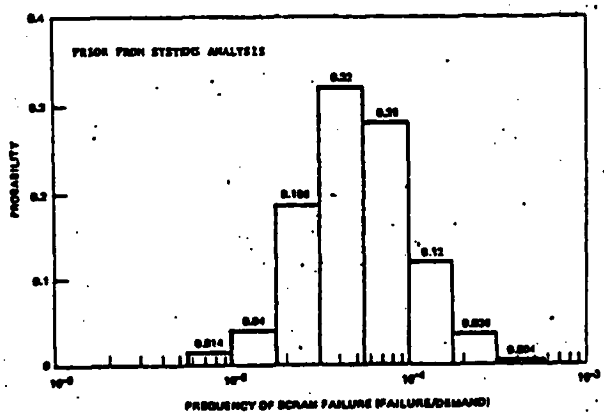

FIGURE A.3 PRIOR PROBABILITY DISTRIBUTION FOR SCRAM SYSTEM FAILURE (19)

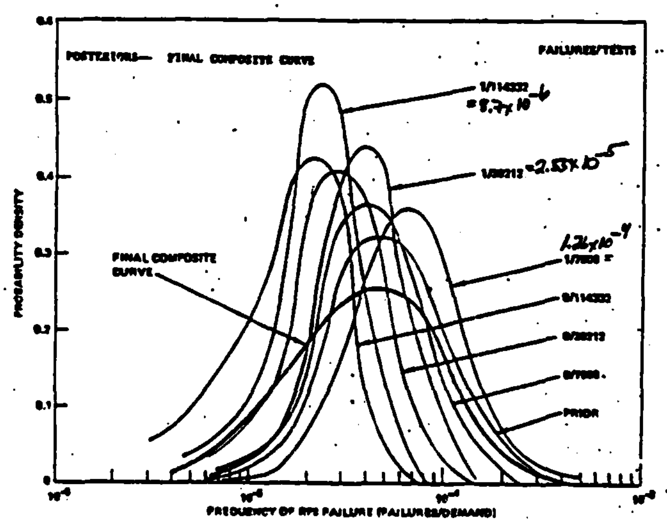

FIGURE A.4 FINAL COMPOSITE PROBABILITY CURVE FOR SCRAM FAILURE RATE (19)

Att. 5

MEMORANDUM

TO: Capt Don Campbell

FROM: Susan C. Malone SCM

DATE: 2 Aug 1985

SUBJ: Maintenance Data Collection System For MILSTAR Warranty Tracking System

Objective

To outline the means by which the MILSTAR SPO can track EDM maintenance data in order to determine system MTBMA, and thus, contractor's earned incentive, which is a function of MTBMA.

Discussion

1. For MTBMA determination, maintenance reports must include at least the following factors: operating and/or flight hours, failure type, corrective action taken, and system component designators. These factors are all included in the Maintenance Data Collection System (MDCS) which, as discussed in the memo of 22 July (see attachment 1), the Air Force is presently using to report maintenance actions. The maintenance data reporting procedure basically follows these steps:

a. Maintenance action is completed;
b. AFTO 349 form is completed by technician;
c. Completed form is checked for accuracy by supervisor;
d. Information from form is keypunched;
e. When keypunched, information is entered into base MDCS;
f. Information goes directly into D056 data base at WPAFB; and
g. A subset of the D056 information enters the Maintenance and Operational Data Access System (MODAS) at WPAFB.

(Total time elapsed from step 1 to step 7 is generally between one and two weeks.)

MODAS is the only one of these data bases which is readily accessible for data manipulation, and according to Mr. Chuck Gross at WPAFB, is the data base generally used for AFLC maintenance data analysis. The primary difference

between MDCS and MODAS is that MODAS excludes much of the manpower and labor related information used by the individual bases to support staffing and scheduling efforts. It does appear to keep all of the information relevant to maintenance and MTBMA determination. However, although the reporting is only one to two weeks in lag, the actual flight operating hours are six to eight weeks behind as they wait until official hours are stated.

2. This reporting procedure currently in use is gradually being phased out so that by 1990 MDCS and MODAS will no longer be in use; the Core Automated Maintenance System (CAMS) will be their replacement. CAMS is a totally computerized system currently under test, and is slated for introduction to all bases over the next few years.

With CAMS, the technicians in the maintenance shop will have computer terminals at their workstations. When they perform a maintenance action, rather than completing a printed AFTO 349 form (see attachment 1, page 5) the information is entered via the keyboard onto an electronic 349 form which is displayed on the terminal screen. Thus, the maintenance data is entered directly into the data base, rather than waiting to be keypunched, allowing the information to be updated daily. Because the 349 form is still being used (although in a somewhat different manner) the format in which the information is reported will be the same in CAMS as in MDCS. This information will be entered into the Sperry 1160 computer system for the particular base. A subset of this data will then be input to one centralized data base, at a location yet to be determined. The CAMS data base, known as the Reliabilty and Maintenance Information System (RAMIS), not only collects the CAMS Data but ascertains its validity as well. For example, if a technician at Offutt inadvertently enters a work unit code for an equipment type which is not repaired at Offutt, he will be alerted to this error. Also, RAMIS will have the capability to check for logic errors in the data entry; for example, if the How Malfunctioned code could not actually be treated with the specified Action Taken code, then attention will be called to this. Thus, the CAMS/RAMIS system will provide many error and logic checks, which is advantageous because data analyses are only as good as the data collected.

3. Initially, different methods may be required to obtain the MILSTAR maintenance data from Offutt and Ellsworth, because Ellsworth is implementing CAMS in 1986, and Offutt is not expecting it until 1989. Therefore, while Ellsworth will be operating under CAMS during the entire EDM period, Offutt may not have CAMS fully operational during the early part of EDM, but probably will convert part-way through. This does not pose a serious problem, however provisions should be made for this occurence and, thus, each base will be discussed separately.

It should be noted that in both MDCS and CAMS, the Work Unit Code (WUC) will be used to identify MILSTAR maintenance actions. The WUC is a five digit alphanumeric code on the 349 form, each digit signifying a succeeding level of component detail. For example:

681AB

68 indicates a satellite system

1 indicates the particular system (AFSATCOM)

A indicates a particular subsystem or assembly (such as an LRU)

B generally indicates the lowest repairable item (often a card, but in certain cases can refer to an even lower level component)

These WUC are developed by Air Logistics Center after the contractor has firmed up the design, and usually are published just prior to IOT&E. Because of the time involved in assigning the correct codes, having the platform manager check them, then having the work unit code manuals printed and distributed, the WUC are often not available to the technicians when the equipment is first fielded. This could make it difficult to track the maintenance data, so if possible, the platform manager could be requested to have the codes developed by the start of EDM, perhaps employing temporary WUC. If the WUC are not developed in time, manufacturers' part numbers may be used track items, although this won't fit the 349 form properly (perhaps they could be keypunched onto the end of the record).

To determine the feasibility of having WUC go down to the component level rather than just the SRU level, the appropriate platform manager would have to be consulted.

a. Offutt AFB

If the MILSTAR EDM phase begins prior to implementation of CAMS at Offutt, then, until CAMS is fully operational, a different maintenance data retrieval method will have to be used. There are three alternatives:

(1) Retrieval. At regular intervals, the maintenance data processing shop at Offutt could dump all of the MILSTAR maintenance data for that period either onto a magnetic tape or onto a printout (listing each maintenance action and its corresponding information from the 349 form), and send it to the SPO. If a tape is sent, then the data could be loaded directly onto a computer system at Hanscom, then accessed via a terminal. There are similar computer systems on base, but it would have to be determined if they were compatible so that data formatted at Offutt could be read at Hanscom; if not, a reformatting program would have to be written. The SI and OCS office could assist in coordinating this. If a printout is sent, then the data will have to be typed into a computer, which would be very time-consuming and prone to error in transcribing the data from the printout to the computer. The magnetic tape would be the more efficient way to obtain the information.

If the retrieval method is chosen, a letter of request must be sent from the SPO program manager to:

55th SRW/MA
Offutt AFB, NE 68113

The letter should request a retrieval of all MILSTAR maintenance data from the MDCS (the first three characters of the work unit code will designate the MILSTAR system, although the specific codes have not been developed yet) for each X week period for Y years (covering the entire EDM period). The data record format will be the same as on the 349 form, i.e., job control number, workcenter, serial number, etc. The sequence in which the records are reported can be specified. For example, it may be useful to sort the records according to work unit code, so that all of the same codes (and therefore the same subsystems) are reported together, rather than in the random order they occur in the data base. The desired sorting procedure must be specified in the letter of request. Also, a report of total operating hours should be requested.

Using the retrieval method, the information obtained would be reasonably current, as the MDCS turnaround time (from maintenance action to entry into the system) is seldom longer than two weeks.

(2) MODAS. As discussed previously, much of the MDCS information serves as input to the MODAS system, and because it can be directly accessed the MILSTAR maintenance data could be obtained from MODAS using an appropriately configured computer terminal at Hanscom. This would facilitate data analysis because there would be no need to wait to receive tapes and transfer the information from tape to computer. However, as already stated, the entire 349 record is not contained in MODAS (although the data relevant to MTBMA determination is there), and the total flight hours are six to eight weeks behind time. An eight-week lag may not provide current enough information to accurately track the warranty. If this lag is determined to be too long, and the MODAS method of maintenance data acquisition is selected, it is possible to obtain more current (although unofficial) flight hour data directly from the individual bases' data processing shops.

If the MODAS method is chosen, one of the following people must be contacted in order to obtain manuals, a user identification number, and the proper switch settings for a terminal:

Mr Chuck Gross
Mr Frank Maguire
WPAFB - AFLC
AV 787-6906

With their assistance, direct access can be arranged from the SPO to the MODAS system to study the MILSTAR maintenance data. No specific type of terminal is required, as long as the proper switch settings are used.

Using the MODAS method, the information obtained would be about as current as in the retrieval method, one to two weeks (assuming unofficial flight hours are used).

(3) Direct Access. It is possible to obtain direct access from the MILSTAR SPO to the MDCS data base at Offutt and retrieve the MILSTAR maintenance data that way. A modem and appropriately - configured terminal or personal computer would be required (an HP 9836 is being tested for this purpose). A program would need to be written to extract the appropriate data from the data base (contact the Field Assistance Branch of the Data Systems Design Office, Gunter AFS, AV 446-4021 if technical assistance is required), and authorization and system configuration would be obtained from:

55th SRW/MA
Offutt AFB, NE 68113

In the letter of request, state the need to access the data, the time frame during which the data will be required, and request information as to the appropriate equipment and/or configuration required.

b. Once CAMS has been implemented, the maintenance data collection procedure will be somewhat modified. There will be three possible methods of obtaining the information.

(1) Direct access to individual bases. With proper authorization, the Offutt data base (i.e., the CAMS data) can be accessed directly from the MILSTAR SPO; only a modem and Sperry 1160 compatible terminal are needed (a UTS-40 or Z-100 with UTS-40 interface would be sufficient). Using this method, any data in the data base can be read, sorted, and stored for future analysis. For example, all records wth MILSTAR work unit codes can be gathered, sorted into a particular order, and stored in a file on the SPOs microcomputer where it can then be manipulated to perform any necessary analysis. The data obtained in this manner would be updated daily, certainly current enough for warranty tracking.

To authorize direct access, the MILSTAR using command would have to send a request to:

SAC LGM (Action)
SIU (Info)
Offutt AFB, NE

AD-A166 177 UNITED STATES AIR FORCE SUMMER FACULTY RESEARCH PROGRAM 05/1
1985 TECHNICAL RE.. (U) UNIVERSAL ENERGY SYSTEMS INC
DAYTON OH R C DARRAH ET AL DEC 85 AFOSR-TR-86-0140
UNCLASSIFIED F49620-85-C-0013 F/G 5/1 NL

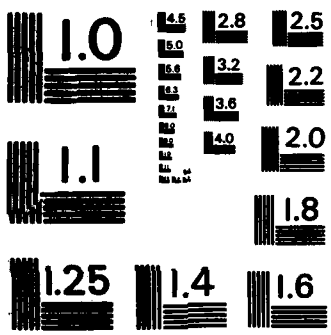

MICROCOPY RESOLUTION TEST CHART
NATIONAL BUREAU OF STANDARDS-1963-A

This request should outline the need to obtain a dial-up port to access the CAMS data base on a read-only basis (i.e., no capability to directly alter the entire data base), a brief description of the intended use of the data, and a request to specify the particular equipment which will be needed (i.e., the ideal computer to interface).

(2) Direct access to collective data base. A large subset of the CAMS/RAMIS data from all bases will enter a collective data base. This data base is updated daily, providing very current maintenance records. Access to this data base could be accomplished using a properly configured computer and modem. The chief advantage to using this collective data base, is that data from all bases can be accessed rather than accessing each base individually and then combining the data. Therefore, during EDM, maintenance data from both Offutt and Ellsworth can be obtained from this one data base, and if this data is going to be tracked during production as well, all bases will input to this one data base. This makes its use seem quite efficient.

To obtain authorization for use of this system, a letter of request should be forwarded (by 1 Sep 85) to:

AFLC LMSC/SMI (RAMIS)
WPAFB OH 45433

This letter should request a remote access hook-up for CAMS/RAMIS, outlining the reason for request, and the type of data desired. The reason for the 1 Sep 85 deadline is that a remote user equipment list is being developed for RAMIS implementation, and the earlier the request is made, the more likely the access will be obtained. If the deadline cannot be met, one of the following people should be contacted:

Dwayne Tucker
Tom Hinkle
Ray Olsky
AFLC
AV 787-5138

(3) Retrieval. As with MDCS, a request can be made for a periodic retrieval of the MILSTAR maintenance data, to be delivered in tape or printout form. The request can either be made to the individual bases (in which case the letter of request is sent to either 55th SRW/MA for Offutt or 28th BMW/MA for Ellsworth) or to the base running the collective data base (the location is yet to be determined). However, with the rapid, efficient computer access available in CAMS, it seems inadvisable to consider retrieval.

c. Ellsworth AFB

Because CAMS/RAMIS is expected to be fully operational throughout the entire EDM phase, there is no need to consider using another system, as there is at Offutt. Obtaining maintenance data from Ellsworth using CAMS is the same as obtaining the data from CAMS at Offutt.

(1) Direct access to individual bases. (see section 3.b.1 for discussion). Authorization for use would be obtained from:

SAC LGM (ACTION)
SIU (Info)
Offutt AFB, NE 68113

(2) Direct access to collective data base. (see section 3.b.2 for discussion). Authorization for use would be arranged in the same letter of request for Offutt.

(3) Retrieval. (see section 3.b.3 for discussion).

Using direct access method, the information obtained would be as current as in the other methods.

4. As discussed in the previous memo (see attachment 1) the MDCS does not code the information from items 26 and 27 on the 349 form, namely, Discrepancy and Corrective Action. Although the maintenance technicians do complete these items, they are in narrative form and thus occupy excessive amounts of space in the computer; that is why they are not coded into the MDCS data base.

If it is decided that this information is important to the MILSTAR warranty tracking system, and that the presently coded How Malfunctioned and Action Taken items do not provide sufficient information, then there are a few alternative ways to obtain it:

a. In MDCS

If MDCS is still in use at Offutt, then there are two methods of obtaining the data from items 26 and 27:

(1) Narrative. The maintenance data processing shop at Offutt maintains a separate narrative file on an HP 9836 personal computer, containing all of the 349 form narratives for items 26 and 27, and their associated work unit codes so they can be matched with their corresponding records in the MDCS to obtain a complete record of each maintenancce action. The information contained in this file can be obtained in four ways, some of which were discussed in the previous memo:

(a) Hardcopy. All of the MILSTAR narratives and their corresponding work unit codes can be printed out periodically, and the printout sent to the SPO. Once at the SPO, the narratives can then be categorized, sorted, coded, entered onto a computer, etc., for further study.

(b) Floppy disk. Rather than dumping the data onto paper, the narratives can be written to an HP floppy disk which can be sent to the SPO. Once at the SPO, the disk can simply be placed into an HP compatible computer and the narratives categorized, sorted, etc. This eliminates the need to type in all of the information from a printout.

(c) Color coding. It is possible to have a particular colored 349 form used specifically to report MILSTAR maintenance actions. The technicians would complete the form as usual (although it may be useful to request them to limit the length of their narratives), and then the keypunch operators would receive the form, recognize the MILSTAR designated color, and code the narratives for items 26 and 27. This would take a great deal of computer space, but it would only be until CAMS was implemented. Unfortunately, there would be no way to automatically search through the narratives; they would have to be read individually.

To authorize color-coded forms, a letter of request would be sent from the SPO to:

55th SRW/MA
Offutt AFB, NE

The request should include the color desired (blue, green, pink, yellow, and salmon are already in use), the expected duration of use, and a brief description of why the special form is needed. Because color-coded forms have been used previously, it is not expected that any difficulty would be encountered in obtaining authorization for their use.

If color coding is selected, then the entire maintenance record will be contained in the base MDCS; items 26 and 27 would not be transmitted to MODAS, because only the base MDCS will be modified. This means that if the MODAS method of retrieval is chosen, color coded forms will be of no use in obtaining items 26 and 27 data.

(2) Codes. It is also possible to develop alphanumeric codes to replace the narratives. This method would be more efficient and less space-consuming, but would require a change in the MDCS Technical Order. However, because MDCS is soon to be eliminated, it would probably be difficult to obtain approval for a modification to the TO, according to Chuck Gross and Dwayne Tucker at WPAFB. Therefore, this method is not recommended for use with MDCS, but may be useful in CAMS, where it is discussed in more depth.

b. In CAMS

There are two ways to obtain the Discrepancy and Corrective Action information from the CAMS/RAMIS system:

(1) Narrative. Arrangements have been made for the item 26 and 27 narratives to be entered into the CAMS/RAMIS data base, from which they can be accessed. Thus, when a user accesses the maintenance data records, a complete record (including the narratives) is obtained. However, the narratives are not indexed in any way, so they can't be searched for keywords. This means that no computer-assisted analyses can be performed on the narrative information; any sorting will need to be done manually.

No separate authorization is needed to access the CAMS narratives; access to the overall system covers the narratives.

(2) Codes. As discussed in 4.a.(2) it is possible to develop alphanumeric codes to be used in place of narratives. These codes would allow for computer sorting and analysis, eliminating the need to manually search throughout the narratives in each record.

To develop the codes, a series of word lists could be designed such that the majority of anticipated discrepancies and corrective actions would be represented. (perhaps looking at AFSATCOM narratives would be helpful in identifying some of the appropriate actions). For example, noun, verb, and adjective lists could be developed, and when completing the maintenance report, the technician would select the code corresponding to the appropriate word, and build a brief narrative of charaters rather than words. This would use less computer space, and would allow computer searching of the narratives to identify trends, etc..

Obtaining authorization to implement this narrative coding scheme may be somewhat difficult; according to Dwayne Tucker of AFLC, similar attempts have failed in the past. However, perhaps because CAMS/RAMIS is still in the growing stages, modifications could be made more easily, particularly if attempted soon. To do this, the MILSTAR SPO program manager would need to send a request to MAJCOM, outlining the requirements, and showing the suggested narrative coding system for CAMS; this request would then be evaluated by the appropriate offices.

5. Implementation

Once arrangements have been made to access the necessary data bases, it is important that this data be easily utilized within the SPO, for data analysis and MTBMA determination.

a. The following steps outline one method by which this system can be used in the SPO, assuming retrieval methods are not used:

(1) Establish access to host system. This will probably be accomplished through dial-up access, using a modem and personal computer. (a Z-100 or HP should be adequate). A personal computer would be better than a terminal, because files could be stored on it.

(2) Use sort routine on host system. All of the systems supporting the maintenance data bases have built-in sort routines. This would allow all MILSTAR maintenance records (identified as such by the first three characters of the work unit code) to be collected from the data base.

(3) Write MILSTAR maintenance data to file on the PC. The data sorted by the host system can be written to a data file on the personal computer and saved there, so the host system does not need to be accessed each time the data is needed.

(4) Assign appropriate component names to work unit codes. A program can be written on the PC which will read the work unit code in each record, assign the corresponding name to it, and keep track of the totals. This will allow easier identification of the components when under study.

(5) Have program output to spreadsheet. As the names are assigned to each record, the records can then be written to a spreadsheet (eg., Lotus 1-2-3 on the Z-100). Spreadsheet use is suggested because fairly large quantities of records can be easily manipulated, allowing for determination of MTBMA (i.e., relating flight hours, malfunctions, number of components by summing, multiplying, etc, appropriate columns of data). Once the records are written to the spreadsheet, any unwanted information can easily be deleted, allowing for compact records containing only essential information.

b. If any retrieval methods are used to obtain the maintenance data, steps 1 and 2 above are no longer needed, but it should be insured that sorted data is sent in the retrieval. Then the data is entered into a system at Hanscom and steps 3-5 can be followed.

Conclusions and Recommendations

It appears that the MILSTAR maintenance data can be tracked efficiently without any major modifications to the standard maintenance data collection methods. It is uncertain whether CAMS will be fully operational at Offutt by the start of EDM, so recommendations have been made for this possibility.

It should be stressed that CAMS is not yet finalized, so modifications may still occur. However, this also allows more flexibility if any changes are desired by the SPO to track the data.

Figures 1-4 briefly summarize some of the options which exist, along with their advantages and disadvantages. This allows for quick, if not detailed comparisons.

Because many of the items require authorization by various offices, it is recommended that ample time be allotted for implementation of any of these recommendations.

Some additional considerations:

- It may be useful to have the contractor complete 349 forms (then return them to the base for processing), to obtain information on factory maintenance.

- It should be determined what computer capabilities exist in the SPO and on base, to determine if any additional equipment is needed.

- If coding of narratives is authorized, the maintenance technicaians should be made aware of the importance of accurate coding.

- It would be interesting to see the contractor's MTBMA determination method, to compare methods as well as results.

- Having the entire maintenance record on hand will be useful if it becomes necessary to resolve discrepancies between contractor results and program office results.

If implemented properly, and with adequate time to become fully operational, the systems described in this report should efficiently track the MILSTAR maintenance data. This will enable determination of MTBMA, and thus contractor's earned incentive.

<u>CONTACTS FOR MILSTAR WARRANTY TRACKING SYSTEM</u>

The following people have all been extremely helpful in researching the MILSTAR Warranty Tracking System:

<u>Andrews AFB</u>

Sgt Jerry Simmons - MDCS, CAMS Information AV 858-3324

<u>Ellsworth AFB</u>

Sgt Deay - Maintenance Data Processing Shop AV 747-2074

Sgt Long - Intermediate Level Maintenance Shop AV 747-7875

<u>Hanscom AFB</u>

Lt Macomber - Information Systems, Computer Facilities 861-5317

Maj Whitehead - RAMIS Program Manager 271-7219

<u>Offutt AFB</u>

Sgt Heath - Maintenance Data Processing Shop AV 271-2507

Sgt Kimmey - Intermediate Level Maintenance Shop AV 271-2004

Chief Knapp - CAMS Implementation AV 271-2231

Capt Lane - CAMS Implementation AV 271-2231

<u>Wright-Patterson AFB</u>

Mr. Chuck Gross - MDCS Information AV 787-6906

Mr. Frank Maquire - MDCS Information and Access AV 787-6906

Mr. Dwayne Tucker - RAMIS Information AV 787-5138

<u>MITRE</u>

Mr. Bob Hassett - Logistics 271-7598

Mr. Rick Wickham - Logistics, Work Unit Codes 271-7094

<u>SSAI</u>

Mr. George Calandrello - Local MODAS User 863-0999

OBTAINING MILSTAR MAINTENANCE DATA
PRIOR TO CAMS IMPLEMENTATION
(OFFUTT)

METHOD	AUTHORIZATION	ALTERNATIVES	ADVANTAGES	DISADVANTAGES	COMMENTS
RETRIEVAL	LETTER OF REQUEST: 55TH SRW/MA/OFFUTT AIR FORCE BASE	MAGNETIC TAPE	QUICK TRANSFER. COMPACT. EFFICIENT.	REQUIRES COMPATIBLE TAPE DRIVE.	TAPE IS BETTER, ALTHOUGH REQUIRES COORDINATION WITH OCS AND SI.
		PRINTOUT	ENTER ON ANY COMPUTER. SET OWN FORMAT.	LOTS OF PAPER. LABOR INTENSIVE. RISK OF ERRORS.	
MODAS	CONTACT: CHUCK GROSS WPAFB AV 787-6906 FOR INSTRUCTION	MODAS FLIGHT HOURS	DIRECT ACCESS. ANY TERMINAL.	NOT ALL 349 DATA. 6-8 WEEK DELAY.	IN LONG RUN, PROBABLY BETTER THAN RETRIEVAL, BUT REQUIRES MORE PREPARATION.
		BASE FLIGHT HOURS	DIRECT ACCESS. ANY TERMINAL. ONLY 1-2 WEEK OLD DATA.	UNOFFICIAL HOURS. NOT ALL 349 DATA.	
DIRECT ACCESS	LETTER OF REQUEST: 55TH SRW/MA/OFFUTT AIR FORCE BASE	NONE	QUICK TRANSFER. EFFICIENT.	REQUIRES COMPATIBLE EQUIPMENT AND INTERFACE PROGRAM. CAN'T ALTER FORMAT.	SOUNDS MORE COMPLEX TO ARRANGE THAN OTHERS.

OBTAINING MILSTAR MAINTENANCE DATA AFTER CAMS IMPLEMENTATION (OFFUTT AND ELLSWORTH)

METHOD	AUTHORIZATION	ALTERNATIVES	ADVANTAGES	DISADVANTAGES	COMMENTS
BASE LEVEL	LETTER FROM USING COMMAND: SAC LGM, INFO SIU	NONE	DIRECT ACCESS. ALL DATA REPORTED.	ACCESS EACH BASE SEPARATELY	COMPUTER ACCESS IS GOOD, BUT ARRANGING WITH DIFFERENT BASES MAY BE DIFFICULT.
COLLECTIVE LEVEL	LETTER FROM SPO TO: AFLC LMSC/SMI (RAMIS) WPAFB	NONE	ALL BASES REPORT TO IT. DON'T HAVE TO ACCESS EACH BASE. DESIGNED FOR REMOTE ACCESS.	MUST ACT QUICKLY TO ARRANGE. SOME DATA DELETED.	PROBABLY MOST EFFICIENT. RECOMMENDED BY AFLC.
RETRIEVAL	LETTER FROM SPO TO EACH BASE.	MAGNETIC TAPE	QUICK TRANSFER.	REQUIRE COMPATIBLE TAPE DRIVE OR REFORMATTING PROGRAM.	NOT RECOMMENDED
		PRINTOUT	NO SPECIAL EQUIPMENT REQUIRED.	LABOR INTENSIVE. RISK OF ERRORS.	

Q. TAINING MILSTAR MAINTENANCE DATA FOR NARRATIVE ITEMS (26 & 27) (MDCS)

METHOD	AUTHORIZATION	ALTERNATIVES	ADVANTAGES	DISADVANTAGES	COMMENTS
NARRATIVE	LETTER OF REQUEST: 55TH SRW/MA/OFFUTT AIR FORCE BASE	HARDCOPY	CAN SPECIFY FORMAT	LABOR INTENSIVE	COLOR CODING WOULD WORK WELL. ALTHOUGH CAN'T SORT. HARDCOPY VERY TEDIOUS.
		FLOPPY DISK	COMPACT. EFFICIENT.	COMPATIBLE TERMINAL	
		COLOR CODING	ALL DATA IN ONE SYSTEM	NOT WITH MODAS	
CODE	DSDO AND SAC	NONE	EFFICIENT. ALL DATA IN ONE SYSTEM	MUST MODIFY TO.	NOT RECOMMENDED.

OBTAINING MILSTAR MAINTENANCE DATA FOR NARRATIVE ITEMS (26 & 27) (CAMS)

METHOD	AUTHORIZATION	ALTERNATIVES	ADVANTAGES	DISADVANTAGES	COMMENTS
NARRATIVE	PART OF OVERALL CAMS AUTHORIZATION	NONE	ALREADY ARRANGED. ALL DATA IN ONE SYSTEM.	CAN'T SEARCH ON KEYWORDS.	NOT AS USEFUL AND EFFICIENT AS CODE.
CODE	LETTER OF REQUEST TO MAJCOM	NONE	ALL DATA IN ONE SYSTEM. CAN SORT ON COMPUTER.	REQUIRES CHANGE TO SYSTEM.	MAY BE DIFFICULT TO IMPLEMENT. BUT WORTH IT.

[illegible]	[illegible]	[illegible]	[illegible]	[illegible]	[illegible]
Access CAMS at the collective level.	Letter to: AFLC LMSC/SMI (BAMIS) WPAFB, OH	SPO Personnel	By 1 Sep 85	Request remote access hook-up, and outline data required.	If deadlin[illegible] be met, ca[illegible] Dwayne Tuc[illegible] AV 787-518[illegible]
Review old AFSATCOM (or other program) MDCS forms to compare narratives with codes, to determine necessity of narratives.	Contact: Sgt Kimmey Maintenance Shop Offutt AFB	SPO Personnel	BY 1 Jan 86	Explain desire to determine necessity of accessing narrative data.	
Develop codes for CAMS narratives.	Letter to: MAJCOM	SPO Program Manager	By 1 Apr 86	Outline the suggested coding scheme and require-	Only if na[illegible] codes are [illegible] mined to b[illegible] important, [illegible] BAMIS narr[illegible] aren't und[illegible]
Access CAMS at the individual base level.	Letter to: SAC LGM (Action) SID (Info) Offutt AFB, NE	Using Command	(EDM - 24 Months) to (EDM - 19 Months)	Request dial-up port for remote access, and list of equipment needed.	
Determine if appropriate equipment is available on base.	Obtain detailed equipment lists from appropriate data processing organizations and compare w/ what's on base.	SPO Personnel	(EDM - 24 Months) to (EDM - 18 Months)		Most of eq[illegible] ment is av[illegible] but some d[illegible] cations a[illegible] ject to c[illegible]
Directly access the MDCS data base at Offutt.	Letter to: 55th SRW/MA Offutt AFB, NE	SPO Program Manager	(EDM - 14 Months) to (EDM - 10 Months)	Request equipment specifications, configuration, contact for assistance.	Only if M[illegible] retrieval [illegible] chosen. [illegible] program.
Retrieve MDCS data from Offutt.	Letter to: 55th SRW/MA Offutt AFB, NE	SPO Program Manager	(EDM - 12 Months) to (EDM - 10 Months)	Specify tape or printout, format, intervals, data desired, operating hours.	Only if M[illegible] not chose[illegible]
Obtain narrative information from MDCS.	Letter to: 55th SRW/MA Offutt AFB, NE	SPO Personnel	(EDM - 12 Months) to (EDM - 10 Months)	Specify hardcopy, disk, color-coding, data desired, time intervals.	Only if n[illegible] data is d[illegible] mined to [illegible] important[illegible]
Access MODAS in order to obtain MDCS data from Offutt.	Contact: Mr. Chuck Gross WPAFB	SPO Personnel	(EDM - 12 Months) to (EDM - 8 Months)	Request instruction, configuration, manuals.	May requi[illegible] visit to [illegible]
Obtain current flight hours.	Letter to: 55th SRW/MA Offutt AFB, NE	SPO Program Manager	(EDM - 12 Months) to (EDM - 8 Months)	Outline the situation.	Only if M[illegible] chosen (t[illegible] pensate f[illegible] week lag)[illegible]
Develop interface program to obtain MDCS data.	Have in-house programmer or contact: Field Asst. Branch Data Sys. Design Ofc. Gunter AFS AV446-4821	SPO Personnel	(EDM - 8 Months) to (EDM - 6 Months)	Need specifics of host system.	Only if d[illegible] access is[illegible]
Have WUC established prior to equipment being fielded.	Letter to: Platform Manager	SPO Program	(EDM - 8 Months) to (EDM - 6 Months)		Important[illegible] done; if [illegible] serial nu[illegible] may be ne[illegible] track.
Transfer data into spreadsheet format.	Write program to specify format of data and output to spreadsheet.	SPO Personnel or Contractor	(EDM - 2 Months) to (EDM - 1 Month)	Want to assign names to WUC.	
Calculate MTBMA.	Develop spreadsheet model to analyze data and calculate MTBMA.	SPO Personnel or Contractor	(EDM - 2 Months) to (EDM - 1 Month)		

page of briefing handout. Shows timetable.

1985 USAF-UES SUMMER FACULTY RESEARCH PROGRAM/

GRADUATE STUDENT SUMMER SUPPORT PROGRAM

Sponsored by the

AIR FORCE OFFICE OF SCIENTIFIC RESEARCH

Conducted by the

UNIVERSAL ENERGY SYSTEMS, INC.

FINAL REPORT

ARTIFICIAL INTELLIGENCE and ROBOTICS PERCEPTION SYSTEM

Prepared by:	Troy F. Henson, Ph.D., P.E.
Academic Rank:	Professor
Department:	Electrical Engineering (EE)
University:	Louisiana Tech University
Research Location:	Wright-Patterson AFB, Ohio Air Force Aerospace Medical Research Laboratory Biodynamics and Bioengineering Division Biological Acoustics Branch
USAF Research:	Timothy R. Anderson
Date:	September 30, 1985
Contract No:	F49620-85-C-0013

ARTIFICIAL INTELLIGENCE and ROBOTICS PERCEPTION SYSTEM

by

Troy F. Henson

ABSTRACT

A comprehensive artificial intelligence (AI) and robotics research effort has been initiated to develop a perception system for a mobile autonomous robot. A document-level review of the publications in AI and robotics was made and an extensive bibliography of books, periodicals, proceedings, and short courses was classified and compiled for future updating and use as a basis for library and research center purchases both at the Air Force Laboratory location and at Louisiana Tech University. Literature describing research and development of robot perception systems and robot GN&C (guidance, navigation, control) systems was reviewed.

A mobile robot was selected as a vehicle for research and development. An initial AI perception system which includes ultrasonic ranging for robot navigation and mapping was described. The primary problems encountered in the use of ultrasonic ranging have been identified and are described and discussed in terms of possible solutions and alternative approaches. A speech recognition system board for command and control of the selected research robot was designed around NEC's Speech Recognition LSI set and the S-100 standard bus.

Recommendations are made for continuing AI/Robotics Perception System and Robot GN&C research including the development of a robot simulation, an ultrasonic sensor array and signal processing scheme, the construction and testing of the speech recognition board, and the development of a vocabulary for robot command and control.

ACKNOWLEDGEMENTS

This research was sponsored by the Air Force Office of Scientific Research/AFSC, United State Air Force, under Contract F49620-85-C-0013. The research was performed at the Biological Acoustics Branch of the Biodynamics and Bioengineering Division of the Air Force Aerospace Medical Research Laboratory, Aerospace Medical Division, Air Force Systems Command, Wright-Patterson Air Force Base, Ohio.

I wish to thank Timothy Anderson, Dr. Nixon, Branch Chief, and all the staff and contractor staff at the Biological Acoustics Branch for their support.

I. INTRODUCTION

I have a Ph.D., am registered as a professional engineer, and have sixteen (16) years of professional experience as an engineer - eight years in industry and eight years as a faculty member. I have remained active professionally via membership and leadership roles in professional organizations, continuing education, participation in professional conferences, and through publishing engineering research, development, and design results.

After earning BS and MS degrees in electrical engineering (EE), I joined the IBM Federal Systems Div. (FSD) Saturn/Apollo Control Systems Design Department. During my engineering career with IBM, 1966-77, I worked in the area of GN&C (guidance, navigation, and control) on the Saturn/Apollo, Skylab, Large Space Telescope, Spacelab, Space Shuttle Projects. I designed control systems utilizing both classical and modern control theory; developed and implemented computer simulations on analog, digital, and hybrid computers; directed teams in software optimization; and managed a software verification department. After an educational leave of absence from IBM FSD, I was graduated with a Ph.D. in electrical engineering from The University of Texas at Austin in 1975 with major course work in computer, control, and information systems and research primarily in optimization and simulation of dynamic systems on digital computers [1], [2].

I left IBM in 1977 to become a university faculty member. From 1977-81, I was at East Texas State University; and since 1981, I have been at Louisiana Tech University, where I am currently an EE professor. My activities have included developing curriculum in the communications/signal processing area; chairing the EE Graduate and Research programs committee;

serving on graduate student advisory committees; and teaching graduate EE courses in communication systems, control systems, digital signal processing, information theory, and random signal analysis. I have also conducted research in digital signal processing as a Research Engineer in adaptive array processing of seismic signals for Mobil Research and Development Corp. [3] and as an Advanced Systems Engineer Specialist in communications signal processing for Lockheed Missiles and Space Company, Austin Div. [4]. My recent research efforts at Louisiana Tech have been oriented toward the areas of control and perception system development for autonomous mobile robots [36], [37], [61].

The Biodynamics and Bioengineering Division of the Air Force Aerospace Medical Research Laboratory (AFAMRL) at Wright-Patterson AFB, Ohio, is active and exercises a leadership role in research into robotics and biocybernetics. Research activities of the BBA (Biological Acoustics Branch of the Biodynamics and Bioengineering Division) include investigation and evaluation under environmental noise, vibration, acceleration stress conditions of automatic speech recognition or voice control systems; the development of artificial intelligence (AI); and the utilization of A.I. for voice/speech processing and in the development of autonomous mobile robotics systems. Goals of this research include the development of "improved systems for pilot protection, decision-making, and weapon system effectiveness", "to protect man against the mechanical force environments created by the flight motion itself or by the propulsion units used", "to provide surrogates" where protection is not possible, and "to accomplish critical tasks not ideally suited to man" [5].

II. OBJECTIVES

The long range goal of the research that I conducted and directed as a participant in the Summer Faculty Research Program (SFRP) is the development of a system that will allow a mobile autonomous robot to plan and execute paths and movements required in order to perform a variety of tasks in a dynamic environment which contains barriers, obstacles, and/or hazards. In other words, the eventual outcome will be a robot capable of performing tasks in environments too hazardous for man. The development of this system will require tools from the fields of A.I., DSP (digital signal processing), control, and communications theory.

The major objective of my SFRP participation was to develop the foundation for continuing research at Louisiana Tech University in the area of AI/Robotics Perception and GN&C systems of interest to the AFAMRL/BBA. Secondary objectives included enhancing my expertise in the AI/Robotics research area, establishing professional relationships with Air Force employees, and furthering the research objectives of the Air Force in the area of AI/Robotics Perception Systems. Specific short range objectives of my SFRP effort included

(1) generating recommendations for AI/Robotics library purchases, hardware and software research lab purchases, short courses for faculty development, curriculum for upper level undergraduate and graduate work at Louisiana Tech University.

(2) reviewing the literature in the area of AI/Robotics Perception Systems, particularly with respect to the use of ultrasonic sensors for navigation and mapping.

(3) developing an algorithm for mapping the walls and obstacles surrounding a robot utilizing the ultrasonic ranging data collected by Clifford and Schneider [58].

(4) directing the research of graduate student Susan Tucker Ebrahimi in the area of speech recognition for robot command and control [76].

(5) developing precursory plans and recommendations for continuing AI/Robotics research into the development of a perception system and an overall GN&C system for a mobile autonomous robot.

III. AI/ROBOTICS LITERATURE and EQUIPMENT REVIEW

Books, conference proceedings, periodicals, and short courses in the area of artificial intelligence (AI) and robotics were reviewed. A bibliography classified into the various areas of AI/Robotics was compiled [12]. This bibliography contains 150 books, 60 conference proceedings, 31 periodicals, 32 short courses classified as follows:

Books:	General	27
	Software	10
	Perception -- Computer/Robot Vision	28
	Perception -- Speech Recognition	6
	Robotics	32
	Expert Systems	8
	Knowledge Engineering	6
	Problem Solving, Heuristics, Search Strategies	8
	Pattern Recognition	5
	Natural Language Understanding	8
	Cognitive Science	5
	Applications	7
Proceedings:	General	15
	Perception	25
	Robotics	20
Periodicals:	General	14
	Perception	9
	Robotics	8
Short Courses		32

A recommendation was made for minimal library purchases of periodicals, books, proceedings listed in order of priority. Also, a recommendation was made for short courses in order of priority for faculty development.

Information was gathered on available, "off-the-shelf", AI computer hardware and software and mobile robots. A classified listing of this equipment will be compiled and forwarded to Timothy R. Anderson, AFAMRL/BBA, and to Louisiana Tech University through Dr. Donald K. Fronek, EE department head, by memorandum in November 1985. Computer hardware and software and a mobile robot, consistent with the AFAMRL/BBA plans, have been selected as a basis for continuing research and are being purchased by the Louisiana Tech EE department for its AI/Robotics Research Laboratory.

Curriculum development in AI/Robotics has also been initiated and will be formerly recommended to Dr. Donald K. Fronek by memorandum in October 1985.

An extensive search for recent literature in the areas of AI/Robotics Perception Systems and Robot GN&C Systems has been conducted. Computer searches plus hand searches through several journals and conference proceedings over the 1983-1985 time frame were made through the search facilities and holdings of the Wright-Patterson AFB Technical Library. Approximately 200 articles and books were reviewed. Those identified as the most relevant are classified into one of six topic areas and included as a bibliography to this report. Copies of the articles are being provided for future reference to the AFAMRL/BBA and to the Louisiana Tech EE AI/Robotics Research Laboratory. Although this set of publications is not claimed to be exhaustive in itself, the set is representative. It is believed to span enough of the field so that when it is combined with all the additional publications which are referenced from the included set, the

total compilation would come close to being the complete set of literature dealing with AI/Robotics Perception Systems and Robot GN&C Systems.

IV. ULTRASONIC RANGING FOR ROBOT MAPPING AND NAVIGATION

For a mobile robot to be autonomous, it must have a means of sensing and responding to its surroundings, i.e., it must have an autonomous GN&C system. Applications projected for autonomous mobile robots include dynamic environments containing obstacles and hazards [5] - [7]. In order to navigate and avoid collisions, the robot needs the equivalent of human senses of seeing, hearing, touching [50].

Seeing (vision) conceivably would provide the most information, and, thus, has become the most prodigious research area [6], [7]. Success has been obtained in the utilization of vision by camera and digital image processing for autonomous mobile robot navigation [13], [14]. However, vision systems are expensive [39]; and, even with the fastest computational equipment, vision is still slow. Moravec's Stanford Cart successfully drove itself through obstacle courses, but it took approximately five hours to traverse a 20 meter course [13]. Touch (or tactile) sensor technology is another active area of research and significant advances are being made [80] - [85]. However, for mobile robot navigation planning (guidance) and collision avoidance, tactile sensors are limited by the close proximity requirements.

Due to the advantages of cost efficiency and speed of processing, the most common sensor systems being considered currently for navigation planning and collision avoidance are ultrasonic rangers, which provide a limited analog to a vision sense. Several experimental research robots as well as some production models are employing ultrasonic ranging for mapping and navigation [8], [11], [57], [59], [60], [67].

The use of ultrasonic ranging does have drawbacks and limitations and cannot be depended on for completely accurate obstacle detection/environment mapping [41], [55], [60]. Problems emanate from the wide beam width (acoustic dispersion) of the transmitted signal, resulting in openings being missed [60]; utltrasonic energy reflection off surfaces, resulting in non-detection of barriers and obstacles with an angle of incidence below a certain critical angle or incorrect range due to the reception of secondary, tertiary, etc., reflection; variation in the reflection characteristics of materials, resulting in reflected energy variation depending upon surface material of an obstacle [61]; variation in the velocity of ultrasonic waves as a function of air currents and temperature, resulting in incorrect range calculations. Partial solutions to these problems can be attained by constructing arrays of ultrasonic sensors for narrowing the beam width [68] (problem of non-detection of openings excluded); combining/correlating/processing data from several ultrasonic "snapshots" of the same scene [67]; utilizing a-priori maps and updating them; adapting range calculations to atmospheric conditions. Also other sensors can be incorporated into an overall perception system, e.g., vision sensors and processing that are switched in on an "as needed" basis for long range, and infrared and bumper or arm length tactile sensors for close proximity.

The most commonly used ultrasonic sensor system is the Polaroid Ultrasonic Ranging Unit consisting of an acoustical transducer and an ultrasonic circuit board that drives it [56], [62], [63]. This unit was used on a test stand to experimentally determine and verify reflection characteristics and beam patterns [61]. Clifford and Schneider built 32 of these sensors into their MARRS-1 robot [58]. Utilizing ultrasonic ranging

data obtained with one to four of these sensors operating simultaneously during remotely controlled test runs of the MARRS-1, they produced rough maps of the robots environment in an off-line, post-run, program.

One of the objectives of my SFRP research was to develop an algorithm for off-line processing of the MARRS-1 ranging data collected by Clifford and Schneider to yield improved mapping and obstacles identification quality. Although incomplete at this writing, a digital signal processing algorithm that will incorporate arc intersection calculations, smoothing, and correlation has been initiated. The effort is continuing at Louisiana Tech University. Progress at the end of November 1985 will be reported by memorandum to Timothy R. Anderson, AFAMRL/BBA, Wright-Patterson AFB, Ohio.

V. SPEECH RECOGNITION FOR ROBOT COMMAND AND CONTROL

For remote, flexible communication with humans, an autonomous mobile robot also needs the equivalent of the human's sense of hearing [5], [50]. Speech recognition analysis and design research was conducted by Louisiana Tech graduate student Susan Tucker Ebrahimi under my direction [76]. Speech recognition theory was studied using the text by Rabiner and Schafer [78]. The performance of a Texas Instruments Speech Recognition System was evaluated under high noise conditions for a pilot cockpit, 15 word vocabulary, voice command system. Also, a speech recognition system board was designed around NEC's Speech Recognition LSI set and the S100 standard bus for communications with a robot.

VI. SUMMARY and RECOMMENDATIONS

An extensive listing of books, periodicals, proceedings, short courses, software, hardware in the area of artificial intelligence (AI) and robotics was classified and compiled, and recommendations for library and research laboratory purchases were made. A review was conducted of recent

research laboratory purchases were made. A review was conducted of recent literature publishing research and development of AI/Robotics Perception Systems and Robot GN&C Systems. After reviewing the literature, decisions were made to purchase a mobile robot research vehicle, consistent with that of the AFAMRL/BBA, for the Louisiana Tech University EE AI/Robotics Research Laboratory.

Performance analysis of an existing speech recognition system was conducted for the pilot/cockpit voice command system. A speech recognition board for the command and control of the selected mobile robot research vehicle was designed. The remainder of the robot perception system was considered, and the development of a signal processing algorithm has been initiated for mapping of the environment and navigation of the robot from ultrasonic ranging units.

It is recommended that an overall AI/Robotics Perception System and GN&C System be modeled for the selected research vehicle and simulated in a modular, top-down form. Initially the simulation would have several empty (null) modules, and it would develop modularly to evaluate individual sensor systems. The simulation would aid the development and design of the perception system and, later, the GN&C system. An array of ultrasonic sensors and an accompanying signal processing scheme should be developed as the first navigation and mapping sensor system for the research robot. The array and processing scheme would be conceived analytically and evaluated first by simulation, then on a test stand, and finally by a proto-type on the robot. The speech recognition board which was designed during the summer [76], should be built and tested and a speech synthesis function added. Then the speech communications board would be installed in the research robot and tested as part of its perception system. A vocabulary

would be developed for command and control of the robot [77], [79]. Performance evaluation similar to that for the pilot/cockpit voice command system [76] including the constructing of confusion matrices, would be conducted to aid the development of the "optimal" vocabulary. Development of the perception system would continue with the addition of vision and tactile sensors and, possibly, infrared, lasar, radar units.

In the long range, a complete GN&C system, incorporating the comprehensive perception system with several types of sensors, an expert guidance system, and an adaptive, hiearchical, control system would be developed for the research robot. The eventual goal is to develop a completely autonomous, mobile robot, that will talk with a human and perform tasks in cluttered and hazardous environments.

REFERENCES

and

BIBLIOGRAPHY

I. SFRP RESEARCHER'S AND AIR FORCE LABORATORY BACKGROUND

1. Henson, T.F. and B.F. Womack, "Digital Simulation by Partitioning and Uncoupling the System Model," Proceedings of the 6th IFAC (International Federation of Automatic Control) Symposium on Automatic Control in Space, Tsakhkadzor, Armenia, USSR, August 1974, Session IV, Paper 3. Published in revised form, Automatica, Vol. 11, November 1975, pp 579-591.

2. Henson, T.F. and B.F. Womack, "Time Domain Desensitized Specific Optimal System Design," Proceedings of the IFAC Sixth Triennial World Congress, Boston/Cambridge, Massachusetts, August 24-30, 1975, Session 37, Paper 1.

3. Henson, T.F., "Adaptive Array Processing of Seismic Land Data," Mobil Research and Development Corp., FRL Memo 113, October 22, 1981.

4. Henson, T.F., "Summer Activity Report," Lockheed Missiles and Space Co., Austin Division, IDC AT-0039-84, August 23, 1984.

5. Lewandowski, P.M. and K.M. Zimmerman, The AFAMRL Mission: 1935-1985, AFAMRL Enhancing Man and Mission, Air Force Medical Research laboratory, Aerospace Medical Division, Air Force Systems Command, Wright-Patterson Air Force Base, Ohio. (Requests for copies may be addressed to AFAMRL/TSA, Wright-Patterson AFB, OH 45433)

II. ROBOTS AND ROBOT RESEARCH

6. Abel, W., Chairman, Committee on Army Robotics and Artificial Intelligence, National Research Council, U.S.A., "Applications of Robotics and Artificial Intelligence to Reduce Risk and Improve Effectiveness," Robotics & Computer-Integrated Manufacturing, Vol. 1, No. 2, 1984, pp 191-222.

7. Albus, J.S., "Research Issues in Robotics," SAMPE Journal, January/February 1985, pp 35-41.

8. Bell, T.E., "Robots in the Home: Promises, Promises," IEEE Spectrum, Vol. 22, No. 5, May 1985, pp 51-55.

9. Bortz, A.B., "Joseph Engleberger: The Father of Industrial Robots Reflects on His Progeny," Robotics Age, April 1985, pp 15-22.

10. Coleman, A., "Robotics Research: The Next Five Years and Beyond," Robotics Age, February 1985, pp 14-19.

11. Everett, H.R., "A Second-Generation Autonomous Sentry Robot," Robotics Age, April 1985, pp 29-32.

12 Henson, T.F., "Artificial Intelligence and Robotics Literature and Short Courses," Memorandum to Timothy R. Anderson, AFAMRL/BBA, September 4, 1985.

13. Moravec, H.P., "The Stanford Cart and the CMU Rover," Proceedings of the IEEE, Vol. 71, No. 7, July 1983, pp 872-884.

14. Moravec, H.P., Robot Rover Visual Navigation, Ann Arbor, Michigan, UMI Research Press, 1981.

15. Nitzan, D., "Development of Intelligent Robots: Achievements and Issues," IEEE Journal of Robotics and Automation, Vol. RA-1, No. 1, March 1985.

16. Reddy, R., editor, "The Special Issue on Robotics and the Factory of the Future," Proceedings of the IEEE, Vol. 71, No. 7, July 1983.

III. ROBOT GN&C (GUIDANCE, NAVIGATION, CONTROL)

17. Astrom, K.J., "Theory and Applications of Adaptive Control-A Survey," Automatica, Vol. 19, No. 5, 1983, pp 471-486.

18. Axelby, G.S., Editor-in-Chief, "Special Issue on Adaptive Control," Automatica, Vol. 19, No. 5, 1983.

19. Bejczy, A.K., T.J. Tarn, and Y.L. Chen, "Robot Arm Dynamic Control by Computer," Proc. 1985 IEEE International Conference on Robotics and Automation, St. Louis, Missouri, March 25-28, 1985, pp 960-970.

20. Cannon, R.H., Jr., "Robots with a Light Touch: Keynote Address to the 1983 Automatic Control Conference," Control Systems Magazine, May 1984, pp 14-16.

21. Chavez, R. and A. Meystel, "Structure of Intelligence for an Autonomous Vehicle," Proc. 1984 IEEE International Conference on Robotics, Atlanta, Georgia, March 13-15, 1984, pp 584-591.

22. Crowley, J.L., "Navigation for an Intelligent Mobile Robot," IEEE Journal on Robotics and Automation, Vol. RA-1, No. 1, March 1985, pp 31-41.

23. Drake, K.C., E.S. McVey, and R.M. Inigo, "Sensing Error for a Mobile Robot Using Line Navigation," IEEE Transactions on Pattern Analysis and Machine Intelligence, Vol. PAMI-7, No. 4, July 1985, pp 485-490.

24. Koch, E., C. Yeh, G. Hillel, A. Meystel, C.Isik, "Simulation of Path Planning for a System with Vision and Map Updating," Proc. 1985 IEEE International Conference on Robotics and Automation St. Louis, Missouri, March 25-28, 1985, pp 146-160.

25. Luh, J.Y.S., "An Anatomy of Industrial Robots and Their Controls," IEEE Transactions on Automatic Control, Vol. AC-28, No. 2, February 1983, pp 133-153.

26. Murray, J.J. and C.P. Neuman, "Arm: An Algebraic Robot Dynamic Modeling Program," Proc. 1984 IEEE International Conference on Robotics, Atlanta, Georgia, March 13-15, 1984, pp 103-114.

27. Neuman, C.P. and V.D.Tourasis, "Discrete Dynamic Robot Models," IEEE Transactions on Systems, Man, and Cybernetics, Vol. SMC-15, No. 2, March/April 1985, pp 193-204.

28. Saridis, G.N., "Intelligent Robotic Control," IEEE Transactions on Automatic Control, Vol. AC-28, No. 5, May 1983, pp 547-557.

29. Shih, L.Y., "Automatic Guidance of Mobile Robots in Two-Way Traffic," Automatica, Vol. 21, No. 2, 1985, pp 193-198.

30. Shin, K.G. and S.B. Malin, "A Hierarchical System Structure for Coordinated Control of Industrial Manipulators," Proc. 1984 IEEE International Conference on Robotics, Atlanta, Georgia, March 13-15, 1984, pp 609-619.

31. Siy, P., "Road Map Production System for Intelligent Mobile Robot," Proc. 1984 IEEE International Conference on Robotics, Atlanta, Georgia, March 13-15, 1985, pp 562-570.

32. Stokic, D. and M. Vukobratovic, "Practical Stabilization of Robotic Systems by Decentralized Control," Automatica, Vol. 20, No. 3, 1984, pp 353-358.

33. Tal, J. and W. Baron, "Motion Control for Automation and Robotics," Robotics Age, December 1984, pp 8-11.

34. Vukobratovic, M., D. Stokic, and N. Kircanski, "Towards Nonadaptive and Adaptive Control of Manipulation Robots," IEEE Transactions on Automatic Control, Vol. AC-29, No. 9, September 1984, pp 841-844.

35. Waldron, K.J., "Mobility and Controllability Characteristics of Mobile Robotic Platforms," Proc. 1985 IEEE International Conference on Robotics and Automation, St. Louis, Missouri, March 25-28, 1985, pp 146-160.

36. Zerkus, J.M., G.L. Mossy, and T.F. Henson, "Platform Control System Design for an Autonomous Robot", Proceedings of the Fifth IASTED (International Association of Science and Technology for Development) International Symposium Robotics and Automation, New Orleans, LA, November 12-14, 1984 pp 66-71.

37. Zerkus, J.M., J.W. Akers, M.J. Spizale, T.F. Henson, and R.H. Thompson, "Control of a Shape Memory Alloy Robotic Actuator via Thermoelectricity," Proc. of Robexs '85, The First Annual ISA Workshop on Robotics and Expert Systems, NASA/JSC, Houston, Texas, June 27-28, 1985, pp. 291-296.

IV. ROBOT/COMPUTER VISION

38. Allen, P., "Surface Descriptions from Vision and Touch," Proc. 1984 IEEE International Conference on Robotics, Atlanta, Georgia, March 13-15, 1984, pp 394-397.

39. Baxes, G.A., "Vision and the Computer: An Overview," Robotics Age, March 1985, pp 12-19.

40. Brady, M., "Representing Shape,", Proc. 1984 IEEE International Conference on Robotics, Atlanta, Georgia, March 13-15, 1984, pp 256-265.

41. Brooks, R.A., "Visual Map Making for a Mobile Robot," Proc. 1985 IEEE International Conference on Robotics and Automation, St. Louis, Missouri, March 25-28, 1985, pp 824-829.

42. Duda, R.O., D. Nitzan, and P. Barrett, "Use of Range and Reflectance Data to Find Planar Surface Regions." IEEE Transactions on Pattern Analysis and Machine Intelligence, Vol. PAMI-1, No. 3, July 1979, pp 259-271.

43. Green, J., "A New Super Camera for Vision Systems," Robotics Age, July 1985, pp 6-9.

44. Jarvis, R.A., "A Perspective on Range Finding Techniques for Computer Vision," IEEE Transactions on Pattern Analysis and Machine Intelligence, Vol. PAMI-5, No. 2, March 1983, pp 122-139.

45. Jarvis, R.A., "A Laser Time-of-Flight Range Scanner for Robotic Vision," IEEE Transactions on Pattern Analysis and Machine Intelligence, Vol. PAMI-5, No. 5, September 1983, pp 505-512.

46. Kanade, T., "Geometrical Aspects of Interpreting Images as a Three-Dimensional Scene," Proceedings of the IEEE, Vol. 71, No. 7, July 1983, pp 789-802.

47. Koivo, A.J., R. Lewczyk, and T.H. Chiu, "Adaptive Path Control of a Manipulator with Visual Information," Proc. 1984 IEEE International Conference on Robotics, Atlanta, Georgia, March 13-15, 1984, pp 556-560.

48. Marr, D., Vision, W.H. Freeman, San Francisco, 1982.

49. ME Staff Report, "Vision Systems Make Robots More Versatile," Mechanical Engineering, January 1985, pp 38-43.

50. Morris, H.M., "Adding Sensory Inputs to Robotic Systems Increases Manufacturing Flexibility," Control Engineering, Vol. 30, No. 3, March 1983, pp 65-68.

51. Pipitone, F.J. and T.G. Marshall, "A Wide-field Scanning Triangulation Rangefinder for Machine Vision", The International Journal of Robotics Research, Vol. 2, No. 1, Spring 1983.

52. Rosenfeld, A., "Computer Vision: Signals, Segments, and Structures", IEEE ASSP Magazine, Vol. 1, No. 1, January 1984, pp 11-18.

53. Teoh, W. and X.D. Zhang, "An Inexpensive Steroscopic Vision System for Robots," Proc. 1984 IEEE International Conference on Robotics, Atlanta, Georgia, March 13-15, 1984, pp 186-189.

54. Villers, P., "Technologies of Robotic and Artificial Vision Systems," Robotics & Computer Integrated Manufacturing, Vol. 1, No. 2, 1984, pp 125-152.

V. ROBOT NAVIGATION AND MAPPING BY ULTRASONIC RANGING

55. Brown, M.K., "Locating Object Surfaces with an Ultrasonic Range Sensor," Proc. 1985 IEEE International Conference on Robotics and Automation, St. Louis, Missouri, March 25-28, 1985, pp 110-115.

56. Ciarcia, S., "An Ultrasonic Ranging System," BYTE, October 1984, pp 113-123.

57. Clemence, G.T. and G.W. Hurlbut, "The Application of Acoustic Ranging to the Automatic Control of a Ground Vehicle," IEEE Transactions on Vehicular Technology, Vol. VT-32, No. 3, August 1983, pp 239-244.

58. Clifford, E. and G. Schneider III, Creating a Mobile Autonomous Robot Research System (MARRS), Thesis, Air Force Institute of Technology, AFIT/GE/ENG/84 D-19, December 1984.

59. Crowley, J.L., "Dynamic World Modeling for an Intelligent Mobile Robot Using A Rotating Ultra-Sonic Ranging Device," Proc. 1985 IEEE International Conference on Robotics and Automation, St. Louis, Missouri, March 25-28, 1985, pp 128-135.

60. Everett, H.R., "A Multielement Ultrasonic Ranging Array," Robotics Age, July 1985, pp 13-20.

61. Gauthier, J.F., J.M. Zerkus, and T.F. Henson, "Autonomous Robot Sensing System Design Utilizing Scanning Ultrasonic Ranging," Proceedings of the Fifth IASTED International Symposium Robotics and Automation, New Orleans, LA, November 12-14, 1984, pp 72-77.

62. Jaffe, D.L., "Polaroid Ultrasonic Ranging Sensors in Robotic Applications," Robotics Age, March 1985, pp 23-30.

63. Maslin, G.D., "A Simple Ultrasonic Ranging System," Proceedings, 102nd Convention of the Audic Engineering Society, Cincinnati, OH, May 1983, 11 pp.

64. Miller, G.L., R.A. Boie, and M.J. Sibilia, "Active Damping of Ultrasonic Transducers for Robotic Applications," Proc. 1984 IEEE International Conference on Robotics, Atlanta, Georgia, March 13-15, 1984, pp 379-384.

65. Mitome, H., T. Koda, and S. Shibata, "Double Doppler Ranging System Using FM Ultrasound," Ultrasonics, September 1984, pp 199-204.

66. Monzingo, R.A. and T.W. Miller, Introduction to Adaptive Arrays, John Wiley & Sons, 1980.

67. Moravec, H.P. and A. Elfes, "High Resolution Maps from Wide Angle Sonar," Proc. 1985 IEEE International Conference on Robotics and Automation, St. Louis, Missouri, March 25-28, 1985, pp 116-121.

68. Mucci, R.A., "A Comparison of Efficient Beamforming Algorithms," IEEE Transactions on Acoustics, Speech, and Signal Processing, Vol. ASSP-32, No. 3, June 1984, pp 548-558.

69. Ouseph, P.J. and J.J. Link, "Variation of Speed of Sound in Air with Temperature," American Journal of Physics, Vol. 52, No. 3, July 1984, pp 661.

70. Schueler, C.F., H.Lee, G. Wade, "Fundamentals of Digital Ultrasonic Imaging," IEEE Transactions on Sonics and Ultasonics, Vol. SU-31, No. 4, July 1984, pp 195-217.

71. Sessler, G.M., "What's New in Electroacoustic Transducers," IEEE ASSP Magazine, Vol. 1, No. 4, October 1984, pp 3-13.

72. Wade, G., H.Lee, C. Schueler, editors, Special Issue on Digital Acoustical Imaging, IEEE Transactions on Sonics and Ultrasonics, Vol. SU-31, No. 4, July 1984.

73. Yokota, T. and Sato, Y., "Super-Resolution Ultrasonic Imaging by Using Adaptive Focusing," Journal of the Acoustical Society of America, Vol. 77, No. 2, February 1985, pp 567-572.

VI. ROBOT COMMAND AND CONTROL BY VOICE/SPEECH RECOGNITION

74. Biermann, A.W., R.D. Rodman, D.C. Rubin, and J.F. Heidlae, "Natural Language with Discrete Speech as a Mode for Human-to-Machine Communication," Communications of the ACM, Vol. 28, No. 6, June 1985, pp 628-636.

75. Doddington, G.R. and T.B. Schalk, "Speech Recognition: Turning Theory to Practice," IEEE Spectrum, Vol. 18, No. 9, September 1981, pp 26-32.

76. Ebrahimi, S.T., "Speech Recognition for Command and Control," Final Report, 1985 USAF-UES Graduate Student Summer Support Program, elsewhere in this document.

77. Jemelka, J.R., "Designing a Reliable Voice-Input Robot Control Language," Robotics Age, February 1984, pp 30-34.

78. Rabiner, L.R. and R.W. Schafer, Digital Processing of Speech Signals, Prentice-Hall, Englewood Cliffs New Jersey, 1978.

79. Saridis, G.N. and J.H. Graham, "Linguistic Decision Schemata for Intelligent Robots," Automatica, Vol. 20, No. 1, 1984, pp 121-126.

VII. ROBOT TACTILE SENSORS

80. Boie, R.A., "Capacitive Impedance Readout Tactile Image Sensor," Proc. 1984 IEEE International Conference on Robotics, Atlanta, Georgia, March 13-15, 1984, pp 370-378.

81. Breen, J., "Force Sensors for Robotic Assembly Systems", Robotic Age, July 1985, pp 11-12.

82. Dario, P. and D. DeRossi, "Tactile Sensors and the Gripping Challenge," IEEE Spectrum, Vol. 22, No. 8, August 1985, pp 46-52.

83. Harmon, L.D., "Automated Touch Sensing: A Brief Perspective and Several New Approaches," Proc. 1984 IEEE International Conference on Robotics, Atlanta, Georgia, March 13-15, 1984, pp 326-331.

84. Raibert, M.H., "An All Digital VLSI Tactile Array Sensor," Proc. 1984 IEEE International Conference on Robotics, Atlanta, Georgia, March 13-15, 1984, pp 314-319.

85. Russell, R.A., "A Simple Thermal Touch Sensor," Robotics Age, October 1984, pp 19-22.

1985 USAF - UES SUMMER FACULTY RESEARCH PROGRAM

GRADUATE STUDENT SUMMER SUPPORT PROGRAM

Sponsored by the

AIR FORCE OFFICE OF SCIENTIFIC RESEARCH

Conducted by the

UNIVERSAL ENERGY SYSTEMS, INC.

FINAL REPORT

THE THERMODYNAMIC, PHYSICAL AND OPTICAL PROPERTIES OF ALUMINUM OXIDE

Prepared by:	Astor Y. Herrell, Ph.D.
Academic Rank:	Professor
Department:	Natural Science
University:	Winston-Salem State University
Research Location:	Arnold Engineering Center Populsion and Diagnostic Section Arnold AFB Tullahoma, Tennessee
USAF Research:	Dr. Wheeler McGregor and Dr. Robert A. Reed

Date:	September 18, 1985
Contract No.	F49620-85-C-0013

THE THERMODYNAMIC, PHYSICAL AND OPTICAL PROPERTIES OF ALUMINUM OXIDE

by

Astor Y. Herrell

ABSTRACT

The scientific literature was reviewed in order to determine the thermodynamic, physical and optical properties of Aluminum Oxide. Its was found that the most stable form of the solid is α- Al_2O_3. It standard enthalpy of formation is -397.6 ± 0.3 K cal mole^{-2}: its heat of fusion is: 26.55 ± 1.0 K cal mole^{-1}, and the melting point, 2324 ± 6K, has been adopted. The data in the literature show that its density at the melting point is 3.01 g/cm^3 and has a temperature dependence given by ρ = 5.632 - 1. 127 x 10^{-3}T. A value for the surface tension of molten Al_2O_3 and its temperature dependence is given. The emissivity of molten Al_2O_3 is about 0.9.

I. INTRODUCTION

The author holds a Ph.D degree in inorganic chemistry and currently serves as Professor and Chairman of the Natural Science Department at Winston-Salem State University in Winston-Salem, NC. The research for my doctoral degree was in the area of chemical thermodynamics and inorganic preparation.

At the Arnold Engineering Center, scientists are interested in the radiative heat from the exhaust plume of rockets using aluminum as a solid fuel. A significant part of the thermal radiation from this exhaust is due to the presence of Al_2O_3 particles. The properties of Aluminum Oxide are needed in order to compute the radiative heat effect.

It was determined that my academic background had the desired elements which would enable me to review the literature concerning Aluminum Oxide and place these properties in a readily accessible document. It was also thought that following this review, I would be in a position to make recommendations concerning further research needed regarding Al_2O_3.

II. OBJECTIVES OF THE RESEARCH EFFORT

The objectives of the research were to determine the thermodynamic, physical and optical properties of Aluminum Oxide that are generally accepted by the scientific community and to make some measurements, using FTIR, of the optical properties of Aluminum Oxide particles obtained from the exhaust plume of a rocket.

The initial activities involved computer searches of the scientific literature as well as a personal search utilizing indexes

to the scientific literature. Publications obtained in these ways gave other references that were followed. Later, the most recently published journals were individually searched in order to obtain publications regarding current work in the area.

Due to the time constraint (10 weeks) of this activity and the time required to secure technical publications for review which were not housed in the library at the base, it was decided that the effort should concentrate on the goal of determining the properties of Alumina. It was the hope that a critical review of the literature would provide information that would suggest additional studies that should be performed on the Al_2O_3 particles from the rocket exhaust plume.

III. THERMODYNAMIC, PHYSICAL AND OPTICAL PROPERTIES OF ALUMINUM OXIDE

Aluminum Oxide particles form a significant portion of the exhaust plume in rockets utilizing Aluminum as a fuel. An understanding of the properties of the oxide is essential to the determination of the radiative heat transfer from these particles.

Aluminum Oxide occurs in nature as corundum (α - Al_2O_3). It has a hardness approaching that of diamond and is inert to acid attack at ordinary temperatures and pressure. However, Foner (1) has developed a high pressure method that readily dissolves Al_2O_3 using hydrochloric acid. Al_2O_3 can occur in several crystal forms but all forms are converted to the alpha structure by heating above 1200°C (2).

Melting Point

A number of investigators have measured the temperature at which Aluminum Oxide melts employing various techniques. Most of the important details of the studies occuring before 1967 are presented in a report by

Schnieder and McDaniel (3). They state that the value (2050°C) obtained in 1914 no longer needs to be referenced due to the changes brought about by the international practical temperature scale (4).

Schnieder and McDaniel (3) investigated the effect of environment on the melting point of Al_2O_3. They employed a susceptor-black body assembly and a photoelectric pryometer for temperature measurements. The environments were: vacuum (10^{-3}torr), helium (1 atm), Argon (1 atm) and air (1 atm). They found that the melting point of Al_2O_3 is influenced by the environment surrounding the sample. Results of the investigation are summarized in Table 1. An estimated precision based on the ability to distinguish one temperature from another in a given set of data is reported to be less than ± 1.5 °C. Using this precision, they concluded that there is a real difference in the melting point of Al_2O_3 in the various atmospheres. In air, the melting of Al_2O_3 occured over a range of temperatures rather than a sharp congruent type of melting as was characterized under other environments. Although they were unable to explain this phenomenon, they did note that a brown-colored crystalline material formed on the surface when the oxide was heated in air above 2020°C. They also reported that water vapor accelerated dissociation. Nelson and co-workers (5) later confirmed the low melting point of AL_2O_3 in oxygen.

From these investigations Schnieder and McDaniel concluded that the melting point of 2051°C mesured in vacuum using a tungsten container was the closest value to the true melting temperature of Al_2O_3. However, they cautioned investigators of indiscriminate use of Al_2O_3 as a reference source until the results of the IUPAC Task Force (6) was made.

The IUPAC Task Force (6) reported its findings concerning the

melting point of Al_2O_3 in 1970. The Task Force was comprised of fourteen scientific gorups representing nine countries. All participating groups used a common source of Al_2O_3, but experimental techniques and equipment used by different investigators varied and no two groups employed the same technique. With the exception of one group, all employed optical pyrometers for temperature measurements. Environmental conditions varied from high vacuum to air or Argon at various pressures.

The melting points of Al_2O_3 that were obtained by individual task force groups ranged from a low of 2043°C to a high of 2073°C. The overall average of the groups was 2054°C (IPTS 1968). The temperature, 2054 ± 6°C was recommended as the melting point of Al_2O_3 and has since been adopted.

Thermodynamic Properties of Al_2O_3

The adopted thermodynamic properties of Al_2O_3 are listed in the JANAF Tables (7) and the literature is critically reviewed. The standard enthalpy of formation of α - Al_2O_3 at 298.15 °C listed is -397.6 ± 0.3 K cal $mole^{-1}$. The enthalpy of fusion of α-Al_2O_3 at its melting point, 26.55 ± 1.0 K cal $mole^{-1}$, represents the average of the data obtained by several investigators. The enthalpy of fusion is obtained from the difference between the enthalpies of the liquid and solid phases at the melting point.

In a recent investigation, Shpil'rain et al. (8) obtained a value of 27.5 ± 1.2 K cal $mole^{-1}$ for α - Al_2O_3. This value falls within the range of values cited in (7).

A search of the literature failed to reveal a single, definitive measurement of the boiling temperature of molten aluminum oxide. However boiling points have been computed on the basis of other data. Brewer and Searcy (9) studied the Al-Al_2O_3 system in an infusion cell and from vapor pressure measurements computed a boiling point of 3800 ± 200 k. They further stated that molten Al_2O_3 undergoes considerable dissociation below this temperature. Other studies (10, 11, 12) confirm the dissociation of molten Al_2O_3. These studies as well as the investigation concerning electrical conductivity (13) show that the molten oxide is an ionic liquid. Vapor species existing above the liquid are aluminum, oxygen and Al O (3,9).

The boiling point, 3260 K, listed in the tables of Kaye and Laby (14) is intuitively more believeable. The value is based on vapor pressure - temperature relationships. However, the original source of the data was not given and could not be found. Using this temperature and the value listed for dt/dp at the boiling point, one can compute a heat of vaporization

$$Hv = RT^2P^{-1}\ (dt/dp)^{-1}. \qquad (1)$$

Substituting in the appropriate values yeilds a heat of vaporization of 104 k cal/m. It is obvious that a need exists for direct measurements of the boiling point of Al_2O_3.

<u>Density of Molten</u> Al_2O_3

The density of alumina in the liquid state has been determined by a number of workers. Kirshenbaum and Cahill (15) used a tungsten sinker and a molybdenum crucible to contain the melt. The technique involved the loss in weight of the sinker over the temperature range of 2375 to 2625K. An inert atmosphere of argon filled the carbon tube resistance

furnace and the temperature was measured by means of an optical pyrometer. They determined a density of 3.053 g/cm^3 and a molar volume of 33.40 cm^3/mole for the molten oxide at its melting point. The volume represents a 22% volume increase going from the solidus to the liquidus phase. The density of the liquid Al_2O_3 (purity 99.96%) showed a linear temperature dependence over the range, 2375 to 2625K, corresponding to the equation:

$$\rho = 5.632 - 1.127 \times 10^{-3}T. \tag{2}$$

Using expansion data for the solid from the literature, they determined a density for the solid of 3.73 g/cm^3. They determined that molten Al_2O_3 does not react with tungsten or molybdenum at these temperatures.

Kingery (16) measured the density of molten Al_2O_3 using the sessile drop technique. The measurements were made just above the melting point. In two runs, he obtained values of 3.02 and 2.91 g/cm^3. The average is 2.97 g/cm^3. He reported a volume change at the transition temperature of a 20.4% increase going from the solid to the liquid. He acutally errored in this report. Based on the reported data, the increase is 25.6% going from the solidus to the liquidus phase. This value, 20.4% is referenced in a 1985 publication (17). His studies were carried out in an atmosphere of purified helium. He also determined a density of the solid at the melting point to be 3.73 g/cm^3.

Rasmussen and Nelson (18) developed an X-radiographic technique for making measurements of the menisus and pendant drops of high temperature melts. A computer program generated a theoretical curve to fit the pendant drop profile. The density of the molten oxide was computed from the calculated volume and the weight of the sample employed. The density was found to be 3.01 g/cm^{3}at the melting point. Rasmussen (19) in a separate article reported a volume increase upon melting of 24.0 ± 1.5%

increase and gave a temperature dependence of density,

$$\rho = 4.55 - 7.52 \times 10^{-4}t, \tag{3}$$

over the temperature range 2050 to 2400°C.

Bates and co-workers (20) determined the density of molten Al_2O_3 at various temperatures and found a temperature dependence identical to that of Kirshenbaum and Cahill (15).

Barkhatov et al. (21) obtained density values using the maximum gas-bubble pressure method. Temperature measurements were made using an EOP-66 pyrometer. The temperature dependence of density was found to be represented by

$$\rho = 5.035 - 0.965 \times 10^{-3}t, \ (t = °C) \tag{4}$$

over the temperature range, 2323 to 3000K.

Elyutin et al (22) measured the density of Al_2O_3 over the temperature range 2325 to 2800K. They obtained a density at the melting point of 2.99 g/cm^3 and the temperature dependence could be represented by,

$$\rho = 3.01 - 1.15 \times 10^{-3} \ (T-2305K) \tag{5}$$

Deviation of the data from the straight line was reported to be ± 3%.

The density, 3.01 g/cm^3, at the melting point appears to be the accepted value for molten Al_2O_3. Based on the data in literature, the temperature dependence of density as given by Kirshenbaum and Cahill (15) appears to be a good approximation of the true variation. The volume change going from the solid to liquid phase corresponds to an increase of aobut 24% (15, 16, 19, 23).

<u>Surface Tension* of Molten</u> Al_2O_3

A number of studies (16-22) have been made of the surface tension of molten alumina. However, most of these studies were made near the

melting point. Results of several studies are summarized in Table 2. Sokolov (24) has computed a theoretical value of 700 dyme/cm based on electrostatic forces.

Three studies (21, 22, 25) have dealt with the temperature dependence of surface tension above the melt point. These studies agree near the melt point. However, the slope of the line for Elyutin's data (22) is quite different from the other works. The most critical study was made by Shpil'rain et al (25). This study employed the maximum gas-bubble pressure method in an inert atmosphere. The temperature dependence of surface tension is given by

$$\sigma = 1560.6 - 522.2 \times 10^{-2} t + 43.2 \times 10^{-6} t^2 \quad (t = °C). \qquad (6)$$

The equation applies over the temperature range, 2054 to 2750°C and is a least square representation of the data. The spread of the data is reported not to exceed ± 1.3%.

Since the difference in the measured values of the surface tension near the melting point of molten alumina is not large, a value of 670 dymes/cm should be close to the true value of the surface tension of molten Al_2O_3 at the melting point. (Kingery's correction of Waterburg's data is employed here in computing an average value.)

Studies (17, 26) have been made concerning the effect of additives on the durface tension of Al_2O_3. Bates and Rasmussen (26) obtained small but inconsistant changes when oxides were added. Lihrmann and Haggerty (17) found oxide additives, TiO_2 excepted, caused a small change in surface tension in the same direction as the melting point was changed.

---

*The surface tension of water at room temperature is about 75 dyme/cm. The large surface tension (~ 400 dyme/cm) causes mercury to form spheres rather than to flow as water does.

TiO_2 additive, up to 0.5 wt. %, caused a rapid decrease in surface tension. They also found that surface tension was changed by environment. Surface tension increased with available oxygen in the atmosphere of the system, and surface tension was lower in a molybdenum crucible than in a tungsten crucible.

Viscosity of Molten Al_2O_3

The viscosity of molten Al_2O_3 has been measured by several investigators (20, 22, 26-29). The preferred technique for viscosity measurements at high temperatures is the oscillating - cup technique described by Bockris (30). Bates and co-workers (20) obtained a linear (logarithmetic) decrease in viscosity in the range 2100 to 2700°C using a high purity single crystal aluminum oxide. Elyutin et al. (22) measured the viscosity of Al_2O_3 (purity not specified) in the temperature range 2325 to 2800K. Although the viscosity decreased with increasing temperature, the decrease was not totally linear. In a separate report (29) Elyutin et al. gave values of viscosity from the melting point to 2620K. The plot of log N vs 1/T deviates from linearity near the melt point. They gave a temperature dependence of viscosity by:

$$N = 660 - 0.195\ (T-2305). \tag{7}$$

They also report an activation energy for viscous flow of $\sim$30 Kcal mole^{-1}.

The most recent study of the viscosity of Al_2O_3 is reported by Blomquist et al (27). Alumina powder (99.99% pure) was used for the study and a decrease in viscosity was observed over the temperature range, 2394 to 2742K. The data are presented in Table 3 and the temperature dependence is give by:

$$\ln N = 11.448/T - 8.2734 \tag{8}$$

The effect of additives to liquid Al_2O_3 on viscosity has been investigated (26, 29). Both groups found that SiO_2 increased viscosity. Compositions less than 20 wt. % SiO_2 gave small increases but large increases resulted from higher concentrations. It was proposed (26) that weak bonds exist between SiO_2 and the ionic species in the Al_2O_3 melt.

Bates and co-workers (26) found no significant differences in surface tension, volume change on melting and liquid density of single crystal Al_2O_3 and lucolox (0.25% MgO). However, there was a significant decrease in viscosity of lucolox compared to single crystal Al_2O_3. They also found that Sm_2O_3 and Y_2O_3 decreased the viscosity as well as the melting point.

Since the viscosity studies by Bates (20, 26) Elyutin (22, 29) and Blomquist (27) involved acceptable experimental techniques, it is not possible, at present, to explain the differences in their values. There is fair agreement between the values of Elyutin and Blomquist but a sufficient difference exists to encourage further studies.

Optical Properties of Al_2O_3

Since Al_2O_3 particles constitute a large part of the exhaust plume of rocket engines using aluminum as a solid rocket propellant, it is necessary to know their optical properties in order to determine their radiative heat effects.

Absorption Coefficient and Refractive Index

The literature concerning the absorption coefficient and refractive index of single crystal Aluminum Oxide (leucosapphire) has been critically

reviewed by Lingart and co-workers (31, 32). The purpose of the work was to determine the most reliable results over a wide range of wavelength and temperature for use in computer programs in calculating the radiative-conductive heat transfer. Since the crystal is anisotropic, they state that the birefriengence can be ignored for radiative heat transfer calculations.

The translucent region of leucosapphire is taken to be from 0.5 to 6.2 um at room temperature. Lingart et al. (31) recommended values, in tabular form,for the absorption coefficients of leucosapphire for the temperature range of 300 to 2300K. They provide details as to the way these values were derived.

In the same report they provide, in tabular form, recommended values for the refractive index of leucosapphire in the translucent region for various temperatures. The recommeded values at room temperature are based on the work of Malitson (33) and those at elevated temperatures are based on the work of Plass (34).

In a further study, these workers (32) reviewed the literature with reference to the indexes of absorption and refraction in the opaque region (6 to 33 um) as well as the optical properties of molten aluminum oxide. They found limited data concerning the index of refraction in the opaque region. However, they gave tables of recommended values for the index of absorption and refraction of the solid in this region and rationalized their conclusions. From their review of the literature regarding molten Al_2O_3, they found the data to be sparse and contradictory, so they were unable to provide recommeded values for its optical properties. Their review showed

that at the melting point transition there is a sharp increase in the absorption coefficient. They stated that this may result from the presence of metallic aluminum or partial melting of the particles.

According to Rubtsov et al. (35), "The data on the complex refractive index of Al_2O_3 crystal Al_2O_3 cannot be applied to material that has been melted." This is due to differences in temperature dependence at the phase transition. They state that the absorption parameter changes step-wise upon melting of single crystal Al_2O_3 but it increases monotonically for the polycrystalline oxide. After single crystal Al_2O_3 melts, the absorption parameter reaches the value for fused particles and then changes with the same temperature coefficient as the polycrystalline material. In this report the authors (35) present a table of values for the absorption parameter for fused Al_2O_3 in the visible and near infrared region at high temperatures.

Emissivity

All objects at high temperatures radiate energy. "Emissivity, as a term, is a fundamental property of materials which have an optically polished surface. It is a dimensionless number expressing the ratio of thermal emission of a non-black body to that of a black body" (37). In a study of the emissivity of ceramic bodies, Blair (37) reported values of emissivity for alumina bodies over a wide temperature range. The total emissivity and the emissivity at 0.64 um varied slightly over the temperature range of $\sim$600 to 1600°C, remaining close to a value of 0.4. The change in emissivity using 1 um was much greater.

The spectral emissivity of several ceramic materials was measured by Bober et al.(36) using a reflectance technique and laser heating. Temeratures as high as 4500K were achieved. They point out that in the

solid state using 0.63 um wavelength only sintered samples of Al_2O_3 were used due to its translucency in the pre-molten solid state. The measured emissivity of Al_2O_3 above the melt point reached a value of $\sim$0.9. At a wavelength of 10.6 um, its spectral emissivity ($\sim$0.9) is essentially constant to about 3500K where it decreases slightly.

The normal spectral emittance of composites made from coatings of Al_2O_3 was found to change appreciably with coating thickness and the substrate emittance by Liebert (38). He found that an oxide coating of 0.4 mm has an emittance of 0.98 at 8.5 um over a wide temperature range which is in good agreement with the work of earlier workers.

In radiative heat transfer it is the hemisperical emissivity that is of interest and the emissivity of microscopic particles in particular. The emissivity from the exhaust plume of rocket motors is much greater than that of Al_2O_3 (38, 40-41). The reasons for this phenomenon is not known and has lead to a number of studies (39, 40, 42-47).

The early studies involving the combustion of Aluminum-Ammonium pechlorate mixtures were performed by Romodanova and Pokhil (48) and Cohen Nir (49). They were primarily interested in determining maximum burning rate. Cohen Nir showed that the maximum burn rate occurred at 10% aluminum composite. This work was confirmed by Verniker et al. (50).

A study of agglomeration of alumimun particles in a rocket motor flowfield was studied by Gany et al. (45). They found that agglomerate size was affected by both pressure and transverse flow rate. Smaller agglomerates were observed under high pressure and high flow rates. High flow rates decreased the time the Aluminum agglomerates could remain on the surface. They also found that the size of aluminum particles determine if they would ignite on the surface or in the gas stream.

In an effort to explain the high emissivity of Al_2O_3 in rocket plumes, Pluchino (39) and Riezer (43) have given theoretical explanations employing impurities of metallic aluminum and carbon in the surface of the particles. They show that a small surface quantity of these elements will enhance the emissivity of Al_2O_3 greatly.

Konopka et al. (47) have investigated the optical properties of Al_2O_3 particles from two rocket motors. The particles with lower contamination had low emissivity which increased with increasing temperature to the melt point. Particles from the second rocket had an emissivity which was essentially temperature independent.

The size of the aluminum oxide particles resulting from the combustion of aluminum in rocket motors is important with respect to the rates at which they will disperse in the atmosphere as well as the light scattering effect (42, 43, 50). Methods for predicting aluminum particle size are presented by Hermsen (51). In this report, he discusses the improved SPP model for size predictions.

Further studies regarding particle size and composition must be made before the emissivity from a rocket plume will be fully understood.

IV. RECOMMENDATIONS

From a review of the literature regarding properties of aluminum oxide, it was found that adopted values have been established for its enthalpy of formation, enthalpy of fusion and its melting point.

On the basis of the studies reported in the literature, it is recommended that the value, 3.01 g/cm^3 be utilized in radiative heat transfer calculations as the density of molten aluminum oxide at its melting point. Further, the temperature dependence of its density is

given by an emperical equation found by Kirshenbaum and Cahill. The recommended value for its surface tension at the melt point is 670 dyme/cm and the temperature dependence of its surface tension be given by the least squares equation reported by Shpil'rain et al.

The data reported in the literature regarding the viscosity of molten alumina are sparse and conflicting. It is recommended that additional studies be made in order to determine an acceptable value for the viscosity of molten Al_2O_3 as well as its temperature dependence.

From a search for the literature, I was unable to find a single report involving a direct measurement of the boiling point of aluminum oxide. Such a study is critically needed and should be done.

The aluminum oxide particles obtained from the exhaust plume of rocket motors is often dark in color. This indicates that the oxide is impure. Until recently, no good method for dissolving Al_2O_3 was known. Foner (Ref. 1) recently developed a method for dissovlving the oxide in hydrochloric acid. This method should be used to dissovlve the Al_2O_3 particles from the rocket motor exhaust and the solution analyzed for chemical constituents.

ACKNOWLEDGEMENTS

Research sponsored by the Air Force Office of Scientific Research /AFSC United State Air Force, Arnold Engineering Center, Tullahoma, Tennessee, under contract F49620-85-C-0013. The author expresses his appreciation to Dr. Wheeler McGregor and Dr. Robert A. Reed for helpful suggestions and the library staff at Arnold Engineering Center for their assistance in securing technical reports.

Temp °C	a Poise	b Poise	c Poise		
2170	0.746	0.500	0.457	(2323)*	
2260	0.648	0.405	0.388	(2423)	
2370	0.584	0.320	0.335	(2473)	K
2475	0.565	0.261	0.295	(2523)	
2575	0.505	0.218	0.265	(2573)	
2675	0.480	0.184	0.246	(2623)	

TABLE 3. Viscosity of Molten Al_2O_3

(a) Values from Bates

(b) Values from Blomquist

(c) Elyutin's Values

*Numbers in parenthesis are actual temperatures of measured values

NOTE: For comparison, the viscosity of water at 0°C is 0.0178 Poise)

ENVIRONMENT	TUNGSTEN CONTAINER	IRIDIUM CONTAINER
	°C. IPTS	°C. IPTS
Vacuum	2051	2046
Argon	2045	-
Helium	2041	2036
Air	-	2038 (liquidus)

TABLE 1. Summary of Al_2O_3 Melting Points

AUTHOR	TECHNIQUE	SURFACE TENSION dyne/cm	COMMENTS
Wartenburg	Vibrating jet and weight of drops	580	Inaccurate density used
Kingery	Hanging drop from Mo rod, (He atm.)	690	
Mawrakh	Falling drop	680	high speed photography used
Yakobashvile	Sessile drop	643	high speed photography used
Rasmussen	Meniscus and drop (vaccum)	638	Mo lowers surface tension
Barkhatov	Maximum gas bubble pressure. (Argon)	672	Experession for temperature dependence given.
Shpil'rain	Maximum gas bubble pressure (Ar & He)	680	least square plot given
Lihrmann	Pendant drop	665	Effect of different environments given.

TABLE 2. Surface Tension of Molten Al_2O_3

REFERENCE

1. Foner, H.A., "High-Pressure Acid Dissolution of Refractory Alumina for Trace Element Determination", Anal. Chem., 56, 856 (1984)

2. Greenwood, N. N. and Earnshaw, A., Chemistry of the Elements, Pergamon Press, New York, 1984 Chpt. 7.

3. Schneider, S. H. and McDaniel, C. L., "effect of Environment Upon the Melting Point of Al_2O_3." J. Of Research - NBS, 71A, 317 (1967)

4. Bedford, R. E., "The International Practical Temperature Scale of 1968 and its Probable Future Development," High Temperatures-High Pressures, 11, 135 (1979).

5. Nelson, L. S., et al., "Effects of Oxygen and Argon Atmosphere on Pendant Drops of Aluminum Oxide Melted with Carbon Dioxide Laser Radiation," High Temperature Science, 5, 138 (1973).

6. Schneider, S. J., "Cooperative Determination of the Melting Point of Al_2O_3," Pure and Applied Chem., 21, 117 (1970).

7. Chase Jr., M. W., Curnutt, J. L., McDonald, R. A. and Syverud, A. N., "JANAF Thermochemical Tables, 1978 Supplement", J. Phys. Chem. Ref. Data, 7, 793 (1978).

8. Shpil'rain, E. E., Kagan, D. N., Barkhatov, L. S., Zhmakin, L. I. and Koroleva, V. V., "A Complex Investigation of the Thermal and Electrophysical Properties of Refractory Oxides in Liquid and Solid Phases." J. of Engineering Phys., 38, 333 (1980).

9. Brewer, L. and Searcy, A. W., "The Gaseous Species of the Al-Al_2O_3 System", J. Am. Chem. Soc., 73, 5308 (1951).

10. DeMaria, G., Drowart, J. and Inghram, M. G., "Mass Spectrometric Study of Al_2O_3," J. Chem. Phys., 30, 318 (1959).

11. Farber, M., "Thermodynamics of Al_2O_3," Jet Propulsion, 28, 760 (1958)

12. Drowart, J., DeMaria, G., Burns, R. P. and Inghram, M. G., "Thermodynamic Study of Al_2O_3isomg a ,ass Spectrometer," J. of Chem. Phys., 32, 1366 (1960).

13. Shpil'rain, E. E., Kagan, D. N., Barkhatov, L. S. and Zhmakin, L. S., "Expwrimental Study of the Specific Electrical Conductivity of Molten Aluminum Oxide at Temperatures up to 3000°K," High-Temepratures, 14, 843 (1976).

14. Kaye, G. W. C. and Laby, T. H., Tables of Physical and Chemical Constants (14th Ed.) Longman Group Limited, London, 1973 p. 174.

15. Kirshenbaum, A. D. and Cahill, J. A., "The Density of Liquid Aluminum Oxide", J. Inorg. Nucl. Chem., 14, 283 (1960).

16. Kingery, W. D., "Surface Tension of Some Liquid Oxides and Their Temperature Coefficients", J. Am. Ceram. Soc., 42, 6 (1959).

17. Lihrmann, J. M. and Haggerty, J. S., "Surface Tensions of Alumina-Containing Liquids", J. Am. Ceram. Soc., 68, 81 (1985).

18. Rasmussen, J. J., and Nelson, R. P., "Surface Tension and Denisty of Molten Al_2O_3", J. Am. Ceram. Soc., 54, 398 (1971).

19. Rasmussen, J. J., "Surface Tension, Denisty and Volume Change on Melting of Al_2O_3 Systems, Cr_2O_3 and Sm_2O_3," J. Am. Ceram. Soc., 55, 326 (1972).

20. Bates, J. L., McNeilly, C. E. and Rasmussen, J.J., "Properties of Molten Ceramics" Ceramics in Severe Environments: Proceedings 6th University Conference on Ceramic Science, North Carolina State Univ., 1970, Plenum Press. P.P. 11-26, 1971.

21. Barkhatov, L. S., Kagan, D. N., Tystsarkin, A. F., Shipl'rain, E. E., and Yakimovich, K. A., "An Investigation of the Thermodynamic Properties of Molten Aluminum Oxide", High Temp., 11, 1063 (1973).

22. Elyutin, V. P., Mitin, B. S. and Nagibin, Yu. A., "Properties of Liquid Alumina:, Advances in Aerosol Phys., 7, 239 (1973).

23. Tyrolerova, P. and Lu, W. K., "Volume Chance on Freezing of Al_2O_3," J. Am. Ceram. Soc., 52, 77 (1969).

24. Sokolov, O. K., "Theory of Molten Salts and Oxides", IZV. Akad Nauk. SSSR, Met. Govn. Delo., 4, 59 (1963).

25. Shpil'rain, E. E., Yakimovich, K. A. and Tsitsarkin, A. F., "Surface Tension of Alumina up to 2750°C and the Wetting Angle near the Melting Point.", High Temp., 11, 894 (1973).

26. Bates, J. L. and Rasmussen, J. J., "Effects of Additives on Volume Change on Melting, Surface Tension, and Viscosity of Liquid Aluminum Oxide, " Final Report, Pacific Northwest Laboratories, June, 1972.

27. Blomquist, R. A., Fink, J. K. and Leibowitz, L., "Viscosity of Molten Alumina", Am. Ceram. Soc. Bul., 57, 522 (1978).

28. Rasmussen, J. J., Bates, J. L., Slagle, O. D. and Nelson, R. P., "Structure - Property Relationships in Liquid Ceramics", Technical Report (N Ro32-501) Office of Naval Research, June (1971).

29. Elyutin, V. P., Kostikov, V. I., Mitin, B. S. and Nagibin, Ya. Al., "Viscosity of Alumina", Russian J. of Phy. Chem., 43, 316 (1969).

30. Bockris, J. O'M, White, J. S., and McKenzie, J. D., Physiochemical Measurements at High Temperatures, Butterworths Scientific Publication, London, 1959.

31. Linghart, Yu.K., Petrov., V. A., and Tikhonova, N. A., "Optical Properties of Leucosapphire at High Temperatures. I. Translucent Region", High-Temp., 20, 706 (1982).

32. Linghart, Yu. K., Petrov, V. A., and Tikhonova, N. A., "Optical Properties of Leucosapphire at High Temperatures. II Single-Crystal Properties in the Opaque Region and Properties of the Melt", High-Temp., 20, 856 (1982)

33. Malitson, J. H., "Refraction and Dispersion of Synthetic Sapphire," J. Opt. Soc. Am., 52, 1377 (1962)

34. Plass, G. N., "Temperature Dependence of the Scattering and Absorption Cross Sections for Aluminum Oxide", J. Appl. Opt., 4, 1616 (1965).

35. Rubtosov, N. A., Emel 'yanov, A. A. and Ponomanev, N. N., "Absorption Parameter of Fused Aluminum Oxide at High Temperatures", High Temp., 22, 240 (1985).

36. Bober, M., Karow, H. U. and Miller, K., "Study of the Special Reflectivity and Emissivity of Liquid Ceramics", High Temperatures-High Pressures, 12, 161 (1980).

37. Blair, G. R., "Determination of Spectral Emissivity of Ceramic Bodies at Elevated Temperatures", J. Am. Ceram. Soc., 43, 197 (1968).

38. Liebert, C. H., "Spectral Emittance of Aluminum Oxide and Zinc Oxide on Opaque Substrates", NASA TN-3115 (1965).

39. Pluchino, A. B., "Emissivity Spectra of Composite Microscopic Particles", Applied Optics, 20, 531 (1981).

40. Pluchino, Al B. and Masturzo, D. E., "Emissivity of Al_2O_3 Particles in a Rocket Plume", AIAA Journal, 19, 1234 (1981).

41. Nelson, H. F., "Influence of Scattering on Infrared Signatures of Rocket Plumes", J. Spacecraft and Rockets, 21, 508 (1984).

42. Strand, L. D. et al., "Characterization of Particulates in the Exhaust Plume of Large Solid-Propellant Rocket," J. Spacecraft and Rockets, 18, 297 (1981).

43. Riezer, T. J., "On the Emissivity of Alumina/Aluminum Composite Particles", J. Spacecraft and Rockets, 16, 438 (1979).

44. Mularz, E. J. and Yuen, M. C., "An Experimenental Investigation of Radiative Properties of Aluminum Oxide Particles", J. Quart. Spectrosc. Radiat Transfer, 12, 1553 (1972).

45. Gany, A. et al., "Aluminized Solid Propellants Burning in a Rocket Motor Flowfield", AIAA Journal, 16, 736 (1978).

46. Morizumi, S. J. and Carpenter, H. J., "Thermal Radiation from the Exhaust

46. Morizumi, S. J. and Carpenter, H. J., "Thermal Radiation from the Exhaust Plume of an Aluminized Composite Propellant Rocket", J. Spacecraft and Rockets, 1, 501 (1964).

47. Konopka, W. L., Reed, R. A., and Calia, V. S., "Measurements of Infrared Optical Properties of Al_2O_3 Rocket Particles." Presented as Paper 83-1568 at the AIAA 18th Thermophysics Conference, Montreal, Canada, June 1-3, 1983. Copyright American Institute of Aeronautics and Astronautics, Inc. 1983. All rights reserved.

48. Romodamova, L. D. and Pokhil, P. K., "Action of Silica on the Burin. g Burning Rates of Ammonium Puthlorate Compositions", Fzika Gareniya, I. Vzryua, 6, 285 (1970).

49. Cohen Nir, E. "Combustion of Powdered Metals in Contact with a Solid Oxidiser", Thirteenth Symposium (International) on Combustion, The Combustion Institute, Pittsburgh, Pa., 1019 (1971).

50. Verneker, V. R. Pai, Sutharamacharyulu, D., and Mallya, R. M., "Combustion of Ammonium Puchlorate - Aluminum Mixtures", Ammonium J. Spacecraft and Rockets, 16, 436 (1979).

51. Lyons, R. B. et al., "Scattering of Radiation by Particles in Low-Attitude Plumes", J. Spacecraft and Rockets, 20, 189 (1983).

52. Hermsen, R. W., "Aluminum Oxide Particle Size for Solid Rocket Motor Performance Prediction", J. Spacecraft and Rockets, 18, 483 (1981).

1985 USAF-UES SUMMER FACULTY RESEARCH PROGRAM/

GRADUATE STUDENT SUMMER SUPPORT PROGRAM

Sponsored by the

AIR FORCE OFFICE OF SCIENTIFIC RESEARCH

Conducted by the

UNIVERSAL ENERGY SYSTEMS, INC.

FINAL REPORT

GEOID MODELLING AND INTERPRETATION

Prepared by: Albert T. Hsui

Academic Rank: Associate Professor

Department and

University: Department of Geology
University of Illinois

Research Location: Division LWG
Air Force Geophysics Laboratory
Hanscom Air Force Base
Bedford, Mass. 01731

USAF RESEARCH: Dr. Thomas P. Rooney

DATE: August 15, 1985

CONTRACT NO: F49620-85-C-0013

GEOID MODELING AND INTERPRETATION

by

Albert T. Hsui

Dept. of Geology, University of Illinois

ABSTRACT

Utilizing SEASAT altimetry data to delineate mantle structure immediately beneath the lithosphere at passive margins has been carried out. A forward modelling approach is followed to study geoid anomalies. Models to simulate thermal mechanical structures within the mantle have been developed. Calculations to translate density anomalies to surface geoid heights have been investigated. It is found that many fundamental problems exist in modelling geoid anomalies for a flat earth. Sensitivity of model parameters have rarely been examined. Although the ten weeks appointment is not long enough to complete the original proposed research, many newly identified problems and the future research direction for surface geoid interpretation will be discussed.

ACKNOWLEDGMENT

I would like to thank D. H. Eckhardt, T. P. Rooney, A. R. Lazarewicz and R. P. Bessette of AFGL for their help to get this project started and for their encouragement and consultation throughout the course of this research. The wonderful hospitality extended by the LWG division of the AFGL is also gratefully acknowledged. This project is sponsored by the Air Force Systems Command, the Air Force Office of Scientific Research and the Air Force Geophysics Laboratory.

I. INTRODUCTION

Understanding the Earth's gravity field has been a major interest of the LWG Division of the Air Force Geophysics Laboratory. For both scientific and practical reasons, it is desirable to gain knowledge about the origin of surface gravity anomalies. Geoid surface represents a reference equipotential surface for the Earth's gravity field. Consequently, geoid undulation from a theoretical ellipsoid surface can be used to infer density inhomogeneities within the earth. Additionally, since geoid undulations represent the first moment of mass anomalies (Turcotte and Schubert, 1982), study of geoid anomalies can provide supplementary information about the vertical structure of internal mass distributions. Since the advent of satellite geodesy, geoid of the Earth has been measured by many satellite altimeters (e.g. GEOS-3 and SEASAT). These data can be analyzed using some inversion techniques to determine corresponding density heterogeneities. Although inversion techniques are perhaps one of the most sophisticated mathematical techniques in geophysics, their solutions are also known to be highly non-unique. Very often, it is more useful to interpret geoid undulations using forward modeling approaches. Such an approach is able to refine the current model of density structure and provide better insight about the origin of geoid anomalies.

This investigator has acquired extensive experience in carrying out mathematical modelling of geophysical problems. Therefore, he is quite capable to construct forward models to interpret geoid undulations. Since AFGL has the SEASAT altimetry data base, it is natural for this investigator to develop collaborative research efforts with the scientists at AFGL.

II. OBJECTIVES OF THE RESEARCH EFFORT

The original objective of this research is to analyze geoid undulation across continental margins to determine the thickness of continental lithospheres. It is hypothesized that a step like discontinuity between an oceanic and a continental lithosphere will cause variations in mantle flow which in turn will be manifested upon the sea surface geoid anomalies. Therefore, by seeking the appropriate geoid undulation signals and by comparison with model computations, the thickness of a continental lithosphere can be estimated. Additionally, during the initial stage of this research, we have also discovered that surface geoid anomalies can also be used to discriminate whether the mantle flow is driving the tectonic motions of the surface plates or the mantle flows passively in response to surface plate tectonics.

As the details of geoid modelling for a flat earth are being implemented, it is found that geoid anomalies are very sensitive to certain parameters such as density contrasts between mantle and crust, ocean depth and thickness of crustal root beneath continents etc. In order to test the reliability of model interpretation, it is necessary to carry out a thorough sensitivity study for all these parameters. Thus, it becomes another goal of our research effort.

Our efforts to realize the above objectives will be elaborated in the following sections.

III. MANTLE FLOW BENEATH A CONTINENTAL MARGIN

Based on bathymetric and surface heat flow studies, oceanic lithospheres are estimated to be about 100 km thick (Parson and McKenzie, 1978). Continental lithospheres are believed to be somewhat thicker because they have remained at the surface of the Earth for a longer period of time and subject to more cooling. However, the exact thickness of a continental lithosphere is controversial. It ranges from 200 km (Anderson, 1979) to over 400 km (Jordan, 1978). One purpose of this study is to see if the geoid data is able to provide some constraints to this problem.

Since oceanic and continental lithospheres have different thickness, a step like structure (albeit there may be some variations in its actual geometry) exists when the two lithospheres meet. Consequently, the thermal-mechanical structure of the mantle beneath continental margins will be altered in response to this special feature. It is this characteristic thermal structure which generates the corresponding density and geoid anomalies that we believe can provide constraints on the thickness of the continental lithosphere.

Thermal mechanical structure of the mantle beneath a continental margin can be modelled following an approach that has been described by Toksöz and Hsui (1978). Similar to Toksöz and Hsui (1978), we choose to use a kinematic model instead of a dynamic model because it will be adequate for regional modelling. Our model is calculated using a finite difference numerical scheme. The mantle flow and its corresponding thermal structure have been successfully simulated. An example is given in Figure 1. Figure 1a is a plot of stream function beneath a continental margin with a vertical wall. It is apparent that there are no flow eddies at the step corner. It is simply because the mantle flow is too viscous to have any flow separation to occur. The corresponding thermal stru-

cture is given in Figure 1b. Based on this temperature distribution, density variations can be calculated and hence the surface geoid anomalies.

The thermal-mechanical model that we have developed is designed to explore a wide range of parameter spaces. For example, it is able to change the angle of the step from 0 degree (i.e. vertical) to 60 degree from the vertical. The flow magnitude and direction can also be varied and even reversed. All the possible models will be examined for a fit with the SEASAT altimetry data.

IV. GEOID MODELING AND SENSITIVITY STUDY

Geoid shape for given mass anomalies has been studied by many investigators. Assuming regional isostasy, geoid anomalies across midocean ridges, continental margins, fracture zones and subduction areas have been investigated (Haxby and Turcotte, 1978; Sandwell and Schubert, 1982; McAdoo and Martin, 1984; Chapman and Talwani, 1979). All these studies attempt to explain the observed geoid anomalies in terms of deformations within the top 100 km of the Earth's surface. Although each of them presented a density model to explain the observed geoid anomalies, none discussed the sensitivity of the parameters used for fitting the data. In order to test the reliability of these models, we decide to carry out a sensitivity study of these parameter spaces. Geoid anomaly across a continental margin is chosen as a working example. First, sensitivity of geoid relief to crustal density is examined. Figure 2 shows the change in calculated geoid relief across a continental margin as a function of crustal density while keeping all other parameters at a fixed value as listed in Table I. Model calculation is carried out following techniques described in Chapman (1979). It is clear that geoid relief is extremely sensitive to the value used for crustal density, a change of 1 meter in geoid height can result with a change of crustal density as small as half a percent. If the mantle density is changed from 3400 to 3300 kg/m^3, identical behavior is observed. We next examine the effect of the depth difference between the bottom of the oceanic crust and that of the continental crust. Again, all the parameter values are fixed at that given in Table I except that of the bottom of the continental crust. Figure 3 shows their relationship. The diagram indicates that geoid relief again is relatively sensitive to this parameter. We next investigate the effect of the burial depth of the mass anomalies. This can be done by

simply increasing or decreasing the crustal thickness of both the ocean and the continent by the same amount. Figure 4 shows the result of that computation. The result indicates that geoid undulation is insensitive to the burial depth of the mass anomaly. It is consistent with the results of Haxby and Turcott (1978) which suggested that geoid anomaly is proportional to the first moment of a density anomaly. This is a very surprising result. Its correct physical interpretation at this time is still not very clear. More investigations are necessary in order to understand its implications.

V. RECOMMENDATIONS

As a result of my ten weeks research in geoid modelling and interpretation, many new problems have been identified and some suggestions can be derived. These are listed as follows.

(1) In most of geoid calculations (e.g. Talwani et al. 1972; Chapman, 1979) for 2-D models, geoid anomaly is often described by a logarithmic profile. However, the expression within the log function is generally dimensional. Consequently, using different dimensional units for the expression will yield different geoid height. It is obviously a deficiency of the formula which should be reconstructed such that it is independent of the dimensional units used for computation. One possible solution is to non-dimensionalize the integral relationship before integrating to obtain the formula. Of course, some more research and careful thinking are necessary in order to choose an appropriate length scale for non-dimensionalization.

(2) Modelling geoid for a spherical earth has been studied by many investigators (e.g. the point mass technique by Blaha et al. 1984). The techniques generally appear to behave well. However, modelling geoid for a flat earth may be problematic, especially for mass anomalies that are buried beneath the lithospheres. As pointed out earlier, most of the current formula suggest the independence of geoid anomalies from burial depth of mass anomalies. This is a result that does not appear to be consistent with physical intuition. More research is necessary so that this problem can be clarified.

(3) A thorough study of parameter sensitivity to geoid modelling is recommended. This is necessary in order to delineate how well constrained the models are.

REFERENCES

Anderson, D. L. (1979) The deep structure of continents. J. Geophys. Res., 84, 7555-7560.

Blaha, G., R. P. Bessette and G. Hadgigeorge (1984) Global point-mass adjustment of the oceanic geoid based on satellite altimetry, submitted to Marine Geodesy.

Chapman, M. E. (1979) Techniques for interpretation of geoid anomalies. J. Geophys. Res., 84, 3793-3801.

Chapman, M. E. and M. Talwani (1979) Comparison of gravimetric geoids with GEOS-3 altimetric geoid. J. Geophys. Res., 84, 3803-3816.

Haxby, W. F. and D. L. Turcotte (1978) On isostatic geoid anomalies. J. Geophys. Res., 83, 5473-5478.

Jordan, T. H. (1978) Composition and development of the continental tectosphere. Nature, 274, 544-548.

McAdoo, D. C. and C. F. Martin (1984) SEASAT observations of lithospheric flexure seaward of trenches. J. Geophys. Res., 89, 3201-3210.

Parsons, B. and D. McKenzie (1978) Mantle convection and the thermal structure of the plates. J. Geophys. Res., 83, 4485-4496.

Sandwell, D. T. and G. Schubert (1982) Geoid height-age relation from SEASAT altimeter profiles across the Mendocino fracture zone. J. Geophys. Res., 87, 3949-3958.

Talwani, M., H. Poppe and P. D. Rabinowitz (1972) Gravimetrically determined geoid in the western North Atlantic, Sea Surface Topography from Space, Tech. Rep. ERL-228-AOML, 7-2, 2, pp1-34, NOAA, Boulder, Colo.

Toksöz, M. N. and A. T. Hsui (1978) Numerical studies of back arc convection and

the formation of marginal basins. Tectonophysics, 50, 177-196.

Turcotte, D. L. and G. Schubert (1982) Geodynamics, John Wiley and Sons, N.Y., 450 pp.

TABLE I. Parameter Values Used for Model Computation.

mantle density ρm (kg/m^3)	3400
crustal density ρc (kg/m^3)	2800
water density ρw (kg/m^3)	1000
sea water depth d_w (m)	5000
depth of the bottom of the oceanic crust (m)	12000
depth of the bottom of the continental crust (m)	25000

FIGURE CAPTIONS

Figure 1. Numerical simulation of thermal-mechanical structure beneath a passive continental margin.

a. Stream lines near a vertical continental corner. The closeness of adjacent stream lines indicates the intensity of mantle flow.

b. The corresponding thermal structure. Solid lines are isotherms.

Figure 2. Geoid undulation as a function of crustal density. All parameter values used are given in Table 1.

Figure 3. Geoid undulation as a function of the depth of crustal roots. All other parameter values are given in Table I.

Figure 4. Geoid undulation as a function of burial depth of mass anomalies.

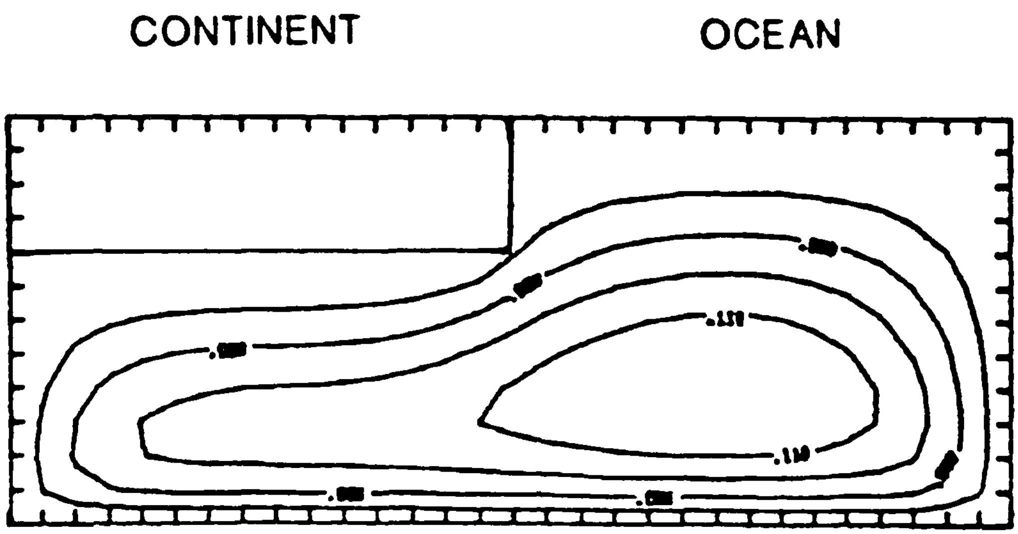

(a) STREAM LINES

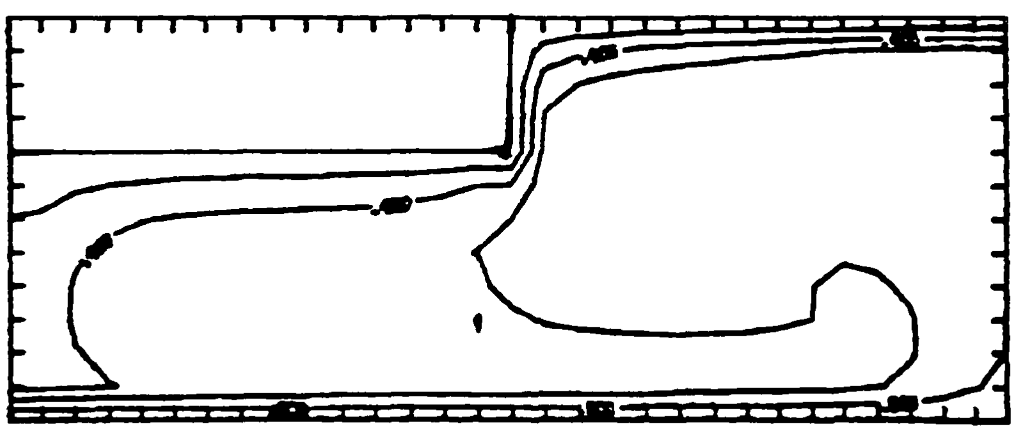

(b) ISOTHERMS

Figure 1

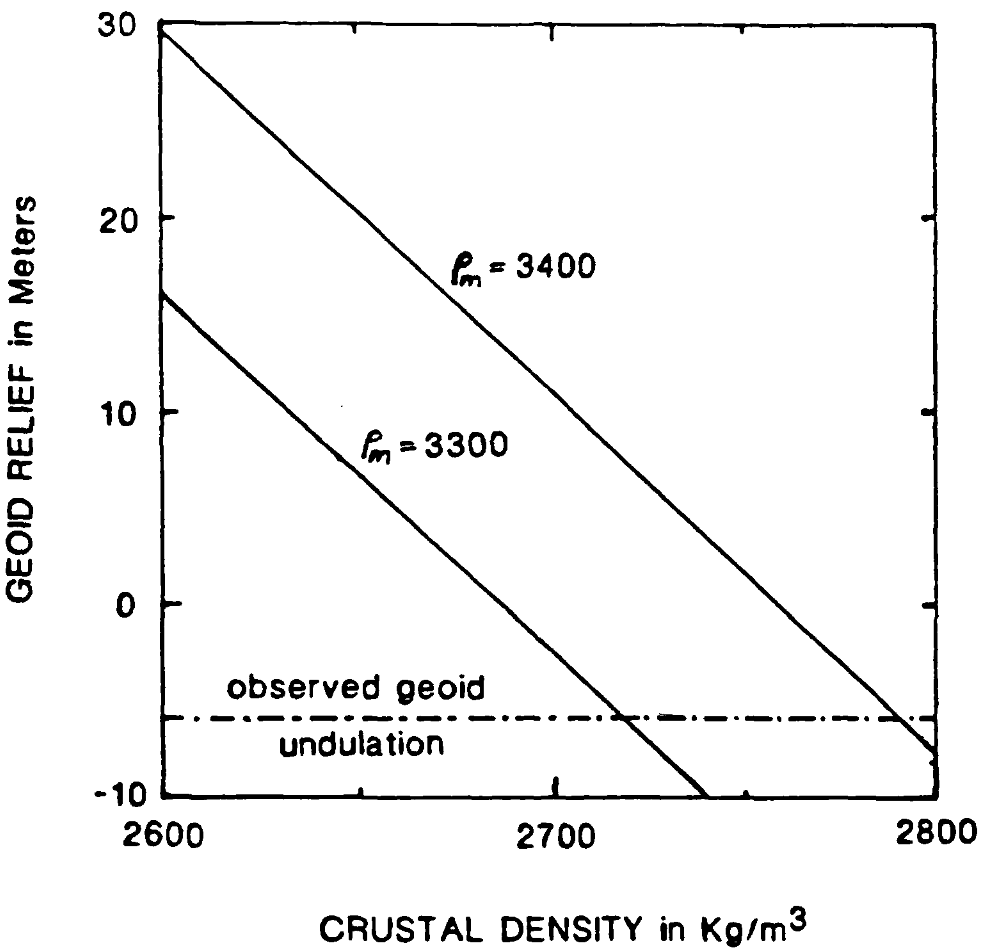

30
20
10
0
-10
GEOID RELIEF in Meters
$\rho_m = 3400$
$\rho_m = 3300$
observed geoid
undulation
2600
2700
2800
CRUSTAL DENSITY in Kg/m^3

Figure 2

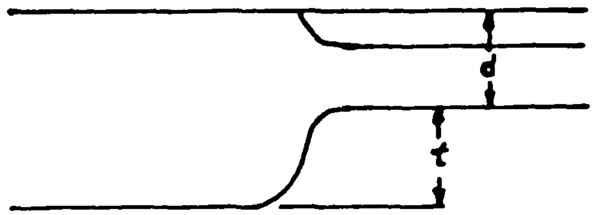
d
t

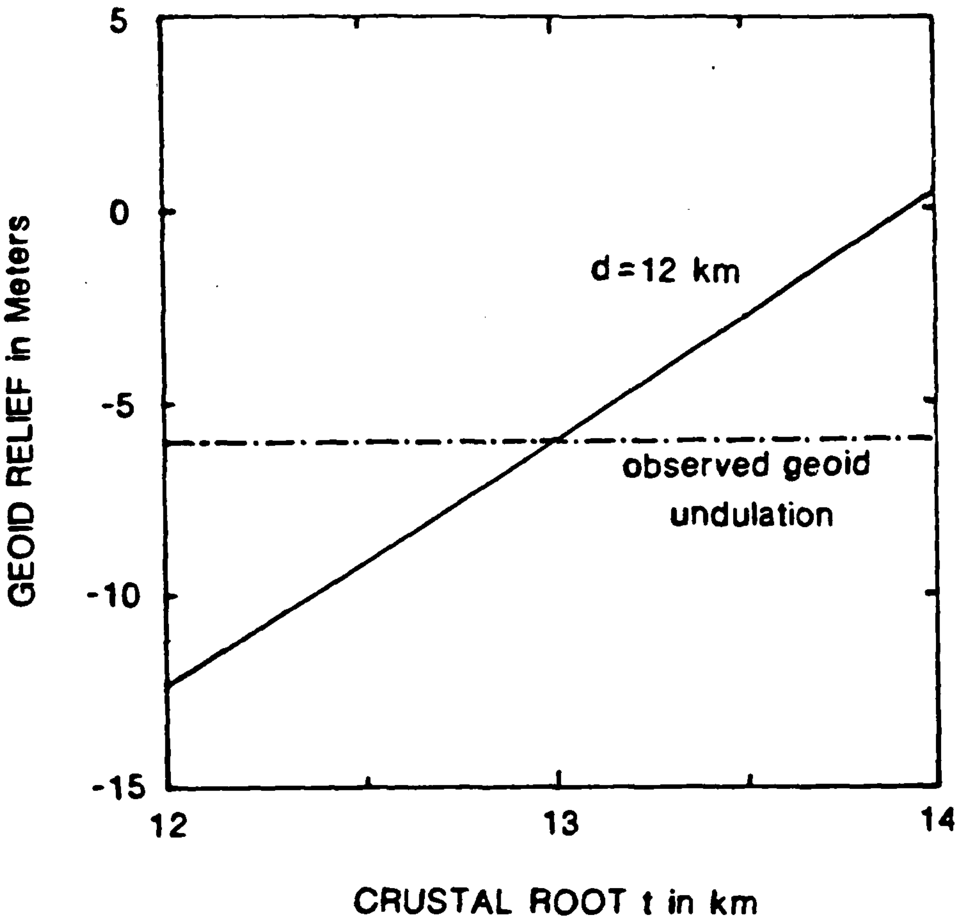
5
0
-5
-10
-15
12
13
14
GEOID RELIEF in Meters
CRUSTAL ROOT t in km
d = 12 km
observed geoid
undulation

Figure 3

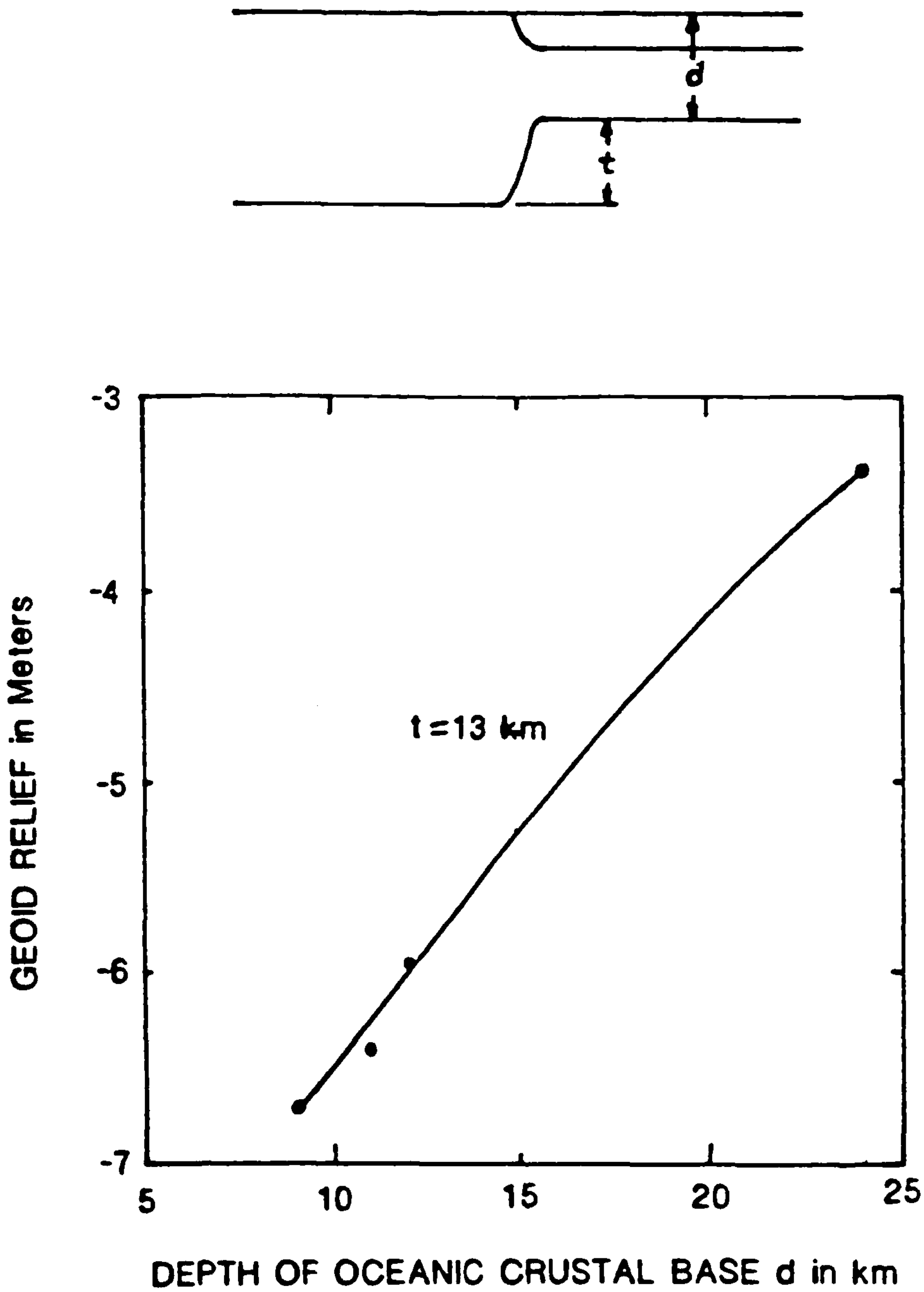
d
t
t=13 km
-3
-4
-5
-6
-7
5
10
15
20
25
GEOID RELIEF in Meters
DEPTH OF OCEANIC CRUSTAL BASE d in km

Figure 4

1985 USAF-UES SUMMER FACULTY RESEARCH PROGRAM

GRADUATE STUDENT SUMMER SUPPORT PROGRAM

Sponsored by the

AIR FORCE OFFICE OF SCIENTIFIC RESEARCH

Conducted by the

UNIVERSAL ENERGY SYSTEMS, INC.

FINAL REPORT

FTIR SPECTROSCOPIC STUDY OF HYDRAZINE INTERACTIONS WITH CLAY MINERALS

Prepared by:	Dr. Clifford T. Johnston
Academic Rank:	Assistant Professor
Department:	Soil Science
University:	University of Florida Gainesville, FL 32611
Research Location:	Environics Laboratory Air Force Engineering and Services Center Tyndall Air Force Base, Fl 32403
USAF Research:	Dr. Daniel A. Stone

Date:	May 13, 1985 to July 20, 1985
Contract No.	F49620-85-C-0013

FTIR SPECTROSCOPIC STUDY OF HYDRAZINE INTERACTIONS

WITH CLAY MINERALS

by

Clifford T. Johnston

ABSTRACT

Fourier Transform Infrared (FTIR) spectra of the [montmorillonite:water], [montmorillonite:hydrazine], and [kaolinte:hydrazine] complexes were obtained in a controlled environment (CE) FTIR cell as a function of pressure. A controlled environment FTIR cell fitted with Irtran (ZnS) windows was constructed for controlling the absolute pressure and gas composition of the vapor phase in contact with the clays during the sorption and desorption studies. Desorption studies of the [montmorillonite:hydrazine] and [kaolinite:hydrazine] complexes in the CE cell indicate that hydrazine is irreversibly adsorbed on the surfaces of these clays. Similar studies of the [montmorillonite:water] complex indicate, however, that water is not irreversibly adsorbed. The results from this study suggest that montmorillonite and kaolinte adsorb hydrazine more strongly than water. The inner hydroxyl stretching band of non-reacted kaolinite, which normally occurs at 3620 cm^{-1}, was observed to increase in frequency to 3628 cm^{-1} after contact with hydrazine vapor. The spectral data indicate that the $-NH_2$ moiety penetrates the siloxane-ditrigonal cavity on the interlamellar surface of kaolinite.

ACKNOWLEDGEMENTS

I would like to thank the Air Force Engineering and Services Center, the Air Force Office of Scientific Research/Air Force Systems Command, and Univesral Energy Systems for their coordinated provision of the Summer Facultly Research Program. The Summer Faculty Program provides an excellent short term research opportunity. Gratitude is also expressed to the personnel of the Environics Division laboratory for their support and providing access to the laboratory.

In particular, I would like to thank Dr. Daniel A. Stone for his collaboration, sponsorschip, and support during the summer program. In addition, I would like to thank Mr. Mike Henley for his technical and administrative assistance.

I. INTRODUCTION

The interaction of organic solute species with interlamellar layer aluminosilicate surfaces is a subject of interest in a number of disciplines including environmental fate and transport, catalysis, pharmacy, and petroleum geology. This area of research has always been a field of interest to soil and environmental scientists since clay-organic complexes are important components affecting the physical, chemical and biological properties of soils. Although the general behavior of clay-organic systems are unerstood, very little is known regarding the chemical mechanisms of solute interaction. Recent appplications of advanced physical methods (Stucki et al., 1980) such as electron spin resonance, nuclear magnetic resonance, quasi inelastic neutron scattering, Raman and Fourier Transform Infrared (FTIR) spectroscopy are providing powerful tools to probe the interfacial region of solute complexes with clay minerals and hydrous metal oxide surfaces.

Fourier transform infrared (FTIR) spectroscopy is a powerful vibrational spectroscopic method which has been developed commercially over the last 15 years. The principle advantages of FTIR spectroscopy over conventional dispersive IR instrumentation are related to (1) the digital file handling capability of the data aquisition system (e.g., multiplexing), and (2) the optical throughput advantage (Fellgets advantages) of the Michelson interferometer (Griffiths, 1985). Sample presentation methods commonly used in FTIR studies include transmission techniques (KBr pellets, self supporting fims), diffuse reflectance, attenuated total reflectance (cylindrical internal reflectance and prism ATR), and grazing angle surface reflection techniques such as internal refelectance absorption spectroscopy. Despite the numerous advantages of FTIR techniques over conventional dispersive instrumentation, this method has not been used previously to investigate organic or inorganic solute interactions with clay minerals.

Hydrazine and its chemical derivatives such as methyl-hydrazine and unsymmetrical dimethyl hydrazine are used extensively throughout the United States Air Force and Space Transportation System. Very little is know regarding the chemical mechanisms of hydrazine interactions with clay minerals and hydrous metal oxides. Barrios et al. (1977) studied stacking faults in kaolinite treated with hydrazine and observed that the IR spectrum of the [kaolinite:hydrazine] complex was perturbed significantly by the presence of hydrazine. Their data, however, was limited in resolution and was obtained with a dispersive instrument which was not capable of digital file comparison. Because of the extreme toxicity associated with these compounds (Lyon, 1974). this model laboratory study was initiated to better understand the fate and transport of hydrazine and its chemical derivatives in the environment.

II. RESEARCH OBJECTIVES

The overall mission of the 10 week study was to develop a FTIR methodology for investigating toxic solute interactions with clay minerals. The intial experimental objectives for the summer faculty program centered around the application of diffuse reflectance and cylindrical internal reflectance sample presentation methods to study hydrazine and water interactions with the selected clay minerals. Initial studies of the clay minerals indicated that the controlled environment (CE) cell would provide a more suitable sample presentation method for the solute interaction studies. The overall objective for the summer project was not altered by the choice of the CE cell over the reflectance sample presentation methods.

The clay minerals chosen for this study were the following:

Kaolinite, a low surface area, highly crystalline clay mineral. Classsified as a 1:1 layer silicate, kaolinite is the most abundant clay mineral in the world and is capable of forming very stable complexes with various organic compounds (Johnston et al. (1984); Olejnick et al. (1974)).

Montmorillonite, a high surface area (> 700 m^2/gram), poorly crystalline clay mineral. Montmorillonite is a highly reactive clay mineral due to the large surface area and abundance of constant charge exchange sites (i.e., functional groups) created by isomorphic substitution.

The solute species of interest were water and hydrazine.

Experimental Research Objectives

Prepare homoionic suspensions of Na-kaolinite and Na-montmorillonite.

Construct a controlled environment (CE) cell with the following requirements:

The IR windows, gas lines and cell body must be chemically inert to hydrazine and water

The IR windows of the CE cell must have suitable optical transmission in the 700 to 4000 wavenumber region.

The CE cell must be connected to a gas manifold and vacuum pumping station. The pumping station must be capable of pulling a vacuum of better than 0.0005 Torr.

Obtain baseline FTIR spectra of montmorillonite and kaolinite in the CE cell.

Introduce solute (e.g., hydrazine) vapor into the cell and observe changes in the FTIR spectra associated with time, absolute CE cell pressure and gas composition.

III. MATERIALS AND METHODS

The clay minerals chosen for this study were the KGa-1 kaolinite and SAz-1 montmorillonite reference clay minerals obtained from the Clay Minerals Source Repository at the Univ. of Missouri. A complete description of these clays including physical and chemical analysis, cation and anion exchange capacities, surface area determinations and a description of the clay genesis and sampling locations are given by Fripiat and van Olphen (1979).

Na-Montromillonite and Na-Kaolinite preparation

The untreated SAz-1 montmorillonite was washed several times in distilled-deionized water and the less-than 0.5 micron size fraction was obtained by centrifugation using the procedures developed by Sposito et al. (1981). Immediately after size fractionation the clay suspension was flocculated by the addition of 0.5 M NaCl. The flocculated montmorillonite suspension was then washed several times with the 0.5 M NaCl solution to insure complete sodium saturation of the exchange complex. Similar procedures were employed for the KGa-1 clay preparation with the exception that the less than 2.0 micron size fraction was collected. A complete description of the Na-kaolinite preparation procedures used in this study are given by Johnston et al. (1985).

FTIR spectrometer

FTIR spectra were obtained on a Nicolet 6000C (160SX) single beam FTIR spectrometer with a Nicolet 1280 data aquisition system operating under the NICOS operating system. A narrow band Mercury-Cadmium- Telluride (MCT) detector was used with an effective range of 700 to 5400 wavenumbers. A 4 mm aperture setting was used with no additonal gain amplification of the detector. All of the montmorillonite spectra were obtained using 4 cm^{-1} resolution corresponding to 4096 data point, data files. A preliminary FTIR study of the kaolinite clay showed that the FTIR spectra of kaolinite were instrument limited at 4 cm^{-1} resolution (i.e., the spectral features in the FTIR spectrum of kaolinite have linewidths (FWHM values) less than 4 cm^{-1}). The data were not instrument limited at 2 cm^{-1} resolution; thus, all FTIR spectra of kaolinite were obtained at 2 cm^{-1} resolution corresponding to 8192 data point, data files.

Controlled Environment Cell

A controlled environment (CE) cell was constructed in order to obtain the FTIR spectra of the clay complexes as a function of pressure and gas composition. The use of the CE cell was essential for working with a volatile, toxic compound such as hydrazine. A 10 cm pathlength, glass, cell body was used with a 25 mm o.d. The windows used in the cell were two 25 mm x 1 mm disk ZnS (Irtran) windows and were attatched to the cell using a metal frame. Silver chloride windows were used in the cell initially; however, hydrazine rapidly reduces Ag(I) to Ag-metal. Consequently, AgCl windows were not suitable for the hydrazine studies. ZnS (Irtran) was found to be chemically inert to hydrazine due to the higer reduction potential of zinc. Irtran windows were chosen for the CE cell despite the relatively high low-frequency cutoff of ZnS (around 700 wavenumbers). The ZnS windows were fitted to the cell using Viton O-rings and were held in place by a metal frame. The cell had a single gas outlet fitted with a teflon stopcock which was connected by glass and stainless steel tubing to the gas manifold and vacuum pumping station. The CE cell was placed within the sample compartment of the FTIR spectrometer with a gas line connecting the cell to the externally mounted gas manifold and vacuum pumping station. This connection allowed the absolute pressure of the CE cell to be changed and solute vapor to be introduced into the cell without breaking the purge in the sample compartment of the spectrometer. The pumping station consisted of a mechanical roughing pump in series with an oil diffusion pump and liquid nitrogen trap. Pressure within the cell was monitored using two pressure gauges, one calibrated for the 760 to 1 Torr region, and the other calibrated for the 0.00 to 10.00 Torr region.

Self-supporting films of Na-Montmorillonite

Self supporting clay films were prepared by depositing an aliquout of the dilute Na-montmorillonite suspension onto a piece of Saran wrap stretched over a flat glass plate. The clay films were dried by placing the glass plate in a drying oven for six hours operating at 50 Torr and 40 deg. C. The saran wrap was removed from the glass plate and the Na-montmorillonite clay films were seperated from the Saran wrap by running the plastic sheet over a knife edge. The resulting self-supporting clay films were then mounted in a 3/8" swagelock fitting and the entire fitting was then placed in the CE cell and the cell windows and metal framework were reinstalled. Several dilutions of the intial clay suspension were required because the intial clay films were too thick optically (IR optical density in the 900 cm^{-1} to 1200 cm^{-1} region was greater than 3 absorbance units {a.u.}). The clay films used in this study were approximately 3 mm x 3 mm and the optical density in the 900 cm^{-1} to 1200 cm^{-1} region was approximately 1.2 a.u. A preliminarly study of the interference fringes in the FTIR spectra of the clay film in the 5400 cm^{-1} to 3700 cm^{-1} region indicated that the clay film was approximately 15 microns thick.

Preparation of Na-KGa-1 kaolinite deposits on IRTRAN windows.

The crystal morphology of kaolinite particles is block like compared to the plate-like morphology of montmorillonite particles. Thus, self supporting films of kaolinite cannot be prepared. FTIR spectra of kaolinite were obtained by depositing dilute aliquots of the *Na-kaolinite suspension directly onto the inner surface of one of the Irtran windows used in* the CE cell. The resulting kaolinite deposit had an optical density of 0.8 a.u. in the 900 cm^{-1} to 1200 cm^{-1} region.

Data Handling

All FTIR spectra were collected and stored as single beam energy spectra. A typical sample-single-beam-energy spectrum is shown in Figure 1a. in the region of 700 cm^{-1} to 4200 cm^{-1}. This spectrum is of a thin, self supporting film of the SAz-1 montmorillonite in the CE cell in the purged FTIR spectrometer. The sharp groups of lines centered arount 1630 cm^{-1} and 3400 cm^{-1} are due to residual water vapor in the spectrometer. The strong doublet at 2330 cm-1 is due to residual CO_2 in the spectrometer and the broad feature at 3000 cm^{-1} is due to the energy response of the detector. The single beam energy spectra shown in Figures 1a-b show the positive energy response of the detector. As IR energy is absorbed by the sample less energy reaches the detector and a negative going band is observed. Absorbance FTIR spectra are obtained by ratioing two single beam energy spectra against each other according to the following equation:

$$(1) \qquad A_{absorbance} = \log_{10}\left(\frac{I_{reference}}{I_{sample}}\right)$$

Figure 1b shows the single beam energy spectrum of the empty , evacuated CE cell. The ratioed spectrum of the clay film (Figure 1c) was obtained by ratioing the single beam energy spectrum of the clay film in the CE cell (Figure 1a - sample) against the single beam energy spectrum of the evacuated empty CE cell (Figure 1b - reference) according to Eqt. (1). The ratioed spectrum corresponds to the IR absorbance spectrum of the clay film in the CE cell. Note that the IR bands due to the residual water and CO_2 vapor within the spectrometer have cancelled out because these IR features were present in both the sample and the reference single beam energy spectra.

The FTIR spectrometer utilizes a rapid scanning Michelson interferometer which is capable of obtaining a complete FTIR scan in the millisecond time domain. With 4 cm^{-1} resolution the Nicolet 6000C spectrometer is capable of collecting a complete scan in approximately 0.8 seconds. Calculating the Fourier transform of the collected interferogram takes approximately 20 seconds for a single interferogram collected at 4 cm^{-1} resolution, so that when kinetic information is desired, the interferograms are collected and stored rapidly and after the experiment is completed the stored data are Fourier transformed into the

frequency domain. The absorbance FTIR spectra of a thin film of montmorillonite obtained as an average of 1, 16, 64, and 512 scans are shown in Figure 2. The sample file used in calculating the absorbance spectrum labeled 1-scan in Figure 2 was collected and stored in less than 0.8 seconds. A scan of comparable quality and resolution using a conventional dispersive IR spectrometer would require a minimum scan time of several minutes. As the FTIR spectra shown in Figure 2 indicate, high quality FTIR spectra of montmorillonite clay can be obtained in less than 1 second. This feature of FTIR spectroscopy has considerable promise for future FTIR kinetic investigations of solute species with surfaces.

IV. RESULTS AND DISCUSSION

Desorption studies

FTIR spectra of the [Montmorillonite:Water] complex are shown in Figure 3 as a function of the $\log_{10}$ value of the absolute pressure of the CE cell. All of the spectra are plotted with the same absorbance dispersion and the y-offset of the plot corresponds to the $\log_{10}$ of the absolute pressure of the CE cell at which the scan was obtained. The absorbance spectrum shown at the top of Fig. 3 corresponds to an absolute pressure of 760 Torr ($\log_{10}(760) = 2.88$); the bottom scan at a $\log_{10}$ value of -3.00 corresponds to an absolute pressure of 0.001 Torr. The absorbance spectra shown in Figure. 3 were obtained by ratioing the single-beam-energy spectra of the clay film in the CE cell obtained at a particular pressure value against the single-beam-energy spectrum of the empty, evacuated CE cell. The resulting IR absorbance spectra correspond to (1) water adsorbed onto the montmorillonite clay film, (2) water vapor within the cell and (3) water adsorbed onto the ZnS windows. An initial study of water sorption in the CE cell without the clay film showed that spectral contributions from (2) and (3) were negligible with respect to the large amount of water (or hydrazine) adsorbed onto the clay film.

The IR bands at 3400 cm^{-1} and 1642 cm^{-1} are the O-H stretching and bending modes respectively of water adsorbed onto the clay. The IR bands at 824 cm^{-1}, 909 cm^{-1}, 1022 cm^{-1}, 1085 cm^{-1}, 1127 cm^{-1}, and 3633 cm^{-1} are IR active vibrational modes of the montmorillonite clay. A complete discussion of the vibrational modes of montmorillonite and related clay minerals is given in a review by Farmer (1974). The observed decrease in intensity of the 3400 cm^{-1} and 1642 cm^{-1} bands as the pressure is decreased in the CE cell indicates that water is being progressively desorbed from the clay. Similar data in the 2800 cm^{-1} to 4000 cm^{-1} region are shown in Figure 4. The 3400 cm^{-1} and 1642 cm^{-1} bands are absent in the bottom spectrum corresponding to a $\log_{10}$ value of -3 (Figures 3-4). This observation indciates that virtaully all of the water has been removed from the surfaces of the clay at this pressure value. The integrated area of the 3400 cm^{-1} and 1642 cm^{-1} bands is

proportional to the amount of water on the clay. Consequently, with the appropriate data analysis of the spectra shown in Figures 3 and 4, a quantitative determination of the amount of the water (or hydrazine) adsorbed on the clay at a particular pressure value is possible.

Sposito and Prost (1982) have reviewed previous IR studies of the [montmorillonite-water] complex and observed that the IR spectra (obtained with dispersive instrumentation) were strongly dependent on the type of exchangeable cation present. They conclude from the IR data that water resides within two distinct environments on montmorillonite: the water adsorbed on interlamellar surfaces and the water on the external and interstitial surfaces of the clay. Quasi inelastic neutron scattering, nuclear magnetic resonance and dielectric relaxation studies (Spostio and Prost, 1982) indicate that the water adsorbed on the interlamellar surface of the clay is: (1) coordinated to exchangeable metal cations, and (2) this water is more tightly bound and less mobile than water adsorbed on the external and interstitial surfaces of the clay.

<u>"Difference desorption" FTIR spectra</u>

A powerful feature of FTIR spectroscopy is the digital file handling capability of the data acquisition system. As discussed in the data handling section, each FTIR absorbance spectrum represents the ratio of a "sample" single-beam energy spectrum ratioed against a "reference" single-beam energy spectrum according to Eqt 1. The method for calculating "difference desorption" spectra in the present study is given below:

Collect a series of single beam energy spectra of the clay film in the CE cell as a function of pressure. The same "raw" single beam energy spectra are used to calculate the absorbance FTIR spectra shown in Figures 3-4 as the "difference desorption" FTIR spectra shown in Figures 5-6, the only difference was the choice of the reference single beam energy files the sample files were ratioed against.

Calculate "difference desorption" spectra corresponding to a given pressure value by ratioing the sample-single-beam energy spectrum against the reference single beam energy spectrum obtained at the next lower pressure value. For example, the "difference desorption" spectrum shown at the top of Figure 5 was obtained by ratioing the single beam energy spectrum obtained at 760 Torr against the 330 Torr single beam energy spectrum.

Plot the "difference desorption" spectra as a function of the $\log_{10}$ value of the pressure at which the sample single beam energy spectrum was obtained.

The difference spectra obtained by this procedure reflect only those <u>changes</u> which occured in the CE cell between the two pressure values. Since both the sample and the reference spectra

correspond to the clay film in the CE cell, the IR bands from the clay are ratioed against each other and effectively cancel out. Pressure assingments for the labeled "difference desorption" spectra shown in Figures 5-6 are given below.

Sample SBES	Reference SBES	Absorbance spectra	
760 Torr	330 Torr	760:330	Figure 5a
330 Torr	180 Torr	330:180	Figure 5b
180 Torr	50 Torr	180:50	Figure 5c
50 Torr	22 Torr	50:22	Figure 5d
22 Torr	17 Torr	22:17	Figure 5e

The "difference desorption" spectra taken at higher pressure values (Figures 5a-c, 6a-c) are relatively featureless indicating that little water is desorbed from the clay at these pressure values. The vapor pressure of waterat 25 degrees Centigrade is 23.7 Torr; thus, the activity of water in the vapor phase would not be expected to decrease until the absolute pressure in the CE cell decreases below 23.7 Torr. The spectral results are consistent with this fact; very little change occurs in the FTIR spectra until the absolute pressure drops below approximately 20 Torr. The large, positve IR bands in the"difference desorption" spectra shown in Figures 5d and 6d indicate that a significant amount of water is removed from the surface of the clay between 50 Torr and 22 Torr. Comparing spectra 5d to 5e and spectra 6d to 6e several significant perturbations are observed. First, the band position fo the 3136 cm^{-1} band (spectra 5e, 6e) increases in frequency to 3201 cm^{-1} in spectra 5f, 6f). The reverse behavior is observed with the 3581 cm^{-1} band which decreases in frequency to 3544 cm^{-1} (Figures 5f, 6f). Similar desorption data, which has not been analyzed, has been obtained for the [montmorillonite:hydrazine] complex (Figures 7-8), and the [kaolinite:hydrazine] complex (Figures 9-10).

These spectral features which are readily apparent in the "difference desorption" spectra (Figures 5-6) are very difficult to distinguish in the absorbance FTIR spectra shown in Figures 3-4. These "difference desoprtion" spectra provide unique spectral information regarding the vibrational energy environment of water molecules being removed from the surface of the clay. Conclusive band assignments for these data have not been made, however, the data indicate that the vibrational energy of water adsorbed on the surface is strongly pressure dependent.

The "difference desorption" spectra presented in Figures 5-6 provide two basic types of information. First, the integrated intensities of the water bands at 1642 cm^{-1} and 3400 cm^{-1} are directly proportional to the amount of water removed from the surface of the clay

during a given drop in pressure. This method could then be used a a quantitative tool to determine the amount of solute adsorbed on the surface of the clay. Secondly, the "difference desorption" spectra provide an extremely sensitive probe to determine the vibrational energy of solute species (e.g., water, hydrazine, etc.) being desorbed from the surface of the clay as a function of pressure. As band assignments for this system become known, this method could provide a useful tool to discriminate between water adsorbed on the external surfaces of the clay versus water on the interlamellar surfaces of the clay.

Long Term Stability of Clay Complexes.

[montmorillonite:water] complex

Absorbance FTIR spectra in the 700 cm^{-1} to 4200 cm^{-1} region of the [montmorillonite:water] complex are shown in Figure 11. Spectrum 11a corresponds to the dry SAz-1 montmorillonite clay film in the CE cell before water vapor was introduced. The bands at 845 cm^{-1}, 919 cm^{-1}, 987 cm^{-1}, 1128 cm^{-1}, 3280 cm^{-1} and 3615 cm^{-1} are all due to IR absorption of the montmorillonite clay (Farmer, 1974). The absorbance FTIR spectrum of the clay film in contact with standing water at 760 Torr is shown in Figure 11b. The strong bands at 3400 cm^{-1} and 1642 cm^{-1} (Figure 11b) are due to water adsorbed onto the clay film. Upon evacuation of the CE cell for 24 hours at a vacuum of greater than 0.001 Torr the absorbance spectrum shown in Figure 11c was obtained. The abscence of the 1642 cm^{-1} and 3400 cm^{-1} bands indicates that virtually all of the water adsorbed onto the clay has been removed. An expanded plot of the absorbance FTIR spectra in the 2800 cm^{-1} to 4000 cm^{-1} region is shown in Figures 12a-c. The observed similarity between the before-exposure spectrum (Figure 11a, 12a) and the after-exposure-vacuum spectrum (Figure 11c, 12c) indicate that water is not irreversibly adsorbed onto the surface of the clay.

[montmorillonite:hydrazine] complex

Similar long term stability FTIR spectra were obtained for the [montmorillonite:hydrazine] complex. Figure 13a shows the absorbance FTIR spectrum of the thin film of montmorillonite before exposure to hydrazine vapor in the evacuated CE cell. The absorbance FTIR spectrum shown in Figure 13b corresponds to the clay film in contact with standing hydrazine at 760 Torr and 25 degrees C. The large bands at 1287 cm^{-1}, 1616 cm^{-1}, 3194 cm^{-1}, and 3342 cm^{-1} correspond to hydrazine adsorbed onto the clay. The significant intensity of the hydrazine bands with respect to the clay bands indicates that a proportionally large amount of hydrazine has been adsorbed onto the clay. To remove (i.e., desorb) the hydrazine from the clay, a high vacuum was applied to the CE cell. The absorbance FTIR spectrum shown in Figure 13c was obtained after a vacuum of 0.001 Torr had been applied on the CE cell for 24 hours. In contrast to the results obtained for the [montmorillonite:water] complex, not all of the hydrazine was removed from the surface of

the clay after the 24 hour evacuation as indicated by the significant intensity of the hydrazine bands at 3194 cm^{-1}, 3284 cm^{-1}, 3365 cm^{-1} (Figure 13c). An expanded plot of the long term stability FTIR spectra for the [montmorillonite:hydrazine] spectra in the 2800 cm^{-1} to 4000 cm^{-1} region are shown in Figures 14a-c. The spectral results presented here provide strong evidence that hydrazine is irreversibly adsorbed onto the surface of clay. This hypothesis is supported by the analogous desorption study of the [montmorillonite:water] complex which showed that using identical analytical procedures all of the water adsorbed onto the clay was removed after a vacuum of 0.001 Torr had been applied for 24 hours. The data presented in Figures 13 and 14 indicate that hydrazine is more strongly adsorbed than water on the surface of montmorillonite.

[kaolinite:hydrazine] complex

Similar long term stability FTIR spectra were obtained for the [kaolinite:hydrazine] complex (Figures 15a-c, 16a-c). The FTIR spectrum of unreacted KGa-1 kaolinite are presented in Figure 15a in the 700 cm^{-1} to 4200 cm^{-1} region, an expanded plot of this spectrum in the 2800 cm^{-1} to 4000 cm^{-1} region is presented in Figure 16a. The sharper lines in the kaolinite spectrum compared to the montmorillonite spectrum are a result of the more crystalline structure of kaolinite. The relatively sharp IR bands at 3620 cm^{-1}, 3652 cm^{-1}, 3669 cm^{-1} and 3692 cm^{-1} have been assigned to the O-H stretching modes of the inner and inner surface hydroxyl groups of kaolinite. The 3620 cm-1 band has conclusively been assigned to the inner hydroxyl group and the 3652 cm^{-1}, 3669 cm^{-1}, and 3692 cm^{-1} bands all correspond to the inner-surface hydroxyl groups (Johnston et al., 1985).

After exposure to hydrazine vapor the intensity of the inner-surface hydroxyl bands are reduced considerably and the position of the inner hydroxyl band has been blue-shifted to 3628 cm^{-1}. The reduced intensity of the inner-surface O-H bands has been reported previously in the literature (Ledoux et al., 1966; Olejnik et al., 1970, Johnston et al., 1984), however, the blue-shift in frequency of the inner hydroxyl group has not been reported previously. This unusual observation suggests that the hyrdrazine molecules residing in the interlamellar region of kaolinite are are small enough to penetrate the siloxane ditrigonal cavity and interact with the inner hydroxyl group. Since the $-NH_2$ functional group is electropositive the increased interaction with the inner -OH group results in a shift in frequency to higher energy due to mutual repulsion. Additional studies of this system using Raman, FTIR, NMR and X-ray diffraction techniques are in preparation.

Similar analytical procedures as those used in the desorption studies of the [montmorillonite:water] and [montmorillonite:hydrazine] complexes were employed to remove the adsorbed hydrazine. After exposure to Hydrazine vapor for 36 hours, a high vacuum of greater than 0.0005 Torr was applied to the CE cell. The absorbance FTIR spectra shown in Figures 15c and 16c were obtained after pulling a vacuum of 0.0005 Torr for 24 hours. Similar to the results obtained for the [montmorillonite:hydrazine] complex not all of

the adsorbed hydrazine is removed after evacuation of the CE cell for 24 hours. The absorbance FTIR spectra presented here provide spectroscopic evidence that kaolinite forms a very strong complex with hydrazine. The position of -OH stretching bands shown in Figure 16c indicate that even after the prolonged evacuation of the CE cell the position of the inner hydroxyl group remains blue shifted from 3620 cm-1 to 3628 cm^{-1}. The position of the hydrazine bands at 3361 cm^{-1} and 3225 cm^{-1} are considerably perturbed from their normal solution values indicating that the intercalated hydrazine molecules are in a more restricted conformation than hydrazine molecules adsorbed on the external surfaces of the clay.

V. RECOMENDATIONS

The application of FTIR spectroscopy to the study of toxic solute interactions with montmorillonite and kaolinte has resulted in several significant findings which are summarized below:

1. The results obtained in this report represent the first application of FTIR spectroscopy to the study of toxic solute interactions with clay minerals. This techniques provides a powerful tool with which to probe solute interactions with environmentally significant substrates such as clay minerals or hydrous metal oxides. This technique is capable of providing two important types of information: first, the amount of solute adsorbed onto a particular surface can be determined and second, the vibrational energy environment of the adsorbed solute species can be studied. The latter information relates directly to the chemical mechanisms of interaction (e.g., bond strength, complex stability etc.)

2. The FTIR data obtained in the CE cell indicate that hydrazine was strongly adsorbed by both montmorillonite and kaolinite. After prolonged evacuation of the CE cell under a high vacuum a considerable amount of hydrazine was observed to remain on the surface of the clay indicating that hydrazine was irreversibly adsorbed.

3. The "difference desorption" FTIR spectra of the [montmorillonite: hydrazine], [montmorillonite:water], and [kaolinite:hydrazine] complexes provide novel information regarding the vibrational energy environment of solute molecules being desorbed as a function of the absolute pressure in the CE cell. The methodology developed during this study may provide a spectroscopic method capable of discriminating between solute molecules adsorbed on interlamellar clay surfaces versus those adsorbed on the external or interstitial surfaces of the clay.

Specific experiments to be considered for future studies in this area are described in detail in a follow-up "mini-grant" proposal submitted to Universal Energy Stystems/Air Force Office of Scientific Research.

REFERENCES

Barrios, J.; Plancon, A.; Cruz, M. I.; and Tchoubar, C. (1977) "Qualitative and Quantitative Study of Stacking Faults in a Hydrazine Treated Kaolinite-Relationship with the Infrared Spectra," Clays and Clay Minerals **25**:422-429.

Farmer. V.C. (1974) "The Layer Silicates" Chap 15 in The Infrared Spectra of Minerals (Bartholomew Press)

Fripiat, J.J; and Van Olphen, H. (1979) Data Handbook for Clay Materials and Other Non-Metallic Minerals Pergamon Press, New York

Griffiths, P.R. (1975) Chemical Fourier Transform Infrared Spectroscopy (Wiley-Interscience) New York.

Johnston, C.T.; Sposito, G.; Bocian, D; and Birge, R.R. (1984) "Vibrational Spectroscopic Study of the Interlamellar Kaolinite-Dimethyl Sulfoxide Complex" J. Phys. Chem. **88**:5959-5964.

Johnston, C.T.; Sposito, G; and Birge, R.R. (1985) "A Raman Spectroscopic Study of Kaolinite in Aqueous Suspension" Clays and Clay Minerals In press.

Ledoux, R. L., and White, J.L. (1966) "Infrared Studies of Hydrogen Bonding Interaction Between Kaolinite Surfaces and Intercalated Potassium Acetate, Hydrazine, Formamide, and Urea" J. Colloid and Interface Sci. **21**:127-152.

Lyon (1974) "Evaluation of Carcinogenic Risk of Chemicals to Man" in International Agency for Research on Cancer.

Olejnik, S.; Posner, A.M.; and Quirk, J.P. (1971) "The IR Spectra of interlamellar kaolinite amide complexes- I. The complexes of Formamide, N-Methylformamide, and Dimethylformamide" Clays and Clay Minerals **19**:83-94.

Sposito, G., Holtzclaw, K.H., Johnston, C.T., and LeVesque-Madore, C.S. (1981) "Thermodynamics of Sodium-Copper Exchange on Wyoming Bentonite at 298 K," Soil Sci. Soc. Am. J. **45**:1079-1084.

Sposito, G. and R. Prost (1982) "Stucture of Water Adsorbed on Smectites" Chemical Reviews **82**:553-573.

Stucki, J.W., and W.L. Banwart, (1980) Advanced Chemical Methods for soil and Clay Mineral Research. Elsevier.

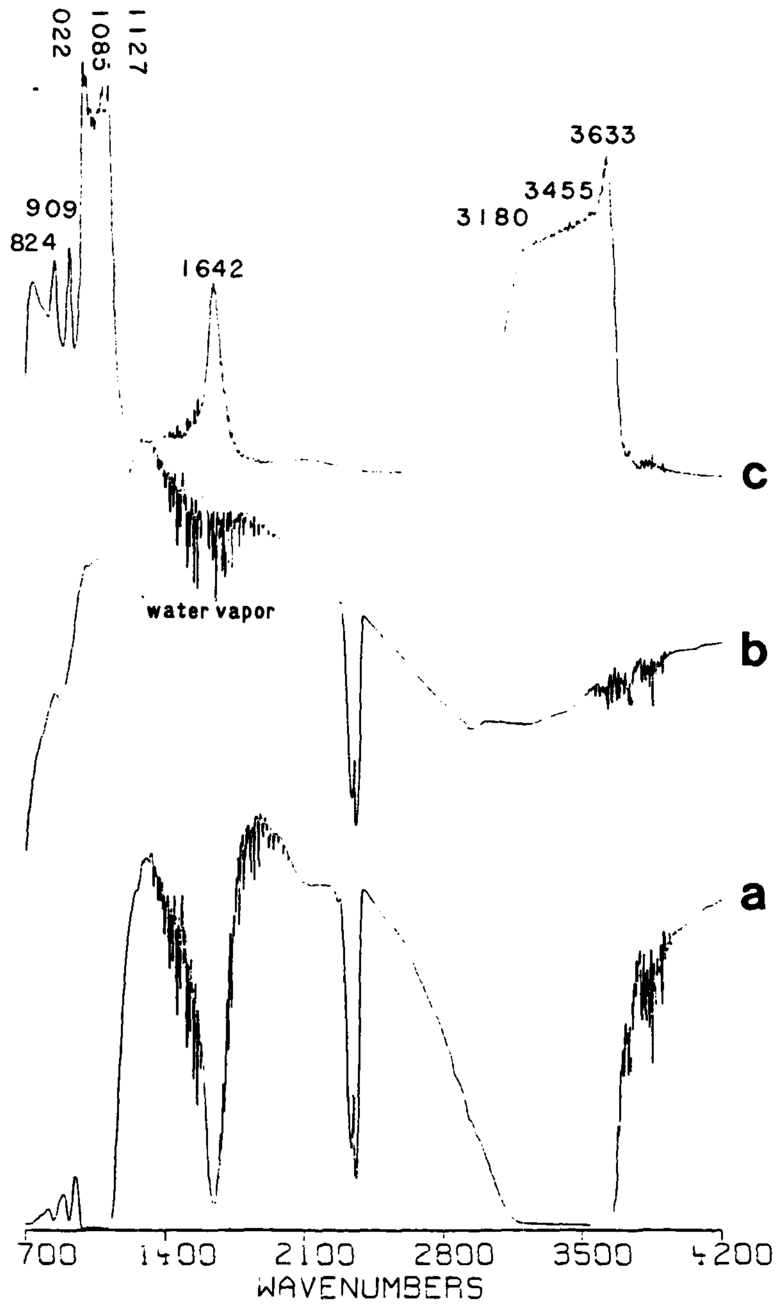

Figure 1 FTIR spectra in the 700 cm^{-1} to 4200 cm^{-1} region. (1a), single beam energy spectrum of clay film in contact with standing water in CE cell at 760 Torr; (1b), single beam energy spectrum of empty, evacuated CE cell; (1c), absorbance spectrum of (1a) ratioed against (1b).

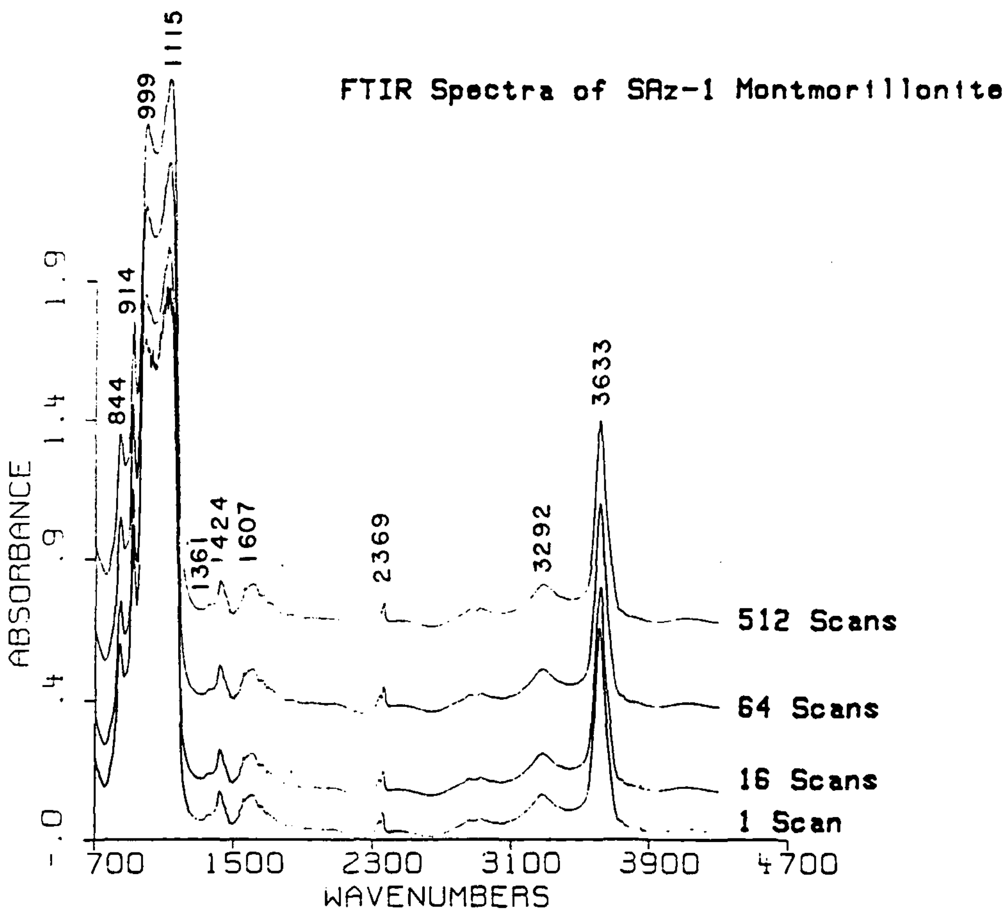

Figure 2 Absorbance FTIR spectra in the 700 cm^{-1} to 4200 cm^{-1} region of a thin film of SAz-1 montmorillonite mounted in the CE cell obtained as an average of 1, 16, 64, and 512 scans.

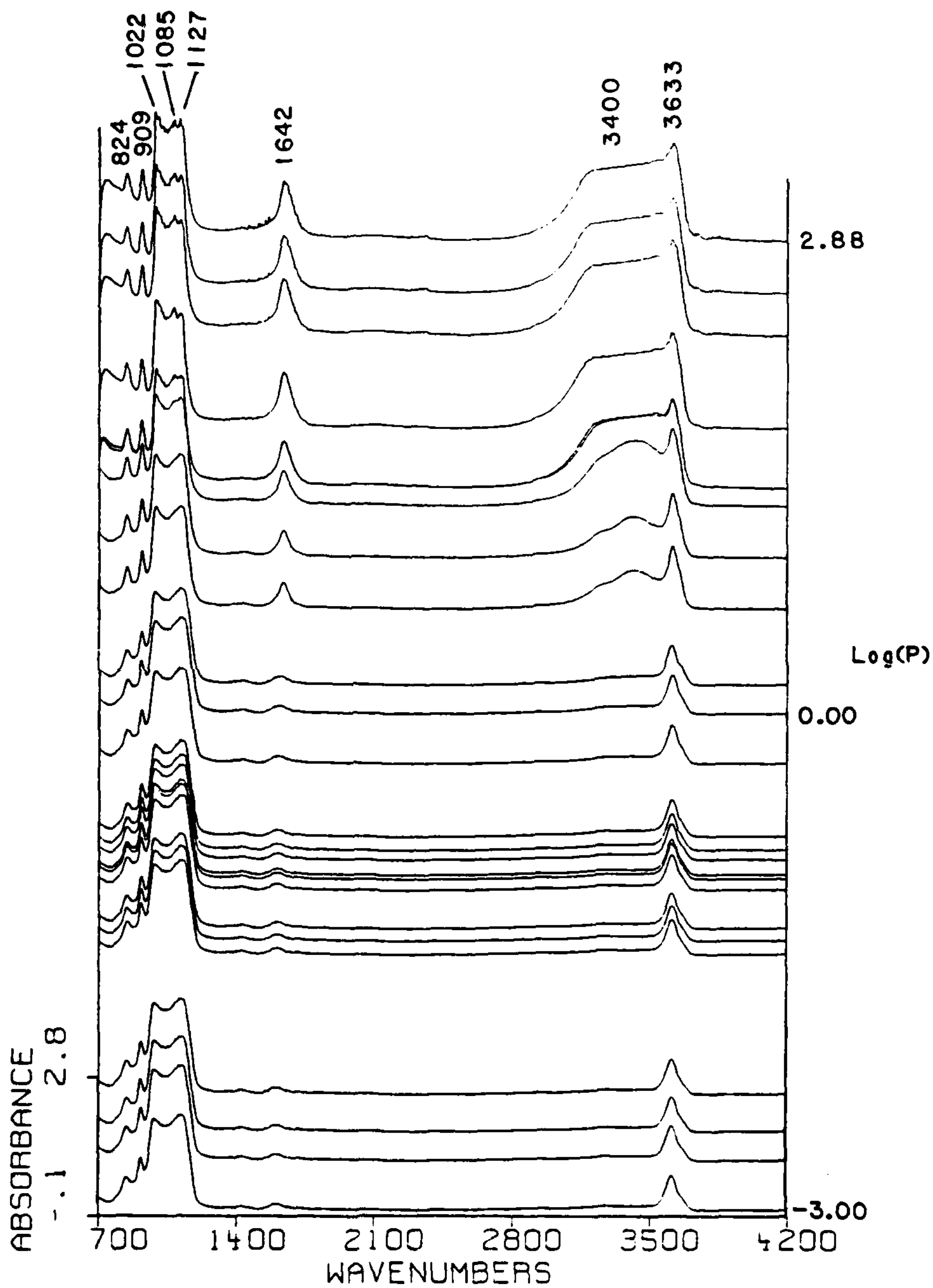

Figure 3 Absorbance FTIR spectra in the 700 to 4200 cm^{-1} region of a thin film of SAz-1 montmorillonite in the CE cell. The y-offset of each spectrum corresponds to the $\log_{10}$ value of the absolute pressure of the CE cell at which the spectrum was obtained. All data files in this plot were ratioed against the reference single beam energy spectrum of the empty evacuated CE cell.

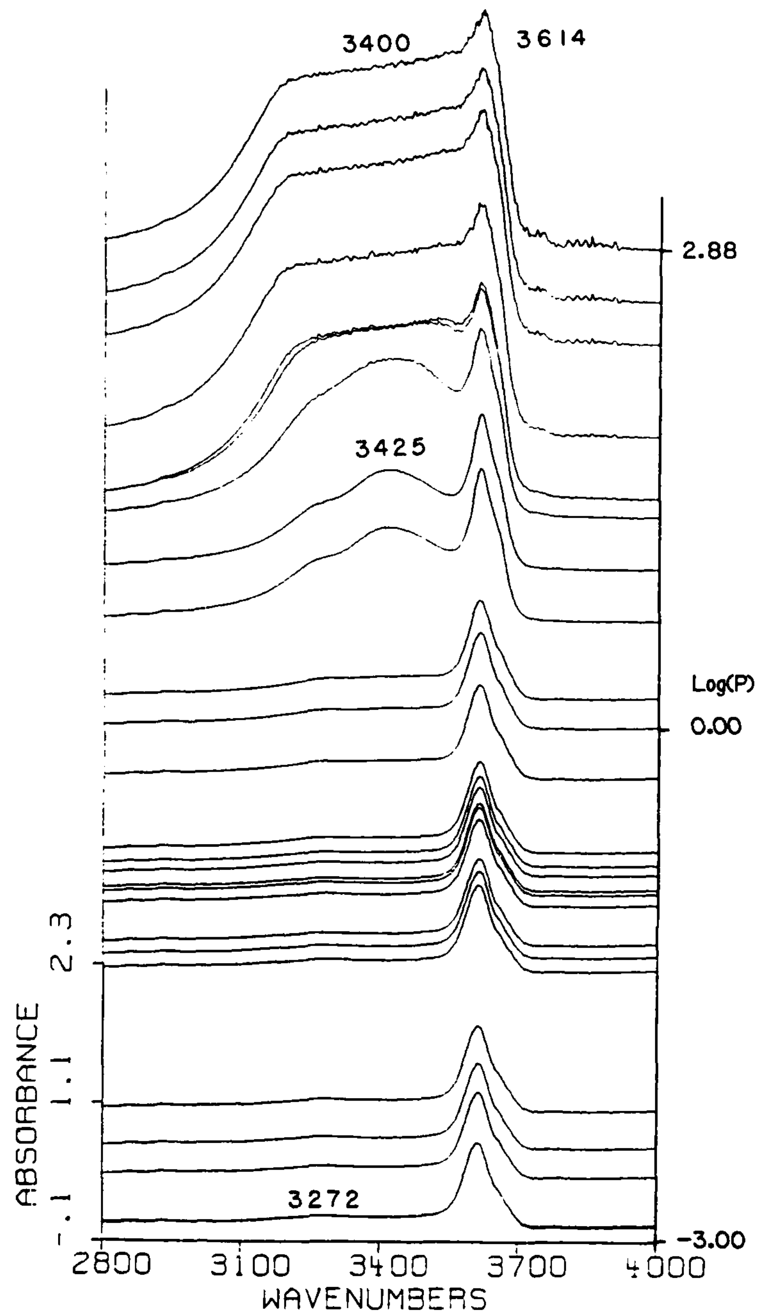

Figure 4 Absorbance FTIR spectra in the 2800 cm^{-1} to 4000 cm^{-1} region of a thin film of SAz-1 montmorillonite in the CE cell. The y-offset of each spectrum corresponds to the $\log_{10}$ value of the absolute pressure of the CE cell at which the spectrum was obtained. All data files in this plot were ratioed against the reference single beam energy spectrum of the empty evacuated CE cell.

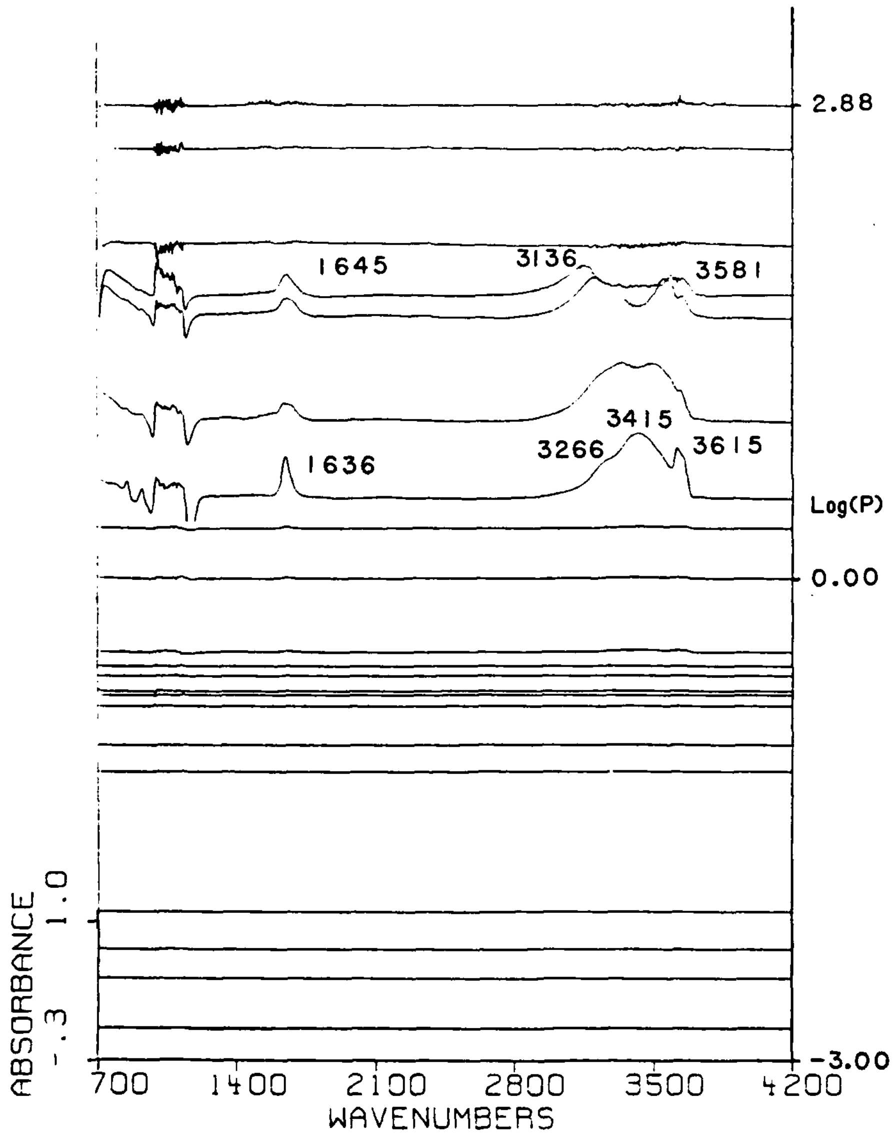

Figure 5 "Difference desorption" FTIR spectra in the 700 cm^{-1} to 4200 cm^{-1} region of the [montmorillonite:water] complex. The y-offset of each spectrum corresponds to the log_{10} value of the absolute pressure in the CE cell at which the spectra were obtained. The spectra were ratioed against the single beam energy spectra of the clay film in the CE cell obtained at the next lower pressure value.

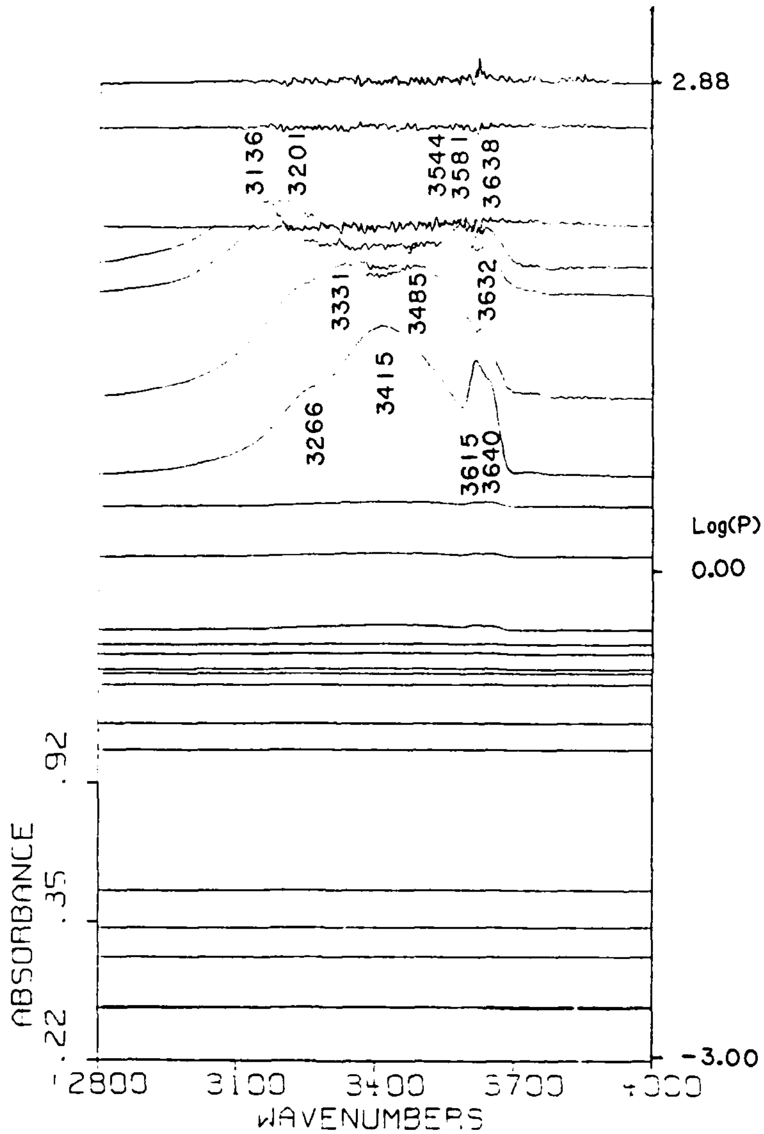

Figure 6 "Difference desorption" FTIR spectra in the 2800 cm^{-1} to 4000 cm^{-1} region of the [montmorillonite:water] complex. The y-offset of each spectrum corresponds to the log_{10} value of the absolute pressure in the CE cell at which the spectra were obtained. The spectra were ratioed against the single beam energy spectra of the clay film in the CE cell obtained at the next lower pressure value.

AD-A166 177 UNITED STATES AIR FORCE SUMMER FACULTY RESEARCH PROGRAM 06/15
1985 TECHNICAL RE (U) UNIVERSAL ENERGY SYSTEMS INC
DAYTON OH R C DARRAH ET AL DEC 85 AFOSR-TR-86-0140
UNCLASSIFIED F49620-85-C-0013 F/G 5/1 NL

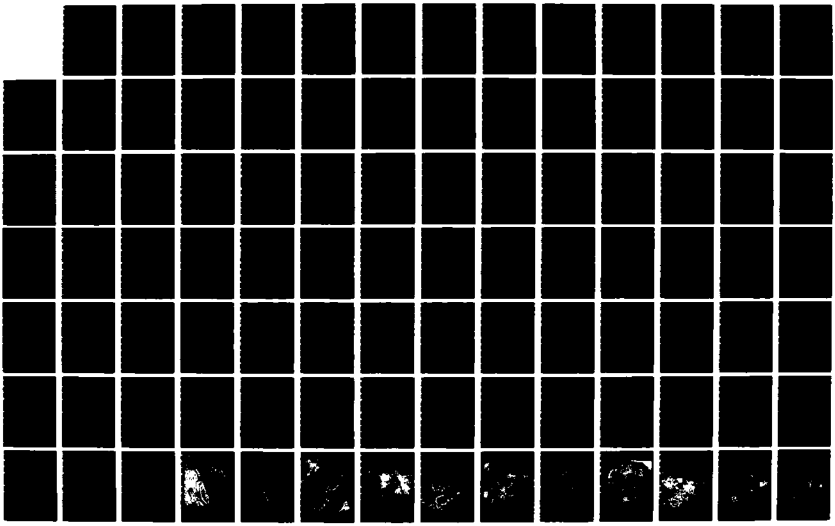

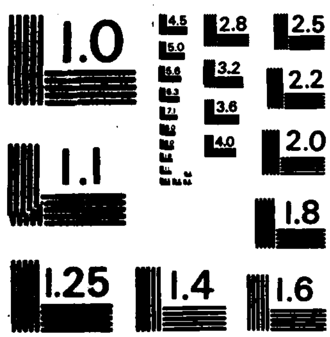

MICROCOPY RESOLUTION TEST CHART
NATIONAL BUREAU OF STANDARDS-1963-A

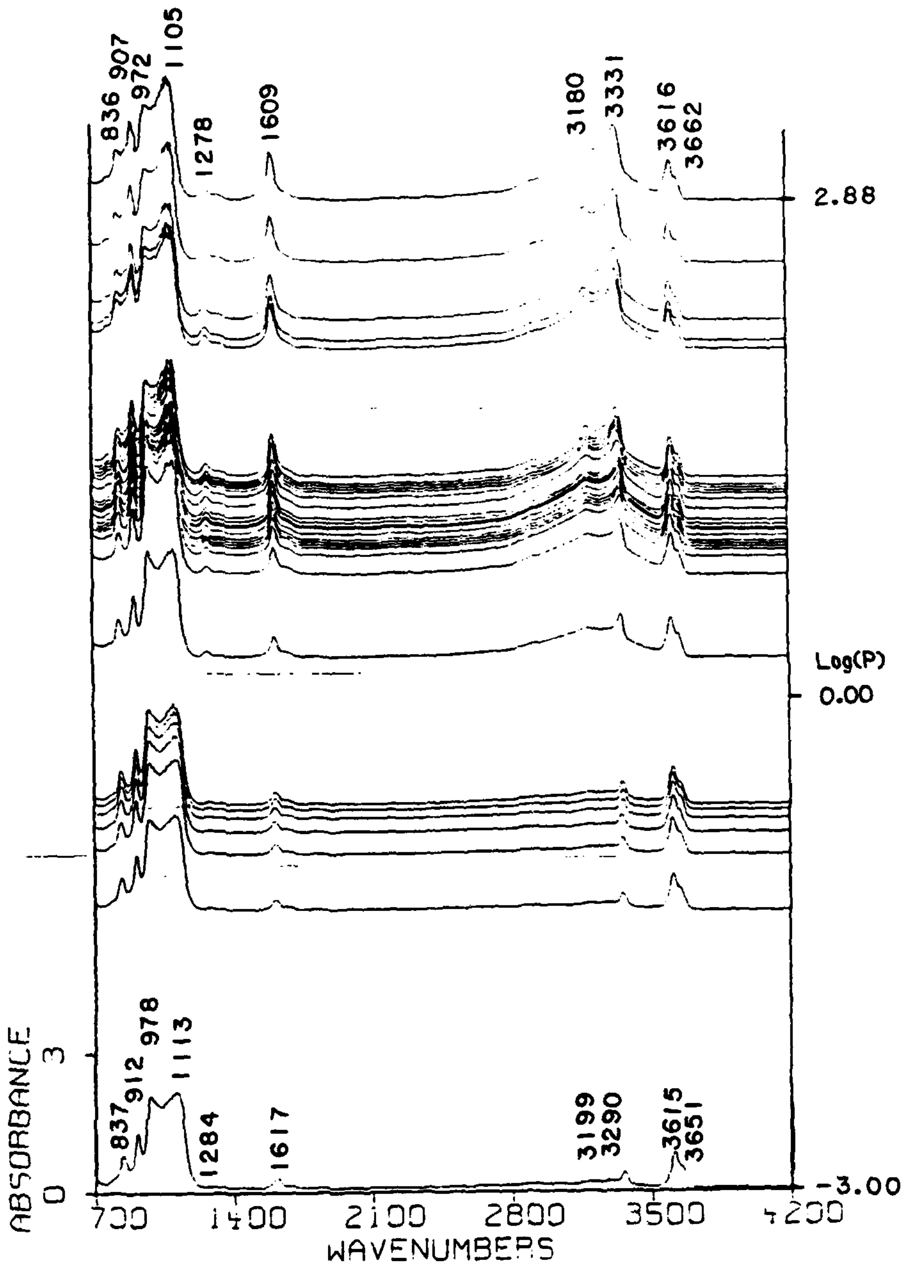

Figure 7. Absorbance FTIR spectra in the 700 cm^{-1} to 4200 cm^{-1} region of the [montmorillonite:hydrazine] complex in the CE cell. The y-offset of each spectrum corresponds to the $\log_{10}$ value of the absolute pressure of the CE cell at which the spectrum was obtained. All data files in this plot were ratioed against the reference single beam energy spectrum of the empty evacuated CE cell.

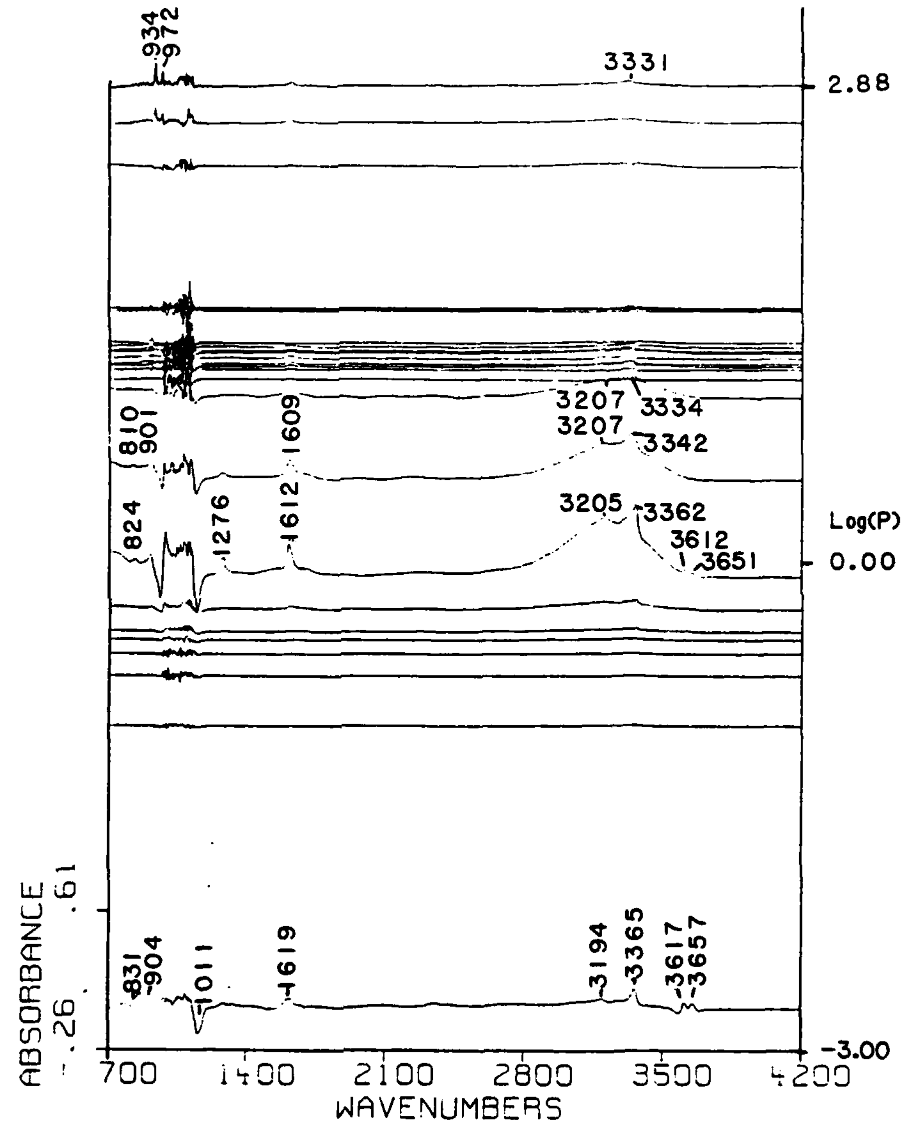

Figure 8 "Difference desorption" FTIR spectra in the 700 cm^{-1} to 4200 cm^{-1} region of the [montmorillonite:hydrazine] complex. The y-offset of each spectrum corresponds to the $\log_{10}$ value of the absolute pressure in the CE cell at which the spectrum was obtained. The spectra were ratioed against the single beam energy spectra of the clay film in the CE cell obtained at the next lower pressure value.

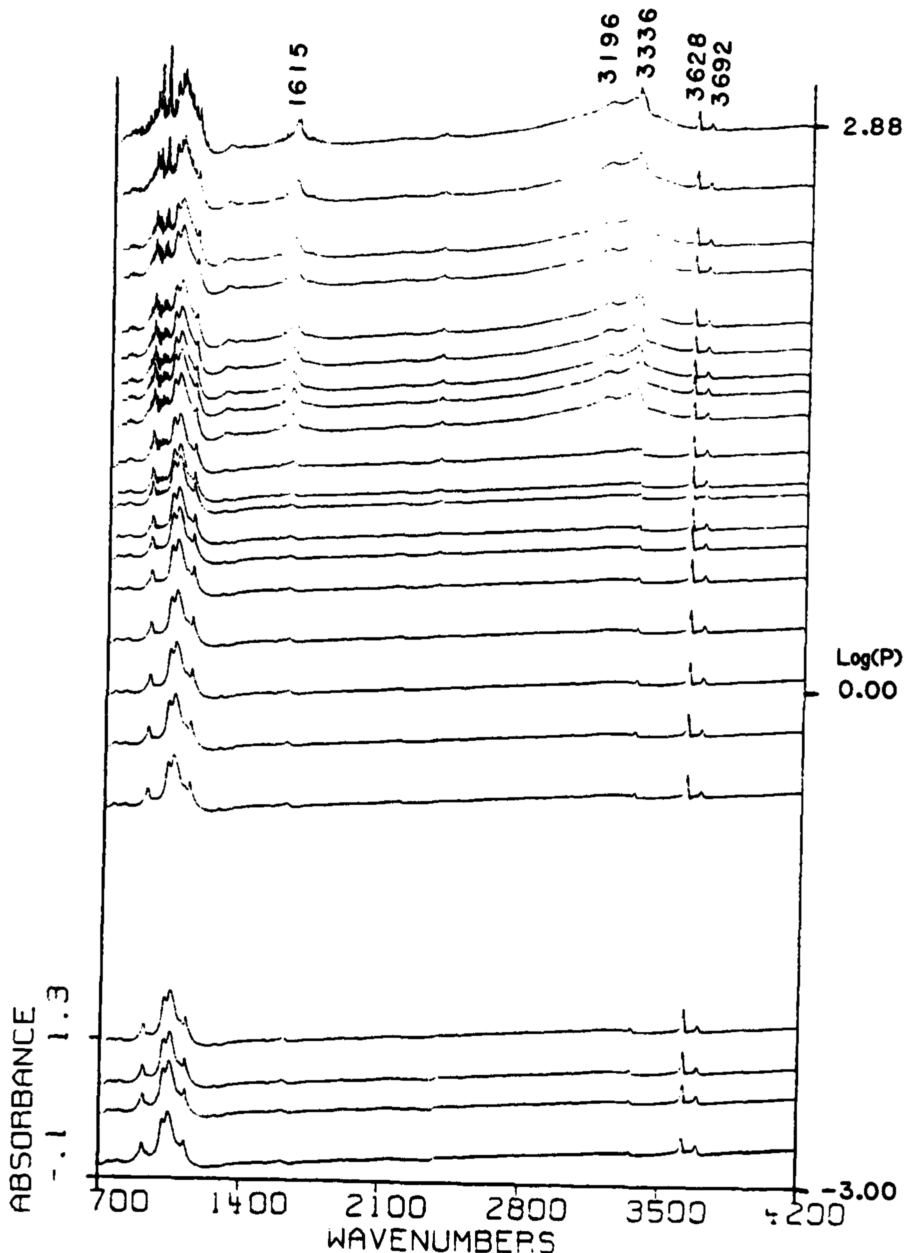

Figure 9 Absorbance FTIR spectra in the 700 cm^{-1} to 4200 cm^{-1} region of the [kaolinite:hydrazine] complex in the CE cell. The y-offset of each spectrum corresponds to the $\log_{10}$ value of the absolute pressure of the CE cell at which the spectrum was obtained. All data files in this plot were ratioed against the reference single beam energy spectrum of the empty evacuated CE cell.

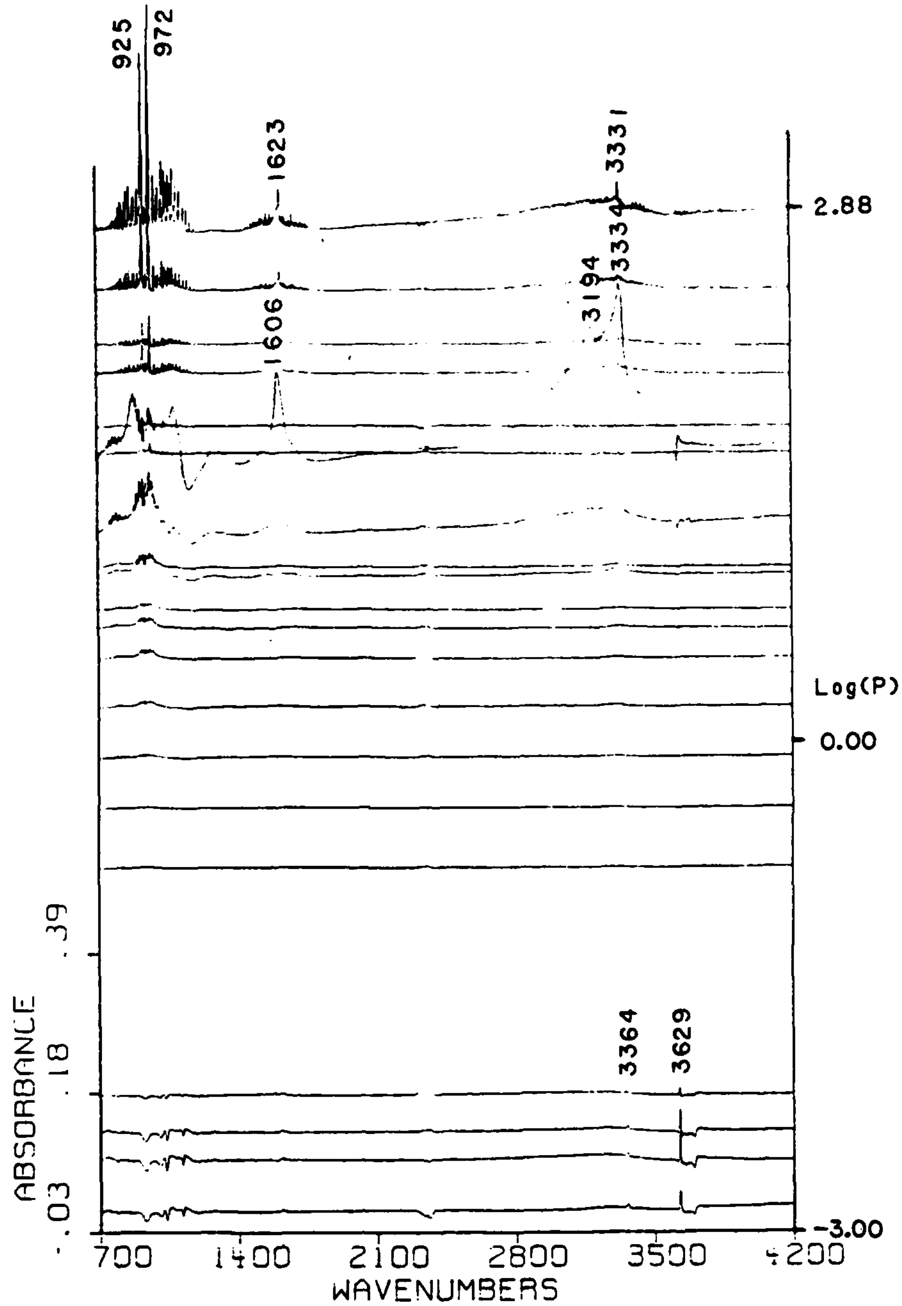

Figure 10 "Difference desorption" FTIR spectra in the 700 cm^{-1} to 4200 cm^{-1} region of the [kaolinite:hydrazine] complex. The y-offset of each spectrum corresponds to the $\log_{10}$ value of the absolute pressure in the CE cell at which the spectrum was obtained. The spectra were ratioed against the single beam energy spectra of the clay film in the CE cell obtained at the next lower pressure value.

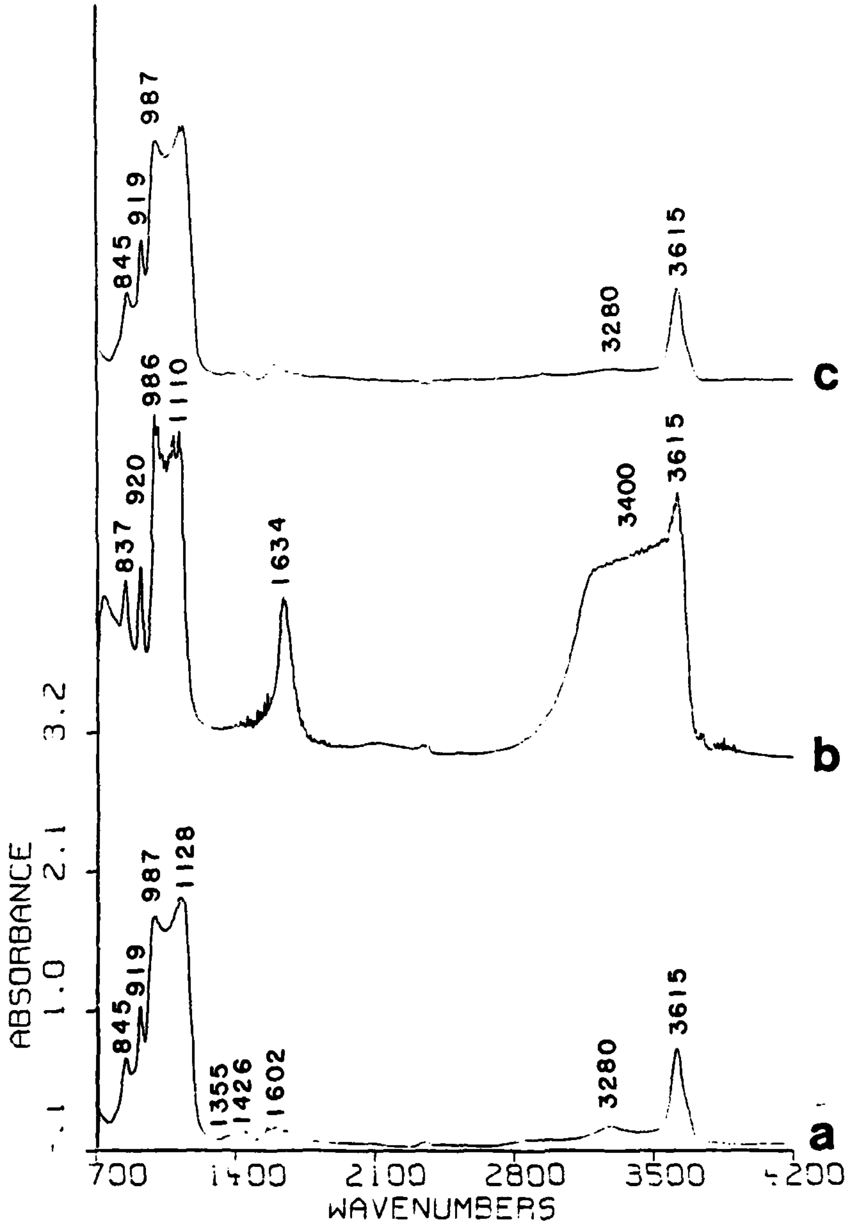

Figure 11 Absorbance FTIR spectra in the 700 cm^{-1} to 4200 cm^{-1} region of the SAz-1 montmorillonite clay film in the CE cell obtained under the following conditions: a) evacuated cell before exposure to water vapor, b) clay film in contact with standing water at 760 Torr, and c) clay film 36 hours after exposure to water vapor under a vacuum of 0.001 Torr.

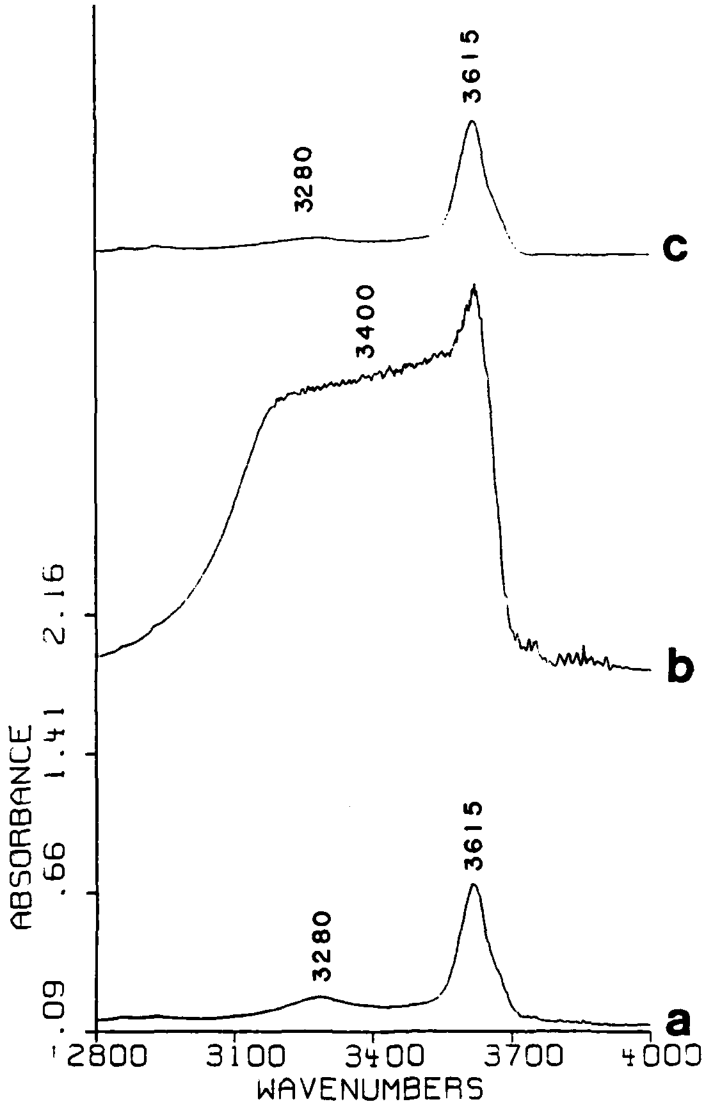

Figure 12 Absorbance FTIR spectra in the 2800 cm^{-1} to 4000 cm^{-1} region of the SAz-1 montmorillonite clay film in the CE cell obtained under the following conditions: a) evacuated cell before exposure to water vapor, b) clay film in contact with standing water at 760 Torr, and c) clay film 36 hours after exposure to water vapor under a vacuum of 0.001 Torr.

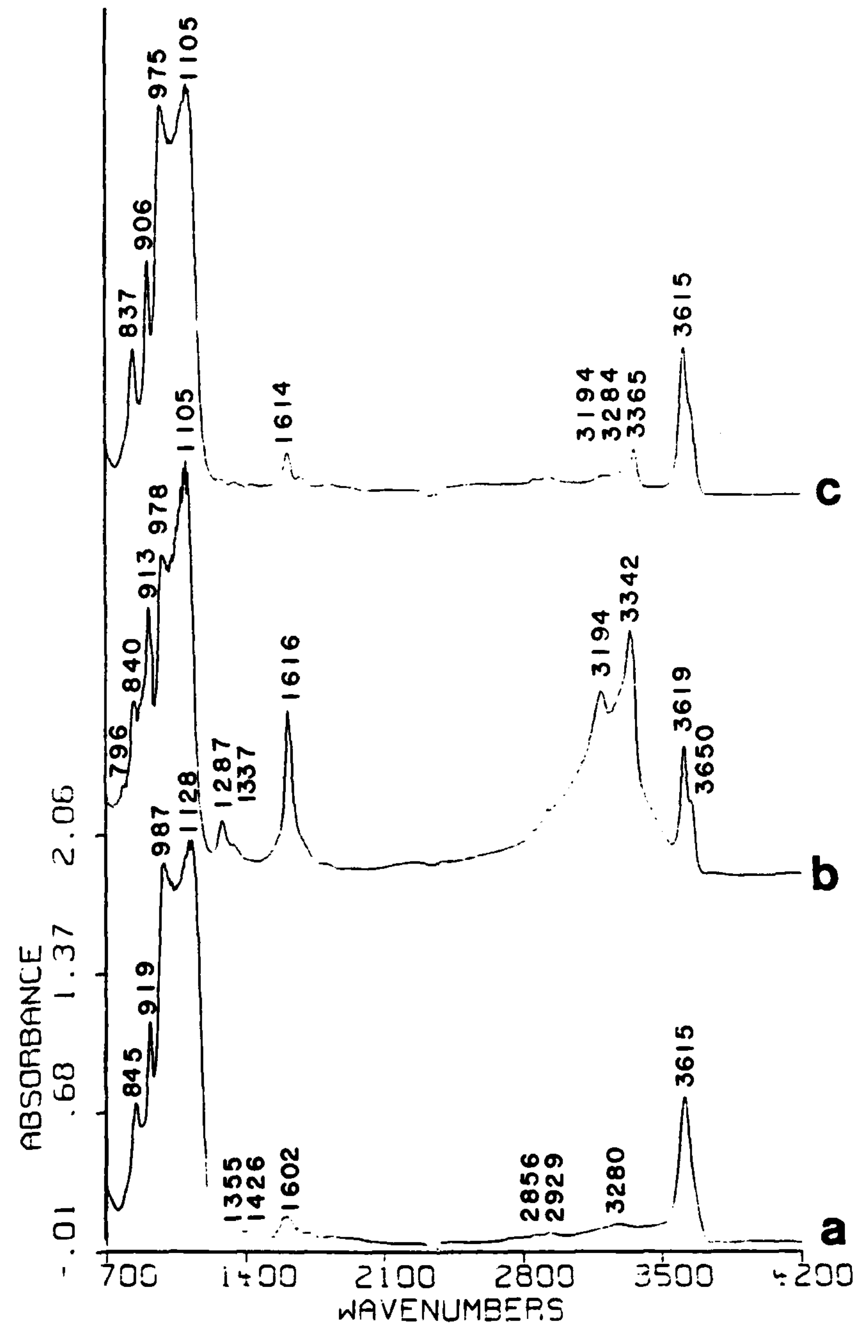

Figure 13 Absorbance FTIR spectra in the 700 cm^{-1} to 4200 cm^{-1} region of the SAz-1 montmorillonite clay film in the CE cell obtained under the following conditions: a) evacuated cell before exposure to hydrazine vapor, b) clay film in contact with standing hydrazine at 760 Torr, and c) clay film 36 hours after exposure to hydrazine vapor under a vacuum of 0.001 Torr.

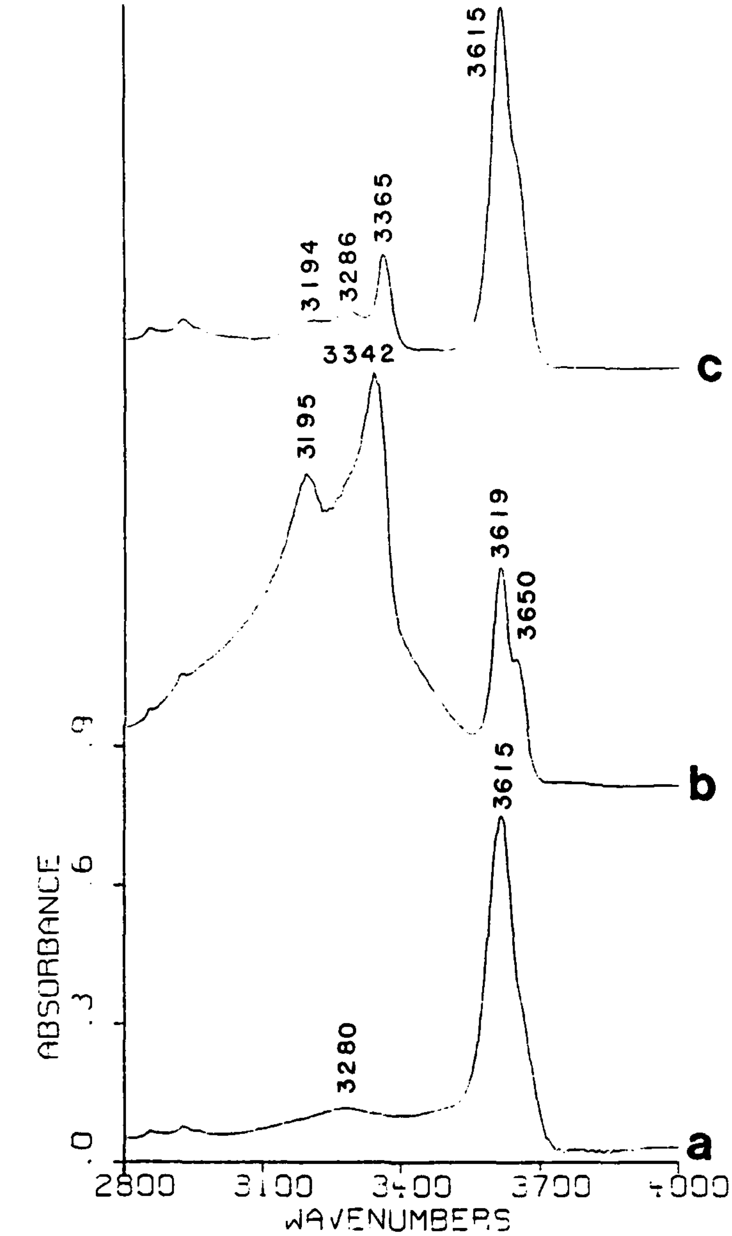

Figure 14 Absorbance FTIR spectra in the 2800 cm^{-1} to 4000 cm^{-1} region of the SAz-1 montmorillonite clay film in the CE cell obtained under the following conditions: a) evacuated cell before exposure to hydrazine vapor, b) clay film in contact with standing hydrazine at 760 Torr, and c) clay film 36 hours after exposure to hydrazine vapor under a vacuum of 0.001 Torr.

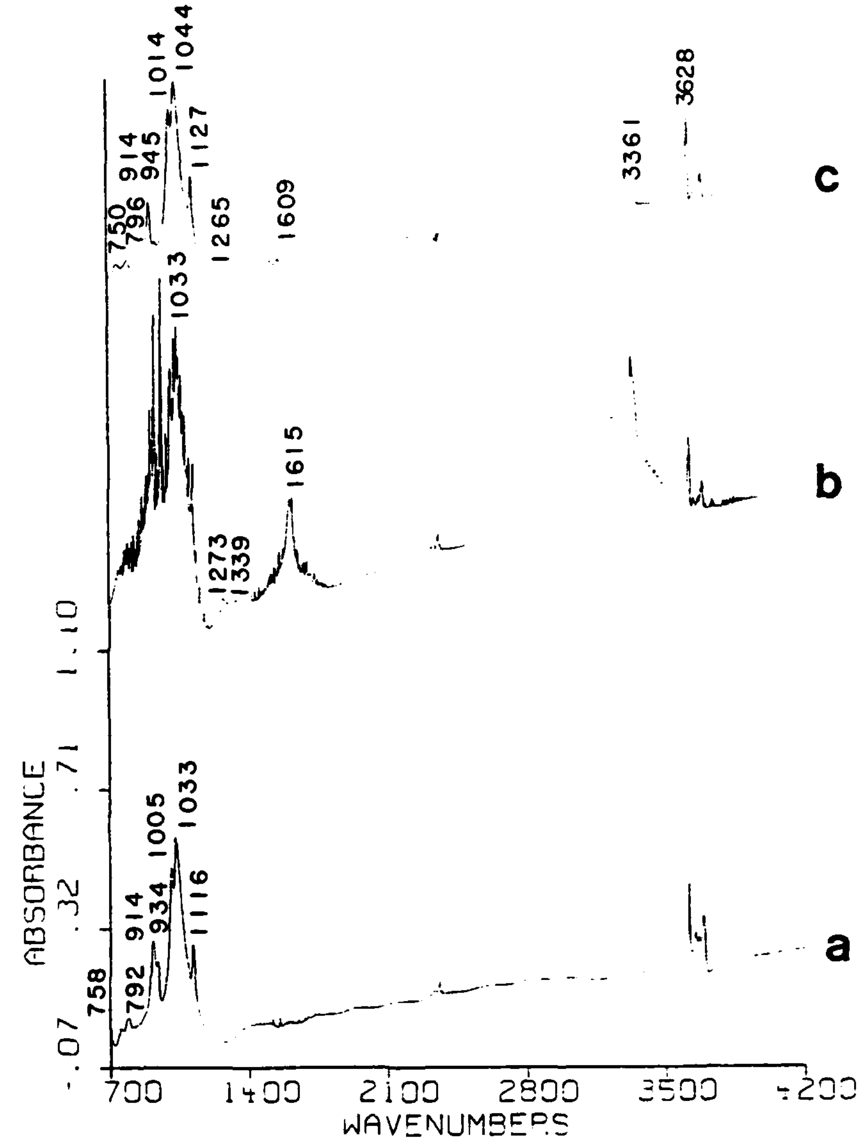

Figure 15 Absorbance FTIR spectra in the 700 cm^{-1} to 4200 cm^{-1} region of the KGa-1 kaolinite deposit on the Irtran window in the CE cell obtained under the following conditions: a) evacuated cell before exposure to hydrazine vapor, b) clay film in contact with standing hydrazine at 760 Torr, and c) clay film 36 hours after exposure to hydrazine vapor under a vacuum of 0.001 Torr.

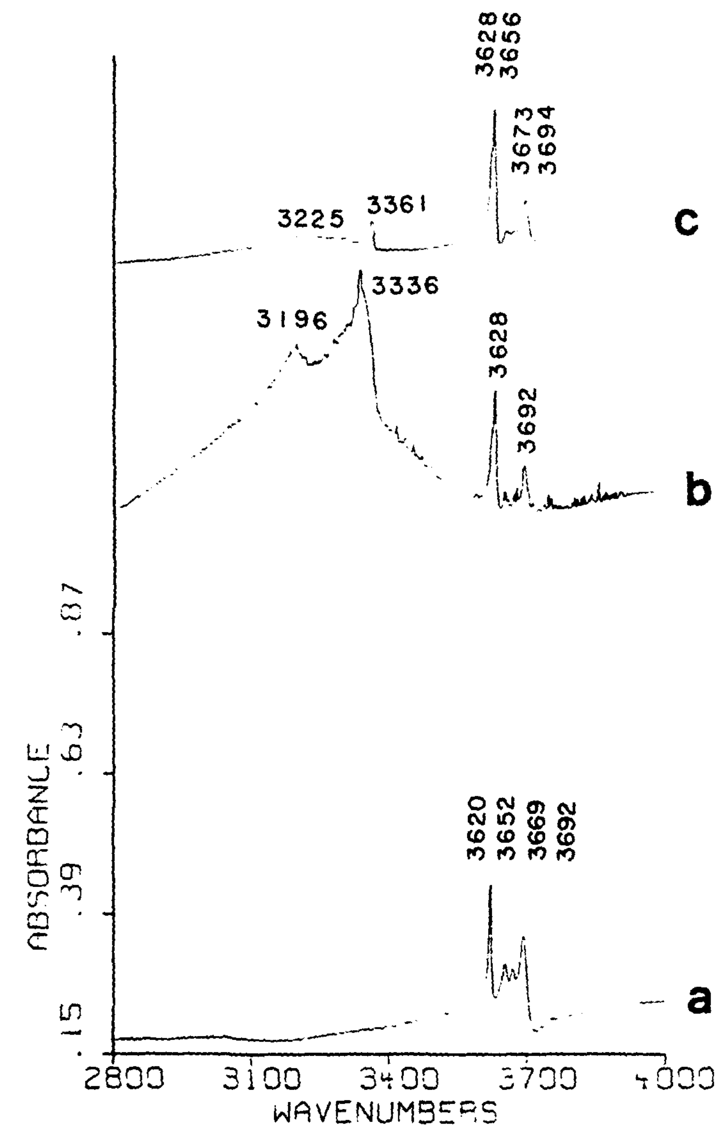

Figure 16 Absorbance FTIR spectra in the 2800 cm^{-1} to 4000 cm^{-1} region of the KGa-1 kaolinite deposit on the Irtran window in the CE cell obtained under the following conditions: a) evacuated cell before exposure to hydrazine vapor, b) clay film in contact with standing hydrazine at 760 Torr, and c) clay film 36 hours after exposure to hydrazine vapor under a vacuum of 0.001 Torr.

1985 USAF-UES SUMMER FACULTY RESEARCH PROGRAM/

GRADUATE STUDENT SUMMER SUPPORT PROGRAM

Sponsored by the

AIR FORCE OFFICE OF SCIENTIFIC RESEARCH

Conducted by the

UNIVERSAL ENERGY SYSTEMS, INC.

FINAL REPORT

EXPERIMENTAL STUDIES RELATED TO III-V SEMICONDUCTOR GROWTH AND CHARACTERIZATION

Prepared by: Dr Patrick L. Jones

Academic Rank: Assistant Professor

Department and University: Chemistry, The Ohio State University

Research Location: Avionics Laboratory, Electronic Technology Division, Electronic Research Branch (AADR), Growth and Characterization Group

USAF Research: Dr. Keith Evans and Dr. Phil Yu

Date: September 23, 1985

Contract No: F49620-85-C-0013

Experimental Studies Related to III-V Semiconductor Growth and Characterization

by

Dr. Patrick L. Jones

ABSTRACT

Experiments in three areas relating to the growth and characterization of semiconductor materials were attempted during this summer fellowship period. Efforts in the first area, photo-assisted molecular beam epitaxy, were aimed at overcoming substrate temperature problems in the growth of heterostructure materials. Attempts to perform preliminary experiments in this area were frustrated by equipment delivery delays and problems. Construction of the apparatus and preliminary measurements were conducted in the second area of research, the kinetics and decomposition of metal organics of interest to metal organic chemical vapor deposition. These results showed difficulties in using the original doser design and quadrupole mass spectrometer. Subsequent changes improved the apparatus performance. Generation of tunable radiation in the region between 700-900 nm enabled studies in the last area of interest, photoluminescence excitation spectroscopy of GaAs using sub band gap excitation, to be conducted and yielded preliminary spectra showing an unexpected Raman feature.

I. INTRODUCTION

High speed and integrated electro-optic semiconductor devices form an area of intense research interest due to their direct application in defense technologies. Many devices such as high electron mobility transistors (HEMT) and heterojunction lasers require the generation of superlattices, for example, AlGaAs/GaAs structures. The growth of uniform and reproducible materials from which these devices may be constucted has proven to be a limiting factor in their developement and use, thus research on the mechanisms of growth and characterization of III-V semiconductors is topical and timely.

For heterostructure devices of III-V compounds molecular beam epitaxy (MBE) is the method that results in the sharpest interfaces.[1] MBE employs ultra-high vacuum technology to provide clean growth conditions and effusive ovens of pure elements to provide molecular beams for growth. Blocking the appropriate beams with mechanical shutters and controlling their temperatures allows one to select the material to be grown. Difficulties in MBE stem from the complexity of the apparatus, the requirements for growth of different materials, for example the optimum substrate temperature for growing epi-layers of GaAS as opposed to AlGaAS, and the MBE's throughput, i.e., number of wafers processed per day.[1]

Recent efforts in metal-organic chemical vapor deposition (MOCVD) represent important advances in the

utility of this method for superlattice manufacture.[2,3] In comparison to MBE technology, MOCVD is far simpler and has the potential for higher throughput. On the other hand the ultimate quality of the material, including interfacial properties, is less than that obtainable at the present time from MBE. Part of the difficulty in MOCVD is the incorporation of impurities from the decomposition of the metal organic into the growing crystal.

It was felt that contributions by me to the on-going research in III-V semiconductor growth and characterization being conducted by the Electronic Research Branch (AADR) of the Avionics Laboratory would be possible because of my background in vacuum and laser technology, and chemical physics. This includes experience in UHV techniques, pulsed and cw lasers. Two initial areas of research were planned, Photo-assisted MBE and Decomposition Behavior of Metal Organics on silicon and gallium arsnide crystals. Involvement in materials characterization using laser raman and photoluminescence excitation spectroscopy were also thought possible with my interests in laser spectroscopy.

II. OBJECTIVES OF THE RESEARCH EFFORT

The original goals of the planned research effort were to explore two areas of interest to III-V semiconductor growth with Dr. Keith Evans and Mr. Larry Kapitan. The first area was photo-assisted molecular beam epitaxy. As pointed out in the introduction, growth of heterostructure materials by MBE can result in contradictory requirements on the growth conditions. One suggestion to overcome incompatible temperature requirements when two materials are being grown is to use intense light sources, such as lasers, to raise the surface temperature for short periods of time.[4] This increase in surface temperature would increase the surface mobility of the more tightly bound atoms without resulting in the unacceptable loss of the more volatile elements. Part of the effort of this summer research period were to be directed towards preliminary experiments to assess the feasibility of photo-assisted MBE.

A second area of interest was the kinetics and decomposition behavior of metal organic species important to MOCVD. Mechanisms of impurity incorporation into the growing crystal when using methylated metals as opposed to ethylated ones are not well understood and the surface chemistry of the reactions important to growth are not well characterized.[5] The objectives of the summer research plan were to reconfigure existing equipment for initial measurements (thermal desorption and fragmentation studies) on the

decomposition behavior of metal organics on silicon and gallium arsenide in order to elucidate the surface decomposition reaction mechanisms.

During the course of the summer research effort involvement in research on the characterization of materials using photoluminescence excitation spectroscopy was possible. In this research effort with Dr. Phil Yu, sub band gap excitation of GaAs using a tunable nitrogen-pumped dye laser while monitoring the luminescence spectrum was to be attempted. The first stage of the research was to create tunable radiation between 700 and 900 nm using existing laser sources within the Branch. The second stage of the research was to excite an existing sample at various wavelengths to look for new impurity features and energy levels in the spectra.

III. Photo-assisted Molecular Beam Epitaxy

a. Approach

This problem required the implementation of planned improvements in the Varian MBE 360 located in the Electronic Research Branch. These improvements included the addition of a reflection electron diffraction (RED) system, a new crystal holder and new load lock to the MBE. The RED system was necessary in order to monitor crystal growth in situ and in real time. A xenon arc lamp was to be used as a test light source and if reconditioning of an existing YAG laser with doubler was possible, it would be made available as well.

b. Results

The promised delivery dates for the equipment required for the MBE modifications were not met. With the recent move of AADR to a new building, a backlog of materials requests existed which precluded use of the MBE for exploatory research. This difficulty was anticipated as a potential problem. Further difficulties caused by a variety of typical vacuum problems, e.g., leaks, resulted in the MBE being down most of the summer. No progress was made in this research area.

My examination of the YAG laser showed it to require modest but critical improvements. Corrosion of the coating for the reflector cavity and degradation of the flashlamps

had occurred during storage. The doubling crystal had suffered burn damage through excessive power loading. A thorough cleaning of the optical components and laser head was undertaken but complete repair of the system was not possible during the 10 week research period.

IV. Kinetics and Decomposition Behavior of Metal Organics Important to MOCVD

a. Approach

This research area required the modification of existing experimental equipment such that low pressure dosing and direct line-of-sight mass spectrometric detection of decomposition products were possible. The aim of the research was to do simple temperature dependent decomposition experiments under constant surface coverage conditions, i.e., constant dosing flux, and to do simple thermal desorption experiments from saturated surfaces. Monitoring of various fragment species was to be conducted to learn more about the decomposition pathways and kinetics for metal organics. The decomposition pathways relate directly to the mechanisms of impurity incorporation in MOCVD grown materials.

b. Results

Modification of an existing unused plasma deposition apparatus for the research was undertaken and completed. This

included the design and construction of a new mass spectrometer housing and gas handling lines. Repair of the quadrupole mass spectrometer was necessitated by a failure in its RF head. Preliminary decomposition mass spectra of trimethyl gallium impinging on a silicon surface as a function of surface temperature were recorded. Based upon the data it was concluded that the background noise levels were too great, most likely as a result of the doser output being too diffuse. A redesign of the doser was implemented. Tests made just before the end of the research period proved promising. Adaptation of the QMS for thermal desorption measurements were conducted. A catastrophic failure of one of the system's small turbo pumps occured and halted the experiments in the last week of research.

V. Photoluminescence Excitation Spectroscopy

a. Approach

The application of photoluminescence and photoluminescence excitation spectroscopy to materials characterization is well documented. The photoluminescence excitation technique relies upon the photoexcitation relaxing quickly down to a strongly emitting level. For excitation out of a common lower level, the technique may be analyzed in terms similar to the autoionization of atoms. As the photon frequency is scanned, changes in absorption (increases,

decreases, or both) result when a bound excited state interacts with a continuum. Thus changes in absorption (photoluminescence) signature quasi-bound levels which may yield data on the energy levels of the crystal or impurities contained within it.

The excitation source in the present experiments was a nitrogen-pumped tunable dye laser. The first goal of the experiments were to obtain tunable radiation straddling and below the band gap of GaAs. If this could be accomplished the first measurements of sub band gap photoluminescence excitation spectroscopy at this facility could be conducted. This would allow among other things an investigation of the existence or non-existence of doubly-excited donors in the sample.

b. Results

The nitrogen pumped dye laser available for these studies was an Avco 20 KW nitorgen laser with an integral cuvette based dye laser. The optical cavity of the dye laser was a simple glass flat output coupler with a grating as the end mirror. After considerable experimentaion, suitable combinations of concentration and solvent were obtained to enable lasing from 700-780 nm in LDS 721 and 830-890 nm in LDS 822 dyes from Exciton Corp. Power level at a 30 Hz repetition rate were the order of 5 microwatts. The laser linewidth was approximately 25 A FWHM. These parameters were

sufficient for the planned experiments. Considerable care was necessary to avoid amplified spontaneous emission which resulted in lasing over the entire gain bandwidth of the dyes.

Run time was limited by the availability of liquid He at the facility. Figure 1. shows some of the raw results for the GaAs sample run at 4 K. The data reveal the presence of an unexpected Raman feature shifted from the excitation line by 12.5 nm which is first observed when the excitation laser wavelength drops below 830 nm. Initial examination of the intensity dependence of the 860 nm peak as a function of excitation wavelength shows that it decreases monotonically as the wavelength (photon energy) drops below the band edge energy. At much longer luminescence wavelengths a small peak corresponding to doubly-excited donors can be observed. Data analysis and interpretation are still in progress.

VI. Recommendations On Photo-Assisted MBE

Since no real test could be made concerning the feasibility of photo-assisted MBE it is recommended that a test be made on the MBE 360 after the new Varian Gen II is up and running and the backlog of materials requests removed. It should be possible to use the doubled output of the refurbished YAG laser as one photon source for this experiment. It is recommended that the modest sums necessary to refurbish the YAG laser be spent independent of its use with this project.

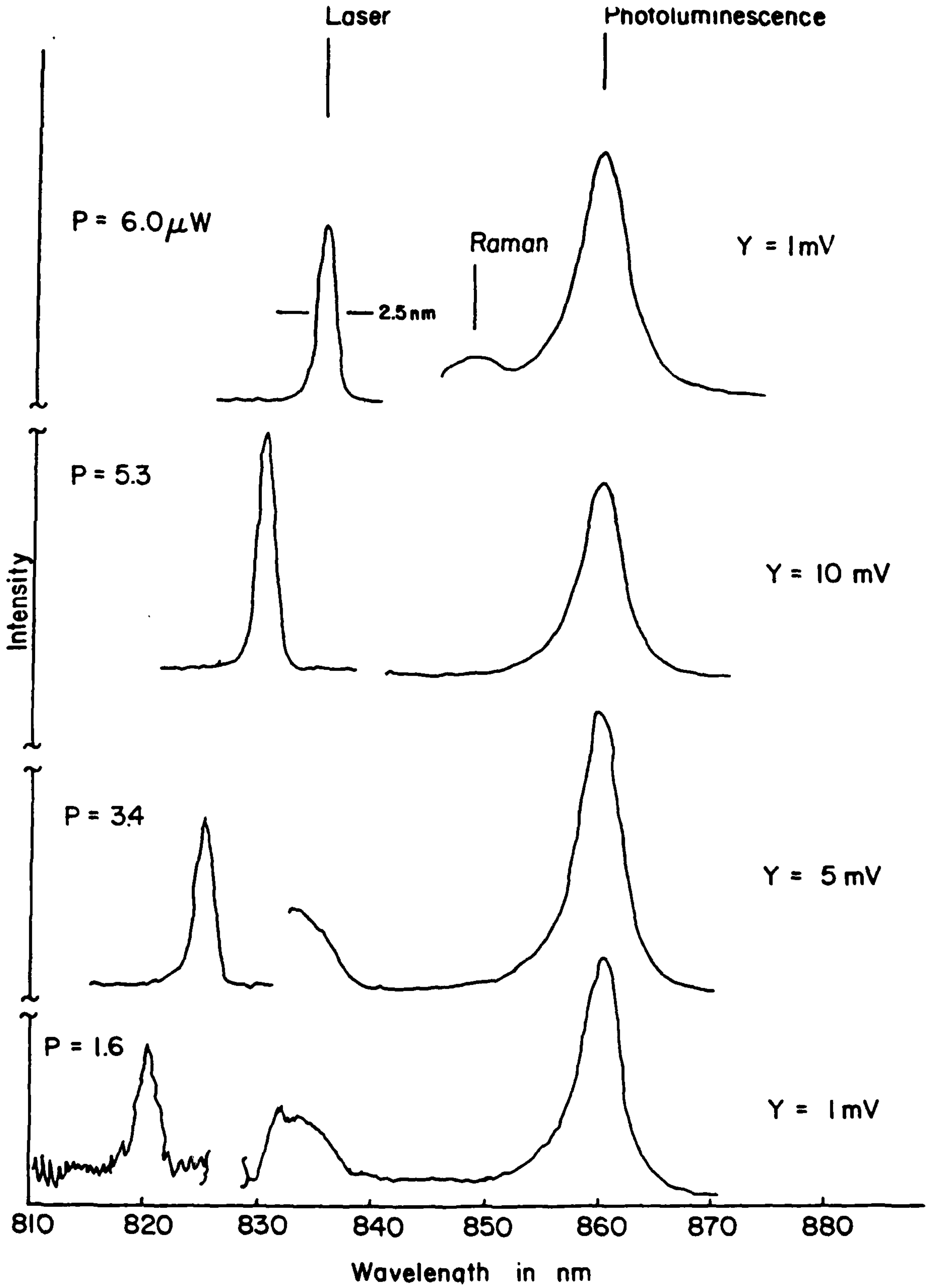

Figure 1. Photoluminescence excitation spectra of GaAs: raw data. To the left are the lineshapes of the excitation pulse with their average power in microwatts. The resulting PLES spectrum is shown to the right with scale factors.

VII. <u>Recommendations for Kinetic and Decomposition Studies of Metal Organics Important to MOCVD</u>

In this research area it is suggested that the apparatus be adapted to use a UTI mass spectrometer instead of the Infocon 200. Restructuring of the gas handling for multiple clean gases is desirable in order to develop a standard crystal preparation proceedure for the measurements. For example heating of the substrate under oxygen dosing to oxidize carbon residues followed by flash heating to desorb oxides. Initial experiments using methane would be desirable to calibrate the system under simple experimental conditions.It is also conceivable that this system can be used for very low pressure MOCVD or a metal organic variant of MBE.

VIII. <u>Recommendations for Photoluminescence Excitation Spectroscopy</u>

The data provide an initial look at low resolution photoluminescence excitation spectroscopy. Of interest is the behavior of the observed Raman feature at wavelengths between the band edge at roughly 820 nm and 835 nm. A specific question is whether or not the Raman feature turns on at a particular wavelength in this range? For example, in normal

photoluminescence a peak is observed at 830 nm (1.489 eV) corresponding to a carbon acceptor level. At long wavelengths this channel for decay is not open and cannot compete with the Raman process. This might explain the apparent turn on of the Raman feature which is observed first in the measurements at roughly 835 nm. Studies at wavelengths below the band gap but above 830nm could help to answer these questions. High resolution photoluminescence excitation spectroscopy using 0.4 A and < 1MHz linewidthlasers available in my laboratory are possible to explore this question. Such work could also examine in greater detail the coupling of impurity levels with the conduction levels.

Acknowledgements

The author thanks co-workers Dr. Keith Evans and Mr. Larry Kapitan of Universal Energy Systems for their help during this work. The co-operation of the people of the Electronics Research Branch, Avionics Laboratory, particularly Dr. Phil Yu and Mr. Greg Smith, and the sponsorship of the Air Force Systems Command, Air Force Office of Scientific Research are greatfully acknowledged.

IX. References

1. Dapkus, P.D., " A Critical Comparison of MOCVD and MBE for Heterojunction Devices," J. Crystal Growth 68, 345 (1984).

2. Fraas, L.M., P.S. McLeod, J.A. Cape, and L.D. Partain, "Epitaxial Films Grown by Vacuum MOCVD," J. Crystal Growth 68, 490 (1984).

3. Nakanisi, T., "The Growth and Characterization of High Quality MOVPE GaAs and GaAlAs," J. Crystal Growth 68, 282(1984).

4. Singh, J., and K.K. Bajaj, "Role of laser enhanced surface kinetics in the low substrate temperature molecular beam epitaxial growth of compound semiconductors: A Monte Carlo study," Appl. Phys. Lett. 46, 577(1985).

5. Stringfellow, G.B., "A Critical Appraisal of Growth Mecahnisms in MOVPE," J. Crystal Growth 68, 111(1984).

1985 USAF-UES SUMMER FACULTY RESEARCH PROGRAM/

GRADUATE STUDENT SUMMER SUPPORT PROGRAM

Sponsored by the

AIR FORCE OFFICE OF SCIENTIFIC RESEARCH

Conducted by the

UNIVERSAL ENERGY SYSTEMS, INC.

FINAL REPORT

A Preliminary Study of Learning Nets and Massive Parallelism

Prepared by:	Jeremy Jones
Academic Rank:	Assistant Professor
Department:	Systems Science Department
University:	University of West Florida
Research Location:	Wright Patterson Air Force Base Avionics Laboratory AFWAL/AAAF-2
USAF Research:	Major James Johnson, and Lt. Bruce Edson
Date:	August 12, 1985
Contract No:	F49620-85-C-0013

Preliminary Study of Learning Nets and Massive Parallelism

by

Jeremy Jones

ABSTRACT

I believe that intractably high control cost of massively parallel systems is the fundamental difficulty of our current technology. Not only does it severly limit our cost effective exploitation of inexpensive VLSI computing units, but in learning research stimies our work to mimic the human brain's massive parallelism with adaptive net learning models. Although I worked in other areas of research and study in this short summer period, this report will be confined to the above research topic because it is so vital for the success of learning systems. Dr. A Harry Klopf (Klopf 1982) has provided the general conceptual framework within which these ideas have been developed. The basic idea comes from recognising the intractability in modeling even a small economy in which every decision affects all other decisions (including the original decision itself!). Given the computational impossiblity of modeling such complexity it is remarkable that self-interest through the pricing mechanism essentially optimizes system-wide resource allocation and other behavior in terms of meeting individual needs. An analogous distributed control Operating System is conceived with tractable coordinating message passing overhead. Just as in the economic case, control is imperfect in the individual case, but optimized in a statistical sense over the system at large. Solutions are proposed for the ubiquitous problems of synchronization, exclusion, deadlock avoidance and determinism.

Outline of this report:

1 Introduction

1.1 Researcher Background

1.1.1 Relevant Experience

At Goodyear Aerospace Corporation/Akron this researcher used autocorrelation methods to help develop systems for pattern recognition for use in target identification and navigation. At Goodyear Aerospace/Arizona I did a phase/amplitude analysis to independently predict the signal/noise(side-look angle) for the

RF-4C synthetic array radar. These projects with the mathematics of optimization through function orthonormalization and sorting helped prepare me to understand and work with Avionics Learning Systems. My experience as a Flight Instructor and Instrument Pilot may add some insight to working with such systems.

1.1.2 Relevant Education

Most relevant to optimization are my two masters degrees relating to functional analysis (math) and the behavior of vector fields (physics) which are the primary source of my insight and analogy for new ideas.

1.2 Assignment to USAF Research Area

I have developed a research interest in Artificial Intelligence and Learning Systems through frequent (often daily) discussions with colleague Dr. Richard Gawronski at the University of West Florida. Since Dr. Gawronski is doing research at Oak Ridge Laboratory on Adaptive Nets, my interest and preparation for the Avionics Lab research on Adaptive Net Learning was suitable.

2 Objectives

2.1 Preliminary Goals

One of the ultimate goals of our research was automatic generation and debugging of software. Preliminary goals of the brief ten-week summer research period were to become adequately familiar with the work of Stephen Grossberg, perceptrons, and the general literature on learning systems to build a basis for future research. Subgoals were to create (i.e. program) an adaptive net learning system and evaluate its performance.

2.2 Additional Goals

After programming a simple adaptive net learning system and

reading the literature it became clear that such methods are currently applicable to only the simplest of idealized textbook problems. Computational intractability seems to be the fundamental reason for this impasse, thus my new goal became the clear identification of thi. severe problem and correcting it.

3 Research Summary

3.1 The importance of Massive Parallelism

3.1.1 The Economics of VLSI

Our new technology of very large scale integrated circuitry has dramatically lowered computation costs. This has radically changed the field of electrical engineering and weapons technology with the replacement of hardware solutions by software solutions in most cases. Along with the greater flexibility, maintainability, reduced development cycle time and portability, the reduced VLSI cost makes an irrestible argument for increased use of computation in systems. Thus parallelism (ideally massive) is upon us if we can master the complexity of controlling it efficiently.

3.1.2 Computational Complexity

One key reason we need massive parallelism is to help inexpensively cope with the computational complexity which makes many of our problems (e.g. optimal resource allocation) unsolvable at this time. Among these many intractable problems are many belonging to artificial intelligence and learning systems.

3.1.3 Analogies with the Human Brain

The human brain seems to consist of a great number of neurons

connected by synaptic junctions. Individual neurons exhibit complex behavior, and parallelism is evident through a number of behaviorial experiments, e.g. involving discontinuous frame and script changes, or filtering of attention triggers.

3.1.4 Real-Time Control and Response Time

Parallel computations are the key to quick response times in many control systems. For example if a weapons system can simultaneously identify, track, arm and evade, it will be more survivable than one which does these necessary things separately.

3.2 The Economic Model and Tractability

3.2.1 Everything Affects everything.

The above tractability problem occurs with a vengence in economic modeling. This is because any decision made by an individual regarding purchase or production directly or indirectly affects every other individual in the economic system including the original individual. This fact seems to make it impossible to model any large economic system. To see this consider a system of n individuals. If each affects all the others as above, there will be at least n^n (pronounced: n raised to the n power) interactions to be considered in a model.

This means that we must consider 10^10 = 10000000000 interactions to understand such a system comprised of only ten individuals. For one hundred individuals the number of interactions we must calculate becomes 100^100 which is far more than the fastest computer could calculate in our lifetime! Hence we use the word intractable. The same combinatorial explosion of coordinating signals chokes a parallel network operating system or adaptive network when such a direct approach is taken for a large problem.

3.2.2 <u>The Invisible Hand and Optimization</u>

3.2.2.1 <u>Tractability Solved by Parallelism?</u>

There is a way out of this combinatorial dilemna as observed by Adam Smith in 'The Wealth of Nations'. If each individual is assumed to have a separate parallel complexity and intelligence, then individual self-interest plus a pricing mechanism can yield statistically optimum system behavior.

3.2.2.2 <u>Seen From a Control Point of View</u>

From an operating systems control point of view, the tractability problem has been solved by distributing control to intelligent subunits. Computational control complexity has been distributed into the intelligent hedonistic behavior (Klopf, 1982) of individuals.

3.3 <u>Smart Nodes: the work of Dr. A Harry Klopf</u>

3.3.1 <u>Neuron Complexity</u>

As Dr. A. Harry Klopf points out, the complexity of the neuron belies its tiny size. Cell complexity becomes quickly apparent in the book, The Lives of a Cell (Thomas 1974), and seems essential for the brain's distributed control in much the same way individual intelligent behavior is neccesary in a free market economy. In much the same way our adaptive net nodes must be complex, optimizing units (Klopf, 1982) to cut the Gordian knot of combinatorial intractability.

3.3.2 <u>Rational Behavior: Supply and Demand</u>

As in a free market economy any process in the operating system process control block chain (ready queue) should make best use of its resource mix. Since this is a systemwide consideration involving RELATIVE cost and availability of resources, it is

affected by all other allocation decisions in the operating system. We develop an operating system blackboard analogous to the free market pricing mechanism to unravel what would otherwise be a combinatorial nightmare.

Supply and demand curves are used to adjust the blackboard values with each production or purchase (i.e. invocation of a ready queue process which produces or uses system resources). Thus each operating system decision affects all other future decisions through the blackboard.

The first trial implementations of this scheme will use simple linear supply and demand blackboard adjustment curves. This is done both for computational speed and simplicity. Of course it is manifestly naive as it theoretically permits infinite values (i.e. takes no account of diminishing returns), but should be adequate to demonstrate feasibility.

3.4 A Possible Implementation

3.4.1 The Blackboard: A Global Variable Pool

There are a few difficulties in implementing this idea. One apparent problem is that if many procedures are similar, and they all act in a systemwide optimal manner, they will all do the same thing with a massive collision. This isn't really a problem though since when any process chooses to supply a function, the value of that function drops through the global blackboard, thereby making it less desirable (i.e. likely) that any other process in the ready queue will choose to perform the same task.

3.4.2 Reducing Collisions through Chance

To further reduce the chance of collisions as described in the last section (3.4.1) we can also used a random number weighted by

the system blackboard relative value table. This means that processes would be more likely to provide results which made best use of their resources, but only in a probabalistic sense. If two processes committed system resources within the interval needed to update the global blackboard they would have a non-zero chance of colliding. This stochastic optimization makes it unlikely the two processes would collide if they were activated within this update time of vulnerability.

3.4.3 The Classical Coordination Problems

Note that collisions are greatly ALLEVIATED by the above two methods, but NOT ELIMINATED. Of course they must be eliminated for correct operation of an operating system. This is done as described below in section 3.4.3.2 on exclusions. But because the chance of collisions is greatly reduced (though not eliminated) by the above two methods, the system OVERHEAD and COST of managing collisions is reduced to a TRACTABLE overhead (i.e. polynomial time/space bounded) as the system approaches massive parallelism.

3.4.3.1 Synchronization

The blackboard would include either semaphore value-pointer pairs, or message slots. This would permit either semaphore or message process synchronization in the classical manner in cases where data tokens or precedence graph relations were needed.

3.4.3.2 Exclusion

Some form of stochastic allocation as illustrated above seems to be necessary to break the combinatorial dilemna of massive parallelism. The nasty side effect of this solution is the unavoidable occurrence of collisions. Thus processes must be

allocated separate workareas (buffers in the case of Input/Output devices) which are invalidated and discarded by backtracking if a collision is later found to have occured.

Thus we see the above scheme includes the 'never wait rule' which says that it is better to have a processor do something which MIGHT be needed, rather than sit idle. In the above we are just attempting to minimize the probability that the computational processor output will not be needed, and have to be discarded.

3.4.3.3 Deadlock Avoidance

Because of the backtracking made possible by the above use of separate duplicate work areas (to avoid collision), deadlock should not occur. To be more precise, there are four conditions, each of which must be separately met, for deadlock to occur. They are 1) hold and wait, 2) non-sharable resources, 3) no preemption of resources of processes held by a separate process, and 4) circular hold and wait condition in the resource request matrix. Since a process uses its own duplicate work buffer, all resources are essentially virtual, hence sharable (because they are separate and independent). Thus at least condition 2) is avoided.

3.4.3.4 Determinism

Determinism simply means that the system will produce the same output (behavior in a control system) in any future run using the same input data. Thus determinism refers to a predictability or dependability of the system. Aside from timing considerations (which is stochastic and must remain only statistically dependable), determinism will be assured if the system can RECOGNIZE prior collisions and backtrack as described above in section 3.4.3.2.

3.5 Characteristics of the System

3.5.1 Imperfect but Low-Cost Control

The blackboard of current function 'prices' (analogous to the stock exchange) must be periodically distributed to regional query centers for unhampered use by procedures deciding what functional output to produce next. Using hierarchical, periodic, and parallel distribution of the blackboard to regional processor centers, control signal overhead can be limited to a logarithmic function of the number of processors. But this makes control tractable at the expense of imperfect resource allocation. This imperfection has a statistical misallocation price, just as more current (i.e. perfect) information has a communication cost (price). By folding this cost of improved information into the blackboard, the optimal compromise between excessive misallocation with backtracking on the one hand, and exponentially nontractable control signal overhead on the other hand, might be achieved.

3.5.2 The Need for Functional [non-procedural] Languages

3.5.2.1 PROLOG

The same reason for PROLOG's notorious inefficiency seems to become an efficiency advantage in a massively parallel architecture. This seems to be for the following reason: In restricting a machine to follow a relatively efficient procedural path (under tight programmer control), the more procedural language constraint in the interest of efficiency, becomes a restraint to developing many procedural paths in parallel. Thus PROLOG's weakness in a sequential machine may become its strength on a parallel architecture. That is, when massive parallelism

becomes commonly available in VLSI hardware, and tractable in control software.

3.5.2.2 LISP

There are a number of reasons LISP is an attractive tool in modeling learning systems: Nets are the natural data structure in LISP, and because of the very late binding may be patched ad-hoc with imbedded procedures (demons) when things don't work as hoped. This less 'structured' and more experimental development method characteristic of a LISP environment is described by Alan Perlis under the name 'the prototypical method' (Perlis, 1981). It seems very suitable for the ad hoc testing and experimenting probably necessary in researching a new and complex field.

On the other hand, this advantage of being able to efficiently direct LISP's control sequence becomes a disadvantage in restricting parallelism. But less of a restriction than in a procedural language, so that LISP may be a best choice because of its large number of practiced users in the AI community.

3.5.2.3 ADA

Because of the DoD edict, and features of ADA for describing parallelism, ADA may be the practical choice. However as ADA is a procedural language, implementation of parallelism will be labor intensive, explicit, and error prone, compared with more applicative languages in which the parallelism will be implicit and more automatically generated.

3.5.2.4 Pascal

While Pascal seems an inapt choice in most ways, it has been my choice in developing a skeleton model for practical reasons: It

is available in a highly interactive form for my microcomputer. This plus the abstraction features of Pascal permit gluing things together in new ways, hence the quick experimentation needed to get anything done in my short summer research period.

3.5.3 Asymptotic Complexity Limit

Let there be n parallel procesors, all in need of coordination through access to the central blackboard. Then if the blackboard is copied twice, and these copies are copied twice to more regional centers, and so on, it will take [log base two of n] units of time and data channel to provide all n processors with copies of the central global blackboard table. Thus one million processors could have access to statistical coordinating information in only twenty units of time and data channel overhead. Of course this data will only be probabilistically helpful, and need updated. So there is a constant k which accounts for the recency of system usage data required for acceptably current decision making. Thus for n processors computing in parallel, there would seem to be k*log(n) time overhead for control. Of course the logarithm is defined as the inverse of the exponential, so inasmuch as the exponential is the paradigm of intractability, then its inverse is tractable.

3.5.4 A Skeletal, Prototype Example in Pascal

I have attempted to simulate the asynchronicity of a heterogenous parallel operating system using random numbers in Pascal to simulate both random times of processing requests, and random resource requests. As a particular generic computational commodity is increasingly requested, its blackboard value

increases according to a linear (simplified) demand curve. These values are sorted from highest value to lowest in the blackboard to minimize random compute times , as the highest valued type of request is most likely to be assigned to a processor. As processors act to fill the indicated needs, their blackboard values decrease, and they are re-insertion sorted to make them less desirable as targets for entrepreneur processors, looking for market opportunities.

I have not included synchronization, and backtracking in the program as my brief research period is drawing to a close.

4 Recommendations

4.1 Further Work Needed

If simulation of the method proves sufficiently encouraging, the next step is to design a modestly massive parallel system of microprocessor based nodes. The blackboard distribution is such an esssential thread that it might be microprogrammed. Cycle stealing would be easier, cheaper and more flexible in distributing the blackboard, but multiport RAM would provide the sharable architecture needed for maximum speed. Either hardware design would seem suitable. The hardware advantage would be the complete decoupling of processors throughout the system. For maximum parallelism, the only physically shared resource would be the system clock. Virtual sharing would occur when results are given to a requesting process through the blackboard, and when distributing the request portion of the blackboard.

4.2 Equipment Needs

Any computer could be used for the feasibility through simulation

phase of study, but of course design tools which facilitate modularity and abstraction of detail would speed design and clarify development.

Because of the portability afforded by the C language. much software is spreading to more powerful, but less popular machines. Thus it would be reasonable to consider the Motorala 68020 or National Semiconductor 16032 mpu because of their address fault trapping and possible systemwide memory usage balancing through MMU IC's now commonly availavle. This would permit more cost effective use of physical memory in a working system.

5 Acknowledgments

This research was sponsored by the Air Force Office of Scientific Research/AFSC, United States Air Force, under Contract F49620-85-C-0013. Work was conducted at the Wright Patterson Air Force Base, Avionics Laboratory with the AFWAL/AAAF-2 Research Group. Extensive use was made of the Air Force technical library and Wright State University Library.

I would like to thank Dr. A. Harry Klopf for his ideas which triggered my interest; Lt. Bruce Edson who educated me to a new field by carefully guiding me through a large maze of interdisciplinary literature; Major Jim Johnson for his interest and encouragement; Major Ken Frankovich for his support, and all the memorable people of the Avionics Lab who helped make my summer productive and pleasant.

6 References

Klopf, 1982: Klopf, A. Harry: The Hedonistic Neuron, A

Theory of Memory, Learning and Intelligence. Hemisphere Publishing Corporation 1982

Perlis, 1981: Perlis, Alan J.: Software Metrics. The MIT Press, 1981.

Thomas, 1974: Thomas, L.: The Lives of a Cell. Viking Press, New York, 1974.

1985 USAF-UES SUMMER FACULTY RESEARCH PROGRAM /

GRADUATE STUDENT SUMMER SUPPORT PROGRAM

Sponsored by the

AIR FORCE OFFICE OF SCIENTIFIC RESEARCH

Conducted by

UNIVERSAL ENERGY SYSTEMS, INC.

FINAL REPORT

APPROXIMATE MATHEMATICAL SOLUTIONS FOR UNIDIRECTIONAL COMPOSITES CONTAINING BROKEN FIBERS

Prepared by:	Dr. Walter F. Jones
Academic Rank:	Assistant Professor
Department and University:	Department of Engineering Science and Mechanics The University of Tennessee, Knoxville
Research Location:	Air Force Wright Aeronautical Laboratories / Flight Dynamics Laboratory, Structures and Dynamics Division, Structural Integrity Branch, Fatigue and Fracture Group
USAF Research:	Dr. George P. Sendeckyj

Date:	September 25, 1985
Contract No.:	F49620-85-C-0013

APPROXIMATE MATHEMATICAL SOLUTIONS FOR UNIDIRECTIONAL COMPOSITES CONTAINING BROKEN FIBERS

by

Walter F. Jones

ABSTRACT

A study of approximate solutions for unidirectional composite laminates containing broken fibers is presented. Assumed displacement fields within finite elements are used to write the element equilibrium equations in terms of displacements. These equations are then solved with appropriate boundary conditions to calculate the stress concentration factors for various numbers of broken fibers. The effect of various types of assumed displacement fields is studied in order to suggest criteria for the selection of optimum displacement functions that will allow the solution of the differential equations, will satisfy appropriate boundary conditions, and will retain proper behavior near the crack for any number of broken fibers.

ACKNOWLEDGEMENTS

The author wishes to thank the Air Force Systems Command, the Air Force Office of Scientific Research, and Universal Energy Systems, Inc. for the opportunity to spend a very rewarding summer at the Air Force Wright Aeronautical Laboratories, Wright-Patterson Air Force Base, Ohio. He would like to acknowledge the Flight Dynamics Laboratory, in particular the Fatigue and Fracture Group of the Structural Integrity Branch, for its hospitality and excellent working conditions.

The author wishes to express his deepest appreciation to Dr. George P. Sendeckyj for his guidance throughout the summer research period. This research project has been a tremendous learning experience and the author looks forward to working with Dr. Sendeckyj on future projects in composite materials research.

I. INTRODUCTION

Much of the recent research in applied mechanics has been directed toward understanding and characterizing the complex behavior of fiber-reinforced composite materials. For example, a designer must know how a composite panel that has some amount of internal damage such as broken fibers or matrix failure will perform under loading and how the internal damage will grow until final failure occurs. This knowledge must be realized before future aircraft composite structures can be certified.

Many investigators, including the author, have studied the growth of damage in composite laminates. Some authors [1-8] have studied damage growth from a very fundamental perspective - the unidirectional lamina (all fibers parallel to the load direction). The fracture behavior of unidirectional composite lamina has been modeled using mathematical models based on the classical shear lag assumption. These models, which assume that the fibers carry all of the axial load and the matrix transmits only shear between fibers, have in their most recent forms taken into account fiber breakage, matrix yielding, and matrix splitting [4-7]. The author used the shear lag model to predict damage growth in unidirectional boron/aluminum composite laminates [8]. The author has also generated improved shear lag models [9-11] for the composite with broken fibers using both first-order and higher-order finite difference approximations for the derivatives that arise in the theories. These models, unlike the early shear lag models, gave reasonable values for the transverse matrix normal stresses as well as the fiber stress concentration factors.

All of the shear lag models have an inherent weakness in that these theories can only deal with quantities at the nodal points (the fibers). If stresses or displacements at points other than the nodes (fibers) are desired, some form of averaging must be employed. Thus the analyst is very limited in his ability to model and understand the complex behavior that exists near a crack in an anisotropic solid.

Finite element models can incorporate displacement functions that are continuous in both the horizontal and vertical coordinates. The analyst can therefore look at stresses and

displacements at any point in the solid and can satisfy boundary conditions at points other than nodal points. For example, if appropriate displacement functions can be generated then the shear stress on the face of a crack can be set to zero at every point instead of being zeroed on the average as in finite difference solutions.

In this investigation, a finite element model using continuous displacement functions will be generated for a unidirectional composite with broken fibers. Careful attention will be given to the model's ability to satisfy appropriate boundary conditions at various points in the lamina. Finally, the effect of various forms of displacement functions on the accuracy of the model will be studied.

II. OBJECTIVES

The major objective of this project was to develop finite element models for the unidirectional composite laminate containing internal damage in the form of broken fibers. Displacement functions would be selected and used to write the element equilibrium equations and to satisfy appropriate boundary conditions. The stress concentration factors could then be calculated and the behavior of the solution studied. Thus the specific objectives of the summer research effort were:

(1) To develop finite element theories for the composite with broken fibers that were consistent with the theory of elasticity and gave correct values for longitudinal fiber stress, matrix shear stress, and matrix normal stress.

(2) To study the effect of various types of displacement functions on the solution for the composite laminate with broken fibers and to determine the optimum displacement function for use in the finite element model.

III. FINITE ELEMENT MODEL FORMULATION

The shear lag theories in the literature [1-11] provide reasonable fiber stresses in all cases and reasonable matrix stresses in the most recent theories. It should be noted, however,

that boundary conditions in the shear lag theories are typically satisfied only at nodal points and therefore there may be some question about their accuracy. To satisfy boundary conditions at every point requires some form of finite element model in which displacement functions allow continuous variation with horizontal and vertical coordinates.

In order to derive the model, consider a unidirectional fiber-reinforced composite lamina undergoing plane deformation. On the micro scale, the composite can be modeled as an elastic matrix reinforced by equally spaced, parallel, elastic fibers as shown below in Figure 1a. Defining b and h as the width and spacing of the fibers, respectively, a typical element of the composite can be isolated as shown in Figure 1b.

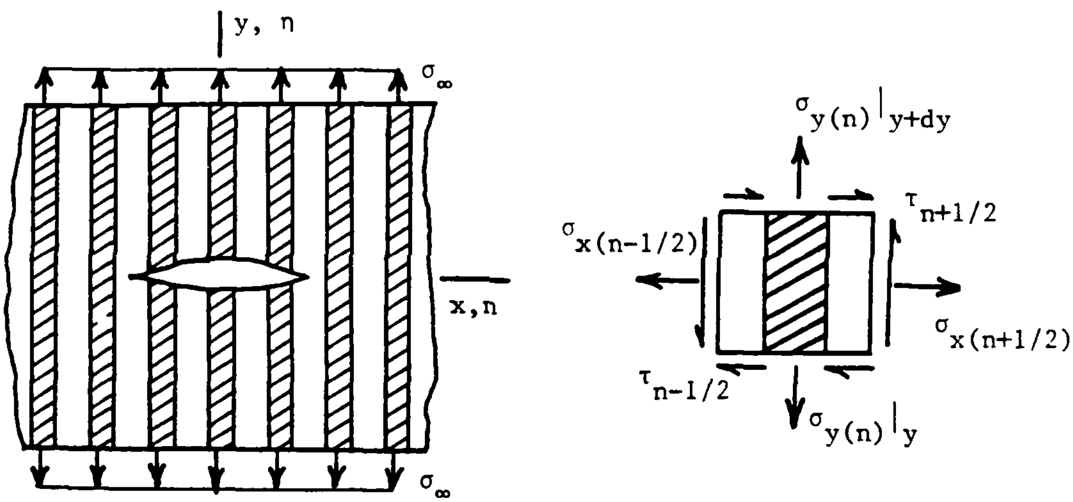

(a) (b)

Figure 1. Lamina Geometry and Typical Element

As seen in Figure 1b, the n^{th} typical element is bounded by the (n+1/2) and (n-1/2) mid-node lines. The equilibrium equations for the element are

$$\sigma_{x(n+1/2)} - \sigma_{x(n-1/2)} + h\tau_{n,y} = 0$$

$$\tau_{n+1/2} - \tau_{n-1/2} + h\sigma_{y(n),y} = 0 \qquad (1)$$

The subscripts following the commas denote partial derivatives with respect to the subscript variable, that is, $f_{,x} = \partial f/\partial x$. The quantities in the above equations are merely the appropriate stresses evaluated at the boundaries of the element. At this point, a selection of appropriate displacement functions must be made in order to derive the stress-displacement relations. Assume that the displacement field in the n[th] typical element can be written as

$$u_n(x,y) = u_{0,n}(y) + (x)u_{1,n}(y) + (x^2 - h^2/4)u_{2,n}(y)$$

$$v_n(x,y) = v_{0,n}(y) + (x)v_{1,n}(y) + (x^2 - h^2/4)v_{2,n}(y) \tag{2}$$

Note that these assumed displacement functions allow for quadratic variation with x in displacement within the element and therefore a linear variation of strain. The advantages of the finite element formulation over the finite difference (shear lag) solution with constant element strains thus become apparent.

As detailed in [12], the stress-strain relations on the element boundaries can be written in terms of displacements as

$$\sigma_{x(n\pm 1/2)} = C_{11}[u_{1,n} \pm (h)u_{2,n}] + C_{12}[v_{0,n} \pm (h/2)v_{1,n}]_{,y}$$

$$\tau_{n\pm 1/2} = C_{66}\{[u_{0,n} \pm (h/2)u_{1,n}]_{,y} + v_{1,n} \pm (h)v_{2,n}\}$$

$$\sigma_x(n) = C_{11}\ u_{1,n} + C_{12}\,[v_{0,n}]_{,y}$$

$$\sigma_y(n) = C_{12}\ u_{1,n} + C_{22}\,[v_{0,n}]_{,y}$$

$$\tau_n = C_{66}\{[u_{0,n}]_{,y} + v_{1,n}\} \tag{3}$$

Using the above relations, the element equilibrium equations can be written in terms of displacements as

$$C_{66}[u_{0,n}]_{,yy} + (C_{66} + C_{12})[v_{1,n}]_{,y} + 2C_{11}u_{2,n} = 0$$

$$C_{22}[v_{0,n}]_{,yy} + (C_{66} + C_{12})[u_{1,n}]_{,y} + 2C_{11}v_{2,n} = 0 \tag{4}$$

Equation (4) can be normalized by letting

$$\eta = y/h \quad , \quad U_{j,n} = h^j u_{j,n} , \quad V_{j,n} = h^j v_{j,n} \quad ,$$

$$F = C_{22}/C_{66}, \qquad E = C_{11}/C_{66}, \qquad H = 1 + C_{12}/C_{66} \tag{5}$$

The resulting differential-difference equations can then be reduced to ordinary differential equations by assuming that the normalized displacements $U_{j,n}$ and $V_{j,n}$ are the Fourier coefficients of functions $U_j(\eta, \theta)$ and $V_j(\eta, \theta)$. For example, U_n can be written as

$$U_{j,n} = (1/2\pi) \int_{-\pi}^{\pi} U_j(\eta, \theta)\, e^{in\theta}\, d\theta \tag{6}$$

with the inverse formula

$$U_j(\eta, \theta) = \sum_{-\infty}^{\infty} U_{j,n}\, e^{-in\theta} \tag{7}$$

Substitution of the transformed expressions for the normalized displacement quantities into Equation (4) gives the following equations to be satisfied:

$$[U_0]_{,\eta\eta} + H[V_1]_{,\eta} + 2EU_2 = 0$$

$$F[V_0]_{,\eta\eta} + H[U_1]_{,\eta} + 2V_2 = 0 \tag{8}$$

These equations can be satisfied using techniques described in detail in [12]. It is important to note that one must examine the inter-element boundary conditions on stress and displacement in order to derive a relationship between the V_0, and V_1, and the V_2 functions along with similar relationships between U_j. For example, the inter-element displacement boundary conditions require that

$$U_1 = 2i\, tan(\theta/2)\, U_0 \quad , \quad V_1 = 2i\, tan(\theta/2)\, V_0 \tag{9}$$

while the inter-element displacement boundary conditions give

$$U_2 = i\, tan(\theta/2)\, U_1 \quad , \quad V_2 = i\, tan(\theta/2)\, V_1 \tag{10}$$

Thus equation (8) can be written as two coupled differential equations in terms of the functions U_0 and V_0. Solutions of the form

$$V_0 = Ae^{-D\eta} \quad , \quad U_0 = iBe^{-D\eta} \tag{11}$$

can then be sought by writing the two coupled characteristic equations and solving for the positive roots of D_i. The boundary conditions that must be satisfied are zero shear stress on the crack surface, unit tensile stress at infinity, zero displacement of the intact fibers, and zero normal stress on the crack surface. The problem is actually solved by imposing a unit compressive stress on the crack surface and then adding this solution to the solution of a uniformly stressed plate with no crack using superposition.

Using details given in [12], the final integral equation that must be solved has the form

$$\sum_m a_m I_{n-m} = H/\phi \tag{12}$$

where

$$I_{n-m} = (1/\pi)\int_{-\pi}^{\pi} [\sin\theta/(3+\cos\theta)]\cos(n-m)\theta\, d\theta$$

and

$$\phi = 4[(1-\sqrt{EF})^2 - H^2]^{1/2}\{\sqrt{F}[\sqrt{EF} - (H-1)]$$

$$+ (1/\sqrt{E})[EF + \sqrt{EF} - H(H-1)](H-1)\}$$

Thus the stress concentration factors can be determined as in the shear lag theories [1-11] as $K_1 = 1 - (I_1/I_0)$, etc. Typical values for the first few stress concentration factors are

$$K_1 = 1.1146 \quad , \quad K_2 = 1.4822 \quad , \quad K_3 = 1.6601$$

It is important to note several features of this solution. First, the integrals do not depend on material properties since all material properties are contained in the function ϕ. It is known for anisotropic elasticity theory that the stress concentration factors should not depend on material properties, thus the present solution represents a significant improvement over previous approximate solutions. It should also be noted that all of the above integrals I_{n-m} can be evaluated closed form without having to resort to numerical integration. This feature represents another significant improvement over earlier theories.

On the negative side, it should be observed that the present theory exhibits non-zero horizontal displacement derivatives (commonly referred to as cusps) for odd numbers of broken fibers. Although the stress concentration factors for odd numbers of broken fibers seem reasonable, the existence of the cusps casts considerable doubt as to their validity. The stress concentration factors for even number of fibers, however, seem reasonable and consistent with the theory of elasticity.

The existence of the cusps in this theory must mean that a problem exists with the selected displacement function. It should be noted that the derivation of the nodal stress-displacement relations in equation (3) was accomplished using a very crude form of averaging. The nodal stresses were assumed to be merely the average of the adjacent mid-node quantities. One might then speculate that proper averaging would eliminate the cusps for any number of broken fibers and lead to accurate results. Averaging the strain quantities to obtain the nodal values, however, leads to a much less desirable solution that cannot be solved closed form and in which the stress concentration factors depend on material properties.

One might also try to take a higher-order displacement function in order to generate more functions which could be used to eliminate undesirable behavior such as the cusps. For example, the following cubic displacement functions could be used

$$u_n(x,y) = u_{0,n}(y) + (2x/h)u_{1,n}(y) + [3(2x/h)^2 - 1]u_{2,n}(y) + [5(2x/h)^3 - 3(2x/h)]u_{3,n}(y) \tag{13a}$$

$$v_n(x,y) = v_{0,n}(y) + (2x/h)v_{1,n}(y) + [3(2x/h)^2 - 1]v_{2,n}(y) + [5(2x/h)^3 - 3(2x/h)]v_{3,n}(y) \tag{13b}$$

One can quickly recognize these functions as normalized Legendre polynomials which are orthogonal and thus should improve the averaging properties. It would seem that as many functions as necessary could be added to match any desired boundary conditions including the no-cusp condition. However, the use of these functions in the form of Legendre polynomials led to an

undesirable uncoupling of the equilibrium equations in which half of the assumed functions were eliminated from the solution. The use of these functions also led to zero displacement at each mid-node which is, of course, physically impossible. Thus it was concluded that the addition of higher-order displacement functions would not solve any of the problems and, in fact, created additional problems in the solution procedure.

IV. RECOMMENDATIONS

While the results from this study are significant on their own, the main objective of this summer program from the beginning was to develop analytical methods that could later be used to analyze more complex composite laminates. The unidirectional lamina is merely a first step in the analysis of general composite laminates with internal damage. The author eventually plans to add other forms of internal damage such as matrix cracking to the model.

Present attention, however, must be focused on the development of a correct finite element model that has reasonable behavior exhibited in the solution. It is clear from this study that the addition of more functions will not solve the apparent problems. Thus it appears that the displacements u and v must each have three functions involved which are chosen to give proper averaging across the element and correct behavior at the mid-nodes.

The choice of these functions would seem to be the area for further study. It is certainly not necessary to limit the three functions of x to a constant term, a linear term, and a quadratic term. Certain combinations of higher-order Legendre polynomials could be used in an attempt to generate displacement functions that have the proper behavior and lead to reasonable stress expressions. It is clear that more study should be placed into the selection of these displacement functions to form a correct finite element theory for the composite with broken fibers. It should also be noted that the functions a_m defined in equation (12) may be defined in a more general manner than previously thought. Since the displacements must be real, it is clear that the a_m may have both real and imaginary parts. Thus it may be possible to choose a more general form for these functions that will satisfy the appropriate boundary conditions through orthogonality

while eliminating the existence of the cusps. It is the cusps (non-zero displacement derivatives) that appear to be the major weakness of the theory in its present form. The study of these proposed functions will constitute a major part of the author's research efforts in the near future.

There are several important applications for a correct finite element model beyond the present unidirectional lamina with broken fibers. It may be possible to add other forms of internal damage such as matrix cracking and yielding to the model by adjustment of the stress expressions for appropriate elements. The author has been involved in this type modeling with shear lag models in the past [6-8]. These models accurately predicted the growth of internal damage in boron / aluminum composite laminates.

The correct finite element model should also provide the basis for a new laminated plate theory. The more accurate stress-displacement relations should provide a significant improvement over current laminated plate theories which are based on relatively simple assumptions for isotropic plates and cannot model interlaminar stress effects. Thus the derivation of a finite element theory which was begun in this summer study warrants continued effort in the near future.

REFERENCES

1. Hedgepeth, J. M., 'Stress Concentrations for Filamentary Structures,' NASA TN D-882, 1961.

2. Zweben, C., 'An Approximate Method of Analysis for Notched Unidirectional Composites,' Engineering Fracture Mechanics, Vol. 6, 1974, pp. 1-10.

3. Eringen, A. C., and Kim, B. S., 'Stress Concentration in Filamentary Composites with Broken Fibers,' Princeton University Technical Report No. 36, September 1973, ONR Contract N-00014-67-A-0151-0004.

4. Goree, J. G., and Gross, R. S., 'Analysis of a Unidirectional Composite Containing Broken Fibers and Matrix Damage,' Engineering Fracture Mechanics, Vol. 13, 1980, pp. 563-578.

5. Goree, J. G., and Gross, R. S., 'Stresses in a Three-Dimensional Unidirectional Composite Containing Broken Fibers,' Engineering Fracture Mechanics, Vol. 13, 1980, pp. 395-405.

6. Goree, J. G., Dharani, L. R., and Jones, W. F., 'Mathematical Modeling of Damage in Unidirectional Composites,' NASA Contractor Report 3453, August 1981.

7. Dharani, L. R., Jones, W. F., and Goree, J. G., 'Mathematical Modeling of Damage in Unidirectional Composites,' Engineering Fracture Mechanics, Vol. 17, 1983, pp. 555-573.

8. Jones, W. F., and Goree, J. G., 'Fracture Behavior of Unidirectional Boron / Aluminum Composite Laminates,' NASA Contractor Report 3753, December 1983.

9. Sendeckyj, G. P., and Jones, W. F., 'A Consistent First-Order Shear Lag Theory for Unidirectional Composites with Broken Fibers,' Engineering Fracture Mechanics, (In press.)

10. Jones, W. F., and Sendeckyj, G. P., 'A Second Order Shear Lag Theory for Unidirectional Composites with Broken Fibers,' Journal of Applied Mechanics. (Submitted for publication.)

11. Jones, W. F., 'Fracture Behavior of Cross-Ply Graphite / Epoxy Composite Laminates,' Final Report USAF Contract F49620-82-C-0035, August 1984.

12. Sendeckyj, G. P., and Jones, W. F., 'Approximate Solutions for Unidirectional Composites with Broken Fibers,' Eleventh Annual DOD / NASA Mechanics of Composites Review, Dayton, OH, October 1985.

1985 USAF-UES SUMMER FACULTY RESEARCH PROGRAM/

GRADUATE STUDENT SUMMER SUPPORT PROGRAM

Sponsored by the

AIR FORCE OFFICE OF SCIENTIFIC RESEARCH

Conducted by the

UNIVERSAL ENERGY SYSTEMS, INC.

FINAL REPORT

LONG TERM LIFE EXPECTANCY RADIATION EFFECTS: AN ULTRASTRUCTURAL STUDY OF BRAIN TUMORS DEVELOPED IN MACACA MULATTA FOLLOWING EXPOSURE TO PROTON RADIATION

Prepared by: Betty Ruth Jones, PH.D
Richard Alexander Hunt, Graduate Assistant

Academic Rank: Associate Professor and Director of the Institute of Electron Microscopy

Department and University: Department of Biology
Morehouse College

Research Location: Brooks Air Force Base
Veterinary Sciences Division
Veterinary Sciences Pathology Branch
Electron Microscopy Section

USAF Research Collaborator:
Major Harold Davis, DVM,PH.D
Chief, Veterinary Sciences Pathology Branch

DATE: September 20, 1985

CONTRACT NO: F49620-85-C-0013

NOTE: Due to the nature of this research project approval has been granted by UES to exceed the required page stipulations.

LONG TERM LIFE EXPECTANCY RADIATION EFFECTS: AN ULTRASTRUCTURAL STUDY OF BRAIN TUMORS DEVELOPED IN MACACA MULATTA FOLLOWING EXPOSURE TO PROTON RADIATION

by

Betty Ruth Jones, PH.D.
Richard Alexander Hunt, Graduate Assistant

ABSTRACT

In 1964 the United States Air Force School of Aerospace Medicine (USAFSAM) and the National Aeronautics and Space Administration (NASA) initiated a series of whole body experiments to determine the effects of space radiation primarily proton radiation on *Macaca mulatta* (Rhesus Monkey). Out of 453 exposed primates, 21 developed brain tumors concentrated at an energy level of 55 MeV and between 200-1200 rads. No tumors were observed in control animals. The focus of one phase of the current research was to study the ultrastructure of these tumors in addition to specifically assessing tumor type and confirming light microscopy tumor diagnosis. As a result of this study techniques of electron microscopy (EM) and the transmission electron microscope have proven to be useful for the precise cellular classification and identification of specific markers for tumor diagnosis.

It has provided an increased specificity, supplemental adjunct and confirmation to light microscopy tumor diagnosis. In addition, new data have been provided on the EM of primate brain tumors following exposure to proton radiation. The data from this study also shows that formalin-fixed material over long periods of time prior to conventional EM methods can provide quality information. The following brain tumors in monkeys were studied at the ultrastructural level following exposure to proton radiation: a malignant meningioma, an ependymoma and four glioblastomas. The findings of each tumor are summarized in the result section of this report.

I. INTRODUCTION:

a. Background Information on Summer Fellow

EDUCATION

1973 B.S., Rust College, Holly Springs, Mississippi. Major: Biology; Minor: Chemistry; Special emphasis in Zoology.

1975 M.S., Atlanta University, Atlanta, Georgia. Special emphasis in Cell Biology and Biological Ultrastructure.

1978 Ph.D., Atlanta University, Atlanta, Georgia. Special emphasis in Parasitology and Ultracytochemistry.

1978-1979 Postdoctoral Fellow (with Dr. J. K. Haynes), Department of Biology, Morehouse College, Atlanta, Georgia.

1981-1983 Postdoctoral Fellow (with Dr. Steve Chia-Tung Pan), Department of Tropical Public Health, Harvard School of Public Health, and Dr. Susumu Ito, Department of Anatomy, Harvard Medical School, Boston, Massachusetts.

1981-1983 Bunting Fellow at The Mary Ingraham Bunting Institute of Radcliffe College, Cambridge, Massachusetts.

ADDITIONAL EDUCATIONAL EXPERIENCE

Workshops and Short Courses

1981 Workshops: (1) Advantages of Plastic Embedding for Light Microscopy;
(2) Histologic Technique and Cytochemical Methods in Hematopathology; sponsored by the Georgia Society for Histotechnology, Jekyll Island, Georgia, May, supported by Morehouse College.

1980 Short Course: Immunobiology; Chautauqua course sponsored by National Science Foundation, University of Georgia, Athens, Georgia. October, 1980 and March, 1981.

1980 Workshop in Geriatric and Gerontology: Duke University Medical Center, Durham, North Carolina; January, Supported by National Caucus on Black Aging.

1979 Short Course: Techniques in Electron Microscopy: TEM, SEM, Freeze-Fracture Replication, X-Ray Microanalysis and EM Autoradiography. Duke University Marine Laboratory, Beaufort, North Carolina; September, Supported by Morehouse College.

1979 Short Course: Immunocytochemistry; Duke University Marine Laboratory, Beaufort, North Carolina; September, Supported by Morehouse College.

1979 Short Course: Frontiers of Neuroscience: Chautauqua course supported by National Science Foundation, University of Georgia, Athens, Georgia. October 1979 and March 1980.

1979 Short Course: Freeze-Etching in Electron Microscopy; Macy Scholar; Marine Biological Laboratory, Woods Hole, Massachusetts; April, Supported by Josiah Macy Award.

1979 Short Course: Quantitative Analysis of Electron Micrographs: Stereology, Morphometry, Optical Diffraction and Three-Dimensional Reconstruction; Marine Biological Laboratory, Woods Hole, Massachusetts; December, Supported by Josiah Macy Award.

RESEARCH PUBLICATIONS

1. Jones, Betty R. (1975).
   Ultrastructural Study of the Cytotoxic Effects of Emetine Hydrochloride in Kidney and Liver Cells of Long-Evan Rats. M.S. Thesis (Cell Biology), Atlanta University, Atlanta, GA.

2. Jones, Betty R. (1978).
   Scanning Electron Microscopy and the Ultrastructural Localization of Alkaline Phosphatase and Acetylcholinesterase Activity in the Tegument of the Cysticercus of *Hydatigera taeniaeformis*. Ph.D. Thesis (Parasitology) Atlanta University, Atlanta, GA.

3. Jones, Betty R., B. F. Smith and W. B. LeFlore (1977).
   Scanning Electron Microscopy of the Scolex of the Cysticercus of *Hydatigera taeniaeformis*. Microbios Letter, 4:71-78.

4. Jones, Betty R., B. F. Smith and W. B. LeFlore (1977).
   Electron Scans of the Bladder of the cysticercus of *Hydatigera taeniaeformis*. Microbios Letters, 4:145-150.

5. Jones, Betty R., and G. A. Ofosu (1978).
   Cytotoxic Effects of Emetine Hydrochloride in the Kidney of Long-Evan Rats. Cytobios, 19:109-118.

6. Jones, Betty R., B. F. Smith and W. B. LeFlore (1979).
   Ultrastructural Localization of Alkaline Phosphatase Activity in the Tegument of the Cysticercus of *Hydatigera taeniaeformis*. Cytobios, 24:195-209.

7. Jones, Betty R., B. F. Smith and W. B. LeFlore (1979). Ultrastructural Localization of Acetylcholinesterase Activity in the Scolex of the Cysticercus of _Hydatigera taeniaeformis_. Cytobios, 26:7-24.

8. Jones, Betty R., B. F. Smith and W. B. LeFlore (1979). Scanning Electron Microscopy of the Infective Eggs of _Hydatigera taeniaeformis_. Microbios, 24:185-193.

9. Jones, Betty R, B. F. Smith and W. B. LeFlore (1979). The Ultrastructural Localization of Acetylcholinesterase Activity in the Scolex of the Cysticercus of _Hydatigera taeniaeformis_. (Abst.) Trans. Amer. Micros. Soc., 98:194.

10. Jones, Betty R., (1979). Application of Scanning Electron Microscopy and X-Ray Microanalysis to Studies on the Infective Eggs of _Hydatigera taeniaeformis_. IRCS Medical Science, 7:391-392.

11. Jones, Betty R., (1980) Surface Topography Features of the Scolex and Strobila of the Cysticercus of _Hydatigera taeniaeformis_. IRCS Medical Science, 8:28-29.

12. Jones, Betty R., (1980). Electron Microscopic Localization of Acetylcholinesterase activity in the Excretory Collection Tubules of the Cysticercus of _Hydatigera taeniaeformis_. IRCS Medical Science, 8:80-81.

13. Jones, Betty R., (1980). Three-Dimensional Surface Topography Ultrastructure and X-Ray Microanalysis of the Cyst Wall of _Cysticercus fasciolaris_. Rivista Di Parasitologia, 61:397-411.

14. Jones, Betty R., J. R. Prince and S. A. Bulls (1980). Electron Microscopic Study of the Effects of Dimethyl Sulfoxide (DMSO) in Mammary Glands of Long-Evan Rats during Fetalogenesis. Cytobios, 20:29-40.

15. Jones, Betty R., (1982). Freeze-Fracture Replication of the Tegument of _Cysticercus fasciolaris_. Rivista Di Parasitologia, 62:281-285.

16. Jones, Betty R., (1983). Structure of the Cyst Wall of _Cysticercus fasciolaris_ through Application of the Freeze-Fracture Replication Technique. Rivista Di Parasitologia, 64:49-59.

RESEARCH PAPERS SUBMITTED

17. Jones, Betty R. and S. C. Pan (1984).
Fine Structure of Granulomas in the Ovotestis of Biomphalaria glabrata infected with Schistosoma mansoni. Submitted to the Journal of Invertebrate Pathology.

18. Jones, Betty R. and S. C. Pan (1984).
Scanning Electron Microscopy of the Cilia of Several Snail Vectors Involved in the Transmission of Schistosomiasis. Submitted to the Journal of Invertebrate Pathology.

BOOKS PUBLISHED

19. Jones, Betty R., (1983).
Electron Microscopy: 39 Basic and Advanced Exercises, A Research Protocol, An Intensive Short Course and Workshop Layout. First Edition, Library Research Associates, Monroe, New York, August, 1983.

20. Jones, Betty R. (1986).
Electron Microscopy: 41 Exercises by 17 Scientists, Library Research Associates, Monroe, New York. (*Second Edition to be released in January).

NUMBER OF ABSTRACT PUBLICATIONS AND PRESENTATIONS AT SCIENTIFIC MEETINGS (34)

NUMBER OF INVITED RESEARCH COLLOQUIUMS (OVERSEAS AND IN THE UNITED STATES, 11)

PENDING INVITED RESEARCH COLLOQUIUMS (6)

NUMBER OF ELECTRON MICROSCOPY WORKSHOPS DIRECTED BY BETTY RUTH JONES (5)

B. Nature of USAF Research Area which Resulted in a Laboratory Assignment

The research reported in this paper took place in the Veterinary Sciences (VS) Division, Veterinary Sciences Pathology (VSP) Branch of the Electron Microscopy Section at Brooks AFB. The ongoing research in this division was very much in accord with some of my research interests and future research goals. My

area of research specialiization in Biology is Medical Parasitology, Tropical Medicine and Electron Microscopy. For many years I have been interested in acquiring further knowledge and skills in Tumor Biology. Some of the parasites we are investigating have been found to form tumorlike masses in various host tissues. My research assignment at Brooks provided me with the opportunity to carry out tumor research with excellent and skillful pathologists trained in Veterinary Medicine (see Acknowledgements). The research project I am involved in has been ongoing since 1964 and is concerned with the effects of Long Term Life Expectancy Radiation on Macaca mulatta (Rhesus monkey). The background information and USAF Relevancy of this project and my specific research role(s) can be found in section II (B) of this report.

II. OBJECTIVES OF THE RESEARCH EFFORT

A. SPECIFIC OBJECTIVES:

i. To carry out a detailed ultrastructural study on brain tumors developed in _Mucaca mulatta_ following exposure to proton radiation

ii. To demonstrate the usefulness of electron microscopy in the diagnosis, classification and pathology of brain tumors developed in _M. mulatta_ following exposure to proton radiation

iii. To study the ultrastructure of the following brain tumors developed in _M. mulatta_ following exposure to proton radiation: A malignant meningioma, an ependymoma and four different glioblastomas

B. BACKGROUND INFORMATION ON PROJECT AND USAF RELEVANCE:

This project is part of a long-term team approach. The following is a cited summary of background information on the project, USAF relevancy and role of the current summer fellow participant. In 1964 the Air Force School of Aerospace Medicine at Brooks AFB and the National Aeronautics and Space Administration began a series of whole body exposure experiments to determine the effects of space radiation, primarily proton on Rhesus monkeys. The hypothesis being tested were as follows: 1) delayed effects from whole body exposure to proton radiation are related to both dose and initial particle energy and occur randomly in time; and 2) that delayed effects from whole body exposure to proton radiation are related to both dose and initial

particle energy, however, latency periods are inversely related to dose.

Initial experiments were designed to examine only the short term or acute effects (i.e. LD_{50} levels). However, as each acute experiment was completed, survivors, both experimental and control, began to accumulate and the idea for a long term study was born. Monkeys surviving the 120-day post-exposure period were banded together to form the "Chronic Radiation Colony." These animals have been periodically evaluated to determine delayed effects from proton radiation. Follow-up reports on the colony have been published at five-year intervals. Table I is a summary of original proton experiments.

Table 1. Summary of Original Proton Experiments.

Proton Energy (MeV)	Tissue Penetration Depth	Dose Rate (Rad/min)	Dose Range (Rad)	Date of Exposure	Facility Site	No. of Animals Exposed (Whole body)
32	1 cm	100	280-2800	July 64	Oak Ridge Isochronous Cyclotron (ORIC)	52
*55	2.5 cm	100	25-1200	Apr 65	ORIC	96
138	Whole body	57	210-1220	Jan 65	Harvard Cyclotron	102
400	Whole body	16	50-1200	Mar 65	University of Chicago Cyclotron	97
2300	Whole body	25	56-1130	Oct 65	Brookhaven Cosmotron	106
						453

*The majority of the Tumors occurred at this energy level.

Several latent post-radiation effects were evident in monkeys from 1960-1984. However, this report will focus on the most dramatic latent effects in the colony. The most dramatic latent effects were neoplasms. Malignant neoplasms were reported and the majority of these were diagnosed in the 55 MeV proton exposed monkeys. Spontaneous neoplasms rarely occur in Rhesus monkeys. Glioblastomas were the predominant tumors occuring in the 55 MeV energy group. No tumors were found below 200 rads and no tumors were observed in control animals. Currently 20 tumors out of 453 exposed monkeys have been confirmed in high energy proton exposed primates. The distribution of these tumors are shown in Figure 1.

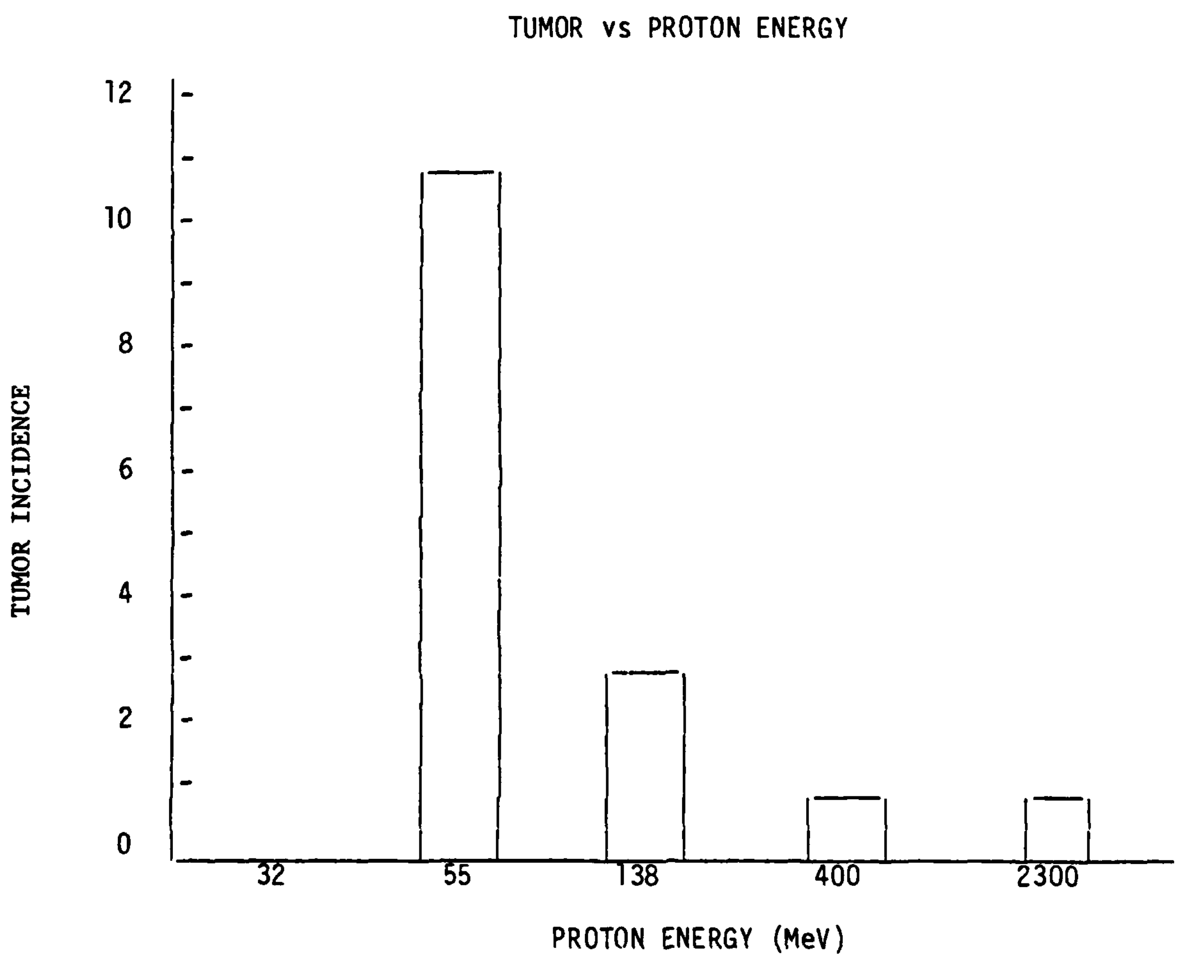

Figure 1. TUMOR DISTRIBUTION VS PROTON ENERGY.

USAF Relevancy and Justification:

Permissible exposure levels for acute radiation effects are well documented. Delayed (latent) effects, 1-20 years post-exposure, are only now emerging. Recent review of personnel exposures during atmosphere testing, reactor maintenance, uranium and nuclear materials fabrication suggests an increased incidence of fatal cancers somewhat above the national average. At some point in time, radiation effects attributed to space flight may also be scrutinized. Current and future findings from the only primate colony in the free world surviving nearly 15 years after radiation exposure (1965), will be highly relevant in establishing safe exposure criteria for extended space flights. In addition, if a reliable RBE for high energy proton particles can be established utilizing data available in the literature and data from x-ray exposed monkeys in the Chronic Radiation Colony, useful predictive information on the long term effects of low levels of radiation encountered in the environment and during nuclear weapons testing may be realized. (Citation for background information; Personal Communication, Radiation Sciences Division, USAFSAM Project Number T64131),

Role of the Current Summer Fellow Participant on the Project:

The primary role of the Summer faculty fellow on this project is to implement a detailed ultrastructural analysis of proton exposed primate brain tumors that occurred between 1966-to the present time; and to confirm and supplement light microscopic histopathology findings on tumor diagnosis and classification. Such electron microscopy

(EM) data from this study should demonstrate the usefulness of EM in the diagnosis of primate brain tumors in addition to essential data on similarities and differences in tumor structure.

C. PERTINENT REVIEW OF LITERATURE ON TUMORS:

In humans, incidence and statistical data show that primary tumors of the central nervous system and its coverings account for about 1.2% of all autopsied deaths and for approximately 9% of all primary neoplasms. Eighty-five percent of them are found within the cranial cavity.

"Among the intracranial tumors, those of central neurogenic origin claim priority in number and complexity. These are the tumors derived from the intrinsic or parenchymatous elements of the central nervous system, excluding the microglia; they are widely credited to account for 40 to 50% of all intracranial tumors both primary and metastatic encountered at all ages of life. These tumors have been termed as tumors of the glioma group. Second to the gliomas in neurosurgical importance in adults are the meningiomas." Meningiomas account for 13 to 18 % of brain tumors. The incidence of ependymomas of all age groups is 6%. Very little is known of the tumor formation in the central nervous system of man (Rubenstein, 1981).

As to our knowledge, no reports have been published on the effects of proton radiation on brain tumors of monkeys at the subcellular level. A few pertinent studies have appeared on the use of electron microscopy in the diagnosis and classification of tumors in general; and numerous papers have appeared in the literature on the ultrastructure of meningiomas, ependymomas and glioblastomas. However, none of

these studies have been carried out on EM of brain tumors occurring in primates. The majority of papers on EM of brain tumors have been from human rats, mice and guinea pigs. Thus, no work has been reported on the ultrastructure of brain tumors of monkeys following long-term proton radiation effects.

Electron Microscopy of meningiomas include references (1-24), Ependymomas, (25-37) and pertinent references on glioblastomas include references (38-59). Since this review is extensive and due to the page stipulations for this report, the faculty fellow has omitted connotations as to the findings of the above papers.

III. EXPERIMENTAL DESIGN:

A. LIGHT MICROSCOPY (Toluidine Blue 1 Micron Thick Sections)

Necropsy, gross anatomical and histological hematoxylin-eosin thick sectioning procedures for brain tumors of primates were carried out by other team researchers in the VSP branch. The following procedure is a detailed account of materials and methods implemented by the summer faculty research fellow and graduate student assistant.

One micron thick sections were cut from the six different brain tumors of *Macaca mulatta* (for tumor type and classification see (B) under electron microscopy). Thick sections were cut from embedded epoxy resin blocks on a Sorvall MT-2 ultramicrotome. Serial sections were placed on glass slides and stained for 2-3 minutes on a hot plate at 40°C. Sections were rinsed in distilled water for 1 minute, and then cleared in 95% ethanol for 5-10 seconds. Tissues were then air-dried and mounted in permount and viewed under a light microscope. Photographs of thick sections were taken at desirable magnifications.

B. ELECTRON MICROSCOPY

All of the brain tumors examined for electron microscopy in this study were previously preserved in 10% formalin. The following is a description of how the six different tumors were prepared following removal from the brain of monkeys. The malignant meningioma, accession number N84-1525, was fixed in Karnovsky's fixative by way of perfusion in 1984, and subsequently prepared for electron microscopy. The ependymoma, accession number N84-2482, was fixed in Karnovsky's fixative by way of the immersion technique in 1984 and then prepared for electron microscopy. The glioblastoma, accession number, A73-403

was prepared for electron microscopy in 1983 using 1% osmium tetroxide as the only fixative, and the immersion method was used. Glioblastomas, accession numbers N66-754, N69-931, and N66-116 were surgically removed from the brain of monkeys between 1966-1969 and preserved in 10% formalin until 1985, after which they were fixed in Karnovsky's fixative using the immersion method.

Following primary fixation in Karnovsky's solution, the glioblastoma tissues were rinsed for 1 hour in 3 changes of 0.25 M of sodium cacodylate pH 7.4, post-fixed for 2 hours in 1% osmium tetroxide buffered with sodium cacodylate at 4°C. Tissues were then rinsed in buffer and dehydrated in a graded series of ethanol (50-100%/15 minutes each, and then 2 changes of 100%). Specimens were infiltrated and embedded in Epon 812 or LX-12 epoxy resin and polymerized for 24-48 hours at 60°C. One micron thick sections were cut from resin blocks using glass and diamond knives. Thick sections were then stained with toluidine blue. Ultrathin sections were cut with diamond knives at 500-800 A° on a Sorvall MT 5000 ultramicrotome and picked up on 400 mesh copper grids. Sections were stained in uranyl acetate and lead citrate in a LKB ultrastainer and viewed in a Hitachi 12-A transmission electron microscope. Photographs were taken at desirable magnifications on electron image film.

IV. ELECTRON MICROSCOPY RESULTS:

NOTE: TO THE REVIEW COMMITTEE

This research project involves a detailed, comprehensive and extensive ultrastructural study of several brain tumors found in Rhesus monkeys following exposure to 55 MeV of proton radiation. Numerous grids were examined for electron microscopy and numerous electron micrographs were taken at desired magnifications. Because of the nature of this study and because of the number of tumors in which ultrastructural data has been obtained, it was necessary to exceed the page stipulations for the final report.

However, the micrographic data for each tumor included in this section of the report is pertinent and has been selected from a very large pool of micrographs. The format for this section consist of descriptions of the results, an explanation of figures and a sequential compilation of micrographs for each tumor. Labeling of micrographs have been omitted due to the large number of micrographs utilized in this report and due to the detailed caption explaining each micrograph.

The following outline has been developed for this section:

a. Electron Microscopy of a Malignant Meningioma #1525

b. Electron Microscopy of an Ependymoma #2482

c. Electron Microscopy of Glioblastomas

  i. Glioblastoma #N69-931

  ii. Glioblastoma #N66-116

  iii. Glioblastoma #N66-403

  iv. Glioblastoma #N66-754

a. Malignant Meningioma #1525

The fine structural results of this study revealed that the appearance of the malignant meningioma was highly variable. We encountered several different patterns of cellular organization based on the overall general profile of cell populations, cell nuclei, the formation of psammoma bodies in cells, and cellular abnormalities. These patterns of cellular variabilities were consistent throughout the entire tumor as revealed from the microscopic examination of several grids.

The following cellular patterns were observed in the meningioma: endothelial cells of meningioma, Type 1, cells showing a fibroblast-like pattern with elongated-blunt nuclei; endothelial cells, Type 2, cells exhibiting a fibroblast-like pattern with pronounced spindle-shaped nuclei; endothelial cells, Type 3A, cells with elongated nuclei but not showing a fibroblast-like organization; endothelial cells, Type 3B, cells with an elongated nuclei and marked indentation of the nuclear membrane; endothelial cells, Type 4, cells with polyhedral-like nuclei; endothelial cells, Type 5, cells showing polygonal-like nuclei, endothelial cells, Type 6, cells characterized by transitional or mixed nuclei; and endothelial cells, Type 7, cells displaying round and oval nuclei.

A large percentage of cellular populations showed the presence of forming psammoma bodies and well differentiated psammona bodies. Primarily, all populations of cells examined showed extensive and pronounced interdigitation of adjacent cell membranes with desmosomes. Collagen fibers and microfilaments were abundant in the luminal spaces of cells. Cellular abnormalities were observed in several populations of mitochondria. The following will present a description of the structural features

and characteristics of malignant meningioma cells.

Type 1 endothelial cells of the meningioma exhibited a fibroblast-like pattern. The dark nuclei appeared elongate-blunt in appearance with indentations of the nuclear membrane. The heterochromatin was regularly distributed peripherally along the nuclear membrane. The cells did not appear to be closely packed but were in close enough proximity to form a somewhat concentric circumscribed profile. Intercellular spaces, mitochrondria irregular in shape and size, some with a disrupted cristae, numerous collagen fibers, microfilaments and microvilli were observed. The fibers and microfilaments occupied the luminal space of the capillary (Figure 1). The fibroblast-like cells in Figure 2 (Type 2 endothelial cells) were characterized by pronounced elongated spindle-shaped nuclei. These fibroblast-like cells tended to lie close to the basal lamina of the capillary wall and contained a small number of mitochondria. The cells were closely packed and intercellular spaces were not evident.

Type 3A endothelial cells of the meningioma were exemplified by elongated nuclei that were somewhat elliptical in appearance. These cells were found in the interstitial space of tumor cells. The cells showed cytoplasmic processes protruding from the surface, were rich in glycogen, contained small, irregular shaped mitochondria, numerous granular endoplasmic reticuli, electron lucent cytoplasm, membrane-bound vesicles, basal bodies on blepharoplasts with rootlets and saccules of golgi. Electron dense granules containing amorphous precipitates of various sizes and interdigitation of adjacent cell membranes were evident (Figure 3).

Type 3B endothelial cells were characterized by elongated nuclei with marked indented nuclear membranes. The organelles in the cytoplasm were loosely distributed and appeared to show degenerative changes. The mitochondria in these cell populations showed shrinkage, irregularities in shape and size, and paucity of the cristae. A few golgi and a scarce number of granular endoplasmic reticuli could be seen in the cytoplasm. Numerous vesicles, double membrane-bound bodies and vacuoles occupied the cytoplasm of these cells (Figure 4).

Type 4 endothelial cells contained polyhedral-like nuclei. These cells showed nuclei with well-defined nuclear membranes and prominent indentations. The cells were found in the capillary wall of the meningioma. The basal lamina of these cells appeared dilated and contained amorphous material. Numerous mitochondria were found devoid of cristae (Figure 5).

Type 5 endothelial cells of the meningioma showed polygonal-like nuclei. These cells occupied the wall of the capillary, and were characterized by several nuclei with a polygonal-like profile. Of particular interest was the presence of two nuclei in the same cell in close proximity to one another. One of the nuclei contained a conspicuous nucleolus with several electron dense membrane inclusions and small electron lucent vesicles. The mitochondria showed shrinkage, and desmosomes were prominent in adjacent cell membranes. The cell membranes showed interdigitation. The collagen fibers were grouped together in bundles, and microfilaments were recognizable in the luminal space. Basal bodies or blepharoplasts with their ciliary rootles and golgi could be seen near the nucleus of a cell. The basal lamina showed marked distention (Figure 6). Other

Type 5 endothelial cells contained large electron dense lysosome-like bodies in the interstitial space and septate desmosomes at the margins of the capillaries (Figure 7).

Type 6 endothelial cells of the meningioma were denoted as showing characteristic transitional or mixed nuclei. These cells contained nuclei that varied in shape and size. The profile for these cells appeared to be somewhat polygonal-like and they were connected to one another by desmosomes. The mitochondria were moderate in number and showed polyploidy (Figure 8).

Type 7 endothelial cells comprising the meningioma were characterized by round to oval nuclei. Cells exemplifying this type of nuclei appeared to be more abundant as compared to the above mentioned types. The nuclei varied in size with well-defined nuclear membranes and regularly formed chromatin areas. The nucleoli of these cell populations when apparent were found close to the nuclear membrane. The cells contained an abundant number of mitochondria that were irregular in size and shape; few granular endoplasmic reticuli; well-developed golgi, forming vacuoles and glycogen occupied the interstitial spaces, and pinocytic vesicles were also recognizable at the membrane surface (Figures 9-10).

Other areas of the meningioma showed Type 7 endothelial cells that were polygonal-like in profile with short processes, highly specialized desmosomes with intracellular plaques, free ribosomes, ciliary rootlets in the cytoplasm and cells devoid of organelles. Another interesting feature of these cells was that various populations contained nuclei of a considerable small size, and a large conspicuous nucleolus was sometimes apparent. These nuclei appeared to be undergoing degenerative changes

(Figure 11).

In addition to variations in endothelial cell types of the malignant meningioma, another interesting feature of several populations of cells was the presence of forming and well-developed mature psammoma bodies. The psammoma bodies appeared to start their formation in the luminal space of the capillaries as membrane vesicles and giant bodies. There appears to be a close association of these vesicles and giant bodies with collagen fibers and filaments. The presence of thick electron dense vesicles varying in size and large giant bodies of various sizes with dense precipitates deposited within varying degrees was seen consistently throughout the luminal spaces of several populations of cells. The dense deposition of precipitate was thought to be hydroxyapatite. In some instances, the giant bodies appeared to be fused. The vesicles and bodies appeared to be primarily dispersed among collagen fibers and microfilaments. The collagen fibers showed different characteristic patterns ranging from a straight-curved profile to that of a circumscribed clumping-like arrangement. Some luminal spaces showed a dramatic increase in the number of microfilaments versus collagen fibers; while others showed a dominance of collagen fibers that appeared to be highly organized.

Several pericyte cells with small round mitochondria, lipid-like dense granules and irregular shaped elongated nuclei with indented nuclear membranes made up the capillaries. At various magnifications, the basal lamina appeared as a filamentous substructure. The surrounding cells comprising the wall of the capillaries showed pronounced interdigitation of adjacent cell membranes with desmosomes and irregular shaped membrane-bound vesicles. Extensive vacuolation, cellular remnants and some

degenerative changes were apparent in some capillary walls. The nuclei of these cells varied in shape and the nucleolus was eccentrically located. Large intracellular spaces were apparent among various areas in the walls of the tumor. The basal lamina in some areas of the tumor showed marked distention; and elongated cell processes projecting in the lumen were rich in lysosome-like dense bodies that varied in size (Figures 12-13).

As the vesicles in the luminal space increased in size and the walls thicken, the collagen fibers appeared to show a more pronounced circumscribed, clumping-like and spatial arrangement. At this stage, the appearance of different stages of psammoma bodies were evident. These psammoma bodies appeared to be fibrous in nature and were found in the luminal space among many vesicles and disorganized collagen fibers. Cellular remnants containing dense lysosome-like bodies could also be seen in the luminal space. The psammoma bodies appeared to show numerous variations in size, the smallest ranging from 3 mm to the largest measuring between 34-36 mm in diameter. The vacant spaces exemplified in some of the psammona bodies are possibly artifacts due to sectioning. The surrounding meningioma cells making up the capillary wall were rich in granular endoplasmic reticuli, ribosomes and mitochondria (Figures 14).

Figure 15 shows numerous fibrous psammoma bodies and several concentric double thick walled psammoma bodies with an electron dense center. Of particular interest was the presence of a large dense body from which smaller psammoma bodies appeared to radiate. This larger body was irregular in shape, had a branched fibrous periphery, and filaments could be seen throughout its center. The fibrous psammoma bodies appeared to be more dominant than the concentric ones. The concentric bodies exemplified

varying degrees of electron dense centers and outer boundaries. However, in all psammoma structures studied, a dark, heavy deposition of material comprised either the entire body (i.e. fibrous psammoma bodies) or dense centers and or outermost membrane areas (i.e. concentric psammoma bodies). The luminal spaces continued to show the presence of numerous smaller vesicles with a dense thick wall.

Other luminal spaces of meningiomas showed well-developed, mature fibrous and concentric double thick walled psammoma bodies. Some of the concentric bodies had a large translucent center, while the mature fibrous psammoma structures were devoid of a center (Figure 16). At high magnifications, some of the fibrous psammoma bodies showed numerous short anastomosing fibers that appeared to form an irregular three-dimensional network (Figure 17).

Occasionally, the interstitial spaces of meningioma cells contained meningiocytic whorls. These whorls showed the presence of psammoma bodies in their center. The whorls and psammoma bodies were fibrous in nature. Degenerative cells with irregular shaped electron dense inclusions could be seen nearby (Figure 18).

Low magnifications of several populations of meningioma cells showed a close compacted arrangement with their membrane boundaries interlocking. A large number of cells contained nuclei round in shape, varying in size, and some contained a distinct nucleolus which was found in close proximity with the nuclear membrane. Patches of heterochromatin appeared to be primarily confined to the peripheral boundaries of the nuclear membrane. A few conspicuous nuclei showed a marked irregularity in size compared to nuclei in surrounding cell populations. Mitochondria were numerous in

number and granular endoplasmic reticuli contained an abundance of ribosomes. The cisternae comprising the golgi appeared to be short and closely packed. Numerous dense and lucent vesicles were found in the cytoplasm. Some cells contained double membrane-bound vesicles. Intercellular spaces were prominent throughout cell populations. Desmosomes were apparent in cell membrane and pronounced membrane interdigitations were observed. Microvilli lined the free membrane surface of some cells, and coated pinocytic vesicles were present in the intercellular spaces (Figures 19-21).

An interesting structural feature of some meningioma cells was conspicuous nuclei. The nucleus of these cells contained a nucleolus and several large irregular shaped membrane-bound bodies. Some of the bodies appeared to be intrinsically located in the nucleolus. The bodies were dense and contained smaller membrane inclusions that were either dense or translucent. Some of the bodies appeared to be surrounded by patches of heterochromatin. Lysosome-like bodies could be seen in some cells, and ciliary bodies could be seen in the cytoplasm near saccules of golgi (Figures 22-23).

The intracytoplasmic processes of meningioma cells were branched, long or short and connected by way of septate desmosomes. The processes of cells were rich in glycogen and mitochondria (Figure 24). Mitochondria of some tumor cells showed extensive paucity of cristae and polyploidy (Figure 25).

EXPLANATION OF FIGURES

Malignant Meningioma #1525

Figure 1. Malignant Meningioma: Endothelial Cells, Type 1, Fibroblast-like Pattern. This area in the meningioma contains endothelial cells that show fibroblast-like characteristics. The cells exemplify an elongated, irregular shape with well-defined dark nuclei containing indentations in the nuclear membrane, and regularly peripherally distributed heterochromatin. The cells do not appear to be closely packed but are in a close enough proximity to form a somewhat concentric circumscribed profile. Intercellular spaces can be seen among cells. The mitochondria of cells are irregular in shape and size, and show a disrupted cristae. Electron dense granules and glycogen can be seen in some cells, and a few microvilli are recognizable along the free membrane surface. Numerous collagen fibers, microfilaments and vacuoles can be seen in the postluminal space. The adjacent capillary shows some disrupted mitochondria; and microfilaments in the lumen. The cells appear to be undergoing some degenerative changes. X 1320.

Figure 2. Malignant Meningioma: Endothelial Cells, Type 2, Fibroblast-like Pattern. These fibroblast like cells appear to be close to the basal lamina of the capillary wall. The nuclei show an elongated profile. Some nuclei show a pronounced spindle-shaped profile. Fenestrations of microvilli can be seen lining the lumen of the capillary. Some cells contain a small number of mitochondria that exhibit disorganized cristae. Other cells show a scarcity of cellular organelles. The basal lamina appears distended. Collagen fibers and membrane bound vesicles can be seen in the post-capillary space. X1320.

Figure 3. Malignant Meningioma: Endothelial Cells, Type 3A, Elongated Nuclei. These cells are found in the interstitial space of tumor cells adjacent to numerous microfilaments. Cytoplasmic processes can be seen protruding from the cell surface, and the cells are rich in glycogen. The mitochondria are small with intact cristae and vary in size. Numerous granular endoplasmic reticuli can be seen in the cytoplasm. The cytoplasm appears electron lucent. Several membrane-bound vesicles of various sizes occupy the cytoplasm. One of the cells contains a basal body, or blepharoplast, and the ciliary rootlet is located in close proximity with the nucleus of the cell. Minute short saccules of golgi can be seen nearby. The nucleus of the cell shows an elongated profile. Interdigitations of adjacent cell membranes can also be seen. Another area of a nearby cell shows the presence of golgi and electron dense bodies containing an amorphous precipitate. The bodies vary in size and are close to the cell membrane. X990.

Figure 4. Malignant Meningioma: Endothelial Cells, Type 3B, Oval-Elongated Nuclei. These tumor cells consist of oval-elongated nuclei with an indented nuclear membrane. The cellular organelles in the cytoplasm are loosely distributed and appear to show degenerative changes. The mitochondria show shrinkage, irregularities in shape and size and paucity of the cristae. A few golgi can be seen near the nucleus. Granular endoplasmic reticuli appear to be scarce in the cytoplasm. Numerous vesicles of various sizes are distributed throughout the cytoplasm, and double membrane-bound bodies containing electron dense inclusions can be seen in some cells. Other cells show large vacuoles and a moderate amount of glycogen. X1320.

Figure 5. Malignant Meningioma: Endothelial Cells, Type 4, Polyhedral-like Nuclei. The capillary wall of this area of the meningioma shows endothelial cells with polyhedral-like nuclei. The nuclear membrane is well-defined and shows indentations. The basal lamina appears dilated and contains amorphous material. Many mitochondria showing a loss of cristae are present in the cells. X1650.

Figure 6. Malignant Meningioma: Endothelial Cells, Type 5A, Polygonal-like Nuclei. The capillary wall of the meningioma cells contain several nuclei with a polygonal-like shape. Note the presence of two nuclei in the same cells in close proximity to one conspicuous nucleolus with several electron dense membrane inclusions and small electron lucent vesicles. The mitochondria of the cells show shrinkage. Desmosomes can be seen in adjacent cell membranes, and cell membranes show interdigitation. Collagen fibers appear to be grouped together in bundles among microfilaments in the luminal space. Basal bodies, or blepharoplasts and ciliary rootlets, and golgi can be seen near the nucleus next to the distended basal lamina. X990.

Figure 7. Malignant Meningioma: Endothelial Cells, Type 5B, Polygonal-like Nuclei. This micrograph shows polygonal-like nuclei in two adjacent capillary walls. The nuclear membrane appears well defined and a large lysosome-like body that is electron dense can be seen in the interstitial space. Septate desmosomes can be seen at the margins of the capillary. X825.

Figure 8. Malignant Meningioma: Endothelial Cells, Type 6A, Transitional or Mixed Nuclei. These endothelial cells contained nuclei of different shapes and sizes. The cells displayed a polygonal-like shape and are connected to one another by desmosomes. The mitochondria are moderate in number and show polyploidy. X1320.

Figures 9 and 10. Malignant Meningioma: Endothelial Cells, Type 7, Round and Oval Nuclei. Note that the nucleolus, when apparent, lies close to the nuclear membrane. The cells contain an abundant number of mitochondria that are irregular in shape and size. Nuclei of a considerable small size can be seen in cells with forming vacuoles and few granular endoplasmic reticuli. The cell membranes of most of the populations of cells show interdigitations with desmosomes. The cell contains a well-developed golgi complex and are rich in glycogen. The cells appear to be closely packed and separated by large interstitial spaces that contain microfilaments. Pinocytic vesicles can be seen at the membrane surface of some interstitial spaces. X990; X1750 respectively.

Figure 11. Malignant Meningioma: Endothelial Cells, Type 7, with Round Nuclei Showing Cells that Exhibit a Polygonal-like Profile with Short Processes. X1320.

Figure 12. An Area Showing Part of the Capillary Lumen of Meningioma ...h Two Psammoma Bodies. One psammoma body has a concentric do... thick wall and an electron dense center. A second body has a... amorphous translucent center and a heavy, irregular outline of electron dense precipitate around the membrane border and outer peripheral area. Numerous vesicles and several giant bodies can be seen among collagen fibers. Note the numerous microfilaments occupying the lumen among psammoma bodies. Some of t... surrounding meningioma cells show extensive vacuolation. X6...

Figure 13. Capillary Lumen of Meningioma Cells Showing Larger Vesicles Dispersed Among Collagen Fibers. Some of the vesicles appear to be fused. The surrounding tumor cells appear to show some degenerative changes. The mitochondria are scarce and presumed remnants of cellular material can be seen in the lumen. The nucleus exhibits an elliptical profile with an eccentrically located nucleolus. X1320.

Figure 14. Capillary Lumen of Meningioma. Note the presence of several fibrous-like psammoma bodies. Vesicles and giant bodies are also present. Collagen fibers show pronounced circumscribed clumping and an irregular profile. X1320.

Figure 15. Numerous Fibrous Psammoma Bodies and Several Concentric Double Thick Walled Psammoma Bodies with an Electron Dense Center. Note the electron dense large center body from which numerous psammoma bodies appear to radiate. The body is irregular in shape, has a branched fibrous periphery and filament can be seen throughout its center. X1320.

Figure 16. Large Fibrous Bodies and Concentric Thick Walled Psammoma Bodies. Note the heavy deposition of precipitate around the outer and inner walls of the body and the electron-lucent center. X4125.

Figure 17. Large Psammoma Body in Luminal Space Showing Numerous, Short Anastomosing Fibers that Appear to Form Irregular Three-Dimensional Networks. X4125.

Figure 18. Part of the Interstitial Space of a Meningioma Showing Psammoma Bodies in the Center of Meningiocytic Whorls. The whorls and psammoma bodies consist of fibers. A degenerative cell can be seen nearby. Note the irregular shaped electron dense inclusions in the area with vesicles and fibers. X1320.

Figure 19. Low Magnifications of Several Groups of Malignant Meningioma Cells. The cells appear closely packed and their membrane boundaries are interlocking. The nuclei are round in shape, varying in size and some contain a distinct nucleolus which lies in close proximity with the nuclear membrane. Patches of heterochromatin appear to be primarily confined to the peripheral boundaries of the nuclear membrane. Conspicuous nuclei show a marked irregularity in size and a few show irregularly small interdigitations of the nuclear membrane. The cells contain numerous mitochondria that are irregular in shape, varying in size and are well distributed in the cytoplasm. The cristae of some mitochondria appear regularly formed while other mitochondria show scarcely any cristae and disruption of the mitochondrial matrix. This disruption of the mitochondrial matrix is thought not to be due to sectioning. X825.

Figure 20. Meningioma Cells Showing Many Desmosomes of Adjacent Cell Membranes. The desmosomes are characterized as short electron dense intracellular plaques in the intercellular spaces of adjacent cell membranes. Smaller, less highly organized densities in opposing cell membranes are encountered in various areas. These structures may sometimes be referred to as desmosome or desmosome-like specializations. X1320.

Figure 21. Pronounced Interdigitations of Adjacent Cell Membranes in Meningioma Cells. Note prominent intercellular spaces and desmosomes. X1320.

Figure 22. Meningioma Cell Showing a Conspicuous Nucleus. The nucleolus contains several large irregular shaped membrane-bound bodies. The bodies are electron dense and consist of smaller membrane-bound inclusions that vary in electron density and lucency. A cilium can be seen in the cytoplasm near saccules of golgi. Microfilaments are present in the extracellular space. X700.

Figure 23. Nuclear Bodies in Another Area of a Meningioma. The bodies are surrounded by patches of heterochromatin. Large electron dense lysosome-like bodies can be seen in the cytoplasm. Note the adjacent cell containing a marked small sized

nucleus. Numerous vacuoles and vacuoles containing membrane-bound inclusions fill the cytoplasm. The mitochondria vary in size and shape. X700.

Figure 24. Electron Micrographs of Meningioma Cells Showing Intracytoplasmic Processes of Cells. The cytoplasmic processes interconnect with adjacent cells by way of desmosomes. The cells are rich in granular endoplasmic reticuli; glycogen and mitochondria. Some of the mitochondria are devoid of cristae. Vesicles and filaments can be seen in the interstitial spaces. Some cells contain large membrane-bound electron semi-lucent bodies. Basal bodies are evident in some of the cells. X1320.

Figure 25. Atypical Mitochondria of a Meningioma Cell Showing Polyploidy. Some mitochondria exhibit paucity of the cristae and varying degrees of shapes and sizes. Dilated granular endoplasmic reticuli can be seen containing an abundance of ribosomes. X495.


(2)

69-33

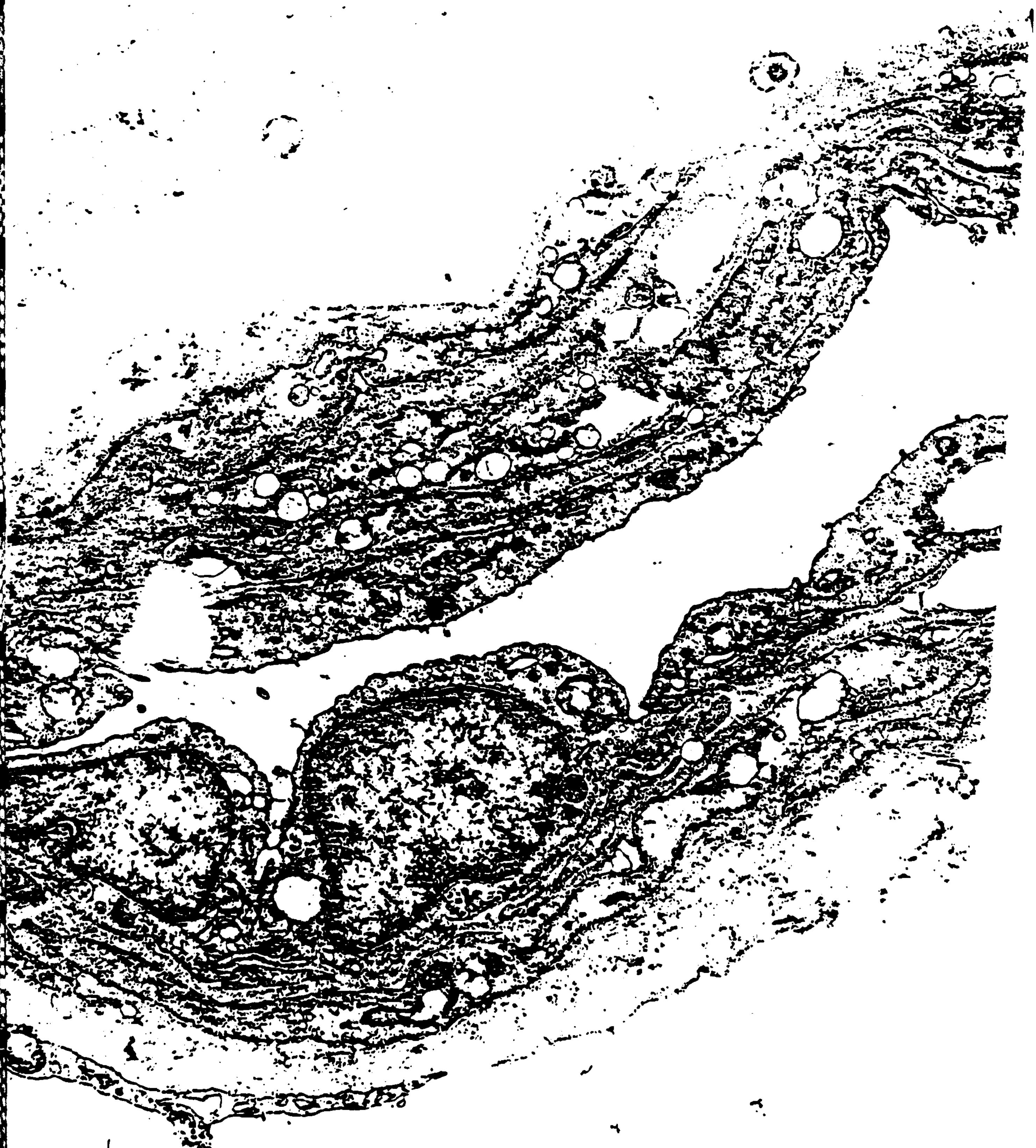

69-35

6940

AD-A166 177   UNITED STATES AIR FORCE SUMMER FACULTY RESEARCH PROGRAM   07/15
1985 TECHNICAL RE..(U) UNIVERSAL ENERGY SYSTEMS INC
DAYTON OH R C DARRAH ET AL. DEC 85 AFOSR-TR-86-0140
UNCLASSIFIED   F49620-85-C-0013   F/G 5/1   NL

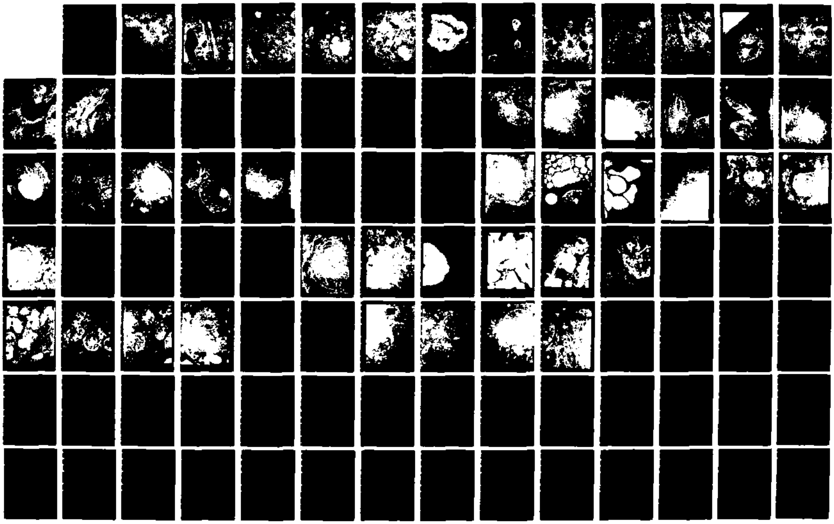

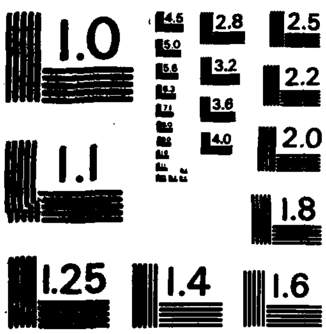

MICROCOPY RESOLUTION TEST CHART
NATIONAL BUREAU OF STANDARDS-1963-A


69-42

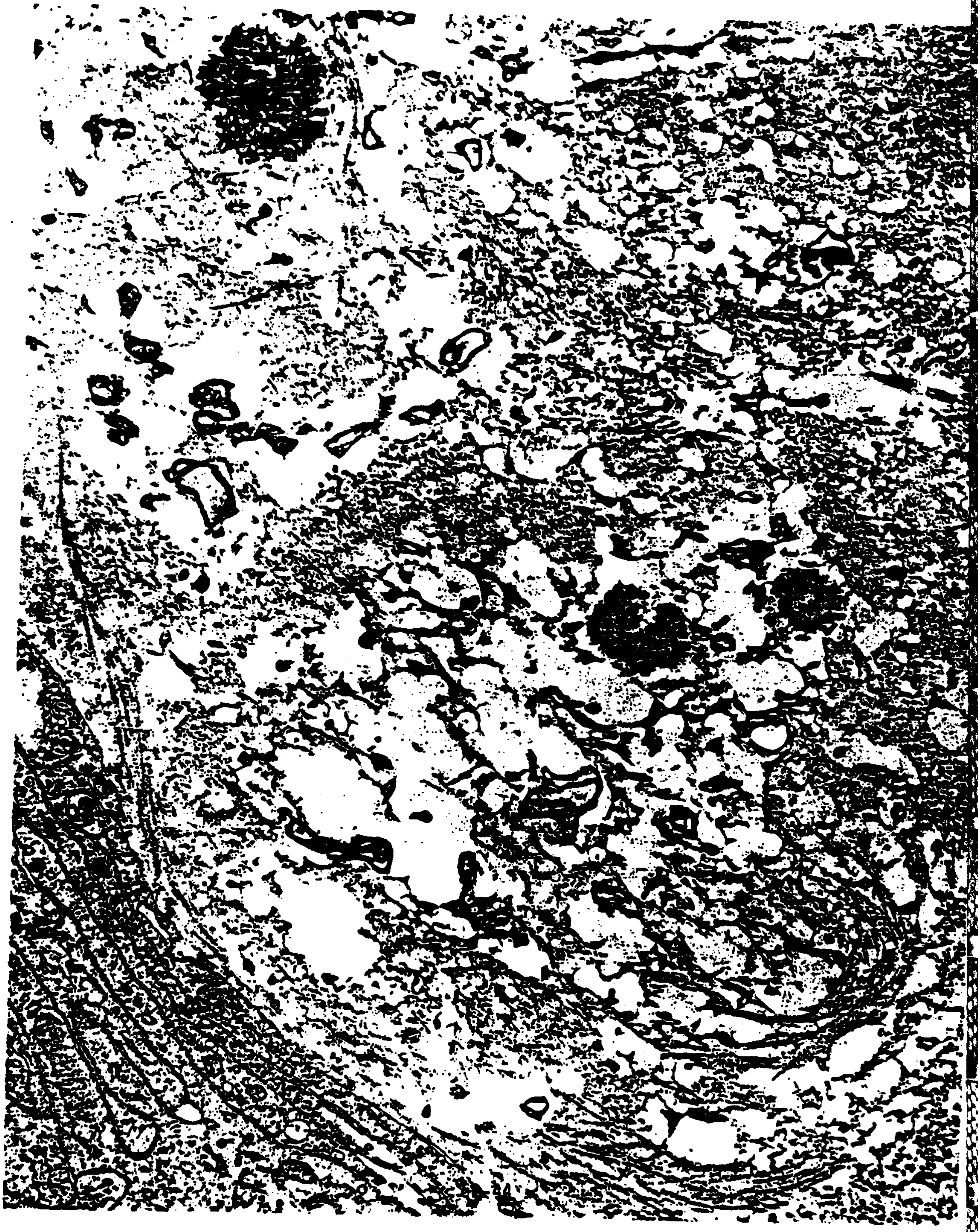

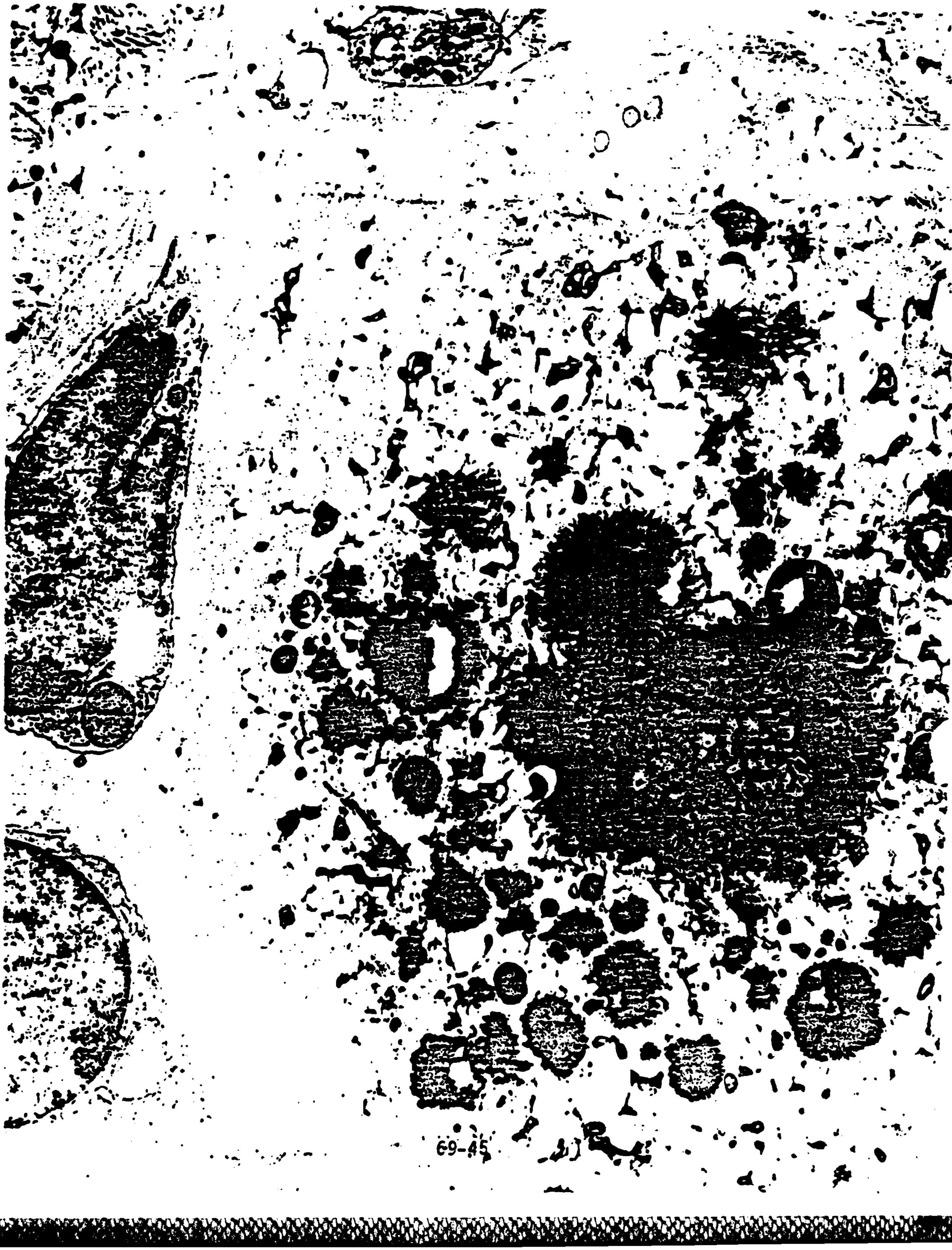
69-45


69-46

69-47


69-46

69-50

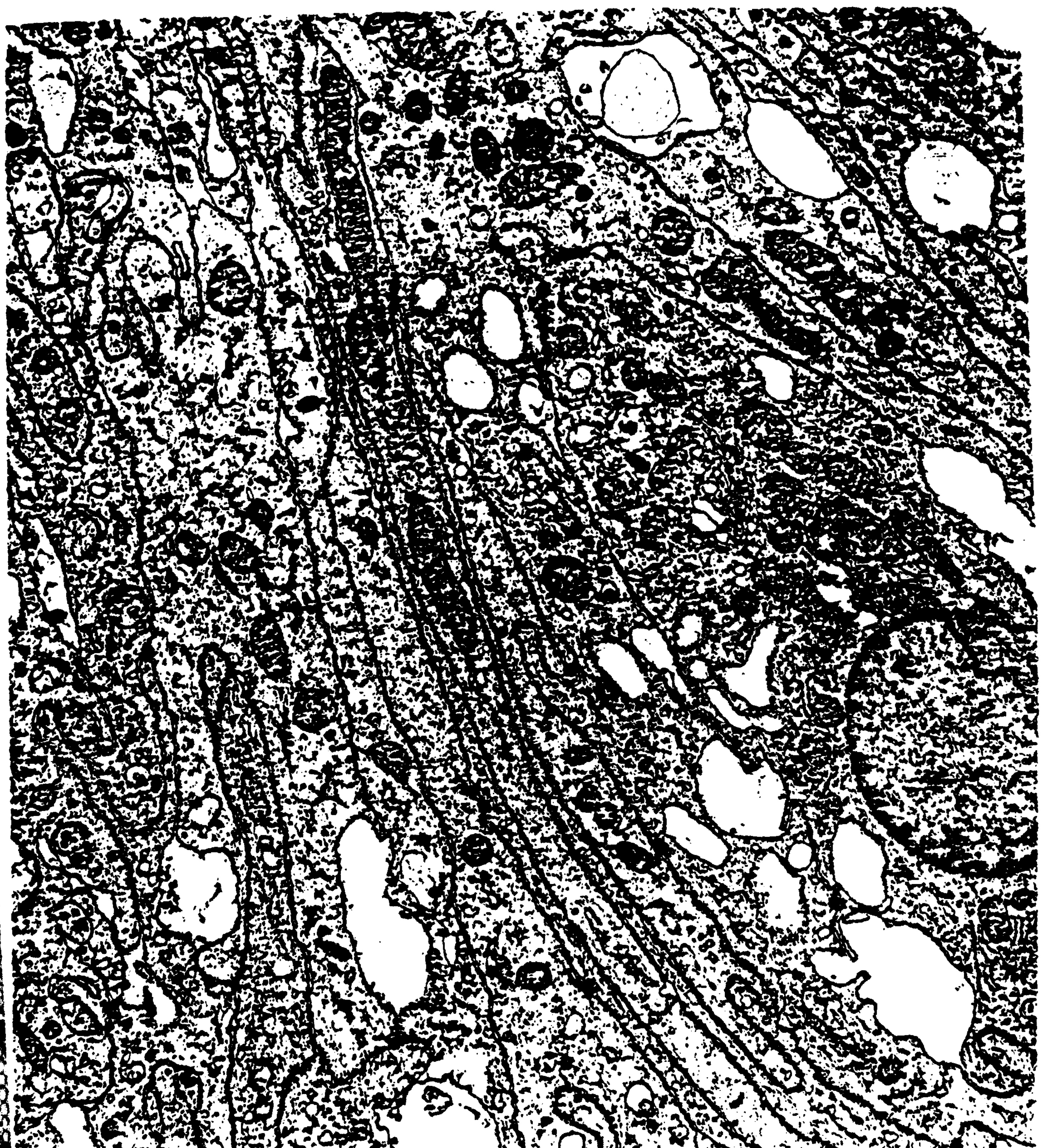


69-52

69-53

that of blepharoplasts (Figure 2). A few blepharoplasts and ciliary rootlets were observed in the cytoplasm of other cells. Highly specialized desmosomes (Figure 3) and gap junctions, and junctional complexes were denoted among adjacent cell membranes and adjoining cells (Figures 1, 3 and 5). The presence of desmosomes and junctional specializations occurred in primarily all cell populations examined. Though the majority of the cells showed bizarre nuclei with pronounced and distinct polymorphism (i.e. remarkable bilobulations and pronounced invaginations of the nuclear membrane), a few cell populations were characterized by oval-round nuclei. Other nuclei exemplified a polyhedral-like shape. A few cells were devoid of nuclei and nucleoli (Figure 10).

A few ependymona cells showed a conspicuous nucleus filled with irregular shaped membrane-bound nucleoplasmic inclusions. The inclusions varied in size and contained smaller membrane-bound bodies. The inclusions appeared to be embedded in patches of dense heterochromatin, and their shape ranged from oval-spheroid to elongated, with a budding-like appearance. Mitochondria of various sizes and a few granular endoplasmic reticuli made up the cytoplasm of this population of cells. A few centrioles were apparent near the nucleus and in other cells (Figure 8). Remaining cells of this area showed a paucity of cellular organelles and an increase in fine cytoplasmic filaments (Figure 9). Various cell populations exemplified large dense membrane-bound bodies in the extracellular space (Figure 5) and large lipid-like bodies occupying a large proportion of the cell's volume (Figure 7). The scarce number of ependymoma cells showed astrocyte-like features. The cytoplasm of these cells was filled with glial filaments, and showed a paucity of mitochondria (Figure 11).

b. ELECTRON MICROSCOPY OF EPENDYMOMAS

Ependymoma #2482

The ultrastructural appearance of the ependymoma studied in this investigation shows a mixture of heterogeneous cells with variations in the structural features of some of the cytoplasmic organelles. These variations in morphological features of cytoplasmic organelles may be categorized as conspicuous, pronounced and bizarre. However, even though the majority of tumor cells examined were manifested by poly-pleomorphic characteristics, various identifying markers and constituents typical of normal ependymal cells were evident.

The majority of the cells were closely packed showing a group-like arrangement and irregular profile. However, extracellular spaces were large and usually contained a scarce to moderate number of fibrous material. Intercellular spaces within cells varied in size and frequently were connected by septate desmosomes. The majority of the ependymoma cell populations contained bizarre polymorphic nuclei of varying sizes. These nuclei appeared to comprise more than one third of the cell's volume (Figures 1-11)

The nucleoli in these cells when apparent showed variations. Some were distinct and located eccentrically near the nuclear membrane (Figures 1, 4). The nucleolonema of the nucleolus of other cells showed a dense and branching anastomosing reticulin-like network (Figure 2). Still other nucleoli consisted of a semi-dense center with a distinct nucleolonema located at the periphery of the center (Figure 3). Of particular interest was the presence of cells containing two nuclei (Figures 3-5). The nucleoplasm of some nuclei showed the presence of inclusions resembling

Mitochondria, golgi, granular endoplasmic reticuli in the majority of cell populations varied in number from scarce to moderate, and showed cellular changes such as dilation, swelling and shrinkage (Figures 1-11). The cell processes of cells were elongated and blunt and occasionally comprised a small number of organelles (Figure 8).

EXPLANATION OF FIGURES

Ependymoma #2482

Figure 1. Electron Micrograph of Several Populations of Ependymoma Cells Showing Bizarre Polymorphic Nuclei which Occupies More Than One-Third of the Cells. The nuclei in some cells show remarkable lobulations and pronounced indentations, while other cells contain nuclei that show an elongated shape and short elevated branched processes. Infoldings of adjacent cell membranes are well defined, and short gap junctions are recognizable. The cells contain an abundant number of irregular shaped mitochondria of variable sizes. The mitochondria located in elongated processes of cells appear to be primarily spindle shaped in comparison to mitochondria in close proximity to the cell nuclei which exhibits a somewhat oval to round appearance. The majority of the mitochondria contains cristae that appears to be intact. Golgi can be seen near the nuclei and in the cytoplasm of cells, and is comprised of stacked short cisternae and irregular sized saccules. A moderate amount of granular endoplasmic reticuli is well distributed in the cytoplasm of cells. A few cells contain a scarce number of typical organelles, and at low magnifications show a translucent cytoplasm. A few spherical dense granules occupy the cytoplasm of some cells. The cells are closely packed showing a group-like arrangement and an irregular profile. The extracellular spaces of cells contain a scarce number of fibers and membrane-bound semi-lucent inclusions. X1980.

Figure 2. Ependymoma Cells Showing an Elongated-Blunt-Like Nucleus With Wide Invaginations. The nucleolonema of the nucleolus shows a dense and branching anastomosing reticulin-like network. An unusual short elliptic inclusion is apparent in the nucleoplasm. The inclusion resembles that of a blepharoplast. The cytoplasm of the cell is rich in granular endoplasmic reticuli. The majority of the granular endoplasmic reticuli show dilated cisternae with an abundance of ribosomes. Swollen mitochondria, golgi and spherical inclusions of a nuclear-like composition can be seen in the cytoplasm. X1800.

Figure 3. Ependymoma Cells Showing Blepharoplasts and Ciliary Rootlets in the Cytoplasm. The blepharoplasts or basal bodies are few in number and are dispersed among irregular shaped mitochondria. Highly specialized desmosomes can be seen adjoining cell membranes. Note the bizarre shaped nuclei in cells. Of particular interest is the presence of two nuclei per cell. The nucleoli when apparent in these cells show a semi-electron dense center and distinct nucleonema located at the periphery of the dense center. X1800.

Figure 4. Ependymoma Cells Showing a Small Number of Mitochondria and Granular Endoplasmic Reticuli. A few membrane-bound inclusions amorphic in shape with a semi-lucent center and dense periphery are contained in vacuoles. Note the unusual bizarre polymorphic nuclei in cells. One cell is comprised of two nuclei showing extensive and pronounced bilobed and cleft-like structural features. Small cells are devoid of nuclei and show few cellular organelles. Some of the mitochondria show a disorganized cristae. X1800.

Figure 5. Ependymoma Cells Showing Microvilli Along the Surface of Cells. Large lucent membrane-bound bodies appear to be forming in the extracellular space. The majority of these structures are in close association with one another. A few intercellular spaces and dense lipid-like inclusions can be seen in some cells. The conspicuous nuclei further shows irregularities in size and shape. The mitochondria appear randomly distributed near the surface of the cells, especially at junctional complexes. The few granular endoplasmic reticuli that are present in the cells show marked dilation of the cisternae. X1800.

Figure 6. Ependymoma Cells Showing Two Different Polymorphic Nuclei, and Pronounced Infolding of Adjacent Cell Membranes. The nuclei, occupies the bulk of the cells, and other cytoplasmic organelles are scarce. Semi-lucent double membrane inclusions measuring around 2 mm in diameter can be seen in the cytoplasm. X1800.

Figure 7. Ependymoma Cells Showing Membrane-Bound Inclusions of Low Electron Density. One of the inclusions show a dramatic increase in size and primarily occupies the entire width of the cell. A small inclusion is located nearby. Several mitochondria with a moderate amount of cristae make up the translucent cytoplasm of the cell. Septate desmosomes can be seen at the margins of the membrane of an intercellular space. The cells show an elongated irregular profile with bizarre nuclei. X2100.

Figure 8. Ependymoma Cells Showing Centrioles, Saccules of Golgi, Dense Small Granules, Swollen Mitochondria, a Scarce Number of Granular Endoplasmic Reticuli and a Number of Free Ribosomes in the Cytoplasm. The cells exhibit a polyhedral-like profile and show interconnections of one cell process to another. The cell processes are elongated and blunt, and occasionally are comprised of a small number of organelles. The cell nucleus exhibits a round shape with chromatin regularly distributed. A scarce number of fibers can be seen in the extracellular space. X1800.

Figure 9. Ependymoma Cells Showing a Conspicuous Nucleus Filled with Irregular Shaped Membrane-Bound Nucleoplasmic Inclusions. The inclusionss vary in size, and many are further comprised of smaller membrane-bound bodies. The inclusions appear to be embedded in patches of dense heterochromatin. The shape of the inclusions range from oval-spheroid to elongated with a budding-

like appearance. Mitochondria of various sizes make up the surrounding cytoplasm and a few granular endoplasmic reticuli. A centriole can be seen adjacent to the nucleus in one cell. Other cells show a paucity of cellular organelles and an increase in fine cytoplasmic filaments. Unusual membrane-bound cytoplasmic bodies filled with material of low density can also be seen in cells. X1800.

Figure 10. Ependymoma Cells Showing Two Distinct Nuclei that Exemplify an Oval and Round Shape. The nucleus of one cell is devoid of a nucleolus and is comprised of several dense small precipitates that are spherical in shape. The chromatin of both cells appear regularly distributed. The mitochondria are swollen and some show polymorphism. The granular endoplasmic reticuli are dilated and show variations in shape. X1800.

Figure 11. Ependymoma Cells Showing Astrocyte-Like Features. The cytoplasm is filled with numerous glial filaments, few mitochondria and vacuoles. The extracellular space contains large pinocytic vesicles and fibers. X480.

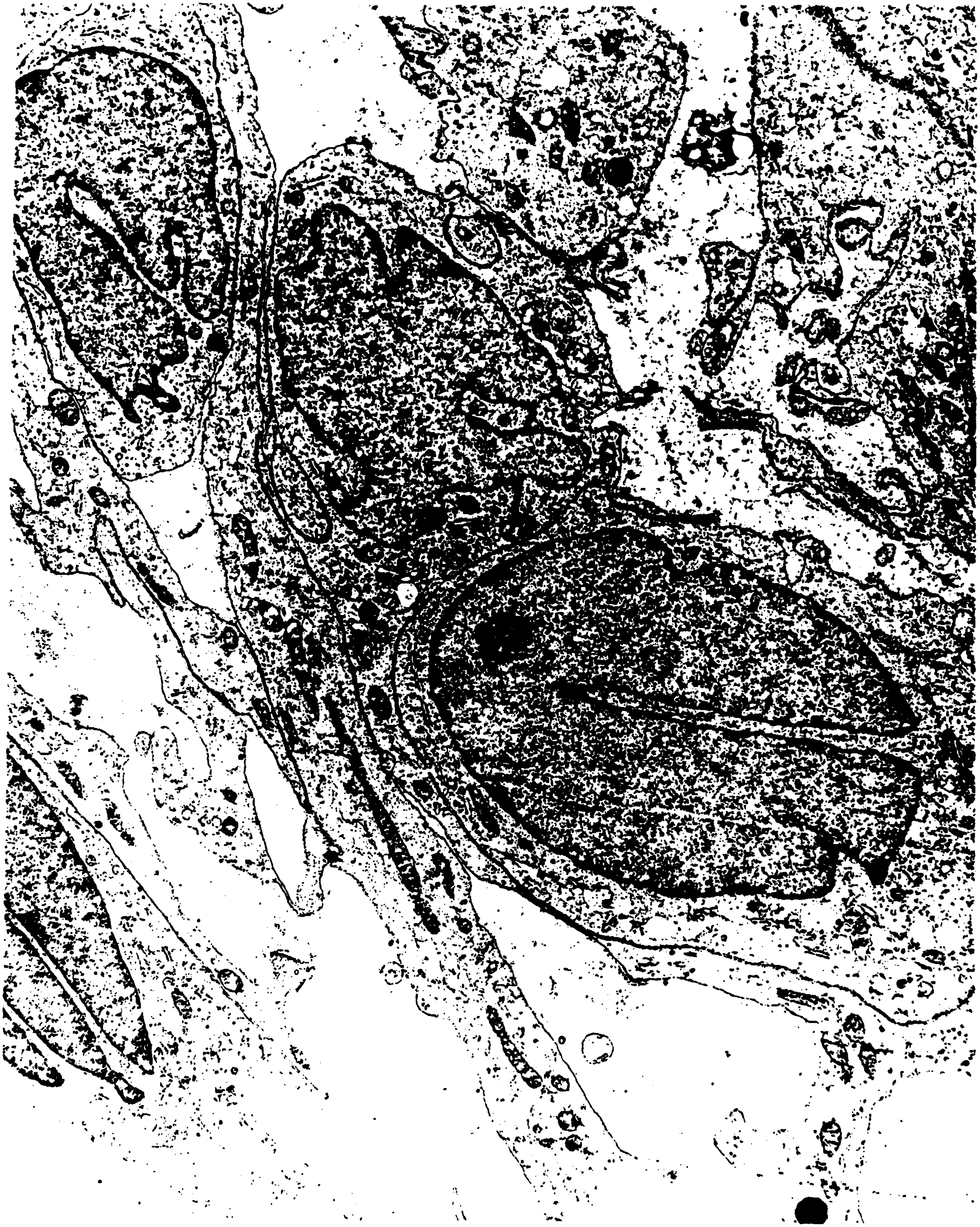

69-62

69-63

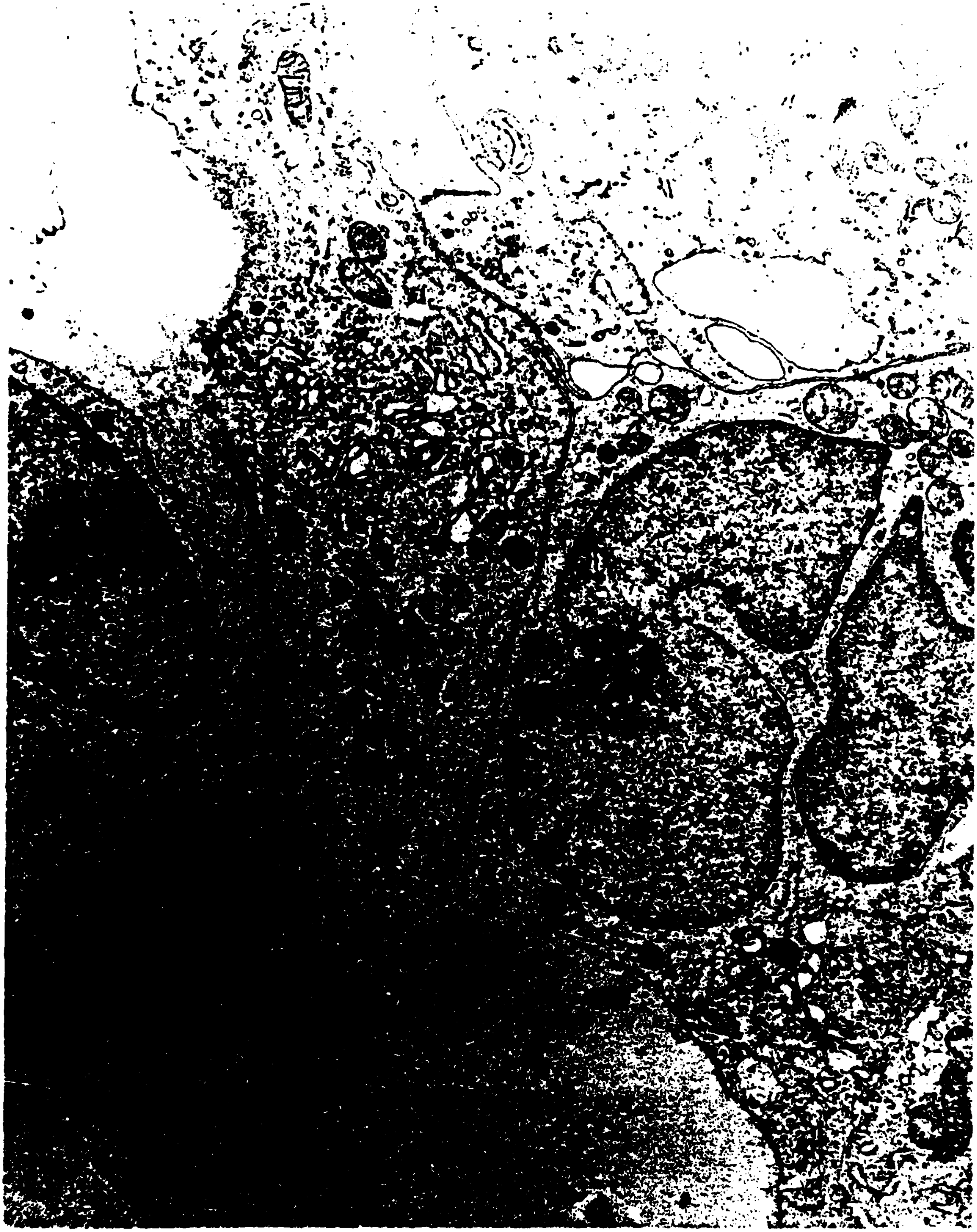

69-64

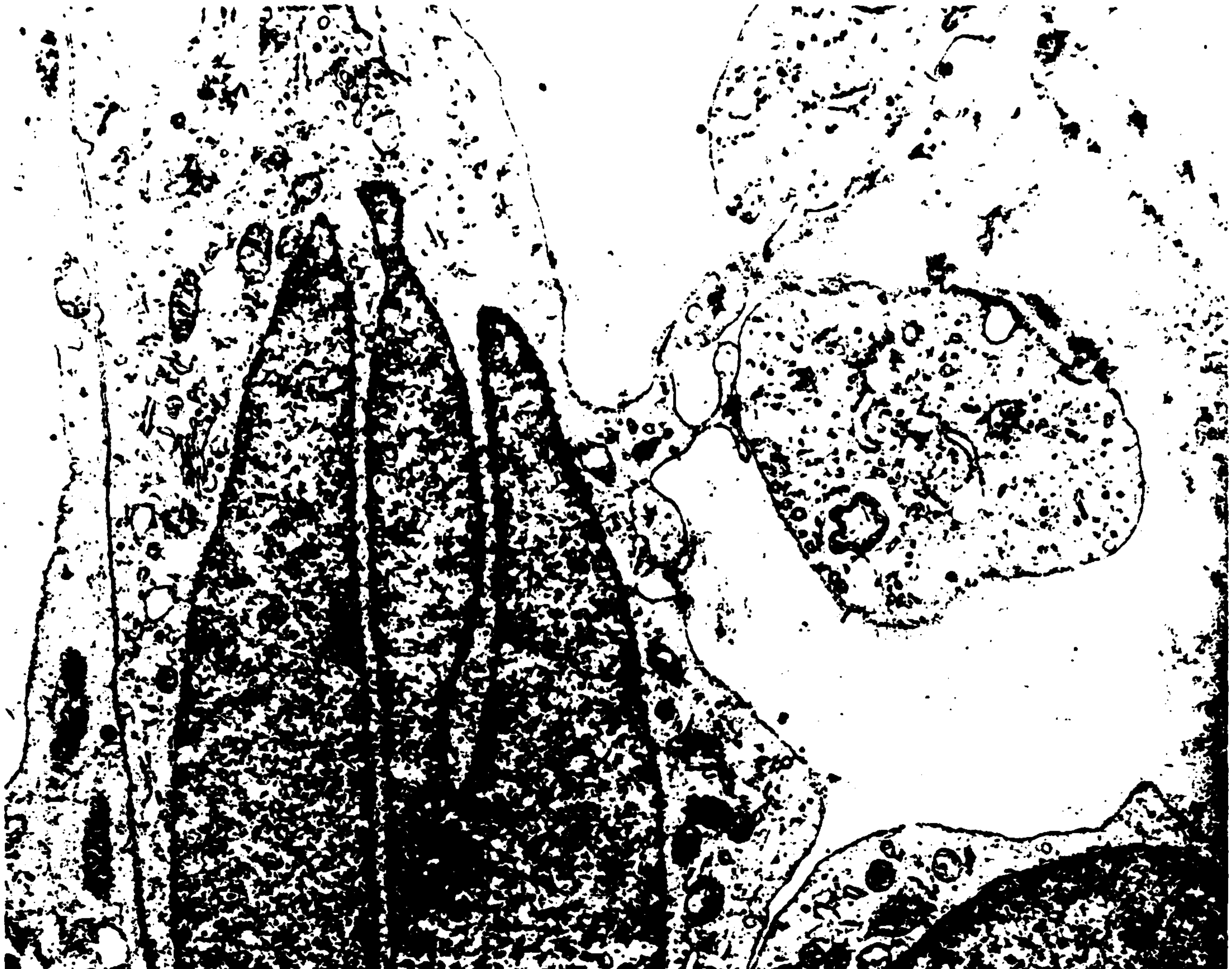

69-65

69-66

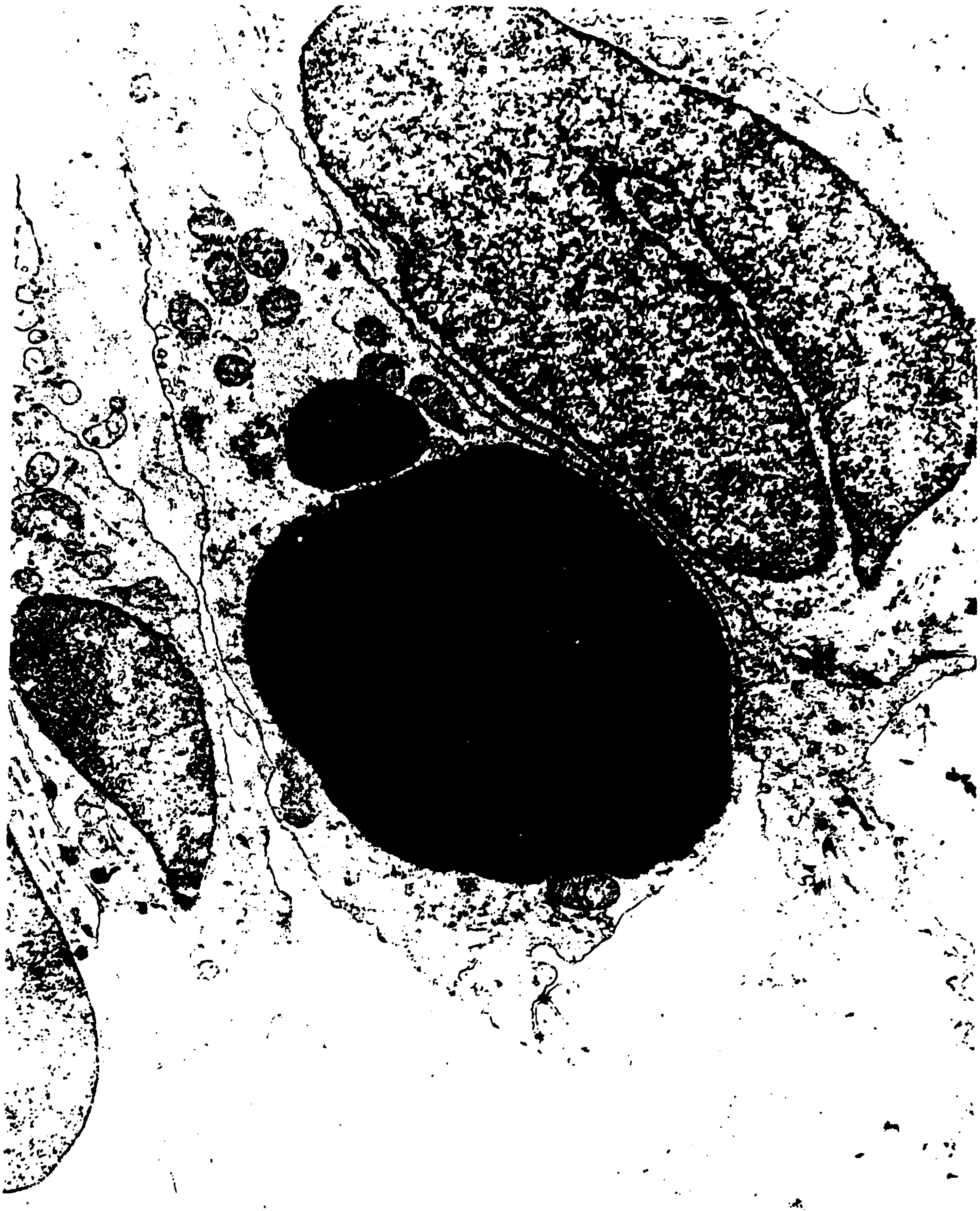

69-68

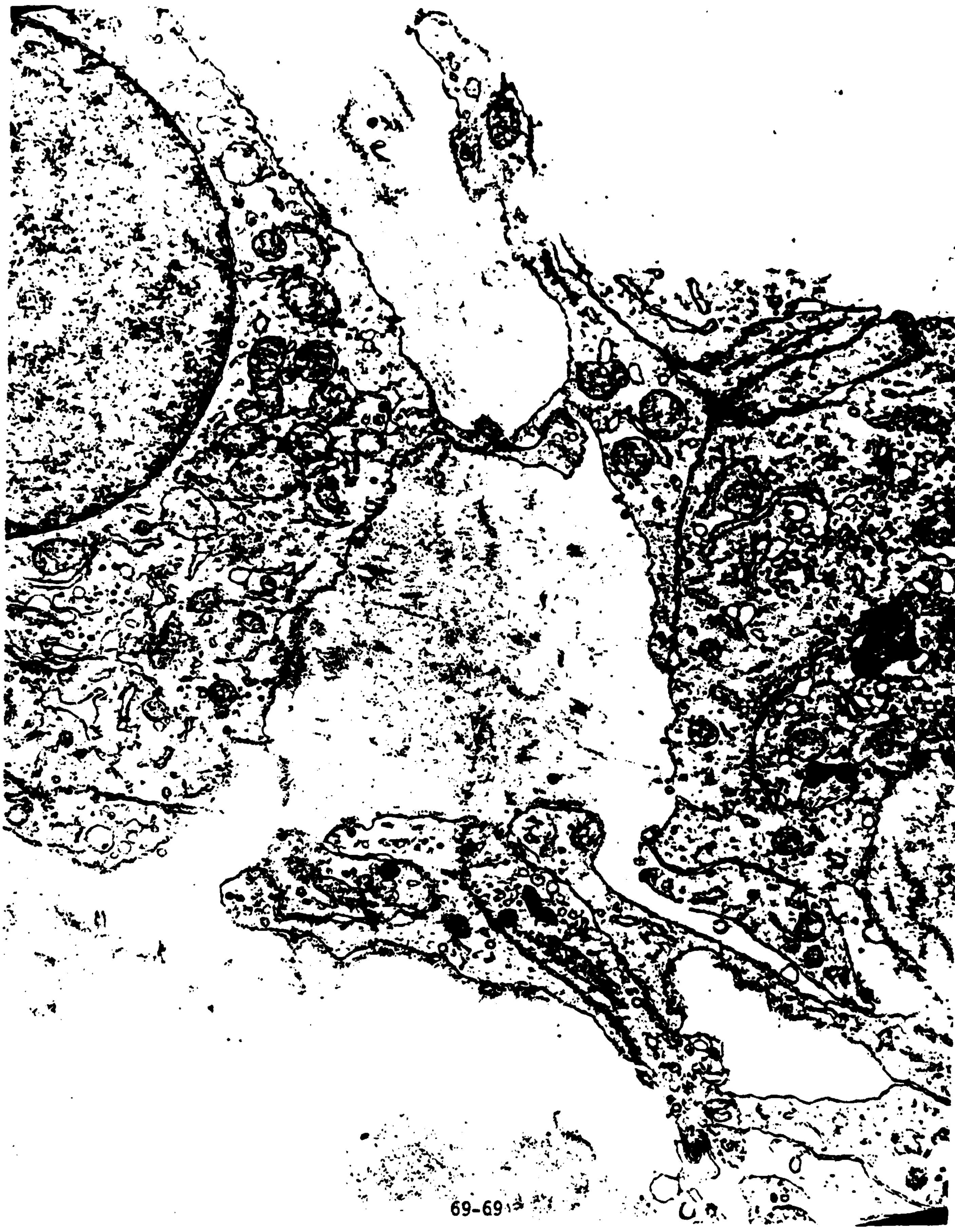
69-69

69-70

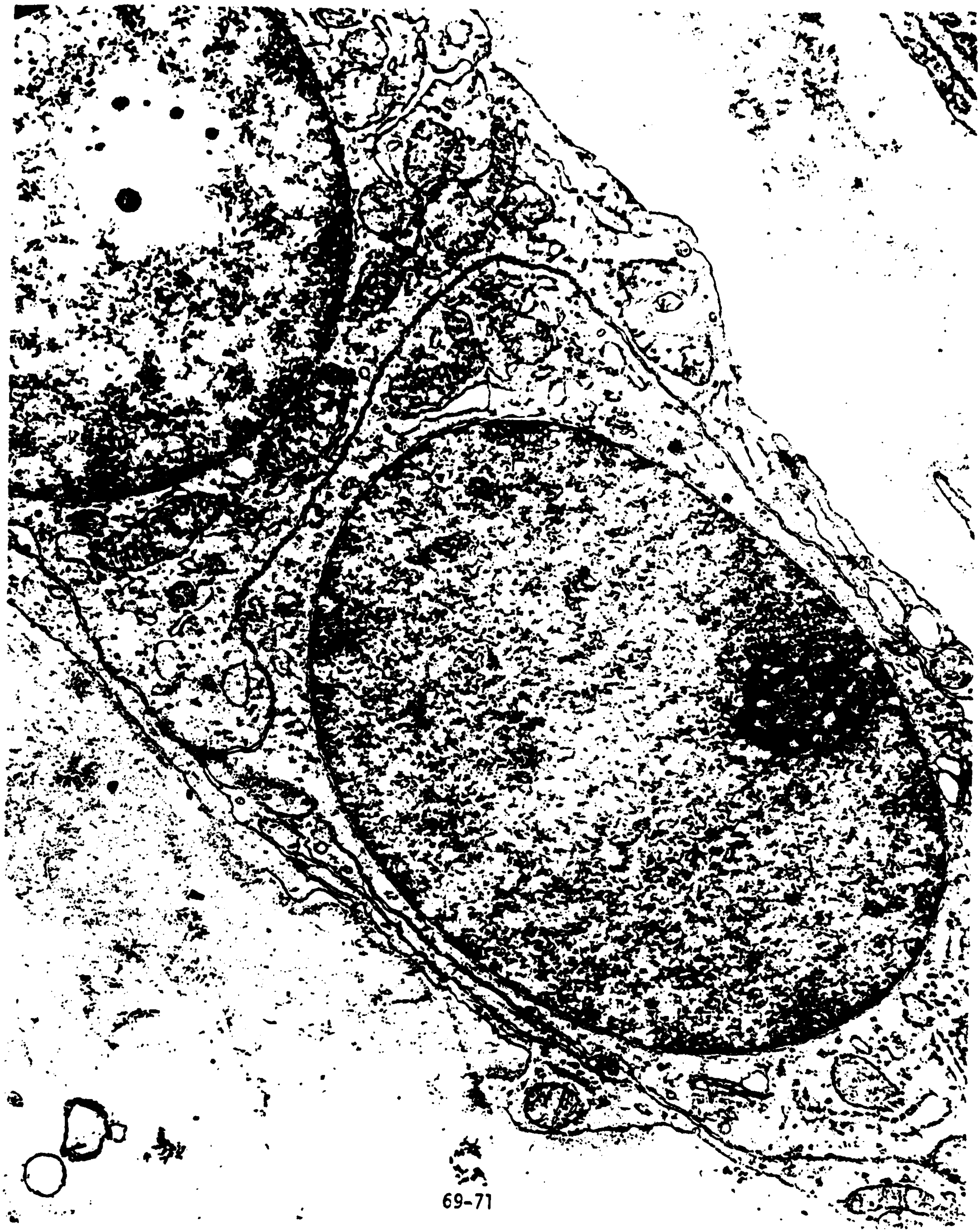

69-71

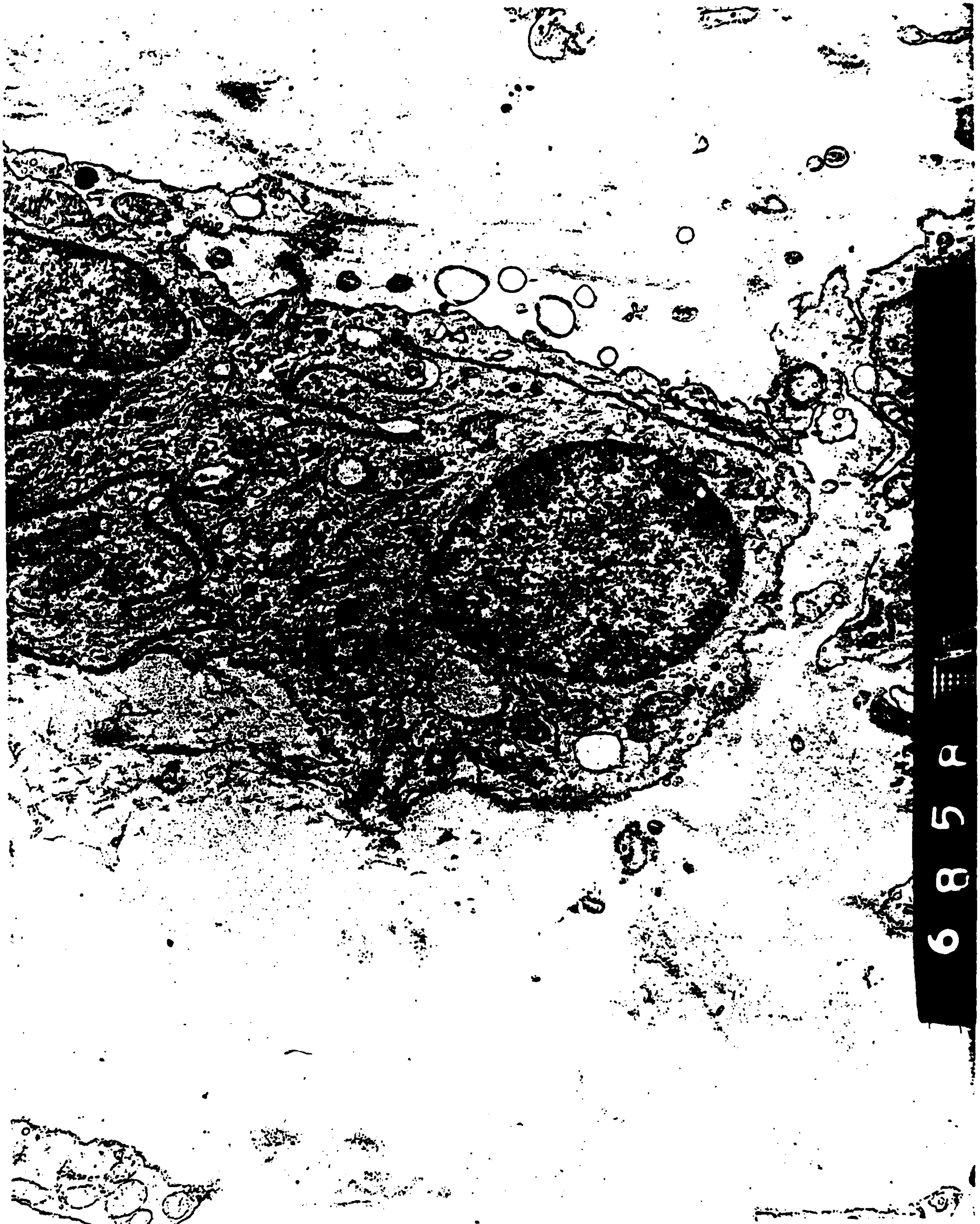
685A

c. Electron Microscopy of Glioblastomas

i. Glioblastoma #N69-931

Glioblastoma cells showed bizarre giant cells. The giant cells ranged from 5-40 mm in diameter and contained a somewhat oval-round semi-dense nucleoli. The nucleoli in most cells appeared to almost be centrally located, but a few cells had nucleoli located eccentrically and close to the nuclear membrane. The nucleoli appeared extensively conspicuous because of their size which ranged from around 4-10 mm. Pronounced indentations of the nuclear membrane were evident in cell populations. The nucleoplasm of most cells exhibited high electron density and appeared to be clumped in various areas of some cells. Heterochromatin of low density was primarily confined to the peripheral membrane border. Of particular interest in observing these cell populations was various degradative and degenerative changes. The membrane profiles of the cells in most sections were not discernable. Numerous amounts of cellular debris were observed filling the cells and extracellular spaces. Swollen mitochondria and granular endoplasmic reticuli were few in number in some cells. Numerous dense granules, varying in size and shape that may be lipid-like in nature filled the extracellular spaces of some cells. Glial filaments and bundles of filaments were also found in the extracellular spaces. (Fig 7.).

The lipid-like inclusions in the extracellular spaces also exhibited degenerative changes. Groups of red blood cells in the extracellular space showed variations in shape and size and were of moderate electron density (Fig. 2-3). Some of the tumor cells contained

well-defined round nuclei and regularly distributed chromatin. A moderate number of mitochondria of various sizes and shapes appeared intact. A moderate number of granular endoplasmic reticuli and a few golgi were recognizable. Desmosomes showing highly specialized areas in the cell membrane could be seen. Numerous infoldings of cell membranes were observed among cells. Of interest was the presence of double-membrane bound structures encapsulating granular ER and free ribosomes. Numerous vesicles and a small number of vacuoles were also present in some cells (Fig. 4). Various areas of the tumor contained membrane whorls. The membrane whorls were encapsulated occasionally by an elongated nuclei with two nucleoli and moderate patches of heterochromatin that appeared confined to the peripheral part of the nucleus. The whorls appeared to show a concentric lamellae-like arrangement with a dense center core. As the whorls were examined from the center to the peripheral area, a translucent area was evident. Cellular organelles could not be well-delineated. Other whorls were not encapsulated by cell nuclei. These whorls displayed dense areas and several spheroid-like structures. These structures appeared to be smaller whorls that were forming in the midst of cellular debris and cellular remnants. Some of the whorls found in giant cells showed a concentric circumscribed profile and dense areas. The giant cells associated with these whorls contained bizarre shaped nuclei. Some of the cells also exemplified degenerative changes (Figs. 5-7).

EXPLANATION OF FIGURES

Glioblastoma #N69-93IJ

Figure 1. Glioblastoma Cells Showing Bizarre Giant Cells. The giant cells ranged from 5-40 mm in diameter and contained a somewhat oval-round semi-dense nucleoli. The nucleoli in most cells appeared to almost be centrally located, but a few cells had nucleoli located eccentrically and close to the nuclear membrane. The nucleoli appeared extensively conspicuous because of their size which ranged from around 4-10 mm. Pronounced indentations of the nuclear membrane were evident in cell populations. The nucleoplasm of most cells exhibited high electron density and appeared to be clumped in various areas of some cells. Heterochromatin of low density was primarily confined to the peripheral membrane border. Of particular interest in observing these cell populations was various degradative and degenerative changes. The membrane profiles of the cells in most sections were not discernable. Numerous amounts of cellular debris was found filling the cells and extracellular spaces. Swollen mitochrondria and granular endoplasmic reticuli were few in number in some cells. Numerous dense granules, varying in size and shape that may be lipid-like in nature filled the extracellular spaces of some cells. Glial filaments and bundles of filaments were also found in the extracellular spaces.

Figure 2. Numerous Lipid-like Inclusions of Various Sizes in the Cells and Extracellular Space of the Tumor. Some of the structures show degenerative changes. X1925.

Figure 3. Groups of Red Blood Cells in the Extracellular Space of the Glioblastoma Exhibiting Variations in Shape and Size and variations in Electron Density. X1925.

Figure 4. An Area of the Tumor Showing Cells with Round Well-defined Nuclei and Regularly Distributed Chromatin. A moderate number of GER and golgi are present. Desmosomes showing highly specialized areas in the cell membrane can be seen. Numerous infoldings of the cell membrane occurs. Of special interest is the presence of double membrane-bound structures, encapsulated GER and free ribosomes. Numerous vacuoles are present. X1650.

Figures 5-7. Membrane whorls of the glioblastoma showing circumscribed profiles and dense areas. The giant cells contain more than one nuclei and they exemplify a bizarre appearance. The cells appear to show degenerative changes. X1500, X1340, X2250.

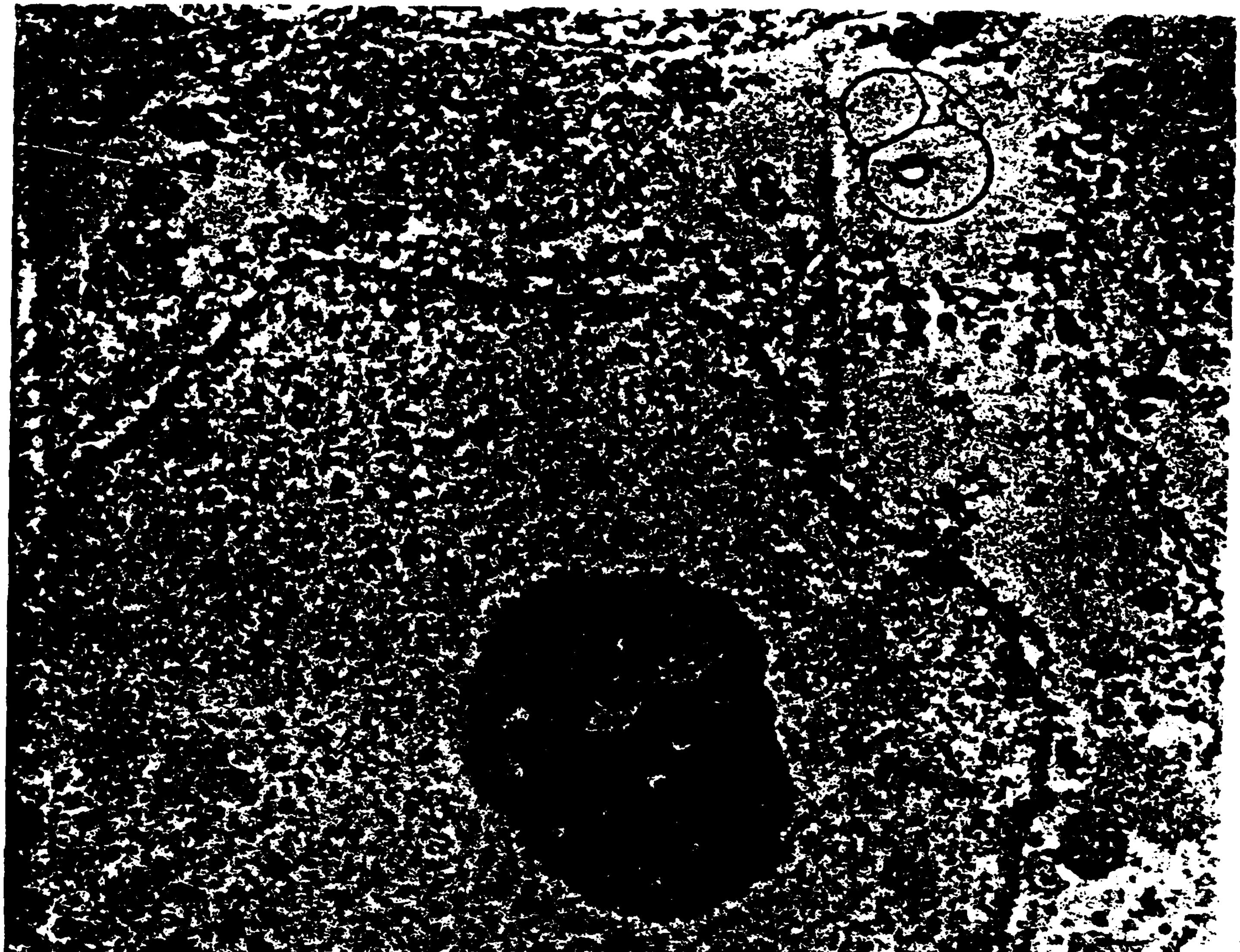

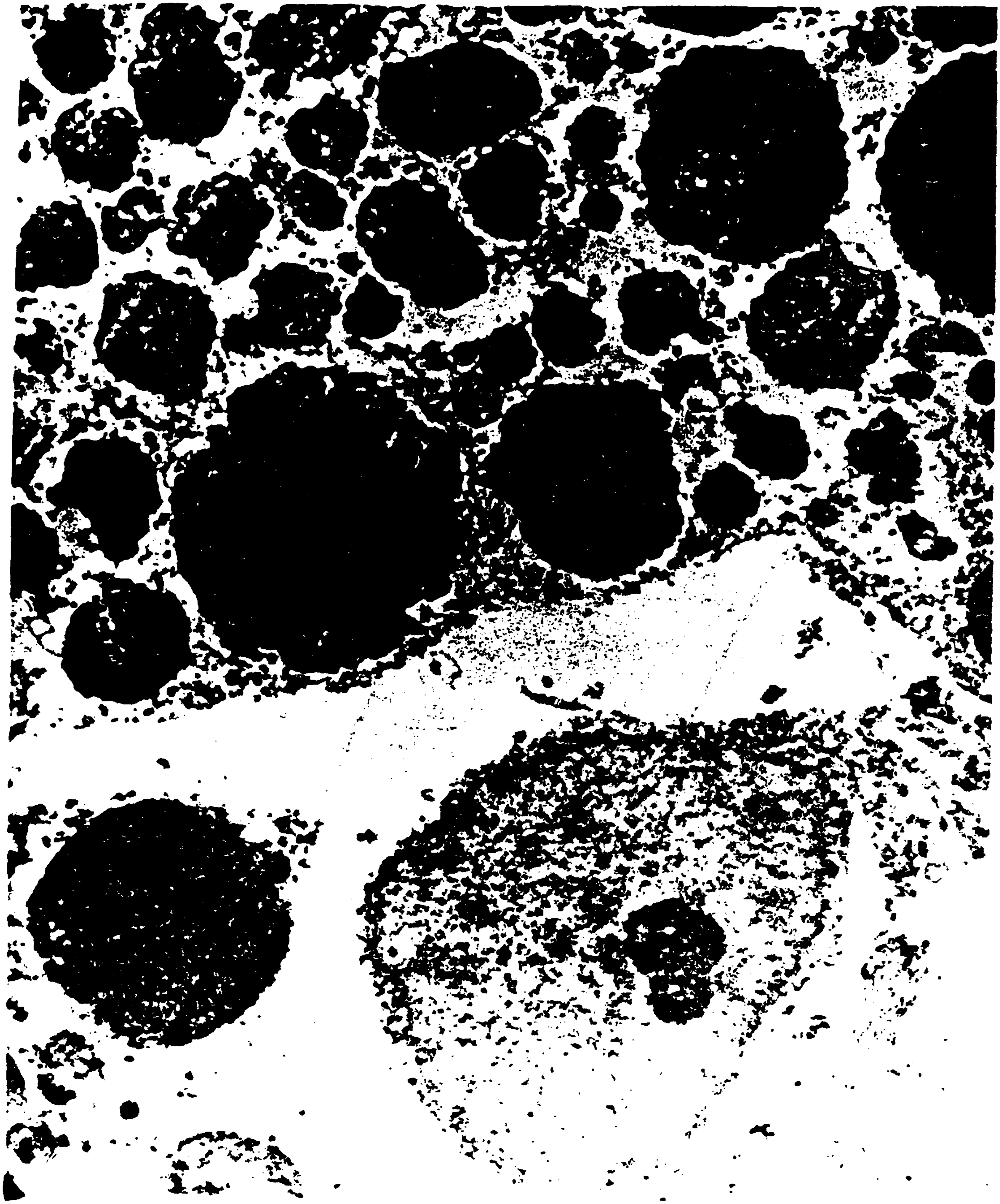

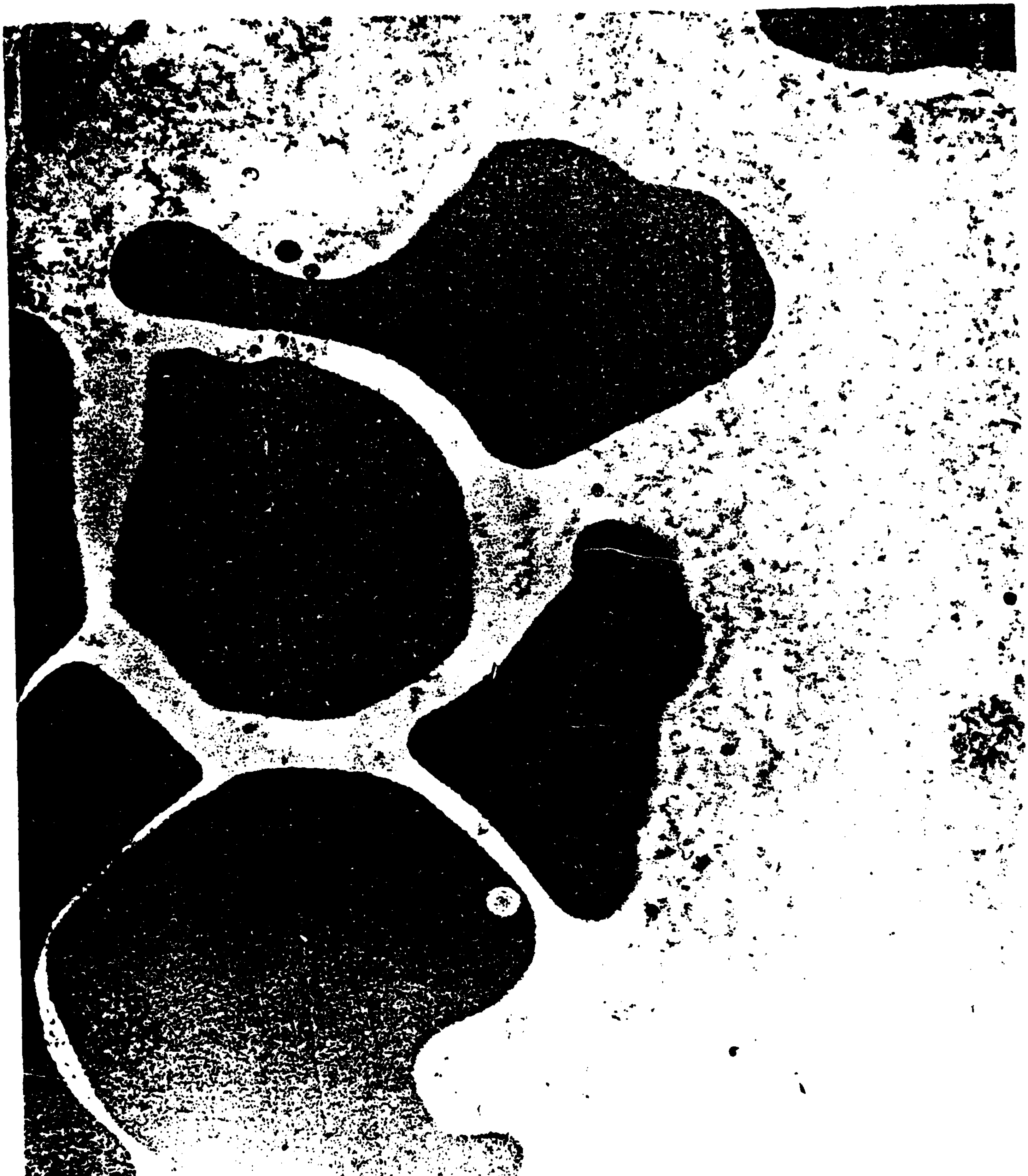

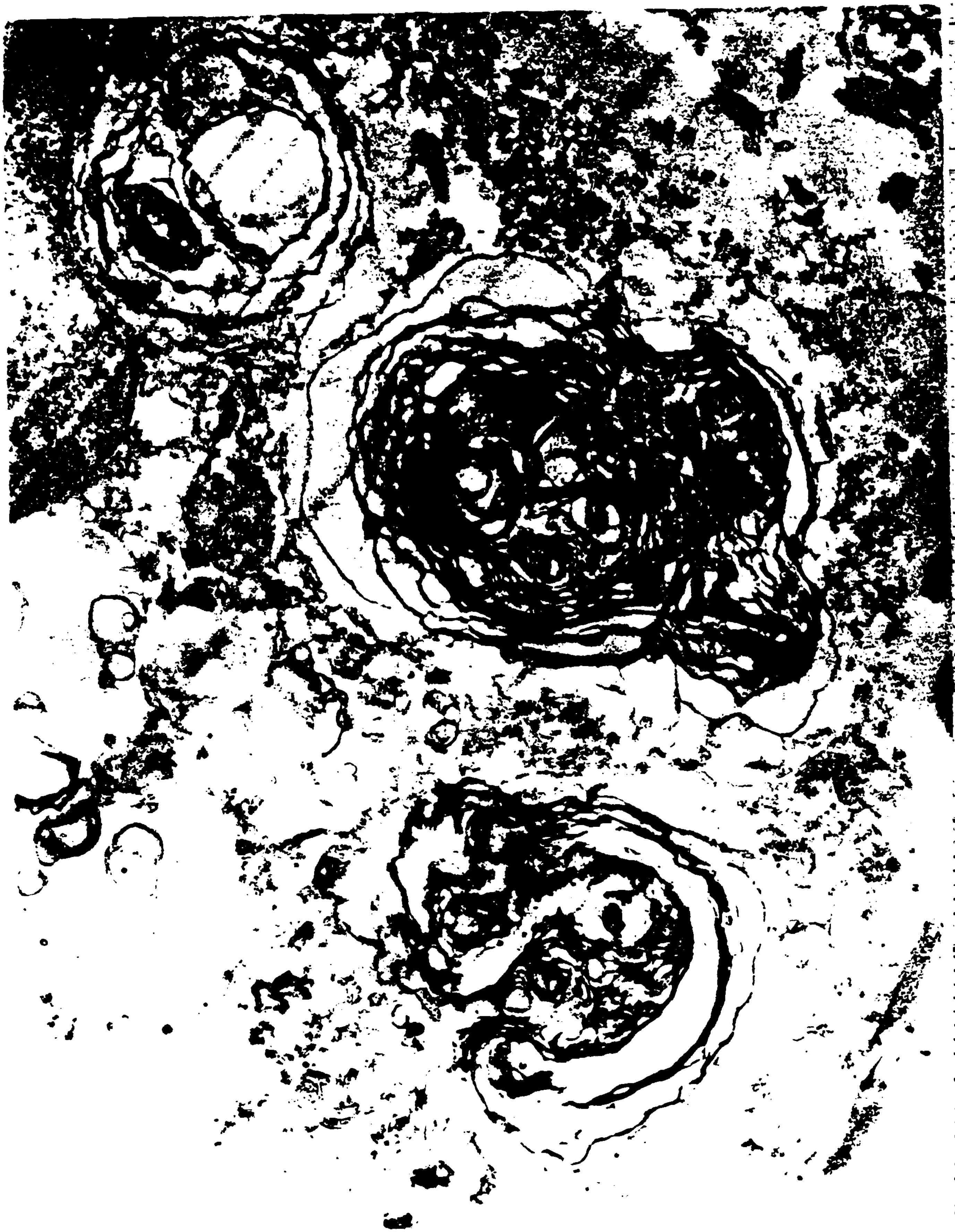

ii. Glioblastoma #N66-116

Populations of glioblastoma cells showed extensive and pronounced dilation of granular endoplasmic reticuli. The cisternae of the ER appeared to form anastomosing networks that were intertwined very closely in circumscribed layers. An abundance of ribosomes were seen on the membrane surface. The reticuli were usually around pleomorphic nuclei. The membranes of the cells were well-delineated and the cytoplasm appeared translucent. Other areas of the tumors showed reticuli revealing a somewhat amorphous appearance with well-defined oval-like saccules. Pronounced dilated reticuli were also evident in the extracellular spaces. The cytoplasm of cells was filled with dense granules, free ribosomes and fine filaments. The extracellular spaces contained glial microfilaments, an abundance of glial fibers, membrane-bound bodies, vesicles, and red blood cells (Figures 1-2).

Cells that appeared to be undergoing degenerative changes were devoid of organelles. Numerous red blood cells in the extracellular space of the tumor showed a fenestrated group-like arrangement. The blood cells exhibited variations in size and shape. Some of the red blood cells showed unusual S-like semi-lucent structures. These structures appeared to be located near the center of the cells and extended the entire diameter. Other red blood cells were found in close association with large bands of glial filaments. The glial filaments, though somewhat filamentous also revealed an amorphous appearance (Fig. 2 and 4). Various glioblastoma cells showed large giant cells that appeared to be undergoing degradative and generative changes. The membrane of these cells showed a

fibrous-like appearance. Numerous dense precipitates were evident in the cytoplasm and unusual and remarkable large-sized amorphous dense bodies. One body measured about 10 mm in diameter and contained several translucent areas (Fig. 3).

The nuclei of the tumor showed atypical variations. Some cells were characterized by polygonal-like nuclei with large amounts of heterochromatin occupying the boundaries of the nuclear membrane and the bulk part of the nucleus. Dense precipitates and granules could be seen in some nuclei (Fig. 5). A few tumor cells contained nucleoli inclusions. These cells showed a scarcity of other organelles (Fig. 6).

EXPLANATION OF FIGURES

Glioblastoma #N66-116

Figure 1. Glioblastoma Cell Showing Extensive and Pronounced Dilation of the Granular Endoplasmic Reticulum System. The cisternae of the granular endoplasmic reticuli appear to form anastomosing networks that are intertwined very closely in circumscribed layers. An abundance of ribosomes can be seen on the membrane surface. The intertwining reticuli are around an unusual pleomorphic nucleus. The membrane of the cell is well-delineated, and the cytoplasm is translucent and filled with small amorphous dense granules, free ribosomes and short fine filaments. The endoplasmic reticulum system shows a semi-lucent amorphous appearance with well-defined oval-shaped saccules. A few large reticuli can be seen in the extracellular space. The extracellular space contains an abundance of thick glial fibers. Some show a band-like configuration. Other small dense irregular-sized granules also occupy the space. X1650.

Figure 2. Extracellular Space of Glioblastoma Showing Numerous Glial Fibers Displaying Several Different Arrangements. Some appear to be flowing straight in the matrix of the extracellular space; others tend to curve, overlap and form a cross-like configuration. Note the spheroid dense bodies among fibers. Some of these bodies show a concentric-like lamellae and others show a dense double membrane of precipitate material. X412.5.

Figure 3. Glioblastoma Cell Showing a Large Giant Cell That Appears to be Undergoing Degradation and Degenerative Changes. The membrane of the cells shows a fibrous-like appearance. Numerous dense precipitates can be seen in the cytoplasm, and an unusual and remarkable large-sized amorphous, dense body 10 mm in diameter is recognizable. Several translucent areas can be seen in the body. Glial filaments surround the cell in the extracellular space. X412.5.

Figure 4. Numerous Red Blood Cells in the Extracellular Space of the Glioblastoma Showing a Fenestrated Group-Like Arrangement. The blood cells exhibit variations in size and shape. Note the few glial fibers and cell remnants that sequester areas of the space. X1200.

Figure 5. Glioblastoma Cell Showing a Polygonal-Like Nucleus With Large Amounts of Heterochromatin Occupying the Boundaries of the Nuclear Membrane and the Bulk of the Nucleus. A dense precipitate can be seen near the center of the nucleus, and a dense granule at one end of the nucleus surrounded by an oval opaque space. The remaining parts of the cell are filled with dense,

numerous membrane-bound bodies of varying sizes, clustered precipitates and a few filaments. Cells also exemplify degradative changes. X1750.

Figure 6. Glioblastoma Cell Showing a Pleomorphic Nuclei With an Unusual Nucleolus. The nucleolus contains semi-lucent inclusions surrounded by a somewhat more dense area. The chromatin appears irregular in distribution. There is an extensive scarcity of cytoplasmic organelles. X1750.

69-74

69-88

iii. Glioblastoma #403

Electron microscopy of this glioblastoma revealed cell populations of varying sizes and shapes. One interesting feature of these tumor cells was the presence of pronounced and bizarre-shaped nuclei. The nuclei were characterized by irregularities in size and shape and marked variations in nuclear membrane indentations. At low magnifications, the tumor cells exhibited a polygonal-like and polyhedral-like arrangement. Groups of cells in various populations were characterized by closely packed nuclei, frequently two unusual nuclei per cell (Figures 1 and 2).

There was a prominent inconstant relationship between the size of the nucleus and the amount of cytoplasm creating the appearance of a conspicuous nucleus and an electron lucent cytoplasm. Some glioblastoma cells showed a polyhedral-like profile. A remarkable characteristic of these cells were not only the presence of two nuclei in one cell, but also bilobulation of the giant cells. The nuclei of these cells showed unusual membrane-bound bodies that appeared to be confined to the peripheral areas of the nuclear membrane. The accumulation of heterochromatin at the nuclear membrane was frequent; although random dispersal was also evident. Fenestrated clusters of nuclei with dense and large amorphous bodies were observed in some cells. The bizarreness of glioblastoma cells was further exemplified in observing spheroid, dense nuclear encapsulated inclusions. The cells showed an elongated profile with intracytoplasmic processes that were branched and lying adjacent to a degenerating cells. Other unusual bodies and processes were in close association with these cells (Figs. 3-4).

EXPLANATION OF FIGURES

Glioblastoma #403

Figure 1. Electron Micrograph of Several Groups of Glioblastoma Cells Showing Varying Degrees of Nuclear Indentations or Invaginations. The indentations or invaginations range from shallow to deep clefts. The chromatin is irregularly dispersed and has a high electron density. There are several polyhedral-like shaped nuclei and a distinct relationship between the size of the nucleus and the amount of cytoplasm. Cellular polymorphism is evident and glial fibers of high electron density can be seen. The cells appear very compact and close with respect to each other. A large vacuole is present which contains numerous large electron dense bodies and granular precipitates. Several of the polyhedral-like cells have two nuclei. A small population of microvesicles can be seen, as well as other electron dense bodies. X495.

Figure 2. Several Glioblastoma Cells of Varying Shapes and Sizes Showing Pronounced Bizarre Irregular Shaped Nuclei. The heterochromatin is irregularly dispersed with moderate clumping or accumulation at the nuclear membrane. The invaginations of the nuclear membrane range from shallow to moderate. Large populations of oval mitochondria with focally indistinct cristae can be seen. A small population of tubular mitochondria with indistinct cristae are also apparent. Free ribosomes and glycogen are dispersed in the cytoplasm. There are no glial fibers present. Desmosomes can be seen connecting adjacent cell membranes. The cytoplasm appears electron lucent and contains glycogen well dispersed within the cells. X1440.

Figure 3. Glioblastoma Giant Cells Showing Nuclear Indentations or Invaginations Ranging From Shallow to Bizarre-Pronounced Deep Clefts. Some of the heterochromatin appears distinct, electron dense, and is randomly dispersed throughout the nuclei; while other heterochromatin is displayed as dense patches confined to the nuclear membrane. Of particular interest is the presence of amorphous, dense, irregularly distributed patches of material within various cells. Cellular polymorphism is distinct: free ribosomes are dispersed in the cytoplasm; a large population of oval tubular mitochondria are present; several populations of golgi can be seen, several small populations of granular endoplasmic reticuli are present; and electron dense patches of amorphous material are randomly dispersed. There is a distinct inconstant relationship between the size of the nucleus and the cytoplasm. When apparent, the nuclei of some cells contain double membrane-bound small inclusions that appear semilucent. X900.

Figure 4. Another Area of Glioblastoma Cells Showing a Large Cell Somewhat Oval in Shape With an Invaginated Short Process. This cell is filled with numerous dense lipid-like structures of varying sizes and shapes. Of special interest is the presence of a distinct nuclei with a well-defined dense deposition of heterochromatin at the nuclear membrane. The euchromatin exemplifies a translucent distinct appearance and comprises the bulk of the nuclei. Other dense inclusions average around 4-6 mm in diameter and show degradative changes. The cytoplasm contains mitochondria that show shrinkage, polyploidy, and are of various sizes. Granular endoplasmic reticuli are also prominent in the cell. Other surrounding cells show large numbers of vacuoles, compact fenestrated nuclei, cellular debris and remnants of cells among fibers in the interstitial spaces. X495.

69-96

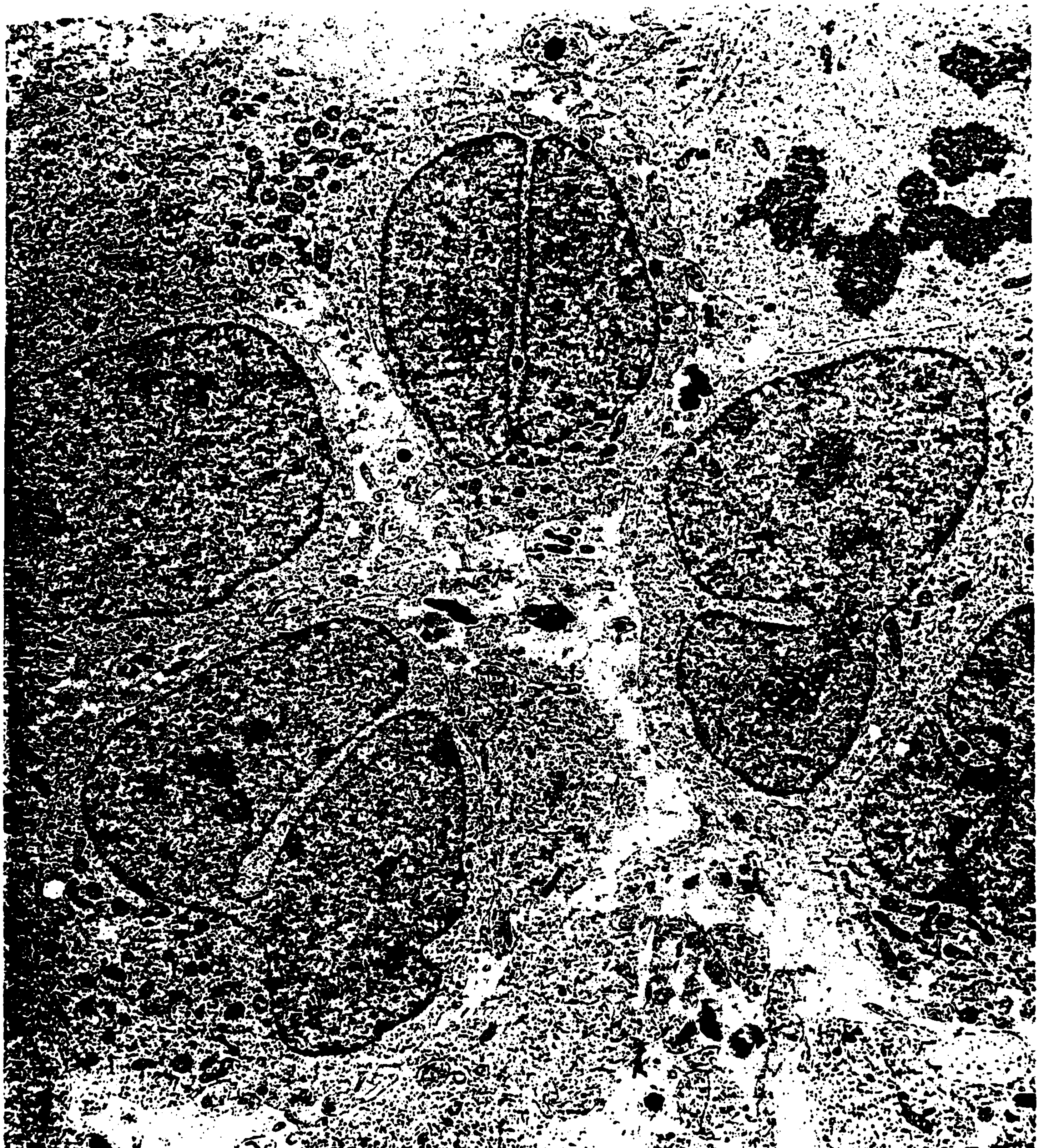

iv. Glioblastoma #N66-754

Glioblastoma cells showed variations in size and shape of nuclei, mitochondria of various sizes and shapes, granular endoplasmic reticuli, dense lysosome-like bodies, golgi and numerous small membrane-bound vesicles. The heterochromatin of nuclei appeared regularly dist ibuted with nucleoli apparent in some cells. Of particular interest was the presence of two nuclei per cell. Mitochondria were scarce-moderate in number and the cells contained a moderate number of endoplasmic reticuli with an abundance of ribosomes on the surface. The mitochondria were occasionally surrounded by a double membrane structure. The nuclear membrane of some cells showed indentations and infoldings of the cell membrane (Figure 1). Some cell populations of cells contained nuclei round in shape. Desmosomes could be seen adjoining adjacent cell membranes. The cytoplasm of various cells showed the presence of membrane encapsulated structures filled with vesicles and free ribosomes. Various inclusions exhibiting various degrees of semi-translucency were also observed. Dense patches of heterochromatin were seen throughout the nuclei (Figs. 2-3). Various cells of the glioblastoma contained bundles of microfilaments and fine microfilaments. The cytoplasm of these tumor cells appeared translucent and occasionally spherical dense granules could be seen (Fig. 4).

EXPLANATION OF FIGURES

Glioblastoma #N66-754

Figure 1. Glioblastoma Cells Showing Variations in Size and Shape of Nuclei, Mitochondria of Various Sizes and Shapes, Granular Endoplasmic Reticuli, Dense Lysosome-like Bodies, Golgi and Numerous Small Membrane-bound Vesicles. The heterochromatin of the nuclei appears regularly distributed. The nucleoli are apparent in some cells. Of particular interest is the presence of two nucleoli per cell. The mitochondria are scarce-moderate in number and the cells contain a moderate number of granular endoplasmic reticuli. Infoldings of the cell membrane are also evident. X1650.

Figure 2. Glioblastoma Cells Exhibiting Round-shaped Nuclei. Desmosomes can be seen adjoining adjacent cell membranes. Double membrane encapsulated structures filled with vesicles and free ribosomes are evident. X1925.

Figure 3. Round Nuclei of Glioblastoma Cells Containing Encapsulated Membrane-bound inclusions that Exhibit Various Degrees of Semi-translucency. Dense patches of heterochromatin can be seen throughout the nuclei. Pronounced invaginated areas in the membrane are apparent in one of the nuclei. X1650.

Figure 4. Glioblastoma Cells Showing Spherical Dense Granules in the Cytoplasm. The cytoplasm is translucent and the mitochondria exhibits polyploidy and are found sometimes in clumps. X1925.

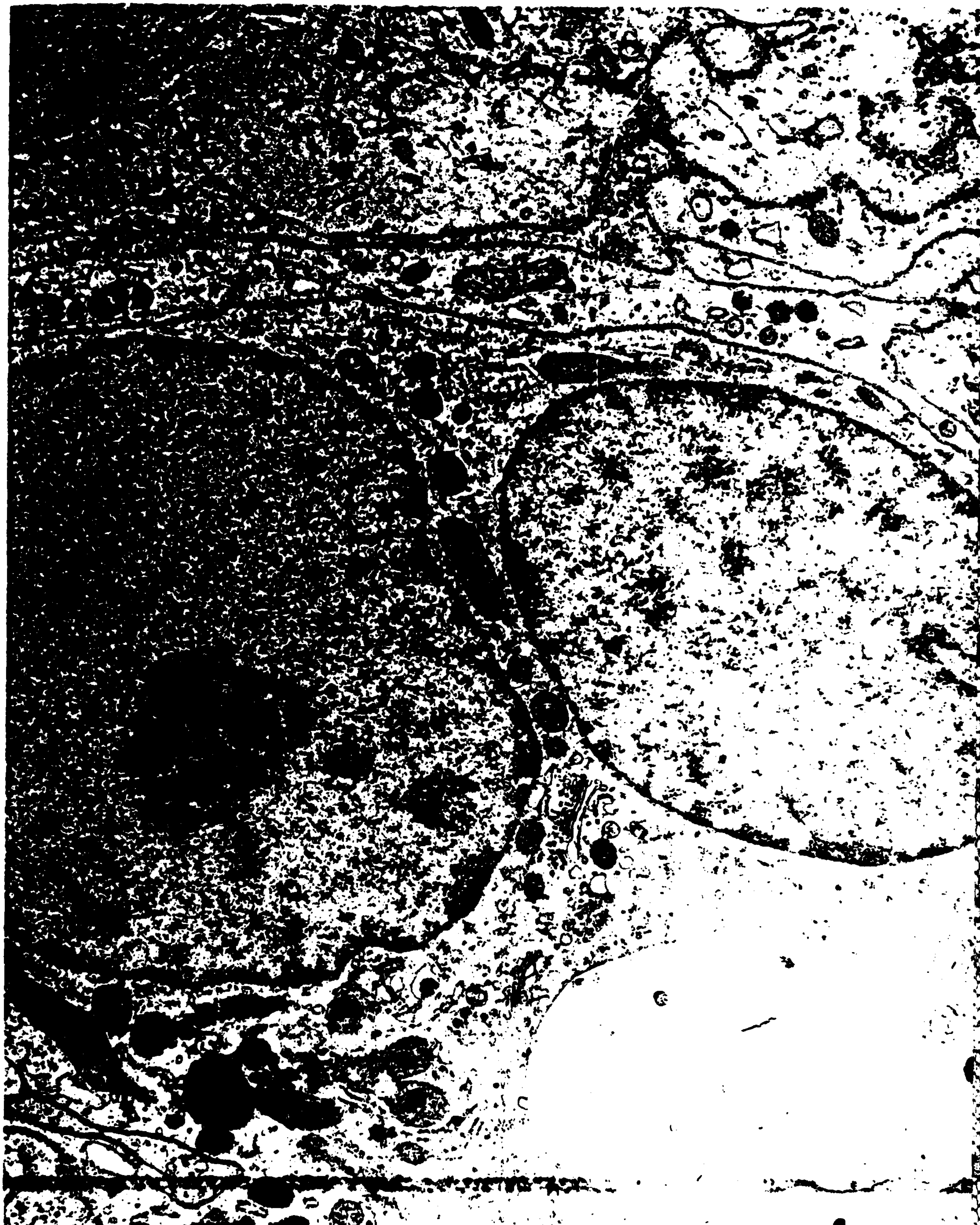

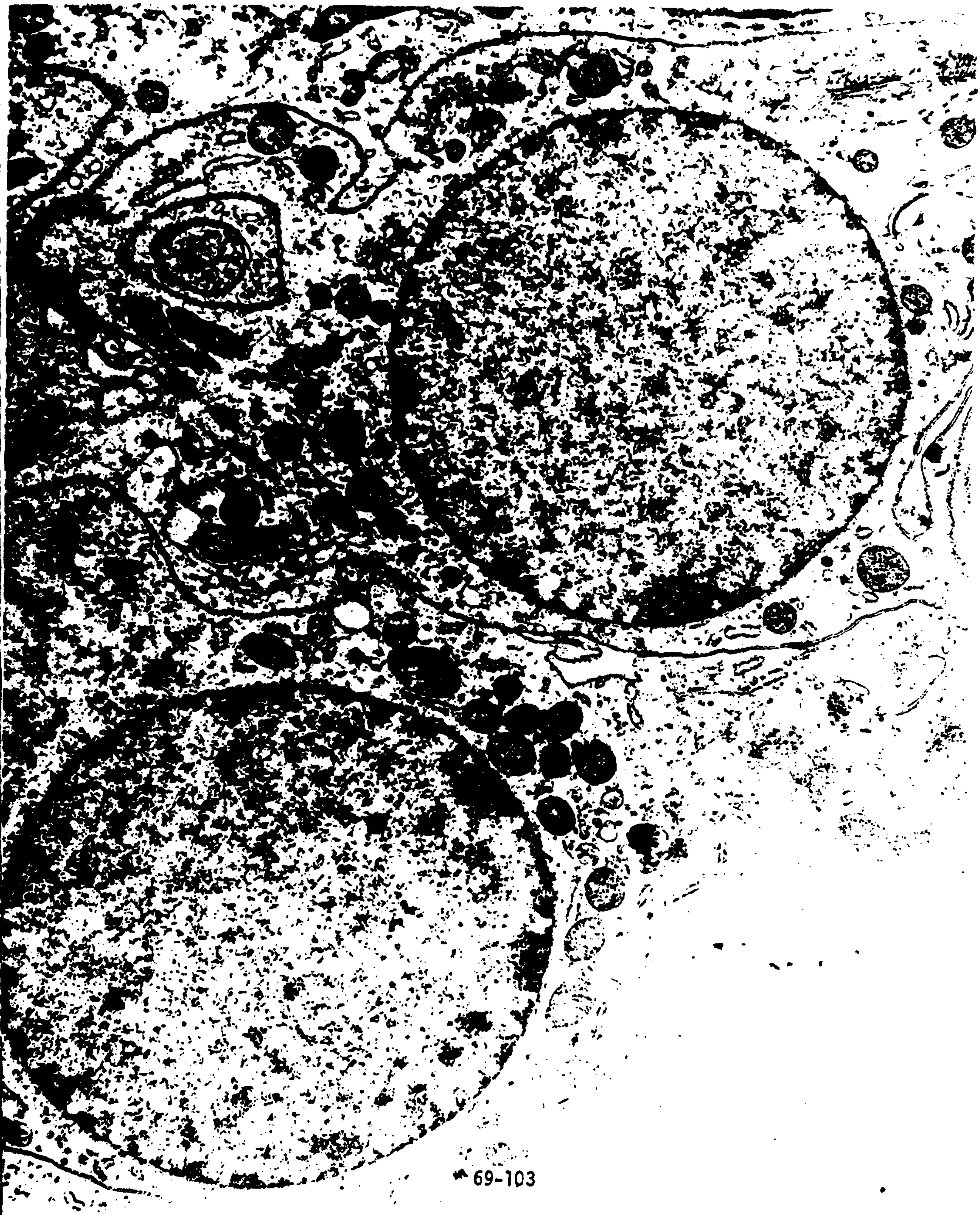
69-103

V. RECOMMENDATIONS:

A. GUIDANCE FOR IMPLEMENTING THE RESULTS OF THE RESEARCH

The recommendations for implementing the results of this research performed over the 10 week summer period are as follows:

i. (1985-1986) Submit abstracts for platform and poster presentations at the following scientific conferences:

- NIH/Minority Biomedical Research Support Symposium, April, 1986, New Orleans, Louisiana
- Southeast Electron Microscopy Society (SEEMS), May, 1986, Columbia, South Carolina
- Electron Microscopy Society of America (EMSA), August, 1986, Albuquerque, New Mexico
- International Congress on Electron Microscopy, August, 1986, Tokyo, Japan
- Other Conferences (i.e. Pathology conferences and etc.) Designated by Dr. Harold Davis, Effort Focal Point Collaboration, USAFSAM/VSP Brooks AFB, San Antonio, TX

ii. (1985-1986) Continue Ultrastructural Work on Brain Tumors at the Following Location:

- Institute of Electron Microscopy
  Department of Biology
  Morehouse College
  Atlanta, Georgia 30314
- Improve on the Following EM techniques: Ultramicrotomy and Darkroom Techniques

- Work Very Closely with Dr. Harold Davis in Preparation of Abstracts for Platform and Poster Presentations at Scientific Conferences and Obtain USAFSAM/VSP Approval

iii. Work Closely with Dr. Davis in Preparation of Manuscripts for Publication

iv. Submit Several Manuscripts for Publication to Refereed Journals

B. SUGGESTIONS FOR FOLLOW-ON RESEARCH

The summer faculty fellow does intend to apply for a mini-grant to continue the research on brain tumors. This will entail a research collaboration between Brooks AFB and Morehouse College. The following is a detailed protocol of follow-on research.

Tentative Title of Project: Long-Term Life Expectancy Radiation Effects: Immunofluorescent and Ultracytochemical Studies on Biogenic Amines, Oxidative and Hydrolytic Enzymes in Brain Tumors of Macaca mulatta Following Exposure to Proton Radiation

USAF/SAM Research Collaborator: Harold Davis, DVM, PH.D. Chief
Veterinary Science Pathology Branch
Brooks AFB
San Antonio, Texas

Principal Investigator: Betty Ruth Jones, PH.D.
Associate Professor of Biology
Director of the Institute of Electron Microscopy
Morehouse College
Acting Director of the Atlanta University Center Scanning Electron Microscopy Research Laboratory

Location Site for Immunohistochemistry and Electron Microscopy Work on Brain Tumors:
Institute of Electron Microscopy
Morehouse College
Atlanta, Georgia

Location Site for Maintenance of Animal Colonies, Radiation Research, Gross and Fine Surgery for Tumor Removal:

Brooks AFB
San Antonio, Texas

Research Objectives:

1) To obtain an understanding of the metabolism and enzyme cytochemistry of brain tumors following exposure to proton radiation

2) To identify and localize biogenic amines, oxidative and hydrolytic enzymes in brain tumors

   i. To identify, localize and study the distribution of the biogenic amines, 5-hydroxytrptamine (serotonin)

   ii. To identify, localize and study the distribution of the following oxidative enzymes (i.e. dehydrogenases): succinic dehydrogenase, malate dehydrogenase, isocitrate dehydrogenase, lactate dehydrogenase, alpha glycerophosphate, alcohol dehydrogenase, glucose-6-phosphate dehydrogenase, 6-phosphogluconate dehydrogenase, glutamate dehydrogenase, beta-hydroxybutyrate dehydrogenase and nicotinamide adenine dinucleotide diaphorase.

   iii. To identify and localize the following hydrolytic enzymes in brain tumors: acid phosphatase, alkaline phosphatase, non-specific esterase, specific acetylcholinesterase, beta-glucuronidase and leucine aminopeptidase.

The proposed objectives for follow-on-research are significant in that new data will be provided on the immunohistochemistry and ultracytochemistry of the identification, localization and distribution of biogenic-amines, oxidative and hydrolytic enzymes in tumors. Such intrinsic data

would lead to an overall understanding of the metabolism of primate brain tumors following exposure to proton radiation. Moreover a better understanding of enzyme-immunohistochemical relationships that exist among various tumor types should emerge.

Experimental Design:

NOTE: The maintenance of primate colonies, exposure to radiation and surgical removal of tumors will be implemented at Brooks, AFB and tissues will subsequently be shipped to Dr. Jones for EM studies.

A. Light Microscopy Immunohistochemistry of 5-Hydroxytryptamine (serotonin) in Brain Tumors by an Indirect Immunofluorescence Technique

NOTE: The PI has experience and training in immunohistochemistry using the indirect immunofluorescence technique. This training was obtained at Harvard Medical School in the Department of Neurobiology with the supervision of Dr. Barbara Beltz (1982-1983). The PI has also been the recipient of a scholarship through The Immunonuclear Corporation for a short course in basic immunohistochemical techniques in whole mounts and sectioned materials. This short course took place at Woods Hole, October 30 - November 4, 1983. The course director was Dr. Barbara Beltz.

Cryosectioned Material: Tumors will be fixed in 4% paraformaldehyde or paraformaldehyde/periodate (PLP) fixative. After 1-2 hours, tumors will be infiltrated with 20% sucrose in 0.1 M phosphate buffer for 1-2 hours. Tumors will then be mounted and frozen with dry ice in preparation for cryostat sectioning. Frozen cryostat sections (6-10 microns) will be cut and mounted on gelatin-coated slides.

Sections will then be incubated at 4°C in a 1:200 dilution of antiserotonin antibody (the primary antibody). Antiserotonin antibodies will be obtained from Immunonuclear Corporation, where they will be generated in rabbits against a formaldehyde cross-linked serotonin-bovine serum albumin (BSA) conjugate. Following primary antibody treatment, the organisms will be rinsed in phosphate/triton x-100/azide for 1 hour, then incubated with the secondary antibody which will be goat antirabbit IgG labeled with fluorescein isothiocyanate (FITC). This antibody preparation will be an affinity-isolated IgG produced by Boehgringer Mannheim Biochemicals.

Tumors will be incubated in IgG-conjugated FITC at 40°C for 6 hours overnight. Excess secondary antibody will be removed by multiple rinses in 0.1 M of phosphate buffer (1 to 2 hours total). Tumors will then be rinsed once in 4 mm of sodium carbonate buffer (pH 9.5), mounted in 80% glycerol in 20 mm of carbonate buffer, and viewed with the proposed Zeiss standard 16 light microscope set up for epifluorescent excitation. Exciter barrier filters and reflector combination cubes will be used containing a blue excitation at 440 to 490 mm and a selective barrier filter at 520 to 560 mm. Specific Controls: Absorption controls will be conducted by preincubating the antiserotonin antibody, at working dilutions, with the following antigens: (1) sertonin creatinine sulfate (1 mg/ml); (2) formaldehyde cross-linked serotonin-BSA in which the BSA concentration will be 300 mg/ml, with a BSA serotonin ratio of approximately 10:1 (w/w); (3) BSA (500 mg/ml); (4) octopamine (1 mg/ml). The serotonin-BSA conjugate will be supplied by Immunonuclear Corporation and the concentration will be determined from analysis of the compound. The antigen/antiserotonin

antibody mixture will be incubated at 4°C for 16 to 24 hours with ocassional gentle agitation, centrifuged at 100,000 x g for 20 minutes, and the supernatant fluid (preabsorbed serum) will be collected. In some experiments tumors will be fixed with PP for 1-2 hours, and rinsed with phosphate/triton x-100/azide. One group of tumors will be incubated with a 1:200 dilution of antiserotonin antibody, and another group will be incubated in pre-absorbed serum.

B. ELECTRON MICROSCOPY CYTOCHEMISTRY OF 5-HT IN BRAIN TUMORS

Tumors will be fixed in Karnovsky's fixative at 4°C for 4-24 hours; washed in 0.3 M phosphate buffer, post-fixed in 1% buffered osmium tetroxide, rinsed in buffer and dehydrated in a graded series of alcohols. Tumors will be infiltrated and embedded in an epoxy resin. Thin sections will be cut on a LKB number V or Porter Blum MT-2 ultramicrotome using diamond knives. Sections will be picked up on uncoated (300-400) copper mesh grids and examined in a Zeiss 9S-2 transmission electron microscope. Electron Micrographs will be taken at desirable magnifications on electron image electron microscope film.

C. HISTOCHEMICAL LOCALIZATION OF OXIDATIVE AND HYDROLYTIC ENZYMES IN BRAIN TUMORS

Cryomicrotomy techniques will be utilized for the localization of oxidative and hydrolytic enzymes in brain tumors. At least 12 dehydrogenases can be demonstrated histochemically. The substrates that will be utilized are sodium succinate for succinic dehydrogenase, sodium-L-malate for malate dehydrogenase, trisodium-DL-isocitrate for isocitrate dehydrogenase, calcium lactate and sodium-DL-lactate for lactate dehydrogenase, disodium-DL-alpha-glycerophosphate for alphaglycerophosphate, ethanol for

enzyme inhibitors and (4) omission of chelating or coupling agents from the incubation medium. Following incubation, sections will be rinsed in distilled water, mounted in gum damar and observed under a light microscope.

NOTE: A few oxidative and hydrolytic enzymes will also be localized at the EM level. Details of these procedures will be included in the mini proposal.

C. OTHER SUGGESTIONS HAVING A BEARING ON THE RESEARCH

1) Through communication with my research collaboration, Dr. Davis, I have been informed that the radiation sciences division and veterinary sciences might initiate a series of experiments to study long term life expectancy radiation effects in rats. If such protocols are developed, we would like to carry out the electron microscopy aspects of the research at the Institute of Electron Microscopy at Morehouse College. Similar studies that are proposed in B of this section can further be implemented.

2) Over the 10 week summer period, the faculty fellow and her graduate obtained a tremendous quantity of EM data on the following tumors: A malignant meningioma, an ependymoma and 4 different glioblastomas. Due to the short research period, EM on two other glioblastomas was not carried out. In addition, other tumors have appeared in the chronic colony since the summer research period ended. We would like to continue to carry out the electron microscopy research at the Institute of EM at Morehouse.

3) Other suggestions for brain tumor study with respect to techniques are to utilize the following: scanning electron microscopy and x-ray Microanalysis and Immunoperoxidase Staining Techniques.

alcohol dehydrogenase, disodium glucose-6-phosphate for glucose-6-phosphate dehydrogenase, barium-6-phosphogluconic acid for 6-phosphogluconate dehydrogenase, Sodium-L-glutamate for glutamate dehydrogenase, disodium DL-beta-hydroxybutyric aid for beta-hydroxybutyrate dehydrogenase, reduced beta nicotinamide adenine dinucleotide for NADH diaphorase, and reduced beta-nicotinamide adenine dinucleotide phosphate for NADPH diaphorase.

Incubations will be carried out for 20 minutes at 37 C or 60 minutes at 25 C. Controls will consist of the following: 1) omission of the specific substrate from the incubation medium, 2) heat-inactivated specimens (held at 90 C for 5 minutes prior to incubation and 3) omission of the specific coenzyme. After incubation frozen sections will be rinsed in distilled water, mounted in glycerol jelly, and observed under a light microscope with a camera attachment.

The following hydrolytic enzymes will be demonstrated in brain tumors: acid phosphatase, alkaline phosphatase, nonspecific esterase, specific acetylcholinesterase, beta glucuronidase and leucine aminopeptidase. The substrates for acid and alkaline phosphatase will be sodium-alpha-napthythyl phosphate. Diazo blue B-tetrazotized-O-dianisidine will act as a coupler. The substrate, 5-Bromoindoxyl acetate will be used for nonspecific esterase and the substrate acetylthiocholine iodide for specific acetylcholinesterase. The substrate for beta-glucuronidase will be 6-Bromo-2-Napthyl-B-D-glucopyruronoside with Fast Blue B salt as the post coupler. For leucine aminopeptidase, L-leucyl-B-Napthylamide HCl will be used as the substrate with Garnet GBS as the simultaneous coupler.

The following controls will be used for hydrolytic enzymes: (1) omission of the substrate, (2) heat inactivation, (3) use of specific

4) Resources and Facilities Available

The institute of electron microscopy is comprised of the following laboratories: preparation laboratory, ultramicrotomy laboratory, electron microscope room, and fully equipped darkroom facility.

The faculty fellow has access to other EM equipment in the Atlanta University Center. A detailed analysis of all resources and facilities available will be given in the mini proposal.

ACKNOWLEDGEMENTS

I am indebted to the Air Force Systems Command, the Air Force Office of Scientific Research and Brooks Air Force Base, Veterinary Sciences Division, Veterinary Pathology Branch in San Antonio, Texas for providing me with the opportunity of further advancing and expanding my research interests. The summer faculty research program sponsored by the Air Force Office of Scientific Research and conducted by Universal Energy Systems has not only enhanced my research capabilities but has provided me an opportunity for follow-on-research at my home institution. In my opinion this is one of the most exciting and attractive components of the program.

My graduate student, Richard A. Hunt and I would like to express sincere appreciation to the Division of Veterinary Sciences at Brooks Air Force Base for a productive summer that allowed us to carry out extensive Ultrastructural Studies on Irradiated Brain Tumors of Monkeys. We are grateful to Dr. Harold Davis for going beyond the call of duty to make our research visit a good and productive one. We wish to thank Ms. Minnie Butcher and Mrs. Lucy Stribling for their assistance in the initial stages of the project and for developing time to allow us to use the EM facility. We wish to thank Dr. Keith Harris for his motivating, stimulating and encouraging remarks throughout the summer and other researchers and staff members in the division that made our stay pleasant.

I also wish to acknowledge the support and assistance of Colonel Toney David, Chief of the Veterinary Sciences Division at Brooks AFB, and

Colonel Harold Powell and Dr. Brice Hartman for administrative arrangements.

With sincere gratitude I am pleased to acknowledge Mr. Rodney Darrah and Ms. Sue Espy of Universal Energy Systems for their patience and support and allowing me to exceed the page stipulations for this final report. Finally, I wish to thank Major Amos Otis, program manager at the Air Force Office of Scientific Research for his assistance throughout the program and for his motivating and positive interactions with faculty members at Morehouse College.

REFERENCES

1. Sobel, H. J. and E. Murquet (1980). Usefulness of Electron Microscopy in the Diagnosis of Tumors, Path. Res. Pract. 167: 22-44.

2. Alwasiak, J., Hajdukiewicz, Karasek, Marek, Majak, and papierz. (1982). Some aspects of the Ultrastructure of Gliomas. Neuropat, Pol. 20: 1-2.

3. Koizumi, J. and S. Minei. (1970) Electron Microscopy of Glycogen in Meningothelial Meningioma. Arch. histol. jap. 32: 347-354.

4. Eimoto, T. and K. Hashimoto. (1977) Vacuolated Meningioma: Light and Electron Microscopic Study. Acta. Path. Jap. 27: 557-566.

5. Pietroszka, M., Hernando, and C. Pena. (1978). Malignant Meningioma: Ultrastructure and Observations on Histogenesis. Pathol. 10:169-173.

6. Kepes, John J. (1975). The Fine Structure of Hyaline Inclusions (Pseudopsammoma Bodies) in Meningiomas. J. Neuropathol. Exp. Neurol. 34:282-92.

7. Virtanen, I., Lehtonen, E., and J. Wartiovaara. (1976). Structure of Psammoma Bodies of A Meningioma In Scanning Electron Microscopy. Cancer 38:824-829.

8. Tedeschi, F., R. Brizzi, A. Lechi, G. Trabattoni, C. Ferrari and F. Tagliavini. (1981). Meningiomas. A Light and Electron Microscopy Study. Acta Neuropathol (Berl). Suppl. VII: 122-125.

9. Humeav, C, P. Vic, P. Senten and B. Vlabovitch (1979). The Fine Structure of Meninglomas: An Attempted Classification. Virchows Arch, A. Path. Anat. and Histol. 382-201-216.

10. Rizzoli, H. J. Randall and D. R. Smith (1978). Psammoma Bodies in Meningioma. Virchows Arch A. Path. Ant. and Histol. 380-325.

11. Bilbao, J., K. Kovacs, and E. Horvath. (1976). Annulate Lamellae in the Pituitary Gland. J. Neuropathol. Exp. Neurol. 35 (3): 360.

12. Gilbert, J. J. O. Paulseth, R. Coates, and D. Malott. (1983). Cerebral Edema Associated with Meningiomas. Neurosurg. 12: 599-605.

13. Markesberry, W. R., P. E. Duffy, and D. Cowen. (1973). Granular Cell Tumors of the Central Nervous System. J. Neuropathol. Exp. Neurol. 32 (1): 92-109.

14. Kubota, T., A. Hurano, K. Sato, and S. Yamamota, (1984). Fine Structure of Psammoma Bodies in Meningocytic Whorls. Arch. Pathol. Lab. Med. 108: 752-754.

15. Font, R. L. and J. O. Croxatto. (1980). Intracellular Inclusions in Meningothelial Meningioma. J. Neuropathol. Exp. H. Neurol. 39 (5): 575-583.

16. Kubota, T. K. Sato, S. Yamamoto, and A. Mirano. (1984). Ultrastructural Study of the Formation of Psammoma. Bodies in Fibroblastic Meningioma. J. Neurosurg. 60: 512-517.

17. Challa, V. R., D. M. Moody, R. B. Marshall, and D. L. Kelly, Jr. (1980). The Vascular Component in Meningiomas Associated with Severe Cerebral Edema. Neurosurg. 7: 363-368.

18. Muller, J. and J. Mealey, Jr. (1971). The Use of Tissue Culture in Differentiation Between Angioblastic Meningioma and Hemangiopericytoma J. Neurosurg. 34: 341-349.

19. Pena, C. (1977). Meningioma and Intracranial Hemangiopericytoma. Acta Neuropath. (Berl) 39: 69-74.

20. Kepes, J. (1975). Fine Structure of Hyaline Inclusions (Pseudopsammoma Bodies) in Meningiomas. J. Neuropath. Exp. Neurol., 34: 282-292.

21. Szymas, J., W. Biczysko, P. Gabryel, and H. Prokopanow (1982). Histological Features of Meningiomas With Their Ultrastructural Aspects. Neuropat. Pol., 2:155-167

22. Cerro's-Navarro, J. and J. J. Vazquez (1969). An Electron Microscopic Study of Meningiomas. Acta Neuropath. (Berl) 13: 301-323.

23. Humeav, V. P. Senten and B. Vlahovitch (1979). The Fine Structure of Meningiomas: (An Attempted Classification). Anat. Histol 382: 201-216.

24. Cerros-Navarro, J., L. F. Martins, and M. C. Lazaro (1980). Ultrastructure of Malignant Meningioma and Meningosarcoma. Advances in Neurosurg. 2:12-22.

25. Zubaidy, A. J. and W. Malinowski (1984). Spontaneous pineal body tumors (pinealomas) in Wistar rats; a histological and ultrastructural study. Laboratory Animal, 18: 224-229.

26. Tani, E. and N. Higushi (1972). Intercellular Junctions in Human Ependymomas. Acta Neuropath., 22: 295-304.

27. Hirano, A. (1978). Some Contributions of Electron Microscopy to the Diagnosis of Brain Tumors. Acta Neuropathol., 43: 119-128.

28. Woyke, S. M.D. and B. Czerniak, M.D. (1978). Fine Needle Aspiration Cytology of Metastatic Myxopapillary Ependymoma. Acta Cytologica, 27: 312-315.

29. Friede, R. L., M.D. and A. Pollak, M.D. (1978). The Cytogenetic Basis for Classifying Ependymomas. J. of Neuropath. and Exp. Neurol. 37: 103-118.

30. Lyser, K. (1975). Human Nervous System Tumors (Observations by High Voltage Electron Microscopy). Aeta Neuropath. 32: 313-324.

31. Nakamura, S. N. Koga and N. Moriyasu (1980). Clinical Application of Diagnostic Ultra-Microscopy. Electron Microscopy, 13, 5-6.

32. Nakahura, S. N. Koga and N. Moriyasu (1979). Cellular Arrangement of the Ependymoma. J. Clin. Electron Microscopy, 12:5-6.

33. Goebel H., H. Cravioto. (1972). Ultrastructure of Human and Experimental Ependymomas: A Comparative Study. J. Neuropath. and Exptl. Neurol. 3:54-71.

34. Woyke, S. and B. Czernaik (1979). Fine Needle Aspiration Cytology of Metastatic Myxopapillary Ependymoma. ACTA Med., 20:1.

35. Moss, T.H. (1984). Observations on the Nature of Subependymoma: An Electron Microscopic Study. Neuropath. Appl. Neurobiol. 10:63-75.

36. Lin, H. M., D. C. McLone and S. Clark (1977). Ependymomas of Childhood: Electron Microscopic Study. Child's Brain 3: 281-296.

37. Virtanen, I. E. Lehtonen, and J. Wartiovaara (1976). Structure of Psammoma Bodies of A Meningioma, In SEM. Cancer 2: 824-829.

38. Herman, M. Adams R. and E. Manuelidig (1966). The Ultrastructure of a Human Glioblastoma Multforme-derived Tumor Heterologously Transplanted To Giunea Pig Eye and Brain. Acta-Neuropath., 8:321-380.

39. Scherneck, S., M. Rudolph, E. Geissler, F. Vogel, L. Lubbe, II., H. Wahhe, T. H. Nisch, F. Weickmann and T. Wolfgangzinmmermann (1979). Isolation of A SV 40-Like Papovirus from a Human Glioblastoma. Intl. J. Cancer, 24: 523-531.

40. Hakanson, C. H. and C. Von Mecklenburg (1981). The Effects of Ionizing Irradiation on Ciliated Cells of the Central Nervous System in Man: A Scanning Electron Microscopy Study. Scanning Electron Microscopy, 4: 93-98.

41. Kusawoki, Tokuro (1969). Electron Microscopic Observations on Glioblastoma Arch. Jap. Chir. 38:12-34.

42. Hadfield, M. G. and S. G. Silverberg (1972). Light and Electron Microscopy of Giant Cell Glioblastoma. Cancer: 4:984-986.

43. Van Der Meulen, J. H. Mouthoroff and E. J. Ebels (1978). Glial Fibrillary Acidic Protein in Human Gliomas. Neuropath. and Appl. Neurobiol., 4:177-190.

44. Nakamura, S. and N. Moriqasu (1981). Usefulness of the Electron Microscopic Study for Diagnosis of Brain Tumors. J. Clin. Electron Microscopy. 14:5-6.

45. Lantos, P. L. (1976). The Role of the Subependymal Plate in the Origin of Gliomas Induced by Ethylnitrosourea in the Rat Brain. Experiential 33: 521-522.

46. Kroh, H., T. Majdecki, K. Renkqwek, and Z. Krebsforsh (1973). Ultrastructure of Experimental Brain Gliomas in Mice 80:159-168.

47. Kumar, S. Kumar, H. B. Marsden, Lynch, and E. Ear Shaw (1980). Weibel-Palade Bodies in Endothelial Cells as a Marker for Angiogenesis in Brain Tumors. Cancer Research, 40:2010-2019

48. Sipe, J. M. Herman, and J. Rubenstein (1973). Electron Microscopic Observations on Human Glioblastomas and Astrocytomas Maintained in Organ Culture System. AM. J. Pathol.,: 73-589-606

49. Ebhardt G. and J. Cervo's-Navarro (1981). The Fine Structure of Cells in Astrocytomas of Various Grades of Malignancy. Acta Neuropathol. (Berl). 7: 88-90.

50. Kroh, H. T. Majdeck:, and K. Renkawek (1973). Ultrastructure of Experimental Brain Gliomas in Mice Z. Koebsforsch. 80, 159-168.

51. Deane, B. R. and P. L. Lantos (1981). The Vasculature of Experimental Brain Tumors, J. Neurol. Sci. 49: 55-66.

52. Sapsford, J. and R. O. Weller (1983) Basement Membrane Surfaces and Perivascular Compartments in Normal Human Brain and Glial Tumors. A Scanning Electron Microscope Study. Neuropath. and Appl. Neurobiol. 9: 181-194.

53. Deck, J. L. Eng, J. Bigbee, and S. Woodcock (1978). The Role of Glial Fibrillary Acidic Protein in the Diagnosis of Central Nervous System Tumors, Acta Neuropath. (Berl.) 42, 183-190.

54. Hamilton, A. M., A. Garner, R. C. Thipathi and M. D. Sanders. (1973). Malignant Optic Nerve Glioma: Report of A Case with the Electron Microscope Study. Brit. F. Ophthal., 57: 253.

55. Gessaga, E. G. (1982). Intracellular Inclusions Called Hirano Bodies. Ultrastructural Path. 3: 199-214.

56. Tascos, J. Parr, N. Gonatas (1982). Immunocytochemical Study of the Glial Fibrillary Acidic Protein in Human Neoplasms of the Central Nervous System. Human. Pathol., 13:454-458.

57. Lantos, P. L. (1977) The Distribution and Role of Microtubules and Filaments in the Neoplastic Astrocytes of Experimental Gliomas. Neuropath. and Appl. Neurobiol. 3, 281-296.

58. Collins, V. R., U. Brank, B., A. Fredrikson and B. Westermark (1980). Transmission and Scanning Electron Microscopy of Whole Glioma Cells Cultured in Vitro. AMF O'Hare, Il, Scanning Electron Microscopy, 2: 223-230.

59. Wang, E., J. Cairncross and R. K. Liem (1984). Identification of Glial Filament Protein and Vimentin in the same Intermediate Filament System in Human Glioma Cells. Proc. Natl. Acad. Sci., 81: 2102-2106.

60. USAFSAM/Radiation Sciences Division, Long Term Life Expect Radiation Effects, Project #T64131 (Personal Communication).

61. Rubinstein, L. J. (1972). Tumors of the Central Nervous System Second Series, Fascicle 6, Armed Forces Institute of Pathology, Washington, D. C.

62. Beltz, Barbara and E. Kravitz. Mapping of Serotonin-like Immunoreactivity in the Lobster Nervous System. J. Neurosci. 3: 585-602.

1985 USAF-UES SUMMER FAACULTY RESEARCH PROGRAM/

GRADUATE STUDENT SUMMER SUPPORT PROGRAM

Sponsored by the

AIR FORCE OFFICE OF SCIENTIFIC RESEARCH

Conducted by the

UNIVERSAL ENERGY SYSTEMS, INC.

FINAL REPORT

Design Considerations for Phase Dependent Voltage Contrast Technique for Application to SEM Analysis.

and

Electrical and Optical and Characterization of Certain Doped Organic Polymers

Prepared by:	Prasad K. Kadaba
Academic Rank:	Professor of Electrical Engineering
Department and	Electrical Engineering
University:	University of Kentucky
Research Location:	AFWAL/MLSA
	Wright-Patterson Air Force Base
Date:	September 23, 1985
Contract No:	F49620-85-C-0013

Design Considerations for Phase Dependent Voltage Contrast Technique for Application to SEM Analysis

and

Electrical and Optical Characterization of Certain Doped Organic Polymers

by

Prasad K. Kadaba

ABSTRACT

A detailed design of the Phase Dependent Voltage Contrast technique (PDVC) that can be used for test and evaluation of IC devices has been outlined. The technique is easy to implement with the SEM and operates on the principle that the detector current due to secondary electrons emitted from a device under test (DUT) in a SEM can be modulated by a suitable signal applied to the substrate of the device. LSI failure analysis is enhanced by image contrast of signal phases, and during LSI complex pulse sequencing, proper control of PDVC gates allows imaging of particular device states. The PDVC technique also has the capability to measure internal propagation delays, which had formerly been possible only with expensive electron beam blanking

Design Considerations for Phase Dependent Voltage Contrast Technique for Application to SEM Analysis.

I. Introduction

Voltage contrast as applied to SEM analysis is based on the following consideration: The collection of secondary electrons depends greatly on the existence of a net positive potential between the specimen and the Faraday cage of the Everhart-Thornley (E-T) detector.[1] If a potential is applied to regions of a specimen, the potential between the specimen and the collector is altered, thus changing the collection efficiency. Therefore, although equal numbers of secondary electrons may leave each point on the specimen, contrast will be developed because of trajectory effects, dependent on the local nature of the surface potential. A positive potential tends to limit the escape of secondary electrons and causes such a region in an image to appear dark. A negative potential tends to enhance secondary collection causing bright regions in an image. Voltage contrast is especially useful for the examination of integrated circuits (ICs). A particular aspect of voltage contrast that will be dealt with in this report is the Phase Dependent Voltage Contrast (PDVC). Figure 1 illustrates the block diagram of the

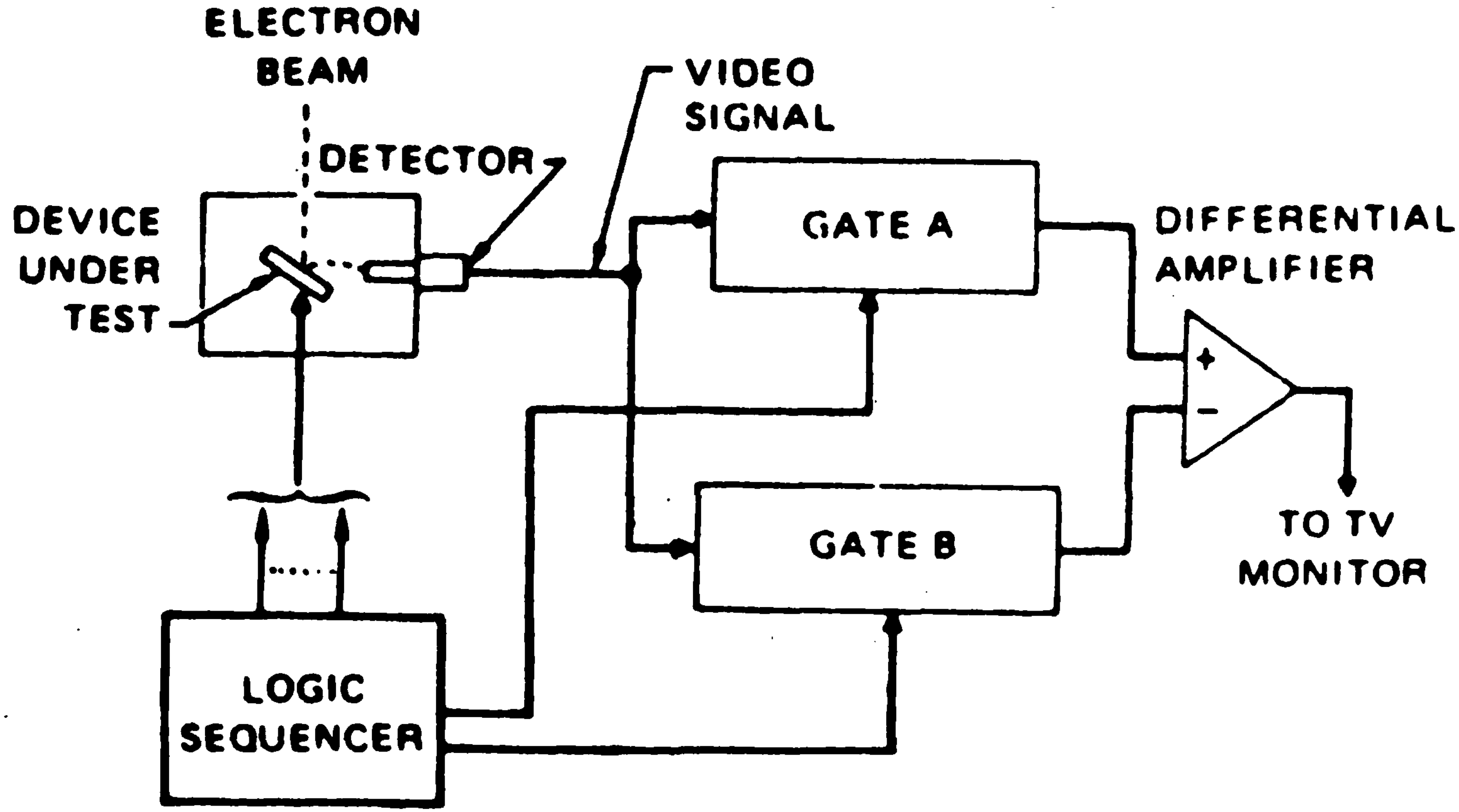

FIGURE 1 PDVC BLOCK DIAGRAM

technique as outlined in a paper by D. Younkin. In this report, a detailed version of the design for (PDVC/SEM) that can be used for test and evaluation of IC devices has been given. The design has been worked out in conjunction with Mr. Jay Harvey* who was formerly a graduate student at the University of Kentucky under the supervision of the author of this report.

II. Objectives

The objective of this part of the investigation is the development of a suitable voltage contrast technique which can be interfaced with the JEOL JSM-35CF SEM equipment that exists in the Electronics Failure Analysis Laboratory (AFWAL/MLSA). The author of this report was in constant communication with Terri Wilkerson, a graduate student who was working on this problem. The research effort of the author of this report was mainly concerned with comprehensive design details of the (PDVC/SEM) that can be used for test and evaluation of IC devices.**

* Mr. Jay Harvey is currently with McDonnell Aircraft Co., St. Louis Division, Mo 63166

** Other aspects of the development of the voltage contrast technique has been given in the final report by Ms. Terri Wilkerson: contract No: F49620-85-C-0013, July 23, 1985.

III. Details of the Design

i) General Considerations:

PDVC/SEM operates on the principle that the detector current due to secondary electrons emitted from a device under test (DUT) in a SEM can be modulated by a suitable signal applied to the substrate of the device. This modulation signal should be a rectangular waveform restricted in voltage to within the supply limits of the device. The electron beam in the SEM may scan the device in either slow-scan or TV-scan rates, and the technique proposed must provide for these modes in such a way as to give an easily interpretable video output signal to an external monitor. It would be desirable to make provisions for viewing either modulated of unmodulated video, normal or inverse video mode, and DC or AC modulation to the device. It is anticipated that video gate delay with respect to device modulation may be required from time to time, and also that various ratios of modulation and gatings may be needed in order to view device performance to the best advantage. Also, it would be desirable to provide for a full range of gated cycle times. All of these features have been incorporated into the design detailed in this report.

ii) Theory of Operation

The individual units of the PDVC/SEM controller are described in this sub-section.

a) Power Supply (Fig. 2). The controller is designed to operate from an external bipolar symmetric DC supply providing between ±15 and ±18 VDC against ground. The Unit will not operate with less than ±14 V and will overheat with greater than ±20 V. Diodes D101 and D102 prevent damage due to reverse connections.

b) Master Clock and Range Dividers (Fig. 3). U201 is a dual oscillator providing an asymmetric rectangle at 20 MHz. One oscillator is disabled and can be used for a colorburst reference at 3579.545 KHz if desired. The 20 MHz signal is divided and symmetrized by the flipflops of U202 to give the master clock MCK which is 10 MHz or 5 MHz depending on the position of NORMAL/HALFRATE switch S201. Cascaded decade dividers U203, U204, and U205 provide counting triggers to the range clock RCK through S202, giving eight selectable cycle times. Because of the 100:1 vernier (see part c), these signals are ranged from 5 KHz to 10 MHz.

c) 100 Division Timing Vernier (Fig. 4). The vernier consists of cascaded decade dividers U301 and U302. It provides a two digit BCD timing word defined by signals B1

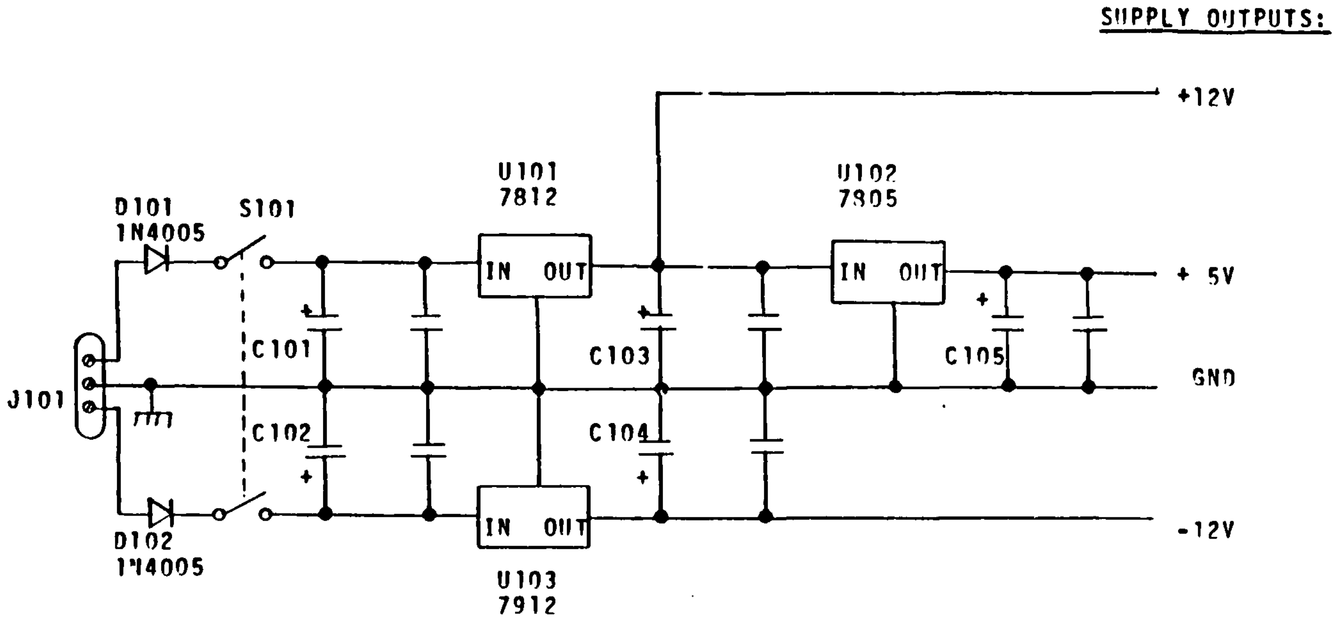

NOTES: C101,102=10 uF 25V. C103,104=10 uF 15V. C105=10 uF 6V
Other capacitors are .1 uF 50V discs. See bypassing figure for layouts.
On 7812 and 7805 middle pin is GND. On 7912 middle pin is IN.
J101 is 3 terminal strip or jack to suit. Input voltage is symmetric bipolar between ±15 and ±18 Volts against GND.
All leads to GND in this figure go to a single tie point.

Figure 2 PDVC/SEM Controller, Power Supply Schematic

NOTES: All capacitors this figure are .1 uF 50V discs. See bypassing figure.
S201 shown in 00KHz-100Hz position. Other position is 50KHz-50Hz.
S202 shown in 100/50 KHz position.
BCD outputs of U202,203,204,205 are not used.

Pins 8,9,10,11 of U201 are not used (reserved for colorburst reference.)

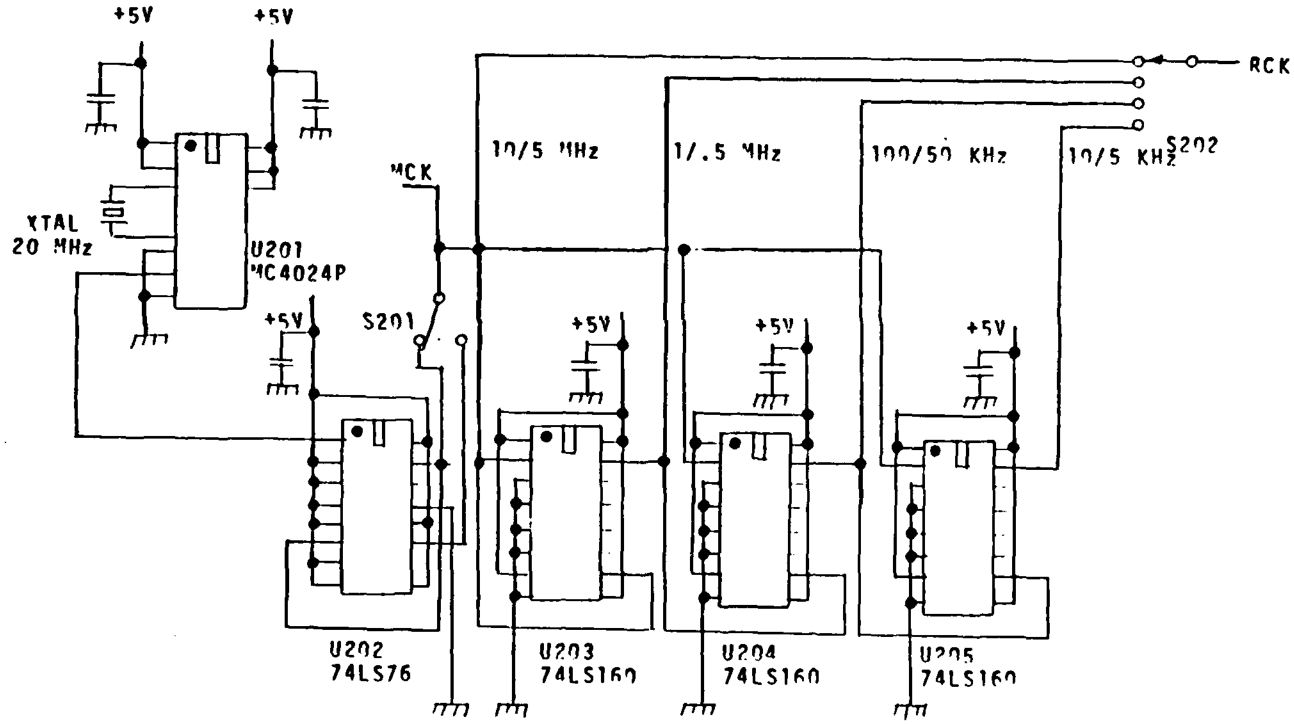

Figure 3 PDVC/SEM Controller, Master Clock and Range Dividers

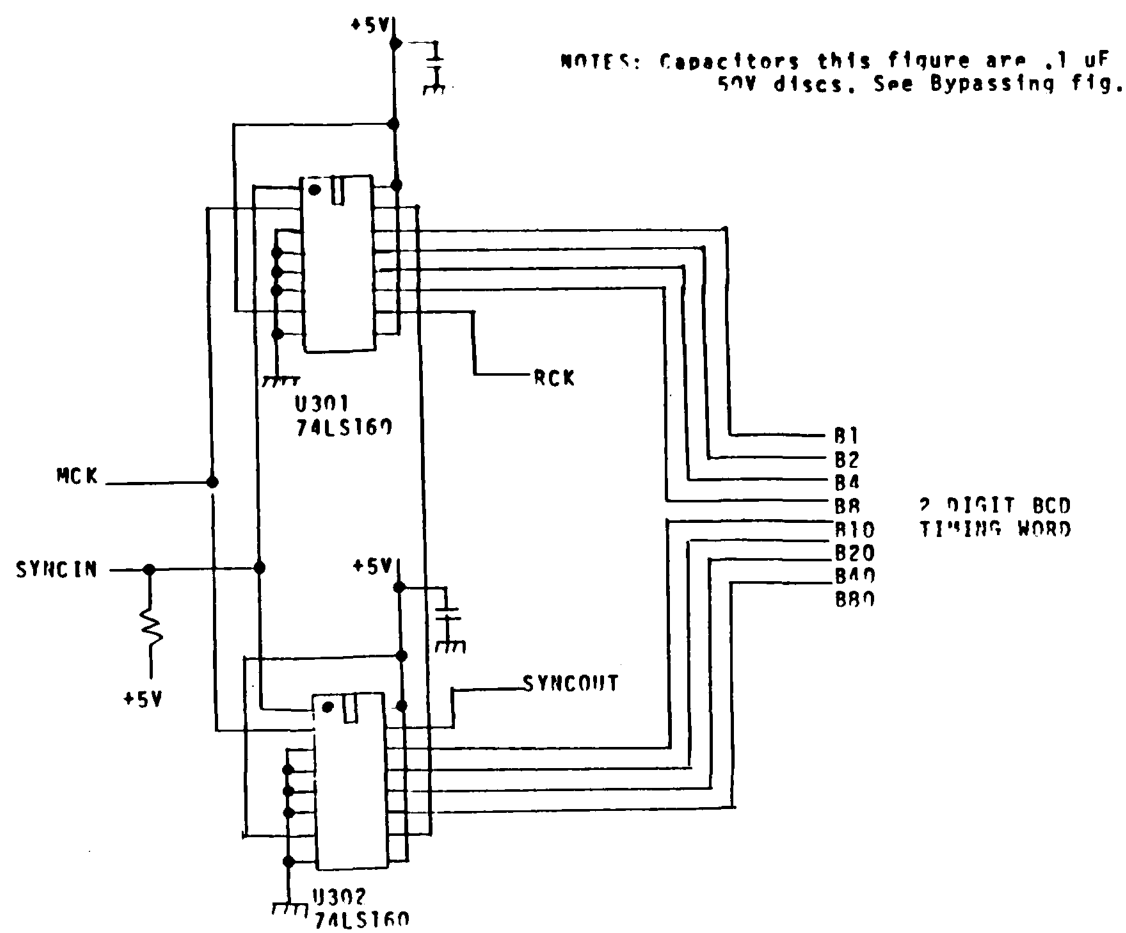

Figure 4. PDVC/SEM Controller, 100 Division Timing Vernier

through B80. The weight of each line is given by its name, viz., B20 has weight = 20. The vernier steps on the trailing edge of RCK and is synchronized by MCK.

d) Modulation and Gate Timing (Fig. 5). There are four of these units, a generic one of which is shown in Fig. 5. Each consists of two four-bit cascaded comparators that output a pulse when ever the word on B1-B80 matches the word (00-99) set on the thumbwheel switch pair associated with that unit. However, unit #4 has no switches, its word being fixed at 00 so that the device modulation waveform always comes up at the start of the cycle. Unit #3, MOD DUTY FACTOR, sets the time when the modulation waveform comes back down. Unit #1, A GATE DELAY, sets the time when the A gate comes on, and Unit #2, END A GATE sets the time when the A gate goes off.

e) Modulation and Gating Latch Gates (Fig. 6). These gates consist of four-input NAND gates whose outputs GLS, GLR, MLS, and MLR are brought low by the word coincidences appearing on the lines TC1-TC4 respectively. These gates are required for two reasons: a) the coincidence pulses are of incorrect polarity to set the latches (see Fig 7); b) set and reset signals to the latches may not appear simultaneously, as would be the case, e.g., if A GATE DELAY = END A GATE or if MOD DUTY FACTOR = 00. If it is desired to have the A gate on all the time, set S501 to A ONLY (similarly for B on always).

NOTES: Capacitors thi fig.
are .1 uF 50V disc
See thumbwheel fig.

UNIT	DEVICES	SWITCHES	OUTPUT
1	U401	S401	TC1
	U402	S402	
2	U403	S403	TC2
	U404	S404	
3	U405	S405	TC3
	U406	S406	
4	U407	*	TC4
	U408		

* Thumbwheels and resistors not used. Connect these 8 lines to GND.

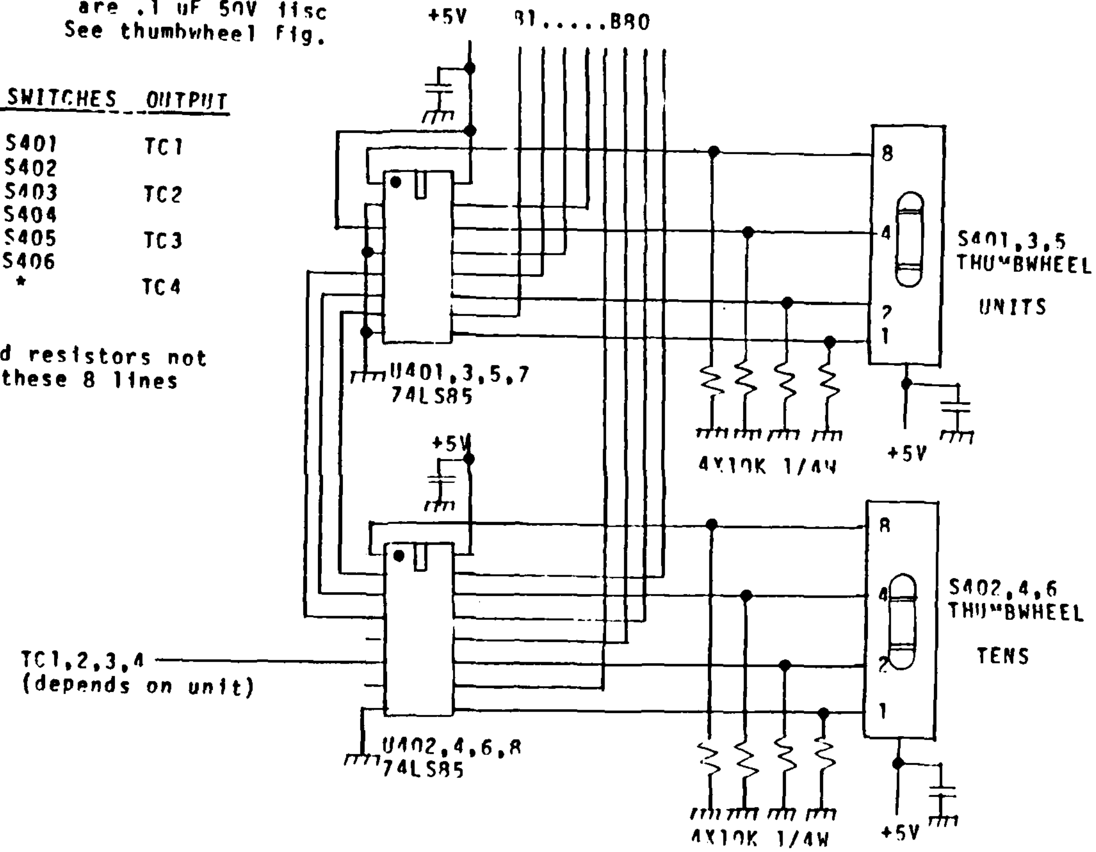

Figure 5 PDVC/SEM Controller, Mod&Gate Timing (one of four units shown.)

NOTES: Capacitors this fig. are 1 uF
50V disc. Resistors are 10K
1/4 W. See bypassing fig.

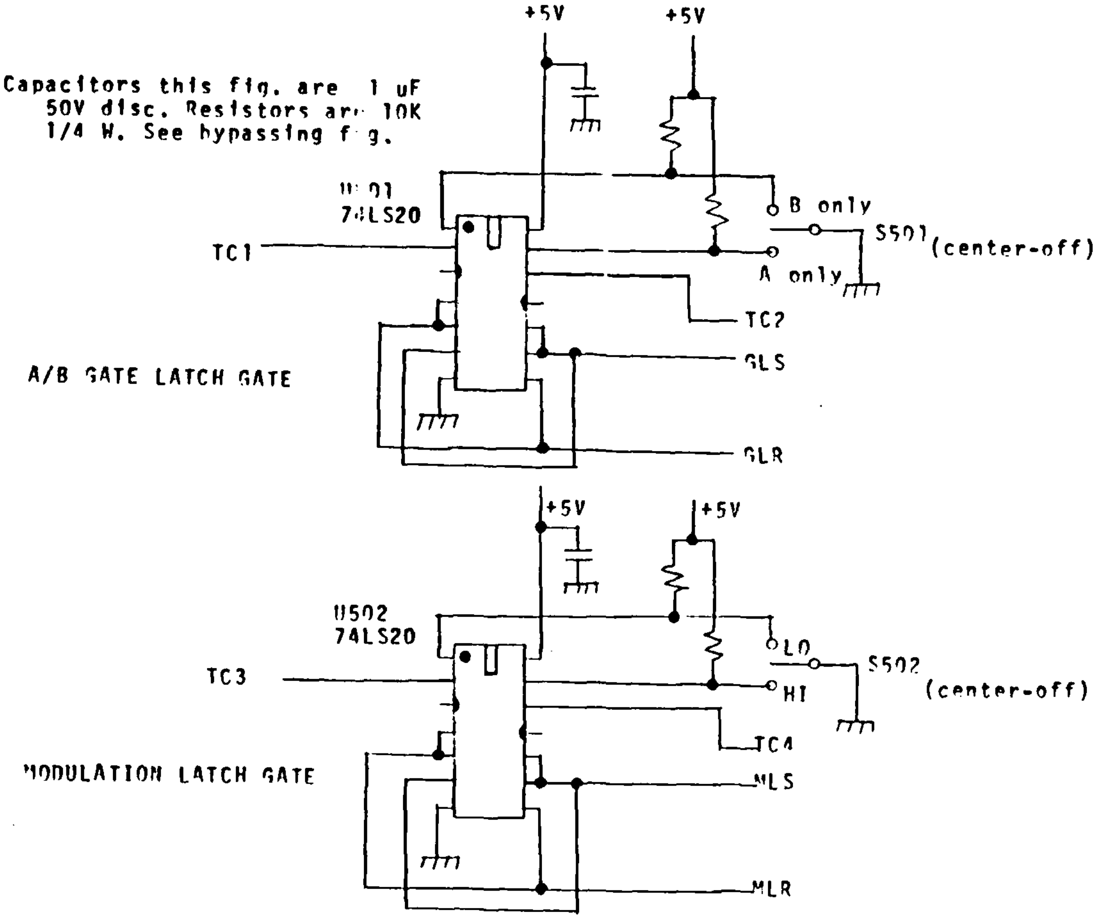

Figure 6 PDVC/SEM Controller, Mod&Gate Latches- Gates

If only one modulation level is to be applied, set S502 accordingly, else place it in center position.

f) <u>Modulation and Gate Latches and A/B Gate (Fig. 7).</u> The flipflops of U601 control the states of the CMOS analog switch U602 and also provide the rectangular modulation signal to the device modulator (see Fig. 8). Switch S601, NORM/INVERSE VIDEO, does not function like its counterpart in the SEM because this switch merely exchanges the roles of the A and B gates. The same effect could have been obtained by exchanging the values of A GATE DELAY and END A GATE, but using S601 is more convenient.

Fig. 7 shows the arrangement for standard TV positive video, 5 MHz bandwidth, and 50 ohm input impedance. The VIDEO GAIN control R601 gives a gain of 1 to 10, but the signal at the output of U603 is limited between 0 and +5 V to protect U602. The A and B analog switches are in series tandem to provide about 80 db (10,000:1) isolation between the channels. The differential amplifier U604 drives the VIDEO OUTPUT at about 50 ohms and 5 MHz bandwidth. A small roll off is provided to reduce switching transients.

g) <u>Device Modulator (Fig. 8).</u> The four opamps of U701 condition the TTL modulation signal from U601 so that it varies between two adjustable voltages in order to bias the device substrate properly. The control R701, P-P MOD,

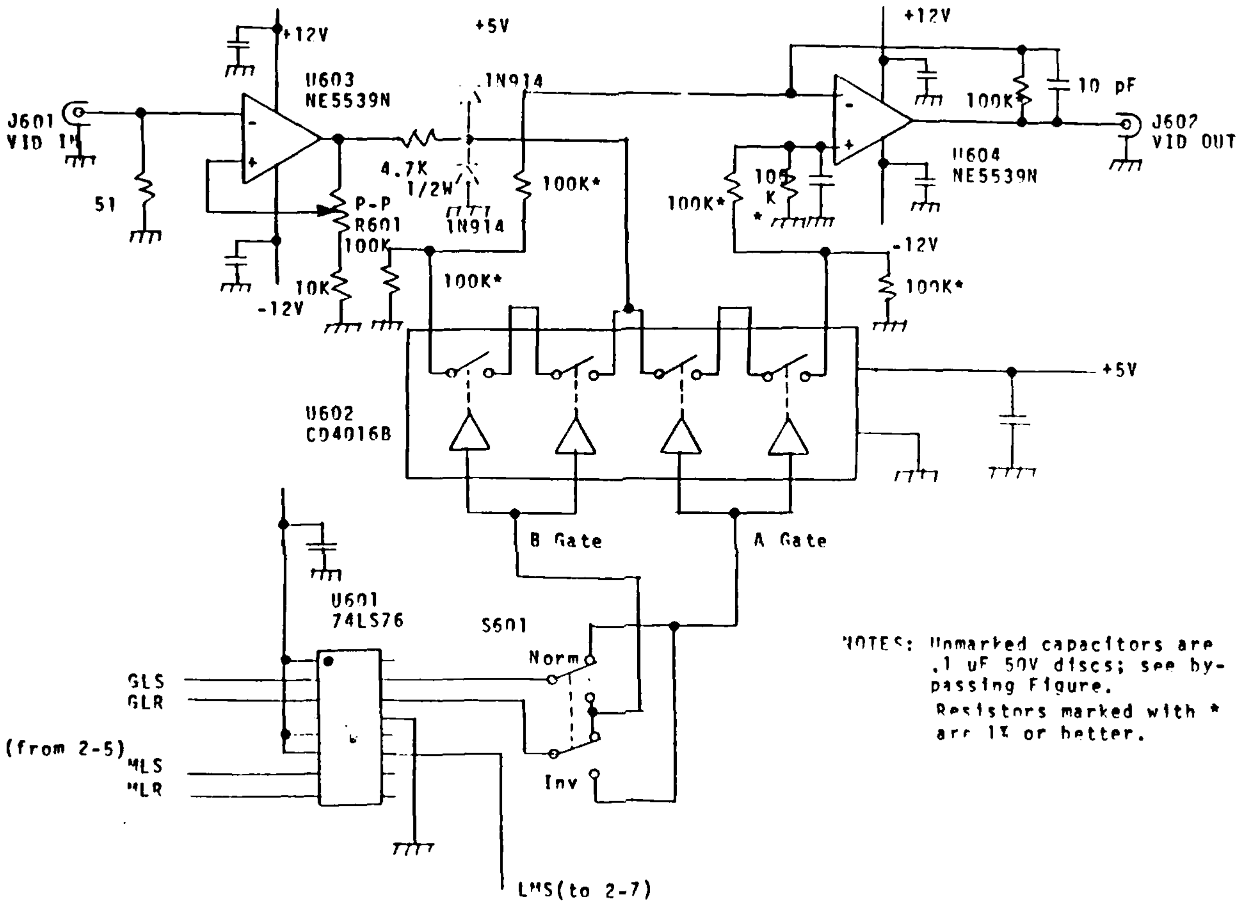

NOTES: Unmarked capacitors are .1 uF 50V discs; see bypassing Figure.
Resistors marked with * are 1% or better.

Fig. 7 Modulation and Gate Latches and A/B Gate.

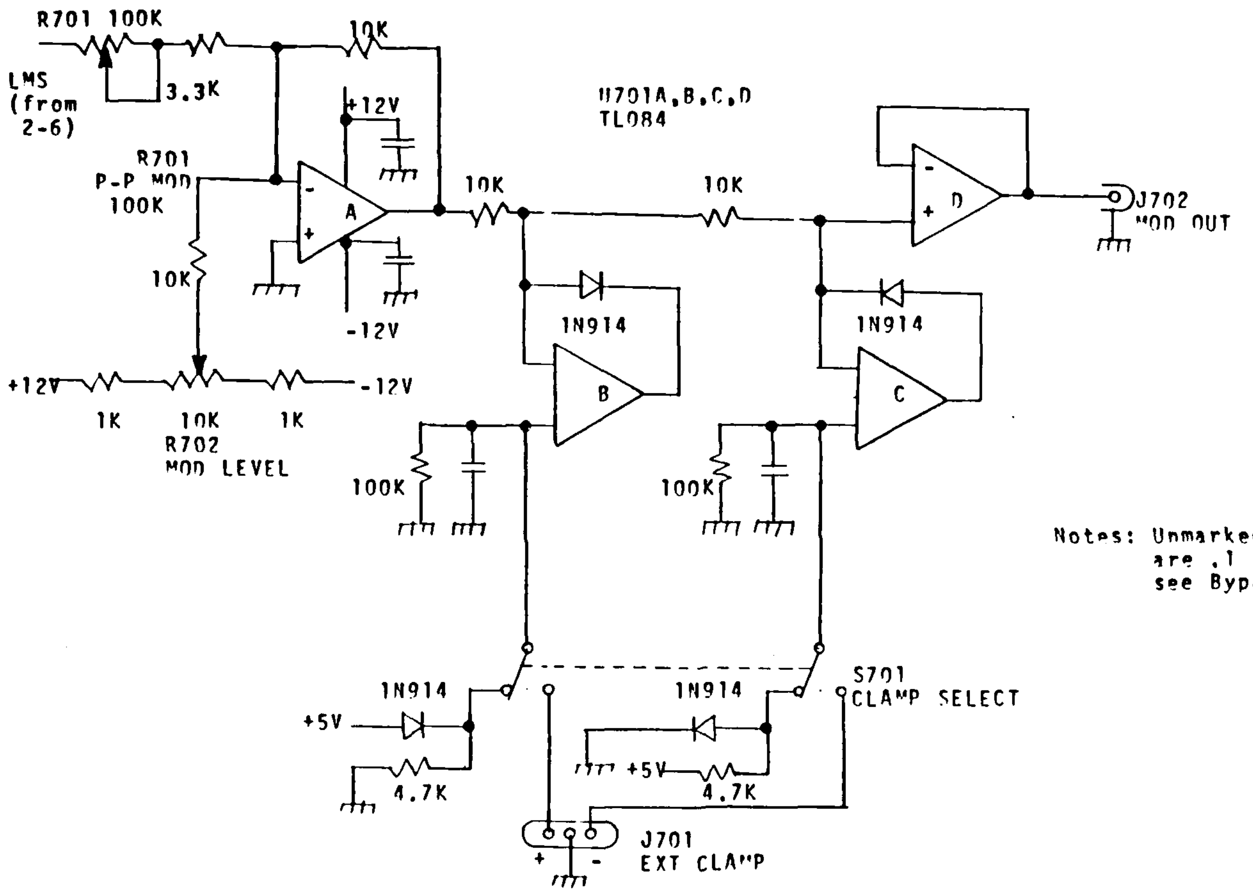

Notes: Unmarked capacitors
are .1 uF 50V discs;
see Bypassing Fig.

Fig. 8 Device Modulator. J701=3 terminal jack or terminal strip to suit.

AD-A166 177 UNITED STATES AIR FORCE SUMMER FACULTY RESEARCH PROGRAM 08/15
1985 TECHNICAL RE (U) UNIVERSAL ENERGY SYSTEMS INC
DAYTON OH R C DARRAH ET AL DEC 85 AFOSR-TR-86-0140
UNCLASSIFIED F49620-85-C-0013 F/G 5/1 NL

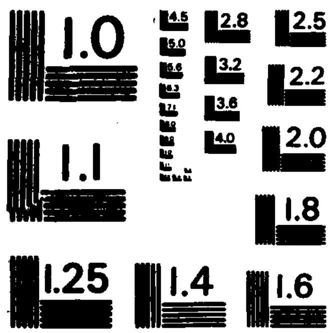

MICROCOPY RESOLUTION TEST CHART
NATIONAL BUREAU OF STANDARDS-1963-A

controls the peak-to-peak amplitude and the control R702, MOD LEVEL, controls the DC reference level of the signal at MOD OUT. This signal can source about 10 ma at a 500 KHz bandwidth. If necessary, video opamps can be substituted for U701 to improve the edge contrast on the 100 KHz range setting. U701B and U701C provide upper and lower clamp levels, respectively, to protect the device under test. With S701 set as shown, these levels are 4.35 V and 0.65 V. Provisions are shown for other clamp references to be applied at J701.

IV. Recommendations

i) It is recommended that the (PDVC/SEM) design detailed in this report be implemented. SEM images of better quality should result when this design is interfaced with JEOL.

ii) Surface charging of the DUT has been addressed to in the report of Ms. Wilkerson that has been cited. In as much as the use of a glowing tungsten filament positioned approximately 1/4 inch from the DUT surface did not produce any significant improvement it is recommended that a commercial source available from Kimball Physics Inc, Wilton, N.H. 03086 be implemented. This dual source charge neutralizer should be effective for both positive and

negative surface charging.

REFERENCES

1. Everhart, T. E., and R. F. M. Thornley., "Wide band detectors for micro-micro-ampere low energy electron currents", J. Sci. Inst., 1960, pp. 246-248.

2. Younkin, D., "Phase Dependent Voltage Contrast - an inexpensive SEM addition for LSI failure analysis", Proc. IEEE, 1981, pp. 264-268.

Electrical and Optical Characterization of Certain Doped Organic Polymers.

I. Introduction

The application of polymers in electronics and computers is expected to grow rapidly during the next decade.[1] The study undertaken has been restricted to electrical and optical characterization of certain doped organic polymers. In particular, the polymers that were chosen for study were: i) polyphenylene benzobis thiozole (PBT), ii) meta-acetylene-terminated-bisphenyl-A (MATB), iii) trans-form 2,5 bi-benzimidazole (ABPBI). Samples of these polymers were obtained from the polymer branch (MLBP) through Dr. Ivan Goldfarb at WPAFB. The doping of these polymers was done by ion implantation rather than by chemical means. The chemical method of doping may not be feasible for lack of suitable solvents. Studies undertaken by other researchers[2] have indicated that the introduction of dopants into the polymer chains by ion implantation results in more stable polymers than the chemically doped polymers. The energy of the bombarding ions and the temperature of the polymer surface should affect the delocalization of the electrons along the chain of the polymers. Data using the following physical

techniques were planned:

i) Ion implantation of the samples with gallium, iodine and argon.

ii) Capacitance measurements to obtain data on permittivity and dissipation factor.

iii) D. C. conductivity vs temperature.

iv) Microwave conductivity vs temperature.

v) ESR studies (Pauli susceptibility).

vi) FTIR studies.

vii) Laser-Raman studies.

viii) Electron diffraction data.

ix) Diffusion length data using the SEM-EBIC technique.

x) Deep-level Transient Spectroscopy (DLTS) Studies to obtain activation energy data.

The completion of the above exhaustive study should lead to a better understanding of the charge transport mechanism. With doped conjugated polymers, the possibility exists to achieve high conductivities (conductive polymers) with a host of applications. The author of this report has research expertise in the characterization of conductive polymers particularly with reference to microwave absorption characteristics of polysulfur nitride with potential application as RAM material. This work was done at the Fort Belvoir Army research facility in the summer of 1983 when the

author spent five weeks as a visiting scientist. The results have been published.[3,4] At the University of Kentucky the author is involved in research effort on the electrical and optical aspects of conductive polymers. A research proposal entitled "Raman and Microwave Studies of Certain Conducting Polymers", is currently pending with the Army Research office (ARO) at Durham, N. C.

II. Objectives

The objectives of the effort on doped polymers are:

i) Understanding the charge transport mechanism in these polymers.

ii) Determination of the nature of the charge carriers.

iii) Evaluation of the d.c. and microwave conductivity data in the light of existing theories. The deviations of the theory from the measured a.c. and d.c. conductivities should yield information on the structure of the density of states in the polymers investigated.[4]

iv) To investigate the Raman spectrum of the ion-implanted samples and to study the effect of the energy of the bombarding ions and temperature of the substrate. The samples will also be analyzed by optical absorption spectra including the infrared region.

v) To obtain supportive data through other physical techniques outlined in part I under Introduction

III. Details of the Study

Because of the limited access to the various equipment and short duration of the effort, many of the experiments proposed in Section I above could not be completed. It is however, planned to continue the research at the University of Kentucky as well as at the W-PAFB with the help of the focal point (Dr. Bill Dobbs). The author of this report plans to apply for a mini-grant to continue the study. In the following some of the tasks which have been completed will be described.

<u>MATB:</u> The unimplanted sample acts like a very good insulator. After gallium ion implant at a fluence of 5×10^{13}/sq.cm at 100 Kev and annealing in argon atmoshpere for 20 minutes at 200 ^{o}C the sample was measured using the Four-point probe method. The measured sheet resistivity was 1.9×10^{17} ohms/sq.cm which translates to a bulk resistivity of 100 - 1000 ohms-cm, assuming an estimated doping depth of about 0.1u. The FTIR spectra of the polymer when compared with the monomer spectra indicated the disappearance of the C=CH bands. Carbonyl bands appear in the polymer spectra.

After increasing the gallium implant to 5×10^{14} /sq.cm and annealing again in argon atmosphere for one half hour at 200°C, the sample behaves like a n-type semiconductor with a sheet resistivity of about -0.23×10^{8} ohms/sq.cm.

<u>PBT:</u> The measured dielectric constant of this sample was 3.2 at 100 Hz. After gallium implant at a fluence of 5×10^{14} /sq.cm and annealing in argon atmosphere at 200°C for one half hour, the sample acted like a p-type, with sheet resistivity of about 9×10^{9} ohms/sq.cm.

<u>ABPBI:</u> After gallium implant at a fluence of 5×10^{14} /sq.cm and annealing in argon atmosphere for one half hour at 200 C the sample acted like a p-type with sheet resistivity of about 0.1×10^{8} ohms/sq.cm.

IV. Recommendations

i) As mentioned in Section III, some of the experiments mentioned in Section I under Introduction could not be completed. The recommendation, therefore, is the need to acquire data from the following techniques: a) data on Pauli susceptibility from ESR studies; b) extended Laser-Raman studies; c) DLTS studies to obtain activation energy data.

ii) The author intends to complete some of the above tasks during the tenure of the mini-grant. If funds become

available through other agencies such as the ARO , the investigation will be extended to other polymers such as polypyrrole, polysulfur nitride, polythiophene and etc.

iii) A detailed understanding of the intricacies of the conduction mechanism in these polymers would be helpful in applications such as solar cells, radar absoubable materials and the future development of molecular computers.

REFERENCES

1. Seminar talk presented by the author in the Materials Lab, W-PAFB entitled "Electrical Characterization of Certain Doped Polymers", 9 August 1985.

2. Aldissi, M. "Review of the Synthesis of Polyacetylene and its Stabilization to Ambient Atmosphere", _Synthetic Metals_, 1984, _9_, pp. 131-141.

3. Bhattacharyya, T. J., and P. K. Kadaba, "Dielectric Constant and Loss of Polysulfur Nitride in the Microwave Region", _J. Mat. Sci., L._, 1983, pp. 727-728.

4. Kadaba, P. K., "Simultaneous Measurement of Complex Permittivity and Permeability in the Millimeter Region by a Frequency-Domain Technique", _IEEE Trans. I and M. Vol. IM-33_, 1984, pp. 336-340.

1985 USAF-UES SUMMER FACULTY RESEARCH PROGRAM/

GRADUATE STUDENT SUMMER SUPPORT PROGRAM

Sponsored by the

AIR FORCE OFFICE OF SCIENTIFIC RESEARCH

Conducted by the

UNIVERSAL ENERGY SYSTEMS, INC.

FINAL REPORT

SYNTHESIS OF NOVEL POLYBENZIMIDAZOLE MONOMERS

Prepared by	James J. Kane, Ph.D and James G. Slagel, B.S.
Academic Rank	Associate Professor and Graduate Student
Department and University	Chemistry Department Wright State University
Research Location	Materials Laboratory, Non-Metallic Materials Division, Polymer Branch, Wright Patterson Air Force Base, OH
USAF Research Colleague	Robert C. Evers, Ph.D.

Date	August 25, 1985
Contract Number	F 49620-85-C-0013

ABSTRACT

Synthesis schemes for the preparation of monomers for poly(1,5(7)-dihydrobenzo[1,2-d:4,5-d]diimidazole-2,6-diyl) and poly(1,5-diphenylbenzo[1,2-d:4,5-d]-diimidazole-2,6-diyl) are proposed. Specific monomers discussed are 1,5(7)-dihydrobenzo[1,2-d:4,5-d]-diimidazole-2,6-dicarboxylic acid, 5,6-diaminobenzimidazole-2-carboxylic acid and N^1,N^4-diphenyl-1,2,4,5-tetraaminobenzene.

The preparation of certain key intermediates for each of the monomers are described. Specific compounds discussed are 5-nitro-2-trichloromethylbenzimidazole, 1,2-di(p-toluenesulfonamido)-4,5-diaminobenzene, 1,2-diamino-4,5-dinitrobenzene, 1-amino-3-(trichloroacetamido)-4,5-dinitrobenzene and N,N′-diphenyl-2,5-diaminoterephthalic acid.

ACKNOWLEDGEMENT

The authors would like to express their appreciation to the Air Force Systems Command, the Air Force Office of Scientific Research and Universal Energy Systems, Inc. for their support and for the opportunity to spend a rewarding and interesting summer at the Air Force Materials Laboratory, Wright Patterson Air Force Base, Ohio. We would like to thank the people of the Polymer Branch in particular for their friendliness and their generosity in sharing their equipment, facilities and ideas.

Finally we would like to thank Dr. Robert C. Evers for suggesting this area of research and for his helpful collaboration and guidance.

I. INTRODUCTION

The Air Force Wright Aeronautical Laboratories and the Air Force Office of Scientific Research are engaged in research and development involving the synthesis and processing of ultra-high strength, thermo-oxidatively stable polymers for use as structural materials in aerospace vehicles. Their objective is production of materials with mechanical properties comparable to the current fiber reinforced composites, but with significantly improved environmental tolerance and without the use of fiber reinforcement. The rigid-rod aromatic heterocyclic polymers are the materials chosen for this effort. Their physical and chemical properties show promise for fulfilling program objectives but they do present certain processing and fabrication problems because of their "all-para" rigid-rod character. Thus, Continuing Materials Laboratory in-house research as well as related contractual programs in academic and industrial laboratories are addressing aspects of the processing and fabrication of these polymers. This research includes synthesis efforts directed toward preparation of novel rigid-rod aromatic heterocyclic polymers which possess improved processing characteristics and/or enhanced mechanical/physical properties.

The present project involves the exploration of synthesis routes to A-A and A-B monomers which would be expected to undergo condensation reactions in polyphosphoric

acid (PPA) to yield the rigid-rod polybenzimidazole, poly(1,5(7)-dihydrobenzo[1,2-d:4,5-d]diimidazole-2,6-diyl), I.

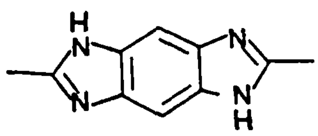

I.

Another polymer of interest in this project is poly(1,5-diphenylbenzo[1,2-d:4,5-d]diimidazole-2,6-diyl, II, an isomer of poly(1,7-diphenylbenzo[1,2-d:4,5-d]diimidazole-2.6-diyl), III,

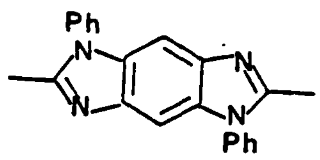

II.

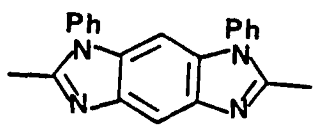

III.

which is the subject of a current in-house synthesis effort in the Polymer Branch.

II. OBJECTIVES

The objectives of this project were to explore routes for the synthesis of the A-A monomer 1,5(7)-dihydrobenzo[1,2-d:4,5-d]diimidazole-2,6-dicarboxylic acid, IV (or certain of its derivatives) and the A-B monomer 5,6-diaminobenzimidazole-2-dicarboxylic acid, V (or certain of its derivatives). Both IV and V are precursors to polymer I.

An additional objective is the exploration of synthesis routes to N^1, N^4-diphenyl-1,2,4,5-tetraaminobenzene, VI.

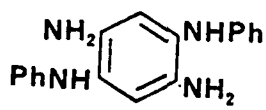

VI

III. DISCUSSION

The condensation reaction of dicarboxylic acids with aromatic tetraamines is one of the classical methods of preparation of polybenzimidazoles.[1] However, the reaction of 1,2,4,5-tetraaminobenzene (TAB) with oxalic acid yields the six membered heterocyclic polydihydro-bisquinoxaline rather than the desired polymer I (1).[2]

Thus, the monomers selected for synthesis of polymer I are the A-A monomer IV and the A-B monomer V. The former on condensation with 1,2,4,5-tetraaminobenzene in PPA would be

expected to yield I (2). Similarly, monomer V on self-condensation in PPA would be expected to yield I (3).

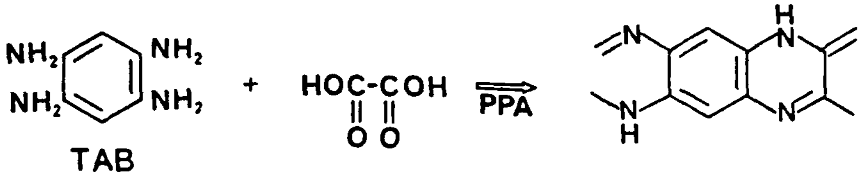

(1)

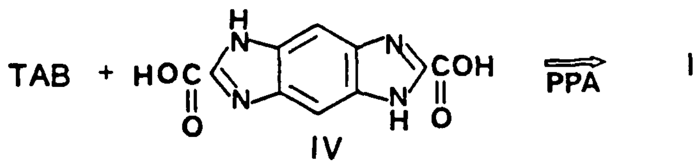

(2)

(3)

In the present project the benzimidazole-2-carboxylic acids are generated by base catalyzed hydrolysis of the corresponding 2-trichloromethylbenzimidazole,[3,4] which are, in turn, conveniently obtained by condensation of the ortho-disubstituted primary amines with methyl-2,2,2-trichloro-acetimidate.

The benzimidazole-2-carboxylic acids are known[4] to be unstable with respect to decarboxylation and there is cause for concern that IV and V might decarboxylate in hot PPA before the desired condensation reaction occurs. Fortunately, a variety of carboxylic acid derivatives are accessible from the 2-trichloromethylbenzimidazoles by reaction with the

appropriate nucleophile.[5] These carboxylic acid derivatives include the nitrile, amides, the methyl and ethyl normal esters and the methyl and phenyl ortho esters. Any of these derivatives should be suitable alternatives for the carboxylic acid in condensation reactions. Moreover, the 2-trichloromethyl derivative itself is known[4] to undergo condensation reactions in PPA to give benzimidazoles.

The required A-A and B-B monomer precursors for polymer III are the tetraamine VI and the dicarboxylic acid 1,7-diphenylbenzo[1,2-d:3,4-d]diimidazole-2,6-dicarboxylic acid, VII. Thus, before any synthetic effort for polymer III can be initiated, synthesis of tetraamine VI must be accomplished.

IV. MONOMER SYNTHESIS ROUTES

The general reaction schemes proposed for synthesis of monomers IV, V and VI are outlined below.

A. Proposed synthesis schemes for Compound IV, 1,5(7)-dihydrobenzo[1,2-d:3,4-d]diimidazole-2,6-dicarboxylic acid.

a. 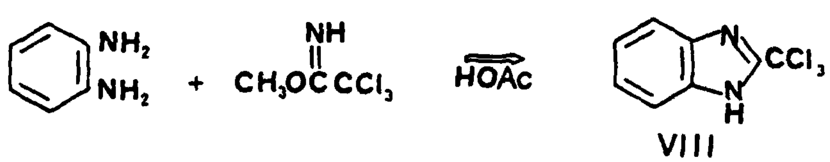

(4)

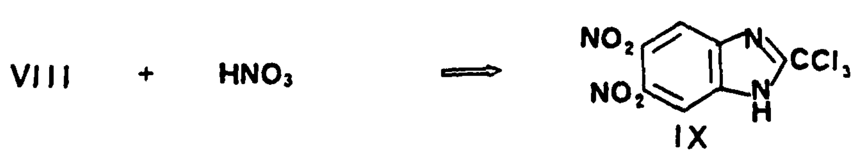

(5)

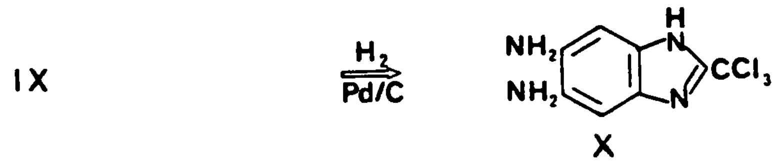

(6)

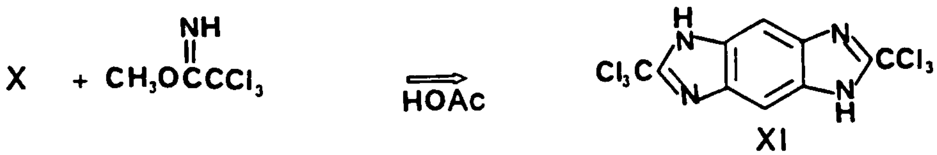

(7)

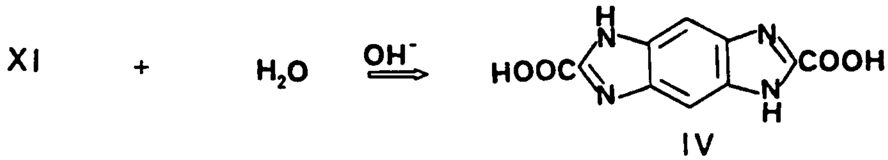

(8)

b.

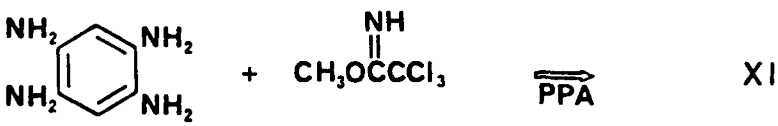

(9)

c.

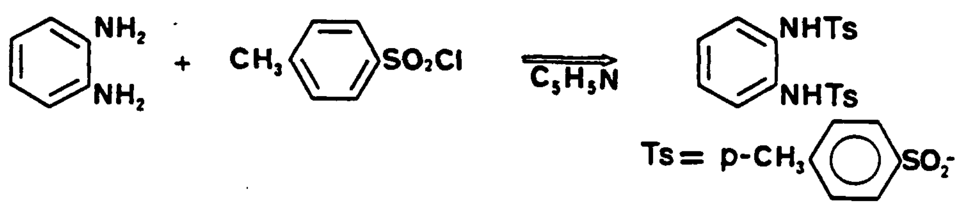

(10)

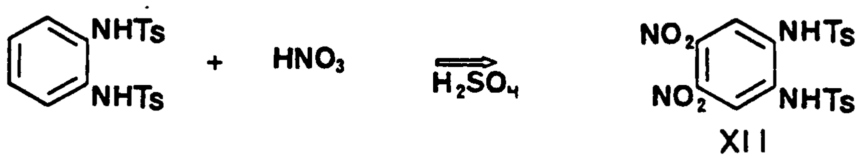

(11)

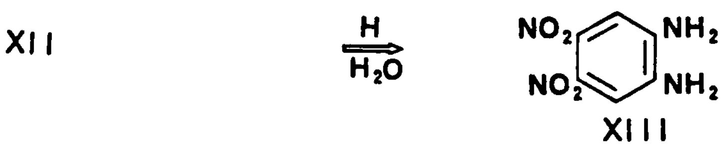

(12)

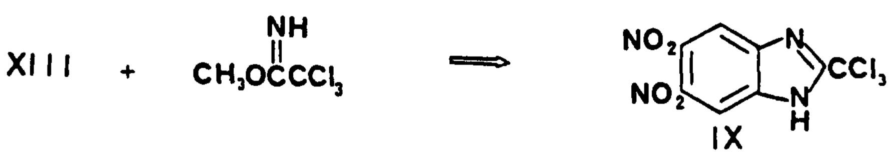

(13)

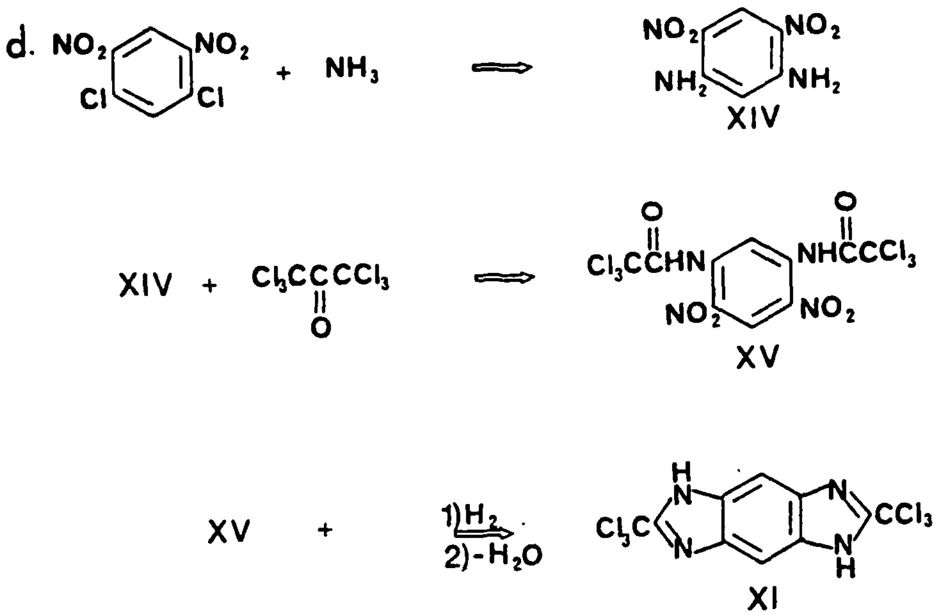

(14)

(15)

(16)

B. Proposed synthesis schemes for Compound V, 5,6-diaminobenzimidazole-2-carboxylic acid.

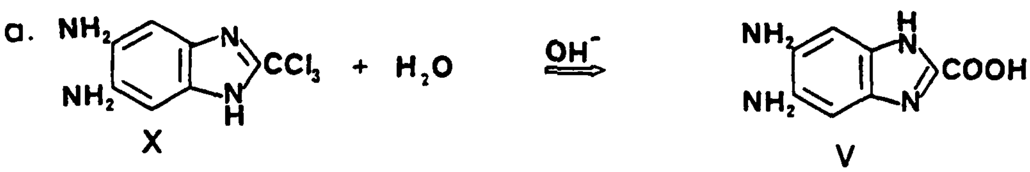

(17)

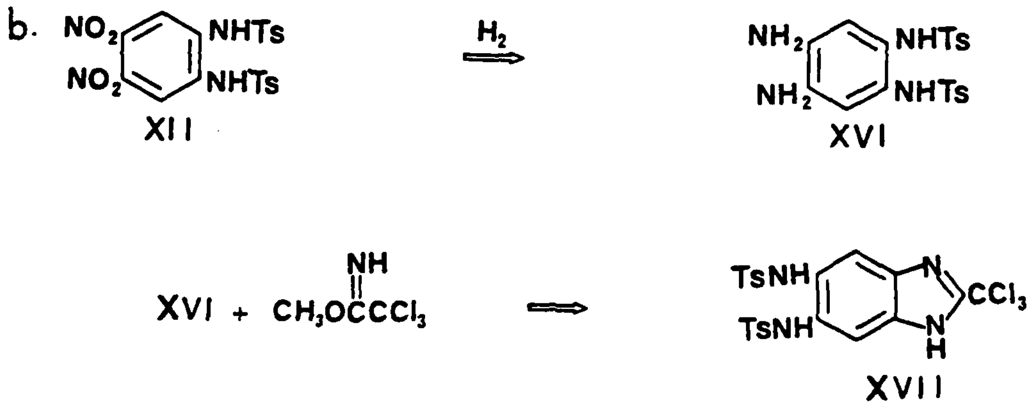

(18)

(19)

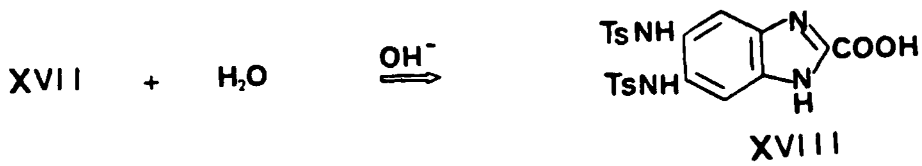

(20)

Compound XVIII, the di-p-toluenesulfonamide of V is an acceptable A-B monomer since it is known[6] that the sulfonamides react in hot PPA to liberate free amines.

C. Proposed synthesis for Compound VI, N^1,N^4-diphenyl-1,2,4,5-tetraaminobenzene.

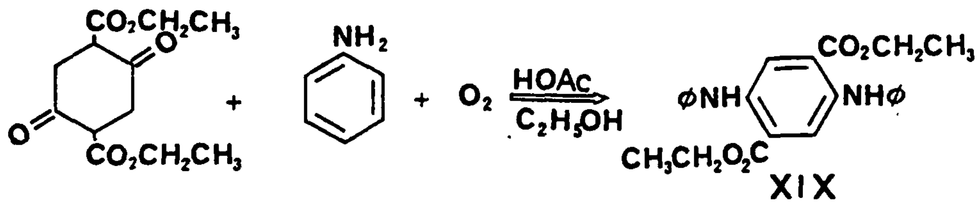

(21)

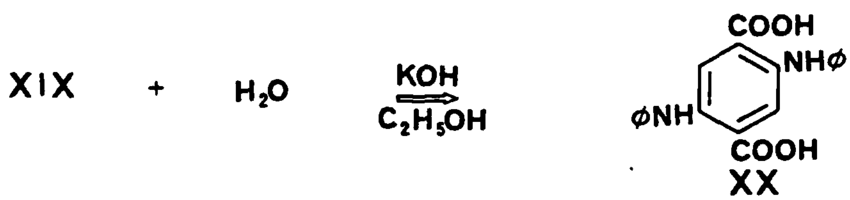

(22)

(23)

V. RESULTS

A. Synthesis of Intermediates

a. Attempted synthesis of 5,6-dinitro-2-trichloromethylbenzimidazole.

The precursor 2-trichloromethylbenzimidazole, VIII, was prepared by reaction of *o*-phenylene diamine and methyl-2,2,2-trichloroacetimidate in glacial acetic acid.[3] Attempted nitration of VIII with fuming nitric acid in glacial acetic acid gave only starting material. Nitration of VIII in fuming nitric acid gave the mono nitro derivative 5(6)-nitro-2-trichloromethylbenzimidazole, XXI.

b. Synthesis of 1,2-di(*p*-toluenesulfonamido)-4,5-dinitrobenzene, XII.

The precursor 1,2-di-(*p*-toluenesulfonamido)benzene was prepared by condensation of *p*-toluenesulfonyl chloride with *o*-phenylenediamine in pyridine. Subsequent nitration with fuming nitric acid in glacial acetic acid gave the desired compound XII.

c. Synthesis of 1,2-diamino-4,5-dinitrobenzene (XIII).
Compound XII was heated in methanesulfonic acid to yield the free dinitro diamine XIII in near quantitative (crude) yield. Interestingly, when this reaction was done using a mixture of glacial acetic acid and methanesulfonic acid, it gave 2-methyl-5,6-dinitrobenzimidazole, XXII, in near quantitative yield.

d. Synthesis of 1,2-di-(p-toluenesulfonamido)-4,5-diaminobenzene XVI).

This compound was prepared by catalytic hydrogenation of the corresponding dinitro derivative XII in DMAC. Compound XVI was also prepared by reduction of XII with aqueous sodium dithionite in pyridine. Interestingly, when the dithionite reduction was done in DMAC, it gave the half reduction product 1,2-di-(p-toluenesulfonamido)-4-amino-5-nitrobenzene, XXIII.

e. Attempted synthesis of 1,3-di-(trichloroacetamido)-4,5-dinitrobenzene (XV).

The precursor 1,3-diamino-4,6-dinitrobenzene was prepared by reaction of 1,3-dichloro-4,6-dinitrobenzene with ammonia in ethylene glycol. Repeated attemps to react XIV with hexachloroacetone in DMAC, DMF and THF gave only starting material. Similarly, reaction of XIV with trichloroacetyl chloride in DMAC provided only starting material. Finally reaction of trichloroacetyl chloride with XIV in THF followed by a non-aqueous workup gave the half amide, 1-amino-3-(trichloroacetamido)-4,5-dinitrobenzene, XXIV.

f. Synthesis of N,N'-diphenyl-2,5-diaminoterephthalic acid (XX).

The precursor, diethyl-N,N'-diphenyl-2,5-diamino-terephthalate was prepared by condensation of aniline with diethyl-4-cyclohexanedione-2,5-dicarboxylate in ethanol-acetic acid with concurrent aromatization by air. The diethylester was then saponified with aqueous-ethanolic KOH

to provide the desired intermediate XX[7].

B. Synthesis of Model Compounds

a. 2,2′-Bibenzimidazole

This model compound was made in seven per cent yield in PPA by reaction of *o*-phenylenediamine with benzimidazole-2-carboxylic acid (XXV) and in two per cent yield when methyl benzimidazole-2-carboxylate (XXVI) was used in place of the free acid. The carboxylic acid XXV was prepared by base catalyzed hydrolysis of the 2-trichloromethylbenzimidazole (VIII) and the methyl ester XXVI was prepared by reaction of VIII with methanol.

b. Attempted synthesis of 1,5(7)-dihydrobenzo[1,2-d:4,5-d]-diimidazole-2,6-bis(2-benzimidazolyl), XXVII.

1,2,4,5-Tetraaminobenzene was condensed with the methyl ester XXV in PPA in an effort to synthesize model compound XXVII. The reaction yielded a black product which according to mass spectral analysis contained small amounts of XXVII.

VI. CONCLUSIONS AND RECOMMENDATIONS

A. Synthesis of 1,5(7)-dihydrobenzo[1,2-d:4,5-d]-diimidazole-2,6-dicarboxylic acid, IV.

a. The attempted dinitration of 2-trichloromethlybenzimidazole (VIII) was done according to a published procedure for for dinitration of the 2-trifluoromethylbenzimidazole.[5] The concern was that the trichloromethyl group, being much more reactive than the trifluoromethyl would not survive the conditions of reaction and aqueous workup. The fact that,

even though only the mononitrated product was obtained, the trichloromethyl function remained intact is encouraging. It appears that future attempts to dinitrate are worthwhile and should probably involve higher reaction temperatures, longer reaction times and/or use of sulfuric acid-nitric acid mixtures.

b. The reaction of tetraamino benzene (TAB) with methyl trichloromethylacetimidate was not attempted because the TAB tetrahydrochloride was insoluble in glacial acetic acid, the usual solvent for this reaction.

The report[2] that 3,3′-diaminobenzidine did not condense with methyl trichloromethylacetimidate made the prospect of preparing XI by a similar reaction of TAB in PPA discouraging and it has not been attempted in this project. However, it is recommended that a future attempt to synthesize XI be done by reaction of TAB with an excess of trichloroacetic acid in PPA.

c. Previous synthesis of the dinitrodiamine XIII in 14 percent yield has been reported[8] by detosylation of XII with concentrated sulfuric acid. The much higher yield obtained by using methanesulfonic acid suggests that the synthetic route outlined be further pursued.

The fact that the use of acetic acid as a solvent in this reaction gives 5,6-dinitro-2-methylbenzimidazole reveals that the desired diamine was formed and underwent the expected condensation and ring closure with the solvent.

This suggests an experiment using trichloroacetic acid as solvent in order to provide 5,6-dinitro-2-trichloromethylbenzimidazole (IX) directly.

d. The failure to obtain N,N′-di(trichloroacetyl)-1,3-diamino-4,6-dinitrobenzene from 1,3-diamino-4,6-dinitrobenzene and trichloroacetyl chloride is surprising. The fact that the mono trichloroacetyl derivative was obtained suggests that the remaining amine function is too deactivated to react further. However, it is recommended that longer reaction times and higher reaction temperatures be tried. It is also suggested that trichloroacetic anhydride be used in place of the acid chloride.

B. Synthesis of 5,6-diaminobenzimidazole-2-carboxylic acid, V.

The synthesis routes proposed in the DISCUSSION section should be pursued. In fact, the "di-tosyl" (XVIII) derivative of V appears very attractive. The next step in this sequence requires condensation of XVI with methyl-2,2,2-trichloromethylacetimidate followed by hydrolysis.

Another recommended route to V makes use of N-trichloroacetyl-1,3-diamino-4,6-dinitrobenzene (XXIV). Hydrogenation of compound XXIV to convert all nitro functions to primary amines would yield X directly after cyclization by loss of water.

C. Synthesis of N^1,N^4-diphenyl-1,2,4,5-tetraaminobenzene, VI.

The next step in this synthesis requires the Schmidt reaction on the terephthalic acid derivative. This should be pursued.

D. Model Compound Synthesis

The failure to obtain a decent yield of 2,2′-bibenzimidazole by reaction of o-phenylenediamine and benzimidazole-2-carboxylic acid suggests that the acid decarboxylates before significant condensation occurs. This is supported by the observation of effervesence during the reaction. This result suggests that it will be necessary to use carboxylic acid derivatives as modifications of monomer II and III. The even poorer yield of bibenzimidazole obtained with methyl benzimidazole-2-carboxylate (XXVI) suggests that the ester is quite unreactive with respect to condensation in PPA.

When the ester XXVI was reacted with tetraaminobenzene, similar results were obtained.

A recent finding showed[2] that phenyl benzimidazole-2-carboxylate reacts with 3,3′-diaminobenzidine in PPA to give a quantitative yield of the corresponding model compound. This suggests that the phenyl esters of IV and V will probably be the monomers of choice for the polymerization reaction.

E. Polymer I

A possible direct route to polymer I might be achieved by reaction of TAB or its "ditosyl" derivative XVI with trichloroacetic acid in PPA. This recommendation is based on the expectation that the tetraamine would first react to form the intermediate XI which would then further react with TAB to form polymer I.

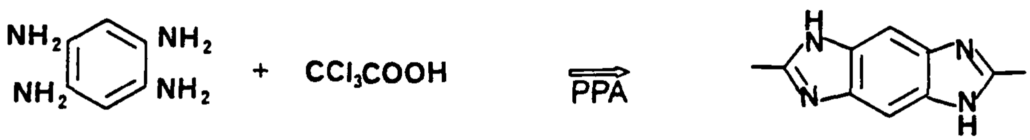

I

(24)

REFERENCES

1. E. W. Neuse, Adv. in Polym. Sci. 47 1 (1982).
2. U. Prabhu and R. C. Evers, AFWAL, Materials Laboratory, WPAFB, OH. Unpublished Results.
3. G. Holan, E. L. Samuel, B. C. Ennis and R. W. Hinde, J. Chem. Soc. (C) 1967, 20.
4. J. J. Kane and R.C. Evers, AFWAL, Materials Laboratory, WPAFB, OH. Unpublished Results.
5. G. Holan and E. L. Samuel, J. Chem. Soc. (C) 1967, 26.
6. F. E. Arnold, J. Polym. Sci. A-1, 8, 2079 (1970).
7. H. Lieberman, Ann. 404 321 (1914); Chem. Abstr. 8 2150 (1914).

1985 USAF-UES SUMMER FACULTY RESEARCH PROGRAM/

GRADUATE STUDENT SUMMER SUPPORT PROGRAM

Sponsored by the

AIR FORCE OFFICE OF SCIENTIFIC RESEARCH

Conducted by the

UNIVERSAL ENERGY SYSTEMS, INC.

FINAL REPORT

A THERMAL EVALUATION OF A PORTABLE, BATTERY-POWERED VAPOR-COMPRESSION COOLING SYSTEM

Prepared by: Amir Karimi

Academic Rank: Assistant Professor

Department & University: Division of Engineering, University of Texas at San Antonio

Research Location: School of Aerospace Medicine, Brooks Air Force Base

USAF Research: Major Charles A. Flick III and Mr. Yasu T. Chen

Date: September 26, 1985

Contract No.: F49620-85-C-0013

A THERMAL EVALUATION OF A PORTABLE, BATTERY-POWERED, VAPOR-COMPRESSION COOLING SYSTEM

by

Amir Karimi

ABSTRACT

The thermal performance of a portable, battery-powered vapor-compression cooling unit, designed by Arthur D. Little, Inc., under contract to The Air Force School of Aerospace Medicine is tested under diverse environmental conditions. The personnel cooler is a portable refrigeration/air conditioning unit to be used with the ground crew liquid-cooled garment.

The cooler consists of a compressor, a condenser, an expansion valve, a fan, a pump to recirculate coolant throughout the vest, and a DC motor to drive the compressor, the fan and the water pump. The cooler is tested in an environmental chamber. The results suggest that the cooler is capable of removing up to 450 W of heat at 25 ^{o}C ambient condition. However, the rate of heat removal drops sharply with the increasing ambient temperature.

An ILC-Dover liquid-conditioned garment (Model 0001684-D1-01) (LCG) is also tested. It is shown that this garment is not optimally compatible with the cooling sytem in that it does not allow for maximum heat removal. Several recommendations are offered to improve the present system. Additionally, it is suggested that further investigations be conducted to improve the cooling system.

ACKNOWLEDGEMENTS

I would like to thank the Air Force Systems Command, Air Force Office of Scientific Research and the Universal Energy Systems, Inc. for providing the opportunity for me to conduct summer research under a UES Faculty Research Fellowship at The School of Aerospace Medicine, Brooks Air Force Base. I would also like to thank the staff of The School of Aerospace Medicine for creating an enjoyable atmosphere for carrying out this research. In particular, I would like to thank Major Charles Flick III for his valuable help in instrumentation, Mr. Yasu Tai Chen for his invaluable assistance in conduction experiments, and Mr. John R. Garza for providing software for the data acquisition system. This summer research opportunity has been an extremely rewarding experience for me and served to stimulate ideas for additional studies.

I. <u>INTRODUCTION:</u> In wartime situations, the threat posed to crew personnel by chemical or biological (CB) agents has long been recognized. In such warfare, USAF groundcrew personnel are expected to perform their assigned combat duties. Therefore, attempts have been made to improve the ability of military personnel to overcome these hazards. To protect groundcrew personnel against these agents, a completely impermeable environment must be created. This requirement can be achieved either by encapsulating the entire operational environment (a macro-environment) or by placing each individual in protective attire (micro-environment). It is clear that the latter presents a more practical and a more cost effective method of protection. Thus special gear has been designed to protect the ground crew personnel while performing their duties during CB warfare. Although these clothing protect the personnel from CB agents, they also places additional thermal stress on them, as the body's metabolic heat cannot be directly dissipated into the environment.

To alleviate the thermal stress, three (3) methods of cooling have been suggested [1]:

- evaporative cooling by circulating a flow of ambient air close to the body;
- convective cooling by circulating a flow of conditioned air close to the body; and
- conductive cooling by circulating a cold liquid through a vest placed in contact with the body.

The studies [2,3] have shown that conductive or liquid

cooling provides the most effective and practical method of cooling for CB warfare situations. In fact, the majority of recent efforts to develop cooling systems have been conducted in this area. In this conductive method, the concept behind the liquid-coupled, indirect-transfer type heat exchanger is used to achieve the desired cooling effect. This heat exchanger as shown in Fig. 1 consists of a heat source (body) and a heat sink coupled together by the circulation of a satisfactory heat transfer medium, such as water.

In this method of cooling, a liquid-cooled vest is placed in direct contact with the body. The cool liquid is pumped through the tubes or channel network panels of the vest which are in direct contact with the heat source (body). Due to the temperature gradient between the body's skin and the circulating coolant, a portion or all of the metabolically generated heat will be removed from the body,

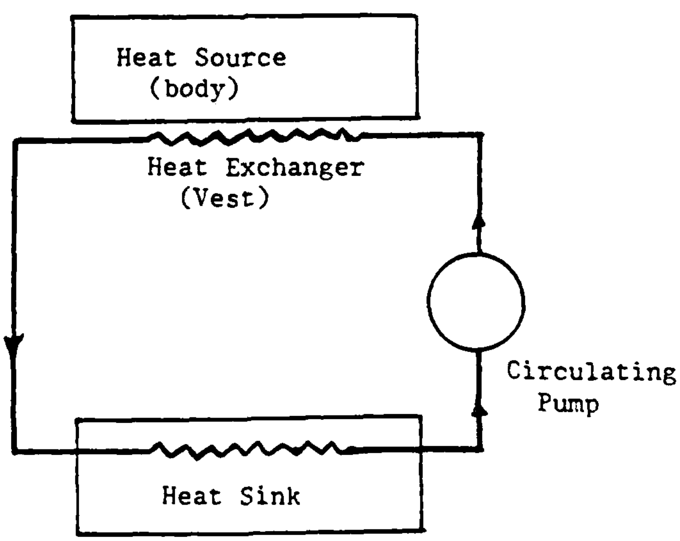

Fig. 1 - Liquid Coupled Indirect-Transfer Type Heat Exchanger

thereby reducing or alleviating thermal stress. On the return cycle, the heat will be rejected to the heat sink.

A heat sink may consist of an ice pack heat exchanger or a small refrigeration air conditioner unit, operating from a vehicle or aircraft power source.

Since the groundcrew personnel must be able to move about freely to conduct their combat duties, a lightweight portable cooler is highly desirable. For this reason, in the most recent efforts to develop portable coolers, ice has been employed as a heat sink medium. Ice, due to its high value for the heat of fusion (325 kJ/kg), provides an excellent heat sink medium. For example, 5 kg of ice can provide 1,625 kJ (1542 Btu) of cooling. However, in recent study of liquid cooled systems [4, 5] and efforts in design [5], we have suggested two main logistic drawbacks in using ice as a heat sink medium: a) this type of heat sink requires a fully portable support system for refreezing of the medium; b) we have shown that the cooling effectiveness drops sharply with the melting process. Therefore, the most recent effort is directed toward the development of a more direct method of cooling. To achieve this, a miniaturized refrigeration/air conditioner system is suggested.

II. <u>OBJECTIVES:</u> Recently, under contract to the U.S. Air Force School of Aerospace Medicine, Arthur D. Little, Inc. developed a small battery-powered, electric motor-vapor compression unit. This replaces ice as a heat sink medium in

a liquid-cooled system. A major objective in their design was to develop a system under 20 lbs., capable of providing a minimum of 1200 Btu/hr. (1264 W) of cooling under harsh environmental conditions.

A breadboard unit was fabricated and delivered to The School of Aerospace Medicine for evaluation. This unit weighs 25 lbs., which exceeds the desired limit, however, the developing company hopes to reduce this weight by design modifications.

The main objective of the present study is to conduct a thermal evaluation of this system under diverse environmental conditions. In the present effort, no attempt was made to redesign the entire system, nor have we completed the thermal evaluation of the system in depth. Because of time limitations, we directed our efforts towards setting up instrumentation for testing the cooling unit and developing an effective procedure for collection of data. Through the course of our study, we will test the system under various ambient temperatures in an environmental chamber. We shall include a brief analysis of the collected data. We shall leave the detailed and more complicated analysis and the task of evaluating the effectiveness of the alternative design modification for future studies.

In order to accomplish our objectives, the study was divided into the following tasks:

1. development of experimental procedures for testing the cooling system;

2. evaluation of coefficient of performance (COP) for the cooling system;

3. determination of the effect of environmental temperature on the cooling effectiveness of the system;

4. determination of the cooling effectiveness of the ILC-Dover liquid-cooled garment (Model 00016814-D1-01) (LCG); and

5. recommendations and suggestions for further studies.

III. <u>A BRIEF DESCRIPTION OF THE COOLING SYSTEM:</u> The cooling system is a battery-powered electric motor compression cycle which consists of a condenser, a thermostatic expansion valve, an evaporator, a fan, a water pump, and a battery-powered DC meter which drives the compressor, the fan and the water pump. A schematic description of the cooling system is shown in Fig. 2.

The DC motor is an Electrocraft motor which weighs 2.2 lbs and provides a shaft output of 190 W (at 56 V). It has an efficiency of 75%. The reciprocating compressor is a modified AE 3425 Tecumseh compressor which weighs 3.5 lbs. and operates at 1500-2000 RPM. The condensor is a spine fin exchanger which consists of 10 feet of copper tubing on the refrigerant side and 20 flat aluminum fins per inch on the air side. The evaporator is a counterflow type heat exchanger which consists of 12 feet of concentric copper tubing. The refrigerant tube is 1/4 inch OD x 0.03 wall thickness and the water tubing is 3/8 inch OD x 0.03 wall thickness. The water pump is a gear pump with a normal capacity of 0.5 l/min while operating at 1800 RPM.

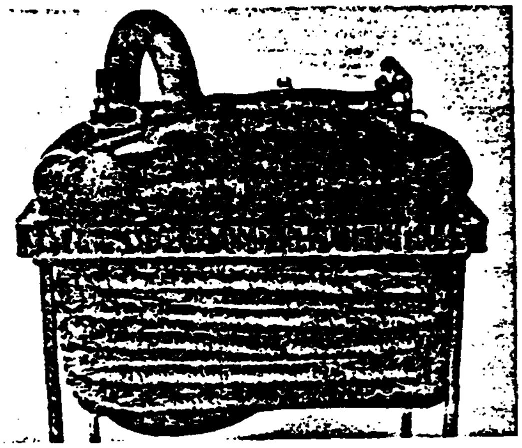

Breadboard Battery Unit
15"W x 9-3/4"D x 13"H

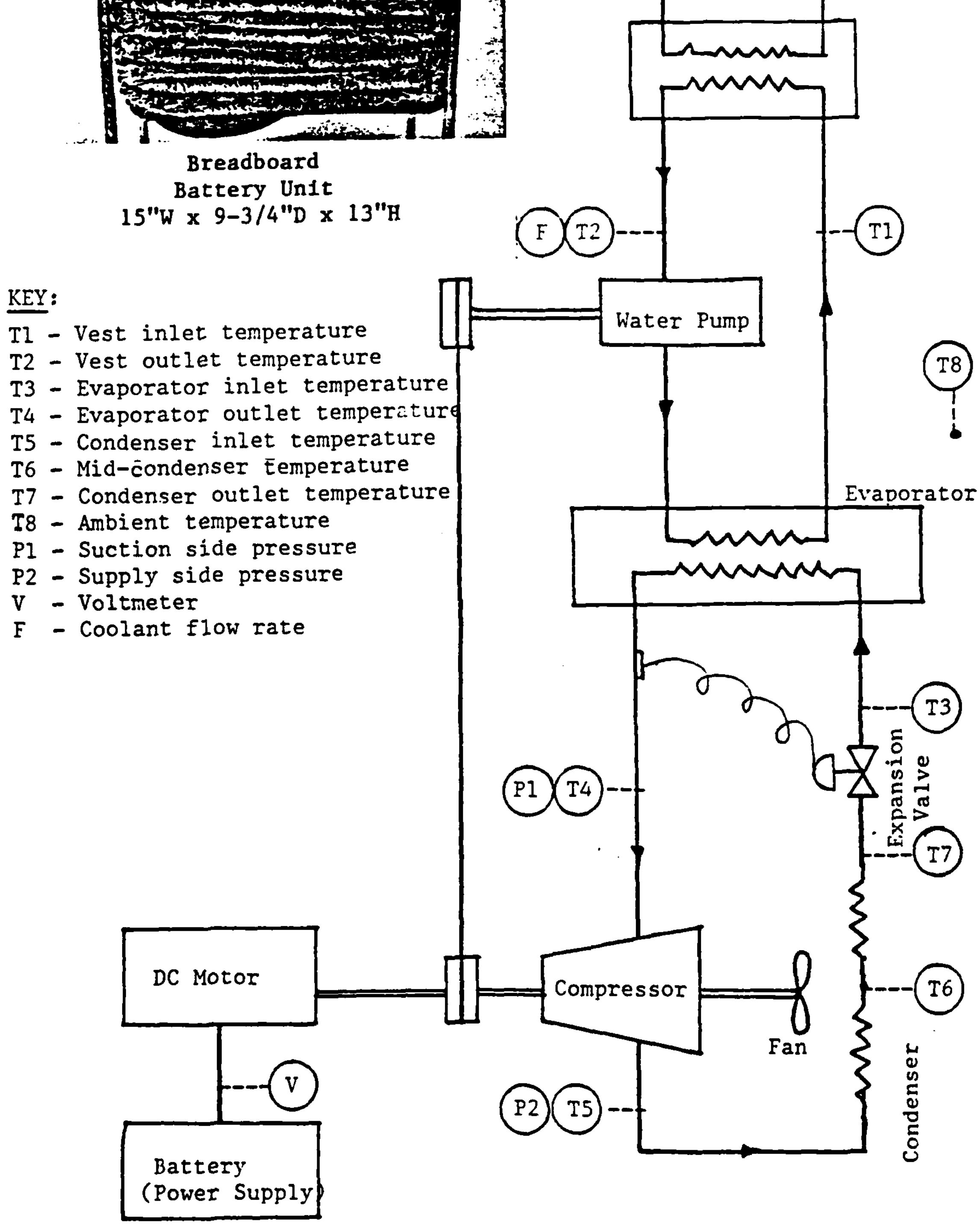

Fig. 2. A Schematic Description of the System and Performance Testing Set Up.

A summary of percentage power consumption by each component of the cooling system is presented in Table 1.

IV. <u>THERMAL PERFORMANCE TESTING OF THE COOLING SYSTEM:</u> A schematic description of the experimental set up to measure the thermal performance of the cooling system is shown in Fig. 2. The thermal load is simulated by a heat source unit which consists of an electrically-heated element inserted into a small cylindrical container. The outer surface of the container is thermally insulated from the environment. The thermal load is controlled by the power input into the heating element. A DC power supply is used to control the power input to the electric motor of the cooler unit.

A flow meter is placed in the water loop to monitor the water flow rate. Two thermistors are used to measure the inlet and the outlet temperature of the water. Five surface thermistors are placed on the cooler tubings to measure the temperature of the refrigerant at the evaporator inlet, evaporator outlet, condenser inlet, mid condenser and condenser outlet. The refrigerant pressure is monitored by placing pressure gauges (pressure transducers) in the suction side (low pressure side) and the supply side (high pressure side) of the compressor.

The evaporator, the water pump, the expansion valve and the water loop tubings are insulated to minimize thermal gains from the environment.

The vapor compression cycle is periodically discharged

TABLE 1. THE POWER CONSUMPTION OF THE SYSTEM COMPONENTS

COMPONENT	% POWER CONSUMPTION
Compressor	62
Fan	9
Water Pump	4
DC Motor (losses)	25
Total	100

and pumped down using a vacuum pump. The system is checked for leakage and recharged by adding 4.5 oz. of Freon-12 refrigerant.

During each thermal performance test, the cooling system is placed in a thermal chamber while the measurement display units and the control units are placed outside the chamber. During the initial stages of data collection, the measurements were recorded manually by monitoring the display units. However, during the latter stages of the investigation, a DEC PDP-11/23+ with a Data Logging Program became available and was used for the collection of test data. The use of this data acquisition system improved the accuracy of the data and enhanced the rate of data collection.

V. RESULTS AND DISCUSSIONS: During each thermal performance test of the cooling unit, we were able to control three variables. These included the control of: a) the thermal load; b) the power input into the vapor compression cooling cycle; and c) the environmental temperature. We have tested the system by providing thermal loads in the range of 50 to

450 W, and the power inputs in the range of 86 to 186 W at environmental temperatures of 25 ^{o}C, 38 ^{o}C and 44 ^{o}C.

Our data indicates that the system undergoes a transient period of operation before a steady state operation is achieved. This transitory period depends on the thermal load, the power supplied to the cooling system and the ambient temperature. Higher environmental temperatures increase the transient period of operation, while an increase in power input into the cooling, or an increase in the thermal load, reduces the transient period of operation. The temperature-time history plotted in Fig. 3 clearly reveals the transient behavior of the cooling system. It is evident that the amount of water in the liquid coupled loop effects the transient period of operation. The larger amount of water in this loop requires a longer period to achieve steady state operation.

The thermal performance test results plotted in Figs. 4 and 5 reveal the effects of environmental temperature and the power input to the cooling system on the rate of heat removal. Figure 4 represents data for the power inputs in the range of 86 to 120 W. Figure 5 represents the data for two power inputs in the ranges of 120 to 140 W and from 160 to 186 W, respectively.

These figures show that the rate of heat removal decreases with increasing ambient temperature. The effect of power input into the cooling system is evident from Fig. 5.

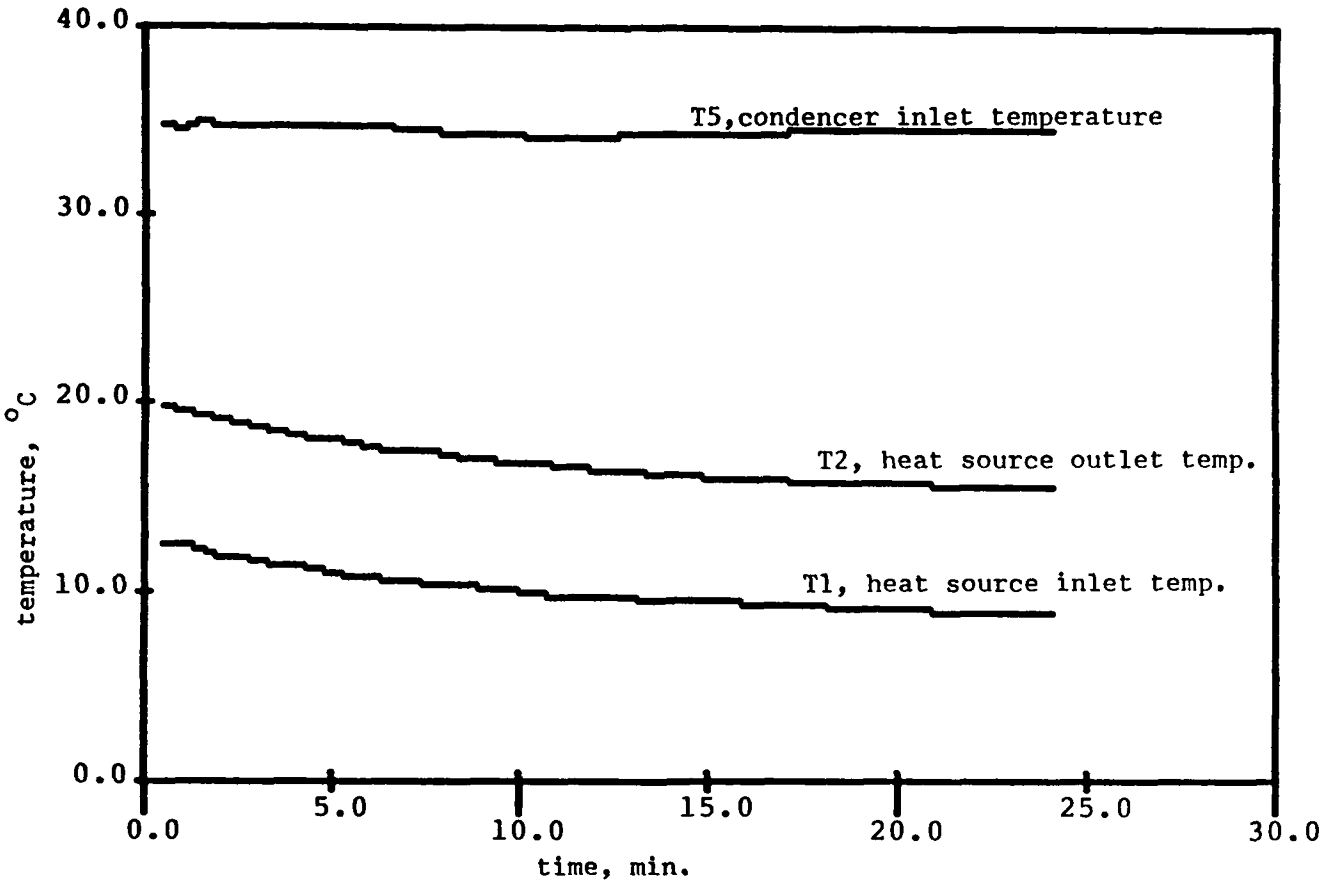

Fig. 3 Temperature - time history -- ambient temperature = 23°C, thermal load = 250 W, power input = 86 W

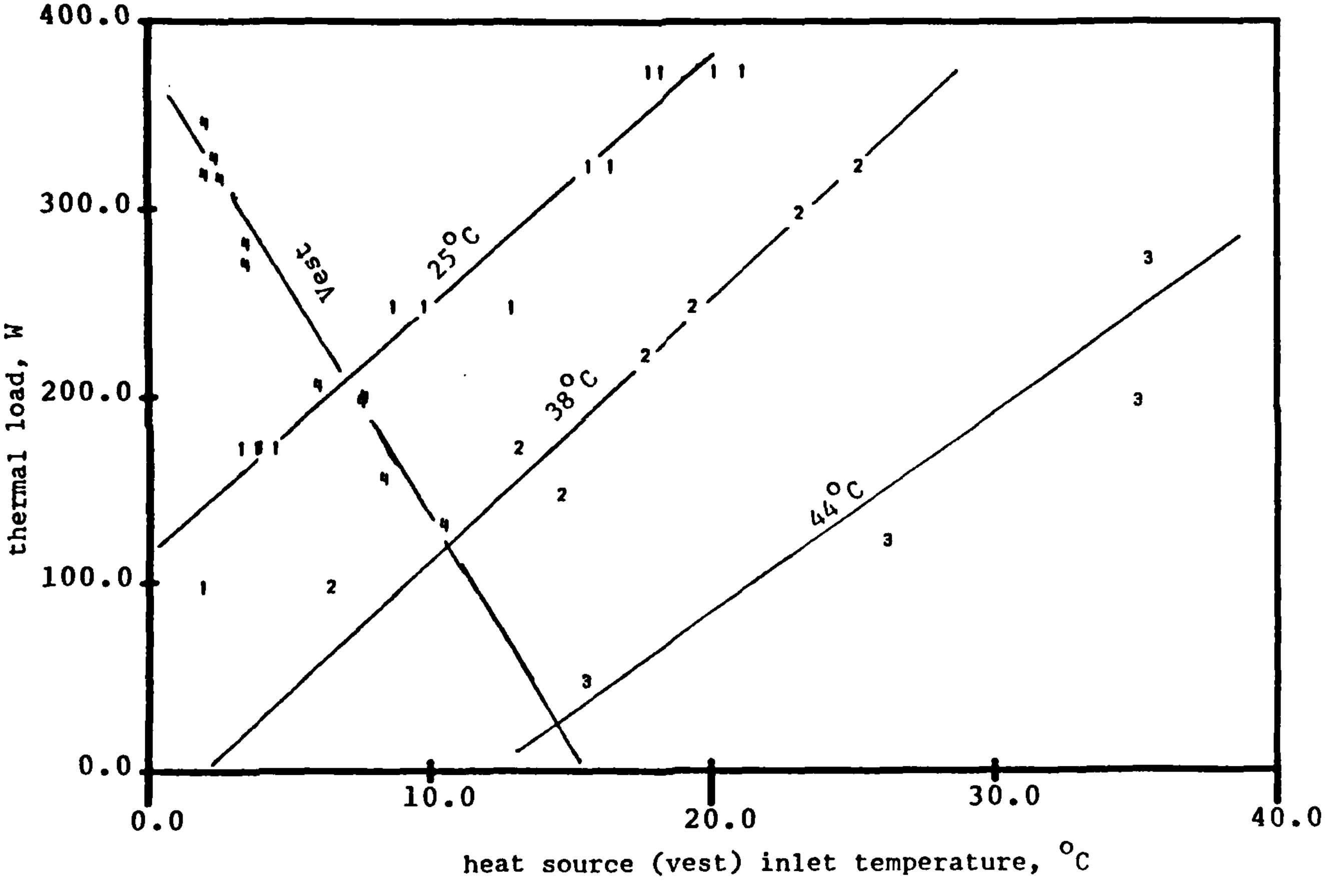

Fig. 4 Test results for the DC motor cooler and the ILC-Dover liquid-cooled vest-- ambient temperatures: 1) 25°C, 2) 38°C, 3) 44°C, 4) ILC-Dover vest

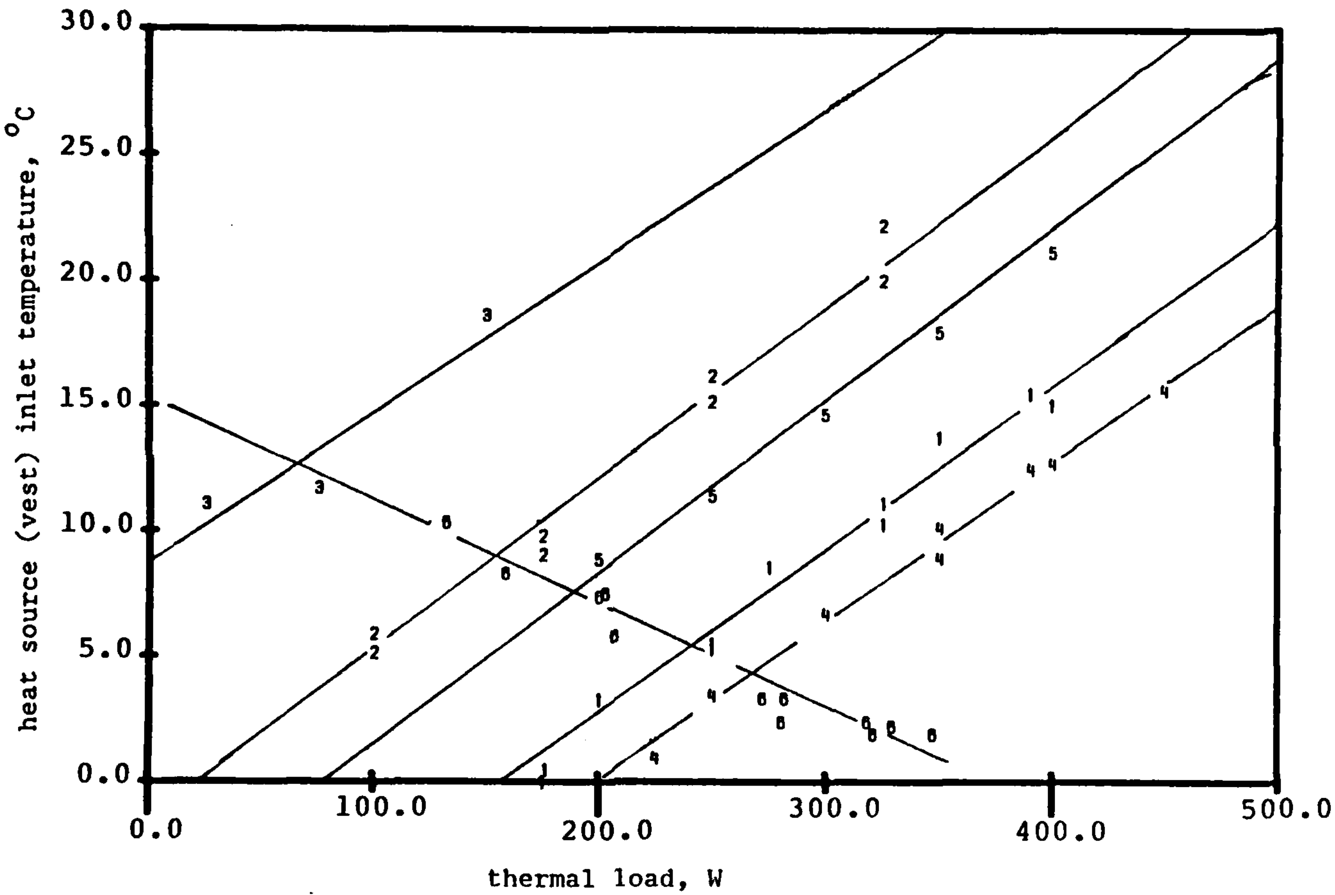

Fig. 5 Test results for the DC motor cooler and the ILC-Dover liquid-cooled vest.
A) Power input = 120-140 W ; ambient temperatures: 1) 25°C, 2) 38°C, 3) 44°C
B) Power input = 160-186 W; ambient temperatures: 4) 25°C, 5) 38°C
6) ILC-Dover vest

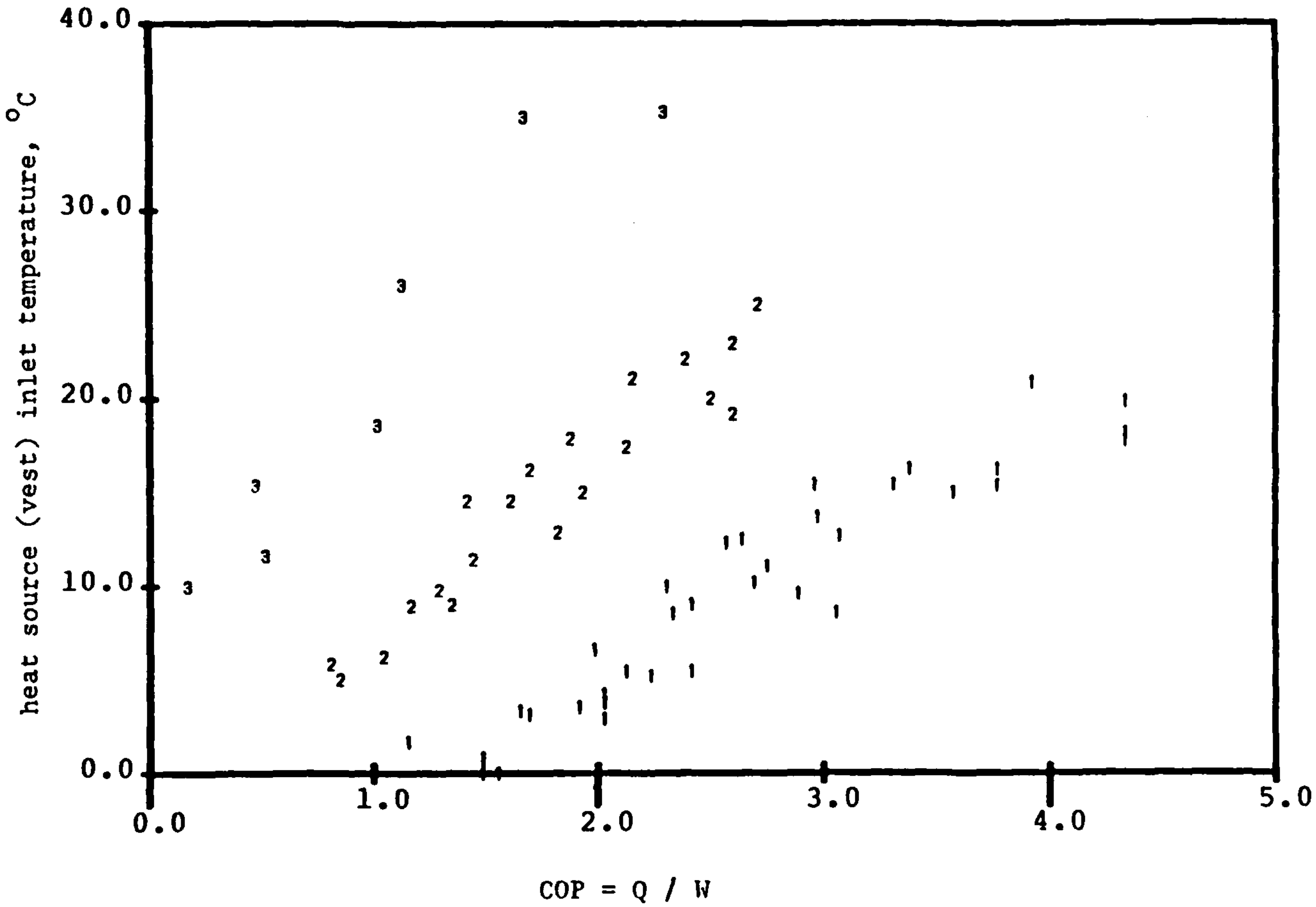

Fig. 6 Coefficient of performance for the DC motor cooler.
Ambient temperatures: 1) 25°C, 2) 38°C, 3) 44°C

It shows that the rate of heat removal increases with power input. Figure 5 also indicates that when removing approximately 350 W of heat at 44 ^{o}C ambient temperature, the vest inlet temperature is at 30 ^{o}C.

The coefficient of performance for cooling is defined as:

$$COP = Q / W \tag{1}$$

where Q is the rate of heat removal and W is the power consumption of the cooling system. Figure 6 shows that the COP decreases with an increase in the ambient temperature.

VI. <u>THERMAL EVALUATION OF THE ILC LIQUID-CONDITIONED VEST:</u>

The ILC Dover liquid-conditioned vest (Model 00016814-D1-01) has often been used by the staff of the Crew Technology Division at The School of Aerospace Medicine (Brooks Air Force Base) to study the effect of cooling on human subjects during physical activities. This vest consists of a series of short tygon tubing parallelly connected. The inside and outside diameter of the tubes are 1/16 inch and 1/8 inch, respectively. The pressure drop across the vest (without the hood and connectors) is 0.59 psi at a flow rate of 1.0 l/min. The pressure drop for a vest with the hood and connectors is 1.5 Psi at 1.0 l/min flow rate.

We have conducted a series of experiments on human subjects wearing this vest while performing various levels of physical activity. The vest was connected to the cooling unit and the vest inlet and outlet temperatures were

monitored. We also monitored the water flow rate.

The rate of heat removal by the vest was determined, using the relation:

$$Q = m\,c\,(T1 - T2) \tag{2}$$

where, Q denotes the rate of heat removal, m is thecoolant mass flow rate, c is the specific heat of the coolant, and T1, T2 the vest inlet and outlet temperatures, respectively.

The rate of heat removal for these experiments is plotted on Figs. 4 and 5 as a function of the vest inlet temperature. The intercepts of the line for the vest and those for the cooling system determine the rate of metabolic heat removed by the vest when it is coupled with the cooling system. Figures 4 and 5 indicate the cooling rate for the vest is always less than 100 W when the cooling unit is operating in 44 ^{o}C or higher ambient conditions.

Figure 5 indicates that the cooling unit is capable of removing heat at a much higher rate if the vest inlet temperature is increased. Therefore, we suggest that other available liquid-cooled vests be tested for compatibility with this cooling unit.

VII. <u>RECOMMENDATIONS:</u> The results of this study suggest two sets of recommendations to be pursued. The first deals with design improvements of the cooling vest. The second requires further investigation prior to implementation of the liquid-cooled system.

1. Design Improvements of the Present Cooling Unit.

a. reduce the weight of the system from 25 lbs. The batteries comprise approximately 40% of the total weight. Therefore, a reduction in battery weight or use of an alternate energy storage medium would reduce the total weight and thereby improve the system.

b. improve the design for maintaining the system. During the course of our investigations, the belt driving the water pump broke several times. In order to replace the belt, it was necessary to remove the motor, the fan, and the compressor drive belt. The design improvements must minimize the time required for routine maintenance.

c) a temperature control unit should be incorporated into the unit, enabling the user to control the circulating liquid temperature according to his level of physical activity and environmental conditions.

2. We suggest further investigation in selection of a liquid-cooled vest suitable for use with this cooling system. Our studies show that the ILC Dover liquid-conditioned vest is not suitable for use with this cooling system, particularly at higher environmental temperatures. Figure 5 suggests that the rate of heat removal increases with the suit inlet temperature. To increase the suit inlet temperature the heat exchange surface area of the vest must be enlarged and the water temperature drop across the evaporator must be minimized. To achieve the latter requirement, the liquid flow rate must be increased. This requires the redesign of the water pump in the cooling unit.

By following the above recommendations, it should be possible to implement compatible improvements in the vest and the cooling system, thereby creating an optimal working system.

REFERENCES

1. Vincent D. Iacono et.al., "Development of Microclimate Cooling System for Combat Vehicles", United States Army Natick Research and Development Laboratories, Natick, Massachusetts, February, 1982.

2. George C. Rannenberg, "Study to Determine the CB Threat and Define Alternative Crew Protective Systems for the Advance Attack Helicopter" (AAH) (Vol.1), United States Army Natick Research and Development Laboratories, Natick, Massachusetts, June, 1981.

3. S. Livingston et. al., "The Effect of Body Cooling on Aircrew in Hot Humid Environments", (Abstract), ASCC Working Party 61 Symposium, November, 1979.

4. A. Karimi, "A Thermal Evaluation of the 'LSSI' Liquid-Cooled System: An Engineering Perspective", USAF-SCEEE Summer Faculty Program, Final Report, Vol. 1/2, Report No. 48, September, 1983.

5. A. Karimi, "An Experimental Study of the Portable Liquid-Cooled System," USAF-SCEEE Summer Faculty Program, Final Report, Control No. F-49620-82-C-0035, December, 1984.

1985 USAF-UES SUMMER FACULTY RESEARCH PROGRAM

Sponsored by the

AIR FORCE OFFICE OF SCIENTIFIC RESEARCH

Conducted by the

UNIVERSAL ENERGY SYSTEMS, INC.

FINAL REPORT

MECHANISTIC STUDIES OF ENERGETIC MATERIALS: ANALYSIS OF 2,4,6-TRINITROTOLUENE THERMAL DECOMPOSITION PRODUCTS

Prepared by:	Daisy White Kimble
Academic Rank:	Instructor
Department and University:	Department of Chemistry Southern University
Research Location:	Frank J. Seiler Research Laboratory USAF Academy, NCX, F305, Colorado Springs, Colorado 80840
USAF Research:	Captain Joseph A. Zirrolli
Date:	August 26, 1985
Contract No:	F49620-85-C-0013

MECHANISTIC STUDIES OF ENERGETIC MATERIALS: ANALYSIS OF 2,4,6-TRINITROTOLUENE THERMAL DECOMPOSITION PRODUCTS

by

Daisy White Kimble

ABSTRACT

High Performance Liquid Chromatography (HPLC) was used to study the thermal decomposition products of 2,4,6-Trinitrotoluene, (TNT). Samples of decomposed TNT were chromatographed to obtain identification and reproducibility of retention times for all peaks, (possible decomposition products). Isocratic and gradient elution runs were made for all samples. Retention times for known standards (possible decomposition products), were obtained from HPLC analysis.

Mobile Phase Liquid Chromatography (MPLC) was used for isolation of the decomposition products. Solvents used in this study were based on polarities, and these are hexane, ethyl acetate, chloroform, acetone and methanol. Solvent fractions were used, they are 100% hexane, 95-5% hexane/ethyl acetate, 50-50% hexane/ethyl acetate, 100% ethyl acetate, 100% acetone, 100% chloroform and 100% methanol.

From HPLC analysis, the 95%-5% hexane/ethyl acetate fraction gave the best chromatogram for isolation of the decomposition products.

With fractions from the MPLC and through multiple injections on the HPLC, enough product could be isolated to obtain a Mass Spectrum and Nuclear Magnetic Resonance for identification of these thermal decomposition products.

ACKNOWLEDGEMENTS

The author wishes to express her sincere appreciation to the Air Force Office of Scientific Research/AFSC, United States Air Force, The Frank J. Seiler Research Laboratory, USAFA, Office of the Commander, and Captains Joseph A. Zirrolli and Jon T. Swanson for their guidance and assistance in the research project.

I. Introduction

A simple method is presented through the use of liquid chromatography for the thermal decomposition of 2,4,6-trinitrotoluene. Chromatography encompasses a diverse and important group of separation methods that permit the scientist to separate, isolate, and identify closely related components of complex mixtures; many of these separations are impossible by other means.

The thermal decomposition of 2,4,6-trinitrotoluene has been a subject of recurring interest for almost 50 years. Several investigators [1] have addressed themselves to the isolation and identification of intermediate products with a view toward elucidation of a stepwise decomposition mechanism.

Samples of TNT were partially decomposed by heating for 15 to 240 minutes at 240 °C. The decomposition product mixtures were shown through High Performance and Mobile Phase Liquid Chromatography. Liquid chromatography is applicable to nonvolatile substances and thermally unstable materials.

My past research experiences involved the use of analytical techniques and mainly wet chemistry. As a result of my research training, I was considered as a candidate to conduct research involving these techniques and analyses.

II. Objectives of The Research Effort

There were three major objectives and goals in which we hoped to have accomplished during the course of our research efforts. These are as follows: (1) to obtain knowledge of the initation and detonation mechanism of explosives, (2) if the structure of representative compounds can be modified, then one may determine the effects on the initiation barrier, and (3) molecules can be tailored to optimize their stability and energetic properties.

The initial phase of the research involved the preparation of the TNT samples for the decomposition process. Exact size sample tubes and weighings had to correlate in all of the TNT samples. A major concern in our research efforts involved the decomposition set-up, (sand bath) in which we used.

Several approaches were taken in an attempt to identify the thermal decomposition products of TNT. They are listed as:

(1) Identification of retention times for all peaks excluding TNT and the solvent acetone by using the 1090 Hewlett-Packard High Performance Liquid Chromatograph.
   (a) Isocratic Elution-45% Methanol/H_2O.
   (b) Gradient Elution-30%/100% MeOH/H_2O-100% Methanol.
(2) Retention times for some known standards (possible decomposition products).
(3) Comparison of the number of decomposition products produced from the sand bath and the Electron Paramagnetic Resonance (EPR)

burned TNT.

(4) Retention times for known standards (possible decomposition products) / dissolved in TNT samples.

(5) Solubility tests for decomposition products in different solvents.

(6) Fraction collection of each peak.

(7) Mobile Phase Liquid Chromatography. FMI Lab Pump-Silica Woelm.

  (a) Isolation of peaks

  (b) Solvents, (hexane, ethyl acetate, chloroform, acetone, and methanol.)

(8) Fraction collection on the HPLC and from the MPLC.

(9) Mass Spectrum data.

(10) NMR data.

III. Experimental

The mixture of decomposition products used in this study were obtained by heating 25 and 80 mg of TNT in a sand bath at 240°C for time intervals ranging from 15 to 240 minutes. These samples were taken up in acetone. Dilutions were made for each acetone sample. Each of these samples were injected in the HPLC. Chromatograms for isocratic, 45% MeOH/H_2O and gradient 30%-100% MeOH/H_2O -100% MeOH were made for comparison. These chromatograms were studied in an attempt to identify retention times for each possible decomposition product. Figures 1 and 2.

TNT was burned in an Electron Paramagnetic Resonance (EPR). These samples were also prepared for the HPLC by the same method as the sand bath burned TNT. These samples gave better chromatograms and the decomposition products were shown to be more concentrated than to that of the sand bath burned TNT. Figure 3

By looking at a few possible mechanisms for the thermal decomposition of TNT, several products are feasible. Standards of possible decomposition products were run on the 1090 HPLC. Retention times for these standards were obtained for an isocratic and gradient elution runs.

Solubility tests were made with the decomposed TNT to see whether or not some of the decomposition products would be soluble in one solvent or the other. The solvents were, chloroform, ether, pyridine, acetone, and methanol. The decomposition products were quite soluble in most of the solvents.

An attempt to collect each peak on the HPLC was made using the 25 and 80 mg samples of decomposed TNT. However, reinjection of each peak

fraction gave a chromatogram indicating all of decomposition products and TNT was still present in a large concentration.

With Mobile Phase Liquid Chromatography (MPLC), 300 mg of dry TNT was placed on a silica packed column and eluted with solvents of different polarities. These included; 100% hexane, 95%-5% hexane/ethyl acetate, 50%-50% hexane/ethyl acetate, 100% ethyl acetate, 100% chloroform, 100% acetone and 100% methanol. Normal phase chromatography was used to elute the non-polar to polar compounds off the column. We hoped to elute the bulk of the TNT off the column in order to see more of our other decomposition products. All of the MPLC fractions were run on the HPLC. The 95%-5% hexane/ethyl acetate fraction was reinjected on the column to its maximum loading. Multiple infections were made and collected as fractions for the NMR and Mass Spectrum.

IV. & V. Results and Discussion

All spectral data was obtained with a Hewlett-Packard 5890A Gas Chromatograph and the JEOL-FX-90Q Fourier Transform NMR Spectrometer, 5610A. Tables 1 and 2 give the retention times for an isocratic, 45% MeOH/H_2O and gradient, 30% MeOH/H_2O-100% MeOH elutions for some standards, (possible decomposition products). Figures 1 and 2 shows the chromatograms for the standards.

Figure 3 shows the comparison between 25 mg of TNT burned at 15 minutes versus 240 minutes. There was not any more decomposition of TNT at 240 minutes than to that for the decomposition at 15 minutes. This situation may have resulted from the preparation of the TNT sample before burning. Also, the uniformity of the burning process may be questionable.

Figure 4 shows the chromatogram for 25 mg of TNT burned at 240 C for 180 minutes in the Electron Paramagnetic Resonance Spectrometer (EPRS). There are approximately six (6) decomposition products shown. In all cases, the EPRS burned TNT gave chromatograms with more decomposition products being shown.

Figure 5 shows the 95%-5% hexane/ethyl acetate fraction collected from the MPLC. The 95%-5% hexane/ethyl acetate fraction gave the best chromatogram for the isolation of the decomposition products.

Figure 6 shows a mass spectrum from one of the 95%-5% hexane/ethyl acetate fraction. Two decomposition products are shown.

HPLC ANALYSIS: HEWLETT-PACKARD 1090A CHROMATOGRAPH

ISOCRATIC 45% $MeOH/H_2O$ SOLVENT

200 x 4.6 mm ODS COLUMN

254 nm UV ABSORBANCE DETECTION

STANDARDS	RETENTION TIMES (MIN)
2-NITROBENZOIC ACID	1.44
2,4-DINITROPHENOL	1.65
TRINITROBENZENE	7.01
1,4-DINITROBENZENE	8.22
NITROBENZENE	11.08
TNT	12.43
2,6-DINITROTOLUENE	15.61
4-NITROTOLUENE	21.83
BIPHENYL	--
TRINITROBENZOIC ACID	1.70
2,4-DINITROTOLUENE	15.24
2-NITROTOLUENE	19.58
p-AZOTOLUENE	--

Table I

HPLC ANALYSIS: HEWLETT-PACKARD 1090A CHROMATOGRAPH

GRADIENT 30% $MeOH/H_2O$-100% MeOH SOLVENT

200 x 4.6 mm ODS COLUMN

254 nm UV ABSORBANCE DETECTION

STANDARDS	RETENTION TIMES (MIN)
2-NITROBENZOIC ACID	1.47
2,4-DINITROPHENOL	1.74
TRINITROBENZOIC ACID	1.82
TRINITROBENZENE	9.50
1,4-DINITROBENZENE	10.67
NITROBENZENE	12.80
TNT	13.45
2,6-DINITROTOLUENE	14.63
4-NITROTOLUENE	16.39
BIPHENYL	24.53
2,4-DINITROTOLUENE	15.24
2-NITROTOLUENE	19.58
p-AZOTOLUENE	28.03 28.92

Table I73-11

STANDARDS

45% $MeOH/H_2O$

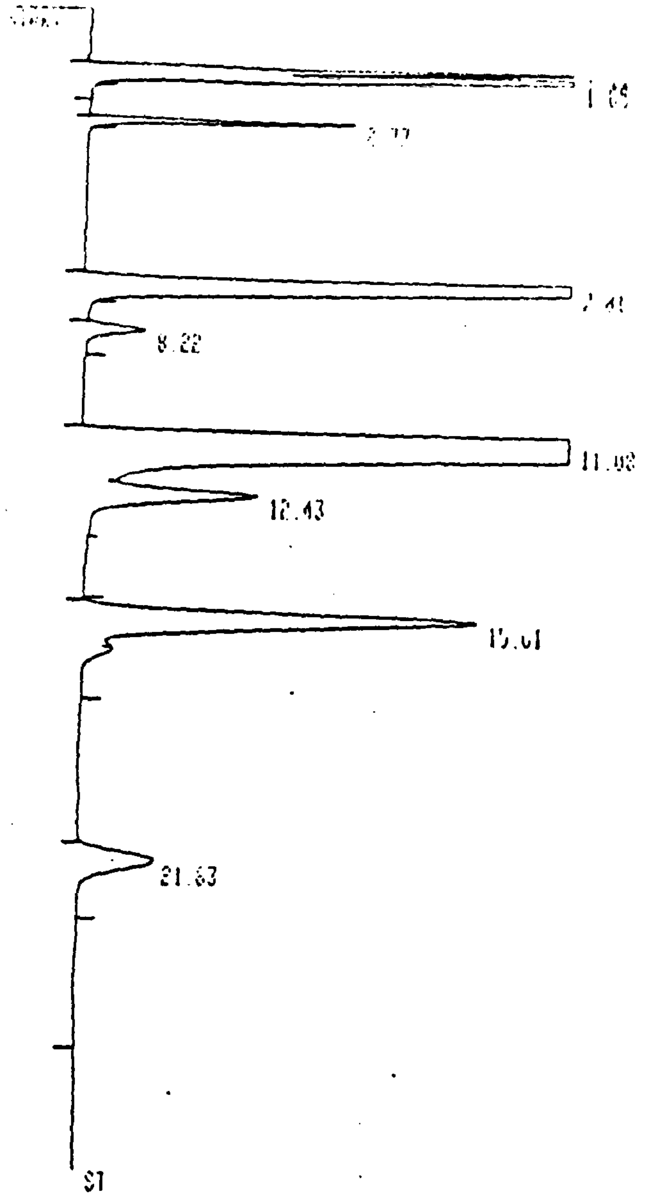

Figure 7

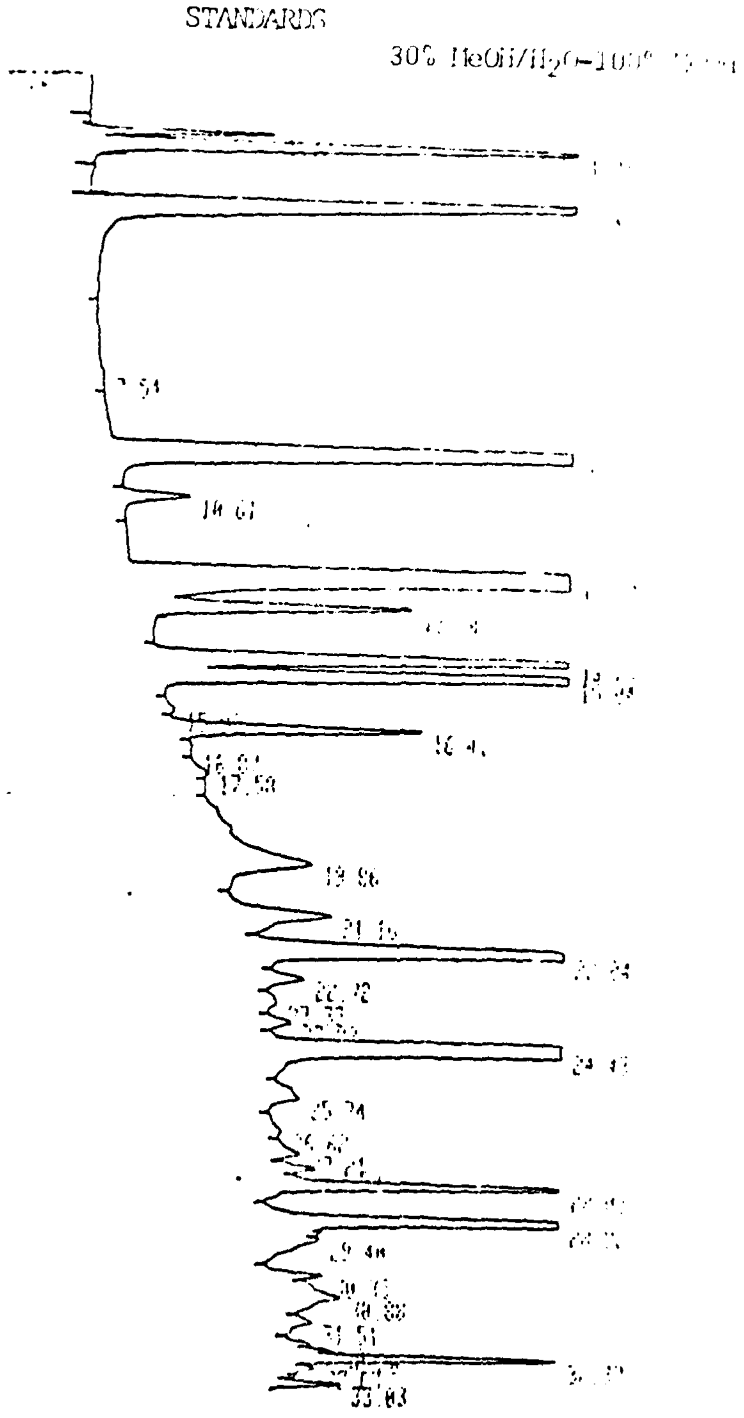

FigureII.

[illegible] mg TNT Burned at 240 [illegible] for 15 min.

25 mg TNT Burned at 240 for 240 min.

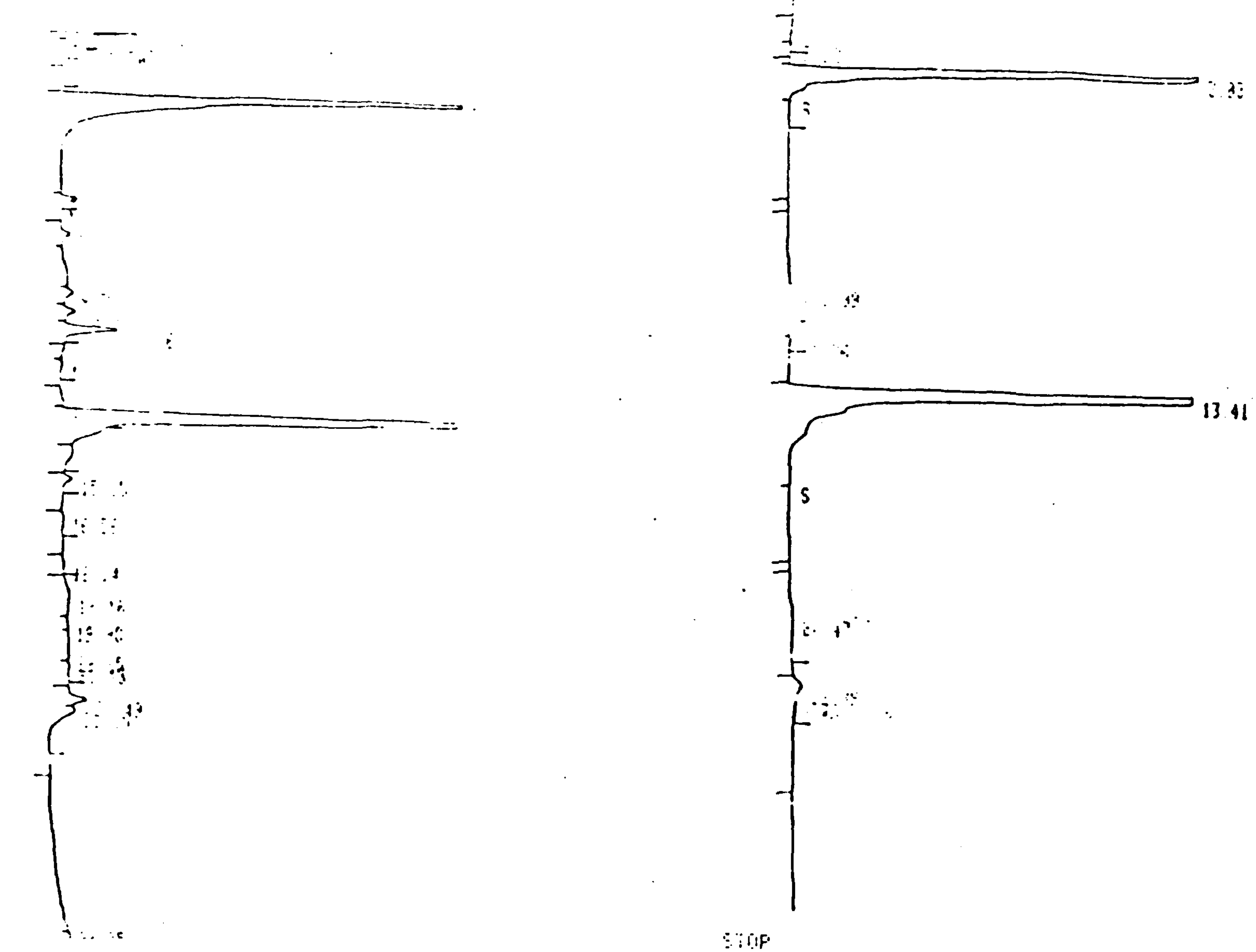

Figure III.

25 mg Burned at 240 C for 180 min. in the EPFC.

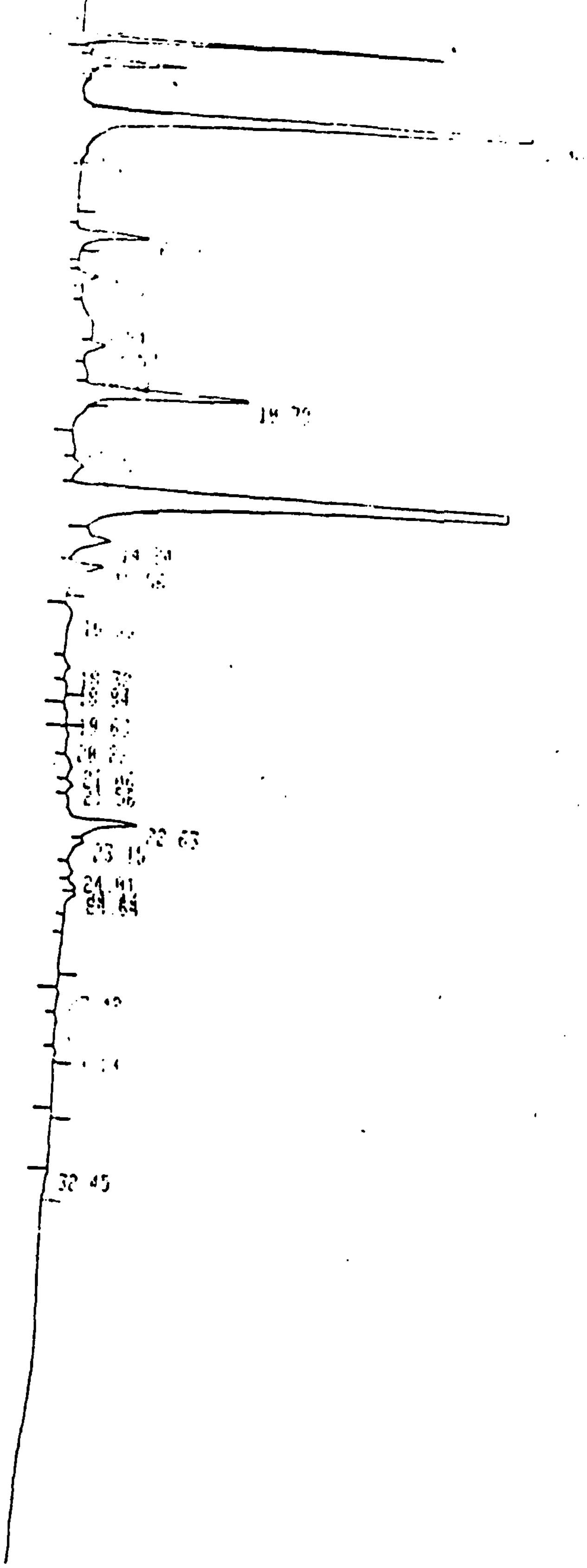

Figure IV.

95%-5% Hexane/Ethyl Acetate Fraction-HPLC

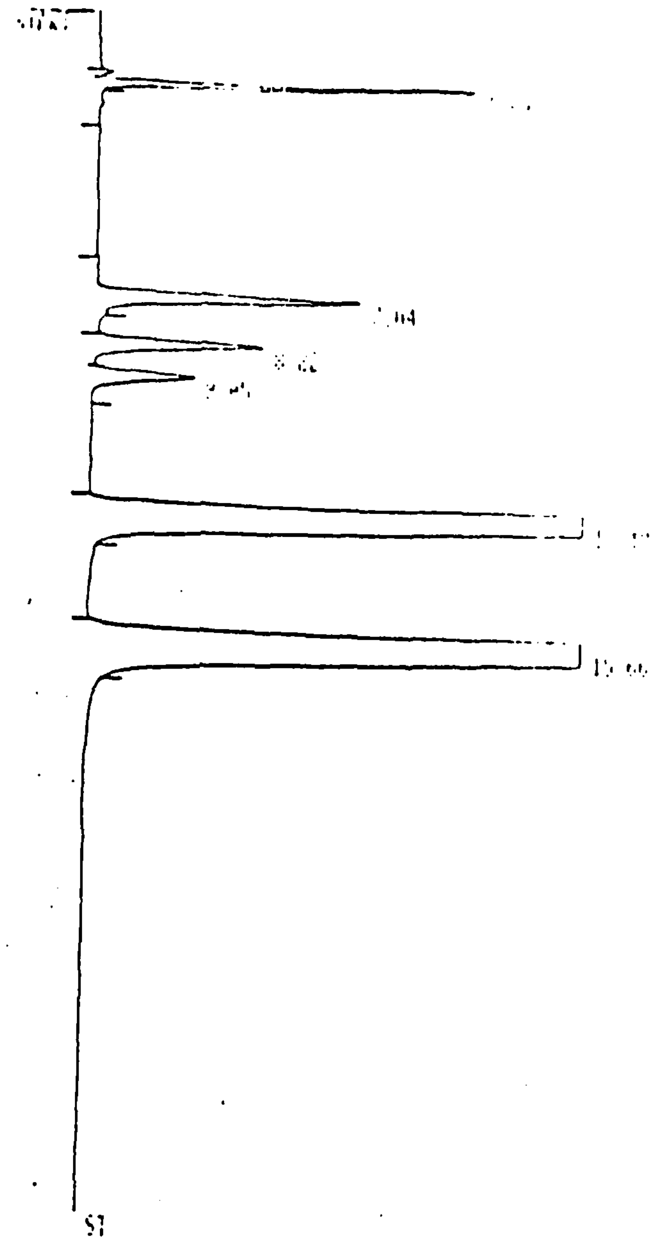

Figure V

DAILY;95/5 ETAC/HEX CRYSTALS; MPLC;12 AUG 85
FT HP PACKED COL(2% OV-101)

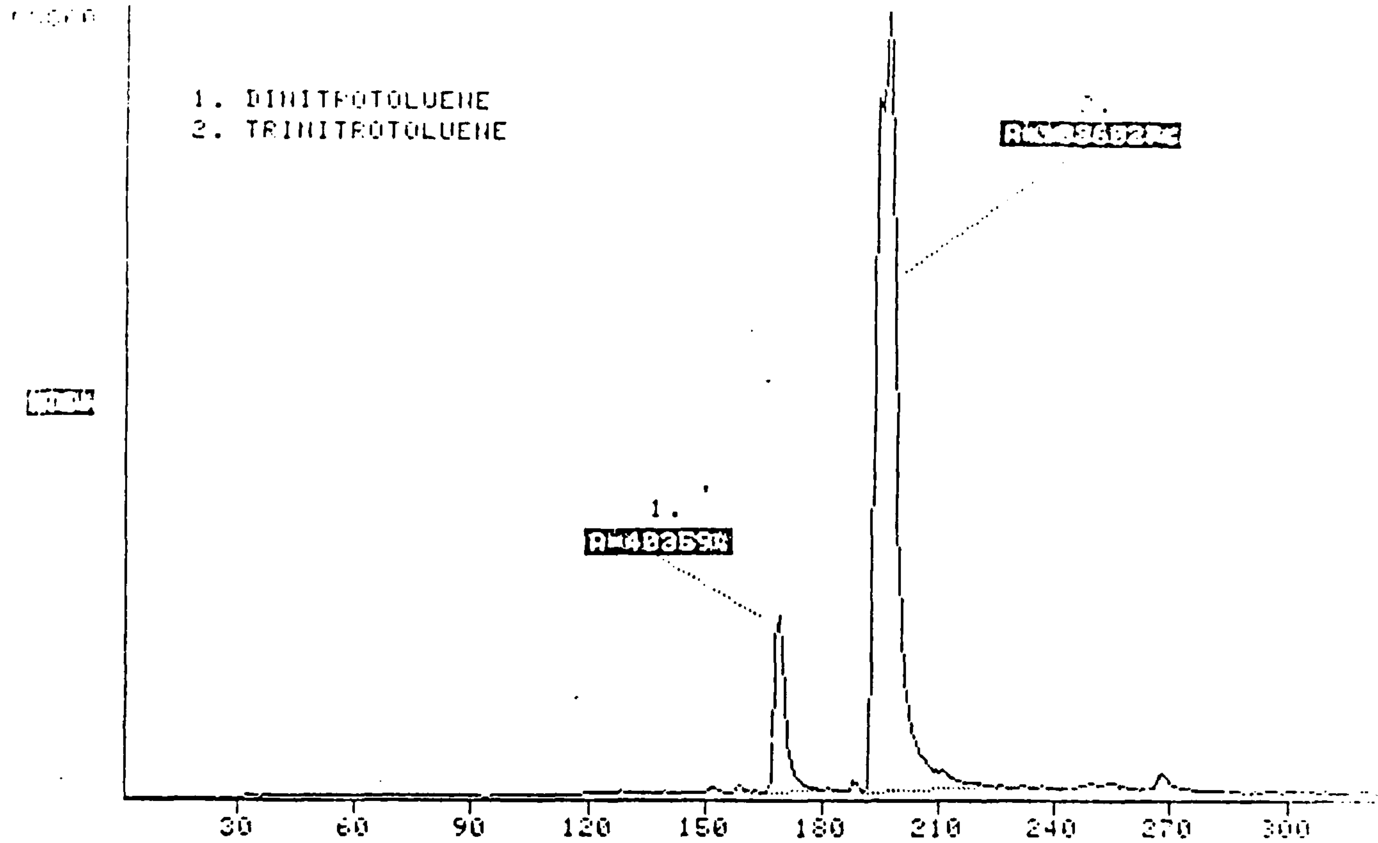

TABLE ENTRIES: FRN 17507

Try	Time	Mass	Area	%
1	6.8	TI	40359.	10.7
	7.8	TI	336027.	89.3

CALCULATE % ON ENTRY #:

Figure VI.

REFERENCES

Conference and journal publications:

1. Rogers, R. N., "Combined Pyrolysis and Thin Layer Chromatography-A Method for the Study of Decomposition Mechanisms", University of California, Los Alamos Scientific Laboratory, P.O. Box 1663, Los Alamos, N. M. 87544

2. Dacons, Joseph C., Horst G. Aldoph, and Mortimer J.Kamlet, "Some Novel Observations Concerning the Thermal Decomposition of 2,4,6-Trinitrotoluene," Advanced Chemistry Division, U.S. Naval Ordnance Laboratory, White Oak, Silver Spring, Maryland 20910

3. Dorey, R. Cameron, W. R. Carper, "Synthesis and High-Resolution Mass-Spectral Analysis of Isotopically Labeled 2,4,6-Trinitrotoluene", Frank J. Seiler Research Laboratory (AFSC), United States Air Force Academy, Colorado Springs, Colorado 80840

Textbooks:

4. Hamilton, R. J., P. A. Sewell, "Introduction to High Performance Liquid Chromatography," 11 NewFetter Lane, London, Halsted Press.

5. Skoog, D. A., D. M. West, "Fundamentals of Analytical Chemistry" CBS College Publishing, Saunders College Publishing. Philadelphia. PA 19105

VI. Recommendations

The techniques involved in the preparation for the burning of the 2,4,6-trinitrotoluene should be modified. Once the techniques and procedures are implemented, then reproducibility and more accuracy can be obtained with better results. The analytical techniques involved in the preparation of the samples for injection in the HPLC should also be refined. Some of the decomposed TNT in the sample tubes have to be chopped to remove it from the pyrex tubes, and also all of the residue cannot be removed for analysis and a considerable amount of the product may be loss due to this technique.

With a more profound preparative procedure for the decomposition, the isolation of the products can be done with the use of Mobile Phase and High Performance Liquid Chromatography. Conclusive results and data will be enchaned with a correction in elemental analysis and with the use of NMR and Mass spectral data, the products can be identified.

1985 USAF-UES SUMMER FACULTY RESEARCH PROGRAM/

GRADUATE STUDENT SUMMER SUPPORT PROGRAM

Sponsored by the

AIR FORCE OFFICE OF SCIENTIFIC RESEARCH

Conducted by the

UNIVERSAL ENERGY SYSTEMS, INC.

FINAL REPORT

ROLE OF STIMULUS UNCERTAINTY IN VISUAL CONTRAST SENSITIVITY

Prepared by:	Dr. David L. Kohfeld	Mr. Brian C. Hayes
Academic Rank:	Professor of Psychology	Graduate Student
Department and University:	Department of Psychology Southern Illinois University, Edwardsville	
Research Location:	Air Force Human Resources Laboratory Operations and Training Division Williams AFB, Arizona	
USAF Research:	Dr. Robert T. Nullmeyer	
Date:	October 1, 1985	
Contract No.:	F49620-85-C-0013	

ROLE OF STIMULUS UNCERTAINTY IN VISUAL CONTRAST SENSITIVITY

by

David L. Kohfeld

ABSTRACT

This research involved the study of contrast sensitivity under conditions of stimulus uncertainty and event uncertainty. In Experiment 1, contrast sensitivity functions (CSFs) were generated at six spatial frequencies when the threshold stimulus was either predictable (i.e., cued or blocked) or unpredictable (uncued and intermixed). The resulting CSFs were the same for the three cueing conditions. Experiment 2 revealed a change in the CSF when the sequence included catch trials (event uncertainty) in conjunction with unpredictable spatial frequencies (stimulus uncertainty). The data were then collected into separate distributions for the catch trial and no-catch trial conditions, and deconvolving the former distribution from the latter resulted in a difference model that was gamma in form. The CSFs in both experiments provided support for a version of multichannel theory which assumes that a wide range of spatial frequency channels can be monitored simultaneously. The distributional analyses revealed that contrast sensitivity measures are composed of at least two component processes, sensory detection and response initiation. It appears that stimulus and event uncertainty have selective influence on the response stage, and a theory of the neural mechanisms that underlie the response process is offered. Finally, a practical implication of this work is that undesired "false alarm" (response criterion) bias can be reduced when the method of increasing contrast includes both catch trials and stimulus uncertainty in the sequence.

Acknowledgements

The data collection, analyses and preparation of this paper were generously supported by the Air Force Systems Command through the Air Force Office of Scientific Research (Contract No. F49620-85-C-0013), as conducted by the Universal Energy Systems, Inc. This work was done while the principal investigator served as a Summer Research Fellow at the Human Resources Laboratory, Williams AFB, Arizona. Computer time and routines, including graphics, were funded by a research grant to the author from the Office of Research and Projects in the Graduate School at Southern Illinois University, Edwardsville. I am indebted to the research staff at AFHRL, Williams AFB, for their encouragement and support, including travel funds, without which this research could not have been accomplished. I am happy to acknowledge the collaboration of Dr. George Geri during this research assignment. Finally, special thanks are extended to my colleague, Dr. Robert Nullmeyer, for his continued advice on how to work effectively in an Air Force laboratory setting.

I. INTRODUCTION

Light energy that strikes the eye is usually distributed as patterns of light that are imaged on the retina. These patterns reflect the spatial properties of a visual display, e.g., its size, shape, or more generally, its form. The quality of a person's vision is often linked to the ability to determine very small spatial patterns in a display. As such, visual acuity, usually measured by the familiar Snellen letter chart, has been the most popular clinical tool for determining the resolving power of the visual system. The use of Snellen-type letters allows the optician to determine the spatial size of the finest detail visible to the individual while other important attributes, such as the contrast between the black letters on the white background of the chart, are held constant.

Over the past thirty years a more sophisticated laboratory procedure has proved useful in the measurement and analysis of spatial resolution. Specifically, acuity gratings consisting of vertical black bars and white bars are presented as sine-wave gratings, so-called because the intensity of the light and dark bars on the display screen changes gradually, in a sinusoidal fashion.[1] The difference between the luminance of the light bars and the dark bars can be reduced until an observer can no longer detect the dark bars on the white background. The coarseness, or widths of the black-white bars in the grating can easily be varied, and the entire test field can be presented as a computer generated display on either an oscilloscope or a video screen. The contrast on the screen is often defined as (L_{max} - L_{min} / L_{max} + L_{min}), where L_{max} is the luminance of the light bars and L_{min} is the luminance of the

dark bars. Thus, when the contrast value is low or zero, the display would appear uniform and unpatterned. In one particular test procedure, $L_{max} - L_{min}$ is gradually increased until the vertical striations are just barely visible, which is the <u>contrast threshold</u>. The reciprocal of this contrast value is usually computed and is plotted as <u>contrast sensitivity</u>.[2,3] Contrast threshold measurements are usually obtained for a number of sine-wave gratings of different <u>spatial frequency</u>, in cycles per degree. The resulting data can then be presented as <u>contrast sensitivity functions</u> (CSFs), in which either contrast threshold[4] or contrast sensitivity[5,6,3] is plotted on a logarithmic ordinate against spatial frequency on a logarithmic abscissa.

The use of sinusoidal gratings to measure contrast sensitivity has contributed a great deal to our understanding of visual pattern perception. In a classic study, Campbell and Robson used simple and compound gratings to evaluate their theory that bars and edges of different orientations and sizes form the basic units of pattern perception, as represented in the visual cortex.[6] Furthermore, Campbell and Robson introduced the revolutionary idea that the visual system is configured in a way that breaks down complex stimulus patterns into specific spatial frequencies, resembling a crude Fourier analysis.[7,1] Such theorizing formed the basis for what is known today as the <u>multichannel theory</u> of pattern perception, i.e., different visual mechanisms are narrowly tuned to specific spatial frequencies and each "channel" is selectively sensitive to a particular frequency.[1,8,9,10,11]

Recently, Ginsburg and his associates have demonstrated that

contrast sensitivity measures, as obtained from acuity gratings, have practical and clinical uses in addition to their traditional role in basic vision research.[12] Moreover, Ginsburg cites growing evidence that Snellen-type measurements provide limited information about visual acuity, i.e., Snellen Charts assess spatial size while contrast is held constant, whereas contrast thresholds reflect both size and contrast. In this vein, Ginsburg and Cannon reported that certain visual abnormalities caused by brain lesions, multiple sclerosis, and cataracts are correlated with measures of threshold contrast sensitivity, but not necessarily Snellen Chart data.[5] Of particular interest to the study of Air Force pilots' performance, Ginsburg and his co-workers found that (a) CSFs predicted pilots' skill in detecting a ground target during fighter-aircraft simulation,[13] and (b) CSFs correlated with the range at which experienced pilots detected approaching aircraft under actual field conditions.[14] One of Ginsburg's general conclusions was that the Snellen-type measures ordinarily employed to determine pilot trainees' visual acuity are unrelated to visual performance in simulation and field-type settings.

II. RESEARCH OBJECTIVES

Numerous experiments have shown that subjects respond more efficiently when a forthcoming stimulus is predictable, i.e., when either a valid cue is provided or the same stimulus is presented repeatedly. More specifically, Davis, Kramer, and Graham found that the number of correct detections of a particular spatial frequency was significantly lower in an Uncued Intermixed condition which produced stimulus uncertainty than in either Blocked Alone or Cued

Intermixed conditions where the forthcoming stimulus was predictable.[8] The results were consistent with a version of multichannel theory which holds that an observer is capable of monitoring all spatial frequency channels simultaneously. Moreover, each frequency channel is thought to contain a certain amount of "neural noise," and when more than one channel must be monitored at once (i.e., in the Uncued Intermixed condition where uncertainty is maximized), there is a probabilistic increase in overall noise, thus resulting in more false alarms.

It should be noted that Davis et al. employed five different spatial frequencies whose contrasts had been subjectively matched beforehand to yield equal detection performance in the Blocked Alone condition where the same frequency was presented repeatedly (predictably). Furthermore, they used a temporal, two-interval forced choice procedure in which a certain number of incorrect choices ("false alarms") is inherent in the methodology. Accordingly, our first experiment was designed primarily to evaluate the effects of cueing and stimulus uncertainty on the actual contrast sensitivity function (CSF). To do this, we employed the psychophysical method of increasing contrast to measure contrast thresholds at different spatial frequencies. Similar to the design employed by Davis et al., the present Experiment 1 included three experimental conditions: (1) <u>Blocked Alone</u>-- data were collected at six spatial frequencies, but the same frequency occurred predictably within a block of trials; (2) <u>Cued Intermixed</u>-- the spatial frequencies were presented in an irregular order across trials, but the sequence was predictable because a correct preview (cue) of each stimulus was presented before

each trial; and (3) Uncued Intermixed— the same sequence of trials used in (2) was rendered unpredictable because no preknowledge cue was provided.

As in previous research, both CSFs and entire distributions of contrast sensitivity measures were evaluated.[3] Thus, an important objective was to analyze the effects of stimulus uncertainty on the forms of contrast sensitivity distributions. A system identification method of deconvolution was used to decompose the distributions into component densities that presumably reflected the separate influence of "pure" contrast sensitivity and response ("false alarm") bias on threshold detections. The general research objective was to identify a valid indicator of contrast sensitivity that is relatively free of undesired false alarm bias, and to theorize about underlying processes which can be inferred from the forms of distributions obtained in different experimental conditions.

III. EXPERIMENT 1

A. Method. The operators (highly motivated, professional people) were three Research Psychologists employed at the Human Resources Laboratory, Williams AFB, Arizona. All had normal or fully-corrected vision. DK, the principal investigator, was 44; a graduate student, BH, was 23; and an undergraduate student, MB, was 21 years old. Operators DK and BH were familiar with the research aims; DK had considerable previous experience as an operator in CSF research, BH had several days of programming and calibration experience with the design, whereas MB had no prior exposure to the present experiment and was unaware of the objectives.

The apparatus was an Optronix Model 200 Vision Tester, which

has been described elsewhere.[3] Briefly, this equipment is capable of displaying sinusoidal gratings at different spatial frequencies. Contrast at the video screen was defined as $(L_{max} - L_{min} / L_{max} + L_{min})$. The Optronix display screen was adjusted to 100 candelas/m^2, as indicated in the calibration procedure for this device. This calibration setting resulted in a display screen with an average luminance of 26.8 apparent foot candles, or 29 millilamberts of white light, as measured by a dark-adapted observer with a Macbeth illuminometer from a distance of three meters. Six spatial frequencies were employed: 0.5, 1.0, 3.0, 6.0, 11.4, and 22.8 cycles per degree. The operators viewed the screen from a distance of three meters; thus, the observed luminance of the uniform (unpatterned) display was the equivalent of 82 decibels of both white light and 1,000-Hz tone.[16]

The psychophysical method employed in Experiment 1 is known as the method of increasing contrast.[3,4,5] Briefly, the contrast on the screen increased at a fixed rate of 4 dB per second from below threshold to where the operator could first detect the presence of the test grating. The operator depressed a switch when the grating on the screen was just barely detectable. Three different experimental conditions employing this method were used in Experiment 1:

1. Blocked Alone-- This condition is available as the Increasing Contrast method in the pre-programmed, menu-driven mode of operation in the Optronix Vision Tester. The time between each threshold detection and the onset of the next trial was varied to discourage the operator from guessing the contrast threshold based on a fixed time interval from the last detection. A block of trials consisted of 12 increasing presentations at each of the six spatial frequencies.

Thus, the term "Blocked Alone" means that one frequency alone was presented in each block of 12 trials. There was a rest period at the end of each series of six trial blocks. An experimental session was comprised of five series of trial blocks, yielding a total of 60 measures in each of the six spatial frequencies for each operator.

2. Cued Intermixed— In this condition, a block of 73 trials was programmed into the Optronix microcomputer (see Appendix 1). The first trial was an unscored warm-up trial which also served to initiate the ensuing 72 scored trials. The six spatial frequencies were presented in an irregular ("intermixed") order with two important restrictions: (a) each spatial frequency occurred 12 times in the 72-trial scored sequence; and (b) the trial-to-trial sequence was arranged so that each spatial frequency was preceded equally often by itself as well as by the other five frequencies in order to control for the sequential (contextual) effects that sometimes occur in psychophysical experiments. Each trial began with a 1-second presentation (cue) of the actual spatial frequency that would occur on that trial. A variable cue-stimulus interval followed which was long enough for cue aftereffects to disappear, and also variable enough to prevent time estimation of when the target frequency would reach threshold. The block of 73 trials was presented five times per operator, with a rest period between blocks. As in the Blocked Alone condition, this resulted in a total of 60 measures per frequency per operator.

3. Uncued Intermixed— This condition was identical to the Cued Intermixed condition, except that no specific cue was presented prior to the onset of the target stimulus. Instead, a non-specific

auditory "beep" signalled the beginning of each trial, and the ensuing tone-stimulus interval was varied to prevent accurate estimation of when the target would appear.

Regardless of previous experience with contrast sensitivity measurements, all three operators received several unscored warm-up blocks in each of the three experimental conditions prior to actual data collection; this was done to minimize the extensive variability due to practice effects. Subsequently, the order of actual data collection was Blocked Alone, Cued Intermixed, and Uncued Intermixed.

B. Results and Discussion. Figure 1 presents log threshold contrast sensitivity as a function of log spatial frequency, in cycles per degree, for the three experimental conditions. Each operator's data are plotted separately (60 measures per data point), and the data means are pooled in the lower-right panel (180 measures per data point). The data form contrast sensitivity functions (CSFs) across the six spatial frequencies (0.5, 1.0, 3.0, 6.0, 11.4, and 22.8 cycles per degree) that are plotted on the logarithmic abscissa.

At least three observations are apparent from the data shown in Figure 1. First, the CSFs reveal the characteristic inverted-U shape found in previous research involving the present range of spatial frequencies.[1,3,5,6] CSFs reveal what Sekuler and Blake term a "window of visibility;" i.e., the resolving power of the visual system is best at intermediate frequencies and progressively less keen at relatively extreme frequencies (e.g., 0.5 and 22.8 cycles per degree). Second, a noteworthy feature of Figure 1 is the overall similarity of the CSFs across the operators for the three conditions shown. It appears that representative CSFs can be

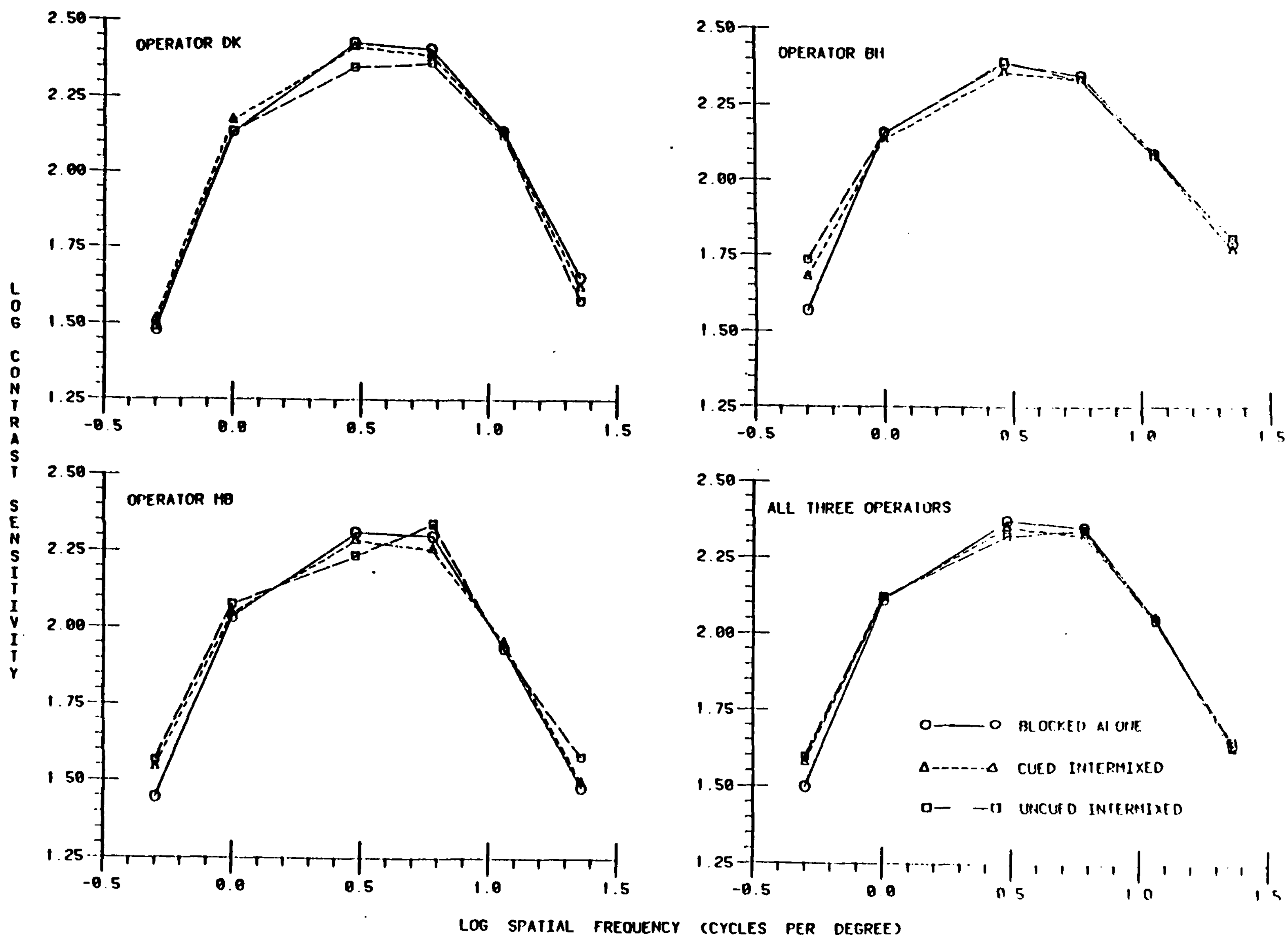

Figure 1. Contrast sensitivity functions for the three experimental conditions in Experiment 1

generated from relatively few operators, at least if these individuals are familiarized with the testing procedures and can generate a reasonably large sample of contrast threshold measures at each spatial frequency. The third, and perhaps most important observation is the obviously small differences among the CSFs for the three experimental conditions. This outcome differs from that reported by Davis et al. who obtained higher contrast thresholds in their Uncued Intermixed condition than in either the Cued Intermixed or Blocked Alone conditions.[8] As noted previously, the present research employed different psychophysical procedures than those used by Davis et al. Moreover, the present data provide even stronger support for multichannel theory than the results reported by Davis et al., a conclusion that will be discussed subsequently more fully.

The next step in this analysis involved the preparation of histograms for each operator (3) at each spatial frequency (6) for the experimental conditions (3), yielding a total of 54 distributions, each comprised of 60 measures. Although these distributions cannot be presented here because of space limitations, it was apparent that the shapes of the distributions were quite similar across operators and spatial frequencies within each of the three experimental conditions. However, the separate groups of distributions for the Blocked Alone, Cued Intermixed, and Uncued Intermixed conditions appeared to differ somewhat in their general form. To evaluate this possibility, the three groups of histograms were collapsed across spatial frequencies by adjusting the 60 raw scores in each distribution to a common origin of 1.0 on the log sensitivity scale, and then collecting these values across the six spatial frequencies. Although this

procedure eradicates information about the actual positions of individual spatial frequency distributions on the contrast sensitivity axis, it does not sacrifice vital information about the nature of log sensitivity as a continuous random variable. The outcome is shown in Figure 2, where proportion of threshold detections is plotted as a function of log threshold contrast sensitivity (bin widths of 0.02 log sensitivity). Thus, each operator's Blocked Alone, Cued Intermixed, and Uncued Intermixed distribution in Figure 2 is based on 360 measures, and the pooled data of all three operators (lower-right panel) includes 1,080 measures per distribution.

In general, the distributions displayed in Figure 2 are most likely from the same Pearson "family" of distributions. That is, the distributions for each of the experimental conditions appear gamma in form; i.e., their means, standard deviations, and positive skewness are correlated. These properties suggest that the three experimental conditions resulted in distributions that were generated by common underlying processes. However, closer inspection of the lower-right panel in Figure 2 reveals that the Uncued Intermixed distribution has the largest variance and skewness, the Cued Intermixed distribution is intermediate, whereas the Blocked Alone distribution is most peaked and least skewed. In other words, although the three conditions have very similar means (as seen in the lower-right panel of Figure 1), the overall shapes of their distributions appear to differ somewhat. These considerations point to the feasibility of a deconvolution procedure that could reveal additional information about possible differences among the processes which

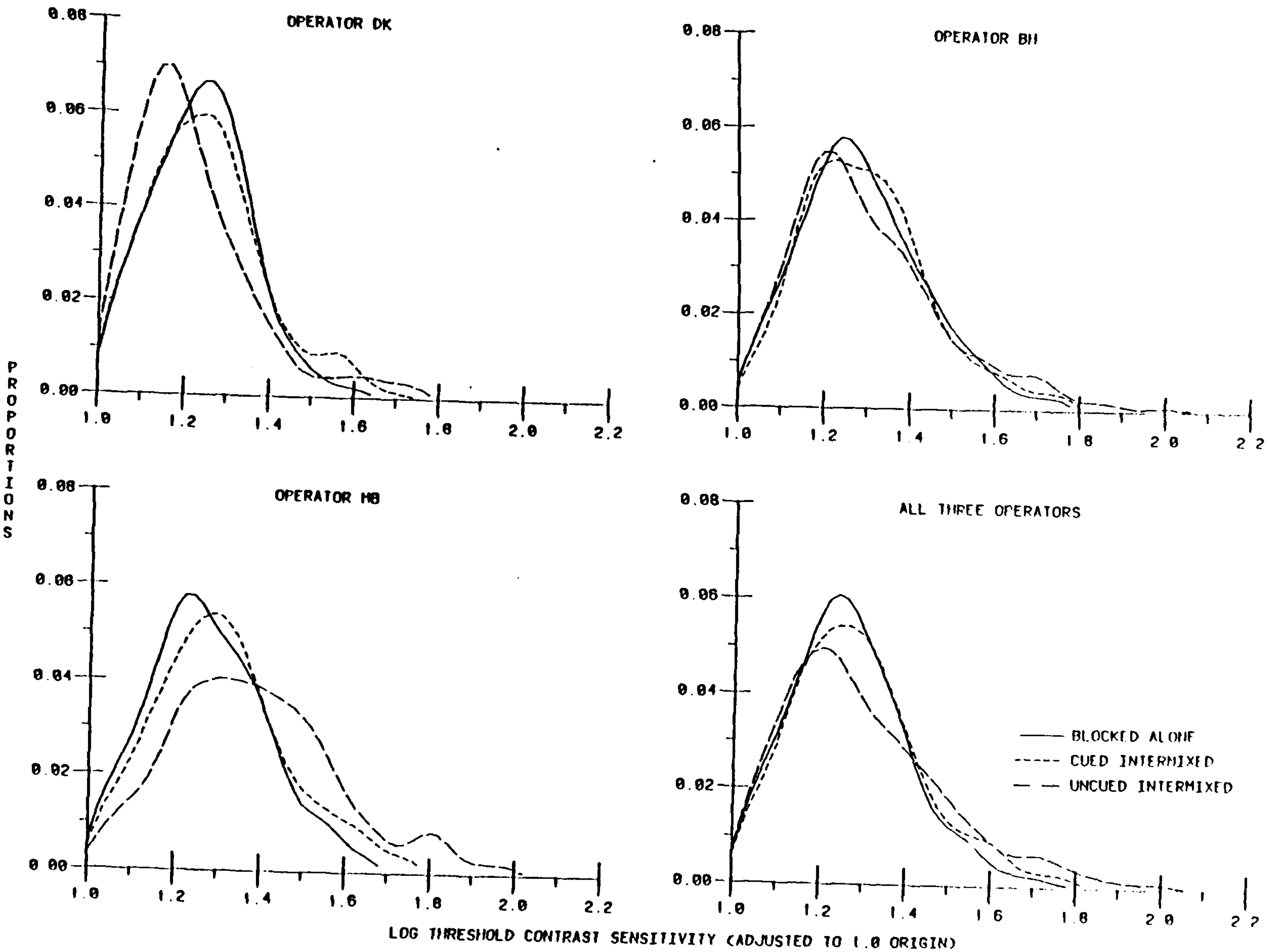

Figure 2. Individual distributions collapsed across spatial frequencies for the three conditions

underlie the distributions shown in Figure 2.[15] The results of this convolution analysis, while informative, were too detailed for presentation in this report. Instead, it was decided to proceed with Experiment 2, where distributional analyses proved to be more conclusive than those attempted in Experiment 1. The convolution method was also applied to the distributions obtained in Experiment 2, and these results are presented subsequently.

IV. EXPERIMENT 2

The main objective of the second experiment was to examine increased stimulus uncertainty by introducing blank ("catch") trials into the stimulus sequence. Catch trials are sometimes used in reaction-time experiments and threshold measurement procedures to prevent a person from guessing that a stimulus has occurred on a particular trial when, in fact, none was presented. Furthermore, the use of blank trials tends to lower false alarm rates, particularly when an operator is instructed to minimize or avoid altogether "getting caught", or responding on trials when no stimulus is presented. In this vein, Yager, Kramer, Shaw, and Graham employed catch trials in their investigation of the detection and identification of acuity gratings.[11] As in Davis et al.'s research,[8] Yager et al. used several spatial frequencies whose contrasts were adjusted to yield approximately the same proportion of correct detections when only one frequency was presented in a block of trials. The results provided further support for a multichannel theory which assumes that an operator can attend to different spatial frequencies simultaneously. However, their results were also consistent with the interpretation that selective attention to one particular channel

(e.g., the one that is cued) facilitates performance when that particular spatial frequency is certain to occur.

Based on these considerations, it was hypothesized that increasing stimulus uncertainty even further by using catch trials would not only decrease the incidence of false alarms, but might also modify both the location and shape of resulting contrast sensitivity functions.

A. Method. The operators were DK and BH, two of the three operators that had served in Experiment 1. The apparatus and general procedures were identical to those used in Experiment 1, except that blank trials were intermixed in the sequence in two of the experimental conditions that were utilized.

Four conditions were evaluated: (1) Blocked Alone/No Catches (same as Blocked Alone in Experiment 1); (2) Blocked Alone/Catches (same as 1. above, except blank trials were included); (3) Uncued Intermixed/No Catches (same as Uncued Intermixed in Experiment 1); and (4) Uncued Intermixed /Catches (same as 3. above, except blank trials were included. In Condition 2, each block of trials was comprised of 9 "go" trials (the same stimulus frequency was presented) and 3 "catch" trials (no stimulus). The catch trials were programmed to occur randomly in each block of 12 trials with the restriction that a catch trial could not occur on more than two consecutive trials. Seven blocks of trials were run at each spatial frequency, yielding a total of 63 measures for each frequency. Condition 4 contained the same sequence of different stimulus frequencies as in Condition 3 (Uncued Intermixed—see Experiment 1), but 18 catch trials were randomly interspersed in each block of 72 trials, 3 catches per frequency. Since each operator ran 7 trial blocks, a total of 63 measures per

frequency were collected. As in Condition 2, the sequence in Condition 4 was programmed so that a blank trial could not occur on more than two consecutive trials. It is to be noted that the overall probability of a catch trial in both Conditions 2 and 4 was .25.

After initial practice sessions in Conditions 2 and 4, it became evident that both operators were occasionally responding on blank trials, that is, they were getting "caught" by pressing the response button when no stimulus was present. Accordingly, both operators continued to practice in both these conditions until a response criterion was achieved in which no errors ("false alarms") were committed. Both operators experienced this as a concentrated effort in which a criterion of no errors was gradually achieved. At this point, no false alarms were permitted, and indeed, none occurred during the collection of the actual data reported in Experiment 2.

B. Results and Discussion. Figure 3 shows the mean threshold values, plotted in the same manner as in Figure 1. There are 60 measures in each data point. As before, the data form orderly CSFs for the two operators across the six spatial frequencies.

A noteworthy feature of Figure 3 is the apparent departure of the lowermost CSF from the other three functions for each operator. That is, the Uncued Intermixed/Catches condition resulted in generally lower contrast sensitivity measures (higher thresholds) than those obtained in the other three conditons. Despite this overall trend, however, the CSFs in all four conditions appear to converge at the lowest spatial frequency, 0.5 cycles per degree, especially for Operator DK. Supporting these observations were the results of a

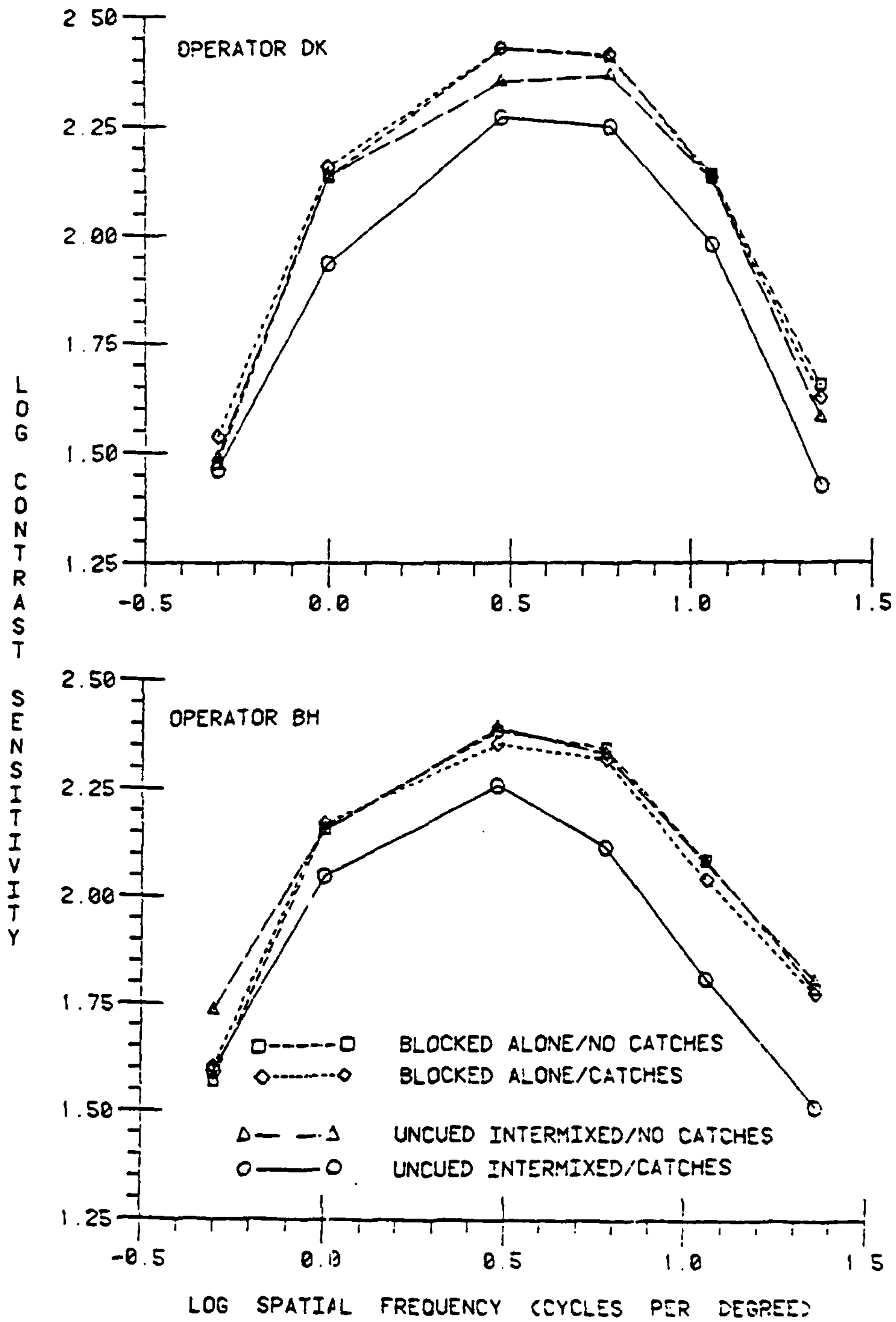

Figure 3. Contrast sensitivity functions for the four experimental conditions in Experiment 2

4 (experimental conditions) X 6 (spatial frequencies) repeated-measures analysis of variance which indicated the following significant effects: Conditions, $F(3,3) = 19.09$, $p < .05$; Spatial Frequency, $F(5,5) = 42.98$, $p < .001$; and Conditions X Frequency, $F(15,15) = 2.72$, $p < .05$. Specifically, the significant main effect of Conditions resulted from the departure of the Uncued Intermixed/Catches CSF from the others, whereas the small, but significant Conditions X Frequency interaction indicates similar contrast thresholds for all conditions at 0.5 cycles per degree only.

The results shown in Figure 3 allow some important conclusions. First, the most obvious effects of stimulus uncertainty on contrast threshold measurements were apparent in the Uncued Intermixed/Catches condition in which unpredictability was maximized. It may be recalled that in this condition the operator was confronted with both stimulus uncertainty (any one of six spatial frequencies could occur on a given trial) and event uncertainty (a stimulus might not be presented on that trial). The other three experimental conditions; stimulus uncertainty only (Uncued Intermixed/No Catches), event uncertainty only (Blocked Alone/Catches), or neither type of uncertainty (Blocked Alone/No Catches), were quite similar in their effect on the CSFs. Second, all four CSFs appeared to converge at the lowest spatial frequency; that is, there are little or no differences among the conditions at 0.5 cycles per degree. This provides support for a version of multichannel theory in which it may be argued that the variable of uncertainty has selective influence on specific channel frequencies.

It is to be noted that the CSFs shown in Figure 3 are based on

measures of central tendency, i.e., arithmetic means of log contrast threshold measures. Although this traditional approach provides important evidence that is relevant to theories about the form of the CSF, additional information about the variability in contrast sensitivity measures is available when entire distributions of contrast threshold data are also evaluated. Accordingly, the data in Figure 3 were re-plotted as distributions, in a manner identical to the way the measures in Figure 1 were presented again in Figure 2. As before, the threshold values in each spatial frequency were adjusted to a 1.0 origin and then collapsed across the six spatial frequencies. The resulting distributions are shown in the top panels of Figure 4. Each distribution with catch trials was based on 378 measures, whereas each distribution with no catches was generated from 360 values. It may also be noted that the Blocked Alone/No Catches and the Uncued Intermixed/No Catches distributions depicted in Figure 4 are identical to the corresponding Blocked Alone and Uncued Intermixed distributions shown in Figure 2 for Operators DK and BH, i.e., these two distributions in both figures are based on the same data, even though the scaling on the ordinate is different.

The results shown in the top panels of Figure 4 reveal that the two distributions obtained when catch trials were employed are considerably more peaked and less skewed than the two distributions generated from the conditions with no catches. In this vein, it is tempting to assume that measures in the upper tails of the distributions reflect <u>higher</u> or "better" contrast sensitivity scores, i.e., the operator can demonstrate higher contrast sensitivity when catch trials are <u>not</u> utilized. It is somewhat ironic, however, that the

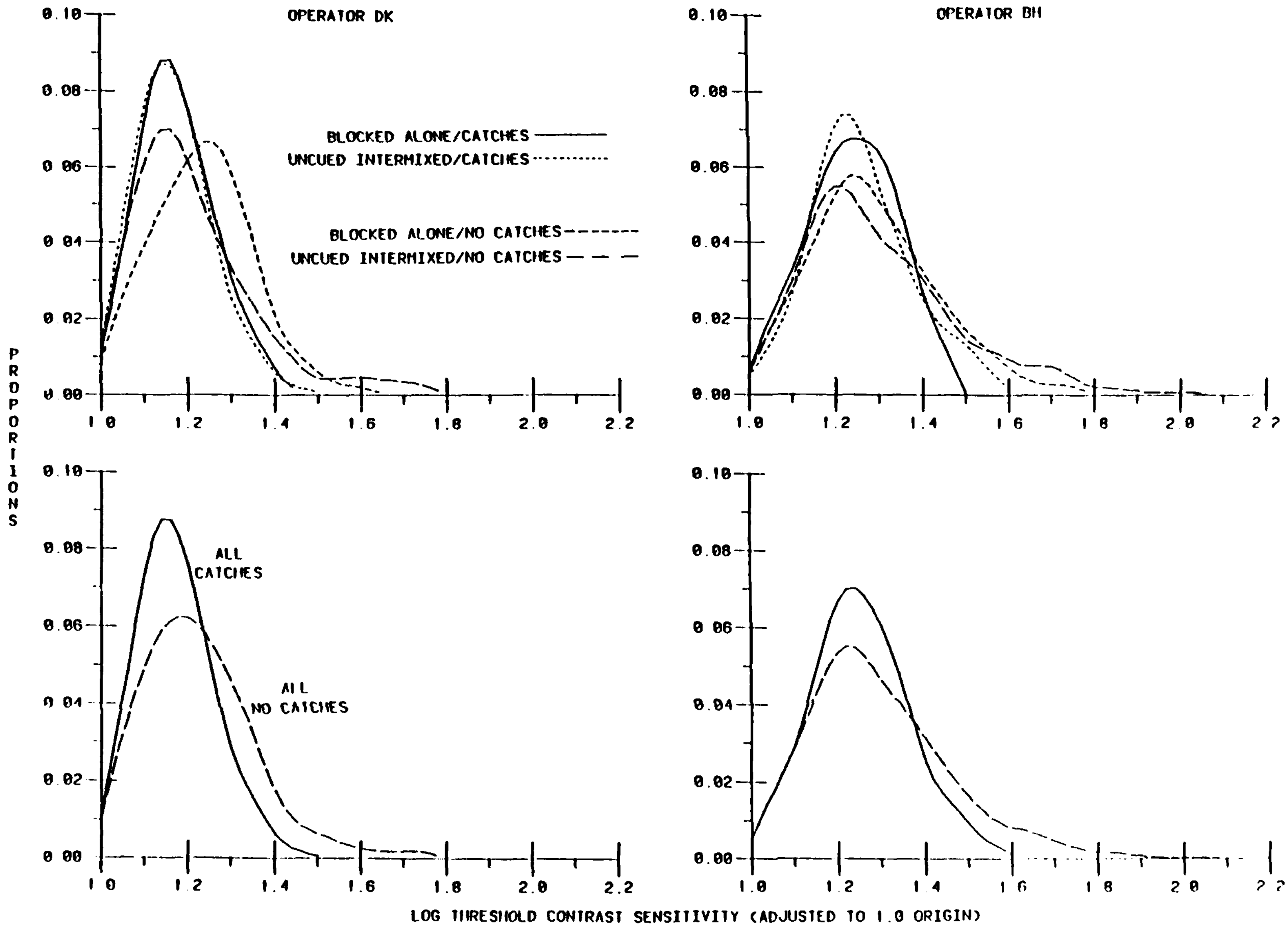

Figure 4. Individual distributions collapsed across spatial frequencies for the four conditions (Top panels) and the same distributions collapsed across the catches and no-catches conditions (Bottom)

contrast measures are more consistent (less variable) when catch trials are employed, as evidenced by less skewness and higher peaks for these distributions. A possible explanation for these results is based on the consideration that the method of increasing contrast is essentially an ascending series of trials for determining a contrast threshold. Thus, when an operator reports the presence of a stimulus it is assumed that the signal was actually detected. As such, the method of increasing contrast, when utilized without catch trials, is susceptible to false alarm data, simply because there is no obvious way to determine whether or not the operator actually detected a threshold stimulus whose probability of occurrence is always 1.0. This implies that when catch trials are not employed, at least some of the measures in the high tails of the resulting distributions are based on false alarms. Unfortunately, premature "guesses" that a threshold stimulus has appeared will yield inflated scores that reflect undesired response bias rather than "true" contrast sensitivity.

In summary, the top panels of Figure 4 reveal that the two distributions resulting from catch-trial procedures are similar in form (especially for Operator DK), regardless of the trial-to-trial sequence (Blocked Alone versus Uncued Intermixed). Correspondingly, the distributions generated from these same two conditions without catch trials are also similar to one another (especially for Operator BH), but are generally different in form from their counterparts in which catch trials were used. Accordingly, the lower panels in Figure 4 portray a summarized version of the data presented in the upper panels; specifically, the two distributions with catch trials are collapsed for each operator, as are the two distributions with

no catches. Both distributions in the lower panel are gamma in form, with differing degrees of kurtosis and positive skewness. As noted previously, this suggests that the processes or events which underlie each distribution are similar, most likely because the same psychophysical method (increasing contrast) was used in all phases of this research. But it is equally apparent that the no-catches distributions for both operators exhibit larger means, variances, and skewness. This points to the possibility that one or more of the component sensory and response processes is behaving differently when catch trials are employed.

C. Convolution Analysis. The next step in this investigation was to identify and separate the component processes that characterize the difference between the catches and the no-catches distributions shown in the bottom panels of Figure 4. The convolution method employed for this task was the Z transform method[17] which is often associated with linear systems identification in engineering.[18,19] This approach incorporates the idea that an observed distribution (e.g., the All No Catches distribution) is often the convolution of a known distribution (e.g., the All Catches distribution) and another theoretical process (e.g., a "false alarm" or response bias component) for which one seeks to identify a model. Conceptually, convolution methods are similar to ordinary subtractive procedures except that the former involve the deconvolution (or "subtraction") of entire distributions rather than just measures of central tendency. Examples of the application of linear systems identification to the analysis of reaction-time distributions,[15,20] distributions of weapon-delivery measures,[21] and contrast threshold distributions[3]

are provided elsewhere.

Using the Z transform method of convolution, a model of the difference between the All Catches and the All No Catches distributions in Figure 4 was obtained by deconvolving the former distribution from the latter distribution for each operator. The resulting difference models are shown in the lower panels of Figure 5. The catches and the no-catches distributions that are plotted as solid lines in the top panels of Figure 5 are the same as the ones in the lower panels of Figure 4. The difference model selected by the convolution method for each operator was also the one whose reconvolution with the catches distribution gave the closest approximation to the no-catches distribution from which it was identified. This reconvolution is the distribution composed of a long-dashed line for each operator, as seen in the top panels of Figure 5. Although tests for goodness of fit were not made, the fits are obviously quite good, which supports the idea that the models describe a linear, additive component that accounts for the difference between the catch trial and the no-catch trial measures obtained in Experiment 2. Finally, it is to be noted the difference models in the bottom panels of Figure 5 are remarkably similar for each operator, despite subtle differences in the forms of DK and BH's observed distributions (top panels) from which each operator's model was identified.

V. THEORETICAL ANALYSIS AND GENERAL DISCUSSION

One basic premise in this analysis is that signal detection and response initiation are the two component stages that govern threshold contrast sensitivity measurements. It follows that observed distributions of contrast sensitivity measures represent a convolution of

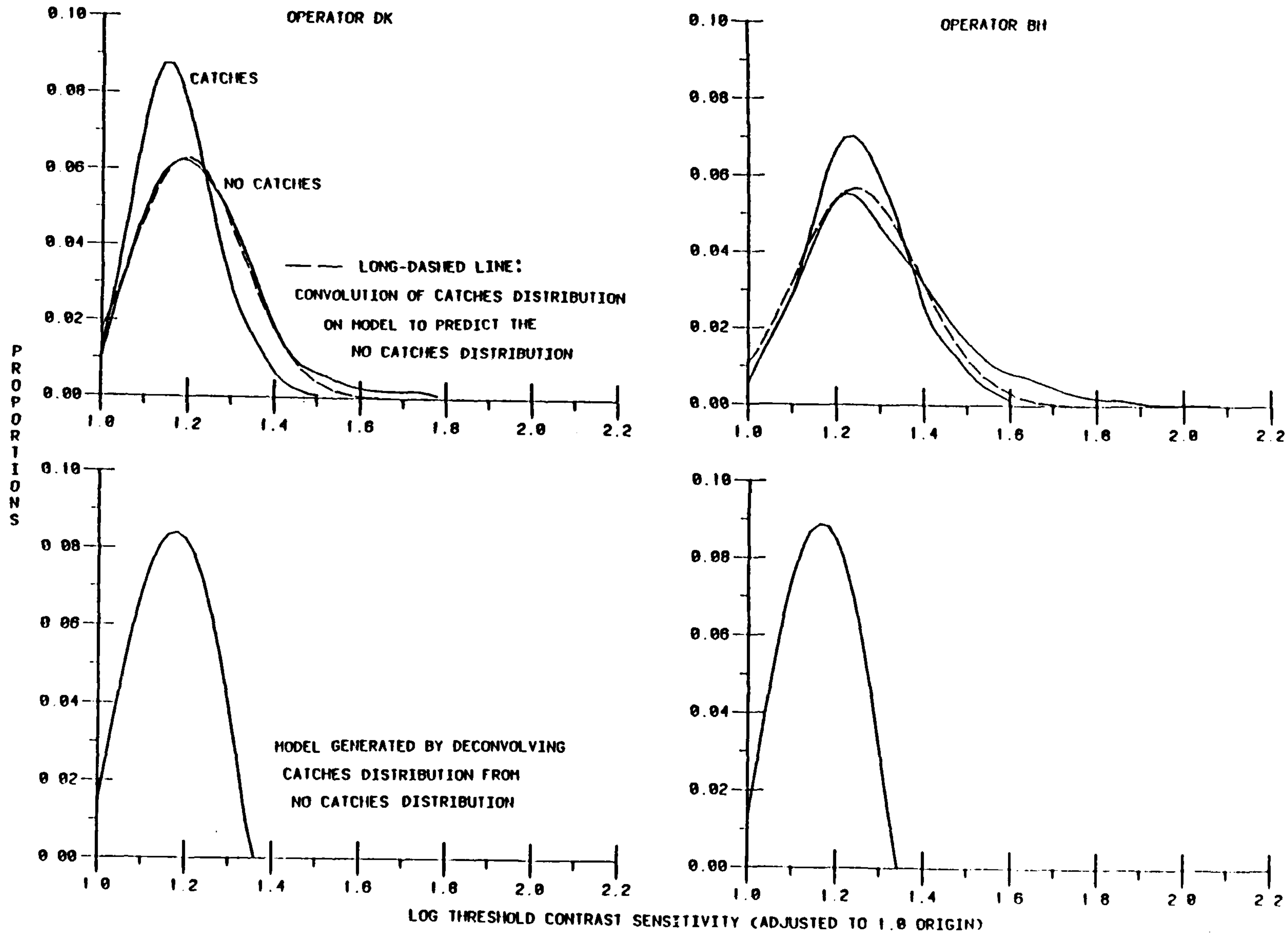

Figure 5. Difference models resulting from the convolution procedures (See text for explanation)

the densities of two component random variables, one of which represents the sensory-detection process and the other having to do with executing the correct response. Conceptually, this approach is derived from the theory of signal detectability (TSD), which holds that an operator is both a sensor and a decision maker. In the present context, TSD implies that the evaluation of contrast threshold measurements requires an independent assessment of the operator's sensory sensitivity, d', and response criterion, β.[22,23] Moreover, TSD assumes that d' and β are independent aspects of task performance, and are selectively influenced by different factors. With respect to contrast sensitivity thresholds, the luminance contrasts on the video screen determined d', whereas β was based on the operator's particular strategy in responding to task demands. Accordingly, the distributions of contrast sensitivity measures should also reflect the behavior of both sensory mechanisms (d') and a response process (β). In other words, the distributions shown in Figures 2, 4, and the top panels of Figure 5 are a composite of two component densities, d' and β, each of which is an independent random variable.

An important assumption in this analysis was that the sensory-detection, or d' component, remained constant in all of the conditions employed in the present experiments. This is because the same six spatial frequencies, the same fixed rate of signal generation (4 dB per second), and the same display-screen luminance and viewing conditions were held constant throughout all of the cueing and catch-trial conditions. In other words, the differences in the forms of the distributions shown in Figures 2 and 5 are attributable to

corresponding differences in each operator's response density (β), since the sensory-detection (d') component for a given operator should retain its distributional form across the various experimental conditions. Thus, cueing conditions and catch trials have selective influence on an operator's response criterion, while the sensory-detection process "holds still" across conditions. It follows that the models depicted in Figure 5 represent a characteristic of the response process that is apparent when no catch trials are used; i.e., the model densities reflect changes in the response stage that are evident when catch-trial measures are separated (deconvolved) from distributions of no-catch measures. This interpretation does not imply that the catches distributions in Figure 5 do not contain a response stage; rather, it simply holds that the no-catches distributions contain a larger, or perhaps different response component.

One manner of conceptualizing the events that underlie the gamma, or possibly normally distributed response-component models for each operator is to assume that the output of the signal detection process is characterized by a flow of neural impulses that is fed into the response mechanism. The response process is triggered (i.e., a response is initiated) when the cumulative impulse count reaches some threshold value that is equivalent to the response criterion. This criterion value depends on the operator's strategy; if the task calls for a conservative criterion, as when catch trials are utilized, the criterion count of impulses is larger than when catch trials are not employed. Of course, a higher or more conservative criterion results in lower contrast sensitivity scores, whereas a lower or relatively liberal criterion yields higher contrast

threshold measures. Larger impulse counts also imply that more "neural" information must accrue before the operator is satisfied that a threshold stimulus is actually present; i.e., responding will not result in a false alarm. This interpretation is particularly compelling when one serves as an operator in the conditions that contain catch trials. Even though both operators in Experiment 2 were highly experienced in conditions without catch trials, and were subjectively certain that responses were not being made until a stimulus was actually detected, both DK and BH were surprised to discover that they were getting "caught" on several trials in each block when they first began practicing in conditions that contained catch trials. By gradually "shaping," that is, raising their response criterion during subsequent practice sessions, both operators experienced an almost abrupt point at which false alarms no longer occurred. This more conservative response strategy was then maintained throughout actual data collection in the catch-trial conditions, and it is noteworthy that neither operator made an error (responding on a blank trial) after the necessary criterion adjustment was made.

Assuming that the models in Figure 5 form gamma distributions, a gamma random variable allows one to make some fairly precise estimates of the number of hypothetical events that characterize these models. Clearly, there is observed trial-to-trial variability in the actual contrast threshold measures that are recorded throughout an experiment. If one assumes that (a) this variation in the measures is due in part to the variability in the rate at which neural impulses accumulate in the response mechanism, and (b) this variability can be described by a Poisson probability distribution,[24] it follows that

AD-A166 177 UNITED STATES AIR FORCE SUMMER FACULTY RESEARCH PROGRAM 09/15
1985 TECHNICAL RE..(U) UNIVERSAL ENERGY SYSTEMS INC
DAYTON OH R C DARRAH ET AL. DEC 85 AFOSR-TR-86-0140
UNCLASSIFIED F49620-85-C-0013 F/G 5/1 NL

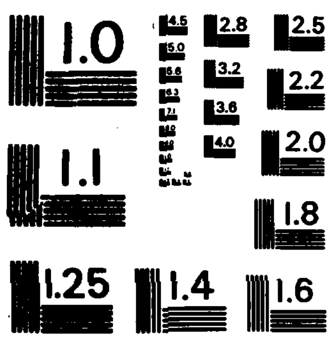

MICROCOPY RESOLUTION TEST CHART
NATIONAL BUREAU OF STANDARDS-1963-A

the trial-to-trial variability in the response process for an operator with a fixed criterion (set number of "required" impulses) should form a gamma distribution with parameters λ (average impulse rate) and n (criterion impulse count). These parameters can be calculated from the models in Figure 5, since it is known that n/λ = mean of the contrast sensitivity distributions, and $n/\lambda^2 = SD^2$. By squaring both sides of the former equality, we get $n^2/\lambda^2 = \text{mean}^2$, and by substitution and reducing to lowest terms, we obtain $n = \text{mean}^2/SD^2$. In Figure 5, the models have a mean value of 1.1686 and 1.1615 for DK and BH, respectively, and corresponding SD values of .0876 and .0818. When the digit to the left of the decimal point of the mean values is dropped in order to allow comparison of the mean and SD values on the same scale, the criterion count of impulses, as calculated by the formula $n = \text{mean}^2/SD^2$, is 3.7 and 3.9 for DK and BH, respectively. In other words, the response models obtained from the deconvolution method indicates that both operators required an average of about four additional neural impulses in order to decide that a response should be initiated when catch trials were included in the sequence. It should be emphasized that these four impulses are to be regarded as an average increase in the criterion count that resulted from the use of catch trials in comparison with no-catch trial procedures. That is, the catch trial conditions resulted in an increase of about four neural events that were needed to reach the adjusted response criterion. The estimated <u>total</u> number of these hypothetical impulses awaits future research that also identifies the response model in no-catch distributions.

VI. SUMMARY AND CONCLUSIONS

The contrast sensitivity functions obtained in Experiment 1 revealed no differences among the cueing conditions that were employed. These results appear to conflict with those reported by Davis et al.[8] who found that predictable (cued or blocked) stimulus presentations resulted in lower contrast thresholds. The discrepancy between the outcomes of the present Experiment 1 and Davis et al.'s study can probably be attributed to methodological differences. As noted previously, Davis et al. used a temporal, forced-choice procedure to measure threshold detections, whereas the present research employed the method of increasing contrast. On the one hand, since the former method plots per cent correct as the dependent variable, the incidence of "false positives" is simply 1 - % correct; these data showed that all subjects performed worse in the Uncued Intermixed condition. On the other hand, the latter method records the same detection response on every trial and provides no obvious way to determine incorrect (false alarm) responses; the resulting CSFs showed no differences among conditions. Although the present operators were unaware of differential response strategies in the three conditions, there was no objective way of determining whether all three operators were making the same response criterion adjustments in the Uncued Intermixed condition that resulted in equivalent CSFs across operators and conditions. Regardless of these considerations, and differences in methodology and results notwithstanding, both investigations provide support for the idea that an observer can monitor a wide range of spatial frequency channels simultaneously.

In particular, the present results indicate that the operator performed just as well when a particular frequency could be predicted as when it could not. Thus, if attention was allocated to one expected channel (cued or blocked conditions), or was divided among all six channels (uncued intermixed), the overall form of the CSFs remained unchanged.

The main purpose of Experiment 2 was to control for false alarm responses by introducing catch trials into the stimulus sequence. In effect, this experiment allowed an evaluation of both stimulus uncertainty (blocked versus intermixed frequencies) and event uncertainty (catch versus no-catch trials) in the same factorial design. As predicted, event uncertainty resulted in an overall lowering of the CSF, but the effect was most obvious when it occurred in conjunction with stimulus uncertainty (i.e., the Uncued Intermixed/Catches condition). However, a serendipitous outcome of Experiment 2 was the tendency for the CSFs to converge at 0.5 cycles per degree, the lowest spatial frequency. One possible interpretation of this finding is that the signal detection process at very low frequencies behaves differently than detection at the wider range of higher spatial frequencies. In this vein, a reaction-time experiment by Tolhurst[10] revealed that the detection of a low frequency signal (0.2 cycles per degree) was relatively sudden, as indicated by a reaction-time distribution whose peak was sharply bounded from below, and quite close to actual stimulus onset. Tolhurst also found that reaction times to a higher spatial frequency (3.5 cycles per degree) had a considerably longer time delay from stimulus onset, and these distributions were less peaked and more variable. The point is that

low-frequency threshold stimuli, when they become visible, produce such a transient change in the signal detector that both stimulus and event uncertainty are less influential on the response process. In contrast, the responses to higher spatial frequencies are determined by the activity of channel detectors that are relatively inert, last longer, and therefore require more analysis by a response system that is governed, at least in part, by stimulus uncertainty. These conclusions receive a degree of support from the subjective accounts of Operators DK and BH, both of whom noticed that whenever the low frequency signal (0.5 cycles per degree) appeared on the screen, regardless of the cueing or catch-trial condition in progress, the compelling experience was that "I definitely could not have pressed the button sooner...the signal appeared too suddenly." However, upon detection of any stimulus between 1.0 and 22.8 cycles per degree, the feeling was that "I might have been able to press the response button earlier and still be correct."

In summary, the CSFs obtained in both Experiments 1 and 2 lend support to a version of multichannel theory in which it is assumed that a fairly wide range of spatial frequency channels can be monitored simultaneously. Furthermore, the evidence provides support for Tolhurst's conclusion that the neural activity in low frequency channels is qualitatively different from the processing that occurs in channels at higher spatial frequencies.

Finally, at the outset of this research it was proposed that contrast threshold measures are influenced by a combination of sensory sensitivity and false alarm bias. The identification of these two components was considered important because "true" contrast

sensitivity, free of response bias, is the variable of importance in studies of this nature. Accordingly, in addition to the more traditional evaluation of CSFs, the present investigation included an analysis of the distributions of contrast threshold measures. The outcome of the convolution methods revealed that stimulus uncertainty, as manipulated by cueing procedures and catch-trial conditions, has a selective influence on the response stage in the contrast threshold process. Although these conclusions are theoretical in nature, they should prove useful in future analyses of the sensory and response processes that are essential components in the contrast threshold task.

VII. RECOMMENDATIONS

What is the recommended method for obtaining contrast sensitivity thresholds? Stated simply, it depends on one's purposes in collecting data. On the one hand, if the goal is to construct theories of the sensory and response components that underlie threshold measurements, experimental designs should include variables that have selective influence on these component stages. On the other hand, if one has a more practical need to obtain measures that are relatively free of false-alarm bias, it is recommended that the method of increasing contrast be used to generate CSFs, provided that both stimulus uncertainty (i.e., a random series of spatial frequencies) and event uncertainty (use of catch trials) are included in the trial sequence.

Assuming that both theoretical and practical goals can be pursued in a properly designed investigation, an important implication is that the resulting measures would serve as a better

predictor of the contrast sensitivity required in other tasks, such as the detection and identification of approaching aircraft, in which precise visual resolution is essential. That is, when the response bias in contrast sensitivity measures is reduced, either by experimental design or analytic methods, better prediction should result. This is because the response bias in a specific predictor task (e.g., threshold determinations) will not necessarily correlate with the unique response bias in a criterion task (e.g., identifying approaching aircraft). Accordingly, two related lines of research are recommended at this juncture, one of which would deal with continued research on the contrast sensitivity process itself, and the other having to do with using the measure as a predictor in an applied setting.

A. Research on Contrast Sensitivity Processes. There are a number of experimental and analytic procedures which can be proposed based on the present investigation; only two are mentioned here.

1. Perform sensory-detection analyses at different spatial frequencies. In the present research, special emphasis was placed on the theoretical analysis of the variables that are thought to have selective influence on the response bias component (i.e., cueing conditions and catch-trial methods). An analysis of the sensory-detection process at each spatial frequency was not attempted, since the data were collapsed across frequencies to yield a common origin necessary for convolution methods. However, if it is assumed that spatial frequency influences the sensory-detection process, the distributions obtained at each frequency could be analyzed separately,

thereby providing insights about the role of spatial frequency in the detection process within each sensory channel.

2. Extend catch-trial procedures to evaluate spatial frequency discrimination. The present research utilized catch trials to reduce the effect of response bias in a threshold detection task; i.e., the presence of any signal was a "go" trial, whereas the absence of a signal was a "catch" trial. An interesting extension of this design would be to program one spatial frequency (e.g., 1.0 cycles per degree) as the go trial, but another adjacent frequency (e.g., 3.0 cycles per degree) as the no-go, catch trial. Thus, a stimulus would appear on every trial, but only a specific spatial frequency would require a response. It is hypothesized that contrast thresholds would be elevated further in this condition, presumably because both detection and discrimination would be required, followed by the usual response process. Convolution methods could then be utilized to identify models of the overall contrast sensitivity process comprised of detection, discrimination, and response stages.

B. Predicting Detection and Discrimination of Approaching Aircraft. During the final week of last summer's research assignment I became interested in using contrast threshold measures to predict an operator's skill in the detection and identification of approaching aircraft. This interest stemmed directly from the work of Ginsburg and his associates,[13,14] who achieved initial success in using contrast thresholds to predict the detection of aircraft in both simulated landings and actual field performance. In this vein, a proposed investigation is to mount a camera on a helicopter and fly

directly toward a ground target at a known speed while taking motion pictures of the target object. Different targets could be utilized, and the resulting tapes could be played on a video screen at different speeds to simulate "approaches" to a target. The advantage is that the display could then be utilized in a controlled laboratory setting for convenient testing of a number of individuals.

The feasibility of this project became more realistic when it was determined that the Media Lab at AFHRL, Williams AFB, has already obtained some excellent aerial footage using a chartered helicopter and an assembled helicopter camera mount. Thus, obtaining quality tapes of approaches to a variety of actual ground targets is a reasonable endeavor. Subsequent design and construction of operator response devices that are synchronized with actual footage of these approaches would yield dependent variables such as detection distance and recognition distance for different targets. The correlation of contrast sensitivity measures at different spatial frequencies with these criterion variables could yield more valid indicators of pilot trainees' effective visual acuity.

REFERENCES

1. R. Sekuler and R. Blake, Perception, New York, Knopf, 1985.
2. J. P. Thomas, "Spatial Resolution and Spatial Interaction," in E. C. Carterette and M. P. Friedman (Eds.), Handbook of Perception V, New York, Academic Press, 1975.
3. D. L. Kohfeld, "An Evaluation of Visual Contrast Sensitivity Measures, " in R. E. Eberts and C. G. Eberts (Eds.), Trends in Ergonomics/Human Factors II, North-Holland, Elsevier, 1985.
4. R. Sekuler and P. Tynan, "Rapid Measurement of Contrast-Sensitivity Functions," American Journal of Optometry & Physiological Optics, Vol. 54, pp. 573-575, 1977.
5. A. P. Ginsburg and M. W. Cannon, "Comparison of Three Methods for Rapid Determination of Threshold Contrast Sensitivity," Investigative Ophthalmology & Visual Science, Vol. 24, pp. 798-802, 1983.
6. F. W. Campbell and J. G. Robson, "Application of Fourier Analysis to the Visibility of Gratings," Journal of Physiology, Vol. 197, pp. 551-566, 1968.
7. M. Georgeson, "Spatial Fourier Analysis and Human Vision," in N. S. Sutherland (Ed.), Tutorial Essays in Psychology: A Guide to Recent Advances. Vol. 2, Hillsdale, N. J., Erlbaum, 1979.
8. E. T. Davis, P. Kramer, and N. Graham, "Uncertainty about Spatial Frequency, Spatial Position, or Contrast of Visual Patterns," Perception and Psychophysics, Vol. 33, pp. 20-28, 1983.
9. R. L. DeValois and K. K. DeValois, "Spatial Vision," Annual Review of Psychology, Vol. 31, pp. 309-341, 1980.

10. D. J. Tolhurst, "Reaction Time in the Detection of Gratings by Human Observers: A Probabilistic Mechanism," Vision Research, Vol. 15, pp. 1143-1149, 1975.

11. D. Yager, P. Kramer, M. Shaw, and N. Graham, "Detection and Identification of Spatial Frequency: Models and Data, " Vision Research, Vol. 24, pp. 1021-1035.

12. A. P. Ginsburg, "Spatial Filtering and Vision: Implications for Normal and Abnormal Vision," in J. A. Proenza, J. M. Enoch, and A. Jampolsky (Eds.), Clinical Applications of Visual Psychophysics, New York, Cambridge University Press, 1981.

13. A. P. Ginsburg, D. W. Evans, R. Sekuler, and S. A. Harp, "Contrast Sensitivity Predicts Pilots' Performance in Aircraft Simulators," American Journal of Optometry and Physiological Optics, Vol. 59, pp. 105-109, 1982.

14. A. P. Ginsburg, J. Easterly, and D. W. Evans, "Contrast Sensitivity Predicts Target Detection Field Performance of Pilots," Proceedings of the Human Factors Society, 27th Annual Meeting, Norfolk, Virginia, 1983.

15. D. L. Kohfeld, J. L. Santee, and N. D. Wallace, "Loudness and Reaction Time: II. Identification of Detection Components at Different Intensities and Frequencies," Perception and Psychophysics, Vol. 29, pp. 550-562, 1981.

16. D. L. Kohfeld, "Simple Reaction Time as a Function of Stimulus Intensity in Decibels of Light and Sound," Journal of Experimental Psychology, Vol. 88, pp. 251-257, 1971.

17. E. I. Jury, Theory and Application of the Z-Transform Method, Harrington, New York, Krieger, 1964.

18. T. C. Hsia, System Identification: Least Squares Methods, Lexington, Massachusetts, Heath, 1977.

19. A. P. Sage and J. L. Melsea, System Identification, New York, Academic Press, 1971.

20. D. L. Kohfeld, "Sensory-Detection Models of Auditory and Visual Reaction Time Processes," Paper Presented at the 17th Annual Meeting of the Society for Mathematical Psychology, Chicago, Illinois, August, 1984.

21. R. T. Nulimeyer and D. L. Kohfeld, "Analysis of B-52 Weapon Delivery Accuracy," Proceedings of the Annual Science and Engineering Symposium, Air Force Command and Naval Materiel Command, Wright-Patterson Air Force Base, Ohio, 1981.

22. D. M. Green and J. A. Swets, Signal Detection Theory and Psychophysics, New York, Wiley, 1966.

23. W. N. Dember and J. S. Warm, Psychology of Perception (2nd Edition), New York, Holt, Rinehart and Winston, 1979.

24. F. Restle, Psychology of Judgment and Choice, New York, Wiley, 1961.

APPENDIX 1

Program Listings for Optronix Model 200 Vision Tester

Cueing and Catch-Trial Conditions in Experiments 1 and 2

Prepared by

Brian C. Hayes

LISTING FOR CONTRAST SENSITIVITY MEASUREMENT

STANDARD PROGRAM

PRESENTS A TOTAL OF 72 TRIALS, THE FIRST AS A WARM-UP TRIALS, THE OTHERS AS ONE OF SIX SPATIAL FREQUENCIES, RANDOMLY SELECTED.

OPTIONS AVAILABLE:

CUED CONDITION: A PREVIEW OF THE PATTERN IS DISPLAYED BEFORE EACH TRIAL

CATCH TRIALS: CATCH TRIALS RANDOMLY PRESENTED AT A PROBABILITY OF .25.

```
100  DIM A$(5),A(5)
105  FOR I=0 TO 5:READ A$(I):NEXT
106  FOR I=0 TO 5:READ A(I):NEXT
110  DATA "0.5","1.0","3.0","6.0","11.4","22.8"
112  DATA 718,1436,4308,8616,16732,32744
115  DATA 1,1,22.8,3,.5,3,11.4,11.4
120  DATA 1,3,6,3,22.8,6,.5,22.8,1
125  DATA 11.4,6,6,22.8,.5,.5,6,1,6
130  DATA 11.4,22.8,22.8,11.4,.5,11.4
135  DATA 3,3,1,.5,1,3,22.8,6,1,6
140  DATA 22.8,22.8,3,11.4,11.4,.5
145  DATA 1,22.8,11.4,3,1,.5,3,6
150  DATA .5,.5,6,6,11.4,1,11.4,22.8
155  DATA .5,11.4,6,3,3,.5,22.8,1,1
156  DATA 999

160  POKE 16629,0:POKE 42001,0
165  POKE 3,108:POKE 5,208
170  POKE 4,23:A=USR(0)
175  POKE 16393,60:POKE 4,29:A=USR(0)
180  POKE 36566,0:POKE 36568,0:POKE 36570...

200  A$="*********************":L$="--------------------"
220  INPUT"MESSAGE";A$:PRINT!A$
230  INPUT"SEED";A:A=RND(-(A))
235  I=PEEK(16629):IF I THEN 400
240  A=120:B=16394:GOSUB 1200
250  POKE 16396,INT(1092.2667/30)
260  A=65535:B=65:GOSUB1200
270  POKE16397,1
280  POKE 4,3:A=USR(2)
285  POKE 4,5:A=USR(0)
295  INPUT"CATCH TRIALS";A$
297  IF LEFT$(A$,1) <> "Y" THEN POKE 16630,0:GOTO 300
299  POKE 16630,1:PRINT!"CATCH TRIALS"
```

```
300  INPUT"CUED CONDITION";A$:IF LEFT$(A$,1) <> "Y" THEN 320
310  POKE 16628,1:PRINT!"CUED CONDITION":GOTO 400
320  POKE 16628,0:PRINT!"NON-CUED CONDITION"

400  INPUT"READY TO BEGIN";A$
420  FOR I=16631 TO 16931:POKE I,0:NEXT
425  POKE 16887,9:POKE 16888,73
430  FOR I=55 TO 69:POKE I,0:NEXT
440  READ A:IF A=999 THEN 900
445  IF A=.5 THEN W=0:GOTO 500
450  IF A=1 THEN W=1:GOTO 500
455  IF A=3 THEN W=2:GOTO 500
460  IF A=6 THEN W=3:GOTO 500
465  IF A=11.4 THEN W=4:GOTO 500
470  IF A=22.8 THEN W=5:GOTO 500
480  PRINT!"ERROR IN DATA";A:GOTO 999
500  GOSUB 1800:B=57:GOSUB 1200
505  POKE 16886,W
510  IF PEEK(16628) THEN GOSUB 1600
520  IF PEEK(16631) THEN A=0:B=57:GOSUB 1200
530  A=0*RND(1):B=65:GOSUB 1200
540  A=255:GOSUB 1700
550  POKE 4,17:A=USR(1305)
560  PRINT PEEK(16639);" <DEL> TO END"
570  POKE 4,11:A=USR(0)
580  POKE 4,17:A=USR(1305)
584  IF PEEK(16631)=0 THEN 590
585  POKE 16896+PEEK(16895),PEEK(16639)
587  POKE 16914+PEEK(16895),PEEK(16886)
588  POKE 16895,PEEK(16895)+1
590  IF ((PEEK(16392) AND 2)=0) THEN 660
600  INPUT"STOP OR REPEAT";A$
610  IF LEFT$(A$,1) = "S" THEN PRINT!"TERMINATED":GOTO 999
620  IF LEFT$(A$,1) <> "R" THEN INPUT"S OR R";A$:GOTO 610
650  PRINT!"REPEAT TRIAL #";PEEK(16639):GOTO 530
660  POKE 16639,PEEK(16639)+1
662  IF PEEK(16639)=1 THEN 430
665  IF PEEK(16631) THEN GOSUB 1900:GOTO 730
670  POKE 16880+W,PEEK(16880+W)+1
680  B=16640+W*40+(PEEK(16880+W)*2-2)
720  POKE B,PEEK(17792):POKE B+1,PEEK(17793)
730  IF PEEK(16639)<=PEEK(16888) THEN 430

900  Y=PEEK(16887)-1:D=0:F=D:G=D:H=D:K=D:L=D
910  PRINT!L$
920  FOR J=16640 TO 16840 STEP 40
930  FOR I=0 TO Y*2 STEP 2:K=K+1
935  A=PEEK(J+I)+256*PEEK(J+I+1)
940  A=(A^2*.5)/65535^2:IF A=0 THEN A=10^-10
945  E=LOG(A)/LOG(10):A=E:B=2:GOSUB 1100:E=A
950  IF I=0 THEN PRINT!"SPATIAL FREQ=";A$(L):PRINT!" "
955  PRINT!SPC(3-LEN(STR$(K)));K;TAB(7);E
960  H=H+E:D=D+E^2:NEXT I
965  F=H/K:A=F:B=3:GOSUB 1100:PRINT!" MEAN=";A
```

```
970  G=D/K-F^2:IF G<0 THEN G=0
975  A=SQR(G):B=3:GOSUB 1100:PRINT!" S.D.=";A
980  F=1/EXP(F*LOG(10)):A=F:B=1:GOSUB 1100
985  PRINT!"SENSITIVITY=";A:PRINT!L$
990  D=0:F=D:G=D:H=D:K=D:L=L+1:NEXT J
995  IF PEEK(16630) THEN GOSUB 2000
999  PRINT!"END OF SESSION":END

1100 A=A*10^B
1105 A=INT(A)-(SGN(A-INT(A)-.5)>1)
1110 A=A/10^B
1120 IF LEN(STR$(A))<10 THEN RETURN
1130 C=1+2*(MID$(STR$(A),10,1)<"5")
1140 A=A+C*10^-(B+1):GOTO 1120

1200 IF A>65535 THEN A=65535
1210 IF A<0 THEN A=0
1220 POKE B,INT(A-356*INT(A/256))
1230 POKE B+1,INT(A/256):RETURN

1600 A=65535:B=65:GOSUB 1200
1610 A=255:GOSUB 1700:GOSUB 1750
1620 PRINT:PRINT SPC(6);"PREVIEW":POKE 4,13:A=USR(0)
1630 GOSUB 1750:A=200:GOSUB 1710:RETURN

1700 PRINT:PRINT SPC(7);"PAUSING"
1710 POKE 4,19:A=USR(A):RETURN

1750 POKE 4,17:A=USR(1034):A=10:GOSUB 1710
1760 POKE 4,17:A=USR(1034):RETURN

1800 POKE 16631,0
1805 IF PEEK(16630)=0 THEN RETURN
1810 IF JJ=1 THEN RETURN
1820 IF PEEK(16889+W)>2 THEN RETURN
1830 IF PEEK(16632)=3 THEN POKE 16632,0:RETURN
1840 R=INT((3-1)*RND(1)-1)
1850 IF R=0 THEN RETURN
1860 POKE16631,1:POKE 16632.PEEK(16632)+1
1870 POKE 16889+W.PEEK(16889+W)+1
1880 RETURN

1900 IF(PEEK(36866) AND 48) THEN RETURN
1910 POKE 16633+W,PEEK(16633+W)+1:RETURN

2000 PRINT!"FALSE ALARM HISTORY":PRINT!" "
2010 PRINT!TAB(3);"S.F.";TAB(10);"#FA'S"
2020 PRINT!TAB(2);"-------";TAB(9);"-------"
2030 FOR I=0 TO 5:PRINT!TAB(3);A$(I);TAB(12);PEEK(16633+I)
2040 K=K+PEEK(16633+I):NEXT
2050 PRINT!" ":PRINT!TAB(2);"TOTAL";TAB(14-LEN(STR$*K));K
2060 PRINT!L$:RETURN
```

MEMORY MAP FOR CONTRAST SENSITIVITY MEASUREMENT

LOCATIONS USED BY ALL CS SERIES PROGRAMS

16628	CUE MODE INDICATOR
16629	REPEAT TEST INDICATOR
16630	CATCH MODE INDICATOR
16631	CATCH ON CURRENT TRIAL INDICATOR
16632	CATCH HISTORY (PAST THREE TRIALS)
16633-16638	COUNTERS: NO. FALSE ALARMS PER SPATIAL FREQUENCY
16639	CURRENT TRIAL NUMBER
16640-16679	RESPONSE CONTRAST BUFFER: 0.5 CYCLES/DEGREE
16680-16719	RESPONSE CONTRAST BUFFER: 1.0 CYCLES/DEGREE
16720-16759	RESPONSE CONTRAST BUFFER: 3.0 CYCLES/DEGREE
16760-16799	RESPONSE CONTRAST BUFFER: 6.0 CYCLES/DEGREE
16800-16839	RESPONSE CONTRAST BUFFER: 11.4 CYCLES/DEGREE
16840-16879	RESPONSE CONTRAST BUFFER: 22.8 CYCLES/DEGREE
16880-16885	COUNTERS: NO. TRIALS PER SPATIAL FREQUENCY
16886	CODE FOR SPATIAL FREQUENCY ('W' IN PROGRAMS)
16887	CONSTANT: NO. TRIALS PER SPATIAL FREQUENCY
16888	CONSTANT: TOTAL NUMBER OF TRIALS PER SESSION
16889-16894	COUNTERS: NO. CATCH TRIALS PER SPATIAL FREQUENCY
16895	COUNTER: TOTAL NUMBER OF CATCH TRIALS
16896-16913	BUFFER: TRIAL NUMBERS ON WHICH CATCH TRIALS OCCURRED
16914-16931	BUFFER: SPATIAL FREQUENCY CODES FOR CATCH TRIALS

NOTES:

1. FOR ALL INDICATORS: 1=ON 0=OFF

2. VALUES IN RESPONSE CONTRAST BUFFERS ARE REPRESENTED IN TWO-BYTE, LSB-MSB FORMAT

3. CODES FOR SPATIAL FREQUENCIES:

0 = 0.5 CYCLES/DEGREE	3 = 6.0 CYCLES/DEGREE
1 = 1.0 CYCLES/DEGREE	4 = 11.4 CYCLES/DEGREE
2 = 3.0 CYCLES/DEGREE	5 = 22.8 CYCLES/DEGREE

THESE CODES ALSO SERVE AS POINTERS TO THE VARIOUS BUFFERS AND COUNTERS.

1985 USAF-UES SUMMER FACULTY RESEARCH PROGRAM/

GRADUATE STUDENT SUMMER SUPPORT PROGRAM

Sponsored by the

AIR FORCE OFFICE OF SCIENTIFIC RESEARCH

Conducted by the

UNIVERSAL ENERGY SYSTEMS, INC.

FINAL REPORT

The Multi-Weapon Multi-Target Multi-Phase Assignment Problem

Prepared by:	Stephan E. Kolitz
Academic Rank:	Assistant Professor
Department and University:	Management Sciences Dept. University of Massachusetts/Boston
Research Location:	ESD/XR-1
USAF Research:	John Kattar
Date:	Sept 22, 1985
Contract No:	F49620-85-C-0013

The Multi-Weapon Multi-Target Multi-Phase

Assignment Problem

by

Stephan E. Kolitz

ABSTRACT

In the Strategic Defense Initiative Battle Management and Command, Control, and Communications (SDI BM/C^3), one of the problems that arises is the multi-weapon, multi-target, multi-phase assignment problem. Weapon platforms are satellites in orbit containing kinetic kill vehicles (projectiles) which can be sent to targets (boosters/missiles). A given weapon platform's projectiles have a known probability of hitting any particular target. A ballistic missile's trajectory is typically described as consisting of four phases; three phases are studied here: boost, post-boost, and midcourse. This assignment problem can be formulated as a large-scale non-linear integer programming problem. While no feasible exact solution technique was developed, efficient near-optimal algorithms have been found.

ACKNOWLEDGEMENTS

I would like to acknowledge the support and assistance of the Air Force Systems Command, Air Force Office of Scientific Research and ESD/XR-1. Without their support, this research would not have been possible.

In particular, there were a number of individuals who were extremely helpful to me and to whom I owe great thanks. In ESD/XR-1, Mr. George Richardson provided excellent logistical assistance and advice, Capt. Dan Cvelbar gave me an excellent military perspective on my research, and Lt. Keith Heien provided absolutely necessary assistance with computer hardware and software.

Lt. Col. Ted Mervosh, made it possible for me to enrich my own professional background, thereby simultaneously benefitting the project. Lt. Col. Richard Paul showed a great willingness to listen to my comments and concerns, in the midst of his extremely busy schedule, providing strong support and encouragement to me.

In the MITRE Corporation, I would like to thank Mr. Burt Noyes, who willingly shared his vast experience and expertise, and Mr. John Kattar, my collaborator in this research, whose analytical and programming skills were in no small part instrumental to the success of this project.

Finally, I would like to thank Mr. Gary Grann of ESD/XR, my Effort Focal Point, whose overall guidance and assistance was critical to the project's success, and who helped make this summer's project a genuine learning experience for me.

I. INTRODUCTION

In the Strategic Defense Initiative Battle Management and Command, Control, and Communications (SDI BM/C^3), one of the problems that arises is the multi-weapon, multi-target, multi-phase assignment problem. Weapon platforms are satellites in orbit containing kinetic kill vehicles (projectiles) which can be sent to targets (boosters/missiles). A given weapon platform's projectiles have a known probability of hitting any particular booster. A ballistic missile's trajectory is typically described as consisting of four phases; three phases are studied here: boost, post-boost, and midcourse. Boost phase is defined to be the phase during which the target is firing its rocket motors. Post-boost is the phase after boost in which the post-boost vehicle (target) releases reentry vehicles. Midcourse phase starts when the reentry vehicle has left the post-boost vehicle and ends when the reentry vehicle enters the atmosphere. This assignment problem can be formulated as a large-scale non-linear integer programming problem. While no feasible exact solution technique was developed, good near-optimal algorithms have been found. This type of problem can be studied using operations research techniques. The author's graduate education was in operations research, providing a good match between the problem and the author's background.

II. OBJECTIVES OF THE RESEARCH EFFORT

The objectives of the research effort were to assist in the development

of efficient algorithms for weapon assignment in the boost phase, and to develop efficient algorithms for weapon assignment across the first three phases (boost, post-boost, and midcourse). Operations research techniques and methodology were used to meet these research objectives.

III. BOOST PHASE ALGORITHM I

Let

$x(k,j)$ = the number of projectiles sent from weapon platform k and aimed at booster j,

$p(k,j)$ = the maximum (over time from now) probability of hitting booster j with a projectile sent from weapon platform k,

$a(k)$ = the number of available projectiles on weapon platform k,

$v(j)$ = the initial value of booster j,

n = the number of targets(boosters), and

m = the number of weapon platforms.

For the time being, let $a(k) = a$ for all weapon platforms.

The probability of booster j surviving is

$$q(j) = \prod_{k=1}^{m} (1 - p(k,j))^{x(k,j)} ,$$

so the expected value of the surviving boosters is

$$E [SBV] = \sum_{j=1}^{n} v(j)q(j).$$

An interesting problem is to

min E [SBV]

subject to

$$\sum_{j=1}^{n} x(k,j) = a$$

$x(k,j) >= 0$ and integer.

In what follows, this problem will be referred to as Problem I. Problem I appeared in Manne [1958], where it was approximated by a transportation problem; it is a non-linear integer programming problem. Complete enumeration would require looking at

$$((a + n - 1)!/a!(n-1)!)^{m}$$

different ways to assign the projectiles to the boosters. See Bogart [1983] page 43. When the problem is large, complete enumeration is clearly out of the question. For example, with 10 weapon platforms, 100 boosters and 10 projectiles per platform, there are approximately 4×10^{130} different ways to assign the projectiles to the boosters.

Let X(s) = a matrix of { x(k,j) } such that

$$\sum_{k=1}^{m} \sum_{j=1}^{n} x(k,j) = s \quad \text{and}$$

$$\sum_{j=1}^{n} x(k,j) <= a.$$

X(s) is a feasible assignment matrix with exactly s projectiles assigned to boosters.

Let P = the matrix of $\{ p(k,j) \}$,

$Q(s)$ = diag ($\{ q(j) \}$) for $\{ x(k,j) \}$ from some $X(s)$,

V = diag ($\{ v(j) \}$), and

$R(s)$ = $PVQ(s)$, consisting of elements

$$\{ \ r(k,j) = p(k,j)v(j)q(j) \ \}.$$

The product $v(j)q(j)$ is the expected value of target j, given $X(s)$. Thus, the element $r(k,j)$ is the expected decrease in booster j's value by sending one additional projectile from weapon platform k.

Let $r(k(s),j(s))$ = maximum (over k and j) of the $r(k,j)$ in $R(s)$ such that

$$\sum_{j=1}^{n} x\,(k(s),j) < a.$$

The best marginal feasible assignment of the next projectile, given the s projectiles already assigned, is from platform $k(s)$ to booster $j(s)$.

<u>Algorithm I</u>

Step 1. Set $s = 0$.

Step 2. Calculate $R(s)$.

Step 3. Find $k(s),j(s)$.

Step 4. Increment $x(k(s),j(s))$ by one, forming $X(s+1)$.

Step 5. Increment s by one, to $s+1$.

Step 6. If $s = a*m$, stop; otherwise go to step 2.

This algorithm first appeared in denBroeder, et.al. [1959]. In this article, it was shown that the algorithm is optimal for Problem I if $p(k,j) = p(j)$ for all k. It is not optimal in the general case, as the following example will illustrate.

$P = \begin{bmatrix} 0.6 & 0.9 \\ 0.0 & 0.7 \end{bmatrix}$ $\quad V = \begin{bmatrix} 1 & 0 \\ 0 & 1 \end{bmatrix}$

$a = 1 \quad m = 2 \quad n = 2$

Step 1. $s = 0$.

Step 2. $R(0) = P$.

Step 3. $k(0) = 1$, $j(0) = 2$

Step 4. $X(1) = \begin{bmatrix} 0 & 1 \\ 0 & 0 \end{bmatrix}$

Step 5. $s = 1$.

Step 6. $1 < 2$; go back to Step 2.

Step 2. $R(1) = \begin{bmatrix} 0.6 & 0.9 \\ 0.0 & 0.7 \end{bmatrix} \begin{bmatrix} 1 & 0 \\ 0 & 1 \end{bmatrix} \begin{bmatrix} 1 & 0 \\ 0 & 0.1 \end{bmatrix}$

$$= \begin{bmatrix} 0.6 & 0.09 \\ 0.0 & 0.07 \end{bmatrix}.$$

Step 3. $k(1) = 2$, $j(1) = 2$ (remembering that it is not feasible to send any more projectiles from weapon platform 1)

Step 4. $X(2) = \begin{bmatrix} 0 & 1 \\ 0 & 1 \end{bmatrix}$ $\quad VQ(2) = \begin{bmatrix} 1 & 0 \\ 0 & 0.03 \end{bmatrix}$

Step 5. $s = 2$.

Step 6. $2 = 2$, so stop.

For this solution $E[SBV] = 1 + (0.1)(0.3) = 1.03$, but

clearly, $X(2) = \begin{bmatrix} 1 & 0 \\ 0 & 1 \end{bmatrix}$ is optimal with $E[SBV] = 0.4 + 0.3 = 0.7$.

Note that since $VQ(s)$ is a diagonal matrix, the eigenvalues are the expected values of the targets, given $X(s)$; thus the trace of $VQ(s)$ is $E[SBV]$.

By doing complete enumeration, the optimal solution can be found for small problems and compared with the solution from Algorithm I. Preliminary empirical evidence suggests that Algorithm I is optimal approximately 80% of the time, and the error made otherwise is less than 5%. In addition to further analytic work on Algorithm I, further systematic running of interesting cases seems to be called for; this would require a great deal of computer time. Also, there appear to be useful modifications of the algorithm which improve performance. Again, this is an open area of research.

IV. BOOST PHASE ALGORITHM II

There is another algorithm which has proved useful in solving Problem I.

Let X(s) = a matrix of { x(k,j) } such that

$$\sum_{k=1}^{m} \sum_{j=1}^{n} x(k,j) = s \quad \text{and}$$

$$\sum_{j=1}^{n} x(k,j) \quad >= a \quad \text{for all } k.$$

X(s) is an assignment of exactly s weapon projectiles to boosters; this assignment is infeasible for a given weapon when the inequality holds, and reaches feasiblity at equality.

Let P^ = { p(k,j)/q(k,j) } and R(s)=P^VQ(s). Let r(k(s),j(s)) = the minimum entry of R(s) such that

$$\sum_{j=1}^{n} x(k(s),j) >= a$$

and $\quad x(\ k(s),j(s)\ ) > 0.$

Elements of R(s) are $p(k,j)*v(j)*q(j)\ /\ q(k,j)$

$$= v(j)*q(j)*(\ 1/q(k,j) - 1\ )$$

$$= -\ v(j)*q(j) + (\ v(j)*q(j)\ /\ q(k,j)\ ).$$

The first term is the negative of the expected value of target j when the s projectiles described by X(s) have been fired. The second term is the expected value of target j if one projectile from weapon k is removed from X(s). Thus element (k,j) of R(s) is the expected increase in target j's value which results from sending one less projectile to it from weapon platform k. The least effective projectile currently sent would be from k(s) to j(s).

Algorithm II

Step 1. Set s

= a * (m * n - the number of zero entries in P).

Step 2. Set X(s) = { a } for all k,j such that p(k,j) >0.

Step 3. Calculate R(s).

Step 4. Find k(s),j(s).

Step 5. Decrease x(k(s),j(s)) by one, forming X(s-1).

Step 6. Decrease s by one to s-1.

Step 7. If s = a * m, stop; otherwise go to Step 3.

Example:

$$P = \begin{bmatrix} 0.6 & 0.9 \\ 0.0 & 0.7 \end{bmatrix} \qquad V = \begin{bmatrix} 1 & 0 \\ 0 & 1 \end{bmatrix} \qquad a = 1,\ m = 2,\ n = 2$$

Step 1. $s = 3$.

Step 2. $X(3) = \begin{bmatrix} 1 & 1 \\ 0 & 1 \end{bmatrix} \qquad Q(3) = \begin{bmatrix} 0.4 & 0.00 \\ 0.0 & 0.03 \end{bmatrix}$

Step 3. $R(3) = P\hat{\ }VQ(3) = \begin{bmatrix} 1.5 & 9.00 \\ 0.0 & 2.33 \end{bmatrix} \begin{bmatrix} 1 & 0 \\ 0 & 1 \end{bmatrix} \begin{bmatrix} 0.4 & 0.00 \\ 0.0 & 0.03 \end{bmatrix}$

$$= \begin{bmatrix} 0.6 & 0.027 \\ 0.0 & 0.700 \end{bmatrix}.$$

Step 4. $k(3) = 1$, $j(3) = 2$ (since weapon platform 2 is already feasible).

Step 5. $X(2) = \begin{bmatrix} 1 & 0 \\ 0 & 1 \end{bmatrix} \qquad Q(2) = \begin{bmatrix} 0.4 & 0.0 \\ 0.0 & 0.3 \end{bmatrix}.$

As noted previously, this is the optimal result. However Algorithm II does not always reach the optimal solution. Based on preliminary empirical results, the performance of Algorithm II is somewhat inferior to Algorithm I in general. It is clearly slower to run; in addition, when some of the p(k,j)'s are close to one, computations necessary to find the elements of Q(s), for large s, are difficult. However, as the example above illustrated, there are times when Algorithm II is superior to Algorithm I. An open area of research would be to study the analytic and empirical behavior of Algorithm II under interesting conditions, including its performance relative to Algorithm I. One interesting result is that when the two Algorithms gave the same value for E [SBV] the result was optimal in all cases run so far.

A straightforward implementation of the algorithms in Pascal (found in the Appendix) can be improved substantially. See Kattar [1985]. In addition, further refinements in the algorithms themselves are possible. This is another open area for further research. Also, preliminary work indicates that an iterative take-away and give-back type of procedure leads to improvements in the solution, when Algorithms I or II do not lead to optimality.

V. THE MULTI-PHASE PROBLEM

There are three phases or layers under consideration: boost, post-boost, and midcourse. All targets which survive boost phase are single targets in post-boost phase; all targets which survive post-boost phase become multiple targets in midcourse phase.

Let X(0) = the number of targets (boosters) at the beginning, X(1) = the number of targets after phase 1 (Boost), X(2) = the number of targets after phase 2 (Post-Boost) and X(3) = the number of targets after phase 3 (Midcourse). These are random variables; in the sequel upper case letters will be used for random variables and lower case letters will be used for specific values. There are m platforms; platform k has a(k,i) weapons available at the start of phase i.

Let u(k,i) = the number of weapons on platform k used on phase i;

p(k,j,i) = the maximum probability of hitting target j from platform k on phase i;

$x(k,j,i)$ = the number of weapons allocated from platform k to target j on phase i (these are the decision variables) and

$v(j,i)$ = the value of target j on phase i.

Then the conditional expected value of the surviving boosters (SBV=surviving booster value) is a function of X(0), X(1) and X(2):

$$E[\ SBV \mid X(0),X(1),X(2)\ ]=$$

$$= \sum_{i=1}^{3} \sum_{j=1}^{X(i-1)} v(j,i) \prod_{k=1}^{m} (1 - p(k,j,i))^{x(k,j,i)}.$$

We would like to

$$\min E[\ SBV\ ] = E[\ E[\ SBV \mid X(0),X(1),X(2)]\ ]$$

subject to

$$\sum_{j=1}^{X(i)} x(k,j,i) = u(k,i) \quad \text{for all } k,\ i=1,2,3$$

$$\sum_{i=1}^{3} u(k,i) = a(k,i) \quad \text{for all } k$$

(In this formulation, after each phase, remaining targets are renumbered 1 to X(i).)

This is a very difficult problem to solve; a perhaps more obtainable goal is to find

1. for all k, $\{a(k,i)\}$ = the initial supply of weapons on platform k and
2. for all k,j,i, $\{x(k,j,i)\}$ = the set of weapon to target allocations such that

   $P\ (\ X(i) \le m(i)\ ) \ge 1 - e$ for $i=1,2,3$ where m(i)

is a predetermined goal and e is a small positive number. Note that a probability is being controlled here, rather than the more usual expected value. The constraint then would have been stated "such that E[SBV] <= K, where K is a predetermined level".

One way to solve the last formulation, called Problem II, is to follow the algorithm described below; but first, some preliminary observations.

Let $Y(j,i) = 1$ if target j is hit on the phase i.

$\quad\quad\quad\quad 0$ otherwise.

$$\text{Then}\quad P(\,Y(j,i) = 0\,) = \prod_{k=1}^{m} (1 - p(k,j,i))^{x(k,j,i)}$$

$$= \prod_{k=1}^{m} q(k,j,i)^{x(k,j,i)} = q(j,i)$$

$$\text{and}\quad P(\,Y(j,i) = 1\,) = 1 - q(j,i) = p(j,i).$$

$$\text{Let } Z(i) = \sum_{j=1}^{X(i-1)} Y(j,i) \quad = \text{the number of hits on phase } i.$$

$$\text{Then}\quad P\,(\,X(i) <= m(i)\,)$$

$$= E\,[\,P(\,X(i) <= m(i) \mid X(0),\ldots,X(i-1)\,)\,]$$

$$= E\,[\,P(\,Z(i) >= X(i-1) - m(i) \mid X(0),\ldots,X(i-1)\,)\,].$$

Algorithm III

The algorithm is stated as follows:

Step 1. Allocate the next weapon optimally on the first phase.

Step 2. Calculate $P\ (X(1) \leq m(1)\ ) = p(1)$.

Step 3. If $p(1) \geq 1 - e$ go to step 4,otherwise go to step 1.

Step 4. Allocate the next weapon optimally on the second phase.

Step 5. Calculate $P\ (\ X(2) \leq m(2)\ ) = p(2)$.

Step 6. If $p(2) \geq 1 - e$ go to step 7, otherwise go to step 4.

Step 7. Allocate the next weapon optimally on the third phase.

Step 8. Calculate $P\ (\ X(3) \leq m(3)\ ) = p(3)$.

Step 9. If $p(3) \geq 1 - e$ done, otherwise go to step 7.

Note: 1) There are assumed to be an infinite number of weapons available on each platform to start. One result of the algorithm is how many weapons are actually needed.

2) Steps 1,4 and 7 can be done using Algorithm I.

3) Calculation of steps 2,5 and 8 is straightforward but tedious; discussion follows. For realistically sized problems, some approximation such as a version of the Central Limit Theorem is clearly necessary. Preliminary analysis follows the discussion mentioned above.

Step 2: Calculation of $P(X(1) <= m(1))$

$P(X(1) <= m(1)) = P (Z(1) >= n - m(1))$. ($X(0) = n$ is assumed throughout.)

Let $A(g,h)$

$= \{ j$: exactly h of the $Y(j,1)$'s $= 1$; pattern number $g\}$,

where

$g = 1,2,\ldots,\binom{n}{h}$. Each element in $A(g,h)$ is a configuration of exactly h hits out of the target set of n targets.

$$\text{Then } P (Z(1) = z) = P \left(\sum_{j=1}^{n} Y(j,1) = z \right)$$

$$= \sum_{g=1}^{\binom{n}{z}} \left[\prod_{j \text{ in } A(g,z)} p(j,1) \prod_{j \text{ in } A(g,z)'} q(j,1) \right]$$

$$\text{and } P (X(1) <= m(1)) = \sum_{z=n-m(1)}^{n} P(Z(1) = z).$$

Since $E[Y(j,1)] = P (Y (j,1) = 1) = p(j,1)$,

$$E [Z(1)] = \sum_{j=1}^{n} p(j,1),$$

$VAR [Y(j,1)] = p(j,1) \, q(j,1)$,

$$VAR [Z(1)] = \sum_{j=1}^{n} p(j,1) \, q(j,1),$$

and the $Y(j,1)$ are uniformly bounded, we have

$$P (X(1) <= m(1)) = P (Z(1) >= n - m(1)) = 1 - \Phi (S(1))$$

where

$$S(1) = ((n - m(1)) - E [Z(1)]) / SQRT (VAR [Z(1)])$$

and Φ is the normal distribution function. See Feller [1968]. Thus Step 3 reduces to checking until the z-value of the goal number of hits is less than or equal to $- z_e$, the z-value with area under the normal curve to the left equal to e.

Calculation of Steps 5 and 8 can be done by conditioning on the configuration of hits made in the previous phase(s) and then taking expectations. The details of these calculations should be finished and coded in further research.

Other open questions involve the degree of communication between the phases and other objective functions - such as minimizing some type of cost function subject to meeting goals similar to Problem II. This area appears to be generating an extremely interesting series of problems.

VI. RECOMMENDATIONS

Without question, the research presented in this report is at an early to intermediate phase. The numerous open questions referred to in the report should be investigated, undoubtedly leading to still further areas of investigation. The need for further research is clear. In addition, there are other applications of the problem in the SDI context, in particular the issue of communications in a chaotic

environment gives rise to similar mathematical formulations.

Attached to the report is an Appendix, containing complete code for Algorithms I and II, and the Boost-Phase part of Algorithm III. This code can run on a VAX-780, using VMS 4.1 and the VAX-11 Pascal compiler.

Summary of Open Questions and Further Research Directions

1) Empirical evaluation of Algorithms I and II
2) Analytic evaluation and refinements of Algorithms I and II
3) Continued quest for different and superior algorithms
4) Completion of analysis and coding of Algorithm III
5) Study of different formulations of multi-phase problem
6) Study of other applications of mathematical results

REFERENCES

1. Bellman, R. and S. Dreyfus, "On a Tactical Air-Warfare Model of Mengel," Operations Research, Vol. 6, pp. 65-78 (1958).

2. Bogart, Kenneth P., Introductory Combinatorics, Pitman Publishing, Inc., Marshfield, Mass., 1983

3. Bracken, J., J.E. Falk, and F.A. Miercort, "A Strategic Weapons Exchange Allocation Model," Operations Research, Vol 25, No. 6, pp. 968-976 (1977).

4. Burr, S.A., J.E. Falk, and A.F. Karr, "Integer Prim-Read Solutions to a Class of Target Defense Problems," Operations Research, Vol. 33, pp. 726-745 (1985).

5. Day, R.H., "Allocating Weapons to Target Complexes by Means of Nonlinear Programming," Operations Research, Vol. 14, pp. 992-1013 (1966).

6. denBroeder, G.G., Jr., R.E. Ellison and L. Emerling, "On Optimum Target Assignment," Operations Research, Vol. 7, pp. 322-326 (1959).

7. Everett, H., III, "Generalized LaGrange Multipler Method for Solving Problems of Optimum Alloction of Resources," Operations Research, Vol. 11, pp. 399-417 (1963).

8. Feller, William, An Introduction to Probability Theory and Its Applications, Volume I, Third Edition, John Wiley & Sons, Inc., New York, 1968

9. Firstman, S.I., "An Approximating Algorithn or An Optimum Aim-Points Problem," Nav Res Log Quart, Vol. 7, pp. 151-167, (1960).

10. Kattar, J., "The Multi-Target Multi-Weapon Assignment Problem," (draft),The MITRE Corporation, October 1985

11. Lemus, F. and K.H. David, "An Optimum Allocation of Different Weapons to a Target Complex," Operations Research, Vol. 11, pp. 787-794 (1963).

12. Manne, A.S., "A Target-Assignemnt Problem," Operations Research, Vol. 6, pp. 346-351 (1958).

13. Matlin, S., "A Review of the Literature on the Missile-Allocation Problem," Operations Research, Vol. 18, pp. 334-373 (1970).

14. Miercort, F.A. and R.M. Soland, "Optimal Allocation of Missiles Against Area and Point Defenses," Operations Research, Vol. 19, pp. 605-617 (1971).

15. Nunn, W.R., D.V. Glass, I. Hsu, and D. Perin, "Analysis of a Layered Defense Model," Operations Research, Vol. 30, No. 3, pp. 595-599 (1982).

16. Passy, U., "Nonlinear Assignment Problems Treated by Geometric Programming," Operations Research, Vol 19, pp. 1675-1690 (1971).

17. Picariello, H.J., "A Missile Allocation Problem," Operations Research, Vol. 10, pp. 795-798, (1962).

18. Soland, R.M., "Optimal Defensive Missile Allocation: A Discrete Min-Max Problem," Operations Research, Vol. 21, pp. 590-596 (1973).

19. Walkup, D.W. and M.D. MacLaren, "A Multiple-Assignment Problem," Math Note 347, Boeing, pp. 14, Apr (1964).

APPENDIX

```
program assign(input,output,outfile);

type
    direction = (forward,backwards);
var
     { There are 100 targets and 10 weapons in this set-up}
    n_weaps,n_targs,weapon,target:                integer;
    targ_val:                       array [1..100] of real;
    pks,cand_value:array [1..10,1..100]       of real;
    alloc:array [1..10,1..100]              of integer;
    min_test_val:                                  real;
    weap_cand : array [1..100] of             integer;
    targ_cand:                                integer;
    global_alloc,actual_supply:               integer;
    exp_val_of_targets:                            real;
    projs_alloc,n_projs:array [1..10]       of integer;
    sn_projs:                                 integer;
    outfile:                                       text;
    way:                                     direction;
    init_seed,seed:                           integer;
    rn,upper_bound_pks,lower_bound_pks      :    real;
    n_steps,n_fired :                         integer;
    hit: array [1..100] of                    integer;
    hitset:                       set of       1..100;
    product,sum:                                   real;
    prob_n_hits:array [0..100] of                  real;
    factor: array [1..100] of                      real;
    n_hits  :                                 integer;
    curr_prob,goal_prob:                           real;
    z_obs,z_alpha :                                real;
    goal_leakage:                             integer;

{------------------------------------------------------------------}

procedure generate_rn;
   var
        multiplier,increment,modulus:       integer;

   begin
        multiplier := 69069;            { 3 x 7 x 11 x 13 x 23 }
        increment :=  1;
        modulus   := 429467807;       { 2**32 -1 }
        seed    := ((multiplier * seed) + increment) mod modulus;
        rn := seed/modulus;

   end; {generate rn}
```

```
{------------------------------------------------------------------}

procedure start_up;
   begin

      writeln('Enter the number of weapons,targets,number of projectiles ',
               'and the seed.');
      read (n_weaps,n_targs,sn_projs,init_seed);
      writeln('Enter the goal probability: ');
      read (goal_prob);
      writeln('Enter the maximum number of surviving boosters acceptable:');
      read (goal_leakage);
      writeln('Enter the lower bound of the pk matrix:' );
      read (lower_bound_pks);
      writeln('Enter the upper bound of the pk matrix:');
      read (upper_bound_pks);
      seed := init_seed;
      for target := 1 to n_targs do begin
         for weapon := 1 to n_weaps do begin
            generate_rn;
            pks [weapon,target] := lower_bound_pks +
                  (upper_bound_pks-lower_bound_pks)*rn;
            end; {for weapon}
         end; {for target}

      end; {start up}

{------------------------------------------------------------------}

procedure forward_initialize;
   begin

      exp_val_of_targets := n_targs;
      global_alloc := 0;
      for weapon := 1 to n_weaps do begin
         projs_alloc[weapon] := 0;
         n_projs[weapon] := sn_weaps;
         end; {for weapon}


      for target := 1 to n_targs do begin
         targ_val[target] := 1;
         for weapon := 1 to n_weaps do begin
            alloc[weapon,target] := 0;
            end; {for weapon}
         end; {for target}
      end; {input_forward_inital_conditions}

{------------------------------------------------------------------}
```

```
procedure print_set_up;

   begin
       writeln(outfile,'There are ',n_weaps:5,' weapons available.');
       writeln(outfile);
       writeln(outfile,'There are ',n_targs:5,' targets to shoot at.');
       writeln(outfile);
       writeln(outfile,'The initial seed is ',init_seed:10);
       end; {print set up}


{--------------------------------------------------------------}


procedure print_pks;

   begin
       writeln(outfile);writeln(outfile);
       writeln(outfile,'The PK matrix follows.');

       writeln(outfile);
       writeln(outfile,'                           WEAPONS ');
       write(outfile,'TARGETS');
       for weapon := 1 to n_weaps do begin
          write(outfile,weapon:8);
          end; {for weapon}
       writeln(outfile);
       for target := 1 to n_targs do begin
          write(outfile,target:4);
          write (outfile,'    ');
          for weapon := 1 to n_weaps do begin
             write(outfile,pks[weapon,target]:8:4);
             end; {for weapon}
          writeln(outfile);
          end; {for target}
       end; { print_pks }



{--------------------------------------------------------------}
```

```
procedure print_alloc;

   begin
      writeln(outfile);writeln(outfile);writeln(outfile);
      writeln (outfile,'                                   WEAPONS ');
      write(outfile,'TARGETS');
      for weapon := 1 to n_weaps do begin
         write(outfile,weapon:8);
         end; {for weapon}
      writeln(outfile);
      for target := 1 to n_targs do begin
         write(outfile,target:4);
         write(outfile,'    ');
         for weapon := 1 to n_weaps do begin
            write(outfile,alloc [weapon,target]:8);
            end; {for weapon}
         writeln(outfile);
         end; {for target}
      writeln(outfile);writeln(outfile);
      writeln(outfile,'Number of ');
      writeln(outfile,'projectiles');
      write(outfile,'allocated');
      for weapon := 1 to n_weaps do begin;
         write  (outfile,projs_alloc [weapon]:8);
         end;
      writeln(outfile);writeln(outfile);
      writeln(outfile,'The total number of projectiles allocated is ',
                 global_alloc);
      writeln(outfile);
      writeln( outfile,
           'The expected number of hits = ',n_targs-exp_val_of_targets:10:5);
      writeln(outfile);writeln(outfile);
      writeln(outfile,'The average success rate is ',
                 ((n_targs-exp_val_of_targets)/global_alloc):8:5);
      writeln(outfile);writeln(outfile);
      writeln(outfile,'   Target    ','   Target Value ');
      writeln(outfile,'--------------------------------');
      for target := 1 to n_targs do begin
         writeln(outfile,target:12,targ_val[target]:12:6);
         end;
      end; {print_alloc}


{-------------------------------------------------------------------------}
```

```
{This is the key procedure in Algorithm I                                }


procedure forward_allocate_weapon;
   begin
      way := forward;
      min_test_val := n_targs;
      for weapon := 1 to n_weaps do begin

         for target := 1 to n_targs do begin
            cand_value[weapon,target] :=exp_val_of_targets
               -targ_val[target]+targ_val[target]*(1-pks[weapon,target]);

            if cand_value[weapon,target] < min_test_val then begin
                min_test_val := cand_value [weapon,target];
                weap_cand [target] := weapon;
                targ_cand := target;

                end;  {if can}
            end; {for target}

       end;  {for weapon}

      exp_val_of_targets := exp_val_of_targets - targ_val [targ_cand] +
         (targ_val [targ_cand]*(1-pks[weap_cand [targ_cand ], targ_cand ]));
      targ_val[targ_cand] := targ_val[targ_cand]*
                              (1-pks[weap_cand[targ_cand],targ_cand]);
      alloc[weap_cand [targ_cand ],targ_cand] :=
                             alloc[weap_cand[targ_cand],targ_cand]+1;
      projs_alloc [weap_cand[targ_cand]] :=
                             projs_alloc [weap_cand[targ_cand]] + 1;
      global_alloc := global_alloc + 1;
      end; {forward allocate weapon}


{-------------------------------------------------------------}
```

```
procedure calc_hit_prob;
var
   i,j,nx,ll:                               integer;
   flag:                                    boolean;
begin

   hit [n_targs] := n_targs;
   hit [ 1 ] := 1;
   nx:=1;
   prob_n_hits [n_hits] := 0;
   while nx > 0 do begin
      for j := nx to n_targs - 2 do begin;
         hit [j+1] := hit [j] + 1;
         end; {for j}
      hitset := [];
      for i := 1 to n_hits do begin
        { write (hit[i]:3);}
         hitset := hitset + [ hit [i] ];
         end; {for i}
      product :=1;
      for target := 1 to n_targs do begin
         if (target in hitset) then begin
            factor [target] := 1 - targ_val [target ];
            end
         else
            factor [target] := targ_val [target];
         product := product * factor [target];
         end; {for target }
      flag := true;
      i := n_hits;
      while (i >= 1) and flag do begin
         nx := 0;
         hit [ i ] := hit [ i ] + 1;
         ll :=n_targs - n_hits + i ;
         if hit [i] <= ll then begin
            nx := i;
            flag := false;
            i :=i+1;
            end;  {if hit }
         i := i - 1;
         end; {while i}
       prob_n_hits [n_hits] := prob_n_hits [n_hits] + product;
       end; {while nx}
     end; {calc prob}
{-------------------------------------------------------------}
```

```
procedure calc_approx_prob;
var
    mean,variance :            real;
begin
   mean := 0;
   variance := 0;
   if goal_prob = 0.99 then z_alpha := -2.33 ;
   if goal_prob = 0.95 then z_alpha := -1.645 ;
   if goal_prob = 0.90 then z_alpha := -1.28 ;
   if goal_prob = 0.80 then z_alpha := -0.84 ;
   for target := 1 to n_targs do begin
      mean := mean + (1-targ_val [target]);
      variance := variance + ((1 - targ_val [target])*( targ_val [target] ));
      end; {for target}
   z_obs := ((n_targs - goal_leakage) - mean )/(sqrt (variance));
   end; { calc approx prob }
{--------------------------------------------------------------------}
procedure meet_goal_exactly;
var
     i:                                integer;
begin
   for n_fired := 1 to n_targs do begin
       forward_allocate_weapon;
       end; {for n_fired}
   repeat
      forward_allocate_weapon;
      curr_prob := 0;
      prob_n_hits [0] := 0;
      for n_hits := 1 to n_targs do begin
         calc_hit_prob;
         if (n_hits >= n_targs - goal_leakage) and (n_hits <= n_targs) then
             curr_prob:=curr_prob + prob_n_hits [n_hits];
         prob_n_hits [0] := prob_n_hits [0] + prob_n_hits [n_hits];
         end;
      prob_n_hits [0] := abs(1 - prob_n_hits [0]);
   until (curr_prob >= goal_prob);
   writeln(outfile,'The probability of less than or equal to ',goal_leakage:3,
       ' boosters getting through is ',curr_prob:8:5);
   print_alloc;
   writeln(outfile);writeln(outfile);
   writeln(outfile,'The histogram of the number of hits');
   writeln(outfile,'# of','   probability');
   writeln(outfile,'hits ');
   for n_hits := 0 to n_targs do begin
      writeln(outfile,n_hits:3,'     ',prob_n_hits [n_hits]:10:6,' ');
      for i:= 1 to round (100*prob_n_hits [n_hits] ) do
         write(outfile,'*');
      end; {for n_hits}
end; {meet_goal_exactly}
{--------------------------------------------------------------------}
```

```
{the following sets up the infeasible starting assignment matrix for    }
{the backward allocation method-Algorithm II                            }


procedure back_initialize;
   begin

      exp_val_of_targets := 0;
      global_alloc := 0;
      for weapon := 1 to n_weaps do begin
         n_projs [weapon] := sn_projs;{scalar n_projs}
         projs_alloc[weapon] := n_projs [weapon] * n_targs; {not feasible}
         global_alloc := projs_alloc [weapon] + global_alloc; {not feasible}
         end; {for weapon}


      for target := 1 to n_targs do begin
         targ_val[target] := 1;
         for weapon := 1 to n_weaps do begin

            alloc[weapon,target] := n_projs [weapon];
            targ_val[target]:= targ_val[target]*
                  ((1-pks[weapon,target])**(alloc[weapon,target]));
            end; {for weapon}
         exp_val_of_targets :=exp_val_of_targets + targ_val [target];
         end; {for target}
      end; {back initialize}

{-------------------------------------------------------------}
```

```
{the following procedure will find the least effective current      }
{weapon-target assignment pair and delete it                        }

procedure back_allocate_weapon;
   begin
      way := backwards;
      for weapon := 1 to n_weaps do begin
       if projs_alloc[weapon] > n_projs[weapon] then begin
         for target := 1 to n_targs do begin
            if alloc [weapon,target] > 0 then begin
               cand_value[weapon,target] :=exp_val_of_targets
               -targ_val[target]+targ_val[target]/(1-pks[weapon,target]);
                 end; {if alloc}
               end; {for target}
            end; {if proj_alloc}
          end;  {for weapon}


  {Find the minimum weapon entry for each target below}

      min_test_val := n_targs;
      for target := 1 to n_targs do begin
        for weapon := 1 to n_weaps do begin
           if (projs_alloc [weapon] > n_projs [weapon] ) and
                      ( alloc[weapon,target] > 0 ) then begin
            if cand_value[weapon,target] < min_test_val then begin
                min_test_val := cand_value [weapon,target];
                weap_cand [target] := weapon;
                targ_cand := target;
                end;  {if can}
            end;  {if projs_alloc}
           end; {for weapon}
         end; {for target}


      exp_val_of_targets := exp_val_of_targets - targ_val [targ_cand] +
       (targ_val [targ_cand]/(1-pks[weap_cand [targ_cand ], targ_cand ]));
      targ_val[targ_cand] := targ_val[targ_cand]/
                              (1-pks[weap_cand[targ_cand],targ_cand]);
      alloc[weap_cand [targ_cand ],targ_cand] :=
                             alloc[weap_cand[targ_cand],targ_cand]-1;
      projs_alloc [weap_cand[targ_cand]] :=
                             projs_alloc [weap_cand[targ_cand]] - 1;
      global_alloc := global_alloc - 1;
      end; {back allocate weapon}


{-----------------------------------------------------------------}
```

```
begin   {program}
   rewrite (outfile);
   start_up;

   print_set_up;
   print_pks;

   { The following is Algorithm I }

   forward_initialize;
   while global_alloc < n_weaps * sn_projs do
         forward_allocate_weapon;
   print_alloc;


   { The following is Algorithm II }

   back_initialize;
   while global_alloc > n_weaps * sn_projs do
         back_allocate_weapon;
   print_alloc;

   { The following give the exact and approximate results of }
   { Step 2. in Algorithm III                                 }

   forward_initialize;
   meet_goal_exactly;
   print_alloc;


   forward_initialize;
   repeat
      forward_allocate_weapon;
      calc_approx_prob;
   until z_obs <= z_alpha;
   writeln(outfile);writeln(outfile);
   writeln('Observed z is ',z_obs:6:3);
   end.  {program}
```

1985 USAF-UES SUMMER FACULTY RESEARCH PROGRAM/

GRADUATE-STUDENT SUMMER SUPPORT PROGRAM

Sponsored by the

AIR FORCE OFFICE OF SCIENTIFIC RESEARCH

Conducted by the

UNIVERSAL ENERGY SYSTEMS, INC.

FINAL REPORT

A STUDY OF THE ELECTROCHEMICAL BEHAVIOR OF THE BROMINE/BROMIDE COUPLE IN MELTS COMPOSED OF ALUMINUM CHLORIDE AND 1-METHYL-3-ETHYLIMIDAZOLIUM CHLORIDE

Prepared by:	Lawrence F. Koons
Academic Rank:	Professor
Department and University:	Chemistry Tuskegee Institute
Research Location:	Frank J. Seiler Research Laboratories United States Air Force Academy Colorado Springs, CO 80840
USAF Research:	Dr. John Wilkes
Date:	30 August 1985
Contract No.:	F49620-85-C-0013

A STUDY OF THE ELECTROCHEMICAL BEHAVIOR OF THE BROMINE/BROMIDE COUPLE IN MELTS COMPOSED OF ALUMINUM CHLORIDE AND 1-METHYL-3-ETHYLIMIDAZOLIUM CHLORIDE

by

Lawrence F. Koons

ABSTRACT

Conventional electrochemical techniques, including cyclic voltammetry and current-voltage scans at a rotating-disk electrode were used to study the title system. Bromine reacts with the melt if aluminum chloride is in excess. The oxidation of the bromide ion is not thermodynamically reversible at Pt, W and glassy carbon electrodes. The tribromide ion is readily formed in melts containing equimolar amounts of aluminum chloride and the alkyl imidazolium chloride. It is both reduced and oxidized at the named electrodes. Mixed trihalide ions appear to be formed in melts containing bromine/bromide and chloride.

ACKNOWLEDGEMENTS

The author wishes to acknowledge the support and assistance of the Air Force Systems Command, The Air Force Office of Scientific Research, United Energy Systems and, in particular, the personnel of the Frank J.Seiler Research Laboratories of the United States Air Force Academy.

I. INTRODUCTION: Systems composed of aluminum chloride and 1-methyl-3-ethylimidazolium chloride (MEIC) are of interest because they are in actuality molten salts at room temperature and below. Their use as electrolytes in batteries is one of several possible applications of them. (1) Among the types of information required for that application is knowledge of the behavior of electrode systems in these melts.

The research done under the auspices of this program was done with the objective of studying the behavior of selected redox couples at electrodes in these melts. Most of the research that I have done and supervised in the past has involved electrochemistry, in particular the study of electrode processes by means of polarography and other potential-sweep methods. Thus I was familiar with the techniques appropriate to the proposed investigation, if not with the details of the system.

II. OBJECTIVES OF THE RESEARCH EFFORT: The original plan was to study the behavior of the Zn(II)/Zn couple in the described melts. Initially some material had to be ordered. It was decided to study the bromine/bromide couple while awaiting the arrival of the ordered material. The objective was to determine the form in which bromine and bromide exist and whether there are conditions under which the electrode reaction corresponding to the interconversion of the two is reversible. It turned out that the entire period was spent on the study of the bromine/bromide system.

III. STUDY OF THE BROMINE/BROMIDE SYSTEM IN MEIC/$AlCl_3$ MELTS: Three approaches were used: 1) The measurement of resting electrode potentials; 2) Cyclic voltammetry; and 3) Current-voltage measurements with rotating-disk electrodes and rotating-ring-disk electrodes. The three methods were used in conjunction with one another, often on the same system.

The MEIC/$AlCl_3$ melts are said to be acidic if the mole fraction of the $AlCl_3$ exceeds 0.5. In the course of attempts to measure the electrode potential of the Br_2/Br^- couple it was discovered that in acidic melts bromine reacts with a constituent of the melt. The reaction is probably the bromination of the MEIC. The rate of disappearance of bromine was followed by measuring both the current at a rotating disk electrode and the absorbance of the solution at 278 nm as a function of time. Both methods showed that in a solution in which the mole fraction (N_A) of aluminum chloride is 0.55, the reaction is of the first order with respect to bromine, and has a corresponding rate constant of 10^{-3} s^{-1} at 25°C.

Electrode-potential measurements in acidic melts were not practical at the conditions used because of the reaction of the bromine. Attempts to make comparable measurements in basic melts did not yield useful, quantitative information. The potential(E)(vs. an Al/melt reference electrode) at a Pt electrode immersed in basic melts containing bromine and bromide ion(added as 1-methyl-3-ethyl imidazolium bromide-MEIB) was measured as a function of the ratio of the concentration of Br_2 to that of bromide. Nernst plots based on

the resultant data had a sigmoid shape, consistent with the hypothesis that bromide and bromine react to form the tribromide ion.

A series of experiments was done in which E was measured as a function of bromide concentration in melts containing a greater than tenfold excess of bromide over bromine. Under these conditions it can be shown, by combination of the equilibrium expression, mass-balance expressions, and Nernst equation that

$$\left(\frac{[Br^-]^*}{[Br^-]}\right)^2 \exp\frac{(E^*-E)2F}{RT} = \frac{1}{1 + K[Br^-]^*} + \frac{[Br^-]}{1 + K[Br^-]^*}$$

E and E^* are the potentials of the Br_2/Br^- electrode, versus a given reference electrode, measured in melts in which the bromide concentrations are $[Br^-]$ and $[Br^-]^*$, respectively. At the described conditions the actual bromide concentrations may be taken as their formal concentrations. K is the equilibrium constant for the

formation of the Br_3^- ion and the other symbols have their standard significance. Thus K can be determined, in principle, from the slope and the zero intercept of a plot of $\exp[(E-E^*)nF/RT)]/[Br^-]^2$ vs. $[Br^-]$, if measurements are made at a series of values of $[Br^-]$. Data obtained from such experiments, done in melts containing equal numbers of moles of $AlCl_3$ and MEIC yielded linear graphs, but the slopes and intercepts did not correspond to physically possible values of K. The same was true when the reverse procedure of using an excess of bromine and varying its concentration was tried.

Bell and Pring (2) studied the formation of mixed trihalide ions in aqueous solutions, using a similar, but more elaborate analysis. It involved measuring electrode potentials at fixed $[Br^-]$ and $[Br_2]$ as a function of $[Cl^-]$. An adaptation of their method was tried, but again the obtained data did not correspond to physically meaningful values for the formation constants of the trihalide ions.

When the above described measurements were being made, the potential appeared to be steady at some chloride concentrations, but at others it drifted at rates as great as several millivolts per hour. The probable reason for the failure of these experiments is that a mixed potential, not indicative of the free-energy change for the reduction of bromine was being measured. It is pertinent that subsequent microscopic examination of the platinum electrode used showed that some erosion of its surface had occurred during these experiments. This could have been the result of haloplatinate formation, although there appear to be no waves on the cyclic voltammetry(CV) scans, done in conjunction with the potential

measurements, that correspond to the oxidation of platinum. It was also determined later that at least while the experiments involving the chloride ion were being done, the atmosphere in the dry box contained a contaminant that reacted with $AlCl_3$, although there is no evidence that this was the cause of the failure of these experiments.

Some insight into the nature of the bromine-bromide interaction was obtained by doing potential-scan experiments in melts containing equal numbers of moles of $AlCl_3$ and MEIC. Melts prepared by mixing equimolar amounts of the two components usually had a slight excess of chloride, possibly because of the loss of $AlCl_3$ as smoke during the mixing. Neutral melts were prepared from these by the addition of increments of $AlCl_3$ until the Cl^--oxidation peak on CV scans was suppressed. (In the following, analyses of potential scan measurements are given in terms of the potential of the working electrode versus a reference electrode. The latter consisted of an Al wire immersed in a melt that made contact with the studied melt via an asbestos wick. It now appears that more attention should have been given to the reference electrode. Inferences drawn from the relative potentials of given features on a given scan are meaningful, but caution should be exercised in comparing features on scans obtained in separate experiments. Essentially by chance, a melt in which $N_A = 0.67$ was used in the reference electrode. This appears not to be a good choice because small changes in the composition of such a melt can produce large changes in its properties. Unfortunately, only after the experiments described below were completed was a check done on the stability of the reference electrode. Two reference electrodes, one

containing a melt with $N_A = 0.60$ and the other containing a melt with $N_A = 0.67$, were placed in the same melt and the potential between them was measured by means of an electronic voltmeter. Initially the potential difference was 0.0793V, but after one hour it had fallen to 0.0146V. After sixty hours it was 0.0462V and remained steady at that value for four hours; over the next four hours it climbed to 0.0550V. It is possible that some of the potential drift that occurred in the resting-potential measurements had its origin in the reference electrode.) The striking characteristic of CV scans obtained in these systems is that after the first cycle, the scans presented the same features, two anodic waves and two cathodic waves, whether the melt contained added bromine, added bromide, or both. The peaks for the anodic waves occur at +0.70±0.02V and 0.95±0.02V (unless stated to the contrary, data for CV scans refer to those obtained at 20mV/s with a Pt working electrode). The peaks of the cathodic waves occur at +0.85±.02V and +0.35±.02V (in these melts, the Cl^-- oxidation wave that appears on the addition of Cl^- has a peak at +1.13V). The relative heights of the peaks depend on the concentrations of the Br_2 and the Br^-. In the concentration range studied, if only one of them were present the two anodic peaks had about the same height, whereas the cathodic peak at the less positive potential was larger by a factor of approximately two than the other cathodic peak.

A possible explanation for these results is that the anodic peaks at +0.7 and +0.95 correspond to the oxidation of Br_3^- and Br^-, respectively, and that the cathodic peaks at +0.85 and +0.35 correspond to

the reduction of Br_2 and Br_3^-, respectively. Evidence in support of this follows.

If the melt contains only Br^-, an initial sweep in the negative direction, starting at +0.6V shows no cathodic waves, but both anodic waves are fully developed on the reverse sweep and both cathodic waves appear on the second cycle. In solutions containing only Br_2, no current flows when the electrode is held at potentials greater than +1.5V, but in a scan starting at such a potential and moving initially in the direction of negative potential, all four waves are fully developed on the first complete cycle. In acidic melts containing Br_2 there is a single cathodic peak at +0.92V. Some additional evidence in support of assigning the cathodic peak at +0,85V to the reduction of Br_2 was obtained in experiments in which CV scans were obtained after the incremental addition of MEIB to neutral melts. In melts containing 3.1×10^{-5} and 8.3×10^{-5} mole Br_2 in 11g melt, the anodic wave for the oxidation of Br^- was somewhat elongated, and there was only a single cathodic wave, which had a peak at +0.85V.Further addition of MEIB to bring the total amount to 1.25×10^{-4} mole resulted in the appearance of the double anodic and the double cathodic waves.

A series of experiments in which peak heights, corrected to a somewhat arbitrarily determined baseline, were determined as Br_2 and Br^- were alternately added to the melt, did not give conclusive results. In general, all four peak heights increased as the concentration of either Br_2 or Br^- was increased. The approximate constancy of some of the peak heights following further addition of one

or the other of the substances after an excess of it, assuming a one-to-one reaction, had been added, suggested the involvement of Br_3^- formation. The height of the peak at +0.85V remained approximately equal to half of the heights of the other three peaks. This is consistent with the assigning of this wave to the reduction of Br_2, the only neutral species, since at the concentrations used, the migration effect probably would not be totally suppressed by the electric charges on the solvent ions.

Current-voltage scans at the rotating platinum disk electrode, with neutral melts, containing only Br_2, had two waves, corresponding to the two waves on the CV scans. At 1000 rpm the two waves were of equal height. The wave heights did not vary linearly with the square root of the rotational velocity and they approached a limiting value as that velocity exceeded 3000 rpm. This suggests kinetic control of the electrode reaction and is consistent with the fact that the CV data imply that the electrode reactions are not thermodynamically reversible. On the other hand, the height of the first oxidation wave obtained when Br^- is added to neutral melts does vary linearly with the rotational velocity of the disk electrode, although the height of the second wave does not. Scans obtained with the rotating disk electrode in melts containing both Br_2 and Br^- show three plateaus. Their heights vary with the concentrations of Br_2 and Br^- in a manner that is qualitatively consistent with the hypothesis that they correspond to the couples, Br^-/Br_3^-, Br_3^-/Br_2 and Br^-/Br_2, in that order, as the potential becomes more positive.Results of experiments done with the ring/disk electrode were

consistent with the interpretations given above, but were not definitive. In melts containing Br^-, the cathodic current at the ring exactly mirrored the anodic current at the disk as the potential of the disk varied from +0.2V to +1.5V while the ring was held at +0.5V, or potentials less positive than that. The ring current increased as the ring potential varied from +0.5V to +0.2V, which accords with other evidence for kinetic control of the electrode reaction. If the waves in the ring current correspond to the reduction of Br_2 and Br_3^-, the migration effect is not important because the heights of the two waves increase by approximately the same factor.

In the reverse experiment ,in which Br_2 was added to the melt, the anodic current at the ring exactly mirrored the cathodic current at the disk as the disk potential varied from +1.3V to +0.1V while the ring was held at a potential more positive than +1.1V. Quantitative correlation of these results with the proposed model, as with those in the paragraph above, would require some knowledge of the diffusion coefficients of the species involved.

Nmr spectra were obtained in an attempt to determine if the Br^- were exchanging with the Cl^- on the $AlCl_3$. The nmr spectrum of a melt prepared by adding 0.117g MEIB to to 5.164g neutral melt showed only a single narrow peak. A melt containing equal numbers of moles of MEIB, MEIC and $AlCl_3$ gave the same peak, which underwent extreme broadening as the melt was cooled, but the extent of the broadening was so great that it was not helpful in resolving the matter of possible halide exchange.

Since evidence for (or against) the hypotheses presented above could be obtained from a knowledge of the equilibrium constant for the reaction for the formation of the Br_3^- ion, a simple spectrophotometric experiment was done to obtain an estimate of its value. The spectrum of a solution containing 0.007g Br_2 in 11.95g neutral melt was obtained. It had a single, broad peak in the visible range, with a maximum absorbance of 0.780 at 402 nm.The plan was to continue to obtain the spectra as increments of MEIB were added. Upon the addition of 0.007g MEIB there appeared to be still only a single peak, but the absorbance became so high (2.3) that any possibility of obtaining quantitative information was lost. Limitations of time and equipment made it impractical to repeat the experiment at lower concentrations of Br_2. It seems worth noting here that acidic solutions containing Br_2 have the color of elemental bromine, whereas solutions containing bromine and an excess of chloride or bromide are yellow.

Most of the work described above was carried out with melts containing equimolar amounts of MEIC and $AlCl_3$. Taking the results obtained therefrom as a starting point, tentative interpretations can be offered for some of the results obtained with melts containing an excess of MEIC. In those basic melts in which the Cl^- concentration exceeds the Br^- concentration by a factor of one hundred, and possibly less, the oxidation of the Br^- ion is represented by a shoulder on the less positive side of the Cl^- oxidation wave. In solutions containing both Br_2 and Br^-, as well as Cl^-, at comparable concentrations scans starting at +0.6V and going toward less

positive potentials have a cathodic peak at +0.45V, the height of which on the initial scan increases with increasing Br_2 concentration. On subsequent scans its height also depends on the Br^- concentration. It is probable that this peak corresponds to the reduction of Br_2Cl^-.

In melts containing Br_2 or Br^- and Cl^- at comparable concentrations the CV scans are somewhat complicated. There are three anodic peaks. There often are nuances of other features -- peaks or shoulders -- that are well less evident than the major features and which shift, appear or disappear with slight changes in the composition of the melt. The three prominent, anodic peaks appear at $+0.85\pm0.05$V, 1.20 ± 0.05V and $+1.45\pm0.05$V. At some compositions there is a slight indication of an additional peak between the ones at 0.85V and 1.2V. The most prominent cathodic peak is at 0.60 ± 0.05V. An increase in the concentration of either Br_2 or Cl^- augments its height. The height of another cathodic peak at 0.85 ± 0.05V diminishes with an increase of the ratio of the concentration of Cl^- to that of Br_2. At some compositions there is evidence of cathodic peaks on either side of the one at +0.85V.

In a series of experiments in which CV scans were obtained after each addition of measured amounts of MEIC or Br_2, the heights of the anodic peak at +1.45V and the cathodic peak at +0.60V were approximately proportional to the concentration of the limiting reagent, assuming that Br_2 and Cl^- react on a one-to-one basis. Because of uncertainties in the peak height, resulting from uncertainties in the base line, any inferences drawn from this must be

qualified, but it suggests that these two peaks correspond, respectively, to the oxidation and the reduction of Br_2Cl^-. Because of the potential at which it occurs and the variation of its height with the Br_2/Cl^- ratio, it appears that the cathodic peak at +0.85V corresponds to the reduction of Br_2. The anodic peak at +1.2V probably corresponds to the oxidation of Cl^-. By default the remaining anodic peak can be assigned to the oxidation of Br^-. The less prominent peaks to which allusion was made may be the result of the formation of other trihalide ions, such as $BrCl_2^-$, for which evidence was sought in the unsuccessful resting-potential measurements.

IV. RECOMMENDATIONS: The work described in the foregoing has provided some insight into the behavior of the Br_2/Br^- couple in the $AlCl_3$/MEIC melts, but the model presented to account for the results is incomplete and there is no unambiguous, confirmatory evidence for it. Some investigations that could resolve the ambiguities in the presented analysis are given below.

It is very likely that trihalide ions are formed in the melts that contain both halide ions and bromine. It seems probable that equilibrium is rapidly established, at least with respect to the immediate reaction between bromine and the halide ion. Confirmation of this in the form of determinations of the equilibrium constants for the reactions between bromine and the halide ions would be a first step toward the resolution of the matter of the nature of the species in the melts. Determination of the spectral absorbance of melts containing bromine and bromide at systematically varied concentrations would

provide useful information concerning the interaction between halogen and halide and very likely would yield values for the equilibrium constant for the formation of the tribromide ion. In order to render the system as simple as possible, probably the intial determinations should be made in a melt composed of MEIB and $AlBr_3$. These experiments could be followed by similar experiments done in neutral MEIC/$AlCl_3$ melts and ultimately in more complex systems containing the chloride ion.

There are several possible reasons for the failure of the experiments based on "open circuit" potential measurements. This series of experiments should be repeated under conditions that would provide some understanding of causes for the observed inconsistencies. This would involve the repetition of that set of measurements, but with controls that would allow one to determine the effects of the pertinent variables. These would include temperature control, rigorous purification of the compounds used, determination of the effects of the electrode material and the state of its surface on the results, and the monitoring of the behavior of the reference electrode.

In addition, although the analysis given in the preceding section leads to results of a qualitative nature, the techniques used are capable of yielding quantitative results. If the spectrophotometric and other experiments provide the expected information concerning the nature of the species in the melts, it would be then appropriate to use standard electrochemical techniques to determine the rate constants of the electrode reactions. The determination, or even estimation, of the diffusion coefficients of the studied species would facilitate the use

of the data from the experiments with the rotating disk and ring/disk electrodes to test the hypotheses concerning the identity of the species involved in the electrode reactions.

Since the rate of disappearance of bromine in the acidic melts can be followed easily by either electrochemical or spectrophotometric means, the determination of the rate law for the corresponding reaction should be easy to accomplish. That should yield insight into the mechanism of the reaction and also provide data that would be of practical value in the design of any cell that might use bromine.

REFERENCES

1. Floreani, D, D. Stech, J. Wilkes, J. Williams, B Piersma, L. King and R. Vaughn. "A New Class of Molten Salts for Room-Temperature Battery Applications," Proc. 30th Power Sources Symp. June 1982, The Electrochemical Society.

2. Bell, R. P., and M. Pring, "Stability Constants and Absorption Spectra of the Ions, Br_2Cl^- and $BrCl_2^-$ J. Chem. Soc. (A) , 1966, 1607-9.

1985 USAF-UES SUMMER FACULTY RESEARCH PROGRAM/
GRADUATE STUDENT SUMMER SUPPORT PROGRAM

Sponsored by the

AIR FORCE OFFICE OF SCIENTIFIC RESEARCH

Conducted by

UNIVERSAL ENERGY SYSTEMS, INC.

FINAL REPORT

THE THERMAL LAYER: A SIMPLIFIED MODEL

Prepared by: Arthur A. Kovitz

Academic Rank: Professor

Department and University: Mechanical & Nuclear Engineering, Northwestern University Evanston, IL

Research Location: Air Force Weapons Laboratory, Nuclear Technology Office, Civil Engineering Research Division, Atmospheric Phenomenology Section (AFWL/NTEDA) Kirtland AFB, NM

USAF Research: Lt. Glenn James

Date: 30 September, 1985

Contract No.: F49620-85-C-0013

THE THERMAL LAYER: A SIMPLIFIED MODEL

by

Arthur A. Kovitz

ABSTRACT

A thermal layer model is described which includes soil properties (void fraction, saturation, density, thermal diffusivity, etc.), blow-off of soil moisture into the atmosphere as a vapor/air exhaust, and time dependent re-radiation into the atmosphere. The radiation heat flux is modeled as "interstitial radiation", dependent on the gradient of the fourth power of the temperature. Use is made of an assumed temperature profile with undetermined functions of time. This is an integral approach which leads to a system of first-order, non-linear differential equations that are solved numerically by Runge-Kutta methods. Results are shown graphically and discussed for a number of parameters: these include surface and vapor/air exhaust temperatures as functions of time; temperature variation with distance in the soil and in the vapor/air exhaust; velocity and massflux of vapor/air exhaust. The model is suitable for coupling with a hydrodynamic calculation such as the HULL code because of its simplicity and qualitative agreement with experiment and other thermal layer calculations.

I. INTRODUCTION

As an individual with a background in fluid mechanics and thermodynamics the opportunity to work on a problem embracing those areas was very attractive. It also was of interest to me that numerical methods would be stressed. The concerns of AFWL/NTEDA focused on developing a model for the thermal layer that avoided experimental correlations, and could be appended to the HULL hydrodynamic code. These tasks compliment both my experience, and my desire to learn more about numerical methods in fluid mechanics.

II. OBJECTIVES OF THE RESEARCH EFFORT

In March 1984 after visiting Major Raymond L. Bell at AFWL/NTEDA, Kirtland AFB, NM it was decided that work on developing a physically based (as opposed to one based on experimental correlations) model for the thermal layer and blast wave precursor was desirable, with the goal of incorporating it into the HULL hydrodynamic code. The emphasis during summer 1984 was concentrated on a one-dimensional version of the problem. This afforded an opportunity to write a one-dimensional HULL code and begin a process of evolving a thermal layer model. During summer 1985 the focus was on simplifying the model mathematically while including more of the soil physics. At the end of summer 1985 a first try was made at running this thermal layer model as a subroutine of the HULL code. Thus, the objective set in March 1984 was, in a preliminary fashion, achieved.

III. BACKGROUND

The irradiation of a ground/air interface results in rapid energy deposition into the ground as well as the neighboring air layer. This observed rapidity of the transfer requires energy transport via mass transport into the air from the ground. The presence of the ejected matter also transforms the air into an absorber of the radiant energy flux. Both processes, injection and absorption, are coupled. In this work a model will be proposed in which the absorption is replaced by an idealized radiant diffusion mechanism; injection will be treated as a "drying" process for moist soil.

The result of the energy deposition is a heated layer of air, the

"thermal layer"; it contains the ejected matter as well. The thermal layer can be important when estimating the effects of large energy releases on objects with thermal layer contact.

The topics noted so briefly above have been extensively discussed in the recent literature. A useful review is that of Allahadadi [1].

IV. THE SIMPLIFIED MODEL

A. Qualitative Description

It is assumed that the dominant processes associated with thermally irradiating moist soil from an atmospheric source are:

(i) the rapid heating of a relatively thin surface layer of soil to the vaporization temperature of the adsorbed moisture; and

(ii) the injection into the atmosphere of a mixture of vapor and air as a result of continued energy absorption at the soil/air interface.

A schematic of the energy transfer mechanisms is shown in Fig. 1. Process (i), Fig. 1a, takes place during the "pre-vaporization period." Heat transfer by conduction is the controlling feature. Process (ii) is a post-vaporization occurrence, more complex than its predecessor; see Figs. 1b, 1c. After the surface reaches the vaporization temperature of the adsorbed water boiling commences. The vaporization front, denoted by $y = G(t) < 0$ moves into the virgin soil, leaving in its wake heated soil whose voids are filled with the vapor/air mixture. There is also a vapor/air exhaust region displacing (as a first approximation) the atmosphere as its front $y = D(t) > 0$, moves to the right.

The point of view taken in this work is that the dominant feature for all portions of the thermal layer development is the imposed thermal radiation flux. In effect, the thermal capacity of the material will be neglected. Thermal flux will, therefore, be a function of time only. An additional assumption will be the adoption of an interstitial radiation model for the soil and vapor/air exhaust. These simplifying features of the radiation energy transfer are taken from studies of pyrolysis [2].

Heat conduction with phase change is inherently non-linear [3]. A

surprisingly effective method of solution for such problems has been developed by Zien [4]; it will be applied in this work.

B. Analytical formulation

The pre- and post-vaporization periods will be treated separately and consecutively.

During the pre-vaporization period conductive heat transfer into the soil occurs, with re-radiation to the air proportional to the fourth power of the time-dependent surface temperature, $T_s(t)$. Zien [4] has shown that an assumed temperature profile of the form

$$T(y,t) = T_\infty + [T_s(t) - T_\infty]\exp[-y/\eta(t)] \tag{1}$$

is well suited to describe conduction heat transfer without phase change. T_∞ is the temperature of the undisturbed medium; $\eta(t)$ is a time-dependent characteristic length for heat conduction into the virgin soil. Zien's [4] integral method requires substitution of the assumed temperature into the heat conduction equation

$$\partial T/\partial t = \alpha_v \partial^2 T/\partial t^2 \quad , \tag{2}$$

and a multiple of this equation (Eq. 2 multiplied by T); these two equations are then integrated from $y = -\infty$ to 0. The result is two ordinary differential equations for the two dependent variables $T_s(t)$ and $\eta(t)$. These equations are

$$d(\omega\eta)dt = -\alpha_v Q/k \quad , \tag{3}$$

$$d(\omega^2\eta)/dt = -4\alpha_v \omega Q/k - 2\alpha_v \omega^2/\eta \quad . \tag{4}$$

In these expressions $\omega = T_s(t) - T_\infty$, k is the virgin soil thermal conductivity, and Q(t) is the heat flux into the soil at $y = 0$.

According to Zien's method Q(t) is <u>not</u> set equal to its Fourier equivalent, $-k(d\omega/dy)$ at $y = 0$; rather, it is set as a specified function of time, as required by the particular problem. In this case

$$Q(t) = Q_o(t) + \sigma\varepsilon_v[(\omega + T_\infty)^4 - T_\infty^4] \quad ; \tag{5}$$

here, $Q_o(t) < 0$ is the imposed thermal radiation flux; σ and ε_v are the Stefan-Boltzmann constant and emissivity of the virgin soil, respectively. Exposing the boundary heat flux Q explicitly in this way is the most significant feature of Zien's method.

Equations (3) and (4) may be put in dimensionless forms that are suitable for fourth-order RUNGE-KUTTA solution. These forms are

$$\dot{\delta} = 2E_1W^{-1}\{W/\delta + q + E_2[(E_3W + 1)^4 - 1]\} \quad , \tag{6}$$

$$\dot{W} = -E_1\delta^{-1}\{2W/\delta + 3[q + E_2((E_3W + 1)^4 - 1)]\} \quad , \tag{7}$$

where

$$\delta(\xi) = [Q_m/k(T_f - T_\infty)]\eta(t), \; W(\xi) = (T_s(t) - T_\infty)/(T_f - T_\infty),$$

$$E_1 = \alpha_v b^{-1}[Q_m/k(T_f - T_\infty)]^2, \; E_2 = \sigma\alpha_v T_\infty^4/Q_m, \; E_3 = (T_f - T_\infty)/T_\infty, \; q(\xi) = Q_o(t)/Q_m;$$

Q_m is the maximum value of the thermal flux $Q_o(t)$; T_f is the vaporization temperature of the adsorbed moisture; ξ is a dimensionless time, $\xi = bt$. Initial and boundary conditions will be discussed in the next section.

At the instant when $T_s = T_f$ the post-vaporization period begins. At the same instant a vapor/air exhaust from the soil wake displaces atmospheric air as it expands; its boundary is denoted by $y = D(t)$.

Zien's method [4] is again used to determine the relationship between temperature and heat flux in the virgin soil. The appropriate temperature distribution is

$$T(y,t) = T_\infty + (T_f - T_\infty)\exp\{[y - G(t)]/\eta(t)\} \quad , \tag{8}$$

where $\eta(t)$ is now a thermal penetration distance relative to the vaporization plane at $y = G(t)$. Substitution of this temperature into Eq. (2), and Eq. (2) multiplied by $T(y,t)$, as in the pre-vaporization case, will yield two equations among the variables $G(t)$, $\eta(t)$, and Q_v.

Q_v is a third dependent variable; it requires a third equation. The first two equations are

$$\dot{\eta} - \dot{G} = -\alpha_v Q_v / k(T_f - T_\infty) \quad , \tag{9}$$

$$\dot{\eta} - 2\dot{G} = -4\alpha_v Q_v / k(T_f - T_\infty) - 2\alpha_v/\eta \quad . \tag{10}$$

It will be seen that Q_v depends upon $T_o(t)$, the temperature at $y = D(t)$, the vapor/air front.

From the general equation for unsteady, one-dimensional heat transfer (neglecting viscous dissipation) in a fluid flow one can get

$$[\rho(c_v T + \frac{1}{2} u^2)]_t = -[\rho u c_v T + pu + Q_{rad}]_y \quad , \tag{11}$$

where the subscripts t and y indicate differentiation with respect to these variables. Q_{rad} is the thermal radiation energy flux. If Q_{rad} is much larger than the other fluxes $\rho u c_v T$ and pu, and internal and kinetic energy changes are small, then eq. (11) requires Q_{rad} to be a function of time only.

It will further be assumed that Q_{rad} is governed by the so-called "interstitial" radiation law [2]; this implies

$$Q_{rad}(t) = -k_r(\partial T^4/\partial y) \quad , \tag{12}$$

where k_r is a coefficient that must be estimated from experiment. Equation (12) may be integrated:

$$Q_{rad}(y - y_c) = -k_r(T^4 - T_c^4) \quad . \tag{13}$$

Since Q_{rad} is a function of time only it may be evaluated at $y = D$. From Fig. 1

$$Q_{rad} = Q_o(t) + \sigma\varepsilon_o(T_o^4 - T_\infty^4) \quad . \tag{14}$$

Furthermore, it is consistent with Eq. (12) to assert that the heat flux into the vaporization front from the soil wake side is

$$Q_f = Q_{rad} \quad . \tag{15}$$

To relate Q_f and Q_v one must characterize the virgin soil so that its moisture content can be expressed in terms of soil properties. These are:

a) porosity N = (void volume)/(total volume); b) saturation S = (water volume)/(void volume); c) water weight fraction w_f = (water wt)/(total wt of soil). The balance of energy for the vaporization interface is then

$$Q_v = Q_f - (\rho_w NS\dot{G})H \quad , \tag{16}$$

where ρ_w is the density of adsorbed water, and H is the heat of vaporization.

Equations (9), (10), and (14), (15), (16) are not yet complete. The temperature $T_o(t)$ must be related to the other variables. This can be done by constructing a mass balance for the region $G(t) < y < D(t)$. The reasoning is outlined in Fig. 2. This gives the third required equation, relating T_o, G, and D by a lengthy first order differential equation, linear in the derivatives.

Linearity in the first order time derivatives allows the governing equations to be expressed separately as functions of the dependent variables, and time. Their form is

$$\dot{W}_i = f_i(W_1, W_2, W_3, t) \quad , \quad i = 1, 2, 3 \quad , \tag{17}$$

which is integrable by fourth-order RUNGE-KUTTA methods. Here the W_i correspond to the variables of η, G, and D, with T_o known from the above noted mass balance.

Boundary and initial conditions may be understood from Fig. 1.

V. SOLUTION OF THE ANALYTICAL MODEL

The equation systems are amenable to RUNGE-KUTTA solution methods; an excellent discussion of this can be found in Ref. [5].

At the initial instant, according to the imposed initial values, the right-hand-sides of equations (6) and (7) are indeterminate. This

is overcome by constructing a series solution valid for sufficiently small times.

The imposed thermal radiation flux Q_o: is

$$Q_o(t) = Q_m q = Q_m\left(-\frac{1}{4}\xi^2 e^{-\xi+2}\right) \quad , \tag{18}$$

where $\xi = bt$, a dimensionless time; b is an inverse characteristic time. The minus sign is required to make $Q_o < 0$ for $Q_m > 0$. In this representation $Q_o = Q_m$ when $\xi = 2$.

It may be verified that series expressions for δ and W which satisfy Eqs. (6) and (7) are

$$\delta = C\xi^{\frac{1}{2}}(1+a_1\xi^{\frac{1}{2}}+a_2\xi+0(\xi^{3/2})), \quad W = D\xi^{\frac{5}{2}}(1+b_1\xi^{\frac{1}{2}}+b_2\xi+0(\xi^{3/2})), \tag{19}$$

$$\text{where } C = (4E_1/13)^{\frac{1}{2}} \quad , \quad D = (13e^4 E_1)^{\frac{1}{2}}/24 \quad . \tag{20}$$

The coefficients a_1, b_1, a_2, b_2 have been evaluated; they are used in the numerical solution.

VI. RESULTS OF THE NUMERICAL SOLUTIONS

All of the results to be discussed have the common parameter values noted in Table I (see last page). Parameters that are varied will be pointed out at the time their effect is observed.

A. Estimation of the interstitial radiation coefficients

An estimate of its value may be obtained from its defining equation; i.e., write Eq. (12) in finite difference form and solve for k_r:

$$k_r = -Q_{rad}(\Delta y)/(\Delta T)^4 \quad . \tag{21}$$

In Eq. (21) the thermal flux, characteristic length, and fourth power of the temperature difference are taken as nominal values associated with the soil wake (to obtain $k_r = k_s$) and vapor/air exhaust (to obtain $k_r = k_e$). These values result in large temperature diffrences from the soil surface,to the vaporization front; on the other hand, the temperature

difference between the soil surface and the leading edge of the vapor/air exhaust is usually much smaller.

B. Surface temperature vs. time

Figure 3 shows the surface temperature $T_s(t)$ for four values of the total energy release (E_{tot}).

It can be shown that $Q_m = bE_{tot}[1 + (R_a/h)^2]^{-3/2}/2\pi h^2 e^2$, where R_a is the ground range and h is the height of burst.

The dotted curve is the dimensionless thermal flux on the same abscisa (time) as the surface temperature results. As expected, the highest surface temperature corresponds to the largest Q_m.

C. Surface temperature vs. time during the transition from pre- to post-vaporization periods: Fig. 4.

This is a magnified view of the region near the origin in Fig. 3. The onset of vaporization causes a temporary reduction in the rate of surface temperature rise.

D. Surface temperature vs. time for a "slower" thermal radiation pulse

Figure 5 shows the time dependence of the surface temperature for the same conditions as in Fig. 3, with the exception of the time required to reach Q_m. In this case the time is 1 second; it was .2 seconds for Fig. 2. The stretched out thermal pulse results in significantly lower surface temperature maxima; e.g., the 1Mt curves peak at 7200K and 4800K for Q_m at .2 and 1. seconds, respectively.

E. Boundary temperatures vs. time with parameter k_e

Figure 6 exhibits the surface and vapor/air exhaust front temperatures, with the interstitial radiation coefficient for the vapor/air exhaust as a parameter. As k_e decreases the surface temperature decreases, and the vapor/air exhaust front temperature increases.

F. Temperature vs. distance in the vapor/air exhaust

Figures 7 and 8 show T(y) in the vapor/air exhaust with time as the parameter. The essentially uniform temperature T(y) for the larger

value of k_e gives way to the perceptible variation of T(y) for the smaller value of k_e.

G. Temperature vs. distance; very early time

Figure 9 exhibits T(y) for several early times on a distance scale that shows the sub-surface and vapor/air exhaust temperature distributions. Post-vaporization temperature distributions (at .0085, .0090, .0095, and .0100 seconds) show the rapid advance of the vapor/air exhaust front into the air compared to the retro-advance of the temperature rise into the soil.

H. Temperature vs. distance in the soil, showing the vaporization front

Figure 10 shows T(y) for the soil over a range of times that includes those of Fig. 9, but with an expanded distance scale. One sees the pre-vaporization T(y) curves evolve into post-vaporization T(y) curves with slope discontinuities at the vaporization boundary.

I. The effect of the vapor/air radiation coefficient

The value of k_e, the vapor/air interstitial radiation coefficient, has a surprisingly complicated effect on the temperature T(y). This is seen in Fig. 11, which shows T(y) at .5 seconds for a range of k_e.

J. Surface massflux and exhaust velocity

Perhaps the most important parameters for future coupling with a hydrodynamic code are the massflux and velocity of the vapor/air mixture at the surface (y = 0). Figure 12 shows the surface exhaust velocity for a range of vapor/air interstitial radiation coefficients.

Figure 13 exhibits the corresponding vapor/air mixture surface massflux. It is worth noting the pronounced shifting of the massflux maximum toward earlier times as k_e is decreased.

VII. RECOMMENDATIONS

The work for the summer stopped with the first attempt to program this model as a subroutine of HULL, a comprehensive hydrodynamic code. Results from this preliminary coupling should be obtainable within a relatively short time (2-4 weeks). These results will provide

information on how and where to modify the thermal layer model so as to make its merging with HULL more realistic from a physics point-of-view.

Substantial revisions of this simplified thermal layer model should embrace

1) making the vapor/air exhaust and soil wake energy absorbers,
2) using a soil equation of state,
3) including solid material entrainment in the vapor/air exhaust,
4) coupling the energy and mass balances at the ground surface with the HULL code.

ACKNOWLEDGMENTS

The author would like to thank the Air Force Systems Command, the Air Force Office of Scientific Research and Universal Energy Systems, Inc. for providing him with the opportunity to spend a very worthwhile and interesting summer at the Air Force Weapons Laboratory, Kirtland AFB, N.M. He would like to acknowledge, in particular, the Civil Engineering Research Division, Technology Branch, Atmospheric Phenomenology Section for its hospitality and excellent working conditions.

As my "EFFORT FOCAL POINT" LT. Glenn James was a continuous source of support and assistance. My thanks are also due to LTC. T. D. McCarson; his leadership made the Technology Branch, Atmospheric Phenomenology Section, an ideal workplace.

References

1. Allahadadi, F. A., "Assessment of the State of the Art of Dust-Entrained Shock Physics," NMERI TA11-3, New Mexico Engineering Research Institute, University of New Mexico, Albuquerque, NM, August 1983.

2. Delichatsios, M. A. and de Ris, J., "An Analytical Model for the Pyrolosis of Charring Materials," Factory Mutual Research, Technical Report J.I. OKOJ1.BU, May 1983.

3. Zien, T. F., "Study of Heat Conduction with Phase Transition Using an Integral Method," AIAA Progress in Astronautics and Aeronautics, Thermophysics of Spacecraft and Outer Planet Entry Probes, Vol. 56, edited by A. E. Smith, New York, 1977, pp. 87-111

4. Zien, T. F., "Integral Solutions of Ablation Problems with Time-Dependent Heat Flux," AIAA Journal, Vol. 16, 12, p. 1287, 1978.

5. Burden, R. L., Faires, J. D., and Reynolds, A. C., "Numerical Analysis," Prindle, Weber, and Smith, Boston, Mass., 2nd Edition, 1981, pp. 200-253.

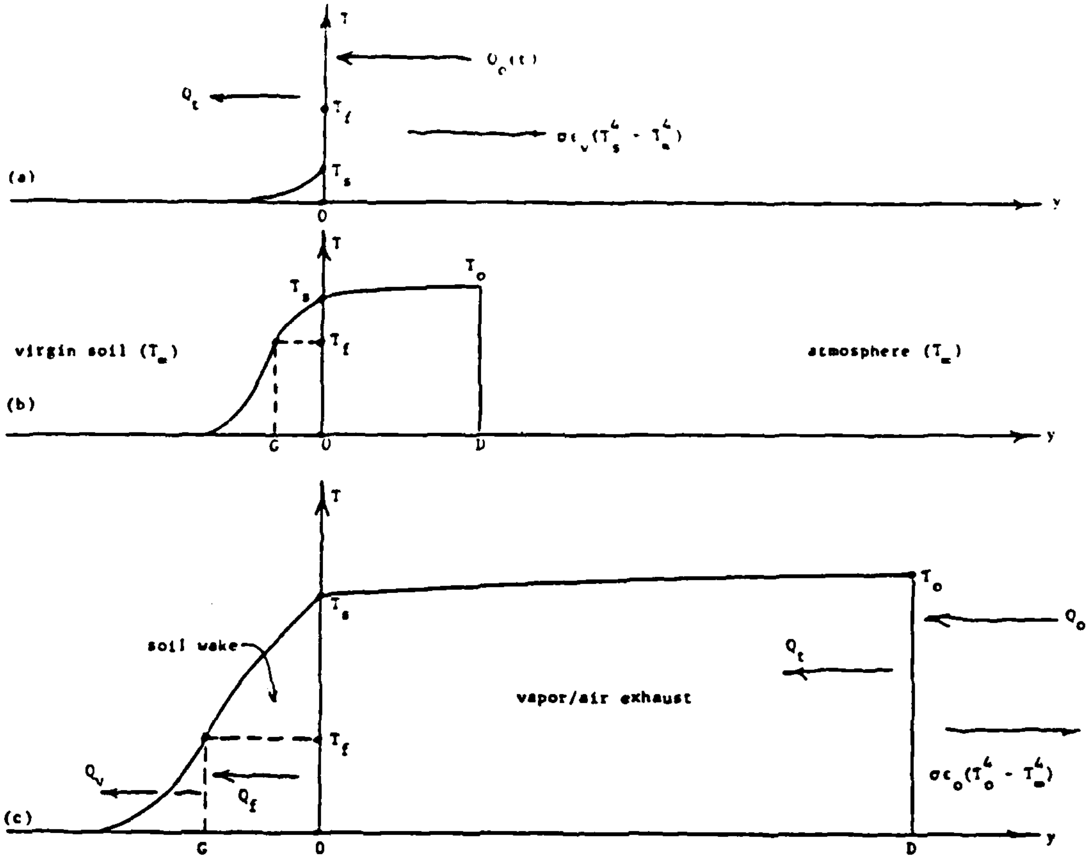

Fig. 1 Schematic of evolution of temperature distribution.
a) Pre-vaporization period: $T_s < T_f$, the vaporization temperature; transmitted radiant flux, $Q_t = Q_o + \sigma\epsilon_v(T_s^4 - T_\infty^4)$.
b) Beginning of post-vaporization period; $T_s > T_f$.
c) Post-vaporization period: virgin soil, $y < G$; soil wake, $G \leq y < 0$; vapor/air exhaust, $0 < y < D$; atmosphere, $y > D$; transmitted radiant flux, $Q_t = Q_o + \sigma\epsilon_o(T_o^4 - T_\infty^4)$.

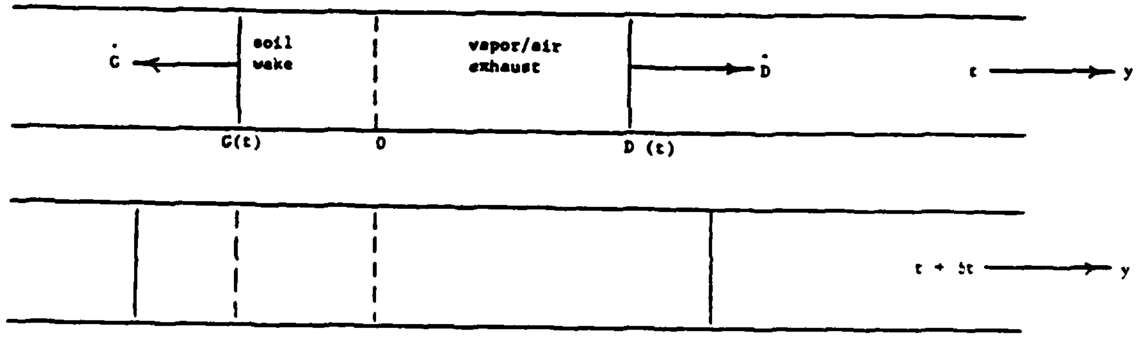

$$M(t) = \int_{y=G(t)}^{0} \rho N dy + \int_{y=0}^{D(t)} \rho dy$$

where ρ is the mixture density $= (p_o/R)/T(y,t)$

$\frac{dM}{dt}$ = rate of increase of vapor air mass

= rate at which front G overruns water + air in virgin soil

$= -N\dot{G}[\rho_a(1-S) + \rho_w S]$

Fig. 2 Schematic, with equations, of the mass balance calculation for the vapor/air exhaust.

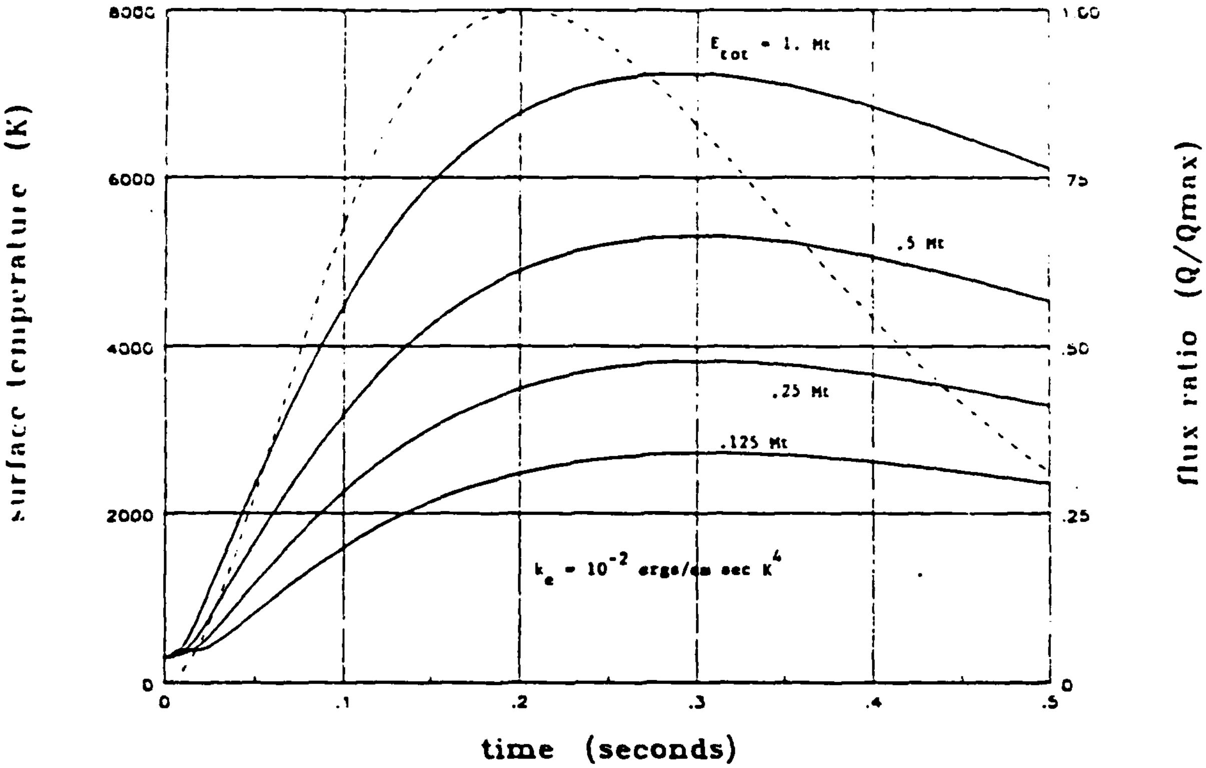

Fig. 3 Surface temperature $T_s(t)$ and heat flux ratio $Q_0(t)/Q_{max}$ for total energy release E_{tot}: 1 Mt = 4.18×10^{22} ergs. Rise time to Q_{max} is .2 seconds (b = 10/sec).

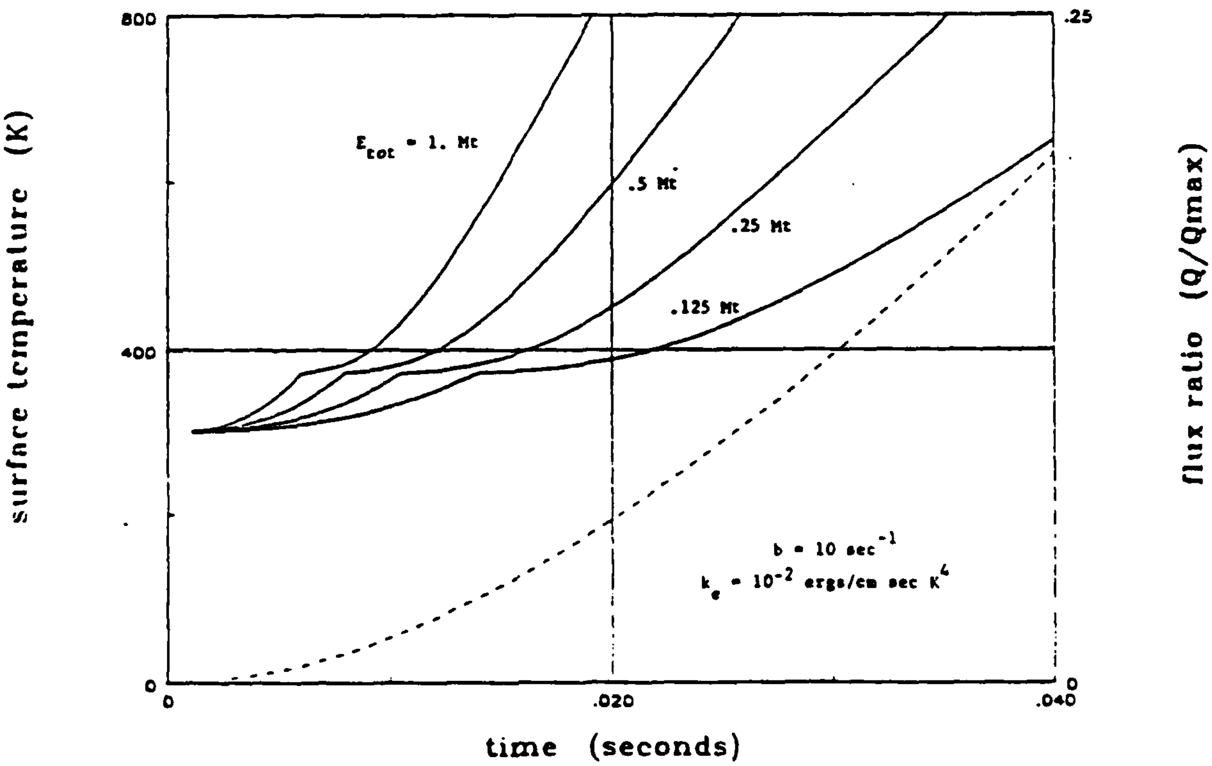

Fig. 4 Surface temperature and heat flux ratio; detail of the early-time behavior seen in Fig. 3. The slope discontinuity at 373 K is due to initiation of vaporization.

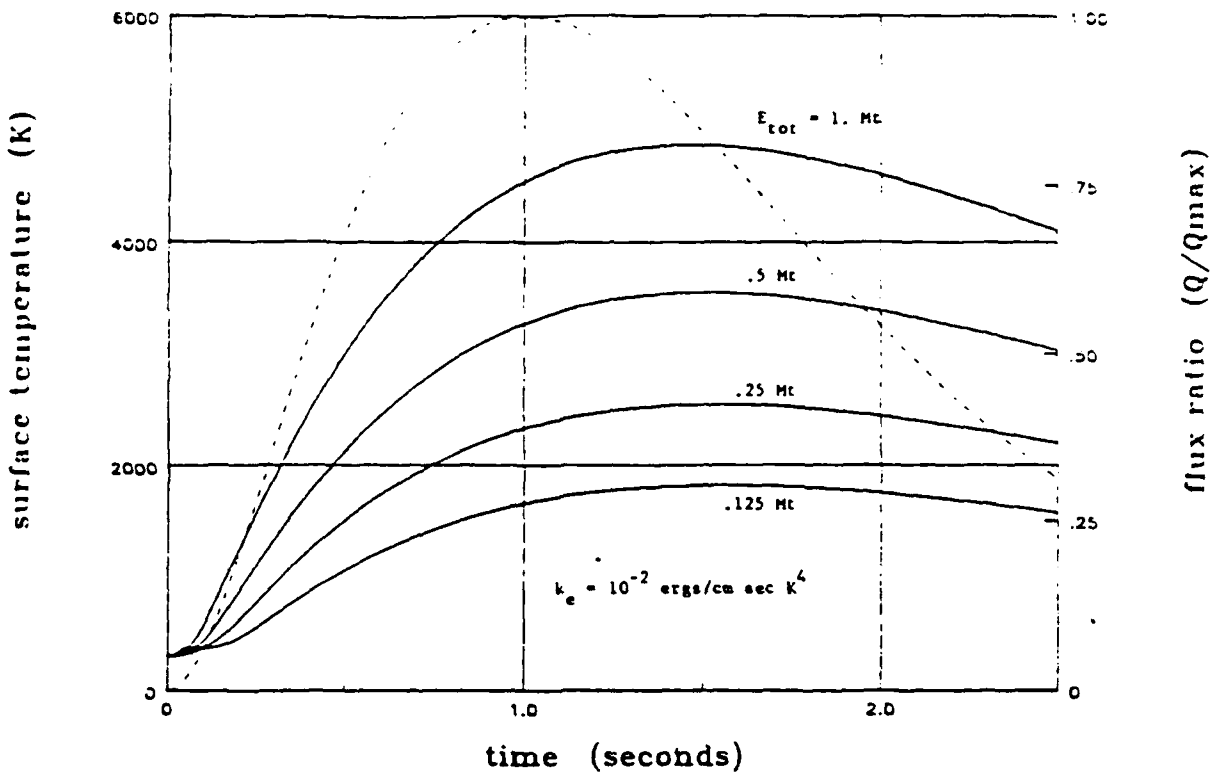

Fig. 5 Surface temperature and heat flux ratio with total energy release as the parameter. Rise time to Q_{max} is 1 second (b = 2/sec).

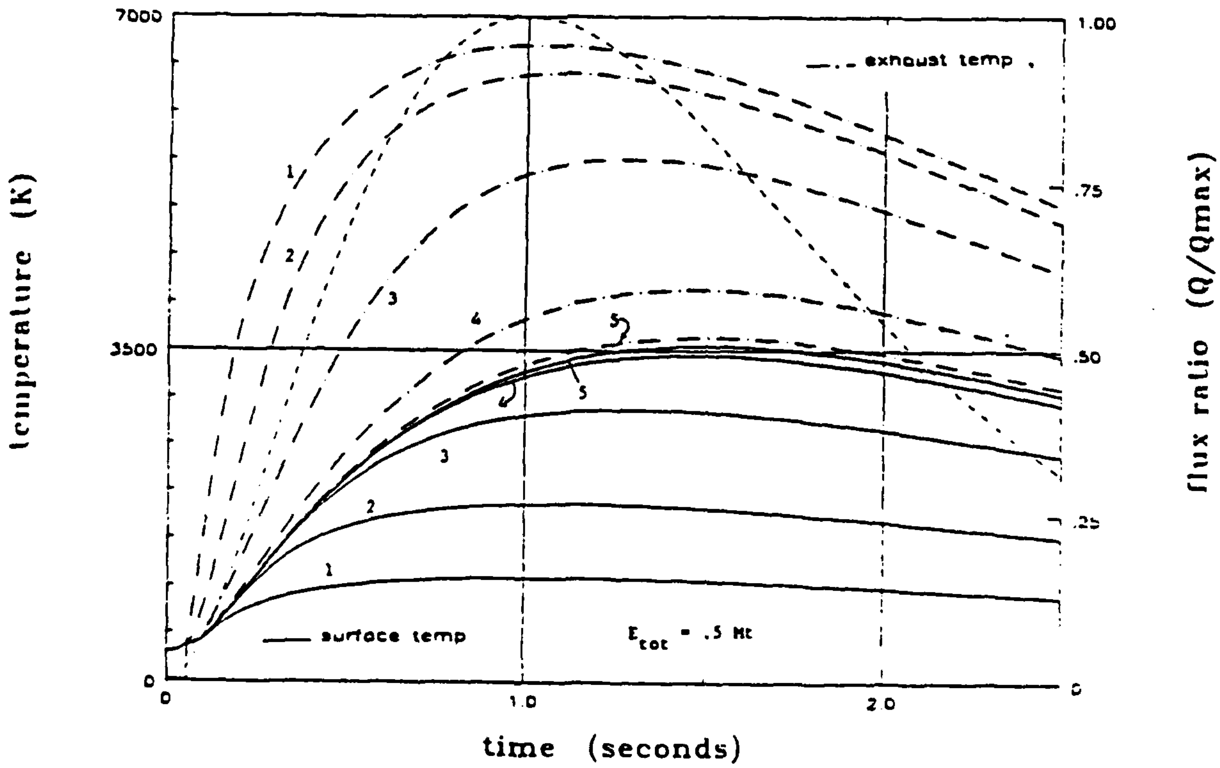

Fig. 6 Surface and vapor/air exhaust temperatures for a range of vapor/air interstitial radiation coefficients k_e. Curve pairs 1 through 5 correspond to $k_e = 10^{-6}, 10^{-5}, 10^{-4}, 10^{-3}, 10^{-2}$ ergs/cm sec K^4, respectively. $E_{tot} = .5$ Mt, b = 2/sec.

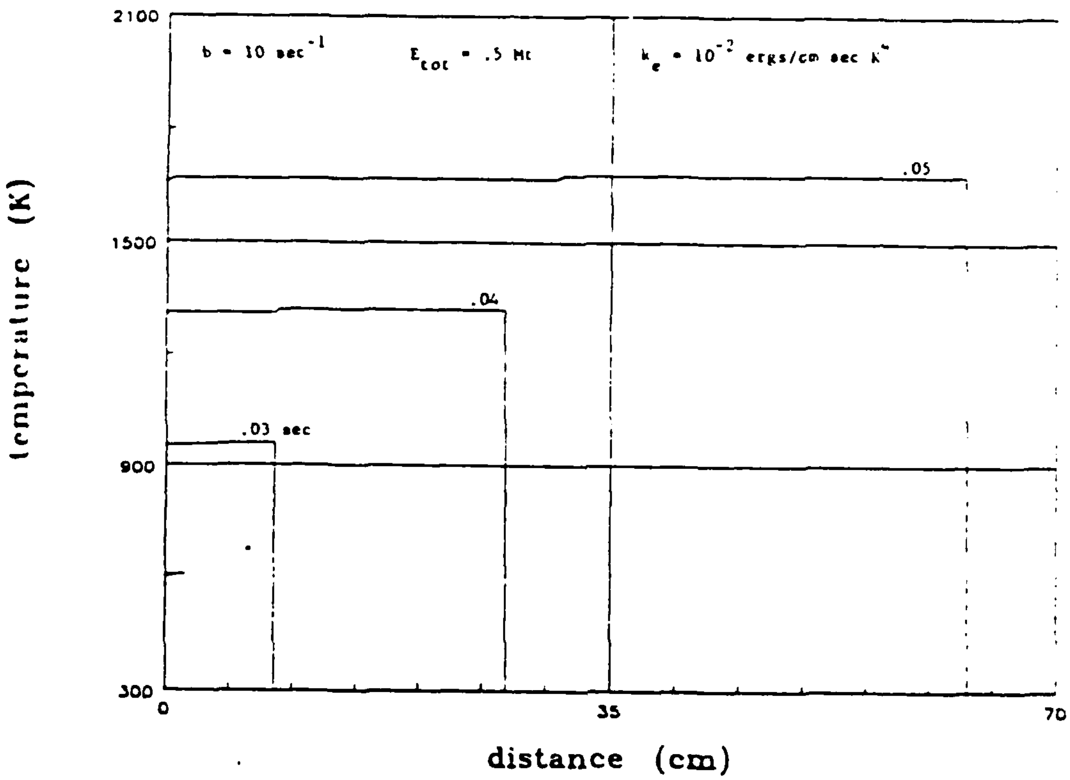

Fig. 7 Temperature vs. distance in the vapor/air exhaust for a range of times: $k_e = 10^{-2}$ ergs/cm sec K^4, b = 10/sec, E_{tot} = .5 Mt.

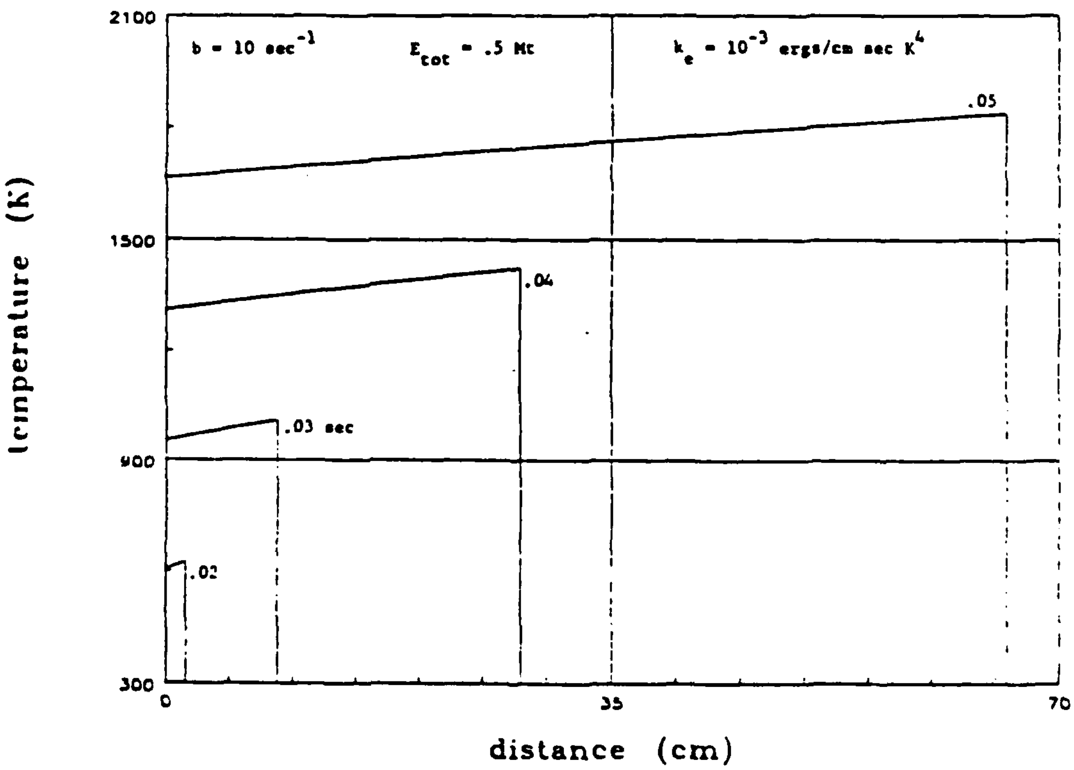

Fig. 8 Temperature vs. distance in the vapor/air exhaust for a range of times, $k_e = 10^{-3}$ ergs/cm sec K^4, b = 10/sec, E_{tot} = .5 Mt.

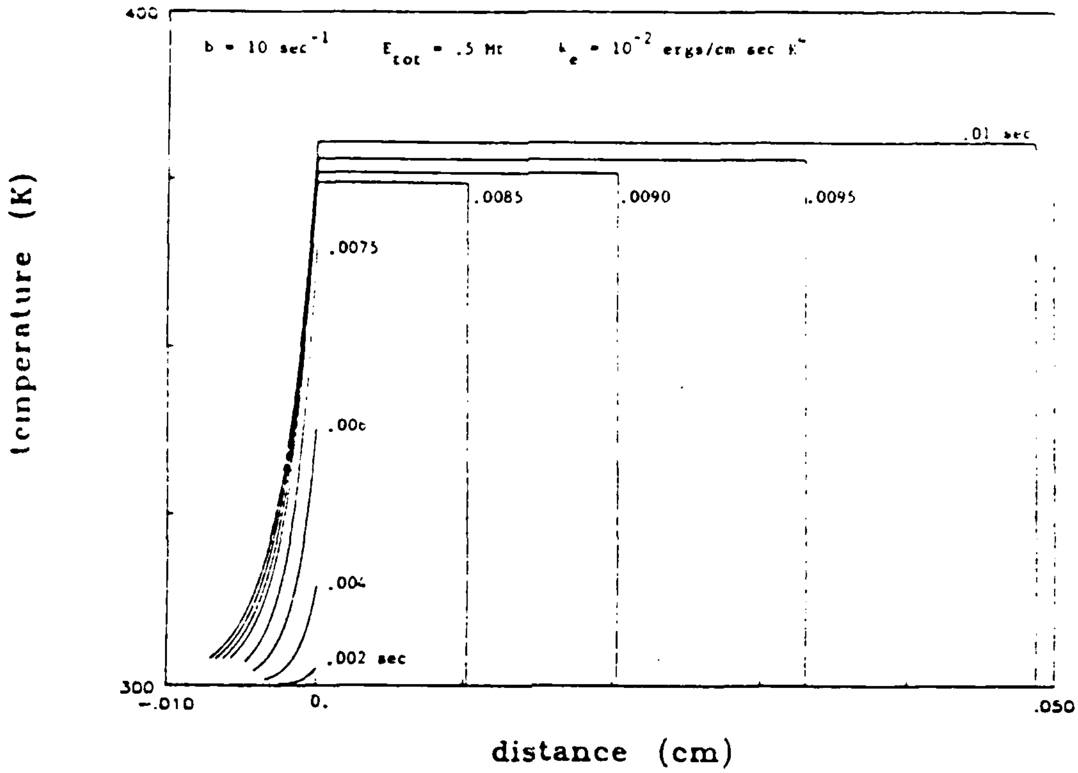

Fig 9 Temperature vs. distance from virgin soil to vapor/air exhaust front for a range of times. Pre-vaporization; t = .002, .004, .0075 seconds: post-vaporization; t = .0085, .0090. .0095, .01 seconds. The post vaporization times are too early, and the distance scale too large to show the vaporization front in the soil.

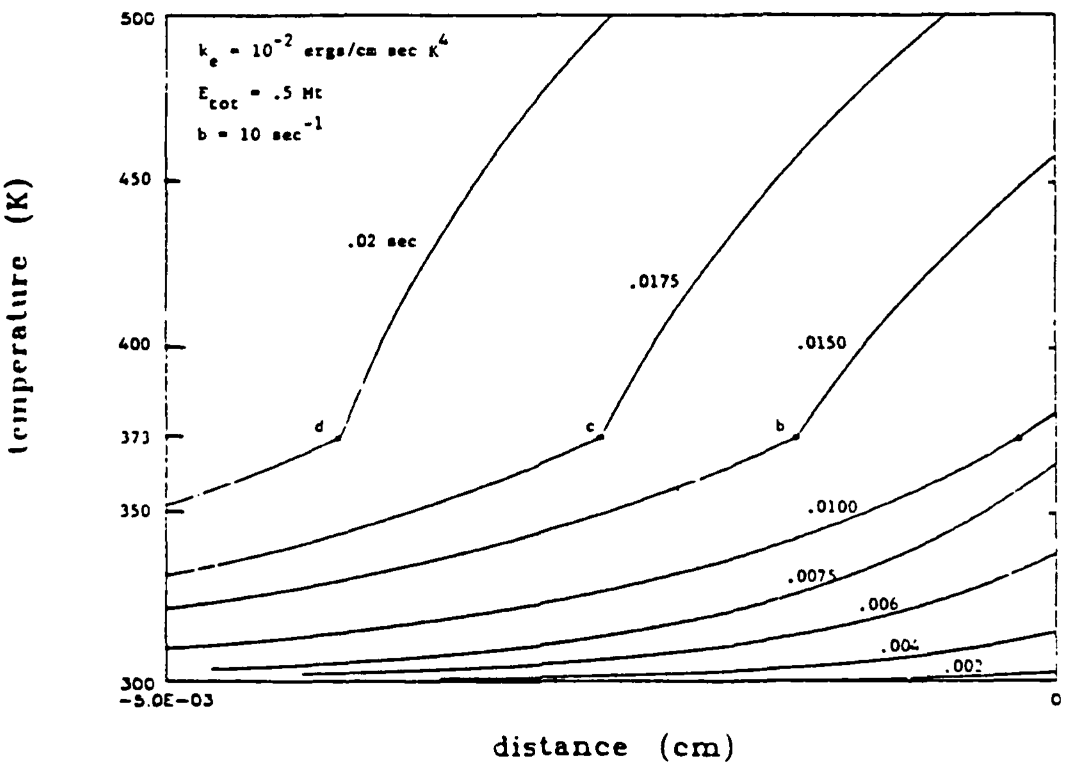

Fig. 10 Temperature vs. distance in the soil (y < 0) showing pre- and post-vaporization periods, and the vaporization front (at a, b, c, d).

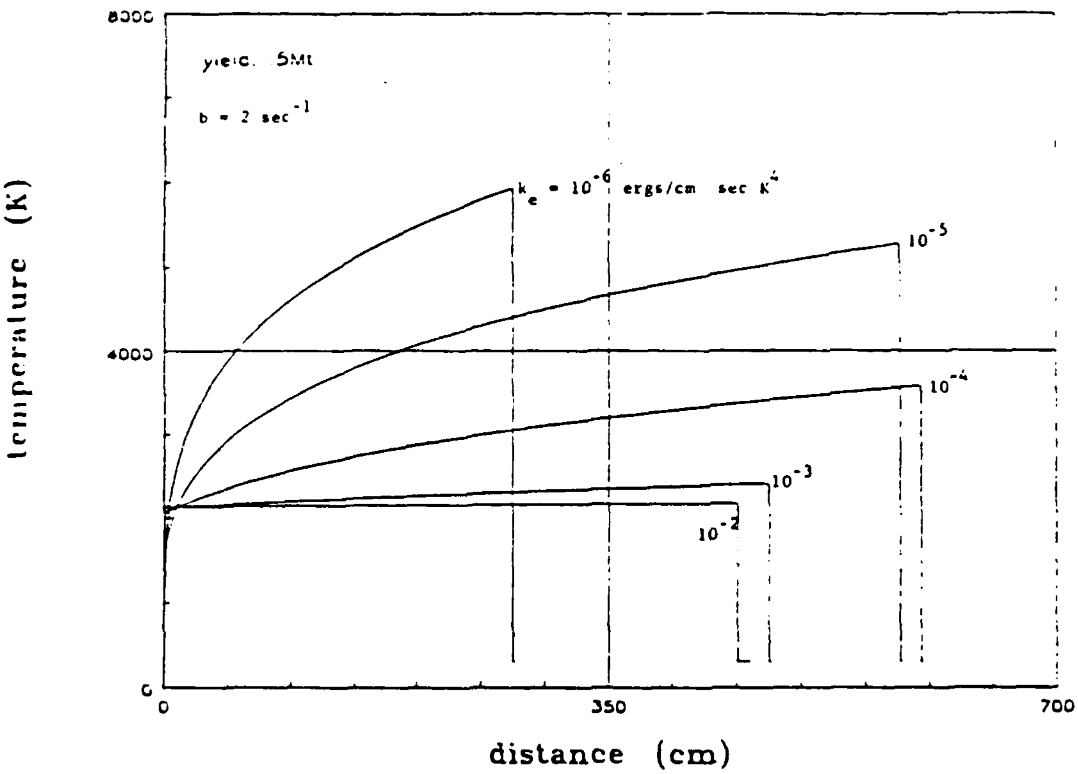

Fig. 11 Temperature vs. distance in the vapor/air exhaust at .5 seconds for a range of vapor/air interstitial radiation coefficients; note the reduction in surface temperature, maximum in extension of vapor/air exhaust, and increase in vapor/air exhaust front temperature as k_e decreases.

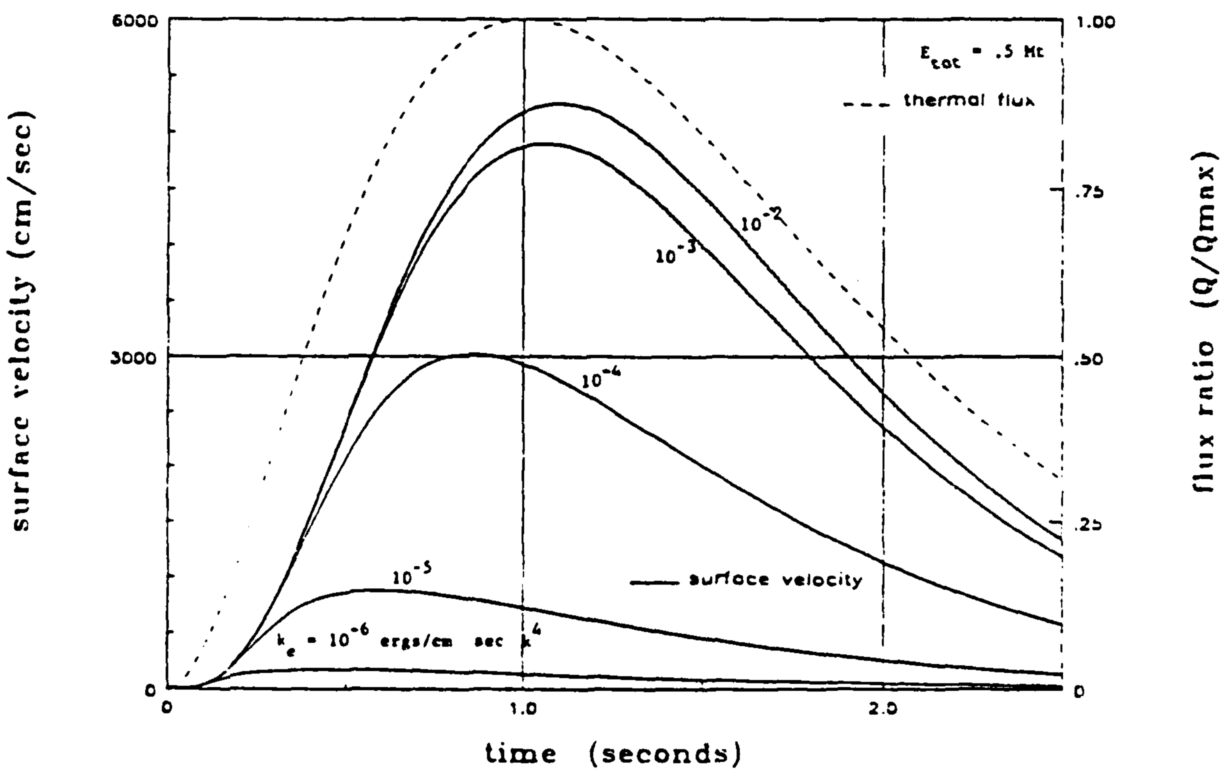

Fig. 12 Vapor/air exhaust mixture velocity at the surface for a range of k_e, the vapor/air interstitial radiation coefficient.

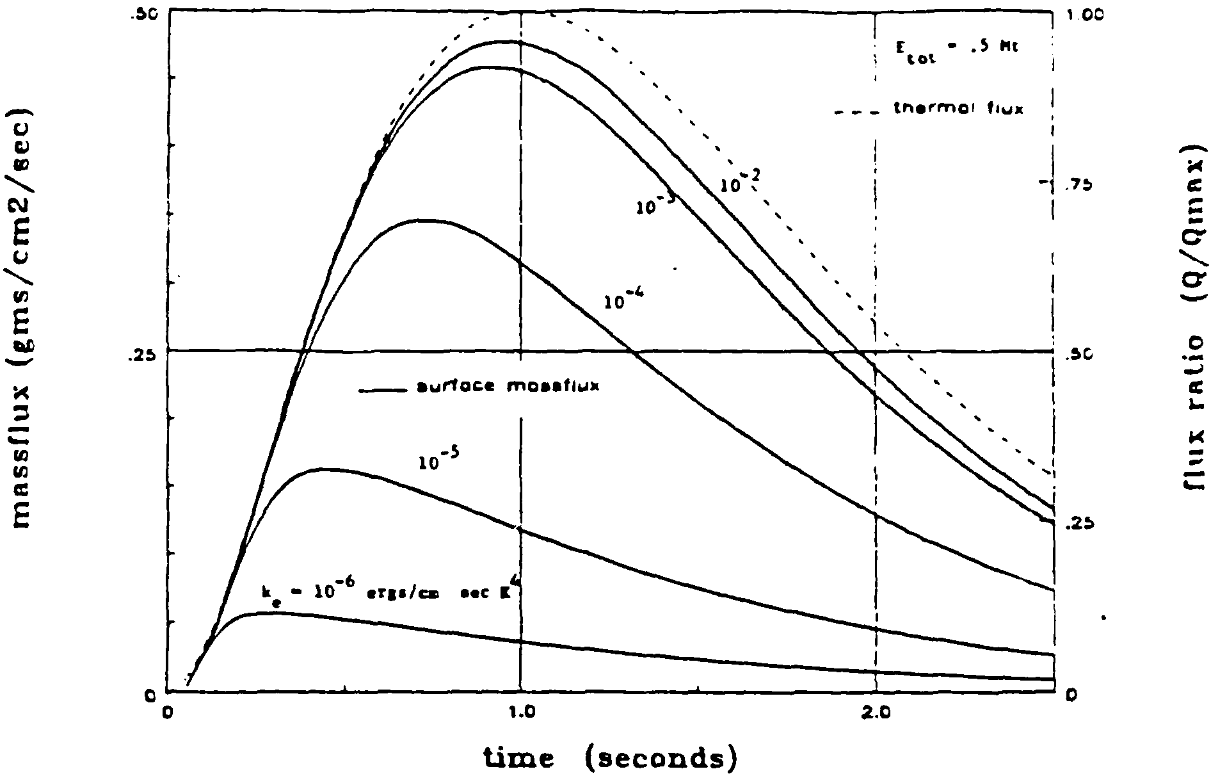

Fig. 13 Vapor/air exhaust mixture massflux at the surface for a range of k_e, the vapor/air interstitial radiation coefficient.

Table 1. VALUES OF PHYSICAL QUANTITIES

Virgin soil	
thermal diffusivity	$\alpha_v = 1.11 \times 10^{-3}$ cm^2/sec
thermal conductivity	$k = 1.63 \times 10^4$ ergs/cm sec K
porosity	$n = .5$
emissivity	$\epsilon_v = .85$
density of soil	$\rho = 1.6$ gms/cm^3
weight of fraction of water	$w_f = .138$
heat of vaporization (of H_2O)	$H = 2.27 \times 10^{10}$ ergs/gm
vaporization temperature	$T_f = 373$ K
Soil wake	
interstitial radiation coef.	$k_s = 4.5 \times 10^{-7}$ ergs/cm sec K^4
Vapor/air exhaust	
pressure	$P_o = 1.01 \times 10^6$ dynes/cm^2
interstitial radiation coef.	$k_e = 10^{-2}$ ergs/cm sec K^4
mixture gas constant	$R = 335 \times 10^4$ cm^2/sec^2 K
emissivity	$\epsilon_o = .10$
ratio of specific heats	$\gamma = 1.3$
Energy release parameters	
height of burst	$h = 6.09 \times 10^4$ cm
ground range	$R_g = 1.53 \times 10^5$ cm
inverse characteristic time	$b = 10$ sec^{-1}
temperature of atmosphere	$T_\infty = 300$ K

1985 USAF-UES SUMMER FACULTY RESEARCH PROGRAM/GRADUATE
STUDENT SUMMER SUPPORT PROGRAM

Sponsored by the
AIR FORCE OFFICER OF SCIENTIFIC RESEARCH
Conducted by the
UNIVERSAL ENERGY SYSTEMS, INC.

FINAL REPORT

ANALYSIS OF RELATIONSHIPS AMONG SELF, PEER, AND SUPERVISORY RATINGS OF PERFORMANCE

Prepared by:	Kurt Kraiger
Academic Rank:	Assistant Professor
Department and University:	Department of Psychology, University of Colorado at Denver
Research Location:	Air Force Human Resources Laboratory, Manpower and Personnel Division Force Utilization Branch, Brooks Air Force Base, San Antonio, Texas
USAF Research:	Dr Jerry Hedge
Date:	22 September 1985
Contract No:	F49620-85-C-0013

Analysis of Relationships Among Self, Peer, and Supervisory Ratings of Performance

by

Kurt Kraiger

Abstract

It is expected that performance ratings will continue to constitute a major portion of the Air Force performance measurement program. The relative quality of self, peer, and supervisory ratings in previous studies was assessed using meta-analysis techniques. Meta-analysis refers to a methodology for statistically cumulating the results of empirical studies. Self ratings were found to be slightly more lenient than peer or supervisory ratings, but subject to less halo. Peer and supervisory ratings showed the greatest convergence though peers appear to diverge from other sources in ratings of interpersonal skills. Self ratings diverge the most in evaluations of leadership. It was concluded that peer and supervisory ratings show considerable overlap in measuring total job performance. Self ratings could be included to ensure broader measurement of the total criterion space. All three forms showed sufficient psychometric quality to be used for validation purposes. Suggestions were given for future research on rating source using the Air Force's performance measurement project data.

ACKNOWLEDGMENTS

The support of a number of individuals and organizations should be acknowledged. I am grateful to the combined efforts of UNIVERSAL ENERGY SYSTEMS and the Air Force Office of Scientific Research for providing the opportunity to spend a ten-week period concentrating solely on a single unit of research. Various members of the Human Resources Laboratory helped make conduct of the research a smooth and pleasant experience. Lt Col Rodger Ballentine facilitated my arrival and start-up at the Lab. Dr R. Bruce Gould provided key input during the planning stages of my research effort. Dr Jerry Hedge deserves particular thanks for providing technical support and helping me mold my thoughts through our discussions. Librarians Orrine Woinowsk and Millie Jones were extremely efficient in providing references for my research. Finally, Rosemary Guerrero deserves special thanks for her fast typing under time pressure.

An Analysis of Relationships Among Self, Peer, and Supervisory Ratings of Performance

1.0 Introduction

1.1 Background. Performance ratings remain the most popular form of employee appraisals, especially for test validation (Landy & Farr, 1983). Though psychologists continue to search for relevant cognitive, objective, and work sampling criteria, it is expected that ratings will remain prevalent due to their adaptability to a wide variety of jobs and appraisal functions. In an example close to home, the Air Force is in the process of developing sophisticated performance measures called "walk-through performance tests" which feature rigorously developed, content valid work samples and interview evaluated by highly trained, external administrators (Gould & Hedge, 1983). The thoroughness of the walk-through is advantageous from a measurement perspective yet may make the tests too costly and time-consuming to develop and administer to all specialties. In addition, many jobs (e.g., managerial) may be too complex or technical to lend themselves to hands-on testing. Thus, it is likely that the Air Force, too, will need to continue to use performance ratings as the principal criterion in many or most specialties.

Work supervisors are the most common source of rating data. Early attempts to incorporate other sources into the measurement system were not motivated by beliefs that these sources could provide worthwhile assessments of past performance. Instead, peers were consulted to provide predictions of behavior in future domains (e.g., leadership roles; Hollander, 1954) and self ratings were obtained to reduce employee defensiveness in performance appraisal interviews (Meyer, Kay, & French, 1965). While researchers have readily embraced supervisory ratings despite awareness that supervisors may distort their ratings for self-serving purposes (Bass, 1956), they have been equally reluctant to implement peer or self rating systems for fear that such ratings will be biased by source factors such as rater-ratee friendship (Wherry & Fryer, 1949) or self-enhancement tendencies (Holzback, 1978).

For example, a frequently expressed concern of personnel researchers is that self ratings will show greater leniency (higher means) than ratings from other sources (Thornton, 1980), presumably for self-enhancement purposes (Schlenker, 1980). Past research does reflect a general tendency of workers to rate themselves higher than their supervisors rate them (e.g., Holzback, 1978; Klimoski & London, 1974; Prien & Liske, 1962). A second method of comparing rating sources has been to assess the degree of convergent and discriminant validity in ratings aligned in a multitrait-multirater matrix. Much of the research on this topic follows the work of Lawler (1967) who proposed that ratings be required to show both convergent validity (agreement between sources on the same dimension) and discriminant validity (a differential ordering of ratees on different dimensions). Studies including all three rating sources have generally reported greater convergence between peer and supervisory than between peer and self ratings or between self and supervisory ratings (Blackburn & Clark, 1975; Klimoski & London, 1974; Lawler, 1967; Morton & MacBeth, 1977) though several other studies have reported considerable agreement between self and supervisory ratings (Pym & Auld, 1965; Williams & Sieler, 1973) or between self and peer ratings (Borg & Hamilton, 1956; Downey, Duffy, & Shiflett, 1975). A third concern has been the relative degree of halo in ratings by different sources. Halo is defined here as a tendency to rate a person similarly across traits in accordance with some global impression of favorability or unfavorability (Bernardin & Beatty, 1984). Halo has been typically operationalized as the level of intercorrelations among dimensions. In an earlier review of self ratings, Thornton (1980) reported relatively smaller intercorrelations for self ratings than other rating sources. There is no research documenting large differences in halo between peer and supervisory ratings.

1.2 Functions of Meta-Analysis. Throughout this introduction, reference has been made to the need to determine the average, typical, or overall relationship between different variables without discussing how this assessment should be done. Meta-analysis (Glass, McGaw, &

Smith, 1981; Hunter, Schmidt, & Jackson, 1982) is an ideal strategy for summarizing relationships between variables across studies. Essentially, in meta-analysis, studies replace individuals as the unit of analysis. A large sample of studies on the same topic and the outcome of each study is represented by a common metric, typically $\underline{r}$ in correlational studies and $\underline{d}$ in experimental studies. Because $\underline{r}$ and $\underline{d}$ are independent of units of measurement, they can be meaningfully compared (i.e., averaged over studies).

2.0 Objectives of the Research Effort

In the present investigation, meta-analytic procedures will be used to examine the leniency, convergent and discriminant validity, halo, and relative weighting of self, peer, and supervisory ratings. Whenever possible, separate analyses will be made for broad job dimensions such as interpersonal skills or job knowledge. Formulas for estimating sampling error variance (Hunter et al., 1982) will be applied to evaluate the severity of study-to-study variance in results. When sampling error variance fails to account for most true variance, potentially relevant moderators will be examined.

After presentation of the study's methodology and results, the final section will discuss the implications of the meta-analysis findings for the Air Force's performance measurement project. Included in this section will be specific recommendations for comprehensive data analysis strategies to be applied to performance data collected on the jet engine mechanic specialty.

3.0 Methods

3.1 Identificaion of Studies. A thorough and comprehensive literature search is necessary in meta-analysis to provide accurate estimates of population parameters. In the present analysis, potential studies were located primarily through keywork searches in major journals and through reference lists of previous reviews in the areas of performance appraisal (Bernardin & Beatty, 1984; Landy & Farr, 1980; 1983), peer ratings (Kane & Lawler, 1978; Lammlein & Borman; Lewin & Zwang, 1976), and self ratings (Mabe & West, 1982; Thornton, 1980). A total of 49 independent samples in 44 different

sources were located.

3.2 Coding Studies. After the studies were located, information necessary for the meta-analysis was extracted from each. All coding was done by the author. Important information was of two types: Statistical and study characteristics. Statistical data recorded were sample sizes and d values, correlations between rating sources by dimensions, intraclass correlations from multitrait-multirater matrices, average dimension intercorrelations, and/or correlations between dimensional and overall ratings within rating source. Not every statistic was typically reported by each study, but each study reported at least one statistic which could be cumulated. To provide meaningful aggregations over rating dimensions, data on specific study dimensions were grouped in five general performance dimensions: Interpersonal skills, personal qualities, job aptitude, leadership and instruction, and level of performance.

Study characteristics were features of the subject or methodology which could be meaningfully related to a study's effect size. The coded study characteristics were where the study was published, ratees' job, type of organization, rating purpose, type of rating scale, and whether rater training was given.

3.4 Meta-Analytic Procedures. Full details of these procedures and computational formulas are presented in Hunter et al. (1982). Briefly for each measure of effect (d, r, or intraclass correlation), its mean and variance across studies was computed within each performance category. Effect sized were weighted by sample size. Next, estimated variance in effect sizes due to sampling error (σe^2) and estimated population variance (true variance less sampling error) were computed. All analyses were performed using a specially written SPSS program and the AFHRL Univac computer.

Estimated population variance represents the study-to-study variation to be expected if all studies were conducted with extremely large samples. The ratio of population variance to true variance suggests the degree to which moderator variables are likely to be present. If the ratio is large, the implication is that sampling

error could not be expected to account for the observed variation in effect sizes: Under these conditions, one or more moderators may be operative.

In several analyses in the present study, the ratio of population variance to actual variance warranted further investigation. Unfortunately, there was too little variation in several study features to effectively analyze their influence on study outcomes. Separate analyses on moderator subsets were typically similar to those based on all studies, though several anomolous results appeared due to the small number of studies in the secondary analyses. Because these moderator analyses revealed no new insights, only the analyses on all studies are presented. 4.0 Results

4.1 Level Differences. Results of the meta-analysis of effect sizes (*d*) between rating sources are presented in Table 1. For a comparison of self ratings with other sources, a positive *d* value indicated higher self ratings. For the comparison of peer and supervisory sources, a positive value indicates higher peer ratings. It should be noted that even after collapsing the eight performance dimensions into five, there were too few effect sizes in some categories to ensure stable population estimates. Thus, interpersonal skills, personal qualities, job aptitude, and leadership and instruction were further collapsed into a single category for this analysis.

On the average, self ratings were higher than supervisory ratings for the collapsed performance dimensions (d = .232) and for level of performance (d = .185). Self ratings were also higher than peer ratings on the collapsed dimensions (d = .295), but somewhat lower on level of performance (d = .048). These latter comparisons though were based on a small number of studies and should be viewed with caution. Finally, comparisons of supervisory and peer ratings reveal virtually no difference in mean levels between these two sources on either the collapsed dimensions or level of performance. It is also clear that the overall leniency effect for self ratings is slight; mean self ratings are typically only two-tenths or three-tenths of a standard deviation higher than mean supervisory on self ratings.

Insert Table 1. About Here

4.2 Convergent and Discriminant Validity. Evidence for convergent validity between sources is presented in Table 2 and 3, Table 2 shows the results of a meta-analysis of bivariate correlations between different sources for each of the performance categories. The results show low agreement between self ratings and either peer or supervisory ratings in all categories. Average correlations within categories ranged between .22 and .30 for comparisons of self and supervisory ratings, and ranged between .07 and .30 for self and peer ratings. In contrast, peers and supervisors showed greater convergence as average correlations ranged from .32 to .52. Self ratings converged the least with other sources on the Leadership and Instruction dimension (r = .16 with supervisory ratings; r = .07 with peer ratings). Similarly, convergence for peer ratings appeared lowest on the Interpersonal Skills dimension (r = .14 with self ratings and r = .32 with supervisory ratings).

Cumulated effects from multitrait-multirater designs are presented in Table 3 and show a similar pattern of results as those in Table 2. The cumulated values in Table 3 are intraclass correlations (ICC's) which equal the ratio of variance due to an effect to error variance within a study. Intraclass correlations for the ratee effect indicate agreement in the ordering of ratees by two or more sources.

As can be seen in Table 3, the convergent validity of rating sources is guite low when studies include all three rating sources (ICC = .25), self ratings and supervisory ratings (ICC = .18), and self ratings and peer ratings (ICC = .30). Convergence between peer and supervisory ratings was the highest (ICC = .35).

Table 3 also presents information regarding the discriminant validity of ratings by different sources. This information is indicated by intraclass correlations for the ratees X traits interaction in a multitrait-multirater analysis. This interaction is desirable since work performance is multi-faceted and workers should be expected to differ in their rank ordering from dimension to

dimension. The results show that regardless of the comparison between sources, discriminant validity is very low (ICC = .08 for self vs. supervisory ratings; ICC = .06 for self vs. peer ratings; and ICC = .11 for peer vs. supervisory ratings).

Insert Table 2 and 3 About Here

4.3 Halo. Cumulated dimension intercorrelations by rating source are displayed in Table 4. Consistent with popular belief, dimension intercorrelations for self ratings are typically lower than for either peer or supervisory ratings. The average dimension intercorrelation for self ratings was .41, the average value for peer ratings was .57, and the average intercorrelation for supervisory ratings was .55.

Insert Table 4. About Here

5.0 Discussion

5.1 Conclusions. The first point to note is how little research has actually been done comparing different rating sources. The number of studies cumulated in most analyses was typically small. Thus, the first conclusion is that has been little systematic research done on different rating sources.

A second conclusion is that the available evidence suggests ratings by any of the three sources would be equally well suited to validation research. Since the comparisons made in this report were between sources and not against any external criteria, no conclusions about the absolute quality of the three sources can be drawn. All three may be good or all three my be bad. While there is a slight leniency effect for self ratings, the effect is not so large that it would cause severe range restriction problems in a validation analysis. Peer and supervisory ratings may be more prone to halo than self ratings but again size of the effect is not so large that it would be a problem in validation studies, particularly when rating dimensions are combined into an overall criterion. The lack of discriminant validity in all three sources revealed by the multitrait-multirater analysis would argue for the formation of composites in

most instances.

Thirdly, convergent validity appears greatest between peer and supervisory ratings. Self ratings typically show a higher mean than peer or supervisory ratings which in turn are nearly equal. Peer and supervisory ratings show nearly equal degrees of dimension intercorrelations and both are greater than self ratings. Dimension intercorrelations and intraclass correlations for convergent validities are highest for peer vs. supervisory ratings.

This information can be interpreted two ways. First, it suggests the use of either of peer or supervisory ratings but not self ratings in validation research if only one source can be used. The consistent divergence of self ratings makes their adoption as a sole criterion problematic. On the other hand, the consistent similarity of results comparing peer and supervisory ratings can be taken as evidence that each is validly measure something. The other interpretation is that self ratings are a highly desirable source if multiple rating sources are to be used and combined. When combining multiple criteria, duplicity in measures is not advantageous. It is apparent that self ratings are often measuring different constructs (or the same constructs differently) than peer or supervisory ratings. Combining this different vantage with one or both ot the other sources would help maximize measurement of the total criterion space.

5.2 Recommendations. A good meta-analysis should raise as many questions as it answers. Most of the recommended offered here are for research questions not addressed or not resolved by the meta-analysis. The first recommendation is the simplest but most important: The Air Force should continue to measure and study all three sources. The paucity of research of different rating sources goes far beyond the small number of total studies cited in the tables. There were few studies of a longitudinal nature. Most studies showed few of the characteristics of first-rate appraisal systems: Rater training programs, rater involvement in scale development, well-defined rating scales, feedback to ratees and raters, etc. Finally, virtually no studies included a meaningful

criterion to validate rating sources against. In each respect, the data base generated by the performance measurement project is far superior to most or all previous attempts to study rating sources.

The second recommendation is that the richness of the Air Force data base should be used to learn why differences by source occur. The motivation of raters to try to give meaningful ratings is fast becoming a major concern of researchers. Yet we know little or nothing of differences between incumbents, peers, and supervisors in rater motivation. In most instances, supervisors may be the most willing to complete rating forms (because it's part of their job) but this is not the same as saying they are the most willing to rate accurately. Raters at each level should be asked if they want to rate accurately and fairly. They should also be asked what they want to rate. It is possible that given a single set of rating dimensions, incumbents, peers, and supervisors would select different subsets of dimensions to actually make their ratings on. This could be assessed by allowing raters a "can't rate" option or asking raters how confident they are in the accuracy of each dimension rating.

More research needs to be conducted on the meaning of ratings to different sources. One approach would be use regression analysis with an overall rating regressed on dimensional ratings within each source. The relative size of the beta weights would indicate the importance of various dimensions to raters' global impressions of ratees (Zammuto, London, & Rowland, 1982). Another strategy would be separate factor analyses of dimensional ratings by each source. Previous attempts to factor analyze ratings by different sources have analyzed both sources in a single matrix. While such an approach is useful for assessing method (rater source) bias in ratings, it is less helpful for understanding the dimensionality or structure of ratings by different sources. Separate exploratory factor analyses by rating source would be more useful for generating hypotheses about how differently raters perceive the performance of ratees. Hopefully, these hypotheses could later be tested using confirmatory factor analysis strategies (Joreskog, 1969).

AD-A166 177 UNITED STATES AIR FORCE SUMMER FACULTY RESEARCH PROGRAM 1985 TECHNICAL RE..(U) UNIVERSAL ENERGY SYSTEMS INC DAYTON OH R C DARRAH ET AL. DEC 85 AFOSR-TR-86-0140 10/15

UNCLASSIFIED F49620-85-C-0013 F/G 5/1 NL

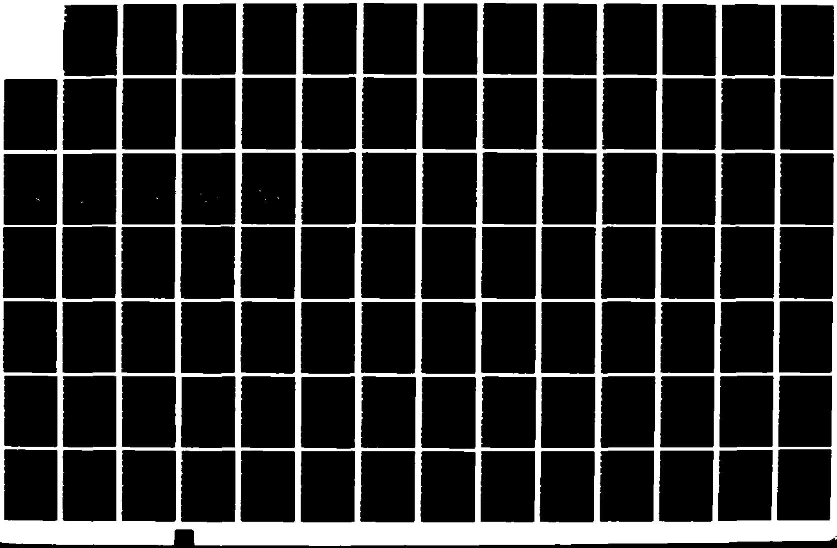

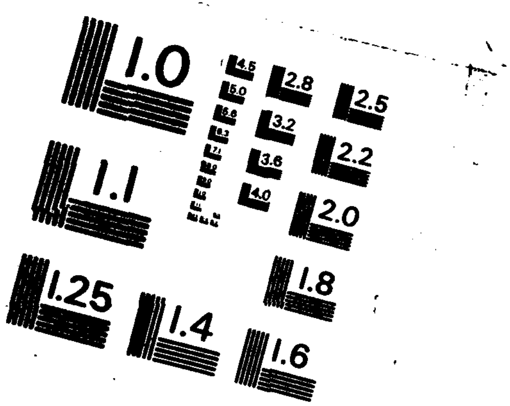

MICROCOPY RESOLUTION TEST CHART
NATIONAL BUREAU OF STANDARDS-1963-A

Finally, efforts should also be made to validate each source against an external criterion. The Air Force data base is also noteworthy for its walk-through performance tests. Most previous studies have not had such a high fidelity measure to compare ratings against. Comparisons of each sources ratings against a measure of job performance can reveal valuable information of the absolute validity of each source and not simply their relative value in comparison with each other.

References

(Note: References with an asterik were studies used in the meta-analysis.)

*Albrecht, P. A., Glaser, E. M., & Marks, J. (1964). Validation of a multi-assessment procedure for managerial personnel. Journal of Applied Psychology, 48, 351-360.

*Baird, L. S. (1977). Self and superior ratings of performance: As related to self-esteem and satisfaction with supervision. Academy of Management Journal, 20, 291-300.

*Bartlett, C. J. (1959). The relationships between self-ratings and peer ratings on a leadership behavior scale. Personnel Psychology, 12, 237-246.

*Bass, B. M. (1954). Validity information exchange (Report 7-045). Personnel Psychology, 7, 279.

Bass, B. M. (1956). Reducing leniency in merit ratings. Personnel Psychology, 9, 359-369.

*Berkeley, M. H. (1955, September). Comparison of supervisor, co-worker, and self-ratings of WAF job performance (AFPTRC-TN-55-25). Lackland AFB, TX: Air Force Personnel and Training Research Center.

Bernardin, H. S., & Beatty, R. W. (1984). Performance appraisal: Assessing human behavior at work. Boston: Kent.

*Blackhurn, R. T. & Clark, M. J. (1975). Assessment of faculty performance: Some correlates between administrator, colleague, student, and self-ratings. Sociology of Education, 48, 242-256.

*Blaha, W. C. (1974). A study of peer and reporting senior ratings in a Marine Corps Rifle Company. Monterey, CA: Naval Postgrduate School.

*Borg, W. R. & Hamilton, E. R. (1956). Comparison between a performance test and criteria of instructor effectiveness. Psychological Reports, 2, 111-116.

*Borman, W. C. (1974). The ratings of individuals in organizations: An alternate approach. Organizational Behavior and Human Performance, 12, 105-124.

*Brief, A. P., Aldag, R. J., & VanSeel, M. (1977). Moderators of the relation-ships between self and superior evaluations of job performance. Journal of Occupational Psychology, 50, 129-134.

*Broedling, L. A. (1975). Relationship of internal-external control to work motivation and performance in an expectancy model. Journal of Applied Psychology, 60, 65-70.

*Chiu, L. -H. (1975). Influence of student teaching on perceived teaching competence. Perceptual and Motor Skills, 40, 872-874.

Dickinson, T. L., Hassett, C. E., & Tannenbaum, S. I. (1985). A meta-analysis of multitrait-multimethod studies of work performance ratings. Report submitted to AFHRL, Brooks AFB, TX.

*Dickinson, T. L. & Tice, T. E. (1977). The discriminant validity of scales developed by retranslation. Personnel Psychology, 30, 217-228.

*Downey, R. G., Duffy, P. J., & Shiflett, S. (1979, June). Construct validity of leader effectiveness criteria (Technical Paper #368). Alexandria, VA: US Army Research Institute for The Behavioral and Social Sciences.

*Doyle, K. D. & Chrichton, L. I. (1978). Student, peer, and self evaluations of college instructors. Journal of Educational Psychology, 70, 815-826.

*Dunnette, M. D., Perry, D. K., & Mahoney, T. A. (1956, June). Criteria of executive effectiveness (AFPTRC-TN-56-73). Lackland AFB, TX: Personnel and Training Research Center.

*Engle, K. B. & Betz, R. L. (1971). Peer ratings revisited. Counselor Education and Supervision, 10, 165-170.

Glass, G. V, McGaw, B., & Smith, M. L. (1981). Meta-analysis in Social research. Beverly Hills, CA: Sage.

*Gordon, L. V. & Medland, F. F. (1965). The cross-group stability of peer ratings of leadership potential. Personnel Psychology, 18, 173-177.

Gould, R. B., & Hedge, J. W. (1983, August). Air Force job performance criterion development. Paper presented at the 91st Annual Convention of the American Psychological Association, Anaheim, CA.

Guion, R. (1965). Personnel testing. New York: McGraw-Hill.

*Hausman, H. S. & Strupp, H. H. (1955). Non-technical factors in supervisors' ratings of job performance. Personnel Psychology, 8, 201-217.

*Heneman, H. G., III. (1974). Comparisons of self- and superior ratings of managerial performance. Journal of Applied Psychology, 59, 638-642.

Hollander, E. P. (1954). Buddy ratings: Military research and industrial implications. Personnel Psychology, 7, 385-393.

*Holzbach, R. L. (1978). Rater bias in performance ratings: Supervisor, self-, and peer ratings. Journal of Applied Psychology, 63, 579-588.

Hunter, J. E., Schmidt, F. L., & Jackson, G. B. (1982). Meta-analysis: Cumulating findings across studies. Beverly Hills, CA: Sage.

Joreskog, K. G. (1969). A general approach to confirmatory maximum likelihood factor analysis. Psychometrika, 34, 183-202.

Kane, J. S., & Lawler, E. E., III. (1978). Methods of peer assessment. Psychological Bulletin, 85, 555-586.

King, L., Hunter, J., & Schmidt, F. (1980). Halo in a multidimensional forced-choice performance evaluation scale. Journal of Applied Psychology, 65, 507-516.

Kirchner, W. K. (1965). Relationships between supervisory and subordinate ratings for technical personnel. Journal of Industrial Psychology, 3, 57-60.

*Kissler, G. D. & Nebeker, D. M. (1970, September). Peer and supervisory ratings of research. San Diego, CA: Navy Personnel Research and Development Center.

*Klimoski, R. J. & London, M. (1974). Role of the rater in performance appraisal. Journal of Applied Psychology, 59, 445-451.

*Kraiger, K. (1981, November). Measuring police officer performance: Criterion development for the Columbus Police Officer Selection Validation Project. Columbus, OH.

*Kraut, A. I. (1975). Prediction of managerial success by peer and training-staff ratings. Journal of Applied Psychology, 60, 14-19.

Lammlein, S. E., & Borman, W. C. (1979, June). Peer rating research: Annotated bibliography (Tech Rep No. AFHRL-TR-79-9). Human Resources Laboratory, Brooks AFB, TX: Personnel Research Division.

Landy, F. J., & Farr, J. L. (1980). Performance rating. Psychological Bulletin, 87, 72-107.

Landy, F. J., & Farr, J. L. (1983). The measurement of work performance: Methods, theory, and applications. New York: Academic Press.

*Lawler, E. E., III. (1967). The multitrait-multirater approach to measuring job performance. Journal of Applied Psychology, 51, 369-381.

Lewin, A. Y., & Zwany, A. (1976). Peer nominations: A model literature critique and a paradigm for research. Personnel Psychology, 29, 423-447.

*Love, K. G. (1981). Comparison of peer assessment methods: reliability, validity, friendship bias, and user reaction. Journal of Applied Psychology, 66, 451-457.

Mabe, P. A., III., & West, S. G. (1982). Validity of self-evaluation of ability: A review and meta-analysis. Journal of Applied Psychology, 67, 280-296.

Meyer, H. H., Kay, E., & French, J. (1965). Split roles in performance appraisal. Harvard Business Review, 43, 123-129.

*Morton, J. B. & MacBeth, W. A. A. G. (1977). Correlations between staff, peer and self assessments of fourth-year students in surgery. Medical Education, 11, 167-170.

*Orpen, C. (1973). An empirical assessment of the job performance of high-level executives by means of a multitrait-multimethod matrix. Psychologica Africana, 15, 7-14.

*Parker, J. W., Taylor, E. K., Barrett, R. S., & Martens, L. (1959). Rating scale content: III. Relationship between supervisory- and self-ratings. Personnel Psychology, 12, 49-63.

*Porter, L. W. & Lawler, E. E., III. (1968). Managerial attitudes and performance. Homewood, IL: Richard D. Irwin, Inc.

*Prien, E. P. & Liske, R. E. (1962). Assessments of higher-level personnel: III. Rating criteria: A comparative analysis of supervisors ratings and incumbent self-ratings of job performance. Personnel Psychology, 15, 187-194.

*Pym, D. L. A. & Auld, H. D. (1965). The self-rating as a members of employee satisfactoriness. Occupational Psychology, 39, 103-113.

*Robinson, D. D. (1970). Predicting police effectiveness from self reports of relative time spent in task performance. Personnel Psychology, 23, 327-345.

Schlenker, B. R. (1980). Impression management: The self-concept, social identity and interpersonal relations. Belmont, CA: Wadsworth.

*Springer, D. (1953). Ratings of candidates for promotion by co-workers and supervisors. Journal of Applied Psychology, 37, 347-351.

*Thornton, G. C. (1968). The relationship between supervisory- and self-appraisals of executive performance. Personnel Psychology, 21, 491-455.

Thornton, G. C.,III. (1980). Psychometric properties of self-appraisals of job performance. Personnel Psychology, 33, 263-271.

Tucker, M. F., Cline, V. B., & Schmitt, J. R. (1967). Prediction of creativity and other performance measures from biographical information among pharmaceutical scientists. Journal of Applied Psychology, 51, 131-138.

Waldman, D. A., & Thornton, G. C., III. (1979). Comparing supervisors' self-evaluations to their administrators' evaluations. Medical Group Management, 26, 22, 24, 58.

Webb, W. B. & Nolan, C. Y. (1955). Student, supervisor, and self-ratings of instructional proficiency. Journal of Educational Psychology, 46, 42-46.

Wheeler, A. E. & Knoop, H. R. (1982). Self, teacher and faculty assessments of student teaching performance. Journal of Educational Research, 75, 178-181.

Wherry, R. J, & Fryer, D. H. (1949). Buddy ratings: popularity contest or leadership criteria? Personnel Psychology, 2, 147-159.

Williams, W. E. & Seiler, D. A. (1973). Relationship between measures of effort and job performance. Journal of Applied Psychology, 57, 79-54.

Zammuto, R. F., London, M., & Rowland, K. M. (1982). Organizational and rater differences in performance appraisals. Personnel Psychology, 35, 643-658.

Table 1

Level Differences: Effect Sizes Between Sources

Comparison	No. Studies	Total Sample	$\bar{d}$[a]	σ_d^2	Est. Pop. Var.	Percent Variance Unexplained
Collapsed Performance Dimensions:[b]						
Self-Supervisor[c]	22	2,110	.232	.1269	.0849	67%
Self-Peer[c]	3	380	.295	.0177	.0000	00
Peer-Supervisor[d]	12	1,552	.002	.1258	.0916	75
Level of Performance						
Self-Supervisor	6	566	.185	.2512	.2086	83
Self-Peer	3	335	-.048	.1122	.0765	68
Peer-Supervisor	5	739	.011	.0188	.0000	00

[a] $d=(X_1 - X_2)/Sd_x$ where X_1, X_2 are means for two sources and sd_x is a pooled standard deviation

[b] collapsed across Interpersonal skills, Personal Qualities, Job Aptitude, and Leadership & Instruction

[c] a positive value of d indicates the mean for self ratings were higher than ratings from other sources

[d] a positive value of d indicates the mean for peer ratings were higher than supervisory ratings

Table 2

Convergent Validity: Correlations Between Sources by Dimension Type

Dimension Type: Comparison	No. Studies	Total Sample	$\bar{r}$	σ_r^2	Est. Pop. Var.	Percent Variance Unexplained
Interpersonal Skills						
Self-Supervisor	7	687	.295	.0243	.0158	65%
Self-Peer	3	272	.136	.0342	.0235	69
Peer-Supervisor	7	953	.316	.0062	.0003	05
Personal Qualities						
Self-Supervisor	7	1,039	.225	.0022	.0000	00
Self-Peer	1	113	.300	.0000	.0000	00
Peer-Supervisor	8	1,085	.383	.0130	.0077	59
Job Aptitude						
Self-Supervisor	4	322	.266	.0070	.0000	00
Self-Peer	-	-	-	-	-	-
Peer-Supervisor	5	660	.384	.0140	.0085	61
Leadership & Instruction						
Self-Supervisor	7	654	.156	.0044	.0000	00
Self-Peer	3	324	.065	.0076	.0000	00
Peer-Supervisor	4	773	.444	.0049	.0024	49
Level of Performance						
Self-Supervisor	18	2,290	.219	.0370	.0299	81
Self-Peer	10	974	.254	.0483	.0394	82
Peer-Supervisor	21	2,629	.521	.0278	.0236	85

Table 3

Multitrait-Multirater Analysis: Intraclass Correlations by Source of Variance and Rater Comparison

Source of Variance: Comparison	No. Studies	Total Sample	$\overline{ICC}$	σ^2_{ICC}	Est. Pop. Var.	Percent Variance Unexplained
Ratee Effect						
(Convergent Validity):						
Self-Peer-Super	4	494	.254	.0018	.0000	00%
Self-Supervisor	7	756	.184	.0109	.0022	.20
Self-Peer	6	531	.296	.0048	.0000	00
Peer-Supervisor	9	916	.354	.0019	.0000	00
Ratee by Trait Effect						
(Discriminant Validity):						
Self-Peer-Super	4	494	.064	.0013	.0000	00
Self-Supervisor	7	756	.082	.0046	.0000	00
Self-Peer	6	531	.061	.0019	.0000	00
Peer-Supervisor	9	916	.112	.0091	.0000	00

Table 4

Halo: Average Correlations Among Dimensions by Rating Source

Rating Source	No. Studies	Total Sample	$\bar{r}$	σ_r^2	Est. Pop. Var.	Percent Variance Unexplained
Self	10	938	.405	.0219	.0144	66%
Peer	12	1,114	.567	.0243	.0193	80
Supervisor	14	1,482	.547	.0154	.0111	72

Table 5

Relative Weights: Correlations with Overall Performance by Rating Source and Dimension Type

Dimension Type: Rating Source	No. Studies	Total Sample	$\bar{r}$	σ_r^2	Est. Pop. Var.	Percent Variance Unexplained
Interpersonal Skills						
Self	6	604	.379	.0038	.0000	00%
Peer	6	869	.604	.0339	.0311	92
Supervisor	8	1,086	.560	.0146	.0111	76
Personal Qualities						
Self	2	188	.473	.0072	.0008	11
Peer	2	339	.643	.0169	.0148	88
Supervisor	4	527	.663	.0058	.0035	60
Job Aptitude						
Self	3	290	.426	.0003	.0000	00
Peer	2	318	.793	.0032	.0023	72
Supervisor	5	608	.715	.0102	.0082	80
Leadership & Instruction						
Self	5	477	.493	.0158	.0098	62
Peer	3	404	.446	.0580	.0532	92
Supervisor	5	543	.645	.0222	.0190	86
Level of Performance						
Self	2	300	.618	.0009	.0000	00
Peer	2	340	.804	.0115	.0108	94
Supervisor	3	457	.821	.0014	.0007	50

1985 USAF-UES SUMMER FACULTY RESEARCH PROGRAM

Sponsored by the

AIR FORCE OFFICE OF SCIENTIFIC RESEARCH

Conducted by the

UNIVERSAL ENERGY SYSTEMS, INC.

FINAL REPORT

NUMERICAL STUDY OF DETONATION NEAR A BARRIER

Prepared by: Dr. Madakasira V. Krishna

Academic Rank: Professor

Department and University: Mathematics and Computer Science, South Carolina State College

Research Location: Explosive Dynamics Laboratory, Air Force Armament Laboratory

USAF Research: Mr. David R. Wagnon

Date: July 30, 1985

Contract No.: F49620-85-C-0013

NUMERICAL STUDY OF DETONATION NEAR A BARRIER

by

Madakasira V. Krishna

ABSTRACT

The Hull (Eulerian) hydrocode developed by Orlando Technology, Inc. has been used to simulate numerically the propagation of detonation between explosives separated by a barrier. The investigation was restricted to two situations. In the first one, a barrier was placed next to the explosive without any medium in between. In the second one, a barrier in between a donor bomb and an acceptor bomb separated by air medium was considered. The main object of this project was to gain familiarity with the complex hydrocode. Suggestions for further research in this area are offered.

ACKNOWLEDGEMENT

The author would like to thank the Air Force Systems Command, Air Force Office of Scientific Research, and Universal Energy Systems, Inc. for providing him with the opportunity to spend a worthwhile and interesting summer at the Explosive Dynamics Lab, Eglin Air Force Base, Florida. He would like to acknowlede the Laboratory for its hospitality and excellent working conditions.

Finally, he would like to thank Mr. David Wagnon for suggesting the area of research, and Mr. Michael Gunger, for his guidance and collaboration during the computation of the problem.

I. INTRODUCTION:

Storage of large quantities of explosives at any Air Force installation is a problem. By reducing storage clearance requirements without endangering safety requirements, significant economic gains can be realized.

Many experimental studies of munition storage concepts have been conducted.[1,3] Tests are time consuming and expensive. Analytical and numerical procedures which could be used with some confidence to predict the effects of detonation of a stack of munitions is very valuable in analyzing new storage concepts. This is also helpful in rational effective planning of future full scale tests as may be required.

If a particular amount of munitions had to be stored on a given area, the safety requirement is primarily to ensure that no fragments landed outside this area. The problem then is to find appropriate combination of munition stack shapes, dimensions and distribution of stacks together with barricade shapes and dimensions and materials to be used in the barricade that would satisfy this requirement.

Many computer codes capable of solving the equations of continum physics associated with the above problem are available.[4] In this project as a first step in solving the above problem, a hydrocode developed by Orlando Technology Inc., is considered. This code is complex and gaining familiarity with the code is essential. The hydrocode (Eulerian) in relation to the problem under consideration consists basically of three parts. The computational process is as follows:

1.	Preprocessor (KEEL)	Initial Geometry Material Description Initial Conditions
2.	Main Program (HULL)	Conservation Equations o Mass o Momentum o Energy o Entropy Material Model o Stress-Strain Equations o Equations of State o Failure Criteria o Post Failure Model
3.	Post Processor (PULL)	Deformation Stress, Strain, Pressure and Temperature Fields Velocities, Accelerations Forces, Moments Energies, Momenta

A second order finite difference scheme is employed in HULL. Here two examples are considered to illustrate the use of the hydrocode in solving the basic problem under consideration.

II. OBJECTIVES:

The main problem under consideration is to find combination of munitions stack shapes together with barricade shapes, dimensions and material to be used in the barricade that would help to store munitions safely and

economically. As a first step in this direction, the HULL hydrocode is used to determine the effect of detonation near a barrier in two problems of practical interest. Pressure and density contours, velocity vectors, velocity (horizontal and vertical) histograms are plotted using the hydrocode. The knowledge gained in using the hydrocode is very useful in further numerical investigation of cost effective and safe weapons storage concepts.

III. BLAST NEAR A BARRIER:

In the first example, effect of a blast near a barrier without any medium in between was considered. The setup is shown in figure 1.

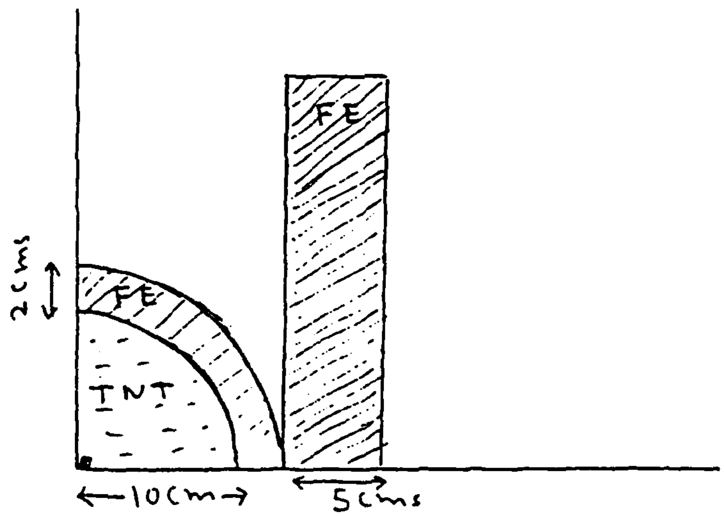

Figure 1: Blast near a barrier with no medium in between

The g ometry employed was 2D plane (cartesian). The left and bottom boundaries are reflective. The mesh size was 0.2 x 0.2 cm^2 with no rezoning of mesh. Programmed burn option was used at the detonation point

which is at center of bomb. Material maps, density and pressure contours, axial velocity histograms are shown in figures 3 to 12, at various times.

IV. BLAST NEAR A BARRIER WITH AIR MEDIUM IN BETWEEN:

In the second problem a donor bomb, an acceptor bomb, separated by a mild steel barrier and air medium, was considered as shown in figure 2. The radius of the bomb is 10.16 cm, thickness of steel casing is 1.2 cms. Material in donor bomb is TNT, in the acceptor bomb it is undetonated, composition B explosive.

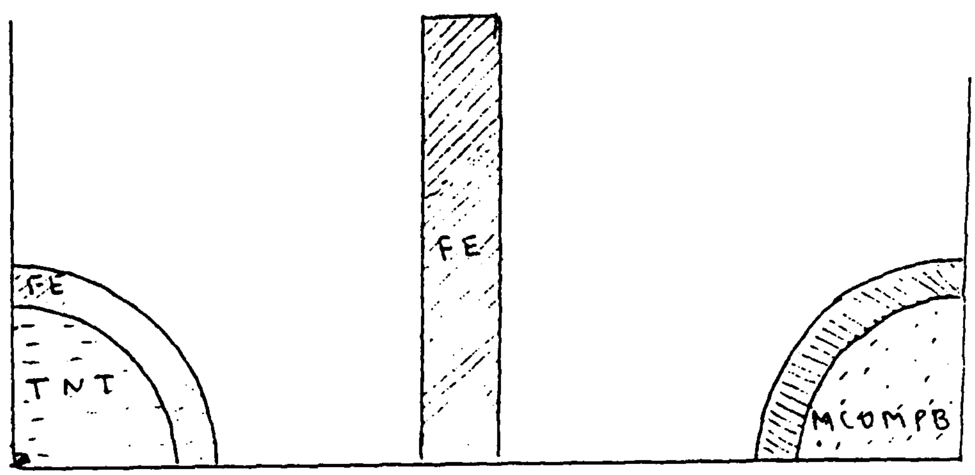

Figure 2: Blast near a barrier with air medium in between

Distance of each bomb from the barrier is 1.27 cms programmed burn option was used at the center of the donor bomb. Barrier thickness is 5.08 cms. Geometry employed was 2D plane (cartesian). The left and bottom bondaries are reflective. Mesh size was 0.2 x 0.2 cm^2. Material

maps, density and pressure contours, axial velocity histograms are shown in figures 13 to 19.

V. RECOMMENDATION:

Numerical procedures can be used economically to predict the effects of detonation of a stack of munitions. The material of the barricade and its shape is one important factor in storing weapons safely. I would like to make hydrocode analysis of effects of a blast by measuring peak pressure and studying shock propagations for the following cases:

1. Vary thickness and materials of the barrier.
2. Vary shapes of the barrier.
3. Vary distance of the barrier from the bomb.

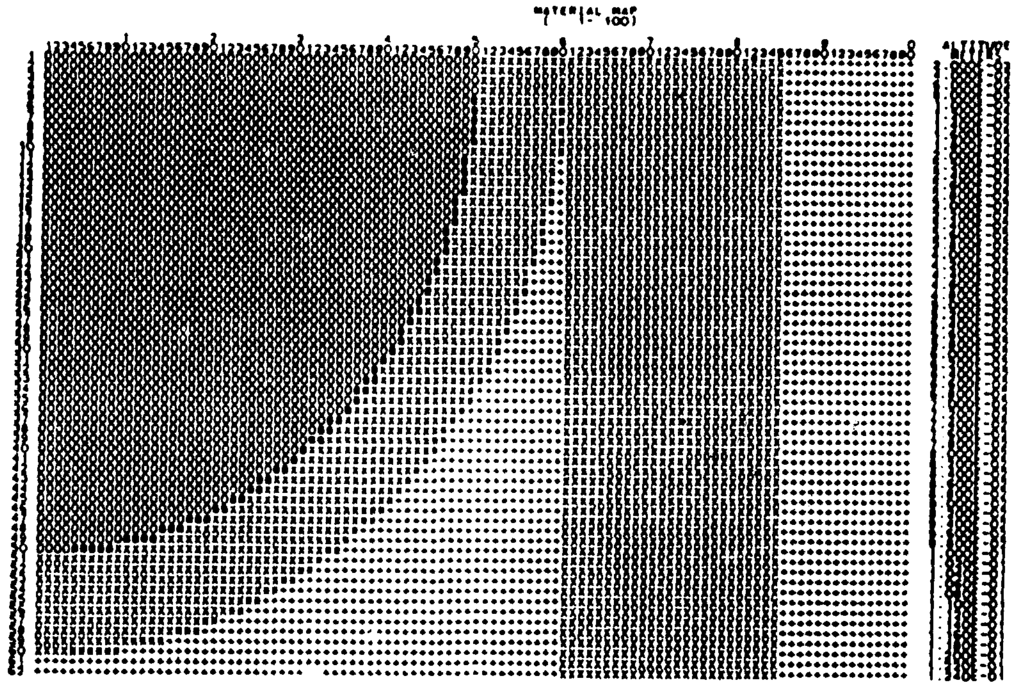

Figure 3 - Material Map

Time 10 μs

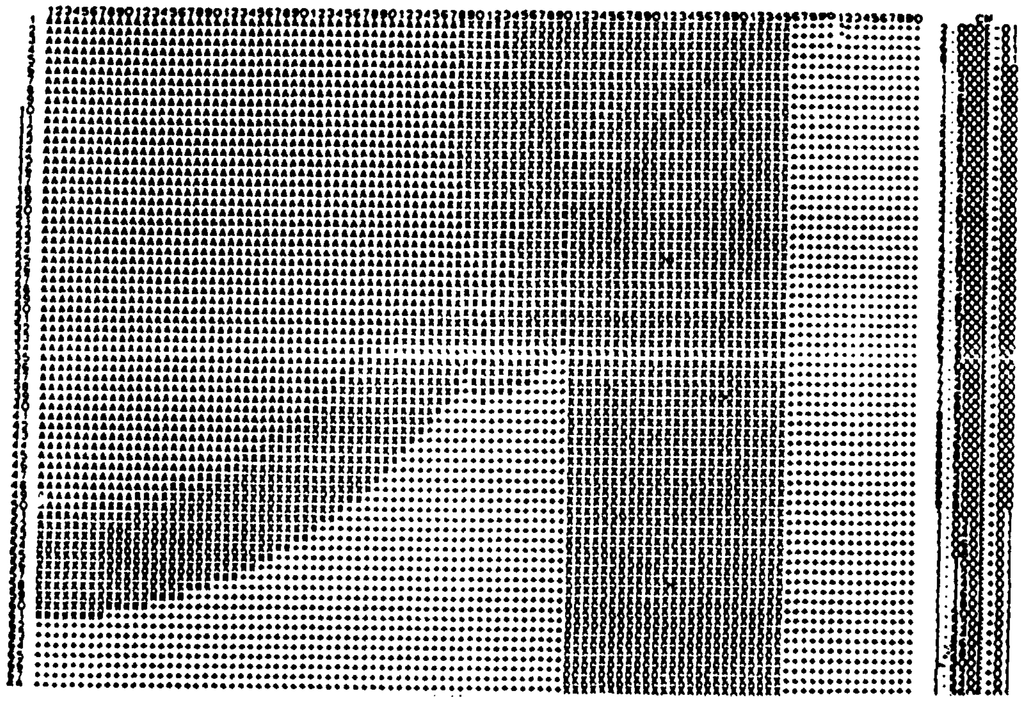

Figure 4 - Material Map

Time 20 μs

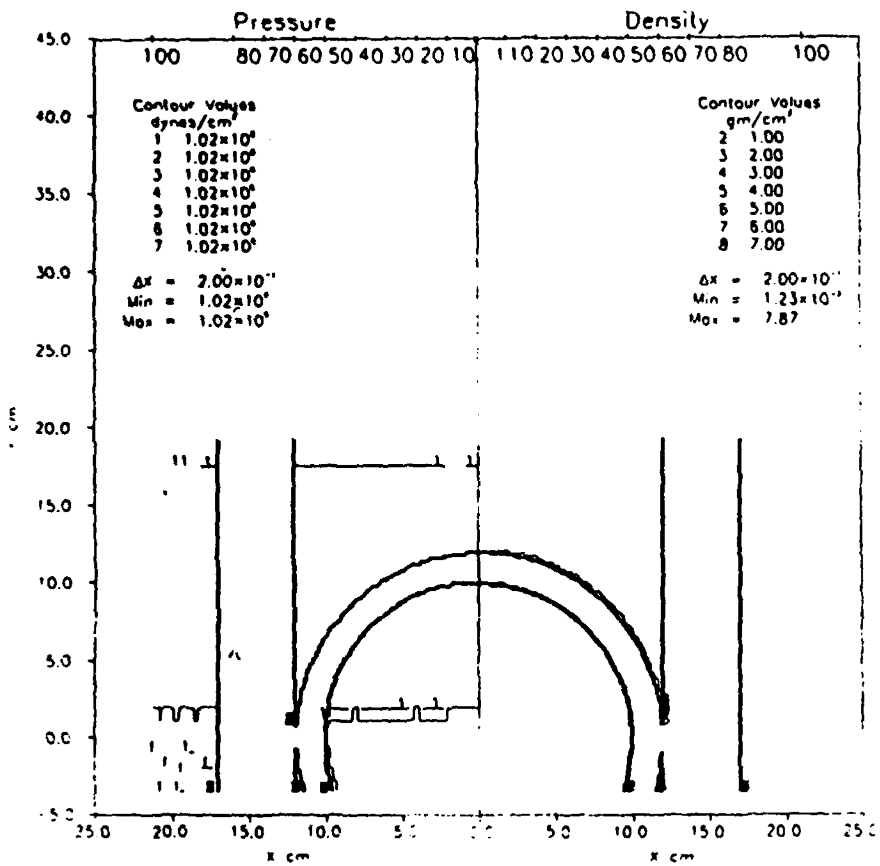

Figure 5 - Pressure and density contours at time = 0

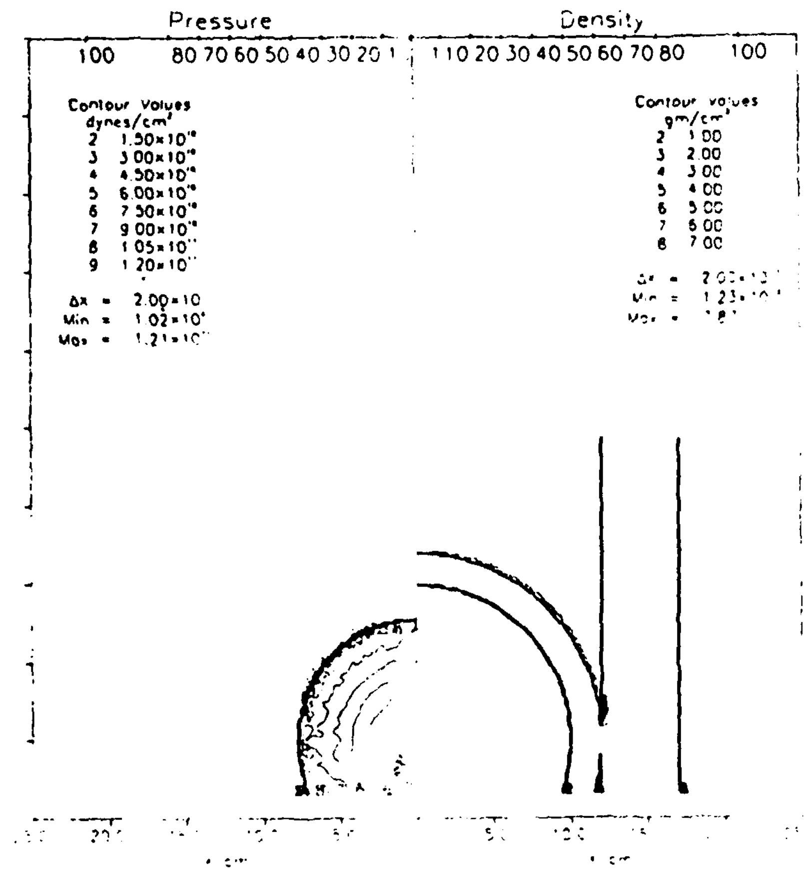

Figure 6 - Pressure and density contours at time - 10 us

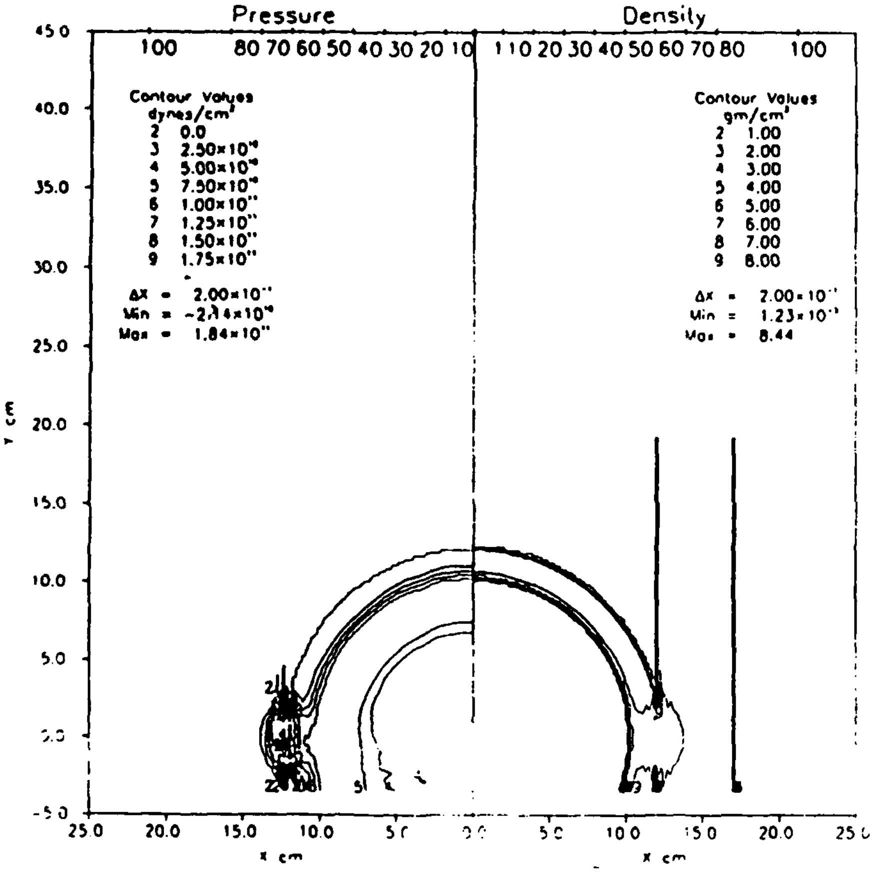

Figure 7 - Pressure and density contours at

time = 20 μs

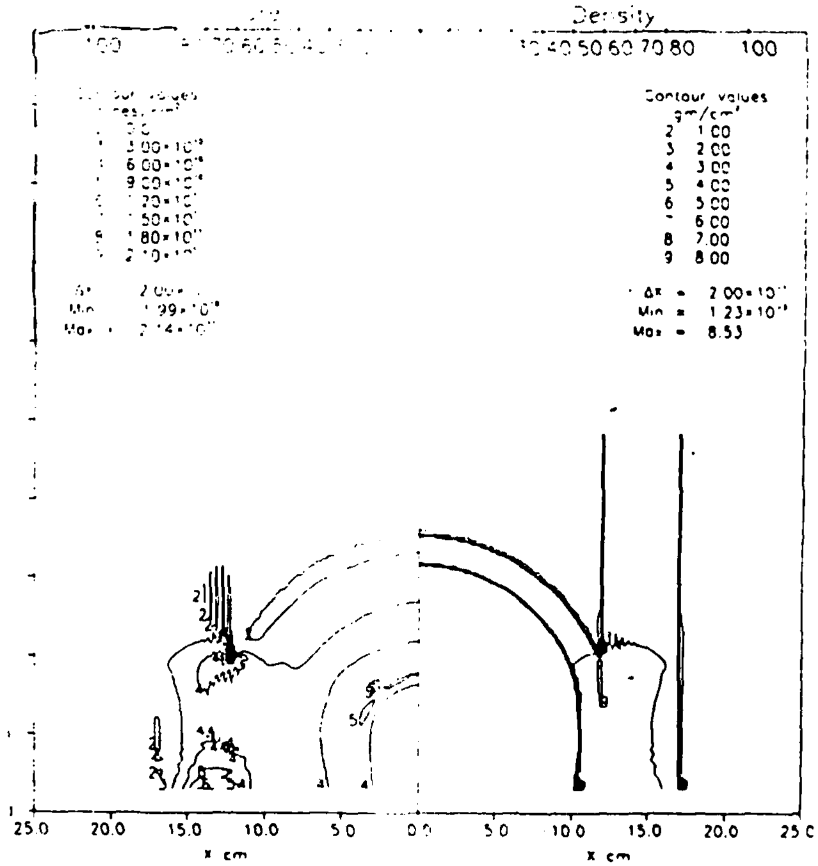

Figure 8 - Pressure and density contours at

time = 30 μs

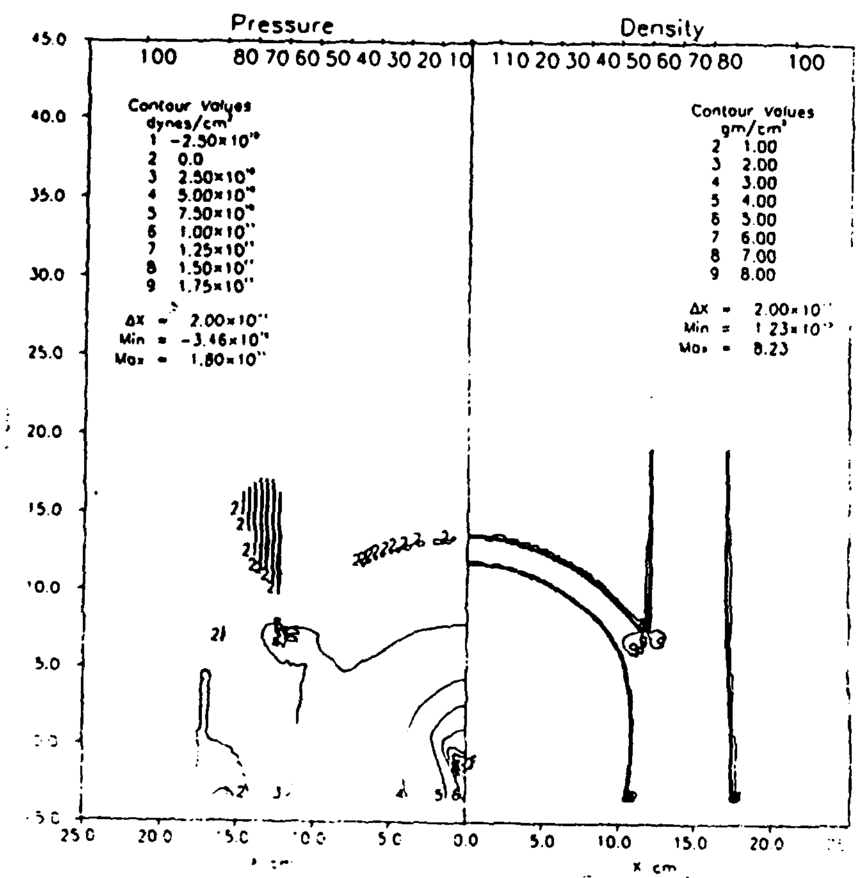

Figure 9 - Pressure and density contours at

time = 40 μs

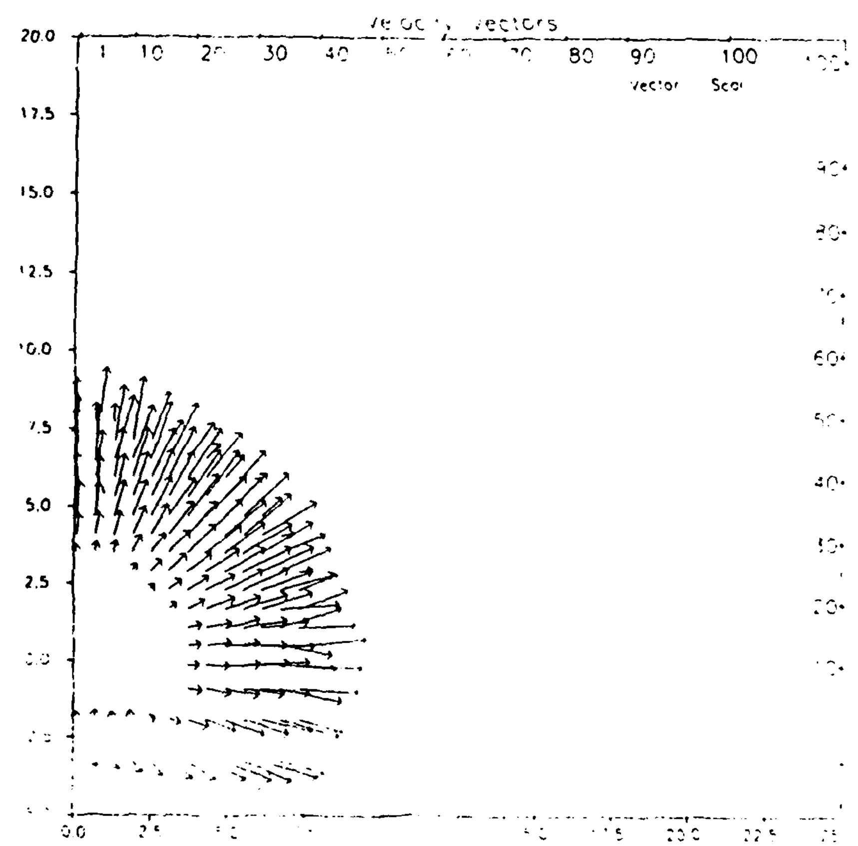

Figure 10 - Velocity vectors at

time = 10 μs

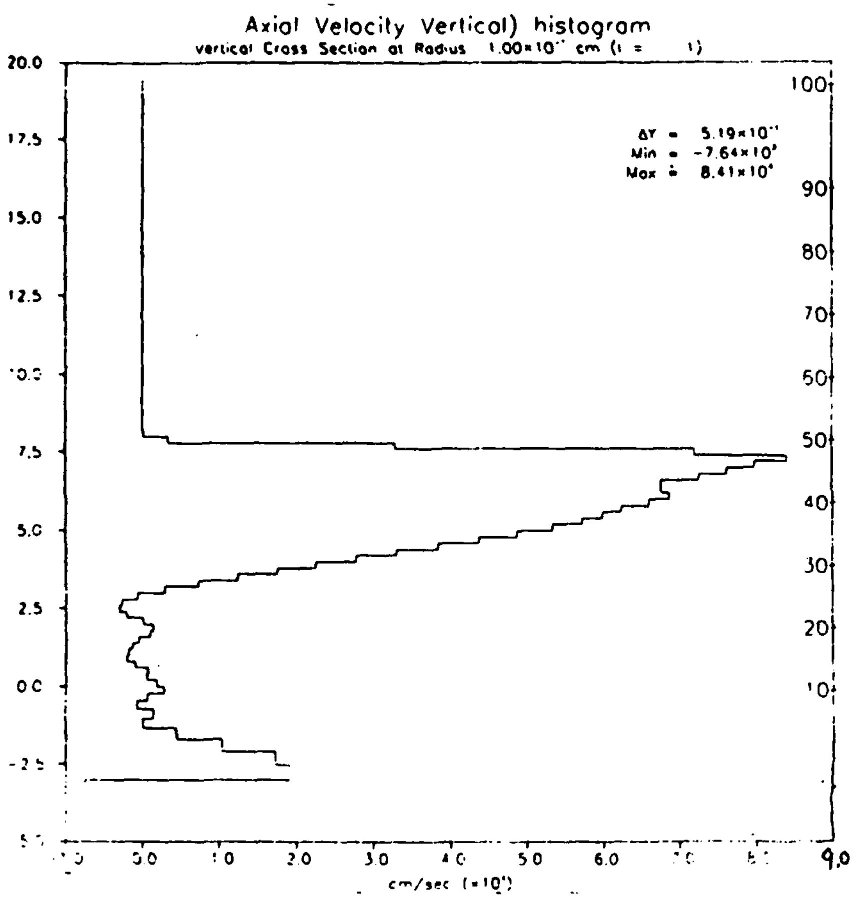

Figure 11 - Axial velocity vertical histogram,

time = 10 μs

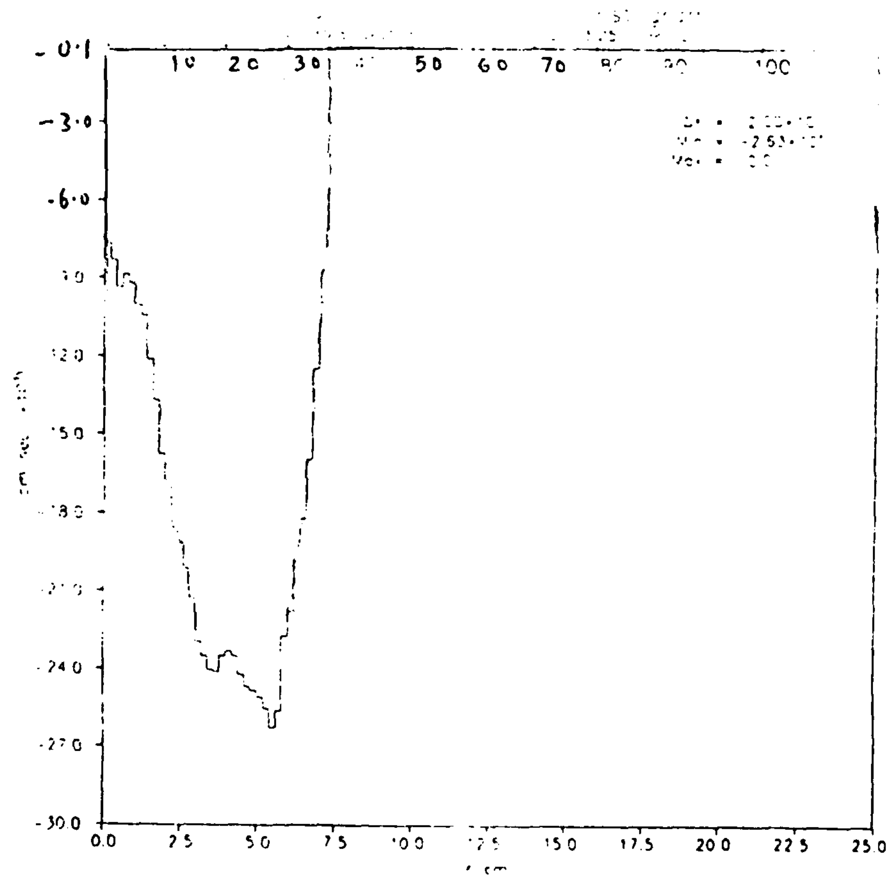

Figure 12 - Axial velocity horizontal histogram,

time = 10 μs

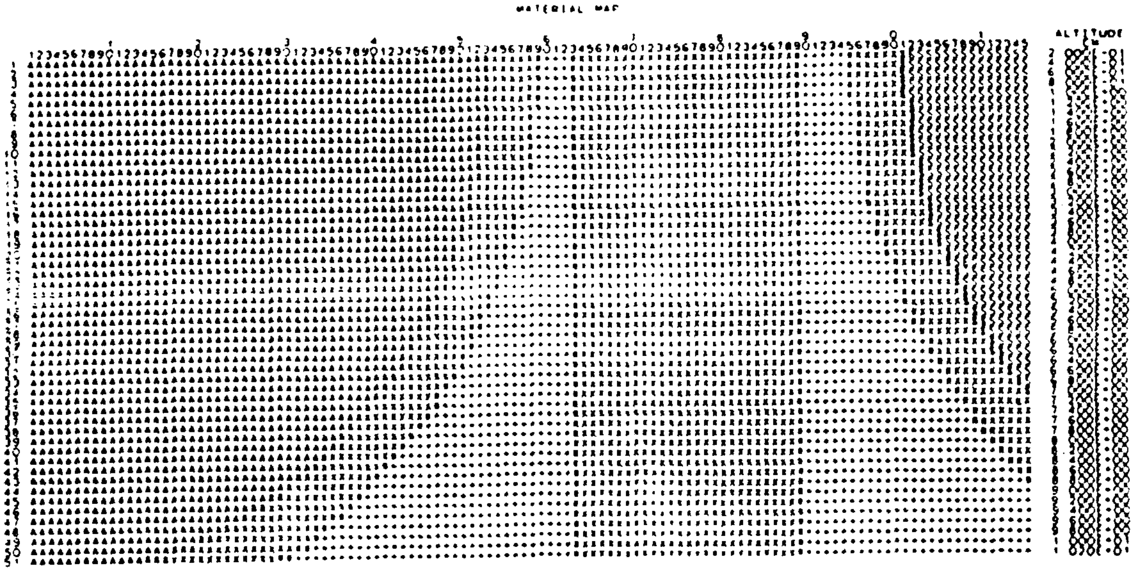

Figure 13: Material Map, time = 0

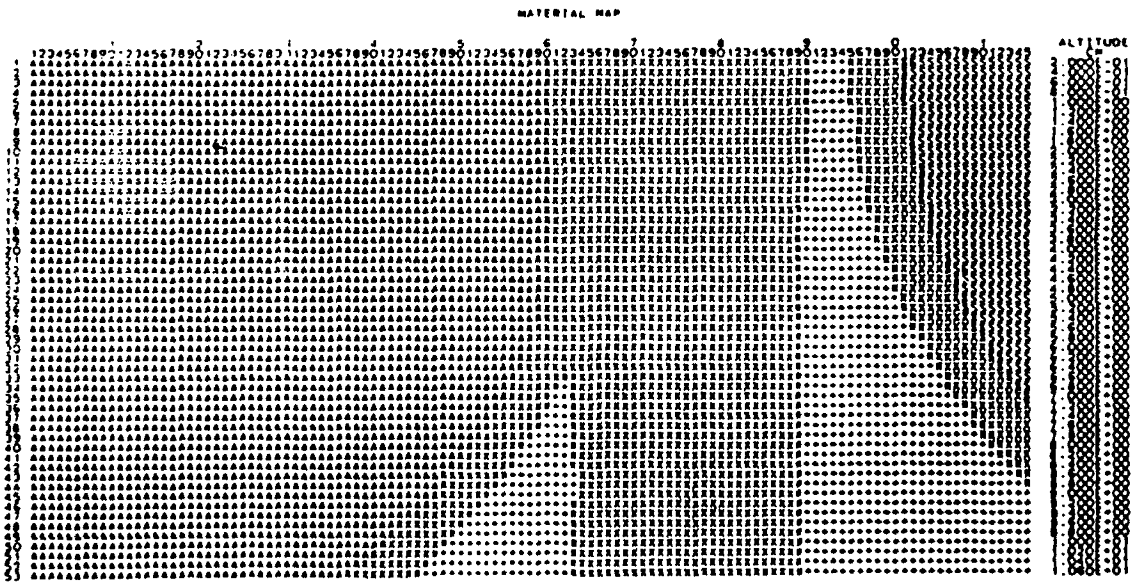

Figure 14: Material Map, time = 10 μs

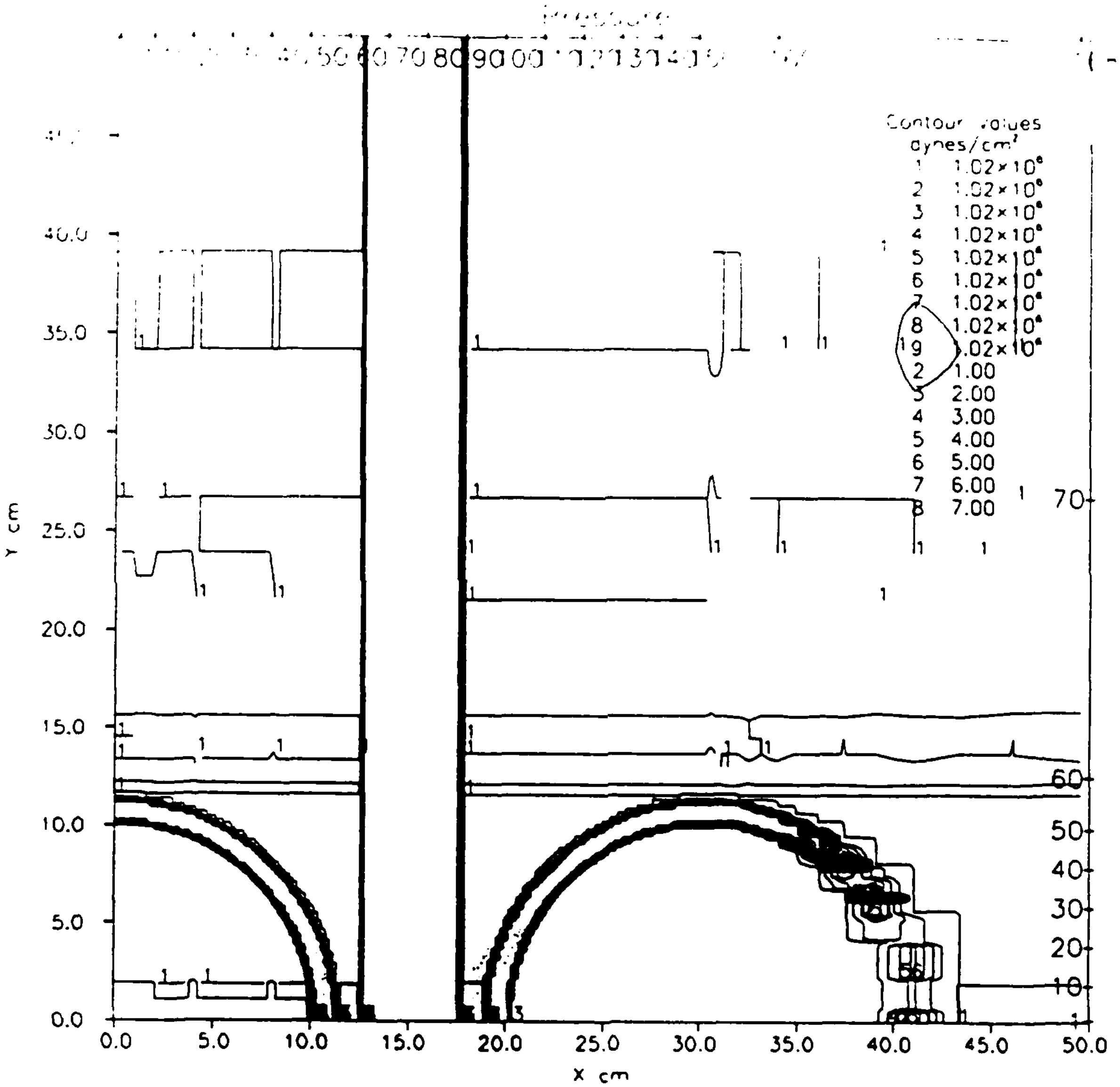

Figure- 15 Pressure contour at time = 0 Sec.

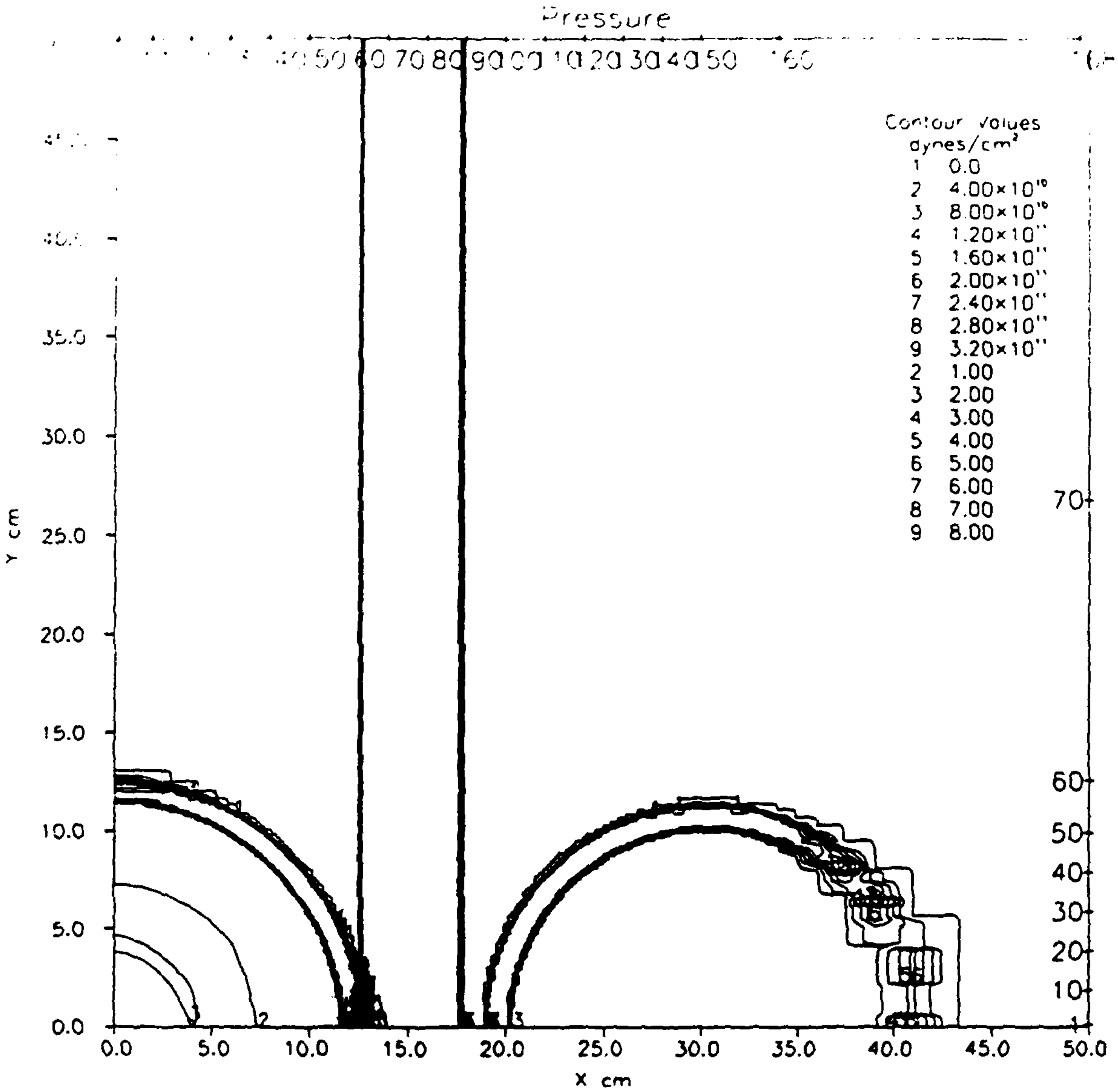

Figure- 16 Pressure contour at time = 30 us

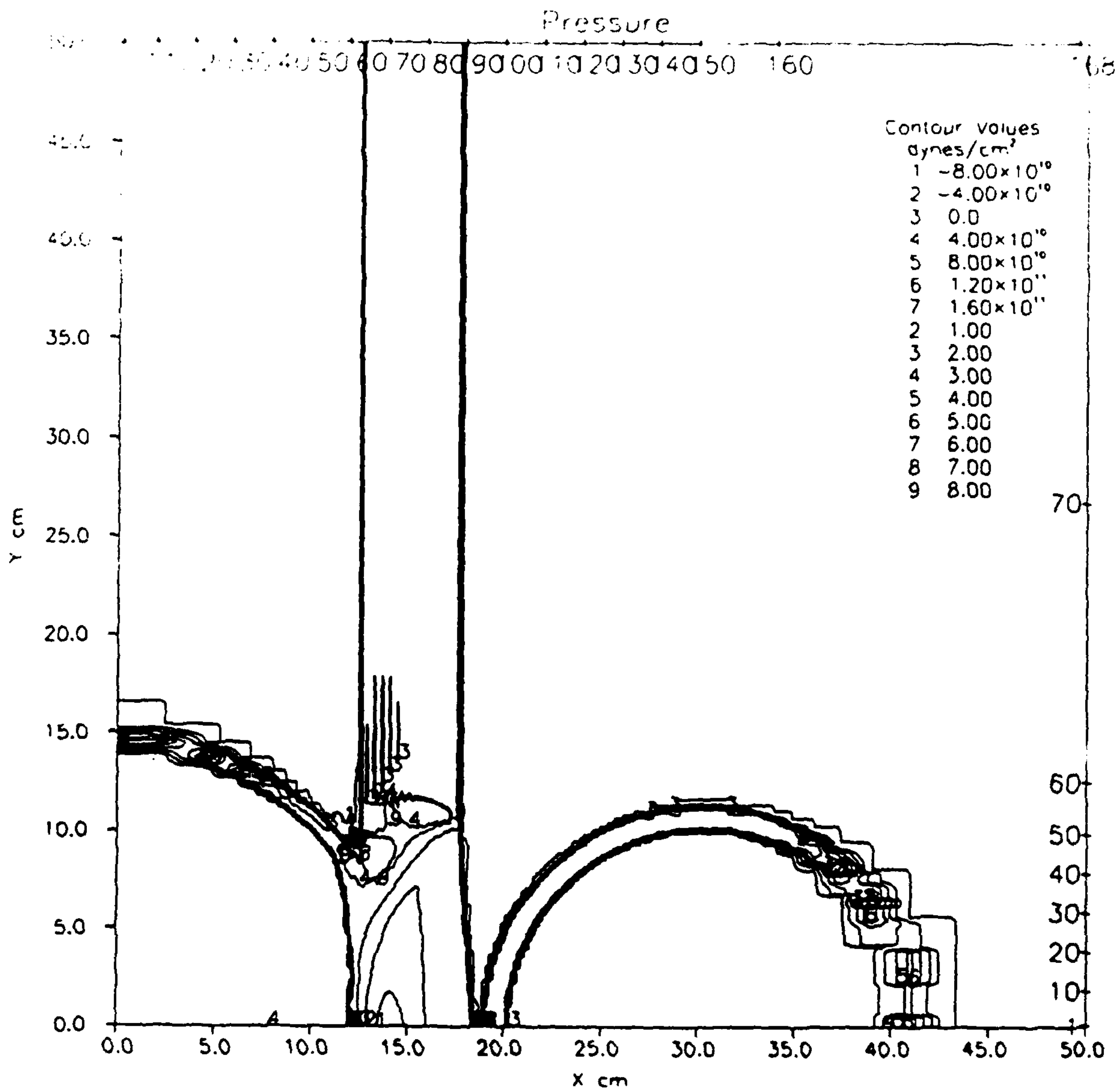

Figure-17 Pressure contour at time = 50 us

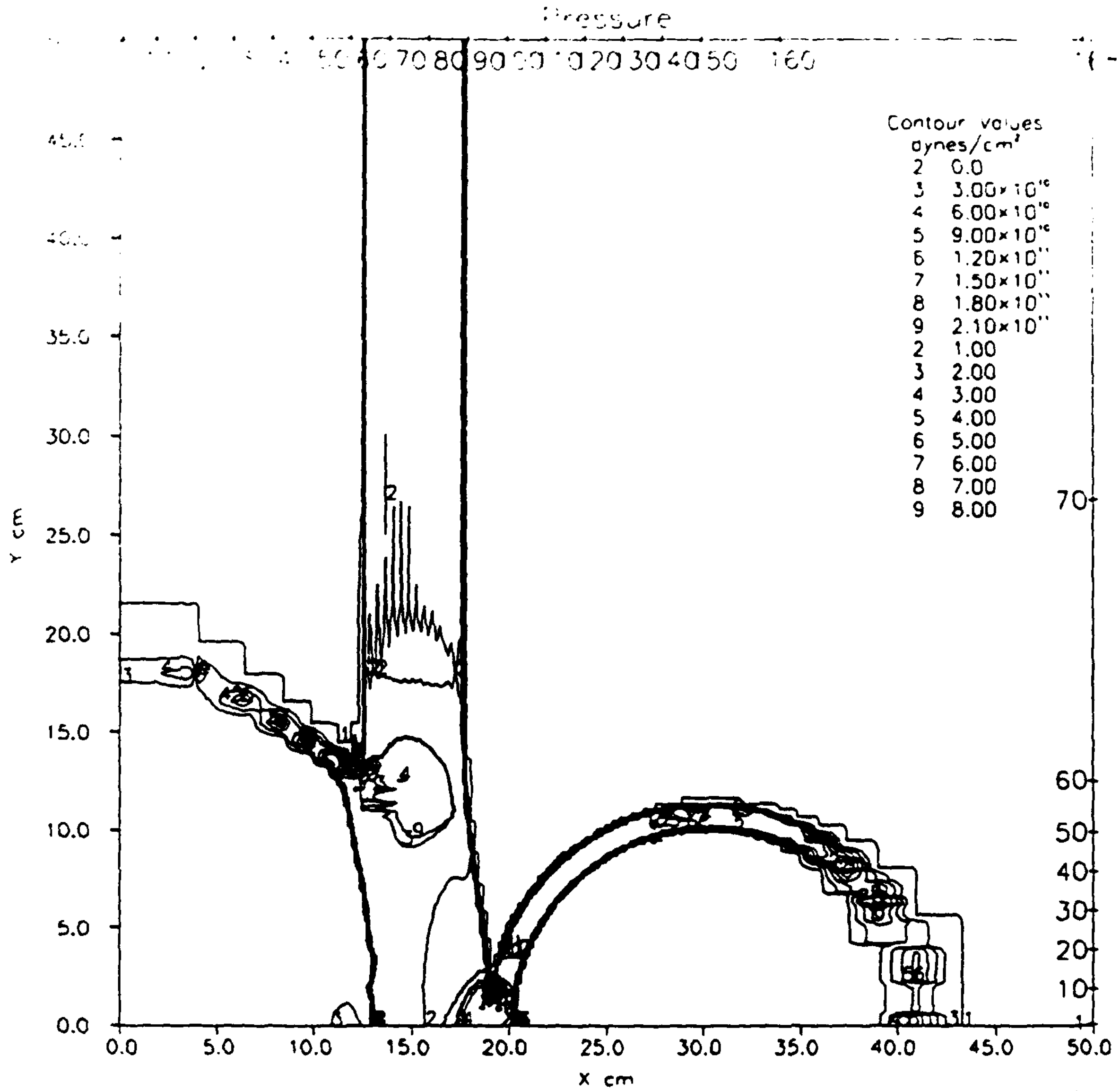

Figure-18   Pressure contour at time = 70 us

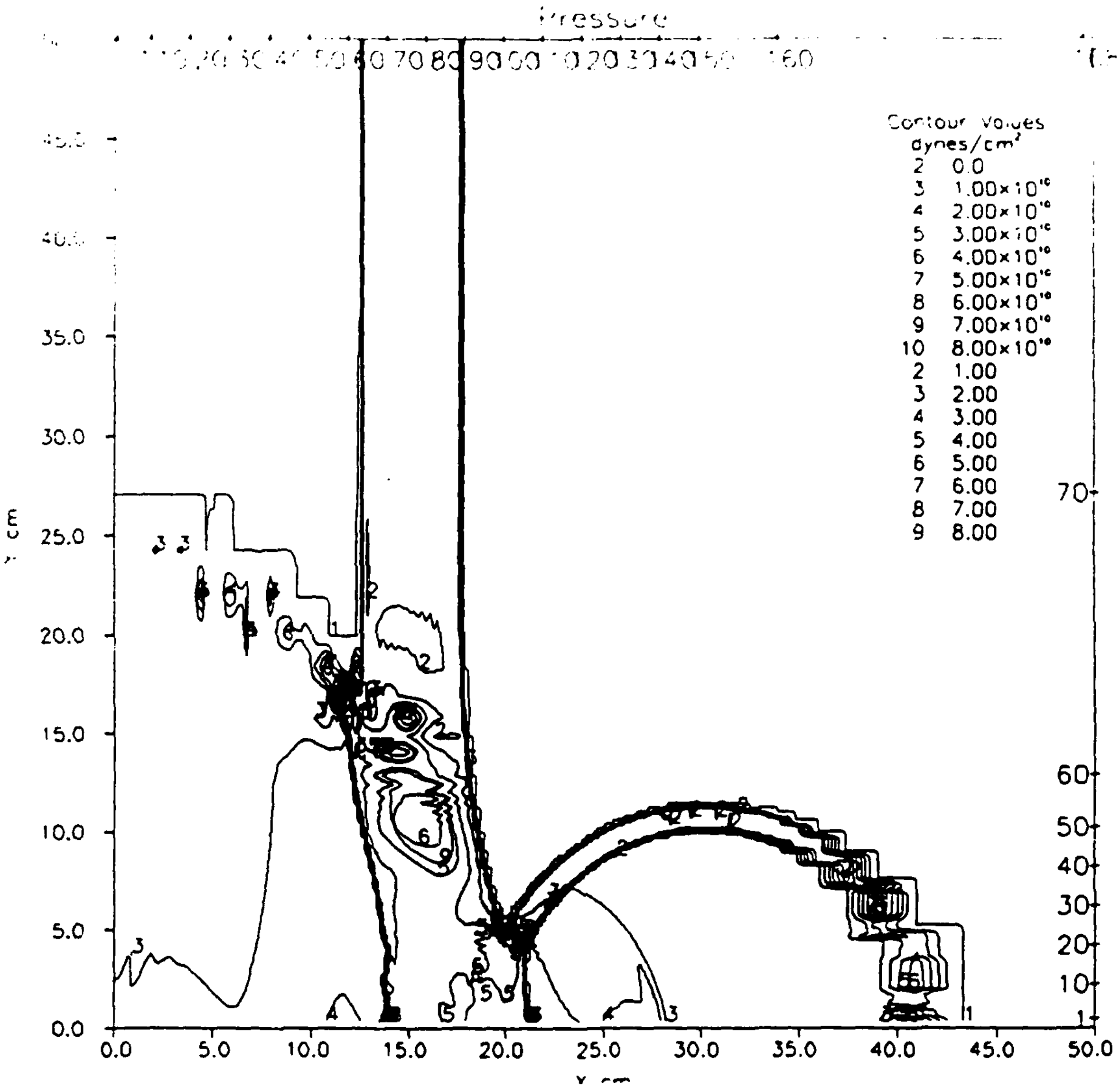

Figure-19 Pressure contour at time = 90 us

REFERENCES

1. Proceedings - Seventh Symposium on Detonation, June 16-19, 1981. NSWC MP 82-334.

2. Suppression of Sympathetic Detonation. J. C. Foster, Jr., M. E. Gunger, B. G. Craig, G. H. Parsons (to be published).

3. Numerical Modeling of Detonations. Charles L. Mader, University of California Press, 1979.

4. Impact Dynamics. Zukas, Nicholas, Swift, Grezczuk, Curran. Jon Wiley and Sons, 1982.

1985 USAF-UES SUMMER FACULTY RESEARCH PROGRAM

Sponsored by the

AIR FORCE OFFICE OF SCIENTIFIC RESEARCH

Conducted by the

UNIVERSAL ENERGY SYSTEMS, INC.

FINAL REPORT

SAMPLING PLAN FOR THE ORGANIZATIONAL ASSESSMENT PACKAGE SURVEY

Prepared by:	PAUL S.T. LEE
Academic Rank:	Associate Professor
Department and University:	Department of Business Administration North Carolina A & T State University
Research Location:	Research and Analysis Directorate, Leadership and Management Development Center, Maxwell Air Force Base, AL 36112-5712
USAF Research:	Maj MICKEY R. DANSBY Director, Research and Analysis

Date:	July 30, 1985
Contract No:	F49620-85-C-0013

SAMPLING PLAN FOR THE ORGANIZATIONAL ASSESSMENT

PAUL S.T. LEE

ABSTRACT

The Organizational Assessment Package (OAP) survey was developed by the Leadership and Management Development Center, (LMDC) U.S. Air Force in the 1970s as means of identifying strengths and weaknesses relative to leadership and management in the Air Force. This report presents a sampling plan as a part of LMDC's effort in searching for a more efficient and scientific survey approach.

The proposed stratified random sampling plan calls for a random selection of about 14,000 individuals on active duty among 12 strata classified by major commands, separate operating units and direct reporting units in the Air Force. The sampling fraction is 1.68 percent for each of the 12 strata as well as for the entire population. Sample sizes among strata range from 600 to 1,987 proportional to sizes of strata. Margins of error range from less than 1 percent to 4 percent. The sampling plan may be inappropriate if changes are to be made in study purposes and statistical assumptions.

ACKNOWLEDMENTS

Many thanks to my friends and colleagues at the Research and Analysis Division, Leadership and Management Development Center, Maxwell Air Force base for their valuable suggestions and comments. This includes Maj M.R. Dansby, Director, LMDC/AN and Drs. I. Mitchell, P. Lewis and R. Niebuhr. For word processing assistance, I am indebted to Cpts K. Ibsen and J. Lowe, CMSgt J. Vermilya, MSgt A. Kopec, TSgt D. Shreeves and Ms. Wanda L. Davis.

Sampling Plan for the Organizational
Assessment Package (OAP) Survey

I. Introduction

The Organizational Assessment Package (OAP) survey was developed by the Leadership and Management Development Center (LMDC), U.S. Air Force for the following purposes:

1. To identify strengths and weaknesses with respect to leadership and management Air Force-wide as well as in its major divisions;
2. To establish a data base in support of Air Force-wide organizational effectiveness research efforts; and
3. To provide feedback to Air Force professional military education schools (6, P.2).

The principal instrument of the OAP survey is a questionnaire consisting of 109 questions and/or statements. The questionnaire was designed to form 21 factors grouped into a system model which assessed three aspects of a work group: Job Enrichment, Interaction Among Group Members and Job Performance.

In striving for efficiency and effectiveness, the Research and Analysis Directorate of LMDC began an effort to systematically improve the OAP system as early as 1981 (5, PP. 7-8). Since then, new factors and new variables have been added. Factors relating to supervision, organizational climate, training and job satisfaction were either combined or consolidated. However, major study purposes and the underlying hypotheses remain unchanged. In the past two years, the revision effort has been temporarily interrupted because of a decision to deactivate the management consulting program. To date, the revised version of the OAP survey has not been field tested.

Since the late 1970s, OAP surveys have been conducted by LMDC's consulting group using an on-site administration approach in preselected commands or agencies. The on-site survey administration was, in reality, a mini-census. During the survey period, the project officers and survey coordinators scheduled survey sessions on-site at a central location. Each member in the unit was asked to attend the session and was given a copy of the questionnaire for completion.

The on-site survey administration approach is generally used as a problem-solving technique rather than a data

collection method since individual objectivity is difficult to maintain in a group environment. Moreover, since probability was not part of the sampling design, findings and conclusions obtained from such a survey may be relevant only to the commands and organizations in which the survey was conducted. Theoretically, they cannot be used to draw any conclusions concerning the entire U.S. Air Force.

Currently, LMDC and its consulting group are in a state of transition. The Research and Analysis Directorate of LMDC (LMDC/AN) is charged with the development of a cost-effective and scientific survey approach. To lower survey costs and increase precision and reliability of sample estimates, an Air Force-wide mail-out survey method and a random sampling procedure have been suggested and are under serious consideration.

II. Objectives

As a Summer Research Fellow, one of my major objectives is to assist LMDC/AN in the development of a cost effective and scientific sampling procedure. After a thorough review of the study objectives, data base composition and data requirements, a stratified random sampling (SRS) procedure is recommended (2, Ch. 5). This paper presents a detailed discussion of the recommended sampling procedure.

III. Sampling Units and Population

According to Air Force Almanac 1985, over 850,000 individuals are currently on active duty in the U.S. Air Force, serving in 13 major commands, 14 separate operating agencies and 3 direct reporting units at approximately 160 Air Force bases (AFBs) and a number of separate installations. Each of these individuals is considered an "elementary sampling unit" and is given an equal chance of being selected in the proposed sampling procedure. All the individuals (or sampling units) as a whole constitute the "population."

IV. Stratification

Stratification was established in accordance with study purposes. In brief, the survey objective calls for large commands to be designated as separate study domains. In addition, major commands and various separate and direct reporting units are to be treated separately because of their differences in functions. Hence, a total of 12 strata were established as shown in Table 1.

Table 1

Stratification of OAP Survey

Strata	Number of Personnel
1. AF Communication (AFCC)	55,338
2. AF Logistics (AFLC)	96,492
3. AF Systems (AFSC)	56,254
4. AF Training (ATC)	84,781
5. Military Airlift (MAC)	94,297
6. Pacific Air Forces (PACAF)	36,612
7. Strategic Air (SAC)	118,064
8. Tactical Air (TAC)	71,477
9. USAF in Europe (USAFE)	71,477
10. Air Univ., Alaska Air, Space, Elect. Security (AU,AAF,SC,ESC)	38,136
11. Separate Operating Agencies (SOAs)	35,650
12. Direct Reporting Units (DRUs)	53,270
Total	854,773

Source: Air Force Almanac 1985. Air Force Association Magazine, May, 1985.

V. Determination of Sample Size

Sample sizes are determined by taking consideration of three factors: (1) the allowable margin of error in estimation, (2) the level of confidence, and (3) the estimated variance of sample estimates. Since most of the statistical analysis takes the form of a sequence of proportions, the maximum variance for proportion is 0.25 (4, P.51). It has also been determined that the maximum allowable margin of error is 4% and the confidence level of estimate is set at 95%. Hence, the sample size for the stratum with the smallest number of elementary sampling units is calculated using the following formula:

$$n = S^2 / V^2 p \qquad \ldots (1)$$

Where n stands for the required sample size; S^2, the estimated variance and V^2p, the estimated variance of sample mean.

Since the level of confidence is set at 95%, and the maximum allowable margin of error is 0.04, the required sample size for the stratum with the smallest number of elementary sampling units is:

$$n = 0.25/(0.0204)^2 = 600.$$

VI. Sample Allocation

To allocate the sample among various strata, the method of "proportionate allocation" is used (2,PP. 91-95). As the name implies, this method allocates total sample to each stratum proportional to the total number of elementary sampling units in that particular stratum.

The proportionate sample allocation method is perhaps the most widely recognized and most frequently used approach in stratified random sampling. It is chosen because of its high degree of representation and of its simplicity to use. This method yields highly representative samples by the notion that "every part of the population is properly represented in the sample" (4,P. 82). The method is simple to use because: (1) the sampling fraction, once calculated, becomes a fixed value. In other words, the sampling fraction in each stratum (nh/Nh, where nh stands for the sample size for the h stratum, Nh for the population size for the h stratum) is equal to the sampling fraction for the population as a whole (2,P.91). (2) The sample is "self-weighting", i.e. the estimated mean for the entire population (Air Force-wide) can be calculated in the same way the estimated mean for each stratum is calculated, without sorting the elements (observation) into different strata (2,P.91; 4, P.83). Table 2 shows the results of the sample allocation along with the estimated maximum margin of error for each stratum.

Table 2

Proportionate Sample Allocation

Strata	No. of Personnel Nh	Sample Size nh	Margin of Error 1/
1. AFCC	55,338	931	0.032
2. AFLC	96,492	1,624	0.024
3. AFSC	56,254	947	0.032
4. ATC	84,781	1,427	0.026
5. MAC	94,297	1,587	0.025
6. PACAF	36,612	616	0.039
7. SAC	118,064	1,987	0.022
8. TAC	114,402	1,925	0.022
9. USAFE	71,477	1,203	0.028
10. AU, AAF, SC, ESC	38,136	642	0.039
11. SOAs	35,650	600	0.040
12. DRUs	53,270	897	0.033
Total	854,773	14,386	0.008

Sampling fraction nh/Nh = 0.0168 or 1.68%

1/ Margin of error was estimated using the maximum variance estimate at the 5% level of significance

As shown in Table 2, the sampling fraction is 1.68 percent for each of the strata as well as for the entire population. Sample sizes range from 600 to 1,987, proportional to sizes of strata. Margins of errors range from less than 1 percent to 4 percent. In reading the table, however, readers are cautioned that the response rate was not taken into consideration in sample size determination. Hence, sample sizes may have to increase to compensate for the expected response rate.

VII. Summary

This report presents a sampling plan as a part of LMDC/AN's effort in searching for a more cost-effective and scientific survey approach. It was designed as a revision of the traditional OAP survey method rather than a substitute. Moreover, the plan was developed in accordance with a set of statistical assumptions and the study purposes set up by LMDC and its consulting group in the 1970s.

The sampling plan may be inappropriate if changes are to be made in the study purposes and the statistical assumptions. For example, sample size could be substantially reduced if major commands are not required to be separate study domains. Sample size could also be altered either if the proportionate allocation is not used or if 1 percent significant level instead of 5 percent is used. If these become apparent, a new sampling plan should be developed.

VIII. Recommendations

The stratified random sampling plan developed in this paper is a scientific and cost effective survey approach. It is highly recommended as an alternative survey approach to the traditional on-site survey administration for data collection needed to accomplish LMDC's major missions.

A two-tier sampling plan was also developed and recommended as a replacement for the traditional OAP survey. Briefly, the two-tier sampling plan calls for the implementation of the stratified random sampling survey at a three-year interval as tier-one plan. This is supplemented by a simple random sampling survey with simplified questionnaire and reduced sample size during the off-years when tier-one plan is not implemented. Details of the two-tier sampling plan will be developed in the form of a mini-grant proposal which will be submitted to UES for approval later this year.

References

1. Air Force Association: Air Force Almanac 1985. Air Force Magazine. May, 1985.

2. Cochran, W.: Sampling Techniques. Third Edition, John Wiley and Sons, New York, 1977.

3. Hansen, M.,W. Hurwitz and W. Madow: Sample Survey--Methods and Theory. John Wiley and Sons, New York, 1953.

4. Kish, L.: Survey Sampling John Wiley and Sons, New York, 1965.

5. Short, L, J. Lowe and J. Hightower: Air Force Organizational Assessment Survey -- Initial Revision and Standarization. LMDC-TR-85-1, Maxwell AFB, Alabama. March, 1985.

6. Short, L.: The U.S. Air Force Organizational Assessment Package. LMDC-TR-85-2. Maxwell AFB, Alabama, March, 1985.

1985 USAF-UES SUMMER FACULTY RESEARCH

Sponsored by the

AIR FORCE OFFICE OF SCIENTIFIC RESEARCH

Conducted by the

UNIVERSAL ENERGY SYSTEMS, INC.

FINAL REPORT

ROUTE PLANNING PROBLEM

Prepared by:	Benjamin Lev, Ph.D
Academic Rank:	Professor and Chairman
Department and University:	Department of Management School of Business Administration Temple University Philadelphia, Pa. 19122
Research Location:	Rome Air Development Center Command and Control Division Applied C2 Systems Branch Decision Aid Section GRIFFISS Air Force Base, N.Y. 13441
USAF Research:	Mr. Yale Smith

Date:	August 20, 1985
Contract No:	F49620-85-C-0013

ROUTE PLANNING PROBLEM

by

Benjamin Lev

ABSTRACT

This report discusses the Route Planning Problem in which one searches for the shortest route from origination point to destination point. There might be threats along the way and in that case we try at all cost to avoid flying through threats. Each threat has a known coordination, known radius and known probability of kill. If we have to fly through threats then we find the route that minimizes total lethality along that route. The problem is solved using Dynamic Programming. The model is operational on LMI machine using LISP. A simple problem with multiple threats is solved in less than 2 minutes. A copy of the code is available at the Decision Aid Section.

ACKNOWLEDGEMENTS

This research was sponsored by the Air Force Office of Scientific Research/AFSC, United States Air Force, under Contract F49620-85-C-0013. The research was done under the supervision of Mr. Yale Smith of the Rome Air Development Center, Griffiss Air Force Base. I would like to thank Major Robert J. Kruchten who introduced me to the Route Planning Problem and assisted me in formulating the problem; and to Lieutenant Peter Priest who helped me with the LISP language.

1. INTRODUCTION: One of the oldest aviation problem is the Route Planning Problem. In planning his route a pilot takes into consideration weather, topography, distance, fuel, weight and many other factors. This problem existed for many years. At the Decision Aid Section we try to assist pilots in determining the route they should fly. Obviously, the straight line between the origination point and the destination point is the optimal solution. If we also consider threats then the problem is to find the shortest route which goes around the threats. If it is impossible to avoid the threats then the problem is to determine the least lethal route (not necessary shortest distance) that passes through the threats.

One can complicate the problem further by providing the pilot with Electronic Warfare (EW) capability through jamming, Wild Weasel etc., whereby he can negate several of the threats. The problem then becomes which threat can he negate and which threat should he negate.

A pilot can fly at various speeds. The faster he flies the higher the probability of a successful mission. But fast flying consumes more fuel and restricts the distance and flying time. A pilot thus should optimize his fuel consumption or his flying speed.

2. OBJECTIVES OF THE RESEARCH EFFORT: A model is a compromise between complexity and accuracy. We can always add additional features but there is a certain cost that is being translated through its complexity. We try to keep the model as simple as possible and yet meet the specifications required by the user.

The Route Planning Problem is currently an ongoing project in the Decision Aid Section being led by Mr. Clark Mollenhauer. Major Kruchten has built an excellent hueristic model. There is a good detailed description in [1] of the problem, the model and a solution.

The objective in this research effort is to build a route planning model that will be accurate enough and can be solved in relatively short period of time. There are several similar models today that vary in sophistication. Some need up to 45 minutes of computer time. Some models are Hueristic and provide a quick solution but the solution may not be an optimal one. The model that we suggest here is in between the two extremes. It is a simple one and can solve the problem in relatively short time.

The model has a list of threats with locations, radius and probability of kill. It finds an optimal route from starting point to its target. The goal here is to keep the model as simple as possible and yet to obtain a meaningful solution. This is only a Decision Aid tool for a pilot who may reject routes suggested by the model.

3. METHODOLOGY: All models have basically two parts. The first is the INPUT/OUTPUT (I/O) portion in which the user communicates with the model. The second part is the ALGORITHM used to solve the problem.

Models that are used for the Decision Aid are heavily weighted toward their Input/Output portion, simply because they are suppose to be "user friendly", they are supposed to have the capability of handling different scenarios, situation and cases. These type of models are different from a problem in which there is a specific problem with a specific data for which the I/O is minimal - just enough to transfer the input to the model and print out the output. In Decision Aid type models the I/O is a major portion of the problem since its purpose is to train the user, to suggest alternatives, and to assist the user in choosing the best decision.

The second part of the model is the algorithm used to solve it. In [1], the procedure is basically to go straight from origin to destination. If there is a threat on the route then avoid the threat by either circling it clockwise or

counterclockwise. This is a short-sighted approach that many pilots use, and probably is the closest to reality. What we suggest in this paper is a global approach which looks at the entire field and select the optimal solution. The technique utilizes Dynamic Programming and is described in [3, Chapter 8]. A detailed formulation of the Dynamic Programming recursive equation is given in Appendix A.

This approach provides us with the optimal solution from the origin to any destination point in the field. In other words, if there is a base from which we wish to dispatch multiple different missions, one does not have to solve the problem more than once. A single solution will provide us with the different optimal routes from the origin point to all targets.

4. PRESENT STATUS OF THE MODEL: At present the user provides the following input to the computer model:

4.1. Origination (start) Point (si,sj)

The size of the field is (500,550) thus $0 <= si <= 500$ $0 <= sj <= 550$.

4.2. Destination (end) Point (ei,ej)

The size of the field is (500,550) thus $0 <= ei <= 500$ $0 <= ej <= 550$.

4.3. Threats

Each threat is represented by (i,j,r,p) where (i,j) is the coordination , r is the radius of the threat and p is probability of kill of the threat. The model can handle as many threats as the user wishes to have.

Both the origin point and the target point can be anywhere in the field including inside threats.

The route starts at the origin. From any point, we can move either vertically, horizontally or diagonally. A vertical or horizontal move costs 10 units. A unit can be measured in distance, fuel consumption, flying time or lethality. A diagonal move costs 14 units (square root of 10**2+10**2 = 14) as described in Figure 1.

First we try to find the shortest route avoiding threats at all cost. Only when this cannot be done we are allowed flying through threats. To reflect the high risk involved in flying through the threats, the cost of a horizontal or vertical move inside a threat is 1000 units, which is 100 times more expensive than normal moves. This order of magnitude will avoid at all cost (if possible) the flight through threats. Similarly, the diagonal move inside a threat is 1400 units.

The next step for the model is to depict on the screen the optimal path with the total cost of that route.

5. <u>THE SEARCH SPACE</u>: The field has a grid size of 500 by 550; thus there are 275,000 cells and each one of them could be part of the optimal route. The first step of the algorithm is to restrict the number of potential points and to consider only those which are serious candidates to be part of the optimal path. Figure 2 describes a problem with two threats, origin point S and target E. Around the threats there is a threat envelope that contains cells which are potentially on the optimal route. Also, from the origin S, there are two tangent lines to the threat envelope and the cells between the two tangent lines are also potentially on the optimal route. Similarly, there are two tangent lines from the target E to the threat envelope and the cells between those are potentially on the optimal route. We have thus restricted the search to only the shaded area which is much smaller than the entire field containing 275,000 points. An optimal solution is most likely either inside the shaded area avoiding the threats or inside the shaded area and through the threats.

The search space is therefore limited to the convex combination created by S, E and the threat envelope.

For the sake of programming simplicity we have taken a slightly different approach. The search space is somewhat larger and is given in Figure 3. Only points inside the shaded region are being considered for the optimal route. The assumption is that the optimal route must pass through the shaded area.

An example of the use of this concept is given in Table 1. The table contains values for each cell. Value of -5 means that the cell is outside the space search. Value of 0 means that the point is outside all threats. Positive value of n=1,2,... means that the point is inside n threats.

6. THE LETHALITY FUNCTION: Every point in the search space has a starting lethality level of 10 units (This is a relatively small number in the algorithm). If in addition a point is also inside a threat with probability of kill of say pk=.8 then there is an additional 1000*pk=800 units of lethality for a total of 10+800=810 units. If the point is inside two threats one with a pk=.8 and the second threat with pk=.7 then the total lethality for the point is 10+1000*.8+1000*.7=1510 units.

Table 2 presents an example of the lethality function. The value of each point is the lethality level computed by 10+1000(p1+p2+...+pi) if the cell is inside i threats.

7. THE ALGORITHM: The algorithm to solve the problem follows these steps:

7.1. Identify the search space

7.2. For all points in the search space which are outside threats compute function FN using (eq.-1).

7.3. Identify boundary points to "dead area" (use it as potential entry points to "dead-area". The term "dead-area" is explained in the Analogy section).

7.4. Compute function FN for all points of previous step using (eq.-1).

7.5. Identify boundary points to threats (use it as potential entering points to threats).

7.6. Compute function FN for all points of previous step using (eq.-1).

7.7. Determine optimal route.

Table 3 presents an example of the function FN. The value of each cell is the shortest lethality distance from the origin to that particular cell using lethality levels of table 2. Table 4 presents the optimal route.

8. ANALOGY: The following is an analogy that might help understand the concept of the solution process. It is not absolutely identical but it is close enough for conceptual purposes.

Suppose we have a pool with water and we drop a rock somewhere in the pool. Assume the pool is large enough to ignore the effect of the waves bouncing back from the walls of the pool. The rock will create a wave which will progress away from its center - the location of the rock. Theoretically, the wave will progress in an even speed at all directions creating perfect centric circles with center at the rock. As time progresses, the circles will get larger and larger. At any point in time one can look at a specific point on the front of the wave and ask himself where did that point come from? (obviously from a previous circle). The process is explained in Figure 4.

At point (x(t),y(t)) we store (remember) that we reached that point from (x(t-1),y(t-1)). This way we have complete knowledge on how we reached every point in the pool. If we track down (reverse the process from (x(t),y(t)) back to the origin - rock) we find the optimal route to any point in the pool. In this simple case all optimal routes will be rays starting at the center and extending to any point.

Now let us complicate the problem by placing some obstacles in the pool. These obstacles will prevent the waves from progressing wherever the obstacles are, but the waves will progress wherever there are no obstacles. The process is presented in Figure 5.

Notice that there is a "dead-area" hidden between the two obstacles. The wave will reach that "dead-area" only after it will get to point A. In fact point A is now being considered as a new source (rock) for waves in the "dead-area". The original wave will continue uninterrupted but there will be a second wave in the "dead-area".

Once we have completed this process we can now consider the obstacles. These are threats with a different medium than the water. Waves move at a different speed in water than in rocks. Each boundary point of the obstacles is a potential source for waves inside the obstacle. One has to generate all possible waves from all possible potential entries and compute the fastest way to reach any interior point of the obstacles. This is a lengthy process but when it is done we have determined the shortest route from the rock to any point in the pool.

9. RECOMMENDATIONS: The basic model is now operational. It is only a demonstration that the methodology is feasible. More work is needed for it to be fully functional. The following is a list of suggestions that could be incorporated in the model to make it functional.

9.1. The computer code was written in the last 6 weeks in a very inefficient way. We intend to improve the computer code so it will be more efficient.

9.2. Improve INPUT/OUTPUT. The INPUT/OUTPUT to the model is limited. It is complicated to modify the input data. We intend to build menus in which users can easily modify input data. We intend to depict more output data on the screen with several options and menus so that a decision maker will be able to obtain all the information he needs before making a final decision.

9.3. The only allowable moves are horizontal, vertical or diagonal at 45 degree moves.

9.4. Target Negating. The model does not allow the negation of targets. We plan to have the capability of selecting the type of targets to be able to negate and the number of targets to negate.

9.5. Multiple Flying Speeds. At present, the model has only one flying speed. We would like to allow several flying speeds, say three speeds (slow, average, fast).

9.6. Target Degrading. Threats degradation through EW is another option currently missing. A pilot can reduce the degree of the threat using EW. We would like to incorporate this capability into the model.

9.7. Navigation Points. The model at present does not include navigation points. It is possible to restrict the optimal route to pass through certain number of navigation points. The path should include a check point on its route at a certain frequency.

9.8. Post Optimality Process. The optimal route derived by the computer might not be feasible to fly. It might contain too many short legs, sharp turns etc. We plan to process the optimal solution to confirm to standard flight patterns.

9.9. Operator Veto Power. The user should be able to observe the optimal path and reject it for his own reason. A rejection could be because of bad weather, position of the sun or any other reason. The model should be able to suggest an alternative solution to the one rejected.

REFERENCES

1. Kruchten, Robert J., Major, USAF, "Decision Aid For Threat Penetration Analysis", 30 may, 1985.
2. Kruchten, Robert J. and B. Lev, "Recent Developments in Route Planning Problem", will be submitted to ORSA/TIMS Conference, April 1986, Los Angeles.
3. Lev, B. and H.J. Weiss, INTRODUCTION TO MATHEMATICAL PROGRAMMING, North-Holland, 1982.

APPENDIX A

In this appendix we will derive the Dynamic Programming recursive equation needed for the model.

Let (i,j) be the coordination

f(i,j) is the shortest distance from the origination point to point (i,j)

r(i+1,j) is the one step distance from (i,j) to its neighbor (i+1,j)

similarly, there are those other one steps distances

r(i-1,j)

r(i,j+1)

r(i,j-1)

r(i-1,j-1)

r(i-1,j+1)

r(i+1,j-1)

r(i+1,j+1)

In our case r(i+1,j) = r(i-1,j) = r(i,j+1) = r(i,j-1) = A

and r(i-1,j-1) = r(i-1,j+1) = r(i+1,j-1) = r(i+1,j+1) = 1.4*A

where A=10 if the point is inside the search space

and A=10+1000*(p1+p2+...+pi) if the point is inside threats 1,2,...,i.

Suppose the starting point is (si,sj) then

f(si,sj)=0

and f(si+1,sj)=r(i+1,j)

f(si-1,sj)=r(i-1,j)

f(si,sj+1)=r(i,j+1)

f(si,sj-1)=r(i,j-1)

f(si+1,sj+1)=r(i+1,j+1)

f(si+1,sj-1)=r(i+1,j-1)

```
f(si-1,sj+1)=r(i-1,j+1)
f(si-1,sj-1)=r(i-1,j-1)
```

The general recursive equation is

```
f(i,j)=minimum([f(i,j-1)+r(i,j-1)],
               [f(i,j+1)+r(i,j+1)],
               [f(i+1,j)+r(i+1,j)],
               [f(i-1,j)+r(i-1,j)],
               [f(i-1,j-1)+r(i-1,j-1)],
               [f(i-1,j+1)+r(i-1,j+1)],
               [f(i+1,j-1)+r(i+1,j-1)],
               [f(i+1,j+1)+r(i+1,j+1)])            (eq.-1)
```

One has to build f(i,j) for all (i,j).
Let (ei,ej) be the destination (end) then f(ei,ej) provides the shortest distance from the origination point to (ei,ej). Once we have the shortest distance we identify the shortest route.

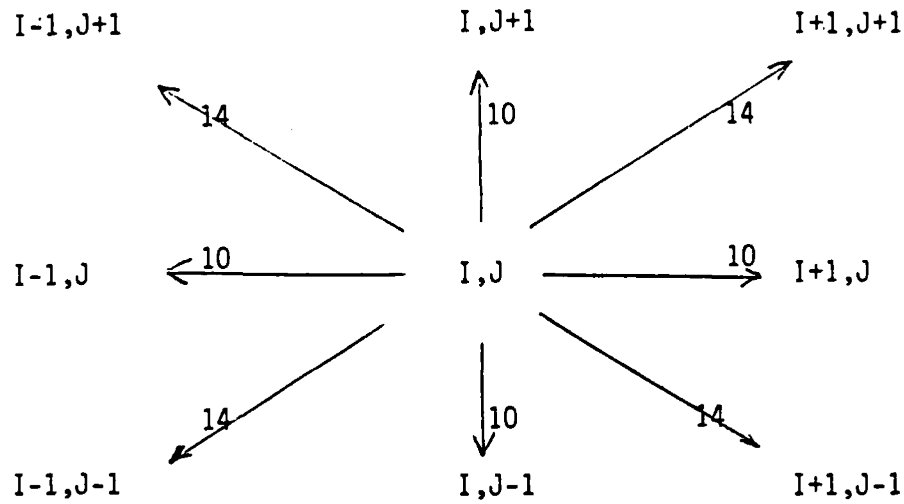

Figure 1: Possible Moves from I,J to 8 Adjacent cells with Costs.

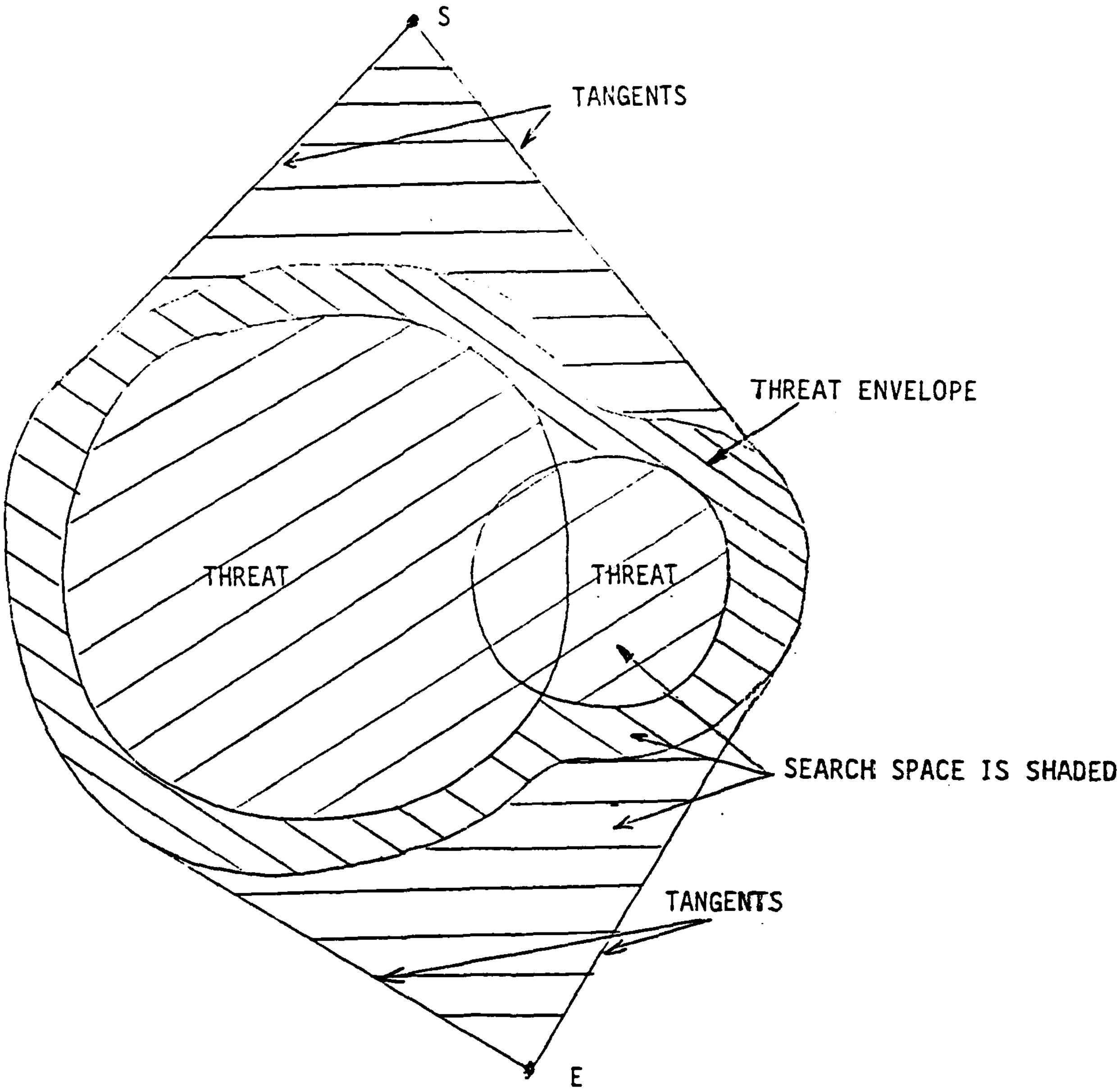

Figure 2: Two Threats with Threat Envelope and Search Space.

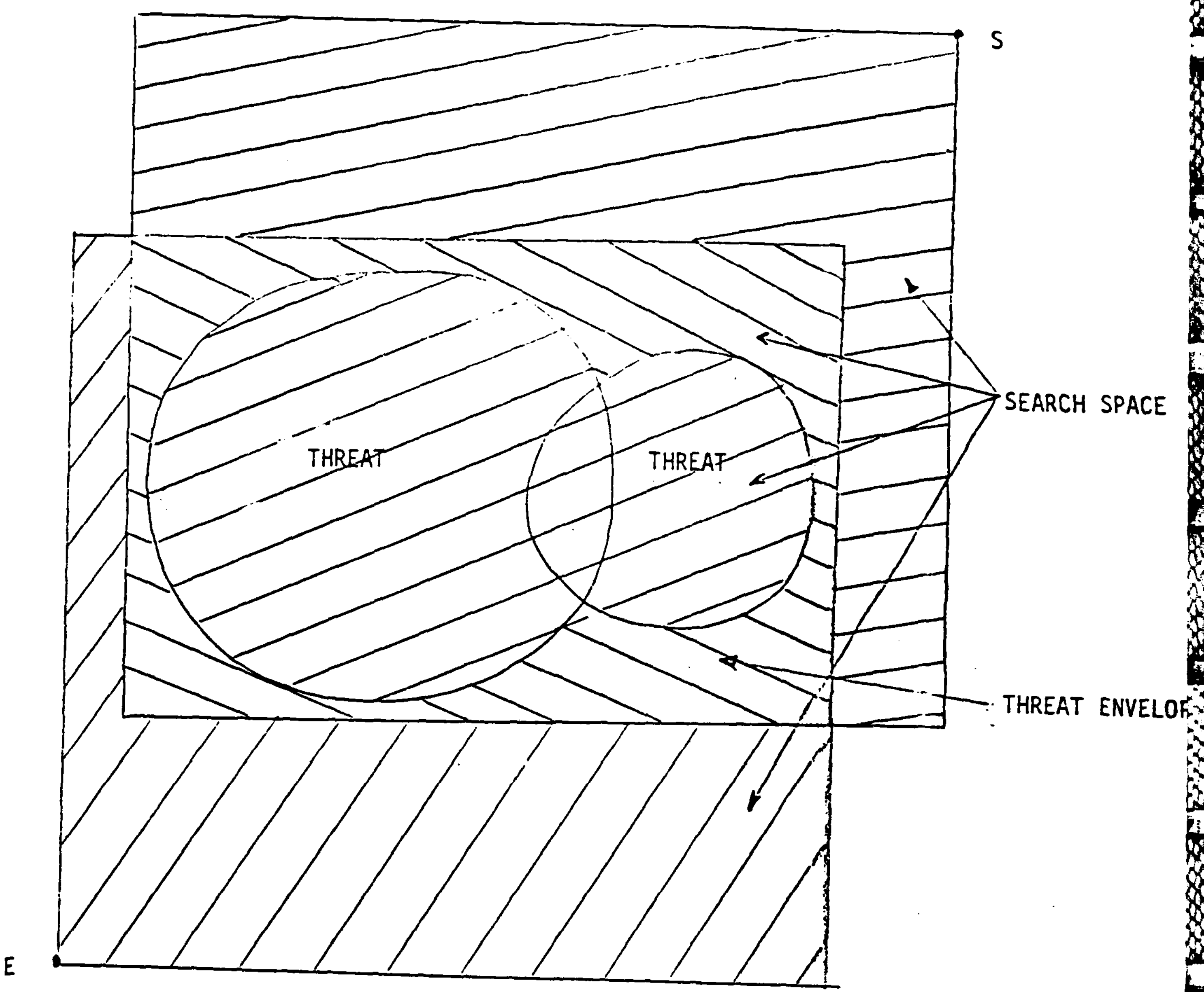

Figure 3: Two Threats with Modified Threat envelope and Search Space.

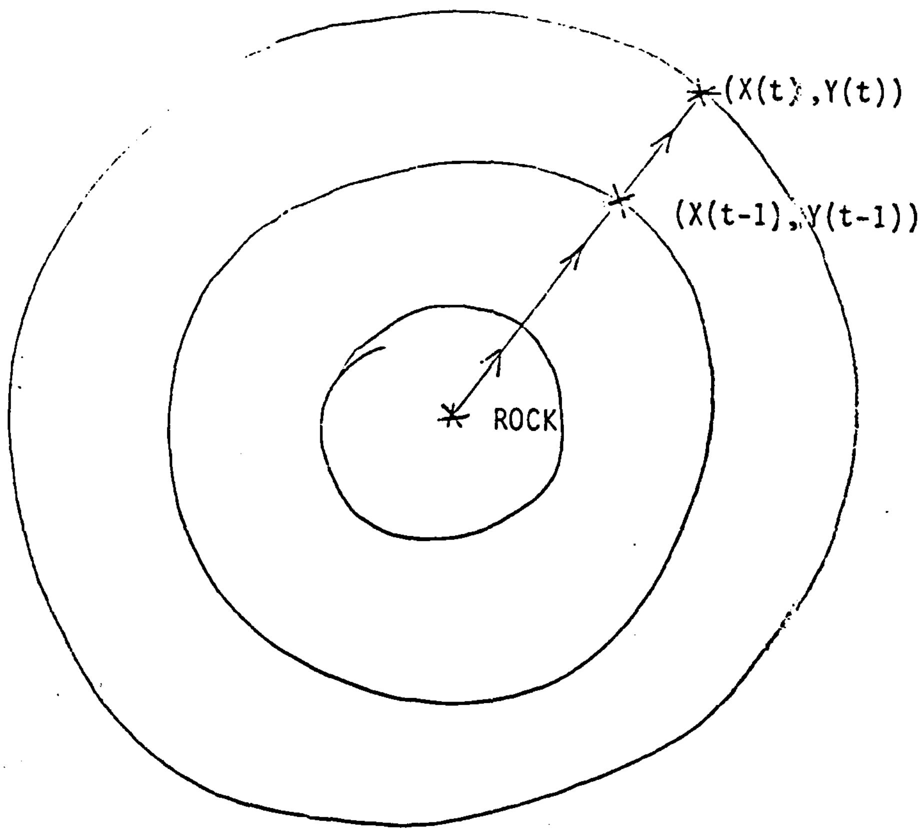

Figure 4: WAVE PROGRESS.

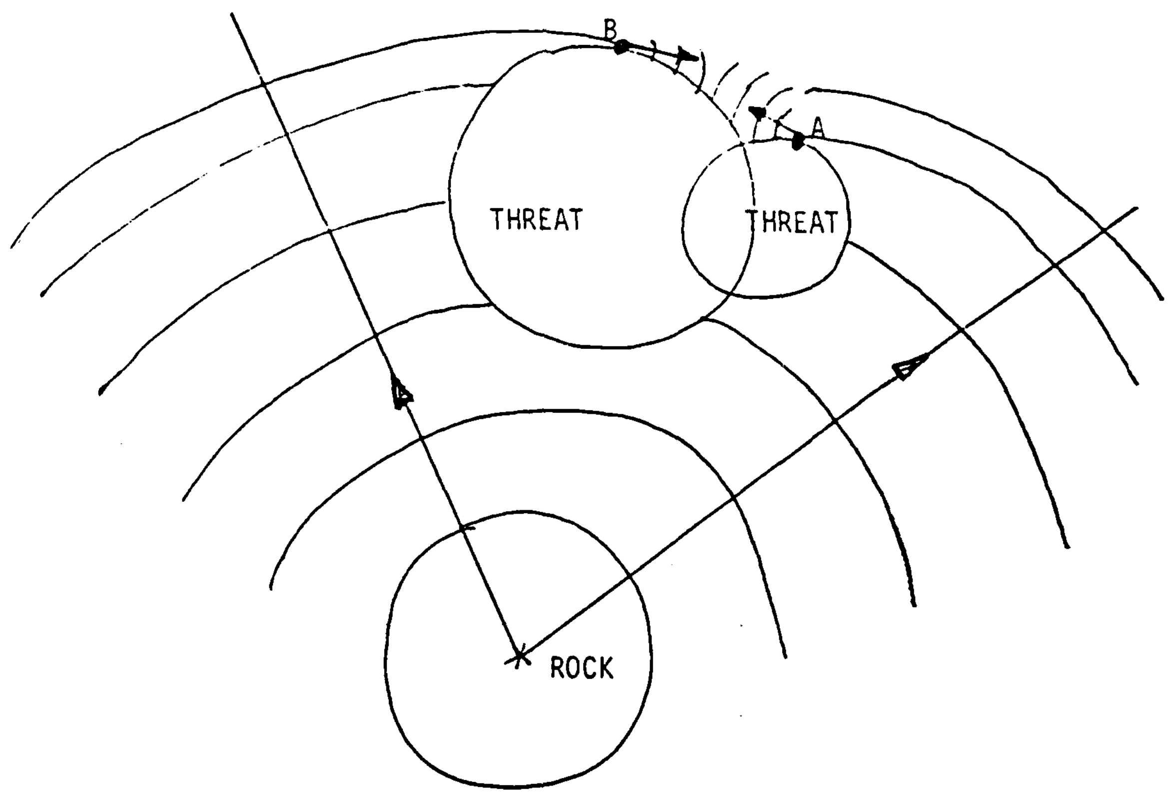

Figure 5: Wave Progress with Obstacles.

[illegible] 25)

	J=25	J=26	J=27	J=28	J=29	J=30	J=31	J=32	J=33	J=34	J=35	J=36	J=37	J=38	J=39	J=40	J=41	J=42	J=43	J=44	J=45	J=46
=20	-5	-5	-5	-5	-5	-5	-5	-5	-5	-5	-5	-5	-5	-5	-5	-5	-5	-5	-5	-5	-5	-5
=21	-5	-5	-5	-5	-5	-5	-5	-5	-5	-5	-5	-5	-5	-5	-5	-5	-5	-5	-5	-5	-5	-5
=22	-5	0	0	0	0	0	0	0	0	0	0	0	0	0	0	0	0	0	0	0	0	-5
=23	-5	0	0	0	0	0	0	0	0	0	0	0	0	0	0	0	0	0	0	0	0	-5
=24	-5	0	0	0	0	0	0	0	0	0	1	1	1	1	1	1	1	0	0	0	0	-5
=25	-5	0	0	0	0	0	0	0	0	1	1	1	1	1	1	1	1	1	0	0	0	-5
=26	-5	0	0	0	0	0	0	0	1	1	1	1	1	1	1	1	1	1	1	0	0	-5
=27	-5	0	0	0	0	0	0	1	1	1	1	1	1	1	1	1	1	1	1	1	0	-5
=28	-5	0	0	0	0	0	0	1	1	1	1	1	1	1	1	1	1	1	1	1	0	-5
=29	-5	0	0	0	0	0	0	1	1	1	1	1	1	1	1	1	1	1	1	1	0	-5
=30	-5	0	0	0	0	0	0	1	1	1	1	1	1	1	1	1	1	1	1	1	0	-5
=31	-5	0	0	0	0	0	0	1	1	1	1	1	1	1	1	1	1	1	1	1	0	-5
=32	-5	0	0	0	0	0	0	1	1	1	1	1	1	1	1	1	1	1	1	1	0	-5
=33	-5	0	0	0	0	0	0	1	1	1	1	1	1	1	1	1	1	1	1	1	0	-5
=34	-5	0	0	0	0	0	0	0	1	1	1	1	1	1	1	1	1	1	1	0	0	-5
=35	-5	0	0	0	1	1	1	1	1	2	2	1	1	1	1	1	1	1	0	0	0	-5
=36	-5	0	0	1	1	1	1	1	1	1	2	2	1	1	1	1	1	0	0	0	0	-5
=37	-5	0	1	1	1	1	1	1	1	1	1	1	1	0	0	0	0	0	0	0	0	-5
=38	-5	0	1	1	1	1	1	1	1	1	1	1	1	0	0	0	0	0	0	0	0	-5
=39	-5	0	1	1	1	1	1	1	1	1	1	1	1	0	0	0	0	0	0	0	0	-5
=40	-5	0	1	1	1	1	1	1	1	1	1	1	1	0	0	0	0	0	0	0	0	-5
=41	-5	0	1	1	1	1	1	1	1	1	1	1	1	0	0	0	0	0	0	0	0	-5
=42	-5	0	1	1	1	1	1	1	1	1	1	1	1	0	0	0	0	0	0	0	0	-5
=43	-5	0	1	1	1	1	1	1	1	1	1	1	1	0	0	0	0	0	0	0	0	-5
=44	-5	0	0	1	1	1	1	1	1	1	1	1	0	0	0	0	0	0	0	0	0	-5
=45	-5	0	0	0	1	1	1	1	1	1	1	0	0	0	0	0	0	0	0	0	0	-5
=46	-5	0	0	0	0	0	0	0	0	0	0	0	0	0	0	0	0	0	0	0	0	-5
=47	-5	-5	-5	-5	-5	-5	-5	-5	-5	-5	-5	-5	-5	-5	-5	-5	-5	-5	-5	-5	-5	-5
=48	-5	-5	-5	-5	-5	-5	-5	-5	-5	-5	-5	-5	-5	-5	-5	-5	-5	-5	-5	-5	-5	-5
=49	-5	-5	-5	-5	-5	-5	-5	-5	-5	-5	-5	-5	-5	-5	-5	-5	-5	-5	-5	-5	-5	-5
=50	-5	-5	-5	-5	-5	-5	-5	-5	-5	-5	-5	-5	-5	-5	-5	-5	-5	-5	-5	-5	-5	-5
=51	-5	-5	-5	-5	-5	-5	-5	-5	-5	-5	-5	-5	-5	-5	-5	-5	-5	-5	-5	-5	-5	-5
=52	-5	-5	-5	-5	-5	-5	-5	-5	-5	-5	-5	-5	-5	-5	-5	-5	-5	-5	-5	-5	-5	-5
=53	-5	-5	-5	-5	-5	-5	-5	-5	-5	-5	-5	-5	-5	-5	-5	-5	-5	-5	-5	-5	-5	-5
=54	-5	-5	-5	-5	-5	-5	-5	-5	-5	-5	-5	-5	-5	-5	-5	-5	-5	-5	-5	-5	-5	-5
=55	-5	-5	-5	-5	-5	-5	-5	-5	-5	-5	-5	-5	-5	-5	-5	-5	-5	-5	-5	-5	-5	-5
=56	-5	-5	-5	-5	-5	-5	-5	-5	-5	-5	-5	-5	-5	-5	-5	-5	-5	-5	-5	-5	-5	-5
=57	-5	-5	-5	-5	-5	-5	-5	-5	-5	-5	-5	-5	-5	-5	-5	-5	-5	-5	-5	-5	-5	-5
=58	-5	-5	-5	-5	-5	-5	-5	-5	-5	-5	-5	-5	-5	-5	-5	-5	-5	-5	-5	-5	-5	-5
=59	-5	-5	-5	-5	-5	-5	-5	-5	-5	-5	-5	-5	-5	-5	-5	-5	-5	-5	-5	-5	-5	-5
=60	-5	-5	-5	-5	-5	-5	-5	-5	-5	-5	-5	-5	-5	-5	-5	-5	-5	-5	-5	-5	-5	-5
=61	-5	-5	-5	-5	-5	-5	-5	-5	-5	-5	-5	-5	-5	-5	-5	-5	-5	-5	-5	-5	-5	-5
=62	-5	-5	-5	-5	-5	-5	-5	-5	-5	-5	-5	-5	-5	-5	-5	-5	-5	-5	-5	-5	-5	-5
=63	-5	-5	-5	-5	-5	-5	-5	-5	-5	-5	-5	-5	-5	-5	-5	-5	-5	-5	-5	-5	-5	-5
=64	-5	-5	-5	-5	-5	-5	-5	-5	-5	-5	-5	-5	-5	-5	-5	-5	-5	-5	-5	-5	-5	-5
=65	-5	-5	-5	-5	-5	-5	-5	-5	-5	-5	-5	-5	-5	-5	-5	-5	-5	-5	-5	-5	-5	-5
=66	-5	-5	-5	-5	-5	-5	-5	-5	-5	-5	-5	-5	-5	-5	-5	-5	-5	-5	-5	-5	-5	-5
=67	-5	-5	-5	-5	-5	-5	-5	-5	-5	-5	-5	-5	-5	-5	-5	-5	-5	-5	-5	-5	-5	-5
=68	-5	-5	-5	-5	-5	-5	-5	-5	-5	-5	-5	-5	-5	-5	-5	-5	-5	-5	-5	-5	-5	-5
=69	-5	-5	-5	-5	-5	-5	-5	-5	-5	-5	-5	-5	-5	-5	-5	-5	-5	-5	-5	-5	-5	-5
=70	-5	-5	-5	-5	-5	-5	-5	-5	-5	-5	-5	-5	-5	-5	-5	-5	-5	-5	-5	-5	-5	-5

3

Table 1: -5 means outside search space. Positive values indicate the number of threats over a cell.

(PRINT-LETHALITY 22 25)

	J=25	J=26	J=27	J=28	J=29	J=30	J=31	J=32	J=33	J=34	J=35	J=36	J=37	J=38	J=39	J=40	J=41	J=42	J=43
I=20	10	10	10	10	10	10	10	10	10	10	10	10	10	10	10	10	10	10	10
I=21	10	10	10	10	10	10	10	10	10	10	10	10	10	10	10	10	10	10	10
I=22	10	10	10	10	10	10	10	10	10	10	10	10	10	10	10	10	10	10	10
I=23	10	10	10	10	10	10	10	10	10	10	10	10	10	10	10	10	10	10	10
I=24	10	10	10	10	10	10	10	10	10	10	810	810	810	810	810	810	810	10	10
I=25	10	10	10	10	10	10	10	10	10	810	810	810	810	810	810	810	810	810	10
I=26	10	10	10	10	10	10	10	10	810	810	810	810	810	810	810	810	810	810	810
I=27	10	10	10	10	10	10	10	810	910	810	810	810	810	810	810	810	810	910	810
I=28	10	10	10	10	10	10	10	810	810	810	810	810	810	810	810	810	810	810	810
I=29	10	10	10	10	10	10	10	810	810	810	810	810	810	810	810	810	810	810	810
I=30	10	10	10	10	10	10	10	810	810	810	810	810	810	810	810	810	810	810	810
I=31	10	10	10	10	10	10	10	910	910	910	810	810	910	810	810	810	810	810	810
I=32	10	10	10	10	10	10	10	910	910	910	810	910	910	810	910	810	910	910	810
I=33	10	10	10	10	10	10	10	910	810	910	810	910	810	810	910	810	910	810	810
I=34	10	10	10	10	10	10	10	10	910	810	810	910	810	810	910	810	810	910	810
I=35	10	10	10	10	910	910	910	910	910	1710	1710	810	810	810	810	810	910	810	10
I=36	10	10	10	910	910	910	910	910	910	910	1710	1710	810	810	810	810	810	10	10
I=37	10	10	910	910	910	910	910	910	910	910	910	910	910	10	10	10	10	10	10
I=38	10	10	910	910	910	910	910	910	910	910	910	910	910	10	10	10	10	10	10
I=39	10	10	910	910	910	910	910	910	910	910	910	910	910	10	10	10	10	10	10
I=40	10	10	910	910	910	910	910	910	910	910	910	910	910	10	10	10	10	10	10
I=41	10	10	910	910	910	910	910	910	910	910	910	910	910	10	10	10	10	10	10
I=42	10	10	910	910	910	910	910	910	910	910	910	910	910	10	10	10	10	10	10
I=43	10	10	910	910	910	910	910	910	910	910	910	910	910	10	10	10	10	10	10
I=44	10	10	10	910	910	910	910	910	910	910	910	910	10	10	10	10	10	10	10
I=45	10	10	10	10	910	910	910	910	910	910	910	10	10	10	10	10	10	10	10
I=46	10	10	10	10	10	10	10	10	10	10	10	10	10	10	10	10	10	10	10
I=47	10	10	10	10	10	10	10	10	10	10	10	10	10	10	10	10	10	10	10
I=48	10	10	10	10	10	10	10	10	10	10	10	10	10	10	10	10	10	10	10
I=49	10	10	10	10	10	10	10	10	10	10	10	10	10	10	10	10	10	10	10
I=50	10	10	10	10	10	10	10	10	10	10	10	10	10	10	10	10	10	10	10
I=51	10	10	10	10	10	10	10	10	10	10	10	10	10	10	10	10	10	10	10
I=52	10	10	10	10	10	10	10	10	10	10	10	10	10	10	10	10	10	10	10
I=53	10	10	10	10	10	10	10	10	10	10	10	10	10	10	10	10	10	10	10
I=54	10	10	10	10	10	10	10	10	10	10	10	10	10	10	10	10	10	10	10
I=55	10	10	10	10	10	10	10	10	10	10	10	10	10	10	10	10	10	10	10
I=56	10	10	10	10	10	10	10	10	10	10	10	10	10	10	10	10	10	10	10
I=57	10	10	10	10	10	10	10	10	10	10	10	10	10	10	10	10	10	10	10
I=58	10	10	10	10	10	10	10	10	10	10	10	10	10	10	10	10	10	10	10
I=59	10	10	10	10	10	10	10	10	10	10	10	10	10	10	10	10	10	10	10
I=60	10	10	10	10	10	10	10	10	10	10	10	10	10	10	10	10	10	10	10
I=61	10	10	10	10	10	10	10	10	10	10	10	10	10	10	10	10	10	10	10
I=62	10	10	10	10	10	10	10	10	10	10	10	10	10	10	10	10	10	10	10
I=63	10	10	10	10	10	10	10	10	10	10	10	10	10	10	10	10	10	10	10
I=64	10	10	10	10	10	10	10	10	10	10	10	10	10	10	10	10	10	10	10
I=65	10	10	10	10	10	10	10	10	10	10	10	10	10	10	10	10	10	10	10
I=66	10	10	10	10	10	10	10	10	10	10	10	10	10	10	10	10	10	10	10
I=67	10	10	10	10	10	10	10	10	10	10	10	10	10	10	10	10	10	10	10
I=68	10	10	10	10	10	10	10	10	10	10	10	10	10	10	10	10	10	10	10
I=69	10	10	10	10	10	10	10	10	10	10	10	10	10	10	10	10	10	10	10
I=70	10	10	10	10	10	10	10	10	10	10	10	10	10	10	10	10	10	10	10

5

Table 2: Lethality values for each point. (The value 1710 is constructed this way: every point gets 10, plus 800 since it is inside threat with pk=.8, plus 900 since it is inside threat with pk=.9.)

ARLJNT-DATA IS 25.

	J=25	J=26	J=27	J=28	J=29	J=30	J=31	J=32	J=33	J=34	J=35	J=36	J=37	J=38	J=39	J=40	J=41	J=42	J=43
I=20	9999	9999	9999	9999	9999	9999	9999	9999	9999	9999	9999	9999	9999	9999	9999	9999	9999	9999	9999
I=21	9999	9999	9999	9999	9999	9999	9999	9999	9999	9999	9999	9999	9999	9999	9999	9999	9999	9999	9999
I=22	9999	$\boxed{2}$	10	20	30	42	50	60	70	80	90	100	110	120	132	140	152	160	170
I=23	9999	12	14	24	34	44	54	64	74	84	94	104	114	124	134	144	154	164	174
I=24	9999	20	24	25	38	48	58	68	78	88	898	914	924	934	944	954	964	158	176
I=25	9999	30	34	38	42	52	62	72	82	892	1222	1724	1734	1744	1754	1764	1322	978	182
I=26	9999	40	44	48	52	55	65	76	686	1216	2025	2355	2544	2554	2556	2435	2112	1315	992
I=27	9999	50	54	58	62	65	70	890	1210	2020	2250	3160	3354	3364	3374	3245	2450	2125	1330
I=28	9999	62	64	68	72	75	80	844	1700	2344	3154	3464	4154	4174	4184	3564	3254	2444	1640
I=29	9999	72	74	78	82	88	92	500	1710	2522	3330	4142	4516	4554	4712	4282	3472	2550	1852
I=30	9999	80	84	88	92	96	102	510	1720	2532	3340	4150	4960	5752	5160	4252	3460	2570	1852
I=31	9999	90	94	98	102	105	110	920	1730	2540	3350	4160	4970	5210	4834	4022	3430	2580	1870
I=32	9999	100	104	108	112	115	120	930	1740	2412	3222	4032	4720	4405	4095	2720	3352	2552	1860
I=33	9999	110	114	118	122	125	130	940	1270	2098	2998	2708	3920	2595	3525	3272	2566	2228	1412
I=34	9999	120	124	128	132	135	142	144	954	1764	2574	3364	3118	2725	2775	2552	2242	1432	1054
I=35	9999	130	134	138	1042	1045	1052	1054	1418	3122	4158	3634	2360	1976	1955	1955	1645	1108	292
I=36	9999	140	144	1048	1412	1955	1958	1964	2328	2692	4482	3288	1498	1165	1155	1145	1122	312	309
I=37	9999	150	1054	1418	2322	2595	2570	2674	3238	3582	3086	2176	1255	255	345	335	225	322	318
I=38	9999	160	1070	1932	2592	3595	3792	3724	4148	4000	3090	2180	1270	360	352	342	335	332	329
I=39	9999	170	1080	1932	2900	3810	4652	4634	4914	4004	3094	2184	1274	354	354	350	345	342	339
I=40	9999	150	1090	2000	2910	3822	4720	5504	4918	4009	3098	2189	1278	358	354	358	255	352	349
I=41	9999	190	1100	2010	2920	3832	4740	4832	4842	4014	3104	2194	1284	374	374	370	365	362	359
I=42	9999	200	1110	2020	2772	3562	3912	3922	3932	3704	2898	2184	1274	364	359	379	375	372	366
I=43	9999	210	1120	1492	2408	2766	3002	3012	3022	2874	2510	1614	1250	354	364	374	384	382	378
I=44	9999	220	224	1134	1512	2032	2092	2102	2112	2122	1600	1235	340	350	362	370	380	390	366
I=45	9999	230	234	236	1146	1172	1182	1192	1202	1212	1222	326	336	346	356	366	376	386	396
I=46	9999	240	244	246	252	262	272	282	292	302	312	322	332	342	352	362	372	382	392
I=47	9999	9999	9999	9999	9999	9999	9999	9999	9999	9999	9999	9999	9999	9999	9999	9999	9999	9999	9999
I=48	9999	9999	9999	9999	9999	9999	9999	9999	9999	9999	9999	9999	9999	9999	9999	9999	9999	9999	9999
I=49	9999	9999	9999	9999	9999	9999	9999	9999	9999	9999	9999	9999	9999	9999	9999	9999	9999	9999	9999
I=50	9999	9999	9999	9999	9999	9999	9999	9999	9999	9999	9999	9999	9999	9999	9999	9999	9999	9999	9999
I=51	9999	9999	9999	9999	9999	9999	9999	9999	9999	9999	9999	9999	9999	9999	9999	9999	9999	9999	9999
I=52	9999	9999	9999	9999	9999	9999	9999	9999	9999	9999	9999	9999	9999	9999	9999	9999	9999	9999	9999
I=53	9999	9999	9999	9999	9999	9999	9999	9999	9999	9999	9999	9999	9999	9999	9999	9999	9999	9999	9999
I=54	9999	9999	9999	9999	9999	9999	9999	9999	9999	9999	9999	9999	9999	9999	9999	9999	9999	9999	9999
I=55	9999	9999	9999	9999	9999	9999	9999	9999	9999	9999	9999	9999	9999	9999	9999	9999	9999	9999	9999
I=56	9999	9999	9999	9999	9999	9999	9999	9999	9999	9999	9999	9999	9999	9999	9999	9999	9999	9999	9999
I=57	9999	9999	9999	9999	9999	9999	9999	9999	9999	9999	9999	9999	9999	9999	9999	9999	9999	9999	9999
I=58	9999	9999	9999	9999	9999	9999	9999	9999	9999	9999	9999	9999	9999	9999	9999	9999	9999	9999	9999
I=59	9999	9999	9999	9999	9999	9999	9999	9999	9999	9999	9999	9999	9999	9999	9999	9999	9999	9999	9999
I=60	9999	9999	9999	9999	9999	9999	9999	9999	9999	9999	9999	9999	9999	9999	9999	9999	9999	9999	9999
I=61	9999	9999	9999	9999	9999	9999	9999	9999	9999	9999	9999	9999	9999	9999	9999	9999	9999	9999	9999
I=62	9999	9999	9999	9999	9999	9999	9999	9999	9999	9999	9999	9999	9999	9999	9999	9999	9999	9999	9999
I=63	9999	9999	9999	9999	9999	9999	9999	9999	9999	9999	9999	9999	9999	9999	9999	9999	9999	9999	9999
I=64	9999	9999	9999	9999	9999	9999	9999	9999	9999	9999	9999	9999	9999	9999	9999	9999	9999	9999	9999
I=65	9999	9999	9999	9999	9999	9999	9999	9999	9999	9999	9999	9999	9999	9999	9999	9999	9999	9999	9999
I=66	9999	9999	9999	9999	9999	9999	9999	9999	9999	9999	9999	9999	9999	9999	9999	9999	9999	9999	9999
I=67	9999	9999	9999	9999	9999	9999	9999	9999	9999	9999	9999	9999	9999	9999	9999	9999	9999	9999	9999
I=68	9999	9999	9999	9999	9999	9999	9999	9999	9999	9999	9999	9999	9999	9999	9999	9999	9999	9999	9999
I=69	9999	9999	9999	9999	9999	9999	9999	9999	9999	9999	9999	9999	9999	9999	9999	9999	9999	9999	9999
I=70	9999	9999	9999	9999	9999	9999	9999	9999	9999	9999	9999	9999	9999	9999	9999	9999	9999	9999	9999

Table 3: Shortest Lethality Distance from Origin (22,26) to all points in Search Space.

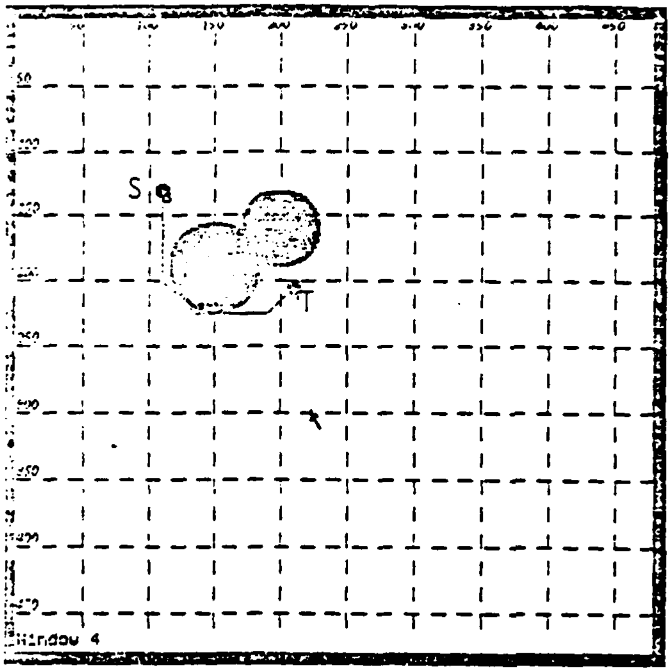

Table 4: Optimal Route from S to T

1985 USAF-UES SUMMER FACULTY RESEARCH PROGRAM/

GRADUATE STUDENT SUMMER SUPPORT PROGRAM

Sponsored by the

AIR FORCE OFFICE OF SCIENTIFIC RESEARCH

Conducted by the

UNIVERSAL ENERGY SYSTEMS, INC.

FINAL REPORT

STATISTICAL PERFORMANCE MEASURES:

RELATING AIR FORCE MISSION CAPABILITY TO BASE SUPPLY MEASURES

Prepared by: Edward Lewis, Ph.D

Academic Rank: Professor

Department and University: Belmont College

Research Location: Air Force Logistics Management Center (LGS), Gunter Air Force Station Montgomery, Alabama 36114-6693

USAF Research: Dr. Douglas Blazer; Major, USAF

Date: September 1985

Contract No: LS840610

STATISTICAL PERFORMANCE MEASURES:

RELATING AIR FORCE MISSION CAPABILITY TO BASE SUPPLY MEASURES

by

Edward Lewis, Ph.D

ABSTRACT

To optimally manage the base supply system and insure the achievement of maximum flying hours the Air Force seeks to determine a small subset of the supply variables at each base that have the highest impact on MICAP (mission capability) when properly managed and which can be used to predict MICAP. Furthermore, once the salient variables for each base have been identified the Air Force seeks a method to determine significant differences in performance between bases and major commands relative to these supply variables and to grade the overall performance of the base supply accounts.

In this study, the salient high impact variables are identified for major commands and bases.

A technique called VA (Value Assessment) is applied to the supply performance data to determine significant differences between bases and major commands, and to create indices to rank the supply performance of bases and major commands.

Recommendations are set forth for a microcomputer-based base Supply Performance Evaluation and MICAP Management System to be used at each base which will increase supply effectiveness and reduce grounding incidents.

Acknowledgements

This research was supported by the Air Force Systems Command, the Air Force Office of Scientific Research, and the Air Force Logistics Management Center, Gunter AFS, Montgomery, Al. The author gratefully acknowledges the sponsorship of these organizations.

Thanks also is owed to the people at the AFLMC who aided me in so many ways throughout the course of the project.

Also, thanks to Major Douglas Blazer, USAF, who provided guidance and procedural helmsmanship at crucial times.

Finally, a special thanks to my wife, Anita, for her patient and enduring support during my many weeks away from home. To her I dedicate this effort.

I: INTRODUCTION:

The research described in this report is essentially statistical in nature and can be divided into two major categories of statistical analysis; identification and multi-criterion decision analysis.

The first objective of the reasearch was to identify; from among a group of over one hundred base supply performance variables tracked and recorded monthly by the Air Force, the variables whih are most directly and strongly related to Air-craft grounding incidents both by base and across bases in each of Air Force major flying commands.

A second objective was to find a method to compare the performance of major commands and bases within commands with respect to individual supply performance variables and groups of such variables.

Third was the objective of being able to combine any or all of the supply performance measures into a grade base by base and major command by major command in order to achieve an overall ranking of overall supply performance base by base and command by command.

Concerning the reasons for my assignment to the project I understand that having educational and professional background in statistics and prior research experience in the statistical areas salient to the current problem contributed to my being chosen as the final candidate.

II. OBJECTIVES OF THE RESEARCH EFFORT:

This research had three objectives which were as follows:

I.) From one hundred and fifteen (115) supply performance measures, reduce these to seventy-eight more aggregate supply performance measures, called the M78 variables (Table 1)and using those develop a predictive model which would:

1. identify the variables which most significantly impact mission capability by base.

2. predict mission capability at a base.

3. be robust enough to allow prediction for all bases in a major command using the same model and a relative few supply performance variables (6-8 variables).

II.) Develop a technique which would identify significant differences between commands and bases within commands with respect to one or more supply performance variables. It is desireable to express these differences as percentages so that meaningful cardinal differences could be expressed (ie. percent differences)

Category 1: Measures of Size

1 - Number of Items Records - Overall Total (Repair Cycle)

2 - Number of Item Records - Overall Total (EOQ)

3 - Number of Item Records - Overall Total (Equipment in Stock)

4 - Dollar Value On-Hand Balance - Overall Total (Repair Cycle)

5 - Dollar Value On-Hand Balance - Overall Total (EOQ)

6 - Dollar Value On-Hand Balance - Overall Total (Equipment in Stock)

Category 2: Activity Measures

7 - Total Transactions (Supplies)

8 - Total Transactions (Equipment)

9 - Total Issues (Supplies)

10 - Total Issues (Equipment)

11 - Total Due-Outs (Equipment)

12 - Total Due-Outs (Equipment)

13 - Total Receipts (Supplies)

14 - Total Receipts (Equipment)

15 - Total DOR - Recoverable

16 - Total DOR - EOQ

17 - Total DOR - Equipment

18 - Total Overall Requisitions - Total Number

Category 2: Activity Measures (Cont'd)

19 - Total Overall Requisitions - Dollar Value Total

Category 3: Effectiveness Measures

20 - Recoverable Issue Effectiveness

21 - EOQ Issue Effectiveness

22 - Recoverable Stockage Effectiveness

23 - EOQ Stockage Effectiveness

24 - Recoverable Release Effectiveness

25 - EOQ Release Effectiveness

26 - Total Item Records with Requisition Objective, Zero accessible Assets - Overall Total

Category 4: MICAP

27 - Total Number MICAP Cause Code A

28 - Total Number MICAP Cause Code B

29 - Total Number MICAP Total All Other Causes

30 - Total Number Deletes Delete Code 8

31 - Total Number Deletes Delete Code 9

32 - Total Number Deletes Total All Other Codes

Category 5: Repair Cycle Information

33 - Average RCT for Total RTS Total All Organizations

Category 5: Repair Cycle Information (Cont'd)

34 - Average RCT for Total NRTS Total All Organizations

35 - Average RCT for Total Condemned Total All Organizations

36 - Average AWP for RTS Total All Organizations

37 - Average AWP for NRTS Total All Organizations

38 - Average AWP for Condemned Total All Organizations

39 - Total Units: RTS Total All Organizations

40 - Total Units: NRTS Total All Organizations

41 - Total Units: Condemned Total All Organizations

Category 6: EOQ/Recoverable Mix

42 - EOQ Line Items Requested as a Percent of Total EOQ and Recoverable

Category 7: Urgency Mix

43 - Line Items Requested, Urgency Need B as a Percent of Overall Total

44 - Line Items Requested, Urgency Need C as a Percent of Overall Total

Category 8: Priority Mix

45 - Total Overall Requisitions Priority Group II As a Percent of Total

46 - Total Overall Requisitions Priority Group III As a Percent of Total

Category 9: Funding Mix

47 - Percent of Total Item Records with Requisition Objective - System Support Division

48 - Percent of Total Item Records with Requisition Objective - General Support Division

Category 10: Bench Stock

49 - Bench Stock Line Items Authorized Total of Overall Summary

50 - Bench Stock Line Items Due Out Total of Overall Summary

51 - Bench Stock Issues and DOR Totals

Category 11: Excess

52 - Dollar Value Excess Supplies General Support Division

53 - Dollar Value Excess Supplies System Support Divison

54 - Dollar Value Excess Supplies Non-Stock Fund

55 - Dollar Value Excess Equipment General Support Division

56 - Dollar Value Excess Equipment Non-Stock Fund

57 - Total Excess Detail Records

Category 12: Special Level

58 - Total Number of Item Records with Special Level - Repair Cycle

59 - Total Number of Item Records with Special Level - EOQ

Category 12: Special Levels (Cont'd)

60 - Total Number of Item Records with Special Level - Equipment in Stock

61 - Total Number of Item Records with Special Level, Date of Last Demand

Category 13: Minimum Level

62 - Overall Total Number of Details Justification 0-Life Cycle Ret

63 - Overall Total Number of Details Justification A ISSL/FOSSL

64 - Overall Total Number of Details Justification - All Others

65 - Total GSD Minimum Level Dollar Value

Category 14: WRSK/MSK

66 - Total WRSL Transactions

67 - Total Type of Details - MSK

68 - Total Type of Details - WRSK

Category 15: Receipts on Time

69 - Total Priority Group 1 - Percent on Time

70 - Total Priority Group 2 - Percent on Time

71 - Total Priority Group 3 Percent on Time

Category 16: Inventory Accuracy

72 - Total Line Items Counted - Complete

73 - Total Line Items Counted - Special

Category 16: Inventory Accuracy (Cont)

74 - Total Line Items Counted - Identity Change

75 - Total Line Items In Lot

76 - Accuracy Percent of Units Complete

77 - Accuracy Percent of Units - Special

78 - Accuracy Percent of Item Records Sampled

Table 1: M78 Variables

III.) To develop statistical indices with which to grade the performance of supply account (bases and for major commands) with respect to one or more supply performance variables.

III. METHODOLOGY

OBJECTIVE I - SALIENT VARIABLE IDENTIFICATION AND PREDICTION OF MISSION CAPABILITY.

FACTOR ANALYSIS

Given a large number of variables as depicted in Table 1 Factor Analysis groups these variables in to "factor" groups in descending rank order of correlation of the "factors" with mission capability (MICAP). From seventy eight variables factor analysis found ten (10) underlying factors (variable groups). as depicted in Table 2. 1.

The underlying factors appear to be associated with variables in the categories shown in Table 2.1

The indicated factor categories are by no means clearly discernable from the Factor Analyses but are vaguely suggested and certainly open to other interpretations.

It was determined, after a number of attempts that, factor analysis would not clearly discriminate a set of variables that could be used over bases or over time to predict MICAP.

Table 2.2 shows the percent coincidence (common variables) between three different time periods called months 01,03 and

Factor	"Apparent" Factor Name"	M78 Variables Involved
1	Total Supply Activity	1,2,4,5,7,9,13,18 21,22,25,44,58,57, 59,63,68,76
2	Inventory Receipts - Timing and Priority (Pipeline)	4,24,25,33,36,37,38 66,69,70,71,76,*VN39
3	Reserves and Stockage Effectiveness	1,2,20,23,25,33,36, 37,38,58,59,63,69 76,77,**VN26,***VN50
4	Order Backlog Processing	4,9,20,21,22,23,24,25, 33,42,43,44,57,66,68, 77
5	Recovery Efficiency Group	20,21,22,23,37,38,42, 43,66,68,77
6	Production (Repair) Backlog	5,23,24,25,33,36,43, 57,69,70,71,*VN39, **VN26,***VN50
7	Inventory Reserves	1,4,5,36,42,44,57,59, 63,77 ***VN50
8	Issues from Inventory	1,2,5,9,20,21,22,23, 33,57,58,59,63
9	Part Shortage	4,5,21,23,24,25,43, 63,66,68,71,77 *VN39
10	Inventory Accuracy & Control	24,57,68,76,77 *VN39

*VN39 = % Reparables this Station

**VN26 - % of the Time a part with a Requisition Objective was Available

***VN50 - % of the Bench Stock Unavailable

Table 2.1: Underlying Factors Identified from Factor Analysis

% Coincidence of Variables

Factor	Months 01 vs 03	Months 01 vs 06	Months 03 vs 06	Average Factor Coincidence
1	55.5	66.7	55.5	59.23
2	0.0	30.8	7.7	12.83
3	0.0	0.0	11.8	3.93
4	6.3	6.3	0.0	4.20
5	9.1	9.1	0.0	6.07
6	0.0	14.3	14.3	9.53
7	8.3	8.3	33.3	16.63
8	7.7	0.0	0.0	2.67
9	0.0	0.0	7.7	2.67
10	0.0	16.7	16.7	11.13
Total	86.9	152.2	14.7	

Table 2.2. Factor Analysis by Month:Variable - Percent Coincidence Matrix

and 06 as repects the percentage of the factor variables that are common to the underlying factors over time. Notice that the largest percent coincidence is 66.7% for factor 1 but that the remaining factors exhibit dismally low percentages of common factors.

Several reasons for the failure of Factor Analysis to clearly discriminate a robust variable set became clear as analysis proceded.

1. The variables that affect MICAP are usually related to MICAP in a lagged fashion.
2. The variables that affect MICAP vary over time different variables being salient at different times.
3. The variables that affect MICAP vary by major command.
4. The variables that affect MICAP vary by base within a command.
5. The variables that affect MICAP vary by weapons systems.

What does appear to be possible, however, is to identify the category of variables (see M78 categories - Table 1). That are most highly correlated with MICAP by command and by base within a command and then to determine within each category the most highly salient variables having the highest impact on MICAP.

Tables 3.1 through 3.4 depict the frequency of occurance of variable categories in the underlying factors identified in Table 2.1 as determined from the many Factor Analyses run.

Notice that the Tables 3.1, 2, 3,4 suggest the possibility of ranking the variable categories in descending order of "affect" on MICAP and that the rankings by time period are very much alike and that some categories appear to be repeatedly ranked high in terms of % of occurances as shown in Table 4 below.

Variable Category	Category Name
1	Measures of Size
3	Effectiveness Measures
5	Repair Cycle Information
11	Special Inventory Levels
13	WRSK War Readiness Spares Rit
15	Inventory Accuracy

Table 4: Six Variable Categories Frequently Occuring in Factor Analysis Factors of the M78 Variable Set

If such variable category rankings of impact on MICAP were possible by Major command and by base within commands and if variables with a category could be similarly ranked then a robust predictive model of MICAP could result, at the very least, by base and perhaps by major command.

Var	Factor Category Name	1	2	3	4	5	6	7	8	9	10	Total	% Total
1- 6	Mea Of Size	4	1	2	1		1	3	3	2		17	12.8%
7-19	Activity Mea	4			1				1			6	4.5
20-26	Efficiency Mea	3	2	3	6	4	3		4	4	1	30	22.6
27-32	MICAP												
33-41	Repair Cycle		4	4	1	2	2		1			14	10.5
42	EOQ Recoverable Mix				1	1		1				3	2.3
43-44	Urgency Mix	1			2	1	1	1		1		7	5.3
45-48	Priority Mix												
49-51	Bench Stock												
52-57	Excess	1			1		1	1			1	5	3.8
58-61	Spec Inv Levels	2		2				3	3			10	7.5
62-65	Min Inv Levels	1		1				1	1	1		5	3.8
66-68	WRSK	1	1		2	2				2	1	9	6.8
69-71	Receipts on Time		3	1			1			1		6	4.5
72-78	Inv Accuracy	1	1	2	1	1	2	1		1	2	12	9.0
VN39	% RTS		1				1			1	1	4	3.0
VN26	% Time IR W/RO Inaccessible			1			1					2	1.5
VN50	% Bench Stock Unavailable			1			1	1				3	2.2
	Total	18	13	17	16	11	14	12	13	13	6	133	

*RO - Requisition Objective

Table 3.1: Frequency of Occurance of Variable Categories in Factors
All Months (1,3,6)

Var	Factor Category Name	1	2	3	4	5	6	7	8	9	10	Total	% Total
1- 6	Mea of Size	4	1		1			3				9	17.3
7-19	Activity Mea	4										4	7.7
20-26	Effectiveness Mea	2			1	1	1			4		9	17.3
27-32	MICAP												
33-41	Repair Cycle			4								4	7.7
42	EOQ Recov'rble Mix				1							1	1.9
43-44	Urgency Mix	1			1	1						3	5.7
45-48	Priority Mix												
49-51	Bench Stock												
52-57	Excess	1						1				2	3.8
58-61	Special Inv lvls	2						2				4	7.7
62-65	Min Inv Levels	1						1				2	3.8
66-68	WRSK	1	1			2					1	5	9.6
69-71	Receipts on Time		3									3	5.7
72-78	Inv Accuracy		1		1					1		3	5.7
VN39	% Reparable this Station										1	1	1.9
VN26	% Time IR W/RO* Inaccessible						1					1	1.9
VN50	% Bench Stock Unavailable						1					1	1.9
	Total	16	6	4	5	4	3	7		5	2	52	

*RO - Requisition Objective

Table 3.2: Frequency of Occurances of Variable Cetegories in Factors
Month 01

Var	Factor Category Name	1	2	3	4	5	6	7	8	9	10	Total	% Total
1- 6	Mea of Size	4			1		1	1	2	2		11	18.3%
7-19	Activity Mea	4			1							5	8.3
20-26	Effectiveness Mea	1		2	2	4	2				1	12	20.0
27-32	MICAP												
33-41	Repair Cycle		4									4	6.6
42	EOQ Recov'rble Mix							1				1	1.7
43-44	Urging Mix				1			1				2	3.3
45-48	Priority Mix												
49-51	Bench Stock												
52-57	Excess										1	1	1.7
58-61	Spec Inv Levels	1							2			3	5.0
62-65	Min Inv Levels			1					1	1		3	5.0
66-68	WRSK	1			2							3	5.0
69-71	Receipts on Time			1			3			1		5	8.3
72-78	Inv Accuracy	1		2		1		1				5	8.3
VN39	% RTS		1							1		2	3.3
VN26	%Time IR W/RO* Inaccessible			1								1	1.7
VN50	% Bench Stock Unavailable			1				1				2	3.3
	Total	12	5	8	7	5	6	5	5	5	2	60	--

*RO-Requisition Objective

Table 3.3: Frequency of Occurances of Variable Categories in Factors
MOnth 03

Var	Factor Category Name	1	2	3	4	5	6	7	8	9	10	Total	% Total
1- 6	Mea of Size	4		2			1	1				8	12.7%
7-19	Activity Mea	4							1			5	7.9
20-26	Effectiveness Mea	1	2	1	4	1	1		2			12	19.0
27-32	MICAP												
33-41	Repair Cycle		1		1	2	2	1	1			8	12.7
42	EOQ Recovr'ble Mix					1		1				2	3.2
43-44	Urgency Mix					1	1	1		1		4	6.3
45-48	Priority Mix												
49-51	Bench Stock						1					1	1.6
52-57	Excess				1		1				1	3	4.8
58-61	Spec Inv Levels	1		2								3	4.8
62-65	Min Inv Levels	1		1								2	3.2
66-68	WRSK	1								2		3	4.8
69-71	Receipts on Time		3	1			1					5	7.9
72-78	Inv Accuracy		1					1			2	4	6.3
VN39	% RTS						1			1	1	3	4.8
VN26	%Time IR W/RO* Inaccessible												
VN50	%Bench Stock Unavailable												
	Total	12	7	7	6	5	9	5	4	4	4	63	--

*RO-Requisition Objective

Table 3.4. Frequency of Occurances of Variable Categories in Factors
Month 06

FILTERING AND SALIENT VARIABLE IDENTIFICATION:

Because the categories of Table 1 contain variables in logical groups and because Factor Analysis did not produce "underlying factors" comprised of variables grouped in sensible ways an alternative identification method was used. The method is comprised of two stages of correlation filtering.

Assume as in Factor Analysis, that high correlation with MICAP means high impact on MICAP. Assume further that each "high impact" variable (hereafter referred to as salient) bears some lagged relationship to MICAP.

The following method was used to rank the variable categories in descending order of salience to MICAP and then to rank variables within a category according to salience.

THE DATA:

It should be noted at the outset that only twelve (12) months of data was available for the M78 variables and therefore the results are only indicative requiring application to more data to establish the generality and robustness of the methodology.

ROTATING VARIABLES:

The twelve monthly values for a given base for each variable including MICAP are imagined to be like the numbers on the face of a clock

For the sake of example each is seen with the monthly values corresponding to the hour marks on the clock faces.

The variable clock face was rotated 12 times, holding the MICAP clock face fixed and twelve correlations were computed representing the twelve possible lag periods of the variable on MICAP. In this way the highest correlation of the variable with MICAP was established and the lag period of the variable with MICAP was established.

Within a major command the variables were rotated for each base and the bases for which statistically significant values (.8230 at α = .005) were obtained (n of them). These were used to obtain an average significant correlation for the variable for the major command. These are known to have a t - distribution with n - 2 degrees of freedom. (1)

Each variable could then be determined to be significant at a base and/or to a major command with respect to MICAP. The level of significance was recorded for each variable that was significant for a major command.

Then within each variable category (Table A-1) the variables were ranked by salience based on level of significance (α).

For the major command under scrutiny the maximum correlation values both significant and not significant were sorted in descending sequence and a rank 1 through 78 assigned. (high rank = low salience).

Then to rank the variable categories according to salience the rank sum of the significant variables in each variable category is computed and divided by the number of variables comprising it yielding the "Average Significant Rank Sum per Variable Category".

From the foregoing analysis the most salient variables in the most salient variable categories can be determined and any or all can be used in a predicative model of MICAP by base or by major command.

As an example of the forgoing consider Figures 1 and 2. Figure 1 shows the variable groups ordered by "average Significant Rank Sum". Figure 2 shows the variables in two of the categories (2 and 3) ordered by maximum average correlation within level of significance. From Figure 1 we see that variable group 3 has salience rank 5 among all groups. From Figure 2 we see that the most salient variables in variable group 3 are 22 and 23, Recoverable Stockage Effectiveness and EOQ Stockage Effectiveness respectively.

It is now possible to clearly identify variable groups in rank order of impact on MICAP both by base and by major command and to identify within these variable groups the most salient variables ranked in order of salience by maximum correlation and level of significance.

The development of a robust predictive model of MICAP will have to be the subject of a follow-on research effort as it is not now clear how such a model should be constructed. It is, however, obvious that a simple regression model will not suffice since we do not seek to explain behavior but rather to predict from a casual relationship.

********** VARIABLE SUM/RANK SUM REPORT **********

SORTED BY SIGNIFICANT RANK-SUM/VARIABLE

SMALLER R-SUM & R/VAR VALUES ARE BETTER(EXCLUDING ZEROS)

VAR	VARIABLE NAME	# SIG	#NOT SIG	TOT VAR	SIG R-SUM	SIG R/VAR	NOT R-SUM	NOT R/VAR	TOT R-SUM	TOT R/VAR
14	MRSK/MSK	0	3	3	0	0.00	151	50.33	151	50.33
6	EOQ RECOVERABLE MIX	1	0	1	10	10.00	0	0.00	10	10.00
8	PRIORITY MIX	1	1	2	12	12.00	74	74.00	86	43.00
4	MICAP	5	1	6	79	15.80	11	11.00	90	15.00
3	EFFECTIVENESS MEASURES	7	0	7	201	28.71	0	0.00	201	28.71
12	SPECIAL LEVELS	4	0	4	115	28.75	0	0.00	115	28.75
15	RECEIPTS ON TIME	3	0	3	87	29.00	0	0.00	87	29.00
1	MEASURES OF SIZE	5	1	6	178	35.60	69	69.00	247	41.17
16	INVENTORY ACCURACY	5	2	7	191	38.20	130	65.00	321	45.86
9	FUNDING MIX	2	0	2	91	45.50	0	0.00	91	45.50
2	ACTIVITY MEASURES	10	3	13	474	47.40	43	14.00	522	40.15
13	MINIMUM LEVEL	3	0	3	147	49.00	0	0.00	147	49.00
7	URGENCY MIX	1	1	2	50	50.00	17	17.00	67	33.50
11	EXCESS	6	0	6	308	51.33	0	0.00	308	51.33
5	REPAIR CYCLE INFORMATION	5	4	9	257	51.40	186	46.50	443	49.22
10	BENCH STOCK	3	0	3	160	53.33	0	0.00	160	53.33

Figure 1: Variable Groups for ATC Ordered by Average Significant Rank Sum

GROUP 2 - ACTIVITY MEASURES NO	VARIABLE NAME	VARIABLES 7 TO 19	RANK	MAX R	SAMP	AV LAG	SD LAG	ZCRIT	ALPHA	RELATION	
7	TOTAL TRANSACTIONS(SUPPLIES)		8	0.7434	2	1.50	2.06	0.0000	0.0000	DIRECT	*** NOT SIG ***
14	TOTAL RECEIPTS(EQUIPMENT)		15	0.9393	2	4.50	4.50	0.0000	0.0000	DIRECT	*** NOT SIG ***
13	TOTAL RECEIPTS(SUPPLIES)		25	0.9322	2	1.75	2.49	0.0000	0.0000	DIRECT	*** NOT SIG ***
10	TOTAL ISSUES(EQUIPMENT)		45	0.9195	6	2.88	2.37	0.9172	0.0100	DIRECT	
17	TOTAL DOR-EQUIPMENT		53	0.9113	6	5.83	2.97	0.8820	0.0200	INVERSE	
17	TOTAL OVERALL REQUISITIONS - $ VALUE		57	0.9107	6	3.10	2.90	0.8120	0.0200	DIRECT	
11	TOTAL DUE-OUTS(SUPPLIES)	R	67	0.8999	6	1.11	1.89	0.8820	0.0200	DIRECT	
16	TOTAL DOR-EQU		60	0.9075	5	1.38	1.87	0.8780	0.0500	DIRECT	
9	TOTAL ISSUES(SUPPLIES)		72	0.8956	5	7.83	1.77	0.8780	0.0500	INVERSE	
15	TOTAL DUR-RECOVERABLE		4	0.9487	4	2.00	3.03	0.9000	0.1000	DIRECT	
18	TOTAL OVERALL REQUISITIONS - TOTAL NO		29	0.9296	4	1.83	1.95	0.9000	0.1000	DIRECT	
12	TOTAL DUE-OUTS(EQUIPMENT)	R	41	0.7205	4	6.57	2.87	0.9000	0.1000	INVERSE	
8	TOTAL TRANSACTIONS(EQUIPMENT)		46	0.9190	4	5.25	1.64	0.9000	0.1000	INVERSE	

GROUP 3 - EFFECTIVENESS MEASURES NO	VARIABLE NAME	VARIABLES 20 TO 26	RANK	MAX R	SAMP	AV LAG	SD LAG	ZCRIT	ALPHA	RELATION
22	RECOVERABLE STOCKAGE EFFECTIVENESS		3	0.9578	6	5.56	4.67	0.9617	0.0050	INVERSE
23	EOQ STOCKAGE EFFECTIVENESS		26	0.9322	7	4.09	4.64	0.9956	0.0050	INVERSE
24	RECOVERABLE RELEASE EFFECTIVENESS		31	[illegible]	6	[illegible]	[illegible]	0.9172	0.0100	INVERSE
26	TOTAL ITEM RECORDS W/PD [illegible]	R	16	0.7387	5	2.81	4.06	0.9161	0.0200	DIRECT
25	EOQ RELEASE EFFECTIVENESS		64	0.9111	6	5.74	4.61	0.8820	0.0200	INVERSE
20	RECOVERABLE ISSUE EFFECTIVENESS		20	0.9371	4	4.88	1.36	0.9000	0.1000	DIRECT
21	EOQ ISSUE EFFECTIVENESS		51	0.9157	4	4.33	3.40	0.9000	0.1000	INVERSE

Figure 2: Variables in Categories 2 & 3 Ordered by Maximum Average Correlation within Significance Level

OBJECTIVE II: IDENTIFYING SIGNIFICANT DIFFERENCES BETWEEN COMMANDS AND BASES WITH RESPECT TO SUPPLY PERFORMANCE VARIABLES

OBJECTIVE III: DEVELOP STATISTICAL INDICES OF PERFORMANCE FOR SUPPLY ACCOUNTS

Both objectives II and III were achieved using the same technique. The technique used was Value Assessment (2) somewhat modified to accomodate special circumstances provided by the current problem setting and the data used.

The paradigm on which Value Assessment is based requires that multiple alternatives (bases, major commands, weapons systems) be characterized by multiple attributes (M78 variables) which can be quantitatively expressed. For example consider the Matrix below which depicts the paradigm.

M78 Variables

	V_{21}	V_{22}	V_{33}	V_{34}	V_{35}	Rank V_j
Base 1	X_{11}	X_{12}	X_{13}	X_{14}	X_{15}	$f_1\ (X_{1j})$
Base 2	X_{21}	X_{22}	X_{23}	X_{24}	X_{25}	$f_2\ (X_{2j}$
	$\vdots$			$\vdots$		$\vdots$
Base k	X_{k1}	X_{k2}	X_{k3}	X_{k4}	X_{k5}	$f_k\ (X_{kj})$

In the matrix above V_{21} V_{22} ... V_{25} represent the M78 variables in the Effectiveness category numbered as indicated by the subscript 21 and 22 and the M78 variables in the Repair

Cycle category numbered 33, 34 and 35. The X_{ij} values are the measurements of the M78 variables for k bases in a major command. The values $f_1(X_{1j})$ ... $f_k(X_{kj})$ represent MCDA (Multiple Criteria Decision Analysis) functions of the X_{ij} in the corresponding row. (3), (4), (5).

The values $f(X_{ij}), i = 1, \ldots, k$ represent indices that allow the alternatives (bases to be ranked relative to their overall composite performance with respect to the five variables (in two categories) shown. This accomplishes objective III.

To accomplish objective II a technique called RIDIT (2) analysis is used which allows the X_{ij} values to be transformed into percentiles which can be added, subtracted and averaged in a way that is commonly understood. Therefore, differences in overall performance base to base can be measured as a percentage as well as differences base to base with respect to one variable, two variables, or any combination of the variables.

Many successful computer analyses were made and are summarized below:

- SAC bases were compared and ranked by weapons systems with respect to M78 variable 20 - "Recoverable Issue Effectiveness".
- Major Commands (SAC, TAC, MAC, ATC, AAC, PACAF, USAFE) were compared and ranked with respect to M78 variable 20 - "Recoverable Issue Effectiveness".
- TAC bases were compared and ranked with respect to M78 variable 20 - "Recoverable Issue Effectiveness".

- SAC and TAC bases within their respective commands were compared and ranked with respect to a number of other M78 variables (21, 22, 23, 24, 25) and variable sets.

Table 5 below summarizes the ranking of weapons systems in SAC with respect to Recoverable Issue Effectiveness. (M78 variable 20)

RANK	SAC WEAPONS SYSTEM
1	B52D/KC135
2	Missiles
3	KC135/Missiles
4	KC135
5	B52G&H/KC135
6	B52G/KC135
7	B52H/KC135
8	FB111/KC135

Table 5: Value Assessment Ranking of SAC Weapons Systems Recoverable Issue Effectiveness

Corresponding to the ranking above VA (Value Assessment) also yields differences in performance between SAC weapons systems expressed as percentages and interpretable as indicating that the performance of bases comprising a particular weapons system is some percentage "better" or "worse" than another weapons system group of bases. Table 6 depicts a matrix of differences for SAC weapons systems. Figure 3 depicts these differences graphically.

Weapons System	B52 KC135	Missiles	KC135 Missiles	KC135	B52G&H KC135	B52G KC135	B52H KC135	FB111 KC135
B520/KC135	—	(0.56)	10.66	23.64	28.55	41.49	34.60	56.55
Missiles	—	—	11.22	24.20	29.11	42.05	35.16	57.11
KC135/Missiles	—	—	—	12.98	17.89	30.83	23.94	45.89
KC135	—	—	—	—	4.91	17.85	10.96	32.91
B52G&H/KC135	—	—	—	—	—	12.94	6.05	28.0
B52G/KC135	—	—	—	—	—	—	(6.89)	15.06
B52H/KC135	—	—	—	—	—	—	—	21.95
FB111/KC135	—	—	—	—	—	—	—	—

Table 6: Matrix of Percentage Performance Differences for SAC Weapons Systems for Recoverable Issue Effectiveness

In Table 6 find a weapons system in the left hand margin, for example, KC135, then read across to a weapon system in the horizontal headings, for example B52H/KC135; the percentage value in the corresponding row and column is 10.96 indicating 10.96% better performance by the bases in the KC135 weapons system category against those in the B52H/KC135 weapons system category with respect to Recoverable Issue Effectiveness. Other comparisons are made in a similar manner from Table 6.

In summary with respect to the stated objectives, it remains only to use the current results to develop a robust predictive model of MICAP by base and by major command.

IV: RECOMMENDATIONS

Develop a predictive model of MICAP involving the salient variables and variable categories which can be identified using the methods described in this work.

Once developed the model should be fashioned to function on a microcomputer at the base supply level.

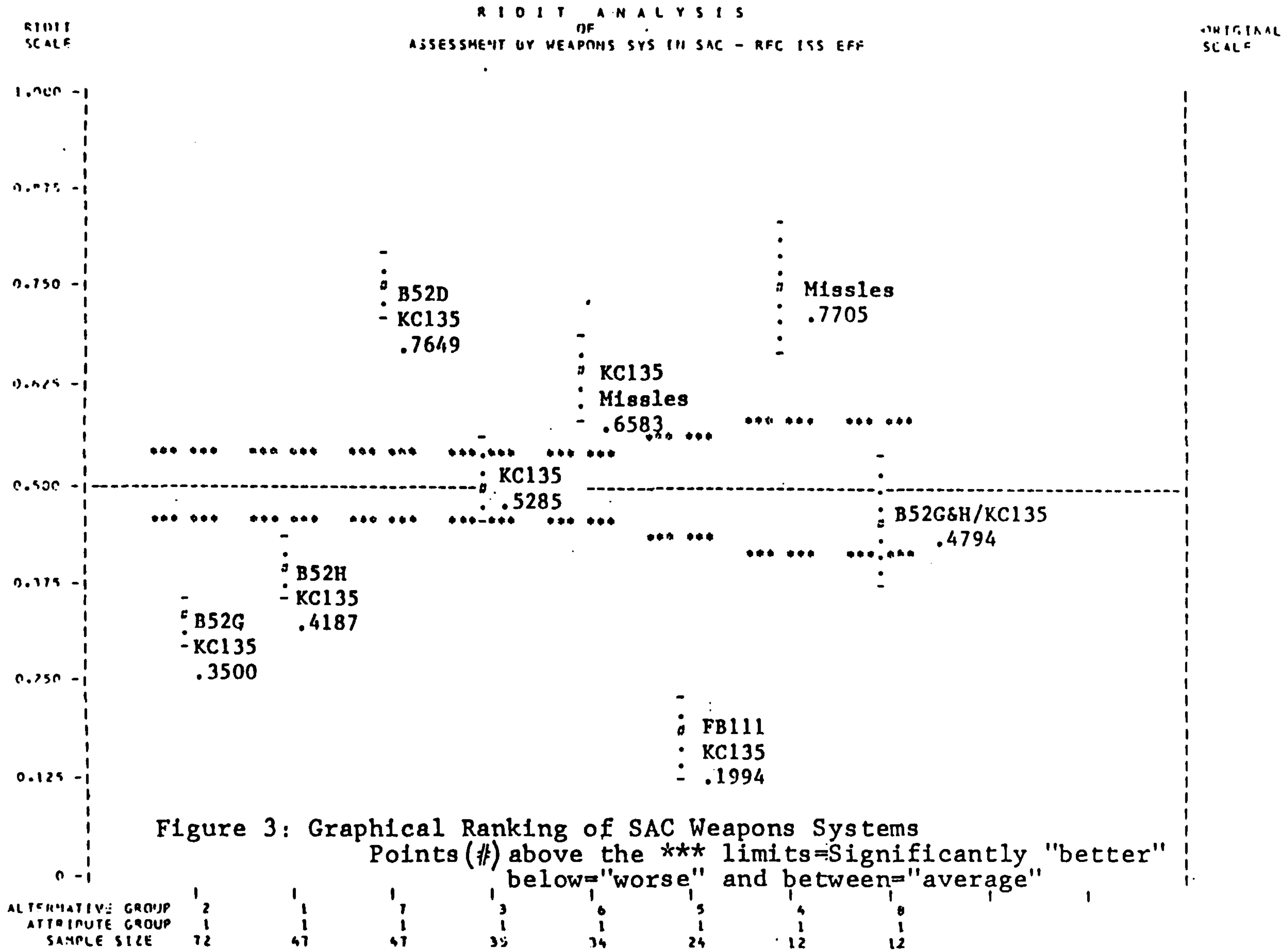

Figure 3: Graphical Ranking of SAC Weapons Systems
Points (#) above the *** limits=Significantly "better"
below="worse" and between="average"

VALUE ASSESSMENT

Value Assessment (VA) now incorporates a statistical method called RIDIT which involves discrete distribution analyses. VA could be generalized and the results made more robust by enhancing the RIDIT portion of VA to perform these same analysis based on the theoretical continuous distribution functions which the discrete analyses now closely approximate.

Also VA should be enhanced to provide greater generality in computing overall indices for alternatives from attribute values by providing a greater number of model forms particularly non-linear ones to accomodate the frequent complex dependencies between attributes that arise in most real problems.

The benefits of this further research would be:

- The ability to predict the rate grounding incidents months in advance.
- The ability to indicate via the "Base Level Model" the salient high impact variables, those that if controlled more diligently and in certain predicted ways, would affect future reductions in grounding incidents.
- The isolation of salient variables for a major command that could be used to predict the rate of grounding incidents over the entire command.
- The ability to compare base performance by variable to determine for a particular base the supply the supply variables with respect to which the base is performing best, worse and above average, and below average.

- The ability to compare the performance of bases within a command with respect to one or more of the supply variables.
- The ability to compare the performance of major commands with respect to one or more of the supply variables.
- The ability to determine the variables for which overall Air Force supply performance is best, worse, above average and below average.
- The ability to determine differences in performance in any of the above ways and express these differences as percentages thus providing a visible mechanism for controlling and improving low performance with respect to selected supply variables.
- The ability to index supply performance by base, by major command and by weapons system.
- The ability to determine a performance standard for the Air Force for each supply variable and then to compare bases, commands and weapons systems performance to the standard.

These enhancements to the current research will be clearly described in detail in the mini-grant follow-on proposal.

REFERENCES

1. Beyer, William H, CRC Handbook of tabbs for Probability and Statistics, 2nd Edition, Boca Raton, Florida, CRC Press Inc, 1983

2. Humphress, G, Lewis, E, "A Value Assessment Aid to Complex Decision Making", FPRI Final Report NA-2507, Project 1391-4, Prepared by Southwest Research Institute, San Antonio, Texas, July 1982

3. Cochrane, J, L, Zeleny, M, Multiple Criteria Decision Making, University of South Carolina Press, Columbia, S.C., 1973

4. Keeney, R, Raiffa, H, Decisions With Multiple Objectives: Preferences and Value Trade Offs, John Wiley & Sons, Inc, New York, New York, 1976

5. Zeleny, M, Multiple Criteria Decision Making, McGraw-Hill Book Co, New York, New York, 1982

1985 USAF-UES SUMMER FACULTY RESEARCH PROGRAM/
GRADUATE STUDENT SUMMER SUPPORT PROGRAM

Sponsored by the

AIR FORCE OFFICE OF SCIENTIFIC RESEARCH

Conducted by the

UNIVERSAL ENERGY SYSTEMS, INC.

FINAL REPORT

TESTING THE EFFECTIVENESS OF SOME USER FRIENDLY ALGORITHMS

Prepared by: Michael Meriwether Lewis

Academic Rank: Assisant Professor

Department and University: Computer Information Science Department, Sorrell College of Business and Commerce, Troy State University, Troy, Alabama, 36082

Research Location: AF Logistics Management Center (AFLMC), Gunter AFS, Alabama, 36115

USAF Research: Captain Ronald E. Travis

Date: 1 November, 1985

Contract No: F49620-85-C-0013

AD-A166 177 UNITED STATES AIR FORCE SUMMER FACULTY RESEARCH PROGRAM 1985 TECHNICAL RE..(U) UNIVERSAL ENERGY SYSTEMS INC DAYTON OH R C DARRAH ET AL. DEC 85 AFOSR-TR-86-0140 11/15

UNCLASSIFIED F49620-85-C-0013 F/G 5/1 NL

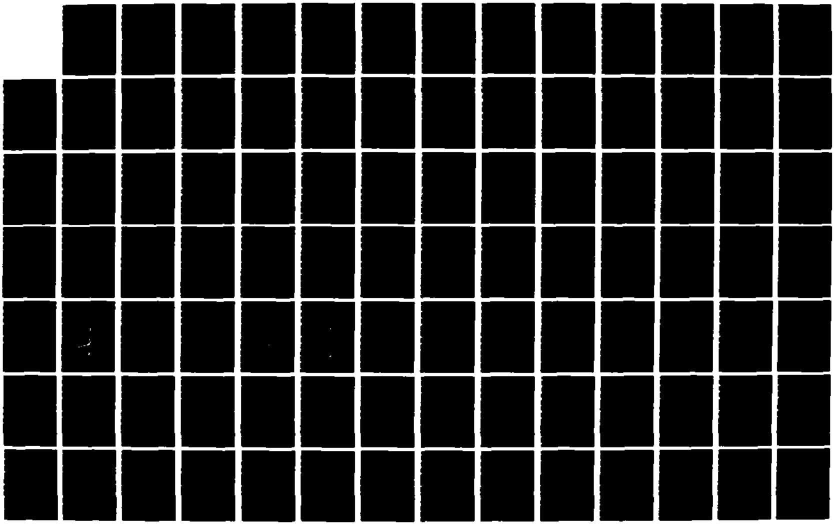

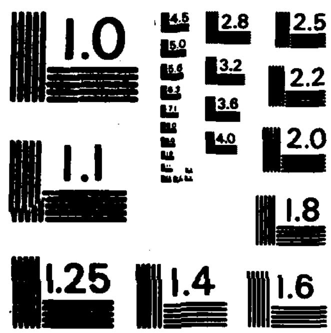

MICROCOPY RESOLUTION TEST CHART
NATIONAL BUREAU OF STANDARDS-1963-A

TESTING THE EFFECTIVENESS
OF SOME USER FRIENDLY ALGORITHMS

by

Michael Meriwether Lewis

ABSTRACT

The objective of this project was to test the effectiveness of some user friendly human-computer interface algorithms. The vehicle chosen to test these algorithms was the AFLMC Project Management System (PMS). This type of computer system is frequently viewed by the lower echelon project manager as an extra work load that intrudes in the effort to complete the project. As a working measurement of "user friendly", I tested the acceptance of two tools (programs) designed to make the job of "keeping up with the paper work" simple enough to cause the project managers to do so as a matter of course rather than as an assigned task to "get done". These programs have several generalized routines that were designed to be transportable to other programs. Included in these routines are: a "field data editor" that allows any or all characters in a field to be manipulated; a set of "date input/output" routines that allow a date to be entered in many acceptable forms; and routines that treat some data as a word processor problem and other data as a spread- sheet problem.

Interviews with representatives at all echelon levels of the organization were done both before and after the introduction of the project manager tools. The prototype tools were user tested and the initial feed back indicated that the project manager needed such tools and they were anxious to have the tools formally implemented (with a few modifications) as soon as possible into the day to day operations.

The time allocated to the project, 10 man-weeks, was insufficient to design, program, and fully test the effectiveness of the tools. It is recommended that a follow on questionnaire should be used to re-evaluate the findings of the initial tests. In addition, other tools should be designed (and tested) to facilitate the human-computer interfaces at other levels of the Project Management System. This would allow investigation of the interactions within the Project Management System to determine some of the practical techniques that should be designed and implemented.

ACKNOWLEDGMENT

The author thanks the Air Force Logistics Management Center (AFLMC) and the Air Force Office of Scientific Research for the opportunity to spend a challenging and rewarding summer with the Plans and Programs Directorate of the AFLMC. I especially appreciate the cooperation of Lt. Col. Len Hall for providing a flexible working environment that enabled this research to be carried out.

In addition I acknowledge the outstanding support of Capt. Ronald Travis. Without the advantage of his extensive knowledge of the existing Project Management System and his willingness to discuss details, problems and possibilities, the initial tools would not have been created in just ten weeks. The AFLMC personnel provided an professional environment in which to do productive work. I especially appreciate the candidness of those interviewed both before the programs were designed and after they were used.

I. <u>Introduction:</u> Mr. Lewis has been in the computer field since 1958 when he joined the US Air Force as a computer operator and board wirer. During the 25 years he was in the USAF, he also worked as a programmer (SPS, AUTOCODER, COBOL, FORTRAN, and RPG II), systems evaluator and quality control tester for world-wide release of standard systems, systems analyst for both batch and on-line systems, and as a data processing manager. He has Master of Business Administration and will complete a master degree in computer science in the fall of 1985. He has a Certificate in Data Processing (CDP). He has built four microcomputers from kits and has written both application and systems programs for them. In 1983, he began teaching courses in computer science at the undergraduate level. He is also a consultant in the microcomputer field.

The historical thrust of computer science has been to efficiently use the computer and to design effective information outputs for the users of the computer. The scale and isolation of the main frame computers caused the emphasis to be placed in the above areas of high cost. The introduction of the personal computer and the online interactive terminal has allowed the user, rather than the trained computer specialist, to be the operator of the equipment. Programs that require little or no training to use are increasingly needed. Little guidance is available in the literature to help the computer scientist design "user friendly" programs.

The AFLMC is project oriented. Typical projects run for 6 to 12 months. There are usually around 100 current projects; some of which are being actively worked and some of which are waiting for the available resources to work them. The pressures to get the projects done (be productive) and the natural tendency to concentrate on the day-to-day work of completing projects causes the project managers to often view the "paper work" necessary to manage the project as intruding on the work itself. This perception is often aggravated by the effort to make the descriptions and justification both clear and politically acceptable. This effort causes the paper work to be typed and retyped many times both for construction changes and for "word smithing" reasons. While some of this "paper churning" can be alleviated by the reduction of retyping for non-critical changes, a more significant reduction could be effected by producing the necessary forms with a word processor and/or spread sheet programs. This approach allows for draft review on either a CRT screen or on hard copy and then making modifications without having to re-input the correct data and thereby reducing the chances of introducing "new" errors in the document. This, of course, is one of the advantages of using the small computer in the office environment.

The automating of paper work without recognizing the problems of the man-computer interface would not solve the perception problems alluded to above. The programs must not only produce the information in a proper form, but them must be user friendly. That is to say, they must be self training, have clear data requests, ask for data in sequences

that are logical to the user, assist the user in his project planning, and help prevent errors from entering the data base.

II. OBJECTIVES OF THE RESEARCH EFFORT:

A. To produce a prototype project management system to aid the project manager in documenting the planning and managing of projects.

B. To design and test user friendly algorithms for use in in the prototype system.

C. To analyze the existing Project Management System to determine other areas of improvement.

III. A PROTOTYPE PROJECT MANAGEMENT SYSTEM: The initial analysis of the existing system showed that there were several forms designed to be used by the project manager to define the project and to report efforts expended in completing the project. The data was typed on the form. There were entry length limitations in the blocks. These lengths were dictated by the field sizes in the mainframe data base system. The typing width of the blocks did not match the required field lengths. The data on the forms was entered into the data base system by a data entry clerk. Various reports could be requested form the data base. Some users did not know how to get reports from the data base. Most

reports were designed for top management rather than for the project manager. The mainframe data base was quite large and report requests had significant impact on the throughput of the mainframe computer.

The initial analysis indicated that there was insufficient time to convert the entire system. Therefore, it was agreed to design and test improvements to the lowest level of the system; the project manager. An overall approach to the total system was determined. The project manager programs were designed to be expandable to a complete project management system. There were two basic types of project manager input: the initial problem definition and planning data, and the project management data. As more time was spent in managing the project, the prototype programs concentrated on the AFLMC Forms 3 and 6.

The Form 3 had much of the management detail: man hour projections, funding projection, and task activity identification. The first section contained identification data such as project title, project responsibilities, and overall project start and completion dates. The second section was for man-hour resource requirements by fiscal quarter not only for the responsible directorate but for supporting directorates as well. In the the third section, up to 15 activities were shown with their actual, current planned, and proposed changed start/stop dates. The fourth section was for remarks concerning the reason for submission of the form and justification for proposed changes. The fifth section contained funds requirements by fiscal quarter for 11 fund different cites. The final section was for signatures by the project manager, the

director, and the AFLMC Commander's approval. The activity section was in the form of a list and the resource and funds requirement sections were in the form of two dimensional grids. The existing form was double sided.

The Form 6, Project Review Data, was used to show which activities had been completed and the activities to be done in the near term. This form was used when a formal review was to be done.

The analysis showed that most projects had less than 15 major activities. In addition, the Form 3 had excessive space for the data to be entered. The data on the Form 6 was a summary of the data on the Form 3. By designing the Form 3 to be printed at 15 characters to the inch and reducing the allocated space for entries, it was possible to print the entire Form 3 on one page with a small computer printer. The printed form included the proper headings and block lines. The Form 6 was redesigned to be a vertical form similar to the Form 3. It was also printed in its final form. The user selected which form was to be printed.

Two prototype programs were were developed and tested. The first allowed the project manager to project his project activities and resource requirements on the CRT screen. Manipulation routines provided a convenient method for rearranging and changing the plan. The data displays were designed to help the project manager to concentrate on the different facets of the project and to move from one part to another

with relative ease. The activities relationships could be viewed in different forms: list, pert, or Gantt chart. A standard screen dump program could print these forms as hard copy. These dumps could be copied to overhead view graphs and used in briefings. The second program printed the AFLMC Form 3 or AFLMC Form 6 in official layout. A print algorithm was designed such that the user could print the Form 3 on a choice of dot matrix printers or on a Diablo daisy wheel printer.

The prototype tools were user tested and the initial feed back indicated that the project manager needed such tools and they were anxious to have the tools formally implemented (with a few modifications) as soon as possible into the day to day operations. However, it must be recognized that part of the initial acceptance was due to a perception that this appeared to be an easier way to keep up with the paper work. The programs were prototype programs and were designed to test some interface techniques. A period of usage patterns must be analyzed before it can be determined whether the interface techniques were in fact "user friendly" or was the positive feedback just a reaction to having someone recognize one of the frustrations of project planning.

IV. <u>USER FRIENDLY ALGORITHMS:</u> The term user friendly interactive process is difficult to define clearly. The reason for this difficulty is that there are many variables to consider in designing a routine to "converse" with a human. Some of these condseration are:

1. Using a program to request data from a human is in some ways

comparable to conducting a conversation with a person you've never met who thinks in a different manner without your being able to see the body language or to be able to react easily to their changes of thought processes.

2. People assign meaning to word, phrase, and sentence tokens. Human speech is rule bound, and normally underlain by prepositional content. When a person "talks" to a computer, he mainly uses only token (symbol) exchanges rather than speech acts. The program responds to strings of alphanumeric characters according to production rules imbedded in the program. These are data transfers rather that idea exchanges. The human may also have to enter relational or positional data; that is, move the cursor to the proper screen position to enter data.

3. The program is requesting a specific class and form of data and must be made "bullet proof" as possible so that invalid data doesn't enter the system.

4. The pre-programmed request must prompt the user for a correct entry, train and help the novice user in entering the data well, and be unobtrusive to the expert user. The demographics of the user class need to be defined before "good" prompts can be designed.

5. The linear order of the requests must follow logical patterns to assist the person in entering "correct" data in thought pattern sequences.

As a working measurement of "user friendly", I tested the acceptance of two tools (programs) designed to make the job of "keeping up with the paper work" convenient enough to cause the project managers to do so as a matter of course rather than as an assigned task to "get done". These programs have several generalized routines that were designed to be transportable to other programs. Included in these routines are: a "field data editor" that allows any or all characters in a field to be manipulated; a set of "date input/output" routines that allow a date to be entered in many acceptable forms; and routines that treat some data as a word processor problem and other data as a spread-sheet problem.

The "field data editor" was designed to function in one field under typical word processor rules. The calling routine must position the cursor, define the field as to length and content (old data or blanks), and call the editor. The field definition is done by setting the field to a value. The editor then inputs the characters one at a time, checks their validity, displays them on the screen, and places them in the field. Cursor keys are used to move around in the field. Character insertion and deletion are provided for. Backspacing will "drag" characters to the left. If the user backspaces out of the field, the original data is redisplayed. Data manipulation can be stopped in any character of the field by pressing the return key and the field will

contain the displayed data. Special characters, such as the cursor keys, backspace key , and return key are passed as control flags to the calling routine to do with as it wishes. This capability allows the user to manipulate data in a known manner.

The "date input/output" routine allows the user to enter a date in the following forms: dd-mm-yy, mm-dd-yy, dd-mm-yyyy, mm-dd-yyyy, yyddd, yyyddd, "dd mon, yy", "dd mon, yyyy", or ddmmmyy. The date was checked for valid days in the month. The output is available to the programmer in any of the listed forms. The internal date was kept in a pseudo-julian date form. In addition, a window could be opened by hitting the HELP key that displayed a calendar of one month that could be pushed either into the future or into the past. This was done so that the user could check to see if a forecasted date was a desired day of the week.

These two routines were used to interface with the user at the field level. Although these techniques helped the user to manipulate the data, they were not sufficient to approach a "user friendly" interface. Each of the sections of the form was displayed on a separate screen with all of the pertinent entry fields displayed at once. The user had the opportunity to move from field to field with the cursor keys. In addition, the fields that could only hold predetermined data, had the choices presented in the proper field to the user one at a time. He could then look at the choices (in an expanded form) with the up/down cursor keys and select the desired code one with the return key. This

was done to help the user enter only valid codes. Standard directorate data was automatically entered. However, the user could over ride the defaults if he needed to do so.

Sections such as 8. RESOURCE REQUIREMENTS IN MAN-HOURS PER QUARTER, and 11. FUNDS REQUIREMENTS IN THOUSANDS PER QUARTER, appeared to the user as two dimensional grids. Movement among the cells was handled in a manner similar to the way standard spread sheet programs perform. For example, movement from cell to cell was done with the cursor keys. Totals were automatically calculated. Section 10. REMARKS, on the other hand, appeared as text and was handled in a manner similar to the way standard word processor programs perform. The purpose of these similarities was to have the user apply skills learned in other programs rather than learn "new" skills and then possibly have to continually adjust to the software they were using.

Section 9. ACTIVITIES (* completed, dated are actual), held other interface difficulties. While sections 8 and 11 had preprogrammed entries, section 9 entries had to be determined by the user. The initial planning of a project holds not only the problem of determining just which steps must be done to complete the project, but it also requires that the activities be ordered in the proper sequence. If the user didn't quite know how to proceed, he could select to start with a "standard" set of activities. These included "standard" start and completion dates. The standards were determined from a study of past projects. This was programmed to give the user a planning framework

with the expectation that modification of the "skeleton" tasks would occur. A management level interface was included in this section. The user could only enter "proposed" dates. The "current" date fields were protected and "proposed " dates were shifted automatically when the plan was approved by upper management and the disk file was processed by the project management directorate. Completed activities could be flagged. When the skeleton was used, section 5 and 6, Project start/completion dates, was automatically calculated. These dates could be over ridden, but could not to be inside the earliest activity start date or latest stop date.

Section 9 manipulation also included the possibility of inserting or deleting activities. It was assumed that the activities had a simple linear relationship. This linear relationship could be augmented (i.e. multiple node linkages) when the activities were displayed in a pseudo PERT chart form. Therefore, this linkage was maintained in the processing of activities. For example, activities could be positionally swapped and the linkage continued to be maintained.

The activities could be displayed in a Ganntt Chart form. This display automatically scaled the entire project to fit on one screen. Weekend indication was added to this display so that the user could see the effects of non-work days in his plan.

V. <u>ANALYSIS OF THE EXISTING PROJECT MANAGEMENT SYSTEM TO DETERMINE OTHER AREAS OF IMPROVEMENT:</u> The small amount of time allocated to this project, 10 man weeks, was insufficient to design and build the prototype tools and to do a complete analysis of the Project Management System. However, some preliminary analysis was possible.

In the prototype programs, the project data was maintained on a disk file and was available to be submitted with the coordinated Form 3 hard copy. A future program could read this disk file and consolidate the data with other project information into an AFLMC project data base. In the case of changed data submission, the updating of the data base could be automated. The prototype project file was designed with this in mind. This approach would eliminate the retyping of data that was required to enter new and/or corrected data into the existing data base.

A test of downloading current/historical project data was done. This test showed the feasibility of building project files for existing project during the initial conversion to this new system. There was also indication of the feasibility of moving the data base processing from the mainframe to a small computer with a 20 megabyte hard disk storage unit. The small system capability of variable length fields, the deletion of blank fields, and the archiving of historical data, would reduce the data base size by approximately 40 per cent. However, before this major change is undertaken, a detailed analysis of the information requirements of the Project Management System should be done. Particular study should be given to determining the needs of the

various levels of management that interface with this system. For example, the planning functions of the project manager, the Director, and the Center Commander all have similar but different needs. These differences must be taken into account in data base design. This does not imply that the initial analysis was not done well. It must be remembered that the existing data base system was designed several years ago. The organization now has the use experience of this system as a basis for analysis of what has worked well and what could be done better.

VI. RECOMMENDATIONS:

A. The prototype project managers system should be used for six months. Initial testing showed it to be usable. Project data (both initial and update) should be passed via floppy diskette among users. During this period, deficiencies, improvements, and general comments should be noted. The general comments should include comment on ease of use and information content derived from the system; good as well as weak features. Use patterns should also be noted. At the end of the six month period, a questionaire testing the effectiveness of the user interface routines should be completed by the actual users of the prototype programs. Analysis of this documentation will show what improvements need to included into these programs. Both user and programmer documentation have been provided to AFLMC to maintain these programs.

B. A second research project should be done to investigate the man-computer interface techniques needed for the intermediate level users; in this case, the project management office personnel. At this level, the human part of the system is typically concerned with the control and manipulation of the information rather than the content and conclusions to be drawn from the data. They are concerned with the integrity of the data base and the production of top management requested reports.

C. Analysis of user requirements at all levels of the organization should be done. It is important to allocate sufficient resources to accomplish this analysis. While it is natural to place emphasis on the job that an organization does, it is equally important to structure job medthodology and to determine if the tools available to do the job can be made more efficient. This includes not only the ability to control today's work, but to analyze the methods used in the past to determine if more effective approaches can be devised to improve productivity.

D. Initial analysis indicates that an detailed analysis will recommend: moving the Project Manager System to the small computer, maintaining a master data base in the project management office, "downloading" directorate information to a directorate small computer for local information analysis, and implementing a center wide local area network to both distribute and gather project and other information.

APPENDIX A

1. Project Number:	2. Title:

3. Phase/Category:	4. Project Manager/Directorate:	5. Phase Start Date:	6. Phase Completion Date:

7. Purpose for Submission:

Initial Form 3 Phase Change Activity Change Resource Change Other

8. Resource Requirements in Man-hours	FY				FY				FY			
Per Quarter	1	2	3	4	1	2	3	4	1	2	3	4
LGM Coordination:												
LGS Coordination:												
LGT Coordination:												
LGC Coordination:												
LGX Coordination:												
LGY Coordination:												
XR Coordination:												
XRP Processing:												

9. Activities	Estimated Start Date	Estimated Completion Date

10. Remarks:

14. Priority:

11. Project Manager's Signature:	12. Director's Signature:	Date:	13. Commander's Approval:	Date:

AFLMC Form 3 Previous Forms are Obsolete

15. Funds Requirements in Thousands Per Quarter	EEIC	FY				FY				FY				TOTAL
		1	2	3	4	1	2	3	4	1	2	3	4	
TDY	40X													
Equip. Lease	473.12													
Equip. Maint.	569													
Contract Studies	592.62													
Equip. Purchase	628													
Equip. Purchase 3080	3080													
ADPE Lease	472													
ADPE Maint.	568													
ADP Services	582													
ADPE Purchase	639													
ADPE Purchase 3080	A3080													
RA Initials:														

APPENDIX B

PROJECT REVIEW DATA
(Please Print or Type)

	DATE LAST REVIEW	CURRENT DATE
TITLE		

ACTIVITIES	PROGRAMMED		ACTUAL	
	START	COMPLETE	START	COMPLETE
PART I: Actions taken since last review:				

	PROGRAMMED		REVISED	
	START	COMPLETE	START	COMPLETE
PART II: Future actions (near term):				

NOTE: When a listed Action corresponds with an Activity identified on an AFLMC Form 3 for the project, then dates for the Action should agree with the AFLMC Form 3 dates.

APPENDIX C

1. Project Number: XP850621	2. Title: Project level PMS tools upgrade.

3. Phase/Catagory:	4. Project Manager/Directorate:	5. Proj. Start Date:	6. Proj. Completion Date:
TE	XRP - Capt Ronald E. Travis	03JUN85	15SEP85

7. Purpose for Submission: Phase extension | 8. PRIORITY:

9. Resource Requirements in Man-hours	FY - 1985				FY -				FY -			
Per Quarter	1	2	3	4	1	2	3	4	1	2	3	4
LGM Coordination:			20									
LGS Coordination:												
LGT Coordination:			20									
LGC Coordination:												
LGX Coordination:												
LGY Coordination:												
XR Coordination:			364									
XRP Processing: Totals 404			404									

10. Activities (* completed, dates are actual)	Current Start Date	Current Stop Date	Proposed Start Date	Proposed Stop Date
* A. Conduct interviews.	05JUN85	19JUN85		
* B. Analysis of the data.	17JUN85	19JUN85		
* C. Design tools.	20JUN85	28JUN85		
D. Develop tools.	01JUL85	12JUL85		31JUL85
E. Prototype test. Start final report.	15JUL85	25JUL85	29JUL85	09AUG85
F. Tool evaluation review.	26JUL85	26JUL85	13AUG85	13AUG85
G. Prepare draft final report.	29JUL85	01AUG85	01AUG85	13AUG85
H. Project review (final report).	02AUG85	02AUG85	14AUG85	14AUG85
I. Publish and distribute final report.	05AUG85	09AUG85	15AUG85	15SEP85

11. Remarks: 1. This Form 3 is to obtain approval for extension of dates. The effort to produce a quality product as well as some system dificulties has caused the development phase of the project to fall behind.

12. Funds Requirements In Thousands Per Quarter	EEIC	FY - 1985 Q1	2	3	4	FY - Q1	2	3	4	FY - Q1	2	3	4	TOTAL
TDY	40X													0
Equipment Lease	473.12													0
Equipment Maintenance	569													0
Contract Studies	592.62													0
Equipment Purchase	628													0
Equipment Purchase 3080	3080													0
ADPE Lease	472													0
ADPE Maintenance	568													0
ADP Services	582													0
ADP Purchases	639													0
ADP Purchases 3080	A3080													0
Total Funds Planned $														

13. Project Manager's Signature:	14. Director's Signature:	Date:	15. Commander's Approval:	Date:

AFLMC Form 3 Previous Forms are Obsolete

APPENDIX D

1. Project Number: XP850621	2. Title: Project level PMS tools upgrade.		
3. Phase/Catagory: TE	4. Project Manager/Directorate: XRP - Capt Ronald E. Travis	5. Proj. Start Date: 03JUN85	6. Proj. Completion Date: 15SEP85
7. Purpose for Submission: Close Activities.		8. PRIORITY:	
9. Resource Requirements in Man-hours Per Quarter. NOT REQUIRED THIS FORM.		Total planned manhours	404
XRP Processing:			

10. Activities (* completed, dates are actual)	Current Start Date	Current Stop Date	Proposed Start Date	Proposed Stop Date
* A. Conduct interviews.	05JUN85	19JUN85		
* B. Analysis of the data.	17JUN85	19JUN85		
* C. Design tools.	20JUN85	28JUN85		
D. Develop tools.	01JUL85	12JUL85		31JUL85
E. Prototype test. Start final report.	15JUL85	25JUL85	29JUL85	09AUG85
F. Tool evaluation review.	26JUL85	26JUL85	13AUG85	13AUG85
G. Prepare draft final report.	29JUL85	01AUG85	01AUG85	13AUG85
H. Project review (final report).	02AUG85	02AUG85	14AUG85	14AUG85
I. Publish and distribute final report.	05AUG85	09AUG85	15AUG85	15SEP85

11. Remarks: 1. This Form 3 is to obtain approval for extension of dates. The effort to produce a quality product as well as some system dificulties has caused the development phase of the project to fall behind.

12. Funds Requirements In Thousands Per Quarter	NOT REQUIRED THIS FORM		Total Funds Planned $
13. Project Manager's Signature:	14. Director's Signature:	Date:	15. NOT REQUIRED

AFLMC Form 6 Previous Forms are Obsolete

1985 USAF-UES SUMMER FACULTY RESEARCH PROGRAM/

GRADUATE STUDENT SUMMER SUPPORT PROGRAM

Sponsored by the

AIR FORCE OFFICE OF SCIENTIFIC RESEARCH

Conducted by the

UNIVERSAL ENERGY SYSTEMS, INC.

FINAL REPORT

FAMILY FACTORS AND THE CAREER INTENT OF AIR FORCE ENLISTED PERSONNEL

Prepared by:	Philip M. Lewis
Academic Rank:	Professor
Department and University:	Department of Psychology Auburn University
Research Location:	Maxwell Air Force Base Leadership and Management Development Center Research and Analysis Directorate
USAF Research Contact:	Maj. Mickey R. Dansby

Date:	August 23, 1985
Contract No:	F49620-85-C-0013

FAMILY FACTORS AND THE CAREER INTENT OF AIR FORCE ENLISTED PERSONNEL

by

Philip M. Lewis

ABSTRACT

The impact of spouse attitudes and attributes on the career intent and job related attitudes of Air Force enlisted personnel was assessed using the Air Force's new Family Survey (AFFS) to measure spouse attitudes and the Organizational Assessment Package to assess the Air Force member's career intent and job attitudes. The Factor structure or the AFFS confirmed its potential utility for assessing critical family variables. Spouses generally viewed Air Force life as more stressful than civilian life, yet most continued to be supportive of and committed to the Air Force. Prominent scources of stress for these families were disruptions caused by work schedules, TDYs, and military exercises and recalls. Reduced employement opportunities and a reduction in family income attendant upon transfer to a new duty location were also viewed as having a negative impact on the family. It proved possible to predict the career intent and job satisfaction of Air Force members from spouse attitudes and other family variables, most importantly from the compatibility of the marital pair's work schedules, the positiveness of the spouse's view of the Air Force and, for career intent only, the perceived stressfulness of the Air Force member's job and of Air Force life for the family. Implications for Air Force policy are briefly discussed.

ACKNOWLEDGMENTS

The research described in this report was conducted under the sponsorship of the Air Force Systems Command, Air Force Office of Scientific Research and the Research and Analysis Directorate of the Leadership and Management Development Center, Maxwell AFB, Montgomery, AL.

Gratefully acknowledged are the advice, support, and overall leadership of Major Mickey R. Dansby and the statistical consultation of Professor Sam Green. Of particular importance was the computer assistance of Ms. Dottie Winther, without which the project would not have been completed.

I. <u>INTRODUCTION</u> Because of this investigator's interests and background in both the psychology of work and marital and family dynamics, application was made to investigate work-family relationships in the Air Force. The Air Force's Leadership and Management Development Center had available a rich data set on the attitudes of spouses of Air Force members, as well as the work attitudes of the Air Force members, and also had personnel willing and able to assist in the proposed research project. Therefore, the Leadership and Management Development Center became the site for the research project which is summarized in this report.

II. <u>OBJECTIVES OF THE RESEARCH EFFORT</u> The main objective of this research effort was to investigate, in a preliminary way, the relationship between married Air Force members' career intent and the demographic characteristics, attitudes, and perceptions of their spouses, as reflected in the spouses' responses to the Air Force Family Survey (AFFS). The most technologically oriented of the military branches, the Air Force invests considerable time and effort in recruiting, selecting, and training high quality personnel. Retention of a high proportion of these individuals is, therefore, a top Air Force priority (Allen, 1980). Because of the demonstrated strong relationship between career intent and employee turnover (Steel & Nestor, 1984), the Family Survey data of the Leadership and Management Development Center offered an opportunity to explore the relationship between a number of theoretically important family variables and the retention of Air Force enlisted personnel. It was hoped that by identifying relationships between Family Factors and Air Force members' career intent, information could be obtained about the ways in which the Air Force could raise retention levels by attending to the impact of Air Force life on the families of Air Force personnel.

III. <u>BACKGROUND</u> There is substantial theoretical and empirical support for the notion that the worlds of work and family life are closely intertwined (see recent reviews by Beeson, 1985; Greenhaus & Beutell, 1985; and Hunter, 1982). However, the exact nature of the reciprocal effects of family and work are still being sorted out. A data set with considerable promise for helping increase our

understanding of the impact of spouse attitudes and attributes on the career intent and job satisfaction of Air Force members is the family and job survey data collected within the last year by the Air Force's Leadership and Management Development Center (LMDC). Of particular interest are data consisting of the job attitudes of married Air Force members and the attitudes, demographic characteristics and perceptions of their spouses. Unlike many previous data sets, where the relationships between family life and work life have been examined from the point of view of a single family member, this LMDC data set includes the responses of both members of the marital dyad.

In 1984 LMDC initiated a revision of its family research instrument, the U.S. Air Force Spouse Survey (Dansby, 1984; Flannery, 1985). The resulting instrument, renamed the Air Force Family Survey (AFFS), represents a systematic attempt to improve the previous instrument, both by improving its psychometric qualities and by adding items that sample areas of theoretical and empirical relevance that were not included in the previous instrument. Because of these improvements it was expected that the new AFFS would provide a more complete understanding of the family-work interface than had the previous Air Force Spouse Survey. The present report summarizes data concerning the factor structure of the new AFFS and the relationship of AFFS factors and demographic items to Air Force members' career intent, job related satisfaction and level of satisfaction with their family's job support.

IV. METHOD The data set utilized in the present investigation consisted of the matched responses of 1170 Air Force members and their spouses for a total of 2340 people. Analyses designed to determine the factor structure of the attitudinal portions of the AFFS were performed using this data set. Fourteen percent of the Air Force members were officers and 84 percent were enlisted personnel. For each pair the Air Force member had completed the Organizational Assessment Package (OAP), a questionnaire designed by LMDC to measure work related attitudes. Their spouse subsequently completed the AFFS. The sample was drawn from a census survey of certain large Air Force organizations (e.g., an entire wing) at four different locations. The married Air Force members who participated in the census survey were

given the AFFS to distribute to their spouses. The return rate from spouses was approximately 39%. Thus, the sample of matched pairs is an "opportunity" sample that cannot necessarily be generalized to all domestically based Air Force families. Nonetheless, it is a relatively large sample and it has the advantage over much previous research of including the responses of <u>both</u> spouses in these Air Force families. For this reason these data permit a direct examination of relationships between the attitudes of military personnel and their spouses.

V. <u>FACTOR STRUCTURE OF THE AFFS</u> The Air Force Family Survey (AFFS) is a 140 item questionnaire that is divided into three main sections. The first 61 items assess the spouses's attitudes about a variety of topics from involvement in the Air Force lifestyle to marital satisfaction and the spouse's gender role orientation. In the middle section are four groups of items concerning 1) frequency of the family's use of various Air Force services, 2) satisfaction with those services, 3) factors perceived by the spouse to be affecting the Air Force member's career intent, and 4) the perceived impact of various factors connected with Air Force life on the family. The final section of the AFFS consists of 23 items that assess demographic characteristics of the spouse or the family. Items from two sections of the AFFS were subjected to factor analyses, the family attitude items (items 1-61) and responses to items in the middle section of the questionnaire having to do with the Air Force member's career intent and the impact of certain Air Force factors on the family.

For the 61 attitudinal items a factor structure was arrived at on the basis of three considerations: 1) initial and confirmatroy factor analyses (Long, 1983), 2) theoretical considerations (Dansby, 1984), and 3) a requirement that each item be included in one and only one factor. The initial method was a principal component analysis followed by a varimax rotation. Using Kaiser's criterion (eigenvalue greater than one) seventeen factors were extracted of which fourteen were easily interpretable. All 61 items were allocated to one of the fourteen factors, and, with the exception of three items, all had factor loadings of at least .27. Following this procedure, a confirmatory factor analysis was conducted using a maximum liklihood

factoring method where 14 factors were specified a priori. This was followed by a varimax rotation to obtain a final factor structure. Twelve of the fourteen factors identified in the exploratory analysis were confirmed in the second analysis. The confirmatory factor analysis divided one of the initial fourteen factors into two factors and failed to identify one of the initial factors. In all, 53 of the 61 items were allocated to the twelve factors identified on both analyses. Because there were good theoretical reasons for retaining the factor not confirmed in the second analysis (Olson's cohesion factor, Olson, Sprenkle and Russell, 1979) and for retaining as a single factor the factor which was split on the second analysis, the original fourteen factors were accepted as the variable structure for use in subsequent analyses. Factor scores were obtained via a simple linear combination of item responses divided by the number of items in the factor. Table 1 lists the fourteen factors and their internal consistencies (Cronbach's alpha).

Table 1

AFFS Attitudinal Factors

Factor	AFFS items*	Name	# items	Alpha
1	13,14,16,22 27,29,36	Air Force Member's Job Stress	7	.72
2	12,19,21,33 34,39	Stress of AF Life for the Family	6	.60
3	28,37,57,58 -59,60,61	Marital Satisfaction	7	.75
4	2,5,7,18 26,32	Positive View of the Air Force	6	.80
5	8,10,23,25 41	Sensitivity of AF to Family needs	5	.75
6	1,3,4,6 9,11,-47	Commitment to AF Lifestyle	7	.74
7	15,20,30,38 -40,42	Perceived Job Satisfaction	6	.72

8	24,43,44	Spouse's Career Orientation	3	.36
9	45,46	Gender role Orientation of Spouse	2	.57
10	52,55	Spouse Independence	2	.46
11**	48,-49	Family Disengagement	2	.59
12	31,35	Member's Career Intent	2	.85
13	17,-51,53	Social Isolation	3	.55
14	50,-54,56	Help Seeking Attitudes	3	.40

*A negative sign indicates that the item loaded negatively on the factor.

**This factor did not emerge on the confirmatory factor analysis.

A second analysis was conducted to determine the factor structure of AFFS items 99-117, the items concerning the Air Force member's career intent and the spouse's view of the effect of a number of Air Force factors on family life. A principal components analysis followed by a varimax rotation yielded four "clean" and easily interpretable factors. Factor loadings of the individual items ranged from .41 to .78, with all items loading on at least one factor. Those factors were perceived favorableness of basic job benefits (items 101, 102, 104, 105, 106, & 108), perceived impact of Air Force moves, exercises, and temporary duty assignments (items 107, 109, 111, 112, & 115), perceived job satisfaction (items 99, 100, 103, & 110), and satisfaction with the current Air Force duty location (items 113, 114, 116, & 117). As with the fourteen family attitude factors, factor scores were obtained via a simple linear combination of item responses divided by the number of items in the factor.

Several observations should be made concerning the factor structure of the first 61 items of the AFFS. First, with the exception of factors 8, 10, and 14, the factors identified had acceptable internal consistencies, particularly considering the small

number of items in some of these factors. Second, the factors which emerged include a number of the kind of variables that are thought to be critical to an understanding of the ways in which families cope with stress and important life transitions (McCubbin, Cauble, & Patterson, 1982). In this regard, there were separate factors concerning perceived stress (Factors 1 and 2), family or spouse coping styles (Factors 10, 11, 13, and 14), and level of social support (Factors 3 and 5). These factors can be expected to be important to an understanding of the career intent of married Air Force members, if one reason for leaving the Air Force turns out to be that one's family is not coping well with the stresses of Air Force life. A third observation concerning the factor structure summarized in Table 1 is that some survey items that might be expected to load on a common factor did not. Most noteworthy was the emergence of separate career orientation and gender role orientation factors. In the present data set, a spouse's orientation toward working is relatively independent of the extent to which he/she holds a traditional or egalitarian view of the roles of husbands and wives. The simple correlation between our Factor 8 (spouse's career orientation) and Factor 9 (gender role orientation of spouse) was only -.04. This independence is further illustrated by the .06 correlation between responses to AFFS item #44 "In our family, it is OK for the wife to work outside the home even if it isn't an absolute financial necessity" and responses to AFFS item #45 "Even if a wife works outside the home, she should still be responsible for running the household." In the past, some researchers have tried to infer gender role orientation or "personal identity" from employment orientation (Beeson, 1985), a strategy that is questionable, given the current pattern of results. The new AFFS permits a direct assessment of role orientation that is relatively independent of career orientation.

VI. SPOUSE ATTITUDES Before moving to a consideration of the relationship between family variables and Air Force members' career intent, a summary of some of the more interesting and relevant attitudes and characteristics of Air Force members' spouses will be presented, particularly those attitudes that might be expected to provide a picture of the current state of Air Force families. In this

summary the focus will be on the responses of the spouses of enlisted personnel, since it is the career intent and job attitudes of enlisted Air Force members that is the focus of the latter half of this paper.

Military life has been characterized in both the technical and popular literature as more stressful and demanding than civilain life (Moskos, 1977; White, 1984). This view matches the perceptions of the current sample of spouses of Air Force enlisted personnel. Fully 76% agree that the special demands of their spouse's Air Force career cause problems for their family that non-Air Force families don't have. Seventy-two percent feel that the Air Force lifestyle causes more stress for a marriage than do non-military lifestyles, and 71% feel their spouse is under "a lot of pressure" as a result of his or her Air Force job. Interestingly, the impact of Air Force life on children is not viewed as negatively, with 55% agreeing that "the Air Force lifestyle offers good conditions for raising children."

Given that over three quarters of the spouses of enlisted personnel surveyed view Air Force life as stressful for families, what do they see as the major sources of stress in the Air Force? Most often viewed negatively in their perceived impact on family life were military exercises and recalls (61%) and TDYs (56%). Fifty-six percent of the spouses surveyed also agreed that their Air Force member's work hours "disrupt our family life more than if my spouse had a non-Air Force job." There were also indications that the effects of being transferred to certain duty location were negative. Forty-five percent of the spouses perceived limited employment opportunities and 42% a negative change in family income due to transfer to the present base (factors that may well be linked). Interestingly, there was <u>not</u> an overall negative perception of PCS moves, with only 23% of the spouses of enlisted personnel agreeing that they moved too often. Factors that were widely viewed as having a positive impact on family life were the convenience of base facilities and acceptance by people in the local area, with 66% and 51% of the spouses viewing these factors as having a <u>positive</u> impact on family life.

Given that Air Force life is generally perceived by these spouses as having a negative impact on the family, we might expect them to

have a somewhat low level of commitment to the Air Force. This was clearly not the case. Fifty-six percent of our respondents indicated that they do feel a part of the Air Force community and 57% feel involved with the Air Force lifestyle. Even a greater proportion (61%) would recommend the Air Force to others as a career. So it appears that the general view of Air Force life as stressful does not translate directly into a lack of support of and commitment to the Air Force. In fact, 66% indicate they want their spouse to make the Air Force a career. And although this is not as high a percentage as those who perceive their Air Force member as wanting to make the Air Force a career (74%), it nonetheless reflects at least a moderate level of commitment by these spouses for continuing with the Air Force, despite some important negative perceptions about Air Force life.

Finally, the spouses surveyed have a high level of both marital satisfaction and general life satisfaction. Eighty-one percent agreed that they are generally happy and fully 95% indicated that they are happy with their marriages. That is not to say that they feel their marriages couldn't be better. In fact, 55% indicated that they wished they communicated better with their spouse.

The overall picture that emerges from the AFFS responses of the spouses of Air Force enlisted personnel is of individuals who are generally quite happy with their lives and very happy, overall, with their marriages. Over half seem committed to and supportive of the Air Force. Yet over three quarters view Air Force life as more stressful for families than civilian lifestyles. The factors seen as most negative in their impact were the disruptions caused by work schedules, temporary duty assignments and military exercises and recalls. Also viewed as having a negative impact by a substantial proportion of these spouses were the effects of the most recent Air force move on their employment opportunities and the (possibly related) factor of reduced family income.

VII. PREDICTING CAREER INTENT One of the primary objectives of the present research effort was exploration of the impact of family variables on the career intent and, by implication, retention of Air Force enlisted personnel. But before proceeding it should be noted

that a variety of factors have been identified in previous research which influence career intent, primarily a number of non-family factors, such as job enrichment, job stress, work group cohesion, role ambiguity et cetera (Mowday, Porter & Steers, 1982). For this reason we can expect the linkages between family variables and career intent to be modest, at best. Yet, modest relationships do not mean that the linkages are not important. The other caveat is that there is a strong link between length of service and career intent (.41 in the present data set). This is due to a number of factors. First of all, in the military those who have been in the longest have passed up a number of opportunities to get out and can be expected, therefore, to have generally high career intent. Secondly, the nature of the military retirement system (no vesting) is such that once an individual has been in the military for a number of years, there are substantial economic incentives for continuing in the military until eligible for retirement. Finally, the longer a person is employed by an organization, the broader their job scope typically is and the higher their compensation level. All of these factors can be expected to strengthen the tenure-commitment relationship and should remind us to interpret with caution the impact of any family variable predictive of career intent which is also significantly correlated with length of service (e.g., length of marriage).

In order to assess the impact of a number of selected AFFS variables on the career intent of Air Force enlisted personnel, a multiple regression analysis was completed using a general linear model. The predictor variables were a number of the AFFS factors identified previously (see Table 1), several demographic items from the AFFS, and several computed variables, including the compatibility between the work schedules of the marital pairs and three dummy coded variables reflecting family life cycle stage. Two AFFS factors (7 and 12) were excluded from the prediction model. Both were expected to have high correlations with the criterion variable (career intent) but for reasons that do little to clarify family-work relationships. Inclusion of the two could obscure other more theoretically meaningful relationships between the AFFS predictors and career intent. Table 2 shows the variables that were included in the regression model.

Subjects for the regression analysis were a subset of the 1170 matched pairs used for establishing the factor structure of the AFFS. Because the dynamics of their career intent were expected to be different from those of the rest of the sample, individuals were eliminated from the data set who indicated that they were expecting to retire within a year or who were married to another Air Force member. These exclusion cirteria reduced the sample to 617 matched pairs, of which 77 included Air Force officers and 540 involved enlisted persons. Multiple regression analyses were conducted on the data for the enlisted personnel and their spouses only, due to the small number of officer-spouse pairs. It is the enlisted personnel where retention is most critical, given their higher turnover rates and proportionally smaller applicant pool.

The criterion variable for the multiple regression analysis was the Air Force member's stated career intent, item 16 from the LMDC's Organizational Assessment Package (Short, 1985). In assessing the significance of AFFS predictors of career intent, a conservative strategy was used. Each predictor variable was entered into the model as if it were entered last, showing the effect of the predictor variable after the effects of all the other predictors had been accounted for. The results of the regression analysis are shown in Table 2.

Table 2

Multiple Regression Analysis of Selected AFFS Factors and Items on the Career Intent of Enlisted Air Force Personnel

Source	df	Type III SS	F
Model (all predictors)	23	266.27	10.87*
Error	517	550.64	
Factor 1 - Job Stress	1	6.50	6.10**
Factor 2 - Family Stress	1	5.10	4.79**
Factor 3 - Marital Satisfaction	1	1.66	1.56
Factor 4 - Positive View of AF	1	14.12	13.26**

Factor 5 - Sensitivity of AF	1	2.59	2.43
Factor 6 - AF Commitment	1	.03	.03
Factor 8 - Career Orientation	1	.01	.00
Factor 9 - Gender Role Orient.	1	.18	.17
Factor 10 - Independence	1	3.86	3.62
Factor 11 - Disengagement	1	.28	.27
Factor 13 - Social Isolation	1	.00	.00
Factor 14 - Help Seeking	1	.09	.08
Item 118 - TDY Frequency	1	.03	.03
Item 119 - TDY Length	1	.93	.88
Item 122 - Marriage Length	1	33.14	31.12**
Item 123 - Living Location	1	.51	.48
Item 127 - Education Level	1	1.90	1.79
Item 128 - No. Children	1	10.19	9.57**
Item 138 - Time Volunteered	1	.17	.16
CWS - Compatibility of Work Sched.	1	10.81	10.15**
PRESCH - Preschooler at Home	1	.11	.10
SCHAGE - School Age Child	1	2.19	2.05
ADOLES - Adolescent at Home	1	.67	.63

* Multiple R for Model = .571

** $p < .05$

Overall, the multiple correlation for the entire regession model (all predictors included) was .571, indicating that is is possible to predict an Air Force member's career intent from their spouses's and family's attitudes and characteristics. Considering each predictor alone, six were able to improve the prediction of career intent to a statistically significant degree over the prediction provided by all the other predictors taken together. In order of magnitude determined by partial correlations with the criterion variable they are as follows: 1) compatibility of work schedules - if the work schedules of the marital pair conflict, then the career intent of the Air Force member is less positive, 2) marriage length - the longer the couple has been married , the more likely the Air Force member is to indicate that he/she intends to make the Air force a career (positive career intent), 3) number of children - the more children they have, the more

positive the Air Force member's career intent, 4) positive view of the Air Force - the more positive the spouse is about the Air Force, the more positive the Air Force member's career intent, 5) stressfulness of Air Force life for the family - the more stressful the spouse perceives Air Force life being for the family, the less committed the Air Force member is to pursuing an Air Force career, and 6) member's job stress - the more stressful the Air Force member's job is perceived as being by their spouse, the more likely the Air Force member is to be intending to make the Air Force a career. This latter finding was unexpected. Inspection of responses to the items in this factor broken down by career intent category (intending to stay, leave or undecided) suggests that the relationship between member job stress and career intent may actually be curvelinear. For example, the spouses of 58% of those intending to stay in the Air Force and 59% of those intending to leave agree with the statement "My spouse's work hours disrupt our family life more than if my spouse had a non-Air Force job." In contrast, only 48% of the spouses of undecided Air Force members agreed with the statement. This same pattern of responses was true for several of the other items making up this factor.

The dynamics of the career intent of enlisted Air Force members can be further clarified by inspection of responses to some of the items which make up the three AFFS factors that were found to be significant predictors of career intent. Fifty-three percent of the spouses whose Air Force members intend to separate from the Air Force agree with the statement "I would urge my spouse to leave the Air Force rather than accept a transfer that didn't fit in our family plans." In marked contrast, only 24% of those whose spouses are either undecided or intend to make the Air Force a career agree with that statement. There was a slight reversal of expected results with regard to spouses' responses to the AFFS item which stated "We move (relocate, 'go PCS', or transfer) too often." Whereas 23% of those with spouses who intend to make the Air Force a career endorsed this item, only 18% of those with a spouse intending to separate from the Air Force endorsed it and an even lower percentage (15%) of the spouses of those who were uncertain with regard to an Air Force career

did so. In this regard it should also be noted that neither TDY length nor TDY frequency was significantly associated with career intent (Szoc, 1982, also failed to demonstrate such a relationship). It may be that TDYs and transfers are an expected part of Air Force life that do not, therefore, significantly affect career intent. On the other hand, the way these potentially disruptive events are actually experienced by the Air Force member's spouse and/or children may have a significant impact on the career intent of enlisted personnel.

Finally, it should be noted that how positively the spouse views the Air Force is significantly correlated with the Air Force member's career intent. Whereas 76% of the spouses of those intending to stay in the Air Force are glad their spouse joined the Air Force, this is true for only 52% of those who intend to leave. Similarly, while 54% of the spouses of those intending to stay would recommend an Air Force career to a son or daughter, that percentage drops to 32% for the spouses of those intending to leave.

Two other variables that researchers have found to be significant predictors of the career commitment of military personnel were examined. Dansby and Hightower (1984), Orthner and Pittman (1984), and Szoc (1982) all found that the perceived level of job support that a military member experiences from his/her family is a significant predictor of career intent, and Szoc (1982) and Woefel and Savell (1978) have confirmed for military personnel the well documented link between job satisfaction and career intent (Mowday et. al., 1982). In the present data set (enlisted subsample) the correlation between career intent and level of satisfaction with the family's attitude toward the job was .26 and the correlation between career intent and job related satisfaction was .23. The relationship of these two additional Air Force member attitudes to spouse and family variables was explored using the same multiple regression approach and predictor variables used with career intent (see Table 2).

With regard to enlisted members' job related satisfaction, there were six significant predictors. In descending order of magnitude determined by their partial correlations they were: 1) compatibility of work schedules, 2) TDY length, 3) the family's attitude toward help

seeking, 4) a positive view of the Air Force, 5) the spouse's gender role orientation, and 6) amount of time the spouse reports spending in volunteer work. Thus, we can describe the more satisfied enlisted personnel as follows: they have a work schedule that doesn't conflict with their spouse's (or their spouse doesn't work outside the home), their spouse has a positive view of the Air Force, they have slightly longer TDYs than their less satisfied counterparts, they have a spouse who reports that their family is more likely to seek outside help for family problems, their spouses report a more egalitarian gender role orientation, and their spouses spend less time doing volunteer work than do the spouses of less satisfied individuals.

Turning to Air Force members' satisfaction with their families' job support, there were only three significant predictors of this criterion variable from among the 23 variables included in the predictor model. These were 1) a positive view of the Air Force by the spouse, 2) compatibility of work schedules, and 3) marital satisfaction. It is worth noting that compatibility of work schedules and the favorableness of the spouse's attitude toward the Air Force were highly significant predictors of all three criterion variables used in the current study. The only new predictor that emerged here was marital satisfaction. And although the relationship was not a strong one, we can conclude that Air Force enlisted personnel tend to be more satisfied with their families' level of support for and pride in their jobs, if their spouses have high marital satisfaction.

Overall, our multiple regression model was less effective in predicting the Air Force member's job related satisfaction and satisfaction with the family's job support (multiple Rs of .405 and .434 respectively) than it was in predicting career intent (multiple R of .571). F tests of the differences in the efficiency of the regression model in predicting the three different criterion variables showed that the model was significantly more effective in predicting career intent (accounted for more variance in criterion variable responses) than it was in predicting either of the other two criterion variables (Sympson, 1980).

VIII. DISCUSSION The findings reported herein confirm once again the close relationship which exists between family life and work life in

the U.S. Air Force. The attitudes and attributes of the current sample of Air Force families were clearly implicated in their Air Force members' career intent. The question of whether the family affects work or work affects the family is probably not a worthwhile question. There is little doubt that family life and work life affect each other in a bidirectional, interactive fashion. In the present study, we were able to show convincingly that family and spouse attitudes can be used to predict work attitudes. Beeson (1985) was just as effective in demonstrating that work attitudes and experiences can be used to predict spouse attitudes. More important than the direction of effect question is the development of a better understanding of the reciprocal interchange between family and work.

Two models have been prominently advanced in the literature that provide an explanatory framework for understanding the work-family interface, the role conflict model (Greenhaus & Beutell, 1985), and the stress model (Burke & Bradshaw, 1981). The role conflict model suggests that work-family conflict may occur when there is a conflict between the role demands of being a family member and the role demands of being an employee. One possible resolution of work-family role conflicts is to change jobs, hence the connection of role conflict theory to the present study's focus on career intent. Family-work role conflicts are expected to be heightened when there is a high level of commitment to one or both roles, the time pressures in either or both roles are high, either role is stressful, or the behaviors required in one role conflict with the behaviors required in the other. From a role conflict perspective, the current findings suggest that the demands of Air Force life may be producing role conflict in a substantial number of enlisted personnel. In the U.S. Air Force there are high performance standards, periods of long and/or irregular hours, and periodic temporary duty assignments away from home. All of these have the potential for interfering with the enactment of one's family roles. The finding in the current study of a strong relationship between work schedule compatibility and career intent and job satisfaction certainly fits predictions from the role conflict model. On the other hand, the lack of a significant relationship between TDY frequency or length and career intent suggest that the

dynamics of the reenlistment decision can not be accounted for by a simple application of the role conflict model.

The other major theoretical model that has been applied to trying to understand the family-work interface is the stress model. As espoused by Burke and Bradshaw (1981) this model essentially says one of three situations may obtain: 1) the family may be a source of stress that negatively impacts one's work attitudes and performance, 2) the job may be a source of stress with a resulting negative impact on the family, or 3) the family may act as a resource, buffering the effects of job stress. It has also been theorized that stressors (whether they come from family or work) do not directly produce strain. Rather the cognitive appraisal of the potential stressor is critical (Lazarus, DeLongis, Folkman, & Gruen, 1985) as are the coping skills and resources that the individual brings to bear on the stressful situation (Heller & Swindle, 1983). In the present study, the perception of the Air Force environment as either stressful or positive by spouses was clearly implicated in the job attitudes of Air Force enlisted personnel. Both the perception that Air Force life is stressful for the family and the perception that the Air Force member's job is more stressful than most civilian jobs were significant predictors of career intent. At the same time a positive view of other aspects of Air Force life may have buffered the effects of the stressful aspects of Air Force life.

How two other significant predictors of career intent, marriage length and number of children, fit with the two explanatory models is less clear. Because the correlation between marriage length and length of service was quite high in our sample ($r = .55$), and because length of service is positively correlated with career intent, for the reasons noted in Section VII above, it could be that the relationship between marriage length and career intent is merely a function of the relationship of marriage length to this third variable (length of service). The same explanation could be used to account for the relationship between number of children and career intent except for the fact that the correlation between the number of children living at home and service length is lower ($r = .38$) and our multiple regression analysis showed that number of children is positively related to

career intent over and above the relationship attributable to marriage length. One explanation is that those with large familites to support may be reluctant to give up a secure career with the Air Force, particularly in light of the finding that the majority of our respondants viewed the Air Force as a good place to raise children.

If a positive family life moderates or buffers the effects of the stressful features of Air Force life, then we could have expected to find that marital satisfaction was a significant predictor of career intent and/or job related satisfaction. This was not found to be true in our sample of enlisted personnel and their spouses. The other possible pattern of results that would support the idea that a positive family life can buffer the effects of work stress would be the finding that marital satisfaction is predictive of job satisfaction and/or career intent in interaction with variables reflecting the perceived stressfulness of Air Force life. When these interactions were assessed in our multiple regression model (the interaction of marital satisfaction with AFFS Factors 1, 2, and 4), there were still no significant effects, although the interaction of marital satisfaction with a positive view of the Air Force just missed statistical significance ($p < .07$) in predicting job satisfaction. It should be remembered, of course, that in our model the marital satisfaction measured was the spouse's marital satisfaction, not the Air Force member's. And although the two are undoubtedly highly correlated, it's possible that stronger marital satisfaction effects would have been obtained if the Air Force member's own marital satisfaction were used as a predictor.

IX. RECOMMENDATIONS The findings of the present study of work-family relationships among Air Force enlisted personnel have several implications for the Air Force. First, Air Force efforts to support their enlisted personnel through support of and sensitivity to Air Force families should be continued. In particular, efforts should be made, where possible, to insure that the work schedules of Air Force members are coordinated with the work schedules of their spouses. How this can be done in a way that doesn't discriminate against those without spouses or whose spouses who don't work outside the home, is not clear. Another finding with important implications for the Air

Force was that a significant number of Air Force spouses (18% in the present enlisted sample) would like to work but indicate they have been unable to find employement. Although the relationship of this factor to career intent was not assessed in the present study, it is very likely that it negatively impacts career intent and job satisfaction. The recently discussed plans of the Air Force's Family Support Centers to establish better employment services for Air Force spouses should be fully supported, since it is likely that the payoff in terms of retention and job productivity will more than offset the cost of the program. Finally, it is recommended that the Air Force continue its support of research into the interface of family life and work life. Factors affecting the retention of officers should be explored, and additional research should be conducted where those families most vulnerable to the stress of Air Force life are identified. There is also considerable wisdom in maintaining ongoing research efforts that can chart changes in the family attitudes and work attitudes of Air Force families, changes that could have important policy implications for the Air Force of the future.

X. REFERENCES

Allen, L. (1980). Air Force policy letter for commanders. Washington, DC: Office of the Secretary of the Air Force.

Beeson, G. W., Jr. (1985). Influence on the identification of wives with the Air Force organization: An examination of the two-person career pattern within the military. Unpublished doctoral dissertation, University of North Carolina, Greensboro, NC.

Burke, R. J., & Bradshaw, P. (1981). Occupational and life stress and the family. Small Group Behavior, 12, 329-375.

Dansby, M. R. (1984). A proposal for the revision of the U.S. Air Force Spouse Survey (Report No. 84-0645). Maxwell AFB, AL: Air Command and Staff College.

Dansby, M. R., & Hightower, J. M. (1984). Family and work in the Air Force. In G. E. Lee & T. E. Ulrich (Eds.), Proceedings, Psychology in the Department of Defense, Ninth Symposium (Report No. US4FA-TR-84-2) (pp. 455-459). Colorado Springs, CO: United States Air Force Academy.

Flannery, P. A. (1985). U.S. Air Force Family Survey revision (Report No. 85-0825). Maxwell AFB, AL: Air Command and Staff College.

Greenhaus, J. H., & Beutell, N. J. (1985). Sources of conflict between work and family roles. Academy of Management Review, 10, 76-88.

Heller, K., & Swindle, R. W. (1983). Social networks, perceived social support, and coping with stress. In R. D. Felner, L. A. Jason, J. N. Moritsugu, & S. S. Farber (Eds.), Preventive psychology: Theory, research and practice (pp.87-103). New York: Pergamon.

Hunter, E. J. (1982). Families under the flag: A review of military family literature. New York: Praeger.

Lazarus, R. S., DeLongis, A., Folkman, S., & Gruen, R. (1985). Stress and adaptational outcomes: The problem of confounded measures. American Psychologist, 40, 770-779.

Long, J. S. (1983). Confirmatory factor analysis: A preface to LISREL. Beverly Hills, CA: Sage.

McCubbin, H. I., Cauble, A. E., & Patterson, J. M. (1982). Family stress, coping, and social support. Springfield, IL: Charles C. Thomas.

Moskos, C. C., Jr. (1977). The all-volunteer military: Calling, profession, or occupation? Parameters, 7(1), 2-9.

Mowday, R. T., Porter, L. W., & Steers, R. M. (1982). Employee-organization linkages: The psychology of commitment, absenteeism and turnover. New York: Academic Press.

Olson, D. H., Sprenkle, D., & Russell, C. (1979). Circumplex model of marital and family systems I: Cohesion and adaptability dimensions, family types and clinical application. Family Process, 18, 3-28.

Orthner, D. K., & Pittman, J. F., Jr. (1984). Linkages between family support variables and military career commitments. In G. E. Lee & T. E. Ulrich (Eds.), Proceedings, Psychology in the Department of Defense, Ninth Symposium (Report No. US4FA-TR-84-2). Colorado Springs, CO: Dept. of Behavioral Sciences and Leadership, U.S. Air Force Academy.

Short, L. O. (1985). The United States Air Force organizational assessment package (LMDC-TR-85-2). Maxwell AFB, AL: Leadership and Management Development Center.

Steel, R. P., & Nestor, K. O., 2nd. (1984). A review and meta-analysis of research on the relationship between behavioral intentions and employee turnover. Journal of Applied Psychology, 69, 673-686.

Sympson, J. B. (1980). Testing differences between multiple correlations (Research Report 79-20). Princeton, NJ: Educational Testing Service.

Szoc, R. (1982). Family factors critical to the retention of Naval personnel (Contract N00125-80-C-1444). Columbia, MD: Westinghouse Public Applied Systems Division.

White, N. J. (1984, December 10). Stress and transience color lives of military marrieds. The Atlanta Constitution, pp. IE, 5E.

1985 USAF-UES SUMMER FACULTY RESEARCH PROGRAM

sponsored by the

AIR FORCE OFFICE OF SCIENTIFIC RESEARCH

conducted by

UNIVERSAL ENERGY SYSTEMS, Inc.

FINAL REPORT

AN ANALYSIS OF LOW DISPERSION IRAS SPECTRA OF CARBON STARS, S STARS AND M VARIABLE STARS

Prepared by:	Dr. Irene R. Little-Marenin
Academic Rank:	Assistant Professor
Department and University:	Department of Astronomy Wellesley College
Research Location:	Air Force Geophysics Laboratory Optical Physics Division Infrared Branch
USAF Research:	Dr. Stephan D. Price

Date:	July 19, 1985
Contract No:	F49620-85-C-0013

AN ANALYSIS OF LOW DISPERSION IRAS SPECTRA OF CARBON STARS, S STARS AND M VARIABLE STARS

by

Dr. Irene R. Little-Marenin

ABSTRACT

My analysis of low dispersion spectra obtained with the IRAS satellite of carbon stars, S stars and M variable stars has shown that 1) about 85% of the carbon stars are surrounded by circumstellar shells as indicated by the presence of the silicon carbide emission feature. The shape of this feature shows little variation from star to star and has a maximum at 11.2 micrometers. The energy emitted in the feature ratioed to the underlying continuum emission is about 20%. 2) Only about one third of the variable M stars are surrounded by circumstellar shells containing silicate dust grains. The shape of the silicate emission feature shows variations from star to star with maximum emission occurring between 9.4 and 10.0 micrometers. The excess emission ratio for M stars is about 30%. 3) About 60% of the known S stars show emission features in the 10 to 11 micrometer region. These features appear to be a composite of emission produced by both silicate and silicon carbide grains.

ACKNOWLEDGEMENTS

I would like to thank the Air Force Office of Scientific Research, the Air Force Systems Command and Universal Energy Systems, Inc. for providing the opportunity to spend a stimulating summer engaged in doing research at the Air Force Geophysics Laboratory, Optical Physics Division.

My indebtedness to Charles Wilton, who wrote most of the computer programs used in this analysis, is gratefully acknowledged. My thanks also go to Len Marcott for writing the programs used in the manipulation of the IRAS data tape. I would like to express my appreciation to all the personnel of the Optical Physics Division, Infrared Branch for making my ten week stay a pleasant and profitable one.

I especially would like to thank Dr. Stephan Price for providing useful and needed guidance for the analysis of infrared data.

I. INTRODUCTION

IRAS, the InfraRed Astronomical Satellite, was launched in January of 1983 and operated for 11 months. During this time IRAS surveyed approximately 96% of the sky in four wavelength bands at 12, 25, 60 and 100 micrometers. Over 250,000 point sources were measured. Simultaneously IRAS operated a low resolution spectrometer in the 8 to 22 micrometer region. About 5000 spectra of point sources brighter than 10 Jy at 12 and 25 micrometers are available.

Many evolved stars are surrounded by a circumstellar shells produced by mass loss from the central star. The 8 to 22 micrometer region is of particular interest since it contains the spectral signature of dust grains found in these shells. In stars with carbon to oxygen ratios less than unity (K and M stars) these dust grains are in the form of silicate grains (SiO in combination with other elements) which have an emission feature centered at about 9.7 micrometers. On the other hand, in stars with carbon to oxygen ratios greater than unity (carbon or C stars) the grains appear to be primarily in the form of silicon carbide (SiC) which emit strongly around 11.3 micrometers. The silicate feature is seen in emission from optically thin and relatively hot shells and in absorption from optically thick and relatively cool shells. The SiC feature has not yet been seen in absorption. The strength of the silicate and silicon carbide feature varies from star to star and in M type Mira variables it appears to increase with the period of light variability (DeGioia-Eastwood et.al. 1981)

II. OBJECTIVE

My primary research effort during the ten week summer fellowship has been the study of the SiO and SiC emission features in three types of objects - carbon stars, S stars and variable M stars. My goal was to answer the following questions:

1) Is the shape of the emission feature (SiO and SiC) uniform from star to star independently of the strength of the emission feature?

2) Can the strength of the emission feature be related to other photospheric parameters of the star such as the photospheric temperatures, the carbon to oxygen ratio, the period of light variability, the amplitude of variability, the magnitude difference (B-V) between blue and visual light?

3) Is the shape of the emission feature in S type stars (stars with carbon to oxygen ratios close to unity) the same as in M stars (i.e. due to SiO) or like the carbon stars (i.e. due to SiC) or is the feature a combination of both types of emission?

4) What is the percentage of carbon and S stars that do and do not show emission features and hence can an estimate of the amount of energy emitted in the these features per star be made?

III. ANALYSIS and RESULTS

All The IRAS spectra are available to us on magnetic tape. Len Marcott from AFGL developed computer programs to read the tapes, produce files and plot the spectra of carbon

stars, S stars and variable stars found in the General Catalogue of Variables Stars (GCVS) by Kukarkin et. al (1969). The SiO and SiC emission features are easily visible if present. Charles Wilton, my graduate student research assistant, and I developed two methods of approach for analysis of the emission features. First we fit a polynomial of order 4 or 6 to the relatively smooth background emission (see Figure 1), subtracted this background emission from the observed flux in the emission feature and then calculated the ratio of this excess emission to the background emission underneath the feature. The shape of the emission feature as a function of wavelength is plotted on the abscissa in Figure 1. Overplotting these emission features (normalized to the maximum emission) allowed us to determine the average shape of the feature. I found that the shape of the SiC emission feature in carbon stars shows very little variation from star to star independent of the strength of the emission (Figure 2). The maximum emission occurs at 11.2 +/- 0.1 micrometers. In a few carbon stars (e.g. Y CVn and UU Aur) I found the short-wavelength side of the emission feature and hence the emission peak to be shifted to longer wavelength by about 0.2 micrometers (Figure 3).

About one third of the variable M stars (semi-regular, irregular and Mira variables) show a silicate emission feature. There is a characteristic shape to the feature but it is not as uniform as the SiC feature in that the widths,

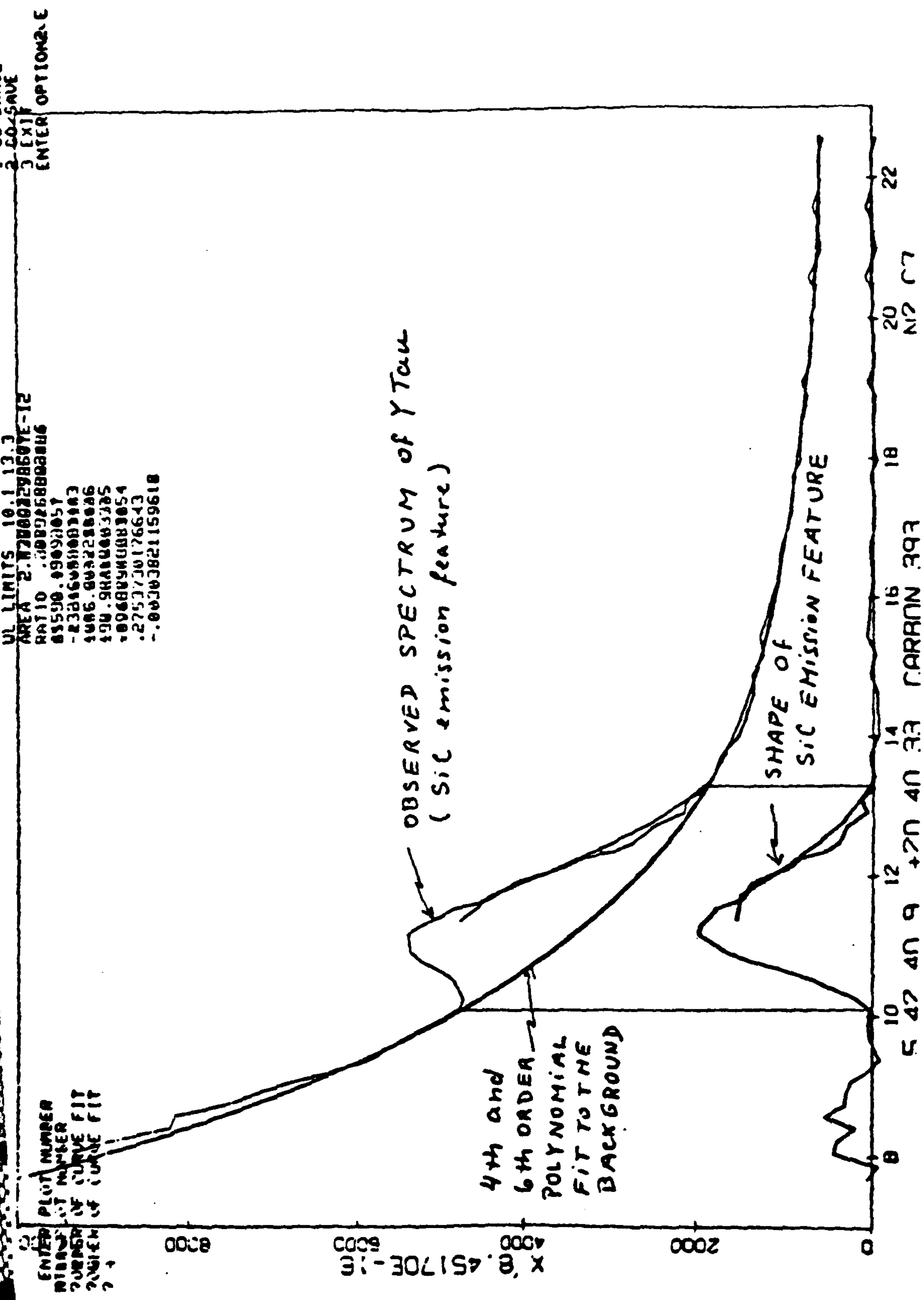
OBSERVED SPECTRUM of Y Tau
(SiC emission feature)
SHAPE of
SiC EMISSION FEATURE
4th and
6th ORDER
POLYNOMIAL
FIT TO THE
BACKGROUND
1 GO/ERASE
2 GO/SAVE
3 [X]T
ENTER OPTION

Figure 1.

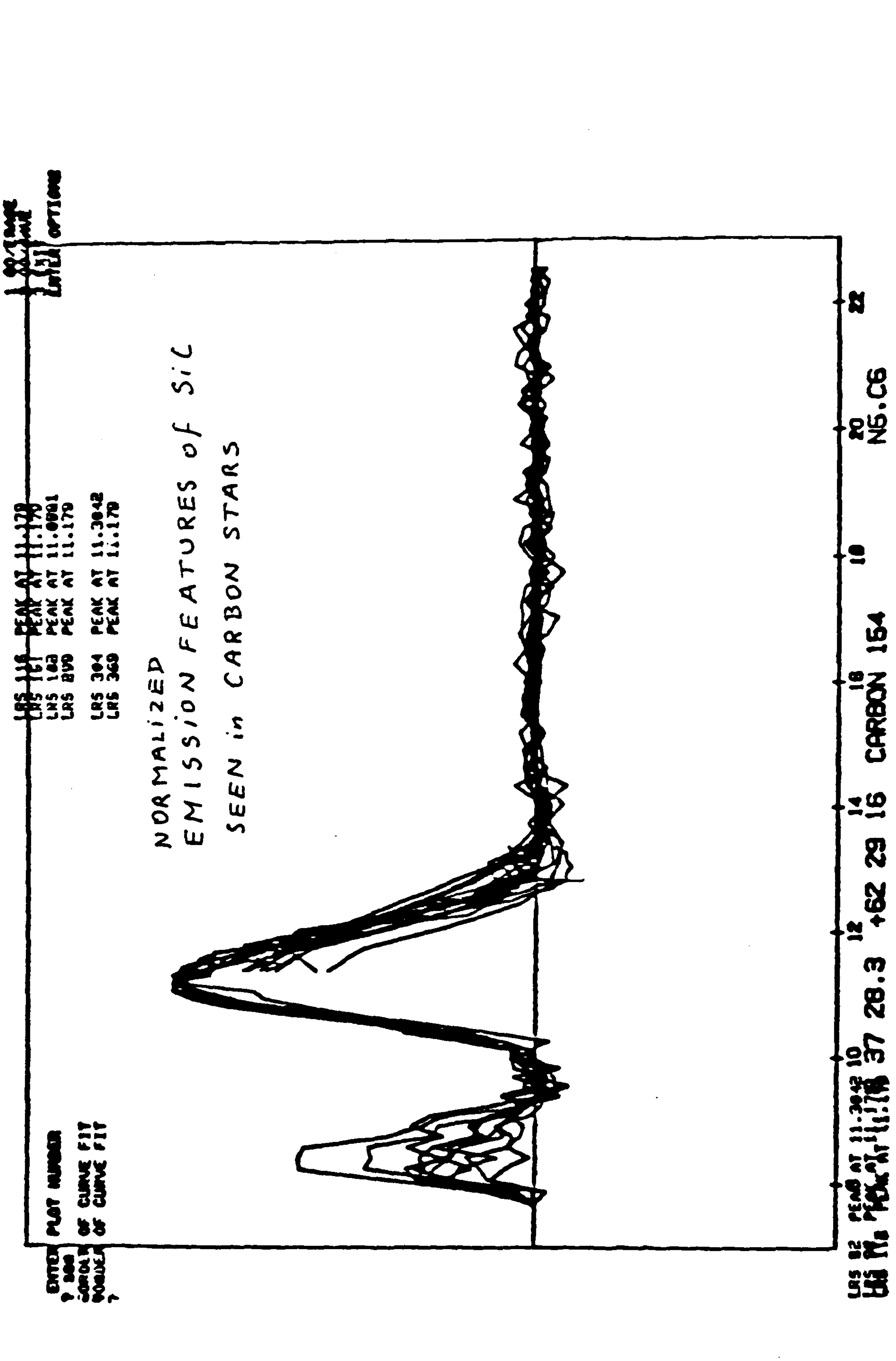
NORMALIZED
EMISSION FEATURES of SiC
SEEN in CARBON STARS
LRS 304 PEAK AT 11.3042
10
12
14
16
18
20
22
CARBON 154

Fig. 2

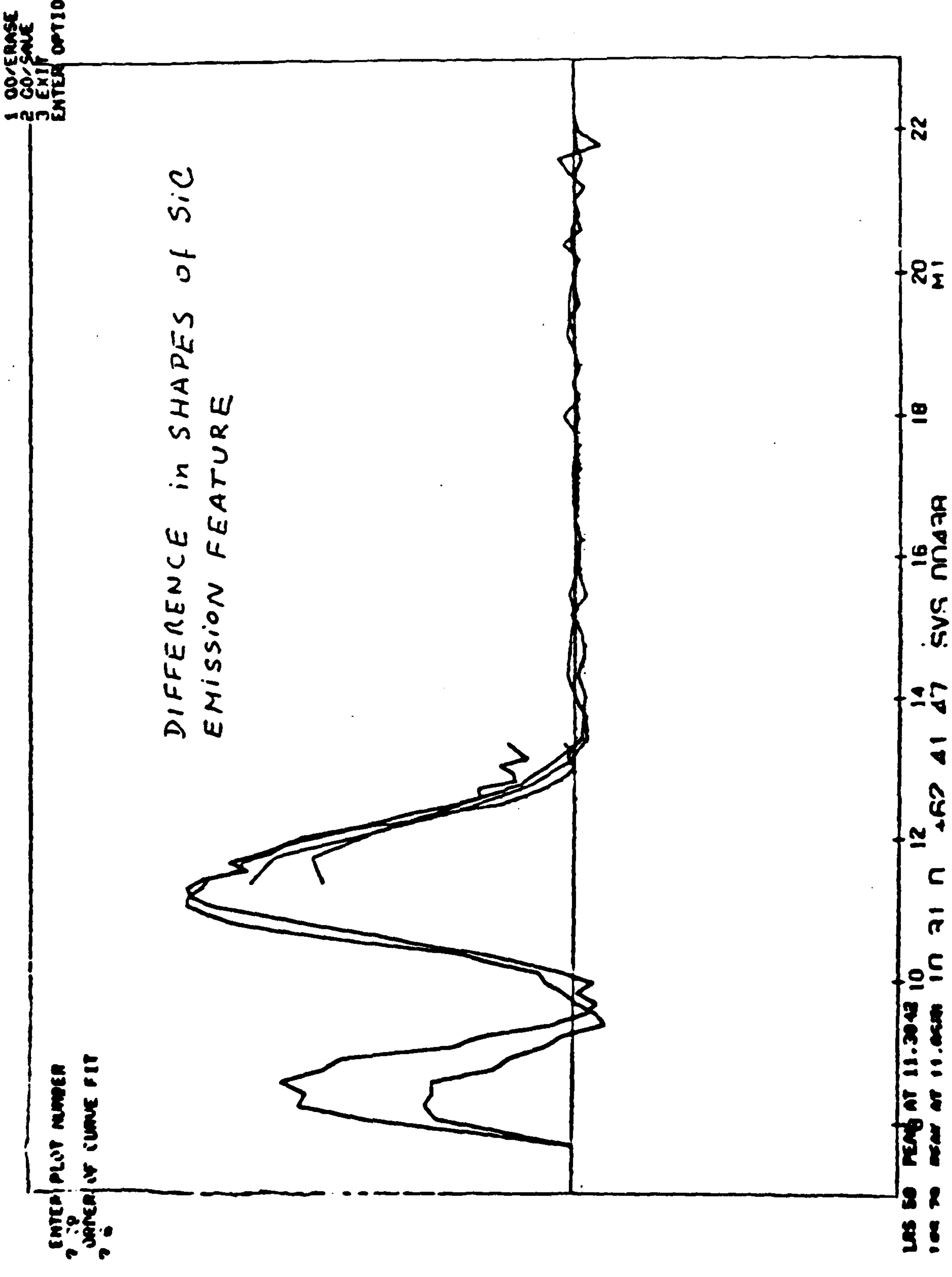
DIFFERENCE in SHAPES of SiC
EMISSION FEATURE
1 GO/ERASE
2 GO/SAVE
3 EXIT
ENTER OPTIONS
ENTER PLOT NUMBER
10
12
14
16
18
20
22

Fig. 3

peak and the shape itself vary (see Figure 4). The average maximum emission occurs at 9.7+/-0.3 micrometers A few of the stars classified as M do show the SiC feature. They may have been misclassified and warrant further study in order to determine their evolutionary status.

About 60% of the S stars show an emission feature in the 10 to 11 micrometer region. The shape of this feature varies from being very similiar to the M star silicate feature to having an emission peak around 11 micrometers (Figure 5). Figure 6 shows the emission feature for a typical M star (R Hor), a representative S star (S Cas) and a typical carbon star (R Lep). The difference in the wavelength dependence of the emission feature for the three type of objects is obvious. I calculated composite emission features based on differing percentages of the average SiO and SiC emission profile. Comparing these to various S star emission profiles shows that the observed feature can be modeled with the percentage of SiC varying from 0% to 50% (Figure 7). Since the C/O ratio in S stars is close to unity it is understable that both SiO and SiC grains may exist in the circumstellar shell. Stellar evolution calculations show that evolving stars are S stars for only a short period of time. Hence the presence of both SiO and SiC emission may indicate a difference in composition between various parts of the circumstellar shell, the outer parts being oxygen rich whereas the inner (more recently ejected)parts are carbon rich.

The excess emission ratio calculated for the carbon stars

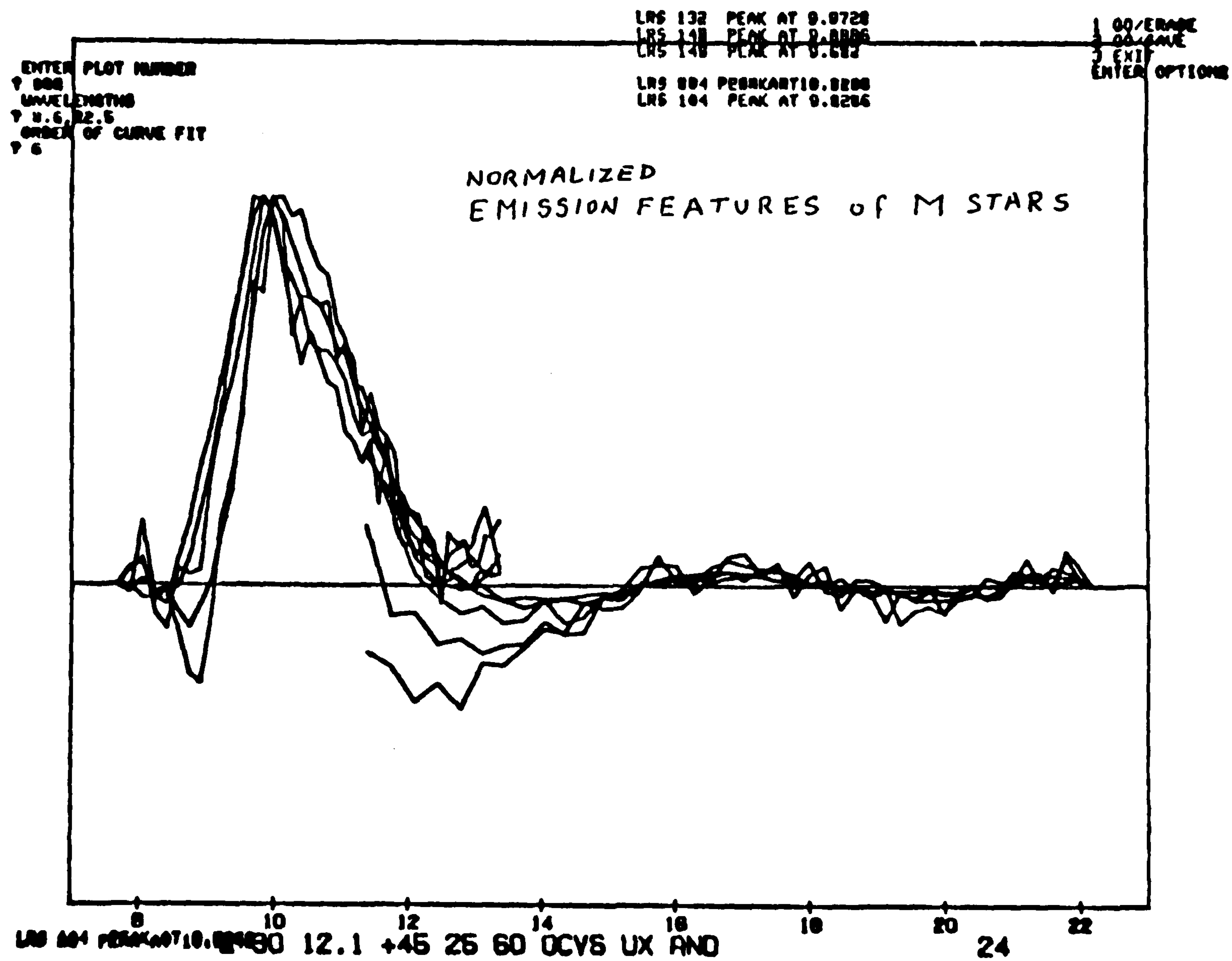
NORMALIZED
EMISSION FEATURES of M STARS
ENTER PLOT NUMBER
ORDER OF CURVE FIT
ENTER OPTIONS
8
10
12
14
16
18
20
22
12.1 +45 26 60 OCVS UX AND
24

Fig. 4

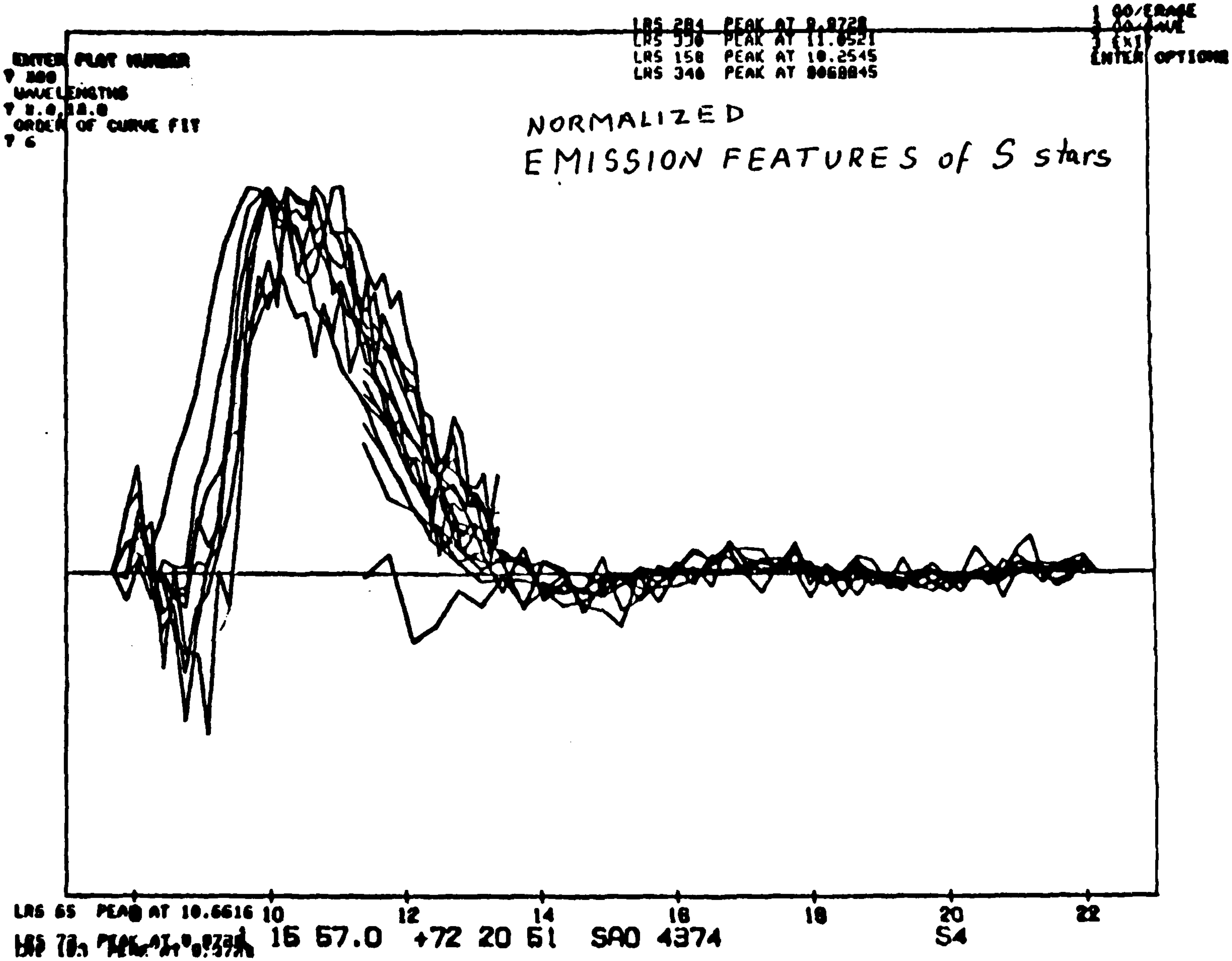
LRS 284 PEAK AT 9.9728
LRS 158 PEAK AT 10.2545
NORMALIZED
EMISSION FEATURES of S stars
ENTER PLOT NUMBER
WAVELENGTHS
ORDER OF CURVE FIT
ENTER OPTIONS
LRS 65 PEAK AT 10.6616
10
12
14
16
18
20
22
16 57.0 +72 20 51 SAO 4374
S4

Fig.5

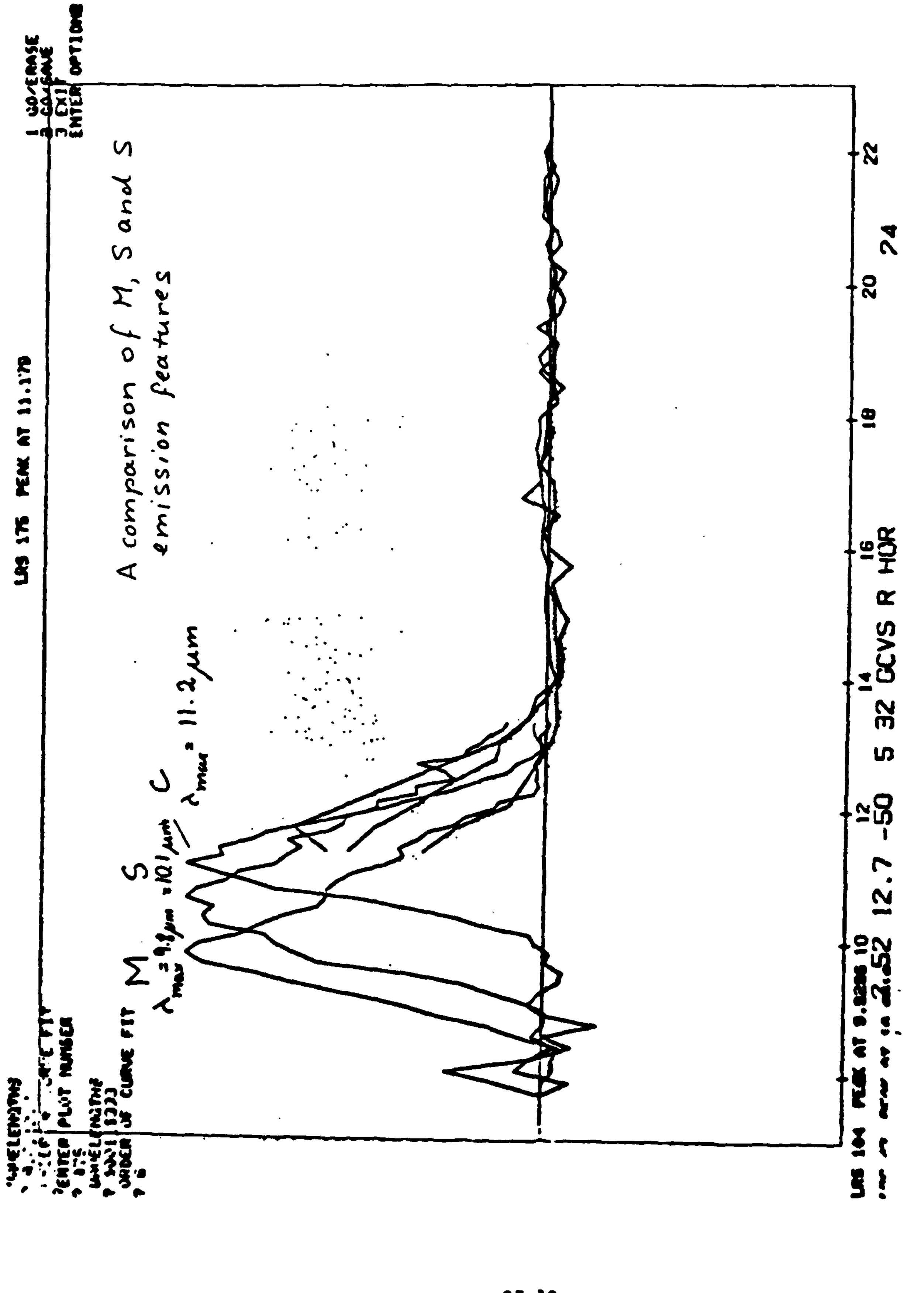
LRS 176 PEAK AT 11.179
1 WO/ERASE
2 GO/SAVE
3 EXIT
ENTER OPTIONS
A comparison of M, S and S
emission features
M
S
C
$\lambda_{max} = 9.8\mu m$
$= 10.1\mu m$
$\lambda_{max} = 11.2\mu m$
10
12
14
16
18
20
22
24
2.52 12.7 -50 5 32 GCVS R HOR
LRS 104 PEAK AT 9.8236
ENTER PLOT NUMBER
ORDER OF CURVE FIT

Fig. 6

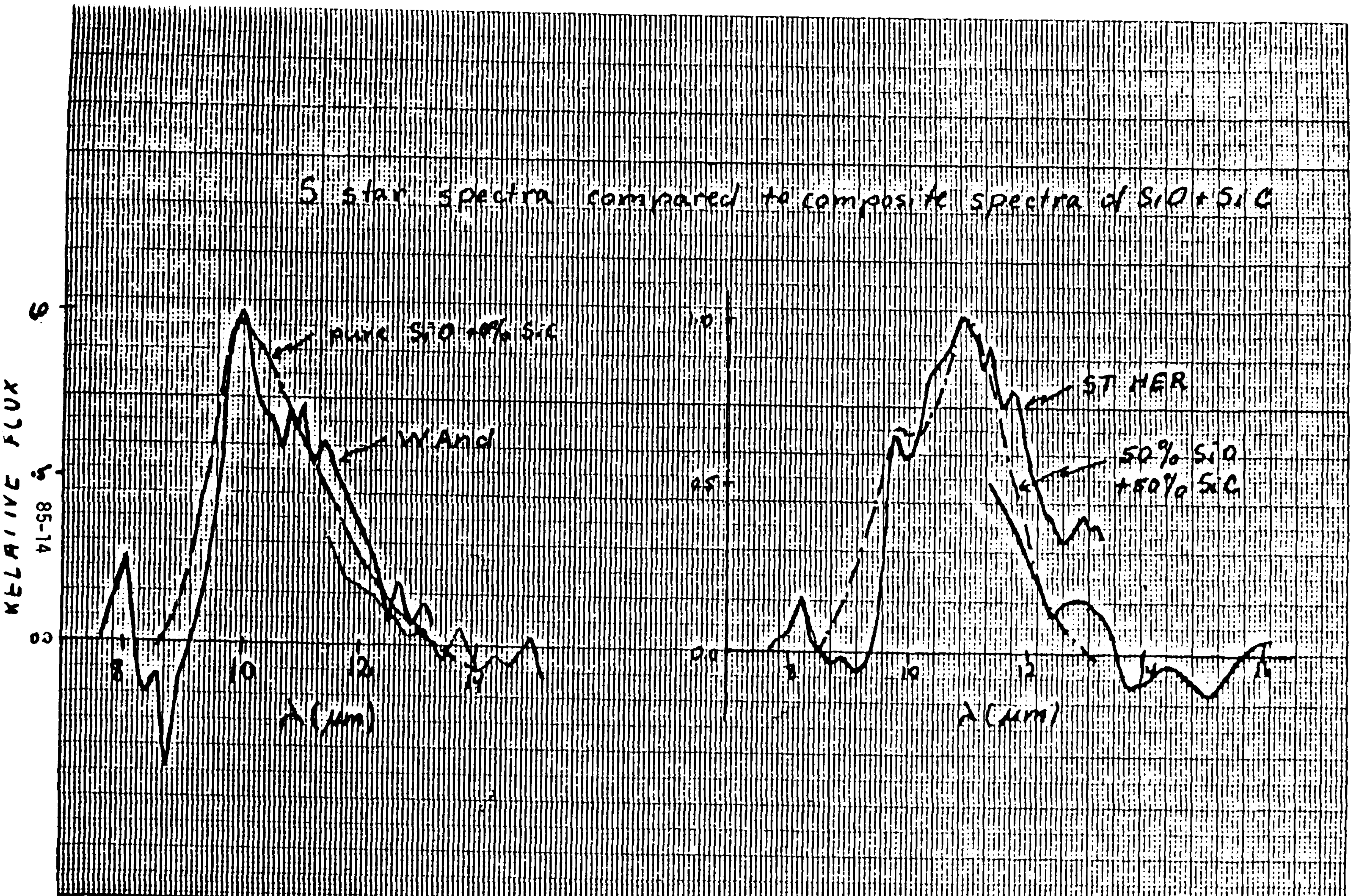
5 star spectra compared to composite spectra of SiO + SiC
RELATIVE FLUX
85-14
pure SiO +0% SiC
W And
ST HER
50% SiO
+50% SiC
λ (μm)
λ (μm)

Fig. 7

averages about 20% (it varies between 5% and 30%). Below 5% the excess emission becomes too weak to be accurately determined. For M stars the average excess emission ratio is about 30%. It is less reliably determined since the 9.7 micrometer emission correlates with an 18 micrometer emission feature (also due to silicates) making it difficult to establish the true background continuum level.

Many of the stars show only a smooth continuum in the LRS spectra. A small percentage of these stars can be fit with a black body continuum of about 2000K to 4000K (Figure 8) which is representative of the stellar photospheric temperature. The others tend to show a continuum that can not be fit with a single temperature. A 2000K continuum fits the spectrum in the 8-12 micrometer region and a 400 to 1000K continuum in the 14-22 micrometer region indicating that we are seeing emission both from the stellar photosphere and the circumstellar shell. We also fit a black body continuum to stars with emission features and calculated the excess emission above this type of continuum. The results are still preliminary but follow the trends previously established with fourth and sixth order polynomial fits. The continuum of these stars for the most part also can not be fit with a single temperature. Figure 9 shows the spectrum of the carbon star Y CVn fit with a 2000K black body continuum. The short wavelength end fits quite well but the black body spectrum falls below the observed spectrum for the long wavelength end. The 14-22 micrometer region is better fit by

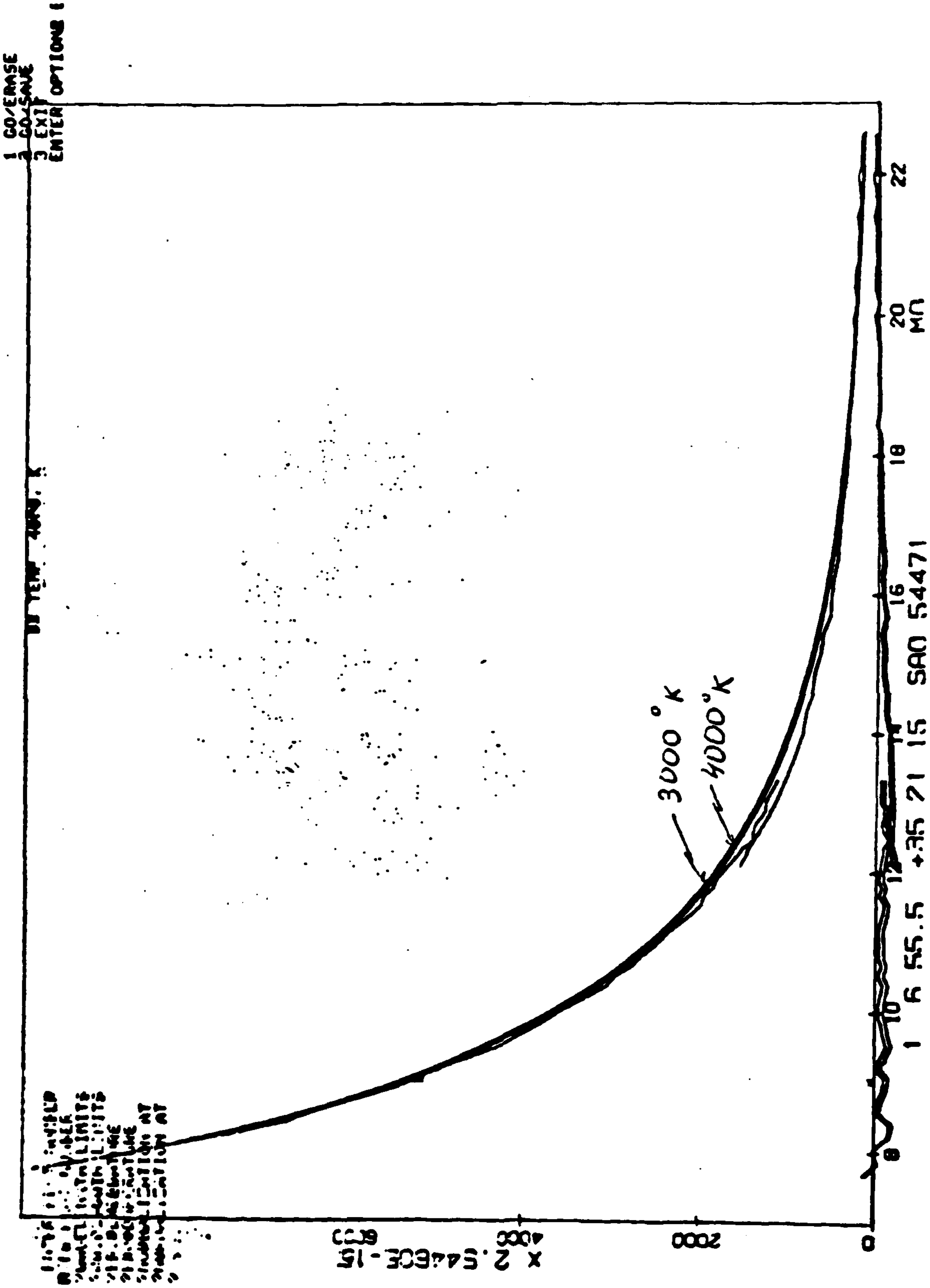
1 GO/ERASE
2 GO/SAVE
3 EXIT
ENTER OPTIONS
SAO 54471
3000 °K
4000 °K
0
2000
4000
8
10
12
14
16
18
20
22

Fig. 8

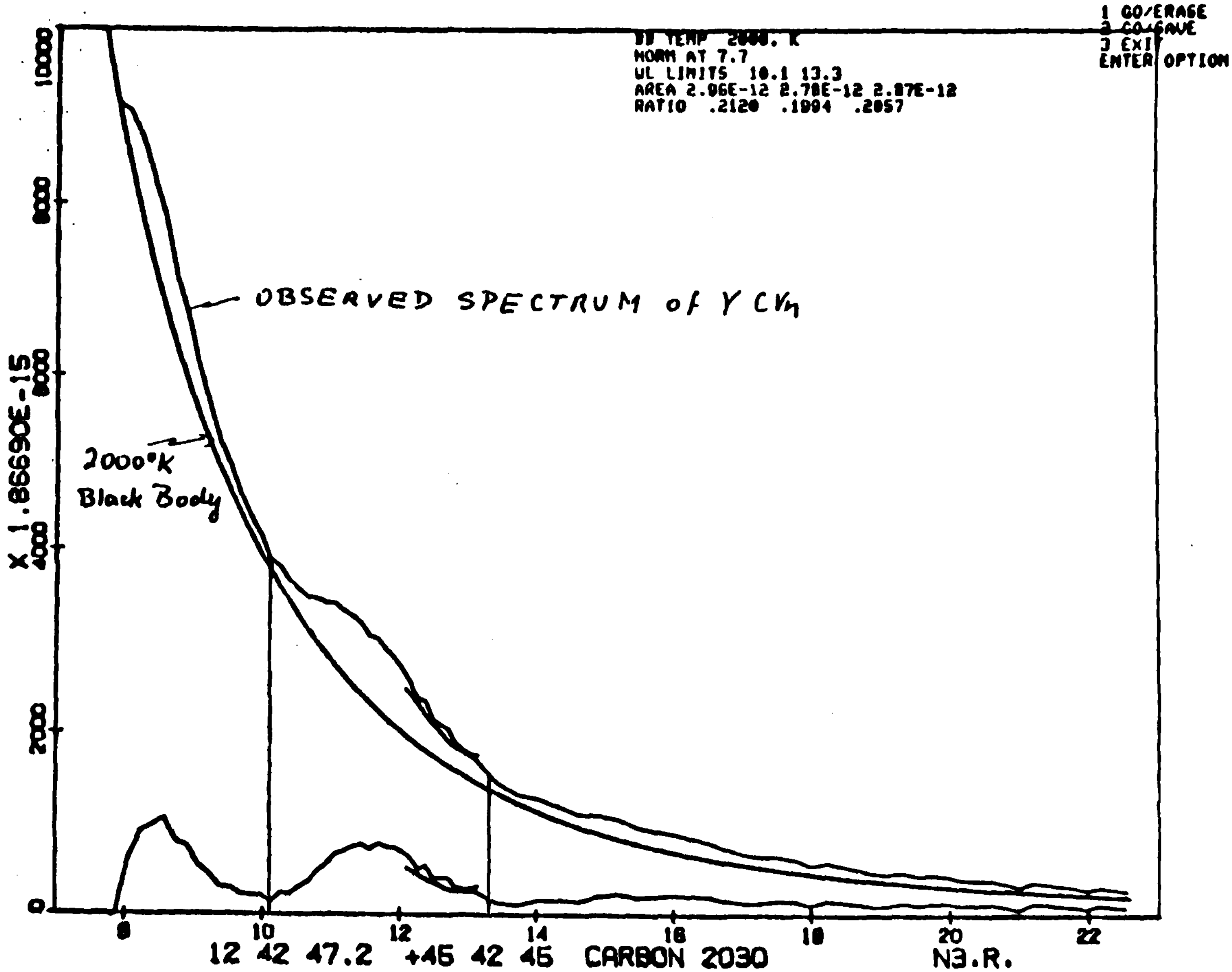

TEMP 2000. K
NORM AT 7.7
UL LIMITS 10.1 13.3
AREA 2.06E-12 2.78E-12 2.87E-12
RATIO .2120 .1994 .2057
1 GO/ERASE
2 GO/SAVE
3 EXIT
ENTER OPTION
OBSERVED SPECTRUM of Y CVn
2000°K
Black Body
X 1.86690E-15
10000
8000
6000
4000
2000
0
8
10
12
14
16
18
20
22
12 42 47.2 +45 42 45 CARBON 2030
N3.R.

Fig. 9

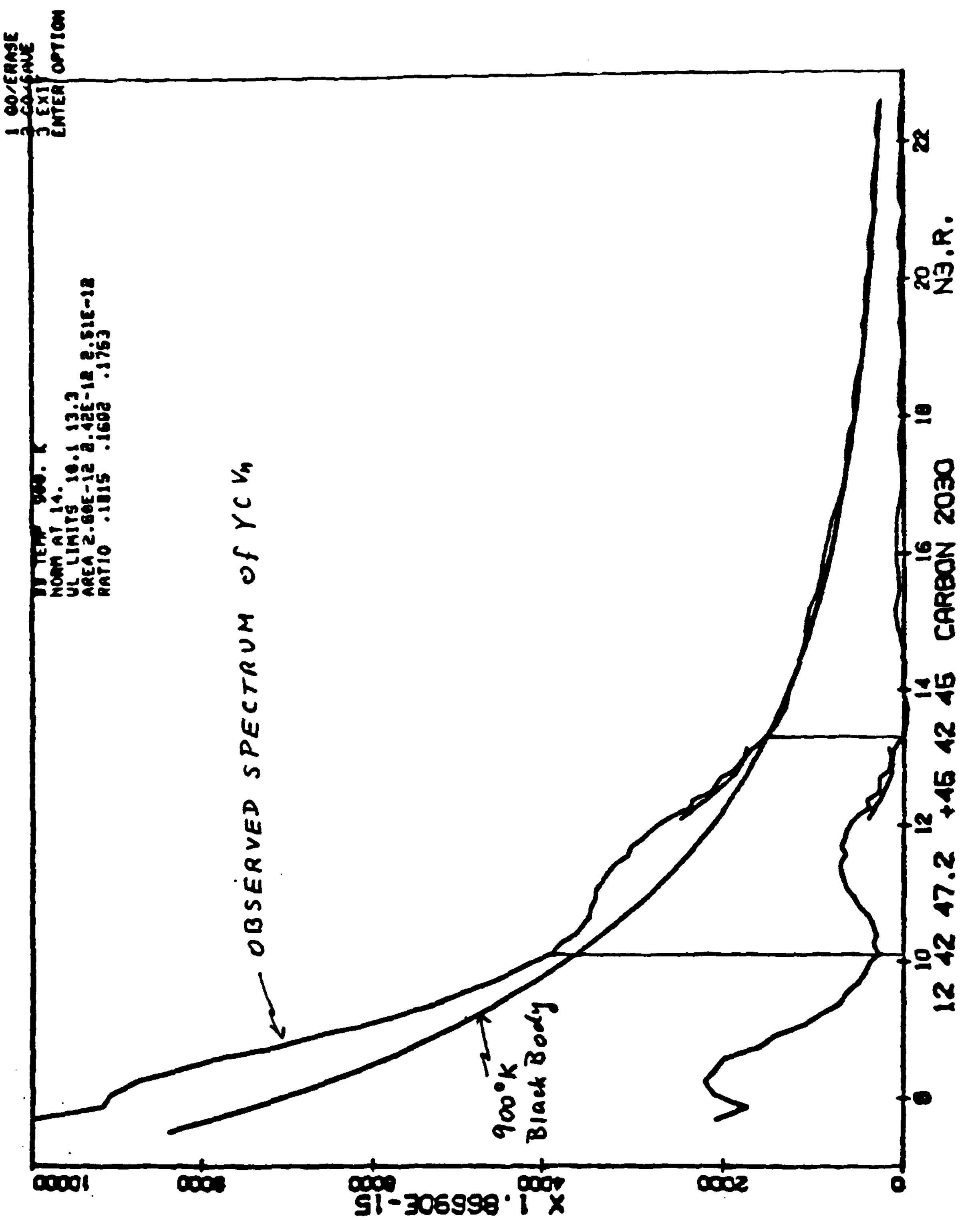

OBSERVED SPECTRUM of YC V_n
TEMP 900. K
NORM AT 14.
UL LIMITS 10.1 13.3
AREA 2.80E-12 2.42E-12 2.51E-12
RATIO .1815 .1602 .1763
1 GO/ERASE
3 EXIT
ENTER OPTION
900°K Black Body
X 1.86690E-15
0
2000
4000
6000
8000
10000
8
10
12
14
16
18
20
22
12 42 47.2 +46 42 46 CARBON 2030
N3.R.

Fig. 10

a 900K black body continumm (Figure 10). But the temperatures derived from these fits depend critically on the absolute calibration of the two detectors used in the IRAS spectrometer. These are not that well established. An error in the absolute calibration of either detector could produce the appearance of two different black body continua. In many spectra it is obvious that the overlap regions of the two detectors differ. A calibration problem in the 8.1 micrometer region may produce the spurious feature seen in the carbon star spectra.

I tried to correlate the excess emission ratio for carbon stars to other photospheric parameters. No clear-cut correlation could be found with the color temperatures and CN strength of Baumert (1972), or the C/O ratio of Gow (1977), or the B-V color index. The excess emission ratio showed almost no correlation with period except that Mira variables (which tend to have the longer periods) show slightly greater excess emission than the semi-regular variables, but the scatter is larger than the mean difference between the excess emission ratio. Some carbon stars show Merrill-Sanford bands in the 4800 A region. These bands are assumed to be produced by SiC_2. The strength of the MS bands as listed by Yamashita (1972, and Stephenson (1973) does not correlate with the excess emission of SiC except that all but one of the stars listed to have MS bands do show SiC emission.

IV. RECOMMENDATIONS

The results of my research suggest a number of follow-up topics that need to be studied:

1. Can the LRS data plus the IRAS photometry be used to obtain a (statistically meaningful) average of the excess emission ratio per star (above the photospheric continuum) for C, S, and M stars? This average would then be used to derive a better stellar luminosity function in the 10 to 100 micrometer region. The existing AFGL model of the infrared celestial background could then be improved.

2. Can the optical depths and temperatures of the circumstellar shells be determined from the shape and strength of the excess emission?

3. Can the excess emission ratio be correlated with the mass loss rates from the central star, hence could this ratio then be used to estimate the mass loss rate of other stars?

There is a large amount of important information about the infrared sky that can be gleaned from the IRAS spectra and photometry. My ten week SFR fellowship allowed me to obtain some important results and suggest directions for future research.

REFERENCES

Baumert, J. 1972 PhD thesis (Ohio State University).

DeGioia-Eastwood, K., Hackwell, J.A., Grasdalen, G.L., and Gehrz, R.D. 1981, Ap.J., 245, L75.

Gow, C. 1977, P.A.S.P., 89, 510.

Kukarkin, B.V., Kholopov, P.N., Efremov, Yu.N., Kukarkina, N.P., Kurochkin, N.E., Medvedeva, G.I., Perova, N.B., Fedorovich, V.P., Frolov, M.S. 1970, General Catalog of Variable Stars.

Stephenson, C.B. 1973, Publ. Warner and Swasey Obs. 1, #4.

Yamashita, Y., 1972, Ann. Tokyo Obs, 13, 175.

FINAL REPORT APPROVED BY: Stephan D. Price 19 July 85

Dr. Stephan D. Price Date

1985 USAF - UES SUMMER FACULTY RESEARCH PROGRAM

Sponsored by the

AIR FORCE OFFICE OF SCIENTIFIC RESEARCH

Conducted by the

UNIVERSAL ENERGY SYSTEMS, INC.

FINAL REPORT

PRELIMINARY INVESTIGATION ON RESOURCE CONTROL STRATEGIES ON DISTRIBUTED COMPUTER SYSTEMS

REAL-TIME vs NON-REAL TIME

Prepared by: DAR-Biau Liu

Academic Rank: Associate Professor

Department & University: Computer Science Department
Old Dominion University

Research Location: RADC/COTD, Griffiss AFB, New York

USAF Research: Richard Metzger and Thomas Laurence

Date: September 15, 1985

Contract No.: F49620-85-C-0013

PRELIMINARY INVESTIGATION ON RESOURCE CONTROL STRATEGIES ON DISTRIBUTED COMPUTER SYSTEMS

REAL TIME vs NON-REAL TIME

by

DAR-Biau Liu

ABSTRACT

Various existing resource control strategies for centralized or decentralized computer systems for real time/non-real time have been studied. Their advantages and disadvantages have been summarized.

The resource management strategies in Arch OS, a decentralized distributed operating system developed at the Carnegie-Mellon University, has been received a great deal of attention in this study. We identify some "new problems" which have to be solved in the design of the decision- making algorithms to determine what "value" the completeness and accuracy of information utilized in what level will contribute the "best quality" of a decision result and their tradeoffs.

ACKNOWLEDGEMENTS

I would like to thank the Air Force Systems Command, Air Force Office of Scientific Research and RADC/COTD, Griffiss AFB for sponsorship of this Summer Faculty Fellowship. Special thanks also goes to Mr. Thomas Laurence and Mr. Richard Metzger of RADC/COTD for their warm accompanyment during my stay at RADC/COTD, and for their great assistance to make this report possible.

I. INTRODUCTION

Distributed systems provide the potential for decentralized control which is usually advocated for increased reliability. Certain distributed processing operating systems use decentralized control to achieve reliability. In this regard, various forms of decentralized control of resources are worthy to discuss: decentralized control that is needed for distributed databases, decentralized control that is needed for stochastic replicated functions such as routing and scheduling, and decentralized control via decomposition see (1).

Only preliminary work has been done in the area of decentralized control for stochastic replicated functions. Possible approaches might include the use of random graphs, decision theory, and stochastic learning automata. The complicated issues for stochastic replicated functions include the need for very low overhead solutions, the operation in the presence of noisy and delayed information, the high degree of interaction between cooperating controllers and the fact that the decisions of each controller affect the others.

In all, the decision-making in the distributed computing system is a complicated issue and the technique to resolve them is still in it's infant stage. More sophisticated techniques and algorithms should be brought into this area. Task assignment problems and job scheduling problems

all need higher power mathematical tools -- like linear programming and dynamic programming techniques, decision theory, estimate theory, etc. to resolve them.

I have the broad training in mathematics and the wide knowledge in the Distributed computing system. Certainly, I am suitable to be assigned to conduct this investigation.

II. OBJECTS OF THE RESEARCH EFFORT

To study the existing resource control strategies for centralized or decentralized distributed computer systems for real time or non-real time. Compare and analyze the various control strategies and summarize their advantages and disadvantages.

At the more centralized computer system, each decision is made by a collection of "entities" which work as a team to improve the overall system's goals. At the other end, in the more decentralized computer system, each member of the decision maker developes their own "strategies" with associated probabilities. To make a decision, members exchange these, reason about and modify them, making compromises as necessary, and in this way, enhance the marginal viewpoints to a more global view. This activity must somehow converge to a single consensus decision, either by a stochastic method used by DeGroot (22) in the "Reaching a Consensus" or by heuristics such as inference rules and algorithms employed by some areas of artificial intelligence such as

problem solving and expert systems.

Drs. E. D. Jensen, Lui Sha and their team at the Carnegie-Mellon University had studied a great deal about the decentralized distributed operating system--ArchOS, and the resource management control in ArchOS. In this study, we follow the same line and identify some "new problems" which have to be solved in the design of the decision making algorithms to determine what "value" the completeness and accuracy of information utilized in what level will contribute the "best quality" of a decision result and their trade-offs.

III. BACKGROUNDS AND SUMMARIES

This section will serve as the main part of the report. Some basic concepts and terminologies are introduced. Quite a few resource control strategies for centralized/decentralized distributed computer systems were reviewed and their advantages and disadvantages were summarized accordingly. The reader might find this as a survey as well as discover some "new problems" in this area of research.

A network which has logically only one native operating system for all the distributed components (physically as well as logically), is called a distributed operating system (DOS). A distributed processing operating system (DPOS) is a DOS that specifically attempts to improve reliability by

using decentralized control where possible to avoid central points of failure, see (1). The advantages and disadvantages of such systems can be seen in (2), (3), and (4). There are quite a few DOS's designed (or being designed) and implemented in a variety of ways, see Table 1 in (1). In this report, we will concentrate on ArchOS (5), and it's related algorithms, policies/mechanisms.

A node in a distributed computer system is a collection of resources and processes, and it is typically an autonomous entity. Processes outside a node access the processes and resources within a node via message-passing or remote procedure call, whereas intra-node communication is normally through shared memory (1).

"Task assignment" and "job scheduling" are two important researches on scheduling for distributed systems. A good survey on this area of research can be found in (1). Most of the research on task assignment can be loosely classified as either graph theoretic, based on mathematical programming, or heuristic. Task assignment is meant that a task is considered to be composed of multiple modules and the goal is to find an optimal policy for assigning the modules of an individual task to processors. Typical assumptions found in task assignment work are: processing costs that are known for each module of the task, the interprocess communication (IPC) costs between every pair of modules is known, IPC cost is considered negligible for

modules on the processor, and reassignment does not occur. Task assignment research where reassignment does allow can be seen in the Domain Structure Operating System by Casey and Shelness (8). Task assignment research for extremely large distributed system was found in MICROS by Wittie and van Talborg (9) -- this is a form of probabilistic scheduling. A graph matching approach to optimal task assignment in Distributed Computer Systems using a Minmax criterion can be seen in Shen and Tsai (21).

Job scheduling can be thought of as assignment of entire jobs which are not decomposed into modules to processors. Whereas modules in task assignment could interact with one another, jobs are independent of each other. Approaches to job scheduling have included bidding (Stankovic and Sidhu (10), Ramamritham and Stankovic (11), queueing theoretics approaches (Chow and Kohler (12), Kleinrock and Nilsson (13), Agrawala, et al (14), the use of estimation theory (Bryant and Finkel (15)) and statistical decision theory (Stankowic (16), (17)).

Bidding schemes attempt to match specific jobs to processors based on the current ability of the processors to perform this work. These schemes are suboptimal, but are more extensible and adaptable than many of the other approaches. However, the cost of making and acquiring bids may become excessive, and the factors to use in making the bids have not been extensively studied (1). The basic bid-

ding approach has been modified in various ways by Stankovic & Sidhu (10) and by Ramamritham and Stankovic (11). In the latter, bidding is used to schedule jobs with real-time constraints, such as deadlines, on a loosely-coupled network. The bidding algorithm is specifically tailored to deal with deadlines, submit delays, scheduling overheads, and delays in the processors. The bidding algorithm is used in conjunction with a locally executed guarantee algorithm which either guarantees arriving tasks that they will neet their deadlines or invokes the bidding algorithms to find a suitable location for execution of the arriving task, if possible. In (18), Zhao and Ramamritham applied the algorithm in (11), using a heuristic approach for solving the problem of scheduling tasks with deadlines and general resource requirements in a dynamic real-time system. The heuristic function is used to select the task to be scheduled next. It is weighted three factors, each factor explicitly considers information about real-time constraints of tasks and utilization of resources.

ArchOS is a physically dispersed operating system, not a network operating system. It is a research vehicle to perform research in the issues of decentralization in the real-time distributed system at the OS level and below. Topics such as Decentralized Resource Management Principles, Robustness and Modularity in Decentralized OS, Atomic transactions at the OS kernel level, Best Effort Decision Making, Time-driven Resource Management, Probabilistic

Algorithms, and Architectural support for Decentralized OS, are receiving a great deal of attention in ArchOS.

Computer systems must make decisions in order to manage resources. In real-time systems, resources must be managed in order to meet time constraints. Resource management decisions must be made on the basis of information regarding the state of computation, the user requirements, and the goals to be achieved. This information may be inaccurate/incomplete or decision algorithms using this information may be intractable. Therefore, the traditional Garbage-In-Garbage-Out concept can not be accepted in such computer decision making. Quite a few computer scientists are pursuing the alternatives of making best effort decisions. The overall objective is to take decentralized local actions which will further the global system objectives based on local information and inaccurate/incomplete global system information. We will focus on the time-driven resource scheduling problem and the Best-effort decision making -- the Load Balance problem in ArchOS.

A. The Load Balance Problem:

Given a set of identical computers (nodes) connected by a bus, assume that workloads are randomly generated at each node and information of workloads at each local node are complete and accurate, but information of all other workloads at other nodes are incomplete/inaccurate (relative to

each node itself). The system goal is to maximize throughputs by balancing the loads. What decision should a local node make when a job is created? Should it be processed at the local node or be sent elsewhere to be processed?

The unattainable idealized situation is when all dynamic workloads are known exactly and instantaneously at each local node. This creates an upper bound on attainable performance. The unrealistic worst situation is when there is no information whatsoever either in local or global. The only control available is for each processor to assign workloads uniformly to all processors. This creates a lower bound for attainable performance. The range between the upper and lower bound is taken as 0 to 100% of performance.

In the worst case for best effort, decentralized load balancing problem, John P. Lehczky and Lui Sha had adopted an adaptive control limit policy (23), if the current workload at a processor is above the "threshold", then the newly created workload is assigned to one of the other processors with equal probability (this is not a good practice, we will discuss this in a later section), and the assignment is permanent (i.e., once assigned, a job will not be transferred to other nodes, again this is not good and will be discussed later).

A properly chosen threshold will yield a probability greater than 1/2 that the job will be assigned to a node

with a queue that is shorter than that of the local node. Typically, the threshold should be taken as the median of queue length distribution.

Their studies show that for realistic system workloads (up to 70%), this control limit policy is at least 62% efficient (compare with the unattainable upper bound). This worst case analysis shows the promise of Best Effort distributed decision making approach for system resource management. The 62% efficiency result is the lower bound for Best Effort decentralized resource management in the context of load balancing. Note that system performance will improve if processors are not identical. For example, if each processor is unique for some type of job, then a local decision which assigns a given type of job to the special processor is also the optimal global decision.

B. Time-Driven Scheduling Problem:

Research into scheduling has continued for many years but all the interesting scheduling problems have been proved to be computationally intractable (NP-complete or NP-hard). Since ArchOS is to be a real-time system in which processes can have explicit time values so time-driven scheduling problem is considered a very important issue in ArchOS. Some optimal deadline driven scheduling has been shown to be computationally efficient only for the simplest computational models which do not hold in actual practice. Very

little research has been performed to define correct and robust scheduling mechanisms in situations in wihch an overlaod condition has occurred -- in which insufficient resources are available to meet time constraints. It is one of the plans in the ArchOS project to construct algorithms to perform efficient best effort scheduling decisions under a realistic time driven scheduling (TDS) model. This model describes the time driven scheduling processing to be done within a single node. In a physically decentralized system, this work must be extended to answer several questions: 1. How can overload conditions be detected (and predicted, if possible? 2. How can the system best determine which processes should be moved to other nodes to avoid missing further deadlines? 3. To which nodes should processes be moved if migration is necessary? An experimental TDS model was constructed in ArchOS as follows: Consider a set of processes P_i to be scheduled. Assume each has a request time R_i, an estimated computation time C_i, and a value function V_i (t). Here V_i (t) represents the relative value of completing task P_i at time t. C_i is assumed to be stochastic and does not include system overhead or premptions. C_i can be estimated from system measurement or predicted by an application programmer, or some combination. Using this model, optimal scheduling consists of computing a process order $(m_1, m_2, \ldots, m_n)$ where P_{m_j} is the j-th process to be scheduled. We do this for each possible sequence by maximizing the sum of all the process value functions evaluated

at their expected completion times according to the process sequences, i.e., to rearrange the process order $(m_1, m_2, \ldots, m_n)$ such that $\sum_{j=1}^{n} V_{m_j}(t)$ to be maximum subject to the constraint $\emptyset \leq t \leq \sum_{j=1}^{n} C_{m_j}$. Note that this model encompasses both periodic and non-periodic processes. Some overload policies are adopted in this TDS model.

Ramamritham and Stankovic in (11) developed: (1) a locally executed guarantee algorithm for periodic and non-periodic tasks, which determines whether or not a task can be guaranteeed to meet it's real-time requirements; (2) a network-wide bidding algorithm suited to real-time constraints; (3) criteria for preempting an executing tasks so that it still meets "its deadline"; and, (4) schemes for including different types of overheads, such as scheduling and communicating. A task is characterized by it's start time, computation time, deadline and possibly, it's period. In addition, a task may have resource requirements, and precedence constraints. Each node in the distributed system has a local scheduler, a bidder and a dispatcher. A set of guaranteed periodic tasks exists at each node. Non-periodic tasks may arrive at any node in the network. When a non-periodic task arrives, an attempt will be made to schedule the task at that node. If it is impossible, the local scheduler will contact schedulers at other nodes by using bidding schemes to determine which node the task can be sent to be scheduled. Upon arrival at the destination node, another attempt is made to schedule the task. Eventually

the task is either guaranteed and executed or it is not guaranteed.

Due to the limit in pages of this report, we could not list all the resource control strategies in a distributed computer system. As a final note, it is worth to mention the Achievable Decentralized Control for D^3AST (Dynamic, Democratic, Decentralized, Adaptive, Stochastic and Time-sensitive) function of a distributed processing operating system developed by Stankovic in (24). It is the first paper that the optimal decentralized control of a system-wide function--D^3AST function, was introduced based on the concepts of controllability, stability and observability and it is in this paper that a lot of optimization problems of control strategies were developed.

VI. RECOMMENDATIONS

ArchOS has a sound theoretical base, as developed by Lui Sha, Lehoczky, P. and Jenson, E.D. in (19) and (20). They used the classical set theoretical techniques to approach the concurrency control, consistency and correctness problem. The database was decomposed into the "consistency preserving" atomic data sets which are not necessarily disjoint, and the notion of compound transactions was introduced. A compound transaction is defined as a partially ordered set of elementary transactions. Each elementary transaction is then independently partitioned into a

partially ordered set of "correct preserving" atomic step segments according to certain modular generalized setwise and serializable scheduling rule. The optimality of concurrency control was proved based on the completeness of the fuzzy set of all modular generalized setwise and serializable scheduling rules. Some failure recovery rules were also introduced based on the notion of atomic commit segments. The resource management control seems to be the weaker spot in the entire ArchOS project. Although some basic techniques were developed, they seem to be not quite good in practice as we mentioned in Section III. For example, in the Load Balance problem, the assumption of equal probability (for assigning a newly created workload to other processors if the current processor is above the "threshold") is too strong, and the assumption that the assignment is permanent even worsens in the sense that the workloads of the new processor which were assigned to receive the newly created workload might itself be over the "threshold". The bidding schemes and guarantee algorithms developed by Ramamritham and Stankovic in (11) seem to be suitable in this problem here. But then, the resources requirement in each node and the overall system-wide optimal control problem still need to be taken care of. The technique deeloped by Zhao and Ramamritham in (18) and the notion of the system-wide optimal control introduced by Stankovic in (24) seems to be good candidates for the research in this direction. One of ArchOS Design goals is the high system modularity --

using the principles of abstract data types and information hiding. Arobject is one of the principal components of an ArchOS computational model; it's structure -- specification and body is exactly the same as the structure of a generic package in Ada language. It seems to be a good idea to develop some software packages in Ada for the algorithms and routines in ArchOS.

To conclude this report, I would like to mention the architecture for control and communicating in Distributed Artificial Intelligence Systems developed by Yang, Hughes and Stephens in (25). A major component in the node architecture is a database of metaknowledge about the expretise of a node's own expert systems and those of the other processing nodes. In order for all related nodes to make optimum use of the information obtained from these problem solving mechanisms, the system dynamically reconfigures itself, thereby improving it's performance during operation. This approach offers the possibilities of increased real-time response, improve reliability and flexibility and lower the processing costs. The resource control strategies on Distributed Artificial Intelligence Systems appears to be a good research direction to go in.

REFERENCES

1. Stankovic, John A.; Ramamritham, K.; Kohler, W.H., "A Review of Current Research and Critical Issues in Distributed System Software", Distributed Processing Technical Committee Newsletter, Vol. 7, No. 1, March 1, 1985.

2. Enslow, P., "What is a Distributed Data Processing System", IEEE Computer, Vol. 11, No. 1, Jan., 1978.

3. Jensen, E.D., "The Honeywell Experimental Distributed Processor--An Overview of It's Objective, Philosophy and Architectural Facilities", IEEE Computer, Vol. 11 No. 1, Jan., 1978.

4. Stankovic, J.A., and A. van Dam, "Research Directions in (Cooperative) Distributed Processing", Research Directions in Software Technology, MIT Press, Cambridge, MA, 1979.

5. Jensen, E.D., and Pieszkocm, N., "ArchOS: A Physically Dispersed Distributed System", Distributed Processing Technical Committee Newsletter, Vol. 6, No. SI-2.

6. Nelson, B.J., "Remote Procedure Call", Xerox Corporation Technical Report CSL-81-9, May, 1981.

7. Hoare, C.A.R., "CSP: Communication Sequential Processes", Communications of the ACM, Vol. 21, No. 8, Aug., 1978.

8. Casey, L. and Shelness, N., "A Domain Structure for Distributed Computer System", Proceedings of the 6th ACM Symposium on Operating Systems Principles, Nov., 1977.

9. Wittie, L., and Andre M. Van Tilborg, "MICROS, A Distributed Operating System for Micronet, A Reconfigurable Network Computer", IEEE Transactions on Computers, Vol. C-29, No. 12, 1980.

10. Stankovic, J.A., and Sidhu, I.S., "An Adaptive Bidding Algorithm for Processes, Clusters and Distributed Groups", Proceeding 4th International Conference on Distributed Computing, May, 1984.

11. Ramamritham, K., and Stankovic, J.A., "Dynamic Task Scheduling in Distributed Hard Real-Time Systems", IEEE Software, July, 1984.

12. Chow, Y.C., and Kohler, W., "Models for Dynamic Load Balancing in a Heterogeneous Multiple Processor System", IEEE Transactions on Computers, Vol. C-28, No. 5, May, 1979.

13. Kleinrock, L., and Nilsson, A., "On Optimal Scheduling Algorithms For Time-Shared Systems", JACM, Vol. 28, No. 3, July, 1981.

14. Agrawala, et al, "Adaptive Routing Using a Virtual Waiting Time Technique", IEEE Transactions on Software Engineering, Vol. SE-8,

No. 1, Jan., 1982.

15. Bryant, R.M., and Finkel, R.A., "A Stable Distributed Scheduling Algorithm", Proc. of the 2nd International Conference in Distributed Computing Systems, April, 1981.

16. Stankovic, J.A., "A Heuristic for Cooperatoin Among Decentralized Controllers", Proceeding of INFOCOM, April, 1983.

17. Stankovic, J.A., "Bayesian Decision Theory and it's Application to Decentralized Control of Job Scheduling", IEEE Transactions on Computers, Feb., 1985.

18. Zhao, Wei, Ramamritham, K., and Stankovic, J.A., "Scheduling Tasks with Resource Requirements in Hard Real-Time Systems", Technical Report, University of Massachusetts, May, 1984.

19. Lui Sha, Lehoczky, P. and Jensen, E.D., "Modular Concurrency Control and Failure Recovery -- Consistency, Correctness and Optimality, Part I, Concurrency Control", to appear.

20. Lui Sha, Lehoczky, P. and Jensen, E.D., "Modular Concurrency Control and Failure Recovery -- Consistency, Correctness and Optimality, Part II, Failure Recovery", to appear.

21. Shen, C.C. and Tsai, W.H., "A Graph Matching Approach to Optimal Task Assignment in Distributed Computing Systems Using a Minmax Criterion", IEEE Transactions on Computers, Vol C-34, No. 3, March, 1985.

22. DeGhoot, M.H., "Reaching a Consensus", J.A.S.A., Vol. 69, March, 1974.

23. Lehoczky, J.P., and Liu Sha, "Best Effort Distributed Decision Making for Decentralized Resource Management", Carnegie-Mellon Univeristy Report, Feb., 1985.

24. Stankovic, J.A., "Achievable Decentralized Control for Functions of a Distributed Processing Operating System", IEEE Transactions on Computers, 1982.

25. Yang, Ju-Yuan, Hughes, M.N., and Stephens, L.M., "An Architecture for Control and Communications in Distributed Artificial Intelligence Systems", IEEE Transactions on Systems, Man, and Cybernetics, May/June, 1985.

1985 USAF-UES SUMMER FACULTY RESEARCH PROGRAM/GRADUATE

STUDENT SUMMER SUPPORT PROGRAM

Sponsored by the

AIR FORCE OFFICE OF SCIENTIFIC RESEARCH

Conducted by the

UNIVERSAL ENERGY SYSTEMS, INC.

FINAL REPORT

MODELLING/ANALYSIS OF SPACE BASED KINETIC ENERGY WEAPON PROJECTILE FLYOUTS

Prepared by: Carl G. Looney

Academic Rank: Associate Professor

Department: Electrical Engineering/Computer Science

University: University of Nevada, Reno

Research Location: Avionics Laboratory (AA)

Mission Avionics Division (AAR)

Applications Branch (AART)

System Concept Group (AART-2)

Wright-Patterson AFB, OH

USAF Research: Lt. Dale Cunningham, Capt. Keith Jenkins

Date: 30Aug85

Contract No: F49620-85-C-0013

MODELLING/ANALYSIS OF SPACE BASED KINETIC ENERGY WEAPON PROJECTILE FLYOUTS

by

Carl G. Looney

ABSTRACT

The most critical capability of Kinetic Energy Weapons is that of hitting a target at large distances in space. Any analysis of the requirements to yield that ability depends upon a model of the projectile flyout that includes the sensor resolution/errors, the tracking errors for both target and projectile, algorithms for computing controls to cause an intercept, and a submodel for moving the target and projectile realistically. In this work we examine the needs and develop algorithms and a computer program for a model that will be usable in trade-off studies. Such trade-off analyses are to be used to define the required state-of-the-arts levels in sensing, tracking, guiding in space based defensive systems, and to compare systems proposed by contractors. The program code needs testing, validation and tuning to be ready for use in trade-off and performance analyses.

I. **INTRODUCTION.** The investigator in this report is Carl G. Looney, Associate Professor of Electrical Engineering/Computer Science, University of Nevada Reno, Reno, NV 89557. He has worked for Hughes Aircraft, Logicon, and Veda, and has background in modelling/simulation, estimation, tracking, software engineering, and artificial intelligence. The graduate student (assistant investigator) is Richard A. Stewart, a graduate student in computer science at the University of Nevada Reno.

Lt. Dale Cunningham and Capt. Keith Jenkins in the System Concept Group are responsible for analysis of space based kinetic energy weapons (KEWs), and are the focal points for the investigators' summer research effort. Lt. Cunningham assisted the investigator in choosing a problem that involves KEWs.

The needs in this area are to be able to:

i) detect and track intercontinental ballistics missiles (ICBMs) and sea launched ballistics missiles (SLBMs)

ii) identify the missile types and estimate their trajectories and burnout times

iii) compute an intercept point for a KEW-fired projectile with the targeted missile, and check that the intercept will occur before burnout time

iv) aim the KEW so the (conic) path of the projectile will hit the target at the intercept point

v) guide the fired projectile to the target by controlling its thruster accelerations

vi) manage a global battle for a constellation of space based platforms versus hostile missile fields

vii) optimize a constellation configuration with respect to coverage of known missile fields

viii) optimally control/schedule the firing from given space based platforms in m platforms on n balistic missiles scenarios

A sensor feeds data into an onboard processor that performs detection and tracking on the sensory data. The processor uses database information to identify the missile type by its plume characteristics (IR signal response over several frequency bands and other information) and estimate its trajectory by missile type. The intercept point is computed from the estimated trajectory of the missile, the velocity of the projectile, and the time-to-go until intercept. The intercept point contains errors, so the projectile and target must be tracked and controls communicated at optimal times to correct the projectile.

The projectile may be command guided by the platform system either part or all of the way to the target. The terminal (homing, or endgame) phase of projectile guidance requires the projectile to have a passive or semi-active sensor system onboard as well as a guidance controller.

KEWs are of two general types. Hypervelocity guns (HVGs) use an electromagnetic rail gun to impart an acceleration of up to 200,000 gravities to a projectile for a few milliseconds to induce a departure velocity to the projectile of up to 15 km/sec (earth escape velocity is approximately 11 km/sec). The other type of KEW uses a cold gas launcher to eject a chemically powered rocket into space where its engines ignite.

Once the projectile departs at hypervelocity, it must be controlled by a closed loop stochastic control system so that it will hit the target. The target is to be destroyed by the instantaneous imparting to it of high kinetic energy, and thus a direct hit is required. Only a few projectiles can be allocated to each missile due to limited resources. The missile must be killed in the boost stage before it can deploy its

multiple reentry vehicles with nuclear warheads, or else the vehicles become responsibility of the next layer of defense with higher risk involved.

II. OBJECTIVES OF THIS RESEARCH EFFORT. The major goal of this summer fellowship effort was to be the development of a simulation model and algorithms, coded in FORTRAN 77 (VAX 11/780) for the analysis of a single projectile flyout against a single target. A second (perhaps a follow-on) objective is the trade-off analysis that requires extensive exercising of the simulation model. We consider the HVG case.

Some of the issues to be addressed by trade-off analyses are:

i) how do the errors in the velocity of departure of the projectile affect the size of the error basket at the time of handover to the terminal (homing/endgame) phase?

ii) how do aiming errors affect the error basket size at handover?

iii) what are the trade-offs between the size of the error basket at handover and the amount of fuel and accuracy required in homing guidance to achieve the required circular error probable (CEP)?

iv) what are the optimal times to apply corrective command guided controls to the projectile?

v) what sensor levels are required to hit the handover error basket?

vi) how do the errors of estimate of the target trajectory affect the error basket?

vii) what is the effect of gravity on the path of the projectile, the amount of fuel required for thrusting, the error basket, CEP, and on the time-to-go until intercept.

viii) what modification to proportional navigation must the homing phase use to achieve the required CEP?

ix) how do errors in control acceleration magnitudes and directions affect error basket size and CEP?

x) how does the relative projectile/target speed affect the error basket size and CEP for a given control system lag?

xi) how does control system lag affect the error basket size and CEP for a given relative speed?

xii) what does a launch envelope look like?

xiii) what sensor resolution and control tolerances are required for the platform based commanded control to guide the projectile for the entire flyout and obtain the required CEP?

xiv) what is the optimal time to hand over the guidance control to the passive or semi-active terminal (homing or endgame) phase?

xv) what is the effect when range rate is sensed in addition to range, azimuth, and elevation?

III. THE SIMULATION MODEL. Our model omits negligible parts of the system. This standard methodology avoids the use of extraneous segments that may introduce errors and complicate the systems analysis, development, verification and validation, and performance analysis.

Our model FLYOUT contains the following sybsystems:

o) FLYOUT - the model executive

i) INITDA - initializes (smoothes and changes perspective from fixed earth to the space platform at each instant) the data for the ICBM trajectory and the space based platform

ii) INITPA - gets input run parameters and error standard deviations, allows changing and saving setup parameter files

iii) FLYSYS - updates the flyout iteratively by moving the target and projectile, sensing, tracking, and computing and applying controls to the projectile (gravity is applied when user selected)

iv) ENDGAM - simulates the homing (terminal) phase of the projectile flyout (not fully implemented at present)

v) WRITIT - writes out all user selected variable values

A higher level hierarchical diagram is shown in Figure III-1. Figures III-2 through III-6 give lower level functional diagrams. The modules FLYSYS and ENDGAM iterate the execution of their submodules. During the initial phase of the flyout, FLYSYS models the command guidance control from the perspective of the space based platform with its sensors and tracking system. During the terminal phase, the control shifts to the homing guidance system aboard the projectile.

FIGURE III-1

HIGHER LEVEL HIERARCHICAL DIAGRAM FOR THE FLYOUT MODEL

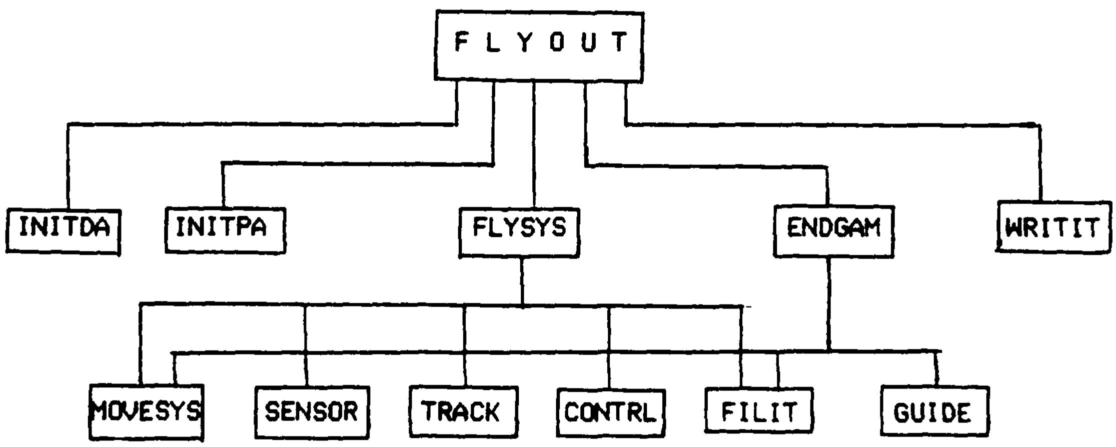

FIGURE III-2

FUNCTIONAL DIAGRAM FOR INITDA

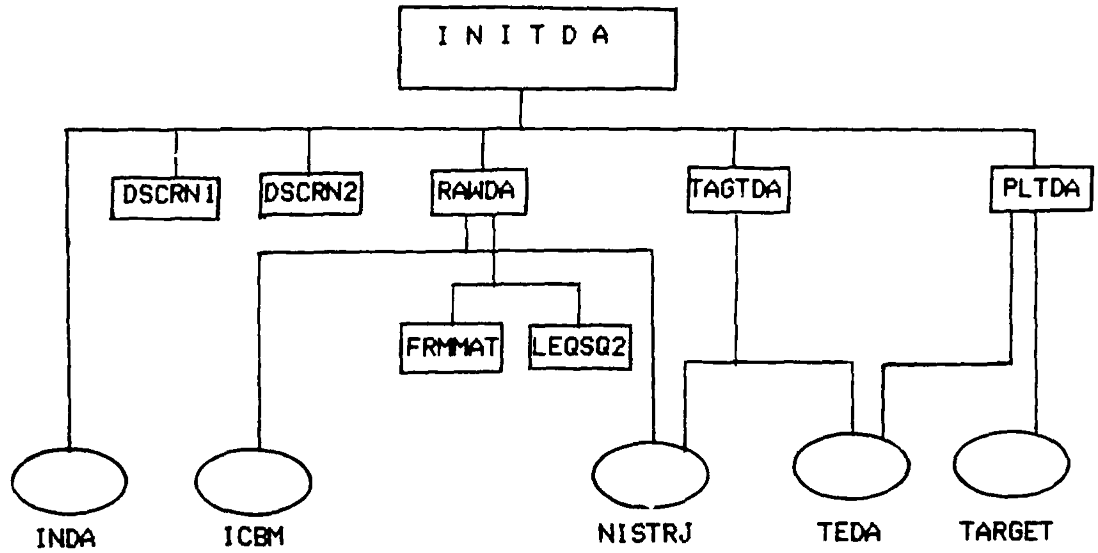

FIGURE III-3

FUNCTIONAL DIAGRAM FOR INITPA

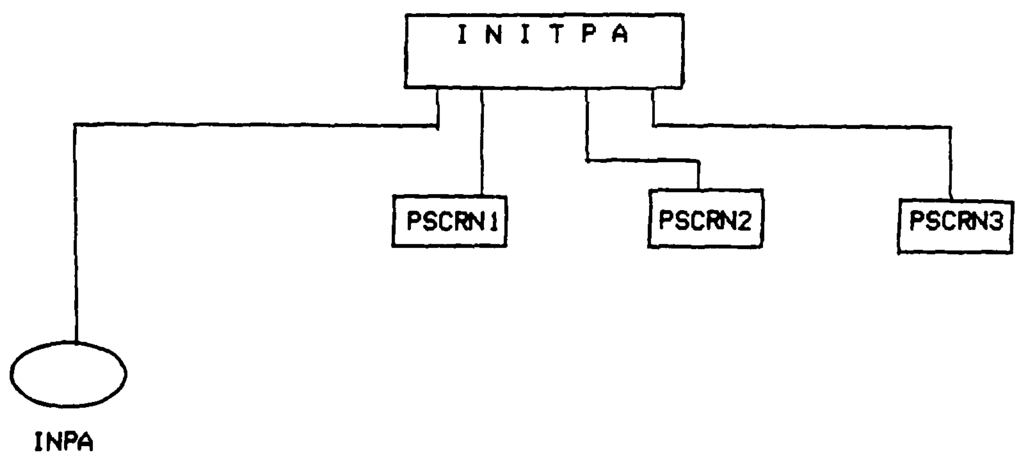

AD-A166 177 UNITED STATES AIR FORCE SUMMER FACULTY RESEARCH PROGRAM 1985 TECHNICAL RE (U) UNIVERSAL ENERGY SYSTEMS INC DAYTON OH R C DARRAH ET AL. DEC 85 AFOSR-TR-86-0140 12/15

UNCLASSIFIED F49620-85-C-0013 F/G 5/1 NL

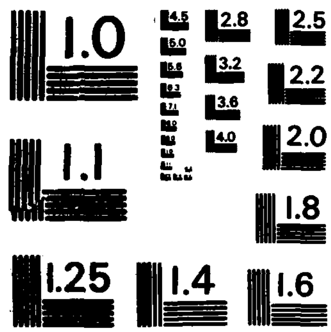

MICROCOPY RESOLUTION TEST CHART
NATIONAL BUREAU OF STANDARDS-1963-A

FIGURE III-4

FUNCTIONAL DIAGRAM FOR FLYSYS

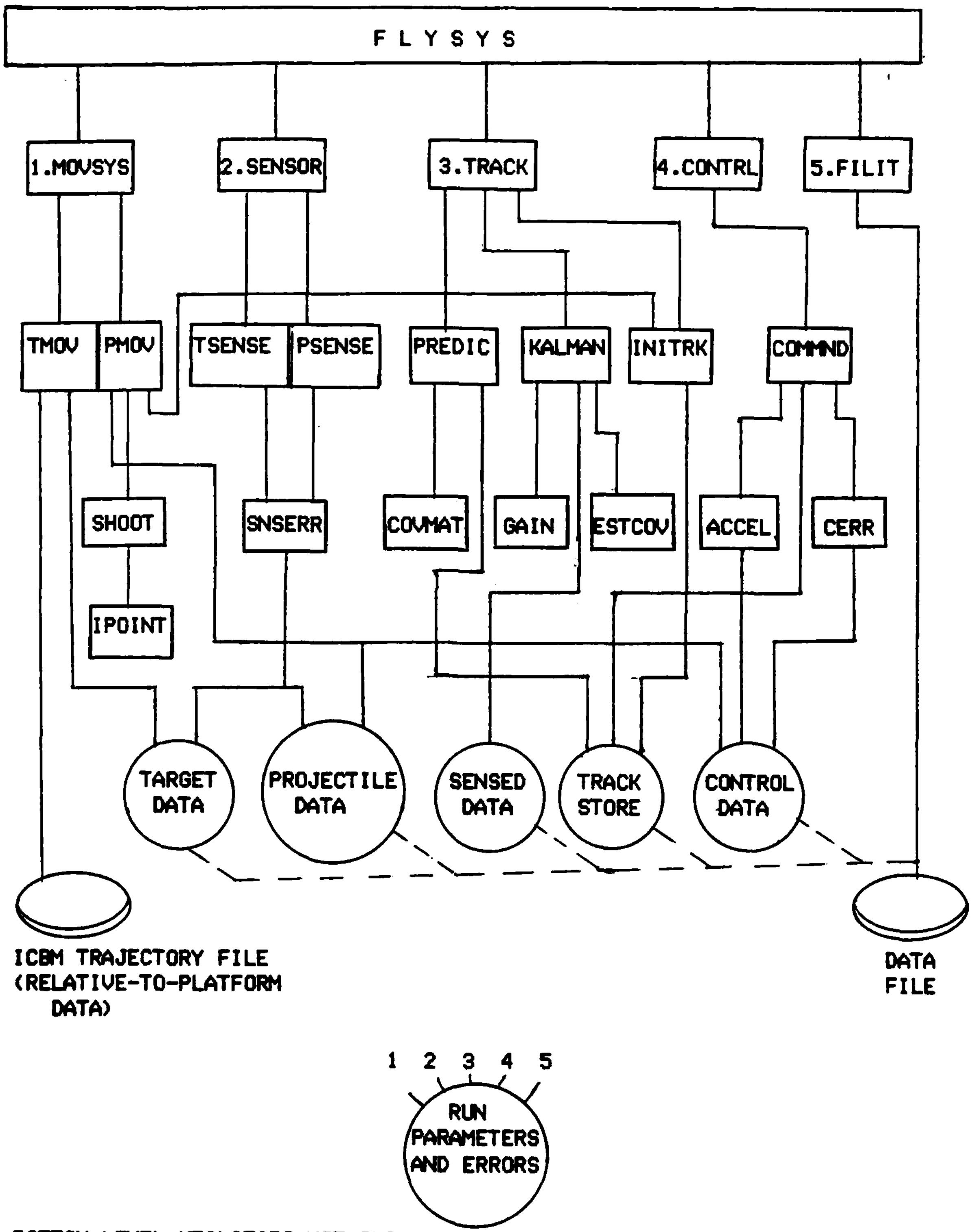

BOTTOM LEVEL UTILITIES NOT SHOWN: RAEXYZ, XYZRAE, MATMUL, GAIN1, ROTATE, EXTEND

FIGURE III-5

FUNCTIONAL DIAGRAM FOR ENDGAM

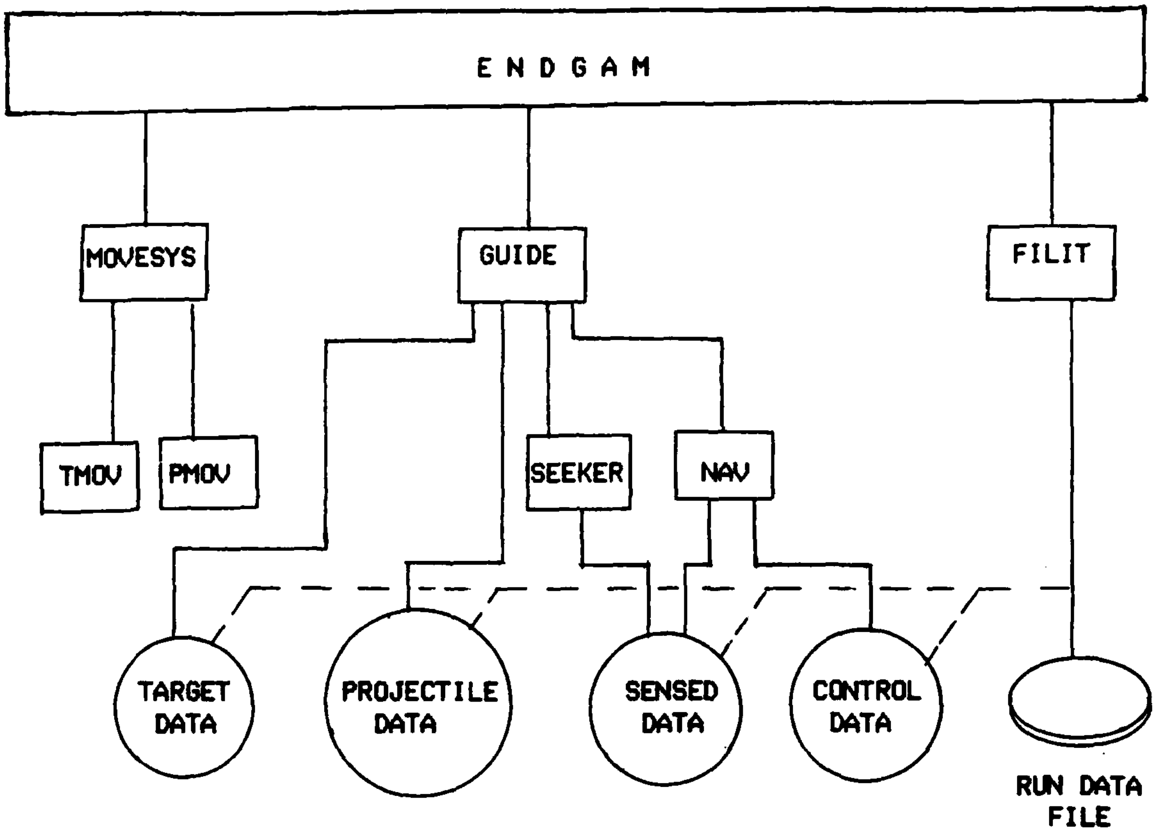

FIGURE III-6

FUNCTIONAL DIAGRAM FOR WRITIT

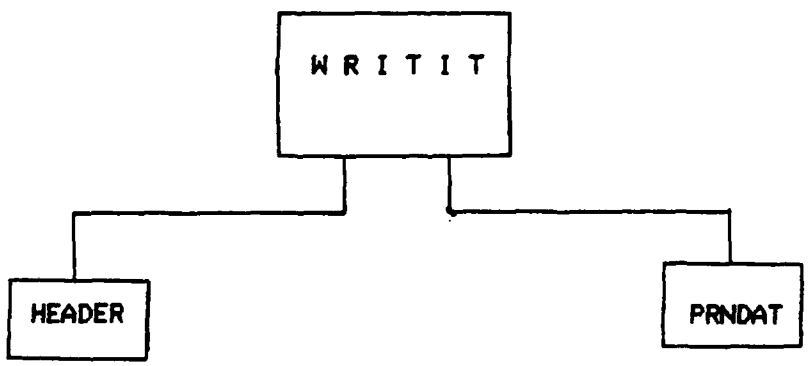

The modules FLYSYS and ENDGAM are the crucial algorithmic parts of the model necessary for analysis. Their sumodules are listed below.

The FLYSYS Subsystem:

0. FLYSYS - executive for the projectile flyout model
   - calls MOVSYS to update the target and the projectile
   - calls SENSOR to sense the target and projectile
   - calls TRACK to track the target and projectile
   - calls CONTRL, if a control application time is reached, to compute control accelerations for the projectile

1. MOVSYS - calls TMOV to interpolate the target trajectory and update the projectile
   - calls PMOV to update the projectile state, apply control accelerations if a control time has been reached, and apply gravity if it has been user selected
   - PMOV calls SHOOT if shoot time has been reached, which in turn calls IPOINT to compute an intercept time and point, and calls INITRK to initialize the projectile track upon shooting
   - PMOV also calls RAEXYZ and XYZRAE to convert to and from space platform polar and cartesian coordinates

2. SENSOR - calls TSENSE to read actual target trajectory position and range rate, and in turn to call SNSERR to generate and add on the sensor errors
   - calls PSENSE to read the actual projectile state, and in turn call SNSERR to generate and add on the sensor errors

3. TRACK - calls PREDIC to propagate (predict) the state of the object being tracked (target/projectile) to the new update time

by use of the track data

- calls KALMAN to call GAIN to obtain the Kalman gain, and then computes the optimal (Kalman, or maximal likelihood) estimate of the state from the measurements (sensed data) the propagated state, and the Kalman gain
- PREDIC calls COVMAT to compute the covariance of the predicted state, which calls MATMUL to multiply matrices
- KALMAN calls ESTCOV to compute the covariance matrix for the Kalman estimate
- GAIN calls GAIN1 to compute the inverse of a special semi-sparse matrix used in computing the Kalman gain
- KALMAN also calls INITRK to initialize the target track on the first iteration

4. CONTRL - calls COMMND to compute the control accelerations to be applied to the y-axis and z-axis of the projectile by computing the time-to-go until intercept and the intercept point, by calling ACCEL to compute the accelerations (controls), and by calling CERR to generate and add on control errors

- ACCEL computes the control accelerations necessary for the projectile to hit the intercept point
- CERR generates uniform random numbers of magnitude given by the standard deviations input by the user to INITPA
- COMMND calls ROTATE to rotate from cartesian platform orientation to the cartesian projectile body coordinate system, or the inverse of this rotation
- COMMND calls EXTEND to propagate states forward in time over a given time increment

- COMMND also calls RAEXYZ to convert from space platform polar to space platform cartesian coordinates

5. FILIT - writes to disk file all trajectory set-up data, run parameters, and error standard deviations on the first iteration, and then writes all variable values on every iteration

The ENDGAM Subsystem:

0. ENDGAM - executive program for the terminal (homing phase)
   - calls MOVSYS to update the target and projectile
   - calls GUIDE to compute the control accelerations to be applied to the projectile to hit the target
   - calls FILIT to write the variable values to disk file
1. MOVSYS - described above, calls TMOV to update the target and calls PMOV to update the projectile
2. GUIDE - computes accelerations to be put on the projectile by calling SEEKER to get the angles and angle rates, and calling NAV to compute the accelerations required
3. NAV - computes the homing control accelerations for the projectile
4. FILIT - described above, writes variable values to disk file

The modules INITDA and INITPA make the trajectory inputs flexible and easy to use. They are described briefly below.

The INITDA Subsystem:

0. INITDA - executive
   - calls the screen menu generating routines DSCRN1, DSCRN2
   - calls RAWDA to read raw trajectory data
   - calls TAGTDA to convert data from earth tangential plane to earth centered fixed coordinates

- calls PLTDA to convert target data to range, azimuth, and elevation of platform coordinates with origin at platform

1. RAWDA - RAWDA calls LEQSQ2 to do piecewise least square smoothing and interpolating of trajectory raw data

The INITPA Subsystem:

0. INITPA - executive

   - calls the screen menu-generating routines PSCRN1, PSCRN2, and PSCRN3 to allow the user to make new run parameter files and error standard deviation files, or to modify old files

IV. HOMING PROJECTILE GUIDANCE. Proportional navigation is the optimal control law for a homing projectile based on the following assumptions:

i) target accelerations are zero, gravity is negligible

ii) the minimized cost functional is miss distance only

iii) all controls are instantaneous, i.e., there are no lags

iv) there is no control acceleration along projectile body reference line

v) line-of-sight (LOS) angles from the LOS to the xy-plane and the xz-plane are nearly zero, so that sinC = C or sinC = 0, and cosC = 1 are valid approximations

vi) the range rate along the LOS is constant so that the time-to-go is equal to

$$-R/\dot{R}$$

However, a ballistic missile accelerates along its trajectory, so the first assumption doesn't hold. We may aim above the intercept point so that gravity will cause the projectile to drop into the intercept point. The effect of gravity on the projectile path will be negligible but the

fuel required to overcome gravity up to 200 seconds is not negligible. In addition, the speeds are sufficiently high that the third assumption also is not valid. The second assumption is valid and crucial because miss distance must be zero. The fourth assumption is also valid for HVGs.

The LOS angles from the projectile body reference line, coincident with the projectile velocity vector, are small only if the projectile speed is much greater than that of the target. In this case the fifth assumption is valid. Figure IV-1 presents the look (LOS) angles A and E, from which the position/velocity state is seen to be:

$$x = R \cos E \cos A \qquad \text{(IV-1)}$$

$$y = R \cos E \sin A$$

$$z = -R \sin E$$

$$\dot{x} = R \cos E \cos A - R E \sin E \cos A - R A \cos E \sin A$$

$$\dot{y} = R \cos E \sin A - R E \sin E \sin A + R A \cos E \cos A$$

$$\dot{z} = -R \sin E - R E \cos E$$

Proportional navigation assumes that A and E are near zero, which yields:.

$$x = R \qquad \dot{x} = \dot{R} \qquad \text{(IV-2)}$$

$$y = R A \qquad \dot{y} = \dot{R} A + R \dot{A}$$

$$z = -R E \qquad \dot{z} = -\dot{R} E - R \dot{E}$$

The optimal acceleration controls for the miss distance criterion are:

$$u_x = 0 \qquad k_1 = -3/t_{go}^2 \qquad \text{(IV-3)}$$

$$u_y = k_1 y + k_2 y \qquad k_2 = -3/t_{go}$$

$$u_z = k_1 z + k_2 z \qquad t_{go} = \text{time-to-go}$$

Proportional navigation uses the sixth assumption to compute the time-to-go.

FIGURE IV-1

LINE-OF-SIGHT ANGLES

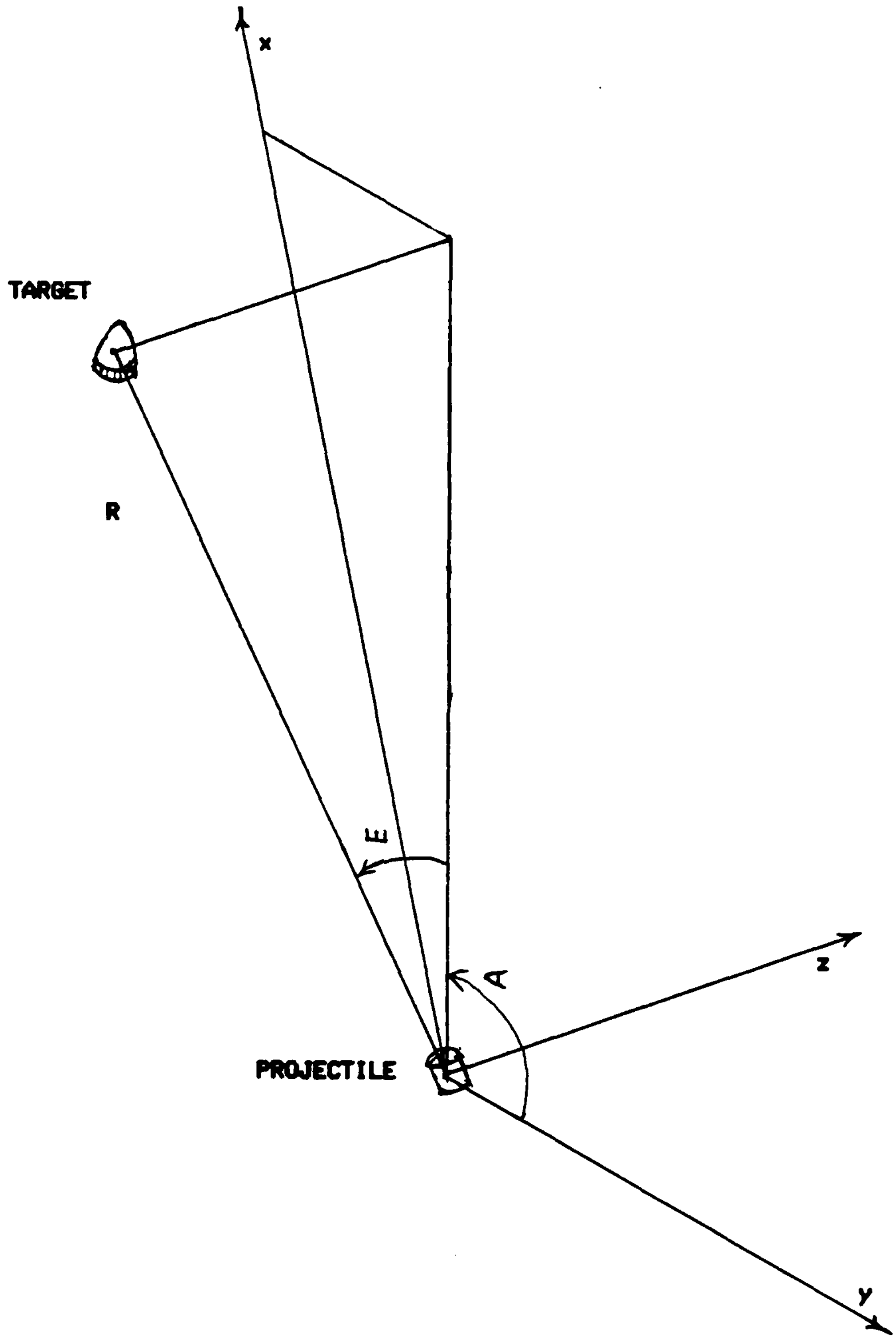

$$t_{go} = - R/\dot{R} \qquad \text{(IV-4)}$$

However, the target is accelerating (while the projectile has constant velocity) and so the range rate is changing. We must account for this acceleration, and so we use:

$${}^{+}t_{go} = - R/[\dot{R} + \ddot{R}(\,{}^{-}t_{go})] \qquad \text{(IV-5)}$$

where

$${}^{-}t_{go} = - R/\dot{R},$$

$\ddot{R}$ = filtered, adjusted acceleration

We may then iterate Equation IV-5 upon setting

$${}^{-}t_{go} = {}^{+}t_{go}$$

The acceleration along R is not constant because the target acceleration is increasing as the mass of the missile decreases with fuel burning. There is also jerk due to staging (the burning out of one rocket motor and the igniting of another). Thus homing guidance is a very difficult problem, and somthing must be known about the missile jerk characteristics before a satisfactory solution can be expected. The tracking of the target should use jerk, by interpolating from appropriate tables [unavailable to the investigators].

The control accelerations for the projectile thrusters along the projectile y-axis and z-axis are obtained by transforming the coordinates in Equation IV-3:

$$u_x = 0 \qquad \text{(IV-6)}$$

$$u_y = (-3/t_{go}^{\,2})RA + (-3/t_{go})[\dot{R}A + R\dot{A}]$$

$$u_z = (-3/t_{go}^{\,2})RE + (3/t_{go})[\dot{R}E + R\dot{E}]$$

When $t_{go} = - R/R$ is used, we get proportional navigation:

$$u_x = 0,\ u_y = 3\ R\ A,\ u_z = -3\ R\ E \qquad \text{(IV-7)}$$

V. **COMMAND GUIDANCE.** During the command guidance phase, only a small number (1 to 3) of corrective guidance controls are to be implemented. To aim the HVG, an initial intercept point must be computed using the target state date in the track store aboard the platform. First the target range and range rate yield a very coarse approximation to time-to-go until intercept (to be refined by iterations)

$$t_{go} = -R/\dot{R}$$

Then the target is extended ahead over time-to-go seconds to obtain a rough intercept point that is then used to compute a corrected time-to-go. This process is repeated until the time-to-go values stabilize. Using the last computed time-to-go, the intercept point is computed by extending the target state forward in time to the intercept time. This latter point is used for aiming.

Corrective times-to-go and intercept points are computed similarly while the projectile is in flight, using the tracks of both projectile and target. The command guided accelerations are computed by setting the projectile and target positions equal at intercept time and solving for the extra accelerations required. These accelerations are along the y-axis and z-axis of the projectile body coordinate system. Shooting delays and control delays are included in the computation, and so is gravity if it is user selected.

VI. **TRACKING.** Tracking is performed in the space based platform coordinate system. The platform tracks the target and projectile by sensing their ranges, azimuths, and elevations, and also their range rates when user selected.

The tracking procedure is the same for both the projectile and the target. Tracks are the states of the target and projectile. The target

state is (with FORTRAN variables given in parentheses):

R_t = range to target (tr(1))

A_t = azimuth to target (taz(1))

E_t = elevation to target (tel(1))

$\dot{R}_t$ = range rate (tr(2))

$\dot{A}_t$ = azimuth rate (taz(2))

$\dot{E}_t$ = elevation rate (tel(2))

$\ddot{R}_t$ = range acceleration (tr(3))

$\ddot{A}_t$ = azimuth acceleration (taz(3))

$\ddot{E}_t$ = elevation acceleration (tel(3))

The projectile state is:

R_p = range to projectile (pr(1))

A_p = azimuth to projectile (paz(1))

E_p = elevation to projectile (pel(1))

$\dot{R}_p$ = range rate (pr(2))

$\dot{A}_p$ = azimuth rate (paz(2))

$\dot{E}_p$ = elevation rate (pel(2))

$\ddot{R}_p$ = range acceleration (pr(3))

$\ddot{A}_p$ = azimuth acceleration (paz(3))

$\ddot{E}_p$ = elevation acceleration (pel(3))

A track is updated by a multistage procedure. Let X be the state vector (9 components as given above) and let A be the linear propagation function (a 9-by-9 matrix to be given in a later paragraph). For

A = 9-by-9 propagation matrix (given in a later paragraph)

X_k = old state at time t_k

X_{k+1} = new state at time t_{k+1}

W = noise of propagation (prediction, plant, or process)

we write:

$$X_{k+1} = A X_k + W$$

This is the plant equation (equation of prediction or propagation of the plant process, where the expected value of the plant noise is zero).

The measurements are in terms of R, A, and E ($\dot{R}$ is user selectable) with additive noises. All of the variables in the state vector are not measured, so some of the components of the measured vector will be zeros. In terms of the state vector, we write the measured state vector as the predicted measured state vector plus noise:

$$Y_{k+1} = H X_{k+1} + V$$

where H = measurement matrix (converts state to measured state)

V = noise of measurement

X_{k+1} = actual state at time t_{k+1}

In the case when R, A, E, and the range rate $\dot{R}$ are measured, we have, by suppressing the subscripts k+1 the matrix equation:

$$\begin{bmatrix} R_m \\ A_m \\ E_m \\ \dot{R}_m \\ \dot{A}_m \\ \dot{E}_m \\ \ddot{R}_m \\ \ddot{A}_m \\ \ddot{E}_m \end{bmatrix} = \begin{bmatrix} 1 & 0 & 0 & 0 & 0 & 0 & 0 & 0 & 0 \\ 0 & 1 & 0 & 0 & 0 & 0 & 0 & 0 & 0 \\ 0 & 0 & 1 & 0 & 0 & 0 & 0 & 0 & 0 \\ 0 & 0 & 0 & 1 & 0 & 0 & 0 & 0 & 0 \\ 0 & 0 & 0 & 0 & 0 & 0 & 0 & 0 & 0 \\ 0 & 0 & 0 & 0 & 0 & 0 & 0 & 0 & 0 \\ 0 & 0 & 0 & 0 & 0 & 0 & 0 & 0 & 0 \\ 0 & 0 & 0 & 0 & 0 & 0 & 0 & 0 & 0 \\ 0 & 0 & 0 & 0 & 0 & 0 & 0 & 0 & 0 \end{bmatrix} \begin{bmatrix} R \\ A \\ E \\ \dot{R} \\ \dot{A} \\ \dot{E} \\ \ddot{R} \\ \ddot{A} \\ \ddot{E} \end{bmatrix} + V$$

When $\dot{R}$ is not measured the 1 in the fourth row is replaced with 0. Thus we have

$$X_{k+1} = AX_k + W \quad \text{(predicted state)}$$

$$\underline{Y}_{k+1} = H\underline{X}_{k+1} + \underline{V} \quad \text{(predicted measurement)}$$

where the plant and measurement noise vector components are independent with zero means, so that their covariance matrices

$$Q = \text{Covariance}(\underline{W}), \qquad R = \text{Covariance}(\underline{V})$$

are diagonal. The variances of the component noises are either known from observed data or from some assumed prior distributions based on knowledge of systemic behavior. We use the following algorithm:

i) predict the expected state

$${}^{-}\underline{X}_{k+1} = A({}^{+}\underline{X})_k$$

where the + denotes the old state estimate and the "-" designates the prediction. In detail, this is

$$R_{k+1} = R_k + \dot{R}_k{}^{\wedge}t + \ddot{R}_k\Delta t^2/2$$
$$A_{k+1} = A_k + \dot{A}_k{}^{\wedge}t + \ddot{A}_k\Delta t^2/2$$
$$E_{k+1} = E_k + \dot{E}_k{}^{\wedge}t + \ddot{E}_k\Delta t^2/2$$
$$\dot{R}_{k+1} = \dot{R}_k + \ddot{R}_k\Delta t$$
$$\dot{A}_{k+1} = \dot{A}_k + \ddot{A}_k\Delta t$$
$$\dot{E}_{k+1} = \dot{E}_k + \ddot{E}_k\Delta t$$
$$\ddot{R}_{k+1} = a\ddot{R}_k + (1-a)[\dot{R}_{k+1} - \dot{R}_k]/\Delta t$$
$$\ddot{A}_{k+1} = a\ddot{A}_k + (1-a)[\dot{A}_{k+1} - \dot{A}_k]/\Delta t$$
$$\ddot{E}_{k+1} = a\ddot{E}_k + (1-a)[\dot{E}_{k+1} - \dot{E}_k]/\Delta t$$

where the k and $k+1$ subscripts denote values at the old and new update times, respectively, and

$$t_{k+1} = t_k + \Delta t$$

and the weight a is taken to be 1 in the standard Kalman filter.

ii) compute the covariance matrix (the mean square errors of the predicted state) of the prediction at the update time

$$P_{k+1} = AP_kA^T + Q$$

where P_k = old covariance matrix

A = 9-by-9 state propagation matrix for updating the state

Q = covariance of $\underline{W}$

[Recall, Covariance$(A\underline{X}_{k+1} + \underline{W}) = AP_{k+1}A^T + Q$]

iii) compute the Kalman gain

$$K_{k+1} = P_{k+1}H^T[HP_{k+1}H^T + R]^{-1}$$

where R = Covariance$(\underline{V})$ = mean square error of the measurement noise.

iv) compute the maximal likelihood estimate

$$^{+}\underline{X}_{k+1} = {}^{-}\underline{X}_{k+1} + K_{k+1}(\underline{Y}_{k+1} - H({}^{-}\underline{X}_{k+1}))$$

where $\underline{Y}_{k+1}$ = the actual measurement

$H({}^{-}\underline{X}_{k+1})$ = predicted measurement

v) compute the covariance matrix of the estimated state

$$P_{k+1} = [I - K_{k+1}H]P_{k+1}$$

Then $\underline{X}_{k+1} = A\underline{X}_k$ in matric form is really

$$\begin{bmatrix} R_{k+1} \\ A_{k+1} \\ E_{k+1} \\ \dot{R}_{k+1} \\ \dot{A}_{k+1} \\ \dot{E}_{k+1} \\ \ddot{R}_{k+1} \\ \ddot{A}_{k+1} \\ \ddot{E}_{k+1} \end{bmatrix} = \begin{bmatrix} 1 & 0 & 0 & \Delta t & 0 & 0 & (\Delta t^2/2) & 0 & 0 \\ 0 & 1 & 0 & 0 & \Delta t & 0 & 0 & (\Delta t^2/2) & 0 \\ 0 & 0 & 1 & 0 & 0 & \Delta t & 0 & 0 & (\Delta t^2/2) \\ 0 & 0 & 0 & 1 & 0 & 0 & \Delta t & 0 & 0 \\ 0 & 0 & 0 & 0 & 1 & 0 & 0 & \Delta t & 0 \\ 0 & 0 & 0 & 0 & 0 & 1 & 0 & 0 & \Delta t \\ 0 & 0 & 0 & 0 & 0 & 0 & 1 & 0 & 0 \\ 0 & 0 & 0 & 0 & 0 & 0 & 0 & 1 & 0 \\ 0 & 0 & 0 & 0 & 0 & 0 & 0 & 0 & 1 \end{bmatrix} \begin{bmatrix} R_k \\ A_k \\ E_k \\ \dot{R}_k \\ \dot{A}_k \\ \dot{E}_k \\ \ddot{R}_k \\ \ddot{A}_k \\ \ddot{E}_k \end{bmatrix}$$

VII. SENSING. The sensing of the projectile and target by the platform sensors is simulated by generating random errors with the user given standard deviations, and then adding them onto the actual positions (and range rates, if user selected). The positions are sensed in terms of

range, azimuth, elevation, and range rate, all relative to the space platform (origin) based coordinate system.

VIII. UPDATING THE SYSTEM. The actual state of the target, with respect to the platform, is read from the target trajectory file and interpolated to the update time. The actual projectile position is obtained by extending the actual projectile state (not the track state of the projectile) ahead to the update time by using its current actual state and any outstanding control accelerations to be applied.

IX. CONCLUSIONS AND RECOMMENDATIONS. We point out here that although our computer model is essentially complete, the ENDGAM module is not completely implemented. Also, the program is not validated/verified. Therefore, no trade-off nor performance analyses have been done. This summer project was rather ambitious, and a lot of work was done for the amount of time and manpower expended.

Our conclusions, which follow, are based on the analysis of requirements for the model.

1. Gravity should be included in the guidance algorithms. If ignored or included as noise, then considerable fuel will be needed onboard the projectile to overcome gravity for up to 200 seconds.

2. The first command control (correction) should be applied immediately after firing to prevent the projectile from travelling a large distance (at hypervelocity) in an erroneous direction, which would result in a wastage of fuel and time.

3. Proportional navigation is not accurate enough at the required speeds and look angles to allow any ICBM targets to be hit.

4. Jerk characteristics of the target must be used to compute corrective interceptive points.

5. Trade-off analyses must be made using one-on-one scenarios first, to determine the allowable error requirements necessary to obtain kills. Indeed, the state of technology must be able to provide the level of errors required for the system to be feasible.

Our recommendations are:

1. The model should be validated.

2. Thorough trade-off and performance analyses of one-on-one type should be done.

3. Additional refinements should be added to allow m-on-n analyses to be completed.

1985 USAF-UES SUMMER FACULTY RESEARCH PROGRAM/

GRADUATE STUDENT SUMMER SUPPORT PROGRAM

Sponsored by the

AIR FORCE OFFICE OF SCIENTIFIC RESEARCH

Conducted by the

UNIVERSAL ENERGY SYSTEMS, INC.

FINAL REPORT

IMAGE FORMATION AND PROCESSING IN SUPERPOSITION EYES: PRECISION LOCATION OF POINT OBJECTS USING THE MOIRE EFFECT.

Prepared by:	James S. Marsh
Academic Rank:	Full Professor
Department and University:	Department of Physics University of West Florida
Research Location:	AFATL/DLMI, Eglin AFB.
USAF Research:	Martin F. Wehling
Date:	July 19, 1985
Contract No:	F49620-85-C-0013

Approved: Dennis H. Goldstein

DENNIS H. GOLDSTEIN
SPONSOR

IMAGE FORMATION AND PROCESSING IN SUPERPOSITION EYES: PRECISION LOCATION OF POINT OBJECTS USING THE MOIRE EFFECT.

by

James S. Marsh

ABSTRACT

An investigation of image formation in insect eyes obeying a superposition model shows that multiple images of point objects are formed. This suggests a method for the precision location of point objects. The optical image is multiplied by a grating into an array of images which are projected onto an analyzer grating. The moire so produced allows location of the image to within a small fraction of the analyzer grating spacing. Replacing the analyzer grating with a photodetector array is proposed. The Fourier coefficient of the detector array corresponding to the period of the moire fringes is investigated. It is shown that the phase of the coefficient furnishes a high precision, relatively noise immune, determination of the image position.

ACKNOWLEDGMENTS

This work was sponsored by the Air Force Systems Command, Air Force Office of Scientific Research, and performed at the Air Force Armament and Training Laboratory, DLMI, at Eglin AFB. The author wishes to thank Rick Wehling for his interest and support of this work, and Dennis Goldstein and David Crane for their assistance and hospitality in the laboratory.

I. INTRODUCTION: The author's speciality is optics. I have done work in holography, moire, diffraction, etc. The research group I joined is concerned with electro-optical guidance. The specific area I chose to work in is multi-aperture optics. Out of several proffered opportunities I chose this because I felt that, with my background, I had the greatest chance of having some impact in the limited time available.

II. OBJECTIVES OF THE RESEARCH EFFORT: The broad objective of my group is to extract, from the operation of segmented eyes of insects and crustacea, ideas for the design of wide aperture high resolution guidance systems with a large field of view. I chose to concentrate on the optical operations of eyes satisfying a superposition model, since little work had been done here and I could immediately bring my expertise to bear. The primary objective was to see if the insects and crustacea were utilizing some mechanism, possibly involving signal processing in addition to clever optics, to achieve superresolution. This study (Phase I) showed that the superposition eye operated in a way that allowed the possibility of superresolution or, more accurately, high precision location of small objects. In Phase II I took the basic mechanism involved and set out to (1) achieve an experimental realization of the simplest form of this mechanism, (2) work out the theory of this mechanism to find a formulation that would aid in the design of devices using the mechanism, and (3) investigate a signal

processing scheme which would achieve good performance in the presence of noise.

III. <u>PHASE I RESULTS</u>: The study of the superposition eyes of insect and crustacea showed that image formation of a point object is achieved without the benefit of focussing by individual segments of the eye. Individual segments direct beams of more or less plane waves onto the retina. Interference of these waves produces an image on the retina which can have the dimensions of the same order of magnitude as the wavelength of light used. However, because the waves come onto the retina from discrete directions determined by the placement of the lens segments, not one but an array of images is produced having the same translational symmetries as the array of segments. Fig. 1 shows the image array produced by a hexagonal array of segments. Fig. 2 is a two dimensional computer simulation of multiple image formation by discrete beams of light intersecting the same region. These calculations are idealized, ignoring spherical and phase aberrations.

The question now became, what does the animal do with this array of images? The retina of the animal consists of an array of light sensitive elements, rhabdomeres, arranged in an array with the same translational symmetries as the image array, but in general with a different period. Thus sometimes an image in the image array would coincide with a rhabdomere, sometimes not. Furthermore, the pattern of coincidences would change as the object moved across the

field of view, dragging the image array with it. It dawned on me that the pattern of coincidences would, on a large scale, produce a two dimensional moire effect and that (1) the phase of the fringes could locate the object to a much higher precision than the size of an individual image would allow and (2) during object motion, the pattern of moire fringes would move with a much higher velocity on the retina than an individual image, so that we would have a very sensitive velocity detector.

IV. PHASE II RESULTS: Phase I showed two things. (1) Images could be formed with discrete cooperating elements, plane mirrors for example, even if the elements did not individually do any focussing. In general such an optical system produces an array of images. (2) An array of images falling on a similar array of light detecting elements could operate by way of a moire effect to locate the image with a much higher precision than the size of the image would alone permit.

I now imagined various metamorphoses of the bugs eye to see how else this scheme might be used and in particular to discover a realization that might conveniently be actualized on the optical bench. The simplest arrangement I found turned out to be a standard Fourier transform set up, as shown in Fig. 3. The lens L_1 puts the source s at infinity. The lens L_2 produces an image of s in the plane of G_2. G_1 is a grating which produces a one dimensional array of images of s with constant spacing d' superimposed on the

analyzer grating G_2 which has slit spacing d. The image array is viewed through the grating G_2. This is a one dimensional analogue of the mechanism discovered in bugs eyes. The spaces of G_2, which is a Ronchi ruling, play the role of detectors. The moire effect is shown in Fig. 4, a photograph of the plane of G_2. In this setup, the fringe period was ~ 15d, allowing a visual location of the actual image to better than d/30 in the image plane. As in ordinary moire with two gratings, relative position of the actual image and the analyzer grating G_2 is determined by the phase of the fringes relative to the reference frame established by G_2.

I now contemplated emulating the bugs eye more closely by placing an array of detectors behind G_2, one for each opening in G_2. The question was how best to process the data from the light detectors to most accurately determine the phase of the fringe system? Locating the maxima or minima of the fringes would not work very well in the presence of noise. I then came up with the idea to numerically Fourier transform the output of the detectors, pick out the Fourier coefficient corresponding to the period of the fringes, and look at the phase of that component. I showed that, under suitable conditions, the phase ϕ was given by $\phi = -2\pi x_0/d'$, where x_0 is the position of the actual image, which is what we want to determine, and d' is the spacing between elements of the image array. The precision within which x_0 can be determined is limited by

the uncertainty in the phase. I did a statistical study on the assumption that the output of each detector had a noise component, and the noise components were independent and had identical Gaussian distributions with variance σ^2. The result was that the uncertainty in x_0 is

$$\Delta x_0 = d'\sigma/(2\pi|C|\sqrt{M}),$$

where $|C|$ is the magnitude of the Fourier coefficient and M is the number of detectors in the array. The appearance of $\sqrt{M}$ in the denominator indicates a high degree of noise immunity for this way of determining x_0. In a low noise environment, using digital processing ($\sigma \sim 1$) with an eight bit processor ($|C| \sim 100$) and a linear array of CCD's for the signal capture ($M \sim 1000$), this would lead to a precision for x_0 of

$$\Delta x_0/d' \sim 1/(6X100X30) \sim 1/18{,}000.$$

With noise comparable to signal ($\sigma \sim |C|$) this still has a precision of

$$\Delta x_0/d' \sim 1/180.$$

These results have been extended to two dimensions, where G_1 is replaced by a two dimensional grating and G_2 is replaced by a two dimensional CCD array with the same translational symmetries as G_1. The result is that the phases of two coefficients of the 2 dimensional Fourier transform of the output of the CCD array suffice to determine the two dimensional location of the image and the precision in the presence of noise is similar to the one dimensional case.

an efficient algorithm for computing radiation from polygonal apertures in the Fresnel approximation needs to be developed. As it happens, I have already done considerable work along this line.

RECOMMENDATION V: Insect and Crustacea eyes have the right size to utilize these effects in visible light. This scale would seem to be too small to fabricate a device to emulate the superposition eye. However it would seem that the scale of millimeter waves or possibly far infrared waves would be such as to allow the fabrication of a device emulating a lobster's eye, which uses only plane mirrors as optical elements. This should be explored.

RECOMMENDATION VI: The idea of producing multiple images for moire processing with plane mirror optics should be further explored by investigating and/or building something that would resemble a multiple-mirror telescope with plane mirrors.

RECOMMENDATION VII: The image array in one dimension could very well be interference fringes produced by a Michaelson interferometer, a Fresnel biprism, or by two plane mirrors. A CCD array used to read and process the fringe system as described above would effectively multiply the finnesse of the fringe system allowing location of the fringe system with high precision. This would be useful, for example, in interferometrically controlled machines. This application should be explored.

V. SUMMARY: There are 3 discrete discoveries to come out of this study. (1) An image array processed with an analyzer grid or CCD array to produce moire can be used to locate the image with a much higher precision than is possible with a single image. (2) The Fourier transform trick proposed here seems to be a particularly favorable and noise immune method for processing the output of the detector array for realizing the precision inherent in (1). (3) Image arrays can be produced by optical systems that do not have focussing elements.

Applications of (1) and (2) to devices for precision location, tracking, or alignment of target objects are obvious.

RECOMMENDATION I: A photodetecting array should be built to replace the grating G_2 in the set up of Fig. 3 to explore the validity of the predictions of the proposed signal processing scheme.

RECOMMENDATION II: A real device using this scheme, performing a real image location job, should be built and evaluated. I have in mind something like a telescope with an image multiplying grating and a photodetector array for measuring star positions.

RECOMMENDATION III: The study of Insect and Crustacea eyes should be continued. In particular a more thorough and detailed study of image formation should be performed, one which takes aberration into account.

RECOMMENDATION IV: With reference to recommendation III,

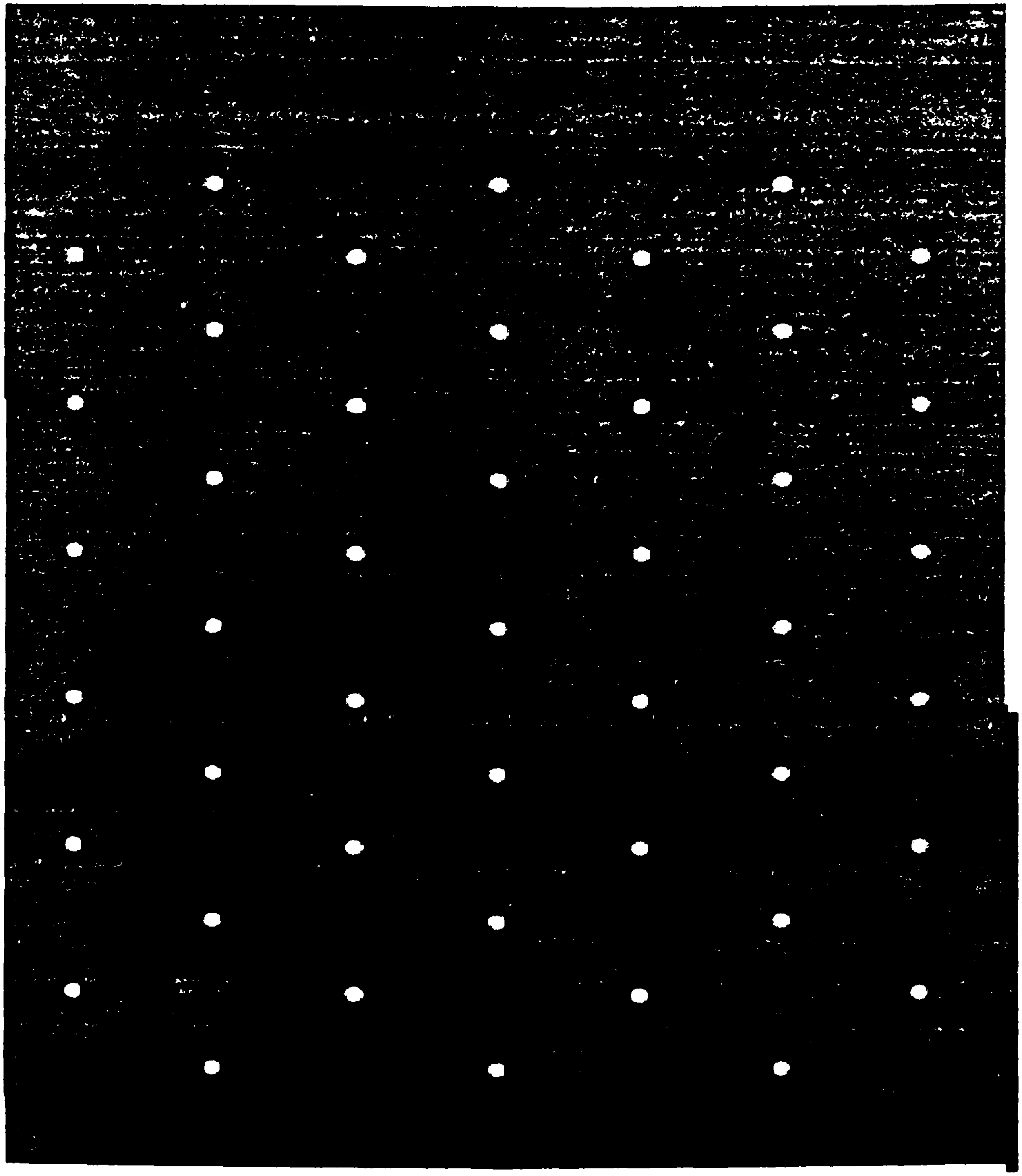

Figure 1

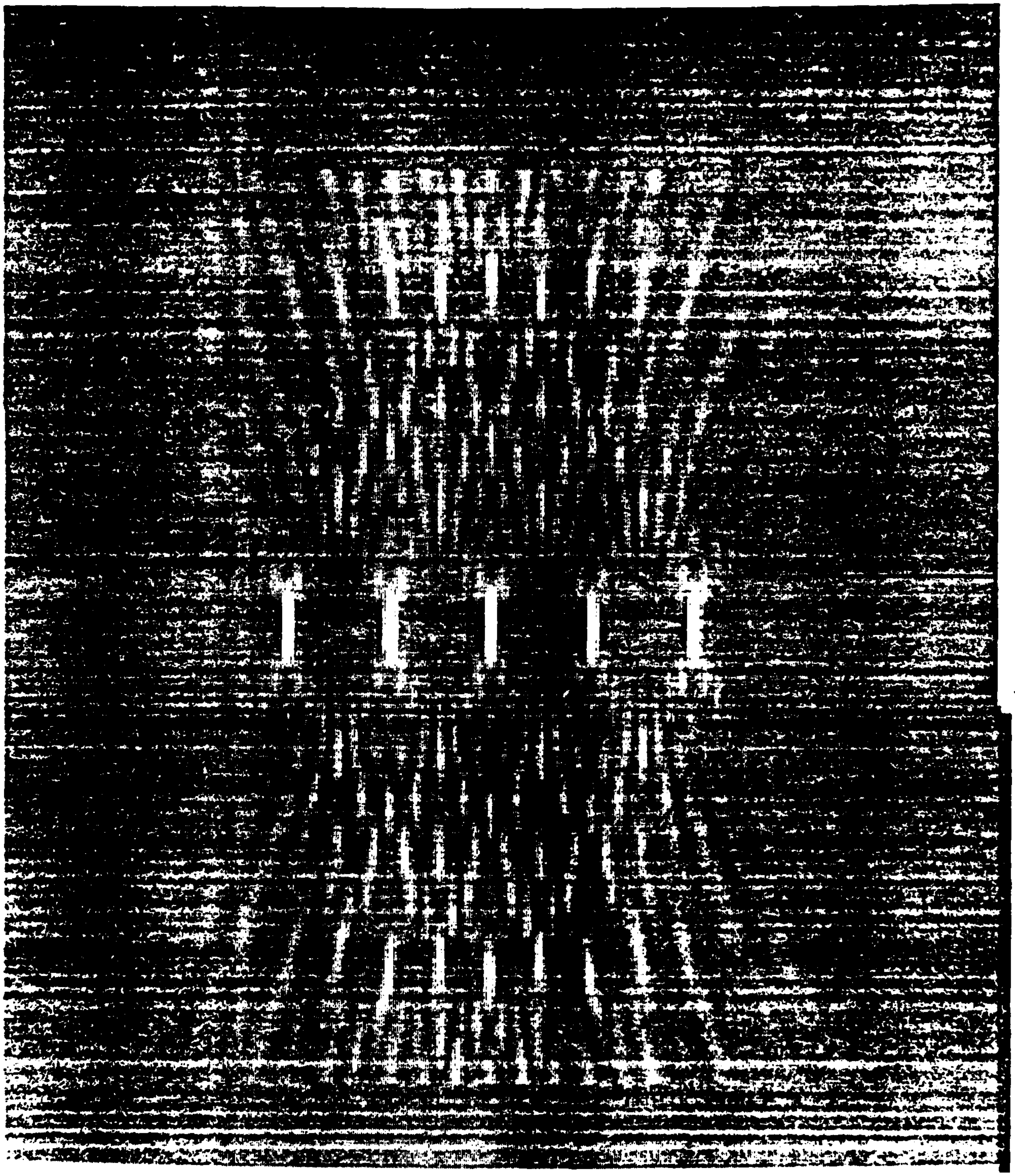

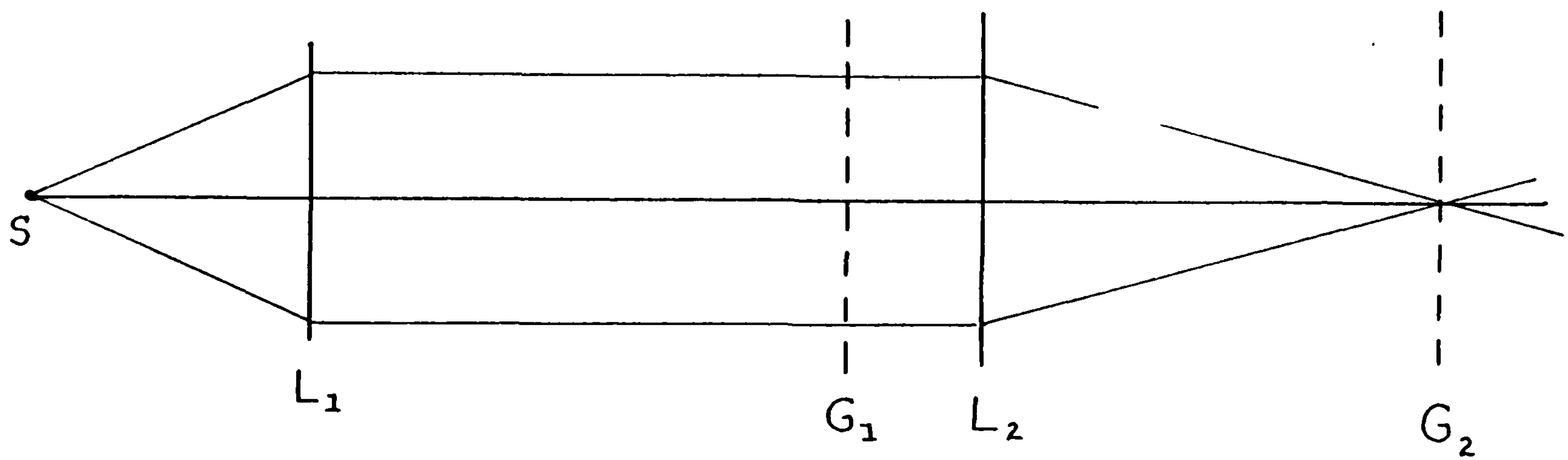

Figure 3.

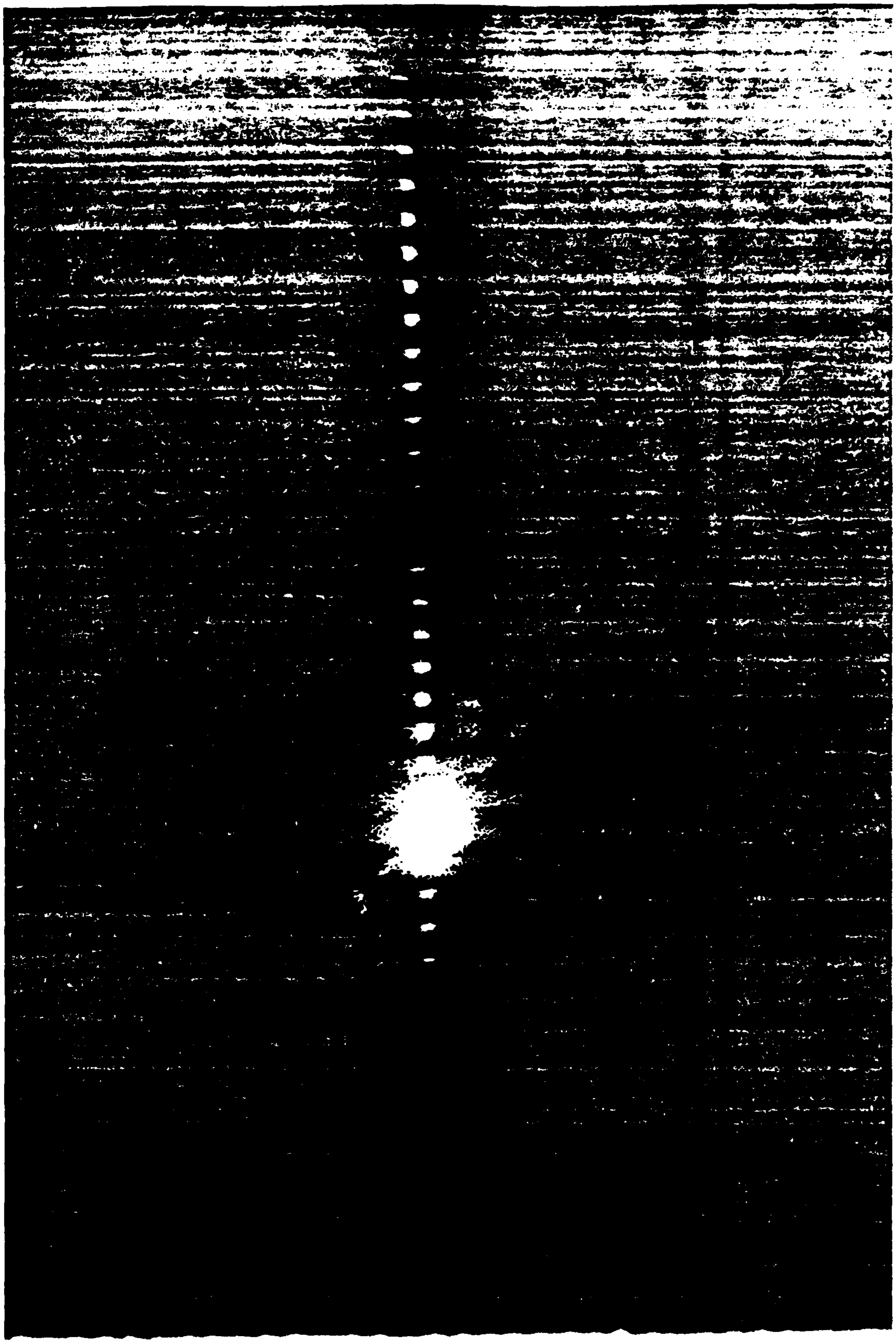

1985 USAF-UES SUMMER FACULTY RESEARCH PROGRAM/

GRADUATE STUDENT SUMMER SUPPORT PROGRAM

Sponsored by the

AIR FORCE OFFICE OF SCIENTIFIC RESEARCH

Conducted by the

UNIVERSAL ENERGY SYSTEMS, INC.

FINAL REPORT

CONTROL FUNCTIONS IN GRID GENERATION

Prepared by:	C. Wayne Mastin
Academic Rank:	Professor
Department and University:	Department of Mathematics and Statistics Mississippi State University
Research Location:	Arnold Engineering Development Center Directorate of Technology
USAF Research	Bharat Soni, Sverdrup Technology, Inc., CFD Group

Date:	August 16, 1985
Contract No:	F49620-85-C-0013

CONTROL FUNCTIONS IN GRID GENERATION

by

C. Wayne Mastin

ABSTRACT

Grid generation techniques based on the solution of elliptic systems or variational problems may be used to make an algebraically generated grid smoother and more orthogonal. In the process, the distribution of points in the original algebraic grid may be altered. This report will develop techniques which include geometric control functions. The purpose of the control functions is to retain the same overall distribution of grid points from the algebraic grid while still giving a grid with a high degree of smoothness and orthogonality. These techniques are applied in the solution of a practical three-dimensional grid generation problem.

ACKNOWLEDGEMENTS

This research would not have been possible without the assistance of Bharat Soni and the Computational Fluid Dynamics Group of Sverdrup Technology, Inc. Support for this program was provided by the Air Force Systems Command, Air Force Office of Scientific Research, and Arnold Engineering Development Center. I am also grateful to Marshall Kingery of AEDC and the staff of Universal Energy Systems for their assistance.

I. INTRODUCTION: The goal of computational fluid dynamics is to simulate the flow about or within complex three-dimensional bodies. The mathematical model of the flow field is a system of partial differential equations. Since exact solutions are a rarity, numerical methods must usually be employed to obtain approximate solutions of the system. These numerical methods reduce the system of differential equations to a system of algebraic equations. The algebraic system is solved, thereby, giving a numerical solution defined at a finite set of points in the flow field. This set of points is referred to as a grid, and the location of the points has a major influence on the accuracy of the numerical solution.

There are two approaches to the construction of computational grids. The first approach uses direct algebraic methods to distribute grid points within a physical region of interest. The techniques employed are multivariant interpolation incorporating weight functions which give a desired distribution of points. A state-of-the-art code which uses this approach is SVTGD3D. The code was developed by Soni [5] at AEDC. The second approach characterizes the grid point coordinates themselves as numerical solutions of some well-posed mathematical problem. The problem is typically stated in terms of

finding a transformation, or mapping, of a rectangular region onto the given region such that the mapping functions are solutions of some elliptic boundary-value problem or variational problem. As with the original physical problem, this mapping problem must generally be solved using some numerical algorithm. The result then is a set of coordinate functions defined at points of a rectangular grid on the rectangular region. These function values are the coordinates of the grid points in the physical region. The two approaches are not completely independent. The mapping functions are usually computed using some iterative method and therefore starting values are needed. The starting values are computed from a simple algebraic grid which may bear little resemblance to the final converged grid. While it is more difficult to control the distribution of grid points with the elliptic and variational methods, there are some clear advantages. A smooth distribution of grid points will occur, irregardless of the shape of the boundary, and the skewness of the grid cells can be controlled to some degree. With an algebraically defined mapping, a good deal of trial and error may be necessary to even obtain a nonvanishing Jacobian. A survey of both grid generation methods may be found in the book by Thompson et. al [4].

II. <u>OBJECTIVES OF THE RESEARCH EFFORT</u>: The objective of this summer's research was to enhance the grid generation capabilities at AEDC. This author has been working on the application of elliptic systems in grid generation for several years. Recently, it was decided by Bharat Soni to incorporate both elliptic and variational methods in the code SVTGD3D. These methods were to be used for a limited purpose. It was to be assumed that the algebraic grid generated by the code was properly distributed, and these iterative methods would only be used to make the existing grid smoother and more orthogonal. Two presently available methods seem well suited for this purpose. The first method uses elliptic equations with control functions developed by Thomas and Middlecoff [3]. The second method is the grid optimization method of Kennon and Dulikravich [1]. An optimal grid is defined as one which solves a particular variational problem. During this summer of research, the method of Thomas and Middlecoff has been extended to give control functions which include more of the geometry of the algebraic grid. The Kennon and Dulikravich algorithm has been added to the existing code and check cases have been run. It was necessary to include control functions so that the distribution of grid points was maintained.

III. <u>SMOOTHING WITH ELLIPTIC SYSTEMS</u>: The elliptic grid generation equations defining the transformation from computational $\xi\eta\zeta$ - space to physical xyz - space is given in vector form as

$$\alpha(r_{\xi\xi}+Pr_{\xi})+\beta(r_{\eta\eta}+Qr_{\eta})+\gamma(r_{\zeta\zeta}+Rr_{\zeta})+\rho r_{\xi\eta}+\sigma r_{\eta\zeta}+\tau r_{\xi\zeta}=0 \tag{1}$$

where r = (x,y,z) and the coefficients are given by

$$\alpha=(r_{\eta}\cdot r_{\eta})(r_{\zeta}\cdot r_{\zeta})-(r_{\eta}\cdot r_{\zeta})^2$$

$$\beta=(r_{\xi}\cdot r_{\xi})(r_{\zeta}\cdot r_{\zeta})-(r_{\xi}\cdot r_{\zeta})^2$$

$$\gamma=(r_{\xi}\cdot r_{\xi})(r_{\eta}\cdot r_{\eta})-(r_{\xi}\cdot r_{\eta})^2$$

$$\rho=2[(r_{\xi}\cdot r_{\zeta})(r_{\eta}\cdot r_{\zeta})-(r_{\xi}\cdot r_{\eta})(r_{\zeta}\cdot r_{\zeta})]$$

$$\sigma=2[(r_{\xi}\cdot r_{\eta})(r_{\xi}\cdot r_{\zeta})-(r_{\xi}\cdot r_{\xi})(r_{\eta}\cdot r_{\zeta})]$$

$$\tau=2[(r_{\xi}\cdot r_{\eta})(r_{\eta}\cdot r_{\zeta})-(r_{\xi}\cdot r_{\zeta})(r_{\eta}\cdot r_{\eta})]$$

The selection of the control functions, P, Q, and R, will be made in two steps. First, only the change in spacing along a grid line will be considered. For this purpose, the one-dimensional form of (1) will be examined. If we assume that the physical region reduces to a straight line $\eta = \zeta = 0$, then

$$r_{\xi\xi}+Pr_{\xi}=0.$$

Now introduce the arc length parameter s and apply the chain rule to arrive at the equations

$$r_{\xi}=r_s s_{\xi},$$

$$r_{\xi\xi}=r_{ss}s_{\xi}^2+r_s s_{\xi\xi}.$$

Since it is assumed that the physical coordinates vary along a straight line which has zero curvature, we have $r_{ss}=0$. Therefore, r_s can be eliminated in the two equations above to yield

$$r_{\xi\xi} = -\frac{s_{\xi\xi}}{s_\xi} r_\xi .$$

From this, and similar analysis in the η and ζ directions, it can be concluded that the proper choice of P, Q, and R should be

$$P_1 = -\frac{s_{\xi\xi}}{s_\xi}, Q_1 = -\frac{s_{\eta\eta}}{s_\eta}, R_1 = -\frac{s_{\zeta\zeta}}{s_\zeta}. \tag{2}$$

One of the purposes in using the elliptic system is to limit the skewness in the grid. If the grid were orthogonal, then the coefficients ρ, σ, and τ, of the mixed derivatives in (1) would vanish. The Jacobian of the transformation would also be equal to the product $\|r_\xi\|\|r_\eta\|\|r_\zeta\|$, provided the Jacobian were positive. Now the change in spacing along grid lines has been considered in the above one-dimensional analysis. If we neglect the change in spacing along a ξ coordinate line, so that $r_{\xi\xi}=0$, and impose the condition $\rho=\sigma=\tau=0$, then when Q and R are eliminated from the system (1), a resulting value for P is produced. Similarly, values for Q and R can be generated. The three control functions generated under these assumptions are

$$
\begin{aligned}
P_2 &= -\frac{(r_\eta \times r_\zeta)\cdot(\beta r_{\eta\eta} + \gamma r_{\zeta\zeta})}{\alpha \|r_\xi\| \|r_\eta\| \|r_\zeta\|} \\
Q_2 &= -\frac{(r_\zeta \times r_\xi)\cdot(\alpha r_{\xi\xi} + \gamma r_{\zeta\zeta})}{\beta \|r_\xi\| \|r_\eta\| \|r_\zeta\|} \qquad (3) \\
R_2 &= -\frac{(r_\xi \times r_\eta)\cdot(\alpha r_{\xi\xi} + \beta r_{\eta\eta})}{\gamma \|r_\xi\| \|r_\eta\| \|r_\zeta\|}.
\end{aligned}
$$

A negative Jacobian would be handled by simply changing the sign of these values.

Whereas the first set of control functions was determined by the distribution of points along coordinate lines, this latter set is determined by the shape of the coordinate surfaces. For a planar surface, $P_2=Q_2=R_2=0$, and for a curved surface these are the control functions needed to maintain a uniform spacing along grid lines passing through the surface. Also it is hoped that the use of the orthogonality assumption would make the resulting grid more orthogonal although we have no rigorous proof. Two sets of control functions have been given only for purposes of development and explanation. The final set of functions which reflects the characteristics of the desired grid is given as

$$P = P_1 + P_2,\ Q = Q_1 + Q_2,\ R = R_1 + R_2.$$

There are two modes of implementing the control functions. The most direct method would be to compute P, Q, and R at each interior point using the coordinates of

the algebraic grid. There are potential problems with this method. A highly concentrated algebraic grid will have cells with small volumes and the denominations in (3) may be nearly zero. Also a lack of smoothness in the algebraic grid would result in large point-to-point variations in the control functions. Either of these occurrences could cause the iterative method for solving the elliptic system to diverge. Therefore, it may be necessary to smooth the control functions before they can be used. An alternate method which may eliminate some of these problems is to evaluate the control functions on the boundary and interpolate to obtain interior values. Of course, some control over the interior grid spacing is lost, and it still may be necessary to employ some smoothing. On the other hand, one could generate control functions if the grid points adjacent to the boundary were given. Little effort would be needed on the interior grid since those points would be modified in the solution of the elliptic system.

It should be noted that the purpose is not to reproduce the algebraic grid. This could be done, of course, by simply solving the three equations in (1) for the three control functions. The desired orthogonality properties have been used in the computation of the control functions.

Once they have been computed, the grid is generated by the complete set of equations in (1). The significance of using the complete system is that, for control functions which are sufficiently small or of a particular form, the transformation can be guaranteed tc have a nonvanishing Jacobian. This would not be the case if the mixed derivative terms were eliminated.

IV. GRID OPTIMIZATION: Many elliptic boundary value problems can be cast in the form of a variational problem. Thus it is not surprising that the popularity of elliptic systems gave rise to grid generation methods based on the solution of variational problems. In order to use one of these methods for our purpose of smoothing and orthogonalizing an existing algebraic grid, properties of the grid must be considered in the formulation of the problem.

The grid optimization method seeks to minimize a convex combination of the following two non-negative quantities.

$$I_o = \int\int\int [(r_\xi \cdot r_\eta)^2 + (r_\xi \cdot r_\zeta)^2 + (r_\eta \cdot r_\zeta)^2]\, d\zeta\, d\eta\, d\xi \tag{4}$$

$$I_v = \int\int\int [(Jw)_\xi^2 + (Jw)_\eta^2 + (Jw)_\zeta^2]\, d\zeta\, d\eta\, d\xi$$

where J is the Jacobian

$$J = r_\xi \cdot (r_\eta \times r_\zeta)$$

and w is a weight function which will be used to control the grid distribution. The optimal grid is thus determined by the transformation

$$x = x\ (\xi, \eta, \zeta)$$

$$y = y\ (\xi, \eta, \zeta)$$

$$z = z\ (\xi, \eta, \zeta)$$

where r = (x, y, z) minimizes the value of the functional

$$I(r) = \alpha I_o + (1-\alpha)\ I_v,\ 0 \le \alpha \le 1.$$

For brevity, the optimization problem has been presented as a continuous problem rather than a discrete problem. In the actual solution procedure, each derivative would be replaced by a difference approximation. One-sided difference approximations are used so that the solution will not decouple at even and odd grid points. This leads to a dilemma since there are four ways to compute $(r_\xi \cdot r_\eta)^2$, a forward or backward difference for either r_ξ or r_ζ. In the same vein, there are four distinct ways to approximate $(Jw)_\xi$. Kennon and Dulikravich [1] decided to form their discrete functional by summing all four approximations as discussed in the next section. Consequently, the minimum value of the functional in their numerical solution is approximately 4 I(r), but this is not important since we are only interested in the solution vector r.

The original grid optimization method of Kennon and Dulikravich uses a constant value of $w=1$. Therefore, the smoothing is achieved by decreasing the variation in grid cell volumes. The grids generated by this method resemble grids generated by the elliptic systems with zero control functions. The objective then is to define the control function w in this optimization method so that the distribution of grid points can be maintained in much the same way that the control functions P, Q, and R were implemented in the elliptic systems. Since there has been no previous research in this area, it was decided to keep the function w relatively simple at first. Suppose an algebraic grid is given and the optimization method is to be applied. If it is desired that the sizes of the grid cells remain about the same, but that the resulting grid be more orthogonal, then one choice would be

$$w = (\|r_\xi\|\|r_\eta\|\|r_\zeta\|)^{-1}.$$

For an orthogonal grid, $Jw = 1$ and thus $I_v = 0$. In the general case, the resulting grid would be more nearly orthogonal, and the cell volumes would be closer to the product of three edges of the original algebraic grid. So far, all the discussion has been on orthogonality, and one might conclude that best choice of α would be one. However, this is generally not the case. Without the

integral I_v, the Jacobian may change signs and result in coordinate lines in one direction crossing over.

The integral I_o in (4) should be modified when constructing grids with extreme differences in cell sizes. In such cases the solution of the variational problem, as it stands, would give a grid which was more orthogonal in regions where the grid spacing was larger but leave the grid relatively unchanged where the grid cells were smaller. A remedy to this deficiency in the original method would be to replace I_o by

$$I_o^1 = \int\int\int \left[\left(\frac{r_\xi \cdot r_\eta}{\|r_\xi\|\|r_\eta\|}\right)^2 + \left(\frac{r_\xi \cdot r_\zeta}{\|r_\xi\|\|r_\zeta\|}\right)^2 + \left(\frac{r_\eta \cdot r_\zeta}{\|r_\eta\|\|r_\zeta\|}\right)^2 \right] d\xi\, d\eta\, d\zeta \tag{5}$$

Now the quotients in the integrand are the cosines of the angles between coordinate lines, and thus the integrand does not depend on the grid spacing.

V. <u>FINITE DIFFERENCE APPROXIMATIONS</u>: The elliptic system and grid optimization methods require the approximation of various derivatives and integrals. For comparison, the difference approximations for both methods will be presented here. A typical grid point will be denoted by using subscripts

$$r_{i,j,k} = (x_{i,j,k}, y_{i,j,k}, z_{i,j,k}).$$

The derivatives appearing in the elliptic equations (1) are approximated by the usual central difference expressions

$$r_\xi \approx \tfrac{1}{2}(r_{i+1,j,k} - r_{i-1,j,k})$$

$$r_{\xi\xi} \approx r_{i+1,j,k} + r_{i-1,j,k} - 2\, r_{i,j,k} \qquad (6)$$

$$r_{\xi\eta} \approx \tfrac{1}{4}(r_{i+1,j+1,k} + r_{i-1,j-1,k} - r_{i+1,j-1,k} - r_{i-1,j+1,k}).$$

With similar expressions for the remaining derivatives. Derivatives of the arc length parameter are required for the calculation of the control functions in (2). If the arc length is computed using a piecewise linear approximation of the grid line, then the central difference approximations yield

$$S_\xi \approx \tfrac{1}{2}(\|\Delta_\xi r_{i,j,k}\| + \|\nabla_\xi r_{i,j,k}\|)$$

$$S_{\xi\xi} \approx \|\Delta_\xi r_{i,j,k}\| - \|\nabla_\xi r_{i,j,k}\|$$

where

$$\Delta_\xi r_{i,j,k} = r_{i+1\,j,k} - r_{i,j,k}$$

$$\nabla_\xi r_{i,j,k} = r_{i\,j,k} - r_{i-1,j,k}.$$

The operators Δ_ξ and ∇_ξ are the standard forward and backward difference operators along the ξ coordinate line.

With the approximations given above, the quasilinear elliptic system (1) becomes a nonlinear system of algebraic equations. Program SVTGD3D uses a nonlinear version of line SOR to solve this system. Since only a small perturbation of the algebraic grid is desired, usually only a few iterations are performed.

The grid optimization method uses the difference approximations given in (6) together with the analogous one-sided approximations in the other two coordinate directions. A typical term in the integrand of I_o in (4) would be calculated from

$$(r_\xi \cdot r_\eta)^2 \approx \tfrac{1}{4}[(\Delta_\xi r \cdot \Delta_\eta r)^2 + (\Delta_\xi r \cdot \nabla_\eta r)^2 + \nabla_\xi r \cdot \Delta_\eta r)^2 + (\nabla_\xi r \cdot \nabla_\eta r)^2]$$

Here it is understood that the vector r is evaluated at (i,j,k). The purpose of averaging the various difference approximations is to give a symmetric expression for the integrand of I_o. The same general idea is used in the approximation of the integrand of I_v. The control function w must first be defined. Since this value is only a target volume, or Jacobian, which will not actually be realized by the final grid, we have simply used

$$w = (\|\Delta_\xi r\| \|\Delta_\eta r\| \|\Delta_\zeta r\|)^{-1}.$$

Now the Jacobian is defined in terms of derivatives so that the integrand of I_v is a second order differential expression. Before constructing the difference approximation, the assumption

$$(r_\eta \times r_\zeta)_\xi = (r_\xi \times r_\zeta)_\eta = (r_\xi \times r_\eta)_\zeta = 0$$

will be used to rewrite the integrand as

$$\left[(wr_\xi)_\xi \cdot (r_\eta \times r_\zeta)\right]^2 + \left[(wr_\eta)_\eta \cdot (r_\xi \times r_\zeta)\right]^2 + \left[(wr_\zeta)_\zeta \cdot (r_\xi \times r_\eta)\right]^2 \qquad (7)$$

This assumption eliminates the need to compute mixed derivative terms, and the integrand may be computed using only the nodal point $r_{i,j,k}$ and its immediate neighbors. Even with this assumption the difference expression is quite complicated, and the gradient of I(r) involves thirteen grid points. A typical term will be approximated using the average of forward and backward difference approximations as above. The j and k indices for w have been retained since different values are used depending on which of four cell faces is determined by the approximations for r_η and r_ζ. The difference expression for the first term in (7) is given by

$$\left[(wr_\xi)_\xi \cdot (r_\eta \times r_\zeta)\right]^2 \approx \tfrac{1}{4}\left\{\left[\nabla_\xi(w_{j,k}\Delta_\xi r)\cdot(\Delta_\eta r \times \Delta_\zeta r)\right]^2 \right.$$
$$+\left[\nabla_\xi(w_{j,k-1}\Delta_\xi r)\cdot(\Delta_\eta r \times \nabla_\zeta r)\right]^2$$
$$+\left[\nabla_\xi(w_{j-1,k}\Delta_\xi r)\cdot(\nabla_\eta r \times \nabla_\zeta r)\right]^2$$
$$\left.+\left[\nabla_\xi(w_{j-1,k-1}\Delta_\xi r)\cdot(\nabla_\eta r \times \nabla_\zeta r)\right]^2\right\}.$$

The other approximations are obtained by a permutation of the variables ξ, η, and ζ.

With all the derivatives in (4) approximated by differences, the next problem is to seek a minimum value for the functional I(r) which is now a nonlinear function of a finite number of variables. The method used here is

the same as that used by Kennon and Dulikravich [1]. The minimum value is found using the Fletcher-Reeves conjugate direction method for solving unconstrained optimization problems. However, the computational steps had to be modified to incorporate a more general functional I(r). This led to convergence problems which have not been resolved at this time.

VI. COMPUTATIONAL EXAMPLES: Several two- and three-dimensional grids have been constructed to verify the numerical algorithms which were developed during this project. Most of the two-dimensional work was performed on the IRIS Graphics Workstation. However, no hard copies could be made. All the described methods were used in the solution of a model three-dimensional problem, and those results will be presented here.

The physical region for the grid problem consists of a finite circular cylinder with a bullet-shaped object imbedded in one end. A screen is located about midway down the cylinder. The objective is to construct a grid with grid points concentrated at the screen and at the imbedded object. An algebraic grid was available. It was constructed using SVTGD3D, and two perspective plots are given in Fig. 1. The grid along a cross-section plane

indicates considerable skewing of the grid along the sides of the bullet. The problem area is indicated in Fig. 2. A good smoothing algorithm would be one which reduces the excessive skewness, smooths out some of the sharp corners of the grid lines, and leaves the distribution of grid points relatively unchanged near the bullet and the screen. The motivation for this research project becomes clear when the system (1), with P=Q=R=0, is solved. The resulting grid, as plotted in Fig. 3, is indeed smooth and more orthogonal. However, the original distribution of grid points is lost. Since SVTGD3D contains an option for using the control functions of Thomas and Middlecoff, a grid using those functions was also constructed and is plotted in Fig. 4. Although the distribution is loosely maintained, there is a considerable difference in grid spacing along the bullet. This is due to the fact that the curvature is not considered. Curvature terms were included in another paper by Thomas [2] but they have not been considered in this report. The control functions used by Thomas and Middlecoff [3] are roughly equivalent to using the functions defined in equation (2). The improvement in spacing along the bullet when the terms from (3) are added to those in (2) is clearly evident in Fig. 5 where the complete set of control functions P, Q, and R developed in Section III have been computed at every interior point.

Only a preliminary partially converged solution can be presented for the grid optimization method. The method used to solve the optimization problem had to be modified so that integrals like those in equation (5) could be incorporated in the objective function. A grid constructed using I_o and I_v in equation (4) with α=.75 is indicated in Fig. 6. Due to convergence difficulties, the optimization method was only applied to the half of the grid near the bullet. Note that the grid has changed, but the change is hardly noticeable where the grid spacing is small. In contrast, the grid in Figure 7, which uses I_v and the value of I_o' from equation (5), exhibits a much higher degree of orthogonality near the surface of the bullet. This grid was also computed using α=0.75. For smaller values of α, the grid lines would cross and some of the grid points would fall outside of the physical region.

VII. <u>RECOMMENDATIONS</u>: Despite the difficulties that were encountered using the method, we believe that the grid optimization method has a lot of potential not only for solving the gridding problems considered here but also in the construction of solution-adaptive grids. Therefore, work should continue on the application of the Fletcher-Reeves algorithm, or possibly some new technique, in the

solution of the grid optimization problem for a general class of objective functions. Once the optimization method is perfected, a test problem in computational fluid dynamics should be solved on an algebraic grid, a grid smoothed by an elliptic system, and a grid computed using the optimization method. An analysis of results should indicate which grid generation method gives the greatest improvement in accuracy and the degree to which grid properties such as smoothness and orthogonality affect the accuracy of the numerical solution. These results should be helpful in the development of adaptive grid methods which is a rapidly growing area of current research in the field of grid generation.

<u>REFERENCES</u>

1. S. R. Kennon and G. S. Dulikravich, "A Posterior Optimization of Computational Grids", AIAA Paper 85-0483, AIAA 23rd Aerospace Sciences Meeting, January 1985, Reno, Nevada.

2. P. D. Thomas, "Numerical Generation of Composite Three-Dimensional Grids by Quasilinear Elliptic Systems", <u>Numerical Grid Generation</u>, (J. F. Thompson, ed.), Elsevier/North-Holland, New York, 1982.

3. P. D. Thomas and J. F. Middlecoff, "Direct Control of the Grid Point Distribution in Meshes Generated by Elliptic Equations", <u>AIAA Journal 18</u>, 1980, 652-656.

4. J. F. Thompson, Z.U.A. Warsi, and C. W. Mastin, <u>Numerical Grid Generation</u>, Elsevier/North-Holland, New York, 1985.

5. B. K. Soni, "Two and Three-Dimensional Grid Generation for Internal Flow Applications of Computational Fluid Dynamics", AIAA Paper 85-1526, AIAA 7th Computational Fluid Dynamics Conference, July 1985, Cincinnati, Ohio.

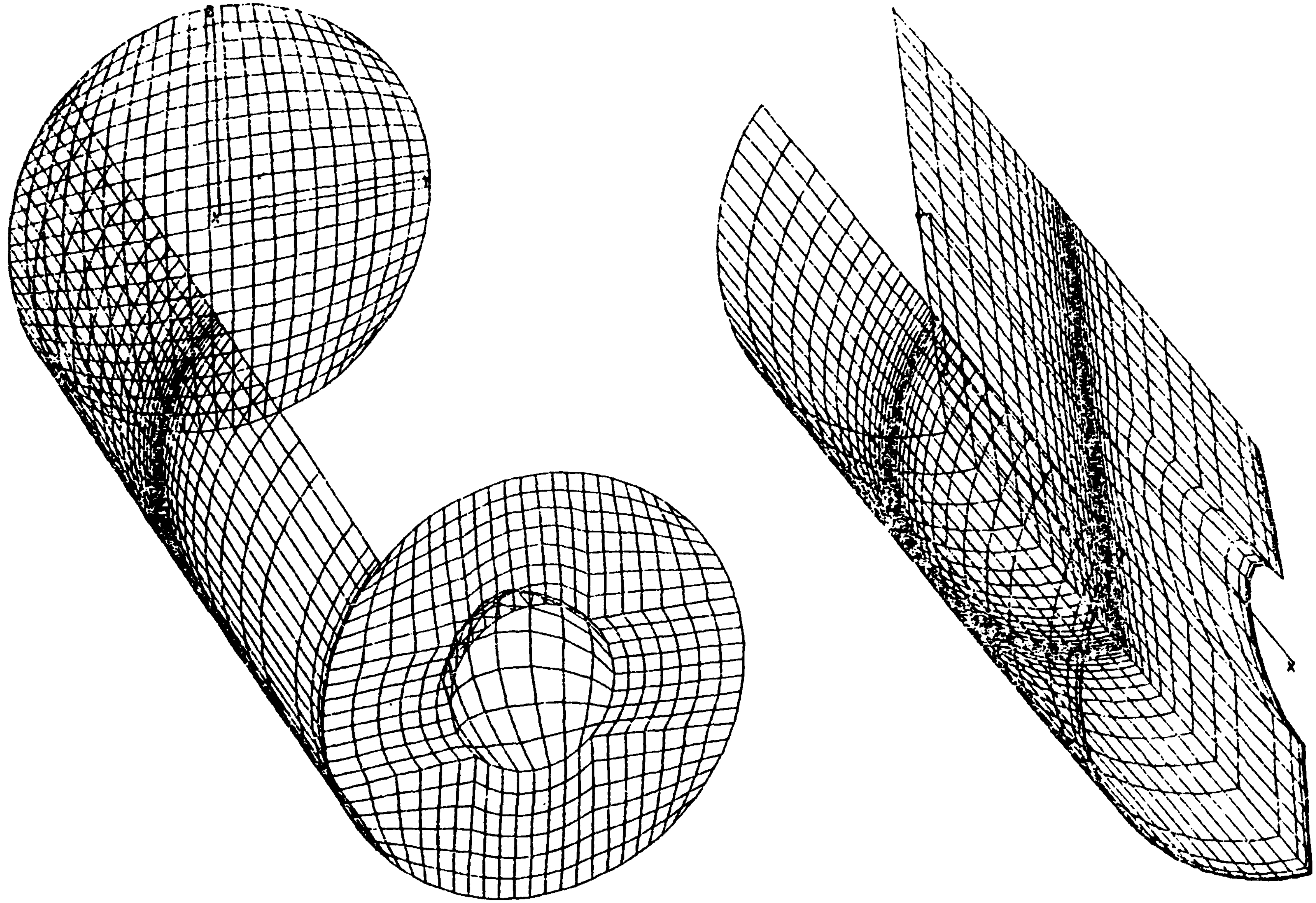

Figure 1. Perspective plots of original grid

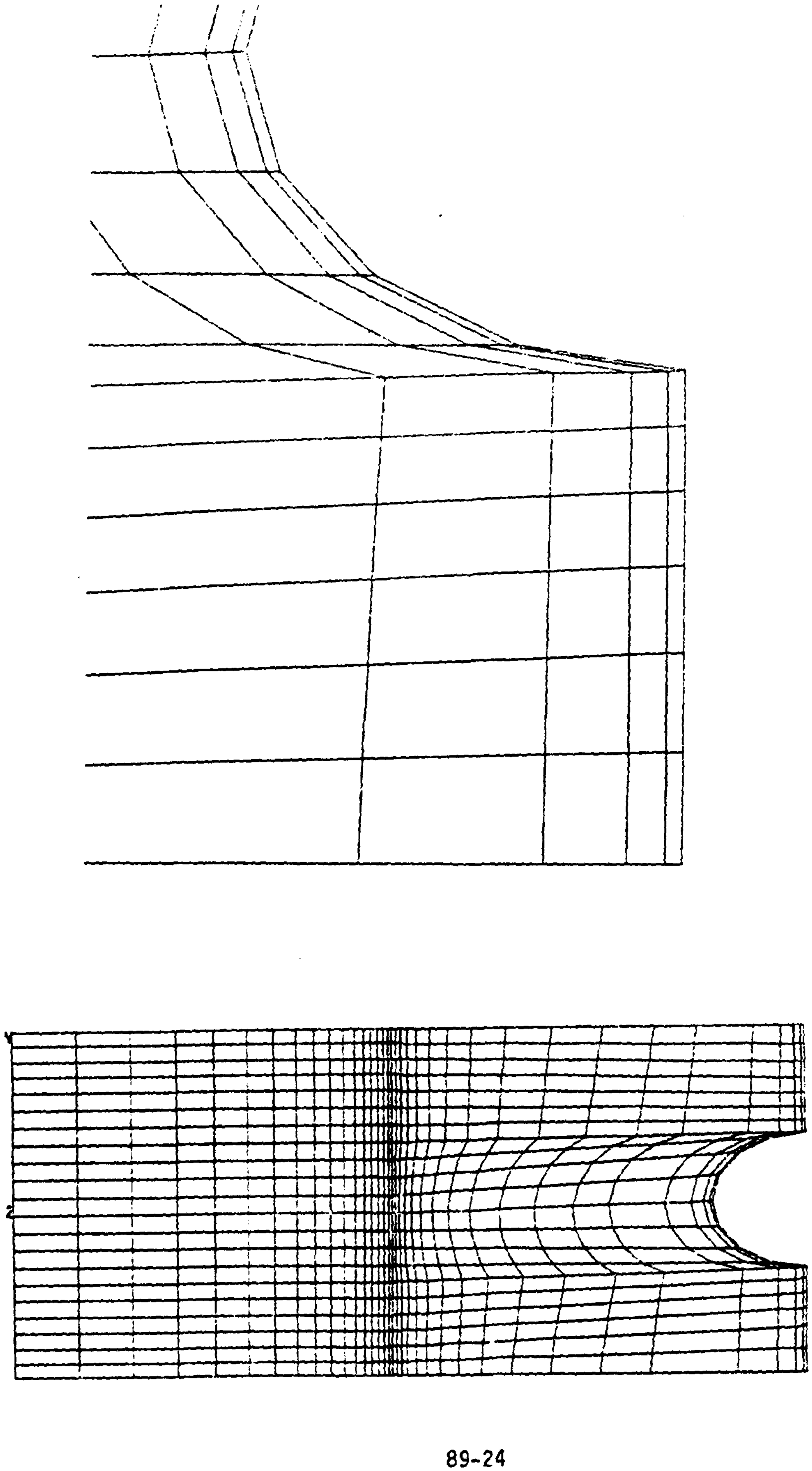

Figure 2. Cross section plots of original grid

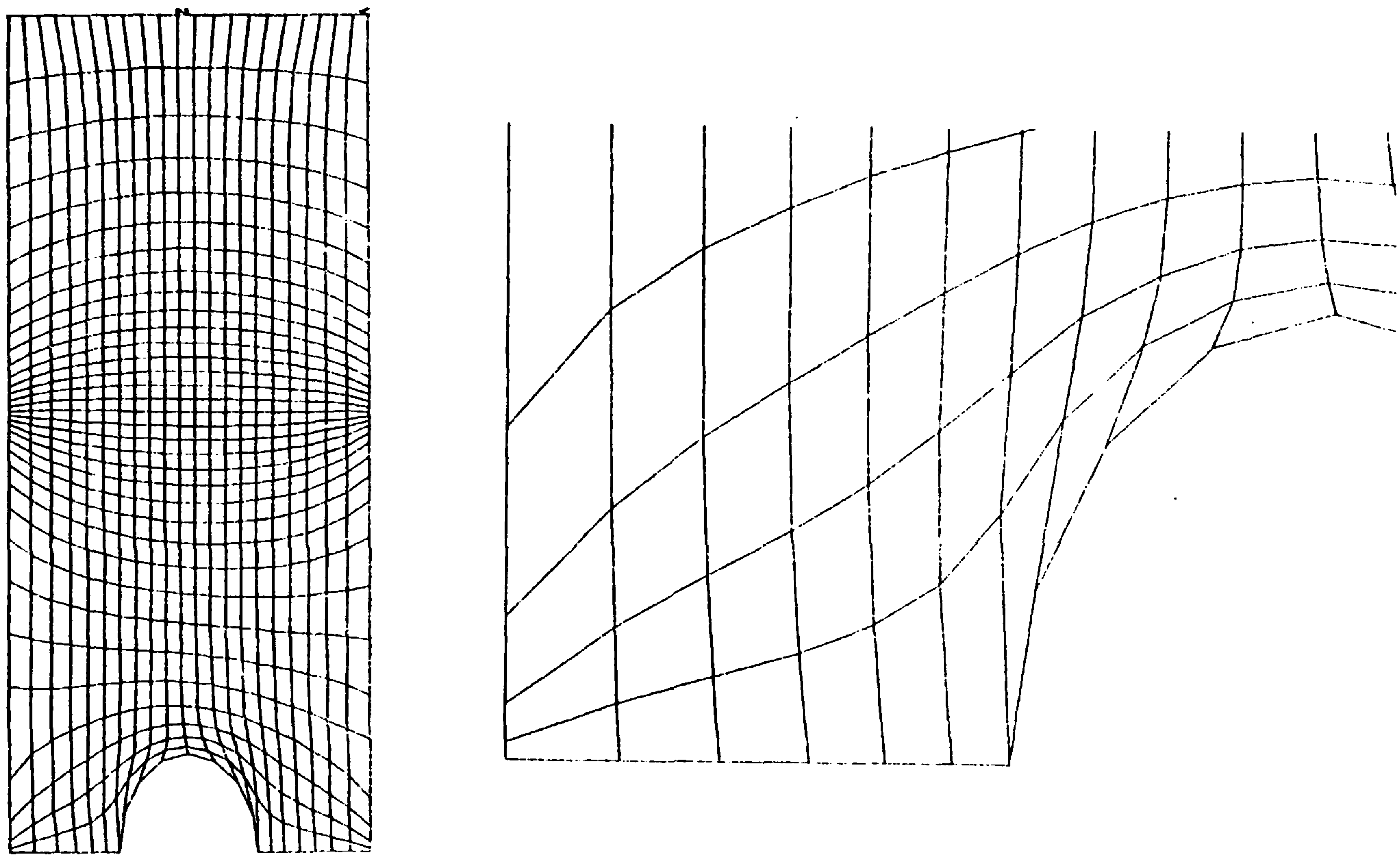

Figure 3. Cross section plots of grid smoothed by elliptic system with zero control functions

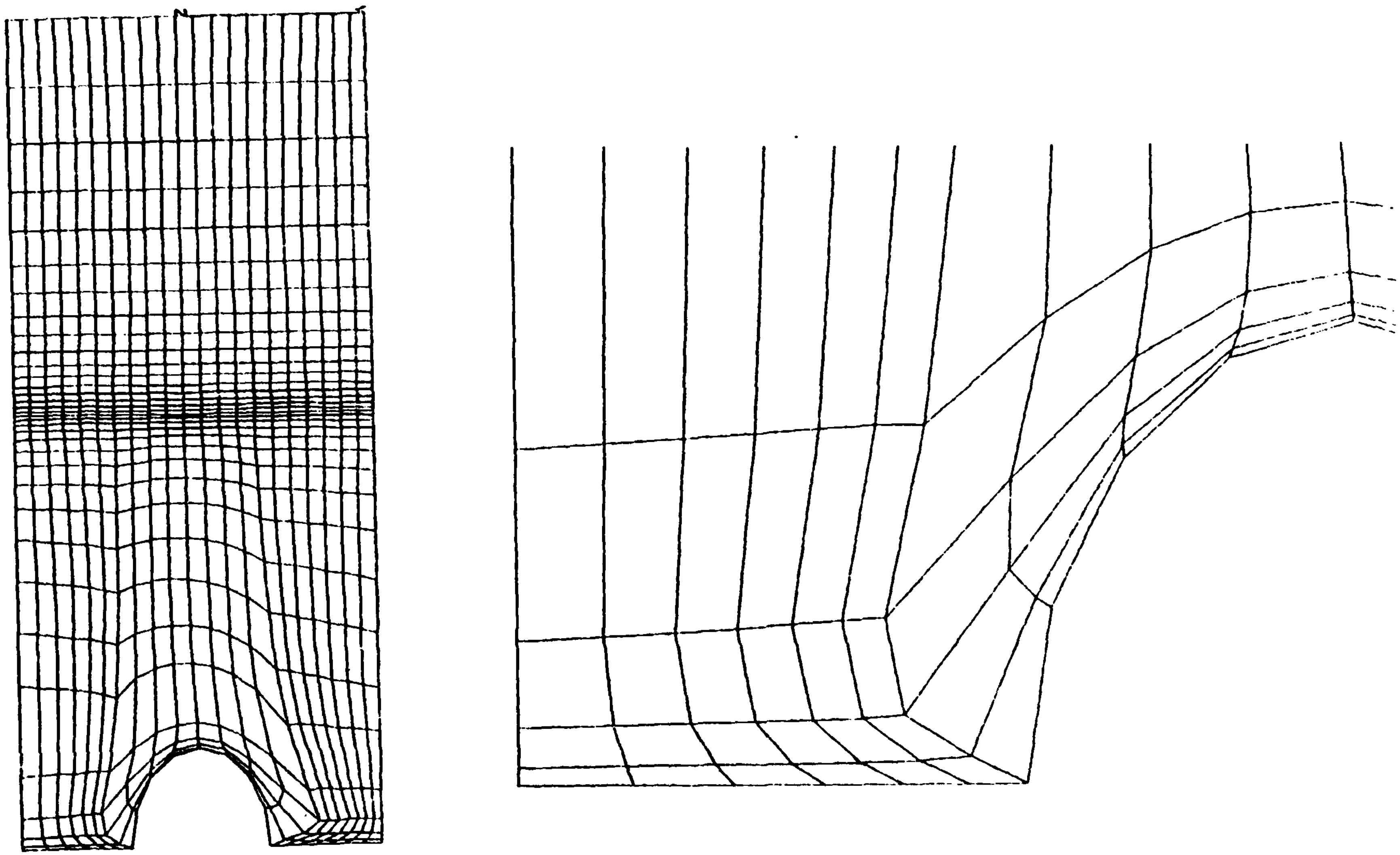

Figure 4. Cross section plots of grid smoothed by elliptic system with control functions of Thomas and Middlecoff[3]

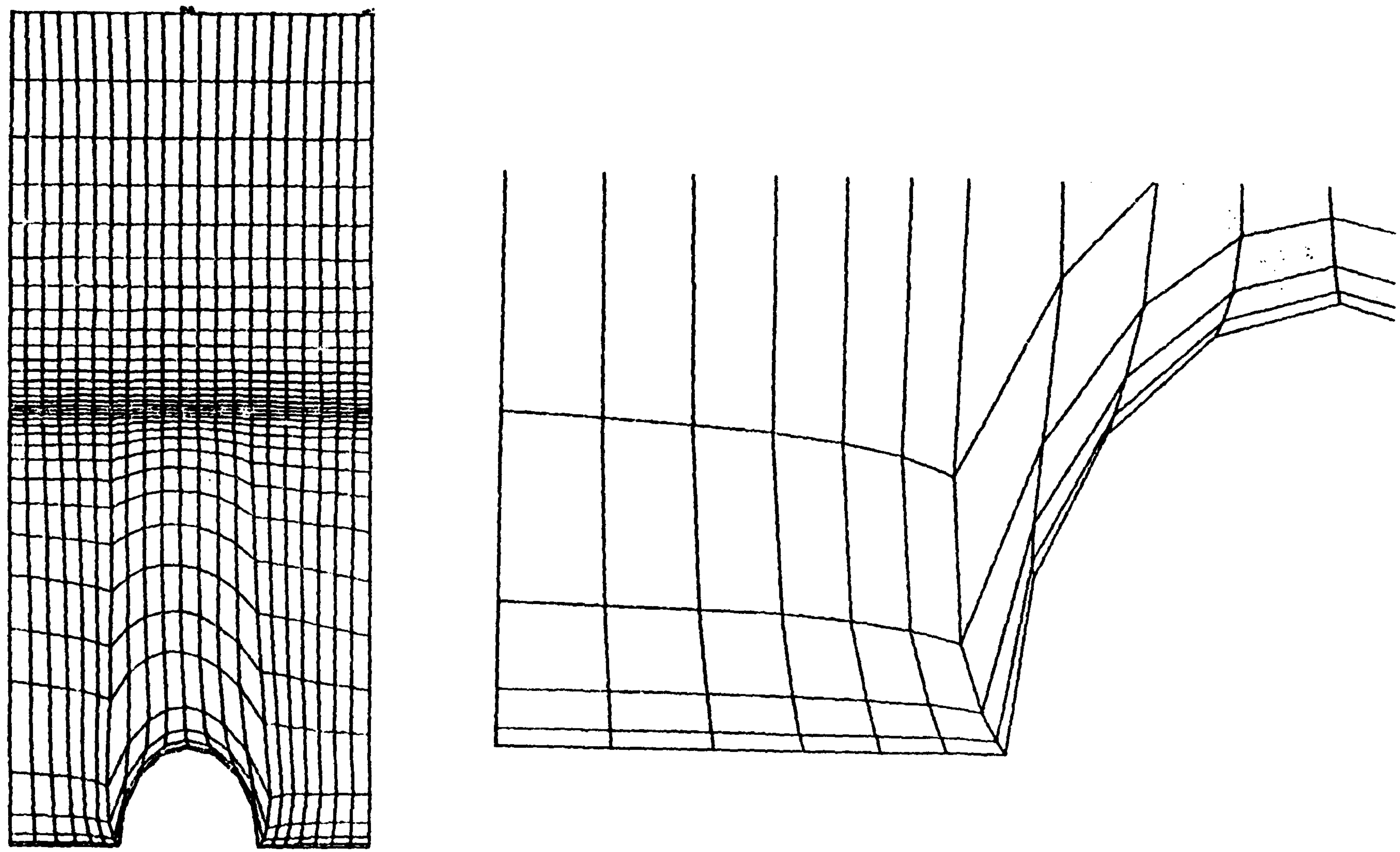

Figure 5. Cross section plots of grid smoothed by elliptic system with new control functions

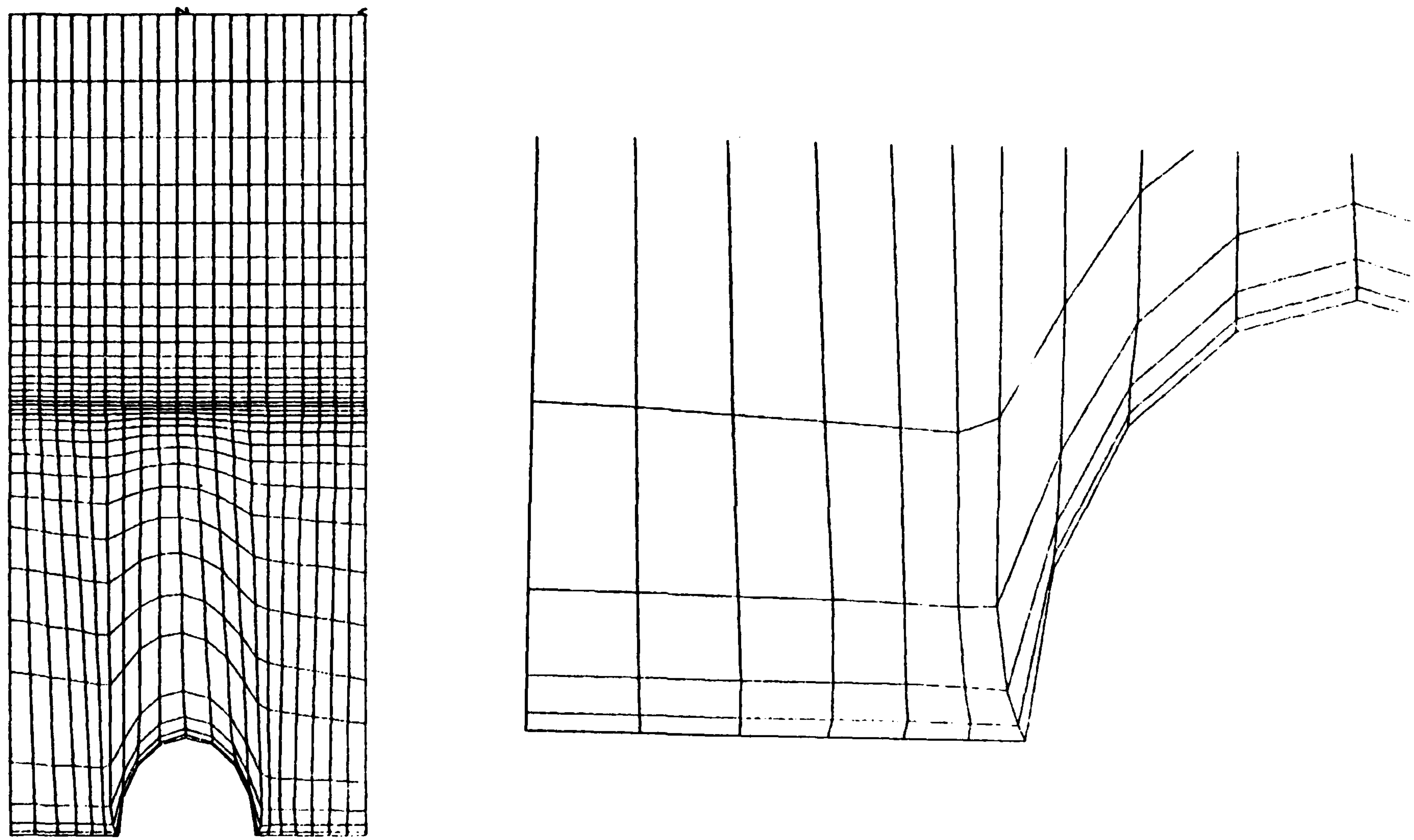

Figure 6. Cross section plots of grid after optimization with volume control

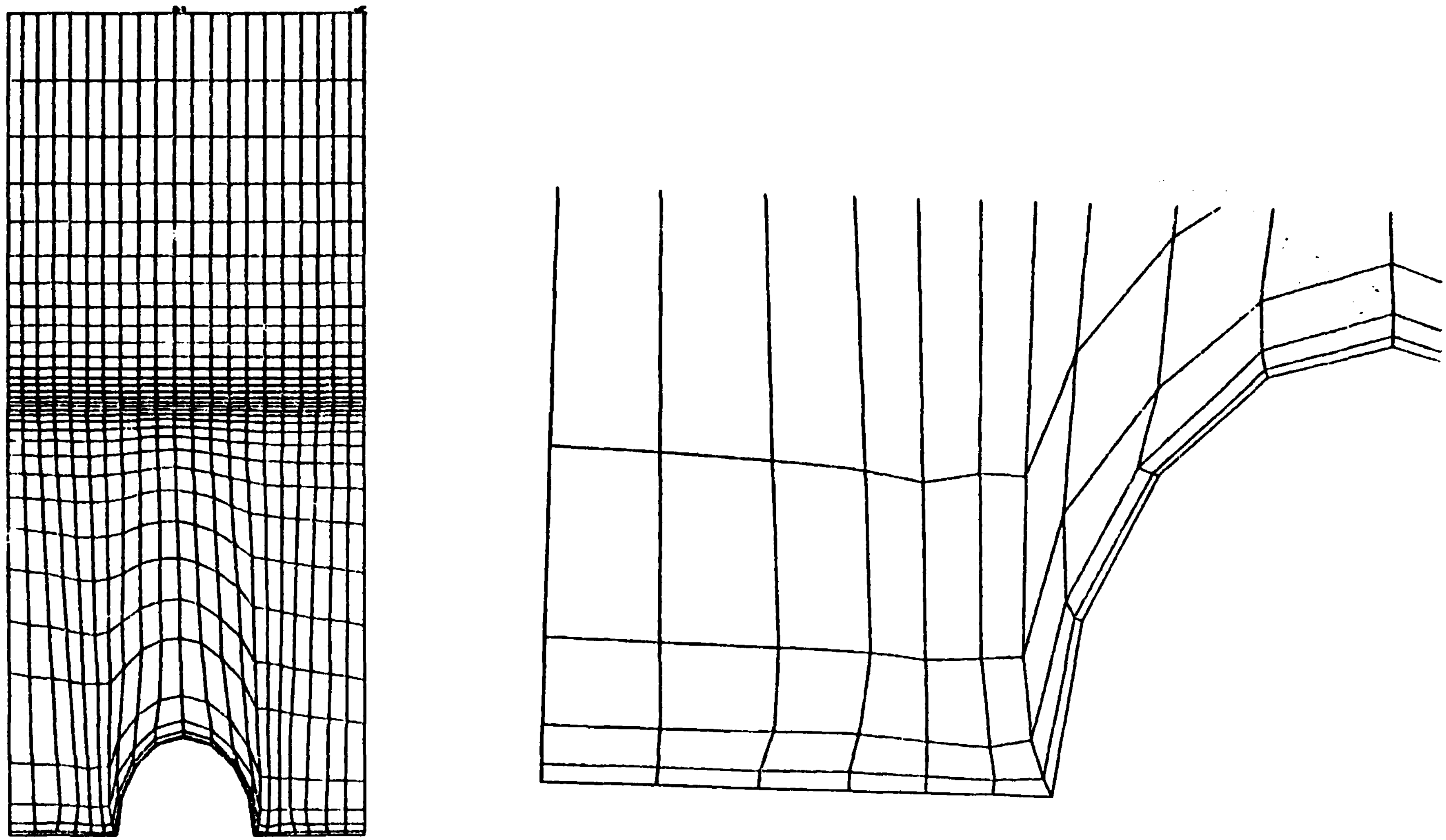

Figure 7. Cross section plots of grid after optimization with volume control and normalized orthogonality measures

1985 USAF-UES SUMMER FACULTY RESEARCH PROGRAM/

GRADUATE STUDENT SUMMER SUPPORT PROGRAM

Sponsored by the

AIR FORCE OFFICE OF SCIENTIFIC RESEARCH

Conducted by the

UNIVERSAL ENERGY SYSTEMS, INC.

FINAL REPORT

ACTIVE MODE-LOCKING TECHNIQUES
FOR ULTRA-SHORT PULSES IN Nd:YAG LASERS

Prepared by:	Dr. Odis P. McDuff
Academic Rank:	Professor
Department and University:	Electrical Engineering Department The University of Alabama
Research Location:	Air Force School of Aerospace Medicine, Clinical Sciences Division
USAF Research:	Dr. John Taboada
Date:	September 23, 1985
Contract No:	F49620-85-C-0013

ACTIVE MODE-LOCKING TECHNIQUES FOR ULTRA-SHORT PULSES IN Nd:YAG LASERS

by

Odis P. McDuff

ABSTRACT

Active mode locking of an actively Q-switched cw Nd:YAG laser was accomplished and the laser's operating characteristics studied. Two-photon fluorescence and second harmonic enhancement were used in the characterization process. The two-photon-fluorescence technique was studied for operation at high cw power levels where thermal effects normally would be a problem. Intracavity etalon effects were considered. The behavior of the pulsed output in the time domain relative to the mode-locker drive signal was studied and related to a possible stabilization precedure.

A scheme was suggested for the attainment of a very stable, but yet relatively simple, synchronously pumped pulsed dye laser.

Acknowledgement

The author would like to thank the Air Force System Command, the Air Force Office of Scientific Research, the Air Force School of Aerospace Medicine, and Universal Energy Systems, Inc. for providing him with the opportunity to spend a very worthwhile and interesting summer at the Air Force School of Aerospace Medicine, Brooks AFB, Texas. He would like to thank the School, and in particular the Clinical Sciences Division, for its hospitality and provision of excellent working conditions.

Finally, the author would like to thank Dr. John Taboada for suggesting this area of research and for his many helpful comments. He would also like to acknowledge the excellent work of Mr. Heinz Jaeger of the School's Machine Shop and the excellent technical assistance of Staff Sgt. Mario Villanea.

I. INTRODUCTION

The Air Force School of Aerospace Medicine (SAM) is interested in non-invasive studies of the eye by the use of optical pulses short enough that physical mechanisms other than thermal effects come into play.[1,2] Stability of the system and reproducibility of the pulses is of paramount importance in work of this nature.

The mode-locked laser, first reported in 1964,[3] provides a means for producing short optical pulses. Since 1964, workers in the field have produced shorter and shorter pulses and used various combinations of active and passive elements within the optical cavity for Q-switching and/or mode locking of various types of lasers.

Simultaneously Q-switched and mode-locked Nd lasers using a saturable absorber for both the Q-switcher and mode-locker produce short, high peak power pulses but tend to have large shot-to-shot variations in pulse width and energy. The use of the colliding pulse technique[4] in an antiresonant ring cavity[5] has been shown to provide shorter and more stable pulsing in a passively Q-switched and mode-locked Nd:YAG laser.[6] A number of active-passive systems have been described[7] in which the Q-switching was done passively and the mode locking done actively.

In the case of a cw Nd:YAG laser, the Q-switching must be done actively but the mode locking could be done either actively or passively. The colliding-pulse, antiresonant cavity mode-locking scheme, with its potentially greater stability over other passive mode-locking schemes and its possibility of producing shorter pulses than active mode locking, seemed a good candidate for the production of a stable pulsed source derived from an actively Q-switched Nd:YAG laser and was

the subject of an experimental investigation by the author during the Summer of 1984.[8] The laser used was a Laser Application Inc. Model 9560T actively Q-switched cw Nd:YAG laser. The conclusion reached was that the laser gain was too low to use saturable absorber mode locking with the mirrors available. Furthermore, there is some doubt whether the active Q-switched, passive mode-locked antiresonant scheme would have been stable enough for the SAM application, based upon the previous work with non-cw Nd:YAG lasers.[6]

Potentially, the active Q-switched active mode-locked system, followed by harmonic doubling, is the most stable configuration. Previous work has shown the mode-locked pulses not to be as short as with passive mode locking; however, regenerative amplification and pulse compression techniques[9,10] could be used to increase the pulse amplitude and reduce pulse width. Furthermore the active mode locking system permits the use of an active stabilization procedure developed by the author.[11] This work and the author's previous experience with active mode locking[12,13] indicated that active mode locking of the Nd:YAG laser would make it a good candidate for the production of a stable pulsed source. The author's effort was directed toward this goal during the period of this research program.

II. OBJECTIVE

The main objective of this work was to actively mode-lock an actively Q-switched cw Nd:YAG laser and to characterize its performance. Included was the determination of whether active stabilizations[11] could be applied.

The laser to be used in the work was a Laser Application Inc.

Model 9560T actively Q-switched cw Nd:YAG laser which had been placed into operation during the author's previous Summer's work at SAM. The construction of this laser, with the various components being mounted on an optical bench and removable, was such that it was a very flexible research tool.

Since the short ten-week length of the project gave no time to order and purchase items other than incidental supplies, a constraint placed upon the project was that items already available in the laboratory would have to be used. Fortunately the excellent machinist support at SAM made it possible to have special hardware fabricated very quickly. The author furnished an acousto-optic mode locker which was purchased under a USAF-SCEEE grant.[11]

III. THE BASIC LASER

The Laser Applications Model 9560T Nd:YAG laser came equipped with a 3mm x 79mm rod having parallel AR coated end faces. This rod was pumped with a Krypton arc lamp, with the rod and lamp mounted in a water-cooled elliptical gold-plated pump cavity. In the later stages of the work the rod was replaced by a similar one having the faces wedged 30' with respect to each other. The laser cavity mirrors were flat, one with a high reflectivity coating and the other with a 10% transmission coating on the interior surface and AR coating on the exterior surface. Removable 0.041 inch diameter apertures were located at either end of the cavity. An electromagnetic shutter and Brewster polarizer were toward one end of the cavity while a water-cooled acousto-optic Q-switcher was near the other end. The RF drive to the Q-switcher was at 24 MHz and could be pulsed on and off

to obtain various Q-switching rates between 500 Hz and 30 KHz. The photo diode mounted at the high reflectivity mirror for monitoring the temporal behavior of the Q-switched pulse was replaced by a high speed photo diode for monitoring the mode locking. The polarizer, normally set at the factory at the polarization direction which gives maximum power output,[14] was rotated to give horizontal polarization. The original optical length between the two cavity mirror reflecting surfaces was measured as approximately 73 cm.

Typical TEM_{00} performance with all elements in the cavity but with the Q-switch drive off was a cw power of 8 watts. Typical Q-switched performance gave 200-nsec wide Q-switched pulses at a repetition rate of 8 KHz and an average output power of 6 watts.

IV. THE MODE LOCKER

An IntraAction model ML-75C acousto-optic mode locker was used in the work. It was constructed of a fused quartz block to which was bonded a lithium niobate transducer. Acoustic resonances were measured by the manufacturer to be at 74.570, 75.041, and 75.523 MHz (The design target specified in the purchase order for the mode locker was 75 MHz ± 1 MHz for the center frequency.) Its diffraction efficiency at 1.06 μm was 50% at a RF drive power of 1.75 watts. The manufacturer's specifications gave a maximum design drive power of 5 watts with water cooling and a temperature sensitivity of the acoustic resonance of 7 KHz/°C. The static optical insertion loss was less than 3% and the windows were wedged at 1°, with high power AR coatings. The overall RF bandwidth of the mode locker was approximately 15% of center frequency.

The mode locker was purchased by the author under support of a

USAF-SCEEE grant[11] in preparation for the Summer research program. In making this purchase an important parameter to be selected was the acoustic drive or resonant frequency. The effective modulation frequency at which the acoustically produced diffraction grating is established and reestablished is twice the RF drive frequency to the acoustic transducer, since the grating results from the acoustic standing wave and is dependent on instantaneous acoustic power. For active mode locking, this effective modulation frequency has to be equal to the c/2L longitudinal mode spacing frequency of the laser.[3] Since the pulse width tends to be a certain fraction of the pulse period in the mode-locked laser, an increase in the c/2L and hence the modulation frequency and pulse repetition rate would produce shorter pulses.[12,15,16] This means shortening the laser cavity length but there were physical limitations as to how short the cavity of the model 9560T laser could be made and still include all the necessary intracavity elements. One also had to be careful that the addition of intracavity elements did not make the cavity too long because based upon the previous Summer's work, this could lead to increased diffraction losses and the accompanying decrease in excess gain and output power (the laser had flat mirrors and therefore had no focusing action present in the cavity.). A modulation frequency of 150 MHz was selected and the mode-locker specified accordingly in making the purchase.

V. INITIAL OPERATION OF SYSTEM

The first step in putting the system into operation was to lengthen the cavity to give a c/2L frequency of 150 MHz. This was done approximately by measuring the physical length and estimating the

foreshortening effects of the rod, Q-switcher, mode-locker, etc. Later, based on the dynamic mode-locked performance the length was "fine-tuned." The mode-locker needs to be near one of the end mirrors to maximize its effect[12] and therefore was placed near the high reflectivity mirror, near the Q-switcher. This necessitated the removal of the rear aperture to give sufficient space. A holder for the mode-locker was fabricated by the machine shop, using a Daedal lens holder as a starting point. The alignment of the cavity with the mode-locker in place proceeded with a minimum of difficulty, the major cavity mirror readjustment being due to the wedging of the mode-locker. Orienting the mode-locker at the 0.64° Bragg angle caused beam offset but it did not cause alignment problems because the cavity mirrors were flat.

The laser output mirror was mounted on a translation-stage mirror holder constructed by the machine shop, with a micrometer head drive so that fine adjustments could be made in cavity length. This was done to facilitate the study of the effect of the differences between the mode-locker modulating frequency and the c/2L frequency, as noted in a later section. In order to match the 75.041 MHz resonance of the mode-locker (the effective modulation frequency is at twice that value as noted in Section IV, or 150.082 MHz) to the c/2L of the laser, precise adjustments in cavity length had to be made. An increase in laser cavity length of 10μm will give a calculated decrease in the c/2L frequency of 1.5 KHz,[17] which can be important when doing active mode locking.

A Boonton model 3200A oscillator, amplified by an Electronic Navigation Industries high-gain, high-power amplifier was used to drive the mode locker. The drive frequency was monitored with a

Sabtronics 8610A frequency counter. It was necessary to leave the Boonton oscillator and Sabtronics counter running 24 hrs a day during the course of the Summer work, in order to prevent frequency drift from becoming a problem. A high bias voltage, high speed fiber optic photo diode, EG&G model FOD 100, was used so that a Tektronix oscilloscope model 519 could be used. The diode was mounted directly on the oscilloscope input terminal, with an optical fiber bringing the optical pulses from the laser at the back or high reflectivity mirror.

Mode locking with Q-switching was readily obtained with performance characteristics generally as expected.[12,15,16] The laser jumped in and out of mode locking as the mode-locker drive frequency was varied about the c/2L frequency. As the mode-locker effective modulating level was increased, the laser initially produced better and better mode locking and then the laser power output decreased as the mode-locker level was increased further, eventually resulting in the extinguishing of the laser. Mode locking without Q-switching was observed but with a poorly shaped pulse. This performance was more sensitive to detuning of the mode-locker drive frequency as expected.

A photograph of the experimental setup is shown in Fig. 1 with a two-photon-fluorescence ring in the left foreground.

VI. SHIFT OF PULSE RELATIVE TO MODULATOR DRIVE SIGNAL

The location of the mode-locked pulse in the time domain, relative to the phase of the mode-locker drive signal, was shown to be dependent upon the frequency of the drive in an early experimental study with loss modulation.[18] A nonlinear theoretical analysis of an inhomogeneously broadened loss-modulated laser[12] and experimental work

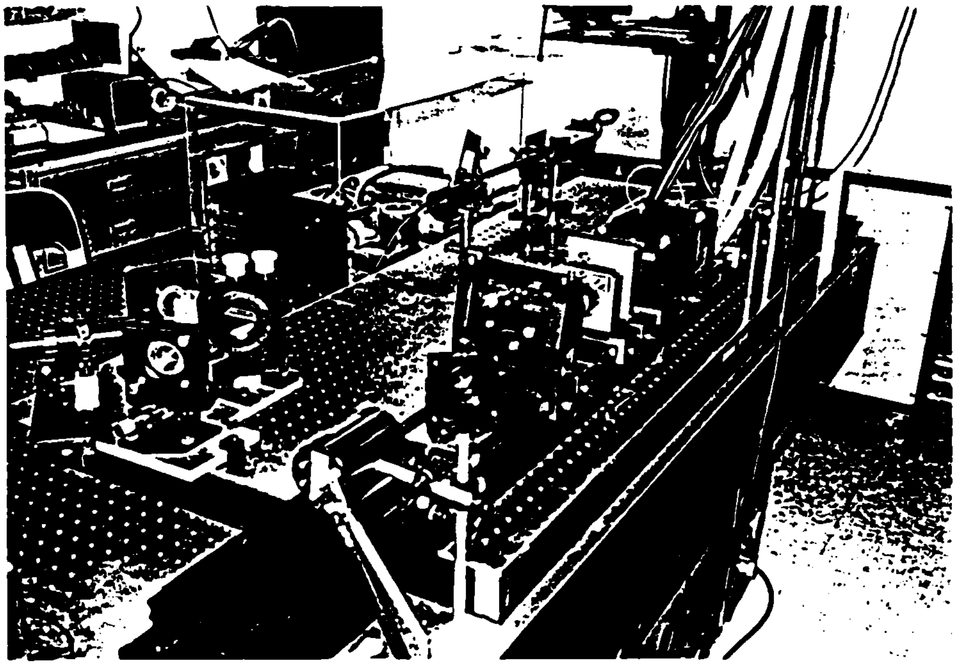

Fig. 1. Photograph of the experimental setup

with an argon loss-modulated laser[19] (argon is largely inhomogeneously broadened) showed the effect to occur. A linearized theory[15] for the homogeneously broadened laser predicted the effect to occur with phase modulation and experimental work showed the effect to occur in a phase-modulated Nd:YAG laser[20,16] (Nd:YAG is largely homogeneously broadened). The effect was predicted to occur in a computer simulation by the author for a homogeneously broadened loss-modulated laser also.[11]

Prior to the work reported here it had not been shown experimentally whether the location of the pulse in the time domain depended upon the modulating frequency in the case of a homogeneously broadened loss-modulated laser such as Nd:YAG. Since the effect, should it occur, would permit the implementation of a feedback stabilization scheme,[11] it was of interest to pursue the matter.

Detuning of the modulator drive frequency from the c/2L was accomplished in two ways. First, the drive frequency was varied, holding the cavity length constant. This procedure was not completely satisfactory because the necessary variation in frequency was a significant fraction of the acoustic resonance bandwidth. Also, electrical phase shift can occur because of the resonance itself and the cable lengths. In the second procedure the drive frequency was held constant and the length of the laser cavity was varied by moving the translation-stage-mounted mirror. Shift of the pulse under Q-switched conditions was noted qualitatively but was difficult to measure. Shown in Fig. 2 are curves showing the experimental non Q-switched results. The data were taken by using a dual-trace oscilloscope to display both the pulse and the modulator signal simultaneously, triggering with the modulator signal. The results

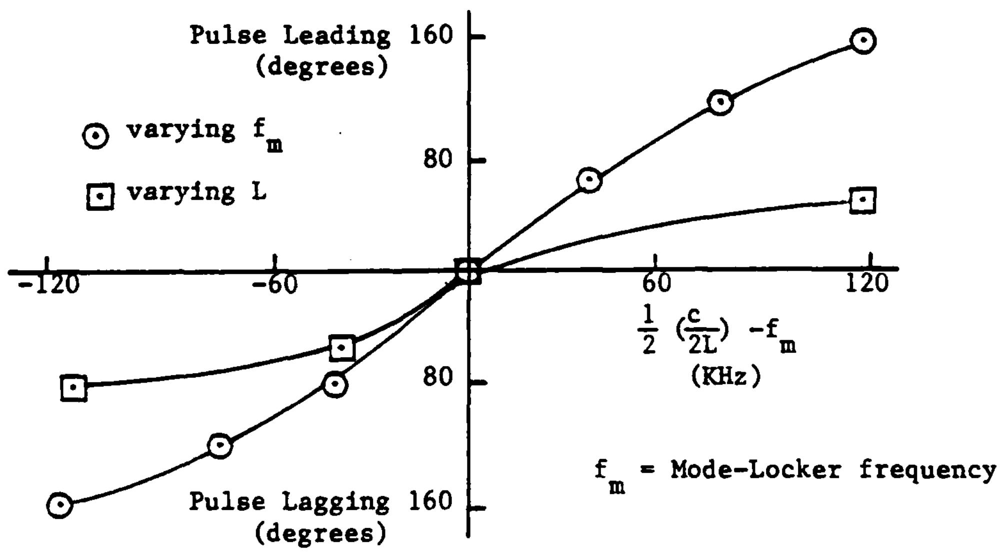

Fig. 2. Effect of detuning the mode-locker from c/2L.

indicate that the stabilization scheme proposed by the author should work with a Nd:YAG laser also, as it did with an Argon laser.[11]

VII. TWO-PHOTON-FLUORESCENCE MEASUREMENTS

Since the high speed photo-diode detector and Tektronix 519 oscilloscope combination was not fast enough to measure the pulse width satisfactorily, effort was directed toward the use of the well known two-photon-fluorescence (TPF) technique of Giordmaine et al.[21] An antiresonant ring cavity[5] used in the colliding pulse[4] work of the previous Summer[8] by the author was modified for use in this work. Since the pulsing pattern as seen using the photo-diode oscilloscope setup was stable on a cw basis, indicating that the pulse pattern was highly repeatable, the TPF measurement also was attempted cw. The laser output beam was directed by a 50% beam splitter into the TPF ring and a solution of Rhodamine 6G dye in ethanol was used in the TPF cell. The plan was to use a Reticon photo-diode array to observe the TPF pattern width and thus a relatively high-level fluorescence signal was desired. Visual observation indicated that a large amount of thermal self-defocusing[22] was occurring in the dye cell. In addition, attenuation of the laser signal due to absorption as it progresses through the cell can reduce the measured peak-to-background contrast ratio.[23]

A beam-expanding telescope was designed using existing lenses so that the optical intensity in the TPF cell could be reduced but yet a high overall fluorescence maintained. This telescope, fabricated by the machine shop, gave a beam magnification of 6. In addition, an extensive study was made to determine the optimum dye concentration for maximum fluorescence output. The work indicated that a high-beam-intensity TPF system using a conventional liquid dye cell would not succeed.

Attention was directed toward the fabrication of a thin, high-

intensity-tolerant cell that could be scanned through the pulse overlap region in the TPF type ring.[24] The fluorescence output was focused into an optical fiber which fed the optical output to a very sensitive photon counter. The head including the focusing lens and fiber input rode along with the cell as it was scanned through the pulse overlap region.

The basic problem was to obtain a thin, damage-resistant cell. A thin liquid dye solution did not work because the beam immediately vaporized the liquid and formed a bubble. Several mixtures of dye solutions (both ethanol and methanol were used as the solvent) with various glues, acrylic resins, etc of various thicknesses were tried. A successful sample was prepared by placing several drops of Ross Household Cement on a microscope slide and mixing in a few drops of a solution of Rhodamine 6G in ethanol. The mixture was permitted to harden in air for 30 minutes and then a second microscope slide was placed on top and the assembly permitted to harden for several days under light pressure.[25] This sample produced a readily measurable fluorescence when placed in the ring, and withstood the beam without damage during runs over an hour long.

Alignment requirements were fairly stringent since the track over which the sample moves must be parallel to the path of the beam, so that the beam illiminates the same portion of the sample as it is scanned. Time was not available to satisfactorily complete the study of this technique but preliminary results indicated that the procedure would work. Peak to background ratios of about 1.7 were the best achieved.

VIII. SECOND HARMONIC ENHANCEMENT

Using the approximate techniques of DiDomenico et.al.,[26] it is possible to estimate the optical pulse length from the enhancement of the second harmonic generation produced by the laser beam when going from unlocked (mode locker drive power equal to zero) to mode-locked conditions. In this work a KDP second harmonic generator was used and the harmonic at 0.53μm was separated from the straight-through 1.06μm beam by means of a polarizer and a filter. A second harmonic enhancement of 10 was measured, using a calorimeter to measure average harmonic power. The average fundamental laser power when locked was 3 watts and the mode-locker drive power was 1.2 watts.

The pertinent equation, which can be used to determine the number of mode-locked modes, is[26]

$$R = \left(\frac{2N_2^2 + 1}{3N_2} \Big/ B\,\frac{2N_1 - 1}{N_1}\right)\left(\frac{P_{1,L}}{P_{1,U}}\right)^2 \tag{1}$$

where

- R = ratio of mode-locked to unlocked average harmonic power
- N_2 = number of mode-locked modes, assumed equal in amplitude
- N_1 = number of uncorrelated modes when unlocked
- B = parameter which depends on amplitude distribution of unlocked modes (=1 for equal amplitudes)
- $P_{1,L}$ = average fundamental power when locked
- $P_{1,U}$ = average fundamental power when unlocked

In using this equation it was assumed that $N_1 = N_2 = N >> 1$ and that $B = 1$. Then, one has

$$N = 3R\,\left(\frac{P_{1,U}}{P_{1,L}}\right)^2 \tag{2}$$

with the measured values of $R = 10$ and $P_{1,U}/P_{1,L} = 1.4$, one obtains

N = 60 modes, giving an oscillating linewidth of $\Delta\nu_{osc}$ = (60)(150 MHz) = 9 GHz. Then, using the pulse-width equation of DiDomenico et.al.,

$$\tau = \frac{3}{\pi}\frac{1}{\nu_{osc}}, \tag{3}$$

one obtains a pulse width of 106 p sec. Interestingly, this agrees almost exactly with a calculated pulse width resulting from a computer simulation.[11]

IX. ETALON EFFECTS

Fabry-Perot etalons are commonly used inside laser cavities for axial mode selection. Also it is possible to use an etalon inside a mode-locked laser to reduce the system bandwidth, which lengthens the pulse width but which may increase the stability.[15,16] Such effects were observed by the author in a computer simulation also.[11] In addition, unwanted etalon effects may occur due to the laser rod, the Q-switcher, the mode-locker, etc. For this reason the windows of such elements are frequently cut at Brewster's angle or they are wedged (the mode-locker used in this work was wedged at 1°).

A 6mm thick available uncoated etalon was tried in the cavity. According to theory[15] the effective linewidth of this etalon can be calculated to be 54 GHz. Since the linewidth of Nd:YAG is 120 GHz, not much effect would be expected and actually not much was observed.

An available 42% reflectivity mirror was combined with the regular laser 90% reflectivity output mirror to form an output coupling "etalon". The spacing of the reflecting faces of this "etalon" could be varied by moving the 90% mirror on the translation-stage holder mentioned earlier. Various spacings were tried with no improvement in pulse shape as viewed on the oscilloscope.

Unfortunately an output coupling etalon does not necessarily provide the advantages that can accrue from an intra-cavity etalon.

X. VARIABLE OUTPUT COUPLING

In the process of working with the two mirrors as an etalon, it was concluded that the regular 90% reflectivily output mirror did not give optimum output coupling under mode-locked conditions. Therefore the decision was made to try a beam splitter inside the cavity to couple out energy and use high reflectivily cavity mirrors. A microscope slide was used as the beam splitter because its calculated etalon linewidth of 385 GHz would be larger than the 120 GHz linewidth of the Nd:YAG and therefore it would cause no "etalon effects."

Varying the angle of the microscope slide relative to the intra-cavity beam varies the *effective output* coupling. With the slide at an angle of 15° from normal to the laser beam, slightly better pulsing was obtained. Unfortunately, one-half of the coupled-out energy is from the other side of the slide in the opposite direction and is lost; thus, the beam-splitter coupler technique is not itself a desirable procedure for actual operation. The results indicated, however, that some slight improvement might be obtained with a slightly higher reflectivity output mirror.

XI. OTHER WORK

Near the end of the project, the laser rod was replaced with a 30' wedged rod, one which theoretically at least would be less susceptible to undesirable etalon effects. Initial results indicated that there might be an improvement but insufficient time was available to study the matter thoroughly.

XII. RECOMMENDATIONS

As has been noted, the stability of a short pulse laser system is of paramount importance when using it for non-invasive studies of the eye. Although the combination of active Q-switching and active mode locking is the most stable configuration, it still requires stabilization. Commercial active-active systems which are becoming available use exotic temperature compensation techniques in stabilizing the laser cavity and the mode locker individually[27] and they are quite expensive.

The active-active system studied in this work performed quite satisfactorily although it was necessary to let the mode-locker source operate 24 hrs a day for stability reasons. The active-active system could be followed by either a synchronously-pumped dye laser or a harmonic doubler and pulse compression scheme to further narrow the pulse and shift it to the visual spectrum.

An active-active Nd:YAG laser followed by a synchronously-pumped dye laser should lend itself to an overall stabilization scheme similar to that employed by the author in stabilizing an argon laser.[11] That scheme uses the fact that the optical pulse shifts in the time domain relative to the modulator drive frequency as the drive frequency departs from the laser c/2L.[12] It is expected that the optical pulse from the dye laser would also shift in the time domain relative to the drive frequency and thus permit a stabilization of the overall system. It is recommended that the concept be given further study. Normally very precise control of both the pumping laser and the dye laser are necessary when using the synchronously pumped technique[28] and this stabilization scheme should eliminate that necessity.

REFERENCES

1. J. Taboada and W. D. Gibbons, "Retinal Tissue Damage Induced by Single Ultrashort 1060 nm Laser Light Pulses," Applied Optics, Vol. 17, pp. 2871-2873, Sept. 1978.

2. W. T. Ham, Jr., H. A. Mueller, A. I. Goldman, G. E. Newman, L. M. Holland and T. Kuwabara, "Ocular Hazard from Picosecond Pulses of Nd:YAG Laser Radiation, Science, Vol. 185, pp. 362-363, July 1984.

3. L. E. Hargrove, R. L. Fork and M. A. Pollack, "Locking of He-Ne Laser Modes Induced by Synchronous Intracavity Modulation," Appl. Phys. Letters, Vol. 5, pp. 4-5, July 1964.

4. R. L. Fork, B. I. Greene and C. V. Shank, "Generation of Optical Pulses Shorter than 0.1 psec by Colliding Pulse Mode Locking," Appl. Phys. Letters, Vol. 38, pp. 671-672, May 1981.

5. A. E. Siegman, "An Antiresonant Ring Interferometer for Coupled Laser Cavities, Laser Output Coupling, Mode Locking, and Cavity Dumping," IEEE J. Quantum Electronics, Vol. QE-9, pp. 247-250, February 1973.

6. H. Vanherzeele, J. L. Van Eck and A. E. Siegman, "Colliding Pulse Mode Locking of a Nd:YAG Laser with an Antiresonant Ring Structure," Applied Optics, Vol. 20, pp. 3484-3486, October 1981.

7. M. A. Lewis and J. T. Knudtson, "Active-Passive Mode-Locked Nd:YAG Oscillator," Applied Optics, Vol. 21, pp. 2897-2900, August 1982. (This paper has a number of references to active-passive systems.)

8. O. P. McDuff, "Techniques for Ultra-Short Pulses in Nd:YAG Lasers," Final Report for 1984 USAF-SCEEE Summer Faculty Research Program, September 28, 1984.

9. H. Nkatsuka, D. Grischkowsky, and A. C. Balant, "Non-linear, Picosecond-Pulse Propagation through Optical Fibers with Positive Group Velocity Dispersion," Phys, Rev. Lett., Vol. 47, pp. 910-913, September 1981.

10. C. V. Shank, R. L. Fork, R. Yen, and R. H. Stolen, "Compression of Femtosecond Optical Pulses," Applied Phys. Lett., Vol. 40, pp. 761-763, May 1982.

11. O. P. McDuff, "Stabilization of Mode-Locked Lasers," 1984 USAF-SCEEE Research Initiation Program grant (Final Report to be published).

12. O. P. McDuff and S. E. Harris, "Nonlinear Theory of the Internally Loss Modulated Laser," IEEE J. Quant. Electronics, Vol. QE-3, pp. 101-111, March 1967.

13. O. P. McDuff, "Techniques of Gas Lasers," Chapter C5 of Laser Handbook, Vol. 2, F. T. Arecchi and E. O. Schulz-Dubois, eds., North Holland Publishing Co., Amsterdam, 1972.

14. Personal communication from Mr. Doug King of Laser Applications, Inc.

15. D. J. Kuizenga and A. E. Siegman, "FM and AM Mode Locking of the Homogeneous Laser - Part I: . eory," IEEE J. Quant. Electr., Vol. QE-6, pp. 694-708, November 1970.

16. D. J. Kuizenga and A. E. Siegman, "FM and AM Mode Locking of the Homogeneous Laser - Part II: Experimental Results in a Nd:YAG Laser with Internal FM Modulation," IEEE J. Quant. Electr., Vol. QE-6, pp. 709-715, November 1970.

17. See Laboratory Notebook, Vol. 1, Summer of 1985, of the author.

18. M. H. Crowell, "Characteristics of Mode-Coupled Lasers," IEEE J. Quant. Electr., Vol. QE-1, pp. 12-20, April 1965.

19. O. P. McDuff, Mode Coupling in Lasers, Ph.D. Dissertation at Stanford University, August 1966.

20. L. M. Osterink and J. D. Foster, "A Mode-Locked Nd:YAG laser," J. Appl. Phys., Vol. 39, pp. 4163-4165, August 1968.

21. J. A. Giordmaine, P. M. Rentzepis, S. L. Shapiro, and K. W. Wecht, "Two-Photon Excitation of Fluorescence by Picosecond Light Pulses," Appl. Phys. Letters, Vol. 11, pp. 216-218, October 1967.

22. S. A. Akhmanov, R. V. Khokhlov, and A. P. Sukhorukov, "Self-Focusing, Self-Defocusing, and Self Modulation of Laser Beams," Chapter E3 of Laser Handbook, Vol. 2, F. T. Arecchi and E. O. Schulz-Dubois, eds., North Holland Publishing Co., Amsterdam, 1972.

23. D. D. Venable and J. Taboada, "Dependence of the Decrease in Contrast Ratios on the Intensity of the Laser Pulse for Two-Photon Fluorescence," J. Appl. Phys., Vol. 50, pp. 5996-5997, September 1979.

24. During the preparation of this report it was discovered that a somewhat similar technique was used earlier at low average power levels where thermal damage was not a problem. See A. R. Clobes and M. J. Brienza, "Passive Mode Locking of a Nd:YAG Laser," Appl. Phys. Lett., Vol. 14, pp. 287-288, May 1969.

25. See Laboratory Notebook, Vol. 2, Summer of 1985, of the author.

26. M. DiDomenico, Jr., J. E. Geusic, H. M. Marcos, and R. G. Smith, "Generation of Ultrashort Optical Pulses by Mode Locking the YAlG:Nd Laser," Appl. Phys. Lett., Vol. 8, pp. 180-183, April 1966.

27. See, for example, advertising brochure for Spectra Physics series 3000 Nd:YAG lasers.

28. T. Sizer and G. Mourou, "Picosecond Dye Laser Pulses using a cw Frequency Doubled Nd:YAG as the Pumping Source," Optics Communications, Vol. 37, pp. 207-210, May 1981.

1985 USAF-UES SUMMER FACULTY RESEARCH PROGRAM

Sponsored by the

AIR FORCE OFFICE OF SCIENTIFIC RESEARCH

Conducted by the

UNIVERSAL ENERGY SYSTEMS, INC.

FINAL REPORT

PLASMA PARAMETER DATA FOR BERT I CHAMBER TESTING

Prepared by: Bernard McIntyre

Academic Rank: Associate Professor

Dept: Electrical Electronics Technology Department

University: University of Houston

Research Location: Air Force Geophysics Laboratory

Space Physics Division

Active Experiments Branch

USAF Research: Herbert Cohen

Date: 13 September 1985

Contract No: F49620-85-C-0013

PLASMA PARAMETER DATA FOR BERT I CHAMBER TESTING

BY

BERNARD MCINTYRE

ABSTRACT

During the BERT I vacuum chamber test at the Johnson Space Center, NASA, cylindrical Langmuir probes were used to monitor the plasma parameters in the vicinity of the payload. Plasma data taken on a Langmuir probe close to the payload shows that during high current electron beam emissions, the return electron current depletes some regions of the test chamber of electrons.

Acknowledgement

The author would like to thank the Air Force Systems Command, The Air Force Office of Scientific Research and the Universal Energy Systems Inc. for providing him with the opportunity to interact with an active research program at AFGL. He would especially like to thank Herbert A. Cohen and the members of his group for all of the help and cooperation extended to him during the summer tenure.

I INTRODUCTION In March 1985 the Air Force Geophysics Laboratory (AFGL) conducted a ground test of electron and ion beam emission systems (BERT I) at the large vacuum chamber test facility of the Johnson Space Center, NASA, Houston, Tex. A main objective of the test was to exercise all aspects of the emission systems in a simulated ionospheric environment. Although the test facility had an ion source used to provide a plasma background for the ionospheric simulation, there were no personnel available who were familiar with the source. When the AFGL conducted a similar test at this facility in 1981, I was an employee of the facility and my function was to interface with the facility and the experimenters and provide the plasma background for the test. During the summer of 1984 I participated in a summer faculty research program at the AFGL and worked on plasma source and diagnostic studies in preparation for the test at the Space Center. Because of my background with the Space Center and the AFGL, I was asked to provide the plasma background and diagnostics for the BERT I testing.

II OBJECTIVES OF THE RESEARCH EFFORT The primary goal of the research effort for the summer research program was to refine the plasma diagnostic data from the BERT I testing in order to define the state of the ambient plasma in the vicinity of the rocket payload and to correlate it with any data from on board instrumentation.

III TEST CHAMBER CONFIGURATION The location of the plasma sources and Langmuir probes for the BERT I test in the large vacuum chamber of the Johnson Space Center is shown in figure 1. The chamber has two catwalks around its inside wall, at the third and fifth levels. These levels are 31 and 62 feet respectively above the ground floor level. Two independent plasma generators were positioned at the third level catwalk 25 feet from BERT and either aimed directly at BERT for a maximum plasma density or at the grounded catwalk to minimize the density. In either case, the plasma beam exiting the generator was in the form of a well collimated beam of argon ions and neutralizing electrons. For the case in which the plasma generator was directed toward the test article, it was expected that approximately 25% to 50% of the beam would be scattered by neutrals, depending on the ambient pressure.

Plasma parameters were monitored with five cylindrical Langmuir probes .010" diameter and one foot long and positioned as shown in figure one. Probes 2-5 were strung from a vertical line dropped from the fifth level rail and twenty feet along the catwalk from the plasma source. These probes were used to indicate the vertical profile of the plasma parameters. Probe #1

was positioned between the plasma source and the test article and ten feet from BERT.

The AFGL monitored a Langmuir probe which was part of the Ernie system shown in figure 1. This probe was at the fifth level vertically but not in the path of the plasma source. From a vertical view of the source and probe set up shown in figure 2, one expects the plasma density of the Ernie probe to be comparable to but larger than that at the fifth level catwalk.

IV TEST DATA The plasma data Ne , KTe and Vp for the probe near Bert is shown as a function of time in figures 3 and 4. N_e is the electron concentration/cc, KT_e is the electron thermal energy and V_p is the plasma potential. Also shown, when available, are the plasma density from the Ernie probe and the reference probe at the fifth level catwalk.

Probe data for the final day of testing was taken on a chart recorder. The probe near Bert was biased at +50V to collect electrons and the probe current was recorded as charge sources on Bert went through a firing sequence. The local plasma density at the probe oscillated as the gun currents increased and decreased and was assumed to be proportional to the probe current on the chart recorder. This data is discussed in the following section.

V Data analysis

Except for a few small time intervals, the plasma source was beaming a collimated plasma towards the Langmuir probe and Bert. As explained earlier, a probe on Ernie, not in the direct beam,

is expected to see a much lower plasma density than the probe near Bert, but more density than a reference probe on the side of the chamber at the fifth level. This is seen in the data, in which the density at Bert was 50-100 times that at Ernie, but 300 times that at the probe near the chamber wall.

During the few brief periods in which the source was not beamed to Bert, it was directed down to the catwalk, to ground the plasma beam. This resulted in a very low ambient plasma density near Bert, 500-1000/cc. In this configuration, none of the probes were in the direct beam of the source, and plasma density variations between the center of the chamber, near Bert, and the fifth level were different by an order of magnitude. This is typical of an ambient plasma in that chamber where there are no effects at the probe from a direct source beam.

During the final day of testing, the probe near Bert was constantly monitored by biasing it at +50 V and putting the voltage converted probe current on a chart recorder. As beam currents were swept on Bert, the probe current oscillated, reflecting changing local electron concentration. The observed electron oscillations at the probe were independent of the gun voltage on Bert but were strongly dependent on current. Electron plasma densities in the ambient plasma went from 5×10^5/cc with the gun off to very nearly zero when the gun current went to 20 ma in rapid steps ($\Delta T \ll 2$ sec.). When the electron gun current built up to 20 ma in 2 second intervals, the electron concentration oscillated from 5×10^5 down to 1×10^4 /cc rather than to near zero. The longer interval apparently allows for a mechanism to replenish the electron depleted region. One

possible mechanism for this is an interaction between Bert and the plasma source. A heavily depleted electron region could result in an ion rich region near the plasma source which could result in more electrons being extracted from the neutralizing filament of the source. Electric fields would also be expected over a large volume of the chamber when the electron gun current is firing. This is due to the very low plasma density outside the beam region of the plasma source. when Bert fires an electron current, its potential will swing positive. the plasma source beams high density 300 - 500 ev argon ions roughly neutralized by 5 ev electrons at Bert. when Bert is floating electrically and the gun current is zero, the electron current density is higher for a neutralized beam because of the electrons having a higher velocity. Bert then should float negative for a neutral beam. Since the beam from the plasma source is not expected to be exactly neutral, there could be some variation in the negative floating potential. A low positive potential on Bert though, due to the electron gun, will result in a rapid net electron current to Bert simply due to the difference in current densities of the electrons and ions. for a large floating positive potential, a sheath around Bert must pull in electrons. These sheaths should be very large on the wake side of Bert where the density is much lower and may even go to the walls or fold around toward the plasma source and its beam. On the plasma source side of Bert, the field from a positive potential should penetrate into the beam to pull in electrons without forming a sheath edge until the floating potential of Bert is enough (300 -

500 ev) to turn the ions around. It is expected then that there will be large sheaths or electric field regions around Bert to which electrons are being attracted. The rising positive potential on Bert should also tend to spread the ions in the beam, so that a Langmuir probe close to the beam will see more energetic ions which will lower the net probe current.

The electron gun was also fired while a strong magnetic field was in the chamber. At peak gun currents, the probe region was severely depleted of electrons since the electrons now have to diffuse across the magnetic field lines. At these peak gun currents, the Langmuir probe could only detect ion current even when biased at +50 volts. At this bias voltage, it is not going to force the energetic ions away from it so it is simply not able to pull in enough electrons to balance the ion current from the beam.

VI Recommendation Section

During most of the testing described in this report, the background plasma provided by the plasma source was very non uniform. The plasma density was very high in its narrow beam but 20 - 50 times lower than in the beam at distant points in the chamber. If a similar situation were to occur again, it would be strongly advised that movable probes be available to make horizontal and vertical scans of the chamber with the payload guns on and off. A mapping of this type may enable one to model the flow of neutralizing charge to the payload. The model would be needed to determine to what extent, if any, the payload couples to the plasma source. If coupling occurs, the assymetric

sheath distribution would differ greatly from that in an actual space test.

FIGURE 1 The experimental configuration in the vacuum chamber for the BERT test. Side view of the chamber

Figure 1

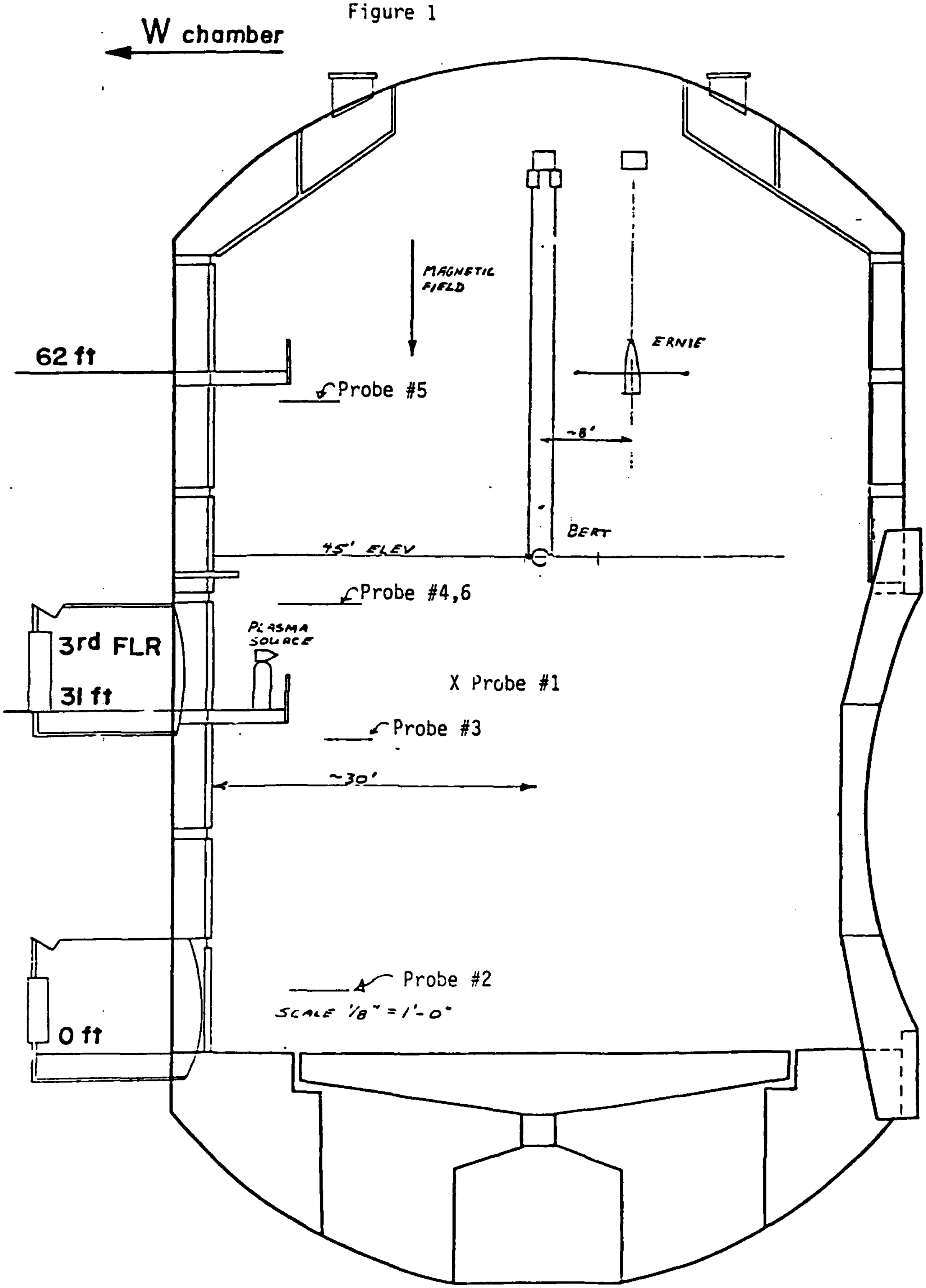

W chamber
MAGNETIC FIELD
62 ft
Probe #5
ERNIE
~8'
BERT
45' ELEV
Probe #4,6
PLASMA SOURCE
3rd FLR
31 ft
X Probe #1
Probe #3
~30'
Probe #2
SCALE 1/8" = 1'-0"
0 ft

FIGURE 2 A vertical view of the experimental configuration for the BERT test.

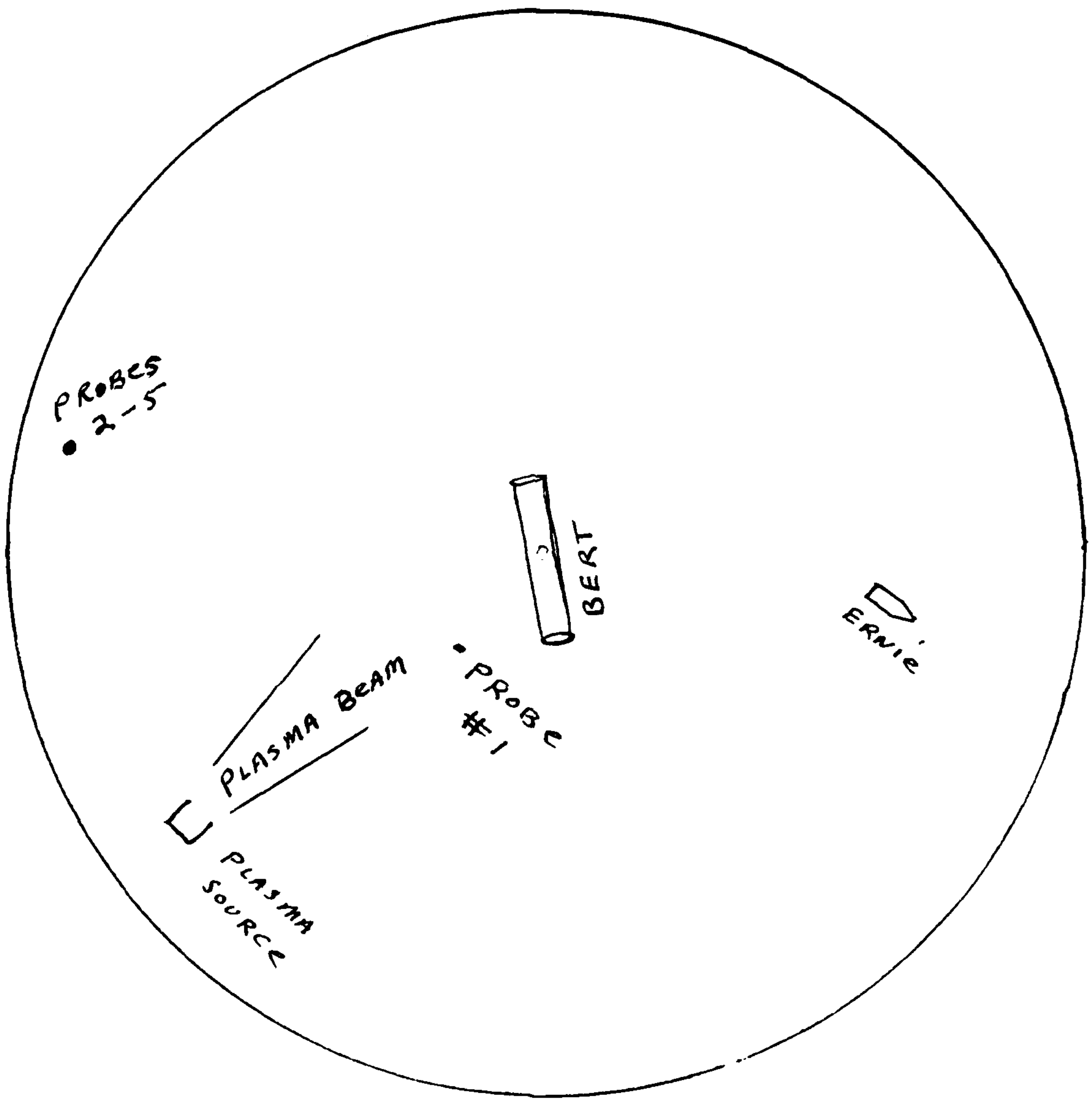
PROBES
2-5
BERT
ERNIE
PLASMA BEAM
PROBE
#1
PLASMA
SOURCE

FIGURE 3 Time display of plasma parameters

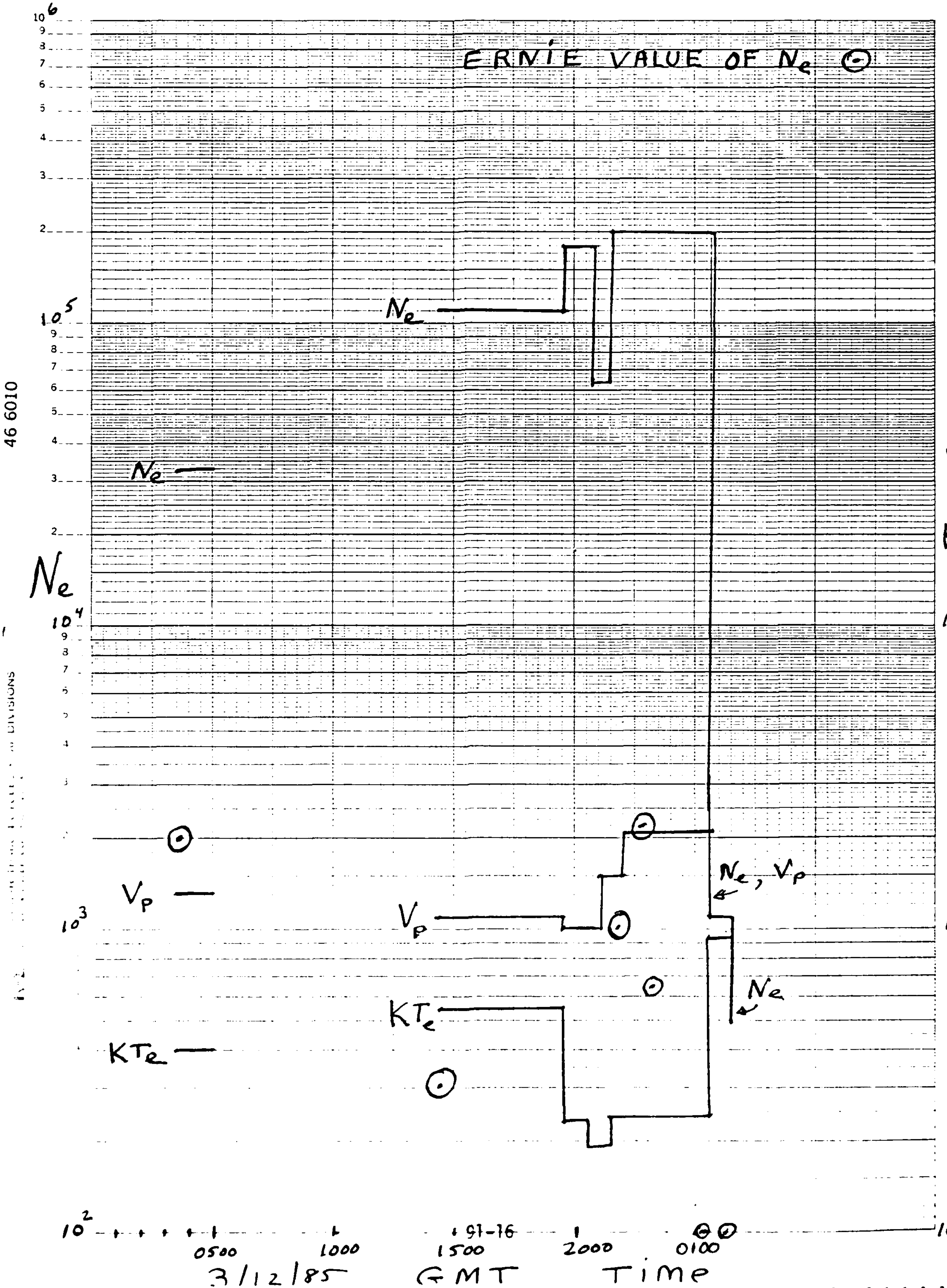

ERNIE VALUE OF Ne ⊙
Ne
Ne
Ne
Vp
Vp
Ne, Vp
Ne
KTe
KTe
10^6
10^5
10^4
10^3
10^2
0500
1000
1500
2000
0100
3/12/85 GMT Time
46 6010

FIGURE 4 Time display of plasma data

AD-A166 177 UNITED STATES AIR FORCE SUMMER FACULTY RESEARCH PROGRAM 13/15
1985 TECHNICAL RE. (U) UNIVERSAL ENERGY SYSTEMS INC
DAYTON OH R C DARRAH ET AL. DEC 85 AFOSR-TR-86-0140
UNCLASSIFIED F49620-85-C-0013 F/G 5/1 NL

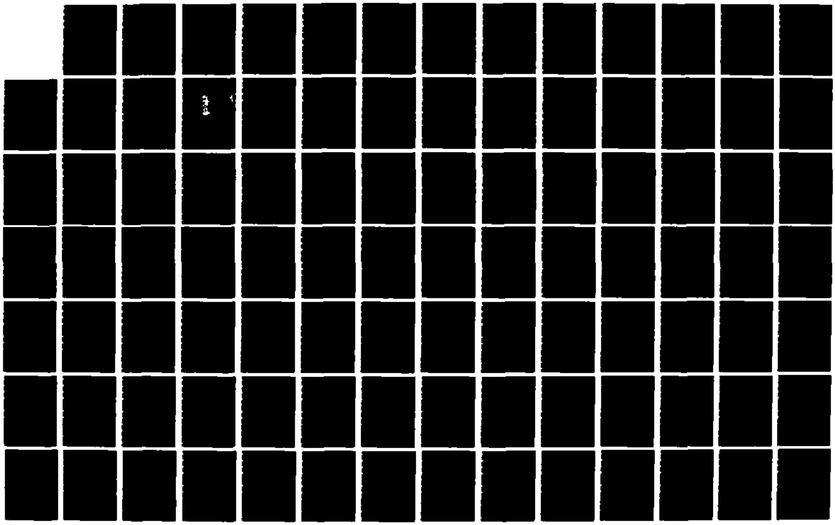

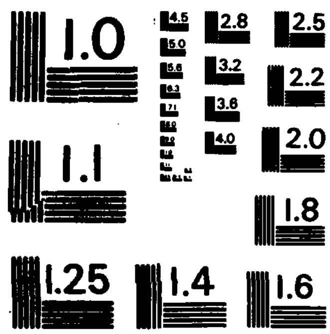

MICROCOPY RESOLUTION TEST CHART
NATIONAL BUREAU OF STANDARDS-1963-A

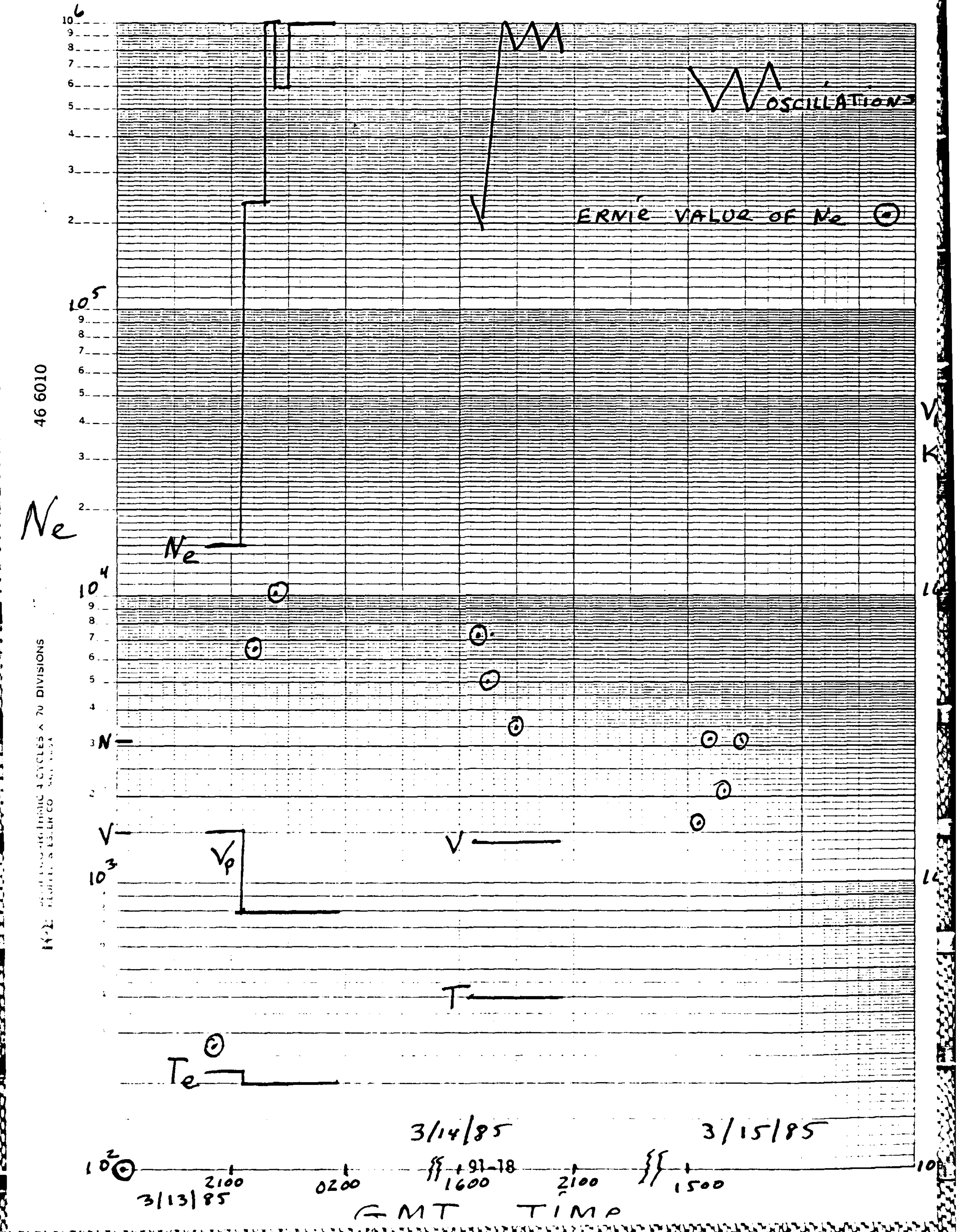

OSCILLATIONS
ERNIE VALUE OF Ne
Ne
Ne
N
V
Vp
V
T
Te
3/14/85
3/15/85
91-18
2100
0200
1600
2100
1500
3/13/85
GMT TIME
46 6010
4 CYCLES X 70 DIVISIONS

FOURIER ANALYSIS OF THE PATTERN ELECTRORETINOGRAM

Final Report

UES-AFOSR SFRP Grant

Leathem Mehaffey,III, Ph.D.

Research Site: Brooks AFB, San Antonio, Texas

Summer, 1985

I wish to extend my thanks to Dr. Donald Farrer and Capt. Robert Cartledge, both of SAM/RZV, Brooks AFB, and to Drs. Fred Previc and Randy Glickman, both of Technology Incorporated, and to all of the support personnel, both military and civilian, at Brooks AFB, for their cooperation and support, without which this project would have been impossible.

FOURIER ANALYSIS OF THE PATTERN ELECTRORETINOGRAM

by

Leathem Mehaffey,III,Ph.D

abstract

The object of the present study is to analyse the pattern electroretinogram (PERG) using Fourier analysis. A Fourier interpretation of the PERG is that the "Luminance ERG" is contained in the fundamental and odd harmonics of the response, while the PERG is contained in the even (nonlinear) harmonics. Three monkeys (macacca mulatta) were used in this study. Stimulus patterns (horizontal bars alternated using either a sinewave or a squarewave counterphase signal) were generated on a monitor by a video pattern generator interactively linked to a computer which controlled both pattern generation and data acquisition. Both VEP's and PERG's were recorded. The signals were stored on the computer for later averaging and Fourier analysis. The preliminary findings presented in this report show that the technique of Fourier analysis as applied to the pattern ERG is sensitive to small changes in the response amplitude and phase; it can reliably detect signals as small as 0.5 to 1 microvolt, using averages of 30 or perhaps fewer responses. Compared to traditional methods this sensitivity represents a substantial improvement, while also providing greater ease of use, and improved objectivity. The study has provided evidence that at least one even harmonic, here the second harmonic, exists and may behave substantially differently from the fundamental. Another finding is the oscillatory nature of the recovery of amplitude of the PERG following a laser flash . This observation has not previously been reported, although a similar phenomenon has been observed in ganglion-cell recovery from laser flashes The correlation of PERG with ganglion cell behavior lends credence to the theoretical origin of the PERG with the ganglion cells.

1 INTRODUCTION

The pattern ERG (PERG) (Arden and Vaegan, 1983) is an electrical response recorded from the cornea of the intact eye in much the same way as the standard clinical ERG (flash ERG or FERG). The PERG differs from the FERG primarily in the nature of the stimulus used to elicit it. While a FERG is elicited by an abrupt change in luminance across the entire visual field, the PERG is elicited by a change in distribution of luminance across the field (i.e., a change in pattern), when the average luminance across the field is constant. Hence the PERG is sensitive to local changes in the field luminance, giving rise to two schools of thought as to the retinal origin of the PERG. Maffei and Fiorentini (Maffei and Fiorentini, 1981) postulate that the PERG is generated by retinal ganglion cells based on the facts that (1) ganglion cells respond briskly to edges and poorly to diffuse light because of the organization of their receptive fields; and (2) the PERG disappears after section of the optic nerve which results in retrograde degeneration of the ganglion cells. This latter result has been observed clinically in humans with unilateral optic neuropathy (Sieple and Siegel, 1983). Spekreijse (Spekreijse, 1973), on the other hand, claims that the PERG does not come from the ganglion cells, but from the same elements in the retina which give rise to the FERG; Spekreijse argues that the PERG is simply a sum of many small FERG's. Baker and Hess (Baker and Hess, 1984) and Schuurmans (Schuurmans, 1985) take a middle ground. Baker and Hess argue that the the ERG recorded to a flickering pattern is composed of the responses of both linear and nonlinear retinal elements. Schuurmans analysed the PERG in two ways. First he recorded the PERG in the normal way, i.e., by averaging a number of responses when the averager was triggered at the onset of each counterphase cycle. That is, each sweep consisted of one full cycle in which a given spot on the stimulus screen went from light to dark to light again. This method produced a standard PERG consisting primarily of a positive response. Schuurmans then recorded the PERG by triggering averages not on each cycle, but on each reversal, i.e., at twice the counterphase frequency. A given sweep then consisted of a sum of responses to both light-to-dark and dark-to-light transitions. When recorded in this way, the PERG showed no positive response, but instead showed a much smaller negative response, Schuurmans argues that the positive response recorded in the usual way is Spekreijse's

luminance response, while the negative response recorded by triggering on each transition is the true PERG.

The object of the present study is to analyse the PERG using Fourier analysis. If Schuurmans's model is correct, then a Fourier interpretation of the model is that the "Luminance ERG" is contained in the fundamental and odd harmonics of the response, while the PERG is contained in the even (nonlinear) harmonics. This follows from Schuurmans's averaging technique: triggering the average at the counterphase rate causes the fundamental and all its harmonics to constructively interfere (add). Triggering on each reversal causes the fundamental and odd harmonics to constructively interfere. Fourier analysis, which looks at both even and odd harmonics, should therefore simultaneously follow both, and so, by Schuurmans' analysis, follow both the FERG and the PERG. Even if Schuurmans's model is incorrect, however, Fourier analysis should provide a sensitive, objective measure of response amplitude unavailable by direct visual measurement.

2 MATERIALS AND METHODS

2.1 Animals

Three monkeys were used in this study. All were rhesus monkeys (macacca mulatta), male, 2 to 3 years of age, maintained in the vivarium of Brooks Air Force Base. All three were refracted using a retinoscope and wore contact lenses correcting their vision to a nominal 0.5 diopters. Final correction was obtained using trial lenses in front of the eye and recording the VEP to a 12 cycle per degree pattern. During the experiments the monkeys were anesthetized with barbiturates, paralyzed with gallamine, and then mechanically ventilated. Anesthesia state was closely monitored using EEG, pCO_2 , and heartrate.

2.2 Stimulus

Stimulus patterns were generated by a Technology Incorporated custom-made video pattern generator interactively linked to a Digital Equipment Corporation 11/34 computer. The computer controlled both pattern generation and data acquisition. Patterns were generally horizontal bars (spatial squarewave) which were alternated using either a sinewave or a squarewave counterphase temporal signal. Patterns were displayed on a Mitsubishi Model C-6911 RGB color video monitor at a distance of two meters from the monkey's eye, so that patterns displayed full-screen subtended a visual angle of 12 . The animals' fixation was precisely controlled using the laser alignment technique of Blankenstein and Previc (Blankenstein and Previc, 1985). Using this technique it could be guaranteed that all patterns were centered on the fovea.

2.3 Electrodes

VEP's were recorded using bipolar stainless-steel electrodes chronically implanted in the visual cortex (Previc et al, 1985). Those electrodes provided a very high signal-to-noise ratio. Where several such electrodes were available in an animal, the one giving the strongest signal was used.PERG's were recorded with one of two active electrode types. First was a Carter and Hogg gold foil electrode (Arden et. al., 1983) which was placed in the lower margin of the orbit. The second type was a custom-made electrode, made electrode, made by vacuum-depositing an annulus of gold on the inner surface of a contact lens which had been made to the prescription of that monkey. PERG's were recorded equally well with both electrodes. In all cases the reference electrode was a "Jet" electrode (Life-Tech, Inc., Houston, TX) placed in the contralateral eye, which was then patched.

2.4 Data Acquisition

PERG and VEP signals were amplified on a Grass EEG polygraph (Model 78D) at gains of from 20,000 to 50,000 , and a standard bandpass of 0.5 to 100 H . Amplified signals were displayed on the polygraph penwriter , and simultaneously sent to a Nicolet Model 535 signal averager for on-line averaging and to the 11/34 computer for digitization and storage for later analysis. The stimulus synchronization pulse was also

displayed and stored to provide a precise stimulus frequency and phase marker for subsequent Fourier analysis. Digitization rates varied from 128/sec to 2048/sec to provide 256 samples per sweep at sweep times of from 2 seconds per sweep to 0.125 seconds per sweep.

2.5 Data Analysis

After collection, the digitized data were averaged. For constant-stimulus runs, all sweeps were averaged together. Usually 90 sweeps were collected and averaged. For variable stimulus conditions, e.g., during a laser flash run, a moving average was used. That is, an averaging "window" of fifteen to thirty sweeps in width was "slid" along the record in fixed increments to produce a series of averages centered around sequential points in time. The averaging program (DATAVG) is included as Appendix A.

Averaged data were subjected to a Fourier analysis using the program FORIER included as Appendix B. This program begin the analysis by precisely determining the stimulus parameters using the digitized stimulus synchronization signal. It first finds the number of full cycles and the time in which they occur, from which data it calculates the stimulus frequency. It then finds the time of the first positive zero-crossing of the stimulus counterphase waveform; this represents the onset of the first pattern reversal in the sweep. Subsequent Fourier analysis of the response is based on these two stimulus parameters.

The data is then analysed by assuming that the equation which describes the data is of the form

$$(1)\ D(t) = A_0 + A_r t + A_1 \cos(\omega t) + B_1 \sin(\omega t) + A_2 \cos(2\omega t) + B_2 \sin(2\omega t) + \cdots$$
$$\cdots + A_n \cos(n\omega t) + B_n \sin(n\omega t)$$

The problem then is to find the coefficients A_0 (the "D.C." term, A_r (the "ramp term"), and $A_1, B_1 \cdots A_n, B_n$, the Fourier terms. We begin by defining an error function as follows:

$$(2)\ E(t) = \int_0^T [F(t) - D(t)]^2 dt$$

where $F(t)$ is the Fourier expansion of equation (1). We then assume that the values of the constants (A) and (B) which cause the equation to best fit the data are those values which cause the partial derivative of the error function to go to zero. Thus:

(3)

$$\frac{\partial E}{\partial A_0} = 0$$
$$\frac{\partial E}{\partial A_r} = 0$$
$$\frac{\partial E}{\partial A_1} = 0$$
$$\frac{\partial E}{\partial B_1} = 0$$
$$\vdots$$
$$\frac{\partial E}{\partial A_n} = 0$$
$$\frac{\partial E}{\partial A_n} = 0$$

This operation sets up a series of $2n + 2$ simultaneous equations which can then be solved for the coefficients. The program FORIER does this by first setting up the coefficients in matrix form, using two subroutines, IRSMAK and SINMAK. SINMAK creates the data-independent terms such as:

$$\int_0^T t dt$$

$$\int_0^T \sin(\omega t) dt$$

$$\int_0^T \sin(\omega t \cos(\omega t) dt$$

etc.

The subroutine IRSMAK creates the data-dependent terms such as:

$$\int_0^T tD(t) dt$$

$$\int_0^T D(t)\sin(\omega t)dt$$

$$\int_0^T D(t)\sin(\omega t\cos(\omega t)dt$$

etc.

The square matrix created by SINMAK and the column created by IRSMAK are then combined in a single matrix and solved in the subroutine SIMQ using a modified Gauss-Jordan elimination method. The results are displayed in terms of n, the multiple of w, or the "harmonic", where n=1 is the "fundamental", n=2 is the "first harmonic", and so forth. For each n the coefficients A[n[and B[n[are displayed. In addition the A_n and B_n terms are used to calculate the constants for the alternative representation of the harmonic as a cosine wave with a phase relation to the stimulus, i.e., $Z_n \cos(\omega t + \phi_n)$. Z_n, calculated from the root mean square of A_n and B_n, gives the amplitude of the component, while ϕ_n, calculated from the arctangent of A_n and B_n, gives the phase relationship of the component to the driving or stimulus frequency. Finally the phase and frequency are used to calculate a latency term which is the temporal relationship of the given harmonic to the stimulus.

Before printing out any coefficients the program FORIER iterates through a series of trial fits in which it begins assuming no periodic components, i.e., a straight line of the form $D(t) = A_0 + A_r t$, and then progressively adds harmonic terms. At each iteration it calculates and displays the sum of squared deviations between the prediction made by the trail equation and the actual data at each point in time for which data exist. The program finds the best-fitting trial equation (up to a maximum of six harmonic terms), and prints out the coefficients from that equation.

Raw data are graphed using the program DATPLT which is included as Appendix C.

3 RESULTS

Figure 1A shows a typical PERG record after averaging. In this case the stimulus is a horizontal bar grating (spatial square wave) which is alternating sinusoidally. The lower trace is the stimulus synchronization signal which is displaying the counterphase rate. The actual alternation rate is twice the counterphase rate, since the stimulus alternates twice during each cycle of the counterphase signal. This can easily be seen in the response (upper trace) which is following not the counterphase but the alternation rate.

Figure 1B shows the Fourier analysis done by the program FORIER on the data of Fig 1A. Note in particular the description of the stimulus in terms of alternation or "reversal rate". Note also the rapid improvement in the "sum of Squares" fit as one goes from no periodic terms (straight-line fit) to one term (the fundamental). This rapid improvement indicates a strong periodic component to the signal. The initial rapid improvement is followed by a very minimal improvement upon iteration with additional periodic terms ("harmonics"). This indicates that there is little contribution to the form of the response by those higher harmonics. The final printout bears out this observation, showing that the first harmonic (twice the fundamental) has an amplitude of less than 1/3 of the fundamental.

Figure 2 shows a similar set of data for a squarewave counterphase In Fig. 2A, note the additional complexity in the shape of the response as the PERG responds not only to the stimulus fundamental but also to its harmonics. Typically the PERG is larger for a squarewave than for a sinewave counterphase. The addition of the higher harmonics to the response is also seen in the Fourier analysis of this response, shown in Fig. 2B.

Figure 3 shows a temporal tuning curve derived from the Fourier analysis of a series of runs on the same monkey. Each point represents the Fourier analysis fundamental frequency derived from a record which was the average of 90 sweeps. The stimulus was a 3.75 cycle per degree horizontal bar (squarewave) pattern with a sinusoidal counterphase waveform. Contrast was 80%, average luminance 22.5 cd/m^2.

The amplitude of the fundamental rises rapidly to a maximum at 2.5 Hz (5 reversals per second), then falls more slowly to reach zero at 15 Hz (30 reversals/sec).

Figure 4 is a spatial frequency tuning curve derived in a manner similar to the data of Fig. 3, but here temporal frequency was fixed at 3 Hz (6 reversals/sec (sinusoidal)) while spatial frequency (horizontal bar pattern, squarewave spatial frequency) was varied. The PERG shows a maximum amplitude at 1 cycle per degree (0.5^o barwidth), then drops, first slowly to 6.3 cycles per degree, then rapidly to 15.8 cycles per degree.

Figure 5 illustrates the dependence of the PERG fundamental amplitude on percent contrast (average luminance 22.5 cd/m^2). Over the range measured, the PERG increases essentially linearly with contrast, showing no appreciable saturation even at 90%.

Figures 6A and B demonstrate the effect of the 514.5nm Argon laser flash (0.1 sec, td-sec). The data shown in the figures were obtained by taking a moving average with a window of 30 sweeps (30 seconds) and sliding it along the 240-second record at 10-second intervals. Thus each point represents the Fourier fundamental amplitude derived from the averaging of 30 sweeps. This "sliding average" effect explains why the amplitude appears to fall even before the flash, which occurred at 60 seconds. That is, each plotted point represents an average of responses from 15 seconds **before** the point to 15 seconds **after** the point, so the 15-second point includes responses in the interval between 50 and 60 seconds, i.e., before the flash occurred. Nonetheless the data show a marked effect of the laser flash. Figure 6A slows the effect of the laser flash on the PERG, while Fig. 6B shows its effect on the VEP. In both figures both the first and second harmonic are plotted. The amplitude of the VEP is much larger than that of the PERG because the VEP was recorded via implanted electrodes. Note that for both VEP and PERG there is a steady-state period before the flash, followed by a rapid drop-off in amplitude immediately after the flash. While both VEP and PERG show recovery following the flash, the recovery patterns are markedly different. The VEP follows the expected monotonic recovery; the PERG recovery, however, follows a non-monotonic time course. The PERG amplitude rises to a local maximum some 60 seconds after the flash, but then

falls spontaneously at 80 seconds post flash, after which it rises rapidly out to 160 seconds, or 100 seconds post-flash. Second-harmonic amplitudes are low for the PERG, but in general seem to follow the first harmonic, except that there is indication of another oscillatory dip in amplitude recovery at 165 seconds (105 seconds post-flash).

Figures 7A and B show representative 30-second averages taken before (7A) and after (8B) the laser flash. For comparison to Figure 6A, the record of Figure 7A yields the 25-second point on Figure 6A, while the record of Figure 7B yields the 85-second point on Figure 6A. It is easy to see the marked drop in amplitude of the first harmonic between Figs. 7A and B. Visual inspection of the two figures indicates, however, that the second harmonic is not equally affected.

Figures 8A and B, and 9A and B are data from replicate laser-flash runs on the same animal taken at subsequent periods during the experiment. They serve to confirm that the difference in recovery pattern between the VEP and the PERG shown in Fig. 6 is not an anomaly, but is a real, reproducible phenomenon, at least in the one animal so far tested.

4 DISCUSSION

While the present document is a final report on the work done under the auspices of the UES-AFOSR Summer Faculty Research Participation program, it reports on what are more in the nature of preliminary findings. There is much room for further work. With this caveat, however, some conclusions can be drawn from the data presented.

The technique of Fourier analysis as applied to the pattern ERG is viable. In its present form it is sensitive to small changes in the Fundamental response frequency, and can reliably detect signals as small as 0.5 to 1 microvolt, using averages of 30 or perhaps fewer responses. Compared to traditional methods this sensitivity represents a substantial improvement. The Fourier technique produces results (Figs. 3,4,5,8,8B, 9b) which are consistent with results produced by earlier methods, while representing greater ease of use, higher sensitivity , and greatly improved objectivity. The analysis program can be improved , however; Figs 7A and B indicate that the program may be losing

valuable second-harmonic information. It may be that there are common instances such as that shown in Fig 7B where the first harmonic is strongly affected by some manipulation while the second harmonic is unaffected or much less affected. The program should be modified to seek out these instances.

The idea that the even harmonics constitute the "true" PERG (nonlinear , pattern-driven) while the fundamental represents the "local- luminance" PERG has been neither substantiated nor disproven so far by this study. Clearly there are even harmonics in the response to a sinusoidally-driven pattern reversal, as shown in Fig 1A and 1B. Whether these even harmonics constitute a response which behaves substantially differently from the odd harmonics has not been substantiated, and will require further analysis of existing data as well as further experimentation. Figures 6, 8, and 9 also provide evidence that an even harmonic, here the second harmonic, exists and may behave substantially differently from the fundamental. It must be pointed out, however, that the stimulus in these three cases was a square-wave counterphasing pattern which itself contains harmonics. It may be, therefore, that the apparent harmonics in the response are simply responses to the harmonics inherent in the stimulus. More work needs to be done to establish the separate identity of response harmonics generated within the retina. One remarkable finding of the present study is the oscillatory nature of the recovery of amplitude of the PERG following a laser flash (Figs 6A, 8A, 9A). This observation has not previously been reported, although a similar phenomenon has been observed in ganglion-cell recovery from laser flashes (Glickman 1985, personal communication). The correlation of PERG with ganglion cell behavior lends credence to the theoretical origin of the PERG with the ganglion cells. What could produce such an oscillatory behavior, and why it is not seen in the VEP, remains a subject for future work, as does its correlation with psychophysical observations such as recovery of pattern sensitivity following laser flashes.

In summary, I feel that the work accomplished under the UES SFRP program has already yielded two significant products, namely the development of a sensitive assay for the PERG and the finding of the oscillatory nature of the recovery of the PERG from laser flashes. In addition, the project has paved the way for a wide variety of future studies.

References

Arden, G.B., and Vaegan. (1983). Electroretinograms evoked in man by local uniform or patterned stimulation. *J. Physiol (Lond)*, *341*, 85-104.

Arden, G.B., R.M. Carter, C. Hogg, I.M. Siegel, and S. Margolis. (1983). A gold foil electrode: Extending the horizons for clinical electroretinography. *Invest. Ophthal. Vis. Sci.*, *24*, 796-798.

Baker, C.L., and R.F. Hess. (1984). Linear and non-linear components of the human electroretinogram. *J. Neurophysiol.*, *51(5)*, 952-967.

Blankenstein, M.F., and F.H. Previc. (1985). Approximate visual axis projection for the rhesus monkey using a funduscope and alignment laser. *Vision Research*, *25*, 301-305.

Maffei,L.,and A.Fiorentini. (1981). Electroretinographic responses to alternating gratings before and after sectioning of the optic nerve. *Science*, *211*, 953-955.

Previc, F.H., M.F. Blankenstein, P.V. Garcia, and R.G. Allen. (1985). Visual evoked correlates of laser flashblindness in rhesus monkeys. I. Argon laser flashes. *Am. J. Opt. Physiol. Optics*, *May*, .

Schuurmans, R.P.,and T. Berninger. (1985). Luminance and contrast responses recorded in man and cat. *Doc. Ophthal.*, *59*, 187-197.

Sieple,William H.,and Irwin M. Siegel. (1983). Recording the pattern electroretinogram: A cautionary note. *Invest. Ophthal. Vis. Sci.*, *24*, 796-798.

Spekreijse, H., O., Estavez, and L.H. van der Tweel. (1973). Luminance responses to pattern reversal. *Doc. Ophthal. Proc. Ser.*, *10*, 205-211.

FIGURE 1A

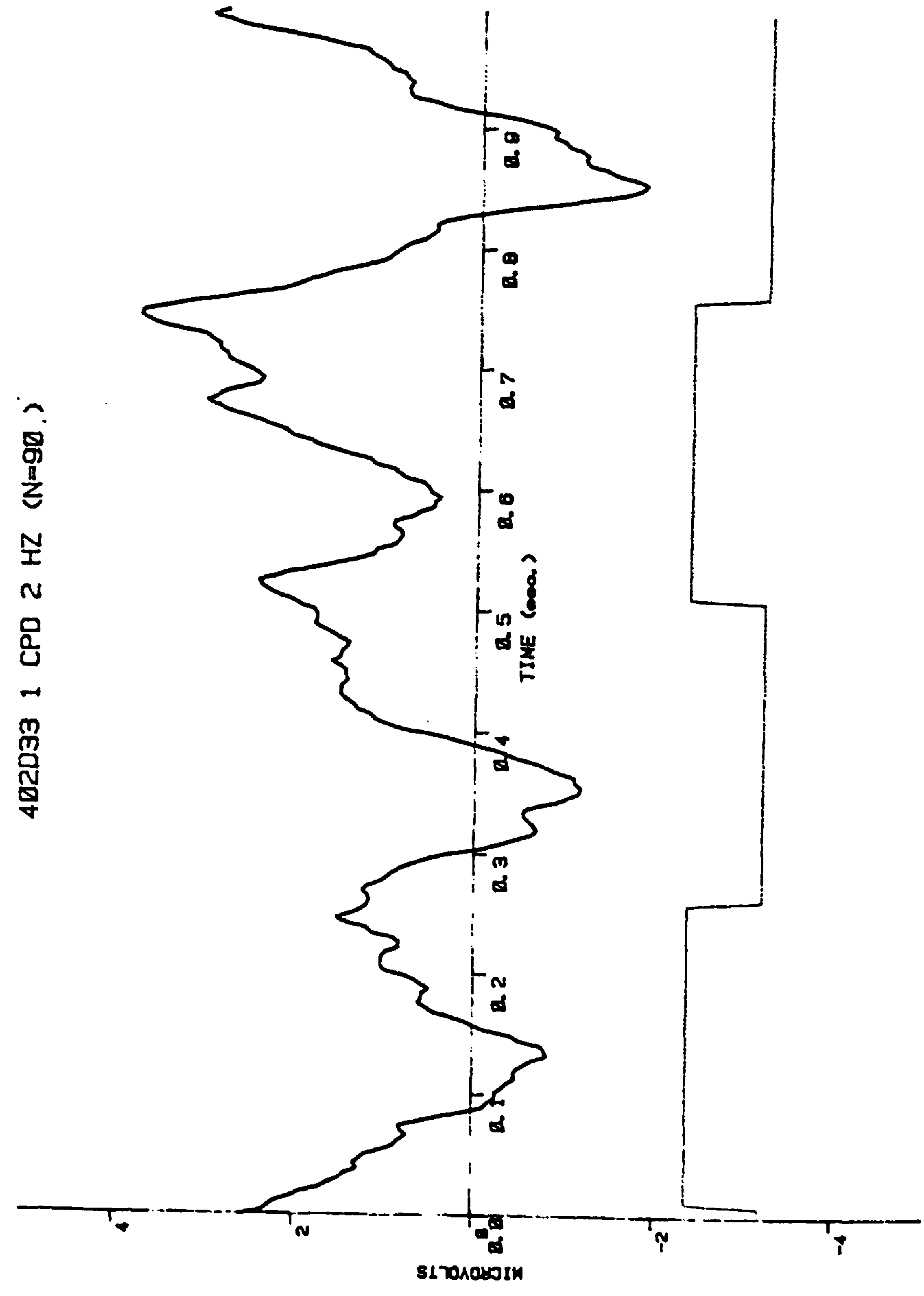
4Ø2D33 1 CPD 2 HZ (N=9Ø.)
TIME (sec.)
MICROVOLTS
Ø.Ø
Ø.1
Ø.2
Ø.3
Ø.4
Ø.5
Ø.6
Ø.7
Ø.8
Ø.9
4
2
Ø
-2
-4

dl

SYNOPSIS OF DATA:

FIGURE 1B

There are 1 cycles in 0.5000 seconds,
giving a reversal rate of 4.0000 Hz.
The sine analysis starts at 0.1250 seconds...
...Giving an analysis window of 224 points.

NUMBER OF SINE TERMS: 0
SUM OF SQUARES: 343.9136

NUMBER OF SINE TERMS: 1
SUM OF SQUARES: 162.3717

NUMBER OF SINE TERMS: 2
SUM OF SQUARES: 155.8407

NUMBER OF SINE TERMS: 3
SUM OF SQUARES: 152.2302

NUMBER OF SINE TERMS: 4
SUM OF SQUARES: 169360.5

COEFFICIENTS:

DC LEVEL: 0.5192
RAMP: 0.6252

Assuming that the stimulus is a sine wave which crosses zero at 0.1250
following are the statistics for the Fourier components of
the response:

Frequency: 4.00 Hz.
Cosine coefficient: 1.1157
Sine coefficient: 0.2181
Peak-to-peak amplitude: 3.0494 microvolts.
Phase : 0.0614 radians.
Response LEADS stimulus by 0.0024 seconds.

Frequency: 8.00 Hz.
Cosine coefficient: -0.0390
Sine coefficient: 0.3877
Peak-to-peak amplitude: 1.1117 microvolts.
Phase : -0.5319 radians.
Response LAGS stimulus by -0.0106 seconds.

Frequency: 12.00 Hz.
Cosine coefficient: 0.1692
Sine coefficient: 0.0591
Peak-to-peak amplitude: 0.3819 microvolts.
Phase : -0.1070 radians.
Response LAGS stimulus by -0.0014 seconds.

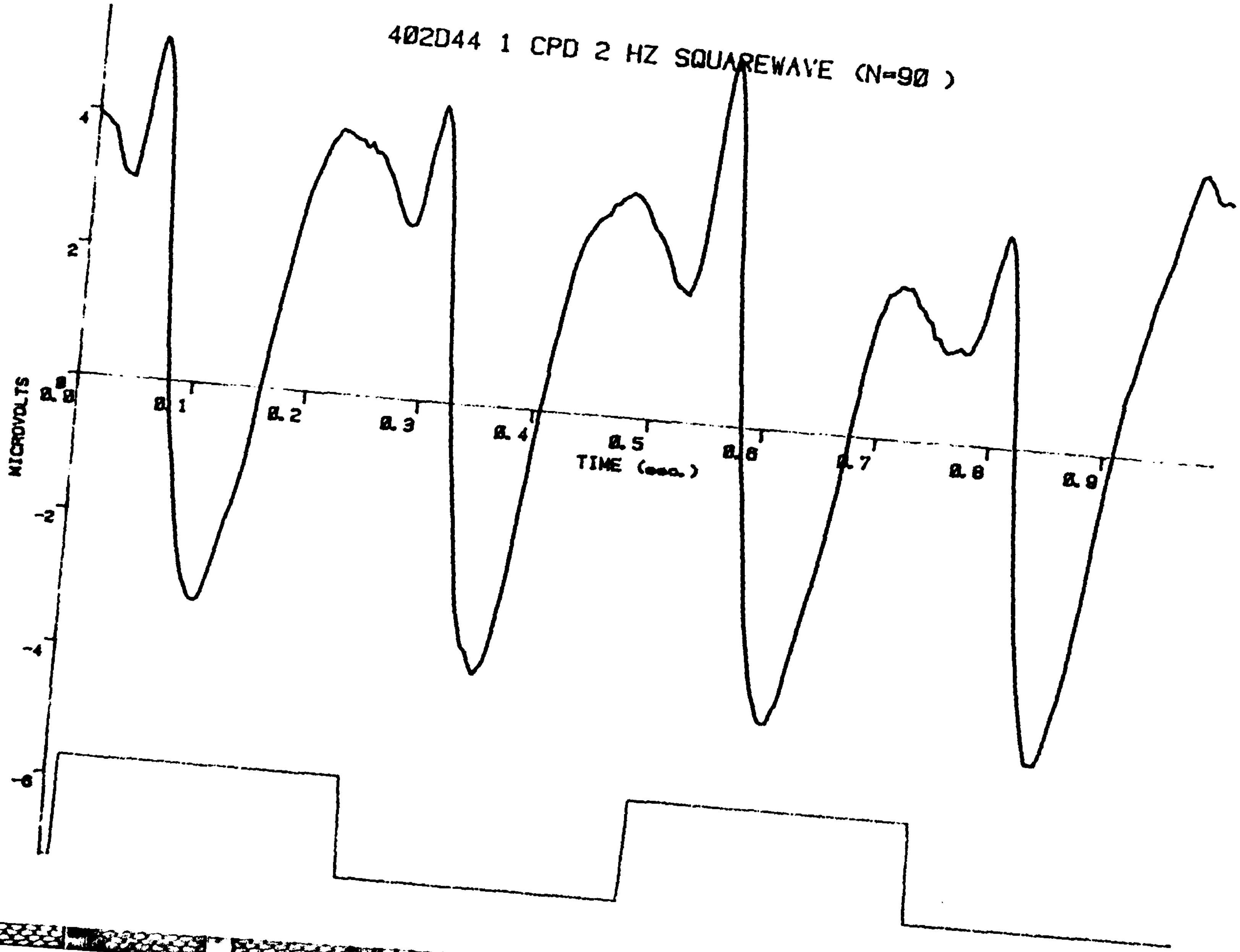

FIGURE 2A
91-26

```
RKING ON FILE UA0:402D44.AVG

NOPSIS OF DATA?                                              FIGURE 2B

   There are    1 cycles in    0.5000 seconds,
    giving a reversal rate of    4.0000 Hz.
   The sine analysis starts at    0.1250 seconds...
   ...Giving an analysis window of    224 points.


UMBER OF SINE TERMS:          0
UM OF SQUARES:     1751.963


UMBER OF SINE TERMS:          1
UM OF SQUARES:     514.8295


UMBER OF SINE TERMS:          2
UM OF SQUARES:     257.2634


UMBER OF SINE TERMS:          3
UM OF SQUARES:     189.3654


UMBER OF SINE TERMS:          4
UM OF SQUARES:     44635.10


OEFFICIENTS:

   DC LEVEL:      2.0540
   RAMP:     -2.3682

ssuming that the stimulus is a sine wave which crosses zero at      0.1250
   following are the statistics for the Fourier components of
   the response:


   Frequency:  4.00 Hz.
        Cosine coefficient:      2.8255
        Sine coefficient:     0.6199
        Peak-to-peak amplitude:      7.7593 microvolts.
        Phase :    -0.0687 radians.
        Response LAGS  stimulus by  -0.0027 seconds.


   Frequency:  8.00 Hz.
        Cosine coefficient:     -1.5174
        Sine coefficient:    -0.1342
        Peak-to-peak amplitude:      4.3457 microvolts.
        Phase :     0.9719 radians.
        Response LEADS stimulus by    0.0193 seconds.


   Frequency: 12.00 Hz.
        Cosine coefficient:      0.3775
        Sine coefficient:    -0.6823
        Peak-to-peak amplitude:      1.6611 microvolts.
        Phase :     0.3391 radians.
        Response LEADS stimulus by 92 9 70045 seconds.
```

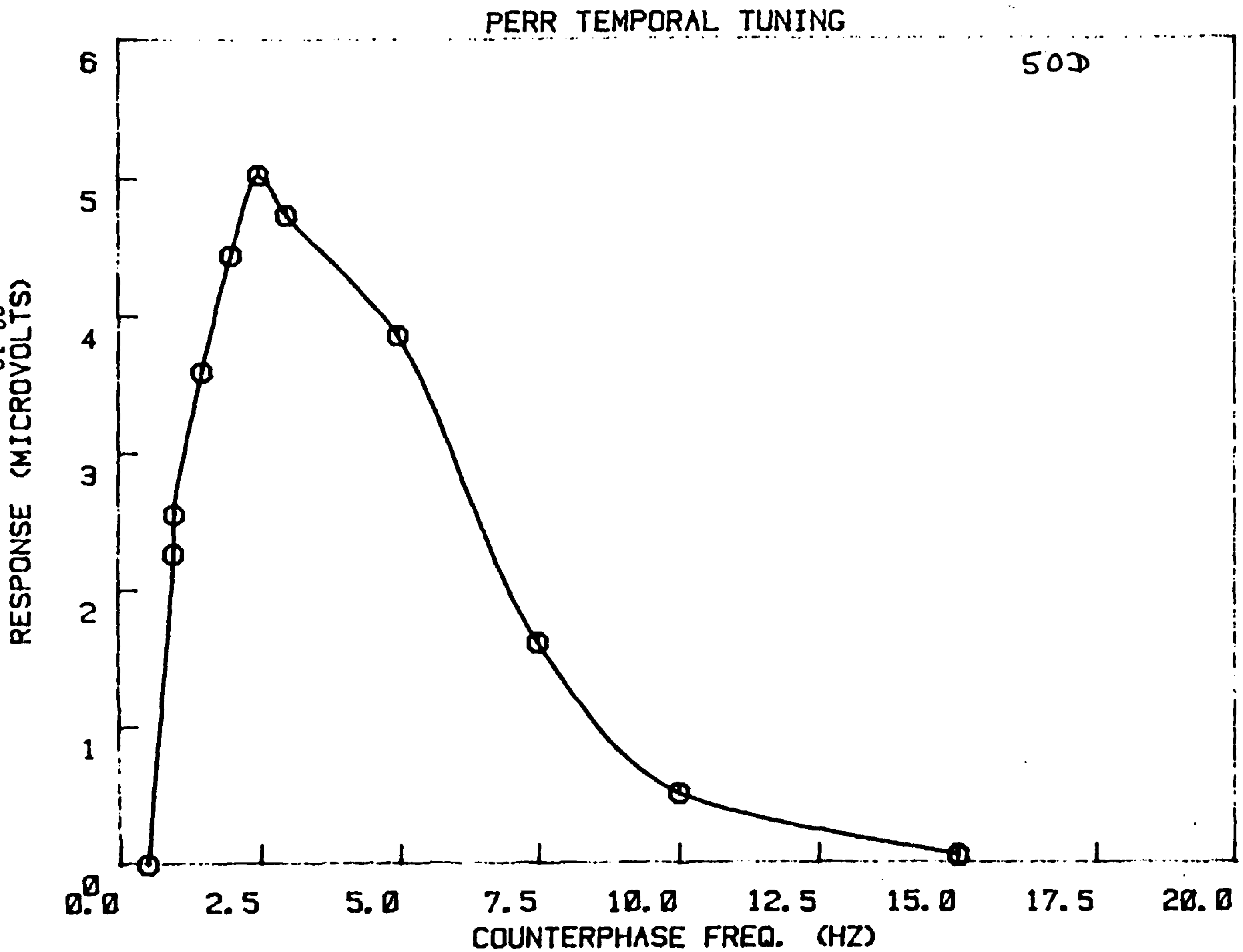

PERR TEMPORAL TUNING
50D
RESPONSE (MICROVOLTS)
0
1
2
3
4
5
6
0.0
2.5
5.0
7.5
10.0
12.5
15.0
17.5
20.0
COUNTERPHASE FREQ. (HZ)

FIGURE 8β-26

PERR SPATIAL TUNING

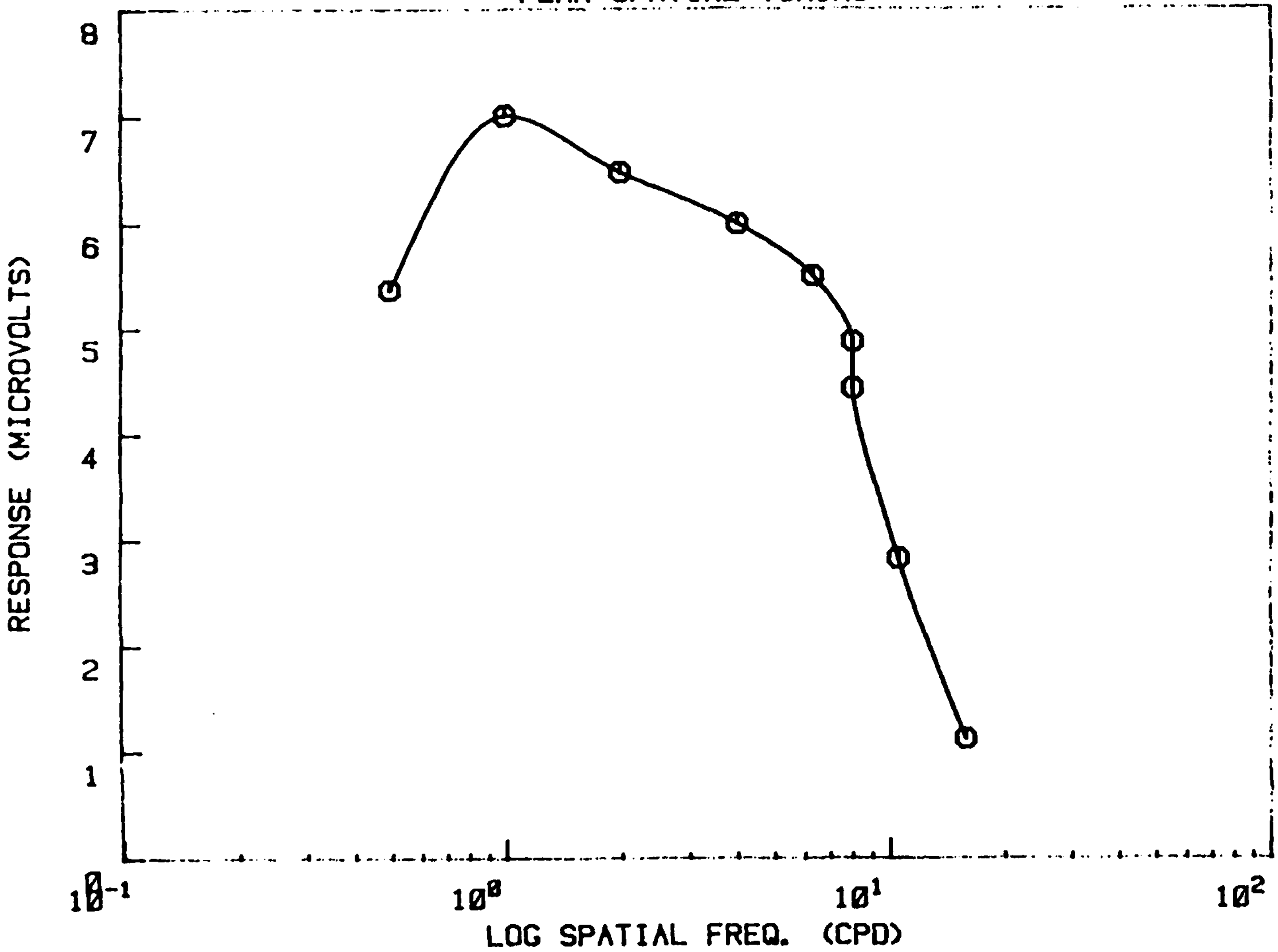

FIGURE 64-26

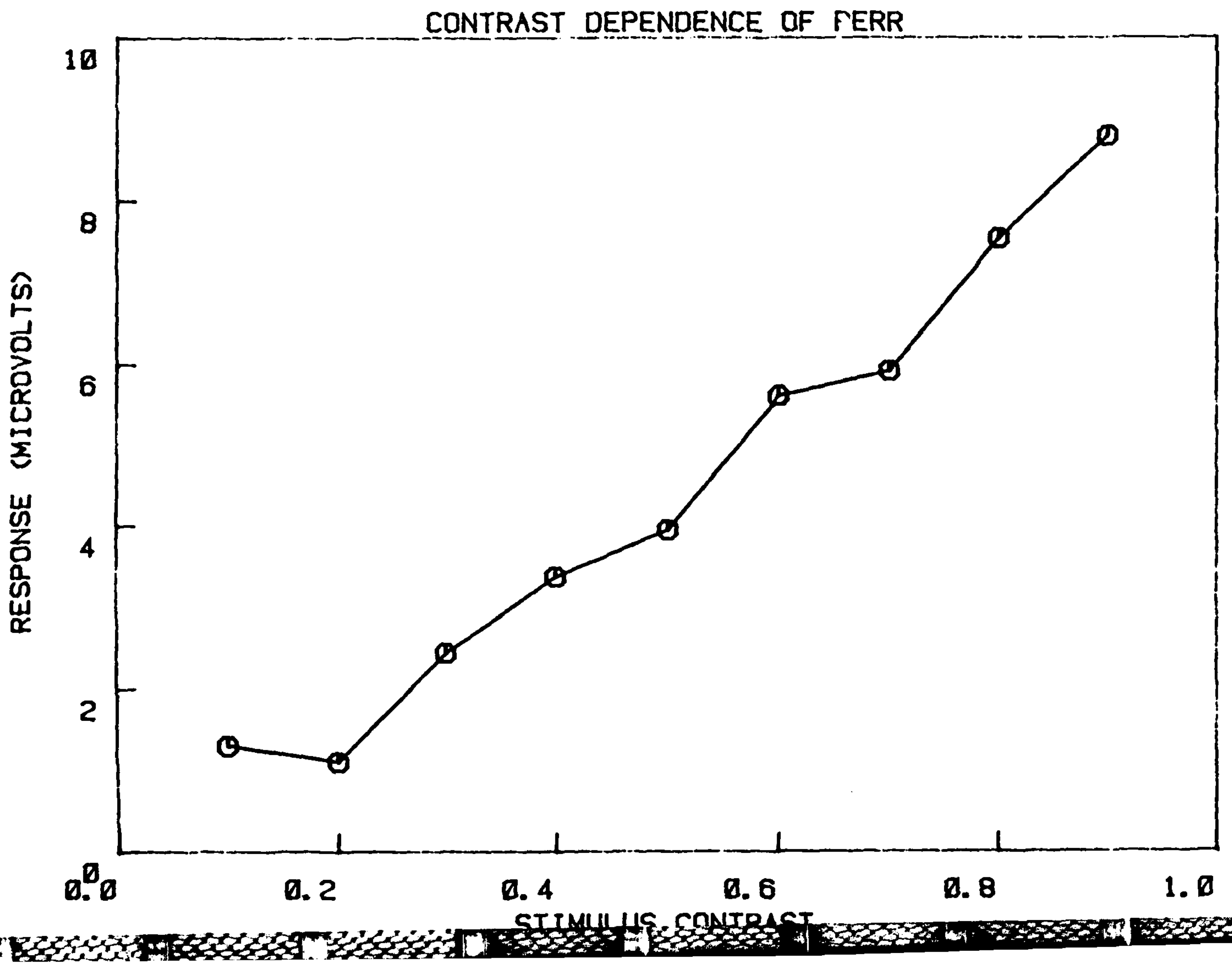

FIGURE 5

02-26

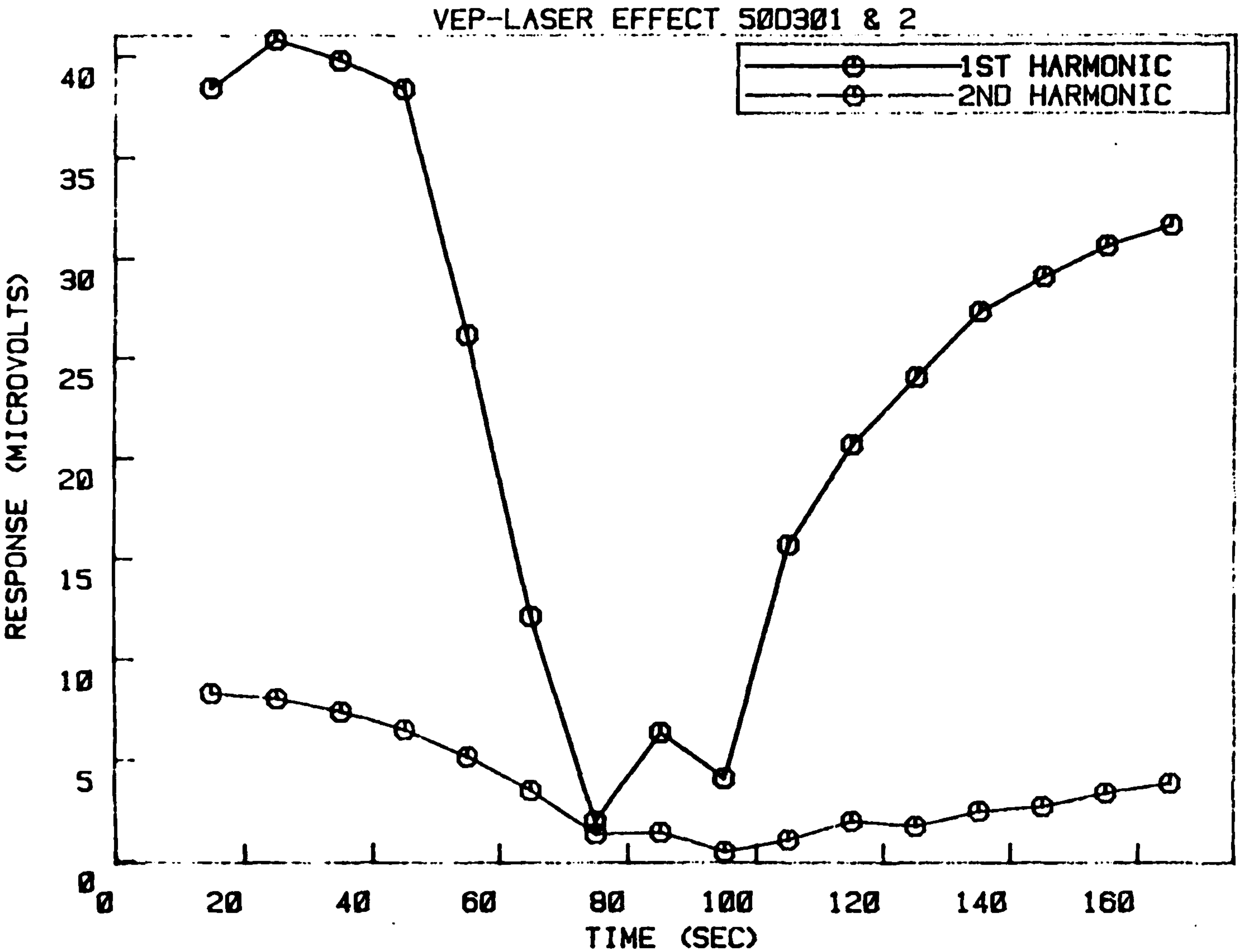

FIGURE 6 B2-26

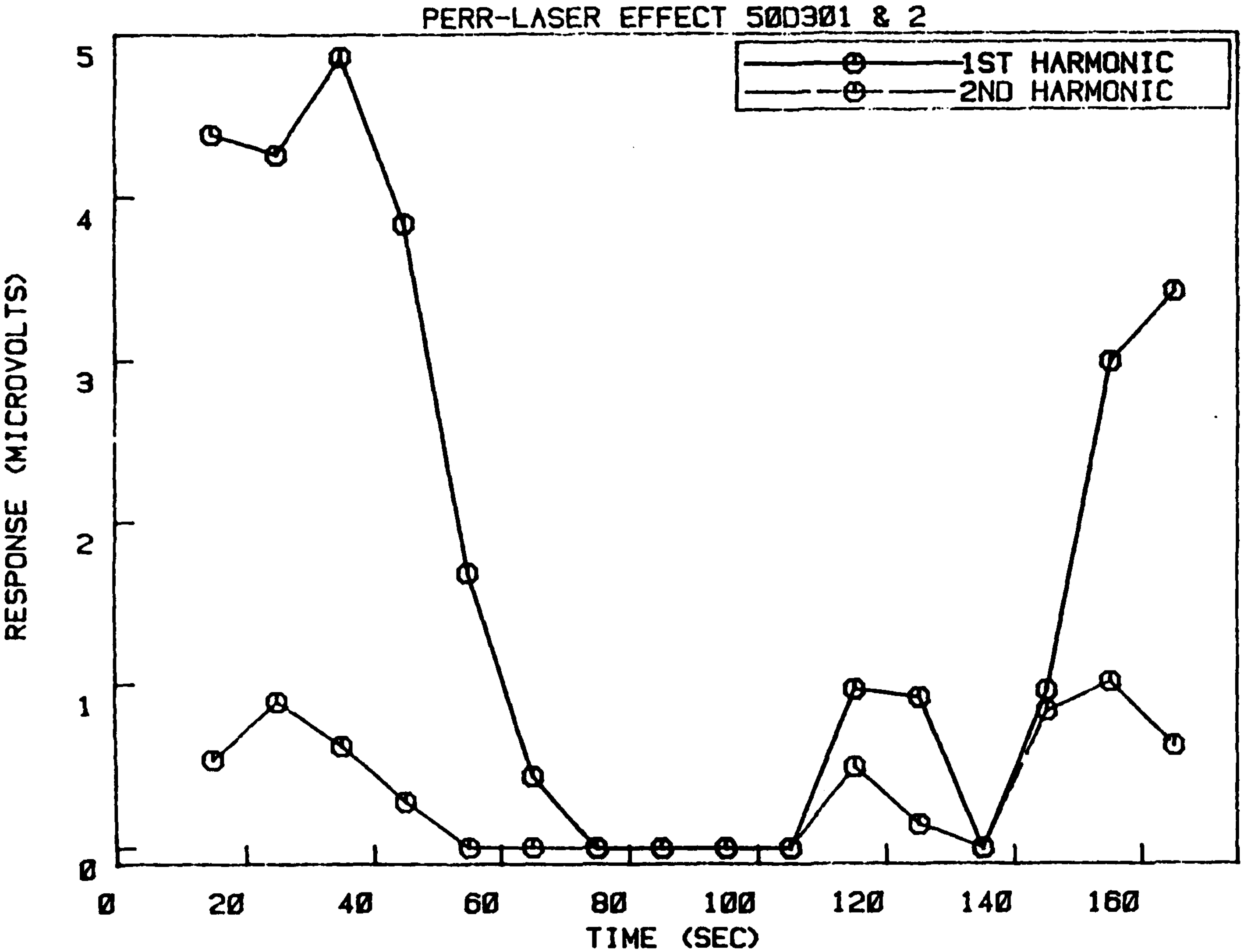

FIGURE 6A 22-26

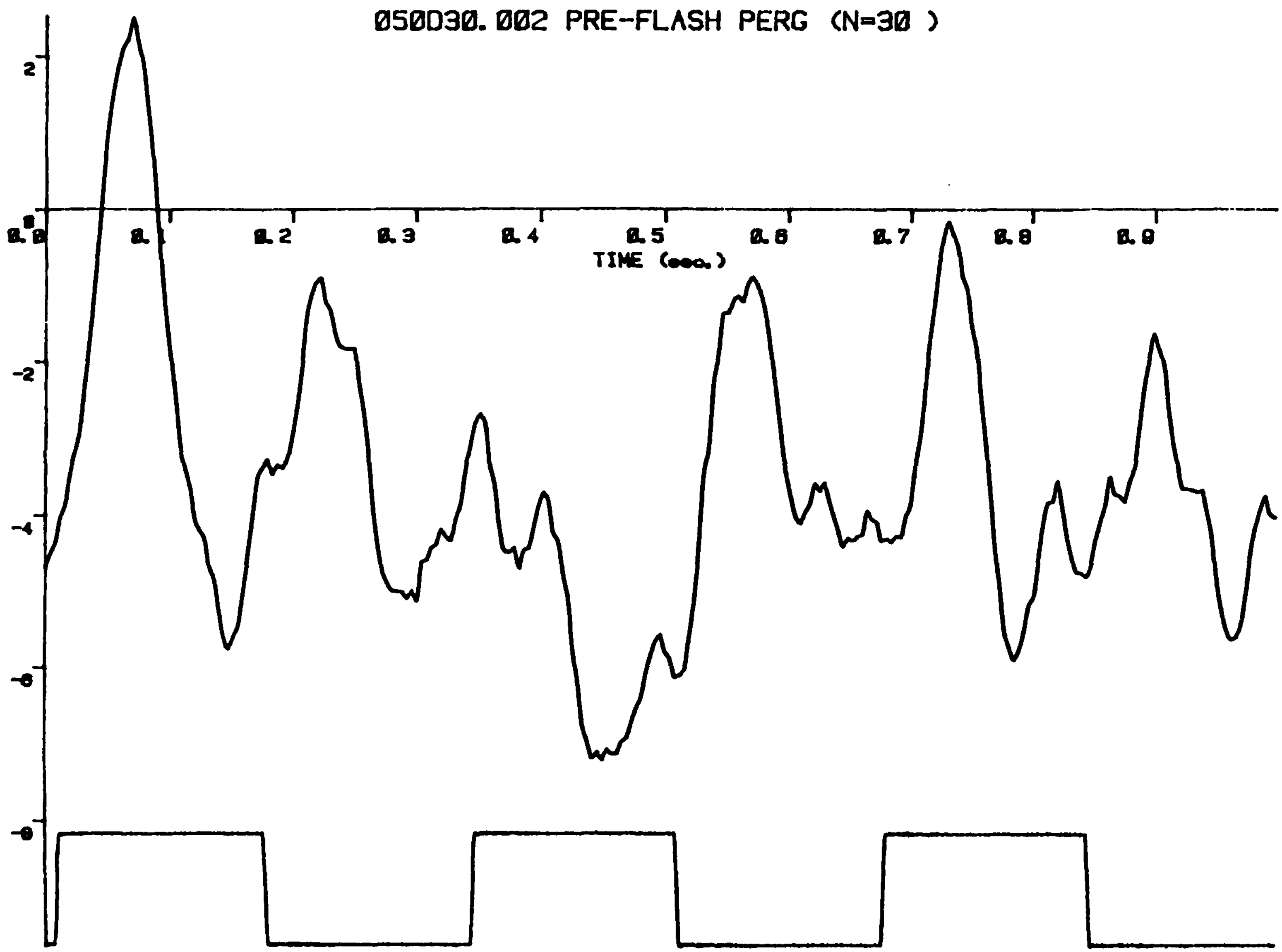
Ø5ØD3Ø.ØØ2 PRE-FLASH PERG (N=3Ø)
MICROVOLTS
2
Ø
-2
-4
-6
-8
Ø.Ø
Ø.1
Ø.2
Ø.3
Ø.4
Ø.5
Ø.6
Ø.7
Ø.8
Ø.9
TIME (sec.)

Figure 7A

050D30.008 POST-FLASH PERG (N=30)

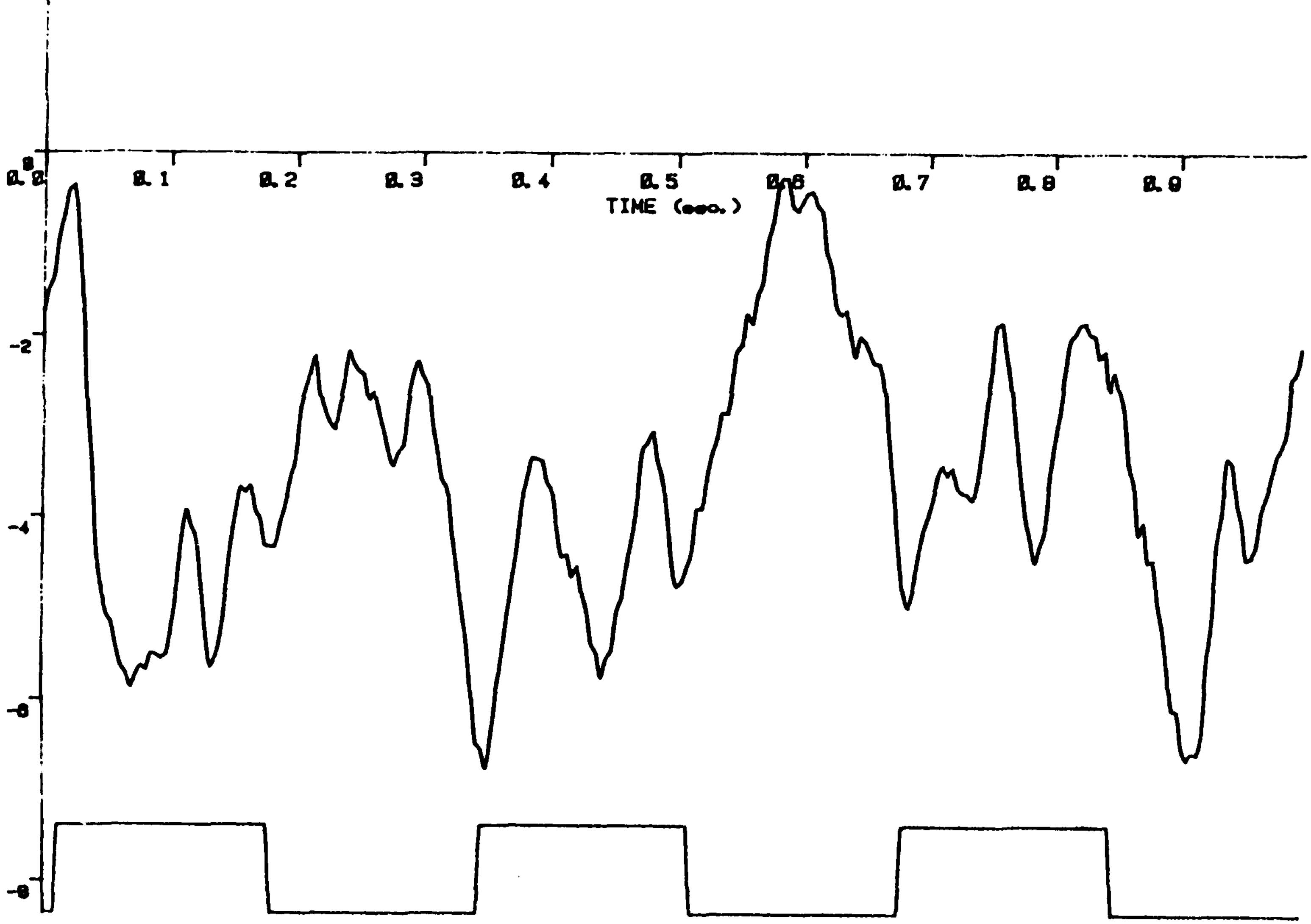

FIGURE 7B

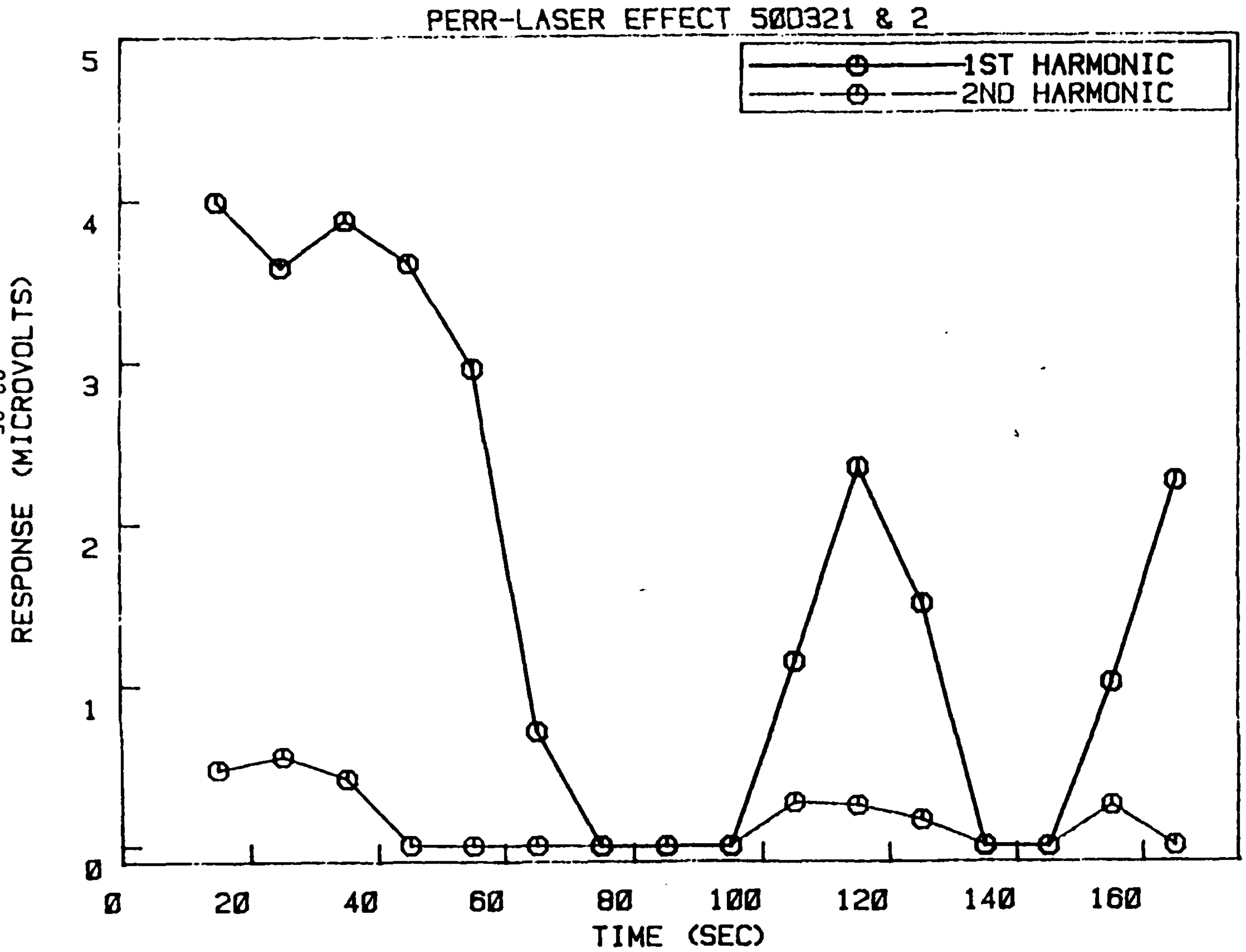
PERR-LASER EFFECT 500321 & 2
1ST HARMONIC
2ND HARMONIC
RESPONSE (MICROVOLTS)
TIME (SEC)
0
1
2
3
4
5
0
20
40
60
80
100
120
140
160

Figure 8A

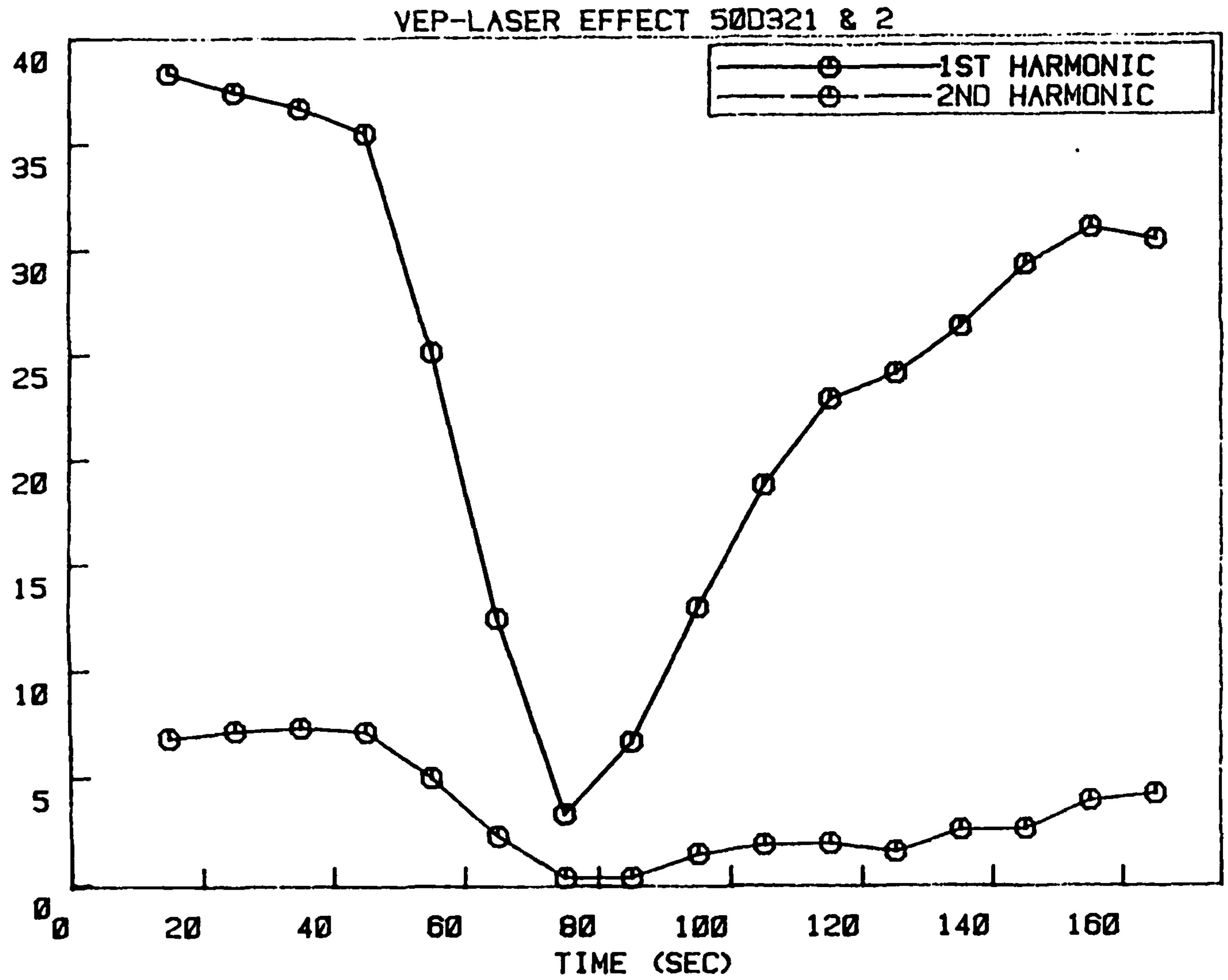
VEP-LASER EFFECT 50D321 & 2
1ST HARMONIC
2ND HARMONIC
RESPONSE (MICROVOLTS)
TIME (SEC)
0
5
10
15
20
25
30
35
40
0
20
40
60
80
100
120
140
160

FIGURE 8B

FIGURE 9A

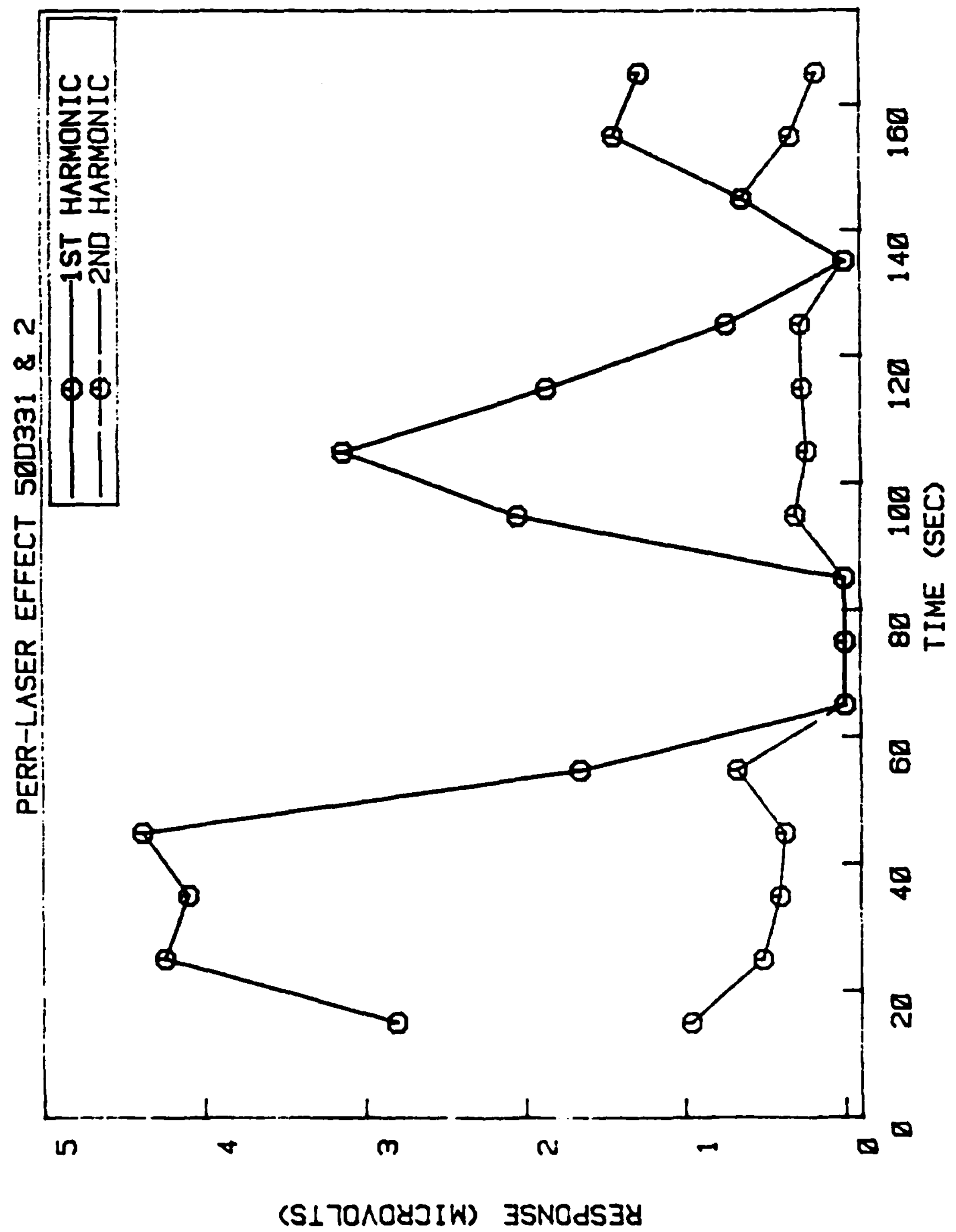
PERR-LASER EFFECT 50D331 & 2
1ST HARMONIC
2ND HARMONIC
TIME (SEC)
RESPONSE (MICROVOLTS)
0
20
40
60
80
100
120
140
160
1
2
3
4
5

FIGURE 9B

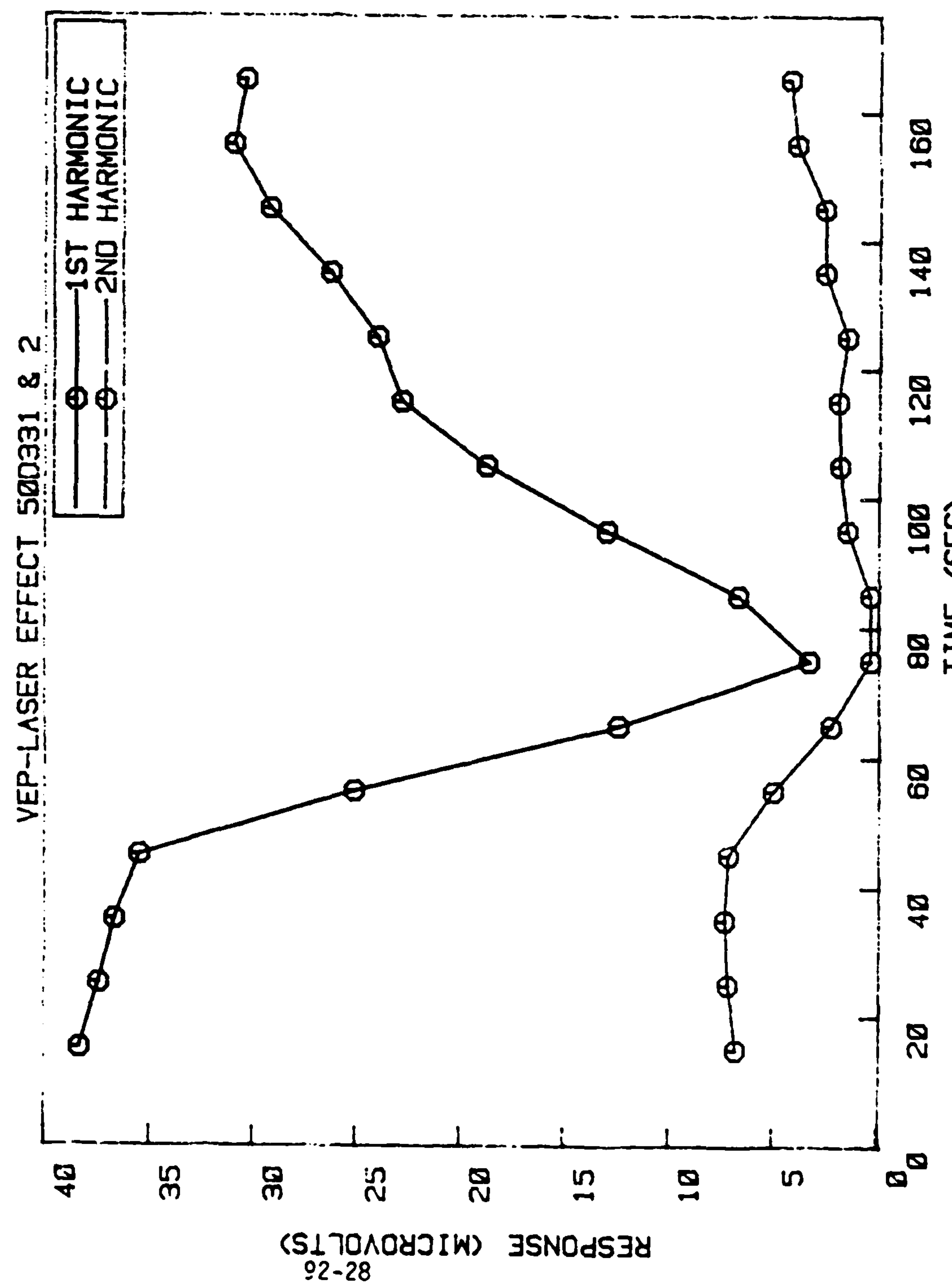

VEP-LASER EFFECT 5Ø0331 & 2
1ST HARMONIC
2ND HARMONIC
Ø 20 40 6Ø 8Ø 100 12Ø 140 160
TIME (SEC)
Ø 5 10 15 2Ø 25 3Ø 35 4Ø
RESPONSE (MICROVOLTS)

HB6578 #3 [MEHAFFEY] - MAJ. CARTLEDGE

```
Listing of save set

Save set:               15SEP85.BCK
Written by:             OPERATORS
UIC:                    [005,004]
Date:                   15-SEP-1985 13:26:52.59
Command:                BACKUP/LIST=MEHAFFEY.LST DRC2:[MEHAFFEY...]*.* MF41:15SEP85.BC
Operating system:       VAX/VMS version V4.1
BACKUP version:         V4.1
CPU ID register:        [illegible]
Node name:              _IRVAX::
Written on:             _MFA1:
Block size:             8192
Group size:             10
Buffer count:           3

[MEHAFFEY]CALIBRATION.DAT;1                        3  17-JUL-1985 11:24
[MEHAFFEY]DATPLOT.PLT;1                            3  17-JUL-1985 11:47
[MEHAFFEY]FOURIER.COM;1                            1   4-MAR-1985 15:55
[MEHAFFEY]FOURIER.EXE;25                          22  30-APR-1985 08:42
[MEHAFFEY]FOURIER.FORV1;1                         12   4-MAR-1985 15:51
[MEHAFFEY]FOURIER.FORV2;1                         13  22-MAY-1985 13:13
[MEHAFFEY]FOURIER.FORV3;1                         13   5-JUL-1985 09:13
[MEHAFFEY]FOURIER.OBJ;3                           10   5-JUL-1985 09:13
[MEHAFFEY]LASMAK.FORV1;1                           2  13-FEB-1985 15:45
[MEHAFFEY]LASMAK.FORV2;1                           3  13-APR-1985 15:11
[MEHAFFEY]LASMAK.FORV3;1                           4   5-JUL-1985 09:11
[MEHAFFEY]LOGIN.COM;3                              1  11-JUL-1985 13:37
[MEHAFFEY]RESP.EXE;1                               4  25-JUL-1985 13:21
[MEHAFFEY]RESP.FOR;1                               1  25-JUL-1985 13:20
[MEHAFFEY]RESP.OBJ;1                               2  25-JUL-1985 13:21
[MEHAFFEY]SCHONK.DAT;1                             1  25-JUL-1985 13:33
[MEHAFFEY]SL4G.FORV1;1                             3  25-JAN-1985 15:11
[MEHAFFEY]SIMUL.FORV1;1                            2   5-JUL-1985 09:14
[MEHAFFEY]SINMAK.FORV1;1                           4  13-APR-1985 15:14
[MEHAFFEY]SINMAK.FORV2;1                           4   5-JUL-1985 09:12
[MEHAFFEY]TEST.DAT;1                               1  11-JUL-1985 13:51
[MEHAFFEY]TEST.DAT;1                               1  15-AUG-1984 17:30
[MEHAFFEY]VARDAT.DAT;6                             2   2-AUG-1985 15:19
[MEHAFFEY]VARDAT.DAT;1                             2   2-AUG-1985 15:14
[MEHAFFEY]VARDAT.DIM;1                             1   2-AUG-1985 15:14

Total of 25 files, 122 blocks
End of save set
```

NOTE: These files were archived by BR, but can be restored at any time. They will, however, be deleted on 18 Sep 86 unless used.

```
C*******************************************************************
C                         PROGRAM DATAVG
C
C To take data from a file collected with the VER program and average
C   it for plotting on the HP plotter
C
C
C*******************************************************************
C
        PROGRAM DATAVG
        DIMENSION IBUF(256),ISTIM(256),DBUF(5,256),GAIN(5)
        BYTE FNAME(16),ONAME(16),IPER(2),NUM(2),EXT(3)
        DATA FNAME/16*0/ONAME/16*0/IPER/'.',0/
        DATA DBUF/1280*0./
        DATA ADMAX/5./ !The maximum +/- swing on the A/D converter
1       TYPE *,'Enter INPUT device (e.g.,DK1:):'
        ACCEPT 100,(FNAME(I),I=1,4)
        TYPE *,'Enter OUTPUT device (e.g.,DK0:):'
        ACCEPT 100,(ONAME(I),I=1,4)
        TYPE *,'Enter starting file name (e.g.,940C01): '
        ACCEPT 100, (FNAME(I),I=5,10)
100     FORMAT(14A1)
C
C Get the last two digits
C
        NUM(1)=FNAME(9)
        NUM(2)=FNAME(10)
        DECODE(2,101,NUM) I1
101     FORMAT(I2)
        FNAME(11)='.'
        FNAME(12)='D'
        FNAME(13)='A'
        FNAME(14)='T'
        TYPE *,'How many files are to be done?'
        ACCEPT 101,NFILES
        TYPE *,'Enter the number of DATA channels: '
        ACCEPT 101,NCHN
        DO 10 I=1,NCHN
        TYPE 102,I
102     FORMAT('0Enter the gain of the preamplifier for channel ',I3,
        1' : ',$)
        ACCEPT 103,GAIN(I)
10      CONTINUE
103     FORMAT(F10.0)
        TYPE *,'Enter the number of sweeps: '
        ACCEPT 105,NSWP
105     FORMAT(I3)
        TYPE *,'Enter the sampling rate (pts/sec): '
        ACCEPT 103,RATE
        TYPE *,'Enter the sweep time (sec per sweep)'
        ACCEPT 103,STIME
        TYPE *,'Enter the time for starting the moving average (sec.):'
        ACCEPT 103,TSTART
        KSTART=IFIX(TSTART/STIME)
        TYPE *,'Enter the time to stop the moving average (sec): '
        ACCEPT 103,TSTOP
        ISTOP=IFIX(TSTOP/STIME)
        IF(ISTOP.GT.NSWP) TYPE *,'Max. time set to ',FLOAT(NSWP)/STIME
        TYPE *,'Enter time increment for the sliding average (sec): '
        ACCEPT 103,AVINT
        INC=IFIX(AVINT/STIME)
```

```
      TYPE *,'Enter the averaging window width (sec): '
      ACCEPT 103,AVWIND
      IWIDTH=IFIX(AVWIND/STIME)

      NSHIFT=IFIX(RATE*12.5E-03) !Calculate the number of points
                                 !to shift the stimulus to compen-
                                 !sate for the synch pulse leading
                                 !the pattern reversal by 12.5 msec

      NDONE=0

C Open the file. If it doesn't exist, try again

      OPEN(UNIT=10, NAME=FNAME,TYPE='OLD',ERR=990)
      TYPE 91,(FNAME(I),I=1,14)
91    FORMAT('OWORKING ON FILE ',14A1)
      IOCHAN=ILUN(10)

C Ok. Now down to business

      ITER=1 !Count the number of iterations of the moving average
      ISTART=KSTART
1     IUPPER=ISTART+IWIDTH-1 !Return point for averaging iterations
      IF(IUPPER.GT.ISTOP) GO TO 3 !We're done.
      IBLK=(NCHN+1)*(ISTART) !locate the stimulus block
      IFLG=IREADW(256,IBUF,IBLK,IOCHAN) !Read in the stimulus block

C First, set the stimulus marker to ON/OFF

      MINST=4096 !Initialize the MAX and MIN values
      MAXST=0
      DO 20 I=1,256 ! Then find the stimulus range
      MINST=MIN0(MINST,IBUF(I))
      MAXST=MAX0(MAXST,IBUF(I))
20    CONTINUE
      MIDL=(MAXST+MINST)/2 !Find the middle
      DO 21 I=1,256 ! Set the stimulus values to ON/OFF
      IF(IBUF(I).GT.MIDL) IBUF(I)="7777
      IF(IBUF(I).LE.MIDL) IBUF(I)="0
21    CONTINUE

C Offset the stimulus to compensate for the 12.5 msec pattern generator
C   offset

      DO 92 I=1,NSHIFT !Zero the first NSHIFT stimulus points.
92    ISTIM(I)=0
      DO 93 I=NSHIFT+1,256 !Shift the stimulus over by NSHIFT points
93    ISTIM(I)=IBUF(I-NSHIFT)

      LL=(ISTART-1)*(NCHN+1)+1 !Initialize the lower limit of channel sc
      DO 30 I=ISTART+1,IUPPER !Now read in the data blocks. There is one
                        !sequence of channels per sweep. Each
                        !channel appears as one block.
      IX=1 !Set the DBUF row counter
      LU=LL+NCHN-1 !Upper limit of the channel scan
      DO 40 J=LL,LU !Do a channel scan by reading a sequence of blocks
                   !of data into DBUF. Each block in the sequence is
                   !one sweep of one channel. They are in channel
                   !sequence.
      IBLK=J !The block pointer.
```

```
      IFLG=IREADW(256,IBUF,IBLK,IOCHAN) !Read a block into IBUF.
      DO 50 K=1,256 !Convert to real and add to appropriate DBUF row
50    DBUF(IX,K)=DBUF(IX,K)+IBUF(K)
      IX=IX+1 !At each read , increment the DBUF row counter
40    CONTINUE
      LL=LL+NCHN+1 !Increment the lower limit of the channel scan.
                   !Add 1 to skip the next stimulus channel.
30    CONTINUE
C
C Average data and convert to microvolts
C
      DATMAX=ADMAX*1.0E6 !A/D bits to Voltage conversion. Note
C                        !that volts become microvolts!!
      DO 60 I=1,NCHN
      DO 60 J=1,256
      DBUF(I,J)=DBUF(I,J)/FLOAT(IWIDTH)!Normalize readings
      DBUF(I,J)=(DBUF(I,J)-2048.)/2048. !Convert averaged data
C                                       !to A/D bit levels
      DBUF(I,J)=DBUF(I,J)*DATMAX/GAIN(I) !Convert to voltage
60    CONTINUE
C
C Get the name of the output file
C
      DO 70 I=5,16 !Base it on the input file name
      ONAME(I)=FNAME(I)
70    CONTINUE
      N=INDEX(FNAME,IPER) !Find the position of the period in FNAME
C
C Change the extension to the iteration number
C
      ENCODE(3,105,EXT) ITER
      DO 90 I=1,3
      IF(EXT(I).EQ.1H ) EXT(I)=1H0 !Fill in the blanks
90    ONAME(N+I)=EXT(I)
C
      OPEN(UNIT=11,NAME=ONAME,TYPE='NEW',ERR=999)
      IOUT=ILUN(11)
C
C Write the results to the output file
C
      TYPE 95,(ONAME(I),I=1,14)
95    FORMAT('0Writing file ',14A1,//)
      DO 80 J=1,256
80    WRITE(11,104) (ISTIM(J),(DBUF(I,J),I=1,NCHN))
104   FORMAT(1H ,I10,2X,5(F10.4,2X))
      CLOSE(UNIT=11)
      IF(INC.EQ.0) GO TO 3 !Averaging whole file
      ISTART=ISTART+INC !Move the average
      ITER=ITER+1 !Increment the iteration count
      GO TO 4 !Back for the next average
C
3     CLOSE(UNIT=10) !All averages done.
      ITER=1 !Resate the iterate count
C
C Make the next filename
C
      I1=I1+1
      ENCODE(2,101,NUM) I1
      FNAME(9)=NUM(1)
      IF(I1.LE.9) FNAME(9)=1H0
```

```
      FNAME(10)=NUM(2)
      NDONE=NDONE+1
      IF(NDONE.LT.NFILES) GO TO 2
      TYPE *,'ALL REQUESTED FILES DONE.'
      GO TO 1
990   TYPE 991,(FNAME(I),I=1,14)
991   FORMAT('OUNABLE TO OPEN INPUT FILE: ',14A1)
      GO TO 1
999   TYPE 99,(ONAME(I),I=1,14)
99    FORMAT(1H ,'UNABLE TO OPEN OUTPUT FILE: ',14A1)
      STOP
      END
```

```
C***********************************************************************
C                          PROGRAM DATPLT
C
C To take data from a file created by the DATAVG program and plot
C   it on the HP plotter
C
C***********************************************************************
C
        PROGRAM DATPLT
        DIMENSION STIM(256),DBUF(5),DATA(256),TIME(256)
        DIMENSION YR(2),XR(2) !Range vectors for JBAXES
        BYTE FNAME(16),XLABL(50),YLABL(50),GLABL(50),NSWP(3)
        BYTE ANS
C
C COMMON and DATA some Simpleplot parameters:
C
        COMMON/JBSYS/KS,KR,CW,CM,IDUMM(14)
        COMMON/JBJUD/KSMP,MISS,IDUM2(18),SYMSZ,IDUM3(9)
        DATA KSMP,MISS,CM/0,0,0./
C
        DATA FNAME/'D','K','O',':',6*0,'.','A','V','G',2*0/
        DATA NPTS/256/
        DATA XLABL/'T','I','M','E',' ','(','s','e','c','.',')',39*0/
        DATA YLABL/'M','I','C','R','O','V','O','L','T','S',40*0/
        DATA NSWP /3*0/
        DATA NXC,NYC/11,10/
1       TYPE *,'Enter file name (e.g.,DKO:TEST1.AVG): '
        ACCEPT 100, (FNAME(I),I=5,14)
100     FORMAT(14A1)
C
C Open the file. If it doesn't exist, try again
C
        OPEN(UNIT=10, NAME=FNAME,TYPE='OLD',ERR=990)
2       TYPE *,'Which data channel is to be graphed?'
        ACCEPT 101,ICHN
101     FORMAT(I2)
        DO 3 I=1,50 !Reset GLABL
3       GLABL(I)=0
        DO 4 I=1,3 !Reset NSWP
4       NSWP(I)=0
        DO 6 I=1,10 !Load the title with the filename
6       GLABL(I)=FNAME(I+4)
        GLABL(11)=1H  !Don't forget the blank.
        TYPE *,'Now to set up the graphing parameters...'
        TYPE *,'  1. Title of graph?'
        ACCEPT 102,NT,(GLABL(I),I=12,50)
102     FORMAT(Q,50A1)
C       TYPE *,'  2. Abscissa (X-axis) label?'
C       ACCEPT 102,NXC,XLABL
C       TYPE *,'  3. Ordinate (Y-axis) label?'
C       ACCEPT 102,NYC,YLABL
        TYPE *,'  2. Length of sweep (seconds)?'
        ACCEPT 103,SLEN
103     FORMAT(F10.0)
        TYPE *,'  3. Number of sweeps averaged?'
        ACCEPT 104,NSWP
104     FORMAT(3A1)
C
C Ok. Now down to business
C
```

```
      GLABL(NT+12)=' '
      GLABL(NT+13)='('
      GLABL(NT+14)='N'
      GLABL(NT+15)='='
      GLABL(NT+19)=')'
      DO 10 I=1,3
      GLABL(I+NT+15)=NSWP(I)
0     CONTINUE
      NT=NT+19
      DO 20 J=1,256 !Read the stimulus and data
      READ(10,105) (STIM(J),(DBUF(I),I=1,5))
      DATA(J)=DBUF(ICHN)
:0    CONTINUE
05    FORMAT(6(F10.4,2X))

: Scale the stimulus for graphing

    First, find the max, min, and range of the stimulus and response data:

      DMAX=-999.
      DMIN=999.
      SMAX=-999.
      SMIN=999.
      DO 40 I=1,256
      DMAX=AMAX1(DMAX,DATA(I))
      DMIN=AMIN1(DMIN,DATA(I))
      SMAX=AMAX1(SMAX,STIM(I))
      SMIN=AMIN1(SMIN,STIM(I))
-0    CONTINUE
      TYPE *,'Data maximum is ',DMAX,' microvolts.'
      TYPE *,'Data minimum is ',DMIN,' microvolts.'
      DRANGE=DMAX-DMIN !Data range
      SRANGE=SMAX-SMIN !Stimulus range
      SRNEW=0.3*DRANGE !New stimulus range is 0.3*data range
      SMAXN=SRNEW/2.   !New stimulus maximum
      FACTOR=SMAXN/SMAX !Factor to convert stimulus to new values
      SMINN=999. !New stimulus minimum
      DO 50 I=1,256 ! Modify stimulus vector
      SNEW=FACTOR*STIM(I)!Convert stimulus values to new range
      STIM(I)=DMIN-(SMAXN-SNEW)-0.1*DRANGE !Shift to position
                                            !below response data
      SMINN=AMIN1(SMINN,STIM(I)) !Find the new stimulus minimum
                                 !for graphing
0     CONTINUE

  Build a time vector for graphing

      TINT=SLEN/256. !Seconds per point
      TIME(1)=0.0
      DO 60 I=2,256
      TIME(I)=TIME(I-1)+TINT
0     CONTINUE
      TYPE 115,(TIME(I),STIM(I),DATA(I),I=1,256,2)
115   FORMAT(1H ,'SCALED DATA:',/,(3(3X,F10.4)))
  Set up the parameters for graphing
  Load the range vectors for graphing
      YR(1)=SMINN !Smallest Y value
      YR(2)=DMAX       !Largest Y value
      XR(1)=TIME(1)    !Starting time
      XR(2)=TIME(256) !Ending time
```

```
      TYPE *,'Do you want to enter your own min/max?'
      ACCEPT 106,ANS
      IF((ANS.EQ."131).OR.(ANS.EQ."171)) GO TO 5
      IF((ANS.EQ.1HN).OR.(ANS.EQ.1Hn)) GO TO 5
      TYPE *,'Enter MAXIMUM: '
      ACCEPT 103,YR(2)
      TYPE *,'Enter MINIMUM: '
      ACCEPT 103,YR(1)
      IF(YR(1).GE.SMINN) TYPE *,'NOTE: Rescaling for stimulus!'
      IF(YR(1).GE.SMINN) YR(1)=SMINN
5     PAUSE 'Set up the HP plotter, then press RETURN.'
C
C Call the subroutine to set up the axes
C
      KSMP=0 !But first set those damned SIMPLEPLOT parameters
      MISS=0
      CM=0.0
C
      CALL JBAXES(XR,2,20.,XLABL,NXC,YR,2,15.,YLABL,NYC)
C
      CALL TITLE(1,2,GLABL,NT) !Put on the title
      CALL PEN(3) !Change the pen color
      CALL DRAW CV(TIME,DATA,256) !Plot the data
      CALL PEN(2) !Change the pen color
      CALL DRAW CV(TIME,STIM,256) !Plot the stimulus
      CALL ENDPLT()
      REWIND 10 !Reset to beginning of file in case.
      TYPE *,'Another Channel? (Y/N): '
      ACCEPT 106,ANS
106   FORMAT(1A1)
      IF((ANS.EQ."131).OR.(ANS.EQ."171)) GO TO 2
      CLOSE(UNIT=10)
      GO TO 1
990   TYPE 90,(FNAME(I),I=1,14)
      GO TO 1
90    FORMAT(1H ,'UNABLE TO OPEN INPUT FILE: ',14A1)
      END
```

```
CCCCCCCCCCCCCCCCCCCCCCCCCCCCCCCCCCCCCCCCCCCCCCCCCCCCCCCCCCCCCCCCCCCCCCCCCC
C
C                                  FORIER
C
C
C
C   A program to perform a Fourier analysis on a data stream given
C       a reference channel which is in the form of a square wave
C       with positive transitions corresponding to positive increases
C       in stimulus (that is, the reference channel serves as a true
C       stimulus frequency and phase marker, but not a true stimulus
C       amplitude marker.
C
C
C
CCCCCCCCCCCCCCCCCCCCCCCCCCCCCCCCCCCCCCCCCCCCCCCCCCCCCCCCCCCCCCCCCCCCCCCCCC
C
C
C
        PROGRAM FORIER
        BYTE FNAME(16),NUM(2)
        REAL*8 PHASE
        DIMENSION COEFFS(14,14),DATA(256),SUMS(14),ISTIM(256),DBUF(5)
        DIMENSION SS(6)
C
        DATA FNAME/16*0/
        DATA PI/3.141593/
        DATA NPTS/256/
C
1       TYPE *,'Enter starting file name (e.g.,DK0:940C01.AVG): '
        ACCEPT 100,(FNAME(I),I=1,14)
100     FORMAT(14A1)
C
C Get the last two digits
C
        NUM(1)=FNAME(9)
        NUM(2)=FNAME(10)
        DECODE(2,101,NUM) I1
101     FORMAT(I2)
        TYPE *,'How many files are to be done?'
        ACCEPT 101,NFILES
        TYPE *,'Enter the sweep length in seconds:'
        ACCEPT 102,SWEEP
102     FORMAT(F10.0)
C
        TYPE *,'Which DATA channel is to be analysed?'
        ACCEPT 101,ICHN
C       TYPE *,'How many frequency terms do you want?'
C       ACCEPT 102,NW
C
        NDONE=0
C
C
C
C Open the file. If it doesn't exist, try again
C
2       OPEN(UNIT=10, NAME=FNAME,TYPE='OLD',ERR=990)
        TYPE 91,(FNAME(I),I=1,14)
91      FORMAT('OWORKING ON FILE ',14A1)
C
C Ok. Now down to business
C
        NW=0 !Trial number of frequency terms.
        KFLAG=0 !Indicator for printout or not
```

```
        DO 20 J=1,NPTS !Load the phase marker and data vectors
        READ(10,103) (STIM,(DBUF(I),I=1,5))
        DATA(J)=DBUF(ICHN)
        ISTIM(J)=IFIX(STIM*1.0E4) !Needed to restore integer
:0      CONTINUE
.03     FORMAT(6(F10.4,2X))
        DWELL=SWEEP/FLOAT(NPTS) !Seconds per point
:
: Find the true frequency
:
        IPOS=-999 !Initialize position of the first positive transition
        INEG=-999 !Ditto for marker for first negative transition
        NCYCLE=0 !Initialize cycle counter.
        ITEST2=ISTIM(1) !Load the test vector
:
:********************
:       IPOS=0      !*Keep this statement if the stimulus marker
:                   !*ALWAYS begins at 0. Otherwise COMMENT it out.
:********************
:
        DO 30 I=2,NPTS
        IFLAG=0 !Set flag for "no transition".
        ITEST1=ITEST2 !Advance the test buffer.
        ITEST2=ISTIM(I)
        IF((ITEST1-ITEST2).GE."4000) IFLAG=-1 !A negative-going transition
        IF((ITEST1-ITEST2).LE.-"4000) IFLAG=1 !A positive-going transition
        IF(IFLAG) 3,30,4 !Test the flag.
3       IF(IPOS.EQ.-999) GO TO 30 !No positive transition yet.
        IF(INEG.EQ.-999) INEG=I-1 !The first negative transition after
:                                 !the first positive transition. Note tha
:                                 !the actual transition BEGAN on the
:                                 !PRECEEDING point.
        GO TO 30
:       IF(IPOS.NE.-999) NCYCLE=NCYCLE+1! If this isn't the first pos-
:                                       !itive transition, increment
:                                       !the cycle counter
        IF(IPOS.EQ.-999) IPOS=I-1 !The first positive transition (TO).
:                         ! Note that the actual transition BEGAN on
:                         !the PRECEEDING point.
        ILAST=I-1!Jot down the position in case this is
                                  !the last transition.
:0      CONTINUE
:
: Calculate the frequency and othe stimulus parameters.
:
        POS=FLOAT(IPOS)*DWELL !POS is the time of the first positive
                              !transition.
        TF=FLOAT(NPTS)*DWELL-POS !The time of the last point.
        TIME=DWELL*FLOAT(ILAST-IPOS) !The time for NCYCLE cycles.
        IF(NCYCLE.EQ.0) GO TO 12
3       FREQ=FLOAT(NCYCLE)/TIME !The alternation frequency
        PERIOD=1./FREQ
        TO=0.25*PERIOD !Time of the first positive zero crossing of the
                       !stimulus sine wave. The beginning time of the
                       !Fourier analysis.
        ITO=IFIX(TO/DWELL)
        FREQ=2.*FREQ !The reversal rate.
        ITO=(INEG+IPOS)/2  !Position of the beginning of the first sine
                           !wave for Fourier analysis (First positive
                           !zero crossing).
```

```
C       TO=FLOAT(ITO)*DWELL !The time of the beginning of the first sine
C                             !wave for Fourier analysis.
        NDAT=NPTS-ITO !The number of data points for analysis
        W=2.*PI*FREQ !The fundamental frequency.
C
C Tell them where we are so far.
C
        TYPE 104,NCYCLE,TIME,FREQ,TO,NDAT
104     FORMAT('OSYNOPSIS OF DATA:'//,5X,'There are ',I3,' cy
        1cles in ',F8.4,' seconds,'/,5X,' giving a reversal rate of '
        2,F8.4,' Hz.',/,5X,'The sine analysis starts at ',F8.4,
        3' seconds...',/,5X,'...Giving an analysis window of ',
        4I5,' points.',//)
C
C  (5): The return point for iterations
C
5       DO 10 I=1,14 !Zero the output vector
        SUMS(I)=0.
        DO 10 J=1,14
10      COEFFS(I,J)=0.
C
C Calculate the inhomogenious terms
C
        CALL IRSMAK(DATA,SUMS,NDAT,NW,W,DWELL,TO,ITO)
C
C Calculate the coefficient matrix
C
        CALL SINMAK(COEFFS,W,NW,TO,TF)
C
        NT=2*NW+2 !Total number of terms in the fitting equation
C
C Solve the equations
C
        CALL SIMQ(COEFFS,SUMS,NT,KS,14,.0001)
        IF(KS.EQ.1) TYPE *,'WARNING!! SINGULAR MATRIX.'
C
C Calculate the coefficients and phases for all terms
C
        IF(KFLAG.EQ.1) TYPE 105,SUMS(1),SUMS(2)
105     FORMAT(1H ,'COEFFICIENTS:',//,5X,'DC LEVEL: ',F10.4,/,5X,
        1'RAMP: ',F10.4)
        IF(NW.EQ.0) GO TO 6
        DO 50 I=1,NW
        J1=(I+1)*2-1
        J2=J1+1
        WN=W*FLOAT(I)
        FN=FREQ*FLOAT(I)
        PHASE='LEADS'
        P=2.*SQRT(SUMS(J1)**2+SUMS(J2)**2) !Peak-to-peak amplitude
        PHI=ATAN2(-SUMS(J2),SUMS(J1))/PI    !Phase relative to sine wave
C
        CALL CALIB(FN,P,PHI) !Convert amplitude and phase by calibration
C                             !factors
        DELT=PHI/WN !Time difference relative to stimulus as sine wave
        IF(PHI.LT.0) PHASE='LAGS'
        IF((KFLAG.EQ.1).AND.(I.EQ.1)) TYPE 107,TO
107     FORMAT('OAssuming that the stimulus is a sine wave which cros
        1ses zero at ',F10.4,/,5X,'following are the statistics for the
        2 Fourier components of',/,5X,'the response:',//)
        IF(KFLAG.EQ.1) TYPE 108,FN,SUMS(J1),SUMS(J2),P,PHI,PHASE,DELT
```

```
)0      CONTINUE
 08     FORMAT(5X,'Frequency: ',F5.2,' Hz.',/,10X,'Cosine coefficient: '
        1,F10.4,/,10X,'Sine coefficient: ',F10.4,/,10X,'Peak-to-peak a
        2mplitude: ',F10.4,' microvolts.',/,10X,'Phase :',F10.4,' radi
        3ans.',/,10X,'Response ',A5,' stimulus by ',F8.4,' seconds.',//)
        TYPE 109
:109    FORMAT(8X,'INPUT',9X,'OUTPUT',/)
        T=TO
        SS(NW+1)=0.
        DO 60 I=ITO,NPTS
        T=T+DWELL
        D=SUMS(1)+SUMS(2)*T
        DO 70 J=1,NW
        H=FLOAT(J)
'0      D=D+SUMS(2*(J+1)-1)*COS(H*W*T)+SUMS(2*(J+1))*SIN(H*W*T)
,0      SS(NW+1)=SS(NW+1)+(D-DATA(I))**2
:60     TYPE 109,DATA(I),D
:109    FORMAT(5X,F10.4,5X,F10.4)
        TYPE *,'NUMBER OF SINE TERMS: ',NW
        TYPE *,'SUM OF SQUARES: ',SS(NW+1)
        TYPE *
        TYPE *
        IF(KFLAG.EQ.1) GO TO 11 !After the printout
        IF(NW.GE.6) GO TO 9 !That's the end. No improvement found.
        IF(NW.EQ.0) GO TO 7 !Always iterate to at least one term.
        IF(SS(NW+1)-SS(NW)) 7,8,8 !Check progress of iterations
7       NW=NW+1 !Getting better...
        GO TO 5
3       KFLAG=1 !No improvement, or worse.
        NW=NW-1 !Set the NW back to the last one.
        GO TO 5 !Go back and do it again, but print out the results
9       TYPE *,'NO IMPROVEMENT FOUND AFTER 6 TERMS. LAST RESULTS:'
        KFLAG=1
        GO TO 5
12      TYPE *,'LESS THAN ONE CYCLE FOUND!!'
        TYPE *,'  Extrapolating frequency from first half-cycle...'
        NCYCLE=1
        TIME=FLOAT(2*(INEG-IPOS))*DWELL
        GO TO 13
11      CLOSE(UNIT=10)
C
C Make the next filename
C
        I1=I1+1
        ENCODE(2,101,NUM) I1
        FNAME(9)=NUM(1)
        IF(I1.LE.9) FNAME(9)=1H0
        FNAME(10)=NUM(2)
        NDONE=NDONE+1
        IF(NDONE.LT.NFILES) GO TO 2
        TYPE *,'ALL REQUESTED FILES DONE.'
        GO TO 1
        CLOSE(UNIT=10)
        GO TO 1
        STOP
990     TYPE 90,(FNAME(I),I=1,14)
        GO TO 1
90      FORMAT(1H ,'UNABLE TO OPEN INPUT FILE: ',14A1)
        STOP
        END
```

```
        SUBROUTINE SINMAK(A,W,NW,TO,TF)
        DIMENSION A(14,14)
        REAL L
        S(Z)=(SIN(Z*W*TF)-SIN(Z*W*TO))/(Z*W)
        C(Z)=(COS(Z*W*TO)-COS(Z*W*TF))/(Z*W)
        S1(Z)=(TF*SIN(Z*W*TF)-TO*SIN(Z*W*TO))/(Z*W)
        C1(Z)=(TO*COS(Z*W*TO)-TF*COS(Z*W*TF))/(Z*W)
        CS(Z)=((SIN(Z*W*TF))**2-(SIN(Z*W*TO))**2)/(2.*Z*W)
        L=TF-TO
C
D       TYPE *,'NOW IN SUBROUTINE SINMAK.'
C
        A(1,1)=2.*L
        A(1,2)=TF**2-TO**2
        A(2,2)=2.*(TF**3-TO**3)/3.
C
        IF(NW.EQ.0) GO TO 2
        IF(NW.LE.1) GO TO 1
        DO 10 J=2,2*NW
        Y=FLOAT(J)
        DO 10 I=1,J-1
        X=FLOAT(I)
        A(2*I+1,2*J+1)=S(X+Y)+S(X-Y)
        A(2*I+2,2*J+2)=S(X-Y)-S(X+Y)
        A(2*I+2,2*J+1)=C(X-Y)+C(Y+X)
10      A(2*I+1,2*J+2)=C(Y-X)+C(Y+X)
C
1       DO 20 J=1,NW
        X=FLOAT(J)
        A(1,2*J+1)=2.*S(X)
        A(1,2*J+2)=2.*C(X)
        A(2,2*J+1)=2.*(S1(X)-C(X)/(X*W))
        A(2,2*J+2)=2.*(C1(X)+S(X)/(X*W))
        A(2*J+1,2*J+1)=L+S(2.*X)
        A(2*J+2,2*J+2)=L-S(2.*X)
20      A(2*J+1,2*J+2)=2.*CS(X)
C
2       DO 30 I=2,2*NW+2 !Fill in the symmetrical terms
        DO 30 J=1,I-1
30      A(I,J)=A(J,I)
C
D       DO 40 I=1,4
D40     TYPE 100,(A(I,J),J=1,4)
D100    FORMAT(1H ,4F10.4)
D       TYPE *,'EXITING SINMAK.'
        RETURN
        END
```

```
      SUBROUTINE IRSMAK(DATA,B,N,NW,W,DWELL,TO,ITO)
      DIMENSION DATA(1),B(1)
C
D     TYPE *,'NOW IN SUBROUTINE IRSMAK.'
C
      T=TO
      DO 10 I=ITO,N
      T=T+DWELL
      B(1)=B(1)+DATA(I)*DWELL
      B(2)=B(2)+T*DATA(I)*DWELL
      IF(NW.EQ.0) GO TO 10 !No sine/cosine terms.
      DO 20 J=1,NW
      B(2*J+1)=B(2*J+1)+DATA(I)*COS(FLOAT(J)*W*T)*DWELL
20    B(2*J+2)=B(2*J+2)+DATA(I)*SIN(FLOAT(J)*W*T)*DWELL
10    CONTINUE
      DO 30 I=1,2*NW+2 !Multiply by 2
30    B(I)=B(I)*2.
D     TYPE 100,(B(K),K=1,2*NW+2)
100   FORMAT('OIRSMAK RESULTS: I  B(I):',(F11.4))
D     TYPE *,'EXITING SUBROUTINE IRSMAK'
      RETURN
      END
```

```
      SUBROUTINE SIMQ (A,B,N,KS,NDIM,TOL)
      DIMENSION A(1), B(1)
      CALL ARRAY(2,N,N,NDIM,NDIM,A,A)
C
C     FORWARD SOLUTION
C
      KS=0
      JJ=-N
      DO 65 J=1,N
      JY=J+1
      JJ=JJ+N+1
      BIGA=0
      IT=JJ-J
      DO 30 I=J,N
C
C     SEARCH FOR MAXIMUM COEFFICIENT IN COLUMN
C
      IJ=IT+I
      IF(ABS(BIGA)-ABS(A(IJ)))20,30,30
20    BIGA=A(IJ)
      IMAX=I
30    CONTINUE
C
C     TEST FOR PIVOT LESS THAN TOLERANCE (SINGULAR MATRIX)
C
      IF(ABS(BIGA)-TOL)35,35,40
35    KS=1
      RETURN
C
C     INTERCHANGE ROWS IF NECESSARY
C
40    I1=J+N*(J-2)
      IT=IMAX-J
      DO 50 K=J,N
      I1=I1+N
      I2=I1+IT
      SAVE=A(I1)
      A(I1)=A(I2)
      A(I2)=SAVE
C
C     DIVIDE EQUATION BY LEADING COEFFICIENT
C
50    A(I1)=A(I1)/BIGA
      SAVE=B(IMAX)
      B(IMAX)=B(J)
      B(J)=SAVE/BIGA
C
C     ELIMINATE NEXT VARIABLE
C
      IF(J-N) 55,70,55
55    IQS=N*(J-1)
      DO 65 IX=JY,N
      IXJ=IQS+IX
      IT=J-IX
      DO 60 JX=JY,N
      IXJX=N*(JX-1)+IX
      JJX=IXJX+IT
60    A(IXJX)=A(IXJX)-(A(IXJ)*A(JJX))
65    B(IX)=B(IX)-(B(J)*A(IXJ))
C
```

```
C        BACK SOLUTION
C
70       NY=N-1
         IT=N*N
         DO 80 J=1,NY
         IA=IT-J
         IB=N-J
         IC=N
         DO 80 K=1,J
         B(IB)=B(IB)-A(IA)*B(IC)
         IA=IA-N
80       IC=IC-1
         RETURN
         END
```

1985 USAF-UES SUMMER FACULTY RESEARCH PROGRAM/

GRADUATE STUDENT SUMMER SUPPORT PROGRAM

Sponsored by the

AIR FORCE OFFICE OF SCIENTIFIC RESEARCH

Conducted by the

UNIVERSAL ENERGY SYSTEMS, INC.

FINAL REPORT

PROFILING AIR FORCE FAMILY WORK GROUPS TO OPTIMIZE SERVICE SATISFACTION AND CAREER COMMITMENT IMPACT

Prepared by: Dr. Ivor S. Mitchell
Academic Rank: Distinguished Professor
Department: Department of Marketing
University: Atlanta University
Research Location: Leadership and Management Development Center
Maxwell Air Force Base
Montgomery, Alabama

USAF Research Contact: Major Mickey R. Dansby

Date: September 5, 1985
Contract No.: F49620-85-0013

PROFILING AIR FORCE FAMILY WORK GROUPS
TO OPTIMIZE SERVICE SATISFACTION AND CAREER COMMITMENT IMPACT

by

Ivor S. Mitchell

ABSTRACT

Air Force members make career commitment decisions on both work and nonwork-related variables. The study shows that while members' own attitudes and demographics are important influencing factors on commitment, the work-family dyadic relationship produces attitudes which account for significant variations in career commitment.

An Air Force career commitment model is presented with frequency of use and satisfaction with Air Force services as mediating factors in career commitment. In order to effect greater precision in targeting, the study identifies attitudinal and demographic profiles of the heavy-user, light-user, and non-user, as well as the highly satisfied, moderately satisfied, and dissatisfied consumer of Air Force services. Based on these identified user-needs and user-categories the study suggests the tailoring of programs to Air Force family work group needs instead of trying to alter their need patterns.

ACKNOWLEDGMENTS

The research described in this report was undertaken through the sponsorship of the United States Air Force Systems Command, Air Force Office of Scientific Research, and the Analysis Directorate of the Leadership and Management Development Center (LMDC), Maxwell AFB, Montgomery, Alabama.

The guidance, advice, support and patience of Major Mickey R. Dansby and his staff are greatly acknowledged. Particularly useful was the computer support of Second Lieutenant Lamb. Brainstorming sessions with Professor Phillip Lewis during the conceptual stage of the project have also been useful.

PROFILING AIR FORCE FAMILY WORK GROUPS
TO OPTIMIZE SERVICE SATISFACTION AND CAREER COMMITMENT IMPACT

1.0 INTRODUCTION

Many factors--individual, family and environmental--have been studied with a view to explaining service satisfaction and career intention/commitment (Sonnenfeld and Kotter, 1980; Mowday, Porter, and Steers, 1982). However, few empirical studies (Mitchell and Beach, 1976; Wheeler and Mahoney, 1981; Wright, 1975) have defined the profiles of work groups as they evaluate choices of alternative attributes which they used as bases for determining the level of service satisfaction and career commitment. Drawing on career choice paradigms, as well as frequency of use and services satisfaction literature, this research effort provides an examination of the effects on career intention and commitment of variables such as family attitudes and demographics, identification with the Air Force and their job, perceived family support, Air Force prestige and status, and access to Air Force services.

Although occupational choice, use frequency and services satisfaction are often characterized as being heavily exposed to individual, family and environmental effects, the explained significance of these effects remains vague, and in some cases researchers have presented contradictory results (Jackofsky, 1984; Bell, et. al., 1976). Despite a decade or more of attempts by the military and civilian managers to solve problems of personnel accession and retention, there still remains much difficulty in explaining career choice and commitment, or even in identifying the effects of specific family attitudes and demogra-

phics, and other factors which significantly impact on career choice.

1.1 Antecedents to Service Satisfaction and Career Commitment

Recent findings from both military and nonmilitary studies support the view that service satisfaction and career commitment are affected by personal characteristics such as length of marriage, number of children, number of children at home, and years in the Air Force (McCubbin, Cauble, and Patterson, 1982); family disruptions due to time at present station (Jones, 1976; Szoc, 1982); dual career considerations due to spousal employment patterns, and compatability with spouse's work schedules (Paloma, Pendleton, and Garland, 1981); spouse's support in terms of their identification with their Air Force job, desire for career retention, desire for information about their spouse's job, compatability between spouses' desires for a military career, and perceived importance of spouses' attitudes on career decisions (Belt and Sweeney, 1973; Schneider and Dachler, 1978; Stanton, 1981; Hickman and Hunter, 1981; Lund, 1978; and Orthner, 1980); and spousal identification with the Air Force (Black, 1982; Belt and Sweeney, 1973; and Orthner and Bowen, 1983).

Another group of general factors relates to Air Force life and families with respect to specific job and employee roles, constituting about six components--work enrichment, stress, conflict/cohesion, coping capability, role ambiguity/clarity, and autonomy.

Several research efforts (Brown, 1969; Buchanan, 1974; Hall, et. al., 1970; Marsh and Mannari, 1977; Steers, 1977; and Stevens

et. al., 1978) have pointed out the increased employee commitment which results from enriching and challenging work, fostered by increased task interdependence among members (Morris and Steers, 1980; Salancik, 1977). Broadening job scope to include task dimensions of autonomy, challenge, feedback, significance, and variety leads to higher levels of organizational commitment, through felt responsibility, because of its enriching effect on the job itself.

Employee stress may originate from at least two main sources--family demands and concerns and work demands and concerns. The former may compound problems in the latter (Greenhaus and Beutell, 1985). A recent Air Force family survey confirmed that while all families may at various times experience some stress, one out of every three is troubled by demands that center on household responsibilities, parents, religion, or the value of spending time together (Orthner, 1980). Work demands among married men and single parents when called upon for extra duty are also a source of stress (Orthner, 1980; McCubbin, Cauble, and Patterson, 1982).

Similar to stress, employee conflict also has two subcomponents. First, family conflict may result from money, children or marital affairs (particularly evident among younger Air Force couples at the lower ranks). Second, conflict at work may result from mistreatment by superiors, who lacking human resource management skills, display insensitivity to work unit family needs (Orthner, 1980). Both conflict types impact on satisfaction and commitment.

Deficiency in cohesion, social interaction and team-work, may also be factors adversely affecting satisfaction and career commitment (Buchanan, 1974; Rotundi, 1975), as will the maintenance of negative attitudes toward the organization. Coping capability may also be affected by difficulties which families experience in "making ends meet" due to economic considerations such as low pay and expensive or unavailable child-care facilities. It may also be affected by the unavailability of marriage counseling services (Orthner, 1980). Then there is coping with the rigor of work itself, which challenge an employee must decide whether or not to take up.

Just how strong a person's commitment is to his/her job has also been linked to clarity (or the removal of ambiguity) in the job role situation. Role ambiguity and clarity are important in career commitment since they may affect directly the career change process (Jepsen and Dilley, 1974). The clarity with which a job role is defined may affect the impact of the influencing variables on career decision process behavior and situations, as well as the process itself by which the employee decides to implement the career change. Ambiguity of job roles may impact differentially on different persons because each individual's cognitive map provides experiences idiosyncratic to that individual (Boneau, 1974), thereby affecting expectations, satisfaction, and career choice decisions. In addition, the presence of multifaceted and contradictory evaluation systems for job performance rewards, as well as the unsystematic, subjective, and vague reward criteria reduce job role clarity (Kahn, _et. al._, 1964). The effects of these evaluation systems and reward criteria are

explained by the concept of role inaccuracy (Walker, Churchill, and Ford, 1977). To the extent that individuals are unclear about their job roles within a particular job context, the gap between their desired and actual career interests is widened, resulting in career dissatisfaction. Whether these individuals will take action to relieve the dissatisfaction by reducing the perceived gap depends on the individual's tolerance, or threshold level, for dissatisfaction reduction.

Despite the plethora of studies in this area, the current evidence remains unclear regarding the impact on career change of satisfaction with various roles and services. While Staines' (1980) work on job role satisfaction contains an indication that it is a significant variable, other studies (Near, Rice, and Hunt, 1978; Schmitt and Mellon, 1980) have produced completely opposite results. Yet other studies report that both work and nonwork roles may in turn be affected by intervening variables such as age and personality (Korman, Wittig-Berman, and Lang, 1981), or by compensation, generalization, and segmentation (Kabanoff, 1980). In terms of service satisfaction, various factors were similarly found to have impact on career change. Among the more remarkable are: limited investment and growth opportunities in present job (Freeman, et. al., 1981); evolution of the family life cycle (Hall, 1976); changing roles based on their lifetime sequence (Super, 1980); role/ability incompatability because of role overload brought about by an individual's inability to cope with work demands (Latack, 1981); and inducement-contribution tradeoffs, one suggestion of which is that an individual's con-

tinuing interests in organizations are induced by rewards received in the attainment of organizational objectives (Barnard, 1938; Simon, 1964; Landy and Trumbo, 1980).

It is important to realize that the antecedent factors outlined above are both intrinsically and extrinsically determined. Work autonomy is one such additional antecedent that originates within the individual creating a sense of self-determination and fulfilment. The latter, by enhancing the individual's self-esteem, may positively impact service satisfaction and career commitment outcomes (Hackman and Lawler, 1971; Hackman and Oldman, 1976). The converse outcome has also been supported. High level constraints in the form of procedural specification were found to negatively affect the level of intrinsic motivation (Zuckerman, et. al., 1978; Fisher, 1978); or individuals displayed lower intrinsic interest when faced with deadlines (Amabile, DeJong and Lepper, 1976). Service satisfaction can increase or decrease career commitment, or can leave it unchanged. However, in the main, higher order service needs become pertinent to an individual only after lower order needs are satisfied (Maslow, 1943).

The above discussion develops the argument that at the micro level, "within the individual forces" impact on feelings of self-determination, and consequently affect service satisfaction and career commitment. At the macro level, structural characteristics, particularly if the organization veers toward the mechanistic polar type, may have strong negative impact through their impact on intrinsic motivation (Sherman and Smith, 1984). According to Deci (1975a, 1975b), greater levels of structural central-

ization, formalization, standardization, and bureaucracy, by reducing worker participation and autonomy, may result in reduced worker responsiveness to voluntarily produce for the organization. Or perhaps, as Selancik (1977) and others have suggested, greater discretion over how the job is performed often improves employee's felt responsibility. The greater discretion to actively participate in decision making is symptomatic of organizations characterized by high degrees of decentralization (Morris and Steers, 1980; Rhodes and Steers, 1978). The latter is likely to increase career commitment. Clearly, for some workers particularly in nonprofit organizations such as the Air Force, this may provide grounds for career change.

1.2 Outcomes of Service Satisfaction and Career Commitment

The outcomes of career commitment are represented by a situation where workers engage or pledge themselves to remain with the organization and work toward its goal attainment. As an outgrowth of this pledge, the individual demonstrates loyalty to the organization. At least five separate consequences have been identified in the literature (Hunt, Chonko, and Wood, 1985; and Mowday, Porter, and Steers, 1982) as being the response of commitment. These include attitude toward the organization, work performance, career with the organization, absenteeism, and turnover. Even though all five outcomes are important, our concern in this study is with them only in terms of feedback provided for the stimulation of antecedent variables.

The behavior of committed individuals is likely to corres-

pond to their attitude--industriousness, eagerness, zealousness, and promptness--toward the organization. By contrast, attitudes which are characterized by reluctance, slackness, and procrastination would be consistent with that found inversely related to commitment (Angle and Porter, 1981).

Committed workers are not necessarily productive workers, because worker performance may be influenced by their motivation level, role clarity, and work ability (Mowday, Porter, and Steers, 1982). Hence, even though a strong commitment-performance relationship per se may not be established, one would expect highly committed workers who are highly motivated, whose job roles are unambiguous, and who are of moderate to high ability to display quantity, quality and efficiency of output of a high order.

Committed workers are also those that are most likely to stay with the organization. To the extent that they firmly believe and support the organization's mission, both the inclination and motivation to stay and contribute will exist, even if the tasks are disliked (Steers, 1977; Mowday, Porter, and Steers, 1982).

The theoretical reasons which would impel workers to stay with an organization are similar to those which will motivate regular work attendance--to facilitate objective and mission attainment. Similarly, participation in the Air Force may take place even in the face of dislike of war, provided there is an overall feeling that a contribution is being made toward national defense and world peace (Steers, 1977). Contrary findings are advanced by Angle and Perry (1981).

Of the five outcomes identified above, the most significant behavioral consequence of career commitment is the reduced likelihood to leave. Much support for this commitment-turnover linkage can be found in the literature (Steers, 1977; Angle and Perry, 1981; Jackofsky, 1984).

The purpose of this paper is to apply a consumer orientation logic to the Air Force approach to creation and dispensation of its services and to gaining commitment. To implement this thinking, this article (1) establishes an Air Force career commitment model adapted from models applied to several occupational areas (Hunt, Chonko, and Wood, 1985; Mowday, Porter and Steers, 1982; Brief and Aldag, 1980; Stevens, Beyer, and Trice, 1978; and Steers, 1977); and (2) utilizes factor analysis, regression analysis, and one-way analysis of variance to reduce the large number of multidimensional variables to a smaller and manageable set, identify significant explanatory variables, and establish multidimensional profiles reflective of Air Force member and family needs as revealed by them. The overall objective is to preserve and/or enhance both Air Force employee and Air Force wellbeing.

2.0 THE AIR FORCE CAREER COMMITMENT MODEL

An individual's career intention may be very much synchronized with his/her current organization, but the everpresent possibility of career changes poses a challenge to supervisors, managers, and commanders responsible for subordinates' activities as these affect commitment to organization goals and objectives. The strength of an individual's commitment may reveal the follow-

ing four distinct types: (i) stable and unchanging; (ii) stable with minor changes; (iii) slowly changing in a predictable manner; and (iv) rapidly changing in an unpredictable manner.

Organizations with employees revealing stable and unchanging career commitment are in an excellent position to operate optimally and make long term tactical decisions and commitments. Should employees seek minor career changes such as seeking promotion within a stable intraorganizational framework, guidelines can be established for orderly promotion changes by expanding certain sectors while contracting others. Organizations like the Air Force recognize that they may be in the third category--slowly changing in a predictable manner. For such organizations, it is necessary to establish continuously new profiles of service satisfaction, to be meshed with personal characteristics, and levels of career commitment. With these profiles, commanders, managers, and supervisors can continuously respond to these newly-profiled needs and wants by adapting their objectives, strategies, structures and systems to optimize service satisfaction and career commitment impact. Some parts of the Armed Forces are today operating in the fourth category--an environment which is rapidly changing in an unpredictable fashion. Thus, during the Eighties, United States Armed Forces in Lebanon, Central America, and Western Europe experienced highly turbulent and unpredictable shocks and surprises, making service satisfaction and career commitment more uncertain.

Individuals, when faced with changes and instability, may choose not to remain with the organization. Alternatively, they

may respond to the threat by either of four types of reactions: (i) continuing in the organization without struggle, even in the face of difficulty; (ii) continuing in the organization, and trying to reverse the difficulty; (iii) trying to modify their own personal attitudes and character, to conform to the organization's expectations; or (iv) leaving the organization altogether. All of the above forces, together with antecedent and moderating variables, are presented in Figure 1 and discussed sections in 2.1 to 2.8.

2.1 The Role of Intrinsic and Extrinsic Job Benefits

The role of both intrinsic and extrinsic job benefits, based on the concept of exchange, is consistent with two of Etzioni's (1961) suggested typologies--moral and calculative involvement--and of March and Simon's (1958) inducements-contributions exchange theory. Commitment by members of the Air Force may be based on their calculation of the cost-benefit equity of the exchange relationship compared to their perceived contributions.

INSERT FIGURE 1 ABOUT HERE

Because commitment is reciprocal--between the member and his organization--a balance of wellbeing must be established between the individual's attachment to his organization and the latter's furtherance of its goals and objectives. Viewed in this light, commitment is more universal and thus differs from service satisfaction which reflects member response to specific provisions important in the performance of duties. In addition, commitment has been found to evolve slowly as a member assesses his exchange

FIGURE 1

THE AIR FORCE CAREER COMMITMENT MODEL [a]

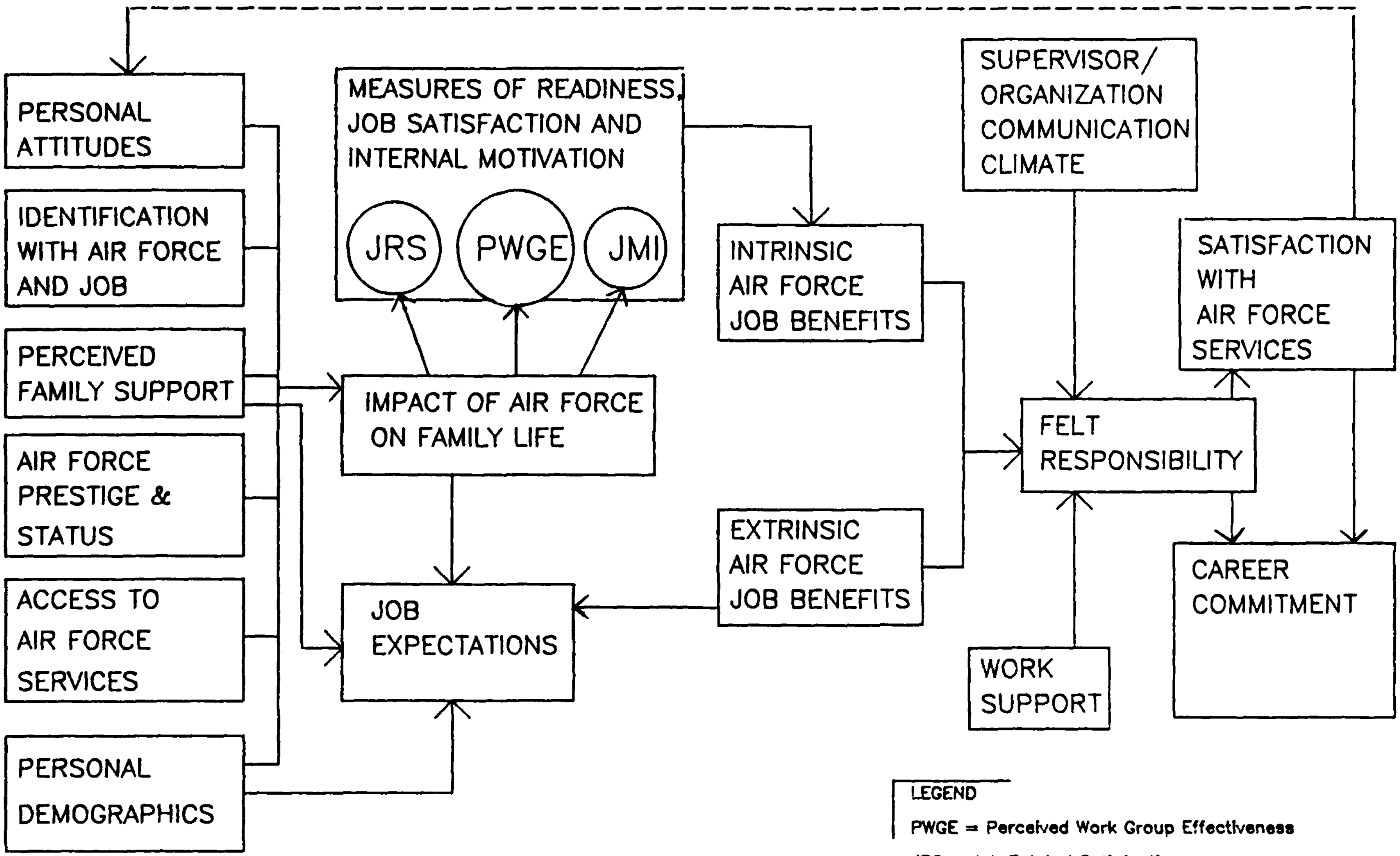

LEGEND

PWGE = Perceived Work Group Effectiveness

JRS = Job Related Satisfaction

JMI = Job Motivation Index (internal).

[a] Adapted from Hunt, Chonko, and Wood (1985); Mowday, Porter, and Steers (1982); Brief and Aldag (1980); Stevens, Beyer, and Trice (1978); and Steers (1977).

relationships with his employer. Service satisfaction, by contrast, is less stable and is affected by a member's day-to-day reactions to provisions (base exchange, commissary, etc.).

2.2 The Role of Perceived Family Support

Despite the large volume of empirical research on commitment, it is generally found that less than 30 percent of the commitment variance is explained. At the same time, nonwork influences on staying and leaving an organization are typically not included in the explanatory variable mix (Mowday, Porter, and Steers 1982). The absence of nonwork factors may account for the small explained variance. Clearly, non-job-related factors, such as transfer of a spouse, may stimulate employee intention to search for a new job (Mobley, 1977); on the other hand, when a spouse finds difficulty in transfering, the Air Force member may be unable to leave his/her current position as desired, and thus immobility can be the result. In both cases, career commitment is affected.

The commitment process may be tempered by perceived family support if the "central life interest" of the employee is shifted to his family and away from work-related tasks. In this case, even though commitment may be low, productivity and contribution may remain high (Dubin, Champoux, and Porter 1975).

2.3 The Role of Identification with Air Force and Job

Depending on the way identification is defined, the concept has been generally reported as positively related to career commitment. Earlier, it was pointed out that members identify

more and have more felt responsibility with their organization when job scope is broadened. Another way in which identification may impact on commitment is through the mediation of tenure on identification. Generally, length of service increases the likelihood of employees broadening their job scope and gaining extrinsic job benefits both of which lead to higher commitment for longer service periods (Hunt, Chonko, and Wood 1985; Mowday, Porter, and Steers 1982; and Angle and Perry 1981). Two other notions are also important with respect to identification. First, members may identify with their organization to the extent that they feel it can be counted on to represent their interests. Secondly, if members feel that their efforts are needed and valued by the organization for the attainment of its mission, positive feelings may be generated and displayed toward the organization (Buchanan, 1974; Steers, 1977). And in general, where job expectations were perceived to have been met, commitment was also positively affected (Steers, 1977).

2.4 The Role of Air Force Prestige and Status

Another way in which job expectations can influence the level of initial and subsequent commitment is through the mediating impact of prestige and status. Employees probably try to establish congruence between the organization's prestige and status and their own. Yet research linking prestige and satus to career commitment remains sparse and limited, although the need for both achievement orientation and the management of impressions has been widely recognized.

2.5 The Importance of Access to Air Force Services

Access to Air Force services provides an important inducement in the member's relationship with their units, and in reenlistment decisions. This would argue for the establishment of a predictive model where access to services is positively related to commitment, especially if the member perceives the exchange contribution to be great. In general, services as compensation for work are normally combined across attributes of each service item so that deficiency in one attribute can be counterbalanced by compensation in another (Wheeler and Mahoney, 1981; Mitchell and Beach, 1976), as members decide to "satisfice" rather than "optimize" overall gain. One aspect--satisfaction with 24 different aspects of Navy life and services--was studied by Szoc (1982) who reported that in general, leavers were dissatisfied with more aspects than those intending to stay. Thus, it appears likely that commitment decision is investment-like, where members incur "costs" (contributions) today in exchange for "benefits" expected in the future (Hunt, Chonko, and Wood, 1985; Sheldon, 1971).

2.6 Personal Attitudes and Demographics

Spousal attitudes--identification and compliance with, or detachment from the Air Force--are singularly important in explaining commitment decisions (Hickman and Hunter, 1981; Orthner, 1980). The member seeks to dove-tail his/her own norms, values, and goals with those of the organization, and may internalize the norms, values, and goals of the organization by seeking moral involvement, for example, through fighting to preserve world peace;

or seeking a calculative involvement, for example, in an exchange of services for income in order to relieve unemployment; or seeking an alienative involvement through military enlistment to get rid of the "unpleasant" obligation of a military draft (Etzioni, 1961).

Demographic correlates of commitment have been studied extensively. Findings indicate that commitment is positively affected by age and tenure (Hunt, Chonko, and Wood, 1985; Mowday, Porter, and Steer, 1982; Angle and Perry, 1981; and Brief and Aldag, 1980). Higher income which constitutes an inducement, has recently been found to be positively related to commitment (Hunt, Chonko, and Wood, 1985; Morrow, 1983). In the past, the linkages found had been weak, although perceived income equity promises to provide a stronger link. In contrast to age and income, education has shown an inverse relationship to commitment (Hunt, Chonko, and Wood, 1985; Brief and Aldag, 1980; and Steers, 1977). The findings on gender, marital status, and ethnic origin are mixed. While Hunt, Chonko, and Wood (1985) found gender and marital status not to be significantly related to commitment, other studies (Szoc, 1982; and Angle and Perry, 1981) found positive relationships. Szoc (1982) also found significant differences in commitment by ethnic groups. Finally, stage in the family life cycle, identified as a determinant of commitment, reflects the possibility that as length of service increases commitment increases likewise (Hall, _et. al._). The effect of family life cycle variable probably reflects the effect of investment in the job, family and social involvements, and job mobility.

2.7 Other Factors--Organizational Climate and Perceived Work Support

The literature is replete with theoretical and empirical arguments suggesting that one way of improving felt responsibility and career commitment is by organizational intervention to "enrich" the organizational climate and the member's job. Members assess their work support and organizational climate by comparison with previous work experience as well as through discussions with other workers. The result of their assessment has been shown to affect their job expectations and subsequent level of commitment attitude. Improvements in organizational climate and work support is intended to cement commitment by improving the scope for member's achievement and recognition as well as expanded opportunities for family growth as member career develops. Hackman and Oldham (1976) provide the theoretical basis for five core job dimensions (skills variety, task identity, task significance, autonomy, and feedback) which provide relief for critical psychological states (feelings of meaningfulness and responsibility, and knowledge of results) thereby leading to outcomes of high intrinsic motivation, high quality of work, high satisfaction, and low absenteeism and turnover. These latter, together with member's anticipated levels of trust reflected in the extent to which the organization is perceived as cooperative and friendly, may be positively related to commitment attitudes.

2.8 Outcomes

Figure 1 shows the several independent antecedent variables which lead, through mediators, to organizational commitment and

satisfaction with Air Force services. The model focuses on career commitment as an outcome to be explained by stimulation of antecedent variables on the left-hand side of the diagram.

3.0 HYPOTHESIS DEVELOPMENT

Based on the above survey of the literature discussion and the developed model in Figure 1 the following hypotheses are tested:

H1: Air Force member career commitment is a positive function of spousal personal attitudes (marital satisfaction, identification with the Air Force and member's job, career orientation, gender role orientation, autonomy) (Beeson, 1985; Greenhaus and Beutell, 1985);

H2: Air Force career commitment is a positive function of member's perceived family support, and perceived job related satisfaction (Hunt, Chonko, and Wood, 1985; Hackman and Oldham, 1976);

H3: Air Force career orientation is a negative function of Air Force member's job stress, move-related family stress, family off-base social interaction, and insensitivity of the Air Force to family needs (McCubbin, Cauble, and Patterson, 1982);

H4: Air Force career commitment is a positive function of member's age, tenure, pay, and a negative function of education (Hunt, Chonko, and Wood, 1985; Mowday, Porter, and Steers; Angle and Perry, 1981; and Brief and Aldag, 1980);

H5: There are significant Air Force career commitment differences between members based on gender, marital status, and ethnic origin (Angle and Perry, 1981; Szoc, 1982);

H6: Based on combined attitudes and demographics, significant group differences exist among Air Force family members with respect to frequency of use and satisfaction with Air Force services (Szoc, 1982);

H7: Air Force member career commitment is a positive function of satisfaction with Air Force services (Hunt, Chonko, and Wood, 1985; Wheeler and Mahoney, 1981; and March and Simon, 1958).

4.0 RESEARCH METHODOLOGY

The research setting consisted of gathering data from the Air Force member and his/her spouse, and linking the separate

matched questionnaires together through a Survey Instrument Linkage Code. The above matched data collection effort constituted a continuation of questionnaire development, validation, and data gathering process using the Organizational Assessment Package (OAP) on members of the United States Air force worldwide. The present OAP survey was first field tested in 1978. Theoretical work by Aldous, Osmond and Hicks (1979) and Kanter (1977), and recent empirical testing by Beeson (1985) and Greenhaus and Beutell (1985) have now established a link between the domains of work and the family. Hence, the development of the Air Force Family Survey (AFFS) was undertaken to test this linkage in the context of the Air Force. The subsequent analysis is based on isolating and rearranging parts of this double-wide data base to accomodate testing of the unverified hypotheses generated by literature search above.

4.1 The Sample

The data base from which the present study's data are extracted consists of a double-wide file. The latter combined OAP work-related attitudinal and demographic information solicited from a sample of 1430 Air Force members, matched to their 1430 spouses. These supplied attitudinal, frequency of use and satisfaction with Air Force services, and demographic information through the AFFS.

The new AFFS questionnaires have been administered to members of the Air Force organization since January, 1985. Administration is still in process (August 1985) by the Leadership and Management Development Center (LMDC) consultants. The survey is

part of the normal consulting process. Questionnaires for the current sample were provided to every member present for duty on the day of administration to selected large Air Force organizations at four different Air Force bases. OAP questionnaire completion was a group-process with answers marked directly on to specially designed computer scan sheets. This was preceded by standard instruction briefings. Respondent groups completed the questionnaire (an average completion time of 45 minutes) during normal working hours with each group scheduled 90 minutes apart.

Because the questionnaire was filled out "on the job" under the explicit sponsorship of the commander virtually all of the members on duty completed the OAP questionnaire. By a show of hands, married respondents were identified and each given a sealed AFFS questionnaire with a randomly generated silcode to be marked on both the member's answer sheet and that to be completed anonymously and returned in a sealed envelope by his/her spouse. In contrast to high participation of members, their spouse's response rate (number of returned completed AFFS as a ratio of married members) to a single wave of the distributed AFFS questionnaire with no followup was 39.0 percent. Thus each sample of matched family members contains responses from both husband and wife in the Air Force, thereby allowing for testing of the effect of spousal attitudes and family demographics on member's career commitment.

4.2 The Data

The data employed in this study were related to the issues revealed in the literature search, including prior theoretical

constructs. After an exhaustive literature search and factor analysis, fourteen attitudinal factors and several demographic variables were identified as the most sensitive to career commitment and satisfaction with Air Force services (see Table 2).

When the combined double-wide OAP/AFFS file data were analyzed, fourteen percent of the respondents were officers and 84 percent were enlisted. The modal categories were white (76.0%), and married between one to three years (23.0%). Variable means both of the Air Force member and spouse are shown in Appendix 1. The average age of the member is 31.0 years, and that of the spouse is 30.3. Most families had two children, with a smaller number (between one and two) living at home. In most families the age of their youngest child was three to five years. Most member's tenure in the Air Force was more than four but less than eight years, having spent between 24 and 36 months in their present career field. Members are clustered modally toward being married to a civilian spouse employed outside the home, and to having less than two years of college education.

4.3 The Measures

A 7-point Likert scale was used on all attitudinal items of the questionnaire. AFFS Items 1 to 61 measured spousal attitudes, and factor analysis was utilized to identify 14 factors shown in the following tables. Items 62 to 79 measured frequency of use of basic and optional Air Force services, while Items 80 to 98 measured the overall level of satisfaction. Items 99 to 108 measured spousal perception of the impact of various factors on the member's intention to make the Air Force a career, while

Items 109 to 117 measured the perceived effects on family life of general Air Force life factors. The remaining independent variables (age, pay, gender, number of children, etc.) are self-explicit. Some of these demographic variables as well as one dependent variable were extracted from the OAP matched questionnaire which collected members' information.

The dependent variables were career commitment and satisfaction with Air Force services. The development of the scale measuring career commitment was based on the member's desire to continue in the Air Force, and is consistent with definitions utilized in other studies (Hunt, Chonko, and Wood, 1985; Mowday, Porter, and Steers, 1982; and Stevens, Beyer, and Trice, 1978). The scale ranged in responses from member's definitely continuing in/with the Air Force to their willingness to seperate/terminate from it as soon as possible. The second dependent variable set, frequency of use and satisfaction with Air Force life and services were extracted from factor analysis.

4.4 Oneway ANOVA, Pearson Correlation, and Regression Equation

R-factor analysis was utilized in order to reduce the large number of items to a more manageable set and to identify a priori conceived underlying themes within the data. Specifically, Items 1 to 61, 62 to 98, and 99 to 117 were each subjected to principal components analysis and varimax rotation. Because sme services such as auto hobby shop and arts and crafts were idiosyncratic to small target groups caution is advised in the interpretation of the use frequency of Air Force services. The scree test, eigenvalues greater than unity, and factor loadings greater than +/-

0.40 were used both to determine and select the number of factors. The independent variables for this study constituted the resulting factors, together with socio-demographic and work-related items selected both from the AFFS and the OAP questionnaires. The dependent variables also consisted of seven factors (frequency of use both of basic and optional services; satisfaction with basic services; satisfaction with optional services; perceived favorableness to basic job benefits; perceived impact of moves, exercises, and TDY; perceived job satisfaction; and satisfaction with current duty location) and a final item--career commitment--selected from the OAP questionnaire. A split-half reliability of 1309 cases produced an alpha of .65 for 19 items in Part One compared with an alpha of .51 for 18 items in Part Two. Appendix 2 reports Cronbach's alpha--a measure of internal consistency (construct validity)--of the 14 factors. More than half of these factors have alpha coefficients of .70 and higher, indicating a high degree of internal consistency.

All of the above resulting and selected variables were then subjected to Pearson pair-wise intercorrelation analysis as a test for multicollinearity among predictor variables to assess the extent to which they reflect the same construct. Table 9 shows that even though intercorrelations are statistically significant, they are small in values, thereby indicating relative construct independence and little overlap among variables.

Dividing the sample into three clearly defined groups, one-way analysis of variance was used to establish mean profiles of these family work-groups on the hypothesized variables.

The regression models used for exploring hypotheses H1 to H4 can be summarized by the following equation:

Career Commitment

$$= B_{01} + B_{11} F1 + \ldots + B_{141} F14 + B_{151} AGE + B_{161} TENURE + B_{171} PAY - B_{181} EDUC + e$$

where Bs are the unknown parameters to be estimated, and e is an error term.

The SPSS stepwise multiple regression software was used for the analysis. This technique was selected because of the large number of independent variables involved in the analysis. The stepwise multiple regression program extracts the most powerful variables that are determinant, and that account for most variation in the criterion variable at a predetermined F-ratio, to enter the equation first. To test for autocorrelation, the Durbin-Watson test of the weighted ratio of the sum of squared differences in successive residuals was employed. The F-ratio was predetermined to correspond to a significance level of 0.10 (i.e., 90 percent). The regression coefficients (including their signs) were used to assess the relationship between the independent and dependent variables, while the coefficient of determination, R^2, was used to assess the amount of variation in the dependent variable that is accounted for by the independent variable. The sign before the regression coefficient was used to confirm the hypothesized direction of association.

5.0 DATA ANALYSIS AND FINDINGS

5.1 Spousal Attitudinal Factors

Table 1 lists the items that loaded most heavily on the 14

Table 1

Air Force Family Survey Attitude Scales

Scale and Title Statements	Factor Loadings	Commun-ality
Factor 5: Sensitivity to AF family needs		
* AF career same status as others	.46	.49
* AF conditions good for child raising	.46	.56
* Leaders aware of AF family needs	.77	.67
* AF tries to make life attractive	.73	.62
* AF leaders sensitive to AF family needs	.78	.67
* Pay, etc., fair for the job	.51	.42
Percent of Variance Explained = 14.0%		
Factor 3: Marital satisfaction		
* Am happy with marriage	.84	.74
* Pleased with how we express affection	.80	.68
* Wish marital communications were better	.50	.38
* We agree on most major issues	.73	.58
* Am happy at present	.67	.61
Percent of Variance Explained = 7.0%		
Factor 7: Perceived job satisfaction		
* Member's abilities are well used	.69	.59
* Member feels positive about contribution	.61	.56
* Member has worthwhile job	.77	.68
* Proud of member's job	.72	.67
* Prefer member have different AF job	.48	.52
Percent of Variance Explained = 5.5%		
Factor 1: AF member's job stress		
* AF career causes unique family problems	.69	.59
* Member is under a lot of pressure	.59	.46
* Member devotes more time to career	.66	.53
* AF lifestyle more stressful than others	.61	.49
* Members hours disrupt family life	.71	.59
Percent of Variance Explained = 3.7%		
Factor 12: Spousal support to commitment		
* Am glad member joined AF	.49	.62
* Want member to make AF a career	.83	.79
* Member plans to make AF a career	.82	.74
Percent of Variance Explained = 3.1%		
Factor 6: Identification with AF and job		
* Feel involved with AF lifestyle	.69	.67
* Feel a part of AF community	.66	.69
* Need to know AF customs and courtesies	.68	.56
* Interested in AF role and mission	.65	.61
Percent of Variance Explained = 2.8%		
Factor 13: Spousal preference for off-base community friendships		

* AF career causes unique family problems	.58	.52
* Friends often visit at our home	.58	.56
* Sometimes feel socially isolated	.72	.65
Percent of Variance Explained = 2.8%		
Factor 2: Move-related family stress		
* We move too often	.54	.43
* Prefer leaving AF to taking a bad PCS	.66	.52
* Children have difficult time with AF life	.55	.49
* We would be happier with a similar non-AF job	.55	.49
Percent of Variance Explained = 2.7%		
Factor 9: Gender role orientation of spouse		
* Wife should run household	.78	.68
* Husband should make family decisions	.75	.69
Percent of Variance Explained = 2.2%		
Factor 10: Spousal autonomy		
* All go own way in family	.40	.54
* Spouse often make decisions for family	.65	.52
* Decide when to do things I want	.75	.64
Percent of Variance Explained = 2.0%		
Factor 14: Help seeking attitudes		
* Don't go outside family for help	.65	.54
* Outside agencies help solve problems	.53	.49
* Seek others help as last resort	.70	.57
Percent of Variance Explained = 2.0%		
Factor 4: Perceived family support		
* Important to know about member's work	.66	.62
* My wishes impact member's career intent	.41	.63
* Spouse's feelings important to member	.50	.50
Percent of Variance Explained = 1.9%		
Factor 8: Spouse's career orientation		
* Important (to spouse) to have own career	.64	.56
* OK for wife to work outside home	.70	.58
Percent of Variance Explained = 1.7%		
Factor 11: Off-base social interaction		
* Prefer member have different job	.47	.52
* Non-AF friends more important	.62	.55
Percent of Variance Explained = 1.6%		
Cumulative Variance Explained = 53.0%		

identified factors. Most of the factors are significantly higher than the cutoff (+/-.40); however, Factor 3, marital satisfaction, and Factor 12, spousal support to commitment, contain items which correlate highest with their respective factors.

A total of 53 percent of the variance was accounted for by the above 14 factors, with "Sensitivity to Air Force family Needs" (Factor 5), "Marital Satisfaction" (Factor 3), and "Perceived Job Satisfaction" (Factor 7) accounting for 14.0, 7.0, and 5.5 percent of the variance explained. The communalities indicated that the 14 factors were least sensitive in explaining the variance of "Wished marital communications were better" (item 3 of Factor 3), "Pay, etc., fair for the job" (item 6 of Factor 5), and "We move too often" (item 1 of Factor 2). The items which produce the factors reveal high construct validity (internal consistency) as indicated by Cronbach's alpha (see Appendix 2). Factors 8, 9, 10, 13, and 14 are below the .60 cutoff for acceptable Cronbach's alpha. However, the magnitude of the alpha value is affected by the number of items loading on that factor as might be the case for Factor 8. In general, the emerging factors were supportive of the translation of the theoretical models of the literature review of our Air Force commitment model.

5.2 Attitudinal and Demographic Profiles by Frequency of Use of Air Force Services

The idea that group differences exist with respect to extrinsic job benefits is almost totally supported by the data. Table 2 shows that moderate and heavy users of Air Force services tend to have significntly different profiles from their nonuser counterparts. The latter report significantly stronger disagreement in experiencing move-related family stress, marital satisfaction, perceived family support, feelings that the Air Force is sensitive to their family needs, perceived job satisfaction, and

TABLE 2

Descriptive Profiles of Air Force Family Work Groups
By Frequency of Use Both of Basic and Optional Air Force Services

Descriptive Variables	Non-user n=304	Moderate n=817	Heavy user n=32	F ratio	F prob
	Groups (means)				
AF member's job stress	5.0796	5.1000	5.2000	0.11	.8973
Move-related family stress	3.5082	3.4204	4.4063	6.83	.0011
Marital satisfaction	5.9975	6.0551	6.8672	7.49	.0006
Perceived family support	5.3355	5.6995	6.1094	9.39	.0001
Sensitivity to AF family need	3.7319	4.1024	4.9062	13.43	.0000
Identification with AF & job	4.9046	5.5268	4.9187	29.62	.0000
Perceived job satisfaction	5.4268	5.6524	6.5313	10.35	.0000
Spouse's career orientation	5.2796	5.4196	6.4375	12.56	.0000
Gender-role orientation	3.7829	3.9235	5.5000	12.03	.0000
Spouse's autonomy	3.4923	3.7222	4.9479	17.63	.0000
Off-base social interaction	4.1678	4.4853	4.6563	4.68	.0095
Spousal support to commitment	5.1436	5.4667	5.2917	3.78	.0234
Spousal preference for off-base community friendships	3.8739	3.4659	4.7187	17.62	.0000
Help seeking attitudes	4.9550	4.7079	5.8750	12.30	.0000
Total number of children	2.4901	2.6365	5.0938	49.73	.0000
Number of children at home	2.2303	2.4443	4.3438	36.09	.0000
Age of youngest child*	1.9243	2.0869	5.4063	48.76	.0000
Other family members in home	1.1349	1.1212	3.6563	120.22	.0000
Sex of AF member*	1.0757	1.0930	1.4375	10.57	.0000
Age of AF member	30.8311	30.6974	40.0313	25.63	.0000
Pay grade of AF member*	5.2158	4.8154	7.4483	30.73	.0000
Personnel category in AF*	1.1645	1.0122	2.1563	17.50	.0000
Years in AF (tenure)	5.4086	5.4491	6.0000	1.77	.1716
Member months in career field	6.1974	6.2559	5.9032	1.08	.3402
Member months on station	4.8482	5.0835	5.6000	3.82	.0222
Member months in position	4.0825	4.0221	5.2333	6.58	.0014
Ethnic group of AF member*	4.8605	4.7549	4.6774	2.73	.0654
Marital status of AF member*	2.3618	2.5324	2.2903	2.34	.0971
Education level of AF member*	2.9670	3.3395	3.1613	10.41	.0000

----

* Means (ratio level) translatable into categories on the questionnaire.

identification with the Air Force and their job. They also express stronger disagreement about spousal career orientation, autonomy, off-base social interaction, commitment support to

member, preference for off-base community friendships, and help-seeking attitudes. The three different user groups reveal no significant differences in terms of Air Force member's job stress. However, heavy users of Air Force services do report having significantly larger numbers of (and older) children (both at large and in the household) than both moderate and nonusers. Heavy users also tend to have a larger extended family. Although heavy users tend to be 10 years older, have higher education, and earn higher pay, yet tenure (years in the Air Force) and months in their career field were the same for all three groups. Nevertheless, heavy users were much longer at their present station and held their Air Force position for a significantly longer period. The suggestion that frequent users are more likely to be from families with older military male members as well as female members (husbands of older lady colonels and senior enlisteds) should be taken with caution, since this is a small part of the overall population. Given this small heavy user category, maybe emphasis should be placed on getting smaller families with younger children to use the services; or alternately, one may create services that appeal to smaller families with younger children.

5.3 Attitudinal and Demographic Profiles by Overall Satisfaction with Basic Services

On a number of personal factors (more attitudinal than demographic), members and spouses who report slight to extreme satisfaction with basic Air Force services reveal significantly different profiles than those who are both extremely or moderately dissatisfied (see Table 3). The latter express much stronger agreement about both member's job and move-related family stress.

TABLE 3

Descriptive Profiles of Air Force Work Groups
By Overall Level of Satisfaction with Basic Air Force Services

Descriptive Variables	Groups (means): Extremely Dissatis-fied n=70	Neutral to Mod Dissat n=428	Slightly to Extre Satisfied n=493	F Ratio	F Prob
AF member's job stress	5.5971	5.3322	4.8548	17.45	.0000
Move-related family stress	3.7893	3.6595	3.2302	11.26	.0000
Marital satisfaction	5.7214	5.9533	6.2490	10.28	.0000
Perceived family support	5.4214	5.5900	5.6856	1.31	.2713
Sensitivity to AF family need	2.8000	3.5861	4.5494	86.27	.0000
Identification with AF & job	5.1486	5.1505	5.5797	14.74	.0000
Perceived job satisfaction	4.9964	5.3873	5.9062	23.99	.0000
Spouse's career orientation	5.0048	5.2998	5.5463	8.29	.0003
Gender-role orientation	3.9929	3.7453	4.1359	4.86	.0079
Spouse's autonomy	3.4524	3.6877	3.7039	1.05	.3519
Off-base social interaction	4.2857	4.3166	4.5588	2.92	.0544
Spousal support to commitment	4.9714	5.2695	5.5463	4.92	.0074
Spousal preference for off-base community friendships	3.9857	3.7383	3.3908	8.69	.0002
Help seeking attitudes	4.9905	4.8076	4.7640	0.75	.4725
Total number of children	2.6857	2.5421	2.7708	2.71	.0670
Number of children at home	2.4857	2.3598	2.5477	2.02	.1328
Age of youngest child*	1.6286	2.0561	2.2394	3.38	.0344
Other family members in home	1.0429	1.1308	1.2941	3.76	.0237
Sex of AF member*	1.0571	1.0724	1.1278	2.06	.1275
Age of AF member	29.6286	30.8447	30.9673	1.02	.3626
Pay grade of AF member*	4.8507	4.8940	4.9621	0.20	.8212
Personnel category in AF*	1.2429	0.9626	1.1724	4.53	.0110
Years in AF (tenure)	5.4429	5.5825	5.2541	4.17	.0157
Member months in career field	6.2319	6.3325	6.0879	3.42	.0330
Member months on station	4.7429	4.9812	5.0286	0.86	.4246
Member months in position	3.9000	4.0000	4.1531	1.17	.3120
Ethnic group of AF member*	4.8116	4.8146	4.7358	1.42	.2418
Marital status of AF member*	2.5143	2.6051	2.4289	2.16	.1160
Education level of AF member*	2.9714	3.3162	3.1850	2.89	.0560

* Means (ratio level) translatable into categories on the questionnaire.

However, this same group reports significantly stronger marital satisfaction, much greater sensitivity to Air Force efforts to satisfy family needs, deeper identification with the Air Force

and job, and higher perception of job satisfaction. Stronger agreement exists about the spouse's career and gender-role orientation. Significant group differences also exist with respect to member and spousal off-base social interaction, as well as spousal commitment support. Three of the attitudinal factors: "Perceived family support", "Spousal autonomy", and "Help seeking attitudes" were indistinguishable among the three groups.

Unlike attitudinal factors, the few demographic variables which were found to distinguish the satisfied from the dissatisfied group were only moderately significant. The satisfied group report having older children at home, a larger extended family, and attained higher educational levels. However, they had shorter tenure in the Air Force and in his/her career field.

5.4 Attitudinal and Demographic Profiles by Overall Satisfaction with Optional Services

While the profiles of those who were satisfied with basic services were not significantly different from those who were dissatisfied on a number of personal factors, the situation for optional services reveals sharper distinctions on a larger number of both types of factors (see Table 4). All but three of the attitudinal factors--both family and member's job stress as well as spousal commitment support--are not important distinguishing variables among the threegroups. The extremely dissatisfied group is most strongly distinguished from slightly to extremely satisfied group on the basis of perceived sensitivity of the Air Force to family needs. Similarly, the latter group express significantly less strong disagreement on gender-role orientation, spousal autonomy and career orientation. The absolute mean score

TABLE 4

Descriptive Profiles of Air Force Family Work Groups
By Overall Level of Satisfaction with Optional Air Force Services

Descriptive Variables	Groups (means) Extremely Dissatis-fied n = 303	Neutral to Mod Dissat n=470	Slightly to Extre Satisfied n=108	F Ratio	F Prob
AF member's job stress	5.1729	5.1519	4.9444	1.13	.3240
Move-related family stress	3.4472	3.4133	3.7847	2.72	.0661
Marital satisfaction	6.1444	5.9920	6.3403	4.51	.0113
Perceived family support	5.5413	5.6489	5.9861	4.13	.0164
Sensitivity to AF family need	3.8020	4.1642	4.4938	10.77	.0000
Identification with AF & job	5.2442	5.5387	5.3407	5.35	.0049
Perceived job satisfaction	5.5371	5.6495	6.0949	7.01	.0010
Spouse's career orientation	5.4325	5.3780	5.8086	5.37	.0048
Gender-role orientation	3.7162	3.9596	4.6065	8.59	.0002
Spouse's autonomy	3.6645	3.7326	4.1914	6.13	.0023
Off-base social interaction	4.2426	4.5138	4.5972	3.20	.0414
Spousal support to commitment	5.2442	5.4695	5.4722	1.63	.1964
Spousal preference for off-base community friendships	3.7470	3.4695	3.8796	5.03	.0067
Help seeking attitudes	4.7745	4.7270	5.2500	5.84	.0030
Total number of children	2.4851	2.6149	3.5463	21.62	.0000
Number of children at home	2.2640	2.4532	3.1296	14.78	.0000
Age of youngest child*	1.7195	2.1234	3.6759	39.74	.0000
Other family members in home	1.1485	1.1021	1.9167	26.94	.0000
Sex of AF member*	1.0660	1.0872	1.2778	8.86	.0002
Age of AF member	29.6291	30.7645	35.0000	22.21	.0000
Pay grade of AF member*	4.7186	4.8293	6.0777	23.73	.0000
Personnel category in AF*	1.0066	0.9957	1.6481	16.09	.0000
Years in AF (tenure)	5.1633	5.4797	5.8302	7.07	.0009
Member months in career field	6.1130	6.2876	6.2617	1.49	.2257
Member months on station	4.8416	5.2047	5.4717	7.25	.0008
Member months in position	3.9637	4.0471	4.8411	10.27	.0000
Ethnic group of AF member*	4.8505	4.7340	4.7103	2.75	.0647
Marital status of AF member*	2.4554	2.5553	2.3832	1.07	.3435
Education level of AF member*	3.2244	3.3226	3.1963	0.81	.4463

----

* Means (ratio level) translatable into categories on the questionnaire.

** Optional services comprise the open mess (club), recreation center, base library, auto hobby shop, bowling center, golf (course/club), arts and craft, child care center, gymnasium, family support center, chapel and chaplains, theater, youth center, base housing, base exchange cafetaria or snack bar, and education services center.

suggests also that among the groups there exists strongest agreement on marital satisfaction and perceived job satisfaction.

In terms of demographics, again Table 4 shows that only four variables--member months in career field, ethnicity, marital status, and education level--are not important in distinguishing among the three groups. Family groups who were slightly to extremely satisfied reported significant difference from dissatisfied groups. The youngest child was older, the extended family was larger, income was higher, the Air Force member was older, and both the total number of children as well as those at home were larger, thereby confirming H6.

5.5 Attitudinal and Demographic Profile by Perceived Favorableness to Basic Job Benefits

The career commitment model (see Figure 1) highlighted the importance of both intrinsic and extrinsic job benefits as factors impacting on satisfaction. Table 5 shows just how these groups are profiled.

Family groups who are somewhat to very positive in their favorableness to basic job benefits, when compared to their negative counterparts, express significantly weaker levels of agreement regarding member's job and move-related family stress and spousal support for off-base community friendships. On the other hand, the positivist group express significantly less disagreement about the Air Force sensitivity to family needs, and greater agreement about perceived job satisfaction,identification with the Air Force and their job, spousal commitment support. Perceived family support, even though at a high level of agreement, reveals only weak distinctiveness among the three groups.

TABLE 5

Descriptive Profiles of Air Force Family Work Groups
By Perceived Favorableness to Basic Air Force Job Benefits

Descriptive Variables	Groups (means) Very Neg Somewhat Negative n=70	Neither Negative Nor Pos n=53	Somewhat to Very Positive n=735	F Ratio	F Prob
AF member's job stress	5.9429	5.2679	5.0305	13.32	.0000
Move-related family stress	4.6500	3.7547	3.3561	25.04	.0000
Marital satisfaction	5.8821	5.8915	6.1374	2.25	.1056
Perceived family support	5.2214	5.5755	5.7320	4.68	.0095
Sensitivity to AF family need	2.6952	3.3050	4.3170	51.39	.0000
Identification with AF & job	4.8314	4.8151	5.5048	16.74	.0000
Perceived job satisfaction	4.6964	4.8302	5.8255	34.07	.0000
Spouse's career orientation	5.0810	5.3711	5.4689	3.11	.0453
Gender-role orientation	3.8643	3.8491	4.0095	0.33	.7219
Spouse's autonomy	3.5619	3.7107	3.6848	0.27	.7638
Off-base social interaction	4.1500	4.2547	4.4803	1.77	.1714
Spousal support to commitment	4.1190	4.5849	5.6798	36.72	.0000
Spousal preference for off-base community friendships	4.2048	4.1509	3.5224	10.29	.0000
Help seeking attitudes	5.1476	4.8491	4.8150	1.66	.1910
Total number of children	2.5857	2.6415	2.7170	0.29	.7471
Number of children at home	2.4286	2.5283	2.5075	0.10	.9017
Age of youngest child*	1.7857	1.9623	2.2653	2.19	.1127
Other family members in home	1.1429	1.4151	1.2095	1.09	.3376
Sex of AF member*	1.1286	1.1132	1.0789	0.71	.4942
Age of AF member	30.0857	30.6731	31.0328	0.06	.9413
Pay grade of AF member*	5.1970	5.0000	4.9789	0.37	.6902
Personnel category in AF*	1.4857	1.0943	1.0585	4.40	.0126
Years in AF (tenure)	5.6957	5.5490	5.4107	1.01	.3653
Member months in career field	6.5429	6.0000	6.1847	2.60	.0748
Member months on station	5.2429	5.0769	4.9863	0.75	.4734
Member months in position	4.1143	3.9615	4.1260	0.20	.8206
Ethnic group of AF member*	4.6571	4.8846	4.7596	1.40	.2476
Marital status of AF member*	2.8857	2.7925	2.4163	6.28	.0020
Education level of AF member*	2.9130	3.1509	3.2861	3.15	.0432

* Means (ratio level) translatable into categories on the questionnaire.
** Basic job benefits comprise rate of pay, AF (or civil service) retirement system, non AF job opportunities, medical benefits, job security, and family needs.

Both positivist and negativist groups moderately agree to experiencing marital satisfaction. In similar vein, spousal career orientation and autonomy, gender-role orientation, and member's

off-base social interaction reveal no significant differences among the groups.

At the 5 percent level of significance, only three demographic variables--marital status, occupation, and education--were reported by the groups as being significantly different.

5.6 Attitudinal and Demographic Profiles by Perceived Impact of Air Force Moves, Exercises and TDY

Results in Table 6 are similar to Table 5 except for the lack of significant group differences in gender-role orientation, spousal autonomy, and member family off-base social interaction. In terms of demographics, the positivists report an expanded but different set of variables. Compared to the negativists, they have significantly more children, a larger extended family, were older, had a much longer job tenure, and earned higher income.

5.7 Attitudinal and Demographic Profile by Perceived Job Satisfaction

The comparative profiles of Air Force family work groups who are positive toward job satisfaction are clearly different from those who are negative toward it. Certain attitudinal variables--marital satisfaction, spousal career orientation and autonomy, and gender-role orientation--are indistinguishable among the positivists and negativists about perceived job satisfaction. However, those who report being positivist about perceived job satisfaction, when compared with negativists who disagree, are in slight agreement about member's job stress and family off-base social interaction, moderately agree about perceived family support, identification with the Air Force and the member's job, perceived job satisfaction, and spousal commitment support. By

TABLE 6

Descriptive Profiles of Air Force Family Work Groups
By Perceived Impact of Air Force Moves, Exercises and TDY

Descriptive Variables	Groups (means) Very Neg Somewhat Negative n=410	Neither Negative Nor Pos n=88	Somewhat to Very Positive n=443	F Ratio	F Prob
AF member's job stress	5.4273	5.0205	5.0370	9.51	.0001
Move-related family stress	3.8915	3.0426	3.4249	17.26	.0000
Marital satisfaction	5.9610	6.0909	6.1061	1.59	.2054
Perceived family support	5.5512	5.4545	5.7302	2.49	.0836
Sensitivity to AF family need	3.4390	4.2936	4.4029	43.66	.0000
Identification with AF & job	5.0585	5.5500	5.4600	12.64	.0000
Perceived job satisfaction	5.2317	5.7131	5.8578	22.75	.0000
Spouse's career orientation	5.2317	5.4545	5.5651	7.48	.0006
Gender-role orientation	3.6293	4.3920	4.0858	9.32	.0001
Spouse's autonomy	3.5569	3.7462	3.8548	5.08	.0064
Off-base social interaction	4.1085	4.4659	4.6433	12.01	.0000
Spousal support to commitment	4.6870	5.9432	5.7562	50.41	.0000
Spousal preference for off-base community friendships	3.9081	3.2008	3.5470	10.88	.0000
Help seeking attitudes	4.9122	4.6629	4.7788	1.51	.2225
Total number of children	2.4927	2.8409	2.7901	5.03	.0067
Number of children at home	2.3659	2.5341	2.5147	1.38	.2515
Age of youngest child*	1.9244	2.6591	2.1603	5.33	.0050
Other family members in home	1.1317	1.1591	1.3047	3.01	.0496
Sex of AF member*	1.0951	1.0341	1.0813	1.79	.1674
Age of AF member	29.8321	32.4318	31.1309	6.46	.0016
Pay grade of AF member*	4.9055	5.4535	4.9598	2.94	.0536
Personnel category in AF*	1.1488	1.0568	1.0293	1.16	.3129
Years in AF (tenure)	5.2525	5.8977	5.4897	5.88	.0029
Member months in career field	6.1373	6.3182	6.3119	1.86	.1565
Member months on station	5.0858	5.0795	4.9750	0.48	.6162
Member months in position	4.0074	4.0682	4.1002	0.28	.7537
Ethnic group of AF member*	4.8329	4.7727	4.7489	1.46	.2324
Marital status of AF member*	2.6244	2.4091	2.4412	2.56	.0782
Education level of AF member*	3.1638	3.2614	3.2721	0.89	.4093

* Means (ratio level) translatable into categories on the questionnaire.

** Factors perceived to impact on spouse's intention to make the AF a career comprise TDY requirements, spouse's TDY, change in family income due to transfer to present base, possibility of future assignment outside continental U.S. (CONUS), and military exercises and recalls.

---

contrast, negativist groups disagree less about spousal preference for off-base community friendship and help seeking attitude.

TABLE 7

Descriptive Profiles of Air Force Family Work Groups
By Perceived Job Satisfaction

Descriptive Variables	Groups (means) Very Neg Somewhat Negative n=90	Neither Negative Nor Pos n=61	Somewhat to Very Positive n=787	F Ratio	F Prob
AF member's job stress	5.5133	5.1869	5.0193	5.00	.0069
Move-related family stress	3.9306	3.9590	3.3161	11.21	.0000
Marital satisfaction	5.8583	5.9344	6.1102	2.14	.1188
Perceived family support	5.3111	5.3033	5.7281	5.83	.0030
Sensitivity to AF family need	3.0463	3.5109	4.2505	33.74	.0000
Identification with AF & job	4.8000	5.0918	5.4915	14.29	.0000
Perceived job satisfaction	3.6861	4.8033	5.9660	150.90	.0000
Spouse's career orientation	5.5185	5.2131	5.4261	1.06	.3464
Gender-role orientation	3.7222	3.6230	4.0623	2.48	.0844
Spouse's autonomy	3.8074	3.5738	3.7039	0.53	.5899
Off-base social interaction	3.7278	3.9098	4.5889	15.47	.0000
Spousal support to commitment	3.8444	4.8798	5.66'2	50.38	.0000
Spousal preference for off-base community friendships	4.1519	3.8852	3.4917	9.02	.0001
Help seeking attitudes	5.4074	4.7432	4.7781	7.81	.0004
Total number of children	2.2222	2.6721	2.7357	4.97	.0071
Number of children at home	2.1111	2.4426	2.4816	2.79	.0617
Age of youngest child*	1.4556	2.1311	2.2846	6.75	.0012
Other family members in home	1.1667	1.1803	1.2147	0.10	.9018
Sex of AF member*	1.1111	1.1311	1.0940	0.32	.7266
Age of AF member	29.1236	30.6393	31.4930	4.12	.0166
Pay grade of AF member*	4.4545	4.8103	5.1013	4.73	.0091
Personnel category in AF*	1.0556	1.1803	1.0801	0.24	.7887
Years in AF (tenure)	4.9333	5.5410	5.5167	5.08	.0064
Member months in career field	5.9101	6.4426	6.2580	3.28	.0382
Member months on station	4.8000	4.9836	5.0575	0.93	.3937
Member months in position	3.8222	3.8197	4.0830	1.32	.2680
Ethnic group of AF member*	4.7865	4.8305	4.7592	0.28	.7532
Marital status of AF member*	2.5889	2.7377	2.4491	1.83	.1616
Education level of AF member*	3.0112	2.8525	3.3244	6.06	.0024

* Means (ratio level) translatable into categories on the questionnaire.

** Variables reflecting perceived job satisfaction comprise job satisfaction, status and prestige, patriotism, and career field (Air Force specialty, type of job) of your spouse.

In terms of personal demographics, those who are positive on job satisfaction tend to be significantly older, attained higher educational levels, have longer tenure, have been longer in their

career field, and earn higher pay. In addition, they have significantly more (and older) children.

5.8 Attitudinal and Demographic Profile by Satisfaction with Air Force Duty Location

Family group profile differences in Table 8 are clearly discerned by the attitudinal but weakly profiled by demographic variables. The positivist and negativist group reaction profile for satisfaction with current Air Force duty location is similar to that for perceived job satisfaction in Table 7. The only differences are the additional significant attitudinal variables --marital satisfaction, spousal career and gender-role orientation--in Table 8 found to significantly differentiate group means. Similarly, in Table 7 more significant demographic variables--total number of children, age, income, tenure, member months in career field, and education--significantly differentiate the positive and negative groups. Thus, hypotheses H5 and H6 suggesting significant group differences with respect to frequency of use and satisfaction with Air Force services is supported by the analysis.

5.9 Regression Results: Career Commitment, Frequency of Use and Satisfaction with Services

The pairwise Pearson correlation matrix (see Table 9) provided the basis for the selection of variables included in the stepwise regression computer run. In general, intercorrelations between pairs of family attitudinal, demographic, and attitudinal -demographic variables are low, and as expected from the large sample size many are significantly related to each other.

TABLE 8

Descriptive Profiles of Air Force Family Groups
By Satisfaction with Current Air Force Duty Location

Descriptive Variables	Groups (means) Very Neg Somewhat Negative n=227	Neither Negative Nor Pos n=111	Somewhat to Very Positive n=541	F Ratio	F Prob
AF member's job stress	5.3480	5.1676	5.0200	4.16	.0159
Move-related family stress	3.8866	3.5495	3.3970	8.31	.0003
Marital satisfaction	5.6971	6.0023	6.1636	11.99	.0000
Perceived family support	5.4361	5.4279	5.7283	4.51	.0112
Sensitivity to AF family need	3.1689	4.2282	4.2794	52.07	.0000
Identification with AF & job	4.8379	5.4432	5.4787	20.65	.0000
Perceived job satisfaction	4.9097	5.4820	5.8452	37.79	.0000
Spouse's career orientation	5.2555	5.1622	5.5656	8.05	.0003
Gender-role orientation	3.5859	3.9234	4.0573	4.81	.0084
Spouse's autonomy	3.6138	3.6486	3.7609	1.04	.3549
Off-base social interaction	4.1586	4.3559	4.4991	3.56	.0288
Spousal support to commitment	4.4831	5.1411	5.6722	37.82	.0000
Spousal preference for off-base communityfriendships	4.2893	3.6937	3.4307	26.70	.0000
Help seeking attitudes	4.9927	4.5766	4.8004	3.23	.0402
Total number of children	2.4537	2.4955	2.7079	2.84	.0590
Number of children at home	2.2863	2.3243	2.5009	2.21	.1098
Age of youngest child*	1.8767	1.8018	2.2052	3.31	.0371
Other family members in home	1.1322	1.1532	1.2810	1.71	.1810
Sex of AF member*	1.1233	1.0901	1.1017	0.34	.7150
Age of AF member	29.8106	30.4182	31.0875	2.56	.0780
Pay grade of AF member*	4.9401	4.5963	5.0172	2.17	.1153
Personnel category in AF*	1.1894	1.0360	1.0832	0.87	.4193
Years in AF (tenure)	5.2455	5.4128	5.4409	1.05	.3502
Member months in career field	6.1416	6.0180	6.2168	0.96	.3845
Member months on station	4.8628	5.0364	4.9944	0.58	.5588
Member months in position	3.8527	4.1532	4.0613	1.41	.2450
Ethnic group of AF member*	4.6830	4.7273	4.7926	1.73	.1791
Marital status of AF member*	2.7665	2.4505	2.4519	4.89	.0077
Education level of AF member*	3.1322	3.4505	3.2416	2.54	.0793

----

* Means (ratio level) translatable into categories on the questionnaire.

** Variables comprising the AF member's intention to make the AF a career include convenience of base facilities, employment facilities for the spouse in the local area, being at the present duty station (base), and acceptance by people in the local area.

5.91 Family Attitudes, Demographics, and Career Commitment

Hypotheses H1, H2, and H3 postulate that the family's per-

Pairwise Pearson Correlation Matrix for Predictor and Outcome Variables

Variables	F1	F2	F3	F4	F5	F6	F7	F8	F9	F10	F11	F12	F13	F14	128	129	130	131	AGE	PAY	V003	V004	V005	V006	V009	FRQ	S1	S2	F91	F92	F93	F94	V019
Family Attitudes																																	
AF member's job stress (F1)	1.00																																
Move-related family stress (F2)	.43a	1.00																															
Marital satisfaction (F3)	-.01	-.02	1.00																														
Perceived family support (F4)	.14a	.12a	.37	1.00																													
Sensitivity to AF family need	-.22a	-.21a	.22a	.19a	1.00																												
Identification with AF & job(F6)	.08c	-.10a	.25a	.27a	.47a	1.00																											
Perceived job satisfaction (F7)	.02	-.09a	.23a	.25a	.42a	.35a	1.00																										
Spouse's career orientation(F8)	-.05	-.02	.13a	.07b	.19a	.11a	.13a	1.00																									
Gender-role orientation (F9)	.06c	.06c	.22a	.14a	.20a	.12a	.14a	-.05	1.00																								
Spouse's autonomy (F10)	.10a	.17a	-.09a	.03	.06c	.03	.05	.22a	.05c	1.00																							
Off-base social interaction(F11)	.01	.01	.14a	.18a	.21a	.27a	.33a	.08b	.06c	.04	1.00																						
Spousal support to commitment	-.01	-.15a	.15a	.25a	.39a	.42a	.42a	.09a	.14a	.05c	.23a	1.00																					
Spousal preference for off-base community friendships(F13)	.32a	.34a	-.16a	-.04	-.20a	-.10a	-.16a	-.05c	.02	.10a	-.09a	-.16a	1.00																				
Help seeking attitudes (F14)	.19a	.21a	.10a	.08b	-.02	-.01	-.04	.06c	.11a	.16a	.05	-.02	.21a	1.00																			
Demographic Variables																																	
Total number of children(128)	.04	.11a	.04	.01	.10a	.03	.13a	.02	.14a	.13a	.08b	.16a	.09a	.08b	1.00																		
Number of children at home(129)	.13a	.17a	.02	.07b	.09a	.08b	.11a	-.03	.15a	.14a	.09a	.19a	.17a	.09a	.72a	1.00																	
Age of youngest child*(130)	.03	.07b	.04	-.01	.11a	.07b	.10a	.08a	.10a	.15a	.10a	.17a	.02	.06c	.51a	.33a	1.00																
Other family member in home(131)	.15a	.22a	.12a	.09a	.16a	.05c	.10a	.17a	.10a	.23a	.11a	.07b	.23a	.10a	.34a	.42a	.28a	1.00															
Age of AF member(AGE)	-.03	-.05c	-.01	-.10a	.05	-.02	.17a	.07b	.05	.12a	.01	.14a	-.06c	-.03	.42a	.22a	.60a	.12a	1.00														
Pay grade of AF member*(PAY)	-.00	-.04	-.05c	-.10a	-.01	-.15a	.10a	.06c	.02	.07b	-.04	.03	.01	-.00	.31a	.15a	.38a	.05	.60a	1.00													
Years in AF (tenure)(V003)	.11a	.02	-.05	-.11a	-.05	.02	.13a	.01	.02	.11a	.06c	.27a	-.00	-.02	.38a	.31a	.42a	.08b	.71a	.51a	1.00												
Member months in career field	.12a	.04	-.00	-.07	-.06c	-.01c	.07b	.01	-.00	.07b	.02	.12a	.03	-.02	.18a	.14a	.17a	.06c	.26a	.29a	.48a	1.00											
Member months on station(V005)	.06	-.02	.01	-.05	.01	-.02	.08b	.05	.06c	.07b	.01	.00	-.04	.02	.11a	.09a	.14a	.05c	.17a	.22a	.21a	.32a	1.00										
Member months in position(V006)	.01	-.03	-.02	-.06c	.02	-.02	.05	-.02	-.01	.07c	-.02	-.04	-.00	-.01	.09a	.05	.11a	.04	.15a	.15a	.10a	.27a	.56a	1.00									
Education of AF member*(V009)	-.07c	-.03	.04	.04	.02	.07b	.10a	-.03	-.06c	-.01	.03	.05	-.13a	-.11a	.05	.03	.15a	.01	.37a	.00	.23a	.02	-.12a	-.08b	1.00								
Outcome Variables																																	
Freq of use of AF services(FRQ)	-.01	.05	.07c	.07b	.13a	.02	.12a	.15a	.13a	.15a	.10a	.03	.07c	.08b	.29a	.25a	.25a	.33a	.16a	.22a	.05	.00	.06c	.04	.04	1.00							
Overall satisfaction—basic services(S1)	-.13a	-.08b	.14a	.08b	.34a	.12a	.19a	.14a	.10a	.05	.08b	.09a	-.08b	.02	.15a	.13a	.15a	.13a	.10b	.06c	-.04	-.05	.05	.06c	.04	.49a	1.00						
Overall satisfaction—optional services(S2)	-.05	.04	.06c	.10a	.16a	.05	.12a	.12a	.11a	.14a	.10a	.06c	.02	.09a	.22a	.20a	.23a	.24a	.12a	.18a	.04	.02	.10a	.10a	-.02	.60a	.47a	1.00					
Perceived favorableness to basic job benefits(F91)	-.06c	-.08b	.10a	.21a	.42a	.25a	.31a	.14a	.15a	.06c	.18a	.30a	-.05c	.00	.13a	.15a	.03a	.21a	-.02	-.03	-.02	-.02	-.04	-.02	.07b	.13a	.32a	.14a	1.00				
Perceived impact of AF moves, exercises, and TDY(F92)	-.02	-.04	.13a	.15a	.36a	.27a	.25a	.14a	.10a	.15a	.24a	.37a	-.04	.06c	.22a	.23a	.13a	.29a	.03	-.02	.00c	.05c	-.01	-.01	.04	.17a	.13a	.16a	.48a	1.00			
Perceived job satisfaction(F93)	-.04	-.07b	.19a	.23a	.33a	.27a	.56a	.09a	.13a	.06c	.33a	.44a	-.13a	-.04	.22a	.19a	.10a	.20a	.14a	.03a	.14a	.07b	.03	.02	.17a	.17a	.20a	.14a	.60a	.49a	1.00		
Satisfaction with current AF duty location(F94)	-.01	-.02	.20a	.18a	.37a	.27a	.29a	.15a	.13a	.10a	.18a	.30a	-.15a	.02	.20a	.22a	.15a	.26a	.09a	-.02	.03a	.04	.05c	.04	.10a	.03a	.29a	.09b	.50a	.51a	.45a	1.00	
Career commitment(V019)**	.05	.16a	.01	.03	-.12a	-.12a	-.25a	-.01	.01	-.07c	-.07c	-.40a	.08b	.06c	-.25a	-.19a	-.28a	-.23	-.46a	-.24a	-.51a	-.15a	-.06c	-.05	-.20a	-.04	-.01	-.05c	-.15a	-.16a	-.28a	-.15a	1.00

a = p < .001; b = p < .01; c = p < .05.

**The signs on this variable should be reversed because of inverse item scaling.

Pairwise Pearson Correlation Matrix For Predictor and Outcome Variables

Variables	F1	F2	F3	F4	F5	F6	F7	F8	F9	F10	F11	F12	F13	F14	128	129	130	131	AGE	PAY	V003	V024	V005	V025	V009	FRQ	S1	S2	F91	F92	F93	F94	V019
Family Attitudes																																	
AF member's job stress (F1)	1.00																																
Move-related family stress (F2)	.43a	1.00																															
Marital satisfaction (F3)	-.01	-.02	1.00																														
Perceived family support (F4)	.14a	.12a	.37	1.00																													
Sensitivity to AF family need	-.22a	-.21a	.22a	.13a	1.00																												
Identification with AF & job(F6)	.00c	-.10a	.25a	.27a	.47a	1.00																											
Perceived job satisfaction (F7)	.02	-.09a	.23a	.25a	.42a	.35a	1.00																										
Spouse's career orientation(F8)	-.05	-.02	.13a	.07b	.19a	.11a	.13a	1.00																									
Gender-role orientation (F9)	.06c	.06c	.22a	.14a	.20a	.12a	.14a	-.05	1.00																								
Spouse's autonomy (F10)	.18a	.17a	-.09a	.03	.06c	.03	.05	.22a	.05c	1.00																							
Off-base social interaction(F11)	.01	.01	.14a	.18a	.21a	.27a	.33a	.08b	.06c	.04	1.00																						
Spousal support to commitment	-.01	-.19a	.15a	.25a	.39a	.42a	.42a	.09a	.14a	.05c	.23a	1.00																					
Spousal preference for off-base community friendships(F13)	.32a	.34a	-.16a	-.04	-.20a	-.18a	-.16a	-.05c	.02	.18a	-.03a	-.16a	1.00																				
Help seeking attitudes (F14)	.19a	.21a	.10a	.08b	-.02	-.01	-.04	.06c	.11a	.16a	.05	-.02	.21a	1.00																			
Demographic Variables																																	
Total number of children(128)	.04	.11a	.04	.01	.10a	.03	.13a	.02	.14a	.13a	.08b	.16a	.09a	.08b	1.00																		
Number of children at home(129)	.13a	.17a	.02	.07b	.09a	.08b	.11a	-.03	.15a	.14a	.09a	.19a	.17a	.09a	.72a	1.00																	
Age of youngest child*(130)	.03	.07b	.04	-.01	.11a	.07b	.10a	.08a	.10a	.15a	.10a	.17a	.02	.06c	.51a	.33a	1.00																
Other family member in home(131)	.15a	.22a	.12a	.09a	.16a	.05c	.10a	.17a	.10a	.23a	.11a	.07b	.23a	.10a	.34a	.42a	.28a	1.00															
Age of AF member(AGE)	-.03	-.05c	-.01	-.10a	.05	-.02	.17a	.07b	.05	.12a	.01	.14a	-.06c	-.03	.42a	.22a	.60a	.12a	1.00														
Pay grade of AF member*(PAY)	-.00	-.04	-.05c	-.10a	-.01	-.15a	.10a	.06c	.02	.07b	-.04	.03	.01	-.00	.31a	.15a	.38a	.05	.60a	1.00													
Years in AF (tenure)(V003)	.11a	.02	-.05	-.11a	-.05	.02	.13a	.01	.02	.11a	.06c	.27a	-.00	-.02	.38a	.31a	.42a	.08b	.71a	.51a	1.00												
Member months in career field	.12a	.04	-.00	-.07	-.06c	-.01c	.07b	.01	-.00	.07b	.02	.12a	.03	-.02	.18a	.14a	.17a	.05c	.26a	.29a	.48a	1.00											
Member months on station(V025)	.06	-.02	.01	-.05	.01	-.02	.08b	.05	.06c	.07b	.01	.00	-.04	.02	.11a	.03a	.14a	.05c	.17a	.22a	.21a	.32a	1.00										
Member months in position(V006)	.01	-.03	-.02	-.06c	.02	-.02	.05	-.02	-.01	.07c	-.02	-.04	-.00	-.01	.03a	.05	.11a	.04	.15a	.15a	.10a	.27a	.56a	1.00									
Education of AF member*(V009)	-.07c	-.03	.04	.04	.02	.07b	.10a	-.03	-.06c	-.01	.03	.05	-.13a	-.11a	.05	.03	.15a	.01	.37a	.00	.23a	.03	-.12a	-.08b	1.00								
Outcome Variables																																	
Freq of use of AF services(FRQ)	-.01	.05	.07c	.07b	.13a	.02	.12a	.15a	.13a	.15a	.10a	.03	.07c	.08b	.23a	.25a	.25a	.33a	.16a	.22a	.05	.00	.05c	.04	.04	1.00							
Overall satisfaction—basic services(S1)	-.13a	-.08b	.14a	.08b	.34a	.12a	.19a	.14a	.10a	.05	.08b	.03a	-.08b	.02	.15a	.13a	.15a	.13a	.10b	.08b	-.04	-.05	.05	.05c	.04	.43a	1.00						
Overall satisfaction—optional services(S2)	-.05	.04	.06c	.10a	.16a	.05	.12a	.12a	.11a	.14a	.10a	.05c	.02	.03a	.22a	.20a	.23a	.24a	.12a	.18a	.04	.02	.10a	.10a	-.02	.68a	.47a	1.00					
Perceived favorableness to basic job benefits(F91)	-.06c	-.08b	.18a	.21a	.42a	.25a	.31a	.14a	.15a	.05c	.18a	.38a	-.05c	.00	.13a	.15a	.03a	.21a	-.02	-.02	-.02	-.02	-.04	-.02	.27b	.13a	.32a	.14a	1.00				
Perceived impact of AF moves, exercises, and TDY(F92)	-.02	-.04	.13a	.15a	.36a	.27a	.25a	.14a	.18a	.15a	.24a	.37a	-.04	.06c	.22a	.23a	.13a	.23a	.03	-.02	.03c	.05c	-.21	-.01	.04	.17a	.13a	.16a	.48a	1.00			
Perceived job satisfaction(F93)	-.04	-.07b	.13a	.23a	.33a	.27a	.56a	.03a	.13a	.06c	.33a	.44a	-.13a	-.04	.22a	.13a	.18a	.22a	.14a	.23a	.14a	.27b	.03	.02	.17a	.17a	.22a	.14a	.60a	.43a	1.00		
Satisfaction with current AF duty location(F94)	-.01	-.02	.20a	.18a	.37a	.27a	.23a	.15a	.13a	.12a	.18a	.30a	-.15a	.02	.20a	.22a	.15a	.26a	.03a	-.02	.03a	.04	.05c	.04	.12a	.03a	.23a	.09b	.50a	.51a	.43a	1.00	
Career commitment(V019)**	.05	.16a	.01	.03	-.12a	-.12a	-.25a	-.01	.01	-.07c	-.07c	-.40a	.08b	.06c	-.25a	-.19a	-.28a	-.03	-.46a	-.24a	-.51a	-.19a	-.06c	-.05	-.22a	-.24	-.01	-.05c	-.15a	-.16a	-.28a	-.15a	1.00

a = p < .001; b = p < .01; c = p < .05.

**The signs on this variable should be reversed because of inverse item scaling.

sonal attitudes might provide significant explanation regarding the Air Force member's decision on career commitment. Table 10 shows that of the 14 attitudinal factors, six (F2, F4, F6, F11, F12, and F13) were found to account for significant variation in career commitment. Two of the three hypotheses were generally supported by at least one factor in the analysis. In H1, contrary to the hypothesis, "Identification with the Air Force and members job" (F6) exhibited a modest but negative influence on career commitment. For H2, again the sign for "Perceived family support" (F4) was in the wrong direction; however, "Member's job satisfaction" (V822) had a positive relationship, as both of these variables were instrumental in determining commitment decision. The testing of the negative relationships in H3 were also supported by the substantial inverse influence of "Move-related family stress" (F2) and "Off-base social interaction (F11). While off-base social interaction of the Air Force member may impact negatively on career commitment, "Spousal preference for off-base community friendships" are perceived to have a positive influence on member's commitment decisions.

Demographic variables were also examined to assess their influence on career commitment. Results support the contention in H4 that career commitment is a positive function of member age and tenure; however the relationship with pay is negative. Some studies have found that expected pay rather than present pay may better explain career decisions. However, that career commitment is a negative function of educational attainment has been confirmed in this study.

TABLE 10

Regression Results of Air Force Family Work Groups To Explain Career Commitment and Satisfaction with Services

Descriptive Variables	Career Commitment			Frequency of Use Of All Services			Satisfaction With Basic Services			Satisfaction With Optional Services		
	Beta	T-Value	T-Prob	Beta	T-Value	T-Prob	Beta	T-Value	T-Prob	Beta	T-Value	T-Prob
AF member's job stress(F1)	.02	0.631	NS	-.06	-2.021	.0435	.01	0.440	NS	-.03	-0.948	NS
Move-related family stress(F2)	-.05	-1.973	.0487	-.01	-0.370	NS	.02	0.799	NS	.02	0.691	NS
Marital satisfaction(F3)	.02	0.002	NS	.01	0.393	NS	.01	0.228	NS	-.05	-1.626	.1042
Perceived family support(F4)	-.06	-2.777	.0056	.05	1.725	.0849	.03	0.942	NS	.07	2.375	.0177
Sensitivity to AF family needF5	-.04	-1.473	NS	.01	0.387	NS	.21	7.079	.0000	.11	3.439	.0006
Identification with AF & job(F6)	-.04	-1.662	.0967	.06	1.811	.0705	.04	1.219	NS	.06	1.721	.0856
Perceived job satisfaction(F7)				.01	0.198	NS	.05	1.641	.1010	.02	0.517	NS
Spouse's career orientation(F8)				.05	1.542	NS	.06	2.139	.0326	-.01	-0.201	NS
Gender-role orientation(F9)	.00	0.328	NS	.02	0.697	NS	.01	0.346	NS	-.01	-0.212	NS
Spouse's autonomy(F10)				.01	0.217	NS	.02	0.671	NS	.07	2.473	.0135
Off-base social interaction(F11)	-.05	-2.253	.0244	.06	2.111	.0350	.04	1.270	NS	.04	1.338	NS
Spousal support to commitment(12)	.31	12.251	.0000	.00	0.107	NS	.01	0.435	NS	.02	0.516	NS
Spousal preference for off-base community friendships(F13)	.06	2.527	.0116	-.00	-0.053	NS	-.01	-0.450	NS	-.06	-2.063	.0393
Help seeking attitudes(F14)	.01	0.611	NS	.02	0.688	NS	.03	0.846	NS	.03	1.097	NS
Total number of children(128)	.03	1.248	NS	.10	3.137	.0018	.04	1.249	NS	.00	0.038	NS
Number of children at home(129)	.04	1.613	.1070?	-.02	-0.457	NS	.02	0.814	NS	.09	3.039	.0006
Age of youngest child*(130)				.04	1.102	NS	.05	1.456	NS	.12	3.166	.0016
Other family members in home(131)				.11	3.500	.0005	-.01	-0.424	NS	-.01	-0.176	NS
Sex of AF member*(SEX)	.00	0.116	NS	.10	3.429	.0006	.02	0.783	NS	.06	2.070	.0387
Age of AF member(AGE)	.28	7.928	.0000	-.04	-1.169	NS	.01	0.175	NS	-.10	-2.710	.0068
Pay grade of AF member*(PAY)	-.07	-2.450	.0144	-.01	-0.269	NS	-.07	-2.534	.0114	.05	1.281	NS
Personnel category in AF*				.01	0.242	NS	-.04	-1.419	NS	-.00	-0.091	NS
Years in AF (tenure)(V003)	.25	7.487	.0000	-.04	-1.398	NS	.02	0.455	NS	-.01	-0.179	NS
Member months in career field(V004)				-.01	-0.450	NS	.01	0.362	NS	.01	0.364	NS
Member months on station(V005)				-.02	-0.816	NS	.02	0.921	NS	.04	1.275	NS
Member months in position(V006)				-.03	-0.953	NS	-.04	-1.406	NS	.01	0.246	NS
Ethnicity of AF member*(V007)	-.00	-0.051	NS	-.10	-3.217	.0013	-.01	-0.345	NS	-.09	-2.925	.0035
Marital status of AF member*(V008)				.06	1.843	.0656	.00	0.144	NS	.02	0.621	NS
Education of AF member*(V009)	-.05	-1.831	.0673	.03	0.911	NS	.00	0.050	NS	-.00	-0.005	NS
Job Motivation Index(V007)	.02	0.705	NS	.01	0.183	NS	-.00	-0.115	NS	.05	1.579	NS
Member Job Satisfaction(V022)	.19	8.134	.0000	-.03	-0.961	NS	-.02	-0.821	NS	.03	1.116	NS
	Adjusted R2 = .45			Adjusted R2 = .05			Adjusted R2 = .06			Adjusted R2 = .06		
	Std Error = .90			Std Error = .37			Std Error = .88			Std Error =1.06		
	Durbin-Watson=2.02			Durbin-Watson=1.88			Durbin-Watson=2.04			Durbin-Watson=1.90		

5.92 Family Attitudes, Demographics, and Service Satisfaction

Table 10 also reveals that a different combination of variables influence Air Force service frequency of use, satisfaction

with basic services, and satisfaction with optional services. The variables that enter the equation to explain frequency of use are "Total number of children" (F128), "Gender of the AF member", "Other family members in the home" (F131), "Ethnic Group of AF Member" (V007), "Off-base social interaction" (F11), and "AF member's job stress" (F1). By contrast, the profile of variables that enter the equation to explain satisfaction with basic services are "Sensitivity of the AF to family needs" (F5), "Pay grade of the AF member", and "Spouse's career orientation" (F8). Even the satisfaction with optional services has a different profile of explanatory variables, somewhat akin to the list explaining career commitment (see Table 10).

Overall, the results reveal that attitudinal and demographic variables were more influential in explaining career commitment (R^2 = .45) than usage frequency of Air Force services (R^2 = .05). The analysis also shows that the accounted-for variation in satisfaction with basic services (R^2 = .06) and optional services (R^2 = .06) explained by variation in attitudinal and demographic variable changes are of relatively diminished importance. Finally, Table 9 reveals that there exists a positive relationship between career commitment and satisfaction with basic and optional Air Force services, thereby supporting H7.

6.0 DISCUSSION

The findings establishing distinct profiles of Air Force family work groups allow us to conclude unmistakeably that (re)-targeting and (re)positioning can be useful in making sure that the Air Force responds to the needs of its members and their

families with much more precision. Profiles of the heavy-user, the highly satisfied, the light-user, and the non-satisfied allow us to (re)design work and services to improve intrinsic and extrinsic job benefits more appropriately.

Since one of the objectives of the Air Force is to improve retention rates, different marketing strategies and promotional appeals can be (re)directed to the targets identified by the above profiles. Thus, now that we have established what different family work groups need we can tailor our program to their needs instead of trying to alter their need pattern.

7.0 CONCLUSIONS AND RECOMMENDATIONS

The results of this study confirmed that services satisfaction is distinct from career commitment, and that the variables important in determining career commitment differ from those determining satisfaction with services. Several user-categories and user-needs were profiled based on frequency and satisfaction. The predictor variables important in explaining career commitment and services satisfaction were also established.

Based on the above results, several recommendations are suggested. First, the Air Force should base its total services design on user-needs and user-categories. Second, commanders should continue to monitor member and family attitudes and demographics as a means of explaining family-work relationships. In particular, they should continue to monitor job and move-related stress, job related satisfaction, off-base social interaction, pay scales and tenure as factors that could influence retention rates. Finally, they should take stock of the portfolio of ser-

vices packaged and offered so that the precision of targeting undertaken can have a decided impact on career commitment.

A logical and necessary extention of the present research is the utilization of clustering procedures to derive stimulus configurations of combined attitudinal, demographic, frequency of use, levels of satisfaction, and career commitment. By obtaining hierarchical and disjoint clusters and positioning them on two-dimensional coordinates one can develop much better precision-engineered marketing strategies to attract existing and potential members.

APPENDIX 1

Descriptive Statistics of Air Force Work Groups
Variables, Cases, Means, and Standard Deviations

Variables	Cases	Mean	Std Dev
AF member's job stress	1170	5.1950	1.1932
Move-related family stress	1170	3.6245	1.2818
Marital satisfaction	1170	5.5922	1.0826
Perceived family support	1170	4.7088	1.4297
Sensitivity to AF family need	1170	4.1142	1.4164
Identification with AF & job	1170	5.0065	1.1962
Perceived job satisfaction	1170	5.4295	1.2234
Spouse's career orientation	1170	5.4157	1.2560
Gender-role orientation	1170	3.9470	1.9045
Spouse's autonomy	1170	4.2385	1.5828
Off-base social interaction	1170	2.5004	1.5078
Spousal support to commitment	1170	5.3282	2.0973
Spousal preference for off-base community friendships	1170	3.6000	1.5045
Help seeking attitudes	1170	4.8046	1.4505
Total number of children	1170	2.6615	1.4896
Number of children at home	1170	2.4231	1.4050
Age of youngest child*	1170	2.1453	1.9900
Other family members in home	1170	1.1590	1.0167
Sex of AF member*	1168	M(mode)	
Age of AF member	1164	31.0034	7.3829
Pay grade of AF member*			
Personnel category in AF*			
Years in AF (tenure)	1170	5.4009	1.7653

Member months in career field	1170	6.2368	1.4183
Member months on station	1170	5.0265	1.7269
Member months in position	1170	4.0786	1.8337
Ethnic group of AF member*	1170	W(mode)	
Marital status of AF member*	1170	M(mode)	
Education level of AF member*	1170	HS(mode)	

----

* Means (ratio level) translatable into categories on the questionnaire.

Appendix 2

AFFS Attitudinal Factors

Factor+	AFFS items	Name	#	Cronbach Alpha
1	14,16,27,36	AF member's job stress	5	.72
2	21,33,34,39	Move-related family stress	4	.60
3	57,58,-59,60,60	Marital satisfaction	5	.75
4	11,28,37	Perceived family support	3	.80
5	5,7,8,10,23,41	Sensitivity to AF family needs	6	.75
6	1,4,6,9	Identification with AF & job	4	.74
7	15,20,30,38,-40	Perceived job satisfaction	5	.72
8	24,44	Spouse's career orientation	2	.36
9	45,46	Gender role orientation	2	.57
10	48,52,55	Spouse's autonomy	3	.46
11**	-40,47	Off-base social interaction	2	.59
12	18,31,35	Spousal support to commitment	3	.85
13	17,-51,53	Spousal preference for off-base community friendships	3	.55
14	50,-54,56	Help seeking attitudes	3	.40

*A negative sign indicates that the item loaded negatively on the factor.
**This factor did not emerge on the confirmatory factor analysis.
+The Scree test was utilized to determine the optimum number of factors.

REFERENCES

Aldous, J., M. W. Osmond, and M. W. Hicks (1979), "Men's Work and Men's Families". In W. R. Burr, R. Hill, F. I. Nye, and I. L. Reiss (Eds.), Contemporary Theories About The Family (Vol. 1) (pp. 227-258), New York: The Free Press.

Amabile, T. M., W. DeJong, and M. R. Lepper (1976), "Effects of Externally-imposed Deadlines on Subsequent Intrinsic Motivation", Journal of Personality and Social Psychology, 34, 92-98.

Angle, H., and J. Perry (1981), "An Empirical Assessment of Organizational Commitment and Organizational Effectiveness",

Administrative Science Quarterly, 26, 1-14.

Barnard, Chester I. (1938), The Function of the Executive, London: Oxford University Press.

Beeson, G. W., Jr. (1985), Influence On The Identification Of Wives With The Air Force Organization: An Examination Of The Two-person Career Pattern Within The Military. Unpublished Doctoral Dissertation, University of North Carolina, Greensboro, NC.

Bell, L. G., R. A. Wicklund, G. Manko, and C. Larkin (1976), "When Unexpected Behavior is Attributed to the Environment", Journal of Research in Personality, 10, 316-327.

Belt, J., and A. Sweeney (1973), "The Air Force Wife: Her Knowledge of and Attitudes Toward the Air Force". Paper presented at the Meeting of the Military Testing Association's Conference on Human Resources, San Antonio, Texas, October.

Black, L. W. (1982), Changing Patterns of Air Force Families. (Report 82-0275). Maxwell AFB, Alabama: Air Command and Staff College, March.

Boneau, C. A. (1974), "Paradigm Regained? Cognitive Behaviorism Restated", American Psychologist, 29 (5), 297-309.

Brief, Arthur P. and Ramon J. Aldag (1980), "Antecedents of Organizational Commitment among Hospital Nurses," Sociology of Work and Occupation, 7, 210-221.

Brown, M. E. (1969), "Identification and Some Conditions of Organizational Involvement", Administrative Science Quarterly, 14, 346-355.

Buchanan, B. (1974), "Building Organizational Commitment: The Socialization of Managers in Work Organizations", Administrative Science Quarterly, 19, 533-546.

Deci, E. L. (1975a), Intrinsic Motivation, New York: Plenum Press.

Deci, E. L. (1975b), "Notes on the Theory and Metatheory of Intrinsic Motivation", Organizational Behavior and Human Performance, 15, 130-145.

Dubin, R., J. E. Champoux, and L. W. Porter (1975), "Central Life Interests and Organizational Commitment of Blue-collar and Clerical Workers", Administrative Science Quarterly, 20, 411-421.

Etzioni, A. (1961), A Comparative Analysis of Complex Organizations. New York: Free Press.

Fisher, C. D. (1978), "The Effects of Personal Control, Competence, and Extrinsic Reward Systems on Intrinsic Motivation", Organizational Behavior and Human Performance, 21, 273-288.

TECHNICAL RE.. (U) UNIVERSAL ENERGY SYSTEMS INC
DAYTON OH R C DARRAH ET AL. DEC 85 AFOSR-TR-86-0140
FIED F49620-85-C-0013 F/G 5/1 NL

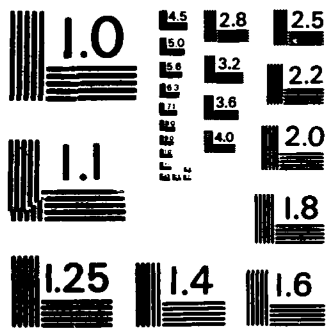

MICROCOPY RESOLUTION TEST CHART
NATIONAL BUREAU OF STANDARDS-1963-A

Freeman, R. D., S. A. Stumpf, E. Weitz, and P. Platten (1981), "Degree of Career Change, Detachment and Job Outcomes", Proceedings of the Eighteenth Annual Meeting of Eastern Academy of Management, 117-122.

Greenhaus, J. H., and N. J. Beutell (1985), "Sources of Conflict Between Work and Family Roles", Academy of Management Review, 10, 76-88.

Hackman, J. R., and E. E. Lawler III (1971), "Employee Reactions to Job Characteristics", Journal of Applied Psychology, 55, 259-286.

Hackman, J. R., and G. R. Oldman (1976), "Motivation Through the Design of Work: Test of a Theory", Organizational Behavior and Human Performance, 16, 250-279.

Hall, D. T. (1976), Careers in Organizations, Glenview, Illinois: Scott, Foresman.

Hall, D. T., B. Schneider, and H. T. Nygren, (1970) "Personal Factors in Organizational Identification", Administrative Science Quarterly, 15, 176-190.

Hickman, R. A., and E. J. Hunter (1980), Military Retention and Retirement: Reciprocal Family/Organization Effects. (Technical Report TR-USIU-81-03). San Diego, California: United States International University.

Hunt, Shelby D., Lawrence B. Chonko, and Van R. Wood (1985), "Organizational Commitment and Marketing", Journal of Marketing, 49 (Winter), 112-126.

Jackofsky, Ellen F. (1984), "Turnover and Job Performance: An Integrated Process Model", Academy of Management Review, 9 (1), 74-83.

Jepsen, D. A., and J. S. Dilley (1974), "Vocational Decision Making Models: A Review of Comparative Analysis," Review of Educational Research, 44, 331-349.

Jones, S. B. (1976), "Corporate Policy on the Transferring of Employees: Sociological Considerations". Paper presented at the meeting of the North Central Sociological Association.

Kabanoff, B. (1980), "Work and Non-work: A Review of Models, Methods and Findings", Psychological Bulletin, 88, 60-77.

Kahn, Robert L., Donald M. Wolfe, Robert P. Quinn, and J. Diedrick Snoek (1964), Organizational Stress, New York: Wiley.

Kanter, R. M. (1977), Work And The Family In The United States: A Critical Review And Agenda For Research And Policy. New York: Russell Sage Foundation.

Korman, A. K., U. Wittig-Berman, and D. Lang (1981), "Career, Success and Personal Failure: Alienation in Professionals and Managers", Academy of Management Journal, 21, 342-360.

Landy, Frank J., and Don A. Trumbo (1980), Psychology of Work Behavior, Homewood, Illinois: Dorsey.

Latack, J. C. (1981), "Person/Role Conflict: Holland's Model Extended to Role-Stress Research, Stress Management and Career Development", Academy of Management Review, 24, 342-360.

Lund, D. A. (1978), "Junior Officers Retention in the Modern Volunteer Army: Who Leaves and Who Stays". In E. Hunter and D. Nice (eds.), Military Families: Adaptation to Change. New York: Praeger.

March, J. G., and H. A. Simon (1958), Organizations. New York: Wiley.

Marsh, R., and H. Mannari (1977), "Organizational Committment and Turnover: A Predictive Study", Administrative Science Quarterly, 22, 57-75.

Maslow, Abraham H. (1943), "A Theory of Motivation", Psychological Review, 50, 370-396.

McCubbin, H. I., A. E. Cauble, and J. M. Patterson (1982), Family Stress, Coping, and Social Support. Springfield Illinois: Charles C. Thomas, Publisher.

Mitchell, T. R., and L. R. Beach (1976), "A Review of Occupational Preference And Choice Research Using Expectancy Theory and Decision Theory", Journal of Occupational Psychology 16, 212-225.

Mobley, W. H. (1977), "Intermediate Linkages in the Relationship Between Job Satisfaction and Employee Turnover", Journal of Applied Psychology, 62, 237-240.

Morris, J. and R. M. Steers (1980), "Structural Influences on Organizational Commitment", Journal of Vocational Behavior, 17, 50-57.

Morrow, Paula C. (1983), "Concept Redundancy in Organizational Research: The Case of Work Commitment", Academy of Management Review, 8 (3), 486-500.

Mowday, R. T., L. W. Porter, and R. M. Steers (1982), Employee-Organization Linkages: The Psychology of Commitment, Absenteeism and Turnover, New York: Academic Press.

Near, J. P., R. W. Rice, and R. G. Hunt (1978), "Work and Extra-work Correlates of Life and Job Satisfaction", Academy of Management Journal, 21, 248-264.

Orthner, D. K. (1980), Families in Blue: A Study of Married and Single Parent Families in the U.S. Air Force. Greensboro, North Carolina: Family Research and Analysis, Inc.

Orthner, D. K., and G. L. Bowen (1983), Families in Blue: Opportunities for Ministry. Arlington, Virginia: Human Resources Research and Development Center, SRA Corporation.

Poloma, M. M., B. F. Pendleton, and T. N. Garland (1981), "Reconsidering the Dual-career Marriage", Journal of Family Issues, 2, 205-224.

Rotundi, T. (1975), "Organizational Identification and Group Involvement", Academy of Management Journal, 18, 892-897.

Salancik, G. R. (1977), "Commitment and the Control of Organizational Behavior and Belief". In B. M. Staw and G. R. Salancik (eds.), New Directions in Organizational Behavior. Chicago: St. Clair Press.

Schmitt, N., and P. M. Mellon (1980), "Life and Job Satisfaction: Is the Job Central?" Journal of Vocational Behavior, 16, 51-58.

Schneider, B., and H. P. Dachler (1978), Work, Family, and Career Considerations in Understanding Employee Turnover Intentions. (Research Report # 19). College Park, Maryland: University of Maryland.

Sheldon, M. E. (1971), "Investments and Involvements as Mechanisms Producing Commitment to the Organization," Administrative Science Quarterly, 16 (3), 143-150.

Sherman, J. Daniel, and Howard L. Smith (1984), "The Influence of Organizational Structure on Intrinsic Versus Extrinsic Motivation", Academy of Management Journal, 27 (4), 877-885.

Simon, Herbert A. (1964), "On the Concept of Organizational Goal", Administrative Science Quarterly, 9 (June), 1-22.

Sonnenfeld, J., and J. P. Kotter (1980), "The Maturing of Career Theory", Paper presented at the 40th annual meeting of the Academy of Management, Detroit.

Staines, G. L. (1980), "Spillover Versus Compensation: A Review of the Literature Between Work and Non-work", Human Relations, 33, 111-129.

Stanton, M. D. (1981), "The Military Family: Its Future in the All-volunteer Context", in E. Hunter and M. Pope (eds.), Family Roles in Transition: In a Changing Military. (Report No. TR-USIU-81-02). San Diego, California: Family Research Center.

Staw, B. M. (1977), "Two Sides of Commitment". Paper presented at the National Meeting of the Academy of Management, Orlando, Florida.

Steers, R. M. (1977), "Antecedents and Outcomes of Organizational Commitment", Administrative Science Quarterly, 22, 46-56.

Stevens, J. M., J. Beyer, and H. M. Trice (1978), "Assessing Personal, Role, and Organizational Predictors of Managerial Commitment", Academy of Management Journal, 21, 380-396.

Super, D. E. (1980), "A Life Span Life Space Approach to Career Development", Journal of Vocational Behavior, 16, 282-298.

Szoc, R. (1982), Family Factors Critical to the Retention of Naval Personnel. Columbia, Maryland: Westinghouse Public Applied Systems.

Walker, Orville C., Gilbert A. Churchill, Jr., and Niel M. Ford (1977), "Motivation and Performance in Industrial Selling: Present Knowledge and Needed Research", Journal of Marketing Research, 14, (May), 156-168.

Wheeler, K. G., and T. A. Mahoney (1981), "The Expectancy Model in the Analysis of Occupational Preference and Occupational Choice", Journal of Vocational Behavior, 14, 11?-122.

Wright, P. (1975), "Consumer Choice Strategies: Simplifying vs. Optimizing.", Journal of Marketing Research, 7, 60-67.

Zuckerman, M., J. Porac, D. Lathin, R. Smith, and E. L. Deci (1978), "On the Importance of Self-determination for Intrinsically-motivated Behavior", Personality and Social Psychology Bulletin, 4, 443-446.

Osama M. Mostafa
No Report Submitted

The <u>OBJECTIVES</u> of this summer research effort, as discussed and fromulated during a pre-summer visit to the Armament Laboratory at Eglin Air Force Base, Florida, would be to evaluate the content of a Research Work Report that was developed in 1981 in connection with InfraRed Imagery and Automatic Target Recognition.

The report is a product of an effort carried on the task of locating man-made objects embedded in low resolution imagery, commonly referred to as "TARGET CUEING".

It is expected that the research effort will address the following undertakings:

1. To investigate the thoroughness of the approaches followed, and the different techniques applied in pursuing the processing of the raw data sets.

   Also, investigate the possiblity of upgrading operations and decision making routines for the purpose of more accurate Image interpretations.

2. To investigate the possiblity of using Aritificial Intelligence (A.I.) Techniques to develop a knowledge-based expert system that will further improve image understanding and classification, and better recognize aerial targets.

3. Investigate the possibility of developing a Skeletal Conceptual Model of a smart Target Recognition System that will utilize A.I. Heuristics as well as standard image processing techniques.

4. To investigate the possiblity of:

   i) Transferring the current Algorithms written in FORTRAN LANGUAGE into a LISP SYSTEM.

   ii) DEVELOPING A LISP SOFTWARE PACKAGE that will execute the analytical functions carried on by the existing FORTRAN Program.

   iii) Developing a LISP/FORTRAN interacting package that will utilize the functional routines embedded in the existing FORTRAN Program, while providing Superior Analytical handling of the Raw Data Sets in InfaRed Imagery and Target Recognition.

1985 USAF/UES SUMMER FACULTY RESEARCH PROGRAM

Sponsored by the
Air Force Office of Scientific Research
Conducted by
Universal Energy Systems, Inc.

FINAL REPORT

CHLAMYDOMONAS PHOTOTAXIS AS A SIMPLE SYSTEM FOR VISION RESEARCH

Prepared by: Dr. Rex C. Moyer
Academic Rank: Associate Professor
Department: Biology Department
University: Trinity University

Research Location: Division of Neurosciences,
School of Aerospace Medicine
Brooks Air Force Base, Texas 78235-5301

USAF Research Colleague: Dr. John Taboada

Date: September 9, 1985

Contract No. F49620-85-C-0013

CHLAMYDOMONAS PHOTOTAXIS AS A SIMPLE SYSTEM FOR VISION RESEARCH

by

Rex C. Moyer, Ph.D.

ABSTRACT

The long term goal of this program is to find a way of testing drugs for their ability to improve night or long wave length vision of pilots. A literature survey pointed to extracts from the plants in the *Panax*, *Eleutherococcus*, and *Schizandra* genera as potential sources of these drugs. A major problem interferring with the attainment of this goal is that no simple inexpensive test system exists that can assess the pharmacological effect of a drug directly upon visual biochemical apparatus without complicating indirect effects. With the discovery that the phototactic unicellular algae, *Chlamydomonas*, employs rhodopsin, the human visual pigment, it becomes theoritically possible to study the effect of drugs on an isolated visual system. Any drugs that enhance or alter phototaxis in *Chlamydomonas* may be of interest in human vision. The goal of this summer fellowship was to set up a phototaxis system in *Chlamydomonas*. Seven strains of *Chlamydomonas reinhardtii* were grown to produce phototactic cells. The basic characteristics of their growth was recorded and qualitative phototaxis of the algal cells to a laser beam was shown. Although a great deal of work remains to be done, this preliminary study suggests that phototaxis in *Chlamydomonas* can be used to construct a relatively simple test to determine if a substance can directly effect the visual system.

ACKNOWLEDGEMENT

I would like to thank the Air Force Systems Command, the Air Force office of Scientific Research, and Universal Energy Systems for providing me the opportunity to participate in a valuable research experience at the Division of Neurosciences, School of Aerospace Medicine, Brooks Air Force Base, Texas. My thanks are particularly directed to Dr. John Taboada and Sergeant Mario Villanea of the Laser Spectroscopy Clinical Application Laboratory and Robotic Vision Laboratory for their help and for making my brief stay very pleasant as well as informative and productive.

My thanks to Dr. Jerome Schmidt, Chief of Microbiology, Division of Epidemiology for allowing me the use of their facilities for the microbiological part of my work and to Microbiology Staff Members, Dr. Vee Davison, Sergeant Aaron Sinclare and A1C Tracy Cole for their help.

My personal thanks to all my research colleagues who made my stay so plesant as well as a vehicle for information exchange: Dr. John Taboada, Dr. Odis McDuff, Dr. Boake Plessy, graduate students Barbara Wilson and Otis Cosby of Neurosciences Division and Drs. Vito Del Vecchio and Gordon Schrank and graduate student Kathy Ryan of Microbiology.

I. INTRODUCTION

Chlamydomonas appears to be an ideal tool to accomplish the research goals. Chlamydomonas is one of the major genera of the Volvocales, with more than 500 described species. Chlamydomonas reinhardtii is typical of the genus. It is a single vegetative cell, 10-15 μm in length, spherical to ovoid in shape, and have a pair of flagella extending from their anterior ends. They possess a single cup-shaped chloroplast surrounding a single nucleus. C. reinhardtii is an aquatic microorganism, and has evolved specialized means of regulating its exposure to sunlight by means of its flagella and directional light antenna which consists of an eye spot plus associated structures.

C. reinhardtii can be grown on simple defined mineral salts media, either in liquid culture or on agar plates. Wild Type cells grow either photoautotrophically, with doubling times of about 5 hours at 25°C when supplied with non-limiting light and CO_2 or heterotrophically in the dark with acetate as a respirable carbon source (doubling time about 15 hours at 25°C). Cell division can be readily synchronized with alternating light-dark cycles (1). The C. reinhardtii cells can be manipulated by standard microbiological techniques.

The simple life cycle of C. reinhardtii and the ease with which it can be grown and manipulated for genetic analysis have contributed to its popularity for research in diverse areas of cell biology and genetics. An impressive body of knowledge and literature base has been accumulated on C. reinhardtii. A genetic map of 18 distinct linkage groups has been developed and an impressive list of mutants of photosynthesis, antibiotic resistance, mating, auxotrophy, cell wall biosynthesis, and others in addition to phototaxis are available (2).

Vegetative cells of C. reinhardtii are haploid. Gametogenesis is induced by nitrogen deprivation. C. reinhardtii is heterothallic and the mating type is determined by a single Mendelian gene, the two alternative alleles being designated mt^+ and mt^-. Mating gametes fuse beginning at specialized structures at the cell's anterior ends. Nuclear fusion and chloroplast fusion occur shortly thereafter. The formation of a hard-walled diploid zygospore follows mating. Restoration of light and nitrogen sources induces the zygospores to undergo meiosis leading to the production of four haploid cells. Segregation of nuclear genes is typically Mendelian, but chloroplast genes of C. reinhardtii show a predominantly uniparental pattern of inheritance: only the chloroplast DNA of the mt^+ parent is transmitted to the meiotic progeny of the majority of zygotes (3).

All photosynthetic organisms have evolved specialized means of regulating their exposure to sunlight. One form this adaption has taken among the flagellated algae is their phototatic response; the ability to swim toward or away from the source of light. Phototatic algae solve the problem of finding the light direction by scanning their environment with an antenna sensitive to light. The antenna is integrated to its response mechanism--the flagella, to allow it to track light.

Chlamydomonas has a red eyespot on its side. The design principles of phototaxis in Chlamydomonas are shown below as described by Foster and Smyth (4). The eyespot and associated structures form a directional antenna. One of the components of the antenna is visibly pigmented, but the visible pigment is not the photoreceptor pigment.

The Chlamydomonas cell swims with its flagella forward, rotating about two times per second. This rotation causes the antenna to scan the environment and the cell thus receives a patterned light signal. This scanning is analogous to a conically scanned tracker used for tracking planes, missiles, and stars (4).

Swimming at a rate of 100 μm per second is caused by the flagellar beat at a beat frequency of 25-50 Hz (varies with different conditions and strains). As the organisms *swim, their bodies rotate* at a frequency of about 2 Hz. During one beat cycle, the cell may turn back and forth through an angle of 20 or 30°.

The intensity range for Chlamydomonas phototaxis is 10^4, extending from 10^{11} to 10^{15} quanta cm^{-2} sec^{-1} at 500 nm (5, 6). This operating range matches the range relevant to the survival of the organism in its natural environment.

Phototaxis also requires that the spectral sensitivity match the color of light the cell can most advantageously use in its response. Both the photoreceptor pigment and the antenna must be effective in the same spectral range. The choice is limited to visible light, the only light appreciably transmitted by water. The photosynthetic pigments, which account for most of the absorption of photosynthetic cells, absorb strongly in the blue and red ranges; in the intermediate wavelength range, the photosynthetic absorption is weaker.

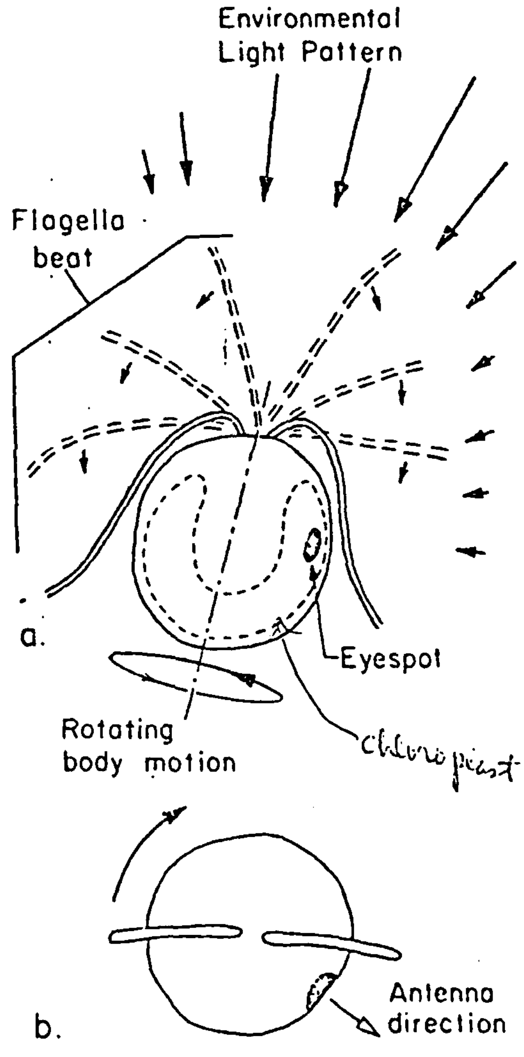

FIG. 2. *Design principles of phototaxis in Chlamydomonas. (a) Side view of cell; (b) end view. The incident light pattern is indicated by solid arrows. The eyespot, which lies inside the chloroplast (dashed line), forms part of the antenna. Rotation of the cell causes the antenna to scan the incident light. This produces a signal that controls the flagellar beat (see Fig. 3). The antenna direction (open arrow) is normal to the cell surface. The antenna is most sensitive to light coming from this direction. Successive positions of the flagella during the power stroke are shown. Flagellar motion causes the cell to translate with the flagellar end forward and to rotate in the left hand sense.*

The phototactic spectral range lies in these intermediate wavelengths. This allows the algae to respond to light even when shaded by overlying photosynthetic organisms.

The eyespot of Chlamydomonas contains four layers of pigmented droplets. A double membrane of 15.4 nm lies at the inner surface of each pigmented layer. Within the layers the pigmented globules are arranged in a hexagonal array 75-100 nm center to center. The pigmented layers consist mostly of β-carotene. The pigmented layers average 69 nm in thickness and the unpigmented layers 77.7 nm in thickness. The spacing of these stacked layers suggest that they act as quarter-wave reflectors-a principle widely used in nature to produce reflection (as in the tapeta of the eyes of nocturnal animals) or colors.

It has been suggested that the $\sim 10^5$ photoreceptor pigment molecules are located in the plasma membrane over the eyespot and thus can provide a means of communication with the flagella since the plasma membrane is continuous with the flagellar membrane. A change in membrane potential is probably involved in conducting the signal from the receptor to the flagella. The minimum time for a behavioral response in Chlamydomonas is 20 milliseconds. Chlamydomonas responds with decreased flagellar beating to an increase in light intensity and vice versa. Large signal effects, which cause the cell to reverse or stop are mediated through internal calcium ion concentration and suggests an ion gate effect.

The receptor pigments in the eyes of all multicellular animals studied so far contain 11-cis-retinal as the chromaphore. Foster et al, (7) have demonstrated that 11-cis-retinal is the natural chromaphore in Chlamydomonas and that the protein environment of this retinal is similar to that found in bovine rhodopsin. This suggests the use of eukaryotic rhodopsins as visual receptors from a variety of species from algae to man and suggests a very ancient origin for the rhodopsin photorecptor.

Foster et al (7) results have established Chlamydomonas as a viable model for studies of rhodopsin photoreceptors without the complications of other tissues such as optic nerves and brain. They have published the phototaxis action spectrum of a Chlamydomonas blind mutant (unable to phototax toward light unless provided 11-cis-retinal). The phototactic action spectrum maximum of Chlamydomonas is 503 nm.

The Russians and the Chinese are intensely interested in using drugs derived from plants to improve worker performance and have published a number of papers on the drugs extracted from several Asian plants related to and including ginseng. The Chinese people have been using ginseng as a "cure-all" drug for thousands of years. Native American Indians have used wild American ginseng for a number of ailments. The Russians have concentrated their work on extracts from Siberian and Oriental ginseng. The Oriental ginseng was reported by the Russians to increase human mental and physical work capacity. Siberian ginseng was also reported to benefit Russian Kosmonaut endurance in space. The pharmacological properties of ginseng is described in the First National Ginseng Conference, Lexington, Kentucky (8). This summary provides an impressive list of pharmacological effects that would be beneficial to pilot performance. Most striking, however, is a Russian article by Sosnova et al. (9) published in Gigiena i sanitarikila, December, 1984. The article, entitled "Prevention of

eye fatigue in color discrimination by Eleutherococcus and Schizandra chinensis extracts," described a study in which young women working on projects requiring color discrimination were given the plant extracts over a 40-day period. The Eleutherococcus extract improved visual sensitivity to red, green, and blue colors by 95.5% and the Schizandra extract improved these factors by 92.5%. Both extracts were effective in lessening fatigue, enhancing color discrimination, and in improving efficiency and productivity.

There are two well-known trade species of ginseng in the family Araliaceae, Panax ginseng (Oriental ginseng) and Panax quinquefolius (American ginseng). In addition, there are other ginseng species found occasionally in the market, Panax pseudo-ginseng varieties (Sanchi ginseng and Japanese ginseng). A related species, Eleutherococcus (Acanthopanax) senticosus, Sibĕrian ginseng, has received much attention from the Russians for its human adaptogenic capabilities.

Drugs from unrelated plant species, Schizandra chinesis and Schizandra sphenanthera have also received a good deal of attention from Chinese and Russian scientists. Schizandra is a perenial woody vine related to the Magnolias. A native American species exists: Schizandra coccinea which is found in Louisiana.

Drugs extracted from Panax ginseng are called ginsenoside saponins and a number of different chemical compounds have been identified which are named Ro, Rb_1, Rb_2 Rb_3 Rc, Rd, Rf, Rg_1, Rg_2, Rg_3, and Rh.

Ginsenosides from American ginseng are named A_2, B_1 and C as well as a number of other related compounds the panosides A to F and the panaquilins.

The structure(s) of the Ginsenosides is given below:

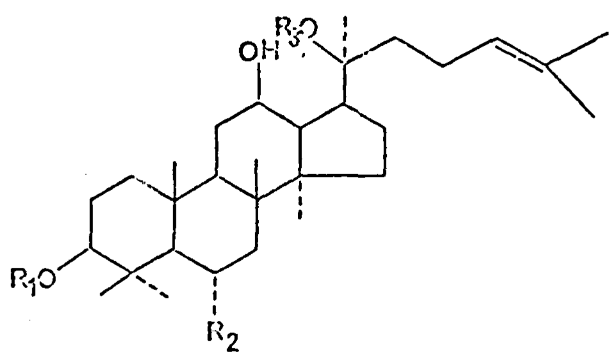

Fig. 1: Ginsenosides from American ginseng leaves and stems.
$A_2(Rg_1)$: R_1 = H; R_2 = D-Glc-O-; R_3 = D-Glc
$B_1(Rd)$: R_1 = D-Glc-β(1→2)-D-Glc; R_2 = H; R_3 = D-Glc
$B_2(Re)$: R_1 = H; R_2 = L-Rha-β-(1→2)-D-Glc-O-; R_3 = D-Glc
C (Rb_2): R_1 = D-Glc-β-1(1→2)-D-Glc; R_2 = H; R_3 = L-Ara-β-(1→6)-D-Glc

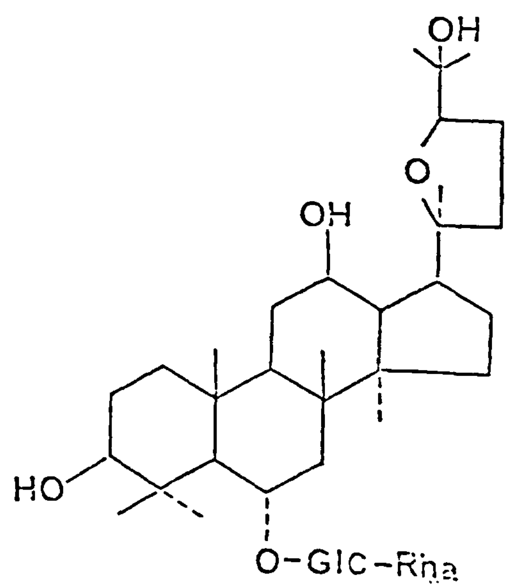

Fig. 2. Ginsenoside AI (Pseudo-ginsenoside F11).

Reports already in the literature support the likely beneficial effects of these plant products on pilot performance (8).

II. OBJECTIVES

The long term goal of this fellowship is to study the possibility of improving the night vision of pilots through pharmacologically active substances (drugs). These drugs may be given to the pilot in his diet, or injected, or as eye drops. The drugs, of course, should have no adverse effect upon the pilot's ability to carry out his mission nor upon his health, but if the drugs enhance his ability to cope with stress as well as his vision--so much the better. However, a major problem associated with testing of drugs in animals and humans is that the drug may affect more than one organ system and the origin of the response observed may be difficult to pinpoint. This surely applies to vision which is closely tied to the brain in its interpretation. What is needed is a test that disassociates the effect of a drug on the vision process itself from other pharmacological effects. Up to a few months ago the existence of a relatively simple experimental system that biochemically mimics human vision process did not exist. Recently, however, Foster et al established that the vision/phototaxis system of the unicellular alga, Chlamydomonas, employs rhodopsin - the human visual pigment. Thus, it becomes theoretically possible to study an isolated visual system in a single-celled organism and to determine the effect of various drugs on that system. Mutants of the phototaxis system of Chlamydomonas have been derived by Hershberg and Stavis and the effect of the drugs on reversing the mutagenic effect would provide valuable information on the biochemical pathways to rhodopsin; but more importantly for our goals, to determine the site of action of the vision-enhancing drugs.

The specific goal of this fellowship this summer (1985) was to set up a phototaxis system using Chlamydomonas reinhardtii and to perform tests of the phototactic response of wild type and phototactic mutants to determine the feasibility of attaining the long term goals of the overall project.

Once the phototaxis system in Chlamydomonas is characterized and the laser doppler method of quantitating phototaxis is perfected and a small collection of phototaxis mutants are on hand, various components (retinoids) and extracts from the plants described in the Introduction (Panax, Eleutherococcus and Schizandra) will be added to the algal phototactic system to determine if their sensitivity to reduced irradiance or longer wave lengths is enhanced. Other drugs that might have an effect upon vision which are of interest to the Air Force can also be tested in this system.

III. MATERIALS AND METHODS

A. Cultures:

1. Chlamydomonas reinhardtii strains CC-124, CC-125, CC-1009, CC-1010, CC-654, CC-656, CC-1101, and CC-1102 were obtained from Dr. Elizabeth Harris, Chlamydomonas Genetics Center, Duke University, Durham, N.C. A brief description of each stain is presented below:

CC-124 wild type mt^-. Levine strain from original wild type strain 137c
CC-125 wild type mt^+. Levine strain from original wild type strain 137c.

Both 124 and 125 have two gene mutations (nit-1 and nit-2) in the nitrate reductase activity and cannot use nitrate as a nitrogen source.

CC-1009 wild type mt^- (UTEX 89)
CC-1010 wild type mt^+ (UTEX 90)
CC-654 Ebersold #191 lnp mt^- (phototaxis mutant)
CC-656 Ebersold #187 y-1 lnp mt^- (phototaxis mutant)
CC-1101 ey mt^- eyespotless mutant from Hartshorne.
CC-1102 ey mt^+ eyespotless mutant from Hartshorne.

B. Culture Media:

1. Trace Elements mix (1000x) from Elizabeth Harris, personal communication.

Trace Element	Weight (g)	ml dist H_2O
Na_2 EDTA	50.0	250
$ZnSO_4.7H_2O$	22.0	100
H_3BO_3	11.4	200
$MnCl_2.4H_2O$	5.06	50
$FeSO_4.7H_2O$	4.99	50
$CoCl_2.6H_2O$	1.61	50
$CuSO_4.5H_2O$	1.57	50
$(NH_4)\ Mo_7O_{24}.4H_2O$	1.10	50

Dissolve each salt in distilled or deionized water as indicated. Disodium EDTA must be dissolved in boiling water. Prepare $FeSO_4$ last since it oxidizes in solution. Mix all solutions except EDTA. Bring the mixed salts solution to a boil and then add the Na_2 EDTA

solution. The mixture should turn green. When all the salts are dissolved, cool the solution to 70°C. Keeping the temperature at 70°C, adjust the pH to 6.7 with 80-90 ml of hot KOH (20%). Standardize the pH meter at 70°C also. Do <u>not</u> use NaOH to adjust the pH.

Let final solution stand for 1-2 weeks in a cotton stoppered flask Shake the solution once a day. The solution should turn purple and leave a rust-brown precipitate. After two weeks, filter the solution through 2 layers of whatman #1 filter paper. Refrigerate or freeze in convenient aliquots.

2. Concentrated Beijerinck's solution:

Salt	wt (g/l)
NH_4Cl	100
$MgSO_4 \cdot 7H_2O$	4
$CaCl_2 \cdot 2H_2O$	2

3. Concentrated Beijerinck's without nitrogen.

Salt	wt (g/l)
$MgSO_4 \cdot 7H_2O$	4
$CaCl_2 \cdot 2H_2O$	2

4. Concentrated phosphate

Salt	wt (g/l)
K_2HPO_4	288
KH_2PO_4	144

5. Media Formulations

Constituent	HSA	Modified Foster	NMM
Conc. Beijerinck's	5 ml	5 ml	--
Conc. Beijerinck's -N	-	-	5 ml
Conc. Phosphate	5 ml	5 ml	1 ml
Trace Elements	1 ml	1 ml	1 ml
Sodium acetate $\cdot$ ($3H_2O$)	2.0 gm	2.0 gm	-
Bacto-tryptone	-	2.0 gm	-
Agar*	-	15 gm	-
Distilled water	990 ml	q.s.1 liter	q.s.1 liter

* Agar Conc. - ordinary agar plates 15 gm/l
agar slants 20 gm/l

C. Procedure for Establishing Phototactic Gametes

1. Routine maintenance of cultures.
Slants of 5 ml of HSA were prepared in screw-capped tubes (for example

pyrex No. 9825). The tubes with media were autoclaved at 121°C for 20 minutes then cooled in a slanted position. Cultures were transferred aseptically with an inoculating loop. All cultures grown on agar medium were incubated at 20°C in an environmental chamber with a 12 hr. light/dark cycle. Lighting was provided by 4 Sylvania 40W cool white bulbs placed 64 cm about the agar cultures. Cultures were transferred weekly.

2. Growth of Chlamydomonas vegetative cells.
Modified Foster's Medium Agar was made up in 1 liter batches and autoclaved for 20 min at 121°C in a 2 liter Erlenmeyer flask. The molten medium was transferred at 20 ml/plate to standard 90 mm plastic petri dishes with the aid of a sterile Cornwall syringe apparatus. Plates were left undisturbed at room temperature for the agar to solidify.
The modified Foster's media agar plates were inoculated with 0.1 ml of HSA agar grown algae cells as follows:
An HSA agar slant was overlayed with 0.25 ml of HSA broth. The cells were resuspended by trituration and 0.1 ml transferred to The Modified Foster's agar. The inoculum was evenly spread over the surface of the agar with sterile glass "hockey sticks". The agar plate cultures were incubated as described above. After about 1 week of incubation the surface of the agar becomes covered with a dense green growth (the density and color varies with the strain--wild type strains were heavier and darker green).

From 3-7 days before phototactic gametes are required, the cultures grown on modified Foster's agar were harvested by adding 5.0 ml of HSA medium to the surface of the agar cultures. The surface was scraped clean with a sterile straight rubber policeman. The cells were removed with a sterile 10 ml pipet and propipet. About 3-4 ml of algal vegetative cell suspension was recovered.

Three ml of the of algae cell suspension were inoculated into 45 ml of previously sterilized HSA broth in 250 ml side-armed Erlenmeyer flasks.

The cultures were incubated at 20-21°C in a rotary shaker at 100 rev/min. under room light. The turbidity of the culture was measured at intervals by spectrophotometry at 600 nm of the culture in the side arm of the flask using sterile HSA broth blank to adjust the absorbance to zero. This culture was incubated from 0-70 hours depending upon the experiment.

3. Induction of gametogenesis.

Rotary shake cultures in HSA broth were harvested at various times after they were initiated and converted to gametes by nitrogen deprivation as follows. Cultures were aseptically poured into sterile 50 ml

centrifuge tubes and centrifuged at room temperature for 5 minutes at full speed in an International Model HN centrifuge. The green cell pellets were resuspended in 10 ml NMM broth medium and again centrifuged under the same conditions. The pellets were washed one more time with NMM. The cell pellet was again resuspended in 10 ml of NMM broth and inoculated into 40 ml of NMM broth. The cultures were incubated at 20-21°C at 100 rev/min as before. The vegetative cells were converted to gametes by 24 hours under these conditions (Foster et al. 1984).

D. Tests for Bacterial Contamination.

To determine if bacteria were contaminating the algal cultures, 0.1 ml of algal material was aseptically pipeted onto a chocolate Agar w/chemically Defined Enrichments (GIBCO, Chagrin Falls, Ohio). The inoculum was spread over the surface with the aid of glass "hockey sticks". The plates were inoculated at room temperature (20-25°C) and duplicates at 37°C. Cultures are examined daily for bacterial growth. The algae do not grow on this medium.

E. Algal cell counts. Cell counts were made both by direct cell count with a hemocytometer or with a Model ZBI Coulter Cell Counter. For both types of counts, 1.0 ml of culture suspension was removed at time intervals and stored at 5°C until the cells were counted.

1. Hemocytometer Count. The culture sample was shaken and a capillary tube of culture removed. Culture was transferred by capillary action to the grids on both sides of the slide underneath the cover slips. The number of cells in 10 small square were counted and the total determined: no. in 10 squares·1000· the dilution factor (if any). At times, the high motility of the cells prevented accurate counting, thus the cells were counted electronically using the model ZBI Coulter Counter.

2. Electronic Counting. Culture samples were diluted in Isoton Solution and counted in the Model ZBI Coulter Cell Counter according to the directions provided by the manufacturer.

F. Measurement of Phototaxis

Our preliminary studies employ an Argon laser (Spectra Physics 164) with a continuous output of 200 mW at 476.2 nm (blue light) and a beam diameter of 1 mm to photostimulate the cells. The cells to be tested for phototaxis are drawn into a 100 µl capillary tube or placed in a cuvette or into a 4-well Lab-Tek slide. The Argon laserbeam is directed through the side of the cuvette or Lab-Tek slide chamber or through the open end of the capillary tube.

The detector is a Helium Neon laser (Hughes Aircraft Co.) (model 3225H-PC) with a continuous output of 10 mW and 632.8 nm (red) light and a beam diameter of 1 mm. The detector laser beam is directed parallel/coincident to the photostimulating light. A 10X objective lens mounted below the vessel housing the algae picks up the scattered light from the detecting red laser beam. The scattered beam is reflected through the microscope and out the 10X ocular lens and into a dull white surface at the focal plane of the ocular lens. At this plane a photo detector picks up the light and converts it to sound via an audio amplifier. As the cells swim toward the phototactic and detector beams the sound changes.

IV. RESULTS

A. Growth Curves of Chlamydomonas reinhardti strains under conditions described by Foster et al for production of phototactic gametes.

Vegetative cells of C. reinhardtii strains 124, 654, 656, 1009, 1010, 1101, and 1102 were grown in HSA broth as described in Materials and Methods. Turbidities of the cultures were measured at intervals over a 68.5 hour culture period. At 30 hrs post inoculation and again at 58.5 hrs post inoculation, 20 ml samples of strains 654 and 1101 were removed from the culture and induced to gametogenesis in NMM medium while a corresponding parallel culture of vegetative cells in HSA broth was likewise monitored for comparison to the gamete cultures. The growth curves are shown in Figs. 1 and 2.

Table 1 lists the important quantitative features of the growth curves. The vegetative cells of strains 654 and 1101 had generation times of 10 and 13 hrs, respectively, whereas these strains gametes had generation times of 6.5 and 8.5 hrs, respectively. The gamete cultures only grew when they were induced at 30 hrs p.i., shortly after the vegetative cells had reached stationary phase. When the vegetative cells were induced to gametogenesis at 58.5 hrs p.i., the gametes failed to grow.

B. Relationship between culture turbidity at 600 nm and cell number as measured in the Coulter Electronic Counter.

The relationships between turbidity and cell number were determined on the cultures at 26.5 and 47.5 hours post inoculation and is shown in Fig 3. The relationship was linear over the range tested and all seven C. reinhardtii strains fit the relationship regardless of whether the cultures were vegetative cells or gametes or whether the cultures were contaminated or not. From the standard curve it could be determined that an increase of 0.17 OD600 units corresponded to a doubling of the population and the time it required to increase in turbidity by 0.17 OD600 units was one generation time.

C. Tests for Bacterial Contamination

After 47.5 hrs of shake culture inculation in the growth curve experiment illustrated in Figs 1 and 2, samples were aseptically removed and

0.1 ml of the algal cultures were evenly spread over the surface of P2306 Gibco chocolate agar and incubated for 24 hrs at 37°C. Strains 1010, 654, 654 gametes at 30 hrs p.i., 654 gametes at 58.5 hr p.i., and 656 all showed contamination by a white colony bacterium within 24 hrs. Strain 1009 showed a different bacterial contaminant which grew on the chocolate agar after an additional 24 hr incubation at room temperature (25°C). Strains 124, 1101, 1101 gametes at 30 hrs p.i., 1101 gametes at 58.5 hrs p.i., and 1102 showed no evidence of bacterial contamination.

D. Measurement of Phototaxis

The growth curves of the Chlamydomonas strains and other studies not shown were performed, in part to obtain vegetative cells and gametes in various stages of their growth cycle and to assess their phototactic ability. Although it was possible to demonstrate phototaxis of some of the algal strains, the development of the quantitative phototaxis assay had not been perfected enough to actually compare the phototaxis of the various strains to each other nor to compare the phototaxis of vegetative cells to gametes.

V. DISCUSSION

A. Growth curves of Chlamydomonas reinhardtii strains under conditions described by Foster et al for production of phototactic gametes.

The seven Chlamydomonas strains grown under conditions described by Foster et al (7) for induction of phototactic gametes showed a wide varaiation in the character of their growth curves. It is also clear that the size of the starting inoculum varied widely even though the preliminary treatment of all the strains in producing the inoculum was identical. Thus there was variation in the amount of growth that could be attained on modified Foster's agar. From culture turbidities obtained at 0 time in the growth curve and the relationship established in Fig. 3, it was possible to calculate the size (cells/3 ml inoculum) of the inoculum used to initiate the HSA broth cultures: strain 654, 166×10^6; strain 1101, 118×10^6; strain 1101, 118×10^6; strain 656, 137×10^6; strain 1009, 96×10^6; strain 1010, 70×10^6; strain 124, 65×10^6; and strain 102, 31×10^6. Since it is likely that the growth characteristics of the seven Chlamydomonas strains in HSA broth will be influenced by the number of cells in the inoculum, it will in the future be necessary to characterize the growth of Chlamydomonas strains first on the modified Foster's agar. Then it will be necessary to repeat these growth curves in HSA broth but using a constant inoculum size in cells/ml.

The procedure of Foster et al for induction of phototactic gametes calls for culturing the vegetative cells for 5-7 days in HSA broth before the cells are shifted to NMM nitrogen starvation medium to induce gametogenesis. Part of the rational for determining the growth curves of these seven C. reinhardtii strains was to see if a 5-7 day culture time is necessary. The growth curves in Figs. 1 and 2 suggest that the

maximum stationary phase of all cultures is attained before 3 days (72 hrs) and if the purpose of the long incubation period is to reach stationary phase of growth, then even slow growing strains do not need to be cultured in HSA broth for 5-7 days to reach stationary phase. If the long incubation period is to exhaust food reserves prior to gametogenesis then it may be necessary to continue it longer than 3 days. It might be possible to achieve the same goal by limiting the nitrogen source supplied in the HSA broth. Until a quantitative assay of phototaxis is perfected and then applied to cells from all stages of the growth curve, we will not be able to test this hypothesis. Since all of the C. reinhardtii strains reached more than one million cells per ml in HSA broth cultures sooner than 3 days I wondered why Foster's group had preliminary cultivation step on modified Foster's agar at all. When questioned about this, Dr. Foster replied (personal communication) that it was necessary to get any growth at all of his FN68 mutant. Thus mutant FN68 must grow poorly on HSA broth much like our 1102 (Fig 1) which is an eye spot mutant (Elizabeth Harris, personal communication).

It was interesting to note that when vegetative cells which had recently reached stationary phase of growth were induced to gametogenesis at 30 hrs p.i., they grew for 15 hours (1.9 - 2.7 generations) before a "gamete" culture stationary phase was reached. However, when the vegetative cell cultures in HSA broth are incubated 33 hrs beyond when they attained maximum stationary phase, that there is no further growth when the vegetative cells are induced to gametogenesis in NMM broth. This could be interpreted that the vegetative cells carried stored nitrogen reserves early in stationary phase but that they depleted their reserve later in the stationary phase. These studies suggested that we must introduce a technic for determining the difference between vegetative cells and gametes. It is at present unclear to me why gametes rather than vegetative cells are used for Foster's studies. Most of the growth curves displayed a faint stimulation of their growth at about 24 hr intervals. This could be a residual diurnal cycle caused by maintaining the modified Foster's agar cultures on a 12 hr light/dark cycle. Another experiment will have to be done comparing the growth of cultures growing in constant light, constant darkness, and 12 hr light/dark cycles to resolve this issue.

It was interesting to note that the minus mating types (mt-) grew better than did the mt+ mating types. If this observation holds, I feel it is a significant finding. I believe these growth curve experiments need to be repeated using equal numbers of cells as inocula and a greater number of strains of known mating type used, before this conclusion is confirmed.

B. Relationship between culture turbidity at 600nm and cell number as measured in the Coulter Electronic Counter.

The linear relationship between turbidity measured at 600 nm and cell number was more direct and uncomplicated than expected. I did not expect both vegetative cells and gametes to fit the same line as they

apparently do. This indicates that they are the same size and contain the same degree of pigmentation. I did not expect that all of the strains would conform to the relationship either, since they appear as different shades of green when growing on HSA or modified Foster's agar. This relationship was convienent to use and was employed to interconvert cell number/ml and turbidity and to estimate generation times. I would like to repeat this experiment utilizing more data points for the different strains and cell types. I would also like to run cell size distributions of the vegetative and gamete cell populations to confirm that they they are of the same size. I would also like to run an absorption spectrum of all the cell populations to confirm their being identical.

C. Tests for Bacterial Contamination.

The algal cultures harboring low level bacterial contaminants did not appear to affect the growth of the algae. The number of contamination organisms/ml was small. Time did not permit additional studies to be performed on this. I would assume that these bacterial contaminants could be eliminated from the algal cultures by growing the algae in media containing antibiotics effective against the bacteria. It is well known among microbiologists that contain pathogenic bacertia such as Legionella attach themselves to algae (especially Chlamydomonas) and are able to grow in environments where they could not grow without the algae. Cases of Legionnaires Disease can be traced to algal blooms, so this area remains one of practical as well of basic interest. It certainly is important to our future work because the bateria may act upon the drugs being tested for activity upon phototaxis. Therefore if they are not eliminated from the algal cultures, we must certainly take into consideration their possible effects. I am well aware of studies involving mammaliar cells in culture that are contaminated with mycoplasma. Such cells certainly do not behave like uncontaminated cells.

D. Progress toward long and short term goals.

The long term goal of this program is to establish way of finding and testing drugs that may improve the night or long wave length vision of pilots. The drugs should have direct effects upon the photoreceptors of the eye and no untoward effects upon pilot performance or health. Literature sources from Russia and China as well as from the USA and Switzerland support that these drugs may be obtained as extracts from the plant genera of Panax, Eleutherococcus, and Schizandra. During the tenure of this 1985 Summer Fellowship, I collected a substantial literature base on these plants and their pharmacological activity. I also found commercial sources for the plant extracts and performed preliminary tests upon myself as to possible improvement of color discrimination. These preliminary tests did improve my color discrimination ability.

Until Foster et al (7) published their paper in 1984, there was no way that I was aware of, to determine if a drug was affecting the visual apparatus directly or whether vision or its mental interpretation was

indirectly affected. With Foster et al discovery that Chlamydomonas reinhardtii employs rhodopsin - the human visual pigment, in its visual/phototaxis system, it became possible to devise ways of determining if phototaxis of these algae could be exploited as a means testing the effects of drugs on the visual pigment system of man.

The specific goal of this preliminary study was to set up a photoaxis system using Chlamydomonas to determine the feasibility of attaining the long term goals of the program. Pursuant to this goal a literature base on the algae and phototaxis was collected, the algal cultures were obtained and the means of culture and maintenance of the algae established. The relevent parts of Foster et al (7) work was repeated and studies of the growth characteristics of seven Chlamydomonas reinhardtii stains were completed.

Qualitative phototaxis of some of the strains was demonstrated using a laser beam and algal cells in a capillary tube.

Unfortunately I was unable to acquire the FN68 mutant from Dr. Foster and the phototaxis quantitative assay system was not perfected before the end of the fellowship. There is no reason to believe that the phototaxis system could not be established directly and progress made toward the long term goals of the program which certainly remain plausable at this point in time.

Fig. 1 Growth curves of Chlamydomonas reinhardtii strains 654, 1009, 1010, 1101, and 1102 under conditions described by Foster et al for production of phototactic gametes.

Cultures of Chlamydomonas strains 654, 1009, 1010, 1101, and 1102 were harvested from HSA agar slants and 0.1 ml inoculated onto modified Foster agar plates at 20°C under a 12 hour light/dark cycle. After one week the cultures were harvested and 3.0 ml inoculated into 45 ml HSA broth cultures and incubated at 20-21°C on a rotary shaker at 100 rev/min. Samples were removed for cell number determination at 26.5 and 47.5 hours post-inoculation. Cultures 654 and 1101 were induced to gametogenesis at 30 hours and another sample at 58.5 hours. Turbidities at 600 nm of the cultures were measured at intervals. Later it was determined that culutres 654, 1009, and 1010 carried an occult bacterial contamination that did not show up when the algae were cultivated on their HSA or NMM broth minimal medium.

Cultures were terminated at 68.5 hours. Solid lines show the turbidity of vegetative cell cultures and dashed lines indicate gamete cultures. This growth curve resembles an earlier growth curve of strains 654, 1009, and 1101 (not shown).

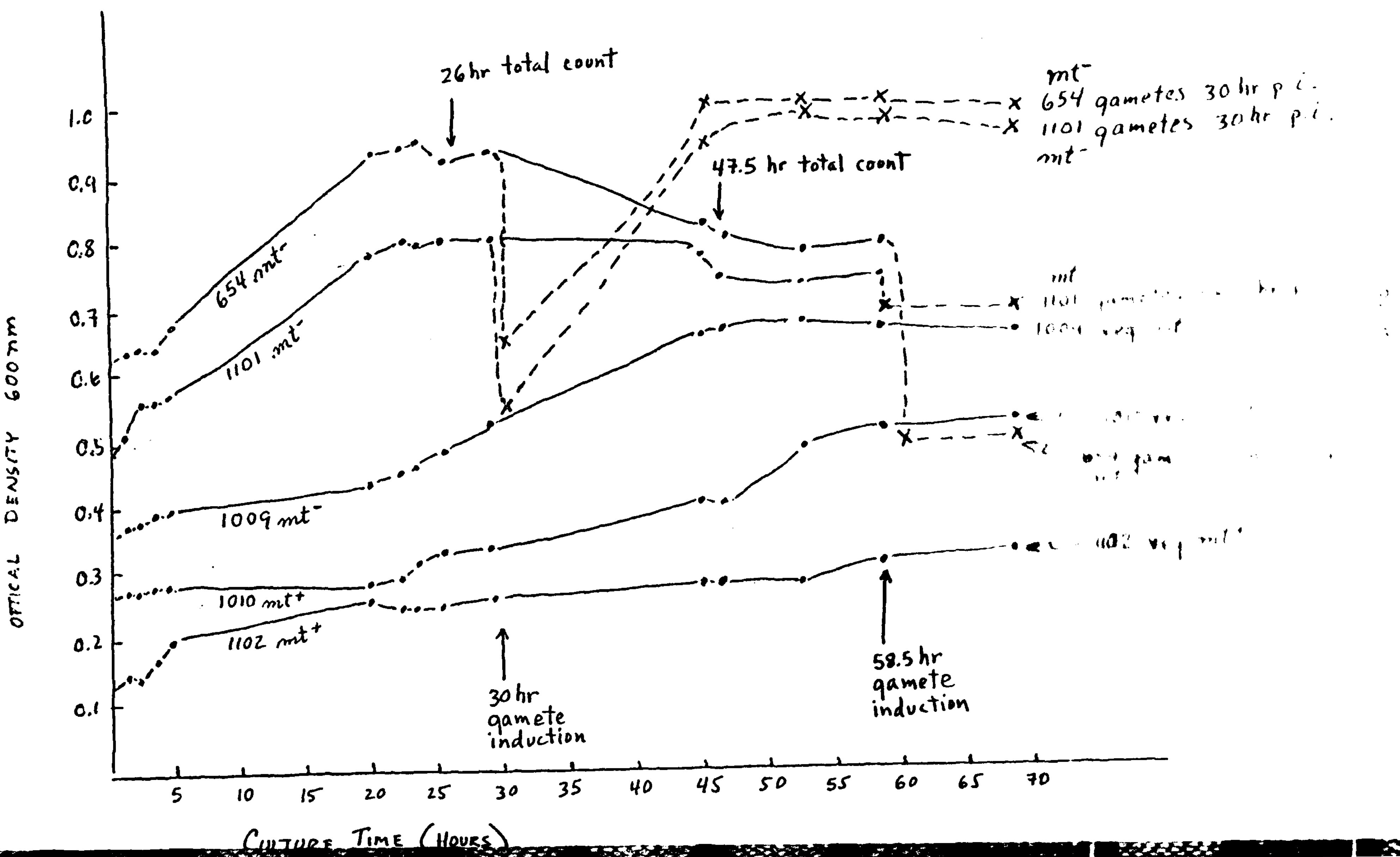

OPTICAL DENSITY 600nm
1.0
0.9
0.8
0.7
0.6
0.5
0.4
0.3
0.2
0.1
5
10
15
20
25
30
35
40
45
50
55
60
65
70
CULTURE TIME (HOURS)
26hr total count
47.5 hr total count
30hr gamete induction
58.5hr gamete induction
654 mt-
1101 mt-
1009 mt-
1010 mt+
1102 mt+
mt-
654 gametes 30 hr
1101 gametes 30 hr
mt-

Fig. 2 Growth curves of Chlamydomonas reinhardtii strains 124 and 656 under conditions described by Foster et al for production of phototactic gametes.

The preparation for growth and measurement of growth of strains 124 and 656 were as described in the legend to Fig 1. Strains 124 and 656 were not induced to gametogenesis. It was later found that strain 656 harbored an occult bacterial contamination.

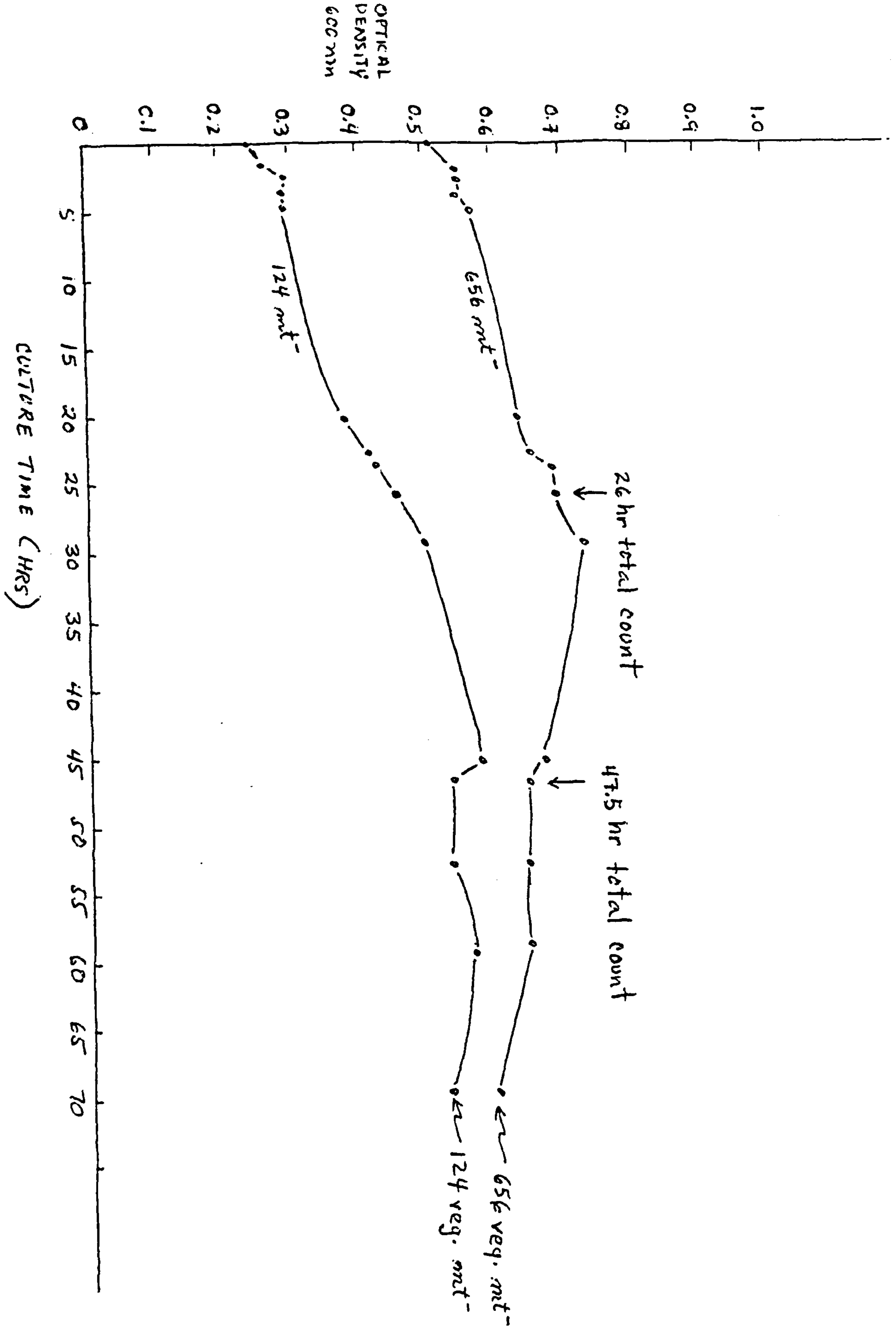
OPTICAL DENSITY 660 nm
0
0.1
0.2
0.3
0.4
0.5
0.6
0.7
0.8
0.9
1.0
5
10
15
20
25
30
35
40
45
50
55
60
65
70
CULTURE TIME (HRS)
656 mt-
124 mt-
26 hr total count
47.5 hr total count
656 veg. mt-
124 veg. mt-

Fig. 3 Relationship between culture turbidity at 600 nm and cell number as measured in the Coulter Electronic Counter.

The growth curve of strains 124, 654, 656, 1009, 1010, 1101 and 1102 were determined as described in the legends of Figs. 1 and 2. At 26.5 and 47.5 hrs post inoculation samples of all cultures were removed for counting in the Coulter Counter. The turbidity of the cultures at 26.5 and 47.5 hrs post inoculation in optical density units at 600 nm was plotted vs cell numbers determined at 26.5 and 47.5 hrs post inoculation.

Those strains noted with an sterisk were later shown to harbor low level bacterial contamination.

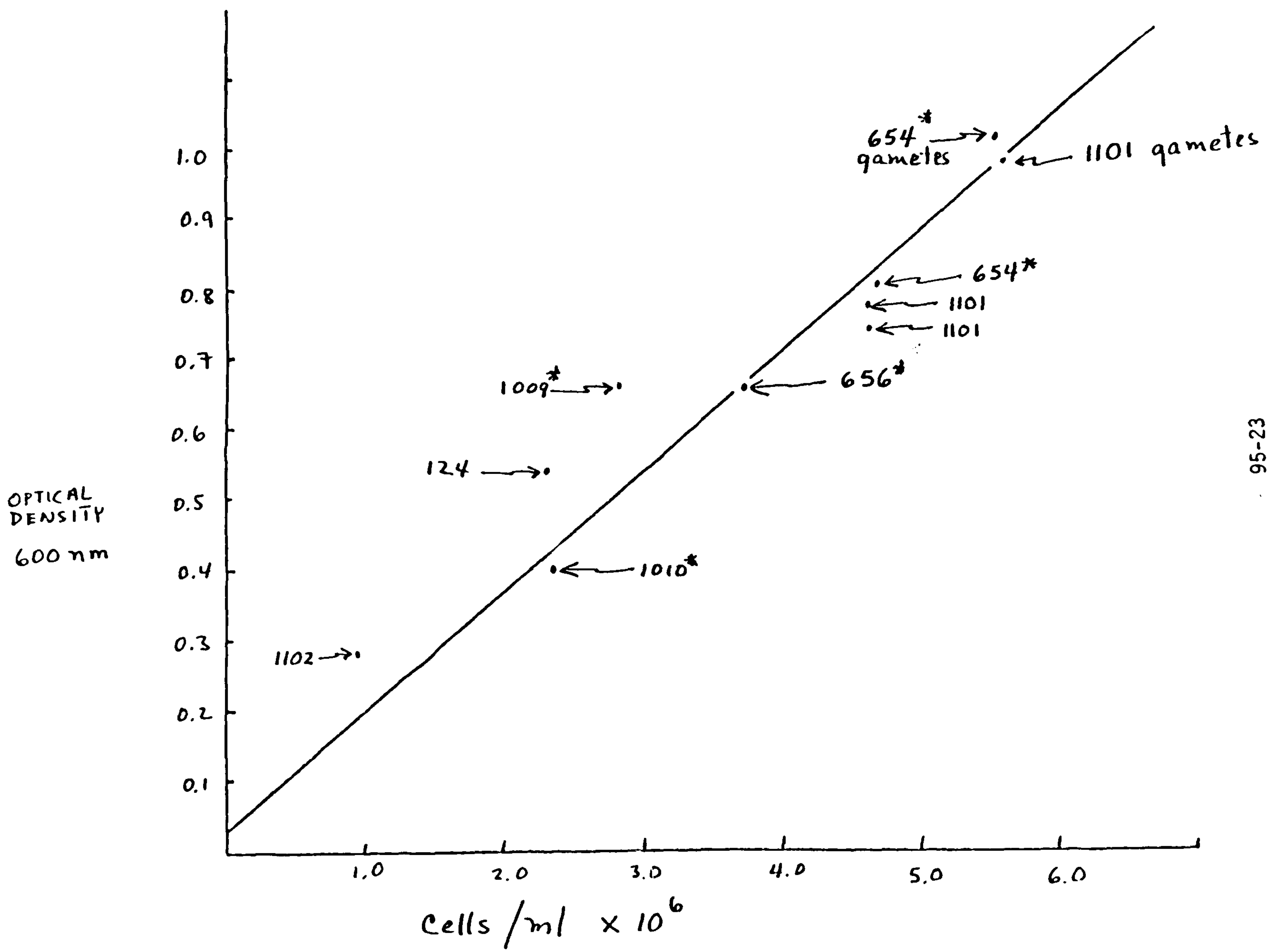

OPTICAL DENSITY 600 nm
1.0
0.9
0.8
0.7
0.6
0.5
0.4
0.3
0.2
0.1
1.0
2.0
3.0
4.0
5.0
6.0
Cells /ml x 10^6
654* gametes
1101 gametes
654*
1101
1101
656*
1009*
124
1010*
1102

Table 1. Important features of the growth of *Chlamydomonas reinhardtii* strains 124, 654, 656, 1009, 1010, 1101, and 1102.

STRAIN NO.	MATING TYPE	LAG PHASE(hrs)	GENERATION TIME(hrs)	TIME TO REACH MAX STATIONARY PHASE (hrs)	OD600 AT MAX STATIONARY PHASE	CELLS/ml AT MAX STATIONARY PHASE
654	mt-	0	10	22	0.92	5.2×10^6
1101	mt-	0	13	22	0.80	4.6×10^6
656	mt-	0	16-27	29	0.72	4.1×10^6
124	mt-	15	12	45	0.59	3.4×10^6
1009	mt-	18	18	47.5	0.68	3.9×10^6
1010	mt+	22	29	55	0.50	2.8×10^6
1102	mt+	0	86	58.5	0.30	1.6×10^6

VI. BIBLIOGRAPHY

1. Kates, J.R., and R.F. Jones (1964). The Control of Gametic Differentiation in Liquid Cultures of Chlamydomonas. J. Cell Comp. Physiol. 63:157-164.

2. Harris, E.H. (1984). The Chlamydomonas Genetics Center at Duke University. Plant Molecular Biology Reporter 2:29-41.

3. Grant, D.M., N.,W. Gillham, and J.E. Boynton (1980). Inheritance of Chloroplast DNA in Chlamydomonas reinhardtii. Proc. Nat'l Acad. Sci. USA 77: 6067-6071.

4. Foster, K.W., and R.D. Smyth. Light Antennas in Phototactic Algae. Microbiological Reviews 44:572-630.

5. Feinleib. M.H., and G.M. Curry (1971). The Relationship between Stimulus Intensity and Oriented Phototactic Response (Topotaxis) in Chlamydomonas. Physiol. Plant 25:346-352.

6. Nultsch, W.G., Thorm, and I. VonRimscha (1971). Phototaktische Utersuchungen an Chlamydomonas reinhardtii Dangeard in Homokontinuierlicher Kultur. Arch. Mikrobiol. 80:351-369.

7. Foster, K.W., J. Saranak, N. Patel, G. Zarilli, M. Okabe, T. Kline, and K. Nakanishi (1984). A Rhodopsin is the Functional Photoreceptor for Phototaxis in the Unicellular Eukaryote Chlamydomonas. Nature 311:756-759.

8. Staba, E.J., and S.E. Chen. (1979). An Overview of Ginseng Chemistry, Pharmacology and Anti-Tumor Effects. In Proceedings, First National Ginseng Conference. Lexington, Kentucky.

9. Sosnova, T.L., V.V. Golubev, N.A. Plevkhanova, and A.N. Afanas'yev. (1984). Prevention of Eye Fatigue in Color Discrimination by Eleutherococcus and Schizandra Chinesis extracts. Gigiyena I Sanitariya 12: 7-9.

1985 USAF-UES SUMMER FACULTY RESEARCH PROGRAM

Sponsored by the

AIR FORCE OFFICE OF SCIENTIFIC RESEARCH

Conducted by the

UNIVERSAL ENERGY SYSTERMS

FINAL REPORT

NORMOBARIC OXYGEN CONCENTRATION EFFECTS ON CULTURED MOUSE MACROPHAGE RESPONSES

Prepared by:	Dr. James J. Mrotek
Academic Rank:	Associate Professor
Department, School and University:	Department of Physiology School of Medicine Meharry Medical College
Research Location:	School of Aerospace Medicine Hyperbaric Medicine Brooks Air Force Base, Texas
USAF Research:	Col. R. Henderson
Date:	October 22, 1985
Contract No:	F49620-85-C-0013

NORMOBARIC OXYGEN CONCENTRATION EFFECTS ON CULTURED MOUSE MACROPHAGE RESPONSES

by

James J. Mrotek

ABSTRACT

This project was initiated to explore the possibility that hyperbaric oxygen accelerates wound healing in Air Force personnel by effects on macrophage free radical production and phagocytic activity.

The purposes of this investigation were: (a) To measure free radical production by these cultures after incubating them at 37° C with oxygen concentrations of 158, 76, 38, and 0 mm Hg (at 1 atm) for 45 min. (b) To develop cell culture models for evaluating hypotheses concerned hyperbaric oxygen effects in wound healing, thereby minimizing animal requirements.

Time-dependent luminescence changes by RAW264 macrophages were determined before and after incubation with various normobaric oxygen concentrations. To control for possible differences in flask envirnment, each flask was bisected, half the cells were scrapped from the flask, and suspensions were immediately assayed for luminescence (pre-gassing control). The unscrapped cells remaining in the culture flask were exposed at 1 atmosphere to constant gas flows containing one of four different oxygen concentrations. Pre-gassed controls were used to normalize data from gassed flasks; the relative uniformity among ratios from a particular flask and, in most cases, between flasks receiving a similar treatment made this approach seem appropriate. Ratios from cells treated using oxygen at 158 mm Hg are from 2 - 20 times higher than those from cells treated using only nitrogen. Future experiments must be more closely examined to determine viability of cells before and after exposure to various oxygen tensions; logistical problems prevented this in the present studies. Because of variablility in data from the three flasks treated with oxygen at 76 mm Hg, no trends can be discerned. It may be that oxygen tensions at 76 mm Hg are threshold concentrations for these macrophages. Treating cells with oxygen at 38 mm Hg may result in increased ability to produce luminol-sensitive products. If this effect is real, it argues that these cells should be cultured in atmospheres more closely approximating those in vivo. Future studies will determine whether oxygen tensions between 38 mm Hg and 0 (i.e., those approximating physiological conditions) improve macrophage function. Our experimental data must be interpreted cautiously because several experiments contained technical difficulties.

Acknowledgement

Acknowledgement is made of the School of Aerospace Medicine, Brooks Air Force Base, Texas, the Air Force Systems Command, the Air Force Office of Scientific Research and Universal Energy Systems for the opportunity to begin investigations to determine the basic mechanisms involved in hyperbaric oxygen effects on wound healing. Project supervisor was Col. Richard A. Henderson, Hyperbaric Medicine to whom appreciation is expressed for an exciting and stimulating summer research fellowship. Associate investigators, to whom I am indebted, were Col. Touhey, Majs. Workman and Philpot, and Sgt. Kee, Hyperbaric Medicine; Maj. Johnathan L. Kiel and Capt. Lenora Wong-Behrning, Radiation Sciences; Dr. Martin Meltz, Department of Radiology, University of Texas Health Sciences Center at San Antonio, Texas; Ms M. Winfree, graduate student in Physiology at Meharry Medical College, my collegue in this project. Because of space constraints, many Sargents in Hyperbarics and Radiation Sciences have not been named specifically; their courtesy and help were, never-the-less, greatly appreciated. This project could not be conducted without the enthusiastic support of Dr. Bryce Hartman. Special mention must be made of the consideration and courtesy of the Epidemiology Division administration, particularly Drs. Blouse and Schmidt. Without the cooperation, technical assistance, tissue culture facilities and supplies from Dr. Vee Davison and the members of her virology laboratory, particularly Cliff Miller, our work would not have been performed. Christina Yee was most courteous and helpful during my experiments at the Health Science Center.

I. INTRODUCTION

Patients with limb ulcerations which were unhealed twenty years or more, exhibit wound healing in as little as eight weeks following treatment with hyperbaric oxygen (7). Chronic ulceration and wound healing pathology are unknown in other animal species (7). Therefore, models are not available to study this phenomenon.

Why certain wounds fail to heal in some humans is unknown. One speculation offered for wound healing pathologies invokes macrophage inefficiency in dealing with wound infections (4). In the following discussion, macrophage literature studied during the Summer Research Fellowship period will be reviewed. Macrophages will be defined, their relation to other phagocytes and to T and B lymphocytes will be discussed, morphological, biochemical, and physiological macrophage characteristics will be reviewed briefly, wound healing will be described and, finally, the relationship of macrophage oxygen consumption and peroxide production will be evaluated.

Monocytes and macrophages are the "oldest" cells in the hematopoietic system (the limulus, or horseshoe crab, an animal unchanged for millions of years, only has a single blood cell, an "amoebocyte" which resembles mammalian macrophages). Terminology relating to monocytes and macrophages is often confusing and inexact (see 2 for details of the following discussion). Hematologists include blood monocytes with lymphocytes as "blood mononuclear cells" although certain macrophages are "poly-

morphonuclear cells" (also called polymorphonuclear leukocytes). Since several mononuclear blood cells are phagocytic and capable of producing hydroperoxide, superoxides, singlet oxygen, and hydroxyl radicals, these cells were called phagocytes or leukocytes during the 1970s. Hematology usage apparently lead to the current "mononuclear phagocyte system (or complex)" for monocytes and macrophages. Macrophages are one of the few normal cells that may be truly multinuclear; current evidence suggests that mononuclear tissue macrophages give rise to multinuclear macrophages during antigen-stimulated differentiation. "Reticuloendothelial system" was also used for these cells, while "tissue histiocyte" was regularly used for macrophages in several Histology texts.

Monocytes and macrophages are part of the mononuclear-phagocyte lineage that is derived from a bone marrow stem cell (30). Monocytes are less differentiated, circulating phagocytes derived directly from bone marrow. Macrophages are mature cells derived from monocytes which invaded damaged tissues and settled there (9, 19). The differentiation from monocytes to macrophages *in vivo* is almost certainly influenced by envirnmental factors such as the presence of infection and inflammatory agents. Although mononuclear macrophages are capable of fusing to form multinuclear cells when they are located in tissues, special stimuli are apparently not

required to initiate this process. Macrophages are defined as "fixed" or "wandering" depending on whether they are concentrated at infection sites or move through tissues (see 2 for details).

Phagocytes represent "antigen-nonspecific" elements in immunity, while T and B lymphocytes are "antigen-specific" cells responsible for immunological specificity (see 2 for details of the following discussion). Although immune response is a continuum, macrophage/T cell interactions are usually separated in two stages: (a) immune system induction during which antigens interact with phagocytes (before lymphocytes are stimulated), and (b) the delayed-hypersensitivity phase of cellular immunity. A macrophage must process an antigen and present it to the T cell to stimulate these lymphocytes to function as helpers to B cells. When T cells receive no macrophage processed antigen, cell-mediated and humoral immune response is impaired. Macrophages greatly enhance foreign substance antigenicity, immunogens presented by macrophages are several thousad times more potent than those that are in a soluble form. The immune response has evolved in such a way that productive interactions take place primarily for antigens that are taken up, to one degree or another, by the phagocytes. These, interestingly, are the same antigens that also need to be eliminated.

When antigen-stimulated macrophage function is studied, several antigen properties are more effective than

others in stimulating function. The particulate antigen (e.g., foreign red cell, microorganism or virus) is an effective stimulant, whereas soluble proteins are weak antigens. Weakly immunogenic proteins, such as monomeric albumin or gamma glubulin, are phagocytized and cleared from the circulation if they are polymerized.

For antigens to be recognized, processed and induce immune system function, macrophages must ingest and kill microorganisms and polymeric antigens by phagocytosis, a process involving internalization of particulates. Before these cells phagosize particulates, an integrated series of events occurs that begins with the chemotactic direction of these phagocytes to the antigen entry site; these chemotactic agents include complement derived agents such as C3a and C5a. Humoral factors produced by lymphocytes, such as antibody immunoglobulins and complement, then bind to microbe surfaces. After coating the antigen with humoral factors, the coated particulate attaches to phagocyte surface IgG and complement receptors, cytotoxic substances, such as hydroperoxides, superoxides, singlet oxygen, and hydroxyl radicals, are released, and pseudopodia engulf the particle to enclose it in a phagocytic vacuole. Thus, macrophage antigen destruction requires soluble T cell products to activate resting macrophages, just as T cells require antigen processing by macrophages for their function.

Monocytes or "resting" macrophages "activated" by anti-

gens or by T lymphocyte interactions undergo a maturation process that makes the cells active as phagocytes, gives them a greater digestive capacity by increasing lysosomal and secretory granule numbers which contain new and/or higher hydrolytic enzyme levels (i.e., acid phosphatase, lysozyme, beta-glucuronidase, lipase, RPN-hydrolase, hyaluronidase, and myeloperoxidase) (reviewed in THE WHITE CELL). Morphologically, activated macrophages are larger than resting cells and contain increased endoplasmic reticulum and greater mitochondrial numbers. During maturation, certain macrophages may fuse with one another to form large, multinuclear cells (found in granulomatous inflammation), although inflammatory stimuli are not required for this polypoidy. Activated macrophages appear to be able to attract more macrophages, cause nearby cells to multiply and produce fibroblasts, stimulate vascular bud formation, and hydrolyze protein to useful amino acids (29).

Biochemically, activated cells increase glucose metabolism via the hexose-monophosphate shunt; mitochondrial enzymatic activity (i.e., cytochrome oxidase) and respiratory activity are also increased (21). With progressive maturation from monocyte to macrophage, the rate of glucose utilization increases; although glycolysis accounts for most glucose utilization (6), mature phagocytes have a more active glucose oxidative metabolism than less mature cells. Glycolysis is the principal energy source for the monocyte/tissue macrophage

even under aerobic conditions (20, 45, 50, 54). Energy requirements for chemotaxis and phagocytosis are principally obtained by anaerobic glycolysis. Relatively small total glucose levels (1 to 2 percent) are metabolized via the hexose monophosphate shunt (54). Monocytes increase the glucose percentage metabolized via the hexose monophosphate shunt during phagocytosis (10). The site where monocytes lodge seems to influence maturation. For example, the enzymatic constituency of pulmonary and peritoneal macrophages is not identical. Pulmonary alveolar macrophages are more active in aerobic envirnments (8, 11). Monocytes and peritoneal macrophages differ from alveolar macrophages in their lower glucose utilization and oxygen consumption rates (6).
The phagocytic process markedly increases the macrophage oxygen consumption rate (26). Within seconds after contact with antigen particles, oxygen consumption rates increase 15- to 20-fold over basal rates (2), the so-called "oxidative burst". Phagocytosis also results in increased generation of hydrogen peroxide (31) and superoxide (1). Evidence that the "oxidative burst" is cytotoxic and microbicidal comes from the genetic leukocyte disorder - chronic granulomatous disease (CGD) - in which macrophages ingest antigens but no microbicidal oxidative burst is generated (25, 47) Studies of CGD leukocytes indicate that NADPH oxidase, a cyanide-insensitive enzyme, uses NADPH produced by the hexose mono-

phosphate shunt along with molecular oxygen to synthesize microbicial hydrogen peroxide and superoxide anion during the oxidative burst (48). Since anti-microbial activities continue to occur when phagocytes are incubated under strictly anaerobic conditions, and since CGD leukocytes offer some disease protection, it follows that not all microbicidal substances are necessarily produced under oxygen-dependent conditions (41). Nevertheless, most efficient leukocyte function requires both oxygen-dependent and -independent anti-microbial systems. Because efficient leukocyte function requires molecular oxygen and injured and/or infected tissues are hypoxic, tissue oxygen deficiencies should limit leukocyte killing capacity and retard wound healing, as suggested by the following observation. Killing of *Staphylococcus aureus* and *Escherichia coli* by normal polymorphonuclear leukocytes was unimpaired at normobaric P O2 levels above 30 mm Hg (see 26 for subsequent discussion). Reducing oxygen concentrations below this level caused progressively large reductions in the killing rate, though phagocytic bacterial uptake was unimpaired. The P O2 range that significantly influences bacterial killing (0 - 30 mm Hg) corresponds well with the P O2 range in tissue wounds. Infected wounds are nearly totally anoxic because the infecting organisms reduce oxygen through metabolism; under these conditions leukocyte function is further impaired (43). This observation is given further significance by the fact that

superoxide production is abolished when leukocytes are incubated in nitrogen atmospheres *in vitro* (15).

In recent years several studies increased understanding of factors involved in the basic physiology of the normal wound healing process (see ref. 40 for review). These studies are of interest since focus is given to previous discussions regarding the role of wound oxygen concentrations, oxygen consumption, and antigen processing by monocytes and macrophages in the healing process. Wounds of soft tissues heal by a process of connective tissue repair and formation of a fibrous scar. Healing is achieved by formation of granulation tissue (a highly vascular and cellular tissue in which collagen and various components of the ground substance are synthesized) within the wound space. Depending on whether wounds are incisions or tissues are lost and/or wound edges are widely separated (e.g., burns, abscesses, or contaminated wounds), repair is different.

This discussion concentrates on the wound resulting from major tissue loss in which granulation tissues form. In granulation tissue formation there are three phases of soft tissue repair. In the first phase, there is wound inflammation and cell mobilization for granulation tissue synthesis. While vasoconstriction and slowed capillary blood flow occurs initially at wound edges, within a short time there is vasodialation. White blood cells, particularly multinuclear macrophages ad-

here to capillary walls. Capillary permiability increases, with gaps that develop between capillary wall endothelial cells giving plasma and white blood cells access to the fibrin coagulum which unites the wound edges. Multinuclear leucocytes and a few lymphocytes present within three hours of wounding are surrounded by a glycoprotein meshwork. While neutrophils increase during the first 48 hours, many of these cells undergo lysis releasing their granules. Few macrophages engage in phagocytosis. A few monocytic cells invade the wound within 24 hours and their number increases during the next few days until they are dominant by the fifth day and actively engaged in phagocytosis. Macrophages have an important role in eliminating effete cells, cellular debris and particulate matter, including activated clotting factors, denatured proteins, and antigen-antibody complexes. Both mobile and fixed phagocytes infiltrate the site, clean the debris resulting from neutrophil infiltration, and destroy invading microorganisms. New blood vessels and fibroblasts appear at wound edges during this phase. Growing endothelium buds are always preceded by macrophage migration into the wound; these buds seem to be stimulated by activated macrophage-produced "angiogenesis factors". Macrophages may determine the rate of new vascular endothelium ingrowth in wound healing (46). In the second phase, at about the fourth or fifth day, granulation tissue is formed in the wound, macrophages still predominate, collegen and

proteoglycans are being synthesized, and the wound mechanical strength is increased. Increasing fibroblast numbers become apparent along with advancing endothelial capillary buds. By the fifth or sixth days wound collagen fibrils interdigitate with wound edge collagen resulting in intrinsic mechanical wound strength. The third phase of indistinct length is characterized by maturation, with the wound undergoing extensive remodelling, including reduction in macrophage numbers and vascularity, and a further increase in strength.

This next section focuses on the role of oxygen in wound healing. The granulocytes and macrophages which invade wounds protect against contaminating antigens and microbes by chemically altering these antigenic substances before phagosizing them. In the course of these actions, large molecular oxygen concentrations are consumed and transformed by enzymes into hydrogen peroxide, hydroxyl radicals, singlet oxygen, and superoxides (21, 22, 24). The central space within wounds is an acidotic and hypoxic envirnment, particularly during early repair phases (49). The significance of hypoxia in wound repair remains uncertain but adequate wound oxygenation is essential to the wound repair process (see above and ref. 40 for review). Oxygen supply influences the susceptibility to wound infection and the rate of bacterial clearance from experimental wounds (28). The oxygen tension profile in the healing wound was recently re-

lated to the cell biology of the repair process (Figure 1) (49).

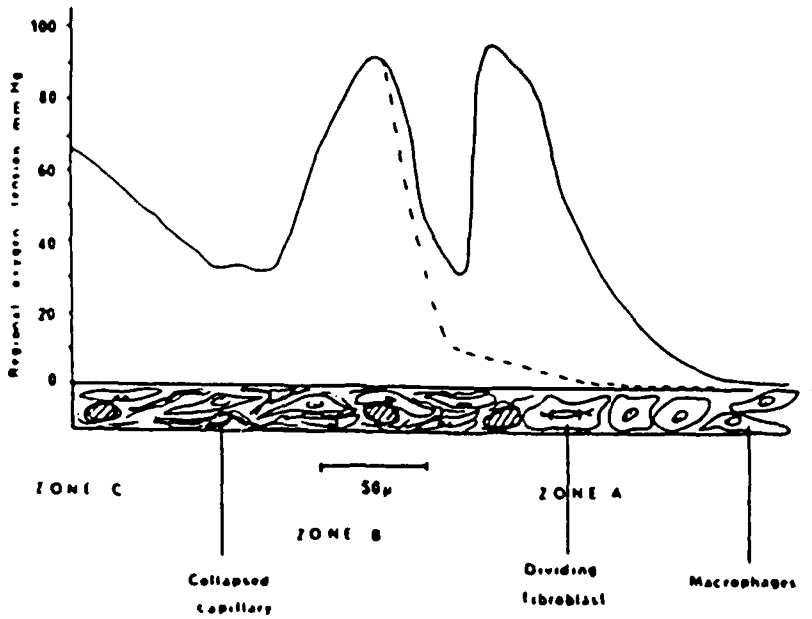

Granulation tissue (fibroblast and endothelial bud) formation is preceded by a layer of macrophages at the extreme wound edge (the most hypoxic zone). These cells may have difficulty with the intracellular digestion process if oxygenation conditions are extremely unfavorable. In areas of slightly better oxygenation, proliferating fibroblasts and endothelial buds are observed (Figure 1, zone A). Extracellular collagen fibrils are found further from the wound edge in conjunction with improved wound oxygenation (Figure 1, zone B). Thus far evidence that exogenous wound oxygenation results in improved wound repair is equivocal (30, 36, 42, 44); this, in part, results from the inability to determine wound oxygen levels accurately (especially during vasoconstriction and when metabolizing microorganisms are

present). The central wound area where vasculature is injured and the inflammatory reaction occurs is characteristically hypoxic. Only 100 microns back from the wound into normal tissue, oxygen is plentiful because vasculature is normal. A steep oxygen gradient, therefore, exists between the central wound and its edges. A wide variety of wounds exist; in addition, regional blood supplies may be compromised by arteriosclerosis, diabetes, and arterial or venous injury. While oxygen delivery to a bacterial entry site is essential for effective leukocyte killing, the exact tissue ocygen tension required for optimal *in vivo* killing has not been rigorously established. *In vitro* studies suggest oxygen tensions as low as 5 mm Hg substantially decrease killing rates (while levels over 30 mm Hg may exceed minimal requirement levels)(26). The repair process is highly susceptible to hypovolaemia and other disorders which cause increasing wound hypoxia (39, 43). When envirnmental oxygen tensions fall below 20 mm Hg, critical cellular energy-dependent processes such as phagocytosis fail in alveolar macrophages (11). In contrast, the phagocytic function of monocytes and other tissue macrophages is not so critically dependent on available oxygen. Phagocytosis by these cells occurs when oxidative metabolic inhibitors are present because of oxygen-independent anti-microbial killing processes, but is depressed by glycolytic inhibitors (9, 10, 12). Inter-

estingly, human alveolar macrophages fail to exhibit the typical monocyte respiratory burst when phagocytosis begins. Whether this burst is affected by reduced oxygen tensions is unknown; however, as discussed above, this respiratory burst is required for superoxide release (32). Macrophages destroy immune complexes and bacteria by using superoxides to digest microbial substances and immune complexes (38). Thus, minimum tissue oxygen tensions seem to be required for hydrogen peroxide, free radical, and superoxide production by phagocytes during antigen processing and wound healing.

Although hyperbaric oxygen seems to accelerate healing in chronic wounds, the mechanisms for these effects are unknown. One hypothesis used to explain hyperbaric effects suggests that phagocytes function more efficiently in the presence of high oxygen concentrations because intracellular superoxide-related enzyme levels increase after experimental subjects are exposured to oxygen (38). This hypothesis implies that certain individuals either are inordinately deficient in oxygen at the wound site or their phagocytes are incapable of using standard oxygen tensions associated with the wound. It is suggested that hyperbaric oxygen has minimal effect within the central wound area, rather more oxygen is dissolved in circulatory fluids providing cells at wound edges with slightly elevated oxygen concentrations (ca. 7 - 8 mm Hg)(17, 23).

Based on postulated hyperbaric oxygen effects on granu-

locyte- and macrophage-efficiency, oxygen consumption, and free radical production during wound healing, the hypothesis will be tested that macrophage free radical production is progressively reduced by exposure to progressively reduced oxygen tensions ranging between ambient air and an envirnment lacking oxygen.

Since animal models examining the relationship of granulocytes and macrophages to pathological wound healing are unknown, other methodologies, such as cell culture, are required to examine postulated relationships between oxygen utilization and macrophage efficiency. Two established mouse macrophage cell culture lines, P388D and RAW264, were attractive for these studies because of their potential capability for producing measurable superoxides in antibody-dependent cell cytotoxicity (34). P388D are a macrophage-like cell line originally isolated from a methylcholanthrene-induced lymphoid neoplasm produced in a DBA/2 mouse. P388D cells are primarily used by others for their high interleukin-1 production rates. These cells phagocytize latex particles and zymosan, they firmly adhere to glass and plastics, and they carry cell-bound receptors for immunoglobulin (Fc) and complement (C3). RAW 264 cells were established from the ascites of a tumor induced in a male mouse by the intraperitoneal injection of Abelson leukemia virus. This macrophage line pinocytoses neutral red and phagocytoses zymosan and latex beads, it

kills antibody-coated sheep RBC, secretes lysozyme and is capable of antibody-dependent lysis of sheep RBC and tumor targets. Receptors for complement and immunoglobulin are also present in this line. P388D and RAW264 are static with regard to nutrient supply, but dynamic with regard to nutrient, immune complex or bacterial comsumption and waste product or metabolite accumulation. Because these cell lines are homogeneous clones, measurement of perturbing-agent effects, such as changing oxygen concentrations, can be conducted in a defined and controlled envirnment without confounding influences of other cell types.

The following reference points serve to define physiological tissue oxygen tensions: P O2 ambient air - 158, human tracheal air - 149, alveolar air - 100, arterial blood -95, mixed venous blood - 40 mm Hg (37). Venous blood P O2 overestimates tissue P O2 because gradients several orders of magnitude less probably exist between capillary blood and cellular sites of oxygen reduction (19). Oxygen tensions in extracellular fluids are estimated to be < 8 mm Hg (23).

Various methods exist for increasing tissue oxygen concentrations. Oxygen can be dissolved in cells and tissues under pressures greater than 760 mm Hg (1 atmosphere). Oxygen concentrations can also be varied over the range from 0 to 760 mm Hg. At 3 atm, a 1 atm room air oxygen concentration decreases from 20% to 7% of the total atmospheric gas. Humans exposed to hyperbaric

oxygen probably have oxygen concentrations which are only a few orders of magnitude higher than physiological tissue concentrations (23). Thus, one should be able to duplicate hyperbaric-related tissue oxygen concentrations for cultured macrophages by incubating cells at 1 atmosphere and varying the oxygen, nitrogen, carbon dioxide mixture to increase oxygen from 0 - 760 mm Hg. In the present study tensions of 158, 76, 38 and 0 mm Hg were chosen for experimentation.

II. OBJECTIVES AND METHODS

Objectives

This project was initiated to explore the possibility that hyperbaric oxygen accelerates wound healing in Air Force personnel by effects on macrophage free radical production and phagocytic activity.

The purposes of this investigation are: (a) To adapt a RZP tissue culture system designed by Maj Johnathan Kiel and coworkers to protocols involving macrophage culture exposured to hyperbaric oxygen. (b) To measure free radical production by these cultures after exposing them to reduced oxygen concentrations at 1 atmosphere [atm] for 45 min. (c) To develop alternative models for evaluating hypotheses concerned with mechanisms for hyperbaric oxygen effects in wound healing, thereby minimizing animal requirements.

Experimental Method/Approach:

a. Cell Lines. The established mouse macrophage lines,

P388D and RAW264, were cultured in plastic T-75 culture plates using standard culture techniques. These cells were grown in RPMI containing sodium bicarbonate and 10% fetal calf serum in a 5% carbon dioxide/95% room air (v/v) atmosphere. Eight days prior to exposure to oxygen treatment, cells from the same generation were removed from flasks using sterile rubber policemen and subcultured into T-150 culture flasks and grown to confluence.

b. Superoxide Measurement. In all experiments to be described, both cells and their incubation medium were examined for superoxide production using the luminol (5-amino-2,3-dihydro-1,4-pthalazinedione) amplified chemiluminescence technique developed by Maj Johnathan Kiel and coworkers, RZP (39, 55). For ten ml of luminol solution 10 mg bovine serum albumin was dissolved in phosphate buffered saline (pH 6.9 - 7.4) then mixed with 10 mg luminol. The resulting mixture was suspended by pipetting up and down 20 times then filtered through a 0.2 micron Millipore filter. Filtered luminol could be stored at 4° C for 2 - 7 days if the pH was 6.9, but only 2 days at 7.4. For a typical assay in this study, 0.2 ml luminol solution was injected into a 1 ml sample contained in a liquid scintillation vial. In this procedure, bovine serum albumin served as antigenic challenge for macrophage suspensions. Background measurements were made with shutter closed, with empty chambers and shutter open, with scintillation vials containing incomplete RPMI and luminol, with vials containing cell

suspension to which phosphate buffered saline was added and with vials containing complete, "used" RPMI and luminol (Table 1). Using a Model 3000 integrating photometer (SAI Technology, Inc., Division of Science Applications, Inc.) set at a sensitivity of 600, a zero of 510, a counting initiation delay of 0.5 sec, and a counting time of 30 sec, brightness readings were taken at room temperature.

c. Basic Approach. To determine incubation conditions for chemiluminescence production, cells were incubated 45 min in continuously flowing atmospheres containing P O2s between 0 and 158 mm Hg at 1 atmosphere. The experiment began with flask removal from the incubator, then used serum-containing RPMI was removed and saved for subsequent replacement in this flask. One-half the flask was washed with 5 ml incomplete RPMI, this was removed and discarded, 2 ml incomplete RPMI was then added to the flask, cells were then scraped from the washed half of the flask into this medium (since cell distribution in the flask was not homogeneous the half chosen for scrapping from each flask was randomized), the cell suspension was removed, and the scrapped portion of the flask was washed with 1 ml RPMI and pooled with the suspension. Before counting the cell suspension with a coulter counter, the used RPMI was returned to the flask, the flask was then connected to a system for flowing a gas mixture of carbon dioxide,

nitrogen and oxygen through the flask, and the flask was placed on a hot plate set to maintain 37° C (carbon dioxide was included in this mixture to provide buffering in conjunction with bicarbonate; since oxygen was being varied, differences in oxygen concentration were adjusted with nitrogen, an inert gas). The gassing system consisted of the pressurized cylinder containing the gas mixture, tubing connected to the cylinder running to a glass tube inserted into a stoppered sidearm flask and immersed in 200 ml of freshly drawn distilled water within the flask, tubing from the side-arm connected to the flask via a glass tube inserted into the stoppered culture flask; a second glass tube inserted into this stopper provided egress for the gas. The side-arm flask was maintained at 37° C and the gas was bubbled through the water at a fixed rate before it entered the flask. The cell suspension removed from the flask was counted and a sample was diluted such that 1 million cells were contained in 1 ml RPMI. Exactly 15 min after these cells were scraped from the flask, 0.2 ml of luminol solution was added to the sample, the sample was continuously mixed for 30 sec, then readings were taken in the luminometer at one minute intervals for 4 min. Each sample was mixed at room temperature between each reading. Preliminary studies indicated that maximum luminescence was reached within 4 min; reading were, therefore, not continued beyond 4 min.

TABLE 1

TIME DEPENDENT LUMINESCENCE CHANGES IN VARIOUS BACKGROUND CONTROL MEANS

INCOMPL. RPMI PLUS LUMINOL			COMPLETE RPMI PLUS LUMINOL			CELLS, INCOMPL. RPMI, LUMINOL		
1*°	2	3	1	2	3	1	2	3
33	37.7±5.5[2]	40.3±4.0	-	32.8±3.5	-	55.6±55.0	36.0±13.5	31.3±4.0
29	37.4±7.5	39.0±3.5	-	32.0±3.0	-	47.4±42.5	34.6±12.5	30.3±6.0
28	36.6±7.5	40.6±3.5	-	30.3±4.5	-	43.1±31.5	35.3±7.5	30.3±1.5
26	37.6±9.5	42.3±5.0	-	30.1±2.0	-	39.9±25.5	34.5±7.0	30.6±1.5
25	36.8±9.5	41.3±5.5	-	32.3±5.0	-	38.0±19.5	34.7±4.5	30.0±4.0

* Experiment number.
° Single determination, all other data are means of eight determinations.
² ±S.E.M.

III. RESULTS

Results obtained using P388D macrophages and sheep or swine spleen macrophages are containing in the report by Summer Research Fellow, Mary Winfree. In general, P388D cells did not produce luminol detectable substances, but did exhibit phagocytosis 30 min after exposure to opsonized sheep red blood cells. While cultures containing sheep or swine macrophages could be produced, methods used to produce these cultures could not be refined enough to permit these cells to be used for the luminol assay.

Various control values were determined during most series of assays (Table 1). These included time-dependent changes in luminescence for RPMI medium which contained no serum (incomplete RPMI), for cells in incomplete RPMI exposed to phosphate buffered saline (the luminol solvent), and for used, complete (serum-containing) RPMI. In addition, luminometer readings were made with the shutter closed and with the shutter open but an empty chamber. Since assayed cells were suspended in incomplete RPMI, only one of the incomplete RPMI series of readings could serve as the assay control. However, there was some uncertainty whether values determined for incomplete RPMI without cells, or with cells, served as the best control. With the exception of two sets of "Cells In RPMI" values (out of eight) from experiment 1, all "Incomplete RPMI Plus Luminol" values were the highest, we, therefore chose to use these values for the

TABLE 2

TIME DEPENDENT LUMINESCENCE CHANGES BY CULTURED RAW264 MOUSE MACROPHAGES BEFORE AND AFTER INCUBATION WITH VARIOUS OXYGEN TENSIONS*

Oxygen Conc. (mm Hg)	Time (Min)	Unincub. Cell Lumin.	Incubated Cell Lumin.	Ratio Incub.: Unincub.	Unincub Cell Lumin.	Incubated Cell Lumin.	Ratio Incub.: Unincub.	Unincub Cell Lumin.	Incubated Cell Lumin.	Ratio Incub. Unincub
Run 2'':					Run 1':			Run 3''':		
158	0.5	38	*16	0.421	234	175	0.781	59	53	0.898
	1.5	43	15	0.372	206	158	0.767	58	45	0.776
	2.5	38	10	0.263	196	146	0.745	47	37	0.787
	3.5	29	6	0.207	170	147	0.865	33	27	0.818
	4.5	25	8	0.320	134	102	0.761	20	18	0.900
76	0.5	60	77	1.283	**124	26	0.210	72	37	0.514
	1.5	48	62	1.292	129	22	0.171	50	32	0.640
	2.5	39	48	1.231	112	24	0.214	40	21	0.525
	3.5	29	31	1.069	88	25	0.284	28	14	0.500
	4.5	26	23	0.885	73	23	0.315	21	8	0.381
38	0.5	41	44	1.073	**64	'92	1.438	43*	37	0.860
	1.5	31	52**	1.677	74	99	1.338	55	35	0.636
	2.5	29	45**	1.552	62	88	1.419	47	23	0.489
	3.5	18	34**	1.889	56	74	1.321	32	20	0.625
	4.5	9	34**	3.778	47	59	1.255	21	13	0.619
0	0.5	75	''3	0.040	**76	''11	0.145	61	30	0.492
	1.5	66	2	0.030	83	12	0.145	65	31	0.477
	2.5	53	2	0.038	71	9	0.127	56	20	0.357
	3.5	41	2	0.049	57	13	0.228	40	13	0.325
	4.5	42	0	0.000	50	14	0.280	33	12	0.364

* Luminescence corrected for time-dependent background produced by RPMI medium without cells.

' Cells used from the 7th population doubling had been subcultured seven days before use. The gas moisturizer device was not maintained at 37° C. The time between scrapping cells and assay was 26 min. Fresh luminol solution was used.

'' Cells used from the 8th population doubling had been subcultured eight days before use. The gas moisturizer was maintained at 37° C. The time between scrapping cells and assay was 15 minutes. One day old luminol was used.

''' Cells from the 7th population doubling were subcultured nine days before use. The gas moisturizer was maintained at 37° C. The time between scrapping cells and assay was 15 minutes. Fresh luminol solution was used; luminescence comparisons between by the solution used in runs 1 and 2 and that used in Run 3 appears in Table 3.

** During the 30 sec mixing between the first and second reading, the vial slipped and one-half the sample was lost. Values are corrected for this loss by multiplying by 2.

* Cylinder pressure gradually declined over the last 25 min of the experiment; 10 min before it ended pressure was lost and compressed air was substituted; this may have affected the data set.

** This experiment was performed while room temperature was steadily rising due to air conditioner shut down. The luminometer is sensitive to temperature changes, therefore, the five data points in this set may be inaccurate.

' Plate temperature was $\geq 1.5°$ C too high, therefore the five data points in this set may be inaccurate.

'' Due to faulty regulators, 5% carbon dioxide/95% nitrogen was not used; 100% nitrogen was used instead. Flask pH was higher than other flasks (≥ 7.6), therefore the five data points in this set may be inaccurate.

* Control cell assay was started 10 min late because of mis-pipetting.

TABLE 3

RPMI LUMINESCENCE PRODUCED BY NEW AND OLD LUMINOL 4 MIN AFTER ADDITION

NEW	OLD
33	43
31	41
44	43

control. The lowest values were obtained from Used, Complete RPMI Plus Luminol; these samples were assayed to determine whether detectable peroxides were released into the medium during incubation with gas treatments. Either peroxides are not released, or serum-containing medium contains antioxidants. With the exception of experiment 1, values determined for the empty luminometer were consistently 18 - 21 units, indicating a lack of untoward changes (e.g., temperature shifts),

In Table 2 are found time-dependent luminescence changes by RAW264 macrophages before and after incubation with various oxygen concentrations. To control for possible differences in flask envirnment (time between using various flasks from the same clone, cell numbers and different gas or medium envirnments), each flask was bisected, half the cells were scrapped from the flask, and suspensions were immediately assayed for production of luminescence (pre-gassing control). We decided to use the pre-gassing controls to normalize data from gassed flasks; this approach seems appropriate because of the relative uniformity among ratios from a particular flask and, in most cases, between flasks receiving a similar treatment. Although raw data (minus RPMI/luminol controls) is presented in Table 1, discussion will be restricted to these ratios. The obvious trends in the data are as follows. Ratios from cells treated using oxygen at 158 mm Hg are from 2 - 20 times higher than

those from cells treated using only nitrogen. These data must be more closely examined in future experiments to determine viability of cells before and after exposure to various oxygen tensions; logistical problems prevented this assessment in the present studies. In addition, luminescence should also be associated with phagocytosis by these cells and no attempt was made to assess this parameter. Because of variablility between each set of ratios obtained from the three flasks treated with oxygen at 76 mm Hg, no trends can be discerned. It may be that oxygen tensions at 76 mm Hg are threshold concentrations for these macrophages causing variability (in a conversation with Major Johnathan Kiel, RZP, October 15, 1985, he indicated he had data from RAWs which might be consistent with this view). There seems to be a suggestion that treating cells with oxygen at 38 mm Hg results in increased ability to produce luminol-sensitive products. If this effect is real, it argues that these cells should be cultured in atmospheres more closely approximating those *in vivo*. Decreased differentiated function by cultured bovine adrenal cells during long-term culture (27) and decreased mitosis by cultured fibroblasts demonstrates that other cultured cell types are exquisitely sensitive to elevated partial pressures of oxygen (2 - 4, 12 -16, 35, 51, 56, 57). Future studies are required to determine whether oxygen tensions between 38 mm Hg and 0 (i.e., those more closely approximating physiological conditions) improve mac-

rophage function. The data in these experiments must be interpreted cautiously because several experiments were flawed. The volume of old serum-containing medium removed from culture flasks incubated with various gas concentrations during experiments 2 and 3 was 9 - 9.5 ml; in the first experiment when the moisturizer was not maintained at 37° C during culture flask incubation the volume was 8 - 8.7 ml. Reduced medium volume suggests medium water loss during incubation which probably resulted in cell dehydration through osmosis. In experiment 1: 26 min elapsed between cell scrapping and assay because exact time required for cell counting was not known (cell trauma seemed to stimulate peroxide release and long times between scrapping and assay lead to increasing luminescence loss; therefore, subsequent experiments used 15 min), the gas moisturizer was maintained at room temperature (subsequent experiments were conducted using moisturizers at 37° C when it was observed that 2 ml medium was lost during gassing), room temperatures became elevated (luminometer readings become unstable at elevated temperatures), plate temperatures rose during incubation with oxygen at 38 mm Hg (cell function could have been adversely affected), the medium pH was increased in the 100% nitrogen flask (cell function may be affected). In experiment 2: oxygen at 158 mm Hg ran out during the incubation and pH became elevated, one-half the 38 mm Hg gassed sample was spill-

ed after the first reading (although subsequent values were doubled, the 4.5 min reading is anomolous), again, 100% nitrogen had to be used to gas the 0 oxygen flask because of a faulty cylinder valve. Except for pipetting twice as many cells as needed and having to restart the 38 mm Hg control 10 min late, experiment 3 was without flaw. Although a new BSA/luminol/PBS solution had to be made for experiment 3, the difference in luminescence between new and old solutions was considered to be within method variability (Table 3). Therefore, data obtained using these solutions was not corrected.

VI. RECOMMENDATIONS:

As noted in the results section, data obtained from RAW macrophages incubated under various oxygen tensions was equivocal because experimental design could not be carefully controlled. Time did not permit additional replications. Future experiments must be carried out using moisturizers maintained at 37° C, a constant 15 min must be maintained between cell scrapping and assay, fresh luminol solutions must be used with each experiment, and carefully controlled gas mixtures containing 5% carbon dioxide must be used to maintain buffer capacity. If, after repeating this experiment, lower oxygen tensions improve macrophage peroxide production, then function should be examined at tensions between 0 and 38 mm Hg. It would also be of interest to determine the time (between 0 and 45 min) required for cells exposed to 0% oxygen to reduce function. The P388D macrophage line

did not produce peroxides, although they were capable of phagocytosis (see 1985 Summer Research Fellowship report by Mary Winfree); these cells represent controls for the RAW line. Experiments run using RAW cells should be repeated with this line as a control.

Since bright field light microscope optics together with time-lapse videomicroscopy permits the detailed examination of time-dependent extra- and intracellular events, macrophage behavior, including phagocytosis, should be monitored using an inverted microscope equipped with bright field optics.

After determining a standardized incubation time and oxygen tension for optimum macrophage chemiluminescence responses in the experiments proposed above, macrophages should be incubated with varying concentrations of E. coli for varying periods of time to determine phagocytic function. To insure that bacteria do not change the optimum macrophage P O2 requirement, at least one additional, higher P O2 concentration should be used in all bacterial experiments in addition to the previously determined optimum P O2. At the end of each incubation medium should be removed from each culture flask, centrifuged at 4° C, and bacterial counts should be made on samples maintained at 4° C to determine changes in bacterial numbers. A control consisting of bacteria added to a culture flask containing medium, but not macrophages, could be incubated under standard condi-

tions. Bacteria should be counted to determine maximum bacterial numbers possible for that culture condition. Bacterial population decrements and phagocytosis could also be observed by bright-field microscopy. Cultured fibroblasts and macrophages cooperate during wound healing. Cooperativity may be affected by changing oxygen tensions. Reduced oxygen tension effects on fibroblast proliferation and macrophage peroxide production during co-culture should be examined. Normal human fibroblast cell lines (i.e., MRC-5) and macrophages could be co-cultured and previosly described macrophage experiments using oxygen tension decrements could be repeated.

REFERENCES

1. Babior, B.M., R.S. Kipnes, and J.T. Curnutte. "Biological Defense Mechanisms. The Production by Leukocytes of Superoxide, a Potential Bactericidal Agent". J. Clin. Invest. 1973, 52:741-9.

2. Baldridge, C.W., and R.W. Gerard. "The Extra Respiration of Phagocytosis". Am. J. Physiol. 1933, 103:235-43.

3. Balin, A.K., D.G. Goodman, H. Rasmussen, and V.J. Cristofalo, "The Effect of Oxygen Tension on the Growth and Aging of WI-38 Cells". In Vitro (Rockville). 1974, 10:384.

4. Balin, A.K., D.G. Goodman, H. Rasmussen, and V.J. Cristofalo, "The Effect of Oxygen Tension on the Growth and Metabolism of WI-38 Cells". J. Cell. Physiol. 1976, 89:235-250.

5. Balin, A.K., D.G. Goodman, H. Rasmussen, and V.J. Cristofalo, "Atmospheric Stability in Cell Culture Vessels". In Vitro (Rockville). 1976, 12:687-692].

6. Bennett, W.E., and Z.A. Cohn, "The Isolation and Selected Properties of Blood Monocytes". J. Exp. Med. 1966, 123:145-54.

7. Boggs, D.R., and A. Winkelstein, "The Phagocyte System (Neutrophils, Monocytes, Eosinophils, Basophils)" in White Cell Manual, Edition 4, F.A. Davis Co., Philadelphia, Pa. 1983, pp. 49-52.

8. Cline, J.J. "Metabolism of the Circulating Leukocyte". Physiol. Rev. 1965, 45:674-85.

9. Cline, M.J., "Bactericidal Activity of Human Macrophages: Analysis of Factors Influencing the Killing of Listeria monocytogenes. Infect. Immun. 1970, 2:156-164.

10. Cline, M.J., and R.I. Lehrer, "Phagocytosis by Human Monocytes". Blood. 1968,32:423-30.

11. Cohen, A.B., and M.J. Cline. "The Human Alveolar Macrophage: Isolation, Cultivation in vitro, and Studies of Morphology and Functional Characteristics." J. Clin. Invest. 1971, 50:1390-1405.

12. Cohn, Z.A. "The Structure and Function of Monocytes and Macrophages". Adv. Immunol. 1968, 9:163-75.

13. Cooper, P.D., A.M. Burt, and J.N. Wilson, "Critical Effect of Oxyger Tension on Rate of Growth of Animal Cells in Continuous Suspended Culture". Nature. 1958, 182:1508-1509.

14. Cooper, P.D., A.M. Burt, and J.N. Wilson, "The Bulk Growth of Animal Cells in Continuous Suspension Culture". J. Gen. Microbiol. 1959, 21:702-720.

15. Curnutte, J.T., and B.M. Babior, "Effects of Anaerobiosis and Inhibitors of O2-, Production by Human Granulocytes". J. Clin. Invest. 1975, 54: 471-9).

16. Dales, S. and K.C. Fisher, "The Effect of Carbon Monoxide on Oxygen Consumption, Glucose Utilization and Growth in Mammalian Cells In Vitro". Can. J. Biochem. Physiol. 1959, 37:623-638.

17. Davis, Jefferson, M.D., Personal communication, Jan. 1984.

18. Ebert, R.H., and H.W. Florey, "The Extravascular Development of the Monocyte Observed In Vitro". Br. J. Exp. Pathol. 1939, 20:342-8.

19. Forster, R.E., Oxygenation of the tissue cell, Ann, N.Y. Acad. Sci., 117:730-735 (1965).

20. Frei, J., C. Borel, G. Horvath, B. Cullity, and A. Vannoti, "Enzymatic Studies in the Different Types of Normal and Leukemic Human White Cells". Blood. 1961,

18:317-29.

21. Fridovich, I., Arc. Chem. Res. 1972, 5:321-8.;

22. Haber, F., and J. Weiss. Proc. R. Soc., London, Ser. A. 1934, 147:332-9.

23. Henderson, R., Personal communication, Sept. 1984.

24. Hertz, F., and Cloarec, A., Pharmacolcogy of free radicals: recent views on their relation to inflammatory mechanisms. Life Science, 34:713-720 (1984).

25. Holmes, B., A.R. Page, and R.A. Good, "Studies of the Metabolic Activity of Leukocytes from Patients with a Genetic Abnormality of Phagocytic Function". J. Clin. Invest. 1967, 46:1422-7.

26. Hohn, D.C., R.D. MacKay, B. Haliday, and T.K. Hunt, "The Effect of Oxygen Tension on the Microbicidal Function of Leukocytes in Wounds and In Vitro.". Surg. Forum. 1976, 27:18-20.

27. Hornsby, P.J., M.H. Simonian, and G.N. Gill, "Aging of Adrenocortical Cells in Culture". International Review of Cytology Supplement. 1980, 10:131-162.

28. Hunt, T.K., M. Linsey, G. Grislis, M. Sonne, and E. Jawetz, "The Effect of Differing Ambient Oxygen Tensions on Wound Infection". Ann. Surg. 1975, 181:35-47.

29. Hunt, T.K., J. Niinikoski, B.H. Zederfeldt, and I.A. Silver, "Oxygen in Wound Healing Enhancement: Cellular Effects of Oxygen". in Hyperbaric Oxygen Therapy Edited by Davis, J.C., and T.K. Hunt. The Undersea Medical Society, Inc., Bethesda, Md. 1977, pp. 111-117.

30. Hunt, T.K., and M.P. Pai, "The Effect of Varying Ambient Oxygen Tensions on Wound Metabolism and Collagen Synthesis". Surg. Gynecol. Obst. 1972, 135:561-9.

31. Iyer, G.Y.N., M.F. Islam, and J.H. Quastel, "Biochemical Aspects of Phagocytosis". Nature. 1961, 192:535-8.

32. Johnston, R.B., Jr., J.E. Lehmeyer, and L.A. Guthrie, "Generation of Superoxide Anion and Chemiluminescence by Human Monocytes During Phagocytosis and on Contact with Surface-bound Immunoglobulin G". J. Exp. Med. 1976, 143:1551-6.)

33. Kiel, J.L., "Microwave effects on immobilized peroxi-

dase chemiluminescence". Bioelectromagnetics. 1983, 4:193-204.

34. Kiel, J.L., Business letter dated 29 March 1985.

35. Kilburn, D.G., M.D. Lilly, D.A. Self, and F.C. Webb, "The Effect of Dissolved Oxygen Partial Pressure on the Growth and Carbohydrate Metabolism of Mouse LS Cells". J. Cell Sci. 1969, 4:25-37.

36. Kirk, D., and T.T. Irvin, "The Role of Oxygen Therapy in the Healing of Experimental Skin Wounds and Colonic Anastomoses". British J. Sur.. 1977, 64:100-103.

37. Lambertson, C., "The Atmosphere and Gas Exchanges with the Lungs and Blood", in: Medical Physiology, 13th edition, Mountcastle, V. (ed.) C.V. Moses Co., St. Louis, Mo. 1974, pp. 1372-1374.

38. Lewis, M.R., "The Formation of Macrophages, Epithelioid Cells and Giant Cells from Leucocytes in Incubated Blood". Am. J. Pathol. 1925, 1:91-6.

39. Lundgren, C.E.G., and B. Zederfeldt, "Influence of low oxygen pressure on wound healing". Acta Chir. Scand. 1969, 135:555-8.

40. Irvin, T.T., "The Healing Wound". in Wound Healing for Surgeons. Edited by Bucknall, T.E., and H. Ellis. Billiere Tindall, Philadelphia, Pa. 1984, pp. 1-15.

41. Mandel, G.L., "Bactericidal Activity of Aerobic and ANAerobic Polymorphonuclear Neutrophils". Infect. Immun. 1974, 9:337-46.

42. Niinikoski, J. "Effect of Oxygen Supply on Wound Healing and Formation of Experimental Granulation Tissue". Acta Physiol. Scand. Suppl. 1969, 334:1-120.

43. Niinikoski, J., G. Grislis, and T.K. Hunt, "Respiratory Gas Tensions and Collage in Infected Wounds" Ann. Sur. 1972, 175:588-93.

44. Niinikoski, J., T.K. Hunt, and B. Zederfeldt, "Oxygen Supply in Healing Tissue".Am J Surg. 1972, 123:247-56.

45. Nungester, W.J., A.M. Ames, and W. Lanning, "Electrophoresis Studies of Leucocytes and Bacteria in Relation to Mechanisms of Phagocytosis". J. Infect. Dis. 1952, 90:61-72.

46. Polverini, P.J., R.S. Cotran, M.A. Gimbrone, Jr., and E.R. Unanue, "Activated Macrophages Induce Vacular

Proliferation". Nature. 1977, 269:804-06.

47. Quie, P.G., J.G. White, B. Holmes, and R.A. Good. "In Vitro Bactericidal Capacity of Human Polymorphonuclear Leukocytes: Diminished Activity in Chronic Granulomatous Disease of Childhood". J. Clin. Invest. 1967, 46:668-76.

48. Rossi, F., and M. Zatti. "Biochemical Aspects of Phagocytosis in Polymorphonuclear Leukocytes: NADH and NADPH Oxidation by the Granules of Resting and Phagocytozing Cells". Experientia. 1964, 20:21-3.

49. Silver, I.A., "The Physiology of Wound Healing". In Wound Healing and Wound Infection: Theory and Surgical Practice Edited by Hunt, T.K., Appleton-Century-Crofts, NY. 1980, pp. 11-28.

50. Stahelin, H., E. Suter, and M.L. Karnovsky, "Studies on the Interaction Between Phagocytes and Tubercle Bacilli. I. Observations on the Metabolism of Guinea Pig Leucocytes and the Influence of Phagocytosis". J. Exp. Med. 1956, 104:121.

51. Taylor, W.G., A. Richter, V.J. Evans, and K.K. Sanford, "Influence of Oxygen and pH on Plating Efficiency and Colony Development of WI-38 Cells and Vero Cells". Exp. Cell Res. 1974, 86:152-156.

52. Unanue, E.R., "Cooperation Between Mononuclear Phagocytes and Lymphocytes in Immunity," The New England J. of Med. 1980, 303:977-85.

53. van Furth, R., Z.A. Cohn, J.G. Hirsch, J.H. Humphrey, W.G. Spector, and H.L. Langevoort, "The Mononuclear Phagocyte System: a New Clasification of Macrophages, Monocytes, and Their Precursor Cells." Bull. WHO. 1972, 46:845-52.

54. West, J., D.I. Morton, V. Esmann, and R.L. Stjernholm, "Carbohydrate Metabolism in Leukocytes. VIII. Metabolic Activities of the Macrophage." Arch. Biochem. Biophys. 1968, 124:85-93.).

55. Wong, L.S., and Kiel, J.L., "Anamnestic chemiluminescence of murine spleen cells". Immunological Commun. 1984, 13:285-290.

56. Wright, G.P. "The Oxygen Tension Necessary for the Mitosis of Certain Embryonic and Neoplastic Cells". J. Pathol. Bact. 1928, 31:735-752.

57. Zwartouw, H.T. and J.C.N. Westwood, "Factors Affecting Growth and Glycolysis in Tissue Culture. Brit. J. Exp. Pathol. 1958, 39:529-539.

1985 USAF-UES SUMMER FACULTY RESEARCH PROGRAM/

GRADUATE STUDENT SUMMER SUPPORT PROGRAM

Sponsored by the

AIR FORCE OFFICE OF SCIENTIFIC RESEARCH

Conducted by the

UNIVERSAL ENERGY SYSTEMS, INC.

FINAL REPORT

ISOTHERMAL DIFFERENTIAL SCANNING CALORIMETRIC STUDIES OF THERMAL DECOMPOSITION OF 1,4-BUTANEDIAMMONIUM DINITRATE

Prepared by: Maurice C. Neveu

Academic Rank: Associate Professor

Department and University: Chemistry Department, State University of New York, College at Fredonia

Research Location: High Explosives Research and Development Facility, Air Force Armament Laboratory, Eglin AFB, FL

USAF Research Colleague: Robert L. McKenney, Jr.

Date: 21 August 1985

Contract No: F49620-85-C-0013

ISOTHERMAL DIFFERENTIAL SCANNING CALORIMETRIC STUDIES OF THERMAL DECOMPOSITION OF 1,4-BUTANEDIAMMONIUM DINITRATE

by

Maurice C. Neveu

ABSTRACT

The kinetic deuterium isotope effect was determined at 265, 270, and 275°C for the induction period of the decomposition reaction of an explosives component, 1,4-butanediammonium dinitrate (BDD), and hexadeutero-1,4-butanediammonium dinitrate (BDD-d_6) in which the hydrogen atoms on the nitrogen atoms have been replaced by deuterium atoms. The k_H/k_D ratio was found to be 1.09, 1.11, and 1.33 at 265, 270, and 275°C, respectively. The faster rate for the protium compound can be interpreted as indicating C-N bond breaking in the rate determining step. The corresponding activation energies are 68.9 and 57.5 kcal/mole for BDD and BDD-d_6, respectively.

ACKNOWLEDGMENTS

The author would like to thank the Air Force Systems Command, the Air Force Office of Scientific Research, and the High Explosives Research and Development Facility, Air Force Armament Laboratory, Eglin Air Force Base for sponsorship of this very interesting and stimulating research project. He would also like to express his appreciation to Universal Energy Systems, Inc. for a well-organized program, and to Ms. Sue Espy and Mr. Rodney Darrah for helpful guidance in the mechanics of the program.

He would especially like to thank his USAF Research Colleague, Dr. Robert L. McKenney, Jr., for a well-coordinated research project and the helpful discussions which led to the success of this fellowship.

I. INTRODUCTION

Some time ago, a program involving the study and determination of the explosive characteristics of 1,2-ethyldiammonium dinitrate (EDD) admixed with ammonium nitrate (AN) and potassium nitrate (KN) was initiated at the High Explosives Research and Development (HERD) Facility at Eglin AFB. In order to develop a system of lower sensitivity than this one, known as EAK, a study of a longer chain homologue of EDD, 1,4-butanediammonium dinitrate (BDD) with ammonium nitrate and potassium nitrate, a mixture referred to as BAK, was begun.

It was felt that a detailed study of the thermal properties of BDD and BAK would provide valuable information for understaning the reaction mechanism of their decomposition which would help in understanding their explosive properties. Such information can conveniently be obtained by Differential Scanning Calorimetry (DSC), a technique that measures the amount of heat absorbed or given off when a substance undergoes physical or chemical transitions.

The author of this report has had previous experience in DSC technique. On a SFRP fellowship at Eglin AFB in 1979, he used this technique in the study of eutectic formation in explosive mixtures of organic substances as fuels and ammonium nitrate as oxidizer. He subsequently continued this project at his campus, State University of New York, College at Fredonia, on an extension grant funded by the Air Force Office of Scientic Research. In these studies, the Perkin-Elmer DSC-1 and DSC-2 Thermal Analysis Systems were used. During the past four summers while on Summer Faculty Research Programs as well as an academic year sabbatical leave at NASA Lewis Research Center in Cleveland, Ohio, he has conducted research on fuels. One phase of this work involved low temperature DSC studies on binary and ternary hydrocarbon mixtures to determine their freezing points and heats of fusion and establish their phase diagrams.

Another phase involved fuel degradation studies using high pressure DSC. In both of these phases the DuPont 1090 Differential Scanning Calorimeter was used.

II. OBJECTIVES OF THE RESEARCH PROJECT

It was decided to measure the kinetic isotope effect in the thermochemical decomposition of liquid BDD by isothermal Differential Scanning Calorimetry in order to obtain mechanistic information for this reaction, specifically, by measurement and comparison of the kinetic parameters of BDD and its deuterated analogue hexadeutero-BDD (BDD-d_6) in which the three hydrogen atoms on each nitrogen atom have been replaced by deuterium atoms.

III. APPROACH

The thermochemical decomposition of an energetic substance such as an explosive can be monitored by Differential Scanning Calorimetry which typically results in a curve like that shown below

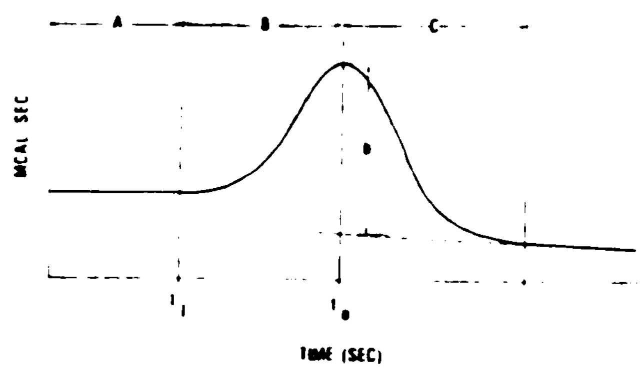

Fig. 1

where A is the induction period, B the acceleratory phase of the decomposition reaction, and C the decay phase. The induction period is represented by t_I and the zero time for the decay phase by t_C. The recorder deflection corrected for the baseline at the point where heat evolution was at a maximum is represented by [illegible]. A plot of t_I

versus $1/T$ where T is the Kelvin temperature of the isothermal scan provides E_{aI}/R as the slope where E_{aI} is the activation energy of the induction reaction and R is the gas constant, 1.98 cal/mol $^{\circ}K$. Other quantities such as the order, n, and the specific rate constant, k, of the decay phase of the decomposition reaction can be obtained from the measurement of t.[1,2] The k values can be plotted against $1/T$ to evaluate the activation energy, E_a, and the entropy of activation, ΔS^*, of the decay phase.

At the temperatures used in this study, the exothermic peak was extremely sharp and measurement of t values was not possible. Determination of t_I, however, was possible and hence values of E_{aI} were able to be calculated.

IV. PROCEDURE

DSC measurements were performed with a Perkin-Elmer DSC-4 equipped with the Thermal Analysis Data Station (TADS). BDD or BDD-d_6 samples weighing 1.55 ± 0.05 mg were placed in Perkin-Elmer aluminum pans (part no. 219-0062). A hole was pierced in the lid to allow the escape of decomposition gases and the lid then sealed to the pan with a Perkin-Elmer sealer assembly (part no. 219-0061). A similar pan assembly containing an equivalent weight of reference standard grade SiO_2 always remained in the reference cell of the calorimeter. The sample was placed in the sample cell of the calorimeter and the lid, in which openings had been machined to allow the escape of decomposition gases, was closed. Dry nitrogen was allowed to flow through the calorimeter cell at a rate of 50 cc per minute.
The sample was heated from $50^{\circ}C$ to the desired isothermal temperature at a rate of 200 $^{\circ}C$/minute and held at that temperature until an exothermic peak was observed and the baseline reestablished. Experiments were carried

out with BDD and BDD-d_6 at 265, 270, and 275 °C. Several experiments were carried out at each temperature for both compounds for statistical analysis. Runs at lower temperatures, 200 and 240 °C, were performed to explore the possibility of obtaining an exotherm that was broader so that b values might be able to be measured in subsequent projects.

V. RESULTS AND DISCUSSION

Data for the induction period of the reaction are presented in Table I. Induction times, t_I, averaged over the given number of runs are shown. A mean standard deviation, s_m, was calculated from the tabulated standard deviation, s, by equation (1)

$$s_m = s/(N)^{1/2} \tag{1}$$

where N is the number of runs. 68% Confidence Limits of the averaged values of t_I were calculated from the expression (2).

$$t_I \pm s_m \tag{2}$$

Table I

Temp. (°C)	Compound	Induction Time, t_I (min)	Standard Deviation	Number of Experiments	68% Confidence Limits, t_I (min)
265	BDD	4[illegible].76	1[illegible].[illegible]3	8	41.30 - 50.22
265	BDD-d_6	50.01	11.57	6	4[illegible].[illegible] - 54.73
270	BDD	22.09	6.50	10	20.03 - 24.15
270	BDD-d_6	24.62	[illegible]	11	[illegible] - [illegible]
275	BDD	14.02	2.13	12	1[illegible].[illegible] - 14.64
275	BDD-d_6	1[illegible].[illegible]	[illegible].[illegible]4	6	1[illegible].[illegible]1 - 19.05

Isotope effects at each temperature calculated from equation (3)[1]

$$\frac{k_H}{k_D} = \frac{t_{ID}}{t_{IH}} \qquad (3)$$

are 1.09, 1.11, and 1.33 for 265, 270, and 275°C. The slower rate for the deuterated compound can be rationalized for a rate determining breaking of the C-N bond when one considers the greater electron donating ability of the N-D group[3] resulting in an increase in the basicity of the departing ND_3 relative to NH_3 and hence, a retardation of the reaction of deuterated compound. This explanation involves a secondary isotope effect which is consistent with the magnitude of the values. It should be noted that there is considerable overlap of the Confidence Limits at 265 and 270°C. However, the totality of the data does seem to indicate a trend of a slower rate for the deuterated compound.

Plots of ln t_I versus 1/T where T is expressed in Kelvin temperature yielded activation energies for the induction period, E_{aI}, 66.9 kcal/mole for BDD and 57.[illegible] kcal/mole for BDD-d_6 (Fig. 2).

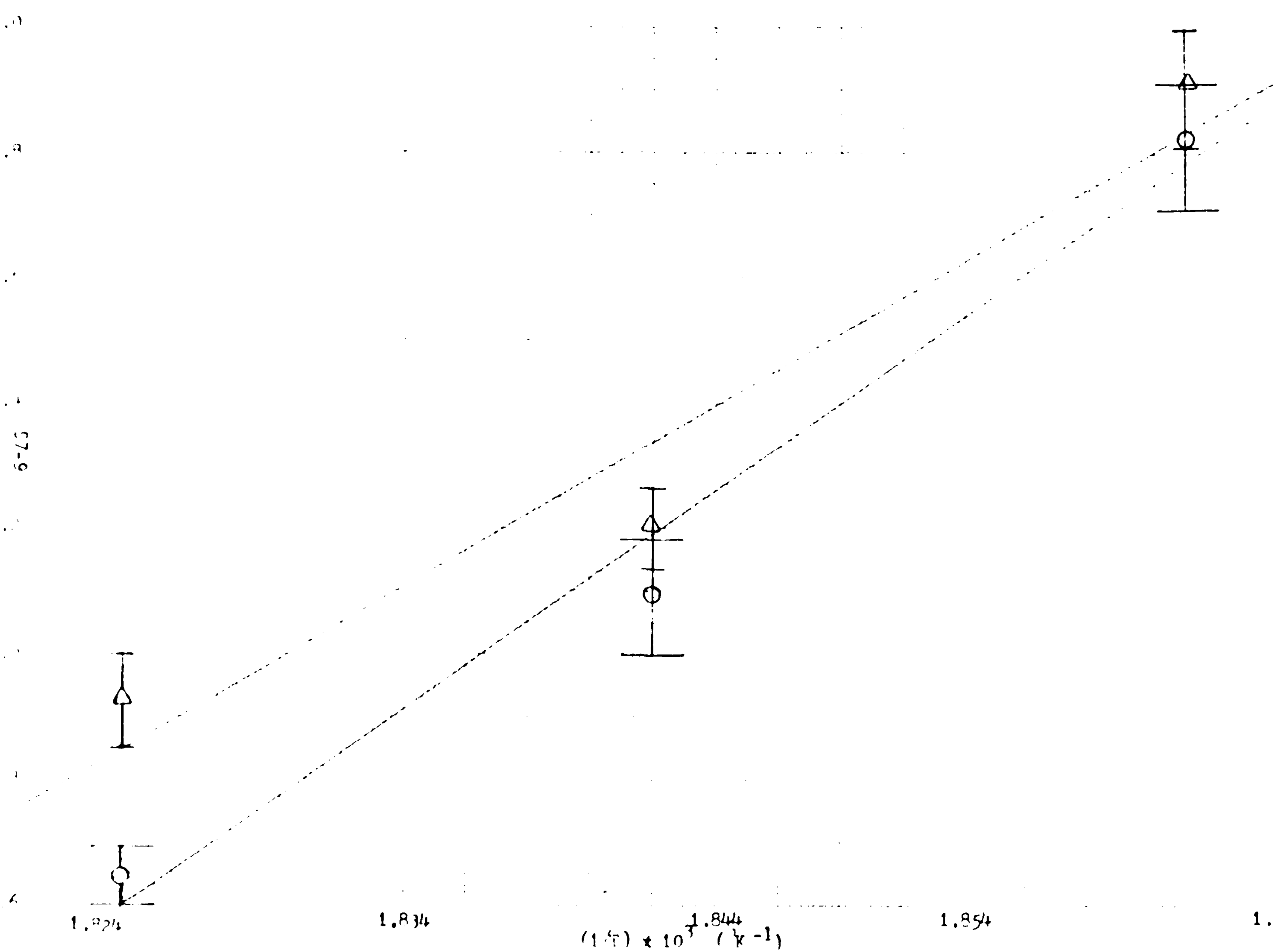
1.824
1.834
1.844
1.854
1.
(1/T) * 10^3 (K^-1)

VI. RECOMMENDATIONS

Due to the sharpness of the exothermic peak, it was not possible to utilize the DSC scan to extract as much information from it as might have been possible had the peak been broader and more bell-shaped. As mentioned in Section III measurement of b (Fig. 1)obtainable in the a broader peak could yield the order, n; the specific rate constant, k; and the activation energy, E_a, of the decay phase of decomposition reaction. The entropy of activation could also be calculated from these results. These kinetic parameters of the decay phase would be very important in elucidating the mechanism of the reaction, especially the entropy of activation which would give information about the nature of the transition state of the reaction. Exploratory DSC isothermal experiments at lower temperatures, 200 and 240°C indicated that such broad and bell-shaped curves are obtainable. Experiments at these and other lower temperatures should, accordingly, be carried out. It might also be useful to obtain more data in the temperature range, 265-275°C, in order to obtain more reliable statistics for the data reported here.

Another avenue of research would involve the use of BDD which has been deuterated on the carbon atoms to investigate the occurrence of primary isotope effects resulting in the breaking of the C-D (or C-H) bond in the rate determining step of induction or the decay reaction.

It might also be possible to stop the reaction during the induction period to isolate any compounds that form during this period which might be responsible for catalyzing the decomposition reaction. This might be done by high-pressure liquid chromatographic analysis.

The nature of fragments formed during decomposition could be investigated by carrying reactions out in the presence of free radical scavengers. If free radicals are formed during decomposition, scavengers such as hydroquinone would react with them and accelerate the reaction.

REFERENCES

Journal publications:

1. Shackelford, S.A., J.W. Beckmann, and J.S. Wilkes, "Deuterium Isotope Effects in the Thermochemical Decomposition of Liquid 2,4,6-Trinitrotoluene: Application to Mechanistic Studies Using Isothermal Differential Scanning Calorimetry Analysis," Journal of Organic Chemistry," Vol. 42, No. 26, 1977, pp. 4201 - 4206.

2. Beckmann, J.W., J.S. Wilkes, and R.R. McGuire, "2,4,6-Trinitrotoluene Thermal Decomposition: Kinetic Parameters Determined by the Isothermal Differential Scanning Calorimetry Technique," Thermochimica Acta, Vol 19, 1977, pp. 111-118.

3. Laszlo, P. and Z. Welvart, "L'Effet Isotopique Secondaire du Deutérium," Bulletin de la Société Chimique de France, No. 7, 1966, pp. 2412 - 2438.

1985 USAF-UES SUMMER FACULTY RESEARCH PROGRAM/

GRADUATE STUDENT SUMMER SUPPORT PROGRAM

Sponsored by the

AIR FORCE OFFICE OF SCIENTIFIC RESEARCH

Conducted by the

UNIVERSAL ENERGY SYSTEMS, INC.

FINAL REPORT

A STUDY OF THE RELATIONSHIP BETWEEN LEADERSHIP AND JOB SATISFACTION/CAREER COMMITMENT AMONG AIR FORCE PERSONNEL

Prepared by: Robert E. Niebuhr

Academic Rank: Associate Professor

Department: Department of Management

University: Auburn University

Research Location: Leadership and Management Development Center
Maxwell Air Force Base
Montgomery, Alabama

USAF Research Contact: Major M.R. Dansby

Date: August 22, 1985

Contract No: F49620-85-C-0013

A STUDY OF THE RELATIONSHIP BETWEEN
LEADERSHIP AND JOB SATISFACTION/CAREER COMMITMENT
AMONG AIR FORCE PERSONNEL

by

Robert E. Niebuhr

ABSTRACT

Using the data base of the Air Force's Organizational Assessment Package (OAP) it was found that a positive correlation existed between leadership behavior and both job satisfaction and career commitment intentions. Additionally, the relationships involving supportive leadership behaviors provided more positive correlations than did instrumental (structuring) leadership behaviors. It was also found that organizational tenure moderated the relationships between leadership behaviors and career commitment intentions--individuals who had been in the service a shorter time (low tenure) had much lower perceptions of leadership supportive behaviors than did high tenure individuals.

This finding is particularly noteworthy given the high attrition rate of first term personnel. The apparent lack of meaningful leader-follower exchanges for low tenure individuals and the corresponding low retention of these same individuals provided sufficient cause for making several specific recommendations regarding military views of leadership and needed leadership training. The results from the study also provided sufficient incentive to investigate further leadership/satisfaction/retention phenomenon across various functional areas (operations, maintenance, resource) and personnel categories (offices, enlisted civilian).

ACKNOWLEDGEMENTS

This research was conducted under the sponsorship of the Air Force Systems Command, the Air Force Office of Scientific Research, and the Leadership and Management Development Center (LMDC) at Maxwell Air Force Base - Montgomery, Alabama.

The contributions of Major M.R. Dansby and the support personnel in LMDC/AN, particularly Capt. K. Ibsen, are gratefully acknowledged.

I. INTRODUCTION

Having had more than ten years of industrial experience and eight more years in an academic environment, my primary emphasis in research activities has been to examine behavioral data from real-life situations in an attempt to make suggestions for improving managerial skills. Consequently, the opportunity to investigate responses to the Air Force Organizational Assessment Package (OAP) (Hendrix & Halverson, 1979) provided an extremely good fit with my own interests. Additionally, my doctoral study at the Ohio State University under Steve Kerr and Ralph Stogdill established a good background and strong interest in studying the concept of leadership as applied to various organizational settings. Although data from the OAP has been collected for some time period there have few research-oriented investigations performed from the data base; the OAP's primary function has been to serve as a source of normative data for action-based interventions by the Leadership and Management Development Center's consultants. The recognition that there was tremendous potential for a number of research studies had to be tempered by the knowledge that the Summer Faculty Research Program was only a ten-week effort.

II. OBJECTIVES OF THE RESEARCH EFFORT

The primary object of this project was to investigate the relationship between leadership behaviors and job satisfaction/career commitment attitudinal responses from data collected with the OAP. As the project developed it was decided to also investigate the moderating influence that organization tenure might have on the above relationships. At the end of

the project some preliminary work was also begun in making comparisons of leadership behaviors across functional areas and personnel categories.

III. RESEARCH BACKGROUND

It is apparent that the concept of leadership is one of the most researched behavioral variables in both military and non-military writings (Bass's (1981) review of leadership research, for example, contains more than 5,000 references). More than fifty articles are included in several recently published books dealing with military leadership (Buck & Korb, 1981; Taylor & Rosenbach, 1984; Hunt & Blair, 1985). Additionally, the Proceedings from the Ninth Symposium on Psychology in the Department of Defense (1984) contained twenty additional articles given in sessions devoted specifically to the concept of military leadership. While the most recent work by Hunt and Blair (1985) contains a number of research-oriented papers, it is apparent from a review of the other compilations cited above that the concept of leadership has an amorphous-like character surrounding it. One author (Yoos, 1984) crystalizes this formless view in his paper title--"There Is No Such Thing as Leadership!" Another (Stokebury, 1981) also suggests this elusiveness in a paper entitled "Leadership as an Art." Washbush (1984) evidences his frustration in suggesting that because military people love the word "leadership" they often misuse or misapply the discoveries regarding this concept. Although principles such as tradition, character, physical fitness and moral courage are important in many organization interactions, the linkage to leadership behavior and follower response appears to be, at best, somewhat unclear. It seems that many writings on "military leadership" stress a more global view of leadership than the dyadic leader-follower interaction process

that is more prevalently investigated in research-oriented studies.

An interesting study by Van Fleet and Yukl (1985) evaluated the content of articles in the three major service publications (Military Review, Air University Review, and Naval War College Review) over a five-yearperiod (1977-1982). They found, for example, that the articles in the Air University Review heavily emphasized criticizing, goal-setting, and disseminating information. Very little emphasis was placed upon developing improved interpersonal relationships between leaders and followers by stressing such topics as showing consideration, facilitating teamwork, and providing praise and recognition. It may be that the traditional image of a strong, directive military leader in combat situations may not allow for alternative pictures of leadership behavior. This "battlefield" context may move leadership from the micro-interpersonal view of leader-follower interactions to a less personal, more global macro-view of leadership. This perceptual inclination might be the underlying reason for some of the apparent lack of clarity surrounding the military concept of leadership.

Figure 1 provides a general model of the specific variables under investigation in this particular study. This model is not a causal model but depicts only the expected correlational relationships between leadership behaviors and job satisfaction/career commitment. Organization tenure is seen as a moderating variable affecting these relationships. There are numerous studies which would suggest that supportive-oriented leadership behaviors would correlate positively with job satisfaction (Bass, 1981) but the evidence for instrumental (structuring) leadership behaviors is less clear. There have been few studies which examine the relationship between leader behaviors and turnover (or career commit-

ment). Fleishman and Harris (1962) found that supportive leadership behaviors were negatively correlated with turnover rate while instrumental behaviors were positively correlated. However, high supportive behaviors would decrease the turnover rate stemming from the high instrumental leader behaviors. A more recent study by Graen, Liden, and Hoel (1982) confirmed these relationships by finding a strong negative relationship between leader-member exchange behavior (supportive-type behavior) and turnover. However, a replication of the study just published by Vecchio (1985) failed to find the same significant relationship. Vecchio proposed that the lack of a relationship may suggest that turnover in the particular situational context he examined may be due to employees being attracted away from their present situation, rather than driven or repelled away from the organization due to dissatisfaction, etc. If the correlations between leadership and turnover had been significant, the results would have suggested the repulsion causal pattern rather than the attraction causal pattern. In many of the retention studies done in the military it appears that both models may be operating.

The high attrition rate (30 to 40% in the first-term enlisted force (USAF) for all reasons (Finstuen & Berry, 1981)) has placed increased emphasis on finding some of these causal factors. Although many studies have examined causes due to attraction models (e.g. economic conditions, education level, internal motivation, occupational classification, retirement policies, etc.) others have also investigated repulsion models (e.g. family attitudes, duty assignment, type of work, military life, etc.). There have also been a few studies of military retention which have investigated the influence of leadership behaviors in career commitment decisions. Stoloff et al (1971) found that Naval personnel's intent to

not reenlist was correlated with low supportive behavior and high instrumental behavior, cmobining the findings reviewed earlier by Fleishman and Harris (1962). A study of Marine Corps recruit attrition by Sarason (1981) found that drill instructors who were more structuring had higher attrition rates than those who exhibited more supportive behaviors. Youngblood and Mobley (1981), however, found no significant impact on retention attitudes due to either instrumental or supportive leader behaviors in a study of 1,500 first-term Marine Corps enlisted personnel.

Based on the above review of both the military and non-military leadership research, it appears that active leadership exchanges (particularly supportive-type behaviors) should be positively correlated with both job satisfaction and career commitment intentions. Consequently, the first hypothesis can be stated as follows:

> A positive correlation will exist between leadership behaviors and job satisfaction/career commitment attitudes. The relationships involving supportive leadership behaviors should be more positive than those involving instrumental (structuring) leadership behaviors.

Organization tenure (length of time in the organization) has been shown previously to be positively related to job satisfaction (Herman, Dunan, & Hulin, 1975; Spencer & Steers, 1981). In addition to job satisfaction, a key component in most turnover prediction models (March & Simon, 1958; Mobley, 1977; Steers & Mowday, 1981) is the influence that organization tenure has in reducing the propensity to search for new job opportunities. Particularly in the military, it might be anticipated that for those individuals who have been with the service only a short period of time the socialization process results in changes in expectations,

motivations, leadership perceptions, etc. which begin to strongly influence the individual's decision to remain with or leave the service. This rationale follows the repulsion causal pattern (Vecchio, 1985) discussed earlier. Hall (1976) indicates that new employees tend to be preoccupied with establishing their own identities and becoming a helpful part of the organization. Learning how to work with one's superior becomes extremely important since, at this tenure level, the individual is likely to have serious concerns about his/her ability to perform job assignments. Therefore, in early socialization stages, job satisfaction and career commitment intentions are likely to be associated with the interpersonal relationships that exist with one's superior. As tenure increases, particularly to the point where a decision is made to reenlist or stay in the service, other variables are likely to affect both job satisfaction and career commitment. These variables may include retirement policies, working conditions, level of advancement, outside opportunities, etc. More elements from an attraction causal pattern of career commitment become evident. By this time the individual has a fairly good perception of how far he/she will advance and adjustments have probably occurred in personal expectations (Hall, 1976).

Using this socialization perspective it is suggested that an individual's job satisfaction/career commitment may be significantly related to leadership perceptions in different degrees, depending upon the particular level of organization tenure. The hypothesis to be investigated is stated as follows:

> Organization tenure will moderate the relationship between leadership behaviors and job satisfaction/career commitment. Specifically, the variables are expected to be more strongly correlated for individuals low in organization tenure than for those high in organization tenure.

IV. METHOD

Subjects

The database for the Organizational Assessment Package (OAP) presently contains responses from more than 200,000 Air Force personnel. For this particular study a 31,980 person segment was chosen to provide a representative sample of various functional area categories (operations, maintenance, and resource) and personnel classifications (officer, enlisted, civilian).

Measures

Leadership Behaviors. The OAP provided nineteen leadership items which were used to produce a single measure of overall leadership. Initial factor analysis (Hightower & Short, 1982) had produced two separate leadership factors but more recent work had collapsed them back into one single factor (Short, Lowe, & Hightower, 1985). To provide some relevance to the leadership research literature six of the nineteen items were chosen on the basis of their content to form a measure of instrumental leadership behavior and four others were chosen to provide a measurement of supportive leadership behavior.

Job Satisfaction. The factor analytic derived seven-item scale called "job related satisfaction" from the OAP was used for this measurement.

Career Commitment. A single item (five response categories) from OAP asking the respondent their feelings about career intentions was used to evaluate career commitment.

Organization Tenure. Demographic data from the OAP provided this information.

V. RESULTS/DISCUSSION

Descriptive statistics and Pearson product-moment correlations among the study variables are presented in Table 1. Scale reliabilities are also reported in this table along the diagonal. The results support the first hypothesis which predicted positive correlations between leadership behavior and both job satisfaction and career commitment. Although the two leadership subscales are highly intercorrelated (as stated earlier these subscales were created from existing items rather than created *a priori*) the stronger relationship between supportive leadership behaviors and both job satisfaction and career commitment is as was hypothesized.

The results of the multiple regression analysis used to evaluate the second hypothesis are presented in Table 2. For moderated regression analysis, the hierarchial inclusion method was used for decomposition of the explained sum of squares into components attributable to each independent variable and the interaction term. The multiplicative interaction term was always entered into the regression in the last step. Therefore, the F test associated with the interaction term indicates the significance of the incremental contribution of this term to the explained variance in the dependent variable after the effects of all other independent variables have been removed.

The interaction of leadership behaviors and organization tenure added significantly to the explained variance in career commitment but did not with respect to job satisfaction. To evaluate these interactions more carefully the data was split into subgroups of low and high organization tenure. Table 3 presents the subgroup means of each of the study variables.

Using Vecchio's (1981) terminology, these results might suggest a repulsion causal model is a stronger rationale for this population's attitudes than an attraction causal model. The correlation between leadership and career commitment intentions was both positive and significant (in Vecchio's attraction causal study the coefficient was slightly negative and non significant) although it did not exceed the level of the correlation between leadership and job satisfaction (as in the repulsion causal study by Graen, Liden, and Hoel (1982)). It is recognized that substantial job irritants affect all personnel, causing dissatisfaction and potential withdrawal intentions. In the case of low tenure individuals, effective supportive-oriented leader behaviors should tend to dissipate these negative feelings in order to reduce the individual's propensity to leave. However, the data in Table 3 indicates that both the perceived supportive leadership behavior and career commitment intentions were lower for low tenure than for high tenure individuals. Apparently, the low tenure individuals do not perceive that their leaders are providing the type of supportive help required to help them deal with their job irritants. This repulsion causal rationale receives support from the study by Sarason (1981), reviewed earlier, which found that high attrition rates were evident among Marine Corps platoon leaders who did not provide sufficient counseling and consideration behavior to new recruits. For high tenure individuals the socialization process has made them more sure of themselves and more comfortable with their environment. Additionally, the vested tenure and shorter time to retirement would tend to increase their career commitment intentions.

VI. RECOMMENDATIONS

The implications of this study suggest several recommendations for both military policy changes and research directions, as follows:

1. Military personnel who function in supervisory roles need to be provided with a clear image of the concept of leadership and its impact on follower attitudes and behaviors.

2. Military training of supervisory personnel needs to be reexamined with respect to content and application of leadership principles. Particular emphasis needs to be placed on those supervisory personnel involved with low organization tenure individuals.

3. Additional research and policy changes need to be accomplished which would isolate and reduce the primary irritants which serve to decrease career commitment.

The first recommendation is a reaction to the apparent lack of specific definition given to the concept "leadership." As discussed in Section II of this study the emphasis of the term "military leadership" may be providing a generalized view of charismatic leadership while those supervising a group of enlisted personnel, officers, or civilians are losing the "battle" with respect to greater degrees of job dissatisfaction and lower retention rates. There are a few glimpses in the military literature of the potential emergence of a more micro-oriented approach to leadership.

> One cannot lead organizations; one must lead individuals. Each follower must feel some linkage with the leader. The inspiration that comes from proper leadership can harness the will of individuals to undertake tasks that may appear impossible (Sarkesian, 1981, p. 246).

and, in a U.S. Army 1985 White Paper <u>Leadership Makes the Difference</u>,

> Leaders must show genuine concern for the individual's well-being and his ability to survive on the battlefield or succeed in the workplace. It is essential for a leader to care. Caring means . . . talking with and listening to subordinates, not simply talking at them; . . . teaching individuals by counseling, not by abusing them. Caring means fostering a command climate where people are challenged, where they feel their contributions make a difference, and where they feel good about themselves . . . (Marshall, 1985, p. 8)

The concern stated in the second recommendation for training supervisory personnel is the recognition of the need to equip them with the skills to handle various situations, to be able to diagnose the critical problems, and provide an appropriate leader-oriented remedy to the situation--not to react with the same directives in the same manner for any situation, perpetuating an image of control but obtaining less than adequate results. Particular attention needs to be addressed to the directing/handling/coaching/counseling of new recruits and those individuals early in the socialization process who do not yet feel comfortable or productive in their environment.

The third recommendation concerns the need to continue the research effort of examining the variables that contribute to both low satisfaction and career commitment intentions. Data analyzed from this study indicated that 52% of the officers and 61% of the civilians responded, with respect to career commitment, that they would most likely not make the Air Force a career. Additional research effort is needed to provide, for example, greater insight into differences in behaviors and attitudes among both functional areas (operations, maintenance, resource) and personnel cate-

gories (officers, enlisted, civilian). On-going programmatic research can provide the key to expanded knowledge and improved professional development of military service personnel.

REFERENCES

1. Bass, B.M. *Stogdill's handbook of leadership: A survey of theory and research*. New York: Free Press, 1981.

2. Buck, S.J. & Korb, L.J., (Eds.). *Military leadership*. Beverly Hills: Sage, 1981.

3. Finstuen, K. & Berry, G. Air Force attrition research: Analysis of pre- and post-enlistment factors. In H. Sinaiko et al (Eds). *Military personnel attrition and retention research in progress* (TR-10). Washington: Smithsonian Institution, 1981.

4. Fleishman, E.A. & Harris, E.F. Patterns of leadership behavior related to employee grievances and turnover. *Personnel Psychology*, 1962, *15*, 43-56.

5. Graen, G.B., Liden, R.C., & Hoel, W. Role of Leadership in the employee withdrawal process. *Journal of Applied Psychology*, 1982, *67*:6, 868-872.

6. Hall, D.T. *Careers in organizations*. Pacific Palisades, Calif.: Goodyear, 1976.

7. Hendrix, W.H. & Halverson, V.B. *Organizational survey assessment package for Air Force organizations* (AFHRL-TR-78-93). Brooks AFB, TX: Air Force Human Resources Laboratory, 1979.

8. Herman, J.B., Dunham, R.B. & Hulin, C.L. Organizational Structure, demographic characteristics, and employee responses. *Organizational Behavior and Human Performance*, 1975, *13*, 206-232.

9. Hightower, J.M. & Short, L.O. *Factor Stability of the Organizational Assessment Package* (LMDC-TR-82-1). Maxwell AFB, AL: Leadership and Management Development Center, 1982.

10. Hunt, J.G. & Blair, J.D. (Eds.). *Leadership on the future battlefield*. McLean, VA.: Pergamon-Brassey, 1985.

11. March, J.G. & Simon, H.A. *Organizations*. New York: Wiley, 1958.

12. Marshall, G.C. *Leadership makes the difference*. (White Paper, DA Pamphlet 600-50). Washington: Department of the Army, 1985.

13. Mobley, W.H. Intermediate linkages in the relationship between job satisfaction and employee turnover. *Journal of Applied Psychology*, 1977, *62*, 237-240.

14. *Proceedings of the ninth symposium: Psychology in the Department of Defense*. Colorado Springs: United States Air Force Academy, 1984.

15. Sarason, I.G. Psychological approaches to Marine Corps recruit attrition. In H. Sinaiko et al (Eds.) Military personnel attrition and retention research (TR-10). Washington: Smithsonian Institute, 1981.

16. Sarkesian, S.C. A personal perspective. In J.H. Buck, & L.J. Korb (Eds.), Military leadership. Beverly Hills: Sage, 1981.

17. Short, L.O. The United States Air Force Organizational Assessment Package (LMDC-TR-85-2). Maxwell AFB, AL: Leadership and Management Development Center, 1985.

18. Spencer, D.G. & Steers, R.M. Performance as a moderator of the job satisfaction-turnover relationship. Journal of Applied Psychology, 1981, 66, 511-514.

19. Steers, R.M. & Mowday, R.T. A model of voluntary employee turnover. In L. Cummings & B. Staw (Eds.). Research in organization behavior (Vol. 3). Greenwich, CT: JAJ, 1981.

20. Stokebury, J.L. Leadership as an art. In J.H. Buck & L.J. Korb (Eds.), Military leadership. Beverly Hills: Sage, 1981.

21 Stoloff, P.H., Lockman, R.F., Allbritton, A.S. & McKinley, H.H. An analysis of first-term reenlistment intentions (CRC 232). Arlington, VA.: Center for Naval Analysis, 1973.

22. Taylor, R.L. & Rosenbach, W.E. (Eds.). Military leadership: In pursuit of excellence. Boulder, Colorado: Westview, 1984.

23. Van Fleet, D.D. & Yukl, G.A. Military-leader behavior: Past, present, and future. In J.G. Hunt & J.D. Blair (Eds.), Leadership on the future battlefield. McLean, VA.: Pergamon-Brassey, 1985.

24. Vecchio, R.P. Predicting employee turnover from leader-member exchange: A failure to replicate. Academy of Management Journal, 1985, 28:2, 478-485.

25. Washbush, J.B. Leadership instruction and officer candidates: Some unholy thoughts. In Proceedings of the ninth symposium: Psychology in the Department of Defense. Colorado Springs: United States Air Force Academy, 1984.

26. Yoos, C.J., II. There is no such thing as leadership! In Proceedings of the ninth symposium: Psychology in the Department of Defense. Colorado Springs: United States Air Force Academy, 1984.

27. Youngblood, S.A. 7 Mobley, W.H. Organizational socialization: A longitudinal analysis of attitude change, turnover, and reenlistment in the military. Columbia, S.C.: Center for Management and Organizational Research, University of South Carolina, 1981.

	M	SD	1	2	3	4	5
1. Overall Leadership	4.79	1.46	(.97)				
2. Instrumental Leadership	4.78	1.54	.96	(.93)			
3. Supportive Leadership	4.75	1.47	.90	.83	(.83)		
4. Job Satisfaction	5.07	1.16	.50	.47	.54	(.81)	
5. Career Commitment	3.74	1.31	.15	.15	.20	.31	
6. Organization Tenure	4.88	1.87	.01	.03	.08	.10	.48

Notes: N = 31,980
Reliability coefficients are in parentheses in the diagonal.
All correlation coefficients above .02 are significant at the .001 level.

TABLE 1

Descriptive Statistics, Reliabilities, and Intercorrelations Among the Study Variables

Dependent Variable	Regression Variables	Interaction Effect R^2	ΔR^2	F
Job Satisfaction	OL, OT, OL x OT	.252	.000	0.07
Job Satisfaction	IL, OT, IL x OT	.229	.000	0.03
Job Satisfaction	SL, OT, SL x OT	.298	.000	0.39
Career Commitment	OL, OT, OL x OT	.256	.001	28.62*
Career Commitment	IL, OT, IL x OT	.254	.001	14.57*
Career Commitment	SL, OT, SL x OT	.264	.001	29.99*

Notes: df = 1, 21811
OL = Overall Leadership
IL = Instrumental Leadership
SL = Supportive Leadership
OT = Organization Tenure
*$p \leq .001$

TABLE 2

Results of Moderated Regression Analysis for Leadership Measures, Job Satisfaction, and Career Commitment

	Low Tenure	High Tenure
Job Satisfaction	4.94	5.23
Career Commitment	3.19	4.49
Overall Leadership	4.73	4.87
Instrumental Leadership	4.70	4.89
Supportive Leadership	4.62	4.93

Note: T-tests on the differences in the subgroup means indicate significance for all comparisons at the .001 level.

TABLE 3

Analysis of Variable Means by Low and High Organization Tenure Subgroups

AD-A166 177 UNITED STATES AIR FORCE SUMMER FACULTY RESEARCH PROGRAM 15/15
1985 TECHNICAL RE. (U) UNIVERSAL ENERGY SYSTEMS INC
DAYTON OH R C DARRAH ET AL. DEC 85 AFOSR-TR-86-0140
UNCLASSIFIED F49620-85-C-0013 F/G 5/1 NL

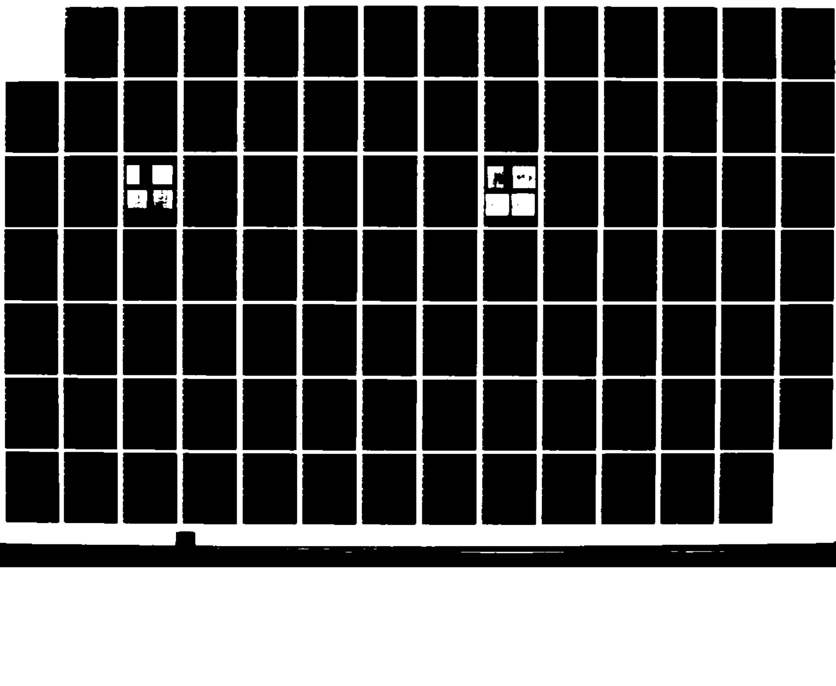

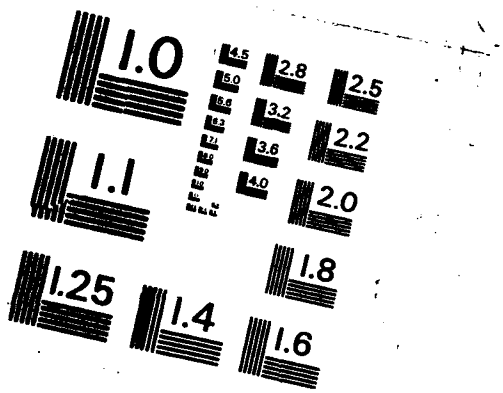

MICROCOPY RESOLUTION TEST CHART
NATIONAL BUREAU OF STANDARDS-1963-A

1985 USAF-UES SUMMER FACULTY RESEARCH PROGRAM/

GRADUATE STUDENT SUMMER SUPPORT PROGRAM

Sponsored by the

AIR FORCE OFFICE OF SCIENTIFIC RESEARCH

Conducted by the

UNIVERSAL ENERGY SYSTEMS, INC.

FINAL REPORT

A Review of Research Literature on the Measurement of Forces/Pressures on the Plantar Surface of the Foot During Gait Using Ambulatory Transducers

Prepared by:	Marion L. Noble
Academic Rank:	Professor
Department and University:	Physical Education, Kansas State University
Research Location:	Armstrong Aerospace Medical Research Laboratory, Biodynamic Effects Branch
USAF Research:	Dr. Leon E. Kazarian
Date:	July 1985
Contract No:	F49620-85-C-0013

A REVIEW OF RESEARCH LITERATURE ON THE MEASUREMENT OF FORCES/PRESSURES ON THE PLANTAR SURFACE OF THE FOOT DURING GAIT USING AMBULATORY TRANSDUCERS

by

Marion L. Noble

ABSTRACT

The development of an instrumentation system to inobtrusively measure the time course of forces/pressures on the plantar surface of the human foot during gait is the beginning of a multi-stage project that aims to increase the knowledge and understanding of bone deterioriation and its prevention during prolonged exposure to microgravity. The most expedient approach to this problem was to review the pertinent research literature so that the appropriate features of systems with similar requirements could be incorporated into the design of the system prior to the development stage. More than 100 studies were collected and reviewed with approximately half of them included in a written report. The report began with an overview of the nature of the various transduction methods including strain gauge, magnetoresistive, capacitive, piezoresistive, and piezoelectric transducers. Recommendations based on this review and the requirements of the measurement system to be developed were made.

ACKNOWLEDGEMENTS

The support for this project of the USAF Systems Command, Air Force Office of Scientific Research and the Armstrong Aerospace Medical Research Laboratory is acknowledged. Special appreciation is extended to the Biodynamic Effects Branch for giving me an opportunity to learn about their research program and the specific projects of great interest to me. Many individuals have treated me with consideration and respect during my tenure as a summer faculty fellow. Dr. Leon Kazarian, Dr. David Toth, Pat Roberts, Lou Muhic, Dr. Arnold Slonim, Clarence Oloff, and Suzanne Smith have taken the time to orient and inform me about research priorities of the branch and division at times when they had little time to give. Mary Agnes Mikalauskas was a tremendous help to me in the conduct of literature searches on which I spent most of my time. Mr. Gary Frank was an invaluable source of information regarding the conceptualization of the instrumentation system proposed in the final part of this report. He was always eager to share his knowledge and expertise with me and enabled me to considerably improve the design of the system. Finally, my gratitude is extended to Ms. Lisa Wooley, the Branch Secretary, who remained cheerful and efficient throughout my stay here even though my presence increased her workload considerably.

I. INTRODUCTION

My background is in the areas of sport biomechanics and sport physiology. My research during recent years has been focused on the mechanics of human movement, especially on skilled athletic performance. I have conducted and supervised research involving electromyographic, cinemetographic, and electronic instrumentation systems. Through my recent work on the forces imparted to the baseball bat during a skilled swing in collaboration with a professor in mechanical enginering specializing in experimental stress analysis I became familiar with strain gauge force transduction and other electronic force measurement systems. This expertise was subsequently applied in a series of studies which involved the measurement of baseball bat impact reaction impulses using strain gauge instrumentation. These projects, merged with years of experience in the cinematographic analysis of human movement, have resulted in a high level of expertise in a variety of human motion analysis techniques.

One of the research goals of the Biodynamic Effects Branch (BBD) of the Armstrong Medical Research Laboratory (AAMRL) is to identify the minimum effective stress for maintenance of bone remodeling. More immediate objectives are to: 1) develop a portable measurement system to accurately provide the pressure-time history of selected parts of the plantar surface of the foot; (2) to inobtrusively quantify these pressure patterns during daily activities, locomotion, and selected contrived activities; (3) to correlate chronic bone remodelling alterations with alterations in plantar stresses; and (4) to identify activities for those exposed to prolonged microgravity which will maintain bone remodeling. The initial phase of this project is the development of an instrumentation system that will provide a pressure time history of the pressure distribution on the plantar surface of the human foot.

The purpose of my selection to work in the BBD branch was to use my expertise and interests to develop an instrumentation system to meet requirements of the aforementioned research program. During the pre-summer visit, I accepted the responsibility of identifying a system already available and assist the BBD in modifying the system to meet specifications. However, no system available for purchase was found with elements that could meet research standards of accuracy and adaptability. Consequently, my task was modified to that of conducting a comprehensive, world-wide literature search of studies involving the measurement of forces/pressures on the plantar surface of the foot during gait. Only those studies involving ambulatory transducers were selected for review because force platforms, pressure mats, and other such stationary devices were deemed inappropriate for use in this project.

II. OBJECTIVES OF THE RESEARCH EFFORT

The objective of this research effort was to conduct a comprehensive, world-wide search related to the measurement of stresses on the plantar surface of the human foot during gait using ambulatory transducers. This effort purported to identify elements, procedures, and other relevent information that would be beneficial in the development of an instrumentaton system that would provide a stress-time history of selected parts of the human foot during all daily activities such as walking, working, exercising and riding in an automobile. The most important feature of the system to be developed is that it be portable and not interfere with normal movement patterns. Also, the system must be adaptable to measure stresses on selected sites of the human and primate foot with a spatial resolution of approximately 1 cm^2. Samples from each of 10 sites at rates varying from 1 to 500 sec^{-1} are required. Signal

processing features need to be adaptable to acquire, store, analyze and present data during very vigorous exercise and mild physical activity on earth as well as during space flight.

III. SUMMARY OF THE LITERATURE REVIEW

More than 100 research studies conducted during the past decade and involving the measurement of stresses on the plantar surface of the foot were collected and reviewed. Approximately one-half of these studies were not included in the final written report because the transducers were stationary. The review only included those studies involving portable transduction elements. Because of the length of the review, only the summary and list of references are included in this report.

The purpose of this review was to provide information to guide the selection and development of an instrumentation system to measure and record the time course of pressure distribution on the plantar surface of the human foot. Requirements of the system to be developed are:

1. The system must be completely portable and not interfere with normal movement patterns.
2. The system must be adaptable to measure pressures and/or forces on selected sites of the human and primate foot with a spatial resolution great enough to measure pressures on specific weight-bearing surfaces of the foot.
3. Samples from each of 5-10 sites at rates varying from 1 to 500 sec^{-1} are required.
4. The system must be sufficiently versatile to acquire, store, and present data taken during slow movements of long duration as well as vigorous movements of short duration.
5. Pressure resolution greater than 1 KPa on observations ranging from 5 kPa to greater than 1 MPa is desired.

Systems using bonded resistance strain gauges, magnetoresistive elements, piezoresistive materials, piezoelectric materials, and capacitive elements as force or pressure transducers were found in recent research studies.

Two devices were identified which may be useful in recording medio-lateral and anterior-posterior shear forces: (1) one using strain gauge elements in the fore and aft portions of a shoe (Spolek, Lippert, and Kirkpatrick, 1975) and (2) another which attached to the foot and consisted of a semi-conductor coil and a small magnet mounted on another disc (Tappin, Pollard and Beckett, 1980).

Many measurement systems using piezoelectric, peizoresistive, strain gauge, and capacitive transducers were reported in the research literature. A majority of the systems were developed for clinical use and do not meet the requirements of accuracy for research purposes. The inherent properties of capacitive and piezoresistive elements limit their accuracy to faithfully transduce rapidly changing forces or pressure. This limits their value for research studies where accurate force or pressure measurement during vigorous movements is required. Recently transducers of this type which meet research standards have become available, but no studies have been found wherein they were used.

Strain gauges have been shown to meet required research standards of accuracy when the appropriate base material and circuitry are used. However, these elements have not been constructed small enough so that they can be placed in the shoe insole or directly onto the surface of the foot and maintain acceptable standards of accuracy. While some transducers of this type have been developed and used for in-shoe use, accuracy has been compromised to the extent that their use for research purposes is limited.

Piezoelectric ceramic elements have emerged during the past decade as a very accurate pressure transducer and appears to be the transducer of choice for studies where accurate measurement of pressure on the foot

during vigorous, short-duration movements are required. The pyroelectric nature of these materials and their very short time constant have been obstacles to their use for events of more than a few seconds in duration. However, very recent improvements in the signal conditioning circuitry seem to have overcome some of these problems.

These transducers have been flush-mounted into the insole of shoes and have been attached directly to the foot. The former application method may be prepared if the elements can be effectively placed beneath the primary weight-bearing areas of the foot. Attachment of transducers to the foot will tend to alter the profile of the planter surface of the foot, even though they are only from 1 to 3 mm in thickness. This altered profile will undoubtedly modify the pressure distribution pattern.

One very recent study (Hennig, 1985) compared the characteristics of capacitive and piezoelectric transducers. The piezoelectric ceramics were demonstrated to be vastly superior in all rated responses, including range of pressure, transducer deformation, frequency response, linearity, hysteresis, and resolution. The only shortcoming of the piezoceramic transducers was that, due to their limited time constant, accurate measurements can only be assured for loads of duration of two seconds or less.

Three studies were found which used telemetry equipment to transfer the signals from the subject to storage, anlaysis and display units. Signals from capacitive, strain gauge, and piezoceramic transducers using as many as 8 channels of data have been used.

Signal storage and processing equipment has improved tremendously in recent years. During the last decade these research studies have

reflected this change. More recent studies have used data storage elements with very large capacities. Data are later accessed and processed with micro- or mini computers. This procedure seems to have replaced the use of the oscillographic recorder as the preferred processing unit.

VI RECOMMENDATIONS

The basic design and features of two proposed measurement system that will meet the requirements of the research project identified in the preparatory portion of this report is presented below.

Design of System to Measure Pressures on Six Selected Sites

This design incorporates the appropriate features of the systems used in the various studies reviewed. This system is designed to provide a pressure/time history of six selected sites on the plantar surface of the foot. Simultaneous measurement of shear force will interfere with the measurement of stresses normal to the foot surface. Consequently, they are not included in the system design.

The base of any measurement system is the transducer. Piezoceramic crystals are the transducer of choice if high accuracy of short-duration events (less than 3 s) are to be measured. However, problems with slowly changing signals of long duration are very difficult to overcome. On the other hand, capacitive transducers are very suitable for measuring static and slowly changing loads. However, transducers that have been reported in the literature suffer from high grave linearity and hysteresis problems when used on high frequency signals. Strain gauges appear to be the best transduction element to accurately measure signals that transcend the frequency range of the signals to be measured in this project. Therefore, use of discs (200 mm diam., 2 mm thick) with a flexible metal top surface as the sensing element is recommended.

Strain gauges are bonded to the bottom surface of this membrane to form a Wheatstone Bridge Circuit. The output is linearly related to the total pressures normal to the top surface of the disc.

Mounting of the transducers in a rubber insole is recommended so that the profile of the foot is not changed. Transducers will be located beneath the (1) center of the distal aspect of the proximal phalanx of the hallux, (2) second metatarsal head, (3) first metatarsal head, (4) fifth metatarsal head, (5) lateral heel condyle, and (6) medial heel condyle. These sites are shown in Figure 1. Each transducer will be flush mounted in a rubber insole 2 mm thick. This arrangement will allow the shoe to be comfortably worn continously for extended periods of time. Wires from the transducers will be routed underneath the insole to a junction box on the heel of the shoe. Figure 2 shows a block diagram of the idealized system. Wires will be connected to the junction box, run up the leg, and connected to a signal conditioner box worn in a belt pack. Output from each channel will then be routed to the multiplexor/encoder/transmitter unit. The encoded signals may either be interfaced in parallel to the microcomputer or multiplexed. The multiplexed signal may be recorded in digital form with a high frequency tape recorder and later transferred to the computer for storage or analysis. A second option is to telemeter the multiplexed system using FM pulse code modulation equipment. If the telemetry option is used, the signal is received and either recorded with a portable tape recorder or sent directly to the microcomputer. Once the data are stored on floppy or hard disk, analysis, hard copy output, and/or graphic display are accomplished. Of course, appropriate software to enable this final process will need to be developed. The strong feature of this system is

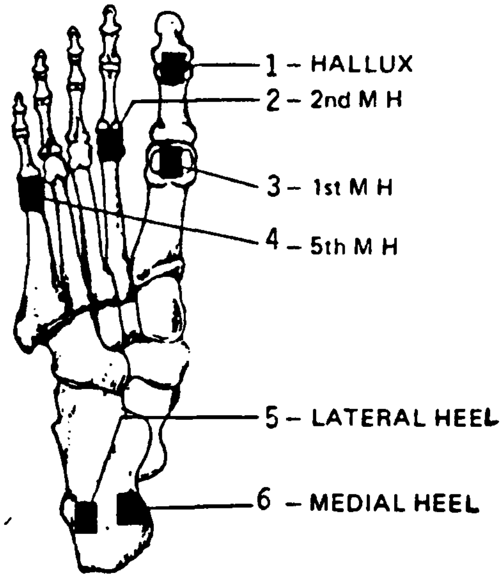

Figure 1. Proposed transducer sites.

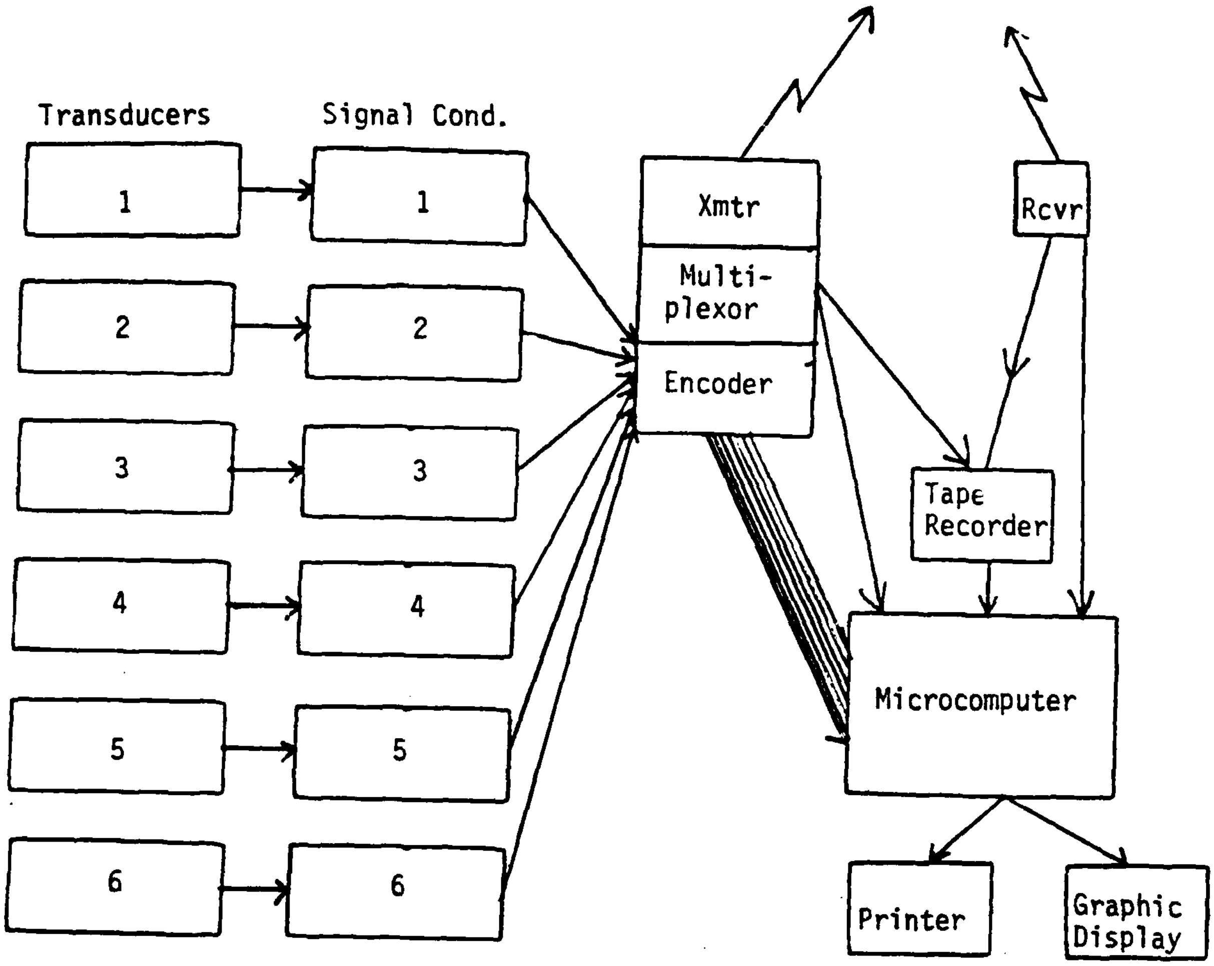

Figure 2. Block diagram of instrumentation system.

that it allows measurements to be made in a natural state to a very great extent. However, some of the signal fidelity may be compromised by use of the tape recorder. This system would allow the received signal to be routed directly into the microcomputer. No additional elements are required.

The modular design of the system will allow this modification to be easily made by simply disconnecting and removing the transmitter from the belt pack and connecting the unit directly to the input port of the demultiplexing card installed in the microcomputer. This modification may be desirable when high signal fidelity and sampling rates are desired and/or when there are problems of interference with the radiotelemetry signals. Yet another modification of this system is to place the recording unit in the belt pack and record processed data over an extended period of time. Data would be retrieved and analyzed at a later time using this modification.

Development Approach

A mini-proposal will be written to initiate the development of the measurement system described above. This proposal will involve the expertise of the author and a colleague and graduate student in the department of Mechanical Engineering at Kansas State University. It is fortunate that the micro-computer and choice of the USAF and Kansas State University is the Zenith. Thus, the prototype unit and software that will be developed at Kansas State University will be immediately usable in the BBD. Also, data collected at Kansas State University can be stored on floppy disks and sent to the BBD during later stages of this project.

The expedient development of this measurement system is crucial to the research objectives of the BBD. Also, the BBD has a very competent group of technicians, engineers, and scientists with expertise and measurement capability to observe a variety of phenomena. The interaction of these personnel with those contracting services to conduct various portions of this project is essential. If more than one contractor is to be involved in this project as it proceeds from phase to phase, periodic meetings and seminars with the different people involved are recommended. This will promote interchange, maintain continuity, and result in greater progress toward the project goals.

V. REFERENCES

Bauman, J. H. and Brand, P. W. (1963). Measurement of pressure between foot and shoe. Lancet, 1, 629-632.

Brewer, V., et. al. (1983). Role of exercise in prevention of involutional bone loss. Medicine and Science in Sports and Exercise, 15, 445-449.

Brown, T. D. and Muratori, D. R. (1979). Miniature piezoresistive transducers for transient soft-body contact-stress problems. Experimental Mechanics, 19, 214-219.

Cavanagh, P. R., Hennig, E. M., Bunch, R. P. and Macmillan, N. H. (1983). A new device for the measurement of pressure distribution inside the shoe. In: H. Matsui and K. Kobayashi (Eds.), Biomechanics VIII-B (pp. 1089-1096). Champaign, Illinois: Human Kinetic Publishers.

Collis, W. J. M. F. and Jayson, M. I. V. (1972). Measurement of pedal pressures. Annals of Rheumatoid Disorders, 31, 215-217.

Durie, N. D. and Shearman, L. (1979). A simplified limb load monitor. Physiotherapy Canada, 31, 28-31.

Eggeman, G. W. and Noble, M. L. (1985). "Design and testing a baseball-bat transducer," Experimental Techniques, 9, 20-23.

Ekstrom and Karlsson, J. (1985). Direct force measurement in biomechanical investigations. In Winter, D. A., et. al. (Eds.) Biomechanics IX-B (pp. 201-205). Champaign, Illinois: Human Kinetic Publishers.

Elftman, H. (1934). A cinematic study of the distribution of pressure in the human foot. Anatomical Record, 59, 481-491.

Frankel, V. H. and Nordin, H. (1980). Basic Biomechanics of the Skeletal System. Philadelphia: Lea and Febiger. pp. 52-60.

Frost, R. B., and Cass, C. A. (1981). A load cell and sole assembly for dynamic pointwise vertical force measurement in walking. Engineering in Medicine, 10, 45-50.

Fung, Y. C. (1984). Biomechanics: Mechanical Properties of Living Tissue. New York: Springer-Verlay New York, Inc. pp. 383-397.

Geddes, L. A. and Baker, L. E. (1975). Principles of Applied Biomedical Measurement (2nd Ed). New York: John Wiley and Sons.

Gindy, S. S. (1985). Force and torque measurement, a technology overview: Part I-Force. Experimental Techniques, 9, 28-33.

Hargreaves, P. and Scales, J. T. (1975). Clinical Assessment of gait using load measuring footwear. Acta Orthopedics Scandinavia, 46, 877-895.

Hennacy, R. A. and Gunther, R. (1975). A piezoelectric crystal method for measuring static and dynamic pressure distributions in the feet. Journal of American Podiatry Association, 65, 444-449.

Hennig, E. M. (1985). Piezoelectric and capacitive pressure distribution techniques and their application in rehabilitation and industry. In Ortengren, R. (ed.). Applications of Biomechanics Proceedings, Linkoping, Sweden, pp. 25-27.

Hennig, E. M., Cavanagh, P. R. and Macmillan, N. H. (1983). Pressure distribution measurement by high precision piezoelectric ceramic force transducers. In: H. Matsui and K. Kobayashi (Eds.), Biomechanics IVIII-B, pp. 1081-1088. Champaign, Illinois: Human Kinetic Publishers.

Hennig, E. M., Cavanagh, P. R., Albert, H. T. and Macmillan, N. H. (1982). A piezoelectric method of measuring the vertical contact stress beneath the human foot. Journal of Biomedical Engineering, 4, 213-222.

Hennig, E. M., Cavanagh, P. R. and Macmillan, N. H. (1981). Human Locomotion I. Proceedings: Canadian Society of Biomechanics, 120-121.

Holden, T. S. and Muncey, R. W. (1953). Pressures on the human foot during walking. Australian Journal of Applied Science, 4, 405-417.

Kljajc, J., Krajnic, J. and Stopar, M. (1985). Relevance of ground reaction pattern for gait analysis and its measurement by force shoes. In Winter, D. A., et. al. (Eds.) Biomechanics IX-B (pp. 196-200). Champaign, Illinois: Human Kinetic Publishers.

Kobayashi, A. S. (Ed.) (1983). Manual on Experimental Stress Analysis (4th ed.). Brookfield Center, Connecticut: Society for Experimental Stress Analysis.

Langer, S., Polchaninoff, M. and Hoerner, F. (1984). Principles and Fundamentals of Clinical Electrodynography. Prepublication Manuscript.

Lereim, P. and Serck-Hanssen, F. (1973). A method of recording pressure distribution under the sole of the foot: Bulletin of Prosthetic Research, 10, 118-125, Fall.

Levin, R. C. et. al. (1976). A system for the measurement of vertical foot forces. Proceedings of 2nd Conference on the Systems and Devices for the Disabled, pp. 104-108.

Leach, C. S., Altchuler, S. I., and Cintron-Trevino, N. M. (1983). The endocrine and metabolic responses to space flight. Medicine and Science in Sports and Exercise, 15, 432-440.

Lord, M. (1981). Foot pressure measurement: A review of methodology. Journal of Biomedical Engineering, 3, 91-99.

Lord, M. and Smith, D. M. (1983). Static response of a simple piezoelectric load cell. Journal of Biomedical Engineering, 5, 162-164.

Mansour, L. M. (1977). Piezoelectric transducers for oral force monitoring. Journal of Medical Engineering and Technology, 1, 95-97, 110.

Minns, R. J. and Craxford A. D. (1984). Pressure under the forefoot in rheumatoid arthritis. Clinical Orthopaedics and Related Research, 187, 235-242.

Miyazaki, S. and Ishida, A. (1984). Capacitive transducer for continuous measurement of vertical foot force. Medical and Biological Engineering and Computing, 22, 309-316.

Miyazaki, S. and Iwakurai, H. (1978). Foot-force measuring device for clinical assessment of pathological gait. Medical and Biological Engineering and Computing, 16, 429-436.

Polchaninoff, M. (1983). Gait analysis using a portable, microprocessor-based segmental foot force measuring system. IEEE 1983 Proceedings of the Seventh Annual Symposium on Computer Applications in Medical Care. pp. 897-899.

Pollard, J. P., LeQuesne, L. P., and Tappin, J. W. (1983). Forces under the foot. Journal of Biomedical Engineering, 5, 37-40.

Pratt, L., Wardlaw, D. and McLauchlan, J. (1979). Load measurement in orthopaedics using strain gauges Journal of Biomedical Engineering, 1, 287-296.

Schwartz, R. P. and Heath, A. L. (1947). The definition of human locomotion on the basis of measurement. Journal of Bone and Joint Surgery, 29, 203-214.

Shereff, M. J., Bregman, A. M. and Kummer, F. J. (1985). The effect of immobilization devices on the load distribution under the foot. Clinical Orthopaedics and Related Research, 192, 260-267.

Soames, R. W. et. al. (1985). Foot pressure patterns during gait. Journal of Biomedical Engineering, 7, 120-126.

Soames, R. W., et. al (1982). Measurement of pressure under the foot during
function. Medical and Biological Engineering and Computing, 20, 489-495.

Spolek, G. A. and Lippert, F. G. (1976). An instrumented shoe - a portable force measuring device. Journal of Biomechanics, 9, 79-783.

Spolek, G. A., Day, E. E., Lippert, F. G. and Kirkpatrick, G. S. (1975). Ambulatory-force measurement using an instrumented-shoe system. Experimental Mechanics, 15, 271-274.

Tappin, J. W., Pollard, J. and Beckett, E. A. (1980). Method of measuring shearing forces on the sole of the foot. Clinical Physiology and Physical Measurements, 1, 83-85.

Tipton, C. M. (1983a). Considerations for exercise prescriptions in future space flights. Medicine and Science in Sports and Exercise, 15, 441-444.

Tipton, C. M. (1983b). Preface to weightlessness and the 1980s. Medicine and Science in Sports and Exercise, 16, 223-227.

Williams, J. A., et. al., (1984). The effect of long-distance running on bone mineral content. Medicine and Science in Sports and Exercise, 16, 223-227.

Wronski, T. J. and Morey, E. R. (1983). Alterations in calcium homeostasis and bone during actual and simulated space flight. Medicine and Science in Sports and Exercise, 15, 410-414.

1985 USAF-UES SUMMER FACULTY RESEARCH PROGRAM

Sponsored by the

AIR FORCE OFFICE OF SCIENTIFIC RESEARCH

Conducted by the

UNIVERSAL ENERGY SYSTEMS, INC.

FINAL REPORT

A SILICON VIDICON SYSTEM FOR PROFILING 1.06 μm LASER PULSES

Prepared by:	Dr. Robert M. O'Connell
Academic Rank:	Associate Professor
Department and University:	Department of Electrical and Computer Engineering
Research Location:	Air Force Weapons Laboratory Kirtland AFB, NM 87117
USAF Research:	Dr. Alan F. Stewart
Date:	September 30, 1985
Contract No.:	F49620-85-C-0013

A SILICON VIDICON SYSTEM FOR PROFILING 1.06 μm LASER PULSES

Robert M. O'Connell

ABSTRACT

A P.A.R. 1252E silicon vidicon and P.A.R. 1216 vidicon controller were interfaced to an RCI Trapix 5500 image processing system for the acquisition, display, and analysis of images of 1.06 um laser pulses. Requirements for the transmission and display of geometrically accurate images were established. It was found that a given pixel clock period and programmed channel time uniquely determine the channel length in pixels that must be programmed to maintain geometric accuracy. Measurements were made of the spatial uniformity and temperature dependence of the vidicon target's dark current and 1.06 um detection sensitivity. The results revealed acceptably low peak-to-peak variations of both dark current and sensitivity throughout the central 3 mm x 3 mm area of the target and an optimum signal-to-noise level at a target operating temperature near 0° C. Efforts to improve the pulsed linearity of the vidicon using the cathode voltage switching method showed that some improvement is possible with a cathode voltage of 6.5 volts. Before higher cathode voltages can be used, however, the Trapix display saturation level has to be raised. With a cathode voltage of 6.5 volts, the pulsed linear dynamic range of the vidicon is approximately 4.

ACKNOWLEDGEMENT

The author extends his thanks to the Air Force Systems Command, the Air Force Office of Scientific Research, and the Air Force Weapons Laboratory for a very enriching summer opportunity. He also thanks Dr. Alan Stewart for his invaluable technical advice.

I. INTRODUCTION

When pulsed, high-power lasers are used in laser damage tests of optical components, the results of the tests can be best understood if profiling information is available for every laser pulse fired. If the laser firings are spaced in time by approximately 30 seconds or more, and if the pulses are not focused to diameters much smaller than approximately 1 mm, certain opto-electronic imaging systems can not only provide the desired pulse-to-pulse profiling information, but they can do it in the time between pulses, thereby providing real-time feedback for subsequent power settings of the laser. A system to do this is currently being developed at the Air Force Weapons Laboratory (AFWL).

The Summer Faculty Research Fellow chosen to participate in the AFWL program has had prior research experience with laser damage generally and with beam profiling in particular. For example, beam profiling was an important component of a study of laser damage in plastics[1,2] and is currently the subject of a graduate student's thesis[3]. Thus the AFWL project was closely suited to the Fellow's interests and abilities.

The system studied during the Summer Fellowship is shown in Figure 1. The device under consideration was a P.A.R. 1252 E silicon vidicon, with the following attractive features:

i. a thicker target for enhanced sensitivity at 1.06 μm.

ii. a large (12.5 x 12.5 mm) target area.

iii. an anti-reflection-coated target to suppress moire' interference.

iv. a built-in refrigeration unit for cooled operation.

Communication with the vidicon was provided by a P.A.R. 1216 vidicon controller, which performed the following functions:

i. setting the vidicon scanning conditions, including channel length, channel time, and number of channels per frame.

ii. delivery of the non-standard video signal from the vidicon to the Trapix computer.

iii. providing a 4 MHz master clock and timing signals every channel and frame as control signals for image transmission from the vidicon to the computer.

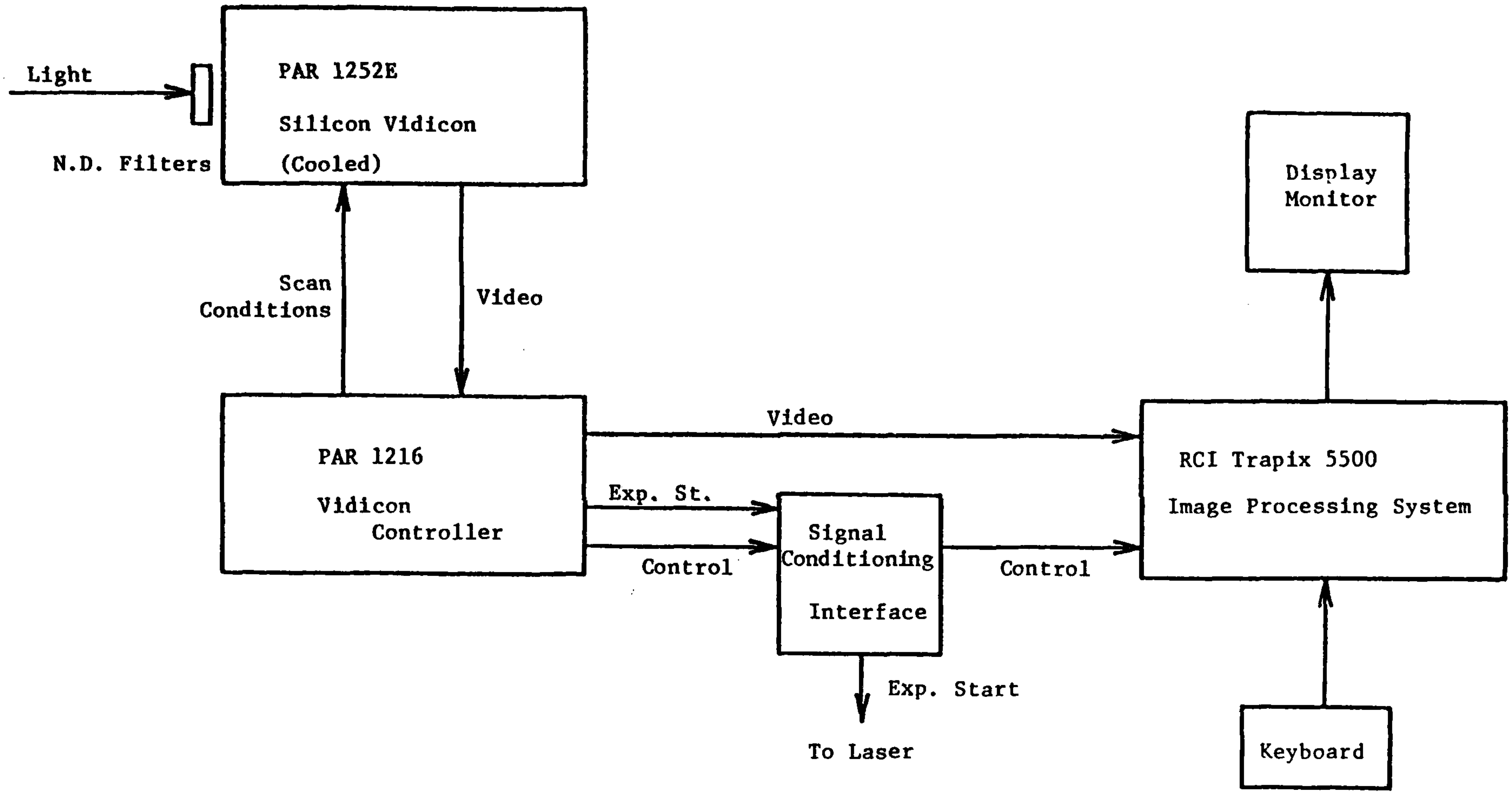

Figure 1. Silicon Vidicon Beam Profiling System

iv. providing a timing signal to fire the pulsed laser and transmit data after a set number of target-pre-equilibration frames.

An R.C.I. Trapix 5500 Image Processing System constituted the final major component of the system. It was used for the following:

i. to digitize, store, and display non-standard video images.

ii. to perform image processing/analysis operations such as pixel grey level averaging, image inversion, histograms, and profiles.

II. OBJECTIVES

In order to contribute to the development of a system for providing accurate, real-time two-dimensional beam profiles of high-power laser pulses, the following objectives were pursued during the project:

i. to develop an interface to permit the flow of data from the vidicon controller to the Trapix computer.

ii. to learn how to use the system to reproduce vidicon images on the Trapix display monitor with the least amount of geometric distortion.

iii. to measure the spatial variation and temperature dependence of vidicon dark current and detection sensitivity at 1.06 μm.

iv. to measure the linearity and dynamic range of the system under pulsed conditions at 1.06 μm.

The approaches taken to achieve these goals, and the results obtained in each case are discussed, in the order of their listing here, in the next four sections.

III. CONDITIONING INTERFACE FOR CONTROL SIGNALS

The vidicon reads images in the non-standard video format set by the operator via the controller. For the Trapix computer to accept the images, they must be transmitted via a pixel clock and synchronization signals for channels and frames. Furthermore, these three control signals must reach the computer in TTL compatible, differential form. After considering several alternatives, the 4.0 MHz master clock, the "clock out" signal, and the "trigger 1" signal, all provided

by the controller and shown in Figure 2, were used as the pixel clock and channel and frame synchronization signals, respectively. They were conditioned for the Trapix computer as shown in Figure 2.

In considering various clock sources, it was found that with the 4.0 MHz master clock from the controller, a certain interference signal, present in the displayed image with other clock sources, was eliminated. Presumably, this is because the clock out and trigger 1 signals are derived from, and thereby phase-locked to, the 4.0 MHz clock.

When the system is used in the pulsed mode, the vidicon target is allowed to pre-equiliberate for 15 "prep" frames at the programmed scanning conditions. The laser is then fired at the start of the next frame, which is transmitted to the Trapix computer. Since the computer is programmed to capture and store the first frame transmitted to it, image transmission from the controller to the computer must be delayed until the laser is fired. This is accomplished with the controller-provided "experiment start" signal, which turns on at the completion of the prep frames. Thus, as shown in the lower portion of Figure 2, after some conditioning, the experiment start signal fires the laser and enables the trigger 1 signal to flow to the differential driver. Delaying the frame synchronization signal this way inhibits transmission of data to the computer until the appropriate time.

IV. TRANSMISSION AND DISPLAY OF GEOMETRICALLY UNDISTORTED IMAGES

After becoming familiar with the entire system, it became clear that geometrically accurate reproduction of a vidicon image on the Trapix display monitor is not automatic with the flow of data. The following conditions must be met:

i. The display monitor must be adjusted, if necessary, for square pixels. The Trapix software program "ROZ" can be used to magnify the display eight times, making it easy to measure the dimensions of a 40 x 40 pixel region. The adjustment can be made with the pixel-width potentiometer VR 503.

ii. The controller must be programmed for symmetric image sampling, i.e., channels and pixels on the display monitor

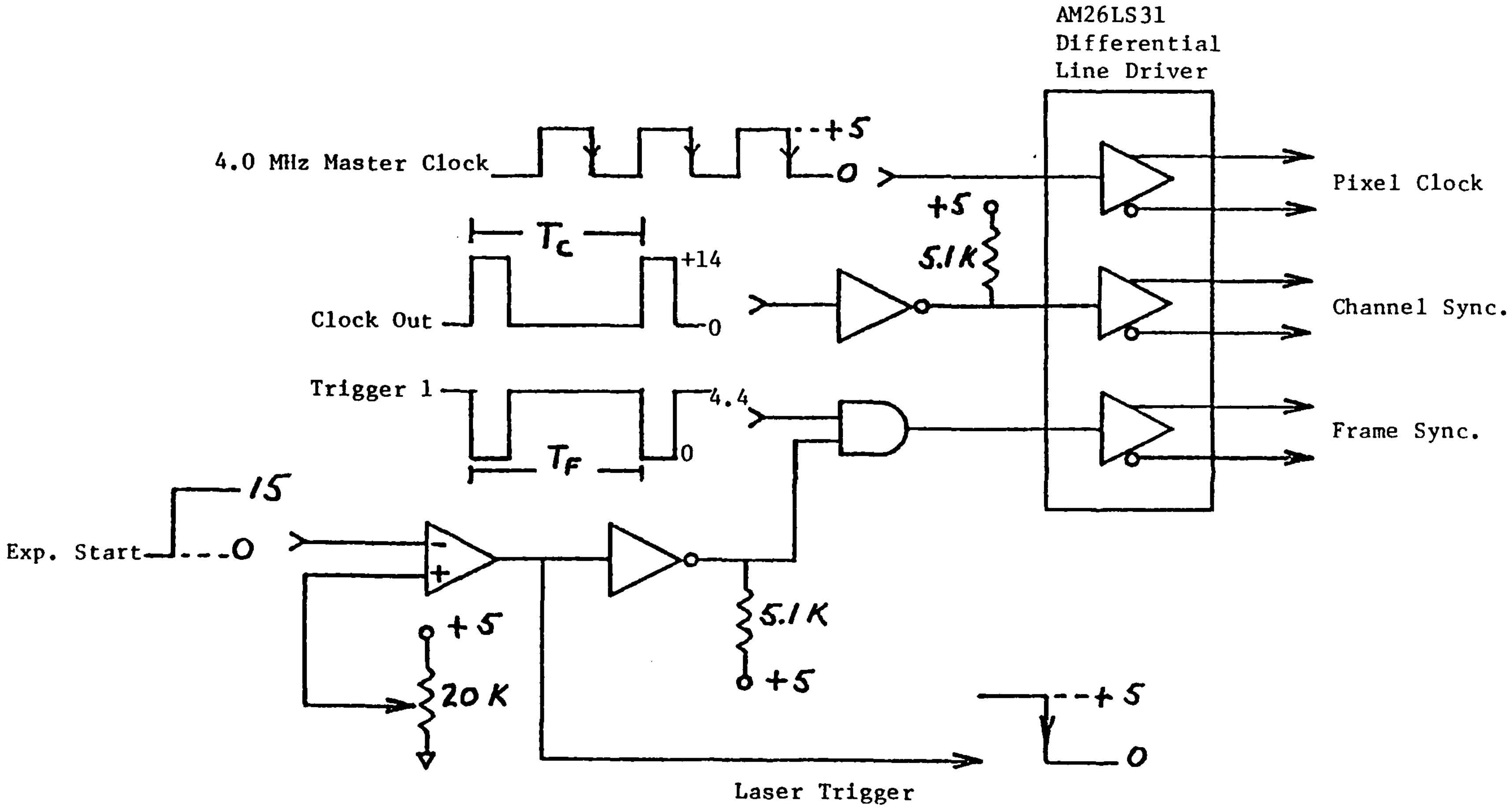

Figure 2. Image Transmission Interface: Signals and Conditioning Circuitry. T_C = Channel Time, T_F = Frame Time.

must correspond to channels and pixels on the vidicon target. The correspondence of channels is assured by the channel synchronization control signal, but pixel correspondence requires more care. Because one pixel of vidicon information is transmitted per period of the pixel clock, pixel correspondence is assured if the operator sets

$$N_C = N_T = (T_C - 10\ \mu sec)/Tcl \qquad (1)$$

where N_C = programmed channel length in pixels.

N_T = number of pixels transmitted per channel.

T_C = programmed channel time.

10 μsec = non-scanning retrace time each channel.

T_{Cl} = pixel clock period.

iii. Finally, the vidicon channel deflection voltage must be adjusted, if necessary, for symmetric image transmission. This can be accomplished by first satisfying steps i and ii, and then by displaying the image of a circular or square object and adjusting the vidicon channel deflection voltage for a circular or square image. The Trapix system program "CUR" can be used to surround the image with a rectangular cursor and count the number of pixels in the x and y directions.

Once the system has been adjusted as just described, the operator has a choice of seven channel times. For symmetric sampling, however, the channel length in pixels must be chosen to satisfy equation 1. Table 1 lists the seven channel times and then respective symmetric-sampling channel lengths.

TABLE 1. Channel Lengths in Pixels for Symmetric Image Sampling.

T_C(μsec)	20	40	60	80	100	120	140
N_C	40	120	200	280	360	440	520

Since the vidicon has a maximum of 512 pixels per channel, the 140 μsec channel time can not be used for symmetric sampling. The 20 μsec and 40 μsec channel times can be used, but the required channel lengths are so small that only rather small images are possible. Thus, it is recommended that only the channel times from 60 - 100 μsec be used for beam profiling measurements.

The photos in Figure 3, which show the circular image of a laser diode transmitted through an optical fiber onto the vidicon target, illustrate the effects of various choices of T_C and N_C on sampled image symmetry. The circular geometry of the object was verified by rotating it 90° (at any T_c, N_c pair) and observing no change in image dimensions. Note that in every photo the ratio of image dimensions Y/X is equal to the ratio of N_C/N_T, as expected.

V. DARK CURRENT AND 1.06 um DETECTION SENSITIVITY MEASUREMENTS

To be useful in two-dimensional beam profiling, the vidicon target's dark current and detection sensitivity at the wavelength of interest should be reasonably uniform throughout the region of interaction with the beam. Measurements of these properties were made using the following procedure:

i. Vidicon operation: T_C = 100 μsec, N_C = 512 pixels, target temperature T = 24° C, 0° C, -30° C.

ii. Illumination conditions: approximate uniform 1.06 μm illumination with a fiber-optic illuminator 1 meter from the target, plus frosted glass and a 1.06 μm band pass filter at the target aperture. Use the *same illumination* level at all three temperatures. Avoid saturation of Trapix pixels.

iii. Dark current conditions: Using vidicon signal as an indicator, verify that no measurable stray light enters the vidicon by covering and uncovering the unilluminated vidicon aperture. Thus background and dark current are identical.

iv. Data acquisition and analysis: Save illuminated and dark current frames at each temperature. Use Trapix software to calculate the mean grey level (0-83) in each of 63 equally spaced 27 x 27 pixel cells throughout each frame. Subtract dark current values from corresponding illuminated-cell values for corrected signal values.

This procedure results in a pair of maps such as those shown in Figure 4 for the case of a target temperature of 0° C. Similar results were obtained at 24° C and -30° C. In all cases, target response is maximum in the center, illustrating the greater efficiency of the reading electron beam in that portion of the target.

A) Symmetric Sampling: T_C=80 μsec, N_C = 280 pixels.

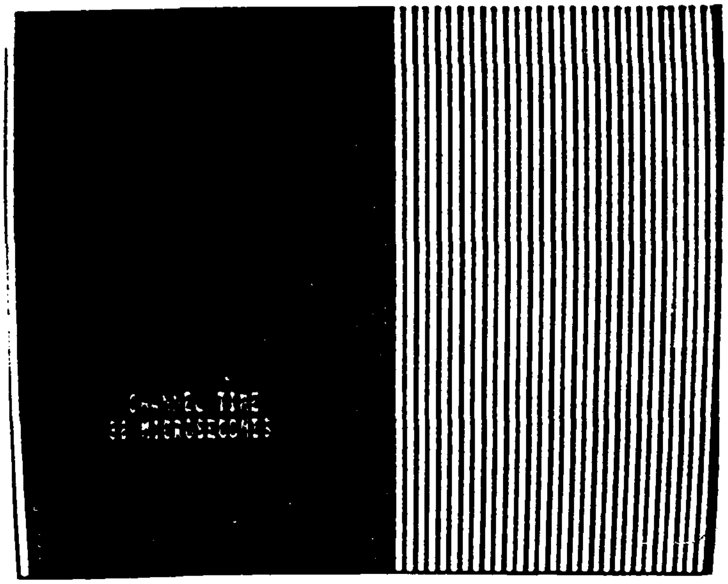

B) Symmetric Sampling: T_C=100 μsec, N_C = 360 pixels.

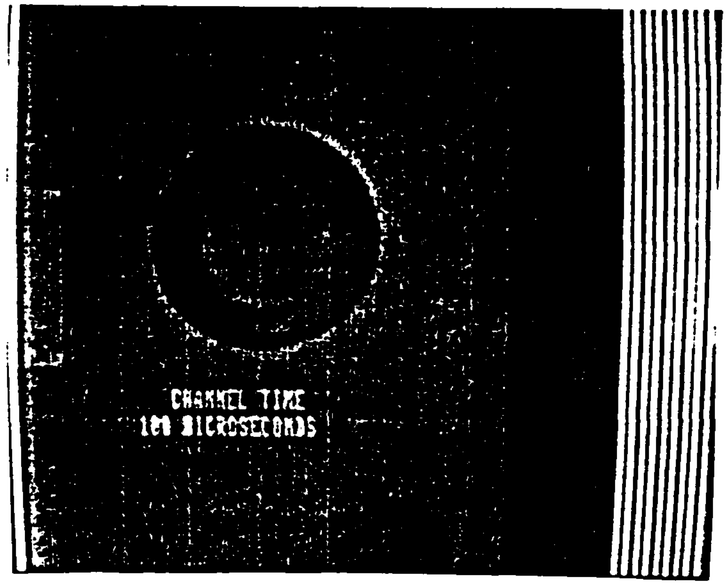

C) Uundersampling: T_C = 100 μsec, N_C = 512 pixels

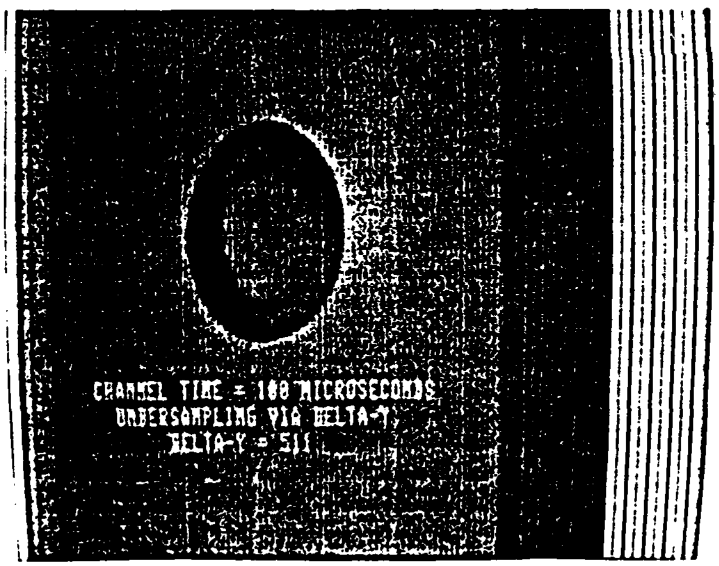

D) Oversampling: T_C = 100 μsec, N_C = 254 pixels.

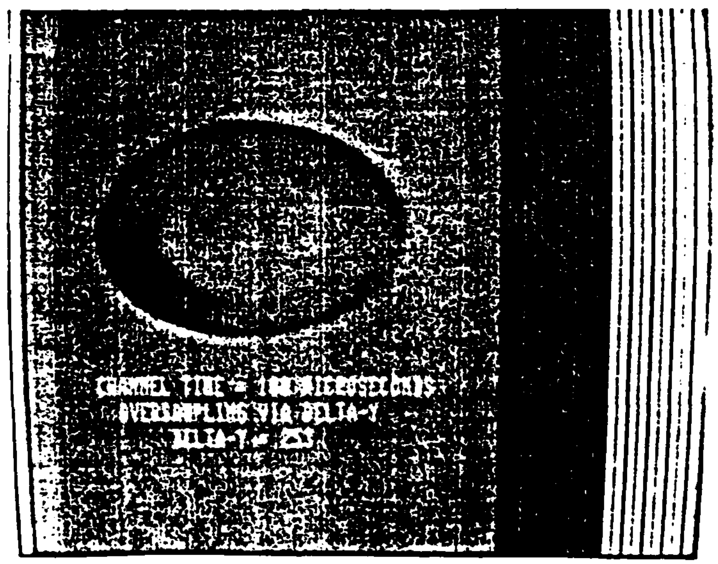

Figure 3. Effects of Controller Programming on Image Symmetry. For Symmetric Sampling, Set $N_C = N_T$. For Undersampling, $N_T < N_C$, so Set $N_C > N_T$. For Oversampling, $N_T > N_C$, So Set $N_C < N_T$. In Each Photo, The X Dimension of the Uniform Background to Each Image is Proportional of N_C.

DARK CURRENT

14.3	14.9	15.3	15.0	15.1	14.6	15.0
14.5	15.1	15.5	15.2	15.3	14.8	15.2
14.5	15.1	15.4	15.1	15.3	14.7	15.2
14.6	15.3	15.6	15.3	15.4	14.9	15.3
15.0	15.6	16.0	15.7	15.9	15.4	15.7
14.7	15.3	15.7	15.4	15.7	15.2	15.5
15.4	16.0	16.2	15.9	16.2	15.8	16.0
15.0	15.4	15.6	15.4	15.6	15.2	15.6
14.6	15.7	15.7	15.4	15.7	15.4	15.7

BACKGROUND - CORRECTED SIGNAL

27.6	35.1	37.0	37.4	37.0	35.9	34.5
27.2	34.9	36.8	37.0	36.7	35.7	34.2
27.3	34.9	36.9	37.2	36.7	35.8	34.3
27.3	34.7	36.7	37.1	36.7	35.6	34.1
27.1	34.6	36.7	37.0	36.2	35.6	34.0
26.8	34.6	35.9	36.5	36.5	35.2	33.2
25.9	33.0	34.4	35.1	34.5	33.0	30.2
26.3	32.8	34.5	34.8	33.7	31.3	29.0
25.7	32.3	32.9	32.1	30.3	29.0	28.3

Figure 4. Mappings of Vidicon Target Dark Current and Background - Corrected Signal in Trapix Grey Levels (0-83) at T=0^{o}C. Bracketed 3X4 Cell Region Corresponds to Central 3.75 X 3.13 mm Region of the Target.

Peak-to-peak variations of the data in Figure 4 are summarized in Table 2, both for the entire target and for its central 3.75 mm x 3.13 mm region.

Table 2. Peak-Peak Variation of Target Response at T = 0° C

	Dark Current	Corrected Current
Whole Target	11.7%	31.3%
Central 3.75 x 3.13 mm	5.6%	3.5%

The numbers in Table 2 suggest that while the whole-target variations are rather excessive, those in the central 3.75 x 3.13 mm region, an area large enough to profile many typical laser beams, are quite acceptable.

The temperature dependence of target sensitivity was established using data from dark current / corrected signal maps (as in Figure 4) measured at the temperatures 24° C, 0° C, and -30° C. The results, plotted in Figure 5, show that while the target signal decreases quite linearly with cooling over the entire 3-temperature range, the dark current improves very little below 0° C. The widest gap between the two curves is in the vicinity of 0° C, thus indicating an optimum signal-to-noise ratio at that temperature.

VI. PULSED MEASUREMENTS AT 1.06 μm

The intended application of the system is to be in profiling 1.06 um pulses from a Nd:Yag laser. The main drawback to the use of vidicons in pulsed applications is a nonlinear response due to the "lag" inherent in all electron beam readout devices[4]. To combat this problem, the method of "cathod-voltage-switching"[5] was incorporated into the system[6], and measurements made to determine its effects on the pulsed-mode linearity of the vidicon. Data were taken according to the following prescription:

i. Vidicon operation: T_C = 100 usec, N_C = 360 pixels for symmetric image sampling, target temperature T = 24° C, 0° C, -30° C.

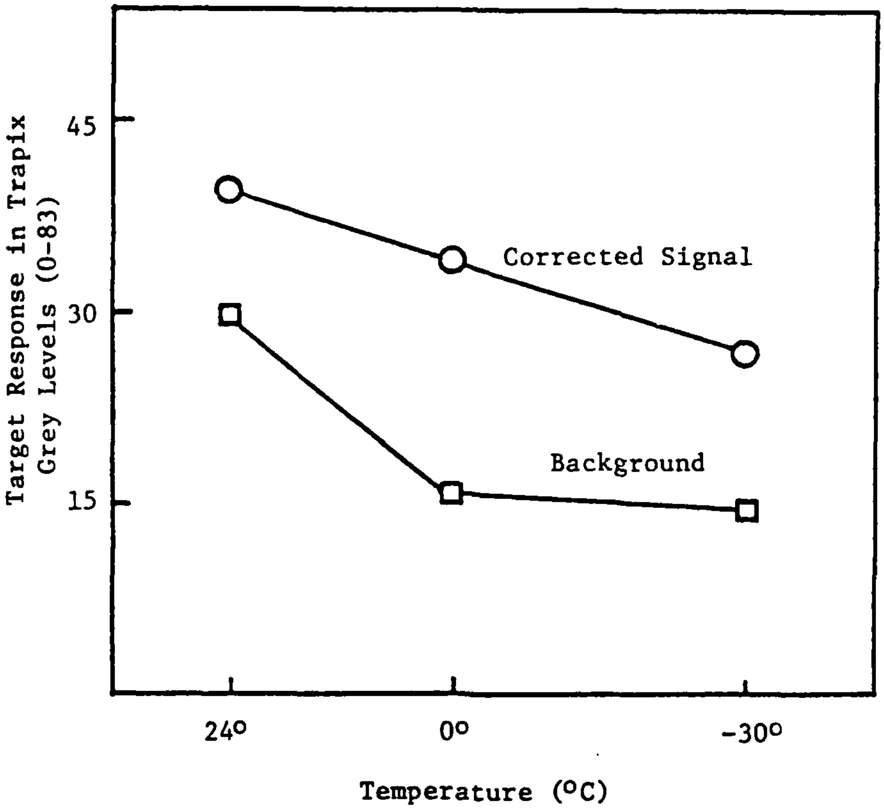

Figure 5. Temperature Dependence of Target Response Using Mean Data from Three Adjacent 27X27 Pixel Cells near the center of the Target

ii. Illumination conditions: Q-switched Nd:Yag laser, pulse width 5 nsec, wave plate attenuator, beam focused to approximately 1 mm diameter on the vidicon target.

iii. Data acquisition: Program the controller to pre-equilibrate the vidicon target for 15 frames, fire the laser at the start of the next frame, transmit that frame to the Trapix computer for storage and analysis.

Results of measurements made with the target temperature at 0° C are shown in Figure 6. Similar results were obtained at 24° C and -30° C. The inset in the figure illustrates the method used to extract vidicon response values from the pulse images.

The V_2 = 6.5 volt curve in Figure 6 shows that significant improvement is possible with cathode voltage switching. The lower end of the curve is still non-linear, however, suggesting that further improvement may be possible with higher cathode voltages. The least encouraging feature of the data in Figure 6 is that it reveals a dynamic range of only approximately 4. But this could also improve with higher cathode voltages.

Each point on the curves of Figure 6 represents the average of approximately ten laser pulses. Pulses were not used in the statistics if they caused saturation of even one pixel on the display monitor. Thus the saturation obvious on the V_2 = 5.0 volt curve (no cathode voltage switching) and possibly just beginning on the V_2 = 6.5 volt curve are evidence of vidicon target saturation. (Different target saturation levels are expected with different cathode voltages, because the cathode voltage controls target saturation[4]). The saturation level of the display pixels was not much higher, however, because with relative pulse energies higher than the upper level shown in Figure 6, significant numbers of display pixels did saturate. This is why the upper end of the V_2 = 6.5 volt curve is not extended further. If cathode voltage switching is to be studied further with this system, it will be necessary to raise the display monitor pixel saturation level.

Finally, Figure 7 shows the image of a typical pulse from the laser used in this section, including some ways of processing and analyzing the image. The results of the image inversion (Fig. 7b) and

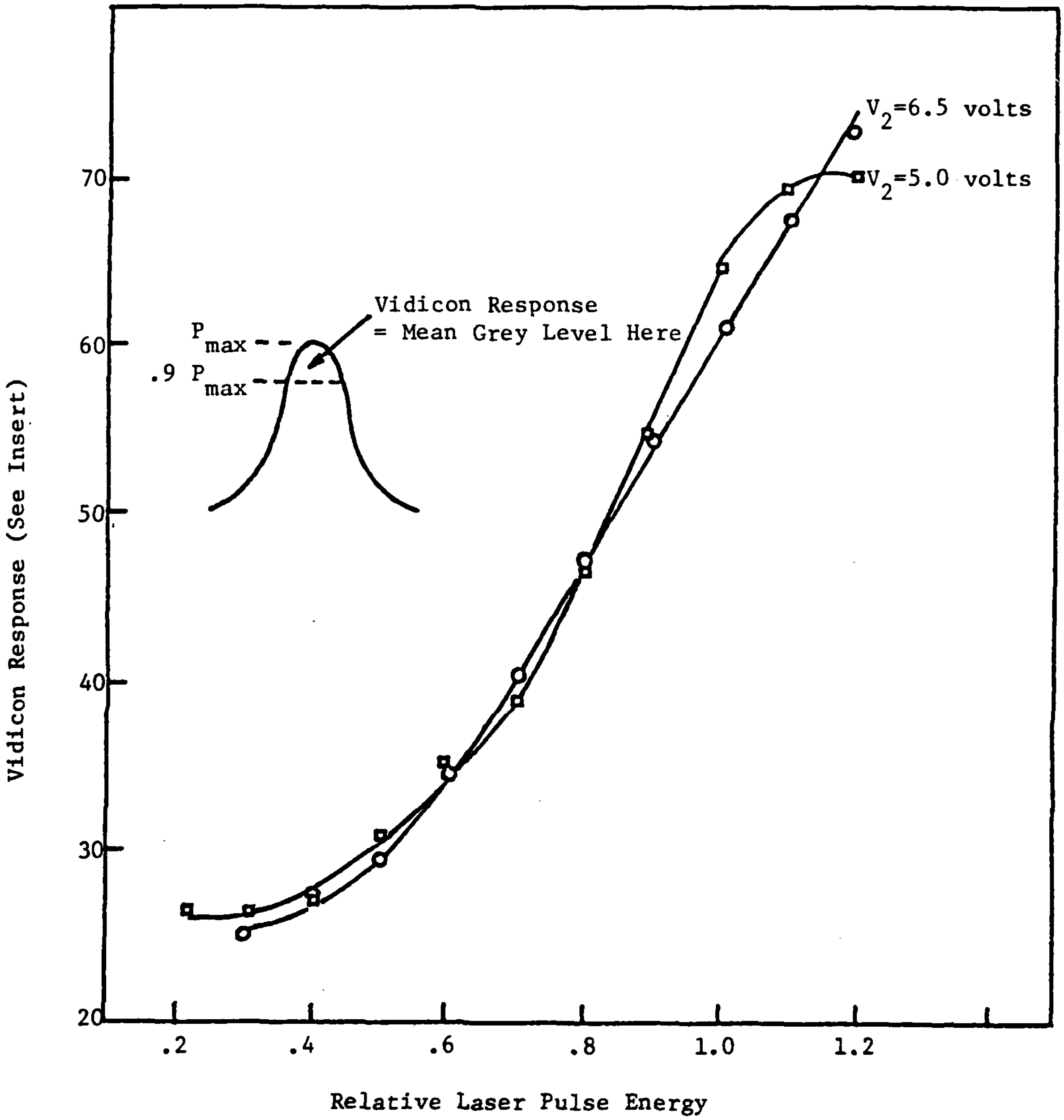

Figure 6. Vidicon Response versus Relative Energy in].06 μm Pulses at T = 0° C. T_C = 100 μsec, N_C = 360 Pixels/Channel. V_2 = 5.0 Volts Curve: Standard Operation. V_2 = 6.5 Volts Curve: Cathode Voltage Switched from 5.0 to 6.5 Volts After Pre-Equilibration Frames. P_{max} = Maximum Pixel Grey Level.

A. Pulse Image. Negative Video Causes Trapix Pixels to Saturate at Zero Grey Level.

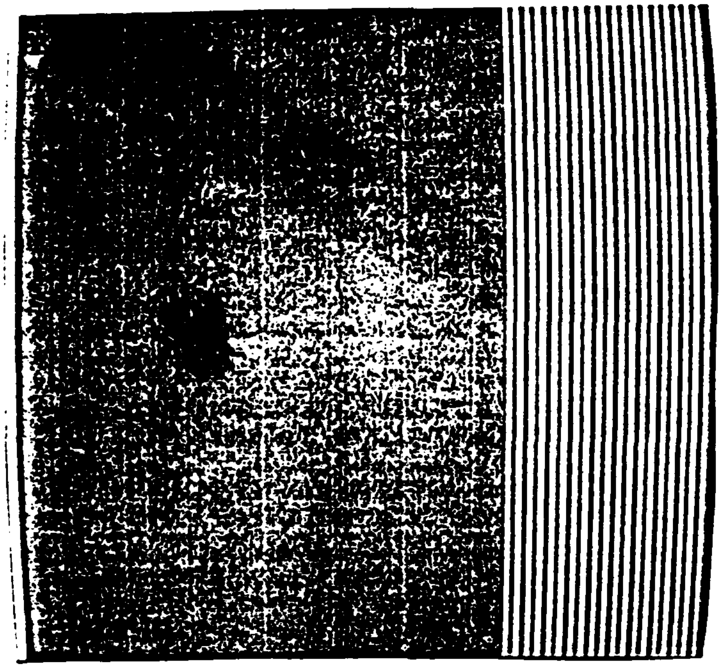

B. Pulse Image Inverted so Trapix Grey Levels Vary from Zero at Low Energy to 83 at Saturation.

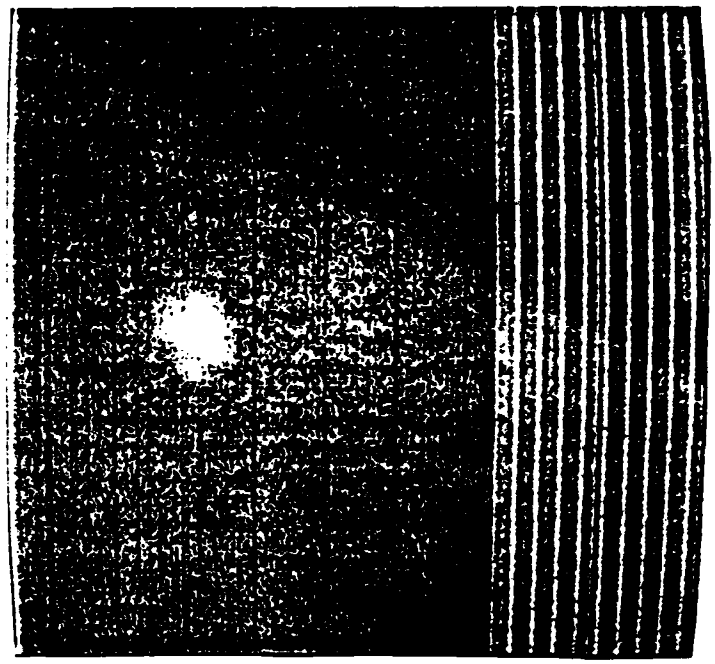

C. Profile of the Inverted Pulse Through the Section Indicated by the Cursor.

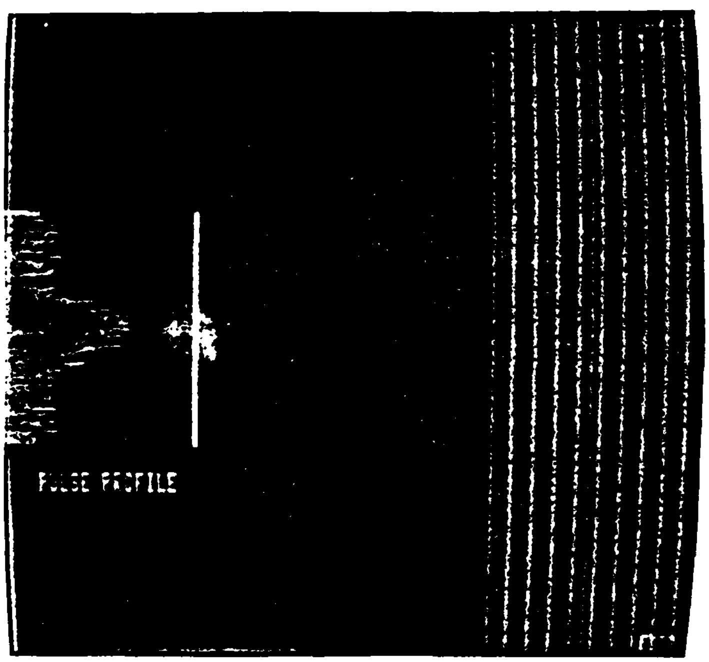

D. Smoothed Profile Obtained by Averaging the Pixels in the Thin Region Outlined by the Cursor.

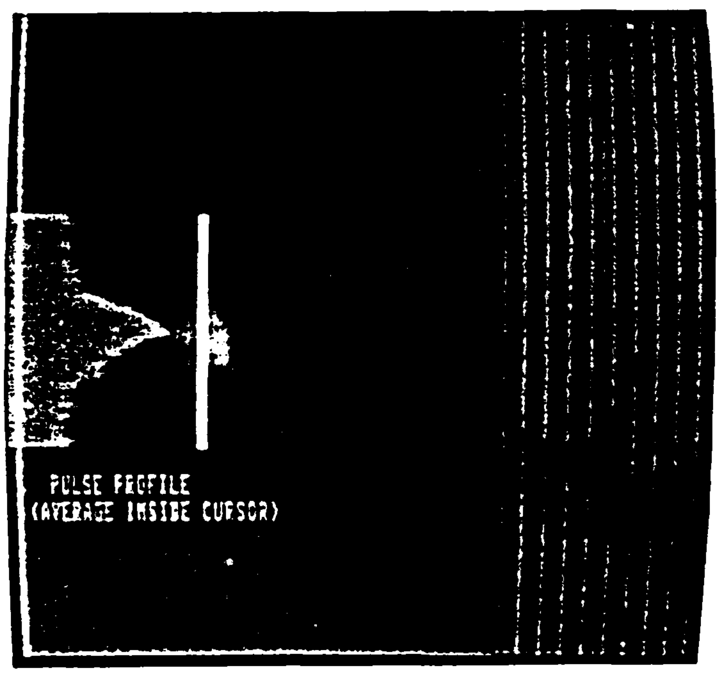

Figure 7. Processed, Analyzed Image of a 1.06 μm, Q-Switched Laser Pulse. T_C = 100 μsec, N_C = 360 Pixels, T = 0° C.

profile smoothing software routines (Fig. 7d) are available approximately 30 seconds after firing the laser. Thus, the system can provide real-time feedback in many laser damage experiments.

VII. RECOMMENDATIONS

Depending on experimental conditions and required accuracy, the system studied here can provide useful, real-time two-dimensional profiling information on fast 1.06 µm laser pulses. Only the central 3.7 mm x 3.1 mm region of the vidicon target should be used, however, where the peak-to-peak variations in dark current and detection sensitivity (≤ 6% and 4%, respectively) are acceptably low. The vidicon target should be cooled to 0° C, too, to benefit from the optimum signal-to-noise behavior at that temperature, although the measurements should be repeated at other temperatures near 0° C to determine the optimum temperature more precisely.

The question of pulsed-mode saturation needs to be considered further. First, a way must be found, hopefully in software, to raise the display pixel saturation level well above that of the vidicon under all useful channel times and cathode voltages. Next, the pulsed linearity measurements should be repeated with higher cathode voltages than the 6.5 volts considered here. Determination of the optimum V_2 will also reveal the maximum dynamic range of the vidicon, which was shown here to be a rather unacceptably low value of 4 for a cathode voltage of 6.5 volts.

If higher cathode voltages do not improve the linear dynamic range of the vidicon, other imaging devices might be substituted for it in the system. For example, the RCA C23250-NTD silicon vidicon was shown to have a linear dynamic range of 20 under pulsed conditions at 1.06 µm[7]. And finally, the family of self-scanned silicon imaging array devices might be considered. For example, because they are digitally scanned (no electron beam), they offer greater geometric accuracy than electron beam devices.

REFERENCES

1. R. M. O'Connell, T. F. Deaton, and T. T. Saito, "Single- and Multiple-Shot Laser-Damage Properties of Commercial Grade PMMA," Appl. Opt. 23, 5, 682 (1984).

2. R. M. O'Connell, A. B. Romberger, A. A. Shaffer, T. T. Saito, T. F. Deaton, and K. E. Seigenthaler, "Improved Laser-Damage-Resistant Polymethylmethacrylate," J. Opt. Soc. Am. B1, 6, 833 (1984).

3. R. M. O'Connell and R. A. Vogel, "Simple, Accurate Inversion of Knife-Edge Data from Radically Symmetric Laser Beams," Proc. 17th Annual symposium on Optical Materials for High Power Lasers, Boulder, Co. (1985).

4. G. W. Liesegang and P. D. Smith, "Vidicon Characteristics under Continuous and Pulsed Illumination," Appl. Opt. 21, 8, 1437 (1982).

5. G. W. Liesegang and P. D. Smith, "Improving Vidicon Linearity in the Pulsed Illumination Mode," Appl. Opt. 20, 15, 2604 (1981).

6. H. E. Cascio, P. D. Smith, and G. W. Liesegang, "Simple Switching Circuit to Improve Vidicon (OMA2) Linearity," Rev. Sci. Instrum. 53, 7, 967(1982).

7. W. L. Smith, A. J. DeGroot, and M. J. Weber, "Silicon Vidicon system for Measuring Laser Intensity Profiles," Appl. Opt. 17, 24, 3938 (1978).

1985 USAF-UES SUMMER FACULTY RESEARCH PROGRAM/

GRADUATE STUDENT SUMMER SUPPORT PROGRAM

Sponsored by the

AIR FORCE OFFICE OF SCIENTIFIC RESEARCH

Conducted by the

UNIVERSAL ENERGY SYSTEMS, INC.

FINAL REPORT

FREE RADICAL SPECTRA OF PO

Prepared by: Ralph Oberly

Academic Rank: Professor of Physics

and

Prepared by: Mary Anne Hudson

Academic Rank: Physics Graduate Student

Department and University: Physics and Physical Science Department, Marshall University

Research Location: Wright-Patterson Air Force Base

Aero Propulsion Laboratory

Power Division

USAF Research: Biswa Ganguly

Date: September 20, 1985

Contract No: F49620-85-C-0013

FREE RADICAL SPECTRA OF PO

by

Ralph Oberly

and

Mary Anne Hudson

ABSTRACT

A spectroscopic study of phosphorus monoxide, or PO, has been undertaken to determine the feasibility of using this spectra as a detection mechanism for certain chemical warfare agents. The B-X band system was selected for study based on equipment available in the laboratory. Several relevant papers were then found through a literature search on this topic.

The preliminary experimental program has produced PO band head emission spectra in the 325 nm region in preparation for looking for LIF band head emission spectra. A computer program has been written for an Apple II computer that calculates the line positions for all branches in the PO B-X band system. These line positions can be used to determine the location of band heads in the spectra.

ACKNOWLEDGMENTS

The authors wish to acknowledge the support of the Air Force Systems Command, Air Force Office of Scientific Research, and the Aero Propulsion Laboratory at Wright-Patterson AFB. In particular, Dr. Alan Garscadden, Dr. Biswa Ganguly, and Lt. Peter Haaland provided the space and equipment for the project as well as many constructive conversations on the technical aspects of the project. In addition, the technical staff provided much valuable support in terms of glass blowing of the plasma tube, plumbing vacuum lines, and finding appropriate equipment items.

I. INTRODUCTION

There is a current military interest in the detection of specific chemical compounds that are used as chemical warfare agents, or that are derivatives of chemical warfare agents. It is essential that quick and sensitive means of detection of such chemical compounds be available to military personnel in the field in order that they know when to take proper protective efforts against the chemical agents. Spectroscopic detection and analysis techniques can be both quick and extremely sensitive to the presence of minute amounts of chemical compounds. Of particular current interest is the diatomic molecule phosphorus monoxide, or PO, as it is a derivative from nerve gas agents containing phosphorus. The current study is a spectroscopic effort to provide analysis techniques for the detection of PO. This study has two principal parallel directions. One is to obtain spectroscopic data for the principal emission bands through conventional emission spectroscopy and through laser induced fluorescence (LIF) techniques. The second part of the work is a computer modeling approach to the spectra. Both parts of the study are to provide background information useful in the development of detection schemes for chemical agents.

The principal investigator on this project has a Ph.D. in physics (1970) from The Ohio State University. His interests are in recording and analyzing spectroscopic data

for small molecules (two to four atoms). His graduate school work consisted of the recording of high resolution infrared spectra for the carbon dioxide molecule, both the common isotope and oxygen-18 enriched isotopes. More recent work has included the modeling of spectra for silicon hydride (SiH) and diatomic sulfur (S_2). He is currently a professor of physics at Marshall University in Huntington, West Virginia. He has been at Marshall since September 1970 and has been chairman of the Physics and Physical Sciences Department since 1973.

The graduate student working on this project is studying physics at Marshall University. She has a B.S. degree (1982) from Ohio University in Athens, Ohio. She has training and experience as a computer systems analyst. She is interested in the computations used to analyze spectroscopic data.

II. OBJECTIVES OF THE RESEARCH EFFORT

The objectives for this project were to obtain information on the emission spectra of the phosphorus monoxide molecule. This included a thorough literature search and a laboratory program to investigate the problems associated with producing and detecting PO spectra. The laboratory part of this investigation was to produce standard emission spectra of PO using a DC-discharge tube and to observe laser induced fluorescence from the PO radical produced within the discharge tube. Moreover, it was determined that the measurement of the current-voltage (I-V) characteristics for the tube before and after the formation of the PO radical would be a useful means of monitoring the effect of the chemical agents on the plasma tube.

A further objective was to write computer software that would simulate the PO spectra based on existing molecular constants available in the literature. In addition, it is desirable to write or acquire software that can be used on computers at the investigators' home institution in order that the study can continue through the academic year. This software is to include programs in regression analysis and matrix operations that can be used in analyzing spectroscopic data.

III. LITERATURE SEARCH

Suchard (1) and Huber and Herzberg (2) have summarized the literature data on the PO molecule up to 1977. This study was directed at laser induced fluorescence (LIF) of the PO molecule. A dye laser is available in the Aero Propulsion Laboratory at Wright-Patterson AFB that can produce 325 nm radiation so the emphasis was on the B-X transition centered at 325 nm. References (3) through (5) were especially helpful in providing current molecular constants for the computer programs. Constants taken from Verma and Singhal (3) are used in the computer program to be described later for calculating the position of PO wavenumbers for the B-X band. References (6) through (8) provide experimental values of the wavenumbers for comparison. References (9) through (15) cover recent work that has used laser excitation of the PO radical. Singhal (16) has additional data on wavenumber positions in his thesis which has been requested through the WPAFB Tech Library but not received yet.

The literature search also tried to find data for the prediction of intensities of spectral lines so that intensities of band heads could be evaluated in the computer programs. Values for the Franck-Condon factors are available in the literature. Smyth and Mallard (12) list values for the PO B-X system for v' from 0 to 8 and for v" from 0 to 10. In addition, Anderson et al (14) have

published a few values for Franck-Condon factors. There does not seem to be good agreement between the two sources. Kovacs (17) has worked out relations for the intensity terms dependent on rotational quantum numbers for diatomic molecules which are applicable here. No literature values were found for the internuclear distance terms, or r-centroids, for the PO molecule. However, it has been learned that values are soon to be published for these factors (18) which will allow the intensity factors to be fully determined.

The computer programs written to date have not accounted for spin-orbit coupling in the rotational structure as it is a minor correction term when band head data is of greatest concern. Veseth (19) has described the general problem of spin-orbit coupling terms. Zaidi and Verma (20) have looked at the quantum number dependence of spin-orbit coupling terms for PO in the ground electronic state.

IV. PO B-X SPECTRA

The PO molecule in the ground electronic state, which is a $X^2\Pi$ electronic state, has a very strong coupling of the electronic motion to the line joining the two atomic centers and a very weak interaction of the nuclear rotation. This makes the state a traditional Hund's case (a). See Herzberg (21). The rotational levels are strongly split into two sublevels with an approximate separation of 324 cm-1. The appropriate expression to describe this splitting is from James (22) and summarized by Klynning (23). The rotational term values become:

$$F_{1,2}(J) = Bx - Dx^2 \mp \sqrt{((A^*-2B^*)^2\Lambda^2)/4 + B^{*2}x} + R \tag{1}$$

where B and D are the rotational and centrifugal distortion constants for the vibrational level considered, R is a simple sum of vibrational and electronic term values given by Klynning et al, and Λ is the orbital angular momentum quantum number. The remaining terms are:

$$B^* = B - \gamma/2 - 2Dx$$

$$A^* = A + A_J x$$

$$x = (J + .5)^2 - \Lambda^2$$

where γ and A are the spin-coupling constants, and A_J gives the J-dependence of A. From equation (1) the rotational energy levels represented by $F_1(J)$ and $F_2(J)$ are separated

by a spin-coupling splitting given by twice the value of the radical term in the equation. For the ground electronic state of PO the value of γ is taken to be zero from the work of Verma and Singhal (3). The additional Λ -type doubling was considered to be sufficiently small to be of no significance at this stage.

The first excited electronic state of the PO radical is the $B\,^2\Sigma$ state. In this state the spin vector is not coupled to the internuclear axis at all. This is characteristic of Hund's case (b). The rotational term values from Herzberg are:

$$F_1(J) = BK(K+1) - DK^2(K+1)^2 + 0.5\gamma K + R \qquad (2)$$

$$F_2(J) = BK(K+1) - DK^2(K+1)^2 - 0.5\gamma(K+1) + R \qquad (3)$$

where B and D are the upper level rotational and centrifugal constants and γ is the spin-coupling constant. For sublevel 1 K is given by $J=K+0.5$ and for sublevel 2 K is given by $J=K-0.5$. Again, R is a term containing the sum of the electronic and vibrational term values.

The selection rules allow transitions from the four possible combinations of upper and lower sublevels (i.e., $1\rightarrow 1$, $1\rightarrow 2$, $2\rightarrow 1$, $2\rightarrow 2$). The traditional R, Q, and P branches are permitted within each sublevel transition so that a total of twelve branches are possible for each

vibrational transition. (If cd-pairs of lines from Λ -doubling splitting were considered twenty-four branches would be considered.) The selection rule values of ΔJ = -1, 0, and 1 correspond to the P, Q, and R branches respectively. For the $1 \rightarrow 2$ and $2 \rightarrow 1$ sublevel transitions there is the additional selection rule that ΔK = -2, -1, 0, 1, and 2 for which superscripts are added to denote O, P, Q, R, and S satellite branches. As an example the notation:

$$^{S}R_{12}$$

represents a transition from an upper sublevel 1 state to a lower sublevel 2 state for which $\Delta J = +1$ and $\Delta K = +2$.

Many branches in the PO system have band heads with very strong emission intensity. For example, the Q branch of the 0-0 vibrational transition in the B-X band system has a band head near the 3247 A wavelength position that is shaded toward the violet. The strong emission intensity in turn makes the band head regions very sensitive for the detection of the PO radical. Several investigators (See references 9 and 11 through 15.) have reported band head emission from the PO radical using laser excitation.

V. SOURCE OF THE PO RADICAL

A number of schemes exist for generating the PO radical. The traditional approach has been to flow a gas mixture containing a trace of oxygen over red phosphorus (4), or to evaporate red phosphorus into a flowing oxygen discharge chamber (7). A radio frequency discharge is then used to excite the PO radical to an excited state. Verma and coworkers (8, 24) have used an r.f. discharge to form the PO radical in a flowing argon stream with a trace of $POCl_3$. Clyne and Heaven (9) have produced the PO radical in a discharge-flow using oxygen and nitrogen atoms to react with PH_3. PO has also been produced in the IR radiation of a carbon dioxide laser used to decompose triethyl phosphite (10). Chou et al (13) and Anderson et al (14) have produced the PO radical from IR photolysis of the dimethyl methylphosphonate (DMMP) molecule and a microwave discharge of the DMMP molecule. Anderson has also successfully used diethyl ethylphosphonate (DEEP). Miziolek et al (15) have used both DMMP and diethyl methyl phosphonothioate (DEMPS) to generate the radical. Davies and Thrush (25) discuss in general the reactions of atomic oxygen and phosphine.

In the current study it was decided to try DMMP as the source for the PO radical. A liquid sample of approximately one liter volume was obtained.

VI. PO PLASMA CELL DESIGN AND TECHNIQUES

Figure 1 shows a schematic of the plasma cell designed for the initial experimental part of this study. A cylindrical tube roughly 30 cm long was constructed with 1 cm diameter cylindrical Kovar electrodes placed approximately 20 cm apart along the tube axis. An input line entered the tube at the bottom center. The input line came from an argon cylinder through a reservoir. The reservoir initially was filled with 15 cc of DMMP so that argon would literally bubble through the room temperature liquid. A thermocouple gauge was connected to the tube through another line just above the argon input line. A third connection to the tube was for the exhaust line to the vacuum pump. Six small quartz windows 1 cm in diameter were attached to the tube. Three were located at 90 degree spacing around the wall of the tube just inside the cathode location. The other three were located about two-thirds of the way from the cathode to the anode with similar 90 degree spacing around the tube. The plasma tube and reservoir containing the DMMP were located in a fume hood at all times during their use.

The initial attempts to see PO emission spectra were made with a DC discharge across the electrodes with voltages ranging from 350 volts up to about 2500 volts. Most of the tube voltages were below 1200 volts. The tube current was limited to 10 mA maximum.

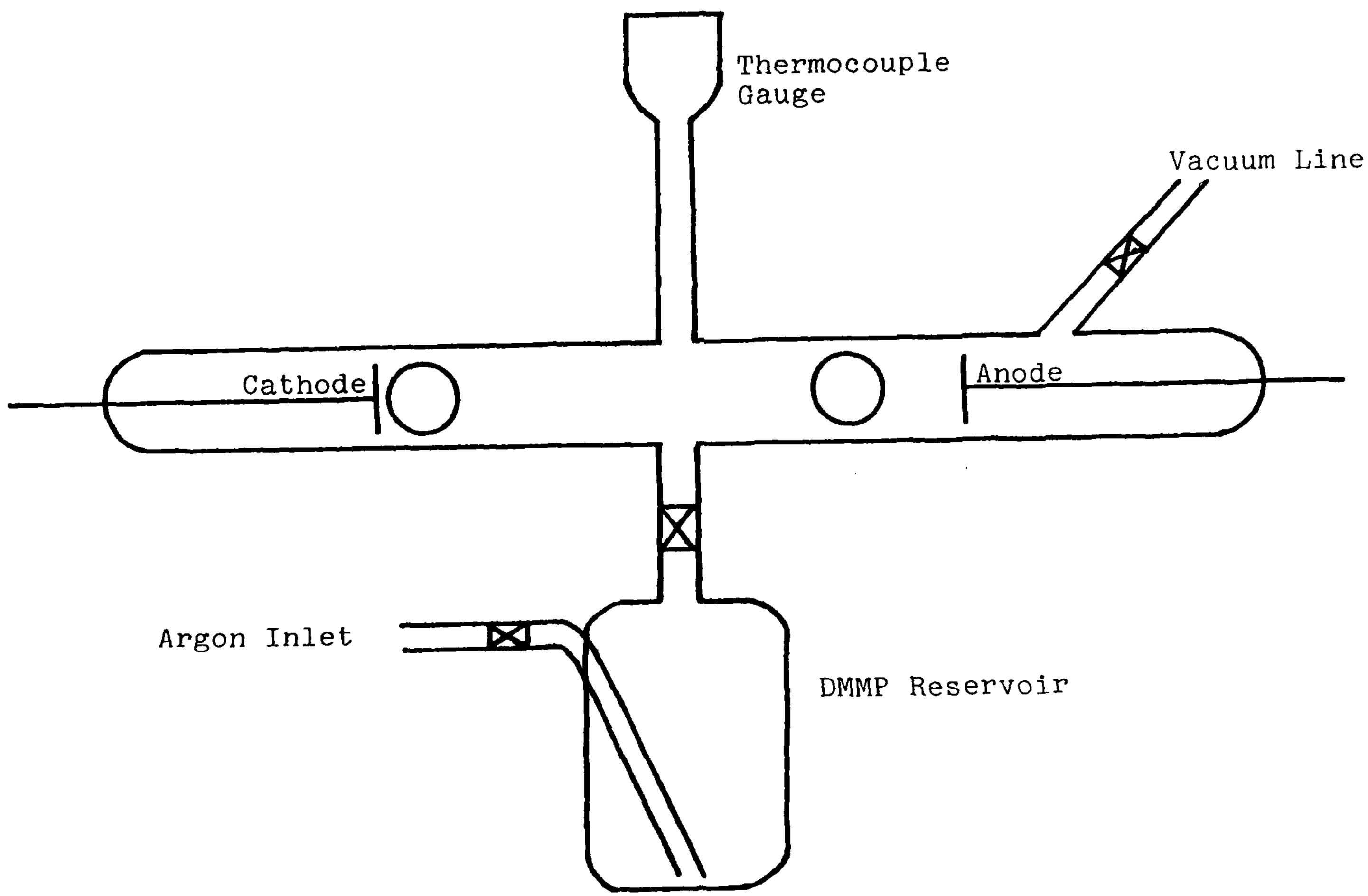

FIGURE 1. ORIGINAL PLASMA TUBE CONFIGURATION

The argon flow rate was initially not monitored quantitatively. The only indication of pressure was of the total pressure inside the tube which read roughly 1 torr on a poorly calibrated thermocouple gauge. The heavy flow of argon bubbling through the DMMP at room temperature established a too high value of the partial pressure of DMMP in the plasma tube creating several problems. A brown film quickly developed on the entire inside of the tube surface with an especially heavy layer near the cathode region. As the tube was used a thick liquid residue collected on the floor of the tube and eventually ran down into the reservoir containing the DMMP. This liquid soon made contact with the cathode surface. In the course of running the discharge tube both electrodes became pitted and caused arcing problems within the plasma discharge, including hot spots between the electrodes and walls of the tube. After about two days of running the plasma tube, it was necessary for the tube to be dismantled and cleaned. The tube was filled with an isopropyl alcohol solution and left to set overnight. Then the solution was emptied and the entire tube and reservoir system was cleaned in an ultrasonic cleaner with a Dynasoap solution. The plasma tube seemed to be restored to original condition by this process with the exception of the pitted electrodes.

Before the tube was used again, four major modifications were made to its design and use. The

reservoir was removed from the tube and reconnected to it through a rubber hose. The reservoir was positioned above the plasma tube so that residue could not enter it by gravity.

The second modification was to run two parallel lines from the argon supply to the plasma cell. See figure 2 for a schematic diagram. A Hastings flow rate meter was placed in the argon line before splitting into the parallel paths so that the total flow rate could be observed. One line went directly to the plasma tube as the major source of argon. The second line went through a needle valve to the DMMP reservoir and then to the plasma tube. A pinch clamp was positioned on the hose between the reservoir and the plasma tube. The combination of pinch clamp and needle valve allowed for sufficient control of the argon flow through the reservoir.

The third change was to only place small amounts of DMMP in the reservoir at any one time. Roughly 0.5 cc was the maximum transferred volume. The argon then flowed over the DMMP droplets rather than bubbling through a liquid.

The fourth change was to maintain the reservoir in a salt and ice water bath with temperatures between -10° C and -6° C. The combination of the four changes just discussed seemed to reduce the residue problems discussed before to easily manageable conditions. Flow rates in the range of 550 sccm to 850 sccm for the total flow rate of argon gave

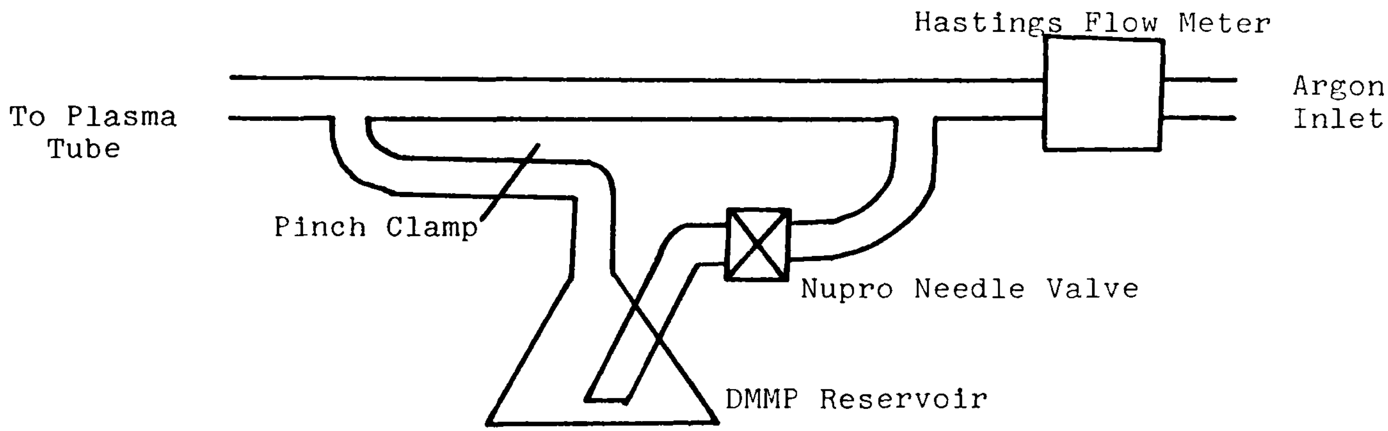

FIGURE 2. MODIFIED ARGON FLOW LINE

prolonged use of the plasma tube.

An additional problem arose due to the assorted sizes and types of vacuum hoses and fittings used in the gas flow lines. Frequent air leaks in the system caused the discharge to be dominated by the nitrogen first positive and second positive band systems. The second positive band system directly overlaps the PO B-X emission region and must not be present in order for the PO B-X system to be observed. Even small amounts of nitrogen in the system create a red or pink tint in the discharge emission. The second problem associated with air leaks is that the presence of nitrogen in the plasma greatly complicates and increases the number of chemical reactions that are possible with the DMMP and its breakdown components.

VII. CURRENT-VOLTAGE (I-V) CHARACTERISTICS

The reaction of the DMMP in the DC-discharge was an unknown both chemically and electrically. It was decided early in the project that I-V characteristic curves be determined at various stages of the project in order to monitor the electrical effects of the resulting chemical reactions on the plasma tube. A current-limited power supply was connected across the tube with moving-coil ammeter and voltmeter. The maximum current was established as 10 mA. I-V values were measured for currents starting at 9 mA and reduced down to values at which the plasma discharge shut off, and then increased up to 9 mA again. In this manner hysteresis curves were obtained for some modes of operation of the plasma tube. Figure 3 shows the I-V characteristics for a clean plasma tube with no DMMP in it. (These values were recorded after the tube was cleaned the first time.) This nearly flat set of curves with no hysteresis is due to a pure argon flow in the tube. The argon flow rate was at 57 sccm with a pressure of about 0.9 torr on the thermocouple gauge.

The I-V measurements were made several times at all stages of using the plasma cell to look for PO emission spectra. Figure 4 shows an example of the characteristics with PO in the cell and the running conditions typical of those with high argon flow rates through the cell. In particular, these points were measured for an argon flow

FIGURE 3
I-V CHARACTERISTICS
CLEAN PLASMA TUBE

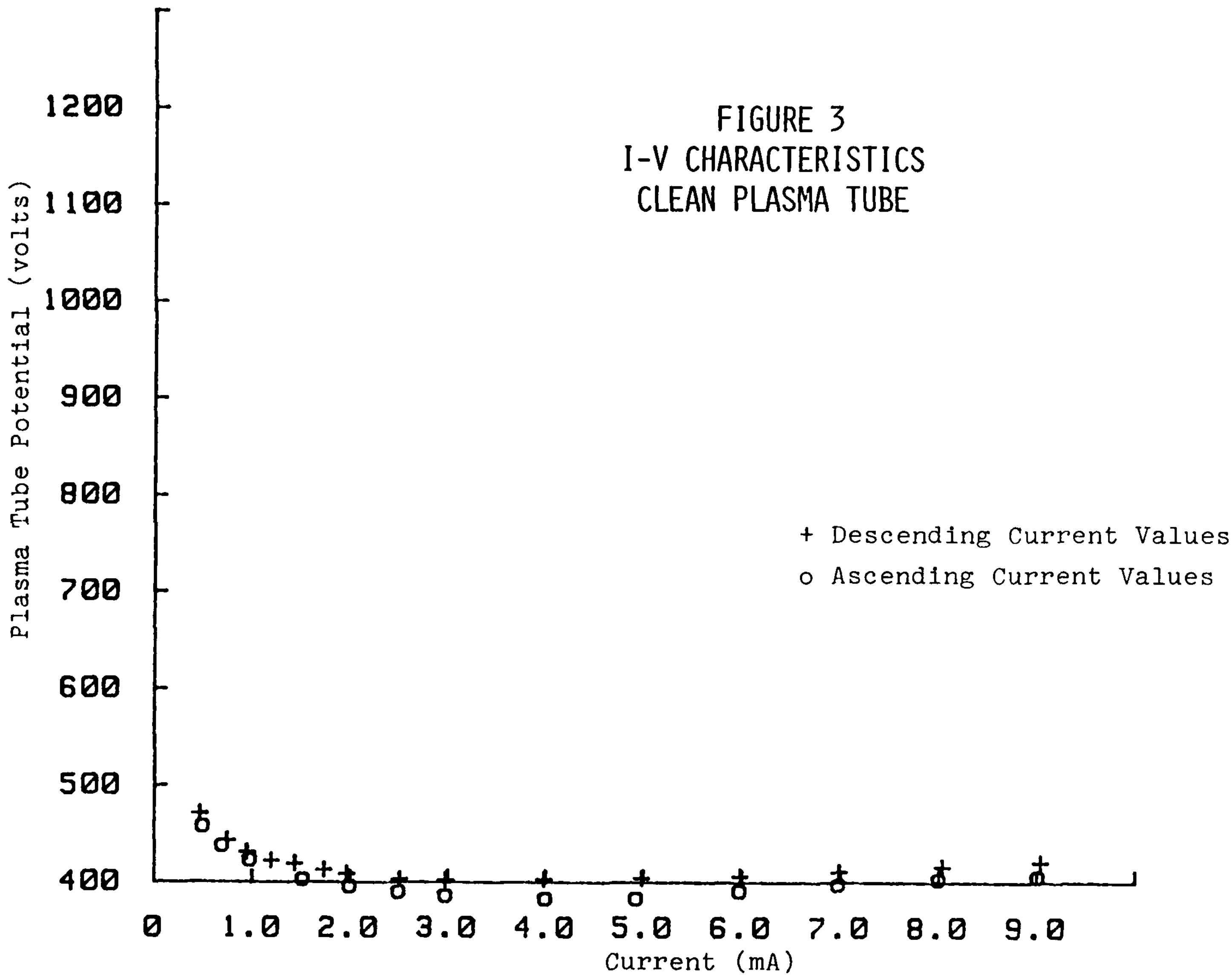

FIGURE 4
I-V CHARACTERISTICS
MODIFIED ARGON FLOW SYSTEM

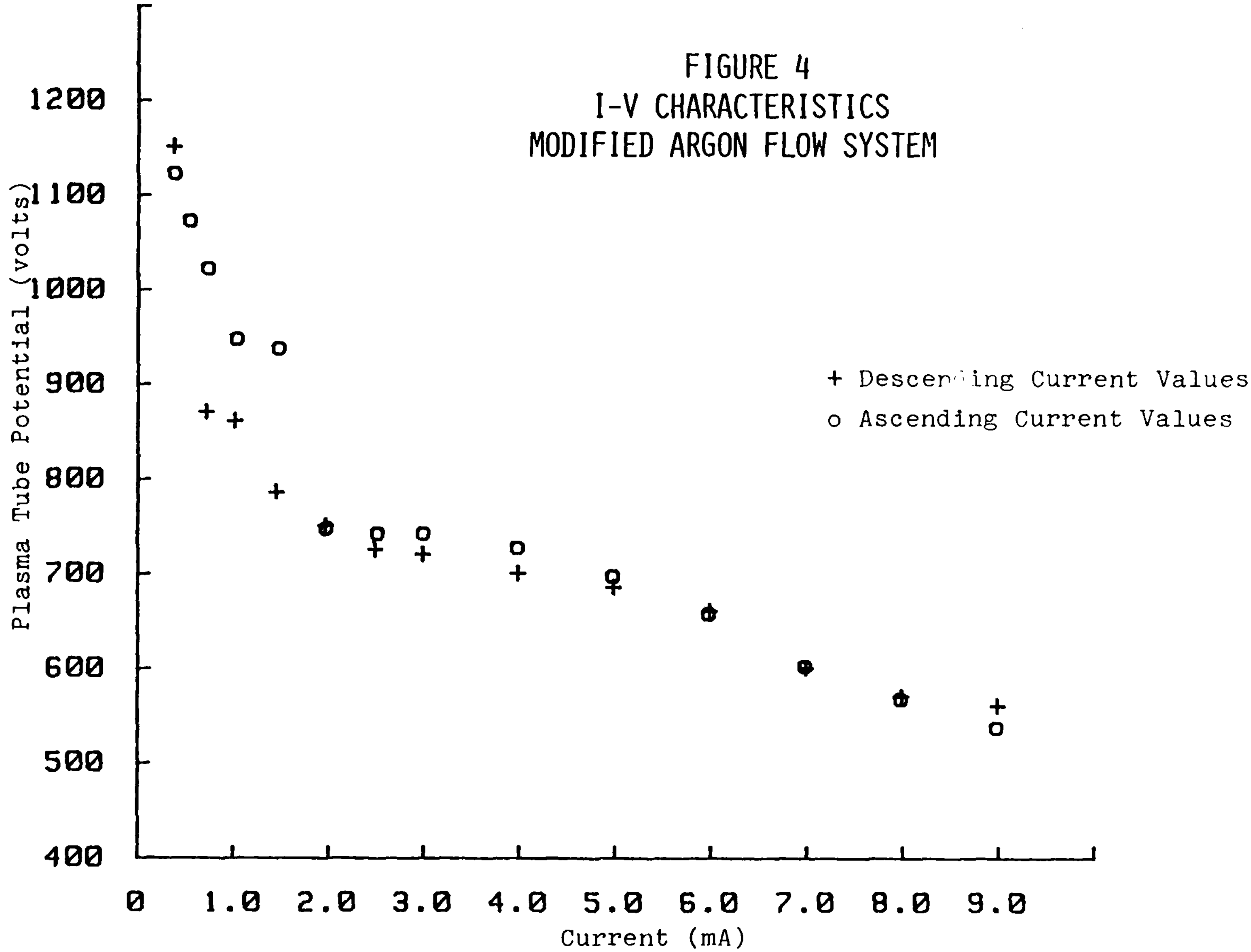

rate of 570 sccm with a cell pressure of 1.0 torr. Even with the current system no quantitative system is available to measure the argon flow rate through the DMMP reservoir. The pinch clamp downstream from the reservoir was removed and the needle valve upstream from the reservoir was opened about 1/5 of a turn. The needle valve was a Nupro stainless steel valve. It is significant that the cell had been in use for several hours with DMMP before these values were recorded yet there is virtually no hysteresis indicating that some or all of the changes were needed.

Figure 5 shows the contrasting situation with similar I-V values recorded before the changes described in section VI. Again, the cell had been in use several hours before these values were recorded. The low argon flow rates and high vapor pressure of the DMMP used initially caused the cell I-V characteristics to change significantly. After some use the voltage range extended to 2400 volts and a prominent hysteresis effect was observed.

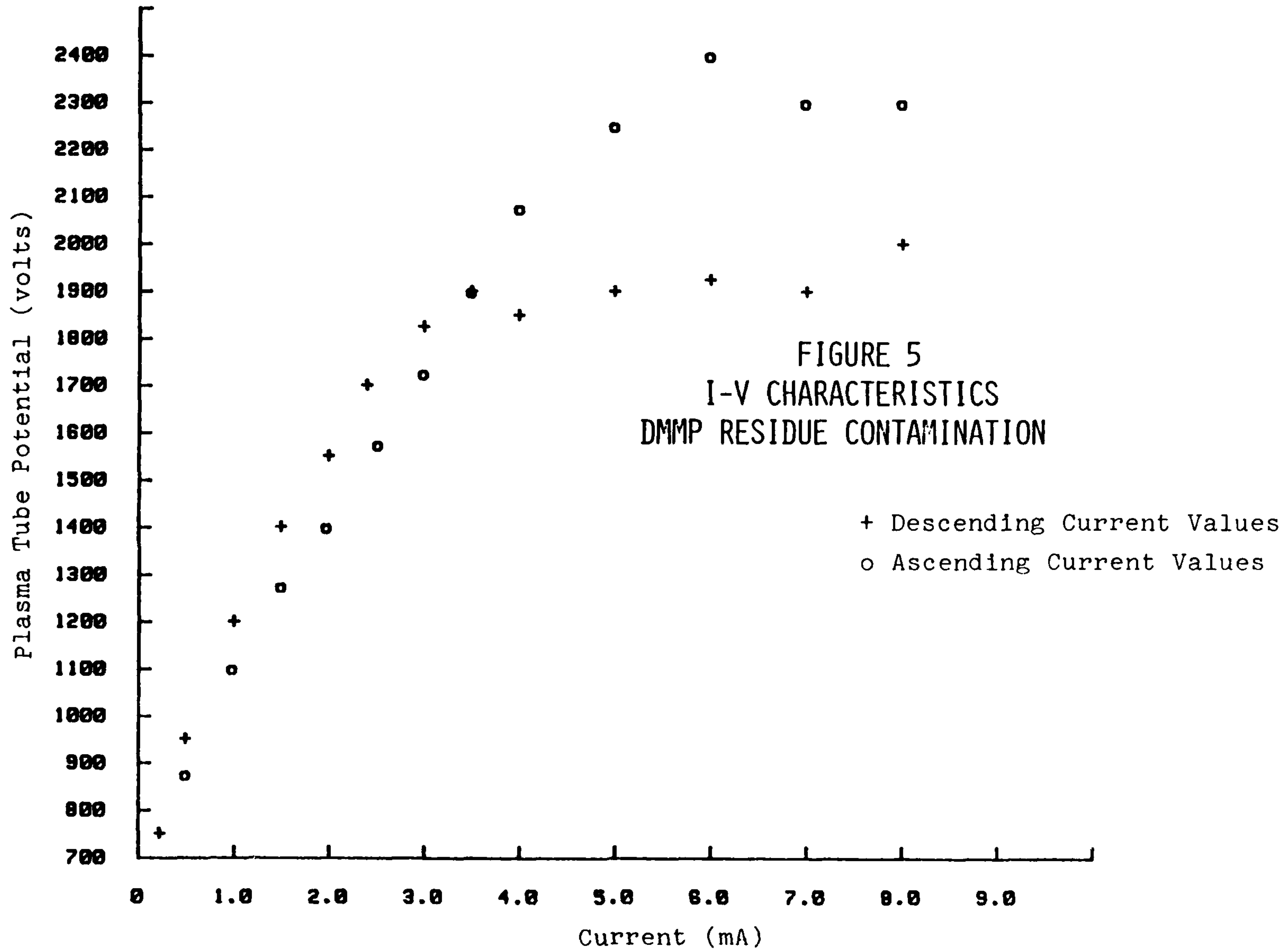

FIGURE 5
I-V CHARACTERISTICS
DMMP RESIDUE CONTAMINATION

VIII. OBSERVED EMISSION SPECTRA

After the modifications to the argon flow lines and the technique for introducing DMMP vapor into the plasma tube additional attempts were made to record PO B-X emission spectra. Lines were observed in the 325 nm region that had the appearance of a strong bandhead as should be observed in the PO spectra. The observed spectra were distinctly due to the presence of DMMP. Each line was checked by setting the spectrometer to the center of the emission line and adjusting the DMMP flow rate to see if the line intensity was affected. Figure 6 shows the strong emission lines at 324.4, 325.2, 326.7, and 327.6 nm. These lines are all affected by the DMMP flow rate and they fall where strong PO bandheads should be observed. Moreover, they occur in pairs showing the ground state splitting expected in the PO molecule. The four lines or bandheads can be identified as belonging to branches of the 0-0 and 1-1 vibrational bands in the B-X system according to the following:

WAVELENGTH	UPPER VIB. LEVEL	LOWER VIB. LEVEL	UPPER SUBLEVEL	LOWER SUBLEVEL	BRANCH
324.4 nm	0	0	1	1	Q
	0	0	2	1	P
325.2 nm	1	1	1	1	Q
	1	1	2	1	P
326.7 nm	0	0	1	2	Q
	0	0	2	2	P
327.6 nm	1	1	1	2	Q
	1	1	2	2	P

It should be noted that the wavelength values listed here are those obtained from the spectrometer counter which was not accurately calibrated. A correction of 1.8 nm for each line has been used to account for the gross inaccuracy of the counter but no system for accurate determination of wavelength existed.

Additional lines, or bandheads, occur at much weaker intensity in the spectral region from 333 nm to 346 nm. Again these lines can be shown to be dependent on the presence of the DMMP in the plasma cell. The appearance of these lines is much less distinctive than for the first case cited above due to the number of lines and the closeness of their positions. A study of the bandheads for this region quickly shows these lines to be the result of vibrational transitions given by 0-1, 1-2, 2-3, etc. The

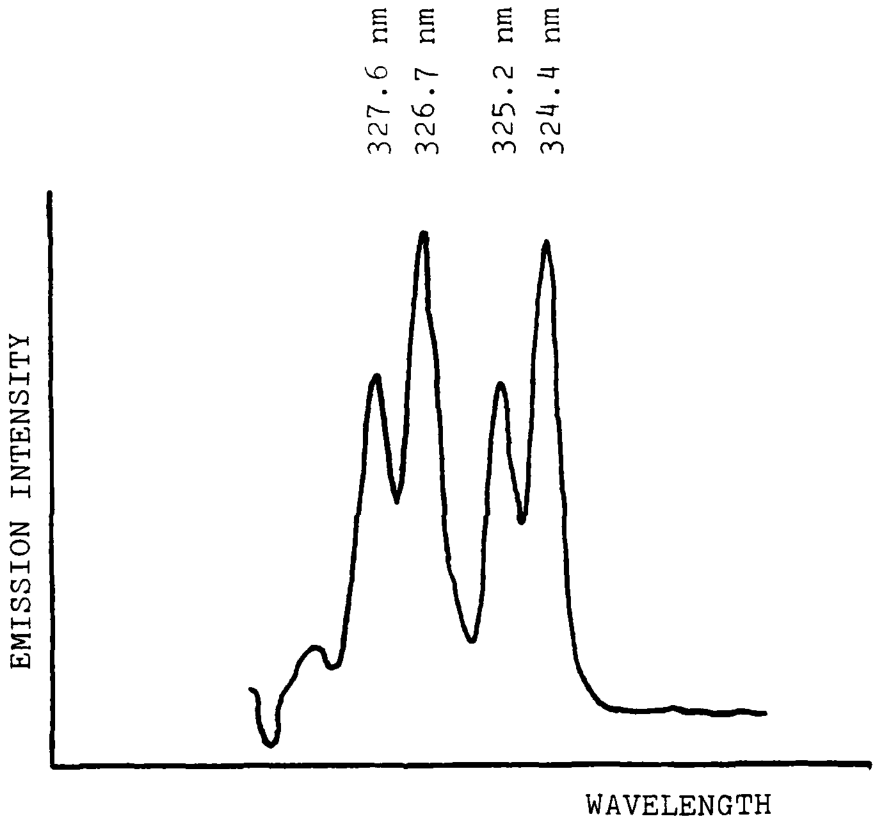

FIGURE 6
PO BAND HEAD STRUCTURE

Q-branches for the 1-1 and 1-2 sublevel transitions and the P-branches for the 2-1 and 2-2 sublevel transitions all give closely overlapping bandheads between 333 and 346 nm. Better resolution and a more accurately calibrated spectrometer are needed to make individual identifications.

IX. COMPUTER PROGRAMS

Two desktop computers were used during the course of this work. A Hewlett-Packard 9836 was used with available programs for linear regression analysis and plotting routines. An Apple II was used to do computations involving the PO B-X spectra. Only the programs specifically written for this project to be run on the Apple II will be discussed here.

The computations for the PO B-X spectra were based on the published data of Verma and Singhal (3). The constants listed in this paper allowed the wavenumber positions for rotational lines of each branch of a vibrational transition to be calculated. The computer operator must select the maximum J-value (J-MAX, half-integer values) for the rotational transitions to be calculated. In addition, the values of the upper vibrational level and the lower vibrational level are input before the computer begins the computations. As noted earlier Λ-type doubling was not considered for the computations as the splitting from this effect is not significant for this study.

Wavenumber values are computed and listed in the order of ascending J-values for each of the twelve branches of the selected vibrational transition. The program cycles through the vibrational sublevels with the 1-1 sublevels (upper sublevel-lower sublevel) first, the 1-2 second, the 2-1 third, and finally the 2-2. For each combination of

sublevels the P-branch ($\Delta J = -1$), Q-branch ($\Delta J = 0$), and R-branch ($\Delta J = +1$) lines are listed in the order just given. As this study is specifically interested in the position of bandheads in the PO spectra the program locates their wavenumber positions. After the listing of a set of wavenumbers for a P-, Q-, or R-branch with a bandhead the message "THE BANDHEAD IS AT   " is printed out to allow quick identification of these features. Branches with no bandhead have no message. The proper specification of J-MAX is important as bandheads occur at J-values from in the teens up to values in the forties. Too low of a value for J-MAX would cause some bandheads to be missed entirely. While high J-value bandheads may have significantly reduced intensity they may still be useful. This program is accessed by the name PONU. A listing for the program PONU is available upon request.

Two programs were written as preliminary projects leading up to PONU. POTERMGS and POTERMES use the same constants from Verma and Singhal to calculate the combined electronic-vibrational-rotational term values for the ground $X^2\Pi$ state (GS) and the excited $B^2\Sigma$ state (ES) respectively. In POTERMGS the values of the rotational quantum number J (half-integer values) and the vibrational quantum number v must be specified. The program then calculates the term values T1 and T2 for the two sublevels. Similarly the rotational quantum number less spin K

(integer values; sublevel 1 has J=K+.5 and sublevel 2 has J=K-.5) and the vibrational quantum number v must be input into POTERMES. T1 and T2 are computed and listed.

A program accessed through the name WN/WL allows wavenumber positions (in cm-1), and wavenumber intervals or half-widths (in cm-1) to be calculated from entered values of wavelength positions (in A) and wavelength half-widths (in A). The reverse calculation from entered wavenumbers to wavelengths is also done by this program.

VAC-AIR is a program written to compute vacuum wavenumbers (in cm-1) from entered values of wavelengths in air (in A). Similarly, wavelengths in air can be computed from entered values of vacuum wavenumbers. This program is useful for correlating data from different published sources where vacuum and air values are listed. The constants for the calculations in this program are from Edlen (26) who has studied the dispersion of standard air.

X. RECOMMENDATIONS

The original objectives of this project included as a primary goal the development of LIF techniques for observing the PO radical in the laboratory. Due to the limited time for the project the LIF work was never done. However, the work done to date has established techniques to generate PO emission spectra. These techniques should be directly applicable to the LIF spectra problem. Therefore it is recommended that the work continue with the next major step being the LIF spectra. For this work to continue it is recommended that a new plasma tube be built along with a more compact and tighter vacuum system. Specific recommendations are itemized below.

The collection of PO spectra is directed at the bandheads in the B-X system. Knowing the relative strengths of the many bandhead regions would help to determine which spectral regions are best suited for the detection of the PO radical. It is recommended that when the r-centroid values for PO become available that intensity information be added to the existing computer program, PONU, in order that sorting and summation routines can be applied to generate an integrated intensity versus wavenumber spectrum for the molecule.

The following is a series of recommendations that have come directly from the experimental program to date.

1. The plasma tube needs to be redesigned as follows

a. A tight vacuum system that is more compact than the original system needs to be designed in order to keep nitrogen out of the system and to allow more flexibility in positioning the tube near the LIF laser spectrometer.

b. The parallel line arrangement for the flowing argon needs to be maintained in the new plasma tube design in order that a flowmeter for total argon flow rate be included and that a calibrated needle valve be included in the line to the PO reservoir for better control of the DMMP vapor pressure.

c. The plasma cell windows need to be removed from the body of the cell on extension arms in order to minimize the buildup of residual from the DMMP on the windows.

d. The electrodes need to be made replaceable as the DMMP and its residuals pitted the surface of the original electrodes and quickly caused hot spots in the discharge.

e. The cathode and anode should be electrically interchanged after several hours of operation to minimize local deposits of DMMP residual.

f. A high argon flow rate directly to the plasma tube in the range of 550 to 850 sccm is needed to remove as much of the DMMP residual from the tube as possible.

2. The argon flow through the DMMP reservoir needs to flow over the DMMP and not through it. The flow rate needs to be small but quantitative rates have not been determined yet. Only small amounts (about 0.5 cc) of DMMP should be in the reservoir at any time.

3. The DMMP reservoir should be cooled at all times that argon is flowing through it. Temperatures between -6 and -10 degrees C seemed to be adequate.

4. It is recommended that the I-V measurements be continued at intervals as a monitoring device for how the plasma tube is changing with use.

5. It is recommended that LIF measurements be made in the regions discussed in section VIII of this report. In particular, the weaker bandheads observed in the emission spectra have not yet been reported as being observed by LIF in the literature.

6. It is recommended that an exhaust system for venting the vacuum pump exhaust and the general area around the plasma tube always be used.

XII. REFERENCES

1. Spectroscopic Data, Volume I: Heteronuclear Diatomic Molecules, edited by Suchard, S. N., (IFI/Plenum, New York, 1975).

2. Huber, K. P., and Herzberg, G., Molecular Spectra and Molecular Structure, Van Nostrand Reinhold Company, 1979.

3. Verma, R. D. and Singhal, S. R., "New Results on the $B^2\Sigma+$, $b^4\Sigma-$, and $X^2\Pi$ States of PO", Can. J. Phy. 53, 411 (1975).

4. Butler, J. E., Kawaguchi, K. and Hirota, E., "Infrared Diode Laser Spectroscopy of the PO Radical", J. Mol. Spectrosc. 101, 161 (1983).

5. Kawaguchi, K., Saito, S., and Hirota, E., "Far-infrared laser magnetic resonance detection and microwave spectroscopy of the PO radical", J. Chem. Phys. 79(2), 629 (1983).

6. Dressler, K., "Ultraviolet- und Schumannspektren der neutralen and ionisierten Moleküle PO, PS, NS, P_2", Helv. Phys. Acta., 28, 563 (1955).

7. Singh, N., "Rotational Analysis of the β Bands of Phosphorus Monoxide", Can. J. Phys. 37, 136 (1959).

8. Verma, R., "Emission spectrum of the PO molecule. I. A new $B^2\Pi - X^2\Pi$ transition", Can. J. Phys. 48, 2391 (1970).

9. Cline, M., and Heaven, M., "Laser-induced Fluorescence of the PO Radical", Chem. Phys. 58, 145 (1981).

10. Merrow, C., and Nogar, N., "Facile Infrared Laser-induced Decomposition of Triethyl Phosphite", Chem. Phys. Lett. 79(1), 69 (1981).

11. Long, S., Sausa, R., and Miziolek, A., "Laser-induced fluorescence Studies of PO Generated by UV Laser Photofragmentation of DMMP", Proceedings of the 1984 Scientific Conference on Chemical Defense Research, November 1984.

12. Smyth, K., and Mallard, G., "Two-photon ionization processes of PO in a C_2H_2/air flame", J. Chem. Phys. 77(4), 1779 (1982).

13. Chou, J., Sumida, D., and Wittig, C., "Two-frequency two-photon ionization of nascent $PO(X^2\Pi)$ from the collision-free IR photolysis of dimethyl methyl-phosphonate", Chem. Phys. Lett. 100(5), 397 (1983).

14. Anderson, R., Bunte, S., and Kotlar, A., "Measurement of Franck-Condon factors for the v'=0 progression in the B-X system of PO", Chem. Phys. Lett. 110(2), 145 (1984).

15. Miziolek, A., Sausa, R., and Long, S., "Eximer laser photofragmentation of organophosphonates I. Detection of the PO radical from dimethyl methyl phosphonate (DMMP)", Technical Report BRL-TR-2611, US Army Ballistic Research Laboratory, November 1984.

16. Singhal, S. R., Ph.D. Thesis, University of New Brunswick, Fredericton, New Brunswick, 1973.

17. Kovacs, I., Rotational Structure in The Spectra Of Diatomic Molecules, Elsevier/North Holland (1969).

18. Private communication from W. Anderson to Greg Schneider.

19. Veseth, L., "Corrections to the Spin-Orbit Splitting in $^2\Pi$ States of Diatomic Molecules", J. Mol. Spectrosc. 38, 228 (1971).

20. Zaidi, H. R., and Verma, R. D., "Quantum Number Dependence of the Spin-Orbit Coupling in the $X^2\Pi$ State of PO", Can. J. Phys. 53, 420 (1975).

21. Herzberg, G., Spectra of Diatomic Molecules, D. Van Nostrand Company, Inc., Princeton, New Jersey, 1950

22. James, T. C., "Rotation-Vibration Interaction and Other Corrections to the Spin Doublet Separation in Diatomic Molecules", J. Chem. Phys. 41, 631 (1964).

23. Klynning, L., and Lindgren, B., "The spectra of silicon hydride and silicon deuteride", Ark. Fys. 33, 73 (1966)

24. Verma, R. D., and Dixit, M. N., "The D and D' states of the PO molecule", Can. J. Phys. 46, 2079 (1968).

25. Davies, P. B., and Thrush, B. A., "The reactions of atomic oxygen with phosphorus and with phosphine", Proc. Roy. Soc. A. 302, 243 (1968)

26. Edlen, B., "The Dispersion of Standard Air", J. Opt. Soc. Am. 43(5), 339 (1953).

1985 USAF-UES SUMMER FACULTY RESEARCH PROGRAM/

GRADUATE STUDENT SUMMER SUPPORT PROGRAM

Sponsored by the

AIR FORCE OFFICE OF SCIENTIFIC RESEARCH

Conducted by the

UNIVERSAL ENERGY SYSTEMS, INC.

FINAL REPORT

ATR PERFORMANCE VS IMAGE MEASUREMENTS

Prepared by/	Won J. Park / Professor and
Academic Rank:	Barbara S. Carruth / Graduate Assistant
Department and	Department of Mathematics and Statistics
University:	Wright State University
Research Location:	AFWAL/AARF Avionics Lab, Mission Avionics Division, Sensor Evaluation Branch, System Engineering Group
USAF Research:	Lloyd Clark
Date:	19 August 1985
Contract No:	F49620-85-C-0013

ATR PERFORMANCE VS IMAGE MEASUREMENTS

By

Won J. Park and Barbara S. Carruth

ABSTRACT

This report describes the theory and methodology use to relate ATR (Automatic Target Recognition) performance with set of image measurements and human target recognition performance. Statistical techniques described include regression analysis, robust regression, and analysis of binary data.

ACKNOWLEDGEMENTS

We wish to express our thanks to the Air Force Systems Command, Air Force Office of Scientific Research, and the AFWAL/AARF Avionics Laboratory for their sponsorship, and also we wish to acknowledge Jim Haley, Edward Gliatti, Jim Rachal, and Lloyd Clark, AFWAL/AARF, for their encouragement and suggestions.

I. Introduction:

The AFWAL/AARF Avionics Laboratory at WPAFB is investigating automatic target recognition performance for the LANTIRN Project. The study requires analyses of multivariate data and it was desired to obtain statistical help for these analyses.

In my affiliation with the Department of Statistics at Wright State University I have a statistical background including regression, factor analysis, principal components, and classification analysis.

II. Objectives of the Research Effort:

The goal of this study is to formulate the relationships between ATR (Automatic Target Recognizer) performance and a set of image measurements by applying statistical techniques such as regression analysis, robust regression, and analysis for binary data.

The first effort was to analyze the data of probability of detection and correct classification by human observer's performance on regressor variables of 19 metrics. This methodology is developed so that it can be applied directly to evaluate the performance of ATR as follow up efforts. This second stage of effort is now in process.

III. Data Organization:

The 19 image metrics for each target, denoted by X1 - X19 are defined as follows:

X1 = Range Code

X2 = RTP of χ^2 on Grayshades

X3 = Values of χ^2 on Grayshades

X4 = RTP of Contrast

X5 = Values of Contrast

X6 = RTP of K-S Min on Connected Edge Gradients

X7 = Values of K-S Min on Connected Edge Gradients

X8 = RTP of K-S Min on Edge Gradients

X9 = Values of K-S Min on Edge Gradients

X10 = RTP of χ^2 of 3 Connected Edges

X11 = Values of χ^2 of 3 Connected Edges

X12 = RTP of χ^2 on Grayshades

X13 = Value of χ^2 on Grayshades

X14 = RTP of TIR^2

X15 = Values of TIR^2

X16 = RTP of K-S Min on Grayshades

X17 = Value of K-S Min on Grayshades

X18 = RTP of K-S abs. on Grayshades

X19 = Values of K-S abs. on Grayshades

The response variable y is related to the proportion, $\hat{p}$, of correct classification out of 63 human performances for each target. Each target generates one data point and there are 221 data points in the analysis.

The later part of analysis involved with the response variable y, which is generated by proportion data by:

$$y_j = \begin{cases} 0 & \text{if } \hat{p}_j \leqslant 0.6 \\ 1 & \text{if } \hat{p}_j > 0.6 \end{cases} \tag{1}$$

This binary response data was used solely to develop statistical methodology for evaluating ATR performance, which has a binary response variable.

IV. Statistical Theory:

We give here a brief description of the statistical theory, that we have applied in our analysis.

a) Least Square Regression: The model is written as

$$y_j = \sum_{i=1}^{k} x_{ij}\beta_i + e_j \qquad j = 1, 2, \ldots, n \tag{2}$$

where y_j is response variable

x_{ij}'s are regressor variables and

e_j is i.i.d. $N(0, \sigma^2)$ random error term.

Equation (1) can be expressed in matrix form as $\underset{\sim}{Y} = X\underset{\sim}{\beta} + \underset{\sim}{e}$ and the estimator $\hat{\underset{\sim}{\beta}}$ of $\underset{\sim}{\beta}$ for minimizing the residual sum of square $RSS = \hat{\underset{\sim}{e}}' \cdot \hat{\underset{\sim}{e}} = (\underset{\sim}{Y} - X\hat{\underset{\sim}{\beta}})'(\underset{\sim}{Y} - X\hat{\underset{\sim}{\beta}})$ is $\hat{\beta} = (X'X)^{-1}X'\underset{\sim}{Y}$.

The coefficient of determination R^2 is given by

$$R^2 = 1 - \frac{RSS}{SYY} \tag{3}$$

where $S_{yy} = \sum_{i=1}^{n} (y_i - \bar{y})^2$.

b) Weighted Least Square:

If $\operatorname{Var}(\underset{\sim}{e}) = \sigma^2 \Sigma$ in the least square regression instead of $\operatorname{Var}(\underset{\sim}{e}) = \sigma^2 I_n$ as in model (2), then the solution is

$\hat{\underset{\sim}{\beta}} = (X'\Sigma^{-1}X)\ X'\Sigma^{-1}\underset{\sim}{Y}$ minimizing

$RSS = \hat{\underset{\sim}{e}}'\Sigma^{-1}\hat{\underset{\sim}{e}}$.

Now suppose that

$$\Sigma = \begin{bmatrix} w_1 & & & 0 \\ & w_2 & & \\ & & \ddots & \\ 0 & & & w_n \end{bmatrix}$$

where $w_j = \operatorname{Var}(y_j)$

then

$$\Sigma^{-1} = \begin{bmatrix} 1/w_1 & & & 0 \\ & 1/w_2 & & \\ & & \ddots & \\ 0 & & & \frac{1}{w_n} \end{bmatrix}.$$

Let

$$C = \begin{bmatrix} \frac{1}{\sqrt{w_1}} & & & 0 \\ & \frac{1}{\sqrt{w_2}} & & \\ & & \ddots & \\ 0 & & & \frac{1}{\sqrt{w_n}} \end{bmatrix}$$

, then $C'C = \Sigma^{-1}$ and

$\operatorname{Var}(\underset{\sim}{e}) = C(\sigma^2\Sigma)C' = \sigma^2 I_n$.

Note that $\underset{\sim}{Y} = X\underset{\sim}{\beta} + \underset{\sim}{e}$ implies $C\underset{\sim}{Y} = CX\underset{\sim}{\beta} + C\underset{\sim}{e}$

and $\underset{\sim}{Z} = W\underset{\sim}{\beta} + \underset{\sim}{d}$ where $\underset{\sim}{Z} = C\underset{\sim}{Y}$, $W = CX$ and $\underset{\sim}{d} = C\underset{\sim}{e}$,

and $\hat{\underset{\sim}{\beta}} = (W'W)^{-1}\ W'\underset{\sim}{Z}$ is the estimate of $\hat{\underset{\sim}{\beta}}$ by the Least Square Method.

c) Robust Regression:

A robust regression procedure is used to dampen the effect of outliers and non-normal distribution of observation $\underset{\sim}{Y}$.

Let $$\rho(t) = \begin{cases} \frac{1}{2}t^2 & \text{for } |t| \le C \\ C|t| - \frac{1}{2}C^2 & \text{for } |t| > C \end{cases} \tag{4}$$

and $\psi(t) = \rho'(t)$.

The robust estimate is obtained from

$$\min_{\underset{\sim}{\beta}} \sum_{i=1}^{n} \rho(e_i) = \min_{\underset{\sim}{\beta}} \sum_{i=1}^{n} \rho(y_i - \underset{\sim}{x}_i' \underset{\sim}{\beta}). \tag{5}$$

Computationally this is accomplished sequentially by solving weighted least square equation

$$(X'W_0X)\underset{\sim}{\beta} = X'W_0\underset{\sim}{y} \qquad i.e. \quad \hat{\beta}_1 = (X'W_0X)^{-1}X'\underset{\sim}{y}$$

where the weight matrix W_0 (diagonal) is defined by

$$w_{i0} = \begin{cases} \dfrac{\psi((y_i - \underset{\sim}{x}'\underset{\sim}{\beta}_0)/s)}{(y_i - \underset{\sim}{x}'\underset{\sim}{\beta}_0)/s} & \text{if } y_i \ne \underset{\sim}{x}_i'\underset{\sim}{\beta}_0 \\ 1 & \text{if } y_i = \underset{\sim}{x}_i'\underset{\sim}{\beta}_0 \end{cases} \tag{6}$$

and $S = \text{median} \left| e_i - \text{median}(e_i) \right| / 0.6745$

d) Linear Logistic Model:

For binary data $y_1, y_2, \ldots, y_n$ of $\{0,1\}$, we have

$$E(y_i) = 1 \cdot \Pr\{y_i = 1\} + 0 \cdot \Pr\{y_i = 0\} = p_i.$$

The linear logistic model is expressed by

$$\lambda_i = \log\left(\frac{p_i}{1-p_i}\right) = \sum_{j=1}^{p} x_{ij}\beta_j + e_i \tag{7}$$

$$= \underset{\sim}{x}_i \underset{\sim}{\beta} + e_i \qquad \text{for } i = 1, 2, \ldots, n.$$

Since

$$p_i = Pr\{y_i = 1\} = \frac{e^{\underset{\sim}{x}_i \underset{\sim}{\beta}}}{1 + e^{\underset{\sim}{x}_i \underset{\sim}{\beta}}} \quad \text{and}$$

$$1 - p_i = Pr\{y_i = 0\} = \frac{1}{1 + e^{\underset{\sim}{x}_i \underset{\sim}{\beta}}},$$

the likelihood function is

$$L(\underset{\sim}{\beta}) = \frac{\prod_{i=1}^{n} e^{\underset{\sim}{x}_i \underset{\sim}{\beta} y_i}}{\prod_{i=1}^{n} (1 + e^{\underset{\sim}{x}_i \underset{\sim}{\beta}})} = \frac{\exp\left(\sum_{j=1}^{p} \beta_j t_j\right)}{\prod_{i=1}^{n} (1 + e^{\underset{\sim}{x}_i \underset{\sim}{\beta}})} \tag{8}$$

where $t_j = \sum_{i=1}^{n} x_{ij} y_i$, and log likelihood function is

$$\log L(\underset{\sim}{\beta}) = \sum_{j=1}^{p} \beta_j t_j - \sum_{i=1}^{n} \log(1 + e^{\underset{\sim}{x}_i \underset{\sim}{\beta}}). \tag{9}$$

The maximum likelihood estimate $\hat{\underset{\sim}{\beta}}$ of β can be obtained by solving

$$\frac{\partial \log L(\underset{\sim}{\beta})}{\partial \beta_k} = t_k - \sum_{i=1}^{n} \frac{x_{ik} e^{\underset{\sim}{x}_i \underset{\sim}{\beta}}}{1 + e^{\underset{\sim}{x}_i \underset{\sim}{\beta}}} = 0 \tag{10}$$

for k = 1, 2, ... , p.

V. Data Analysis:

[A] $y_j = \hat{p}_j$;

a) Least Square Regression

The results of the least squares regression procedures for all 19 variables are presented in

Table 4.A.1. In all cases the total degrees of freedom was 220.

The λ_i transformation,

$$\lambda_i = \log\left(\frac{\hat{p}_j + 1/126}{1 - \hat{p}_j + 1/126}\right) \tag{11}$$

is derived from one suggested by Cox (1970) as an adaption of the logistic transform

$$\lambda_i = \log\left(\frac{\hat{p}_j}{1 - \hat{p}_j}\right) \tag{12}$$

If the transformation

$$\lambda_i = \log\left(\frac{R_j + 1/2}{n_j - R_j + 1/2}\right) \tag{13}$$

is used, where R_j = number of successes

n_j = number in group

$P_j = \frac{R_j}{n_j}$ = proportion of successes in group

then the cases in which $R_j = 0$ or $R_j = n_j$ which result in undefined expressions, would not have to be excluded from the analysis.

In the specific case where $n_j = 63$

$$\left(\frac{R_j + 1/2}{n_j - R_j + 1/2}\right) \cdot \frac{1/n_j}{1/n_j} = \frac{\hat{p}_j + 1/126}{1 - \hat{p}_j + 1/126}$$

Table 4.A.1

Least Squares Regression for Y_j and Transformations of the Dependent Variable

Transformation	R^2	F	Residual Plots: Normal Probability Plot	Residual Plots: Residual vs. Predicted
$y_j = \hat{p}_j$	0.5248	11.685	nearly linear	double bow
$y_j = \lambda_j = \log\left(\frac{\hat{p}_j + 1/26}{1 - \hat{p}_j + 1/26}\right)$	0.5320	12.028	linear	double bow
$y_j = \sin^{-1}(\sqrt{p_j})$	0.5381	12.323	linear	double bow
$y_j = \frac{\lambda_j}{\sqrt{V_j}}$ where $V_j = \mathrm{Var}(\lambda_j)$	0.4900	10.164	nearly linear	double bow
$y_j = \frac{\lambda_j}{V_j}$	0.3340	5.304	nearly linear	double bow

Although all cases of the least squares analysis did indicate a significant regression ($p < 0.0001$), the R^2 values were low, and the normal probability plots and double bow pattern of residuals indicated violation of the distribution assumptions, $\epsilon \sim N(0, \sigma^2)$.

Table 4.A.2

Weighted Least Squares Regression

Weight	R^2	Total df	F	Residual Plots: Normal Probability Plot	Residual Plots: Residual vs. Predicted
(14)	0.8327	170	39.547	non-linear	4 outliers
(15)	0.9102	220	107.272	non-linear	4 - 8 outliers

b) Weighted Least Squares Regression

For the weighted least squares analyses if

$$y_j = \hat{p}_j \text{ and}$$

$$w_j = \sqrt{63/\hat{p}_j(1 - \hat{p}_j)} \qquad (14)$$

then all $\hat{p}_j = 0$ or 1 were excluded from the analysis

If $y_j = \hat{p}_j + 1/126$ and

$$w_j = \sqrt{63/(\hat{p}_j + 1/126)(1 - \hat{p}_j + 1/126)} \qquad (15)$$

Then all 221 observations were included in the analysis.

Results are presented in Table 4.A.2.

In both cases the regression was significant ($p < 0.0001$).

c) Variable Selection

To select a subset of 5 to 6 variables from the weighted least squares regression, each combination of dependent variable, $Y_j W_j$, with the weighted independent variables was

analyzed by PROC RSQUARE of SAS. Since it is recommended to limit the number of independent variables to 14 for this procedure, those input to PROC RSQUARE were those variables:

- indentified by Northrup as selected for analysis
- with the highest correlations with the dependent variable, $\hat{p}_j$
- indicated as most significant in the weighted least squares regression of all 19 variables
- indicated by the SAS STEPWISE procedure

Results of the RSQUARE analysis indicate: X4, X6, X7, X8, X9, and X15 as a subset of 6 regressors. The six variables selected by Northrup were X3, X5, X7, X15, X16, X17.

Table 4.A.3 gives the results of the weighted least squares regression procedures for selected subsets of regressors. In all cases total degrees of freedom was 220 and regression was significant ($p < 0.0001$).

d) Robust Regression

Since the residual plots for the weighted least square regression for the subsets of regressors indicate outliers and non-normal error distributions, application of the robust procedure produced the results given in Table 4.A.4. In all cases: the initial estimates were from the weighted least squares regression; the total degrees of freedom was 220; regression was significant ($p < 0.0001$); $C = 1.5$; in (4) and a satisfactory resid vs. predict plot implies that the residuals appeared to be randomly scattered within a band about zero.

Table 4.A.3

Weighted Least Squares for Selected Subsets of Regressors

Variables	R^2	F	Residual Plots Normal Probability Plot	Residual vs. Predicted
X4, X6, X7, X8, X9, X15	0.9010	324.662	Non-Linear	6 outliers
X3, X5, X7, X15, X16, X17	0.8691	236.713	Non-Linear	6 outliers
X20, X21, X22	0.8834	548.238	Non-Linear	6 outliers

NOTE: Collinearity diagnostics (not included in table) did indicate ill conditioning in all but the X20 = (X6)(X8), X21 = (X7)(X9), X22 = (X4)(X15) model. In the cases with collinearity the associated regression coefficients may be poorly estimated. This is the case when variance inflation factors (VIF) are greater than 5 and $k = \lambda max/\lambda min$ is greater than 1000. If $100 < k < 1000$, then it is an indication of mild collinearity.

[B.] Binary (0,1) Data;

a) Least Squares Regression

The least squares analysis of the binary data for all 19 variables produced by conversion of the Northrup data:

$$y_j = \begin{cases} 0 & \hat{p}_j < 0.6 \\ 1 & \hat{p}_j > 0.6 \end{cases}$$

Table 4.A.4

Robust Regression for Selected Subsets of Regressors

Variables	R^2	F	No. of Iterations	Residual Plots Normal Probability Plot	Residual vs. Predicted
X4, X6, X7, X8, X9, X15	0.9858	2478.320	3	Linear	Satis-factory
X3, X5, X7, X15, X16, X17 Northrup	0.9853	2397.193	3	Linear	Satis-factory
X7, X15	0.9515	2137.779	3	Nearly Linear	Satis-factory
X20 = (X6)(X8) X21 = (X7)(X9) X22 = (X4)(X15)	0.9830	4183.283	3	Nearly Linear	Indication of Possible Decreasing Variance For e
X20 X21 X22	0.9923	9365.653	6	Non-Linear	Satis-factory

resulted in an $R^2 = 0.3957$, $F = 6.927$, $p < 0.0001$, total df = 220, with a non-linear probability plot and a resid vs predict plot indicative of non-equal variance.

b) Catagorical Analysis

PROC FUNCAT (PROC CATMOD is SAS 508), a procedure for analysis of catagorical data with logistic regression analysis, produced the results summarized in Table 4.B.1.

NOTE: For 200 df the critical value for the Chi Square statistic $\chi^2_{0.05} \doteq 234$:

$$\chi^2_\alpha = n(1 - 2/9n + Z_\alpha\sqrt{2/9n})^3 \qquad (16)$$

Where Z_α = normal deviate.

The FUNCAT (or CATMOD) procedure does generate parameter estimates for each of the variables. Comparison of these parameter estimates with those from the weighted least squares and robust procedures are included in Table 4.B.3.

c) Robust Regression

Applying the robust procedure to the binary data was not successful in improving the least squares R^2 value of 0.3957 because of the small range of residual values.

Table 4.B.1

Catagorical Analysis With Logistic Regression

Variables	Likelihood Ratio χ^2	df
X1 - X19	135.23	201
X4, X6, X7, X8, X9, X15	161.72	214
X3, X5, X7, X15, X16, X17 (Northrup)	152.40	214
X7, X15	166.40	218
X20 = (X6)(X8) X21 = (X7)(X9) X22 = (X4)(X15)	162.02	217

d) Variable Selection

The methods used for variable seletection for binary data are as follows:

i) PROC FUNCAT (CATMOD): This SAS procedure is designed specifically for catagorical data. Criteria for variable selection from this procedure was $p < 0.10$ for χ^2.

ii) PROC FACTOR with varimax rotation: The advantage of this procedure is that only the independent variables are involved in the analysis, so there should be no difference between the analyses for binary and p data. The criteria for variable selection with this procedure is that the factor loadings be high (>0.7) within the factors accounting for 70% - 90% of the variability. This, however, did identify more than 6 variables in this anaylsis.

iii) Retaining the most significant variables ($p < 0.15$) from the least squares regression, $\hat{Y} = X\hat{\beta}$ where $Y = 0$ or 1 is another method for variable selection.

iv) PROC RSQUARE will identify the combination of variables (from procedures previously mentioned) which will maximize the R^2 for a given number of variables in the model.

The results of these methods for the Northrup converted data are presented in Table 4.B.2.

e) Binary Conversion to $\hat{p}_j$

To apply the results of the $\hat{p}_j$ analyses, i.e., weighted least squares and robust regression, to the binary data a conversion is possible of binary to $\hat{p}_j$ format by caluclating

Table 4.B.2

Results of Methods for Variable Selection for Binary Data

FUNCAT (CATMOD)	Factor Analysis (Varimax, Rotation) Principal Components	Maximum Likelihood	Least Squares Regression	RSQUARE for 6 Var
X5	X2 - X9	X3 - X9	X3	X3, X5,
X12 - X16	X14 - X19	X14	X5	X6, X9,
		X17 - X19	X12 - X16	X16, X17

$\hat{p}_j = R_j/n_j$ for each cell created when up to 4 selected variables are divided into 4 levels each, where each level = range of variable / 4. Unfortunately this analysis can only be efficiently run after the variable selection has been accomplished since the nubmer of cells could be large as 4^p where p = number of variables.

Use of PROCS SUMMARY, MEANS, and REG where

$$y_j = \hat{p}_j + 1/(2\cdot n) \quad \text{and}$$

$$w_j = \sqrt{n/(\hat{p}_j + 1/(2\cdot n))(1 - \hat{p}_j + 1/(2\cdot n))} \qquad (17)$$

will accomplish this analysis.

A comparison of the results of this conversion to $\hat{p}_j$ from binary with the WLS (Weighted Least Squares), robust procedure, and FUNCAT procedures is given in Table 4.B.3.

Table 4.B.3

Comparison of Analyses for Variables X20, X21, X22

Method:	Binary -> p , WLS			
Variable	$\hat{\beta}_j$	F	df	R^2
X20	0.66804191	415.486	22	0.9850
X21	0.29020239			
X22	0.26967359			
Method:	WLS, $\hat{p}_j$			
X20	0.497260	548.238	220	0.8834
X21	-0.210140			
X22	0.627884			
Method:	Robust Regression, $\hat{p}_j$			
X20	0.81189578	4183.283	220	0.9830
X21	-0.28729008			
X22	0.32290284			
Method:	FUNCAT, Binary data	χ^2	df	
X20	-1.1108	162.02	217	
X21	-14.5102			
X22	-2.16365			

V. Recommendations:

To analyze the ATR (Automatic Target Recognition) data which is binary, it is recommended that the number of variables be reduced using the FACTOR with varimax rotation and CATMOD procedures, most significant regressors in the least squares regression, PROC CATMOD, and PROC RSQUARE.

After reduction of the model to 4 regressors, convert the binary data to $\hat{p}_j$ format as described in section e, then apply the weighted least squares approach and, if necessary due to errors not being distributed $N(0,\sigma^2)$, robust regression.

REFERENCES

Conference and journal publications:

1. Huber, Peter J., "Robust Regression: Asymptotics, Conjectures and Monte Carlo," The 1972 Wald Memorial Lectures, IMS Annual Meeting, Hanover, New Hampshire, August 28 - September 1, 1972; The Annuals of Statistics, 1973, Vol. 1, No. 5, pp. 799 - 821.

Textbooks:

2. Cox, D. R., Analysis of Binary Data, London, Methuen and Company Ltd., 1970.

3. Duda, Richard O. and Hart, Peter E., Pattern Classification and Scene Analysis, New York, A Wiley - Interscience Publication, 1973.

4. Montgomery, Douglas C. and Peck, Elizabeth A., Introduction to Linear Regression Analysis, New York, John Wiley and Sons, 1982.

5. Morrison, Donald F., Multivariate Statistical Methods, New York, Mc Graw-Hill Book Company, 1976.

END

DTIC

5-86